

EXTERIOR BALLISTICS OF ROCKETS

by

LEVERETT DAVIS, Jr.

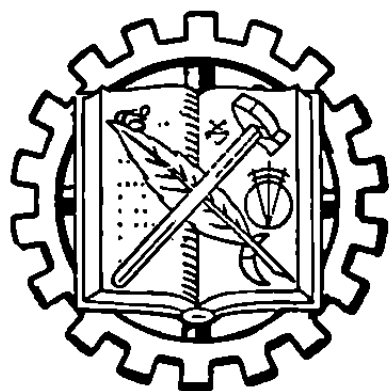
*Professor of Physics
California Institute of Technology*

JAMES W. FOLLIN, Jr.

*Applied Physics Laboratory
The Johns Hopkins University*

LEON BLITZER

*Professor of Physics
University of Arizona*



D. VAN NOSTRAND COMPANY, INC.

PRINCETON, NEW JERSEY

TORONTO

NEW YORK

LONDON

PREFACE

This book develops the basic theory of the exterior ballistics of simple rockets, that is, rockets without moving control surfaces. Emphasis is placed on the physical understanding of rocket behavior as well as on the mathematical formulation of the theory. The concepts and methods were thoroughly tested for the classes of rockets considered during the five years of intensive experimental work that paralleled the theoretical development. The equations of motion are formulated and solutions are worked out for many different cases. Because each mode of presentation has its own advantages, these solutions are usually given both in analytical and graphical form. Care was taken to use the simplest mathematical methods that will yield the desired result. In general, unfamiliar concepts that go beyond elementary analytical mechanics, differential equations, and vector analysis are explained in some detail. The formulation of the dynamics of axially symmetric rigid bodies that is developed in Chapter 9 should be of value in any study of their motion, whether or not rockets are involved. Although complicated rockets and guided missiles are not considered explicitly, they could be treated by an elaboration of the methods used for simple artillery rockets; and an understanding of these methods should form the basis for a study of more advanced missiles.

To understand the form and content of this book, one must know something of its history and of the recent history of rocketry. Rockets have been used in both peace and war for centuries; but their design and theory remained a very primitive art, in contrast with the highly developed interior and exterior ballistics of conventional weapons. With World War II this changed rapidly when several nations realized the unusual potentialities of rockets in a number of important special situations. Large research programs proceeding on a crash basis were devoted to developing a scientific understanding of rockets and to the design and construction of a large number of rockets of various sizes and types. Some of these found extensive and effective employment before the end of war. Of the types considered in this book, one could mention, among others, the anti-tank bazooka, the barrage rockets used in amphibious operations, and the rockets fired forward from aircraft.

The development of such weapons and the necessary fundamental background research were carried out at a number of laboratories in this and other countries. From late 1941 until 1946 various phases of rocket research were conducted at the California Institute of Technology under a contract (OEM sr-418) with the Office of Scientific Research and Development. This was the work of Section L, Division 3, of the National Defense Research Committee. The extensive knowledge of rocketry that was developed was in large part contained in the many separate reports and memoranda that were issued, but its effective use depended on individuals who had organized the mass of information into a systematic understanding of the subject. When OSRD was about to be dissolved at the end of the war, it was realized that this knowledge should be put into a more permanent, useful, and easily communicable form. Accordingly, the individual reports were reorganized and rewritten, where possible by those who could produce

an essentially new synthesis of the knowledge. In this way a comprehensive series of texts on the general subject of rockets was produced.

The summary report on the exterior ballistics of rockets, referred to as "The Exterior Ballistics of Fin and Spin Stabilized Rockets" in the California Institute of Technology Monographs—and planned as a companion piece to "Internal Ballistics of Solid-Fuel Rockets" by R. N. Wimpers, McGraw-Hill, 1950—was assigned to the three senior members of the project's theoretical section. It was planned to be an unclassified basic treatment of the subject. Unfortunately, the manuscript was not completed by the time OSRD support was withdrawn in 1946 because of the approaching end of OSRD. The following year the authors proposed to the Naval Ordnance Test Station, Inyokern, California, that the book be completed as originally planned. Meanwhile the Office of Naval Research, along with the Bureau of Ordnance and Army Ordnance, recognized the need for an extensive, unified treatise on the exterior ballistics of rockets. Accordingly in mid-summer of 1947 ONR undertook the sponsorship and the financial support of the completion of the book, NOTS providing editorial assistance and administration. Because of many difficulties, completion of the manuscript took several years. The resulting classified manuscript was published by ONR as "Exterior Ballistics of Rockets" NAVEXOS P-1002, 17 July 1953. This edition was very ably edited at the Naval Research Laboratory and produced by the Government Printing Office. During the next three years the authors, with much assistance from NOTS and ONR, prepared and secured the declassification of the slightly modified version which became the present volume. In the interest of economy, it was prepared by a photo-offset process from the ONR version, the deletions needed to secure declassification being filled in by the authors, a number of typographical errors being corrected, and new figures being added.

Most of the book was written shortly after the conclusion of World War II. Since that time, significant progress has been made in the field of rocketry and hence some of the predictions are subject to some reconsideration in the light of more recent developments. The basic concepts and treatment of the exterior ballistics of solid-fuel rockets are still pertinent, however, and should be permanently useful as a foundation on which to build more advanced treatments. The main changes suggested by the passage of time would be the addition of new, more complete data on aerodynamic forces and on more recent rockets, but this would raise classification difficulties.

The basic content of this book is the product of the efforts of a great many people, and even the original classified papers do not always contain an adequate record of the sources of the ideas. Most of the basic ideas that were fed into the mathematical analysis and that form its essential content came from those who claimed to be mainly experimentalists or from collaboration with experimentalists; the way in which the ideas are developed is the work of the authors. Of the many who made important contributions, explicit mention must be made of Dr. I. S. Bowen for first pointing out to the group at the California Institute the basic cause of rocket dispersion and for first setting up the problem mathematically, and of Dr. W. A. Fowler for his long-continued guidance, inspiration, and leadership. Although the detailed theoretical and experimental work under OEM sr-418 proceeded essentially independently of somewhat parallel developments elsewhere and did not seem to be greatly influenced by them, there were substan-

tial exchanges of information in spite of the hampering effects of distance and wartime secrecy. In particular, it is a pleasure to take note of the cordial relations with Dr. J. B. Rosser of the Allegheny Ballistic Laboratory. Many others have also contributed much toward building up this scientific knowledge in the field of rockets; it is most regrettable that footnote references to their work are often excluded by security regulations.

Individuals in all of the organizations mentioned above have contributed invaluable services in the preparing, reviewing, and editing for publication of the successive versions of this book; and the authors are most grateful to all of them. Our gratitude, and that of the reader, should also go to those who pointed out errors in the ONR edition. Many difficult administrative problems have arisen and if they had not been solved by hard and skillful work, there would be no book. Any attempt to list all the individuals to whom we extend our thanks would be too long and too incomplete to be of value; but a special acknowledgment must be made to the Armament Branch of ONR for supporting the completion and printing of the classified version of this book. If the final result assists the reader in becoming familiar with the science of rocket ballistics and increases the number of those skilled in this field, the efforts of those who have worked on this book will seem worthwhile.

LEVERETT DAVIS, JR.
JAMES W. FOLLIN, JR.
LEON BLITZER

January, 1958

CONTENTS

	Page		Page
PREFACE	iii	Chapter 3. The Motion During Burning—	
		Cont.	
Chapter 1. Introduction	5	3.11 Effect of Gravity	62
1.1 Delimitation of the Subject	5	~ 3.12 Effects of Linear and Angular	
1.2 Description of a Fin-Stabilized Rocket	6	Thrust Malalignment	65
1.3 General Characteristics of Rockets	7	~ 3.13 Effect of Mallaunching	68
		3.2 General Equations of Motion During	
		Burning	70
		3.21 Coordinate Systems and Forces	70
		3.22 General Dynamical Equations	75
		3.23 Forces and Torques	79
		3.231 The jet forces and mo-	
		ments	79
		3.232 Gravity	79
		3.233 Aerodynamic forces	80
		3.24 Equations of Motion—Reduction	
		to Two Dimensions	81
		3.25 Reduction of the General Solution	
		to the Linear Combination	
		of a Number of Particular	
		Solutions	82
		~ 3.3 Solutions When the Tangential Acceleration	
		Is Constant	85
		3.31 Velocity and Distance Functions	86
		3.32 Yaw Oscillation Distance, σ	87
		3.33 Reduction of the Equations to	
		Integrable Form—The Characteristic	
		Functions	91
		3.34 Solutions of the Homogeneous	
		Equations	96
		3.35 Effect of Initial Yaw	99
		3.36 Effect of Mallaunching or Initial	
		Angular Velocity	102
		3.37 Solutions of the Inhomogeneous	
		Equations by Means of	
		Green's Functions	105
		3.38 Effect of Gravity	108
		3.39 Effect of a Constant Linear	
		Thrust Malalignment	114
		3.391 Effect of σ or fin size	117
		3.392 Effect of launcher length	118
		3.393 Approximate formulas	119
		3.394 Limitations of the theory	
		—Experimental confirmation	
		of the theory	120
		3.4 Further Solutions	121
		3.41 Effect of a Constant Angular	
		Thrust Malalignment	121
		3.42 Effect of Fin or Aerodynamic	
		Malalignment	122
Chapter 2. Description of a Fin-Stabilized			
Rocket and Its Force System	13		
2.0 Introduction	13		
2.1 Description of Fin-Stabilized Rockets	13		
2.11 Definitions	13		
2.2 Jet Forces	18		
2.21 Conservation of Momentum and			
Linear Acceleration	18		
2.22 Effective Acceleration and Effective			
Burning Time	23		
2.23 Effective Launcher Length	27		
2.24 Linear and Angular Thrust Mal-			
alignment	28		
2.25 Sources of Linear Thrust Mal-			
alignment	30		
2.26 Angular Acceleration and Jet			
Damping Torque	33		
2.3 The Effective Rocket Temperature	37		
2.4 Aerodynamic Forces	37		
2.41 Definitions	38		
2.411 Dimensions and units	41		
2.412 The center of pressure			
and of lift	42		
2.42 Effects of Changes of Air Density	43		
2.43 Effects of Changes of Mass and			
Changes of the Position of the			
Center of Mass	43		
2.44 Drag	44		
2.441 Experimental values of			
drag	44		
2.442 Theoretical calculation of			
drag coefficients	50		
2.443 After-burning	54		
2.45 The Restoring Moment	54		
2.46 The Lift	57		
2.47 Fin Malalignment	58		
2.48 The Damping Moment	59		
Chapter 3. The Motion During Burning	62		
3.0 Introduction	62		
3.1 The Vacuum Approximation	62		

	Page
Chapter 3. The Motion During Burning—Cont.	
3.43 Effect of a Uniform Wind Normal to the Launcher Line ..	124
3.44 Effect of a Uniform Wind Parallel to the Launcher Line	131
3.5 Effect of the Damping Terms	133
3.51 Effect of the Cross Force	134
3.52 Effect of the Aerodynamic Damping Moment	136
3.53 Effect of Jet Damping	136
3.6 Effects of Slow Spin	137
3.61 The Vacuum Case	139
3.62 The Aerodynamic Case	142
Chapter 4. The Launching Process	149
4.0 Introduction	149
4.1 Rounds Constrained at a Point that Slides Along the Launcher	150
4.11 Equations of Motion	151
4.12 Tip-off	152
4.13 Effects of Launcher Motion ...	153
4.2 Rounds Constrained at a Point that is Fixed on the Launcher	154
Chapter 5. The Motion After Burning	157
5.0 Introduction	157
5.1 The Equivalent Shell	158
5.11 The Equivalent Initial Conditions	159
5.2 Ballistics of Shells	160
5.21 The Vacuum Approximation ..	161
5.22 The Didion-Bernoulli Method ..	161
5.23 The Otto-Lardillon Method ...	164
5.24 The Siacci Method	165
5.25 Other Methods	166
5.3 Differential Corrections	167
5.31 Green's Functions	167
5.32 Connection Between the Green's Functions and the Adjoint Equations	170
5.33 Some Approximate Differential Corrections	173
5.4 The Effect of Wind	174
5.41 Derivation of Formulas	174
Chapter 6. The Ballistics of Rockets Fired Forward from Aircraft	176
6.0 Introduction	176
6.1 Trajectory During Burning	176
6.11 Connection Between Forward Firing and Ground Firing—Equations of Motion	177
6.12 Effect of Air Drag on Velocity and Acceleration	178
6.13 Solution for the Deflection of the Tangent to the Trajectory ..	179

	Page
Chapter 6. The Ballistics of Rockets Fired Forward from Aircraft—Cont.	
6.14 The Gravity Term and Effective Launching Line	181
6.15 The Launching Factor	182
6.16 The Angular Velocity Factor ..	183
6.17 Summary	183
6.2 Approximate Trajectory During Burning—Equations and Solutions for $\sigma = 0$	184
6.3 Trajectory After Burning	185
6.4 Summary and Simplifying Procedures for Trajectory Calculations	189
6.41 Transformation of Trajectory from Effective Launching Line to an Arbitrary Reference Line	189
6.42 Transformation of Trajectory Drop for Various Dive Angles	191
6.43 Empirical Analytic Expressions for Gravity Drop and Angle of Fall	191
6.44 Effect of Small Changes in Burning Time and Velocity on Trajectory Drops	192
6.45 Differential Corrections to Trajectory Drops for Aircraft Rockets Fired at Targets Above Sea Level	194
6.5 The Sighting Problem	195
6.51 Speed-Attitude Relations	195
6.52 Sight-Setting Equation—Wing Launchers	196
6.53 Sight-Setting Equation—Lanyard Launching	197
6.54 Effective Angle of Attack of Aircraft for Rocket Firing ..	200
6.6 A Theory for the Difference Between the True Angle of Attack and the Effective Angle of Attack	201
6.7 Sources of Error and Dispersion	205
6.71 Effect of Linear Thrust Malalignment	205
6.711 Approximate formulas for long-burning rockets .	207
6.712 Low airplane speeds ...	207
6.713 High airplane speeds ..	209
6.72 Effect of Angular Thrust Malalignment	209
6.73 Effect of Fin Malalignment ...	211
6.74 Other Effects	211

II. SPIN-STABILIZED ROCKETS

Chapter 7. Introduction to Spin-Stabilized Rockets .. .	215
7.1 Purpose	215
7.2 General Characteristics ...	215

	Page
Chapter 8. Description of a Spin-Stabilized Rocket and Its Force System	218
8.0 Introduction	218
8.1 Description of a Spin-Stabilized Rocket	218
8.2 Definitions of the Aerodynamic Forces	220
8.21 Introduction of Vector Notation for Yaw, Cross-Spin, and Moment About a Transverse Axis	221
8.22 Definition of the Force and Moment Due to Yaw	222
8.23 Definition of the Forces and Moments Due to Cross-Spin	225
8.24 Summary of Numerical Data	226
8.25 Comparison of Notations	230
8.3 The Detailed Analysis of the Aerodynamic Forces	230
8.31 General Considerations	231
8.32 Lift, Drag, and Overturning Moment	235
8.33 Magnus Force and Moment, Spin Deceleration	236
8.34 The Damping Moment	239
8.35 Magnus Moment Due to Cross-Spin	243
8.4 Aerodynamic Forces on a Projectile with Fins	243
8.41 Lift, Drag, and Side Force	243
8.42 Overturning Moment and Axial Torque	244
8.43 Effect of Unsymmetrical Forces and Moments on the Motion	245
8.5 The Jet Forces	246
8.51 The Thrust and the Malalignment	246
8.52 An Elementary Theory for the Spin Produced by Inclined Jets	247
8.53 A More Accurate Theory Based on Conservation of Angular Momentum	250
Chapter 9. The Motion During Burning and During Launching	256
9.0 Introduction	256
9.1 Derivation and Reduction of the Equations of Motion of a Symmetrical Rotating Projectile	256
9.11 Approximate Equations of Motion	257
9.12 Properties of the Solutions	264
9.13 Solution of the Inhomogeneous Equations by Means of Green's Functions	267
9.14 A Rigorous Geometrical Description of the Motion; Euler's Equations	268

	Page
Chapter 9. The Motion During Burning and During Launching—Cont.	
9.15 The Energy Integrals	275
9.16 Exact Definitions of the Coordinates—The Angular Motion	276
9.17 Motion of the Center of Mass	281
9.18 Complex Representation of the Forces and the Yaw	283
9.19 Exact Equations of Motion in Complex Form and the Effects of the Errors in the Approximate Equations	287
9.2 The Vacuum Approximation	291
9.21 Equations of Motion	291
9.22 Solutions for Initial Yaw, Initial Cross-Pointing, and Gravity	291
9.23 Solution for Mallaunching	292
9.24 Linear Malalignment	296
9.25 Approximate Treatment of Malalignment	301
9.26 Derivation of the Approximate Malalignment Solution from the Green's Function	309
9.27 Angular Malalignment	312
9.3 Motion with Finite Stability Factor and Constant Acceleration	313
9.31 Equations of Motion	313
9.32 Solutions for Initial Cross-Pointing and for Mallaunching	314
9.33 Solution for Initial Yaw	321
9.34 Solution for Gravity	322
9.35 Effect of a Cross Wind	331
9.36 Malalignment	338
9.4 General Aerodynamic Effects During Burning	338
9.41 The Equations of Motion	338
9.42 Approximate Solutions of the Equations of Motion	340
9.43 Effects of Wind During Burning	341
9.5 Aircraft Firing of Spin-Stabilized Rockets	344
9.51 Qualitative Discussion of Aircraft Fired Spinners	345
9.52 Equations of Motion	346
9.53 Approximate Gravity Solution	347
9.54 Discussion of the Solutions for Initial Yaw and Mallaunching	349
9.55 Sighting of Forward Fired Spinners	355
9.6 Miscellaneous Effects During Burning	356
9.61 Effect of Regressive Burning	356
9.62 Effect of Varying Stability Factor	357
9.63 Effect of a Liquid Pay Load	357

	Page		Page
Chapter 9. The Motion During Burning and During Launching—Cont.		Chapter 10. The Motion After Burning—Cont.	
9.7 The Launching Process	358	10.2 Motion with Nonlinear Aerodynamic Moments and Constant Velocity and Spin	381
9.71 Description of Motion During Launching	358	10.21 Description of the Motion in Terms of Nutations and Precessions	381
9.72 Theory of the Mallaunching Produced by Unbalance . . .	359	10.22 Nutations and Precessions with an Overturning Moment Only	386
9.73 Expressions for the Unbalance Due to the Addition of a Small Mass	362	10.23 Damping of the Nutations . .	387
9.74 Effect of Unbalance on Malalignment	363	10.24 Precessions with a Nonlinear Overturning Moment Only	391
9.75 Effect of Malalignment During Launching	364	10.25 Precessions with General Nonlinear Aerodynamic Moments	395
9.76 Variation of Dispersion with Launcher Length for Rigid Launchers	366	10.26 Types of Instability in Spin-Stabilized Projectiles	402
9.77 Effect of Elliptical Bourrelets .	367	10.3 The Solar Yaw Camera	405
9.8 Inertial Forces on Spinning Rockets	368	10.31 Methods of Exterior Ballistics Measurements	405
9.81 Acceleration of the Parts of the Rocket	368	10.32 Analysis of Yaw Camera Records	408
Chapter 10. The Motion After Burning	370	10.4 The Effect of Aerodynamic Forces on the Trajectory	412
10.0 Introduction	370	10.41 Approximate Treatment of Right Drift	412
10.1 The Motion with Linear Aerodynamic Moments and Constant Velocity and Spin	371	10.42 Approximate Treatment of Lift	413
10.11 Motion with an Overturning Moment Only	371	Appendix A. Glossary of Symbols	417
10.12 Motion with Overturning and Magnus Moments Only . . .	373	Appendix B. Integrals, Series, and Asymptotic Expansions	425
10.13 Motion with All Transverse Aerodynamic Forces and Moments	374	Appendix C. Tables of Fresnel Integrals and Characteristic Functions	433
10.14 Effect of Gravity	380	INDEX	453

CHAPTER 1

INTRODUCTION

1.1 Delimitation of the Subject

In the broadest sense of the word, a rocket would be any device propelled by the ejection of material originally contained within itself. The term would thus include the familiar fire-works devices, the military rockets of the early nineteenth century, the artillery rockets of World War II, the jet devices used to assist the take-off of airplanes, the rocket-powered airplanes, and the V-2. Here, in this text, we consider but one of these, the artillery rocket, which is essentially a weapon that replaces an ordinary gun in a situation where weight or recoil is a serious handicap. Velocity is imparted to the projectile by one or more rearward-directed jets of gas produced by the burning of a solid propellant such as ballistite. The rockets considered range in diameter from about 2 to 12 inches, in length from about 1 to 10 feet, in weight from about 1 to 1,200 pounds, and in velocity from about 100 to 1,500 feet per second. It is not, however, the presence or absence of these characteristics that determines whether or not the theory developed here can be applied to the exterior ballistics of a rocket projectile; it is, rather, whether our assumptions as to the nature and relative magnitudes of the forces are appropriate. Hence we consider first the salient characteristics of the projectiles whose exterior ballistics we treat.

The most important limitation—the one that excludes the jet plane, the guided missile, and the V-2 from our considerations as a rocket—is that there be no movable control surfaces or variable jets manipulated by a human or automatic pilot. The projectiles to be considered must maintain their orientation because of (a) their inertia combined with the aerodynamic effect of symmetrical fixed fins or (b) the gyroscopic stability produced by rotation about a longitudinal axis. During the period in which it acts, the jet force must be much larger than all the other forces so that sufficient accuracy is obtained if these relatively minor forces are dealt with by easily handled approximations. As an associated property, all deflecting forces must be small enough so that during the short period of jet action, usually about one second, the deflection of the trajectory is small. The equations of motion during burning can then be linearized. The acceleration due to the jet action is regarded in the first approximation as being constant, and the change in mass and moment of inertia during the consumption of the propellant is regarded as having no significant effect on the motion. Although the appropriate differential equations of motion are given for the more general case, these quantities, namely, acceleration, mass and moment of inertia, are regarded as constants in the only solutions considered. The only forces considered to act after the short burning period are the force of gravity and the aerodynamic forces appropriate to an axially symmetrical body with, perhaps, radial fins. Thus no gliding action, as in an airplane, is contemplated.

It was mentioned above that a rocket can be stabilized either by fins at the rear, as in the case of an arrow, or by the gyroscopic effects of spin as in the case of an ordinary shell. The fin-stabilized rocket is much simpler to treat theoretically and is easier to design in practice. Hence it was the first to be developed. The first six chapters will be devoted to this type of rocket, and the last four to the complications introduced by axial spin.

What is the distinction between exterior and interior ballistics? Both for a gun and a rocket, exterior ballistics is concerned with where the rocket goes while interior ballistics is concerned with the forces that make it go. Thus interior ballistics considers the details of propellant combustion and the resultant forces on the projectile. In the case of a gun, the trajectory is completely prescribed while the shell is inside the barrel, and the details of the

motion are important only because they have a very great effect on the burning of the propellant. Hence all phases of the behavior while the projectile is inside the gun and the propellant is burning are treated under interior ballistics, while exterior ballistics is restricted to the treatment of the motion after the projectile has emerged from the gun and is no longer driven by the propellant.

In the case of a rocket, on the other hand, its motion usually has little effect on the burning of the propellant, but the trajectory is greatly affected by the motion during burning. Thus, with rockets, interior ballistics is restricted to the study of the burning of the propellant, the flow of the gases out through the nozzle, and the production of the force that accelerates the rocket. Little attention is paid to the rocket's motion. Exterior ballistics does not consider the origin of the force but does treat its influence on the motion during burning. This is the principal problem in the exterior ballistics of rockets. Also included in exterior ballistics is the study of the motion after the jet force ceases, but here the analysis is very similar to that for shells.

Since this text deals essentially with the exterior ballistics of rockets, the only mention of interior ballistics will be those statements required to understand the motions produced by the propellant forces. The behavior of a rocket or shell at the end of its trajectory as it passes through water, earth, concrete, or steel at the target, or just before reaching it, lies in the field of terminal ballistics and is outside the scope of the present treatment.

1.2 Description of a Fin-Stabilized Rocket

A typical fin-stabilized rocket (fig. 1.2) has two main parts, the head and the motor, the former containing what is to be delivered and the latter the device for providing the necessary velocity. The head may be solid or may contain a cavity to be filled with explosive or any other substance. If it is not solid, there will be a fuze either in the nose, as shown in the figure, or in the base, at the junction between the head and motor, or possibly both. The functioning of all these parts is beyond the scope of the present volume which considers the head merely as a load to be pushed by the motor.

The motor is a hollow chamber, usually cylindrical, containing one or more large pieces of propellant called grains. To produce uniform burning, these grains are so designed that the surface area remains nearly constant during combustion; a typical shape is a hollow cylinder burning on both inside and outside. A nozzle is located at the back of the motor to increase the momentum of the escaping gas. Other components include an igniter, which is

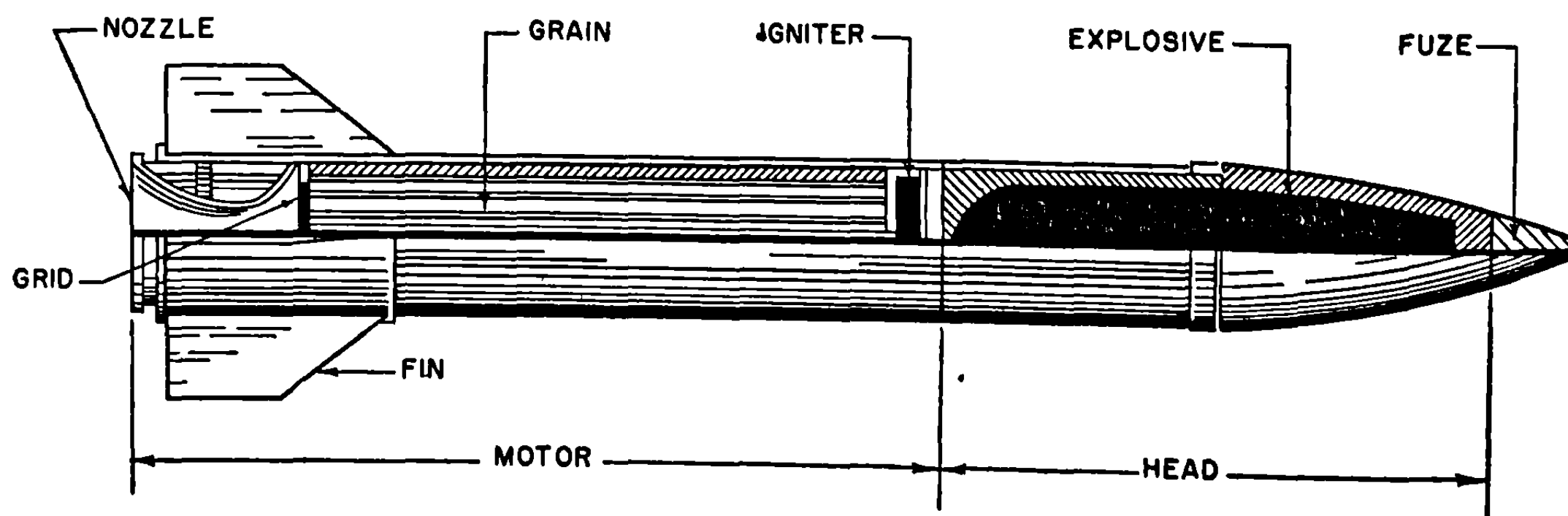


FIGURE 1.2.—Cross section of a typical fin-stabilized rocket.

usually fired electrically, and a grid to confine the propellant grain. More detailed descriptions of the motor and its functioning belong to interior ballistics; here we regard it merely as a device which produces specified accelerations.

At this point we must emphasize that the jet forces depend strongly on the temperature of the propellant before ignition, varying over the working range by as much as a factor or two. The higher the original temperature, the faster the propellant burns and the greater the acceleration of the rocket during the burning period. Fortunately, the final velocity depends only slightly on temperature so that exterior ballistics after burning is not directly affected by the propellant temperature. However the exterior ballistics during burning is strongly affected by temperature and hence the complete trajectory is changed because of the modified position and direction of motion at the end of burning.

For aerodynamic stability in a nonspinning rocket it is necessary that the center of pressure (the effective point of application of the aerodynamic force) be to the rear of the center of gravity. To meet this requirement for most rocket configurations requires the use of fins on the rear of the rocket. Such fins—designed for the velocity of the rocket, the stabilizing moment needed, and the drag that can be tolerated—are undesirable because they increase the difficulties of handling, storage, and launching. There are a number of fin types, each with advantages and disadvantages, as discussed in later chapters.

Although the rocket shown in figure 1.2 is typical and all rockets have the general features described above, great latitude in proportions is possible. Rockets are constructed with many different grain shapes, with multiple grains and frequently with multiple nozzles. It is even possible to make such drastic modifications as placing the motor ahead of the load, the nozzles being placed in a ring at the center of the rocket.

1.3 General Characteristics of Rockets

It seems desirable to consider briefly the salient characteristics of rockets since they determine when rockets will be used in place of shells and hence what demands will be made on the theory of rocket ballistics. The outstanding advantages of the rocket over the gun are that the rocket produces no recoil and that the weight of the launcher, from which the rocket is fired, is trivial compared with that of a gun. Both features are of great importance when firing heavy projectiles from a small vehicle such as an airplane, truck, or small boat, which would be greatly handicapped by the weight and recoil of a gun. It is also easy to fire many rockets in a very short time merely by providing many launchers or simple reloading devices. These can be much simpler than for a gun since it is merely necessary to lay the rocket on suitable rails; no breach mechanism is required. These features, then, enable an airplane to fire a salvo comparable to that of a cruiser, or enable a few landing craft to saturate a beach with rocket fire.

A less important feature is the relative slowness of the acceleration as compared to that of a projectile fired from a gun. Thus more delicate fuzes can be used and, if desired, the head can have thinner walls and a greater capacity in applications where penetration of the target is not important.

The fact that the ratio of length to diameter is greater for rockets than for most shells has turned out to be advantageous in cases where penetration of water or earth is desired. To understand the reason for this, we must digress briefly into terminal ballistics. When a rapidly moving projectile enters water, the nose abruptly pushes the water aside beyond the body of the projectile which then moves in an air-filled cavity or bubble. A short projectile will turn so far sideways in the bubble that it tumbles, thereby losing velocity very rapidly.

Also the trajectory is irregular, the fuze action uncertain, and the strain on the projectile very great. On the other hand, a long projectile cannot turn far before the tail strikes the side of the bubble. Then, particularly if the center of mass is well forward (a probable condition because the rear consists of a burned-out motor), the projectile rides along in the bubble touching only at the nose and tail. By properly shaping the nose, the bubble can be made relatively small, thus reducing the resistance to a minimum and increasing the range. The trajectory can be made nearly straight by using a small hemispherical cap on the nose, or the trajectory can have a curvature which will be greater the sharper the nose. That the motion is nearly parallel to the axis favors reliable fuze action. The behavior in earth is somewhat similar although the range is less because of the greater density.

It has sometimes been said that the spin of a shell tends to produce tumbling on entering the water or earth; but careful analysis shows that this is not the case. The difficulty must arise from the pointed nose and short length which are usually typical of shells. If suitably proportioned, either shells or spin-stabilized rockets would have underwater trajectories not greatly different from those of fin-stabilized rockets.

The outstanding disadvantages of rockets as compared with guns result from the rockets being less accurate, having lower velocities, and weighing more than the corresponding shells. The greater weight for the same useful load arises from the metal parts of the motor and much more propellant than is needed for a shell of comparable mass and velocity. In case only a few projectiles are to be fired, this does not matter since the elimination of the gun's weight more than compensates for the rocket weight. If a great many projectiles are to be fired over an extended length of time so that only one gun is needed, a point is reached where the total weight and shipping expense is less for the gun than the rockets. Rockets can be given high velocities, if desired, by increasing the amount of the propellant and reducing the useful load, but this greatly accentuates the above-mentioned difficulties with weight.

The most important of the rocket's defects is its increased dispersion over that of shells, running from 20 to 40 mils for most typical ground-fired, fin-stabilized rockets. Although this dispersion may be useful in some barrage applications and may not be a serious handicap in firing at large targets or with poor sights or with unfavorable conditions of launcher motion, it is a major limitation in many situations. For practical purposes, one can say that the entire dispersion arises during burning. It can be produced by many causes such as bent fins, poorly fitting launchers, moving launchers, inaccurately assembled rockets, warping during burning due to heat or pressure, wind, variation in mass, temperature, or other properties of the rocket from round to round, or by nonuniform flow of the gas through the nozzles. With care in the design and construction of the rockets and launchers and with good fire control to correct for the wind, it seems possible to reduce all but the last of these to the point where the nonuniform flow of gas, the so-called gas malalignment, is the limiting factor in the attainment of accuracy. Because it is so difficult to overcome, gas malalignment becomes the most important factor that limits the accuracy and hence the usefulness of rockets, and its action must therefore be understood. Hence we summarize here the results of the more extended discussions of chapters 2 and 3. The nonuniform gas flow produces a resultant jet thrust which does not pass through the center of mass and which, therefore, tends to rotate the rocket about a transverse axis. As soon as the nose starts to point in the wrong direction, the thrust has a component normal to the trajectory and the rocket is thus deflected from its proper course. The obvious methods of reducing the dispersion due to gas malalignment are to smooth out the flow of gas and to provide some means of constraining the rocket so that it points in the proper direction in spite of the torque.

Thus far it has not proved possible to change the design of the grid and nozzles so as to reduce the gas malalignment below its value in standard rockets. If the rocket is rotated rapidly about its axis of symmetry, the malalignment is directed first to one side and then to the other. In this way its average value can be made small enough so that it is a negligible source of dispersion. The rotation is usually produced by suitably inclining the jets. Since such spin-stabilized rockets are treated in chapters 7 through 10, we need only note here that their dispersion is easily reduced to 5 mils, and a lower value seems possible.

If one does not eliminate, or average out, the malalignment, one can still try to reduce its effects by restraining the transverse rotation of the rocket. Lengthening the launcher is an obvious procedure and a very helpful one since it applies the constraint during the crucial first part of the motion. However, since long launchers are impractical and since the gain per unit added length goes down fairly rapidly as the length increases, it is usually not practical to use launchers much longer than 5 to 8 feet. Another possibility is to try to shorten the burning distance by using higher accelerations, thus getting a greater fraction of the burning finished while the rocket is still constrained. The higher burning rate produces greater pressures which have many disadvantages; stronger and heavier motors are needed, the gas malalignment is greater, and the rocket is much more difficult to design. In spite of extensive efforts along these lines, they have not led to a significant decrease in dispersion. After the rocket leaves the launcher the rotation is reduced by the aerodynamic stability provided by the fins. Increasing the size of the fins should thus decrease the dispersion. However, extending the fins farther from the rocket makes the projectile difficult to handle and increasing the fin length along the rocket moves the aerodynamic center of the fins forward and cancels out most of the benefit of increasing the area. During the important first few feet, the air speed is low and hence the fins produce but little restoring moment during the time it is most needed. One concludes that the fins should be made as large as is convenient but that for a significant decrease in dispersion below that of standard fin-stabilized rockets, one must look to spin stabilization.

An exception to this statement is found when one fires rockets forward from airplanes. Then the air speed of the rocket is never smaller than the relatively high air speed of the plane, and the aerodynamic restoring moment is large from the start. If one does not try to use fast-burning rockets with their large torques due to gas malalignment, it is relatively easy to reduce the dispersion to a few mils since the aerodynamic moment strongly counteracts the attempt of the malalignment to produce transverse rotation. Rockets thus become quite accurate when fired from airplanes. It is necessary, however, to fire them forward since the fins turn them strongly in this direction if one attempts to aim them elsewhere. It is also clear that, for accuracy, the airplane must be flown in such a way that one knows the direction in which it is moving as well as that in which it is pointing. All these complications are discussed in chapter 6.

A list of the most important English and Greek letter symbols used throughout this report has been included as appendix A. The symbol is followed by the name of the quantity designated by each symbol, and, in many instances, the section where it is defined.

I
FIN-STABILIZED ROCKETS

•

CHAPTER 2

DESCRIPTION OF A FIN-STABILIZED ROCKET AND ITS FORCE SYSTEM

2.0 Introduction

All that is really required in studying exterior ballistics of rockets are the values of a few parameters that characterize the mass distribution, the force system, and the constraints imposed by the launcher. If the description is not given in terms of these parameters, it should be detailed enough so that they can be computed or estimated.

The only important parameters required to characterize the mass distribution are the mass, the position of the center of mass, and the radius of gyration about a transverse axis through the center of mass. The forces that act on the rocket are of three kinds: gravitational forces, jet forces, and aerodynamic forces. The effects of gravity are determined when one knows the mass and the position of the center of mass of the projectile. The treatment of the jet forces is mainly in the province of interior ballistics. Our main concern, therefore, will be with the introduction of parameters that describe the magnitude and direction of the linear and angular accelerations produced by the jet forces. We shall also make a brief excursion into rudimentary interior ballistics in order to derive some basic equations and to treat the jet damping torque. The aerodynamic forces that should be considered in the exterior ballistics of fin-stabilized rockets are the drag, the lift, the aerodynamic restoring moment, and the aerodynamic damping moment. When these forces and moments are given as functions of the velocity, the yaw, and the transverse angular velocity, we have a complete description of the aerodynamic force system. This information can be obtained from wind tunnel measurements or by varying the aerodynamic coefficients in theoretical computations of the motion until the theoretical motion agrees with that observed experimentally. Much information can also be obtained by means of a water tunnel. In the absence of these sources of information, one can usually compute a reasonably satisfactory approximation to the drag if given the shape of the projectile, provided the shape is relatively simple and smooth without large projecting lugs or fin braces. It is much more difficult to compute the other aerodynamic forces; but a knowledge of the aerodynamic coefficients of a number of different projectiles may serve as a guide in estimating the coefficients of any particular projectile of relatively conventional design.

2.1 Description of Fin-Stabilized Rockets

In this section we shall give a table and figures which show the important characteristics of a number of rockets. These will enable the reader to substitute numerical values in the various formulas to be developed in later chapters and hence to determine the magnitude of the effects under consideration. An attempt has been made to include rockets of a variety of types so that such comparisons need not be confined to a single type of rocket. The table and figures will give only the average values of the most important quantities, and will give them for only one model of each type.

2.11 Definitions.—Let us first consider some of the important dimensions. Little need be said regarding the length of the rocket except that it may vary slightly from the value given

in the table with changes of the fuze. The diameter given in the table is the diameter of the largest part; it does not include lug bands that clamp around a rocket, but it does include bourrelets. The diameters of other cross sections and the separate dimensions of the head, motor, and grain can be determined from the figures. The number, type, and dimensions of the fins are also shown in the figures, as are the positions of the points at which the round is supported by the launcher. The table gives the distance from the rear of the rocket to the center of mass of the rocket after burning; i.e., the distances from the floor to the center of mass when the rocket is resting upright on the floor with its nose in the air. The moment of inertia of the projectile, after the end of burning, about a transverse axis through the center of mass is given in the table in terms of the radius of gyration, the moment of inertia being the mass times the square of the radius of gyration.

The masses of the rocket before and after burning are listed in the table together with the mass of the propellant before burning. The mass of the parts remaining after burning is designated as the mass of the projectile, while the initial mass, which could be determined by weighing just before firing, is referred to as the mass of the round. This conforms to the convenient convention in which the parts of the rocket remaining after burning are called the projectile while the complete rocket as it rests on the launcher just previous to firing is called the round. The listed mass of the grain does not include that of the igniter. Thus the mass of the round is greater than the sum of the masses of the projectile and the propellant by the mass of the igniter, the seals in the jets, the ignition wires, and similar parts.

The velocity immediately after burning (often referred to as the burnt velocity), effective burning time, effective acceleration, and gas velocity with respect to the rocket are quantities having obvious meanings; the exact definitions will be given in 2.21 and 2.22. Only the values at 70° F. are listed; values at other temperatures are to be found in connection with more detailed specifications.

TABLE 2.11
CHARACTERISTICS OF ROCKETS

Designation of rocket	BR	3.5 AR	5.0 AR	5.0 HVAR	11.75 AR
Shown in figure number.....	2.11a	2.11b	2.11c	2.11d	2.11e
Diameter (inches), D	4.5	3.5	5.0	5.0	11.75
Length (inches), l	30.0	54.7	65.0	68.3	123.0
Distance of center of mass from rear (burnt) (inches), l_J	18.5	34.5	42.0	36.8	42.0
Radius of gyration about a transverse axis through CM (burnt) (inches), K	8.3	18.6	19.6	21.8	37.2
Mass of projectile (pounds), m_b	27.2	46.0	72.4	111.3	1,133.0
Mass of propellant (pounds), μ_b	1.43	8.5	8.5	24.0	146.0
Mass of the round ¹ (pounds), m_t	28.7	55.2	81.6	137.1	1,285.0
Burnt velocity, 70° F. (ft./sec.), v_b	353	1,120	734	1,370	813
Effective burning time, 70° F. (seconds), t_b37	.89	.89	.87	.91
Effective acceleration, 70° F. (ft./sec. ²), G	954	1,260	825	1,570	894
Gas velocity, 70° F. (ft./sec.), V_g	7,050	6,660	6,660	7,000	6,700
Deceleration coefficient (low vel.) (ft. ⁻¹), c	7.0×10^{-5}	3.5×10^{-5}	2.4×10^{-5}	2.0×10^{-5}	0.9×10^{-5}
Deceleration coefficient (high vel.) (ft. ⁻¹), c	7.2×10^{-5}	4.2×10^{-5}	4.1×10^{-5}	1.5×10^{-5}
Characteristic distance (feet), σ	265	200	200	320	650
Characteristic time, 70° F. (seconds), t_σ74	.56	.70	.64	1.21
Characteristic velocity, 70° F. (ft./sec.), v_σ	711	710	570	1,000	1,080

¹ Mass of round may be greater than sum of projectile and propellant by the mass of the igniter, seals, ignition wires, etc.

The aerodynamic drag is given in terms of the deceleration coefficient which is defined in 2.41 as the deceleration produced by the aerodynamic drag divided by the square of the velocity. The deceleration coefficient, c , is independent of velocity up to about 800 ft./sec., since in this range the drag is nearly proportional to the square of the velocity. Above this velocity the drag increases more rapidly than the square of the velocity and hence c is no longer constant. Therefore, in the case of high-velocity rockets, the table lists the deceleration coefficients of the projectiles both at low velocities and at a velocity of 1,300 ft./sec. The aerodynamic restoring moment is inversely proportional to the square of σ , the distance traversed by the projectile while the yaw oscillates through one cycle. The exact equation connecting the two is 2.41 (8). The values of σ listed in the table are those for low velocities, below 800 ft./sec. As the velocity approaches the velocity of sound, σ can either increase or decrease, depending on whether or not the forward motion of the center of pressure more than compensates for the extraordinary increases in the aerodynamic forces. Since the most important part of the burning period in the

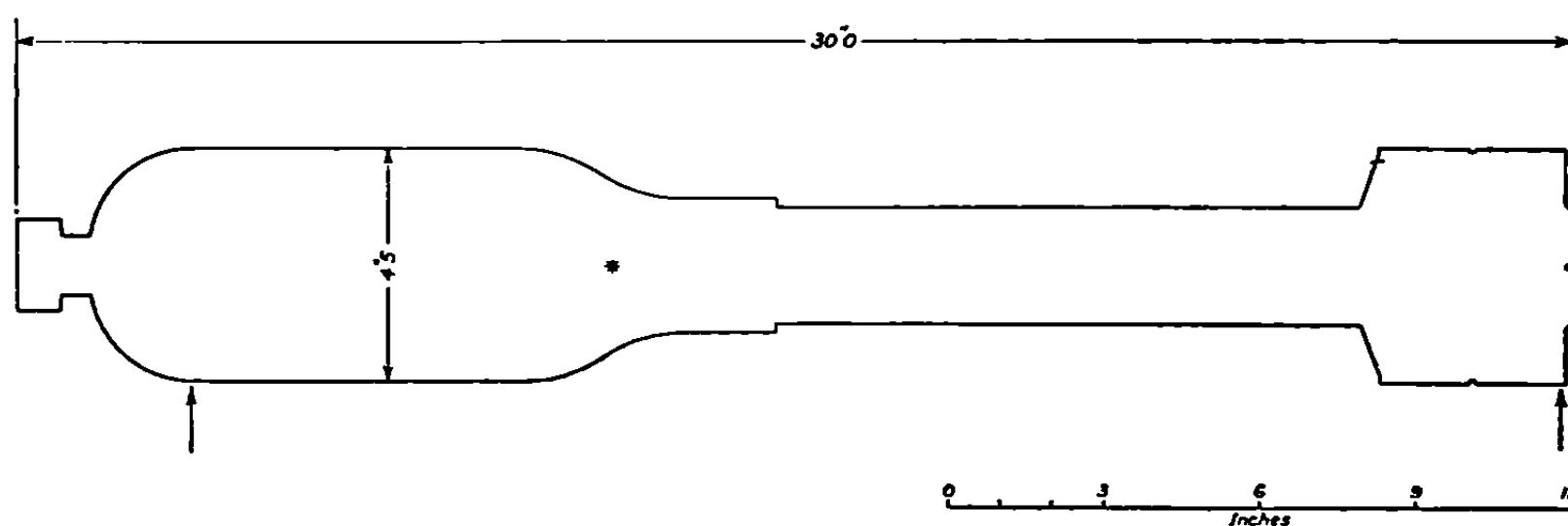


FIGURE 2.11a.—BR. Tail: Drum.

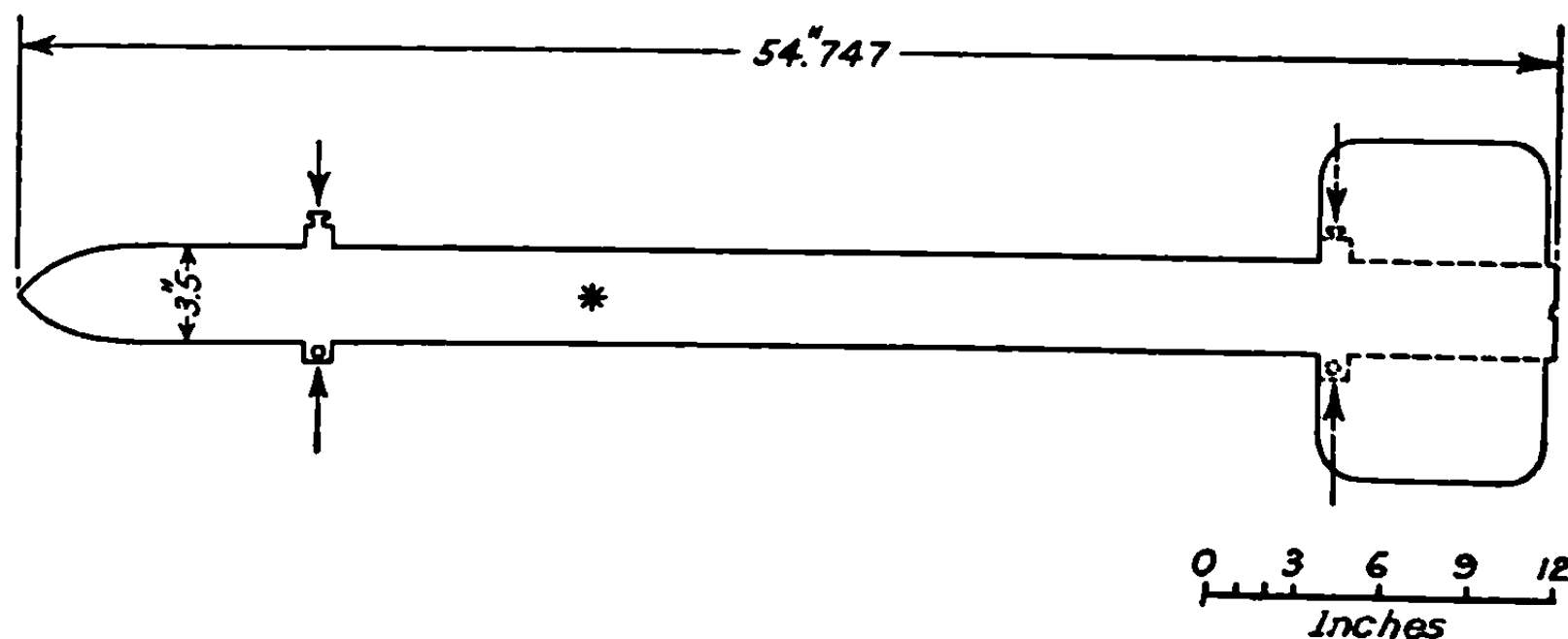


FIGURE 2.11b.—3.5 AR. Tail: 4 fins.

FIGURE 2.11.—Outlines of various rockets. The asterisk designates the center of mass and the arrows the points of support by the launcher. Figures 2.11b–2.11e show both the fins and the lugs in the same vertical plane in order to facilitate scaling off dimensions. Actually, when the lugs are in the vertical plane, the fins are inclined at 45° .

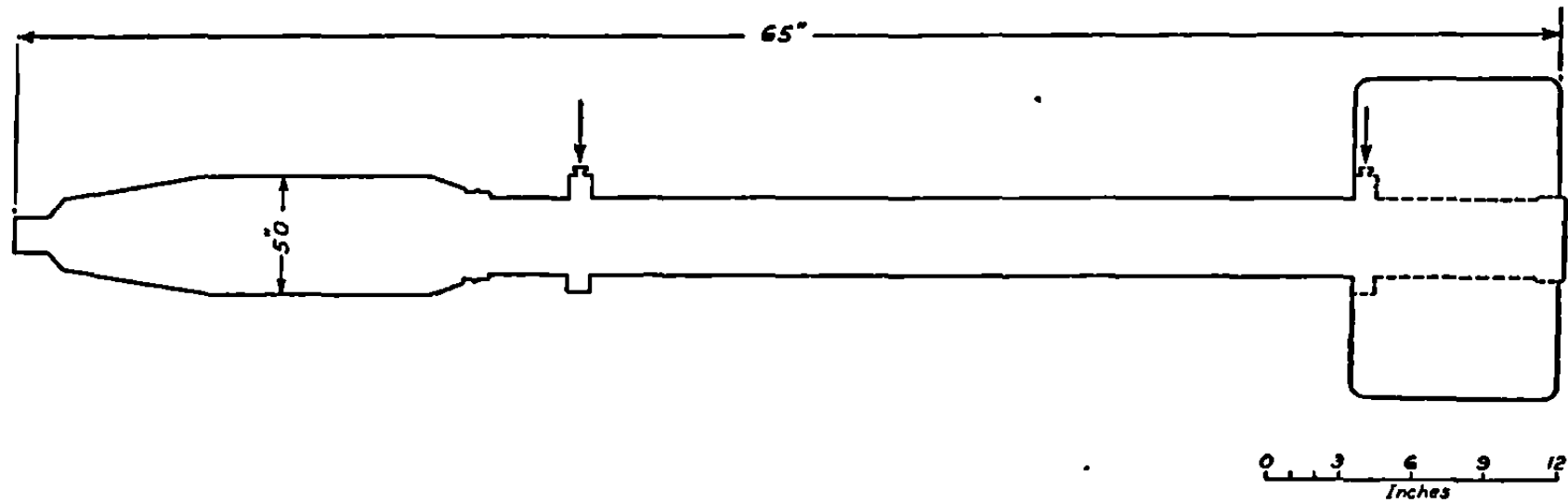


FIGURE 2.11c.—5.0 AR. Tail: 4 fins.

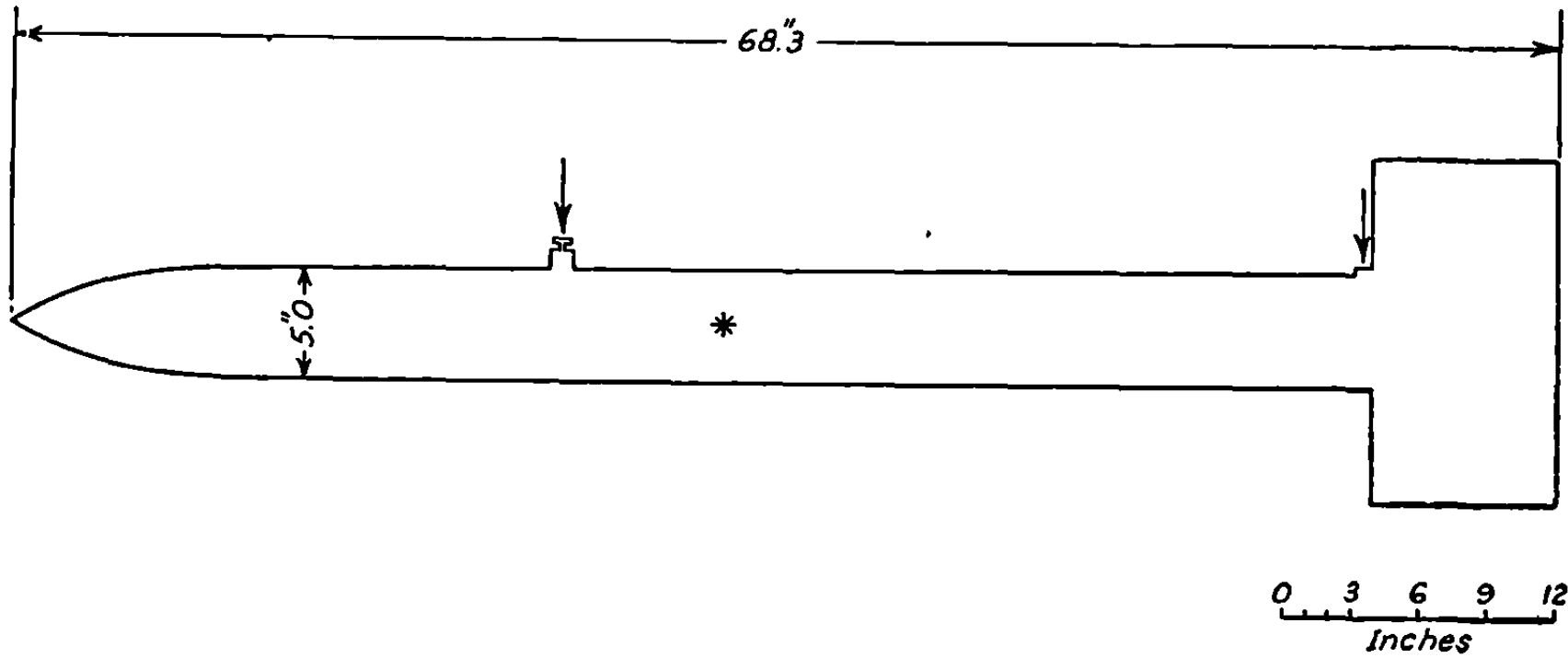


FIGURE 2.11d.—5.0 HVAR. Tail: 4 fins

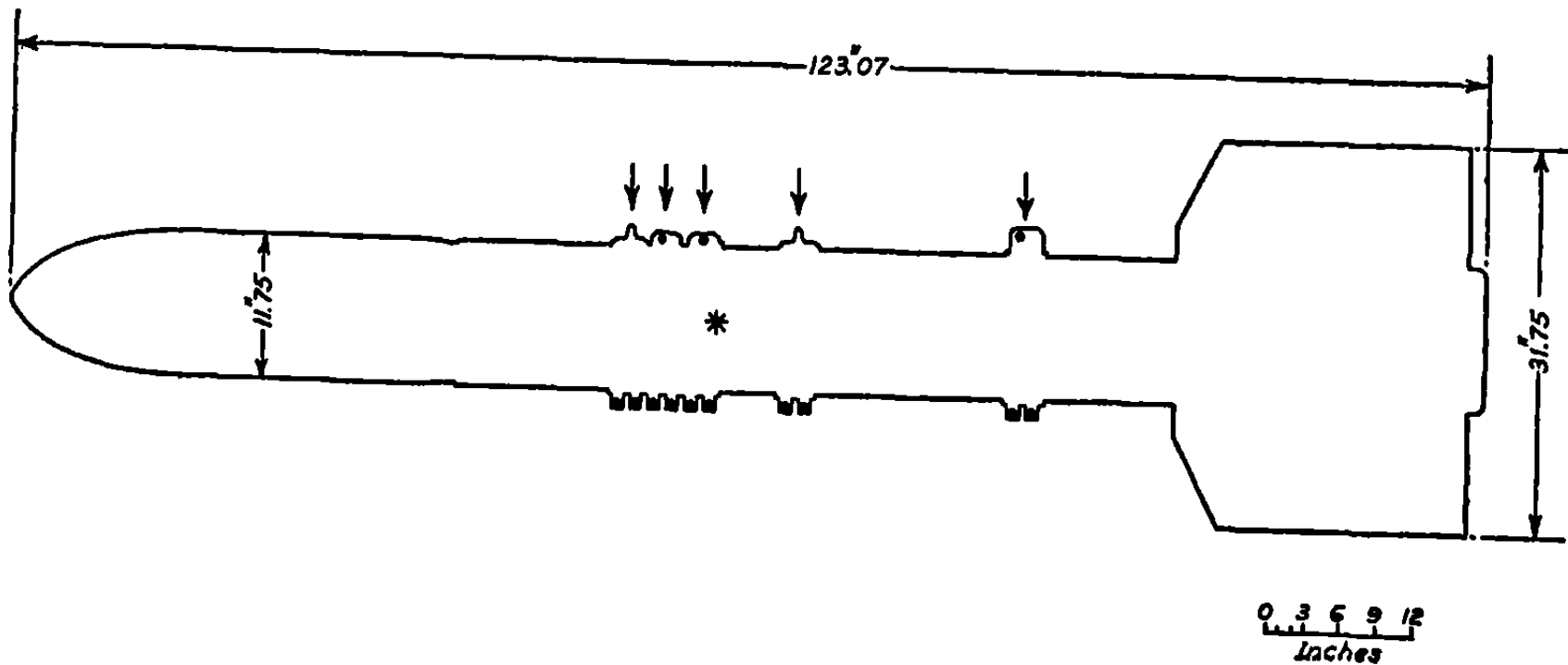


FIGURE 2.11e.—11.75 AR. Tail: 4 fins.

determination of deflections and dispersion is the early part, the low velocity value of σ is used throughout the theory. It is determined photographically from range firings, in the case of high-velocity projectiles by firings with reduced charges so that the burnt velocity is only about 600 ft./sec. It could also be determined from wind- or water-tunnel data. Two quantities important in the theory can be derived from σ and from G , the effective acceleration of the rocket. They are

$$t_\sigma = (2\sigma/G)^{1/2}, \quad v_\sigma = (2G\sigma)^{1/2}. \quad (1)$$

Evidently they depend on temperature since G does. We call t_σ the characteristic time; it is the time required for the rocket to traverse the distance σ , starting from rest and moving with the acceleration G . We call v_σ the characteristic velocity; it is the velocity attained under these circumstances at the time t_σ .

2.2 Jet Forces

The study of the forces and the accelerations produced by the flow of gas out of the motor of a rocket lies primarily in the field of interior ballistics.² It is necessary, however, to consider the subject briefly here because the results obtained from a study of interior ballistics are needed as a basis for exterior ballistics. Moreover, our point of view is quite different from that of the usual treatment, which is concerned with many questions that we disregard since they have little influence on exterior ballistics; but we must investigate some aspects of the jet forces that are of relatively little interest in the usual treatment. For example, we shall find it convenient to give much greater emphasis to momentum considerations, in contrast to the usual emphasis on pressure distribution.

Our only interest in the jet forces concerns the accelerations, both linear and angular, that they impart to the rocket. In the following sections (2.21 and 2.26) we shall consider the equations of motion of a rocket on the basis of conservation of momentum. This will give insight into the meaning of these equations and into the energy and momentum relationships that hold for rockets. It will also disclose the existence of a somewhat unexpected torque that may be called the jet damping torque. At first we shall consider the most elementary cases in which the only acceleration is along the trajectory and is determined empirically by field measurements of the acceleration or by static firing measurements which give the rocket thrust when the rocket is held stationary in the laboratory. Our principal problem will be the definition of a suitable effective acceleration and effective burning time, to be used in subsequent chapters. Next we shall describe the force system more completely, including accelerations normal to the trajectory and angular accelerations about a transverse axis. The sources of these latter undesirable accelerations will then be considered and it will be seen that probably the most important uncontrollable source of dispersion in fin-stabilized rockets is gas malalignment, a term used to describe the fact that the thrust produced by a jet does not coincide in practice with the axis of symmetry of the nozzle.

2.21 Conservation of Momentum and Linear Acceleration.—In an extensive study of interior ballistics the thrust is usually computed from the pressure distribution. This is necessary in any treatment that considers the details of the gas flow and of the burning of the propellant. It is also necessary if the question of nozzle expansion ratio is to be considered. On the other hand, if one considers not a stationary rocket on a static firing block but rather a rocket in flight having a variety of linear and angular accelerations, and if only the accelera-

² N. Wimpess, "The Interior Ballistics of Solid-Fuel Rockets," McGraw-Hill, New York, 1950.

2.2 JET FORCES

tions are desired, it is usually more convenient to obtain the thrust from momentum considerations.

The fundamental assumption underlying this treatment is that each element of gas is ejected from the rocket with a certain velocity, V_g , called the gas velocity. This velocity is with respect to the nozzle from which it is ejected, being along the axis of the nozzle. Since in the present chapter, we shall consider only cases in which the rocket does not rotate about its longitudinal axis, it is immaterial for our present purpose whether the rocket has one nozzle or many, since all the gas can be assumed to have the same velocity. We assume further that the gas velocity is independent of the acceleration and angular velocity of the rocket. This assumption is reasonable as long as the change in the velocity of the rocket during the time required for any element of gas to move the length of the rocket motor is very small compared to the gas velocity. Since the nozzle is accelerated it is important that the gas velocity be taken to be the velocity of the gas with respect to the nozzle at the instant of emission, rather than at some other time. The principal theoretical difficulty with the momentum method lies in determining the exact instant at which any particular element of gas stops interacting with the rocket. However, this is not an important practical difficulty since we define the gas velocity as having the value necessary to produce the observed acceleration or thrust.

As an introduction to the momentum method let us consider a rocket moving along a straight trajectory and ejecting the burnt gas backward along the trajectory. We shall let v be the velocity of the metal parts and unburned propellant with respect to the coordinate system in which the rocket was initially at rest. We shall let m_b be the mass of the projectile after burning, μ be the mass of the propellant ejected up to any particular time, and μ_b be the initial mass of the propellant; i. e., the total mass ejected by the end of burning. Thus the total mass of the rocket before burning is $m_i = m_b + \mu_b$, the mass of the solid parts at any time during burning is $m = m_i - \mu$, and the mass of propellant remaining is $\mu_b - \mu$. After burning m becomes equal to m_b ; thus we can write m in place of m_b in cases where the context makes it clear that we are considering the mass after the end of burning. In an infinitesimal interval of time, dt , during which the velocity of the solid parts increases from v to $v + dv$ the mass $d\mu$ is ejected from the rocket with velocity V_g relative to the rocket and velocity $v - V_g$ relative to our stationary coordinate system.

Now just before the mass $d\mu$ is ejected, the momentum of the rocket and the unburned propellant is

$$mv = (m_i - \mu)v. \quad (1)$$

Immediately afterward, the momentum of the rocket and the remaining unburned propellant is

$$(m_i - \mu - d\mu)(v + dv), \quad (2)$$

while the momentum in the same direction of the gas ejected during the interval is

$$d\mu (v - V_g). \quad (3)$$

We neglect the momentum of the gas inside the motor because the change in its momentum is small compared to the momentum of the ejected gas. This follows, in spite of the fact that its high velocity might give this gas appreciable momentum, since the amount of gas inside the motor and its high velocity can be regarded as nearly constant during the time dt , unless the interval is taken just at the beginning or end of burning. Since the linear momentum of the rocket plus the ejected gas is constant, we have, if we neglect all other forces

$$(m_i - \mu)v = (m_i - \mu - d\mu)(v + dv) + d\mu(v - V_g). \quad (4)$$

If we neglect second order infinitesimals, this can be reduced to the equation of motion

$$m dv = (m_i - \mu)dv = V_g d\mu. \quad (5)$$

Equation (5) can now be integrated by separation of variables to give the velocity as a function of μ , the mass of propellant ejected. The appropriate initial condition is that $v=0$ when $\mu=0$. We are particularly interested in v_b , the velocity at the end of burning, at which time $\mu=\mu_b$. We find that ⁴

$$v = V_g \ln \frac{m_i}{m_i - \mu} = V_g \ln \frac{m_i}{m}, \quad (6)$$

and

$$v_b = V_g \ln \frac{m_i}{m_b} = V_g \frac{\mu_b}{m_b} \left(1 - \frac{\mu_b}{2m_b} + \frac{\mu_b^2}{3m_b^2} + \dots \right). \quad (7)$$

This leads to the convenient approximate formula, valid when $v_b \ll V_g$,

$$v_b = V_g \frac{\mu_b}{m_b + \frac{1}{2} \mu_b}, \quad (8)$$

which, when expanded by the binomial expansion, differs from (7) by a term of order $V_g \mu_b^3 / 12 m_b^3$. Equation (8) is easily remembered since $m_b v_b$ is the momentum imparted to the projectile while $\mu_b(V_g - \frac{1}{2}v_b)$ is approximately the momentum imparted in the opposite direction to the gas. The term $-\frac{1}{2}\mu_b v_b$ allows for the fact that the velocities given the gas range from V_g to $V_g - v_b$. Equation (8) is not exact since relatively more propellant is ejected with velocities in the neighborhood of V_g because $dv/d\mu$ is greater near the end of burning. We can regard (6) as giving v as a function of μ . Since we can find μ as a function of the time t from static firing, and since we can usually assume that through most of the burning period the rate of burning is independent of the acceleration, we can obtain v as a function of t from (6).

Examination of (7) shows that if $(m_b + \mu_b)/m_b > e = 2.72$; that is, if $\mu_b > (e-1)m_b = 1.72m_b$, then v_b will be greater than V_g . An equivalent condition is that μ_b be greater than $0.67m_i$. In other words, if enough propellant is used, the burnt velocity of a rocket fired in vacuum and in the absence of gravitational forces can be made greater than the gas velocity by any specified amount. This should not seem surprising if it is realized that during the early stages of burning of a rocket having a large portion of its mass in the form of propellant, the rocket accelerates relatively slowly, the gas is ejected with a high velocity relative to our coordinate system, and a great deal of momentum is stored in the unburned propellant. Toward the end of burning the ejected gas has relatively little velocity, and hence momentum, from the point of view of an observer in our coordinate system. Since the momentum of the system as a whole is conserved, the momentum that the unburned propellant had acquired must be transferred to the metal parts, thereby increasing their velocity.

It is instructive to divide (5) by dt , thus getting

$$m \frac{dv}{dt} = V_g \frac{d\mu}{dt}. \quad (9)$$

⁴ We will denote log_e by ln.

This equation states that at any instant the acceleration multiplied by the total mass of the system at that instant is equal to the gas velocity multiplied by the rate at which the mass is ejected. Now the right-hand side of (9) is independent of v and is just the thrust as measured in static firing. This follows since the thrust in static firing is equal to the rate of change of the momentum of the system of constant mass consisting of the unburned propellant plus the burnt gases; and this is just the right side of (9). Hence (9) states that the jet thrust is equal to the acceleration times the instantaneous mass of the system. It should be noted that when dealing with a system consisting of a projectile plus a changing amount of unburned propellant, it is not correct to equate the jet force to the rate of change of momentum. If such a statement were true, the term $v d\mu/dt$ would be added to the left side of (9). It is true that one can regard the external force as being equal to the rate of change of the momentum of the system of constant mass consisting of the projectile, the unburned propellant, and the ejected gas. This point of view is not profitable in the case we have been considering since both the external force and the rate of change of momentum are zero. The jet force is an internal force of the system from this point of view.

It may be argued that our treatment is not valid since it neglects the interaction of the jet with the air into which it emerges and because it assumes that the interaction between the ejected gas and both the rocket and the gas that is still interacting with the rocket ceases abruptly when the ejected gas attains the velocity V_g . Moreover it is essential from our point of view that the ejected gas acquire the velocity V_g while it is still relatively close to the nozzle since otherwise the analysis becomes complicated. But if we choose to define V_g in terms of the statement that the thrust is given by the right side of (9) and that the thrust is to be determined by experiment or by a rigorous theoretical method, then our procedure will always give the proper acceleration along the trajectory and that is all that really matters. It may not give the precise value of the jet damping torque in 2.25, but there an accurate value is not needed and no other method gives as good results.

Up to this point we have assumed that there are no aerodynamic, gravitational, or other external forces besides the jet force acting on the rocket. If we assume that the component along the trajectory in the direction of motion of all such forces is $F(t)$, they will add the momentum Fdt during the interval dt , and (5) will become

$$m dv = (m_t - \mu) dv = V_g d\mu + F dt. \quad (10)$$

Hence we can write the equations of motion as

$$\frac{dv}{dt} = \frac{1}{m_t - \mu} \left(V_g \frac{d\mu}{dt} + F \right) = G_J + \frac{F}{m_t - \mu}, \quad (11)$$

where

$$G_J = V_g \frac{1}{m_t - \mu} \frac{d\mu}{dt}$$

is the acceleration produced by the jets alone. In this form the equation of motion expresses the fact that the acceleration of the rocket at a particular instant is equal to the total force, including the jet force, acting on the rocket divided by mass of the rocket at that instant. It is worth noting that the velocity and acceleration referred to are those of any point that is fixed with respect to metal work of the rocket (such as the tip of the nose, the geometrical mid-point, or the center of mass of the rocket after all the propellant has been burned). Except in the unusual case in which the center of mass of the propellant coincides with the center of

mass of the projectile after burning, the instantaneous center of mass of solid parts of the rocket during burning (i. e., the center of mass of the mass $m_t - \mu$) moves with respect to such fixed points and hence, strictly speaking, its velocity or acceleration should not be used. Since the motion of the instantaneous center of mass with respect to points fixed in the metal is only of the order of a few inches during the whole of burning, the difference in the velocities and accelerations will be completely insignificant. Since we shall find when we come to treat lateral and rotational motions that it is necessary to treat the motion of the instantaneous center of mass, rather than that of any other point, we shall assume that v in the above expressions is also the velocity of the center of mass.

It may be of interest to consider briefly some of the energy relations involved in rocketry. In static firing the ejected gas acquires a kinetic energy $\frac{1}{2}\mu_b V_g^2$ which we shall regard as being equal to the available potential energy of the propellant. When a rocket is fired into the air from a stationary launcher, its kinetic energy at the end of burning is $\frac{1}{2}m_b v_b^2$. In the absence of gravity and aerodynamic forces this leaves the energy $\frac{1}{2}\mu_b V_g^2 - \frac{1}{2}m_b v_b^2$ in the ejected gas, which has less energy than in the static firing case because it has less velocity. A detailed calculation of the energy in the ejected gas will verify this statement. If we use the approximate equation (8), we find that the fraction of the available energy that is imparted to the rocket is

$$\frac{m_b v_b^2}{\mu_b V_g^2} = \left(\frac{m_b}{\mu_b} + \frac{\mu_b}{4m_b} + 1 \right)^{-1} \quad (12)$$

Perhaps the principal value in obtaining such an expression is the opportunity given to point out that no useful purpose is served by defining this expression as the "efficiency" of a rocket. The desirable qualities of a rocket are not measured by its effectiveness in converting available propellant energy into kinetic energy.

It is instructive to derive (10) from energy rather than from momentum considerations by considering the energy changes during an interval dt in which the mass of gas ejected is $d\mu$, the velocity increases by dv , and the rocket moves a distance vdt . The kinetic energy at the start is

$$\frac{1}{2}(m_t - \mu)v^2, \quad (13)$$

the potential energy of the propellant converted into other forms of energy during the interval is

$$\frac{1}{2}(d\mu)V_g^2, \quad (14)$$

and the energy added by the external force F , which acts in the direction of motion, is

$$Fvdt. \quad (15)$$

The kinetic energy of the rocket at the end of the interval is

$$\frac{1}{2}(m_t - \mu - d\mu)(v + dv)^2 \quad (16)$$

and the kinetic energy of the ejected gas is

$$\frac{1}{2}(d\mu)(v - V_g)^2. \quad (17)$$

If we equate the sum of (13), (14), and (15) to the sum of (16) and (17) we get (10) by discard-

ing second order infinitesimals, thus indicating that we have correctly allowed for all forms of energy involved.

2.22. Effective Acceleration and Effective Burning Time.—The thrust produced by a rocket motor is its most important characteristic, and our principal interest in the thrust is in connection with the resulting acceleration along the trajectory. An empirical determination of the acceleration of the rocket as a function of time during burning for all propellant temperatures in the range of interest forms the basis for the exterior ballistics of the rocket. The acceleration is never constant throughout burning and there is no precisely defined end of burning; nevertheless, in the development of the theory in subsequent chapters it is necessary for practical reasons to assume a constant acceleration and a definite instant at which burning ends. Our present problem is the discussion of the considerations that govern the choice of suitable effective accelerations and effective burning times. Since there is considerable variation from round to round in the acceleration-versus-time curves, the deflections and dispersions computed theoretically from suitable average constant values of the acceleration and burning time will usually agree as satisfactorily with the mean of the observed values as will the results computed from any other more complicated assumptions.

It is possible to lay down specific rules for the evaluation of the parameters. It is obviously necessary to adopt such rules before turning the calculation over to computers, and it is desirable to maintain the same system of rules throughout any program in which results are to be compared, or in which they should be self-consistent. Nevertheless it must be remembered that any rules are based on experience and good judgment. The rules that are best under one set of circumstances may not be best under another. The more competent the person is who determines the values of the parameters from the experimental data and the better his physical intuitions, the less he need be bound by specific rules and the more freely he can make exceptions. It must always be remembered that the use to which the parameters are to be put may properly influence the values of the acceleration and burning time chosen. For example, since the gravity drop is relatively more affected by what happens immediately after launching, while the wind deflection is relatively more sensitive to what happens a little later in burning, one might well weigh the acceleration close to the launcher more heavily in choosing an average acceleration for gravity drop than in choosing an average acceleration for wind deflections. In almost all cases, however, the early acceleration is the more important; and, fortunately, it usually happens in practice that the acceleration is nearly constant throughout the first half or three-quarters of burning. When this is the case, this constant value should be chosen as the effective acceleration.

It is necessary to keep in mind the following factors⁵ that affect the acceleration and its dependence on the time. The burning rate of the propellant depends on its composition, its shape, the pressure in the vessel in which it is burned, and the temperature of the propellant. We shall regard the composition as fixed. The shape is chosen when the grain is designed to give as satisfactory as possible characteristics during burning. The pressure in the vessel depends on the burning rate and the exit area through which the gas escapes, and the temperature is more or less under the control of the person firing the rocket. Both the gas escape rate and the burning rate, or rate of production of gas, increase with pressure, but the burning rate increases somewhat more slowly. Thus, under any specified circumstances, there is an equilibrium pressure at which the two rates are equal; but the equilibrium is relatively delicate and shifts markedly for small changes in conditions.

⁵ For a more complete discussion, see Wimpress, *op. cit.*

When the temperature is increased the burning rate increases as does the pressure and the thrust, while the burning time decreases. A complicating factor is the erosion of the nozzles, which increases the exit area during the latter part of the burning period, and thereby decreases the burning rate and the thrust, and increases the burning time. The erosion is much greater at high temperatures than at low. Well-designed grains are usually nearly neutral burning; i. e., have constant thrust. In this way efficient use is made of the motor wall strength, since otherwise some of the weight is needed for strength during a fraction of the burning time only. For a variety of reasons, including the use of designs that allow for the weakening of the motor wall as it heats up, there is frequently some tendency to regression; i. e., the thrust decreases with time throughout burning. Since the mass also decreases during burning, the acceleration will be more nearly constant than the thrust in these cases.

Although the curve showing the thrust as a function of time may vary appreciably from round to round, the integral giving the area under the curve and hence the burnt velocity of the rocket is much more nearly constant. This can be understood in terms of the language of the previous section in terms of the assumption that the gas velocity is nearly constant although the burning rate may vary appreciably. Not only is this true for a group of rounds all of the same temperature, it also tends to hold as the temperature is changed, although here the velocity usually tends to fall off at very low or very high temperatures due to various inefficiencies. This effect is well illustrated by the following table.

TABLE 2.22
CHARACTERISTICS OF 3.5-IN. AIRCRAFT ROCKET

Characteristic	Temperature (° F.)			
	0	40	70	100
Effective burning time (sec.).....	1.40	1.12	0.93	0.75
Effective acceleration (ft./sec. ²).....	780	1,010	1,240	1,520
Velocity at end of burning (ft./sec.).....	1,090	1,130	1,150	1,140
Gas velocity (ft./sec.).....	6,450	6,700	6,800	6,750

If the acceleration is constant throughout burning, a knowledge of any two of the four quantities—acceleration, burning time, burnt velocity, and burning distance—is sufficient to determine the other two. If the acceleration is not quite uniform, then we must define average or effective values of two of the quantities, the effective values of the other two thereby being determined. Basically, the velocity is probably the most important quantity during burning and the burnt velocity is the most important parameter in determining the motion in the post-burning period. Consequently, the observed burnt velocity is usually taken as one of the basic parameters. The next most important factor in determining the motion during burning is the acceleration during the first half or three-quarters of the burning period; hence the average value of the acceleration during this interval, excluding the time on the launcher during which the value of the acceleration is unimportant, is taken as the effective acceleration, G_{eff} . The effective burning time and effective burning distances are computed from the equations

$$t_{b, eff.} = v_b / G_{eff.} \quad (1)$$

$$d_{b, eff.} = \frac{1}{2} v_b / G_{eff.} \quad (2)$$

In practice the burnt velocity and effective acceleration are usually determined from range firing records showing the velocity as a function of time during burning or from static

firing records showing thrust as a function of time. The procedure is simpler and more direct if range firing data are available. Figure 2.22 shows an illustrative example which is fairly typical of the 3.5 *AR* except that the deviations from linearity are somewhat exaggerated. The velocities are measured photographically and a smooth curve is drawn through the experimental points. Well after the end of burning this curve becomes nearly horizontal; it is not exactly horizontal because gravity and air drag slow the rocket down slightly. Since the expected slope of this part of the curve can be computed, a useful refinement in cases in which it is not well defined by the experimental points is to draw a straight line with the computed slope in the best position through the point, or points, giving the velocity well after the end of burning. The nearly horizontal straight line obtained in this way, or directly from the experimental points as in figure 2.22, is extended backwards into the burning period. Next a straight line is drawn that represents as nearly as possible the velocity during the first half or three-quarters of burning. Just how this line is to be drawn is a matter that may take some judgment, although in many cases the acceleration is so nearly constant throughout most of the burning period that there is essentially only one line that can be drawn. The slope of this line determines G_{eff} . The velocity corresponding to the intersection of this line and the nearly horizontal line is v_b ; effective burning time either can be read from the figure as indicated or can be computed from (1).

It may be desirable to correct the effective acceleration, burning time, and burnt velocity for the effects of gravity and air drag in order to determine the values, v_0 and $G_{0,\text{eff}}$, that would be obtained in the absence of gravity and air. This could be done by correcting the curve of velocity versus time, but it is probably sufficient merely to use an expression derived in 5.11 for v_0 ,

$$v_0 = v_b + t_b(g \sin \theta_0 + \frac{1}{3} c v_b^2), \quad (3)$$

and to replace G_{eff} by

$$G_{0,\text{eff}} = G_{\text{eff}} + g \sin \theta_0, \quad (4)$$

where θ_0 is the quadrant elevation of the launcher, c is the deceleration coefficient, and v_0 is the velocity that the rocket would have at the end of burning if it were not for the effects of

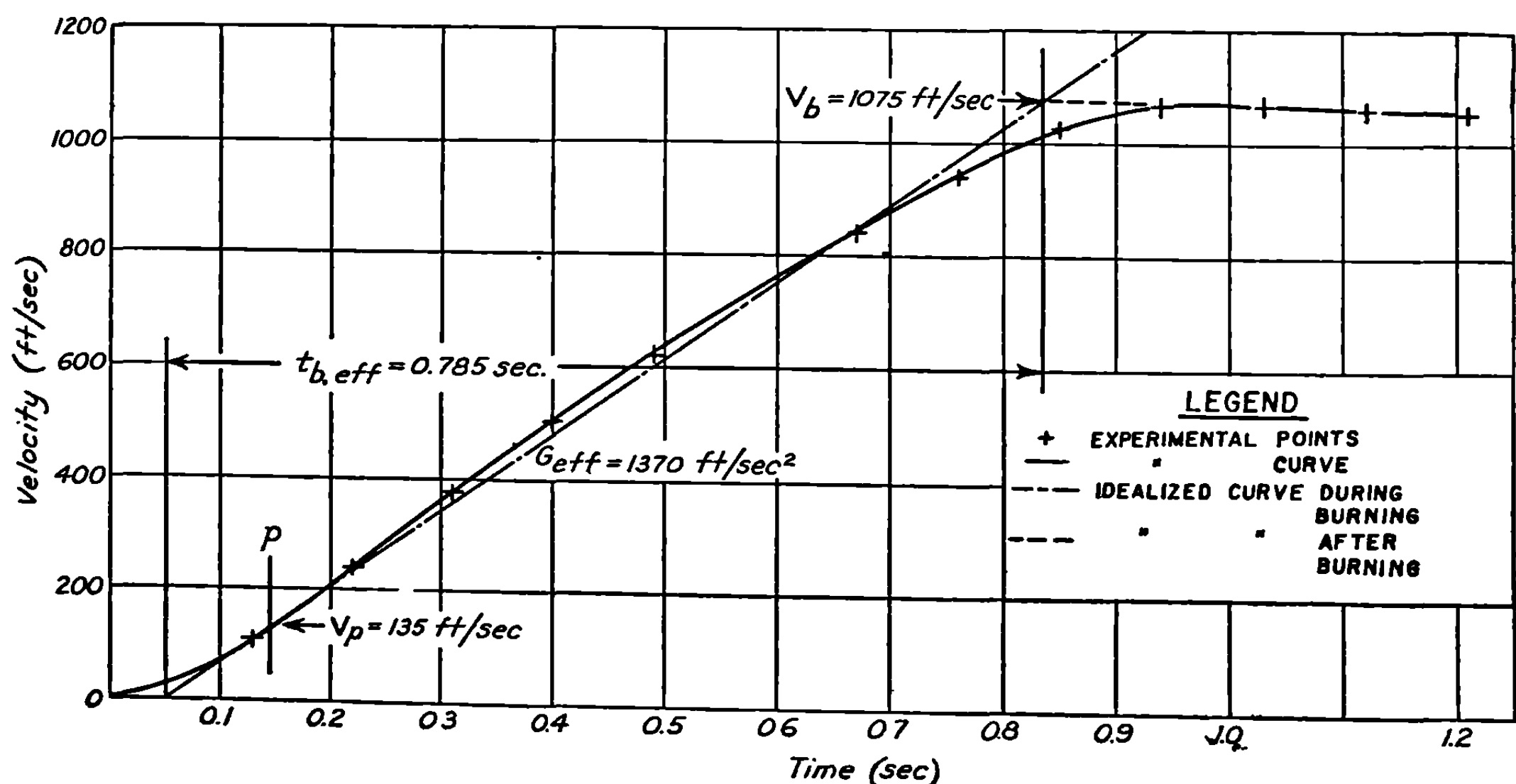


FIGURE 2.22.—Illustrative velocity-time curve.

gravity and air drag. Note that v_b is corrected for air drag but G_{eff} is not so corrected because the effect of the air drag is important only during the latter part of burning; and while v_b is the value of v at the end of burning, G_{eff} is the value of G averaged over only the early part of burning. If these corrections are made, $t_{b,\text{eff}}$ should be taken to be

$$t_{b,\text{eff}} = \frac{v_0}{G_{0,\text{eff}}} = \frac{v_b}{G_{\text{eff}}} + \frac{c v_b^3}{3 G_{0,\text{eff}}^2}. \quad (5)$$

The difference between (1) and (5) is unimportant in most cases.

It is possible to get the above data from static firing measurements of thrust versus time. This is a less desirable procedure, both because of the necessity for making the corrections described below, and because burning may not proceed in exactly the same manner in static firing as in field firing. For example, in field firing the setback (the force required to accelerate the grain or other part under consideration) and, in the case of spinners, the centrifugal force, may tend to break up the grain toward the end of burning, thus increasing the burning area momentarily and increasing the amount of propellant that blows out through the jet before burning. However, if field firing data are not available, it is usually possible to get fairly satisfactory values of the parameters from static firing data. If one assumes that the gas velocity is constant throughout burning, then the mass of propellant burned at any time is proportional to the area under the thrust-versus-time curve out to this time. Thus if $F_J(t)$ is the thrust of the jet and if

$$A(t) = \int_0^t F_J(t) dt, \quad (6)$$

and $A(\infty)$ is the total area under the curve, we have

$$\mu = \mu_b \frac{A(t)}{A(\infty)} \quad (7)$$

for the mass of propellant burned at any time. Thus from the thrust-versus-time curve we get both the thrust and the mass at any time. By using 2.21 (11), we see that the acceleration is the thrust divided by the mass of the rocket including the unburned propellant. There are now two possible methods of procedure. The acceleration can be integrated numerically very easily, giving the velocity as a function of time. If this curve is plotted, one gets a figure analogous to figure 2.22 and one can proceed as in the case where the figure is obtained from experimental data. The other method of procedure is useful when field measurements of burnt velocity are available but no complete velocity-versus-time curve has been obtained. In such cases the burnt velocity should be taken from the field data. The acceleration is calculated at a number of times equally spaced over the first half or three-fourths of the burning, and the average of these values is taken as the effective acceleration. Equation (1) then gives the effective burning time.

In treatments of internal ballistics and static firing it is usual to define a "reaction time" or a "burning time" in a way that is convenient for the purpose at hand. For example, the reaction time is frequently defined as the length of time during which the pressure is more than half of the final pressure, the final pressure being the pressure at the end of the relatively steady state that lasts throughout most of the burning. It is evident that this is not the same as the effective burning time and the two must not be confused. The effective burning time is useful in exterior ballistics; while the reaction time is useful in interior ballistics, in describing the results of static firing, and in setting up specifications to be met by statically fired samples.

Since burning time can be defined in a variety of ways, it is important to check the definition lying behind any values used. In the present work we shall always use the effective burning time as defined above, unless another definition is explicitly given.

When one is attempting to draw up specifications for the manufacture of propellant grains one would like to specify the effective burning time in order to guarantee uniform exterior ballistics; but it is easier to specify the reaction time. Fortunately if one determines the average value of the ratio of the two for a number of samples of the grain under consideration, one can, in practice, use this ratio to convert the range of effective burning times satisfactory for exterior ballistics into a range of reaction times to be used in the specifications. For example, in one particular case of a grain which was used in high-velocity rockets it was found that the ratio of t_{reaction} to $t_{b,\text{eff}}$ is 1.14 at 70° F. This value was deduced from static firing curves. The reaction time could be obtained directly from the curves, and the effective burning time was obtained by the method described above. Since it was desired that the mean effective burning time should be 0.52 second with a standard deviation of 0.14 second, the specifications require that the mean reaction time shall be $0.52 \times 1.14 = 0.59$ second with a standard deviation of $0.14 \times 1.14 = 0.16$ second.

2.23 Effective Launcher Length.—Another point that must be considered is the connection between the actual and effective launcher lengths. It is very convenient to express the initial conditions used in the theoretical formulas derived in subsequent chapters in terms of the launcher length. If the acceleration on the launcher is the same as G_{eff} , and this is true in the usual case in which the idealized velocity-versus-time curve passes through the origin of a figure such as figure 2.22, then the effective launcher length is just the true launcher length. On the other hand, it really does not matter what the acceleration on the launcher may have been; the only things that affect the motion after launching are the velocity at launching and G_{eff} , the effective acceleration after launching. Hence we define the effective launcher length

$$p_{\text{eff}} = \frac{v_p^2}{2G_{\text{eff}}}, \quad (1)$$

where v_p is the actual velocity at launching. For example, in figure 2.22, the time at which the photographs show the launching to occur is indicated by the vertical line marked “ p .” Since the velocity at this instant is $v_p = 135$ ft./sec., and $G_{\text{eff}} = 1,370$ ft./sec.², $p_{\text{eff}} = 6.6$ feet. An actual measurement of the launcher, or an integration of the velocity-time curve would give a length of 7.5 feet. The difference between the actual and the effective launcher lengths is frequently even less and hence may be neglected. In some cases the difference may be of more importance. For example, in forward firing from airplanes, there is almost no correlation between the two kinds of launcher length, since, as will be shown in chapter 6, in this case one must use the velocity of the rocket with respect to the air for v_p in (1) and hence p_{eff} depends primarily on the velocity of the airplane.

Another thing to be considered in determining launcher length is the definition of the instant of launching. Ideally this is taken to be the instant at which an ideal round loses contact with an ideal launcher. Actually, looseness of fit and flexibility of the launcher mean that the constraint will not be complete for as long a time as in the ideal case. This could be allowed for by decreasing the launcher length used in computations. Another example where it may be advisable to use a shorter launcher length than the actual one is the following. When long slender aircraft rockets are launched from rail launchers, the center of mass starts to drop as soon as the front supporting point clears the launcher. At the time that the rear supporting point slides off the launcher, the center of mass is dropping, the rocket is pointing

down, and the rocket is rotating about a transverse axis. If this is taken to be the instant of launching and the launcher length is therefore computed from the velocity at this instant, the initial conditions are quite complicated. If, however, one takes the instant at which the front supporting point slides off the launcher as the instant of launching and computes the launcher length from the velocity at this instant, the initial conditions are very simple and it is relatively easy to compute the deflection due to gravity by neglecting all further interaction of the round and the launcher. Moreover, the deflection computed on this basis is frequently an entirely satisfactory approximation to the deflection computed by the more complicated procedure. It is evident that a judicious choice of effective launcher length will enable one to make a partial allowance for some of the things that can happen during launching whose effects cannot be computed rigorously.

2.24 Linear and Angular Thrust Malalignment.—In the previous sections we assumed that the thrust of the jet acted along the axis of the rocket and passed through its center of mass. It is impossible to build such ideal rockets because metal parts cannot be made and aligned perfectly and because the gas stream will not be perfectly uniform even if the metal parts are perfect. If the line of action of the thrust does not pass through the center of mass, it produces a torque tending to rotate the rocket about a transverse axis. Since the thrust always tends to drive the rocket off in the direction in which it points, the rocket will move in a curved path and not go in the expected direction. If the line of action passes through the center of mass but is not parallel to the axis of the rocket, it deflects the rocket to the side. Imperfections of the former type are referred to as linear malalignments, the linear malalignment being the distance from the thrust axis to the center of mass; imperfections of the latter type are referred to as angular malalignments, the angular malalignment being the angle between the thrust axis and the rocket axis. A precise definition that is rigorously applicable to the general case in which both types of malalignment are simultaneously present is given below. A consideration of malalignment is important since in most cases the principal source of dispersion in fin-stabilized rockets is the linear malalignment due to nonuniform gas flow. Forward firing from airplanes forms an exception to this statement since there the high velocity through the air at launching reduces the deflection of the rocket due to linear malalignment to a point where the resulting dispersion is less than the dispersion due to imperfect fire control.

The jet forces are produced by a complicated distribution of pressure over the entire interior of the motor and the nozzle or nozzles. It is not necessary to consider this force system in detail since we can make use of the theorem that insofar as the motion of a rigid body is concerned all the applied forces and moments can be replaced by a single force F_J acting at an arbitrarily chosen point plus a moment M_J about this point. We take the point to be the center of mass and we assume that the moment is perpendicular to the axis of the rocket. Cases in which the moment has a component parallel to the axis can be treated by the methods used for spin-stabilized rockets. The resultant force acting at the center of mass, O , can be resolved into a component parallel to and a component normal to the axis of the rocket. For the component parallel to the rocket axis we write $mG_J\mathbf{k}$ where m is the mass of the rocket, \mathbf{k} is a unit vector along its axis, and G_J is the acceleration in this direction. For the component normal to the rocket axis we write $mG_J\boldsymbol{\beta}_M$ as shown in figure 2.24a. This statement defines $\boldsymbol{\beta}_M$ both in magnitude and direction. In order to appreciate the significance of the quantity defined in this way, consider the resultant force which is $mG_J(\mathbf{k} + \boldsymbol{\beta}_M)$. Thus the resultant force acts through the center of mass and makes an angle $\tan^{-1} \beta_M \doteq \beta_M$ with the axis of the rocket. Hence we can say that $\boldsymbol{\beta}_M$ is a vector whose magnitude, β_M , is equal to the angle between the rocket axis and the direction of the resultant force, and whose direction lies in

the plane of this angle and is normal to the rocket axis. For this reason β_M is called the angular malalignment.

Since the moment M_J is normal to the rocket axis, it could be produced by the force $mG_J k$ acting at the end of a vector R_M which is drawn from the center of mass normal to the rocket axis as shown in figure 2.24b. Hence a specification of R_M will define the moment. In vector notation the moment can always be written as $mG_J R_M \times k$; and this statement defines R_M if we require that R_M be normal to the axis of the rocket. Since R_M can be regarded as being the distance from the center of mass to the line of action of the jet force, it is called the linear malalignment. The vector f_R is included in figure 2.24b for use in chapter 3 where it will be defined.

If it happens that the system of forces actually applied to the rocket is equivalent to a single force acting in the proper direction and applied at a properly chosen point, then R_M locates the point of application and β_M defines the direction of action. This special case has a particularly simple interpretation in which we picture the jet as producing only a single thrust force that can be specified by giving its magnitude, mG_J , its point of application, R_M , and its direction in terms of β_M . This simple interpretation is still roughly valid in the general case; but it is not strictly correct since in general both a force and a moment are required, no matter where the force acts.

To see that it is not possible to reduce any general system of forces to a single force applied at a suitably chosen point, it is only necessary to try to reduce the system consisting of the force $mG_J(k + \beta_M)$ acting at the center of mass plus the moment $mG_J\beta_M$ about the center of mass. The necessary and sufficient condition that such a reduction be possible is that β_M and R_M be parallel. When limiting oneself to the two dimensional case in which β_M and R_M lie in the plane of the motion, this condition is always satisfied. A sufficient, although not necessary, physical condition that the jet forces be reducible to a single force is that the ejected material shall appear to diverge from a single point.

The angular thrust malalignment is defined in terms of the axis of the rocket. Now actually the rocket has many axes and there is no basis, except convenience, for singling out one and calling it the axis of the rocket. Among the many axes are the axis of symmetry of the head, the axis of symmetry of the motor, the axis through the center of mass defined by the total thrust of the jets, the aerodynamic axis, which is the direction of motion when the restoring moment is zero, and the axis through the center of mass parallel to the direction in which the rocket is constrained to move by the launcher. In the ideal case all of these axes coincide, but in actual rockets no two are precisely coincident. When some line is chosen as the axis, the directions of all the other axes with respect to the chosen one take on fixed values; that is to say, definite values can be given for the angular thrust malalignment, the fin malalignment, and the initial yaw. If a different choice is made for the axis, different values will

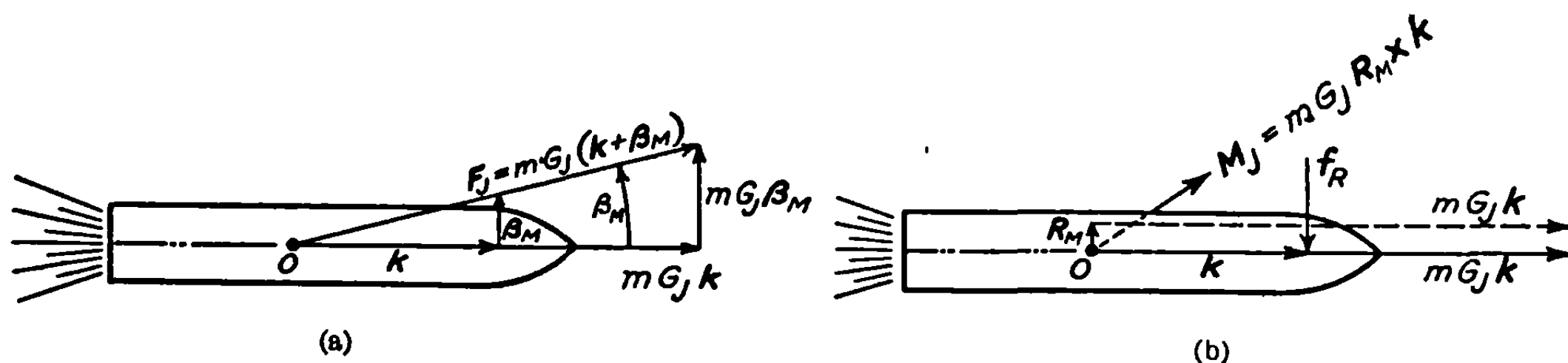


FIGURE 2.24.—Angular and linear thrust malalignments.

(a) Angular malalignment.

(b) Linear malalignment (M_J is perpendicular to the plane of the paper.)

be obtained for the various malalignments, but the trajectory of any particular rocket will not be changed. This shows that the division of the deflection into parts is to a considerable extent artificial; that the results of a comparison of the deflection due to angular malalignment, the deflection due to fin malalignment, and the deflection due to initial yaw depend on the axis selected.

It is of course possible to compare the deflection due to linear thrust malalignment with the total deflection due to these other malalignments. When this is done it is found that in most cases the linear malalignment gives the main contribution to the dispersion. In the next section we shall see that the principal cause of linear malalignment in well-built rockets is the irregular flow of gas. This causes the thrust axis of a nozzle to differ from its geometrical axis and is called gas malalignment. In rockets having a number of nozzles, gas malalignment is the result both of the lack of coincidence of the thrust and the geometrical axis of the individual nozzles and of inequalities in the thrusts at the various nozzles. The gas malalignment varies from rocket to rocket even when they are otherwise identical; it even varies during the burning period of a single rocket. It might appear that this would destroy the usefulness of the mathematical solutions given in the next chapter which enable the deflection produced by a constant malalignment to be computed. But in practice it turns out that if the average gas malalignment of a given rocket motor is computed from the observed dispersion under any set of circumstances, then the dispersion under any other circumstances can be computed from the theory. Moreover if one has had enough experience to estimate the average gas malalignment to be expected from a given motor design, the theory enables one to predict the dispersion to be expected.

2.25 Sources of Linear Thrust Malalignment.—As soon as it was clearly understood⁶ that linear thrust malalignment would produce a deflection of the trajectory and that therefore random malalignment would produce dispersion, efforts were made to check the theory and to reduce the dispersion by reducing the malalignment. The distance, called the mechanical malalignment, from the axis of the nozzle to the center of gravity was measured before firing by a device which located the axis of the nozzle by means of a conical mandrel and which located the center of mass by balancing. Field firings showed a very good correlation between the average deflection produced by a given mechanical malalignment and the value expected on the basis of theory. But the deflections of the individual rounds showed a great deal of dispersion about the expected value. After an extensive investigation it was concluded that while such factors as wind, launcher motion, variation in burning rate, etc., could produce dispersions that were large under some circumstances, under ordinary circumstances they were less important than the fact that the thrust axis during burning did not coincide with the position of the geometrical axis of the nozzle before burning. Various hypotheses have been suggested to account for this, and a considerable amount of work has been done to try to determine which hypotheses are the most acceptable. It has been concluded that because of nonuniform gas flow, with rockets of the usual design such as the 4.5 BR or the 5.0 HVAR, the thrust axis of the jet differs from the geometrical axis of the nozzle during burning by enough to produce linear malalignments of the order of 0.025 inch. Another possibility is that the geometrical axis of the rocket is displaced by the pressure inside the motor so that it does not occupy the same position before and during burning. This can occur for a variety of reasons, including the straightening of a crooked motor tube under pressure (the Bourdon gauge effect), the warping of a motor tube as it is heated, or the displacement of an improperly

⁶ At CIT this was discovered by I. S. Bowen.

2.2 JET FORCES

supported nozzle with respect to the motor tube. Although it is possible to build rockets in which the axis of the nozzle is displaced during burning, it may be concluded that in most well designed rockets the only important effect is the nonuniform flow; this is called gas malalignment.

Because of the great practical importance of the conclusion that the limiting factor in determining the lower bound of the dispersion of fin-stabilized rockets is the gas malalignment, it will be worth while to consider further the evidence upon which the conclusion is based. The theoretical treatment of the motion of a malaligned rocket to be given in chapter 3 enables one to compute α_R , the deflection of the trajectory, in mils (milli-radians) produced by each 0.001-inch mechanical malalignment. To check the theory, one measures, as described above, the mechanical malalignments of a number of rockets and fires them at low quadrant elevation with the rockets oriented on the launcher so that the mechanical malalignment will make them go alternately right and left. If the mechanical malalignments are purposely made large by unsymmetrical heads, the displacements due to mechanical malalignment will be relatively large compared to those due to gas malalignment which will be randomly distributed. By firing a number of rounds, the effects of the unknown gas malalignment and of the other causes of dispersion can be averaged out and the value of α_R determined experimentally. The experimental value has been compared with the theoretical for a number of rockets, and in all cases any discrepancies have been within the experimental error. Perhaps the best test involved 50 rounds of 5.0 HVAR rockets fired in the Mojave desert in 1944 from a zero-length launcher. The mechanical malalignments, which were of the order of 0.1 inch, were produced by replacing the filler of the head with lead cast off center. The experimental value of α_R was 0.98, while the theoretical value was 1.06. If in such a test each deflection is corrected by the amount computed from the measured mechanical malalignment and the remaining dispersion is all attributed to gas malalignment, one can compute from α_R what the "gas" malalignment must have been to produce the dispersion. (The quotation marks are usually used with values of the gas malalignment obtained in this way, since actually they include the effects of all causes of dispersion and need not be due to irregular gas flow.) In the test referred to above the "gas" malalignment was found to be 0.029 inch. For the 4.5 BR it has been found to be 0.023 inch. It is easy to get very much larger values than these, but very difficult to get appreciably smaller values. One precaution that is worth noting in connection with experimental determinations of α_R is that it is not always safe to try to produce large mechanical malalignments by bending the motor tubes, since they may straighten somewhat during burning due to the Bourdon gauge effect.

In order to determine whether the residual dispersion could properly be attributed to gas malalignment, experiments were carried out in which the torques about a transverse axis were measured when small rocket motors were static fired and when miniature nozzles were fed by freely flowing compressed air. On the basis of these experiments and the range firing of various standard and special types of rockets, Wilson and Kron at the California Institute concluded that:

1. A nozzle fed by a uniform flow of gas produces a uniform torque about a transverse axis which is correlated with the mechanical malalignment. The precise shape of the nozzle is unimportant.
-

2. A nozzle fed by a grain of burning ballistite in close proximity is subject to a constant torque plus an erratically varying additional torque of considerable magnitude. This torque is sufficient to produce the dispersion ascribed to "gas" malalignment. With the same nozzle it varies from one firing to the next and varies appreciably during burning on any one firing, the sign of the torque sometimes changing part way through burning. The fluctuations are not rapid enough so that any significant averaging out to zero takes place.

3. The mechanical malalignment force is controllable, and may be predicted and measured. It may be reduced to small values by proper balancing of the round. There is no evidence that rocket motors in their usual forms become distorted from temperature or pressure effects during burning to such an extent that mechanical alignment is seriously affected.

4. The observed dispersion of rounds having low mechanical malalignment is caused by the effects of wind, mallaunching, fin malalignment, and gas malalignment. Of the causes listed, gas malalignment is usually by far the most important uncontrolled phenomenon contributing to the dispersion of rocket fire.

5. Gas malalignment is produced by the flow of gas past the grid or any other obstructions near the entrance of the nozzle (compare item 1) and perhaps in other ways. Long slender nozzles are somewhat better than shorter, thicker ones in smoothing out the effects of non-uniform gas feed. Nozzles having the proper aerodynamic shape to give freedom from shock waves are somewhat better than conical nozzles, but the difference is not enough to justify the added expense. The only effective methods that have been found for decreasing the dispersion due to gas malalignment are to use spinning rockets, or to use very short burning times and very long launchers.

It has been proposed by some of those who have carried out experiments on these problems that the discrepancy between the observed dispersion and that predicted from the mechanical malalignment measured before firing is due to motion of the venturi relative to the rocket tube under the influence of the pressure in the motor. They base this conclusion on correlations between what would be called above "gas" malalignment and the peak load on the venturi, the peak load being a function of the propellant temperature. They find that the unexplainable dispersion is proportional to the peak pressure and that it correlates well with the estimated rigidity of the nozzle assembly which varies with the type of rocket and with the method of manufacture. Thus their displacement theory appears quite plausible on the basis of the data they consider. It is important to determine whether the displacement theory or the gas malalignment theory is correct since in the former case the dispersion of fin-stabilized rockets can be markedly reduced by making them more rigid and by eliminating circumferential variations in weld strength in their manufacture while in the latter case one must either try to smooth out the gas flow or, if this appears impossible, must use rotating rockets. The most direct test of the displacement theory would be an observation during static firing of the motion or absence of motion of the nozzle of a properly mounted motor.

In the absence of such direct evidence as to the validity of the displacement theory, all of the available indirect evidence available at CIT has been reconsidered. It appears quite certain that, as stated above, there is no appreciable displacement of the nozzle or nozzle assemblies in CIT rockets. For example, the dispersion of the 3.5 AR is essentially independent of the propellant temperature over a range of temperature in which the pressure just inside the nozzle varies by a factor of 2.8. It also appears certain from the studies mentioned above that there is a nonuniform flow of gas in rockets that does produce torques about a transverse axis; that is, that there is a true gas malalignment. There is no reason to suppose that, with certain

types of grids and propellants, the gas malalignment should not increase with motor pressure and should not vary with apparently minor variations in design. There is no evidence to show that this will account for all of the effects observed with the other rockets, but it seems most probable that gas malalignment is an important factor and that it will be the dominating factor in all rockets that are sufficiently rigid.

2.26 Angular Acceleration and Jet Damping Torque.—By extending the treatment of 2.21 to cases in which the rocket is rotating about a transverse axis, we can investigate the effects of the variation in the transverse moment of inertia and in the position of the center of mass on the equations governing the lateral and rotational motion of the rocket. It will be found that the equations have exactly the form to be expected if we interpret them as being the equations of motion of the center of mass, rather than of any point fixed with reference to the metal parts. Also we shall obtain expressions for the so-called jet damping torque. The existence of this torque was first called to our attention by Dr. J. B. Rosser, who pointed out that if a rocket rotates about a transverse axis during burning, the gas must be accelerated laterally as it flows down the motor tube. The reaction on the motor tube tends to damp the rotation.

Let us consider what happens to a rocket whose motion during burning is confined to a single plane. We concern ourselves only with the changes that occur during an interval dt in which, in the notation of 2.21, the rocket ejects a mass of gas $d\mu$. As the propellant burns, the center of mass will move forward along the axis of the rocket. We denote by C the point occupied by the center of mass at the beginning, and by C' the point occupied at the end, of the interval, these points being fixed with respect to the metal parts of the rocket. We assume that the propellant burns symmetrically so that C_p , the position of its center of mass, does not move with respect to the metal parts. If, as indicated in fig. 2.26, l_p is the distance from C back to C_p and $l_p + dl_p$ is the distance from C' to C_p , then the distance that the center of mass moves during our interval is dl_p . If m is the mass of the rocket and unburned propellant at the beginning of the interval, $m - d\mu$ will be the mass at the end. In order to calculate dl_p , consider the system as it is at the end of the interval, taking the origin temporarily at C' . If now we add the mass $d\mu$ at C_p , the center of mass will shift the distance dl_p from C' to C . Hence

$$m dl_p = d\mu (l_p + dl_p),$$

and, to terms of the first order

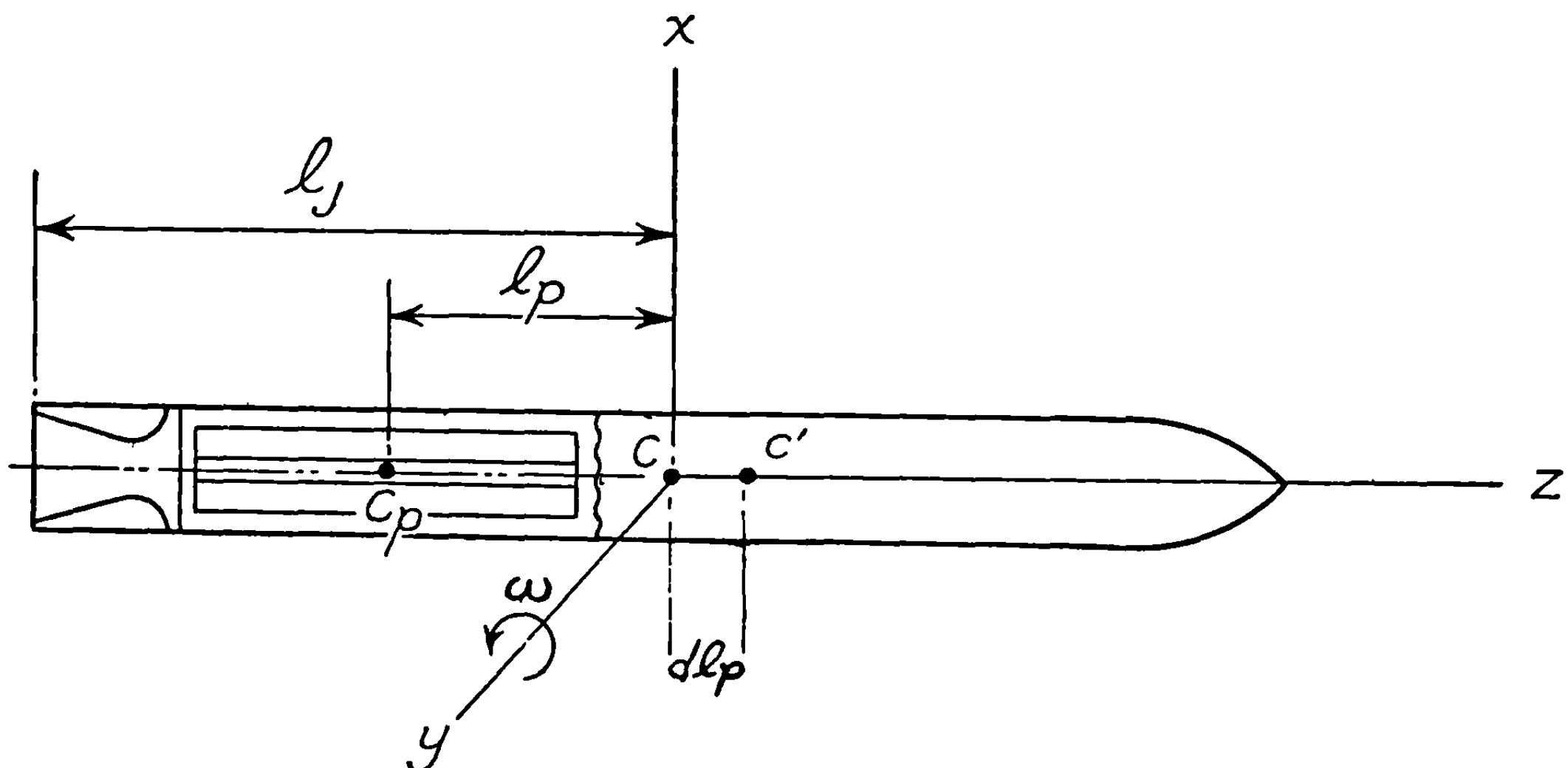


FIGURE 2.26.—Displacement of the center of mass.

$$dl_p = \frac{l_p}{m} d\mu. \quad (1)$$

We must now introduce a Newtonian coordinate system with reference to which we can describe the motion of the rocket. It is most convenient to use an unaccelerated, nonrotating system whose origin, O , coincides, at the beginning of the interval, in position and velocity with C and whose Oz -axis coincides with the rocket axis. The Ozx -plane is taken as the plane of motion so that the rocket must rotate about the Oy -axis, the angular velocity being ω . Since the rocket experiences an acceleration G , while the coordinate system is unaccelerated, by the end of the interval the point C will have moved a distance $\frac{1}{2}G(dt)^2$ with respect to O . This is a second order infinitesimal, as is the motion of C with respect to O due to rotation; and all second order infinitesimals can be neglected in our treatment.

At the beginning of the interval both the z - and x -components of the velocity of C are zero while the components of the velocity of C' are zero and ωdl_p , respectively. The components of the velocity of C' at the end of the interval are denoted by dv_z and dv_x , respectively. Hence at the end of the interval the z -component of the velocity of C is dv_z and the x -component is $dv_x - \omega dl_p$. It will be noted that dv_z is the change in the lateral velocity of the center of mass in the interval dt and includes both the effects of the acceleration of the metal parts of the rocket and the motion of the center of mass with respect to the metal parts. We assume that the gas acquires the velocity V_g by the time it reaches the center of the exit plane which lies at a distance l_J behind C . Thus the z - and x -components of the gas velocity are $-V_g$ and $-\omega l_J$ with respect to our coordinate system. At the beginning of the interval both the z - and x -components of the linear momentum of the solid parts are zero. At the end of the interval the sum of the linear momentum of the remaining solid parts and that of the ejected gas must equal the momentum imparted by the external forces, such as gravity and aerodynamic forces, whose components are F_z and F_x . Thus

$$dv_z(m - d\mu) + (-V_g)(d\mu) = F_z dt,$$

or

$$mdv_z = V_g d\mu + F_z dt. \quad (2)$$

This is exactly equation 2.21 (10) and shows that the rotation does not affect the acceleration along the trajectory. The entire discussion of 2.21 can be applied to this component of the acceleration. Likewise for the x -direction

$$dv_x(m - d\mu) - \omega l_J(d\mu) = F_x dt$$

or

$$mdv_x = \omega l_J d\mu + F_x dt, \quad (3)$$

or

$$\frac{dv_x}{dt} = \frac{\omega l_J}{m} \frac{d\mu}{dt} + \frac{F_x}{m}. \quad (4)$$

This equation states that the lateral acceleration of the center of mass is equal to the applied force divided by the mass plus an additional term that is proportional to the angular velocity about a transverse axis. This additional term is negligible under ordinary circumstances since the entire lateral velocity imparted by it during burning will be of the order of $\omega l_J \mu_b / m$. By 2.21 (8) this is approximately $\omega l_J v_b / V_g$, and hence the angular deflection of the trajectory is of the order of $\omega l_J / V_g$ radians. Since ωl_J would rarely be greater than 2 ft./sec. while V_g is usually 7,000 ft./sec. the deflection will be of the order of 0.3 mil at most. It should be noted that,

strictly speaking, (4) gives the lateral acceleration of the moving center of mass while (2) gives the longitudinal acceleration of C or C' .

In the above discussion we obtained changes of velocity and accelerations with respect to a uniformly moving coordinate system. If we take any other inertial coordinate system, including the one with respect to which the rocket was initially at rest, the velocities will be different, but the changes of velocity and the accelerations will be the same. Hence the above formulas apply generally.

Let us now consider the angular acceleration. We shall use the theorem that for any system of fixed mass the rate of change of the angular momentum with respect to the origin of any inertial system is equal to the moment with respect to this origin of the applied exterior forces. Consider the change in angular velocity, $d\omega$, during the interval dt . It is most convenient to continue to use the coordinate system whose origin coincides with the center of mass of the rocket at the beginning of the interval and whose velocity is the velocity of the solid parts at that instant. The angular momentum of the solid parts with respect to O at the beginning of the interval is

$$I\omega \quad (5)$$

where I is the moment of inertia of the rocket, including the propellant, at this instant. The angular momentum about O of the solid parts remaining at the end of the interval (as calculated from the theorem that the angular momentum of a rigid body about some point is the sum of its angular momentum about its center of mass plus the angular momentum about the chosen point of the entire mass concentrated at the center of mass) is

$$I'(\omega + d\omega) + (m - d\mu)dl_p dv_x = I'(\omega + d\omega) \quad (6)$$

to terms of the first order. In (6) I' is the moment of inertia with respect to C' of the solid parts remaining at the end of the interval. The two components of the velocity of the ejected gas are $(-V_g, -\omega l_J)$, the coordinates of the point of emission are $(-l_J, 0)$, and the mass involved is $d\mu$. Hence the angular momentum with respect to O of the ejected gas is

$$d\mu(-l_J)(-\omega l_J) = \omega l_J^2 d\mu. \quad (7)$$

If the aerodynamic forces or any other exterior forces produce the torque L_v , they will increase the angular momentum by

$$L_v dt \quad (8)$$

during the interval. Combining all these results, we see that (6) plus (7) minus (5) must equal (8). Thus

$$I'd\omega = (I - I' - l_J^2 d\mu)\omega + L_v dt. \quad (9)$$

Let us now obtain an expression for $I - I'$. The moment of inertia about an axis through C' of the solid parts at the beginning is

$$I + m(dl_p)^2 \doteq I. \quad (10)$$

We defined I_p to be the moment of inertia of the propellant about a transverse axis through C_p , its center of mass, at the beginning of the interval. Thus I_p is a function of time and varies from I_{p0} at ignition to zero at the end of burning. The change in I_p during the interval is denoted by dI_p , which is negative since I_p is decreasing; hence $(-dI_p)$ is the moment of inertia about an

axis through C_p of the material of mass $d\mu$ that is burned during the interval. The moment of inertia with respect to a transverse axis through C' of this material is

$$-dI_p + d\mu(l_p + dl_p)^2 \doteq -dI_p + l_p^2 d\mu. \quad (11)$$

Subtraction of (11) from (10) gives us

$$I' = I + dI_p - l_p^2 d\mu. \quad (12)$$

Substitution of this in (9) gives

$$I \frac{d\omega}{dt} = -\omega \left[(l_J^2 - l_p^2) \frac{d\mu}{dt} + \frac{dI_p}{dt} \right] + L_y. \quad (13)$$

This equation states that the moment of inertia times the rate of change of angular velocity is equal to the sum of two terms. The second term is just the torque due to the applied forces, while the first term may be called the jet damping torque since it is due to the jet and since in rockets of the usual type it tends to damp out any angular velocity that may be imparted to the rocket. We denote the jet damping torque by M_{JD} and express it in terms of the jet damping torque coefficient K_{JD} where

$$M_{JD} = -K_{JD}\omega, \quad (14)$$

and

$$K_{JD} = \left[(l_J^2 - l_p^2) + \frac{dI_p}{d\mu} \right] \frac{d\mu}{dt}. \quad (15)$$

Equation (13) is of exactly the same form as the equation for the rotation of a rigid body of constant mass except for two things. The first is the presence of the jet damping torque; the second is the fact that I is not constant, the value to be used at each instant being the moment of inertia about a transverse axis through the center of mass at the instant.

To investigate the magnitude of the effect of the jet damping torque, consider the case in which $L_y = 0$, so that (13) can be written as

$$I \frac{d\omega}{dt} = -K_{JD}\omega. \quad (16)$$

If we neglect the variation of I and K_{JD} during burning, we can integrate this subject to the initial condition that $\omega = \omega_0$ when $t = 0$, getting for ω at the end of burning

$$\omega_b = \omega_0 \exp \left(-\frac{K_{JD}t_b}{I} \right). \quad (17)$$

Calculations of $K_{JD}t_b/I$ for a variety of rockets show that it averages about 0.4 for high-performance rockets; while in the case of a typical low-velocity rocket such as the 4.5 BR $K_{JD}t_b/I$ is about 0.15. If the 0.4 value is used, one finds that $\omega_b \approx 0.7\omega_0$, indicating that if the rocket were fired in vacuum, the jet damping would decrease any initial transverse angular velocity to 70 percent of its original value by the end of burning. Thus the effect of jet damping is much less than the effect of the applied torques under all ordinary circumstances. For example, the aerodynamic forces on an HVAR launched with an initial transverse angular velocity will make the angular velocity oscillate through $1\frac{3}{4}$ complete cycles during burning. Hence the jet damping torque will usually be neglected.

2.4 AERODYNAMIC FORCES

The fact that the moment of inertia varies with time is also usually neglected. If a suitable average value is chosen, the error introduced in this way is no larger than the errors introduced due to the lack of knowledge of L_y . The torque L_y is uncertain both because of the unknown magnitude of the gas malalignment and because sufficiently precise aerodynamic data are usually unavailable.

2.3 The Effective Rocket Temperature

The burning time of a rocket varies over a wide range with varying propellant temperature, and the total impulse and the extent of the progression or regression of the reaction may also vary with temperature, although to a lesser degree. It follows that G_{eff} and $t_{b, \text{eff}}$ depend on the temperature of the propellant and that consequently the entire exterior ballistics of a rocket depends on the temperature. Consequently, in practice, the features of interest are worked out for enough different temperatures so that the behavior at any other temperature can be determined by interpolation. When the rounds are stored at constant temperature for a considerable length of time before firing, this storage temperature is the temperature of the propellant and few complications arise. But if the rounds have been exposed to changing temperatures during the period preceding firing, different parts of the propellant will be at different temperatures, since the temperature at the center will tend to lag behind that of the outer parts, thus resulting in a relatively complicated situation. One way out is to introduce an "effective rocket temperature" so chosen that the quantity of interest, usually the gravity drop of the trajectory, has the same value for a rocket having the actual temperature distribution as for one whose entire propellant is at the "effective rocket temperature."

This procedure turns out to be applicable to aircraft forward firing in cases in which the rocket is hung out in the air stream. Under such circumstances rockets are placed in a rapidly moving air stream for considerable lengths of time. The temperature of the air is usually quite different from that of the magazine in which the rockets were stored, so that the effective rocket temperature would be expected to differ from the storage temperature by an amount that will lead to appreciable errors in sighting. Since the air temperature at a given altitude can be predicted approximately, and since the cooling effect of air is independent of air speed above about 30 ft./sec., it is possible to calculate a useful "effective rocket temperature." In the case of ground-fired rockets the usefulness of the concept is small since, because of the effects of the sun's radiation and the difficulties of predicting or measuring the air temperature, it is very difficult to calculate the effective temperature. A still more troublesome difficulty is the fact that the cooling effect of an air stream depends markedly on the velocity of the air flow past the rocket at velocities below about 30 ft./sec.

2.4 Aerodynamic Forces

The only aerodynamic forces whose effects are of real importance in the ballistics of fin-stabilized rockets are the drag and the righting, or restoring, moment; although on some occasions it is desirable to include the effects of the cross force and the damping moment. The principal effect of the drag is to decrease the velocity of the rocket, while that of the righting moment is to stabilize the rocket and to produce oscillations in the orientation of the rocket

whenever it is given a yaw. The principal effect of the cross force and of the damping moment is to damp these oscillations. It will be seen in chapters 3 and 5 that, contrary to what one might naively suppose, the cross force is not important in producing the deflections due to a cross wind. These four forces and moments do not constitute the complete system of aerodynamic forces acting on the rocket; but the additional forces and moments, which are discussed in chapter 8, can be neglected completely here.

In discussing the aerodynamic forces, one usually considers the forces as measured in a wind tunnel or a water tunnel; that is, the forces that act on the rocket when there is no jet present. However, the presence of the jet certainly decreases the part of the drag that is due to the partial vacuum behind the blunt afterbody of the rocket. Since this effect is relatively small and since it is difficult to see how it can be separated from the thrust produced by the jet, it seems satisfactory to assume that the drag is the same with and without the jet and that the jet force is that required to produce the observed acceleration. Whether the presence of the jet affects the moment or cross force appreciably is not known definitely, and although the jet certainly produces an appreciable increase in the flow of air along the rocket, it is usually assumed that the effect of this flow is negligible. This is plausible since the increased flow should be symmetrical and since its velocity is probably small enough so that the induced aerodynamic forces are small. So far as is known, no effects have been observed that invalidate this assumption as applied to rockets in flight. However, rockets fired from tubes are sometimes observed to have a lower launching velocity than those fired from rails, a fact ascribed to the partial evacuation of the part of the tube behind the rocket by the jet. During a period of a few seconds immediately after burning, hot gases continue to stream forth from the motor, and it is sometimes thought that this markedly changes the drag; a possibility which will be considered further in the section on afterburning.

We shall now define the various aerodynamic forces and moments, and introduce the coefficients in terms of which they are expressed. Next we consider them individually, discussing their variation with yaw and velocity, and taking up briefly the experimental and theoretical determination of the various coefficients.

2.41 Definitions.—Consider a projectile moving in a plane with linear and angular velocities as indicated in figure 2.41, the angular velocity, ω , being about an axis perpendicular to the plane of the figure. This sketch is drawn for the case in which the projectile is moving with velocity V through still air, but the forces are of course the same if the projectile is at rest in a wind tunnel and the air is flowing from right to left with velocity V . Although the aerodynamic forces are produced by the distribution of pressure over the entire surface of the projectile, we need not consider the distribution in detail. The effect of any system of forces on the motion of a rigid body is the same as the effect of a suitable single force acting at an arbitrarily chosen point plus a suitable torque about this point, the single force being the vector sum of the forces of the system, and the torque being the vector sum of the moments of the forces of the system with respect to the chosen point. We take the point to be the center of mass, O_M , and designate the resultant force as F_A and the resultant torque as $M + M_q$. By symmetry F_A is in the plane of the figure, and $M + M_q$ is perpendicular to it. We assume that the resultant force is independent of ω ; that is, we neglect any possible variation of F_A with ω (ch. 8). The total moment, on the other hand, is divided into two parts, of which M is independent of ω , and M_q is any additional torque that is present when ω is not zero.¹⁸ M is called the restoring moment, since it tends to reduce the yaw, and M_q is called the damping moment because it tends to reduce the transverse angular velocity.

¹⁸ The subscript q is used since we shall usually write q for the magnitude of the transverse angular velocity.

The total force, F_A , is customarily resolved into two components. The lift, L , is the component normal to V and the drag, D , is the component parallel to V . Thus, to describe the aerodynamic force system on a nonrotating rocket, we must specify the variation of D , L , and M , with V and δ , the yaw, and must also specify the variation of M_q with V , δ , and ω . The lift is sometimes called the cross force or the cross force due to cross velocity. Although some authors use the term cross force to mean the component of F_A normal to the projectile rather than that normal to the direction of motion through the air, we shall always use the resolution normal to the direction of motion except on rare occasions when the contrary is explicitly stated.

For velocities between about 100 and 800 ft./sec., D , L , and M are nearly proportional to V^2 , and all the forces and moments are proportional to ρ , the density of the air or other medium in which the projectile moves. If geometrically similar projectiles of different dimensions are considered, D and L are proportional to the square of the linear dimensions, and hence to A , the cross-sectional area of the projectile, while M is proportional to the cube of the linear dimensions or to Al , where l is the length. Because of these facts, which can be demonstrated experimentally or indicated by dimensional analysis, it is customary to write

$$D = \frac{1}{2} C_D \rho A V^2, \quad (1)$$

$$L = \frac{1}{2} C_L \rho A V^2, \quad (2)$$

and

$$M = \frac{1}{2} C_M \rho A l V^2. \quad (3)$$

On similar grounds the contribution of the angular velocity to the moment can be written as

$$M_q = \frac{1}{2} C_q \rho A l^2 V \omega. \quad (4)$$

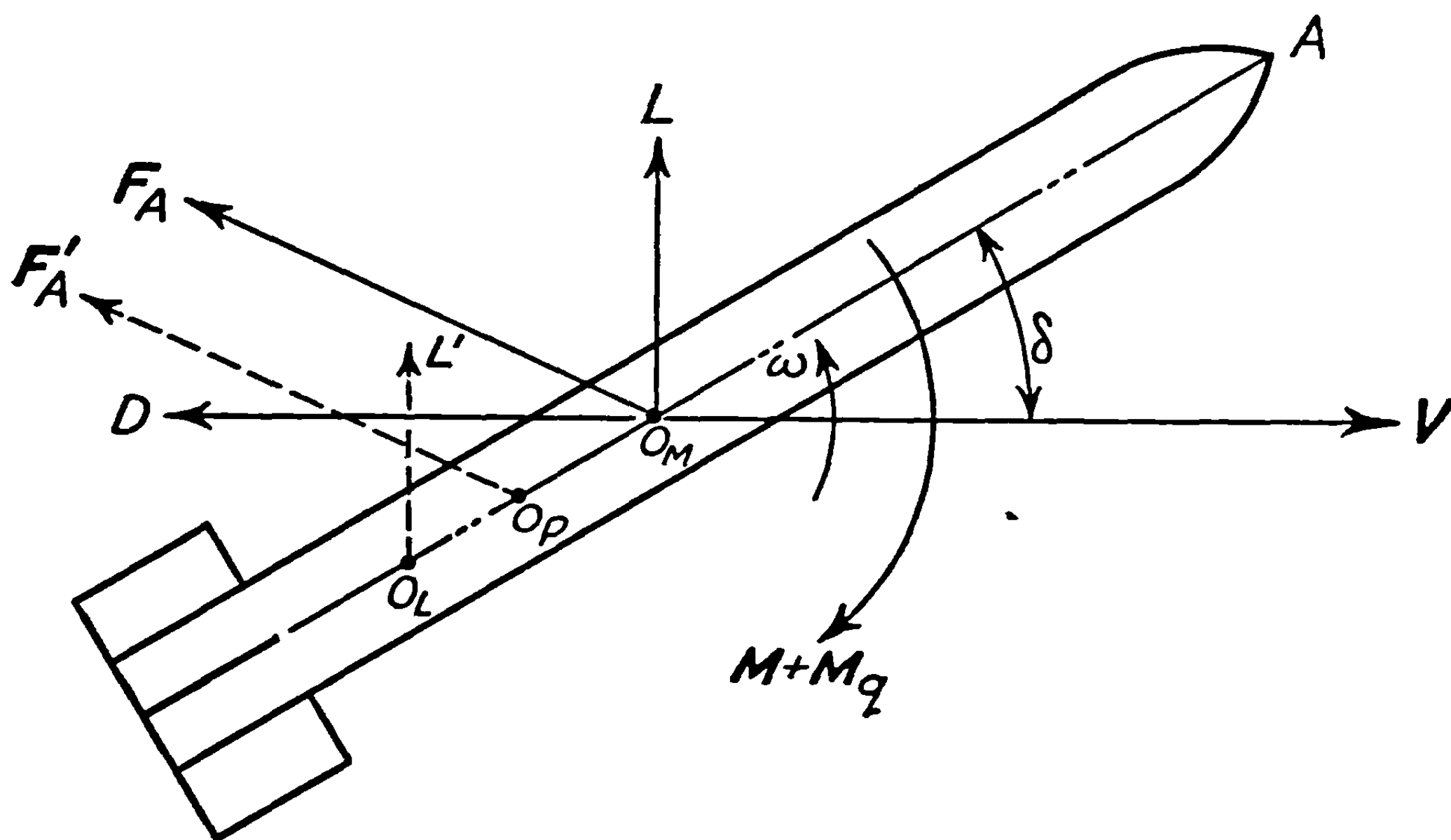


FIGURE 2.41.—Aerodynamic force system of a nonspinning projectile.

The values of the dimensionless coefficients C_D , C_L , C_M , and C_q as functions of δ characterize the aerodynamic forces on a projectile. These coefficients are not, strictly speaking, independent of V , but they vary much more slowly with velocity than do D , L , M , and M_q . For small yaws, that is to say, yaws up to 10° for most projectiles and up to about 20° for many projectiles, C_L and C_M are nearly proportional to δ while C_D and C_q are nearly constant.

In considering the variation of the coefficients with velocity, it is not proper to disregard the variation of other quantities such as the air temperature, the air density, or the viscosity of the air. It is much better to assume that these coefficients are functions of the Mach number, which is V/a where a is the velocity of sound under the circumstances, and of Reynolds number, which is $\rho V l / \eta$ where η is the viscosity of the air. The dependence on Reynolds number can usually be neglected, but in precise work the coefficients should be regarded as functions of the Mach number rather than as functions of V in order to allow for the effects of variations in the velocity of sound. The main variation in the velocity of sound arises from the fact that the velocity is proportional to the square root of the absolute temperature. Curves or tables giving, say, C_D as a function of V are to be regarded as valid only when the velocity of sound is $a_0 = 1,120$ ft./sec., the velocity under standard ballistic conditions. If the velocity of sound is different, then the table should be entered not at V , the velocity of the rocket, but at

$$V_T = (a_0/a)V = (T_0/T)^{1/2}V, \quad (5)$$

in order to enter at the correct Mach number. Here T is the absolute temperature and T_0 is the absolute temperature under standard ballistic conditions. If the Fahrenheit scale is used, T_0 is 518° , corresponding to 59° F; while on the Centigrade scale it is 288° A., corresponding to 15° C. In practice this refinement has not been made in rocketry since the available data and measurements are not sufficiently accurate to justify it. Unless the temperature varies by more than 50° F. from the standard temperature, a will differ from a_0 by less than 5 percent. Since C_D , C_L , C_M , and C_q vary slowly with respect to V , the error in the coefficient will be very small indeed except in the neighborhood of the velocity of sound. Here small changes of Mach number with changes in air temperature are important when one is making experimental measurements of the coefficients. Detailed consideration of the variation of the coefficients with velocity will be postponed to later sections.

The forms used in (1)–(4) for expressing the aerodynamic forces in terms of coefficients are the standard forms of aerodynamics and hydrodynamics; but conventional ballistic theory usually replaces the combination $\frac{1}{2} C_D A$ by $K_D d^2$, where d is the diameter, and makes similar changes in the other coefficients. In the present treatment we use the forms listed above as the basic definitions; in the equations of motion we use certain derived coefficients that reduce the equations of motion to more convenient form. The relations between the forms used and the conventional ballistic forms is given in table 8.1.

In dealing with the motion of a projectile it is usually more convenient to use the deceleration coefficient

$$c = \frac{1}{2} (\rho A/m) C_D, \quad (6)$$

rather than the drag coefficient, C_D , as a means of specifying the drag. Here m is the mass of the projectile. The deceleration coefficient multiplied by V^2 gives just the rate of change of velocity due to drag, since

$$c V^2 = \frac{1}{2} C_D \rho A V^2 / m = D/m. \quad (7)$$

Experimental measurement of deceleration in flight gives c more directly than C_D ; the converse being true of the measurement of D in a wind or water tunnel. For Mach numbers less than 0.7 or 0.8, c is essentially constant; above this point it increases sharply. Typical values of c for rockets lie in the range from 10^{-5} to 10^{-4} ft.⁻¹, the larger values corresponding to rockets having larger drag and lower mass; values of c for a variety of rockets are given in table 2.11.

In theoretical treatments it is almost always necessary to make use of the fact that for small yaws C_M is approximately proportional to δ . Evidently the analysis is simpler if a suitable constant, which we denote by C_m , is introduced for the value of $C_M(\delta)/\delta$ averaged over the range where C_M is essentially linear. In the treatment of fin-stabilized rockets the most convenient procedure is to introduce the constant σ defined by

$$\sigma = 2\pi \left(\frac{2mK^2}{\rho Al C_m} \right)^{1/2} \text{ or } C_m = \frac{C_M}{\delta} = \frac{8\pi^2 m K^2}{\rho Al \sigma^2}, \quad (8)$$

where K is the radius of gyration and mK^2 the moment of inertia of the projectile about a transverse axis through the center of mass. Physically, as shown in 3.32, σ is the distance traveled by the projectile while the yaw oscillates through one complete cycle if all the forces and torques other than the restoring moment are small. In such a case V is constant in magnitude and direction, while $d^2\delta/dt^2$ is the angular acceleration of the rocket about a transverse axis. Since the moment of inertia times the angular acceleration is equal to the torque acting, we have

$$mK^2 \frac{d^2\delta}{dt^2} = -M = -\frac{1}{2} C_M \rho Al V^2 = -\left(\frac{2\pi V}{\sigma} \right)^2 mK^2 \delta, \quad (9)$$

the minus sign being used because the aerodynamic moment is a restoring moment. The solution of this equation is

$$\delta = \delta_1 \cos \left(\frac{2\pi V t}{\sigma} + \epsilon \right) = \delta_1 \cos \left(\frac{2\pi d}{\sigma} + \epsilon \right), \quad (10)$$

where δ_1 and ϵ are constants of integration and $d = Vt$ is the distance traveled. Evidently δ oscillates through one complete cycle every time d increases by σ so that photographic measurements of δ in flight after the end of burning give σ directly. As may be seen in table 2.11, typical values of σ for rockets lie in the range from 200 to 700 feet, the larger values belonging to rockets having small restoring moments and large moments of inertia.

In terms of the coefficient $C_m = C_M/\delta$ defined above, (3) can be written

$$M = \frac{1}{2} C_m \rho Al V^2 \delta = \frac{1}{2} C_M \rho Al V^2. \quad (11)$$

In a similar fashion C_l can be defined to be the average value of C_L/δ over the range where C_L is essentially linear in δ . Thus for small yaws (2) can be written as

$$L = \frac{1}{2} C_l \rho AV^2 \delta = \frac{1}{2} C_L \rho AV^2. \quad (12)$$

2.411 Dimensions and units—A brief treatment of the dimensions of the various quantities and of the units to be used may be helpful. Any absolute system of units can be used with the above equations. Physicists normally use a system in which forces are in poundals, masses in

pounds, distances in feet, and times in seconds, or one in which forces are in Newtons, masses in kilograms, distances in meters, and times in seconds; while engineers generally measure forces in pounds and masses in slugs. The coefficients C_D , C_L , C_M , and C_q are dimensionless and hence have the same values in all systems. Angles and angular velocities are measured in radians and radians per second, respectively. Since cV^2 is an acceleration, c will have dimensions of $(\text{length})^{-1}$, and in either of the two English systems c will be measured in ft.^{-1} while in the metric system it will be measured in meters^{-1} . For any given projectile the value of c in ft.^{-1} is 0.3048 times the value in meters^{-1} . The yaw oscillation distance, σ , has the dimensions of length and is measured in feet or meters.

2.412 *The center of pressure and of lift.*—If the rocket is not rotating, M_q is zero and the force F_A , applied at the center of mass, and the torque M about an axis perpendicular to the plane of figure 2.41 are equivalent to the actual distribution of pressure over the surface. This is not, however, the only system of forces and moments that will produce the same acceleration of the rigid body as does the actual pressure distribution. Since M is perpendicular to F_A , it is possible to find a point on the axis of the rocket such that the force F_A applied at this point gives the moment, M , about the center of mass and hence is equivalent to the pressure distribution. This point, which is labeled O_P in figure 2.41, is called the center of pressure. It must lie to the rear of the center of gravity in order that a nonrotating projectile be stable.

The distance, l_P , from the center of pressure to the center of mass can be computed if L , D , and M are known. Since the moment about O_M of F_A applied at O_P must be M , and since F_A is the vector sum of the lift and drag, the total moment about O_M of the lift and drag when applied at O_P must also be M . But the moment due to the drag is $Dl_P \sin \delta$, and the moment due to the lift is $Ll_P \cos \delta$. Hence, from 2.41 (1), (11), and (12),

$$l_P = \frac{M}{D \sin \delta + L \cos \delta} = \frac{lC_M}{C_D \sin \delta + C_L \cos \delta} \doteq \frac{l(C_M/\delta)}{C_D + (C_L/\delta)} \doteq \frac{lC_m}{C_D + C_i} \quad (1)$$

In the approximation in which δ is small compared to unity and for rockets where C_M and C_L are proportional to δ for small yaws, the position of the center of pressure is independent of the yaw. At zero yaw all but the last two forms of (1) are indeterminate since C_M , C_L , and $\sin \delta$ are all zero when $\delta=0$ for symmetrical projectiles. The position of the center of pressure at zero yaw is defined as being the limiting position as the yaw goes to zero. The ratio of l_P to the total length of the projectile is called the center of pressure eccentricity; in normal fin-stabilized rockets it is usually about 0.2. This eccentricity is a measure of the stability since it must be positive and not too small, or else a rocket that gets an accidental yaw will be rotated back to the direction in which it was originally moving so slowly; i. e., σ is so long, that the lift will have time to produce a significant deflection of the trajectory.

There are occasions when the ratio $M/lL = C_M/C_L$ occurs in the analysis of ballistic problems. This ratio has a convenient interpretation in terms of the distance, l_L , from the center of mass to the point, O_L , called the center of lift, at which the lift force would have to be applied in order to produce the moment M . In this case the drag is applied at the center of mass. Since the moment produced by the lift applied at O_L is $Ll_L \cos \delta$ and since this must equal M , it follows from 2.41 (11) and (12) that, for small angles of yaw,

$$\frac{l_L}{l} = \frac{M}{Ll \cos \delta} = \frac{C_M}{C_L \cos \delta} \doteq \frac{C_M}{C_L} = \frac{C_m}{C_i} \quad (2)$$

This ratio is called the center of lift eccentricity. Since $C_D \sin \delta$ is usually much less than C_L , comparison of the third terms of (1) and (2) shows that the center of lift eccentricity is usually

only slightly greater, say from 3 to 10 percent, than the center of pressure eccentricity. In this respect figure 2.41 is a gross exaggeration since it shows the center of lift to be about twice as far from the center of mass as is the center of pressure. This could happen only in a rocket that is stabilized more by the drag than by the lift of the fins.

2.42 Effects of Changes of Air Density.—The values of the dimensionless coefficients C_D , C_L , C_M , and C_q are independent of the air density. In fact, for comparable Reynolds numbers, the values are essentially the same in both air and water provided that V is well below the velocity of sound in each case, and, in water, less than the velocity at which cavitation becomes important. Because of this, one can use coefficients determined in a water tunnel when coefficients determined in a wind tunnel are not available.

The values of the parameters c and σ , on the other hand, depend on the air density, according to 2.41 (6) and (8), c is proportional to ρ , and σ is inversely proportional to $\rho^{\frac{1}{2}}$. Since only approximate values of c and σ are known from experiment or needed in rocketry, minor variations of ρ are of little concern, but if major changes in elevation are involved, the corresponding changes in ρ may become important. For example, a 3,000-foot decrease in elevation usually involves about a 10-percent increase in ρ and hence a 10-percent increase in c and a 5 percent decrease in σ .

In precise work it would be advisable to correct all experimental values for the variation of ρ from ρ_0 , the density under standard ballistic conditions; i.e., a density of 0.07513 lb./ft.³, a temperature of 59° F., and a pressure of 750 mm. of Hg. Thus all tabulated experimental values would be for standard conditions, and if values were wanted for other conditions appropriate corrections could be made. However, if the uncertainty in the experimental values of c and σ is greater than the corrections involved, it is hardly necessary to correct the experimental values. This is particularly true if almost all firings are done at the same altitude. In that case the experimental values are the appropriate ones to use in any calculations that are to be checked against further firings under essentially the same conditions. All values of c and σ given in this text are the values at an elevation of about 3,000 feet. Hence when range tables are computed for sea level conditions, c must be increased by 10 percent, and similar corrections must be made in any other calculations of the behavior of rockets at elevations other than 3,000 feet.

2.43 Effects of Changes of Mass and Changes of the Position of the Center of Mass.—It often happens that the aerodynamic coefficients C_D , C_L , C_M , and perhaps C_q or else the parameters c and σ are known for a particular rocket, but that the design is then modified in a way that does not alter the exterior shape, or alters it only slightly. A very common example of this is a change in the filler used in the head, although a modified motor design sometimes has the same effect. It is then necessary to determine the effect of this change on the aerodynamic coefficients and the parameters, and it is desirable that this be done without further experimentation.

If the only changes are in the mass of the projectile from m_1 to m_2 and in the moment of inertia from $m_1 K_1^2$ to $m_2 K_2^2$, the position of the center of mass remaining the same, then the aerodynamic forces and coefficients will be unchanged since they depend only on the linear and angular velocities of the projectile with respect to the air. In accordance with 2.41 (6) and (8), however, c will be changed from c_1 to

$$c_2 = (m_1/m_2)c_1, \quad (1)$$

and σ will go from σ_1 to

$$\sigma_2 = (m_2 K_2^2 / m_1 K_1^2)^{\frac{1}{2}} \sigma_1. \quad (2)$$

If the new design has a different position for the center of mass as well, moving it forward a distance h from O_{M1} to O_{M2} , then the aerodynamic coefficients are affected. If we consider the case in which ω is zero so that we are concerned only with C_D , C_L , and C_M , then moving O_M forward the distance h along the axis while keeping δ constant does not affect the local pressure distribution or the flow of air past the rocket. Hence the resultant aerodynamic force, F_A , its two components D and L , and the aerodynamic coefficients C_D and C_L will be unaffected by the change. The new deceleration coefficient is still given by (1). On the other hand, the moment, M_2 , of the applied aerodynamic forces will now be computed about the new origin and will be greater than the moment, M_1 , about the old origin. Since, in accordance with the discussion of 2.412, either moment can be produced by the forces L and D acting at O_P in figure 2.41, we have

$$M_1 = (\overline{O_P O_{M1}}) (L \cos \delta + D \sin \delta)$$

$$M_2 = (\overline{O_P O_{M2}}) (L \cos \delta + D \sin \delta)$$

$$= (\overline{O_P O_{M1}} + h) (L \cos \delta + D \sin \delta)$$

$$= M_1 + h(L \cos \delta + D \sin \delta).$$

Hence from 2.41 (1), (2), and (3), the restoring moment coefficient changes according to the equation

$$C_{M2} = C_{M1} + (h/l) (C_L \cos \delta + C_D \sin \delta). \quad (3)$$

For small angles, this can also be written as

$$C_{m2} = C_{m1} + (h/l) (C_L + C_D). \quad (4)$$

The effect on σ of a change in the position of the center of mass can then be computed by 2.41 (8).

The effects of changes in the position of the center of mass in cases in which ω is not assumed to be zero are much more complicated. Evidently the coefficient C_e will be affected, but, in practice, one rarely knows the value of this coefficient with sufficient accuracy to make it worth while trying to compute the change. A more serious difficulty arises from the fact that when ω is not zero, the velocity vectors of the various points along the axis of the rocket in figure 2.41 are not parallel. Hence for each origin one must take a different value of the yaw and must resolve the total force into lift and drag in a different way, even though the motion of the surface of the projectile with respect to the air and the pressure distribution are independent of the choice of origin. This line of argument leads to results of some theoretical interest (see 8.2), although they are of little practical importance in the usual problems concerning the ballistics of fin-stabilized rockets.

2.44 Drag.—Gravity and aerodynamic drag are the only forces of importance in determining the trajectory after burning. The variations of drag with velocity and yaw must be determined for each projectile so that theoretical trajectories can be computed. A large body of experimental data on numerous types of projectiles exists and with this as a basis a semi-empirical theoretical technique has been developed for computing the drag. We shall first give a summary of some of this data and then give the theoretical methods of calculating the drag.

2.441 Experimental values of drag.—We use the deceleration coefficient c to specify the drag because it gives the most direct connection between the drag and its effect on the

motion. The drag coefficient, C_D , can always be obtained from the deceleration coefficient by means of 2.41 (6) or by means of the following expressions for the drag:

$$D = \frac{1}{2} C_D \rho A V^2 = m c V^2 = -m \frac{dV}{dt}. \quad (1)$$

The deceleration coefficient can be determined experimentally in several different ways including direct measurements of deceleration in flight, measurements of range, and wind-tunnel measurements. Perhaps the most direct way is to launch the projectile essentially horizontally, measuring its velocity photographically or by other means at two points a known distance, d , apart. If d is small enough so that we can neglect the effects of gravity during the time required to travel this distance, then, by (1), the equation of motion is

$$\frac{dV}{dt} = -c V^2, \text{ or } \frac{dV}{dd} = -c V. \quad (2)$$

If c is constant, this can be integrated to give

$$V(d) = V_0 e^{-cd}, \text{ or } c = \frac{1}{d} \ln \frac{V_0}{V(d)} = \frac{V_0 - V(d)}{V_0 d}, \quad (3)$$

where V_0 is the velocity at the beginning of the interval and $V(d)$ is the velocity after traveling the distance d . By using a variety of different initial velocities, one can obtain the deceleration coefficient as a function of the average velocity over the interval. If necessary, corrections can be made for the effect of gravity, which produces a curvature of the trajectory and a decrease in velocity and drag at the summit. Since this method of determining c can be used only when the section of trajectory involved is relatively straight, the corrections can be made by means of the Didion-Bernoulli method described in chapter 5.

The advantages of the above method of determining the deceleration coefficient are that it is direct, and that it measures the deceleration for the same values of average yaw and velocity that are important in computing the trajectory. A possible exception to this statement must be made for rockets intended to be fired forward from airplanes since if the standard rocket is fired on the ground, the air velocity will be much lower than the velocities of interest in forward aircraft firing, but if light, hollow heads are used in ground firing in order to get the proper velocity, the average yaw might be changed. Another exception must be made for spin-stabilized rockets whose average yaw depends on the angle between the trajectory and the horizontal, although the error introduced by this variation is small. The disadvantages of this method are that neither the variation of drag with yaw nor high accuracy are attainable. For if d is small, it is difficult to measure $V_0 - V(d)$ with the desired accuracy; while if d is large, the corrections due to curvature of the trajectory become large, one can no longer assume that c is independent of V in the integration of (2), and one becomes uncertain as to just what value of V to associate with the value of c obtained. This method is better adapted to high velocities than low since with large V_0 , the curvature of the trajectory is small, and d may be made large, giving, by (3), larger values of $V_0/V(d)$ for a given c .

If the dependence of c on V is known except for a factor of proportionality, one can determine the desired factor, and hence c , by range firings. This method is only practical if tables are available which present range and time of flight as a function of the factor of proportionality and of the initial conditions. If the initial conditions are measured it is easy to obtain the

deceleration coefficient from the observed range or time of flight. The experimental error may be reduced by firing at a quadrant elevation of 45° because then the range is very insensitive to quadrant elevation and only the initial velocity need be measured carefully. Unfortunately tables covering high quadrant elevations are available only for the Gâvre resistance law and for the case in which c is constant. (See ch. 5.) The deceleration coefficient obtained in this manner is a function of the velocity and yaw along the whole trajectory but does not vary much with quadrant elevation or initial velocity and, if the drag is required only for the construction of range tables, the use of the tables from which c was determined gives very accurate results.

This method is a good supplement to the previous one since it is useful for subsonic velocities where the highly curved trajectories make a direct measurement of the deceleration difficult, but where it is legitimate to assume that c is constant. This method gives a relatively more accurate value of c than does the previous one since it does not require the measurement of a small difference, although it is more difficult to make proper wind corrections. It suffers from the same lack of control over the yaw. The principal objection to this method is that one does not determine the dependence of the drag on the velocity; this is assumed as known. The assumption made can be tested by firing with a variety of initial velocities and quadrant elevations to see whether one gets the same value of the proportionality factor under all circumstances.

Experimental values of the drag can also be obtained from wind or water tunnels by measuring the forces on a projectile or a scale model while it is supported at rest in a stream of moving air or water. This method has the advantage that the forces can be measured with considerable precision and that they can be measured as a function of yaw. However, the accuracy of the results is always open to a certain amount of question because corrections must be applied for the forces on the supports, and corrections may be necessary to allow for the effects of the walls of the tunnel and for scale effects if full scale models are not used. An advantage of the wind tunnel is that the velocity of the air is easily controlled and measured, but this is more than compensated for by the fact that the highest velocity available is usually relatively low so that only the value of the drag in the square-law range can be obtained. In the case of the water tunnel the situation is even worse than for the wind tunnel since it is evidently impossible to get a flow pattern in water that corresponds to that in air at velocities where compressibility is important. Consequently all one gets from the water tunnel are values of the aerodynamic coefficients in the subsonic region where the square law can be used. If the proper experimental technique is used, the water tunnel values of c and σ have been found to be accurate enough to use as a basis for ballistic calculations in low-velocity rocketry. The decision as to the method to be used to measure the aerodynamic coefficients is, more often than not, based not on considerations such as the above, but rather on the relative availability, quickness, and cost of the various methods.

Figure 2.441a shows how the drag coefficient varies with yaw in two cases. The 3.5 GPSR is a spin-stabilized rocket but is included since wind tunnel data out to yaws of 90° are available for it. This rocket has no fins but does have a length-diameter ratio of 7 to 1 that is common for rockets. At yaws of 30° , 60° , and 90° the drag coefficient increases to 1.4, 6.0, and 6.2, respectively. The characteristics of the 3.5 AR are listed in table 2.11; the length-diameter ratio is 15.7 and the rocket has four fins.

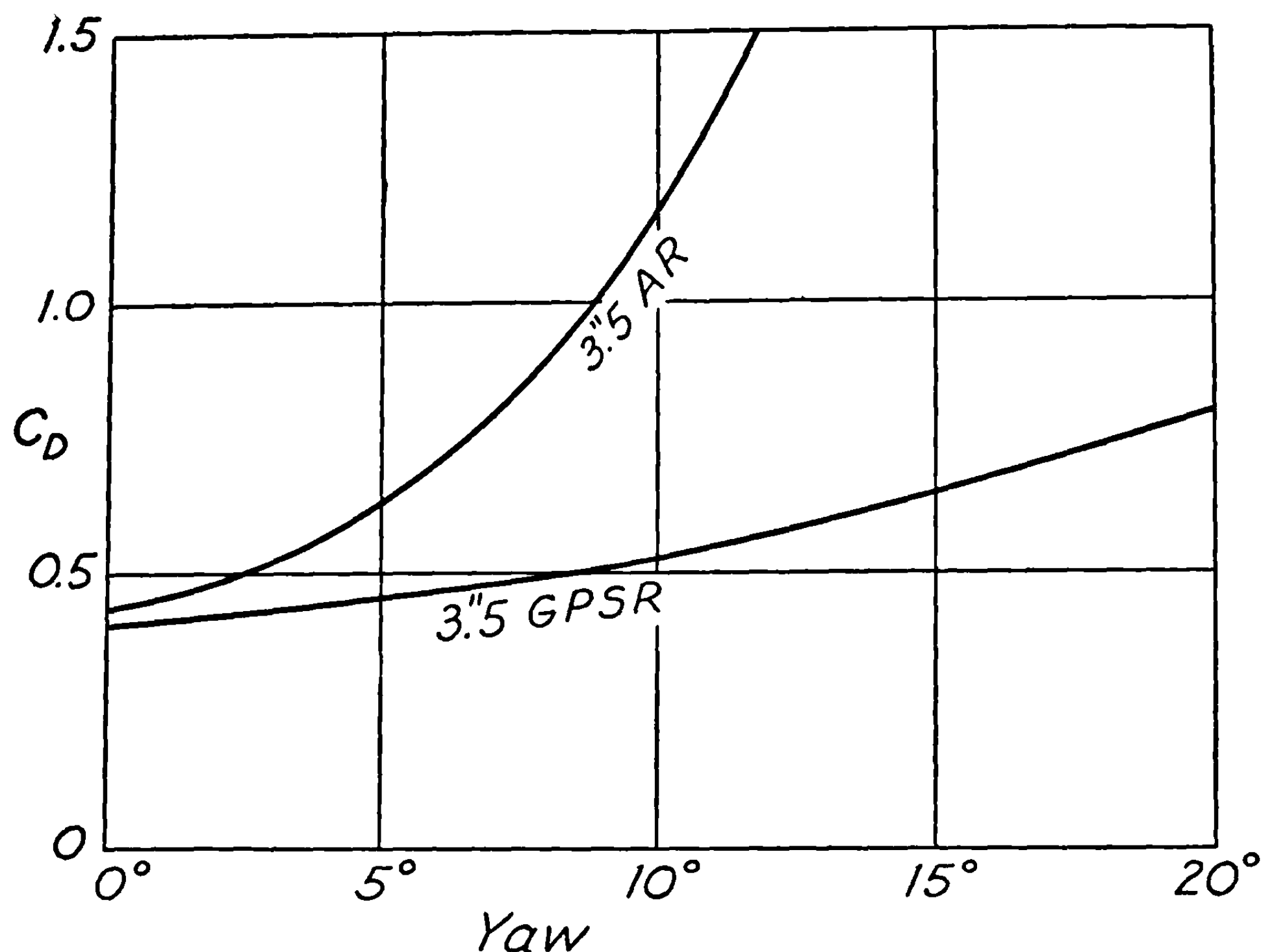


FIGURE 2.441a.—Drag coefficient of two rockets versus yaw.

The variation of drag with velocity is of more interest than the variation with yaw. Below about 800 ft./sec. the drag may be assumed to be proportional to the square of the velocity so that the deceleration coefficient is constant. In the neighborhood of the velocity of sound, the deceleration coefficient rises rapidly, reaching a maximum at about 1,500 ft./sec., followed by a slow decline as the velocity increases.²² As discussed in 2.41, one should treat the drag as a function of the Mach number rather than of the velocity since then the curves hold under nonstandard conditions. However, by using 2.41 (5), the usual curves showing the deceleration coefficient as a function of velocity under standard conditions can be used in the more general case.

As indicated by figure 2.441b the shape of the curve varies considerably from projectile to projectile. All the curves shown apply to shells since there is not enough data available to draw corresponding curves for any rocket. Consequently all estimates of the drag of rockets must be based on curves for the drag of shells, modified as described in 2.442. Unless one has available a modern mechanical or electrical integrator, a precise knowledge of the deceleration coefficient as a function of velocity for a particular projectile is of very little use in trajectory calculations. It is much more practical to use a function that applies only approximately to the projectile, but for which ballistic tables are available. In such cases the methods considered in chapter 5 enable one to make ballistic calculations much more readily than with resistance functions for which no one has prepared ballistic tables. Hence we shall confine our attention to functions that are useful in trajectory calculations.

Even after eliminating resistance functions for which there are no useful ballistic tables, there remains a bewildering number of notations used by various authors. Any one of the

²² For more complete discussions than the one given here, see C. Cranz, "Lehrbuch der Ballistik," Vol. 1, Springer, 1935 (Edwards Bros., 1943), pp. 36-107, and E. H. Herrmann, "Exterior Ballistics, 1935," Annapolis, 1935, Chapter 4. The treatment by Herrmann is more modern but in some ways Cranz's discussion of obsolete shells is more useful in rocketry.

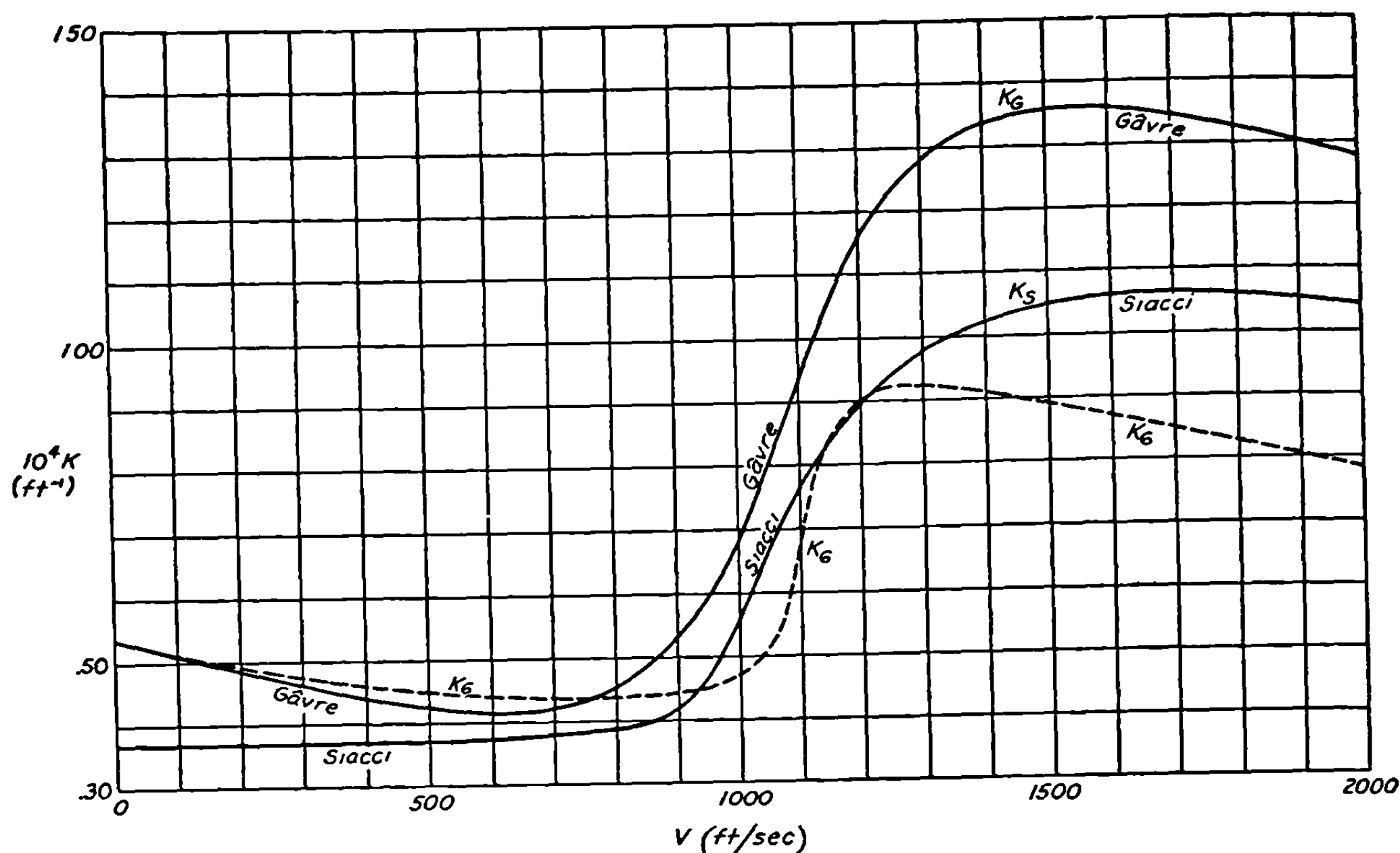


FIGURE 2.441b.—Deceleration coefficient of various shells versus velocity.

notations by itself is quite satisfactory, but the only way to avoid confusion in a discussion like ours is to introduce, for use in this section and in chapter 5, the subscript notation defined in table 2.441. One cannot translate everything into one of the notations, say Siacci's, since then it is very confusing to use tables based on any other notation. By equating the equivalent expressions for the deceleration in the fourth column of the table, it is easy to convert from one notation to another. For example, if one knows the ballistic coefficient, C , in the Gâvre system, and wishes to find the deceleration coefficient, c , at a particular velocity, the use of the table and the precise notation gives

$$c_D(V) = (\rho/\rho_0) C_G^{-1} K_G(V), \quad (4)$$

where K_G can be obtained from figure 2.441b. If one wants the connection between the constants in the Siacci and the Gâvre laws, one gets

TABLE 2.441

THE RELATIONS BETWEEN VARIOUS NOTATIONS FOR THE DECELERATION FUNCTIONS USED IN EXTERIOR BALLISTICS

Resistance law	Reference	Value of $-dV/dt$ in usual notation	Value of $-dV/dt$ in precise notation	Value of constant *	$\frac{K_{max}}{K_{min}}$
n 'th power.....	(†)	cV^n	$c_n V^n$		
Siacci.....	(‡)	$cV^2 K(V)$	$c_s V^2 K_s(V)$	$c_s = \frac{896(2R)^3 \rho_0}{P \rho_0}$	2.87
Gâvre.....	(§)	$(\rho/\rho_0) C^{-1} V^2 K(V)$	$(\rho/\rho_0) C_G^{-1} V^2 K_G(V)$	$C_G = m/i_0 d^2$	3.28
G_s or J_s		$(\rho/\rho_0) C^{-1} V^2 K_s(V)$	$(\rho/\rho_0) C_s^{-1} V^2 K_s(V)$	$C_s = m/i_0 d^2$	2.12
Form used in this volume.....		$c(v) V^2$	$c_D(V) V^2$		
Form used in aerodynamics.....		$\frac{1}{2} m^{-1} C_D \rho A V^2$	$\frac{1}{2} m^{-1} C_D A V^2 \rho$		

*In column 5 one must use the units: $2R$, diameter in meters; P , mass of projectile in kilograms; m , mass in pounds; d , diameter in inches.

†C. Cranz, "Lehrbuch der Ballistik," Vol. 1, p. 54, p. 160 Springer, 1935 (Edwards Bros. 1943).

‡Cranz; op. cit., p. 58, p. 175, p. 572.

§Ordnance Department, U. S. Army, "Exterior ballistics tables based on Numerical Integration." vol. I. 1924.

$$c_s K_s(V) = (\rho/\rho_0) C_G^{-1} K_G(V), \text{ or } c_s C_G \approx 1.25 (\rho/\rho_0), \quad (5)$$

where the last form is based on the fact that $K_G(V)/K_s(V) \approx 1.25$.

The earliest ballistic laws assumed that the deceleration, $-dV/dt$, was proportional to the n 'th power of the velocity, where n was usually taken to be an integer. This is still a useful assumption when one is considering only a relatively short trajectory since then the velocity does not change greatly and it is usually possible to find values of c_n and n that give a satisfactory fit over the limited range of interest.

From about 1870 to 1914 it was usual to assume that the deceleration of all projectiles could be expressed in either of the equivalent forms

$$-\frac{dV}{dt} = \frac{D}{m} = c V^2 K(V), \quad (6)$$

or

$$-\frac{dV}{dt} = \frac{D}{m} = (\rho/\rho_0) C^{-1} V^2 K(V). \quad (7)$$

In these expressions $K(V)$ is either a function defined by a table, a complicated empirical function, or a function defined by a series of n 'th power laws each good in a particular zone of velocities. $K(V)$ is taken to have the dimensions of (length)⁻¹, while the constant c , or C , which is chosen to fit the particular projectile under consideration, is usually taken to be dimensionless. The dependence of the deceleration on air density is included in the constant c used in (6) but is expressed explicitly in (7). The constant C used in (7) is usually known as the ballistic coefficient. We shall have occasion to refer to two of the functions used during this period, that of Siacci and that of the Commission de Gâvre. These functions are essentially the same except for a common factor; if K_s in figure 2.441b is multiplied by 1.25 it agrees with K_G to within 8 percent or better. Since all projectiles in use during this period were approximately equally inefficient aerodynamically, the resistance law of any projectile could be derived with satisfactory accuracy by multiplying either of these functions by a suitable constant which was usually expressed in terms of i , the form factor, as indicated by the fifth column of table 2.441. The function $K(V)$ was chosen so that i was unity for projectiles of the most common shape, which for both the Gâvre and Siacci functions was about 3 calibers long with an ogival head of 2 calibers radius of curvature. Cranz²³ gives an extensive discussion of the variation of i with nose shape, such considerations being of considerable use at supersonic velocities. At subsonic velocities, on the other hand, the drag is less sensitive to projectile shape and it is probably better to use a form factor of unity with either the Siacci or the Gâvre law for all reasonable projectile shapes. This is illustrated in figure 2.441b by the curve labeled K_6 which applies to a shell of modern design having low drag at high velocities. In order to fit the drag of this shell by a function of the Gâvre type, it is necessary to take $i \approx 0.6$ at high velocities while at low velocities the two curves agree quite closely when $i \approx 1.0$. If the projectile is boat-tailed; i. e., tapered in the rear, the corrections to be discussed in 2.442 should be made.

The introduction of shells having boat-tailing and long slender noses led to such departures from the older resistance functions that a variety of new functions have been obtained. Because there are a number of functions, and because no one believes that any one of them is correct for all projectiles, less extensive ballistic tables are available in connection with the new

²³ Cranz, op. cit., pp. 84-89.

functions than with the older ones where each computer could hope that his ballistic tables would be universally valid. The only one of the new resistance laws that should concern us is one obtained at Aberdeen and usually denoted by G_6 or J_6 ; it is particularly useful since it agrees with the relatively few experimental values of the deceleration coefficient of aircraft rockets better than any other resistance function for which ballistic tables are available. This function was obtained from measurements on a shell about four calibers long having a square base and an ogival nose whose radius of curvature is 7 calibers. The fact that rockets obey more or less the same resistance law, with a much smaller ballistic coefficient, does not hold because their shape resembles that of this shell. Rather, the relatively blunt noses of rockets would make their drag follow the Gâvre law were it not that their great length tends to add a nearly constant skin friction term to the drag. The total drag, then, is like that of a G_6 shell having a large form factor.

In deciding which of these resistance laws to use, one is usually guided more by whether tables are available (see ch. 5) that permit the desired ballistic calculations rather than by whether the chosen function gives the best possible values of the resistance. When considering low quadrant elevation firing, or forward firing from airplanes, or any other case in which the trajectory curves through no more than about 20° , one should choose from the Siacci law, the Gâvre law, and the G_6 law, the particular function that gives the best fit to the experimental or theoretical values of the rocket resistance in the velocity range to be used. If the velocity range includes the velocity of sound, the best fit is usually obtained by choosing the law for which the ratio of K_{\max} to K_{\min} is closest to the experimental value. Siacci type tables can be used for ballistic calculations in such cases as described in chapter 5. If these tables are not available one can often use the n 'th power law by choosing n properly. If the velocities involved are less than about 800 ft./sec., the square law is best, and, when it can be used, chapter 5 gives several good methods for carrying out calculations. When high-angle fire at supersonic velocities is contemplated, one must use the Gâvre resistance law since all of the available ballistic tables that can be used under such circumstances are based on this law. If sufficient accuracy can not be obtained in this way, one can fall back on numerical or mechanical integration based on any desired resistance law.

2.442. *Theoretical calculation of drag coefficients.*—Aerodynamics has not progressed to the point where the drag coefficient of a projectile can be computed on purely theoretical grounds, but by a combination of theory and empirical results it is possible to make surprisingly close estimates of the drag coefficient of an aerodynamically "clean" projectile. However, if the projectile has large lugs, fin braces, or other irregular projecting parts that tend to produce large contributions to the drag, it is much more difficult to estimate the drag. The methods described below for estimating the drag become particularly valuable when one or two experimental values of the deceleration coefficient are known and one needs to know the coefficient as a function of velocity over an extended range.

The basis of this method ²⁴ is the division of the total drag into five parts:

1. Head resistance.
2. Base drag due to reduced pressure at the rear.
3. Skin friction of the cylindrical body.
4. Skin friction of the fins.
5. Drag due to lugs and other irregularities.

We compute or estimate the contribution of each part to the drag coefficient, adding these to get the total drag coefficient of the rocket. The deceleration coefficient can then be obtained in the usual way by 2.41 (6).

²⁴ The authors owe their knowledge of this method to Dr. H. S. Tsien, California Institute of Technology.

The drag coefficients or deceleration coefficients of a number of shells are known as functions of velocity. In addition to the data given in the previous section and in the references therein, two useful curves will be found in Fowler, Gallop, Lock, and Richmond.²⁵ In computing the drag coefficient of a rocket, one starts with the values of C_D for a shell having a nose shape as much as possible like that of the rocket under consideration. This drag coefficient includes the head resistance,²⁶ the base drag due to reduced pressure at the rear, and the small skin friction of the shell. It therefore gives one a good estimate of the head resistance plus base drag of the rocket if the area of the rocket base is equal to the cross-sectional area of the head. Then if the motor is smaller than the head as in the 5.0 AR shown in figure 2.11i; this gives an overestimate of the base drag. Now the base drag can be estimated from the expression.²⁷

$$\text{Base drag} = \frac{1}{2}(0.20)\rho A_B V^2, \quad (1)$$

where A_B is the base area, and 0.20 is the average value of the base drag coefficient. Hence if A_B is less than A , the cross-sectional area of the head, we must subtract $0.20(A - A_B)/A$ from the drag coefficient of the shell, getting

$$C_{DH} = C_{Ds} - 0.20(1 - A_B/A), \quad (2)$$

for the contribution of the head resistance and the base drag to the drag coefficient of the rocket. If the shell is boat-tailed to reduce its base drag, then, strictly speaking, the 1 in equation (2) should be replaced by the ratio of the area of the base of the shell to its cross-sectional area. This correction for the decrease in base area of the rocket can be made only if the transition from the head to the motor is properly streamlined. If the taper is too abrupt for the velocities considered, one should not make the correction.

The contributions to the drag coefficient of the skin friction of the cylindrical body and of the fins are calculated from the formula²⁸

$$C_{Df} = \frac{0.455 (A_f/A)}{[\log_{10}(RN)]^{2.58}}, \quad (3)$$

where (RN) is Reynolds number, and A_f is the surface area whose skin friction is being computed. If ρ is the density of the air, V is the velocity, L is the length of the part whose skin friction is being computed, and η is the viscosity of air, then Reynolds number is given by

$$(RN) = (\rho VL/\eta) \approx 532 V(\text{ft./sec.})L(\text{in.}), \quad (4)$$

where the approximate form holds in air under normal conditions provided V is in ft./sec. and L is in inches. Since Reynolds number for the fins is much smaller than that for the rocket as a whole, the fins contribute more drag per unit area than does the cylindrical body of the rocket, and (3) must be evaluated separately for the fins and for the motor. If desired, one could make a precise allowance by means of (3) for the skin drag of the shell included in (2). However, the accuracy of these calculations is not sufficient to warrant such a refinement. If

²⁵ Fowler, Gallop, Lock, and Richmond; Phil. Trans. of Royal Soc. of London (A), 221, p. 295, Figs. 4 and 5, 1920.

²⁶ The head resistance can also be computed theoretically by modern methods; however, they are too laborious for our purposes.

²⁷ Th. von Kármán and N. B. Moore, "Resistance of Slender Bodies Moving with Supersonic Velocities, with Special Reference to Projectiles." Trans. of ASME, Vol. 54, pp. 303-310, 1932.

²⁸ L. Prandtl, W. F. Durand's "Aerodynamic Theory," vol. IV, p. 153, 1935.

desired, A_f can be reduced by the area of the shell without any attempt being made to distinguish between Reynolds number of the shell and that of the rocket.

If one adds to (2) the two contributions of the skin drag computed from (3), one gets the total drag coefficient of the projectile in cases where one can neglect the contribution of the lug bands or other irregularities. Calculations made on the above basis for various rockets have given values of the drag and deceleration coefficients that agree with experiment to within the rather large experimental error characteristic of most of the measurements that have been made. The drag of rockets which have large lug bands is considerably greater than the theoretical value obtained in this way, and is very difficult to compute. Probably the best that can be done is to measure the drag of such rockets experimentally at one or two velocities and then either multiply the theoretical value of the drag by an empirical factor or add an empirical constant to get a new curve that agrees as well as possible with the observed values. In the case of the 3.5 AR rocket, which had two lug bands that projected more than an inch, it was found that the drag was increased by about 50 percent by the lug bands.

The procedure outlined above may be illustrated by the calculation of a theoretical curve for the drag coefficient of one 5.0 AR rocket. Considerable care is needed with regard to units and with regard to using the correct definitions of the various quantities. The nose shape of this rocket resembles that of the shell from which the G_6 resistance law was obtained. The connection between the $K_6(V)$ of figure 2.441b and the drag coefficient of the shell, $C_{D_s}(V)$, may be deduced from table 2.441 to be

$$C_{D_s}(V) = \frac{2m K_6}{A \rho_0 C_6} = \frac{2i_6 d^2 K_6}{A \rho_0} = 4,860 K_6(V) \quad (5)$$

The numerical value is obtained by taking $\rho_0 = 0.07513$ lb./ft.³ the form factor $i_6 = 1$, and $d^2/A = 576/\pi$ since d is measured in inches while A is measured in square feet. Since the diameter of the head is 5 inches, while the diameter of the base of the rocket is only 3.25 inches, the correct expression for the part of the drag coefficient due to head resistance and base drag is given by (2) as

$$C_{DH} = 4,860 K_6(V) - 0.11. \quad (6)$$

Next we compute the contributions of the skin drag. We assume that the skin drag of the rocket head is about equal to the skin drag of the corresponding shell and hence is included in (6). Since the length of the motor tube is 45 inches, Reynolds number for the motor is

$$(RN) = (532) V(45) = 2.4 \times 10^4 V.$$

The surface area of the motor divided by the cross-sectional area of the head is 23.6. Hence the contribution of the motor skin friction is given by (3) as

$$C_{DM} = \frac{0.455(23.6)}{[\log_{10}(RN)]^{2.58}} = \frac{10.7}{[\log_{10}(2.4 \times 10^4 V)]^{2.58}}. \quad (7)$$

The length of the fins is 8 inches; hence for them

$$(RN) = (532) V(8) = 4,360 V.$$

The surface area of both sides of the four 8 x 5 inch fins is 320 in.², and this divided by the cross-sectional area of the motor is 16.3. Hence we get the contribution of the skin friction of the fins to the drag coefficient of the rocket from (3). However, because of the finite thickness of the fins, part of the resistance is due to eddy drag which will depend on the nature of the edges of the fin. For lack of more accurate information, the drag of the fins will be assumed to be twice the skin friction so that we write

$$C_{DF} = 2 \frac{0.455(16.3)}{[\log_{10}(RN)]^{2.58}} = \frac{14.8}{[\log_{10}(4,260V)]^{2.58}} \quad (8)$$

The sum of C_{DH} , C_{DM} , and C_{DF} gives the estimated drag coefficient, C_D , of the rocket. The relative magnitudes of the various components are evident from Fig. 2.442 in which they are plotted as functions of velocity.

Three experimental values of the deceleration coefficient are known from measurements of the change of velocity while the rocket traverses a known distance, and from the range when fired at a quadrant elevation of 45° at 740 ft./sec. The drag coefficient corresponding to these deceleration coefficients can be computed from 2.41 (6), which becomes

$$c = 6.05 \times 10^{-5} C_D, \quad (9)$$

where we take $m = 76.2$ pounds for this particular model and $\rho = 0.9\rho_0$ to allow for the fact that the experimental measurements of deceleration coefficient were made at an elevation of 3,000 feet. The fact that the theoretical curve is everywhere too low should not be surprising. In the first place, the actual nose shape is somewhat blunter than that of the shell from which the G_6 resistance law was obtained and, in addition, the lugs are fairly large relative to the size of the rocket and hence would be expected to produce an appreciable drag not included in the theoretical calculations. If the theoretical curve is multiplied by 1.3, the resulting curve agrees with the experimental data to within 7 percent, which is less than the experimental errors and is more accurate than is needed for most trajectory computations.

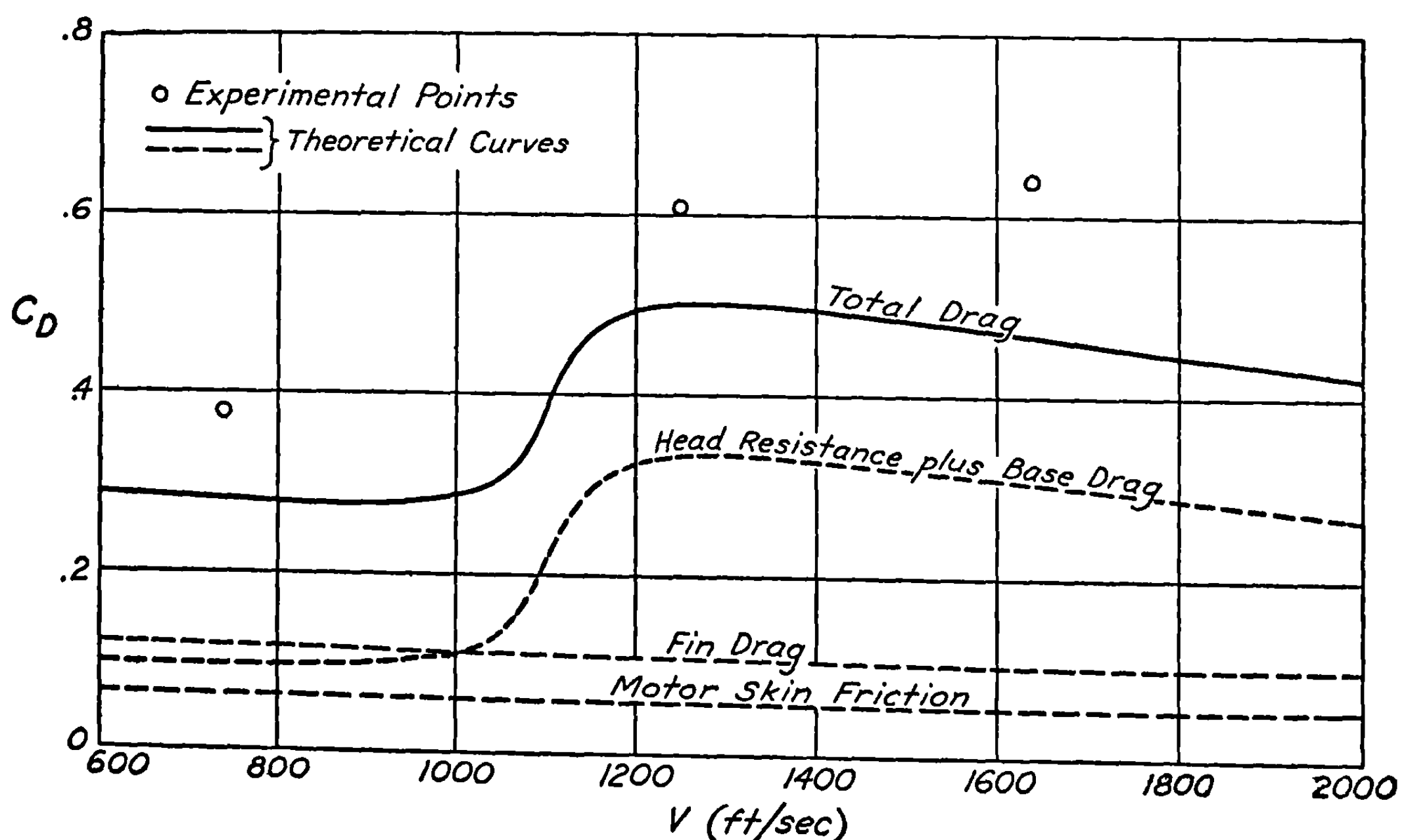


FIGURE 2.442.—Drag coefficient of the 5.0 AR versus velocity.

2.443 After-burning.—There is a considerable body of experimental data that has been interpreted as indicating that for several seconds after the time usually taken to be the end of burning, a rocket does not behave like an ordinary projectile. On the contrary it appears to behave like a projectile having a very low drag, or, in some cases, a small jet thrust that more than compensates for the drag, so that the velocity continues to increase slightly when one would expect it to decrease. This phenomenon has been attributed to “after-burning”; that is, to the relatively slow burning of inhibitor strips or other solid and gaseous residue in the hot motor. However, it is difficult to find any mechanism that will adequately account for this phenomenon, and none of the experimental evidence seems to establish conclusively its existence. Hence at present it appears reasonable to conclude that after-burning produces no marked effect on the motion of the rocket.

One must, of course, be careful to distinguish between the actual end of burning of the propellant and the expiration of the effective burning time or the reaction time as defined in 2.22. Static firing records show that within a small fraction of the burning period after the thrust starts its final drop toward zero, there is no appreciable thrust or pressure inside the motor. Since there is no reason to suppose that the situation would be different in range firing, one must conclude that there is no jet thrust due to after-burning that lasts for several seconds.

Even though the after-burning produces no thrust, it is recognized that a stream of hot gas may pour forth from the motor for several seconds. It has been suggested that this may reduce the drag appreciably, but, it is difficult to see how this could do more than remove part, or at most all, of the base drag. This would decrease the drag coefficient by no more than $0.20 A_B/A$ in the notation of 2.442 (2); and inspection of figure 2.442 shows that the decrease in C_D would be less than 25 percent in the case in which all of the base drag vanished, although in rockets in which the base is the same size as the head, the base drag is a bigger fraction of the total. However, in these cases it is very difficult to see how enough hot gas could be produced to fill in the entire volume swept out by the rocket, and one is forced to conclude that the after-burning produces no pronounced decrease in the drag.

2.45 The Restoring Moment.—The restoring moment is the most important of the aerodynamic moments in determining the orientation of the rocket, since the greater the restoring moment the more rapidly will the rocket oscillate about its equilibrium position and the less it will be displaced from equilibrium due to any applied torques or impulses. During burning, the orientation of the rocket and hence the restoring moment are important in determining the trajectory since the jet accelerates the rocket in the direction in which it is pointing. After burning no forces depending on the yaw are of importance in determining the motion, so that it is not necessary to know the yaw or the restoring moments. As will be shown in Chapter 3, most of the deflection of the trajectory during burning occurs near the launcher where the velocity is subsonic, so that we are primarily interested in the moment in the velocity range where it is proportional to the square of the velocity.

Since we are principally interested in the oscillations of the rocket rather than in the torques exerted on it, it is usually more convenient to express the restoring moment in terms of σ , the yaw oscillation distance, rather than in terms of C_M or C_m . The connections between these quantities, the restoring moment, M , and the angular acceleration about a transverse axis, $d^2\varphi/dt^2$, are given by 2.41 (3) and (8) as

$$M = \frac{1}{2} C_M \rho A l V^2 = \frac{1}{2} C_m \rho A l V^2 \delta = m K^2 \left(\frac{2\pi V}{\sigma} \right)^2 \delta = -m K^2 \frac{d^2\varphi}{dt^2}. \quad (1)$$

Here δ is the yaw, $m K^2$ the moment of inertia about a transverse axis through the center of mass, and φ is the orientation angle; i. e., the angle between the rocket axis and the launcher.

The yaw oscillation distance can be determined either by direct photography or from a knowledge of $C_M(\delta)$ as determined in a wind or a water tunnel. It is much easier to determine σ than c by measurements on motion-picture records of a rocket in flight since the determination of σ does not involve obtaining a second derivative. In the range in which the moment is proportional to the square of the velocity, σ is independent of V , and the effects on σ of the change in V due to drag and gravity and of the change in the direction of motion due to gravity and cross-force are completely negligible. All that is necessary is to plot the yaw measured photographically beyond the end of burning as a function of distance along the trajectory and to fit the best possible damped sine curve to the data. The distance between successive maxima and minima or between successive zeros is $\sigma/2$. In the case of high-velocity rockets, the amount of propellant should be reduced so that the burnt velocity is well below the velocity of sound, in order to give a value of σ in the desired velocity range. If a relatively accurate value of σ is required, corrections should be made for the wind since σ is the distance traveled with respect to the air, not the distance traveled with respect to the ground. If the rockets are given a thrust malalignment in the vertical plane, one will get relatively large yaws in this plane, thus facilitating the measurement of σ . When only the order of magnitude of σ is required, one can measure the orientation angle rather than the yaw. The determination of σ from wind or water-tunnel measurements of C_M is less direct than the above-described photographic determination which requires no knowledge of the position of the center of mass or of the moment of inertia. On the other hand, measurements of C_M which, of course, involve corrections for the effects of the support and, sometimes, for wall effects and scale effects, may be preferable for some purposes since they give more detailed information on the variation of the moment with yaw and hence on the range over which one can assume that C_m and σ are independent of δ .

It is very difficult to give directions for the calculation or even the estimation of σ or C_M from a knowledge of the shape of a rocket. Although the fins are very important in producing the restoring moment, even in estimating orders of magnitude one cannot neglect the aerodynamic torque on the remainder of the rocket or the interaction of the fins and the rest of the rocket. However, if the characteristics of enough different projectiles are known, it is often possible to find one that resembles the new projectile and hence to get an estimate of its characteristics. If the only important differences between the projectile whose σ is known and the new projectile are the radius of gyration and the position of the center of mass, we may use the equations of 2.43. Values of σ for a number of rockets will be found in table 2.11 and values of C_M or C_m for particular shells, bombs, and rockets can be found in a variety of places. Figure 2.45a, shows the variation of C_M with δ for the 3.5 AR and the 5.0 HVAR; the general characteristics of these rockets are given in table 2.11 and figure 2.11. Figure 2.45a does not go out to large enough yaws to show the marked deviation from linearity that sets in between 10° and 20° .

The choice of fin size is usually a difficult compromise. For convenience in stowing, handling, and firing it is desirable that the fins be as small as possible, and in particular that their width (the dimension normal to the rocket axis) be small; while in order to get high accuracy it is necessary that σ be small and hence that the fins produce a large restoring moment. Several investigations have shown that increasing the fin length (the dimension parallel to the rocket axis) is a very inefficient way to increase the moment. For

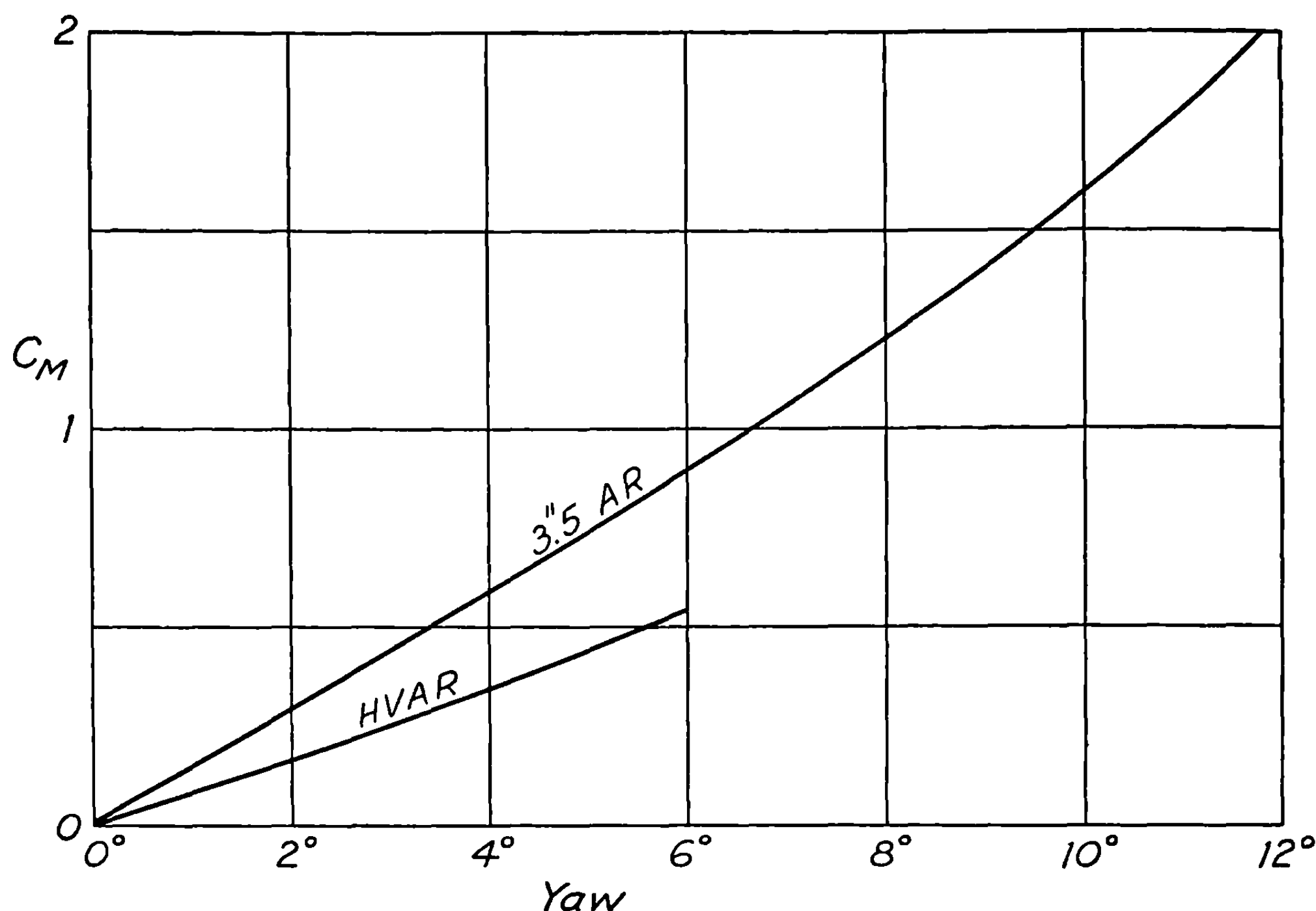


FIGURE 2.45a.—Moment coefficients of two rockets versus yaw.

example, figure 2.45b, which gives the variation of C_M with length of fins for several different widths, shows that lengthening the fins beyond a certain point actually decreases the restoring moment. Increasing the width (or diameter) of the fins has a much greater effect than increasing the length, not only for tails that consist of four or more fins but also for tails in which a shroud ring surrounds the fins. Such a ring tail is considerably more efficient than a fin tail of the same size. To illustrate the magnitude of these differences, table 2.45 gives the dimensions of a number of different tails for a particular rocket that give the same moment coefficient, $C_M=0.225$, at 3° yaw.

TABLE 2.45

DIMENSIONS (IN CALIBERS) OF TAILS PRODUCING THE SAME MOMENT

	Fin tails			Ring tails		
Length.....	1.6	0.8	0.4	1.0	0.5	0.25
Outside diameter.....	2.9	3.28	4.0	2.06	2.22	2.5

The results of extensive investigations of this rocket may be summarized as follows:

1. For fin tails which are flush with the rear of the rocket, the moment increases very rapidly with increasing outside diameter; it increases rapidly with increasing fin length up to a length of about 1.0 caliber but increases little, if at all, as the length is increased beyond 1.5 calibers.

2. For ring tails which are flush with the rear of the rocket, the moment increases very rapidly with increasing outside diameter of the ring; it increases rapidly as the length of the

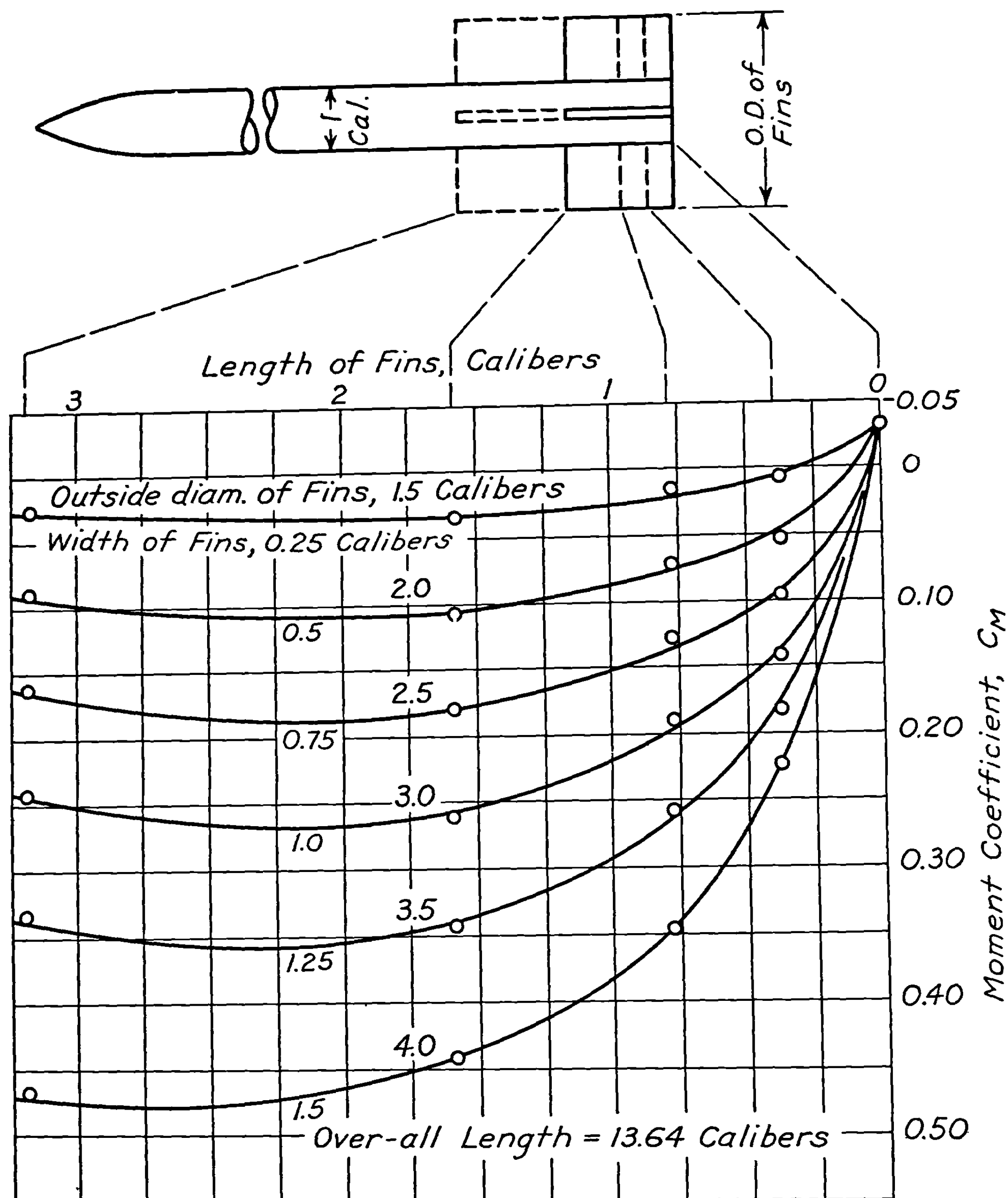


FIGURE 2.45b.—Moment coefficient of a fin tail as a function of fin size at 3° yaw.

ring is increased up to a length of approximately one-half the ring diameter, with little, if any, increase in moment resulting from a further increase in length.

3. The stabilizing moment is much larger with ring tails than with fin tails of the same dimensions.

Other investigators have arrived at similar conclusions for other projectiles.

2.46. The Lift.—The effects of the lift or cross force are of relatively minor importance in dealing with fin-stabilized rockets because the rocket oscillates about a position of zero yaw, and over a complete cycle most of the effects of the lift cancel out. The lift does however damp the oscillations and superposes a small sinusoidal motion on the trajectory. If one is

interested in the damping or in making measurements of position to within a few inches during the period immediately after the end of burning, the effects of the lift must be considered. The phase of the sinusoidal motion at the end of burning affects the direction of motion, but this effect, as shown in 3.32, is very small compared to other sources of deflection and dispersion. Probably the most important use that can be made of a knowledge of the lift is in the calculation, by means of 2.43 (3), of the change in the restoring moment when the center of mass is shifted by a change in design.

In principle, one could find the lift coefficient experimentally by measuring σ and c for two different rockets of the same shape but different centers of mass. From the two values of σ one would calculate the corresponding values of C_m and from c one would calculate C'_D . One could then obtain the lift coefficient from 2.43 (4). In practice this method would not be expected to be very convenient or accurate and recourse is usually had to wind tunnel or water tunnel measurements which give the lift coefficient as a byproduct of the measurement of the more important drag and moment coefficients. Information on the lift coefficients of projectiles will be found in conjunction with most of the discussions of the moment coefficient referred to in the previous section. Figure 2.46 shows the variation of the lift coefficient with yaw in the essentially linear region for the two rockets whose moment coefficients were shown in figure 2.45a.

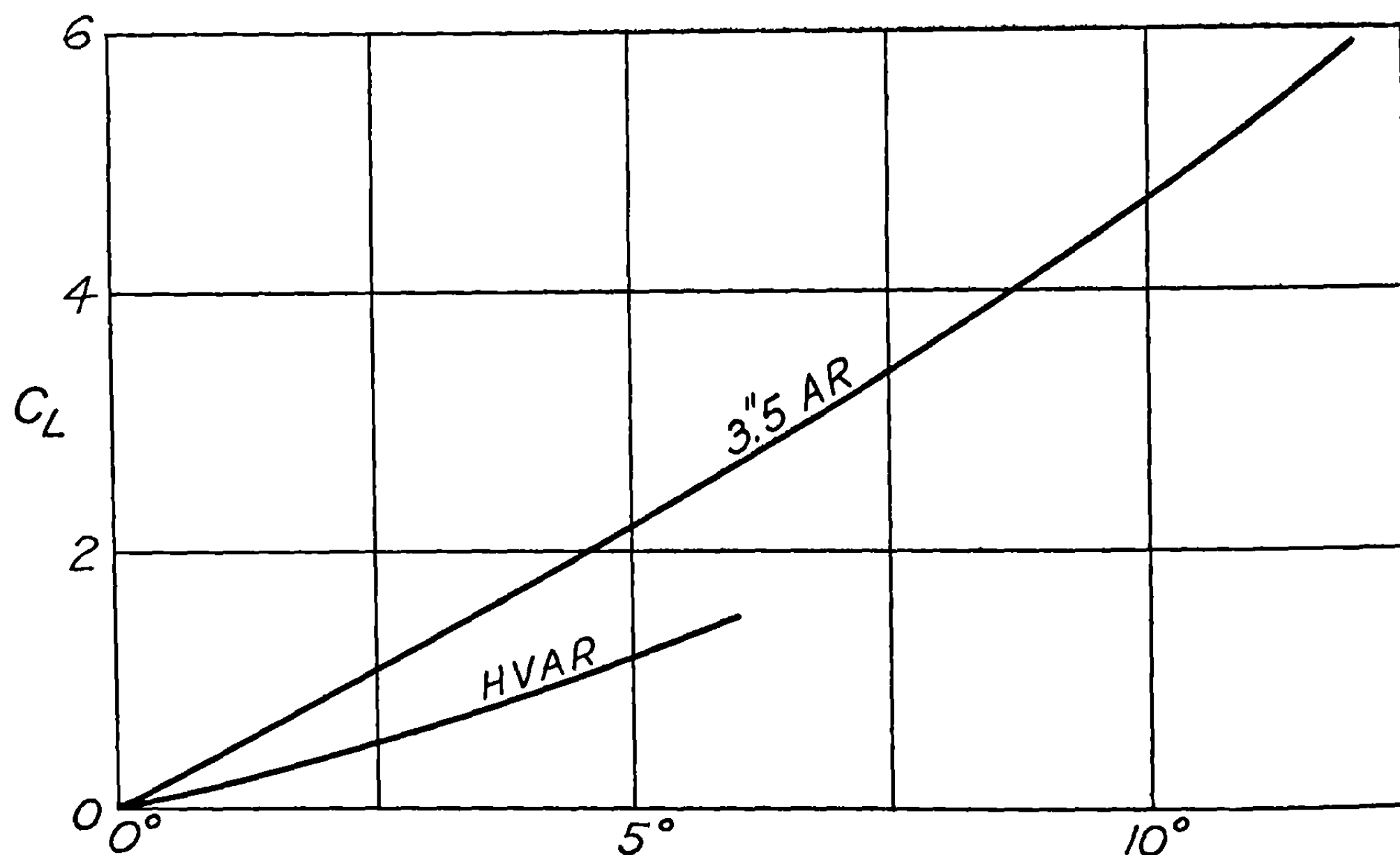


FIGURE 2.46.—Lift coefficients of two rockets as a function of yaw.

2.47 Fin Malalignment.—Thus far we have tacitly assumed that we were dealing with ideally symmetrical rockets whose restoring moment and lift are zero when the longitudinal axis is parallel to the direction of motion. In practice this is usually not the case since the fins may be bent or malaligned or the motor and head may not be perfectly aligned. A rocket for which the restoring moment is zero when the yaw of the axis is δ_0 ($\delta_0 \neq 0$) is said to have fin malalignment and δ_0 is said to be the fin malalignment whether the structural defect is in the fins or elsewhere. This defect is sometimes known as aerodynamic malalignment. To allow for it we modify 2.41 (11) to read

$$M = \frac{1}{2} C_m \rho A l V^2 (\delta - \delta_0). \quad (1)$$

We make this correction to the overturning moment since M is of considerable importance in determining the motion of the rocket during burning and since this correction is sufficient to account for practically all of the dispersion introduced by fin malalignment. We do not make the corresponding modification of the expression for the aerodynamic lift since this force is relatively unimportant in determining the motion and consequently need not be expressed precisely. After we have developed a notation that will let us describe the yaw in three dimensions rather than in a plane, we shall make the obvious modification of (1) to cover the general case.

An actual rocket usually has no unique axis of symmetry but has many lines that could be taken as the rocket axis. For example, one could take as the axis of the rocket the line through the center of mass and the tip of the nose, the line through the center of mass and the center of the nozzle, the line through the center of mass and in the direction in which the center of mass is constrained to move by the launcher, the line through the center of mass and parallel to the total jet force, or the aerodynamic axis, which is the axis through the center of mass such that the aerodynamic moment is zero when the yaw of this axis is zero. For each choice, the fin malalignment, the yaw at launching, and the angular thrust malalignment will be different. For a particular rocket the direction of motion at the end of burning is the same no matter what line we choose to call the axis, but the mode of division of the deflection during burning into the sum of the deflection due to fin malalignment, the deflection due to initial yaw, and the deflection due to angular thrust malalignment depends on our choice. Once this point is realized, no difficulty should arise from the fact that in practice, the axis is chosen in a convenient but arbitrary manner.

There is no reason to expect that in an actual rocket the lift will be zero when the moment is zero. Since the yaw oscillates about the equilibrium value δ_0 , the average value of the lift or cross force is its value when $\delta = \delta_0$. Hence one might expect that, although the lift is too small to produce an appreciable effect while the rocket travels the distance $\sigma/2$ during a half oscillation, this small but nonzero average lift would produce an appreciable deflection over an entire trajectory, particularly at long ranges. This would indeed be the case were it not that rockets always have a certain amount of rotation about the longitudinal axis. Since the moment of inertia about this axis is small, it requires very little torque to produce sufficient angular velocity so that the rocket will make several revolutions during flight. The aerodynamic torques due to imperfect fins would be expected to do this even if no angular velocity were imparted during launching or by the jet. If the rocket makes one or more revolutions every time it travels a distance of three or four σ , the dispersion introduced by the lift will be negligible.

2.48. The Damping Moment.—The aerodynamic torque about a transverse axis has been divided into two parts: one a function of the yaw only, the other a function of ω , the angular velocity about a transverse axis. We assume as a first approximation that this second part can be expressed in the form

$$M_q = -\frac{1}{2} C_q \rho A l^2 V \omega, \quad (1)$$

and is therefore independent of the yaw. This equation is the same as 2.41 (4) except that it has been expressed in vector form to indicate that the torque is opposed to the angular velocity producing it. This aerodynamic damping moment is of little importance; its main effect is

to contribute to the damping of the oscillations. Since burning takes place during only one or two yaw oscillations, and since the direction of motion at the end of burning is largely determined by what happens during the first oscillation or less, the damping has little effect during burning. Its effect on the amplitude of the oscillations after burning is appreciable, but the influence of these oscillations is negligible because there is no jet thrust. This is fortunate since it is difficult to determine C_q , and little is known of its variation with velocity and yaw.

One experimental method of determining C_q is to observe the ratio of the amplitudes of successive oscillations of the yaw in the experimental measurement of σ . From this ratio and a knowledge of C_i and C_D one can deduce the average value of C_q by the methods given in 3.32.

The value of C_q can also be measured in a wind tunnel by supporting the projectile so that it can rotate about a transverse axis through the center of mass and either determining the rate at which free oscillations die out or determining the power that must be supplied to maintain oscillations having a constant amplitude. Examination of data covering a number of bombs whose lengths vary from 4 to 10.5 times their diameter shows that the ratio C_q/C_i averages about 1/3, ranging from 1/4 to 2/5. This ratio appears to be roughly independent of the ratio of length to diameter and of C_q , which varied by a factor of 5. However, if one considers very short projectiles or those of unusual design, the rule of thumb that $C_q/C_i \approx 1/3$ may not hold.

The relation between C_q and C_i may be seen from the following heuristic argument. Consider a projectile whose center of mass lies midway between the two ends as indicated in figure 2.48, and assume that the aerodynamic forces act at the ends only, being proportional to the yaw when the projectile is not rotating about a transverse axis. Thus we can write the lift as

$$L = (F_R + F_N) V^2 \delta, \quad (2)$$

where F_R and F_N are the constants of proportionality for the rear and nose forces, respectively, and are independent of V and δ . Now at some instant the rocket will have no yaw but will be rotating about a transverse axis with angular velocity ω . The nose then has a transverse velocity $\omega l/2$, so that the local situation is exactly the same as though the rocket had a yaw equal to $\omega l/2V$. Consequently the force on the nose is

$$F_N V^2 \frac{\omega l}{2V} = \frac{1}{2} F_N V \omega l.$$

Likewise the force on the rear is

$$\frac{1}{2} F_R V \omega l,$$

and the moment about the center of mass is

$$M_q = \frac{1}{4} (F_R + F_N) V \omega l^2. \quad (3)$$

It follows from (2), (3), and 2.41 (4) and (12) that

$$\frac{C_q}{C_i} = \frac{M_q / \frac{1}{2} \rho A V l^2 \omega}{L / \frac{1}{2} \rho A V^2 \delta} = \frac{1}{4}. \quad (4)$$

If the centers at which the forces $F_R V^2 \delta$ and $F_N V^2 \delta$ act are closer together than was assumed in the above argument, C_q/C_i will be less than $1/4$. On the other hand, when the center of mass is nearer the nose than the rear, C_q/C_i depends on the center of lift eccentricity and may be somewhat greater than $1/4$ for stable projectiles and considerably less than $1/4$ for unstable ones. It is clearly unprofitable to pursue this line of argument further in search of more detailed conclusions.

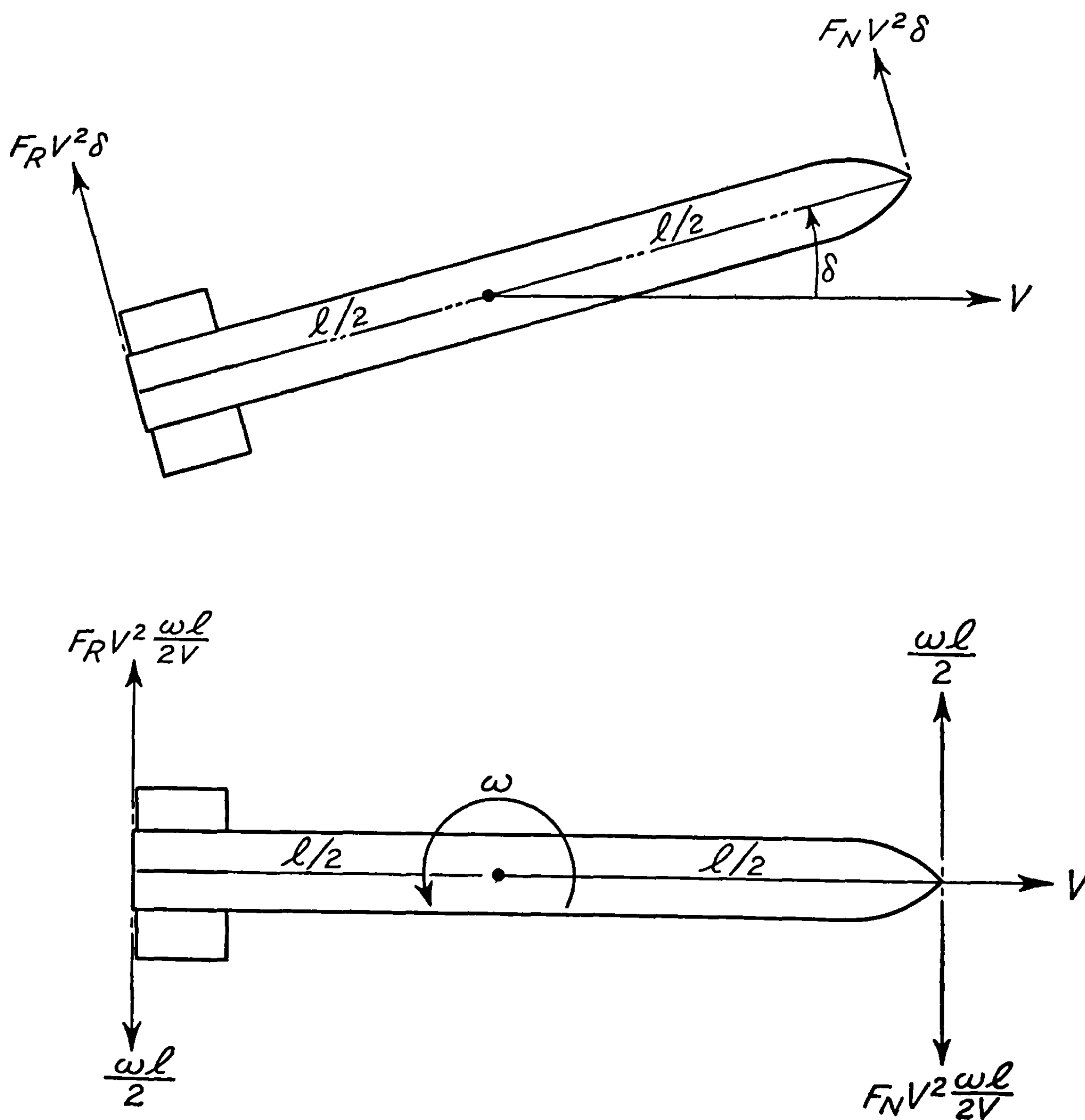


FIGURE 2.48.—The relation between L and M_q .

CHAPTER 3

THE MOTION DURING BURNING

3.0 Introduction

Having introduced, in chapter 2, the forces acting on the rocket we are now in a position to set down the equations of motion and thence determine the elements of the motion—position, velocity and orientation of the projectile—as functions of time. The complete ballistics problem requires the determination of the trajectory from the point of launching to the impact point. However, because of the fact that the jet forces, which are the dominant forces during the period of burning, cease to act after burning, the problem is naturally resolved into two distinct parts: (1) The determination of the relatively short trajectory during burning, when all of the forces—jet, aerodynamic and gravity—are present; and (2) the determination of the trajectory after burning, when only the aerodynamic forces and gravity are present. The consideration of the former problem constitutes the subject matter of the present chapter.

3.1 The Vacuum Approximation

It will prove useful to consider first the ideal case of a rocket fired in a vacuum; that is, in the absence of aerodynamic forces. Although this treatment will not lead to results applicable to the actual case of firing in air, nevertheless it will provide considerable insight into the nature of the effects of the various disturbing factors on the trajectory. Moreover, the results should apply fairly well to the early part of the actual trajectory, during which the velocity and hence the aerodynamic forces are small, as well as to the case of rockets which are neutrally or barely stable.

To simplify as much as possible the treatment of the motion during burning in vacuum, each of the effects of gravity, linear and angular thrust malalignment, and mallaunching will be considered separately. No loss of generality is entailed thereby, for it will be shown in 3.25 that the contributions of the above disturbing factors to the yaw and deflection in any plane superpose linearly.

Our main object will be to determine the direction of motion of the center of mass of the rocket during and particularly at the end of burning; that is, the angular deflection of the tangent to the trajectory from its initial direction as determined by the orientation of the launcher. Any linear deflections of the rocket from the launcher line that are introduced during the burning period will be small compared to the deflections introduced after burning because of the altered direction of motion of the trajectory as a whole, for the burning distance is generally only a small portion of the entire path.

3.11 Effect of Gravity.—The coordinate system we shall use is shown in figure 3.11a, in which the origin is taken at the position of the center of gravity of the rocket at the instant of ignition, the Z_0 -axis along the direction of the launcher, and the Y_0 -axis normal to it and pointing downward. The rocket is assumed to be perfectly symmetrical in shape with the axis of thrust along the axis of symmetry. Since the only forces acting on the rocket are the jet force through the center of mass and the force of gravity, the orientation of the projectile will remain unchanged during its motion. We use the following notation.¹

¹ See also the glossary of symbols, appendix A.

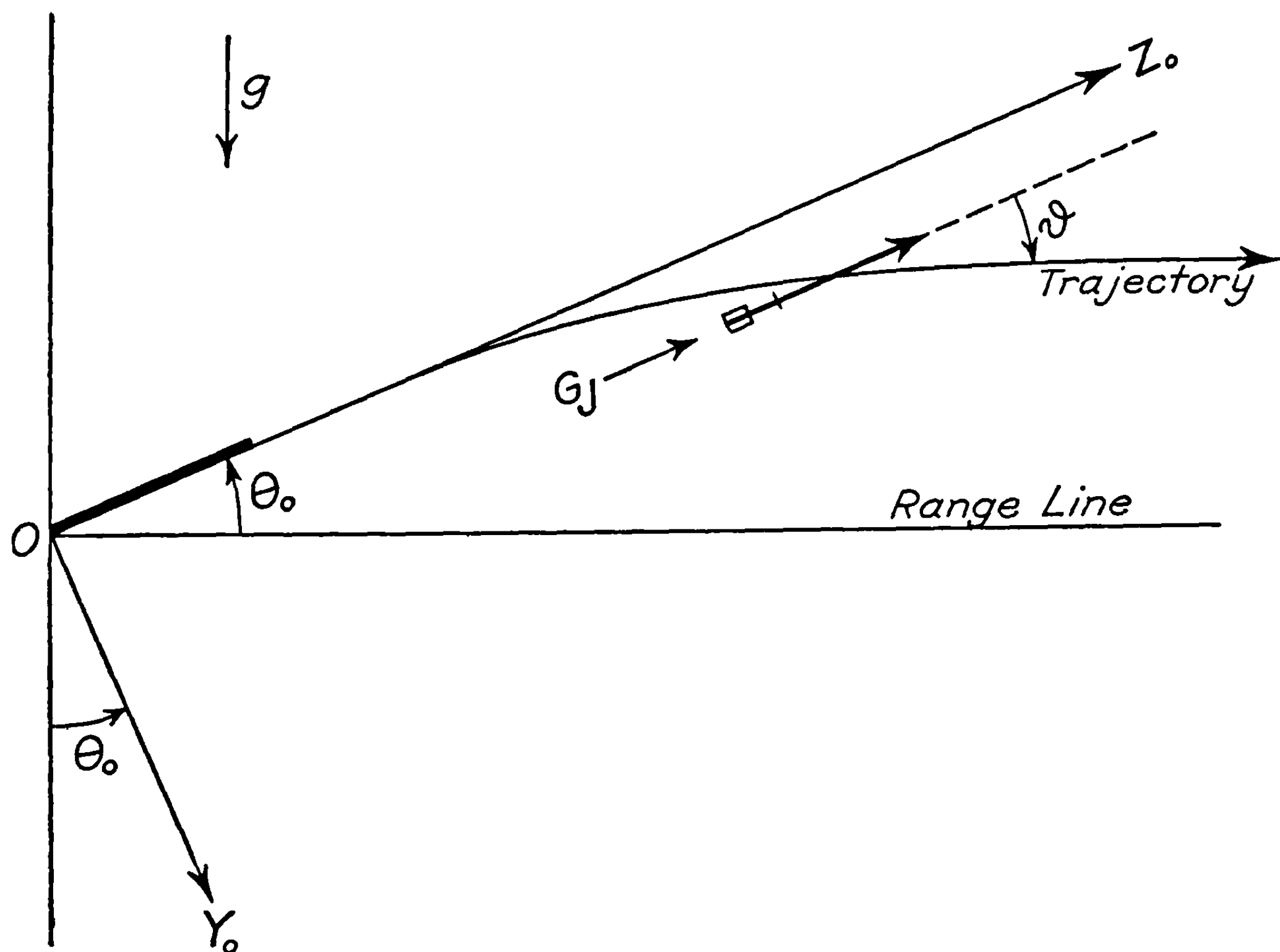


FIGURE 3.11a.—The coordinate system.

g = acceleration due to gravity,
 G_J = acceleration due to jet propulsion forces (assumed constant),
 $G = G_J - g \sin \theta_0$ = total acceleration along Z_0 -axis,
 p = effective launcher length; that is, the distance the rocket moves before the constraint of the launcher is removed,
 t = time from start of burning,
 t_p = time at which rocket leaves launcher; $t_p = (2p/G)^{1/2}$,
 t_b = burning time of the rocket,
 θ_0 = quadrant elevation of the launcher above the horizontal,
 φ = deflection of the tangent to the trajectory from the launcher line.
 The equations of motion of the rocket during burning are:

$$\ddot{Z}_0 = G_J - g \sin \theta_0, \quad (1)$$

$$\ddot{Y}_0 = g \cos \theta_0, \quad (2)$$

and

$$\varphi = \tan^{-1}(\dot{Y}_0/\dot{Z}_0) \doteq \dot{Y}_0/\dot{Z}_0. \quad (3)$$

for small angles.

When the rocket leaves the launcher, that is at $t = t_p$, the boundary conditions are that $Y_0 = \dot{Y}_0 = 0$. Hence the integrated equations are:

$$Z_0 = \frac{1}{2}(G_J - g \sin \theta_0)t^2, \quad (4)$$

$$Y_0 = \frac{1}{2} g \cos \theta_0 (t - t_p)^2, \quad (5)$$

$$\vartheta = \frac{g \cos \theta_0}{G_J - g \sin \theta_0} \left(1 - \frac{t_p}{t} \right). \quad (6)$$

Writing $\vartheta_{g, \text{vac}}$ for ϑ to indicate that it is the deflection due to gravity in vacuo, we have in terms of distance,

$$\vartheta_{g, \text{vac}} = \frac{g \cos \theta_0}{G} [1 - (p/d)^{\frac{1}{2}}]. \quad (7)$$

In the above equation d is the distance measured along the Z_0 -axis. Since ϑ is generally quite small, however, the quantity d might just as well be taken to mean the distance along the trajectory. For zero-length launchers we note that $\vartheta_{g, \text{vac}}$ is a constant regardless of the burning distance. That is, the trajectory is a *straight line* at an angle $(g/G) \cos \theta_0$ with the launcher line. For $p > 0$, the deflection increases with the burning distance d , approaching the limit $(g/G) \cos \theta_0$ as $d/p \rightarrow \infty$. The function defined by (7) is shown graphically in figure 3.11b.

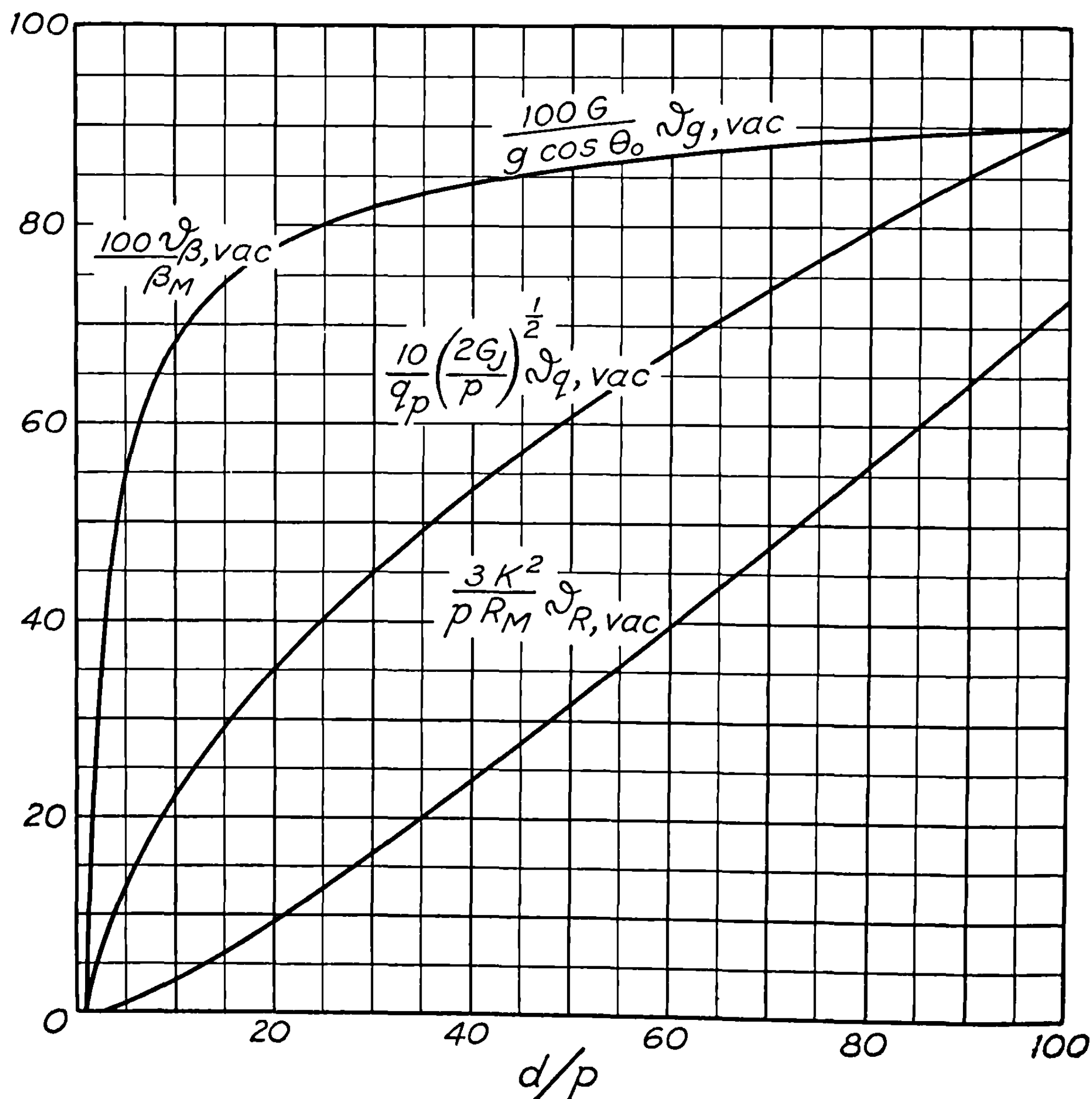


FIGURE 3.11b.— Effects of gravity (ϑ_g), linear (ϑ_R), and angular (ϑ_β) malalignment, and mallaunching (ϑ_q) on the deflection of the trajectory in vacuum.

3.12 Effects of Linear and Angular Thrust Malalignment.—We take the Z_0 -axis along the launcher, as before, and the Y_0 -axis in the plane of the trajectory. As shown in figure 3.12, the angle between the tangent to the trajectory and the Z_0 -axis is denoted by ϑ and the angle between the axis of the projectile and the Z_0 -axis by φ . The equations of motion of the center of mass of the rocket are:

$$\ddot{Z}_0 = G_J \cos \varphi - G_J \beta_M \sin \varphi \cong G_J, \quad (1)$$

and

$$\ddot{Y}_0 = G_J \sin \varphi + G_J \beta_M \cos \varphi \cong G_J \varphi + G_J \beta_M. \quad (2)$$

The equation for the rotation about a transverse axis is

$$mK^2\ddot{\varphi} = mG_J R_M, \quad (3)$$

while the deflection of the tangent to the trajectory is given by

$$\vartheta = \tan^{-1}(\dot{Y}_0/\dot{Z}_0) \cong \dot{Y}_0/\dot{Z}_0. \quad (4)$$

In the above equations the usual approximations have been made for small angles ($\varphi, \vartheta, \beta_M \ll \pi$).

The symbols have the same meaning as in 3.11, the additional ones being:

K =radius of gyration of the rocket about a transverse axis through its center of mass (assumed constant),

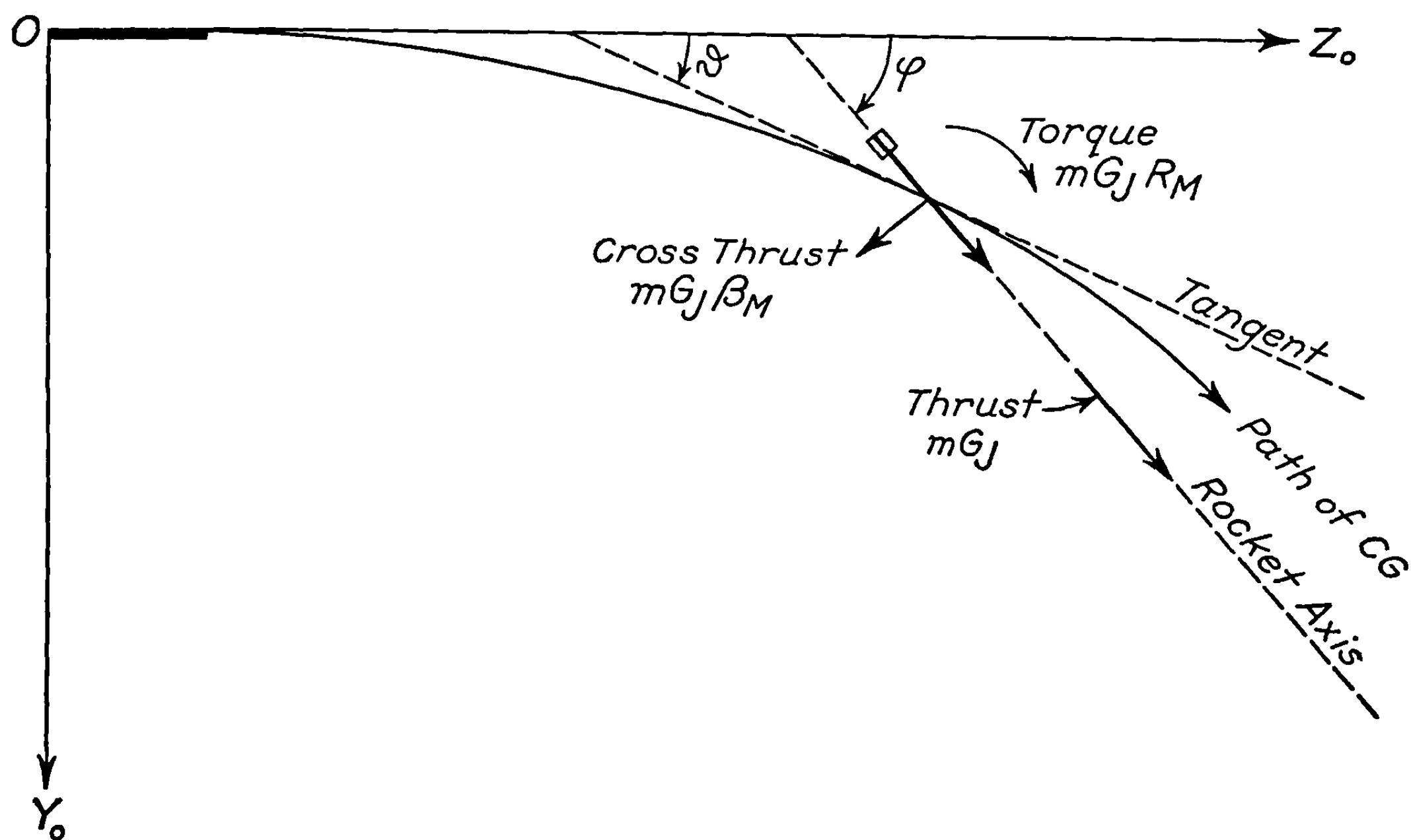


FIGURE 3.12.—The coordinate system for thrust malalignment.

m = mass of the rocket, and

φ = orientation angle; that is, angle between rocket axis and launcher line.

As discussed in 2.24, the force system produced by the jet does not consist exclusively of a thrust, mG_J , along the axis of the rocket, but includes a cross force, $mG_J\beta_M$, normal to the longitudinal axis and a torque, mG_JR_M , about an axis normal to the longitudinal axis. The quantities R_M and β_M are known as the *linear* and *angular malalignments*, respectively, on the basis of the geometric interpretation given in 2.24. We shall now consider the motion in vacuum of a rocket having these malalignments but not acted on by gravity, since, as mentioned above, the effect of including gravity is obtained by adding the deflections obtained in 3.11. The effect of a constant angular malalignment is essentially the same as that of gravity, since it is a constant force acting normal to the trajectory and hence nearly in a fixed direction. The effect of the torque due to the linear malalignment is to rotate the rocket about a transverse axis through the center of mass with constant angular acceleration. As the rocket rotates, the thrust produced by the jets rotates with it and tends to drive the rocket in the direction the axis is pointing, rather than parallel to the launcher. This, it will be shown, is the primary cause of the dispersion of fin-stabilized rockets; although the angular malalignment and other effects contribute in a minor way.

We consider the case in which the motion takes place in a single plane which contains the longitudinal axis and the trajectory. This requires that the transverse thrust due to angular malalignment lie in this plane and that the torque due to linear malalignment must be about an axis normal to this plane in order that it not rotate the rocket out of the plane. This restriction of the motion to a single plane does not result in any essential limitation of the generality of our final result, for we can always say that we are considering only the projection of the general three dimensional motion on this plane, that the transverse force due to angular malalignment which we consider is the component parallel to this plane of the actual force, and that the torque due to linear malalignment that we consider is the component normal to this plane of the complete torque. If we successively project the force system and motion on two perpendicular planes, we get a complete three dimensional description of the motion as the vector sum of the deflections in each plane. We assume that there is no torque or initial angular velocity about the longitudinal axis of the rocket; this case will be postponed to 3.61.

It is assumed that although m and the moment of inertia, mK^2 , vary during burning, G and K remain constant. It is worth noting that if both the linear and the angular malalignments are due to a deflection of the axis of thrust, as when the nozzle is improperly aligned, they will have opposite signs in the usual case in which the thrust axis intersects the rocket axis to the rear of the center of mass. In this case the deflections due to the two causes will be in opposite directions; but it is quite possible for the two effects to be in the same direction, particularly when the nozzle is close to the center of mass.

The boundary conditions are that when the rocket leaves the launcher; i. e., at $t=t_p$,

$$Y_0 = \dot{Y}_0 = 0,$$

and

$$\varphi = \dot{\varphi} = 0.$$

Integrating (3), we have

$$\varphi = \frac{G_J R_M}{2K^2} (t - t_p)^2. \quad (5)$$

Substituting into (2) and integrating once,

3.1 THE VACUUM APPROXIMATION

$$\dot{Y}_0 = \frac{G_J^2 R_M}{6K^2} (t - t_p)^3 + G_J \beta_M (t - t_p). \quad (6)$$

Now from (1),

$$\dot{Z}_0 = G_J t; \text{ and } Z_0 = \frac{1}{2} G_J t^2 \cong d. \quad (7)$$

Thus the deflection of the tangent to the trajectory is

$$\vartheta = \frac{G_J R_M}{6K^2} \left(1 - \frac{t_p}{t}\right)^3 t^2 + \beta_M \left(1 - \frac{t_p}{t}\right). \quad (8)$$

Since the two effects are linear, we may write

$$\vartheta = \vartheta_R + \vartheta_\beta. \quad (9)$$

Hence, placing subscripts on the terms to indicate vacuum conditions, and rewriting with distance, d , as the independent variable, we have

$$\vartheta_{R, \text{vac}} = \frac{R_M}{3K^2} [1 - (p/d)^{\frac{1}{2}}]^3 d \quad (10)$$

for the deflection due to linear malalignment in vacuum; and for the deflection due to angular malalignment

$$\vartheta_{\beta, \text{vac}} = \beta_M [1 - (p/d)^{\frac{1}{2}}]. \quad (11)$$

Graphs representing the above relations are given in figure 3.11b. Examination of (10) and (11) and the curves in figure 3.11b leads to the following conclusions:

(1) The contributions of the linear and angular malalignments to the deflection of the trajectory are algebraically additive and are directly proportional to the magnitudes of the respective malalignments. For most rockets, however, the deflections will be in opposite directions.

(2) For zero-length launchers, the angular deflection due to the linear malalignment increases linearly with the burning distance, while the deflection due to the angular malalignment is constant and equal to the angular malalignment β_M . For $p > 0$, both deflections are less than for the zero-length launcher case, approaching the condition for $p = 0$ as the burning distance increases.

(3) The effect of the angular malalignment on the deflection is identical with the effect of gravity, see 3.11 (7), with β_M replacing $(g/G) \cos \theta_0$.

(4) As long as the rocket acceleration remains constant, the deflections due to malalignment are independent of the acceleration, depending only on launcher length and burning distance.

(5) If the burnt velocity remains constant, the burning distance, d_b , is inversely proportional to the acceleration. Hence in vacuum, the greater the acceleration the smaller the deflections due to linear and angular malalignment, the decrease in the deflection due to linear malalignment being particularly great. One of the most important results of 3.33 is that this conclusion is usually reversed when one allows for the aerodynamic moment.

(6) For a given malalignment the deflection due to β_M is independent of the geometry of the rocket, while the deflection due to R_M is inversely proportional to the square of the radius of gyration. Since for a given shape of rocket R_M and K will vary approximately as the length of the rocket, a longer rocket should give a smaller deflection.

(7) The deflection at the end of burning due to the angular malalignment is generally negligible compared to that of the linear malalignment. To get an order of magnitude for this ratio, consider a slender rocket fired from a zero-length launcher. Assuming $K^2 \approx l^2/12$ and $R_M \approx \beta_M l/2$, where l is the length of the rocket, we have for the desired ratio:

$$\frac{\text{angular deflection}}{\text{linear deflection}} = \frac{3K^2\beta_M}{R_M d} \approx \frac{l}{2d} \ll 1.$$

When the burning distance, d_b , is not very much greater than the launcher length, this result may be modified somewhat.

3.13 Effect of Mallaunching.—In the above sections it was assumed that the constraints imposed on the rocket by the launcher are removed instantaneously at the moment of launching and that the initial conditions at this instant are the ideal ones considered in the previous sections. Such a situation is of course an idealization; for in any actual launching process as the rocket begins to leave the launcher and is supported at but one point, interactions between the rocket and the launcher, resulting from gravity, blast effects, etc., will result in the rocket receiving some net impulse. This situation we call *mallaunching*. In precise discussions we usually reserve the term *mallaunching* for the initial angular velocity about a transverse axis, and we use the terms *initial cross pointing* and *initial cross velocity* for the changes in orientation of the rocket and the velocity normal to the launcher, respectively. Since the mallaunching produces by far the biggest deflection under ordinary circumstances, we sometimes refer to all three phenomena together as mallaunching in cases where no confusion will result. A discussion of the mechanism of mallaunching will be reserved for chapter 4. For the present we assume that at the instant of launching; that is, when all constraints are removed, we have the initial conditions

$$t=t_p, Z_0=p, Y_0=Y_{op}, \varphi=\varphi_p, \dot{Y}_0=\dot{Y}_{op}, \dot{\varphi}=\dot{\varphi}_p.$$

The coordinate system, figure 3.12, is so chosen that the Z_0 -axis is again the launcher line, while the Y_0 -axis is in the plane in which the rocket is deviated; that is, the Y_0 -axis is in the direction of the impulse imparted to rocket by the launcher and is normal to the axis about which the rocket starts rotating. Just as in the previous section, this implies no real loss in generality since any three dimensional motion can be regarded as resolved into the sum of two motions in perpendicular planes. Since the only force acting is the thrust, which is along the axis of symmetry of the rocket, the equations of motion are:

$$\ddot{Z}_0 = G_J \cos \varphi \doteq G_J, \quad (1)$$

$$\ddot{Y}_0 = G_J \sin \varphi \doteq G_J \varphi, \quad (2)$$

$$\ddot{\varphi} = 0, \quad (3)$$

$$\vartheta = \tan^{-1}(\dot{Y}_0/\dot{Z}_0) \doteq \dot{Y}_0/\dot{Z}_0. \quad (4)$$

Integrating (3) twice, and applying the boundary conditions, we have

$$\varphi = \dot{\varphi}_p (t - t_p) + \varphi_p. \quad (5)$$

Substituting (5) into (2) and integrating, we have

$$\dot{Y}_0 = \frac{G_J \dot{\varphi}_p (t - t_p)^2}{2} + G_J \varphi_p (t - t_p) + \dot{Y}_{0p}. \quad (6)$$

Now from (1),

$$\dot{Z}_0 = G_J t. \quad (7)$$

Therefore,

$$\begin{aligned} \vartheta &= \frac{\dot{Y}_0}{\dot{Z}_0} = \frac{\dot{\varphi}_p}{2} \left(1 - \frac{t_p}{t}\right)^2 t + \varphi_p \left(1 - \frac{t_p}{t}\right) + \frac{\dot{Y}_{0p}}{G_J t} \\ &= \frac{\dot{\varphi}_p}{(2 G_J)^{\frac{1}{2}}} [1 - (p/d)^{\frac{1}{2}}]^2 d^{\frac{1}{2}} + \varphi_p [1 - (p/d)^{\frac{1}{2}}] + \frac{\dot{Y}_{0p}}{(2 G_J d)^{\frac{1}{2}}}. \end{aligned} \quad (8)$$

We shall now show that the dominant term in (8) is the one due to the angular velocity $\dot{\varphi}_p$. To get the order of magnitude of the second term, we can assume that $\varphi_p \approx \frac{1}{2} \dot{\varphi}_p (\Delta t)_p$, where $(\Delta t)_p$ is the time interval during which the impulse is received by the rocket. Hence, the ratio of the second term in (8) to the first term is

$$\frac{\varphi_p (1 - t_p/t)}{\frac{1}{2} \dot{\varphi}_p (1 - t_p/t)^2 t} \approx \frac{\frac{1}{2} \dot{\varphi}_p (\Delta t)_p}{\frac{1}{2} \dot{\varphi}_p t} = \frac{(\Delta t)_p}{t} \ll 1.$$

Assuming $\dot{Y}_{0p} \approx \frac{1}{2} l \dot{\varphi}_p$, where l is the length of the rocket, we have for the ratio of the last term to the first term in (8)

$$\frac{\dot{Y}_{0p}}{(2 G_J d)^{\frac{1}{2}}} \cdot \frac{(2 G_J)^{\frac{1}{2}}}{\dot{\varphi}_p [1 - (p/d)^{\frac{1}{2}}]^2 d^{\frac{1}{2}}} \approx \frac{l}{2d} \ll 1.$$

Hence the dominant term in the deflection resulting from mal-launching is that due to initial angular velocity $\dot{\varphi}_p = q_p$, namely

$$\vartheta_{q, \text{vac}} = \frac{q_p}{(2 G_J)^{\frac{1}{2}}} [1 - (p/d)^{\frac{1}{2}}] d^{\frac{1}{2}}, \quad (9)$$

for which the deflection increases approximately as the square root of the burning distance. The variation of this term with p and d is shown in figure 3.11b.

3.2 General Equations of Motion During Burning

The following treatment of the motion of fin-stabilized rockets during the period of burning will be limited to the case of firing from a stationary launcher in the absence of wind. The extension of the problem to forward firing from aircraft or from moving launchers will be found in chapter 6; while the special case of firing in the presence of a wind will be discussed in 3.43. Furthermore, it is assumed that the rocket does not rotate about its longitudinal axis. Such rotations could be caused by a rifled launcher or by a variety of other means, accidentally or intentionally introduced. In the presence of any of these causes of rotation, the problem could be treated either by the methods adopted for slow spin in 3.6 below, or, in the case of fast spin, by the methods of chapter 9. Finally, all angular deviations and rotations of the rocket and trajectory from the initial direction as determined by the orientation of the launcher will be assumed sufficiently small ($\varphi \ll \pi$) so that the usual approximations for small angles, $\sin \varphi \doteq \tan \varphi \doteq \varphi$, and $\cos \varphi \doteq 1$, will be valid. This restriction is not as serious as might at first appear, for it will be seen later that even in the case of long-burning rockets, the deflections during burning are generally not over three or four degrees. Instead of attempting to obtain the exact equations of motion we shall make use of approximations based on the smallness of the yaw and orientation angle in order to get useful linear equations. The solutions of these approximate equations are usually as useful as the solutions of the exact equations would be, if such exact solutions could be obtained; since our knowledge of the aerodynamic and jet forces and moments is rarely precise enough to justify the use of the exact equations. If a more exact analysis is desired it can easily be modeled on the treatment given in 9.1.

3.21 Coordinate Systems and Forces.—In the absence of gravity, malalignments and mallaunching the trajectory of the rocket would be a straight line in the direction of the launcher, with the only forces being those due to thrust and drag, acting in antiparallel directions. When a single additional force (or torque, or initial transverse velocity) comes into play, the motion will take place in a plane, namely the plane determined by the disturbing force vector and the launcher. If two or more forces come into play the motion will be in a single plane only in the unlikely situation that the forces are all coplanar. In general, though, the motion will be three-dimensional, and the trajectory will not lie in a plane. However, it will be shown in the following section that for small displacements the motion can be resolved into independent motions in two perpendicular planes.

Figure 3.21a shows in perspective the relationships among the launcher, range line and coordinate systems which we shall use. To represent both the translational and rotational motions of the rocket we make use of the two parallel right-handed rectangular coordinate systems shown in the figure. One of them, $O_0X_0Y_0Z_0$, is fixed with the origin at the position of the center of gravity of the rocket at the instant of ignition, the X_0 -axis horizontal and pointing to the right as seen from the rear of the launcher, the Y_0 -axis normal to the launcher and pointing downward, and the Z_0 -axis along the direction of the launcher. The other system, $OXYZ$, moves in such a manner that its origin is at the center of gravity of the rocket, the orientation of the axes remaining always parallel to the $X_0Y_0Z_0$ axes. The linear motion of the rocket will be referred to the fixed coordinate system, while the angular motion will be referred to the moving system.

The details of the angular displacements in the XYZ system are shown in figures 3.21a, b, and c. For the purpose of specifying angles, a sphere of unit radius is drawn about the center of gravity, O , of the rocket, and all angles are measured as arcs on this sphere. The point

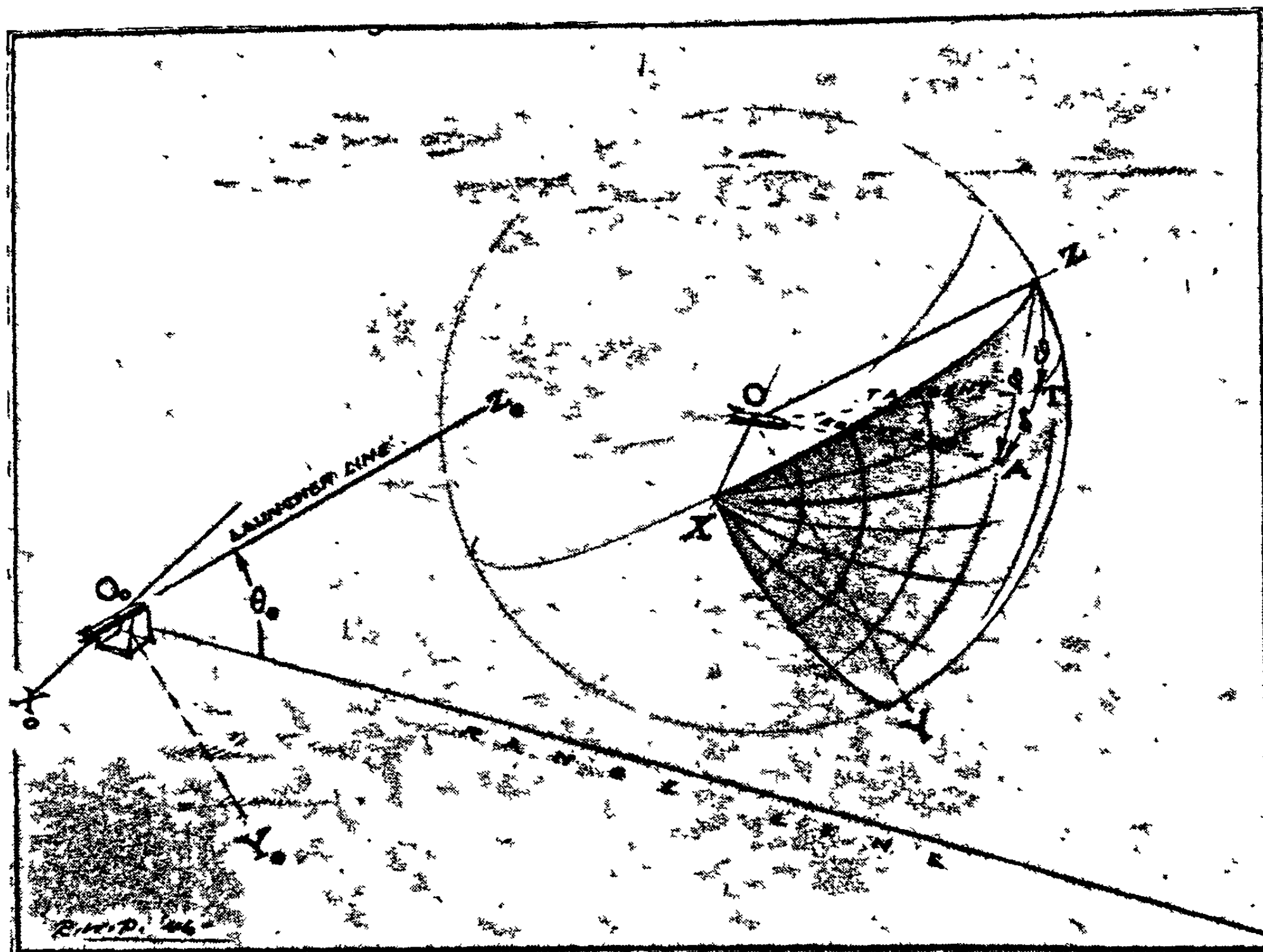


FIGURE 3.21a.—Location of the coordinate systems in space.

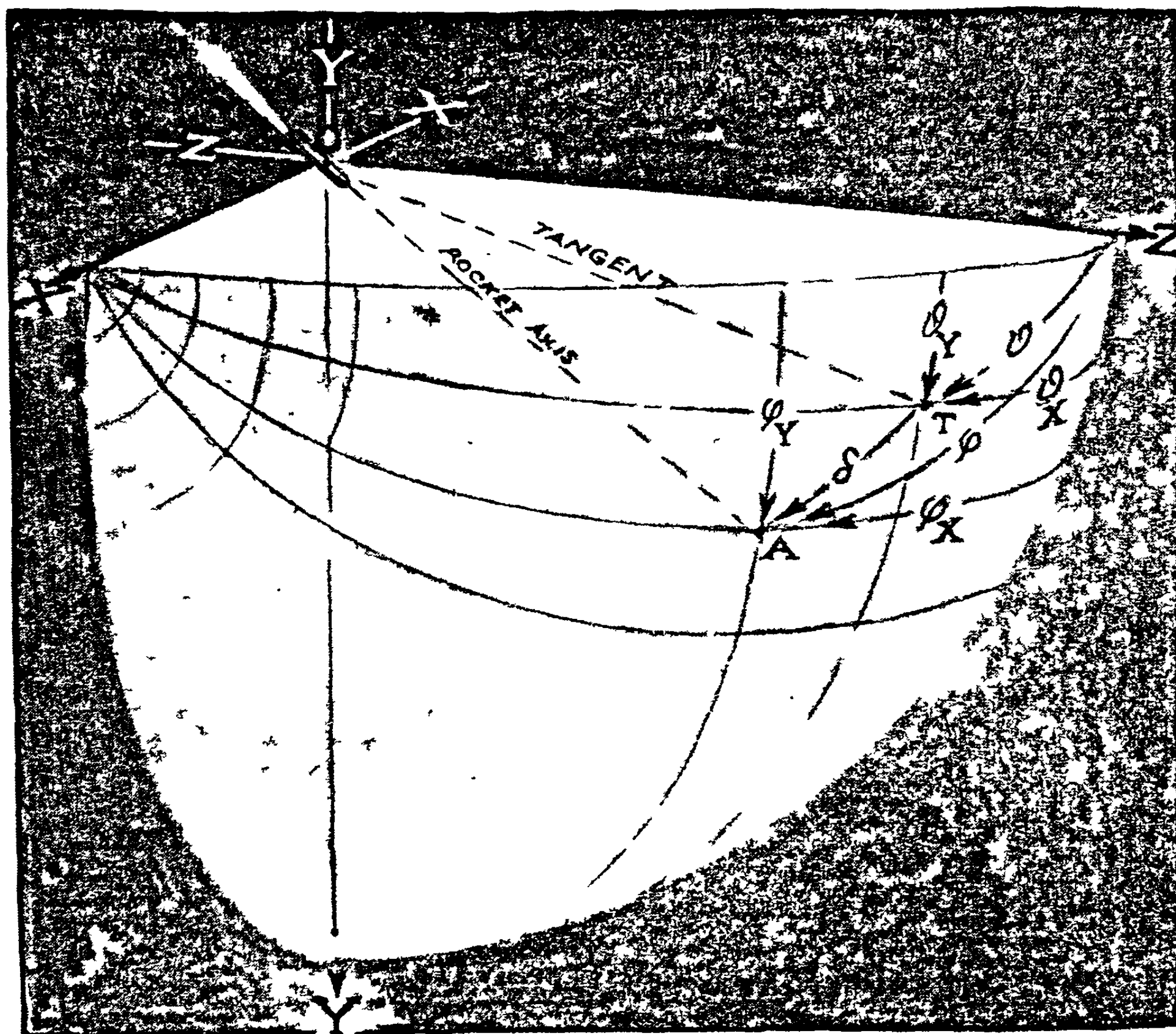


FIGURE 3.21b.—Angular coordinates as seen from ahead of the rocket.

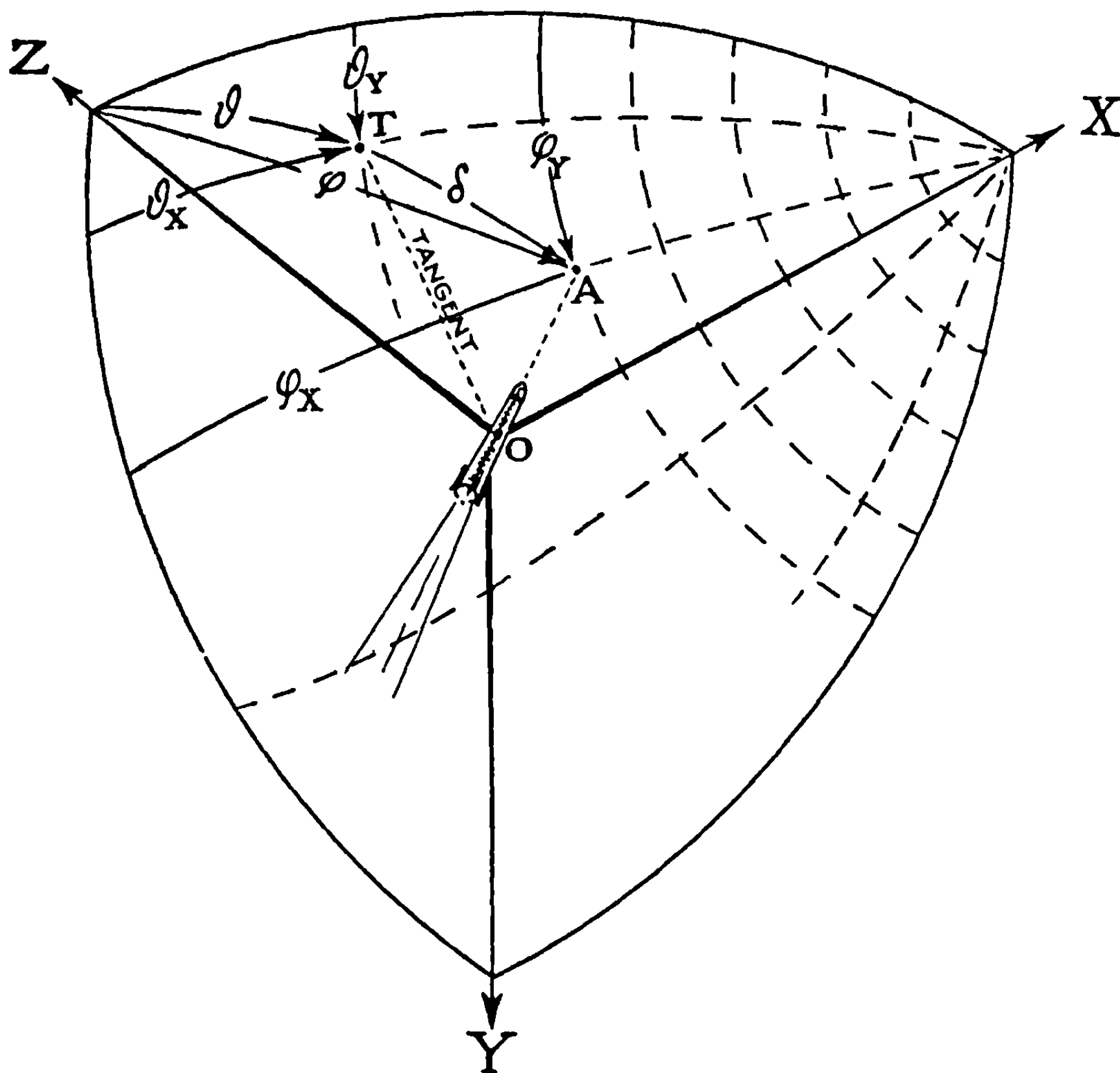


FIGURE 3.21c.—Angular coordinates as seen from behind the rocket.

where the geometrical axis of the rocket pierces the sphere is designated by the letter A , and the point where the tangent to the trajectory cuts the sphere by the letter T . The angle between the Z -axis and the rocket axis is the angle through which the rocket has rotated from its original direction on the launcher and is called the *orientation angle*, φ . To indicate the direction in which angles are measured from the Z -axis, it is convenient to represent them as complex vectors on the sphere. For example, we write $\varphi = \varphi_X + i\varphi_Y$; where i is $(-1)^{\frac{1}{2}}$, φ_X is the angle measured from the YZ -plane to the point A along the arc of the great circle through A and the X -axis, and φ_Y is the angle measured from the XZ -plane to the point A along the arc of the small circle parallel to the YZ -plane. In similar manner, the deflection of the tangent to the trajectory may be represented in complex form by $\vartheta = \vartheta_X + i\vartheta_Y$, where the magnitude of the deflection, ϑ , is the angle between the tangent to the trajectory OT and the Z -axis. The angle of yaw is the angle between the lines OA and OT and is represented in complex form by

$$\delta = \delta_X + i\delta_Y.$$

We note that

$$\varphi = \vartheta + \delta, \tag{1}$$

since

$$\varphi_X = \vartheta_X + \delta_X, \tag{2}$$

and

$$\varphi_Y = \vartheta_Y + \delta_Y. \tag{3}$$

Also, in view of the restriction to small angles,

$$\varphi = |\varphi| = (\varphi_x^2 + \varphi_y^2)^{\frac{1}{2}}, \quad (4)$$

$$\vartheta = |\vartheta| = (\vartheta_x^2 + \vartheta_y^2)^{\frac{1}{2}}, \quad (5)$$

and

$$\delta = |\delta| = (\delta_x^2 + \delta_y^2)^{\frac{1}{2}}. \quad (6)$$

What has really been done above is to represent the angular displacements as complex linear displacement vectors on a two-dimensional rectangular coordinate system tangent to the sphere with the origin on the Z -axis. (See fig. 3.21d.) For small displacements this is an adequate representation, since any deviations of the plane from the sphere will introduce negligible errors.

Let us now consider the resolution of the forces and moments acting on the rocket into components. In dealing with the equations of motion, one obtains convenient forms only if the forces are resolved into components parallel to and normal to the trajectory while the moments are resolved into components parallel to and normal to the axis of the projectile. In general, neither of these components will be quite parallel to the axes of the XY coordinate system:

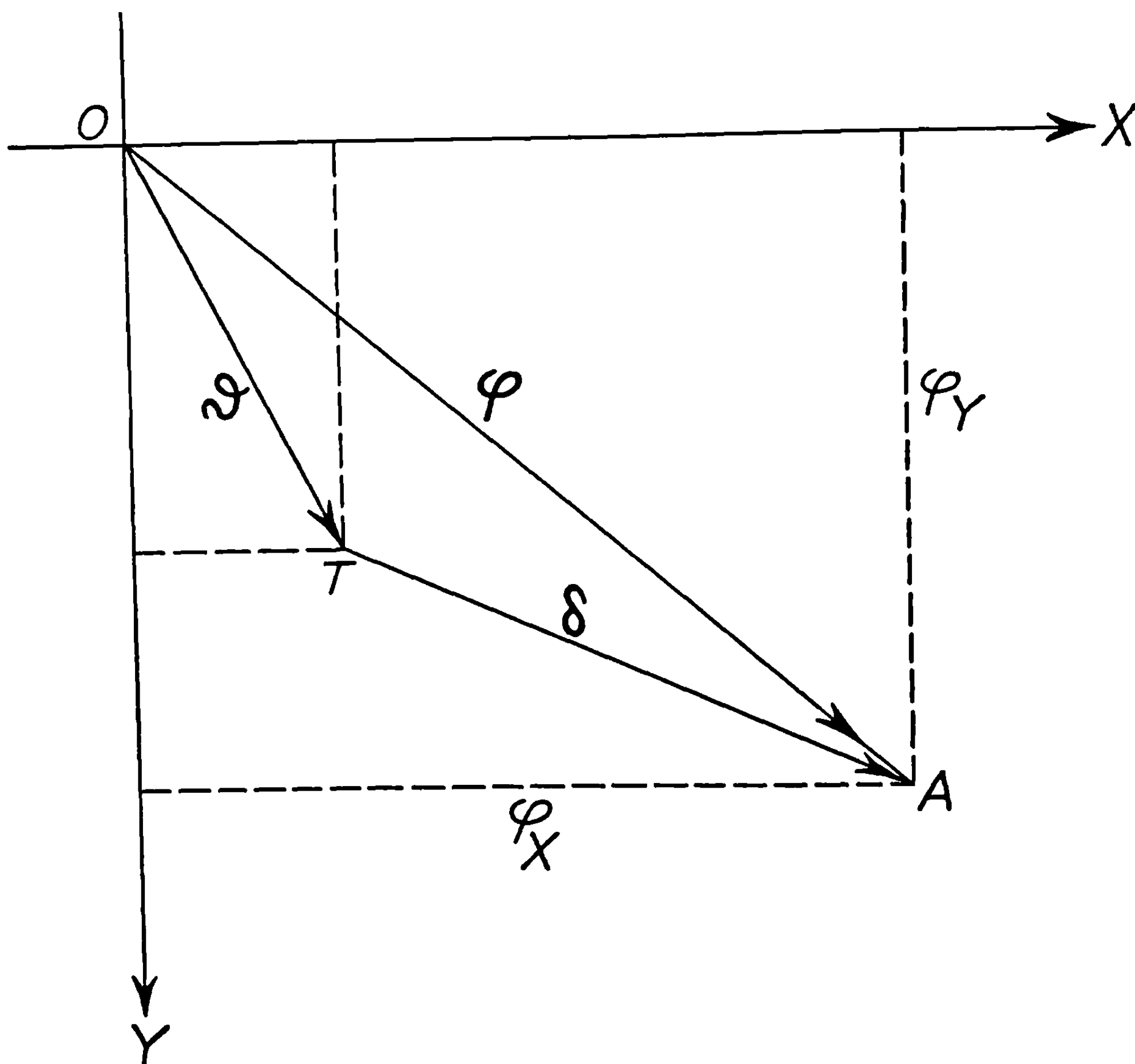


FIGURE 3.21d.—Coordinate system on a sphere, looking along the Z -axis.

although, because of the small values of ϑ and φ involved, they will be nearly parallel. We adopt the convention that the components of a force will be denoted by F_x , F_y , and F_z ; where F_z is the component parallel to the *tangent* to the trajectory. It is *not* the component parallel to the Z -axis. Likewise F_x and F_y are the components normal to the trajectory along the axes on which ϑ_x and ϑ_y , respectively, are measured. The components of a torque or moment will be denoted by M_x , M_y , and M_z , where M_z is the component parallel to the *axis* of the rocket. It is not the component parallel to either the Z -axis or the tangent of the trajectory. Likewise M_x and M_y are the components of the moment normal to the axis of the rocket along the axes on which φ_x and φ_y are measured. M_z is usually taken to be zero for fin-stabilized rockets.

It is, of course, possible to introduce two new sets of subscripts for designating the components of the forces and torques along the rocket axis or along the tangent. However, it is felt that the resulting confusion would be worse than the possibility that small errors may be introduced when one forgets that *throughout the treatment of fin-stabilized rockets forces are always resolved with respect to the tangent to the trajectory, while moments are always resolved with respect to the axis of the projectile*. Since φ and ϑ are small, the reader can usually ignore these distinctions between the coordinate axes and the directions used in taking components except at one or two obvious points in the derivation of the equations of motion. A more extensive discussion of these problems, including the effects of allowing φ and ϑ to become large, is given in 9.1.

3.22 General Dynamical Equations.—We are now in a position to apply Newton's laws of motion to obtain the equations of motion in terms of the above coordinates. For the motion along the path we know that the mass times the tangential acceleration of the rocket is equal to F_z ; that is,

$$m\dot{V} = F_z. \quad (1)$$

In view of the fact that $\dot{Z}_0 = V \cos \vartheta \doteq V$, we can also use the approximate form

$$m\ddot{Z}_0 = F_z. \quad (2)$$

The lateral motion of the center of mass is most conveniently deduced from the direction of the tangent to the trajectory by means of the relations

$$\tan \vartheta_x = \dot{X}_0 / \dot{Z}_0 \doteq \vartheta_x,$$

and

$$\tan \vartheta_y = \dot{Y}_0 / \dot{Z}_0 \doteq \vartheta_y. \quad (3)$$

The equations whose solutions give ϑ_x and ϑ_y are obtained by equating the component of the total force normal to the trajectory to the mass times the acceleration normal to the trajectory. Since F_x and F_y are the two components of the total force normal to the direction of motion, while $V\dot{\vartheta}_x$ and $V\dot{\vartheta}_y$ are the corresponding components of the acceleration, this gives

$$mV\dot{\vartheta}_x = F_x,$$

and

$$mV\dot{\vartheta}_y = F_y. \quad (4)$$

To see that $V\dot{\vartheta}_x$ is the component of the acceleration that is both normal to the trajectory and in a plane through OX consider figure 3.22a, which shows the projection of the trajectory on this plane. If O_c is the center of curvature of the projection and R_c is the radius of curvature,

then $mV^2/R_c = mV\omega$ is the centrifugal force, where $\omega = V/R_c$ is the rate at which R_c turns as the projectile passes through O . Since the tangent to this projection of the trajectory is normal to R_c , the tangent turns at the same rate and $\omega = \dot{\vartheta}_x$. Hence the acceleration along R_c must be $V\dot{\vartheta}_x$. A similar argument holds in the Y direction.

Equations (4) are of sufficient importance to justify our giving another derivation in which the physical concepts used are simpler, although they do not lead so directly to the desired result. Since F_x and F_z are the components of the total force in the directions indicated in figure 3.22a, the component along the OX axis is

$$F_x \cos \vartheta_x + F_z \sin \vartheta_x \doteq F_x + F_z \vartheta_x. \quad (5)$$

By Newton's second law this is equal to $m\ddot{X}_0$, which by (3) and (2) is

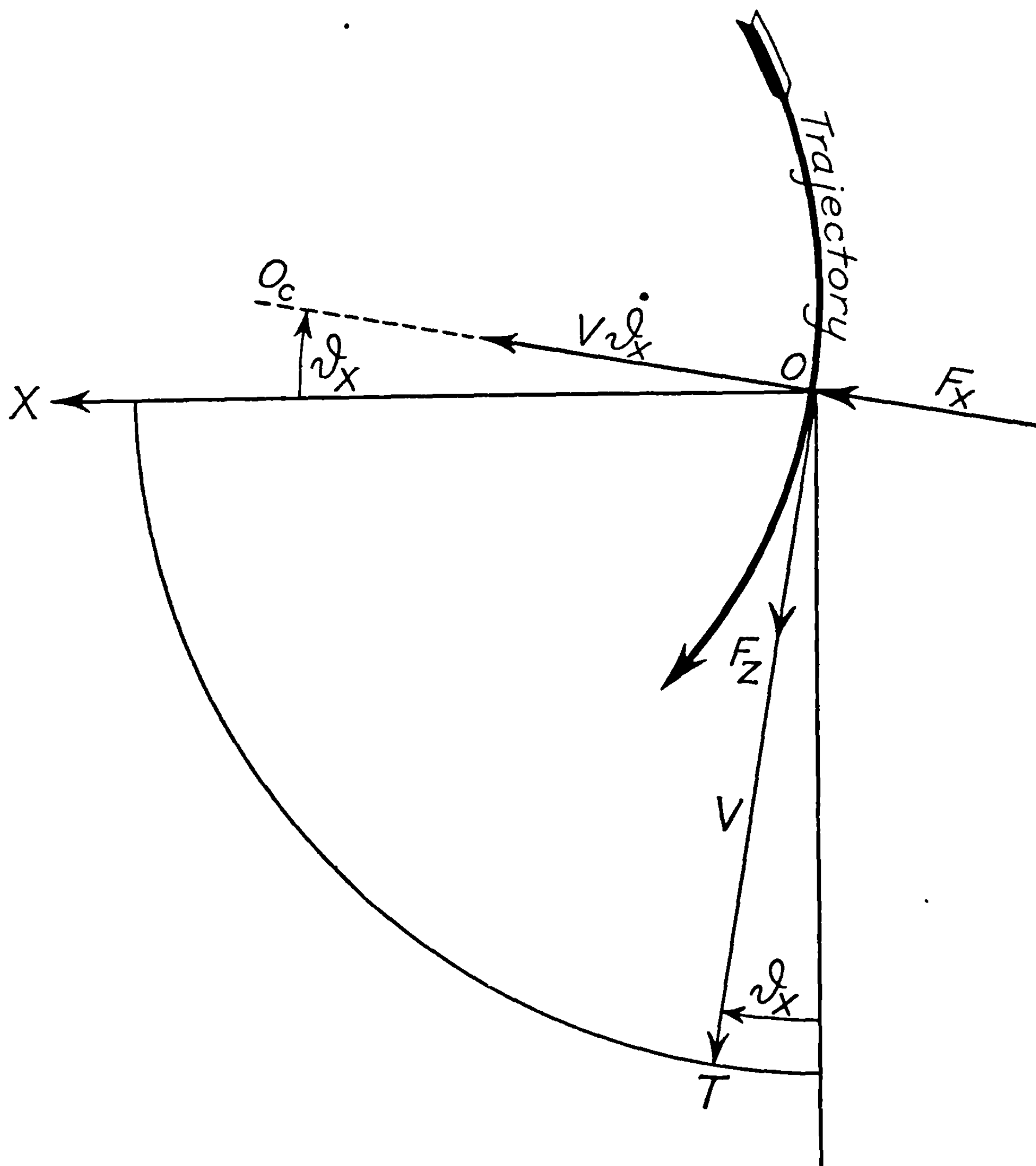


FIGURE 3.22a.—Acceleration normal to the direction of motion.

$$m\ddot{X}_0 = m \frac{d}{dt} (\dot{Z}_0 \vartheta_X) = m\dot{Z}_0 \dot{\vartheta}_X + m\ddot{Z}_0 \vartheta_X = mV \dot{\vartheta}_X + F_Z \vartheta_X. \quad (6)$$

If we equate (5) and (6) we get the first of equations (4). The second equation can be obtained similarly.

The equations for the rotation about the OX and OY axes are easily obtained when φ , the orientation angle, is small and the rocket has neither rotation nor torque about its longitudinal axis. From figures 3.21 b or c, it is evident that the angular velocity about the OY axis is $\dot{\varphi}_X$. Hence the statement that the moment of inertia times the angular acceleration is equal to the applied torque becomes

$$mK^2 \ddot{\varphi}_X = M_Y, \quad (7)$$

where mK^2 is the moment of inertia about a transverse axis through the center of mass and M_Y is the component of the total torque along the arc on which φ_Y is measured. M_Y is nearly but not quite equal to the component of the total moment in the OY direction. A more precise derivation which shows that here the difference is negligible will be found in chapter 9. Inspection of figures 3.21b or c will show that the angular velocity about the positive OX axis is $-\dot{\varphi}_Y$. Hence, proceeding as in the derivation of (7), we get

$$mK^2 \ddot{\varphi}_Y = -M_X, \quad (8)$$

where M_X is the component of the total torque along the arc on which φ_X is measured and is nearly equal to the component of the moment in the OX direction.

The minus sign in (8) and the variation in subscript between the right- and left-hand sides of (7) and (8) is an awkward feature that can be eliminated by introducing a vector \mathbf{f} which is normal to the axis of the rocket and is defined by

$$f_X = M_Y, f_Y = -M_X. \quad (9)$$

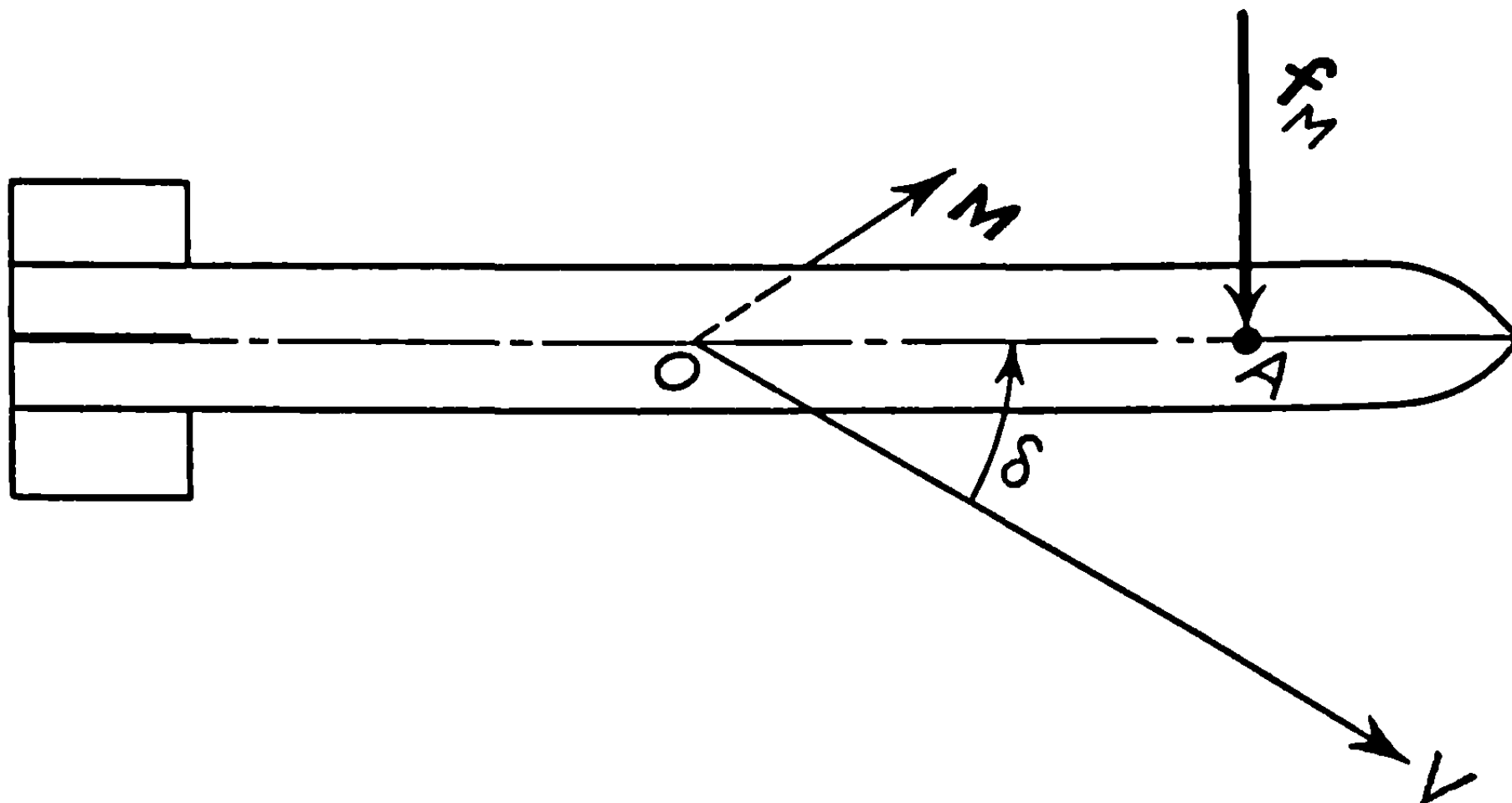
Then (7) and (8) become

$$mK^2 \ddot{\varphi}_X = f_X,$$

And

$$mK^2 \ddot{\varphi}_Y = f_Y. \quad (10)$$

Not only does the introduction of \mathbf{f} simplify the equations of motion, but in addition, its physical interpretation provides a very desirable representation of moments or torques about transverse axes of the rocket. If the force \mathbf{f} acts at A , the point on the axis of the rocket unit distance ahead of the center of mass, and if the force $-\mathbf{f}$ acts at the center of mass, the moment of this couple has the components M_X and M_Y , where \mathbf{f} and \mathbf{M} are connected by (9). Thus the use of the vector \mathbf{f} to describe any particular moment is equivalent to the specification of the force that would have to be applied at A normal to the axis of the rocket in order to produce this moment about O , the center of mass. This kind of representation is very convenient in the case of moments such as the aerodynamic restoring moment. To describe the restoring moment in the usual way requires a vector normal to the plane of the yaw and hence to the plane of the figure such as figure 3.22b. The moment is connected with the direction in which the rocket tends to move only through the right-hand rule. The vector \mathbf{f}_M , on the contrary, lies in the plane of the figure and points in the direction in which the restoring moment tends to move the rocket. By using the vector \mathbf{f}_M to represent the

FIGURE 3.22b.—Physical significance of f .

moment we can easily give 2.41 (11) the useful vectorial form

$$\mathbf{f}_M = -\frac{1}{2}C_{m\rho}AlV^2\delta, \quad (11)$$

which indicates that the direction of \mathbf{f}_M is opposite to that of the vector δ . Further examples of the convenience of \mathbf{f} will be given in 3.23. There are two points that must be emphasized in connection with the use of \mathbf{f} to represent moments. The first is that the method can be used only to represent moments about a transverse axis, or the component along the transverse axis of a general moment. The other is that \mathbf{f} is tangent to the unit sphere shown in figures 3.21b and c and hence, strictly speaking, f_x and f_y are *not* the components in the OX and OY directions but are the components along the arcs φ_x and φ_y at O . That is, \mathbf{f} is resolved in the same way that moments are.

In terms of the complex quantities defined in 3.21 and the additional complex representations

$$\mathbf{F}_\perp = F_x + iF_y, \quad (12)$$

$$\mathbf{f} = f_x + if_y, \quad (13)$$

equations (4) and (10) become

$$mV\dot{\vartheta} = \mathbf{F}_\perp, \quad (14)$$

and

$$mK^2\ddot{\varphi} = \mathbf{f}. \quad (15)$$

It is quite clear that a one-to-one correspondence exists between the complex quantities defined above and the two-dimensional vectors formed by the X and Y components of the various forces and moments. In fact the same quantity may be thought of as being a complex quantity, or a two-dimensional vector, in the XY -plane. For this reason the same **bold-face** type is used to designate both vectors and complex quantities.

3.23 Forces and Torques.—In order to proceed with the solution of the equations of motion, we must first obtain expressions for the various forces and torques considered in chapter 2 in terms of our present notation and in a form suitable for substitution in 3.22 (14) and (15).

3.231. The jet forces and moments.—In 2.24 the jet forces were found to be equivalent to a force mG_J along the axis of the rocket and $mG_J\beta_M$ normal to the axis. The contribution of these forces to F_Z , the component of the force tangent to the direction of motion, is

$$F_{JZ} = mG_J \cos \delta \doteq mG_J, \quad (1)$$

in which we have neglected the small term, of order $mG_J\beta_M \sin \delta$, contributed by the angular malalignment. (The exact magnitude of the term depends on the angle between δ and β_M .) Because of the yaw, the axial force mG_J also has a component normal to the trajectory of magnitude $mG_J \sin \delta \doteq mG_J\delta$. In addition, the angular malalignment force $mG_J\beta_M$ acts nearly normal to the trajectory. Hence if we neglect the difference between 1 and $\cos \delta$, the contribution of these two forces, expressed in components, is

$$F_{JX} = mG_J\delta_X + mG_J\beta_{MX}, \quad (2)$$

and

$$F_{JY} = mG_J\delta_Y + mG_J\beta_{MY};$$

or, in the complex notation,

$$F_{J\perp} = mG_J(\delta + \beta_M). \quad (3)$$

For brevity throughout the remainder of this section we shall use the complex notation to represent two-dimensional vectors tangent to the unit sphere of figures 3.21a, b, and c. However, if desired, one can readily replace each equation by the two equations in terms of components and thus carry through the entire treatment without the use of complex numbers.

The moment resulting from the linear thrust malalignment is equivalent to that produced by a force f_R applied unit distance ahead of the center of mass, where inspection of figure 2.24b shows that

$$f_R = -mG_J R_M. \quad (4)$$

In addition, the jet produces the jet damping torque (see 2.26) which may be written as

$$M_{JD} = -K_{JD}\omega, \quad (5)$$

where K_{JD} is given by 2.26 (15), ω is the transverse angular velocity of the rocket, and M_{JD} is the moment which opposes this velocity. In terms of our coordinates, the transverse angular velocity is specified by giving $\dot{\varphi}_X$ and $\dot{\varphi}_Y$ or by the single vector or complex number $\dot{\varphi}$, which points in the direction in which the nose of the rocket moves. The torque opposing this motion is represented by a vector f_{JD} in the opposite direction, the vector being

$$f_{JD} = -K_{JD}\dot{\varphi}. \quad (6)$$

3.232. Gravity.—This force, of magnitude mg , acts vertically downward in the YZ -plane. If θ_0 is the quadrant elevation of the launcher, and hence of the OZ axis, above the horizontal, and if ϑ_Y is the downward deflection of the trajectory below the OZ axis, then the components of the force of gravity along and normal to the trajectory are, respectively,³

³ Certain infinitesimals in ϑ_X have been neglected in (7) and (8) since they are completely unimportant during burning. For further discussion, see 9.17.

$$F_{gz} = -mg \sin (\theta_0 - \vartheta_Y) \doteq -mg \sin \theta_0 + (mg \cos \theta_0) \vartheta_Y, \quad (7)$$

and

$$F_{gY} = mg \cos (\theta_0 - \vartheta_Y) = mg \cos \theta_0 + (mg \sin \theta_0) \vartheta_Y. \quad (8)$$

During burning the last term in each of these equations can be neglected, since, when (1) and (7) are added to get the total F_z , $mg \cos \theta_0 \vartheta_Y$ will be extremely small compared to mG_J ; while, when (2) and (8) are added to get the total F_Y , $mg \sin \theta_0$ will be small compared to mG_J , and ϑ_Y will be of the same order as δ_Y . This considerably simplifies the treatment during burning without introducing discrepancies between theory and experiment larger than those due to the fluctuations in G_J . After the end of burning, however, these terms must be retained. If we wish to express in a single equation both (8) and the fact that $F_{gx} = 0$, we can write

$$F_{g\perp} = img \cos \theta_0. \quad (9)$$

Gravity exerts no torque about the center of mass.

3.233. *Aerodynamic forces.*—Reference to figure 2.41 shows that the contribution of the aerodynamic forces to F_z , the component of the force tangent to the direction of motion, is just the negative of the drag so that, in accordance with 2.41 (1),

$$F_{Az} = -\frac{1}{2} C_D \rho A V^2. \quad (10)$$

The contribution to the force normal to the trajectory is given by the lift, which is in the direction of the yaw. Hence from 2.41 (12)

$$F_{A\perp} = \frac{1}{2} C_l \rho A V^2 \delta. \quad (11)$$

The aerodynamic restoring moment was found in 3.22 (11) to be representable by the force f_M applied unit distance ahead of the center of mass on the axis. That is

$$f_M = -\frac{1}{2} C_m \rho A l V^2 \delta. \quad (12)$$

Unless δ is determined essentially by means of (12) as the yaw of the axis of aerodynamic symmetry, then as pointed out in 2.47 zero moment will not in general correspond to zero yaw. Slight asymmetries in projectile shape or in the fins will result in a situation in which the restoring moment is zero for a yaw, δ_0 , which is different from zero. We call this phenomenon *fin malalignment*, and in such cases the aerodynamic moment is given by

$$f_M = -\frac{1}{2} C_m \rho A l V^2 (\delta - \delta_0). \quad (13)$$

The aerodynamic damping moment is given by 2.48 (1) as

$$M_d = -\frac{1}{2} C_d \rho A l^2 V \omega. \quad (14)$$

If we represent this moment by the force f_a , and the angular velocity ω by $\dot{\phi}$, then, just as in the derivation of (6) from (5), we have

$$f_a = -\frac{1}{2} C_{a\rho} A l^2 V \dot{\phi}. \quad (15)$$

3.24 Equations of Motion—Reduction to Two Dimensions.—In terms of the forces and torques listed in the previous section, the equations of motion take the following forms. If we add together 3.23 (1), (7), and (10) to get the total F_z , 3.22 (1) and (2) become

$$m\dot{V} = m\ddot{Z}_0 = mG_J - mg \sin \theta_0 - \frac{1}{2} C_{D\rho} A V^2. \quad (1)$$

If we add 3.23 (3), (9), and (11) to get the total F_\perp , 3.22 (14) becomes

$$mV\dot{\vartheta} = mG_J\delta + mG_J\beta_M + img \cos \theta_0 + \frac{1}{2} C_{I\rho} A V^2\delta. \quad (2)$$

If we add 3.23 (4), (6), (13), and (15) to get the total f , 3.22 (15) becomes

$$mK^2\ddot{\phi} = -mG_J R_M - K_{JD}\dot{\phi} - \frac{1}{2} C_{m\rho} A l V^2(\delta - \delta_0) - \frac{1}{2} C_{a\rho} A l^2 V \dot{\phi}. \quad (3)$$

In order that the meaning of these equations may be completely clear, let us separate (2) and (3) into real and imaginary parts, thus getting the equations of motion that would have been derived if we had carried through the entire development of the previous section in terms of X and Y components. Thus

$$mV\dot{\vartheta}_X = mG_J\delta_X + mG_J\beta_{MX} + \frac{1}{2} C_{I\rho} A V^2\delta_X, \quad (4)$$

$$mV\dot{\vartheta}_Y = mG_J\delta_Y + mG_J\beta_{MY} + mg \cos \theta_0 + \frac{1}{2} C_{I\rho} A V^2\delta_Y, \quad (5)$$

$$mK^2\ddot{\phi}_X = -mG_J R_{MX} - K_{JD}\dot{\phi}_X - \frac{1}{2} C_{m\rho} A l V^2(\delta_X - \delta_{0X}) - \frac{1}{2} C_{a\rho} A l^2 V \dot{\phi}_X, \quad (6)$$

and

$$mK^2\ddot{\phi}_Y = -mG_J R_{MY} - K_{JD}\dot{\phi}_Y - \frac{1}{2} C_{m\rho} A l V^2(\delta_Y - \delta_{0Y}) - \frac{1}{2} C_{a\rho} A l^2 V \dot{\phi}_Y. \quad (7)$$

The above equations constitute the fundamental equations of motion of the rocket. It is important to note that (1) can be solved for $V \doteq Z_0$ and $Z_0 \doteq d$ independently of the others. More important, however, is the fact that there are no cross-terms in the X and Y equations. That is, equations (4) and (6) in ϑ_X and $\dot{\phi}_X$ depend only on the X -components of the various quantities that enter into the equations; and, similarly, equations (5) and (7) for ϑ_Y and $\dot{\phi}_Y$ depend only on the Y -components of the various quantities that determine the motion. Thus there is complete independence of the two motions; and hence (4) and (6) can be solved independently of (5) and (7). Of course, (1) must first be solved for V in either case. In other words, as a

consequence of the restriction to small angles of deflection, our three-dimensional problem has been reduced to two separate problems, each in two dimensions.

The solution of the equations for φ_x , ϑ_x and δ_x will represent the projection of the actual space motion onto the XZ plane; while the equations for φ_Y , ϑ_Y , and δ_Y represent the projection of the actual motion onto the vertical plane, YZ , passing through the launcher. It will suffice to determine the motion in the vertical plane only, since if g is set equal to zero in the equations for this motion, one gets equations of precisely the same form as the equations of motion in the XZ plane. We can, therefore, concentrate our attention on solving (5) and (7). The subscript Y in each term can now be omitted without danger of confusion,⁴ the equations becoming

$$\ddot{\varphi} + \left(\frac{C_q \rho A l^2 V + 2 K_{JD}}{2 m K^2} \right) \dot{\varphi} + \frac{C_m \rho A l V^2}{2 m K^2} \delta = - \frac{G_J R_M}{K^2} + \frac{C_m \rho A l V^2}{2 m K^2} \delta_0, \quad (8)$$

$$V \dot{\vartheta} - G_J \delta - \frac{C_l \rho A V^2}{2 m} \delta = G_J \beta_M + g \cos \theta_0. \quad (9)$$

In addition, from 3.21 (3),

$$\varphi - \delta - \vartheta = 0. \quad (10)$$

3.25 Reduction of the General Solution to the Linear Combination of a Number of Particular Solutions.—The solution of the above equations is uniquely determined as soon as V is known as a function of t from 3.24 (1) and as soon as the initial conditions are specified. For the complete statement of the initial conditions it is sufficient to specify that at the instant $t=t_p$ at which the final launcher constraint is removed, the values of φ , δ , and $\dot{\varphi}$ are

$$\varphi(t_p) = \varphi_p,$$

$$\delta(t_p) = \delta_p,$$

and

$$\dot{\varphi}(t_p) = \dot{\varphi}_p = q_p. \quad (1)$$

In practice the values of φ_p , δ_p , and q_p are usually determined either from photographic measurements or from a mathematical analysis of the motion during the launching period. Occasionally one of them has been determined by the condition that the theoretically computed deflection agree with the observed deflection. When the values of φ , δ , and $\dot{\varphi}$ are given at any instant, 3.24 (8)–(10) determine the values of ϑ and of all derivatives of $\dot{\varphi}$, δ , and ϑ at this instant and at all later times. We might have taken φ , ϑ , and $\dot{\varphi}$ instead of φ , δ , and $\dot{\varphi}$ to define our initial conditions, but the former choice is usually less convenient.

The solution of 3.24 (8)–(10) subject to the initial conditions (1) is obviously relatively complicated if all of the constants and parameters are given arbitrary values. Much simpler particular solutions can be obtained by making the proper assumptions. If one assumes that $R_M = \beta_M = \delta_0 = 0$, so that the rocket is free of any malalignment, and also that $\varphi_p = \delta_p = q_p = 0$, so that the rocket is perfectly launched, one gets the deflection produced by gravity under ideal circumstances. On the other hand, if one assumes that $g = \beta_M = \delta_0 = 0$, but that $R_M \neq 0$, and furthermore that $\varphi_p = \delta_p = q_p = 0$, one gets the deflection produced by linear thrust malalignment in an otherwise ideal rocket and in the absence of gravity. Or if one obtains the

⁴ Another method of interpreting (8), (9), and (10) is to regard φ , δ , ϑ , δ_0 , R_M , β_M , and g as complex quantities, using bold-faced type, and to let $g = ig$. Thus these equations become (2) and (3) and can be regarded as giving the complete three-dimensional motion.

solution in the case in which $g=R_M=\beta_M=\delta_0=0$ and in which $\varphi_p=\delta_p=0$, but $q_p\neq 0$, one will have the motion of an ideal rocket that is mallaunched in the absence of gravity. Evidently a large number of particular cases could be considered, but since the differential equations are linear, the deflection in complicated cases can frequently be obtained by superposing the deflections in the appropriate simple cases. For example, if we add together the deflections in the three cases considered above, we get the deflection produced when a rocket having linear thrust malalignment is mallaunched in a gravitational field. That is, we get the solution in the case in which $\beta_M=\delta_0=0$ and $\varphi_p=\delta_p=0$ but $g\neq 0$, $R_M\neq 0$, and $q_p\neq 0$.

Two points that must be considered in this connection are the extent to which this superposition principle is valid and the number of independent particular solutions that need be considered before one can build from them every other particular solution. That there are some improper applications is shown by a consideration of what happens if the term $\vartheta_Y mg \sin \theta_0$ is not discarded from 3.23 (8) in the derivation of the equations of motion. It is still possible to compute separately the deflection due to mallaunching when $g=0$ and the deflection due to gravity when $q_p=0$, but the deflection due to mallaunching when gravity is present will not be the sum of these two deflections. This condition arises because in setting $g=0$ in the first of these solutions, we alter one of the homogeneous terms of the equation rather than confine the changes to the inhomogeneous terms, usually collected on the right side, or to the initial conditions. For our present purposes the above two points will be adequately covered by the theorem that we are about to develop. Any cases not specifically covered by this theorem can generally be handled in an analogous manner.

Our attention will be confined to the solution of the system of simultaneous linear differential equations 3.24 (8)–(10) subject to the initial conditions (1). These equations are not homogeneous in φ , ϑ , and δ because of the presence on the right-hand side of terms in R_M , δ_0 , β_M , and g . As is usual, we consider first the case in which these last four quantities are zero so that we have homogeneous equations. Since the discussion following (1) above showed that there were only three independent initial conditions, there are just three independent sets of solutions of the homogeneous equations, any other solution being expressible as a linear function of the three solutions chosen as the basic ones. It will be convenient to designate these basic functions by capital letters having suitable subscripts and to call them *characteristic functions*.

As the first of our basic sets of solutions let us choose the functions φ , δ , and ϑ that satisfy 3.24 (8)–(10) when the right-hand sides are set equal to zero and when the initial conditions⁵ are that $\varphi=1$, $\delta=0$, and $\dot{\varphi}=0$ at $t=t_p$. To distinguish this particular solution from other possible solutions we designate the three functions defined above as $\Delta_\varphi(t_p, t)$, $\Phi_\varphi(t_p, t)$, and $\Theta_\varphi(t_p, t)$. We can summarize the definitions in this paragraph as follows:

The characteristic functions for initial cross-pointing,

$$\left. \begin{array}{l} \Delta_\varphi(t_p, t), \Phi_\varphi(t_p, t), \Theta_\varphi(t_p, t), \\ \varphi_p=1, \delta_p=q_p=R_M=\delta_0=\beta_M=g=0. \end{array} \right\} \quad (2)$$

In precisely the same way we define the two remaining sets of characteristic functions in the homogeneous case.

⁵ It is entirely proper to obtain mathematical solutions of these equations for value of φ_p and δ_p of one radian even though these solutions are not valid in any actual case since the approximations made in deriving the differential equations break down for such large angles. In practice these mathematical solutions are always multiplied by small coefficients, and the resulting angles are small enough so that the derivations are valid.

The characteristic functions for initial yaw,

$$\left. \begin{array}{l} \Delta_\delta(t_p, t), \Phi_\delta(t_p, t), \Theta_\delta(t_p, t), \\ \delta_p = 1, \varphi_p = q_p = R_M = \delta_0 = \beta_M = g = 0. \end{array} \right\} \quad (3)$$

are the solutions subject to

The characteristic functions for mallaunching,

$$\left. \begin{array}{l} \Delta_q(t_p, t), \Phi_q(t_p, t), \Theta_q(t_p, t), \\ q_p = 1, \varphi_p = \delta_p = R_M = \delta_0 = \beta_M = g = 0. \end{array} \right\} \quad (4)$$

are the solutions subject to

The general solution of the homogeneous differential equation is a linear combination of these three particular solutions. The general solution of the inhomogeneous equations is obtained by adding to this linear combination a particular solution of the inhomogeneous equation. In our case we have four inhomogeneous terms, and it is best to consider first the particular solutions when all but one of the inhomogeneous terms are zero. Since we want only particular solutions we shall take the simplest possible initial conditions; $\varphi_p = \delta_p = q_p = 0$. We can summarize the resulting solutions by the statements:

The characteristic functions for gravity

$$\left. \begin{array}{l} \Delta_g(t_p, t), \Phi_g(t_p, t), \Theta_g(t_p, t), \\ g = 1, \varphi_p = \delta_p = q_p = R_M = \delta_0 = \beta_M = 0. \end{array} \right\} \quad (5)$$

are the solutions subject to

The characteristic functions for linear malalignment

$$\left. \begin{array}{l} \Delta_R(t_p, t), \Phi_R(t_p, t), \Theta_R(t_p, t), \\ R_M = 1, \varphi_p = \delta_p = q_p = g = \delta_0 = \beta_M = 0. \end{array} \right\} \quad (6)$$

are the solutions subject to

The characteristic functions for fin malalignment

$$\left. \begin{array}{l} \Delta_F(t_p, t), \Phi_F(t_p, t), \Theta_F(t_p, t), \\ \delta_0 = 1, \varphi_p = \delta_p = q_p = g = R_M = \beta_M = 0. \end{array} \right\} \quad (7)$$

are the solutions subject to

The characteristic functions for angular malalignment

$$\left. \begin{array}{l} \Delta_\beta(t_p, t), \Phi_\beta(t_p, t), \Theta_\beta(t_p, t), \\ \beta_M = 1, \varphi_p = \delta_p = q_p = g = R_M = \delta_0 = 0. \end{array} \right\} \quad (8)$$

are the solutions subject to

It is worth noting that each of these sets of characteristic functions satisfies 3.24 (10) so that

$$\Theta = \Phi - \Delta. \quad (9)$$

In 3.37 we shall find that the four sets of characteristic functions for the inhomogeneous terms can be expressed in terms of integrals involving the characteristic functions for the initial conditions.

Having defined these seven sets of characteristic functions, one for each of the independent initial conditions and one for each inhomogeneous term, we can now express the most general solution of 3.24 (8)–(10) in terms of them. By direct substitution in the differential equations we find that

$$\delta(t) = \varphi_p \Delta_\varphi + \delta_p \Delta_\delta + q_p \Delta_q + g \Delta_g + R_M \Delta_R + \delta_0 \Delta_F + \beta_M \Delta_\beta, \quad (10)$$

$$\varphi(t) = \varphi_p \Phi_\varphi + \delta_p \Phi_\delta + q_p \Phi_q + g \Phi_g + R_M \Phi_R + \delta_0 \Phi_F + \beta_M \Phi_\beta, \quad (11)$$

and

$$\vartheta(t) = \varphi_p \Theta_\varphi + \delta_p \Theta_\delta + q_p \Theta_q + g \Theta_g + R_M \Theta_R + \delta_0 \Theta_F + \beta_M \Theta_\beta, \quad (12)$$

satisfy 3.24 (8)–(10);⁶ and if we let $t=t_p$ we find that they satisfy (1). Thus the general solution of the differential equations has been expressed as a linear combination of seven particular solutions, and we have proved that these particular solutions can be superposed. It must be remembered that this solution is in the vertical plane and that the initial conditions used in (10)–(12) are really the Y components of corresponding vectors. A similar resolution holds in a horizontal plane except that then the gravity term is omitted. A further discussion of this point is given in 3.33.

It should be noted carefully that throughout this entire discussion it has been completely unnecessary to have explicit formulas for any of the characteristic functions. All of our conclusions follow merely from the fact that the characteristic functions satisfy certain linear differential equations and boundary conditions.

3.3 Solutions When the Tangential Acceleration Is Constant

The actual integration of the differential equations 3.24 (8)–(10) as they stand is a hopeless task; for none of the quantities m , K , G_J , R_M , β_M remains strictly constant during the burning period. Similarly, the aerodynamic coefficients will vary with velocity, especially near the velocity of sound. In order to reduce the equations to integrable form it is necessary to assume that these quantities remain constant during burning. (Moreover one's knowledge of the true variation of some of the quantities is usually so meager that the assumption of constancy is as good as any other) This is not true of m or K ; but for rockets in which the propellant mass is a relatively small fraction, say one fifth, of the total mass, the effects of the variation of m or K are negligible compared to the effects of variations of G_J and the malalignments during the burning of a single round and from round to round.

We shall now proceed with the detailed solution of the equations of motion under these conditions, and we shall derive analytic expressions from which numerical values of the orien-

⁶ The reader should note carefully that in 3.3 and 3.4 a slightly different definition of characteristic function is needed because ξ rather than t is used as an independent variable. The only important consequence of this is that (10), (11), and (12) cannot be used with the values of the characteristic functions obtained from the figures and formulas of these later sections; instead, one should use 3.33.

tation angle, the yaw, and the direction of motion can be computed. The solutions involve trigonometric functions, Fresnel integrals, and certain more complicated integrals. By using the formulas of Appendix B, one can obtain power series and asymptotic expansions for the various solutions. All important solutions are also presented in graphical form so that the calculations in practical problems usually consist of multiplications of numbers read from the graphs by the parameters characterizing the rocket under consideration.

3.31 Velocity and Distance Functions.—The equation for the translation of the rocket parallel to the Z_0 -axis is given by 3.24 (1) as

$$\dot{V} = G_J - g \sin \theta_0 - \frac{C_D \rho A V^2}{2m} \quad (1)$$

$$= G_J - g \sin \theta_0 - c V^2, \quad (2)$$

where

$$c \triangleq \frac{C_D \rho A}{2m} \quad (3)$$

is the deceleration coefficient of the rocket, as defined in 2.41 (6).

We now assume that the jet acceleration G_J and the deceleration coefficient c are constant throughout burning. In practice, for most rockets G_J is very nearly constant during the important early stages of burning; while for velocities less than about 800 ft./sec. c is very nearly constant. The deceleration coefficient will of course vary with the mass of the projectile during burning; but, since $c V^2 \ll G_J$ anyway, the over-all effect of any small changes in mass on c , and hence on V , will be inappreciable.

Under these conditions (2) can be solved by separation of variables and direct integration, under the condition that $V=0$ when $t=0$. The result is

$$V = (G/c)^{\frac{1}{2}} \tanh (c G t^2)^{\frac{1}{2}} \quad (4)$$

$$= G t \left(1 - \frac{1}{3} c G t^2 + \frac{2}{15} c^2 G^2 t^4 - \dots \right) \quad (5)$$

$$\doteq G t, \quad (6)$$

where

$$G \equiv G_J - g \sin \theta_0. \quad (7)$$

Now

$$\frac{1}{3} c G t^2 \approx \frac{2}{3} c d,$$

where

$$d \approx \frac{1}{2} G t^2 \text{ is the distance traversed.}^7$$

Since c is of the order of $3 \times 10^{-5} \text{ ft.}^{-1}$ and the burning distance d is of the order of $5 \times 10^3 \text{ ft.}$, we have $\frac{2}{3} c d$ of the order of 10^{-2} at the end of burning. Hence the effect of the drag on the

⁷ Although it would undoubtedly be less confusing to use a different symbol, such as r or s , for path length, in so doing one would conflict seriously with the common notation used in the rest of this report. In any case, little ambiguity will arise between the symbols for distance and that for ordinary differentiation.

velocity is negligibly small, especially during the early part of burning. It will be shown later that it is during the early part of burning, while the rocket transverses about half its yaw oscillation distance, that practically all of the deflection of the trajectory occurs. Hence it is the acceleration of the rocket during this period that should be used in the equations 3.24 (8)–(10) for φ , ϑ , and δ . Thus we write

$$\dot{Z}_0 \doteq V = Gt = (G_J - g \sin \theta_0)t \quad (8)$$

where G_J is the average jet acceleration during the early part of burning.⁸

The distance the rocket travels along its path during burning is given by integration of (4) as

$$d = \frac{1}{c} \log \cosh (cGt^2)^{\frac{1}{2}} \quad (9)$$

$$= \frac{1}{2} Gt^2 \left(1 - \frac{1}{6} cGt^2 + \dots \right) \quad (10)$$

And by the same reasoning as above

$$d \doteq \frac{1}{2} Gt^2. \quad (11)$$

Another point of view is to say that actually G_J is never constant. What we do is to assume that the mathematical solutions, obtained when G_J is regarded as a constant in the equations, are very satisfactory approximations to the actual motions. This is particularly satisfactory in the present case where our main interest lies in obtaining expressions for V to use in the differential equations for ϑ and φ . Now we can just as well assume that it is G that is constant during burning and that consequently (6) and (11) are exact. By this we mean to say that the mathematical solution obtained in this manner is a sufficiently close approximation to the actual motion for our purposes.

3.32 Yaw Oscillation Distance, σ .—We now consider briefly the effect of the aerodynamic forces alone on the motion of the rocket. This will enable us to determine which aerodynamic forces are important, and which are relatively unimportant and hence can be neglected during burning. It will also enable us to introduce the parameter σ which we shall henceforth use to specify the restoring moment. For this purpose, we set $G_J = g = 0$, and treat the motion *after* burning. Under these conditions the equations of motion 3.24 (1), (8), (9), and (10) become

$$\frac{dV}{dt} = -\frac{C_D \rho A}{2m} V^2, \quad (1)$$

$$\ddot{\varphi} + \frac{C_q \rho A l^2}{2mK^2} V \dot{\varphi} + \frac{C_m \rho A l}{2mK^2} V^2 \delta = 0, \quad (2)$$

$$\dot{\vartheta} - \frac{C_l \rho A}{2m} V \delta = 0, \quad (3)$$

and

$$\varphi - \delta - \vartheta = 0. \quad (4)$$

⁸ See ch. 2 for a discussion of the method of determining the effective acceleration and burning time.

We have taken $\delta_0=0$ in (2) in order to simplify the problem slightly. The only effect on the yaw of this change is to add a constant term, proportional to δ_0 .

Now from (4) and (3)

$$\dot{\varphi} = \dot{\delta} + \dot{\vartheta} = \dot{\delta} + \frac{C_l \rho A}{2m} V \delta, \quad (5)$$

and from this and (1)

$$\ddot{\varphi} = \ddot{\delta} + \frac{C_l \rho A}{2m} V \dot{\delta} - \frac{C_l C_D (\rho A)^2}{(2m)^2} V^2 \delta. \quad (6)$$

Substituting for $\dot{\varphi}$ and $\ddot{\varphi}$ in (2), we have

$$\ddot{\delta} + \left[\frac{C_l \rho A}{2m} + \frac{C_q \rho A l^2}{2m K^2} \right] V \dot{\delta} + \left[\frac{C_m \rho A l}{2m K^2} + \frac{C_l C_q \rho^2 A^2 l^2}{4m^2 K^2} - \frac{C_l C_D \rho^2 A^2}{4m^2} \right] V^2 \delta = 0. \quad (7)$$

We now transform to distance, d , as the independent variable, by means of the relations

$$\frac{d\delta}{dt} = \frac{d\delta}{dd} \frac{dd}{dt} = V \frac{d\delta}{dd}$$

or

$$\dot{\delta} = V \delta'$$

and

$$\ddot{\delta} = V^2 \delta'' - \frac{C_D \rho A}{2m} V^2 \delta',$$

where the primes indicate differentiation with respect to distance. Equation (7) then becomes

$$\delta'' + 2\alpha \delta' + \kappa^2 \delta = 0, \quad (8)$$

where

$$2\alpha = \frac{C_l \rho A}{2m} + \frac{C_q \rho A l^2}{2m K^2} - \frac{C_D \rho A}{2m}, \quad (9)$$

and

$$\kappa^2 = \frac{C_m \rho A l}{2m K^2} + \frac{C_l C_q \rho^2 A^2 l^2}{4m^2 K^2} - \frac{C_l C_D \rho^2 A^2}{4m^2}. \quad (10)$$

On the basis of the data given in chapter 2 for the 3.5 AR and the 5.0 HVAR, we shall assume that for a "typical" rocket, about 5 feet long,

$$\begin{aligned} \frac{C_l \rho A}{2m} &\approx 10^{-3} \text{ ft.}^{-1}, \quad \frac{C_q \rho A l^2}{2m K^2} \approx 3 \times 10^{-3} \text{ ft.}^{-1}, \\ \frac{C_D \rho A}{2m} = c &\approx 3 \times 10^{-5} \text{ ft.}^{-1}, \quad \frac{C_m \rho A l}{2m K^2} \approx 6 \times 10^{-4} \text{ ft.}^{-2}; \end{aligned} \quad (11)$$

and, therefore,

$$2\alpha \approx 4 \times 10^{-3} \text{ ft.}^{-1}, \quad \kappa^2 \approx 6 \times 10^{-4} \text{ ft.}^{-2}.$$

Hence (8) is the equation of motion of a free under-damped oscillator, which has the well-known⁹ general solution

$$\delta = Ae^{-\alpha d} \cos \left(\frac{2\pi d}{\sigma} + \epsilon \right), \quad (12)$$

where A and ϵ are arbitrary constants, and the natural wavelength σ is given by

$$\sigma = 2\pi(\kappa^2 - \alpha^2)^{-\frac{1}{2}} \approx 250 \text{ feet.} \quad (13)$$

But, in view of the relations (11),

$$\alpha^2 \ll \kappa^2,$$

and

$$\kappa^2 \approx \frac{C_m \rho Al}{2mK^2}. \quad (14)$$

Thus, to a high degree of approximation the distance traveled by the rocket in one yaw oscillation depends only on the restoring moment: that is,

$$\sigma = \frac{2\pi}{\kappa} = 2\pi \left(\frac{2mK^2}{C_m \rho Al} \right)^{\frac{1}{2}}. \quad (15)$$

The aerodynamic moment can then be expressed in terms of σ as

$$M = -\frac{C_m \rho Al}{2} V^2 (\delta - \delta_0) = -\frac{4\pi^2 m K^2}{\sigma^2} V^2 (\delta - \delta_0), \quad (16)$$

in which we no longer assume that δ_0 is zero.

This relation between the aerodynamic stabilizing moment and the wavelength of yaw oscillation holds exactly only in the absence of lift, drag, and damping. In that case (8) reduces to

$$\delta'' + \frac{C_m \rho Al}{2mK^2} \delta = 0.$$

an equation for simple harmonic oscillation with wavelength

$$\boxed{\sigma = 2\pi \left(\frac{2mK^2}{C_m \rho Al} \right)^{\frac{1}{2}}}.$$

However, since the effect of these forces on σ is extremely small (16) is a very good approximation. Its great importance lies in the fact that σ can be determined photographically while the rocket is in flight, and hence one can get a rapid, indirect measure of the aerodynamic moment.

It is of some interest to compute the ratio of the amplitudes of successive oscillations. It follows immediately from (12) that this ratio is

$$R = \exp(-\alpha\sigma) \approx 0.9 \quad (17)$$

for the particular values assumed in (11). No careful measurements of R have been made, but occasional investigations of the amplitude of the oscillations at the beginning and end

⁹ See Leigh Page, "Introduction to Theoretical Physics," p. 63, New York: D. Van Nostrand, 1928.

of a trajectory indicate that this is of the right order of magnitude and hence that $(C_q \rho A l^2 / 2mK^2)$ either has a value of the order of magnitude of 3×10^{-3} as assumed in (11) or a smaller value. In practice, the problem is complicated considerably by the effect of gravity. It is probable, however, that one of the best methods for determining C_q experimentally is the measurement of σ and R . If C_l and C_D are measured in the wind tunnel (17) and (9) will give C_q .

With the equations at hand it will be useful at this point to determine the effect of the cross-force on the motion of the rocket after burning. (In 3.51 it will be shown that the effect on the trajectory during burning is negligible.) For this purpose we consider the rocket acted on by lift and restoring moment only. Hence the velocity, V , will be constant.

Neglecting the damping due to lift in (12), we have for the yaw due to the restoring moment

$$\delta = \delta_M \cos\left(\frac{2\pi d}{\sigma} + \epsilon\right), \quad (18)$$

where δ_M is written for the amplitude of the oscillation. Substituting (18) into (3) and making use of the fact that

$$\dot{\vartheta} = \frac{d\vartheta}{dd} \frac{dd}{dt} = V \frac{d\vartheta}{dd},$$

we get

$$\frac{d\vartheta}{dd} = \frac{C_l \rho A}{2m} \delta_M \cos\left(\frac{2\pi d}{\sigma} + \epsilon\right). \quad (19)$$

For the deflection of the tangent to the trajectory, we have then

$$\vartheta = \frac{\sigma C_l \rho A}{(2\pi)2m} \delta_M \sin\left(\frac{2\pi d}{\sigma} + \epsilon\right). \quad (20)$$

Now

$$\vartheta = \frac{\dot{r}}{V} = \frac{dr}{dd}, \quad (21)$$

where \dot{r} is the lateral velocity of the rocket. Therefore,

$$\frac{dr}{dd} = \vartheta = \frac{\sigma C_l \rho A}{(2\pi)2m} \delta_M \sin\left(\frac{2\pi d}{\sigma} + \epsilon\right);$$

whence the linear displacement of the trajectory is

$$r = -\frac{\sigma^2 C_l \rho A}{(2\pi)^2 2m} \delta_M \cos\left(\frac{2\pi d}{\sigma} + \epsilon\right). \quad (22)$$

In terms of the moment coefficient, C_m , we have in lieu of (20) and (22)

$$\vartheta = \frac{2\pi K^2 C_l}{\sigma l C_m} \delta_M \sin\left(\frac{2\pi d}{\sigma} + \epsilon\right), \quad (23)$$

and

$$r = -\frac{K^2 C_l}{l C_m} \delta_M \cos\left(\frac{2\pi d}{\sigma} + \epsilon\right). \quad (24)$$

It is clear from the above that the yaw, deflection of the tangent to the trajectory, and

the linear displacement of the trajectory are all sinusoidal functions in distance with a wavelength equal to the yaw oscillation distance σ . Now, by (11) and (13),

$$\frac{K^2 C_l}{l C_m} \approx 1.7 \text{ feet,}$$

and

$$\sigma \approx 250 \text{ feet.}$$

Thus, the maximum values of ϑ and r are

$$\vartheta_{\max} = \frac{2\pi K^2 C_l}{\sigma l C_m} \delta_M = 0.043 \delta_M, \quad (25)$$

and

$$r_{\max} = \frac{K^2 C_l}{l C_m} \delta_M = 1.7 \delta_M \text{ feet} \quad (26)$$

Hence, we see that for a yaw of 1° ($=0.0175$ rad) the maximum deviation of the tangent is only 0.00075 rad or 0.75 mil, while the linear displacement of the trajectory is only about 0.03 feet. The above deflections resulting from the cross-force on the rocket might be considered as an additional source of random dispersion, for the actual values of ϑ and r will depend upon the particular phase of the yaw at the instant burning ceases. It is clear, however, that this is an extremely small effect, since the yaw at the end of burning is usually of the order of 2 or 3 degrees.

The effect of the damping terms, which have been neglected, would be to reduce the above displacements still further. For then the yaw would be damped according to the exponential term in (12). In any case we can conclude that after burning, in the absence of gravity, the trajectory is essentially a straight line.

3.33 Reduction of the Equations to Integrable Form—The Characteristic Functions.—The differential equations for the orientation, direction of motion, and yaw of the rocket were given in 3.24 (8)–(10) in terms of V , the velocity. If we substitute into these equations the expression $V=Gt$ given by 3.31 (8), we get

$$\ddot{\varphi} + \frac{(C_q \rho A l^2 G t + 2K_{JD})}{2mK^2} \dot{\varphi} + \frac{C_m \rho A l G^2 t^2}{2mK^2} \delta = -\frac{G_J R_M}{K^2} + \frac{C_m \rho A l G^2 t^2}{2mK^2} \delta_0, \quad (1)$$

$$t \dot{\vartheta} - \frac{G_J}{G} \delta - \frac{C_l \rho A G t^2}{2m} \delta = \frac{g \cos \theta_0}{G} + \frac{G_J \beta_M}{G}, \quad (2)$$

and

$$\varphi - \delta - \vartheta = 0. \quad (3)$$

Now it would be advantageous to replace G_J by G throughout. This should be possible since the difference between the two is small. Furthermore, in practice R_M and β_M are neither known with great precision nor are they actually constant. Hence it is no worse to assume that those two inhomogeneous terms contain the constant factors GR_M and $G\beta_M$ than to assume that $G_J R_M$ and $G_J \beta_M$ have some particular values.¹⁰ The remaining term containing G_J is the second term of (2). In accordance with 3.31 (7), we find that

¹⁰ If a situation arises in which it is significant to distinguish between G_J and G in the terms containing R_M and β_M , it is only necessary to replace R_M by $R_M G_J/G$ and β_M by $G_J \beta_M/G$ throughout the rest of this chapter.

$$-\frac{G_J}{Gt} \delta - \frac{g \sin \theta_0}{V} \vartheta = -\frac{\delta}{t} - \frac{g \sin \theta_0}{Gt} \varphi. \quad (4)$$

The second term on the left in (4) is the term that we found we could omit in going from 3.23 (8) to 3.23 (9). But if the term $-g \sin \theta_0 \vartheta / V$ can be neglected it is equally proper to neglect

$$-\frac{g}{Gt} \sin \theta_0 \varphi. \quad (5)$$

Hence we can cancel the two G 's in the second term of (2) and can regard (5) as giving the sum of the quantity omitted in 3.23 and the quantity omitted in the cancellation.

We may express the aerodynamic restoring moment in terms of σ , the yaw oscillation distance, by means of the relation, derived in 3.32 (15),

$$\frac{C_m \rho A l}{2} = \frac{4 \pi^2 m K^2}{\sigma^2}.$$

We also change the independent variable from t (or V or d) to the dimensionless parameter ζ , proportional to t , and defined by ¹¹

$$\begin{aligned} \zeta &= t \left(\frac{G}{2\sigma} \right)^{\frac{1}{2}} = \frac{t}{t_\sigma} \\ &= \frac{V}{(2G\sigma)^{\frac{1}{2}}} = \frac{V}{v_\sigma} \\ &= \left(\frac{d}{\sigma} \right)^{\frac{1}{2}}, \end{aligned} \quad (6)$$

where it is convenient to write

$$t_\sigma \equiv \left(\frac{2\sigma}{G} \right)^{\frac{1}{2}}; \quad v_\sigma \equiv (2G\sigma)^{\frac{1}{2}} \quad (7)$$

The quantities t_σ and v_σ may be regarded as a characteristic time and a characteristic velocity, since t_σ is the time required for the rocket to travel the distance σ , starting from rest; and v_σ is the velocity acquired in this time. Denoting differentiation with respect to ζ by primes, we get in lieu of (1), (2) and (3)

$$\varphi'' + \frac{(C_a \rho A l^2 \sigma \zeta + t_\sigma K_{JD})}{m K^2} \varphi' + 16 \pi^2 \zeta^2 \delta = -\frac{2 \sigma R_M}{K^2} + 16 \pi^2 \zeta^2 \delta_0, \quad (8)$$

$$\zeta \vartheta' - \delta - \frac{\sigma C_l \rho A}{m} \zeta^2 \delta = \frac{g \cos \theta_0}{G} + \beta_M, \quad (9)$$

$$\varphi - \delta - \vartheta = 0. \quad (10)$$

These equations can be simplified still further, since during burning we can neglect the terms containing C_a , K_{JD} and C_l . We shall see in 3.5 how to get an approximate expression

¹¹ It will prove convenient, especially when considering the motion of a rocket fired from a moving launcher or in the presence of a wind, to let V represent the velocity of the rocket relative to the air, and to let v represent the velocity relative to the launcher. In firing from a stationary launcher in the absence of wind, as in the present case, $V=v$. The characteristic velocity, $v_\sigma \equiv (2G\sigma)^{\frac{1}{2}}$, is always written as lower case.

for the effects of these terms; but in the meantime the following consideration will justify their omission. To show that the term containing C_i is small, consider the ratio of the third term of (9) to the second term. If the origin of these terms is considered, it is seen that this is equivalent to taking the ratio of the aerodynamic cross force to the component of the jet force normal to the trajectory. The ratio is

$$\frac{\sigma C_i \rho A}{m} \zeta^2 \approx 0.5 \zeta^2, \quad (11)$$

since, according to 3.32 (11) and (13), $\sigma \approx 250$ feet and $C_i \rho A / 2m \approx 10^{-3}$ ft.⁻¹. Thus this ratio is rather small during the early part of burning ($\zeta < 1/2$) when the major features of the motion are determined.

Next let us consider the ratio of the second term of (8) to the third term; that is

$$R = \frac{(C_q \rho A l^2 \sigma \zeta + t_o K_{JD}) \varphi'}{16 \pi^2 m K^2 \zeta^2 \delta} = \frac{C_q \rho A l^2 \sigma \varphi'}{16 \pi^2 m K^2 \zeta \delta} + \frac{K_{JD} t_o \varphi'}{16 \pi^2 m K^2 \zeta^2 \delta}. \quad (12)$$

This is the ratio of the torque due to damping to the torque due to the aerodynamic restoring moment. The first term contains the aerodynamic damping and the second the jet damping. Now φ' and δ tend to be 90° out of phase in their oscillations, so that if we happen to compare these terms at a time when the yaw is zero the ratio will not be small. If we substitute for φ' its maximum value and for δ its maximum, the comparison will be fair. For then if the ratio is small, the maximum torque contributed by the second term of (8) will be small compared to the maximum torque, or the average torque, contributed by the third term. Now inspection of 3.34 (10) and (12) will show that for both mallaunching and initial yaw the ratio of the maximum of φ' to the maximum of δ is $4\pi\zeta$. Hence we assume that this is the correct order of magnitude under all circumstances. If we accept the estimates $C_q \rho A l^2 / 2m K^2 \approx 3 \times 10^{-3}$ ft.⁻¹, and $\sigma = 250$ feet, given by 3.32 (11) and (13); and if we accept the estimate $K_{JD} t_o / m K^2 \approx 0.4$, from 2.26, we get for (12)

$$R = \frac{1}{3\pi} + \frac{1}{10\pi\zeta\zeta_b}, \quad (13)$$

where ζ_b is the value of ζ at the end of burning. Evidently the first term, which gives the relative effect of the aerodynamic damping moment, is always small. The second term will also be small as long as $\zeta > 0.1$, which includes most of the burning period. Even for very small values of ζ where the second term of (13) is large, we cannot conclude that the jet damping torque is large, since the aerodynamic moment, with which we are comparing the jet damping, is very small there. This point could be examined in greater detail, if desired, by comparing the jet damping torque with the torque due to linear malalignment.

When these terms that we have been considering are omitted, our equations of motion become

$$\varphi'' + 16\pi^2 \zeta^2 \delta = -\frac{2\sigma}{K^2} R_M + 16\pi^2 \zeta^2 \delta_0, \quad (14)$$

$$\zeta \vartheta' - \delta = \frac{g}{G} \cos \theta_0 + \beta_M, \quad (15)$$

and

$$\varphi - \vartheta - \delta = 0. \quad (16)$$

In actual firing of rockets it turns out that the above equations predict the motion to within the limits of the observed experimental errors. Hence these may be considered to be the basic equations of this chapter in the sense that it is their solutions that give most of the information of practical importance about the motion of fin-stabilized rockets.

The initial conditions that characterize the position and motion of the rocket at the instant

$$\zeta = \zeta_p = \frac{t_p}{t_\sigma} = \left(\frac{p}{\sigma}\right)^{\frac{1}{2}}, \quad (17)$$

when the constraints of the launcher are removed, are obtained from 3.25 (1), which becomes $\varphi(t_p) = \varphi_p$, $\delta(t_p) = \delta_p$, $\dot{\varphi}(t_p) = \dot{\varphi}_p = q_p$, on making the change of variables (6). This yields for the initial values, subject to which (14), (15), and (16) are to be solved,

$$\varphi(\zeta_p) = \varphi_p, \quad \delta(\zeta_p) = \delta_p, \quad \varphi'(\zeta_p) = t_\sigma q_p = \varphi'_p. \quad (18)$$

It should be noted that φ'_p is defined by (18) and is, of course, not equal to $\dot{\varphi}_p = q_p$.

Now the differential equations (14), (15), and (16) and the initial conditions (18) are of the same general form as the differential equations 3.24 (8), (9), and (10) and the initial conditions 3.25 (1). A few very small terms have been neglected, and we have changed the independent variable. These changes are enough to make it inappropriate to use the characteristic functions defined as functions of t_p and t in 3.25. However, we can proceed to apply to equations (14), (15), (16) and (18) exactly the same reasoning used in 3.25, thus defining the new set of characteristic functions of ζ_p and ζ listed below. Contrary to our practice in 3.25, we now take pains to make all the characteristic functions dimensionless. These new definitions will be used throughout the remainder of this chapter.

As the first of our basic sets of solutions we choose the functions δ , φ , ϑ that satisfy (14), (15) and (16) when the righthand sides are set equal to zero, and when the initial conditions are that $\varphi_p = 1$, $\delta_p = 0$, $\varphi'_p = 0$. We denote this particular set of functions by means of the symbols $\Delta_\varphi(\zeta_p, \zeta)$, $\Phi_\varphi(\zeta_p, \zeta)$, and $\Theta_\varphi(\zeta_p, \zeta)$. We can summarize this definition and the definitions of the remaining characteristic functions by means of the following statements.

The characteristic functions for initial cross-pointing,

$$\left. \begin{array}{l} \Delta_\varphi(\zeta_p, \zeta), \quad \Phi_\varphi(\zeta_p, \zeta), \quad \Theta_\varphi(\zeta_p, \zeta), \\ \varphi_p = 1, \quad \delta_p = \varphi'_p = R_M = \delta_0 = g = \beta_M = 0. \end{array} \right\} \quad (19)$$

The characteristic functions for initial yaw,

$$\left. \begin{array}{l} \Delta_\delta(\zeta_p, \zeta), \quad \Phi_\delta(\zeta_p, \zeta), \quad \Theta_\delta(\zeta_p, \zeta), \\ \delta_p = 1, \quad \varphi_p = \varphi'_p = R_M = \delta_0 = g = \beta_M = 0. \end{array} \right\} \quad (20)$$

The characteristic functions for mallaunching,

$$\left. \begin{array}{l} \Delta_q(\xi_p, \xi), \Phi_q(\xi_p, \xi), \Theta_q(\xi_p, \xi), \\ \text{are the solutions subject to} \\ \varphi'_p = q_p t_\sigma = 1, \varphi_p = \delta_p = R_M = \delta_0 = g = \beta_M = 0. \end{array} \right\} \quad (21)$$

The characteristic functions for gravity,

$$\left. \begin{array}{l} \Delta_g(\xi_p, \xi), \Phi_g(\xi_p, \xi), \Theta_g(\xi_p, \xi), \\ \text{are the solutions subject to} \\ \frac{g \cos \theta_0}{G} = 1, \varphi_p = \delta_p = \varphi'_p = R_M = \delta_0 = \beta_M = 0. \end{array} \right\} \quad (22)$$

The characteristic functions for linear malalignment,

$$\left. \begin{array}{l} \Delta_R(\xi_p, \xi), \Phi_R(\xi_p, \xi), \Theta_R(\xi_p, \xi), \\ \text{are the solutions subject to} \\ -2 \frac{\sigma}{K^2} R_M = 1, \varphi_p = \delta_p = \varphi'_p = \delta_0 = g = \beta_M = 0. \end{array} \right\} \quad (23)$$

The characteristic functions for fin malalignment,

$$\left. \begin{array}{l} \Delta_F(\xi_p, \xi), \Phi_F(\xi_p, \xi), \Theta_F(\xi_p, \xi), \\ \text{are the solutions subject to} \\ \delta_0 = 1, \varphi_p = \delta_p = \varphi'_p = R_M = g = \beta_M = 0. \end{array} \right\} \quad (24)$$

The characteristic functions for angular malalignment,

$$\left. \begin{array}{l} \Delta_\beta(\xi_p, \xi), \Phi_\beta(\xi_p, \xi), \Theta_\beta(\xi_p, \xi), \\ \text{are the solutions subject to} \\ \beta_M = 1, \varphi_p = \delta_p = \varphi'_p = R_M = \delta_0 = g = 0. \end{array} \right\} \quad (25)$$

We note that the first three sets of characteristic functions arise from the boundary conditions and that the last four come from the four inhomogeneous terms in the differential equations. In 3.37 we shall find that the last four sets of functions can be expressed in terms of integrals involving the characteristic functions of (20) and (21). The relation

$$\Theta = \Phi - \Delta \quad (26)$$

is satisfied by each of the seven sets, thus making it unnecessary to solve separately for the Θ functions.

We can now express the general solutions of (14), (15), and (16) in terms of these characteristic functions as

$$\delta(\xi) = \varphi_p \Delta_\varphi + \delta_p \Delta_\delta + q_p t_\sigma \Delta_q + \frac{g \cos \theta_0}{G} \Delta_g - 2 \frac{\sigma}{K^2} R_M \Delta_R + \delta_0 \Delta_F + \beta_M \Delta_\beta, \quad (27)$$

$$\varphi(\zeta) = \varphi_p \Phi_\varphi + \delta_p \Phi_\delta + q_p t_\sigma \Phi_q + \frac{g \cos \theta_0}{G} \Phi_g - 2 \frac{\sigma}{K^2} R_M \Phi_R + \delta_0 \Phi_F + \beta_M \Phi_\beta, \quad (28)$$

$$\vartheta(\zeta) = \varphi_p \Theta_\varphi + \delta_p \Theta_\delta + q_p t_\sigma \Theta_q + \frac{g \cos \theta_0}{G} \Theta_g - 2 \frac{\sigma}{K^2} R_M \Theta_R + \delta_0 \Theta_F + \beta_M \Theta_\beta. \quad (29)$$

It will be recalled (see 3.24) that the equations with which we are dealing are really those representing the component of the motion in the vertical plane through the launcher, the subscript Y having been omitted from the various quantities. Hence δ , φ , and ϑ above represent merely the vertical deflections due to the components of initial yaw, orientation, angular velocity, etc., in this vertical plane. At the same time reference to 3.24 (2)–(7) reminds us that the equations for the motion in the lateral plane through the launcher are completely symmetrical with those for the motion in the vertical plane, with the term in gravity missing. In view of this, the solutions of the equations for the *lateral* motion must be identical with those written above, with the single exception that φ_p , δ_p , q_p , R_M , δ_0 , and β_M represent the components of initial orientation, yaw, angular velocity, and the various malalignments in the lateral direction. The *characteristic functions* Δ , Φ , and Θ remain *unaltered*. We conclude then that if the quantities φ_p , δ_p , q_p , g , R_M , δ_0 and β_M be regarded as complex quantities (as in 3.24), then the equations (27), (28) and (29) give the complete three-dimensional motion of the rocket.

A simpler way of writing the above equations and one which shows the linearity of the various effects is

$$\delta = \delta_\varphi + \delta_\delta + \delta_q + \delta_g + \delta_R + \delta_F + \delta_\beta, \quad (30)$$

$$\varphi = \varphi_\varphi + \varphi_\delta + \varphi_q + \varphi_g + \varphi_R + \varphi_F + \varphi_\beta, \quad (31)$$

and

$$\vartheta = \vartheta_\varphi + \vartheta_\delta + \vartheta_q + \vartheta_g + \vartheta_R + \vartheta_F + \vartheta_\beta, \quad (32)$$

where

$$\delta_\varphi = \varphi_p \Delta_\varphi, \delta_\delta = \delta_p \Delta_\delta, \delta_q = q_p t_\sigma \Delta_q, \quad (33)$$

$$\delta_g = i \frac{g \cos \theta_0}{G} \Delta_g, \delta_R = -\frac{2\sigma}{K^2} R_M \Delta_R, \delta_F = \delta_0 \Delta_F, \delta_\beta = \beta_M \Delta_\beta.$$

with corresponding expressions for the φ 's and ϑ 's.

3.34 Solutions of the Homogeneous Equations.—Let us now consider the homogeneous differential equations that result when we take $R_M = \delta_0 = g = \beta_M = 0$ in 3.33 (14)–(16). The solution of these equations will give us the three sets of characteristic functions defined by 3.33 (19)–(21).

The equations we wish to solve are

$$\varphi'' + 16\pi^2 \zeta^2 \delta = 0, \quad (1)$$

$$\zeta \vartheta' - \delta = 0, \quad (2)$$

and

$$\varphi - \vartheta - \delta = 0. \quad (3)$$

Eliminating φ from (1) by means of (3) and the ϑ'' that this process introduces by means of (2), we get an equation in δ alone, namely

$$\delta'' + \frac{1}{\zeta} \delta' + \left(16\pi^2 \zeta^2 - \frac{1}{\zeta^2}\right) \delta = 0. \quad (4)$$

This equation can be simplified by introducing a new variable, w , defined by

$$\delta = \frac{w}{\zeta}. \quad (5)$$

In place of (4) we then get the equation

$$\frac{d^2 w}{d\zeta^2} - \frac{1}{\zeta} \frac{dw}{d\zeta} + 16\pi^2 \zeta^2 w = 0. \quad (6)$$

Now transforming to distance as the independent variable by the relation [3.33 (6)]

$$d = \sigma \zeta^2, \quad (7)$$

we have

$$\frac{d^2 w}{dd^2} + \frac{4\pi^2}{\sigma^2} w = 0. \quad (8)$$

But (8) is the well-known equation for simple harmonic motion in d with wavelength σ , whose general solution is

$$\begin{aligned} w &= A_1 \cos\left(\frac{2\pi d}{\sigma}\right) + A_2 \sin\left(\frac{2\pi d}{\sigma}\right) \\ &= A_1 \cos 2\pi \zeta^2 + A_2 \sin 2\pi \zeta^2. \end{aligned} \quad (9)$$

Thus we note that the statement that σ is the yaw oscillation distance has meaning *during* as well as after burning. The general solution of (4) is therefore

$$\delta = \frac{w}{\zeta} = \frac{1}{\zeta} (A_1 \cos 2\pi \zeta^2 + A_2 \sin 2\pi \zeta^2), \quad (10)$$

where A_1 and A_2 are arbitrary constants.

To solve for φ , we find from (2), (3) and (5) that

$$\varphi' = \vartheta' + \delta' = \frac{\delta}{\zeta} + \delta' = \frac{1}{\zeta} \frac{d(\zeta \delta)}{d\zeta} = \frac{1}{\zeta} w'. \quad (11)$$

Hence, from (10)

$$\varphi' = -4\pi A_1 \sin 2\pi \zeta^2 + 4\pi A_2 \cos 2\pi \zeta^2, \quad (12)$$

and

$$\begin{aligned} \varphi &= 4\pi \int (-A_1 \sin 2\pi \zeta^2 + A_2 \cos 2\pi \zeta^2) d\zeta \\ &= -2\pi A_1 S(2\zeta) + 2\pi A_2 C(2\zeta) + A_3, \end{aligned} \quad (13)$$

where C and S are the ordinary Fresnel integrals ¹² defined by

$$\frac{1}{2} C(2u) = \int_0^u \cos 2\pi r^2 dr, \quad (14)$$

and

¹² See appendix B for a further discussion of these functions, and appendix C for a table of their values.

$$\frac{1}{2}S(2u) = \int_0^u \sin 2\pi r^2 dr. \quad (15)$$

To complete our solution, we get ϑ from (3); that is

$$\vartheta = \varphi - \delta. \quad (16)$$

The next step is to determine the values that must be given the arbitrary constants A_1 , A_2 , and A_3 in order to satisfy the initial conditions. Now the initial conditions that give us the characteristic functions for cross-pointing are listed in 3.33 (19) as $\varphi=1$, $\delta=\varphi'=0$, when $\zeta=\zeta_p$. Substituting in (10), (12), and (13) we find that $A_1=A_2=0$, and $A_3=1$. Therefore

$$\Delta_\varphi(\zeta_p, \zeta) = 0, \Phi_\varphi(\zeta_p, \zeta) = 1, \text{ and } \Theta_\varphi(\zeta_p, \zeta) = 1. \quad (17)$$

The characteristic functions for initial yaw are obtained, according to 3.33 (20), by finding the values of A_1 , A_2 , and A_3 required to make $\delta=1$, $\varphi=\varphi'=0$ at $\zeta=\zeta_p$. These values are

$$A_1 = \zeta_p \cos 2\pi \zeta_p^2,$$

$$A_2 = \zeta_p \sin 2\pi \zeta_p^2,$$

and

$$A_3 = 2\pi \zeta_p [S(2\zeta_p) \cos 2\pi \zeta_p^2 - C(2\zeta_p) \sin 2\pi \zeta_p^2].$$

Hence,

$$\Delta_\delta(\zeta_p, \zeta) = \frac{\zeta_p}{\zeta} \cos 2\pi(\zeta^2 - \zeta_p^2), \quad (18)$$

$$\begin{aligned} \Phi_\delta(\zeta_p, \zeta) = 2\pi \zeta_p \{ [C(2\zeta) - C(2\zeta_p)] \sin 2\pi \zeta_p^2 \\ - [S(2\zeta) - S(2\zeta_p)] \cos 2\pi \zeta_p^2 \}, \end{aligned} \quad (19)$$

and

$$\begin{aligned} \Theta_\delta(\zeta_p, \zeta) = \Phi_\delta - \Delta_\delta = 2\pi \zeta_p \{ [C(2\zeta) - C(2\zeta_p) - (2\pi\zeta)^{-1} \sin 2\pi \zeta^2] \sin 2\pi \zeta_p^2 \\ - [S(2\zeta) - S(2\zeta_p) + (2\pi\zeta)^{-1} \cos 2\pi \zeta^2] \cos 2\pi \zeta_p^2 \}. \end{aligned} \quad (20)$$

In a similar manner we find that the characteristic functions for initial mallaunching, as obtained from condition 3.33 (21) that $\varphi'=1$, $\varphi=\delta=0$ when $\zeta=\zeta_p$, are

$$\Delta_q(\zeta_p, \zeta) = (4\pi\zeta)^{-1} \sin 2\pi(\zeta^2 - \zeta_p^2), \quad (21)$$

$$\begin{aligned} \Phi_q(\zeta_p, \zeta) = \frac{1}{2} \{ [C(2\zeta) - C(2\zeta_p)] \cos 2\pi \zeta_p^2 \\ + [S(2\zeta) - S(2\zeta_p)] \sin 2\pi \zeta_p^2 \}, \end{aligned} \quad (22)$$

and

$$\begin{aligned} \Theta_q(\zeta_p, \zeta) = \Phi_q - \Delta_q = \frac{1}{2} \{ [C(2\zeta) - C(2\zeta_p) - (2\pi\zeta)^{-1} \sin 2\pi \zeta^2] \cos 2\pi \zeta_p^2 \\ + [S(2\zeta) - S(2\zeta_p) + (2\pi\zeta)^{-1} \cos 2\pi \zeta^2] \sin 2\pi \zeta_p^2 \}. \end{aligned} \quad (23)$$

If we wish to obtain the general solution of the homogeneous equations in terms of arbitrary initial values for φ_p , δ_p , and $q_p = \varphi'_p/t_\alpha$, we find from 3.33 (27)–(29) that they are

$$\delta = \delta_p \Delta_\delta(\zeta_p, \zeta) + q_p t_\sigma \Delta_q(\zeta_p, \zeta), \quad (24)$$

$$\varphi = \varphi_p + \delta_p \Phi_\delta(\zeta_p, \zeta) + q_p t_\sigma \Phi_q(\zeta_p, \zeta), \quad (25)$$

and

$$\vartheta = \varphi_p + \delta_p \Theta_\delta(\zeta_p, \zeta) + q_p t_\sigma \Theta_q(\zeta_p, \zeta), \quad (26)$$

where we have simplified by substitution from (17).

Following the argument preceding 3.33 (30), the coefficients of the characteristic functions in the above expressions may be regarded as complex quantities, so that the equations in reality represent the complete three-dimensional motion of the rocket.

3.35 Effect of Initial Yaw.—In the above section it was shown that the contributions of initial yaw to the yaw and orientation of the rocket and to the deflection of the tangent to the trajectory at all times during burning are

$$\delta_\delta = \delta_p \Delta_\delta(\zeta_p, \zeta), \quad (1)$$

$$\varphi_\delta = \delta_p \Phi_\delta(\zeta_p, \zeta), \quad (2)$$

and

$$\vartheta_\delta = \delta_p \Theta_\delta(\zeta_p, \zeta), \quad (3)$$

where δ_p is the complex yaw at the instant $\zeta = \zeta_p$; while the characteristic functions are given by 3.34 (18), (19), and (20). Since the characteristic functions are *real* quantities, it follows from (1)–(3) that the motion of the rocket will take place in the plane determined by δ_p . Thus if δ_p is real, the motion due to this cause will take place in the lateral plane, while if δ_p is pure imaginary the motion will be in the vertical plane.

From the expression for Δ_δ , 3.34 (18), namely,

$$\Delta_\delta(\zeta_p, \zeta) = (\zeta_p / \zeta) \cos 2\pi(\zeta^2 - \zeta_p^2),$$

we observe that the yaw is a simple periodic function in distance ($d = \sigma \zeta^2$) with wave length σ , with the amplitude of oscillation decreasing as $1/\zeta$ or $1/d^{1/2}$. The quantity of greatest interest, however, is the deflection of the tangent to the trajectory ϑ_δ , for this gives us the direction of motion at the end of burning. To see how this varies during the burning period, we have plotted ¹³ in figures 3.35a and b the characteristic function $\Theta_\delta(\zeta_p, \zeta)$ as a function of $(2)^{1/2} \zeta$ for various values of $(2)^{1/2} \zeta_p$. It might appear paradoxical at first that $\Theta_\delta(\zeta_p, \zeta)$ is negative; that is, an initial positive yaw will result in a *negative* deflection. On further thought, however, one realizes that this must be so; for the only way in which the initial yaw can be positive while the orientation φ_p and angular velocity q_p are both zero is for the rocket to be launched with a lateral motion in the negative direction. Mathematically the situation is described by the fact that when $\varphi_p = 0$, $\delta_p = 1$, then $\vartheta_p = \varphi_p - \delta_p = -1$, and ϑ is initially negative. Since the action of the air stream on the fins will turn the rocket into the direction of motion, the net effect will be a negative deflection of the trajectory. To launch a rocket in this way one can either give it an impulsive lateral blow at the center of mass at the instant of launching or can have the launcher moving laterally. A similar situation occurs when the rocket is

¹³ An apology is due the reader for the obvious lack of consistency in the manner in which the graphs of the various characteristic functions will be plotted. The reason for this is that the computations were made at widely separated intervals over a period of 3½ years, and it was often convenient for the immediate purpose to plot the various quantities as functions of $V/(\sigma G)^{1/2} = (2)^{1/2} \zeta$, or $d/\sigma = \zeta^2$, etc. The effort required to recompute the functions seems excessive merely for the sake of consistency, since one can easily use the following graphs, if one allows for the odd constants that enter.

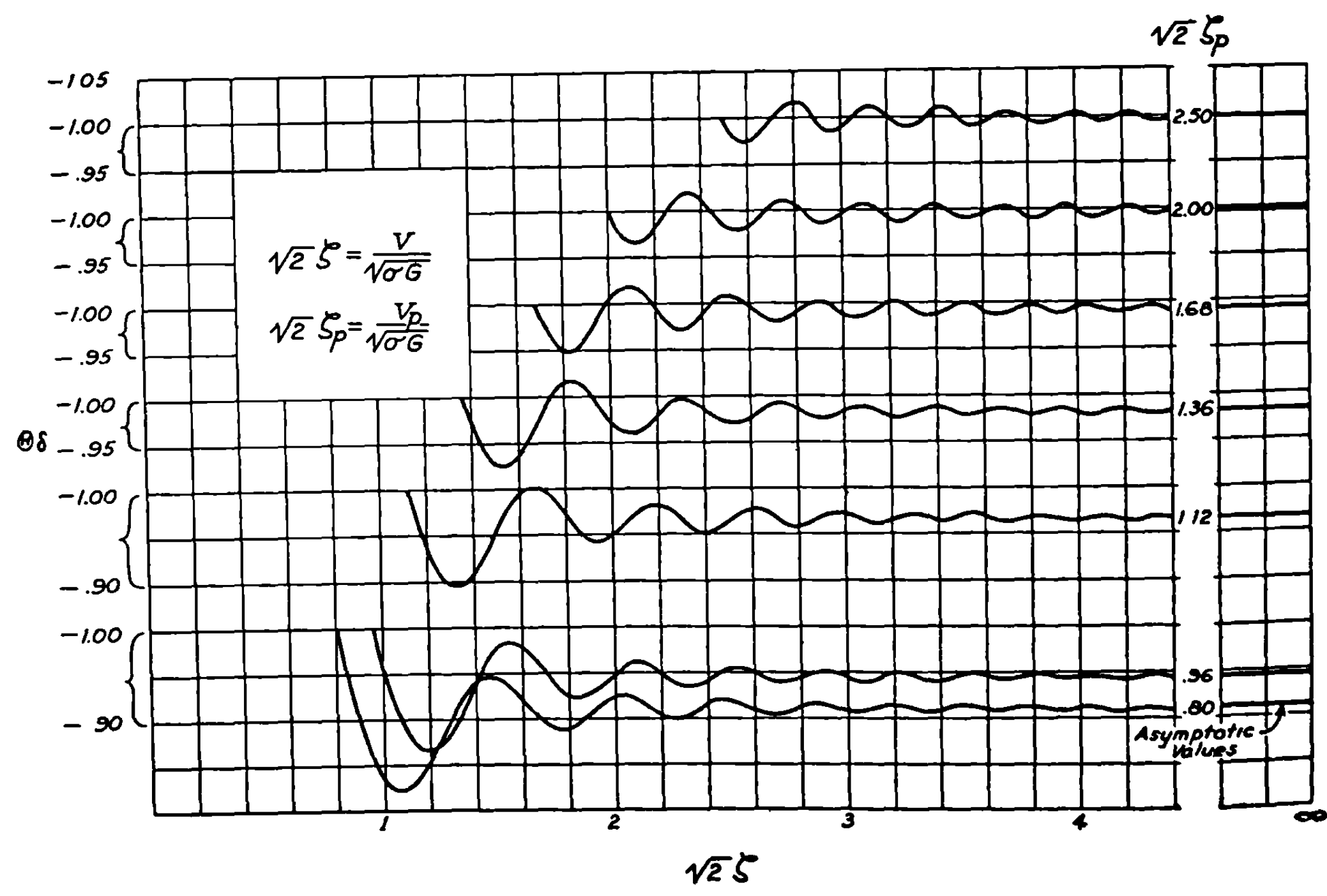
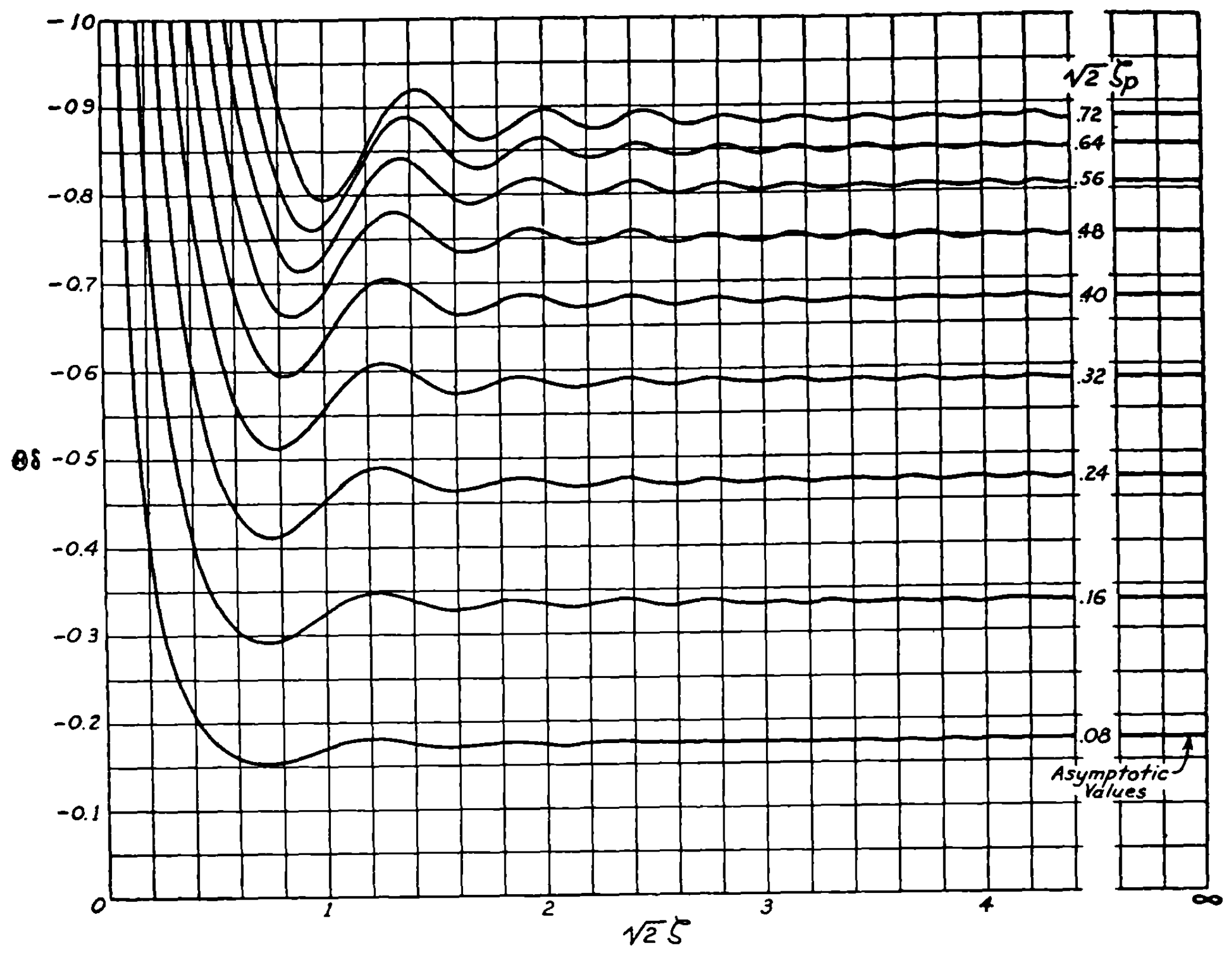


FIGURE 3.35a, b.—Characteristic function $\Theta(\zeta_p, \zeta)$.

launched in the presence of a cross-wind. (See 3.43.) In such a case the rocket has initial yaw, relative to a coordinate system at rest with respect to the air mass, while the initial orientation and angular velocity are both zero.

It may be seen from the figure that $\Theta_s(\zeta_p, \zeta)$ attains its maximum value¹⁴ within half a yaw oscillation $[(2)^{\frac{1}{2}}\zeta = (2d/\sigma)^{\frac{1}{2}} = 1]$ and thereafter oscillates with decreasing amplitude about a value very nearly equal to its asymptotic value. These limiting values are plotted to the right of the figure and were obtained by taking the limit of $\Theta_s(\zeta_p, \zeta)$ as $\zeta \rightarrow \infty$. The asymptotic expression for $\Theta_s(\zeta_p, \zeta)$, valid for burning distances greater than or equal to the yaw oscillation distance ($d \geq \sigma$), is given by¹⁵

$$\Theta_s(\zeta_p, \zeta) \sim 2\pi\zeta_p \left\{ \left[\frac{1}{2} - C(2\zeta_p) \right] \sin 2\pi\zeta_p^2 - \left[\frac{1}{2} - S(2\zeta_p) \right] \cos 2\pi\zeta_p^2 \right. \\ \left. + \sin 2\pi(\zeta^2 - \zeta_p^2) \sum_{n=0}^{\infty} \frac{(-1)^n(4n+1)!}{(2n)!2^{6n+3}\pi^{2n+2}\zeta^{4n+3}} + \cos 2\pi(\zeta^2 - \zeta_p^2) \sum_{n=1}^{\infty} \frac{(-1)^n(4n-1)!}{(2n-1)!2^{6n}\pi^{2n+1}\zeta^{4n+1}} \right\}, \quad (4)$$

the first term of which is the limit value plotted in figures 3.35a and b. For convenience mainly in computational work of related characteristic functions (see 3.37) the quantities Θ_s and Φ_s are tabulated in appendix C for the most useful range of values of ζ_p and ζ .

An initial yaw will also result in a linear deflection of the rocket from the Z_0 -axis (the launcher line, see fig. 3.21a). Let the complex linear deflection be

$$\mathbf{r}_s = X_{0s} + iY_{0s}. \quad (5)$$

Then from 3.22 (3), 3.31 (8), and (3) above,

$$\dot{\mathbf{r}}_s = \dot{X}_{0s} + i\dot{Y}_{0s} = \dot{Z}_0(\vartheta_{Xs} + i\vartheta_{Ys}) = Gt\vartheta_s, \quad (6)$$

and

$$\mathbf{r}_s = G \int_{t_p}^t t\vartheta_s dt = 2\sigma \int_{\zeta_p}^{\zeta} \zeta\vartheta_s d\zeta \\ = 2\sigma\delta_p \int_{\zeta_p}^{\zeta} \zeta\Theta_s(\zeta_p, \zeta) d\zeta. \quad (7)$$

This can be written as

$$\mathbf{r}_s = \sigma\delta_p R_s(\zeta_p, \zeta), \quad (8)$$

where the characteristic function R_s is gotten by substituting from 3.34 (20) and carrying out the integration with the aid of the expressions in appendix B. Thus

$$R_s(\zeta_p, \zeta) = 2 \int_{\zeta_p}^{\zeta} \zeta\Theta_s(\zeta_p, \zeta) d\zeta, \\ = \zeta_p \left\{ \zeta_p - \zeta \cos 2\pi(\zeta^2 - \zeta_p^2) \right. \\ \left. + [C(2\zeta) - C(2\zeta_p)] [2\pi\zeta^2 \sin 2\pi\zeta_p^2 - \frac{1}{2} \cos 2\pi\zeta_p^2] \right. \\ \left. - [S(2\zeta) - S(2\zeta_p)] [2\pi\zeta^2 \cos 2\pi\zeta_p^2 + \frac{1}{2} \sin 2\pi\zeta_p^2] \right\}. \quad (9)$$

¹⁴ That is, the curves drop to their lowest point. This is the maximum since the scale at the left has $-\infty$ at the top and $+\infty$ at the bottom.

¹⁵ This expression is obtained from 3.34 (20) by making use of asymptotic representations of the various functions which are given in the mathematical appendix along with other properties of the functions.

In terms of the characteristic functions defined in 3.34 and which are also tabulated in appendix C, we have in lieu of (9)

$$R_s = \zeta^2 \Theta_s - \zeta_p \Phi_s + \zeta_p^2. \quad (10)$$

In practice, when it is necessary to compute a series of values of R_s or the other characteristic functions for linear deflection it is simpler to do so by numerical integration of $\zeta \Theta_s$ or with the aid of (10) than by the use of the complicated expression (9). In most practical cases, however, r_s is of little importance as compared to ϑ_s , since the displacement produced by r_s at a point down range from the end of burning is just the value of r_s at the end of burning; and this is very small compared with the deflection produced by ϑ_s , this deflection being the value of ϑ_s at the end of burning multiplied by the distance traveled beyond the end of burning. The same is true for all causes of deflection. Therefore, in general, the total lateral linear displacement of the rocket from the launcher line is

$$r = r_b + (d - d_b) \vartheta_b. \quad (11)$$

For example, for a "typical" rocket with $G = 1,000$ ft./sec.², $\sigma = 250$ feet, $V = 1,000$ ft./sec., and $p = 5$ feet $= 0.02\sigma$, so that $V_p = 100$ ft./sec. and $d_b = 500$ feet $= 2\sigma$, (9) or (10) tells us that at the end of burning $r_s/\delta_p = -203$ feet, while from (4) we have that $\vartheta_s/\delta_p = -0.410$. Thus even for initial yaws up to 0.017 rad $= 1^\circ$, r_s is of the order of only 3.5 feet, while ϑ_s is 0.0070 radians. Thus 3,000 feet down range from the end of burning, the linear deflection will be $3.5 + 3,000 \times 0.0070 = 24.5$ feet. The quantity r_s is important, however, when one wants to know the deflection during burning.

3.36 Effect of Mallaunching or Initial Angular Velocity.—We have defined mallaunching to be the angular velocity about a transverse axis possessed by the rocket when $\zeta = \zeta_p$. When, as is usual, this is the value at the instant the constraint of the launcher is removed, the terminology is appropriate since such an angular velocity results from the influence of the launcher on the rocket. We shall also use the same terminology on the rare occasions when it is desirable to take ζ_p at a later time.

It was shown in 3.34 that the contributions of initial angular velocity to the yaw and orientation of the rocket and to the deflection of the tangent to the trajectory during burning are

$$\delta_a = q_p t_\sigma \Delta_a(\zeta_p, \zeta), \quad (1)$$

$$\varphi_a = q_p t_\sigma \Phi_a(\zeta_p, \zeta), \quad (2)$$

and

$$\vartheta_a = q_p t_\sigma \Theta_a(\zeta_p, \zeta), \quad (3)$$

where q_p represents the complex angular velocity at the instant $\zeta = \zeta_p$, t_σ is the characteristic time $(2\sigma/G)^{1/2}$; while the characteristic functions are given by 3.34 (21), (22), and (23).

As was the case in the previous section, it follows from (1)–(3) that the motion of the rocket will take place in the plane determined by q_p , since the characteristic functions are *real* quantities. Thus if q_p is real the motion due to this cause will be entirely in the lateral plane; while if q_p is pure imaginary the motion will take place in the vertical plane.

From 3.34 (21) it is apparent that the yaw is a simple periodic function in distance ($d = \sigma \zeta^2$) with wavelength σ , with the amplitude of oscillation decreasing as $1/\zeta$ or $d^{-1/2}$. Our attention is centered, however, on ϑ_q ; for the tangent to the trajectory at the end of burning gives the direction of motion of the rocket after burning. To see how ϑ_q varies during burning, we have plotted in figures 3.36 a and b the characteristic function $\Theta_q(\zeta_p, \zeta)$ as a function of $2^{1/2}\zeta$ for various values of $2^{1/2}\zeta_p$; i. e., various launcher lengths. It may be seen therefrom that $\Theta_q(\zeta_p, \zeta)$, like Θ_s , attains its maximum value within half a yaw oscillation distance [$2^{1/2}\zeta = (2d/\sigma)^{1/2} = 1$] and thereafter oscillates with decreasing amplitude about a value very nearly equal to its asymptotic value. These limiting values are plotted to the right of the figure and were obtained by taking the limit of $\Theta_q(\zeta_p, \zeta)$ as $\zeta \rightarrow \infty$. The asymptotic expression for $\Theta_q(\zeta_p, \zeta)$, valid for burning distances greater than or equal to σ , is, from 3.34 (23) and the asymptotic formulas given in Appendix B.

$$\begin{aligned} \Theta_q(\zeta_p, \zeta) \sim & \frac{1}{2} \left\{ \left[\frac{1}{2} - C(2\zeta_p) \right] \cos 2\pi \zeta_p^2 + \left[\frac{1}{2} - S(2\zeta_p) \right] \sin 2\pi \zeta_p^2 \right. \\ & - \cos 2\pi(\zeta^2 - \zeta_p^2) \sum_{n=0}^{\infty} \frac{(-1)^n (4n+1)!}{(2n)! 2^{6n+3} \pi^{2n+2} \zeta^{4n+3}} \\ & \left. + \sin 2\pi(\zeta^2 - \zeta_p^2) \sum_{n=1}^{\infty} \frac{(-1)^n (4n-1)!}{(2n-1)! 2^{6n} \pi^{2n+1} \zeta^{4n+1}} \right\}. \end{aligned} \quad (4)$$

The first term of this is the limiting value plotted in figures 3.36a and b. Mainly for convenience in computing related characteristic functions (cf. 3.37) the quantities Θ_q and Φ_q are tabulated in Appendix C for the most useful range of values of ζ_p and ζ .

There is also a contribution to the linear deflection of the rocket from the Z_0 -axis (the launcher line), which, by analogy with 3.35 (5)–(8) is given by

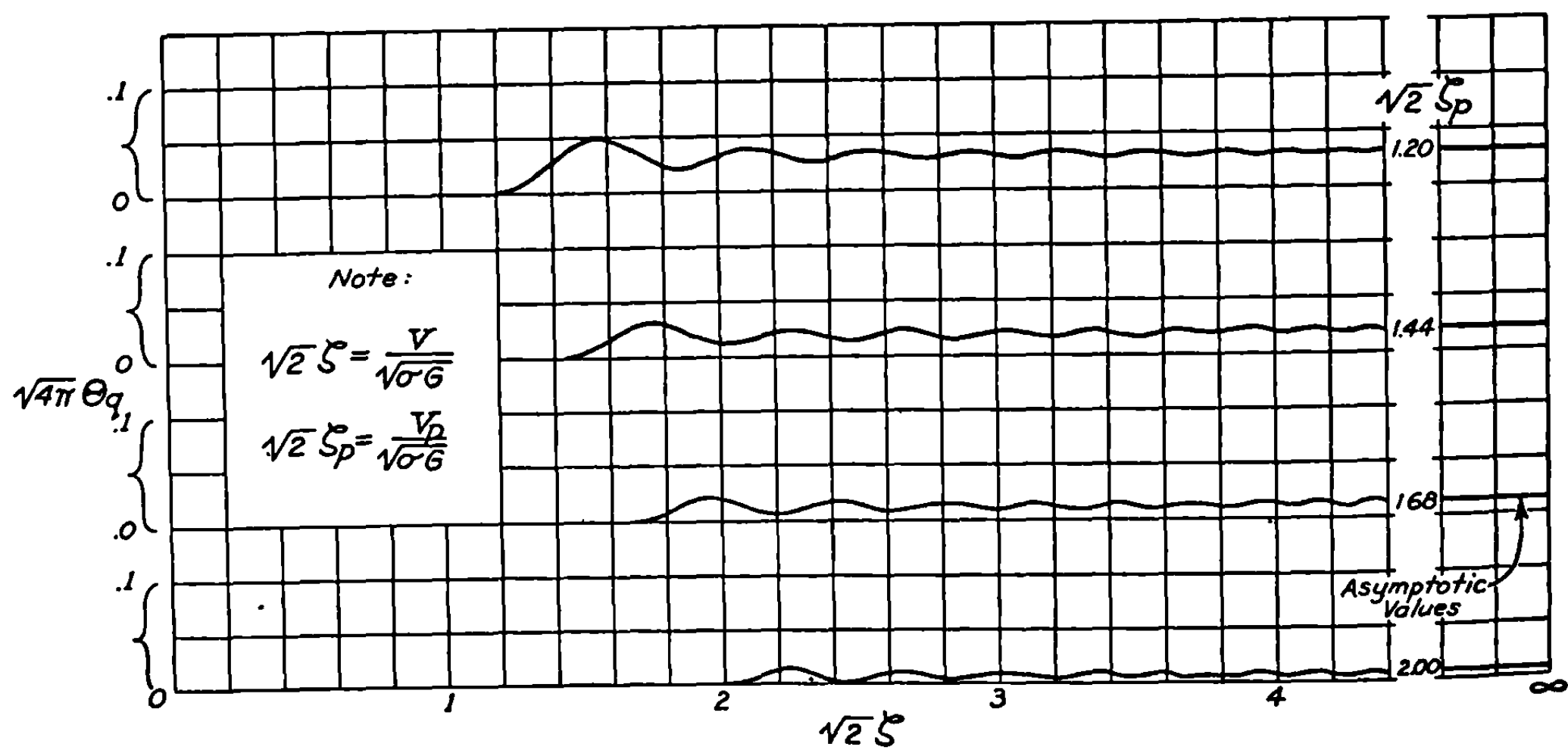
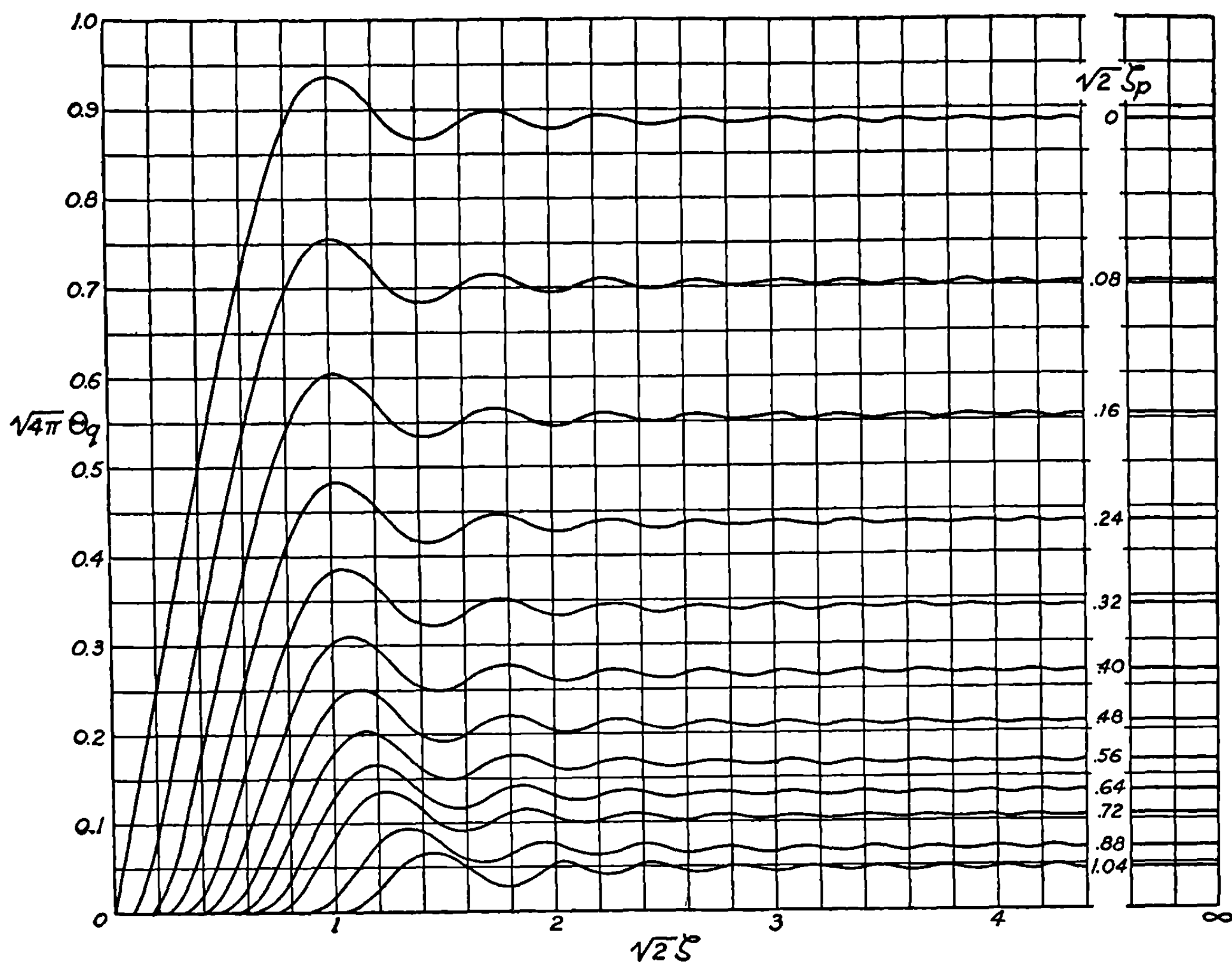
$$\begin{aligned} r_q &= 2\sigma \int_{\zeta_p}^{\zeta} \zeta \vartheta_q d\zeta = 2\sigma t_\sigma q_p \int_{\zeta_p}^{\zeta} \zeta \Theta_q(\zeta_p, \zeta) d\zeta \\ &= \sigma q_p t_\sigma R_q(\zeta_p, \zeta). \end{aligned} \quad (5)$$

Carrying out the integration with the aid of the integrals in appendix B, we find that the characteristic function R_q is given by

$$\begin{aligned} R_q(\zeta_p, \zeta) &= 2 \int_{\zeta_p}^{\zeta} \zeta \Theta_q(\zeta_p, \zeta) d\zeta \\ &= \left\{ [C(2\zeta) - C(2\zeta_p)] \left[\frac{1}{2} \zeta^2 \cos 2\pi \zeta_p^2 + \frac{1}{8\pi} \sin 2\pi \zeta_p^2 \right] \right. \\ &\quad + [S(2\zeta) - S(2\zeta_p)] \left[\frac{1}{2} \zeta^2 \sin 2\pi \zeta_p^2 - \frac{1}{8\pi} \cos 2\pi \zeta_p^2 \right] \\ &\quad \left. - \frac{\zeta}{4\pi} \sin 2\pi(\zeta^2 - \zeta_p^2) \right\} \end{aligned} \quad (6a)$$

$$= \zeta^2 \Theta_q + \frac{1}{16\pi^2 \zeta_p} \Phi_s. \quad (6b)$$

This linear deflection resulting from mallaunching is much greater than that resulting from initial yaw, although it is still relatively small compared to the deflections that enter

FIGURE 3.36a, b.—Characteristic function $\sqrt{4\pi} \theta_q(\zeta, \zeta_p)$.

after burning. For example, for our "typical" rocket with $G=1,000$ ft./sec.², $\sigma=250$ feet, $V=1,000$ ft./sec. and $p=5$ feet ($V_p=100$ ft./sec.), equation (6) tells us that $r_a/q_p=45.8$ ft./ (rad./sec.). Thus for an initial angular velocity of 0.3 rad./sec. $r_a \approx 14$ feet. For comparison, ϑ_a is 0.029 rad. under similar circumstances, and the deflection 3,000 feet down range is from 3.33 (10), $(14+3,000 \times 0.029)=101$ feet.

3.37 Solutions of the Inhomogeneous Equations by Means of Green's Functions.—In order to obtain the characteristic functions for gravity and for linear, angular, and fin malalignment, as defined in 3.33 (22)–(25), we must solve a set of differential equations which can be written as

$$\varphi'' + 16\pi^2 \zeta^2 \delta = f(\zeta), \quad (1)$$

$$\zeta \vartheta' - \delta = h(\zeta), \quad (2)$$

and

$$\varphi - \vartheta - \delta = 0, \quad (3)$$

where $f(\zeta)$ and $h(\zeta)$ are functions of ζ whose forms can be obtained from 3.33 (14), (15), and (16), and where either f or h may be zero depending on which characteristic function one is solving for. Solutions of these equations are required subject to the initial conditions $\varphi=\delta=\varphi'=0$ at $\zeta=\zeta_p$. These solutions can be obtained by the well-known method of variation of parameters in terms of integrals involving the solutions of the homogeneous equations. However, we shall generalize Cauchy's relatively little known method¹⁶ of solving a single linear differential equation and obtain a method of solving a system of simultaneous inhomogeneous equations. The solution will be expressed as an integral of the product of the inhomogeneous term and a solution of the homogeneous equation. It seems appropriate, because of this form, to call this a Green's function method for solving differential equations—the function by which we multiply the inhomogeneous term is the Green's function. This Green's function method turns out to be particularly satisfactory because of its simple physical interpretation and because it yields solutions of just the form defined in 3.33 (22)–(25). Moreover, it leads to analytic expressions for the solutions of the inhomogeneous equations in cases where f and h are sufficiently simple functions of ζ . Even for the most complicated f 's and h 's it gives solutions in the form of integrals whose value can be estimated if we are interested in orders of magnitude only or whose value can be calculated by numerical quadrature formulas whenever accuracy is desired. Furthermore, the Green's functions do not need to be determined separately; they are included among the characteristic functions found in 3.34.

We commence with a discussion that will illustrate the physical interpretation of the theorem as well as indicate its form. The functions $\Delta_a(u, \zeta)$, $\Phi_a(u, \zeta)$, and $\Theta_a(u, \zeta)$ defined by 3.33 (21) give the motion of the rocket when the inhomogeneous terms f and h are zero and when the rocket is given the transverse angular velocity $\dot{\varphi} \equiv \varphi'/t_\sigma = 1/t_\sigma$ at $\zeta=u$. This transverse angular velocity could have been imparted by means of an impulsive moment of suitable magnitude applied at this instant. If an impulse of any other magnitude is applied when $\zeta=u$, the effect produced is proportional to the magnitude of the impulse. The term $f(\zeta)$ appears in (1) because terms representing torques about transverse axes appeared on the right

¹⁶ See H. Bateman, "Partial Differential Equations of Mathematical Physics," p. 57, Dover, 1944.

side of 3.24 (8); $f(\zeta)$ is proportional to these torques, but the value of the constant of proportionality is not important in the present discussion. Now when h is zero then in any particular infinitesimal interval of time these torques can be regarded as merely supplying an infinitesimal impulse whose effect is computable from the functions Δ_a , Φ_a , and Θ_a . And since we are dealing with a linear system, we may expect that by summing up the effects of each infinitesimal impulse into which f can be resolved, we would get the desired solution of the inhomogeneous equation. Similarly the inhomogeneous term $h(\zeta)$ is due to a force applied at the center of mass. The effect of such a force applied over an infinitesimal length of time in the neighborhood of $\zeta=u$ is the same as though the rocket were launched at this instant with an initial transverse velocity, V_\perp , proportional to the applied impulse. An initial transverse velocity V_\perp imparted at the instant when $\zeta=u$ and the forward velocity is $V=v_\sigma u$ corresponds to an initial deflection $\vartheta_p = V_\perp/v_\sigma u$ and hence to the initial orientation and yaw

$$\varphi_p = 0, \quad \delta_p = \varphi_p - \vartheta_p = -V_\perp/v_\sigma u.$$

Therefore by 3.33 (27)–(29) the effect, at any arbitrarily chosen later value of ζ , of this initial transverse velocity is that

$$\begin{aligned} \delta &= -(V_\perp/v_\sigma u) \Delta_\delta(u, \zeta), \\ \varphi &= -(V_\perp/v_\sigma u) \Phi_\delta(u, \zeta), \\ \vartheta &= -(V_\perp/v_\sigma u) \Theta_\delta(u, \zeta). \end{aligned} \tag{4}$$

The effect of a continuously applied h is then obtained by summing, in the form of a definite integral, the effects of the infinitesimal impulses into which h can be resolved.

Such arguments suggest that the desired solutions of the inhomogeneous equations are of the forms given in (5)–(10) below. A proof that the forms given are correct and that the proper factors have been used to allow for the change of variables from t to ζ is best developed, as indicated below, by direct substitution in the differential equations rather than by elaboration of the arguments of the previous paragraph. Expressed in terms of the functions defined in 3.33 (20)–(21) the solutions of (1), (2), and (3) subject to the conditions $h = \varphi_p = \delta_p = \varphi'_p = 0$ are

$$\delta_f(\zeta_p, \zeta) = \int_{\zeta_p}^{\zeta} f(u) \Delta_a(u, \zeta) du, \tag{5}$$

$$\varphi_f(\zeta_p, \zeta) = \int_{\zeta_p}^{\zeta} f(u) \Phi_a(u, \zeta) du, \tag{6}$$

and

$$\vartheta_f(\zeta_p, \zeta) = \int_{\zeta_p}^{\zeta} f(u) \Theta_a(u, \zeta) du. \tag{7}$$

The solutions subject to $f = \varphi_p = \delta_p = \varphi'_p = 0$ are

$$\delta_h(\zeta_p, \zeta) = - \int_{\zeta_p}^{\zeta} \frac{h(u)}{u} \Delta_\delta(u, \zeta) du, \tag{8}$$

$$\varphi_h(\zeta_p, \zeta) = - \int_{\zeta_p}^{\zeta} \frac{h(u)}{u} \Phi_\delta(u, \zeta) du, \tag{9}$$

and

$$\vartheta_h(\zeta_p, \zeta) = - \int_{\zeta_p}^{\zeta} \frac{h(u)}{u} \Theta_h(u, \zeta) du. \quad (10)$$

It should be noted that in these expressions we integrate with respect to u from ζ_p , the value of ζ at launching, to ζ , the value at the instant of interest. The function that is integrated is the inhomogeneous term¹⁸ in the differential equation, with ζ replaced by u , multiplied by the appropriate characteristic function, with ζ_p replaced by u . It will not always be possible to carry out the indicated integrations in terms of known functions. In such cases, with the aid of the tables of Θ_e and Θ_h given in Appendix C, it is a simple matter to evaluate the functions ϑ_e and ϑ_h , for any specific values of ζ_p and ζ , by numerical integration of (7) and (10). The functions φ_e and φ_h can be evaluated in a similar manner.

If a solution with both applied forces and moments is desired we need only add corresponding terms from the two sets of solutions. Our main use of these solutions will be to obtain the characteristic functions defined in 3.33 (22)–(25). It is usually simplest to determine δ by the Green's function method, but is often most convenient to determine φ and ϑ from

$$\varphi(\zeta_p, \zeta) = \int_{\zeta_p}^{\zeta} \frac{h(v)}{v} dv + \int_{\zeta_p}^{\zeta} \frac{1}{v} \frac{d[v\delta(\zeta_p, v)]}{dv} dv + \varphi(\zeta_p, \zeta_p), \quad (11)$$

or

$$\vartheta = \varphi - \delta = \int_{\zeta_p}^{\zeta} \frac{h(v)}{v} dv + \int_{\zeta_p}^{\zeta} \frac{\delta(\zeta_p, v)}{v} dv. \quad (12)$$

Equation (11) is readily derived from (2) by following the procedure used in deriving 3.34 (11), while (12) follows directly from (2) and (3). Besides giving the characteristic functions, the above equations will also be used to obtain other solutions of the inhomogeneous equations.

To prove that the functions defined above are the desired solutions, consider (8), (9), and (10). They contain the functions Δ_h , Φ_h , and Θ_h which, from the definitions given in 3.33 (20), satisfy the differential equations.

$$\Phi_h''(u, \zeta) + 16\pi^2 \zeta^2 \Delta_h(u, \zeta) = 0, \quad (13)$$

$$\zeta \Theta_h'(u, \zeta) - \Delta_h(u, \zeta) = 0, \quad (14)$$

and

$$\Phi_h(u, \zeta) - \Theta_h(u, \zeta) - \Delta_h(u, \zeta) = 0. \quad (15)$$

By 3.33 (20), or by 3.34 (18) and (19), these functions also satisfy the conditions

$$\Delta_h(\zeta_p, \zeta_p) = 1, \therefore \Delta_h(\zeta, \zeta) = 1; \quad (16)$$

$$\Phi_h(\zeta_p, \zeta_p) = 0, \therefore \Phi_h(\zeta, \zeta) = 0; \quad (17)$$

and

$$\Theta_h(\zeta, \zeta) = \Phi_h(\zeta, \zeta) - \Delta_h(\zeta, \zeta) = -1. \quad (18)$$

If (8), (9), and (10) are substituted in (3), one gets just the left side of (15), multiplied by $h(u)/u$, under the integral sign; and (3) is obviously satisfied. In order to substitute in (2) differentiate (10) and use (18), getting

¹⁸ Since the differential equation can be multiplied through by any arbitrary function of ζ , thus multiplying the inhomogeneous term by any arbitrary function, this statement is meaningless until a standard form is adopted for the differential equation. The proper standard form for (2) is the one in which the coefficient of ϑ' is unity. This explains the use of $u^{-1}h(u)$ rather than $h(u)$ in (8)–(10).

$$\begin{aligned}
\vartheta_n'(\zeta_p, \zeta) &= -\frac{h(\zeta)\Theta_\delta(\zeta, \zeta)}{\zeta} - \int_{\zeta_p}^{\zeta} \frac{h(u)}{u} \Theta_\delta'(u, \zeta) du \\
&= +\frac{h(\zeta)}{\zeta} - \int_{\zeta_p}^{\zeta} \frac{h(u)}{u} \Theta_\delta'(u, \zeta) du.
\end{aligned} \tag{19}$$

Now substituting (8) and (19) in the left-hand side of (2) we have, with the aid of (14),

$$\zeta \vartheta_n' - \delta = h(\zeta) - \int_{\zeta_p}^{\zeta} \frac{h(u)}{u} [\zeta \Theta_\delta'(u, \zeta) - \Delta_\delta(u, \zeta)] du = h(\zeta),$$

which is the right-hand side of (2). In a similar fashion it can be shown that (1) is satisfied when $f=0$. It is immediately evident from (8) and (9) that these definitions are consistent with the requirement that $\delta_p=0$, $\varphi_p=0$; and if we differentiate (9) and make use of (17) we see that $\varphi'_p=0$. Thus (8), (9), and (10) fulfill the specified initial conditions. Similar arguments show that (5), (6) and (7) satisfy the differential equations subject to the specified conditions.

This Green's function method can be applied to any system of linear differential equations. Only minor variations in terminology would be required to make the above theorems apply to 3.33 (8), (9), and (10) or 3.24 (8), (9), and (10) rather than to 3.33 (14), (15), and (16). The theorem applies also to the equations of motion of spin-stabilized rockets in 9.13, where the additional term in the equations merely lengthens the proof.

Those who are familiar with the usual use of Green's functions in the solution of differential equations will note at once that the integrals have just the usual forms. It appears, though, that the Green's functions Δ_a , $-\Delta_\delta$, etc., do not have the customary forms since our functions are defined and continuous functions of ζ_p and ζ for all $\zeta_p \geq 0$ and all $\zeta > 0$. Of course the values of ζ that are less than ζ_p are rarely of physical significance and one rarely computes the values of the functions for such values of ζ . The usual Green's function, $G(\zeta, u)$, is either discontinuous or has a discontinuous derivative at $\zeta=u$. However, if we had wished to define a Green's function

$$G(\zeta, u) = \begin{cases} 0 & \text{when } \zeta_p \leq \zeta < u \\ \Delta_a(u, \zeta) & \text{when } u < \zeta \leq \infty \end{cases} \tag{20}$$

and had integrated this with respect to u from ζ_p to ∞ , (5) would take on just the expected form; but this is not done since the forms (5)–(10) are more convenient for our purposes.

In the following sections we shall make use of (5)–(10) to determine the explicit functions defined by 3.33 (22)–(25).

3.38 Effect of Gravity.—The effect of gravity is given by the characteristic functions identified by the subscript g and defined in 3.33 (22). Comparison of 3.37 (2) and 3.33 (15) shows that in this case $h(\zeta) = (g/G) \cos \theta_0$. Hence if we use 3.37 (8), (9), and (10) together with 3.33 (22) to determine the characteristic functions, we find that they are

$$\Delta_g(\zeta_p, \zeta) = - \int_{\zeta_p}^{\zeta} \Delta_\delta(u, \zeta) \frac{du}{u}, \tag{1}$$

$$\Phi_g(\zeta_p, \zeta) = - \int_{\zeta_p}^{\zeta} \Phi_\delta(u, \zeta) \frac{du}{u}, \tag{2}$$

$$\Theta_g(\zeta_p, \zeta) = - \int_{\zeta_p}^{\zeta} \Theta_g(u, \zeta) \frac{du}{u}, \quad (3)$$

where Δ_g , Φ_g , and Θ_g are given explicitly by 3.34 (18), (19), and (20).

It will be simplest to evaluate first the integral for Δ_g . Substituting from 3.34 (18) into (1) above, we have

$$\begin{aligned} \Delta_g(\zeta_p, \zeta) &= - \int_{\zeta_p}^{\zeta} \frac{u}{\zeta} \cos 2\pi(\zeta^2 - u^2) \frac{du}{u} \\ &= - \frac{1}{\zeta} \cos 2\pi\zeta^2 \int_{\zeta_p}^{\zeta} \cos 2\pi u^2 du - \frac{1}{\zeta} \sin 2\pi\zeta^2 \int_{\zeta_p}^{\zeta} \sin 2\pi u^2 du. \end{aligned} \quad (4)$$

Finally,

$$\Delta_g(\zeta_p, \zeta) = - \frac{1}{2\zeta} \{ [C(2\zeta) - C(2\zeta_p)] \cos 2\pi\zeta^2 + [S(2\zeta) - S(2\zeta_p)] \sin 2\pi\zeta^2 \}. \quad (5)$$

Substituting from 3.34 (19) into (2) above, we find

$$\Phi_g(\zeta_p, \zeta) = - 2\pi \int_{\zeta_p}^{\zeta} \{ [C(2\zeta) - C(2u)] \sin 2\pi u^2 - [S(2\zeta) - S(2u)] \cos 2\pi u^2 \} du \quad (6)$$

$$\begin{aligned} &= - 2\pi C(2\zeta) \int_{\zeta_p}^{\zeta} \sin 2\pi u^2 du + 2\pi S(2\zeta) \int_{\zeta_p}^{\zeta} \cos 2\pi u^2 du \\ &\quad + 2\pi \int_{\zeta_p}^{\zeta} [C(2u) \sin 2\pi u^2 - S(2u) \cos 2\pi u^2] du; \end{aligned} \quad (7)$$

from which

$$\Phi_g(\zeta_p, \zeta) = \pi \{ [C(2\zeta) - C(2\zeta_p)] S(2\zeta) - [S(2\zeta) - S(2\zeta_p)] C(2\zeta) + J_I(2\zeta) - J_I(2\zeta_p) \}, \quad (8)$$

where the function J_I is defined by

$$J_I(2\zeta) = 2 \int_0^{\zeta} [C(2u) \sin 2\pi u^2 - S(2u) \cos 2\pi u^2] du. \quad (9)$$

It is not necessary to compute the characteristic function Θ_g by (3), for

$$\Theta_g = \Phi_g - \Delta_g; \quad (10)$$

or

$$\begin{aligned} \Theta_g(\zeta_p, \zeta) &= \pi [J_I(2\zeta) - J_I(2\zeta_p)] \\ &\quad + [C(2\zeta) - C(2\zeta_p)] \left[\pi S(2\zeta) + \frac{1}{2\zeta} \cos 2\pi\zeta^2 \right] \\ &\quad - [S(2\zeta) - S(2\zeta_p)] \left[\pi C(2\zeta) - \frac{1}{2\zeta} \sin 2\pi\zeta^2 \right] \end{aligned} \quad (11)$$

Hence the yaw, orientation and deflection of the tangent due to gravity are

$$\delta_g = \frac{g \cos \theta_0}{G} \Delta_g(\zeta_p, \zeta), \quad (12)$$

$$\varphi_z = \frac{g \cos \theta_0}{G} \Phi_z(\zeta_p, \zeta), \quad (13)$$

$$\vartheta_z = \frac{g \cos \theta_0}{G} \Theta_z(\zeta_p, \zeta). \quad (14)$$

Since the differential equations 3.33 (14)–(16) refer to the motion in the vertical plane, the above quantities represent only the motion in this plane. However, gravity does not enter into the equations for the motion in the lateral plane; hence (12), (13), and (14) above represent the *entire* motion due to gravity. One can write these equations in complex form by introducing the imaginary unit i on the right-hand side. Thus

$$\delta_z = i \frac{g \cos \theta_0}{G} \Delta_z(\zeta_p, \zeta), \quad (15)$$

$$\varphi_z = i \frac{g \cos \theta_0}{G} \Phi_z(\zeta_p, \zeta), \quad (16)$$

$$\vartheta_z = i \frac{g \cos \theta_0}{G} \Theta_z(\zeta_p, \zeta), \quad (17)$$

which emphasizes the fact that these motions are confined to the vertical plane. A graph of the characteristic function $\Theta_z(\zeta_p, \zeta)$ showing the variation with $2^{1/2}\zeta$ for various constant values of $2^{1/2}\zeta_p$ is given in figure 3.38a. It will be observed that Θ_z does not approach a finite limiting value as ζ increases, but that after a single yaw oscillation [$2^{1/2}\zeta = (2d/\sigma)^{1/2} = 2^{1/2}$] its oscillations die down and become inappreciable, and the function takes on the asymptotic value¹⁹

$$\Theta_z(\zeta_p, \zeta) \sim K + \ln \frac{\zeta}{\zeta_p}, \text{ for } \zeta \gg 1, \quad (18)$$

where the constant K is given by

$$K = 1.901 - \pi J_I(2\zeta_p) - \frac{\pi}{2} [C(2\zeta_p) - S(2\zeta_p)] + \ln \zeta_p. \quad (19)$$

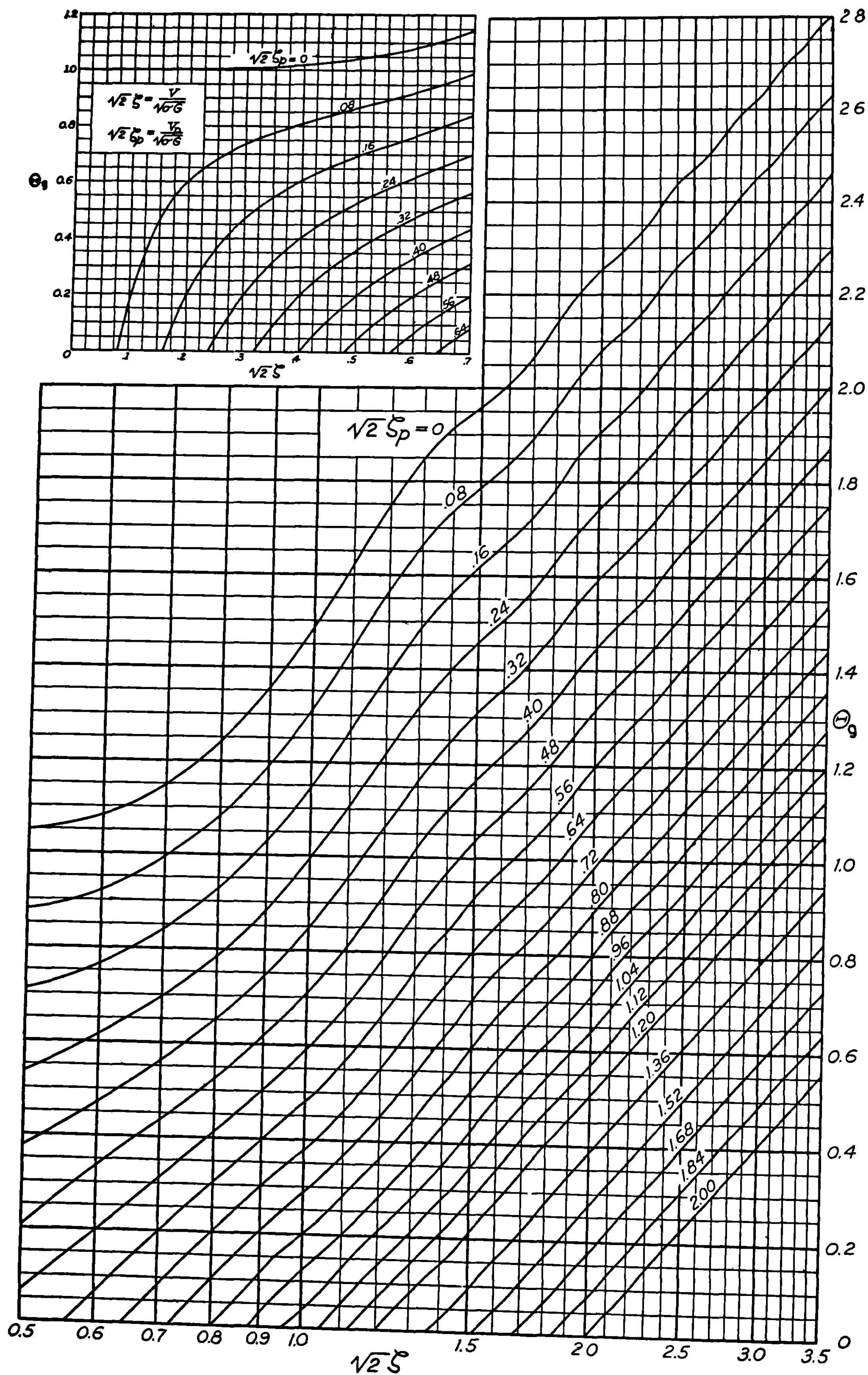
The linear deflection of the rocket from the launcher line or Z_0 -axis is

$$\begin{aligned} r_z &= \int_{t_p}^t V \vartheta_z dt = 2\sigma \int_{\zeta_p}^{\zeta} \zeta \vartheta_z d\zeta \\ &= i \frac{2\sigma g \cos \theta_0}{G} \int_{\zeta_p}^{\zeta} \zeta \Theta_z(\zeta_p, \zeta) d\zeta. \end{aligned} \quad (20)$$

We can write this as

$$r_z = i \frac{\sigma g \cos \theta_0}{G} R_z(\zeta_p, \zeta), \quad (21)$$

¹⁹ See appendix B.

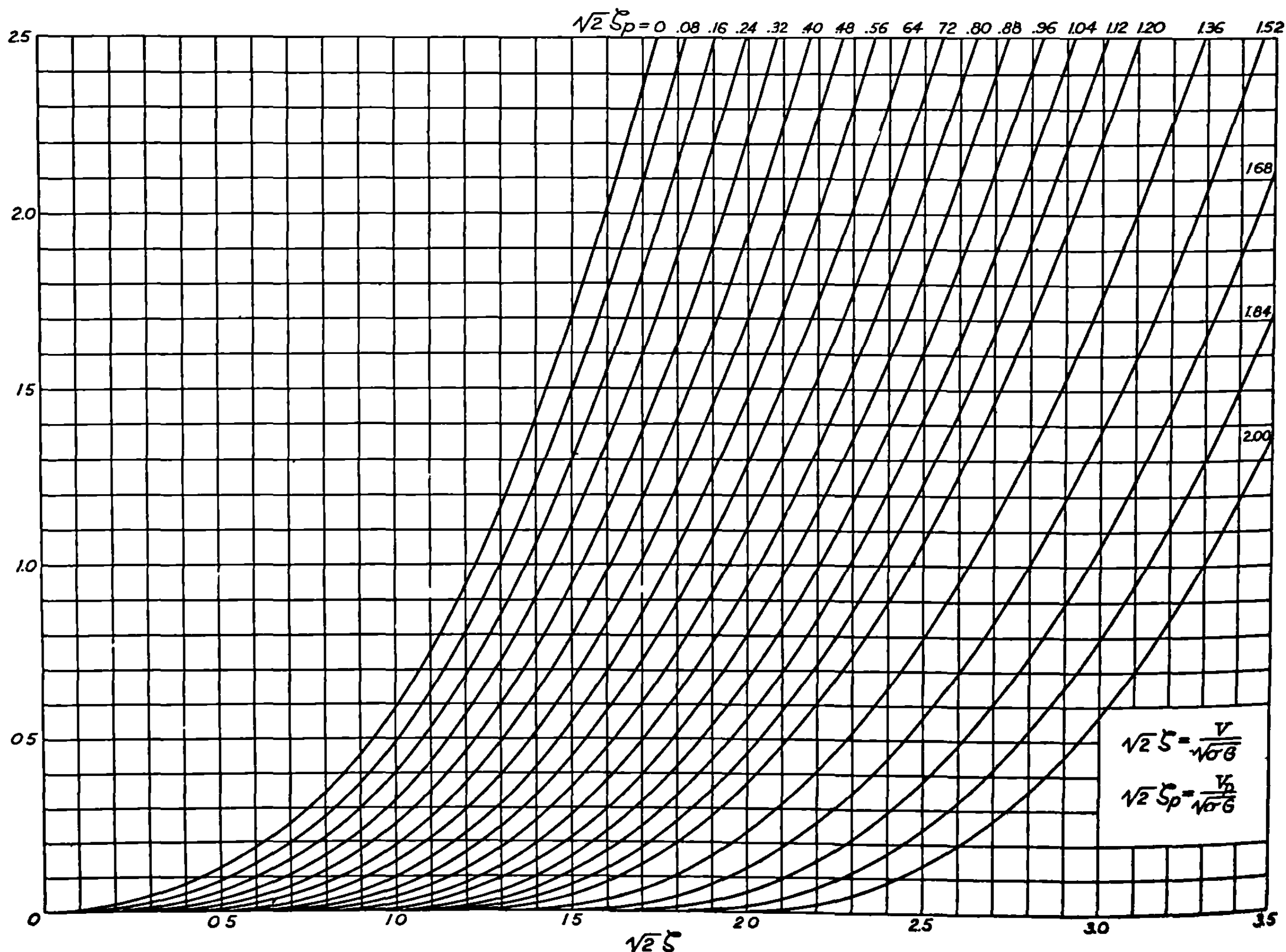
FIGURE 3.38a.—Characteristic function $\Theta_s(\zeta, \xi)$.

where the characteristic function R_g is given by

$$\begin{aligned}
 R_g(\zeta_p, \zeta) &= 2 \int_{\zeta_p}^{\zeta} \zeta \Theta_g(\zeta_p, \zeta) d\zeta \\
 &= \zeta^2 \Theta_g(\zeta_p, \zeta) - \frac{1}{2}(\zeta^2 - \zeta_p^2) \\
 &\quad + \frac{1}{8}[C(2\zeta) - C(2\zeta_p)]^2 + \frac{1}{8}[S(2\zeta) - S(2\zeta_p)]^2 \\
 &= \zeta^2 \Theta_g - \frac{1}{2}(\zeta^2 - \zeta_p^2) + \Phi_R.
 \end{aligned} \tag{22}$$

We evaluated R_g by integrating by parts, but it could also have been done by a Green's function method using R_g as a Green's function. However, it is usually easier to use (20) rather than a Green's function to get r .

This quantity is of considerable importance for calculating the trajectory of the rocket up to the end of burning. To facilitate rapid calculation of gravity deflections, the quantity $R_g(\zeta_p, \zeta)$ has been plotted in figures 3.38b and c as a function of $2^{\frac{1}{2}}\zeta$ for various values of $2^{\frac{1}{2}}\zeta_p$. For our "typical" rocket with $V_b = 1,000$ ft./sec., $G = 1,000$ ft./sec.², $\sigma = 250$ feet and $p = 5$ feet ($V_p = 100$ feet), we have from the figure $R_g(\zeta_p, \zeta) = 2.68$. Hence for low angle firing, $\theta_0 \leq 10^\circ$ the vertical displacement of the rocket normal to the launcher line at the end of burning is 21.4 feet; while at 45° quadrant elevation, the normal deflection is 15.1 feet.



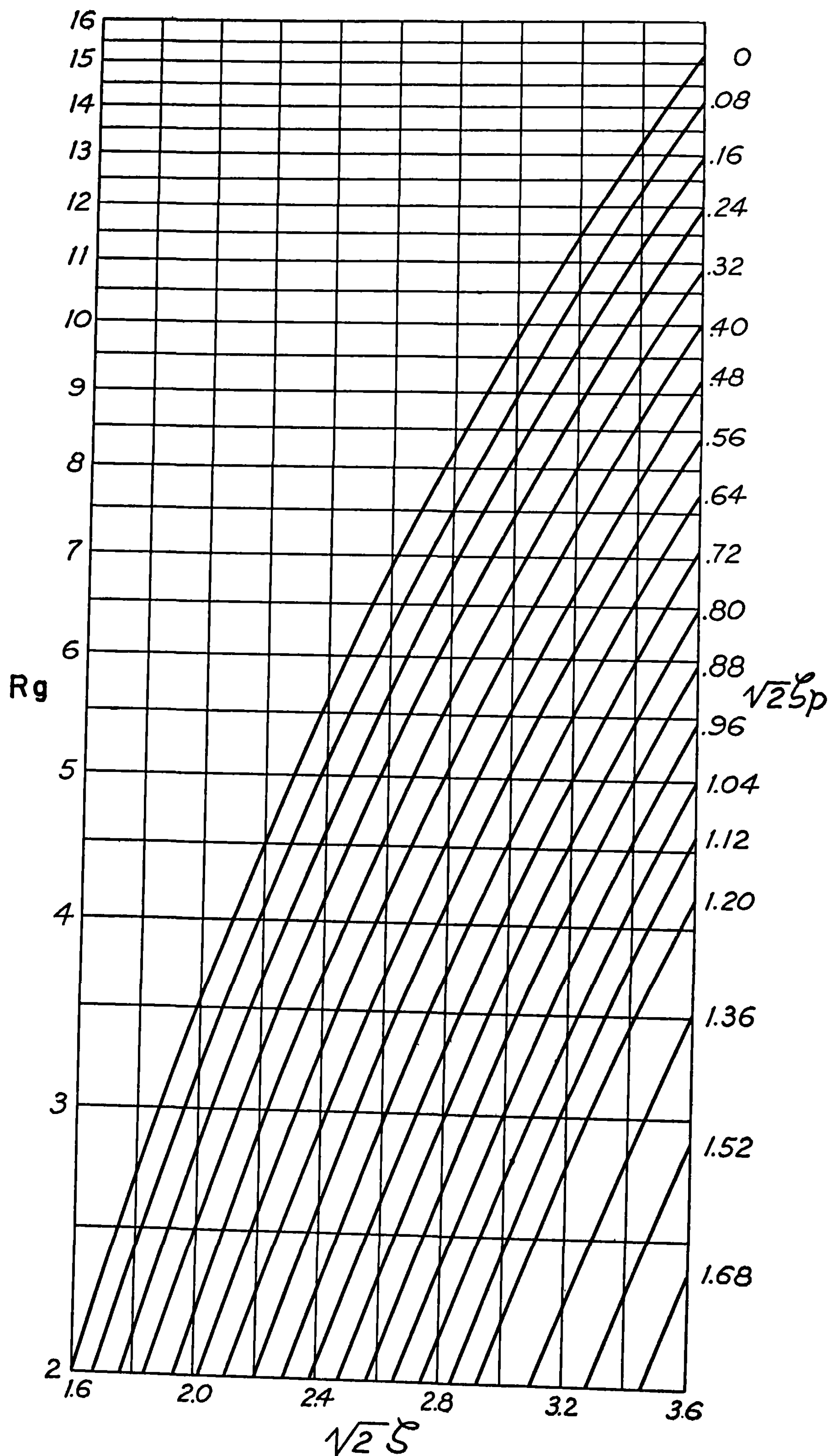


FIGURE 3.38c.—Logarithmic plot of $R_g(\zeta_p, \zeta)$.

3.39 Effect of a Constant Linear Thrust Malalignment.—The effect of the linear thrust malalignment R_M is given by the characteristic functions identified by the subscript R and defined in 3.33 (23). Comparison of 3.37 (1) and 3.33 (14) shows that in this case $f(\zeta) = -(2\sigma/K^2)R_M$. Hence if we use 3.37 (5), (6), and (7) in conjunction with 3.33 (23) to determine the characteristic functions, we find that they are given by

$$\Delta_R(\zeta_p, \zeta) = \int_{\zeta_p}^{\zeta} \Delta_q(u, \zeta) du, \quad (1)$$

$$\Phi_R(\zeta_p, \zeta) = \int_{\zeta_p}^{\zeta} \Phi_q(u, \zeta) du, \quad (2)$$

and

$$\Theta_R(\zeta_p, \zeta) = \int_{\zeta_p}^{\zeta} \Theta_q(u, \zeta) du, \quad (3)$$

where Δ_q , Φ_q , and Θ_q are given explicitly by 3.34 (21), (22), and (23).

Substituting from 3.34 (21) into (1) above, we have

$$\Delta_R(\zeta_p, \zeta) = \int_{\zeta_p}^{\zeta} \frac{1}{4\pi\zeta} \sin 2\pi(\zeta^2 - u^2) du \quad (4)$$

$$\begin{aligned} &= \frac{1}{4\pi\zeta} \sin 2\pi\zeta^2 \int_{\zeta_p}^{\zeta} \cos 2\pi u^2 du \\ &\quad - \frac{1}{4\pi\zeta} \cos 2\pi\zeta^2 \int_{\zeta_p}^{\zeta} \sin 2\pi u^2 du \\ &= \frac{1}{8\pi\zeta} \{ [C(2\zeta) - C(2\zeta_p)] \sin 2\pi\zeta^2 \\ &\quad - [S(2\zeta) - S(2\zeta_p)] \cos 2\pi\zeta^2 \}. \end{aligned} \quad (5)$$

The solution for Φ_R is similarly obtained by substituting from 3.34 (22) into (2) above. Thus, by using some of the formulas in appendix B, we get

$$\begin{aligned} \Phi_R(\zeta_p, \zeta) &= \frac{1}{2} \int_{\zeta_p}^{\zeta} \{ [C(2\zeta) - C(2u)] \cos 2\pi u^2 + [S(2\zeta) - S(2u)] \sin 2\pi u^2 \} du \\ &= \frac{1}{2} C(2\zeta) \int_{\zeta_p}^{\zeta} \cos 2\pi u^2 du - \frac{1}{2} \int_{\zeta_p}^{\zeta} C(2u) \cos 2\pi u^2 du \\ &\quad + \frac{1}{2} S(2\zeta) \int_{\zeta_p}^{\zeta} \sin 2\pi u^2 du - \frac{1}{2} \int_{\zeta_p}^{\zeta} S(2u) \sin 2\pi u^2 du \\ &= \frac{1}{4} C(2\zeta) [C(2\zeta) - C(2\zeta_p)] - \frac{1}{8} \{ [C(2\zeta)]^2 - [C(2\zeta_p)]^2 \} \\ &\quad + \frac{1}{4} S(2\zeta) [S(2\zeta) - S(2\zeta_p)] - \frac{1}{8} \{ [S(2\zeta)]^2 - [S(2\zeta_p)]^2 \}. \end{aligned} \quad (6)$$

Finally,

$$\Phi_R(\zeta_p, \zeta) = \frac{1}{8} \{ [C(2\zeta) - C(2\zeta_p)]^2 + [S(2\zeta) - S(2\zeta_p)]^2 \}. \quad (7)$$

The function Θ_R is merely the difference between Φ_R and Δ_R , or

$$\begin{aligned} \Theta_R(\zeta_p, \zeta) = \frac{1}{8} \left\{ [C(2\zeta) - C(2\zeta_p)] \left[C(2\zeta) - C(2\zeta_p) - \frac{1}{\pi\zeta} \sin 2\pi\zeta^2 \right] \right. \\ \left. + [S(2\zeta) - S(2\zeta_p)] \left[S(2\zeta) - S(2\zeta_p) + \frac{1}{\pi\zeta} \cos 2\pi\zeta^2 \right] \right\}. \end{aligned} \quad (8)$$

Following the argument preceding 3.33 (30) we can represent both the lateral and vertical components of the motion by considering R_M as a complex vector. Hence the yaw, orientation and deflection of the tangent resulting from the linear thrust malalignment are given by

$$\delta_R = -(2\sigma/K^2) R_M \Delta_R(\zeta_p, \zeta), \quad (9)$$

$$\varphi_R = -(2\sigma/K^2) R_M \Phi_R(\zeta_p, \zeta), \quad (10)$$

$$\vartheta_R = -(2\sigma/K^2) R_M \Theta_R(\zeta_p, \zeta). \quad (11)$$

Since the characteristic functions are real quantities, it follows from the above that the motion of the rocket will take place in the plane determined by R_M . Further, a positive malalignment will lead to a negative deflection of the trajectory. This is not surprising, since a positive linear thrust malalignment results in a torque tending to turn the head of the rocket and hence the thrust axis toward the negative direction. To see how the deflection of the tangent ϑ_R varies during the burning period, we have plotted in figure 3.39 the characteristic function $(1/6)\Theta_R(\zeta_p, \zeta)$ as a function of $2^{1/2}\zeta$ for various values of ζ_p^2 . It will be observed that the function rises rapidly to a maximum within roughly half a yaw oscillation [$2^{1/2}\zeta = (2d/\sigma)^{1/2} = 1$] and thereafter oscillates with decreasing amplitude about a value which slowly approaches its asymptotic value. These limiting values are plotted to the right of the figure and were obtained by taking the limit of $(1/6)\Theta_R(\zeta_p, \zeta)$ as $\zeta \rightarrow \infty$. The asymptotic expansion for $\Theta_R(\zeta_p, \zeta)$, valid for burning distances greater than or equal to σ , is given by ²⁰

$$\begin{aligned} \Theta_R(\zeta_p, \zeta) \sim \frac{1}{16} + \frac{1}{4} J_R(2\zeta_p) - \frac{1}{8} [C(2\zeta_p) + S(2\zeta_p)] - \frac{1}{32\pi^2\zeta^2} \\ + \frac{1}{32\pi^2\zeta^2} \left\{ \left[C(2\zeta_p) - \frac{1}{2} \right] \cos 2\pi\zeta^2 + \left[S(2\zeta_p) - \frac{1}{2} \right] \sin 2\pi\zeta^2 \right\}, \end{aligned} \quad (12)$$

the first term of which leads to the limit value plotted in figure 3.39.

* The linear deflection of the rocket from the Z_0 -axis is given by

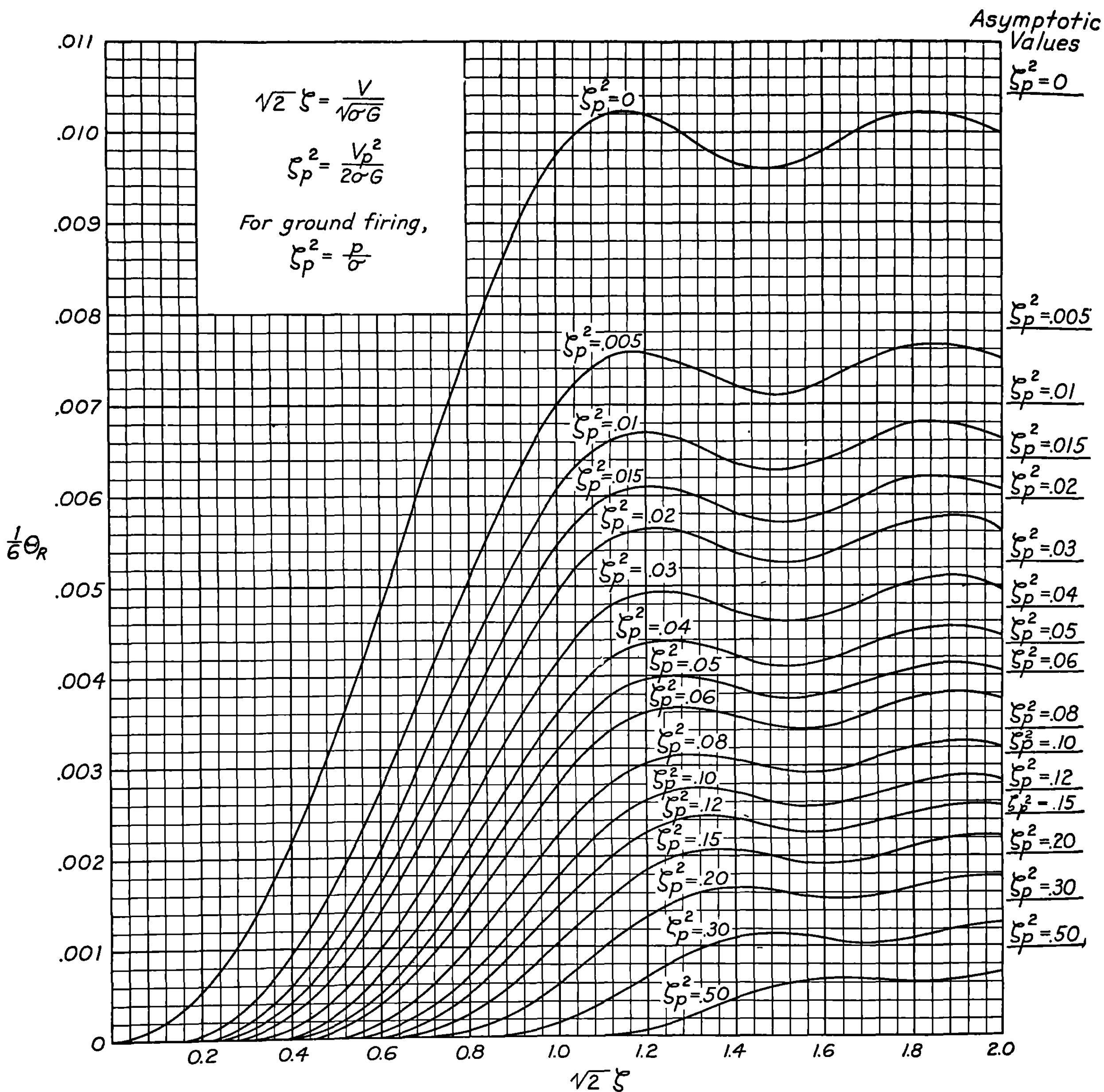
$$\begin{aligned} r_R &= \int_{t_p}^t V \vartheta_R dt = 2\sigma \int_{\zeta_p}^{\zeta} \zeta \vartheta_R d\zeta \\ &= -\frac{4\sigma^2}{K^2} R_M \int_{\zeta_p}^{\zeta} \zeta \Theta_R(\zeta_p, \zeta) d\zeta, \end{aligned} \quad (13)$$

$$= -\frac{2\sigma^2}{K^2} R_M R_R(\zeta_p, \zeta), \quad (14)$$

where the characteristic function R_R is given by

$$R_R(\zeta_p, \zeta) = 2 \int_{\zeta_p}^{\zeta} \zeta \Theta_R(\zeta_p, \zeta) d\zeta. \quad (15)$$

²⁰ From appendix B.

FIGURE 3.39.—Characteristic function $(1/6)\Theta_R(\zeta_p, \zeta)$.

Carrying through the integration, with the aid of integrals given in the appendix, we find

$$R_R(\zeta_p, \zeta) = \zeta^2 \Theta_R(\zeta_p, \zeta) + \frac{1}{16\pi} [C(2\zeta_p)S(2\zeta) - S(2\zeta_p)C(2\zeta)] - \frac{1}{16\pi} [J_I(2\zeta) - J_I(2\zeta_p)]. \quad (16)$$

This linear lateral deflection resulting from the malalignment is really of little consequence, for the deflections are generally quite small. For example, for our typical rocket with $G=1,000$ ft./sec.², $\sigma=250$ feet, $V=1,000$ ft./sec., $p=5$ feet ($V_p=100$ ft./sec.), and $K=1.0$ foot, we have (assuming $G_J \approx G$) $r_R/R_M=7,020$ ft./ft. Hence, even for a malalignment as large as 0.025 inch=0.002 feet, we get a lateral deflection of only $r_R=0.002 \times 7,020=14$ feet. At 3,000

feet down range from the end of burning the total lateral deflection under the same conditions is, from 3.35 (11), $14 + 3,000 \times 0.0354 = 120$ feet.

3.391 *Effect of σ or fin size.*—In figure 3.391 the results of the above solution for ϑ_R have been plotted so as to show more clearly the effect of fin size, or σ , on the deflection due to linear thrust malalignment. As a standard of comparison we have taken the deflection for $\sigma = \infty$; that is, the condition for neutral stability, which is identical with the vacuum case. The function [3.39 (11)]

$$\vartheta_R = (2\sigma/K^2) R_M \Theta_R(\zeta_P, \zeta) \quad (1)$$

has been divided by the corresponding expression [3.12 (10)] for the vacuum case,

$$\vartheta_{R, \text{vac}} = \frac{R_M}{3K^2} [1 - (p/d)^{\frac{1}{3}}]^3 d, \quad (2)$$

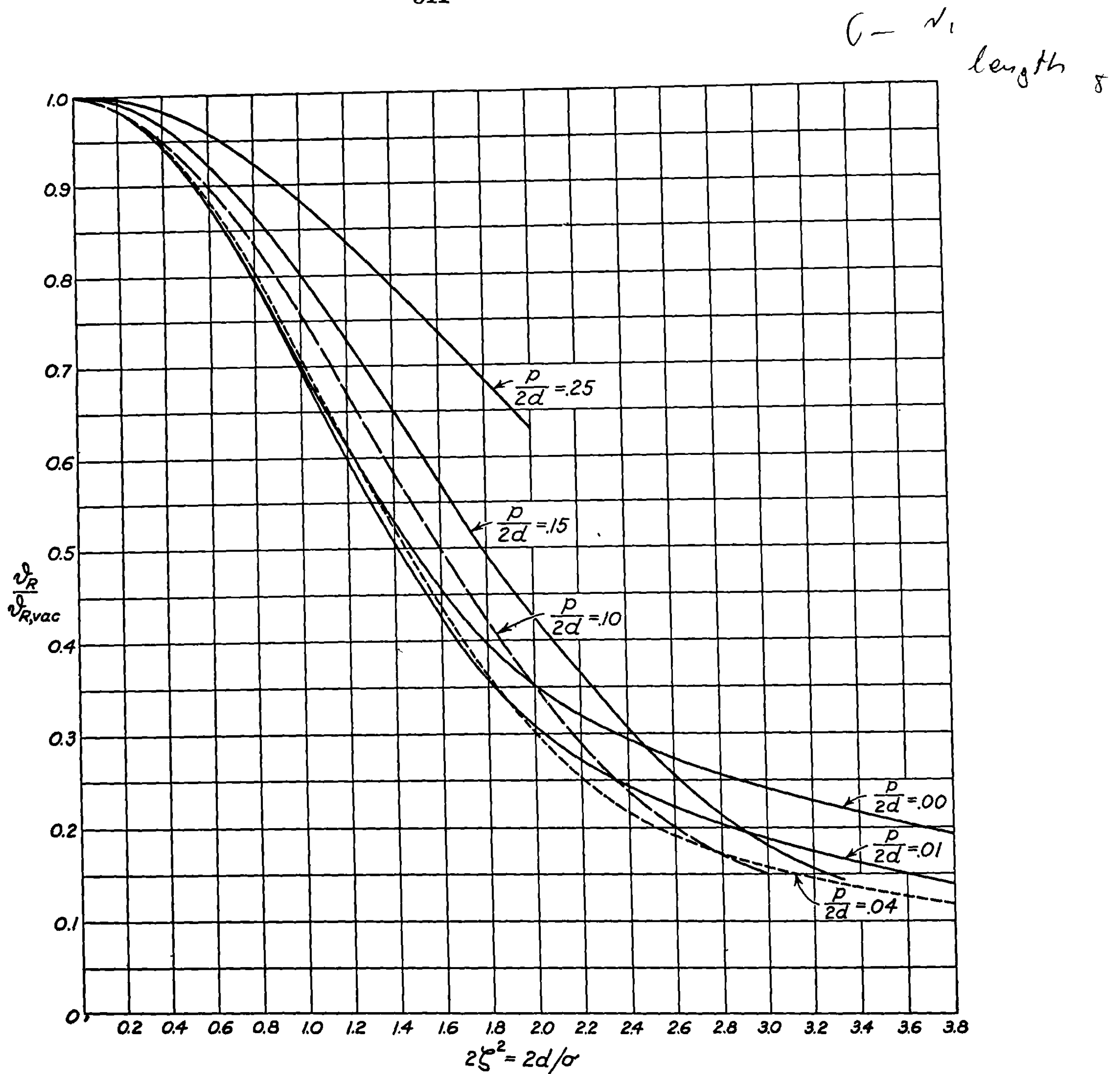


FIGURE 3.391.—Effect of fins (σ) on deflection due to linear malalignment;
Plot of $\vartheta_R / \vartheta_{R, \text{vac}}$ versus $2d/\sigma$.

to give

$$\frac{\vartheta_R}{\vartheta_{R, \text{vac}}} = 6 \frac{\Theta_R[(p/\sigma)^{\frac{1}{2}}, (d/\sigma)^{\frac{1}{2}}]}{(d/\sigma)[1 - (p/d)^{\frac{1}{2}}]^3}, \quad (3)$$

or

$$\frac{\vartheta_R}{\vartheta_{R, \text{vac}}} = 6 \frac{\Theta_R(\zeta_p, \zeta)}{\zeta^2(1 - \zeta_p/\zeta)^3}. \quad (4)$$

For various constant values of $p/2d = \zeta_p^2/2\zeta^2$, the ratio $\vartheta_R/\vartheta_{R, \text{vac}}$ has been plotted as a function of $2d/\sigma = 2\zeta^2$; where σ refers, of course, only to the real case, while d and p are the same for both the real and vacuum conditions.

In cases for which $p/2d < 0.10$; that is, in which the launcher length is less than one-fifth of the burning distance, the results of the figure may be summarized as follows: *Fins of such size as to make the yaw oscillation distance equal to twice the burning distance ($2d/\sigma = 1$) decrease the dispersion to about 70 percent of the dispersion that would be obtained with fins just large enough to give the rocket neutral stability.* For fins of greater size, down to $\sigma = d$ or slightly less, the dispersion is roughly proportional to σ . If σ is reduced still further, the resulting gain in accuracy is relatively small as may be seen from figure 3.391.

3.392 Effect of launcher length.—In figure 3.392 the results of the same solution are plotted so as to show more clearly the effects of launcher length on deflection. The abscissa is the logarithm of the ratio of effective launcher length to twice the burning distance ($p/2d$); while the ordinate $\vartheta_R/\vartheta_{R, p=0}$ is the ratio of the deflection for the given value of $p/2d$ to the deflection of the same rocket fired under the same conditions from a zero length launcher. Curves are given for a number of constant values of $2d/\sigma$. It will be observed that for launcher lengths

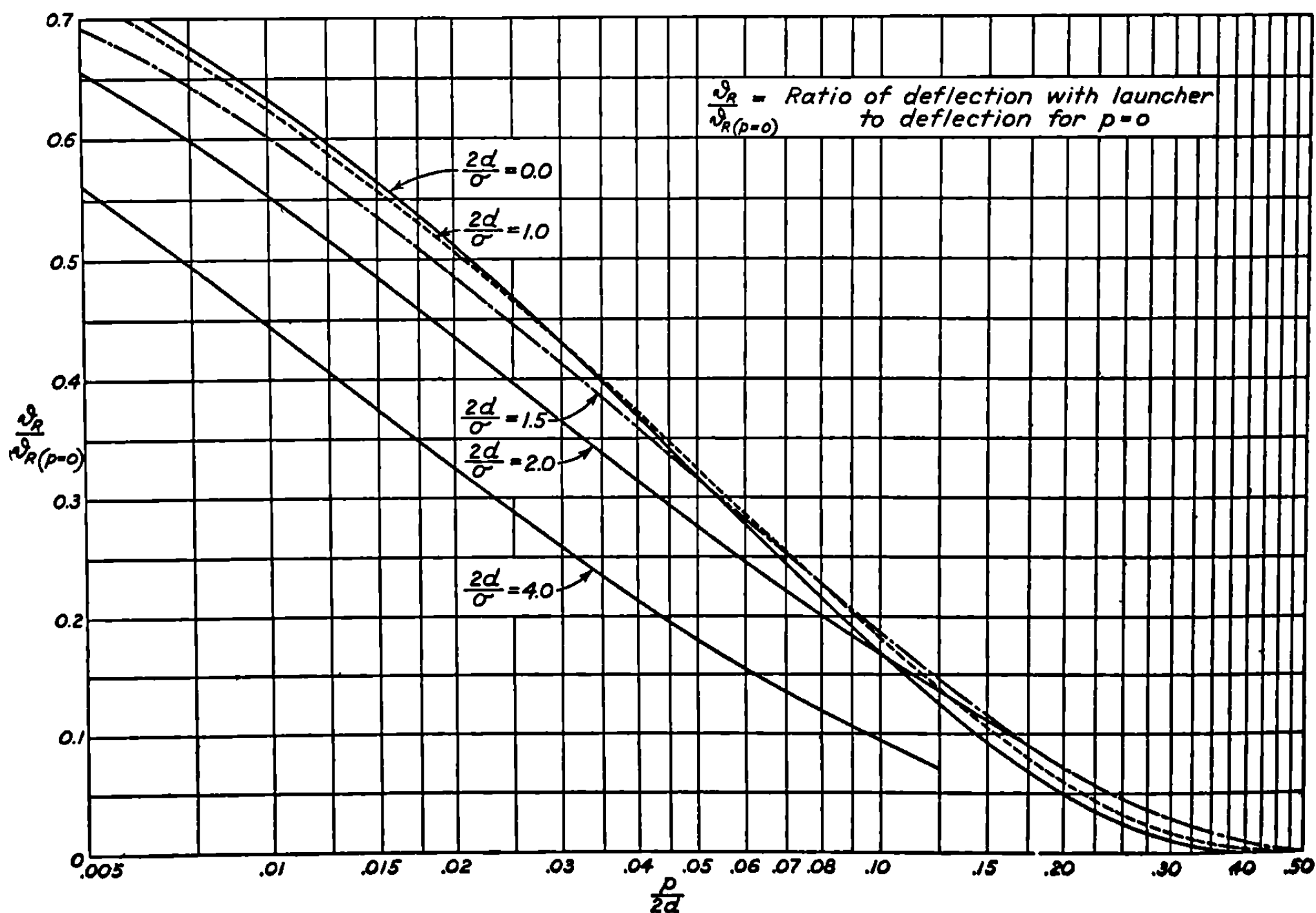


FIGURE 3.392.—Effect of launcher length on deflection due to linear misalignment.

between $1/1000$ and $1/2$ the burning distance the dispersion decreases roughly linearly with the logarithm of the effective launcher length.

3.393 Approximate formulas.—The complete expression [3.39 (11)] for the deflection due to linear malalignment is generally too difficult to handle when one is interested in getting an analytic expression for the effect of changes in σ , d or p on ϑ_R . Hence it is often useful to have simple approximate formulas for ϑ_R which, though restricted to narrow regions of validity, may be easily applied to advantage.

For *short-burning* rockets; that is, those for which $p/\sigma \leq 0.1$ and $d/\sigma \leq 0.6$, the first two terms of the power series expansion²¹ for $\Theta_R(\zeta_p, \zeta) = \Theta_R(\sqrt{p/\sigma}, \sqrt{d/\sigma})$ lead to the following approximate formula:

$$\frac{K^2 \vartheta_R}{p R_M} = \frac{1}{3} \frac{d}{p} \left[1 - \left(\frac{p}{d} \right)^{1/2} \right]^3 \left[1 - \left(\frac{d}{p} \right)^2 \left(\frac{p}{\sigma} \right)^2 \right]. \quad (1)$$

As $\sigma \rightarrow \infty$, this reduces to the simple vacuum expression 3.12 (10); namely,

$$\frac{K^2 \vartheta_{R, \text{vac}}}{p R_M} = \frac{1}{3} \frac{d}{p} \left[1 - \left(\frac{p}{d} \right)^{1/2} \right]^3. \quad (2)$$

On the other hand, for *long-burning* rockets; that is, those for which $p/\sigma \leq 0.1$ and $d/\sigma \geq 0.6$ the following formula fits the asymptotic expression 3.39 (12) for ϑ_R quite well:

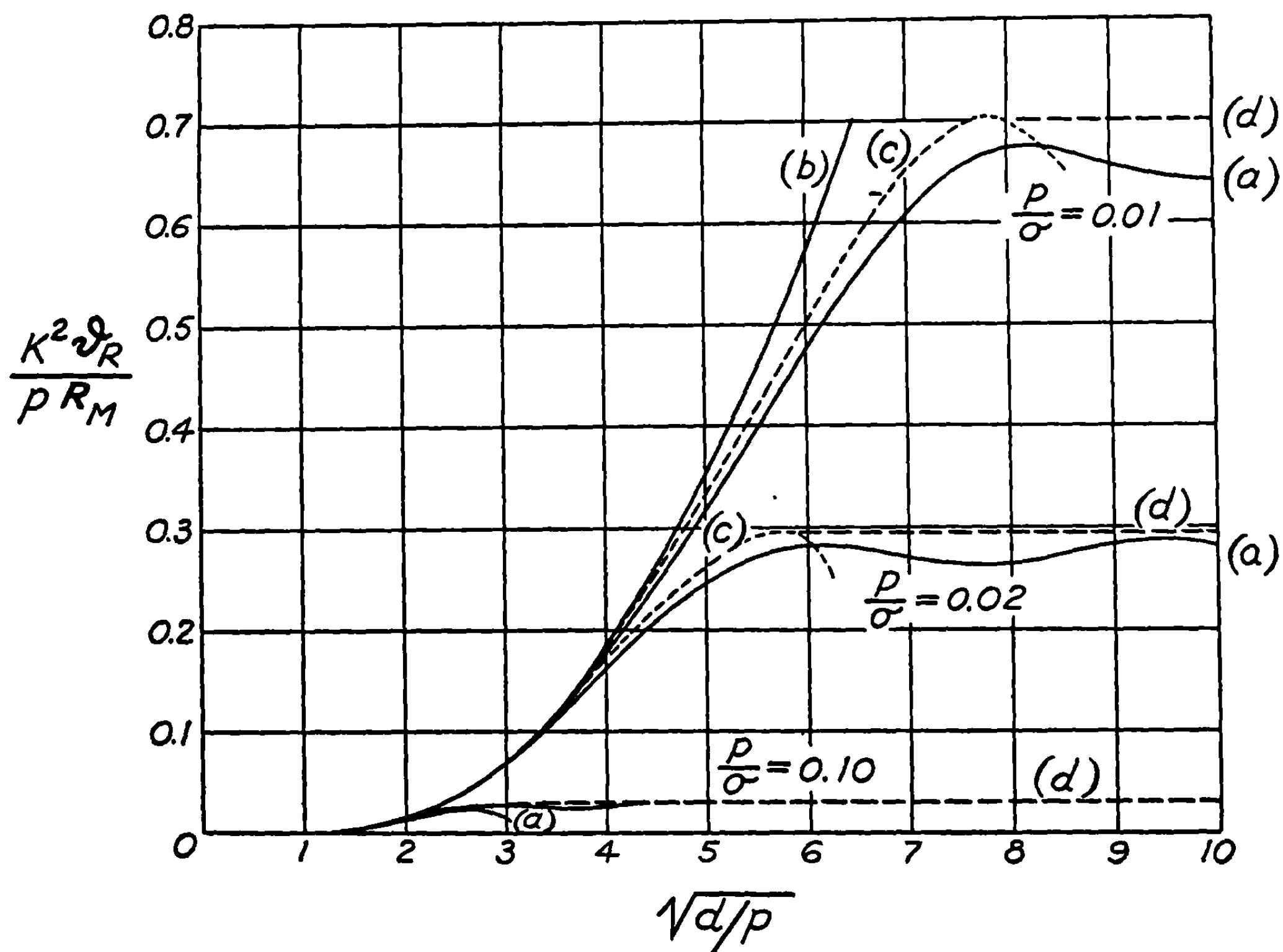


FIGURE 3.393.—Approximate curves for ϑ_R .

- (a) No approximation.
- (b) Vacuum case ($\sigma = \infty$).
- (c) Approximation for short-burning rockets.
- (d) Approximation for long-burning rockets.

²¹ See Appendix B. The coefficient of $(d/p)^2(p/\sigma)^2$ in (1) was determined by curve fitting.

$$\frac{K^2 \vartheta_R}{p R_M} = \frac{1}{8} \frac{\sigma}{p} \exp \left\{ -4 \left(\frac{p}{\sigma} \right)^{\frac{1}{2}} \right\}. \quad (3)$$

Graphs of the expressions (1) and (3) are plotted in figure 3.393 for $p/\sigma=0.10$, 0.02, and 0.01, together with the vacuum expression (2). For comparison the exact curves for $K^2 \vartheta_R/p R_M$ taken from figure 3.39, are also shown.

3.394 *Limitations of the theory—Experimental confirmation of the theory.*—The earlier effects—gravity, mallaunching and initial yaw—which have been discussed are essentially systematic effects, for they depend only on the particular type of rocket and the mode of launching. Hence the resulting deflections can be determined theoretically, or experimentally. However, in the case of the thrust malalignment, the disturbances are essentially random in magnitude and direction; and one can make no predictions regarding the resulting deviations unless one has measured beforehand the magnitude of the malalignment and the orientation of the malalignment plane when the rocket is on the launcher. Since in practice little or nothing is known about the thrust malalignment at the time of launching, and since the ratio ϑ_R/R_M is significantly large, this item is the largest single cause of the dispersion of fin-stabilized rockets.

It should be emphasized that R_M is the distance from the axis of thrust of the gas jet to the center of mass of the rocket, and that this is *not* necessarily the same as the distance from the geometrical axis of the nozzle to the center of mass, that is the *geometrical* malalignment. As discussed in chapter 2, because of asymmetries in the burning of the propellant or irregularities along the path of the gas that might introduce turbulence or shock waves into the flow of the gas, the axis of this flow may deviate from the geometrical axis of the nozzle, and such asymmetries in the gas flow may vary rapidly during the burning period. This additional random malalignment has been termed the *gas* malalignment. Indeed, a considerable amount of evidence has developed that indicates that such deviations may be as large as, or larger than, the geometrical malalignment of the nozzle. All of this means that the absolute values of the deflections or dispersions calculated on the basis of 3.39 (11) or figure 3.39 and the measured geometrical malalignments can only be relied on as to order of magnitude. While these uncertainties may affect the absolute values of the dispersion, they should not appreciably change the relative dispersions to be expected when fin size, or burning time, or launcher length is varied for a given projectile.

It is possible by mechanical means to determine the geometrical malalignment, that is the distance between the center of mass of a rocket and the axis of the nozzle. If the gas malalignments are considerably greater than the measured geometrical malalignments one would expect little or no correlation between the observed deflections and the known mechanical malalignments. On the other hand, if the measured geometrical malalignments are considerably greater, there should be a rather good correlation.

The results of one such test on the 4.5 BR Rocket with excessively large measured geometrical malalignments are plotted in figure 3.394a. The solid line is the theoretically expected slope on the basis of linear thrust malalignment alone. The dotted line is the correlation curve; that is, the best linear fit to the actual set of points. Such decided correspondence between deflection and malalignment—and between the observed and theoretically predicted lines—is seldom observed, since the geometrical malalignments are generally of the same order of magnitude as the gas malalignments. The fact that the two lines do not coincide in the present case is presumably due partly to possible systematic effects, such as wind, and partly

to the fact that a completely random distribution of the gas malalignment was not attained with only 25 rounds. The presence of this gas malalignment effectively establishes an upper limit to the accuracy of rocket fire, with unrotated, fin-stabilized rockets.

Values of the deflection-malalignment ratio, ϑ_R/R_M , for the 4.5 BR have been computed from the slopes of a number of plots of the type shown in figure 3.394a. These have been reduced to zero quadrant elevation and plotted as a function of burning time (which depends on temperature) in figure 3.394b, together with the theoretically expected curve for this rocket. Each point represents one day's test, the number of rounds differing in each. The results presented in the above figures constitute probably as good experimental evidence as one can find that rockets, at least the 4.5 BR, follow the general theory of yaw and deflection as given in 3.39.

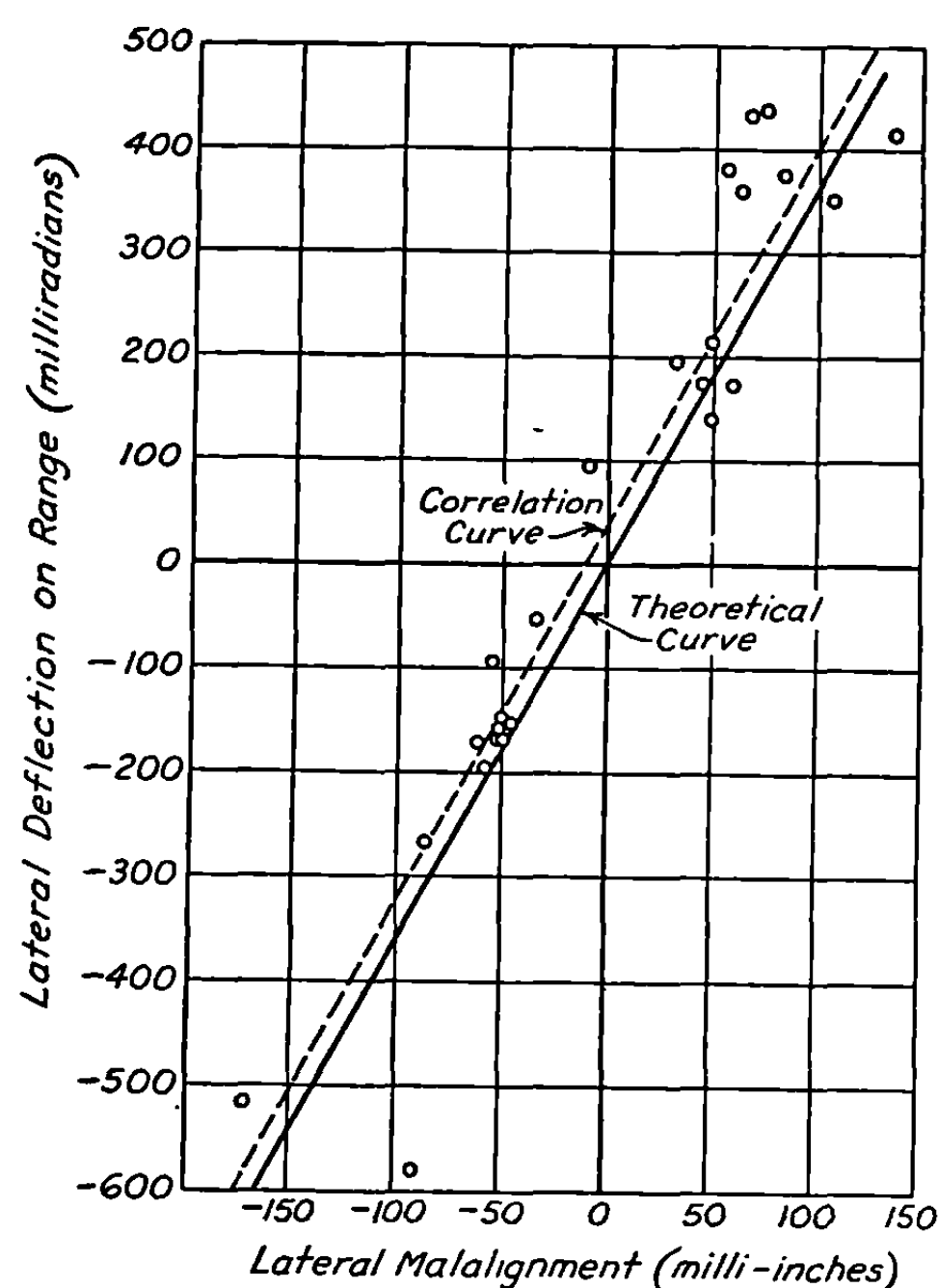


FIGURE 3.394a.—Experimental deflection-malalignment curve for the 4.5 BR.

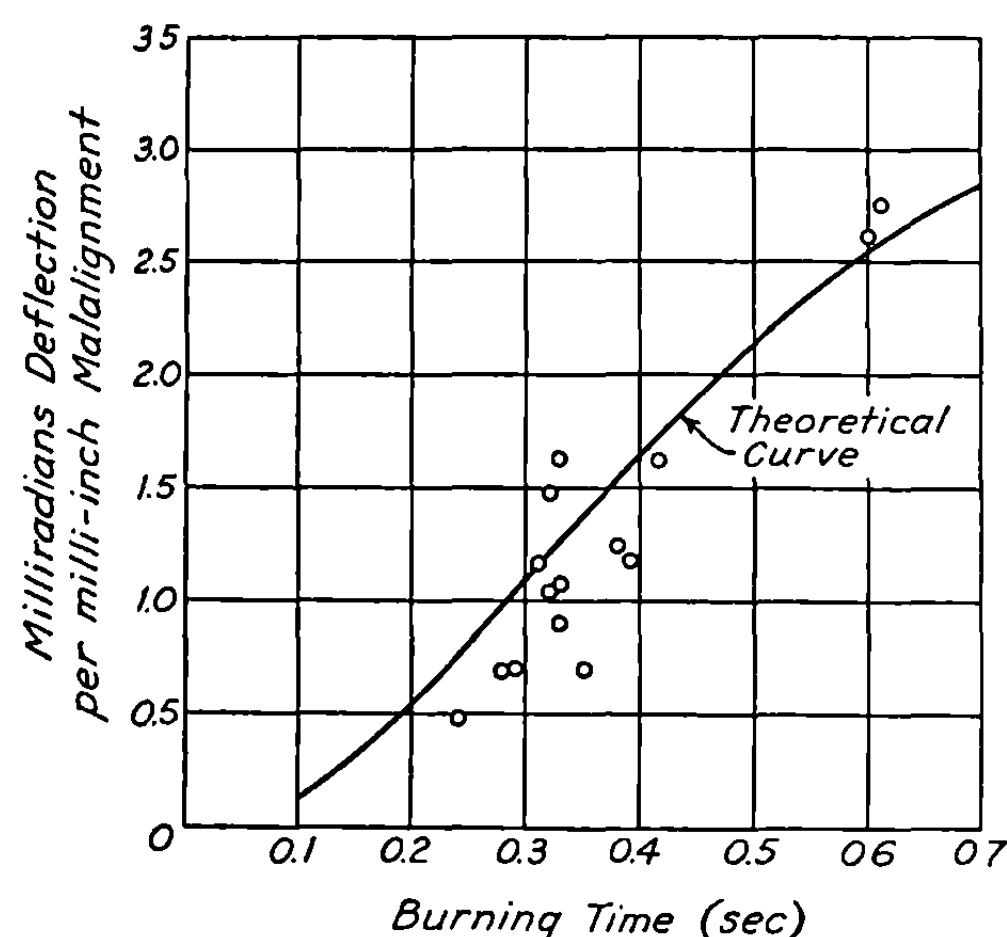


FIGURE 3.394b.—Deflection-malalignment ratio for the 4.5 BR.

3.4 Further Solutions

3.41 Effect of a Constant Angular Thrust Malalignment.—The angular thrust malalignment arises from the fact that the axis of thrust is generally not parallel to the axis of the rocket, the angle between the two axes being β_M . This enters merely as an inhomogeneous term, β_M , in 3.33 (15); and we shall determine its contribution to the yaw and deflection by using the appropriate Green's functions.

Comparison of 3.37 (2) and 3.33 (15) shows that in this case $h(\zeta) = \beta_M$. Hence if we use 3.37 (8), (9) and (10) together with 3.33 (25) to determine the characteristic functions for angular malalignment, we find that they are

$$\Delta_\beta(\zeta_p, \zeta) = - \int_{\zeta_p}^{\zeta} \Delta_\delta(u, \zeta) \frac{du}{u}, \quad (1)$$

$$\Phi_\beta(\zeta_p, \zeta) = - \int_{\zeta_p}^{\zeta} \Phi_\delta(u, \zeta) \frac{du}{u}, \quad (2)$$

$$\Theta_\beta(\zeta_p, \zeta) = - \int_{\zeta_p}^{\zeta} \Theta_\delta(u, \zeta) \frac{du}{u}, \quad (3)$$

where Δ_δ , Φ_δ , and Θ_δ are given explicitly by 3.34 (18), (19), and (20).

It will be recognized, however, that the above integrals are identical with the ones that enter in the case of gravity, 3.38 (1)–(3); and hence without repeating the integrations we can state that the characteristic functions for the angular thrust malalignment are identical with those for gravity. One could have come to the same conclusion more readily by recognizing the similarity in the two inhomogeneous terms in 3.33 (15). Since they are both constant, the corresponding characteristic functions must be identical. Therefore

$$\Delta_\beta(\zeta_p, \zeta) \equiv \Delta_\delta(\zeta_p, \zeta), \quad (4)$$

$$\Phi_\beta(\zeta_p, \zeta) \equiv \Phi_\delta(\zeta_p, \zeta), \quad (5)$$

$$\Theta_\beta(\zeta_p, \zeta) \equiv \Theta_\delta(\zeta_p, \zeta), \quad (6)$$

where Δ_δ , Φ_δ and Θ_δ are given explicitly by 3.38 (5), (8), and (11), respectively.

As with the linear thrust malalignment, the term in β_M enters into the equations for the motion in the lateral direction exactly in the same manner as it entered into the equations for the motion in the vertical plane, as given above. To generalize, then, for the complex angular thrust malalignment β_M , the contributions to the motion are given by

$$\delta_\beta = \beta_M \Delta_\beta(\zeta_p, \zeta), \quad (7)$$

$$\varphi_\beta = \beta_M \Phi_\beta(\zeta_p, \zeta), \quad (8)$$

and

$$\vartheta_\beta = \beta_M \Theta_\beta(\zeta_p, \zeta), \quad (9)$$

the motion taking place in the plane determined by β_M .

The resulting linear deflection from the launcher line or Z_0 -axis is given by

$$r_\beta = \int_{t_p}^t V \vartheta_\beta dt = 2\sigma \int_{\zeta_p}^{\zeta} \zeta \vartheta_\beta d\zeta, \quad (10)$$

or

$$r_\beta = \sigma \beta_M R_\beta(\zeta_p, \zeta), \quad (11)$$

where

$$R_\beta(\zeta_p, \zeta) \equiv R_\delta(\zeta_p, \zeta), \quad (12)$$

as given by 3.38 (22).

3.42 Effect of Fin or Aerodynamic Malalignment.—The fin or aerodynamic malalignment arises, as discussed in 2.47, from the fact that, in general, slight asymmetries in projectile shape will result in the rocket having a nonzero moment for zero yaw, the yaw angle δ_0 , corresponding to zero moment, being the so-called fin malalignment. The term in δ_0 enters in the form of $16\pi^2 \zeta^2 \delta_0$ in the inhomogeneous part of 3.33 (14). As with the other effects, we can determine the characteristic functions Δ_F , Φ_F and Θ_F for the fin malalignment by the Green's function method of 3.37.

Comparison of 3.37 (1) and 3.33 (14) shows that in this case $f(\zeta) = 16\pi^2 \zeta^2 \delta_0$. Hence if we

use 3.37 (5), (6) and (7) together with 3.33 (24) to determine the characteristic functions for fin malalignment, we find

$$\delta_F = \delta_0 \Delta_F(\zeta_p, \zeta) = \delta_0 \int_{\zeta_p}^{\zeta} 16 \pi^2 u^2 \Delta_q(u, \zeta) du, \quad (1)$$

$$\varphi_F = \delta_0 \Phi_F(\zeta_p, \zeta) = \delta_0 \int_{\zeta_p}^{\zeta} 16 \pi^2 u^2 \Phi_q(u, \zeta) du, \quad (2)$$

and

$$\vartheta_F = \delta_0 \Theta_F(\zeta_p, \zeta) = \delta_0 \int_{\zeta_p}^{\zeta} 16 \pi^2 u^2 \Theta_q(u, \zeta) du, \quad (3)$$

where Δ_q , Φ_q , and Θ_q are given explicitly by 3.34 (21), (22) and (23).

It is possible to obtain the solutions for Δ_F , Φ_F , and Θ_F by direct integration of (1)–(3) above. However, such a mathematical procedure is not necessary in this case, for the solutions can be obtained in terms of functions previously determined by proper physical arguments. In discussing fin malalignment by itself, we have assumed that the thrust axis and launcher line are co-linear, this line being chosen as the rocket axis, and that δ_0 is the angle between this line and the aerodynamic axis, the latter being the line whose yaw is proportional to the restoring moment. If now we redefine the rocket axis as being *along* the aerodynamic axis, then the rocket in this latter case has no apparent fin malalignment. However, in so orienting the rocket axis, we have introduced the angular thrust malalignment δ_0 , for the thrust now has a component normal to the rocket axis of magnitude $mG\delta_0$. It is obvious, too, that at the instant of launching the initial yaw and orientation of the new rocket axis are $\delta_p = \varphi_p = -\delta_0$. Under these conditions the yaw, orientation and deflection of the tangent are, from 3.33 (27), (28), and (29),

$$\delta_F = \delta_0 \Delta_\beta(\zeta_p, \zeta) - \delta_0 \Delta_\delta(\zeta_p, \zeta) - \delta_0 \Delta_\varphi(\zeta_p, \zeta) + \delta_0, \quad (4)$$

$$\varphi_F = \delta_0 \Phi_\beta(\zeta_p, \zeta) - \delta_0 \Phi_\delta(\zeta_p, \zeta) - \delta_0 \Phi_\varphi(\zeta_p, \zeta) + \delta_0, \quad (5)$$

and

$$\vartheta_F = \delta_0 \Theta_\beta(\zeta_p, \zeta) - \delta_0 \Theta_\delta(\zeta_p, \zeta) - \delta_0 \Theta_\varphi(\zeta_p, \zeta), \quad (6)$$

where the final δ_0 in (4) and (5) has been added in order to give the yaw and orientation of the original (i. e., thrust) axis rather than of the new (i. e., aerodynamic) axis.

Comparison of (4), (5), (6) with (1), (2), (3) shows that since $\Delta_\varphi = 0$, $\Phi_\varphi = \Theta_\varphi = 1$, $\Delta_\beta = \Delta_g$, $\Phi_\beta = \Phi_g$, and $\Theta_\beta = \Theta_g$, the characteristic functions we are seeking are given by

$$\Delta_F(\zeta_p, \zeta) = \Delta_g(\zeta_p, \zeta) - \Delta_\delta(\zeta_p, \zeta) + 1, \quad (7)$$

$$\Phi_F(\zeta_p, \zeta) = \Phi_g(\zeta_p, \zeta) - \Phi_\delta(\zeta_p, \zeta), \quad (8)$$

$$\Theta_F(\zeta_p, \zeta) = \Theta_g(\zeta_p, \zeta) - \Theta_\delta(\zeta_p, \zeta) - 1, \quad (9)$$

where Δ_g , Φ_g and Θ_g are given explicitly by 3.38 (5), (8) and (11); and Δ_δ , Φ_δ and Θ_δ are given by 3.34 (18), (19), and (20).

Since, as with all the other effects except gravity, the term in δ_0 enters into the equations (see 3.24) for the motion in the lateral direction exactly in the same manner as it entered into the equations for the motion in the vertical plane as given above, the solution for the effect of

fin malalignment on the motion in the lateral plane will be identical with (3) above, with δ_0 as the component of the fin malalignment in the lateral plane. We can generalize for any fin malalignment angle by writing (3) in the complex vector form as

$$\vartheta_F = \delta_0 \Theta_F(\zeta_p, \zeta), \quad (10)$$

or

$$\vartheta_F = \delta_0 [\Theta_g(\zeta_p, \zeta) - \Theta_\delta(\zeta_p, \zeta) - 1], \quad (11)$$

which points out directly that the motion takes place in the plane determined by δ_0 .

The resulting linear deflection from the launcher line or Z_0 -axis is given by

$$r_F = \int_{t_p}^t V \vartheta_F dt = 2\sigma \int_{\zeta_p}^{\zeta} \zeta \vartheta_F d\zeta, \quad (12)$$

or

$$r_F = \sigma \delta_0 R_F(\zeta_p, \zeta), \quad (13)$$

where

$$R_F(\zeta_p, \zeta) = 2 \int_{\zeta_p}^{\zeta} \zeta \Theta_F(\zeta_p, \zeta) d\zeta. \quad (14)$$

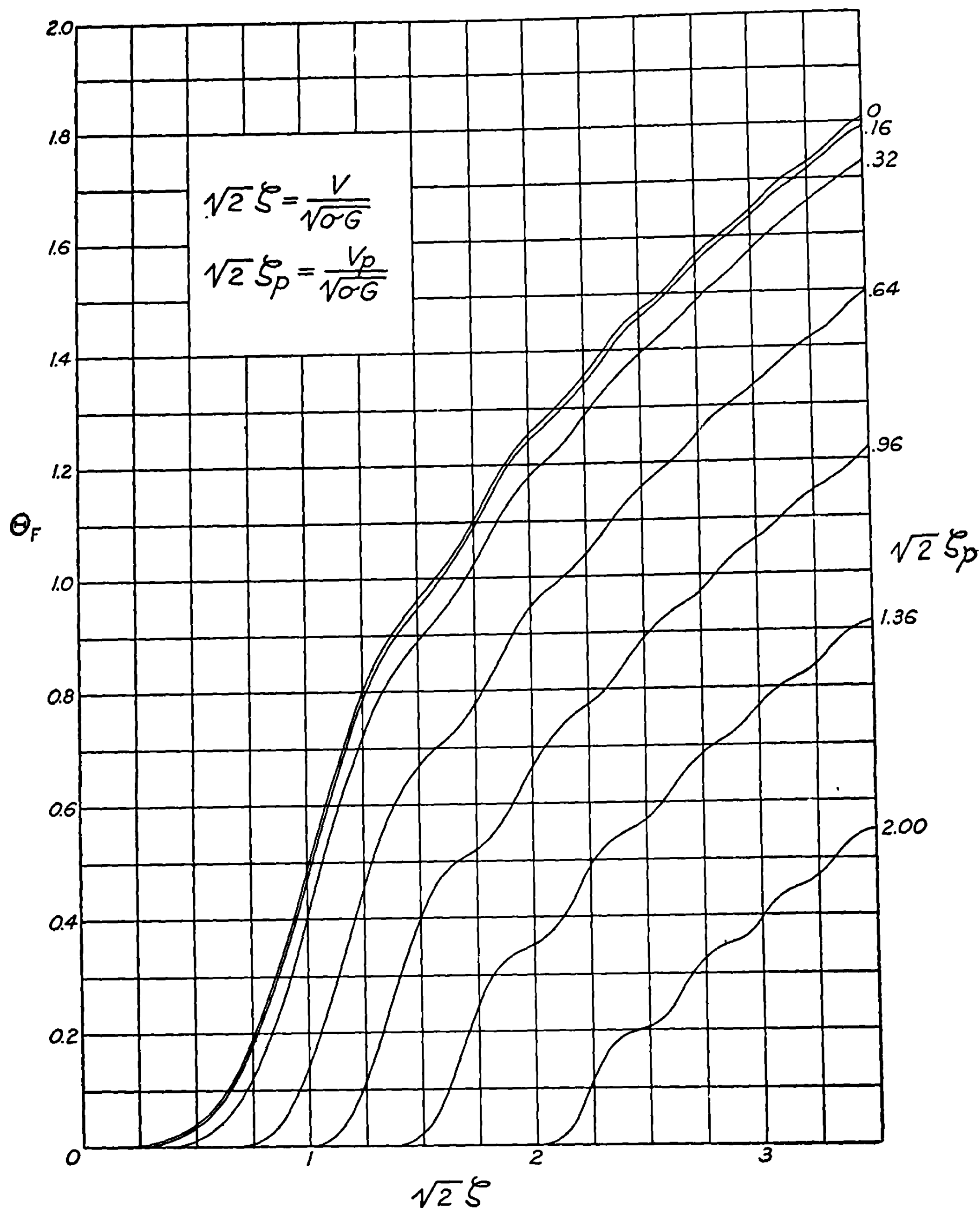
However, in view of (9),

$$\dot{R}_F(\zeta_p, \zeta) = R_g(\zeta_p, \zeta) - R_\delta(\zeta_p, \zeta) - (\zeta^2 - \zeta_p^2), \quad (15)$$

where $R_g(\zeta_p, \zeta)$ and $R_\delta(\zeta_p, \zeta)$ are given explicitly by 3.38 (22) and 3.35 (9). In figure 3.42, Θ_F has been plotted as a function of $2^{\frac{1}{2}}\zeta$ for a number of values of $2^{\frac{1}{2}}\zeta_p$. It will be observed that the function rises very sharply immediately after launching, but after the rocket has made about one yaw oscillation the slope decreases and the function behaves very much like Θ_g . Since the characteristic quantity Θ_g does not approach a finite value as $\zeta \rightarrow \infty$, it follows that Θ_F similarly will continue to increase as the burning progresses. This is of importance, then, in the case of long-burning rockets. In practice, however, rockets are generally assembled carefully enough so that δ_0 is extremely small. In that case $\vartheta_F = \delta_0 \Theta_F$ will be negligible. Similar remarks apply to the linear deflection r_F . As a particular example, for our "typical" rocket with $G = 1,000$ ft./sec.², $\sigma = 250$ feet, $V_b = 1,000$ ft./sec., $p = 5$ feet ($V_p = 100$ ft./sec.), $r_F/\delta_0 = 378$ ft./rad. Hence, even for δ_0 as great as $1^\circ (= 0.017$ rad.), $r_F \doteq 6.5$ feet, which is quite small.

3.43 Effect of a Uniform Wind Normal to the Launcher Line.—It has been assumed in the previous discussions that the rocket was launched in a uniform atmosphere free from wind. In that case the velocity of the rocket relative to the ground was identical with the velocity relative to the air. In the case of firing in the presence of a wind, one can write and proceed to solve the equations of motion, allowing for the fact that the aerodynamic forces and moments depend upon the velocity of the rocket relative to the air.

We are now in a position, however, to calculate the wind effect rather simply by means of a suitable change in the coordinate system. We assume that the wind is parallel to the ground, uniform in magnitude and direction, does not vary with altitude, and is small compared to the velocity of the rocket at the end of burning. We shall find that, contrary to what one might expect, the effect of the aerodynamic lift or cross-wind force on the rocket is small and can be neglected.

FIGURE 3.42.—Characteristic function $\Theta_F(\xi_p, \xi)$.

The relation of the wind velocity vector \mathbf{W} to the fixed $O_0X_0Y_0Z_0$ coordinate system of figure 3.21a is shown in figure 3.43a. In order to specify both the direction and magnitude of \mathbf{W} , it will usually be given in terms of W_{\parallel} and W_{\perp} , the components of the wind velocity parallel and perpendicular, respectively, to the range line. W_{\parallel} is positive when the wind blows in the direction in which the launcher is pointed; W_{\perp} is positive when the wind blows from left to right as one looks down range. $W_{\perp} = W_x$ is just the component of \mathbf{W} along the X_0 -axis, while W_{\parallel} can be resolved into the components normal to, and parallel to, the launcher.

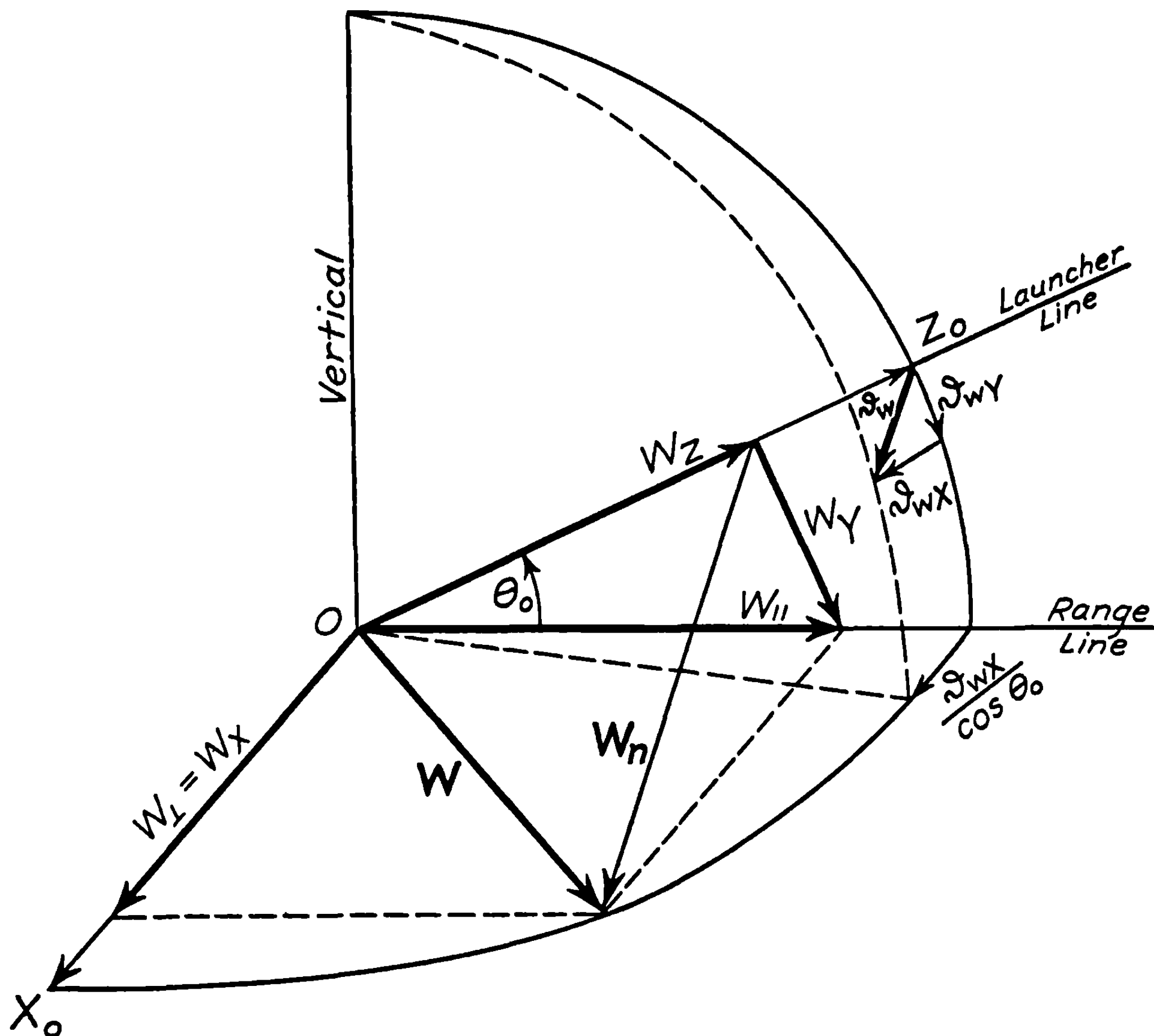


FIGURE 3.43a.—Components of the wind.

$$W_Y = W_{\parallel} \sin \theta_0,$$

and

$$W_Z = W_{\parallel} \cos \theta_0. \quad (1)$$

We now combine W_X and W_Y into a single vector, W_n , which is normal to the launcher and which is represented in our usual complex form by the expression

$$W_n = W_X + iW_Y = W_{\perp} + iW_{\parallel} \sin \theta_0. \quad (2)$$

The effects of the wind perpendicular to the launcher are different from those due to the parallel component and will be treated separately.

We consider first the effect of the normal component, W_n , of the wind vector. The deflection due to this cross wind will lie in the plane containing W_n and the launcher line; hence, again we have essentially a two-dimensional problem. It will be convenient to refer the motion of the rocket to an $O_a X_a Y_a Z_a$ coordinate system that *moves with the air*, thus having the velocity W_n relative to the fixed $O_0 X_0 Y_0 Z_0$ system and remaining parallel to it. We shall use the subscript a to designate the values of angles as measured by an observer in this moving, or air, coordinate system; while for velocities we shall use V to designate velocity with respect

3.4 FURTHER SOLUTIONS

to the air coordinate system and v to designate velocity with respect to the fixed system. This is not inconsistent with our usage up to this point, since previously the two coordinate systems coincided and either symbol could be used for velocity. As seen by an observer fixed with respect to the launcher, the situation at any instant will be as indicated²⁵ by the left half of figure 3.43b. The velocity v of the rocket can be resolved into a component v_z along the O_0Z_0 -axis and a component v_n normal to it; while the trajectory angle, ϑ , is

$$\vartheta = \tan^{-1} \frac{v_n}{v_z} \doteq \frac{v_n}{v}. \quad (3)$$

An observer who moves with the air and the $O_aX_aY_aZ_a$ coordinate system will have the transverse velocity W_n with respect to the fixed system, and hence the transverse velocity of the rocket will appear to this moving observer to be $V_n = v_n - W_n$. Both observers will regard the rocket as having the same velocity in the Z -direction, so that $V_z = v_z$. Hence from the point of view of the observer in the air coordinate system,

$$\vartheta_a = \tan^{-1} \frac{V_n}{V_z} \doteq \frac{V_n}{V} = \frac{v_n - W_n}{v} \doteq \vartheta - \frac{W_n}{v}. \quad (4)$$

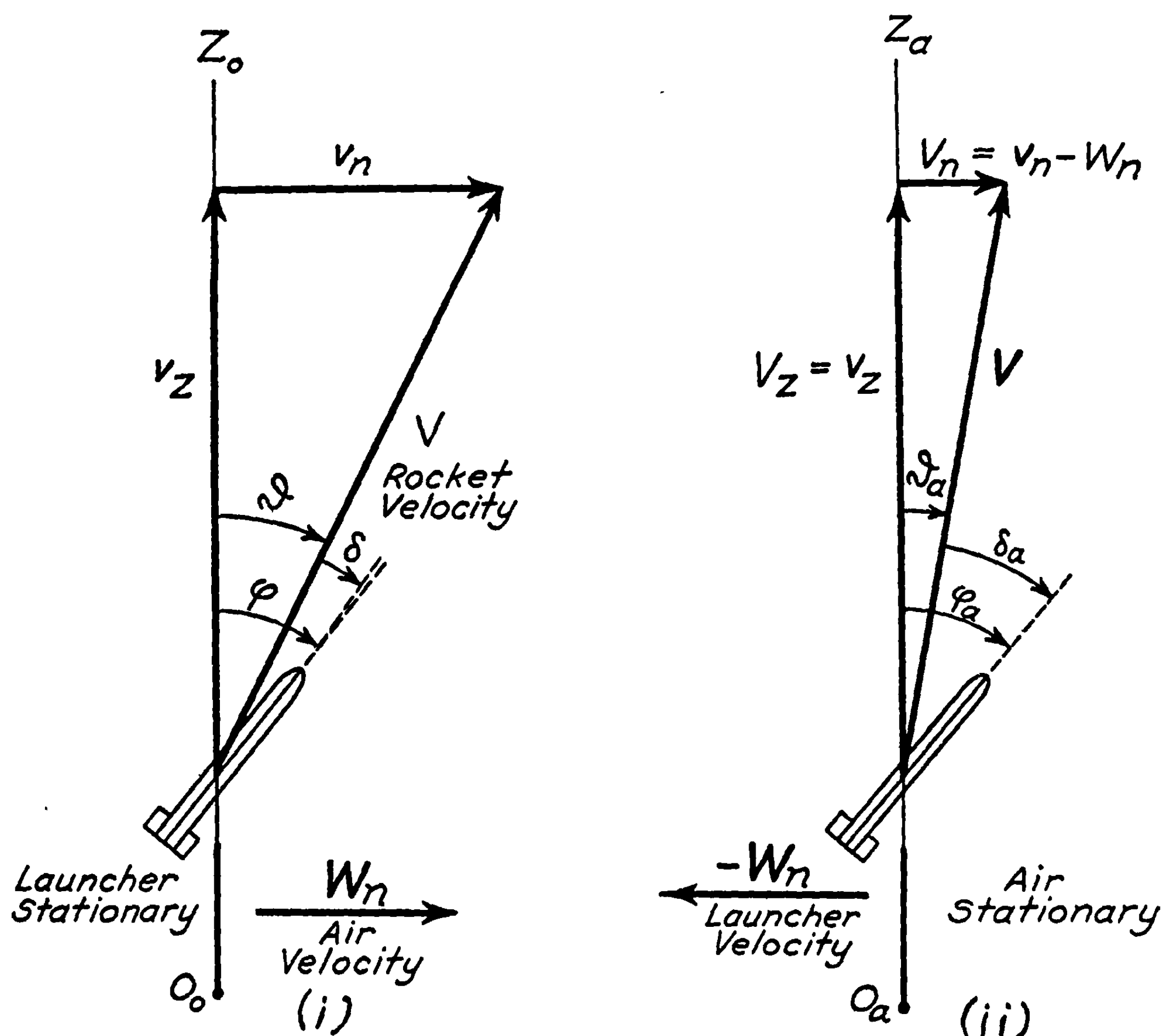


FIGURE 3.43b.—Velocity diagram in fixed and moving coordinate systems.

- (i) Situation as seen by an observer fixed with respect to launcher.
- (ii) Situation as seen by an observer moving with the air.

²⁵ The deflection due to cross wind is actually up wind. This figure is designed to show the general connections between the transverse velocities and the angles in the two cases, not to show the deflection due to cross wind.

Since the orientations of the rocket and of the axes are the same in the two systems, we have

$$\varphi_a = \varphi, \quad (5)$$

$$\delta_a = \varphi_a - \vartheta_a = \varphi - \vartheta + \frac{W_n}{v} = \delta + \frac{W_n}{v}, \quad (6)$$

and

$$\dot{\varphi}_a = \dot{\varphi}. \quad (7)$$

It is now evident that the problem of finding the motion of a rocket launched in a cross wind with $\varphi_p = \dot{\varphi}_p = \delta_p = 0$ becomes, in the moving system, identical with the problem previously solved in 3.34 and 3.35, the initial conditions being ²⁶

$$\varphi_{ap} = 0, \quad (8)$$

$$\dot{\varphi}_{ap} = 0, \quad (9)$$

and

$$\delta_{ap} = \varphi_{ap} - \vartheta_{ap} = \frac{W_n}{v_p}. \quad (10)$$

Thus the solution for the motion in this air coordinate system is that given in 3.34 and 3.35 for initial yaw. From 3.35 (3), the deflection of the tangent is given by

$$\vartheta_{aw} = \vartheta_{ad} = \delta_{ap} \Theta_\delta(\zeta_p, \zeta) = \frac{W_n}{v_p} \Theta_\delta(\zeta_p, \zeta), \quad (11)$$

where $\Theta_\delta(\zeta_p, \zeta)$ is given explicitly by 3.34 (20), and ϑ_{aw} will now be used in place of ϑ_{ad} in order to indicate that the ultimate cause of the yaw is the cross wind.

Returning now to the stationary system by using (4) we have

$$\vartheta_w = \vartheta_{aw} + \frac{W_n}{v} = \frac{W_n}{v_p} \Theta_\delta(\zeta_p, \zeta) + \frac{W_n}{v}, \quad (12)$$

for the deflection due to the wind from the point of view of a stationary observer. Since $v = v_\sigma \zeta$ and $v_p = v_\sigma \zeta_p$ we have

$$\vartheta_w = \frac{W_n}{v_\sigma} \left(\frac{1}{\zeta_p} \Theta_\delta(\zeta_p, \zeta) + \frac{1}{\zeta} \right), \quad (13)$$

or

$$\vartheta_w = \frac{W_n}{v_\sigma} \Theta_w(\zeta_p, \zeta), \quad (14)$$

where the characteristic function Θ_w is given by

$$\begin{aligned} \Theta_w(\zeta_p, \zeta) &= \frac{1}{\zeta_p} \Theta_\delta(\zeta_p, \zeta) + \frac{1}{\zeta} \\ &= 2\pi [C(2\zeta) - C(2\zeta_p)] \sin 2\pi \zeta_p^2 \\ &\quad - 2\pi [S(2\zeta) - S(2\zeta_p)] \cos 2\pi \zeta_p^2 \\ &\quad - \frac{1}{\zeta} \cos 2\pi(\zeta^2 - \zeta_p^2) + \frac{1}{\zeta}. \end{aligned} \quad (15)$$

²⁶ Of course, as the launcher length approaches zero, $v_p \rightarrow 0$, while $\varphi_{ap} = -\tan^{-1}(W_n/V_p) \rightarrow -\pi/2$. This violation of the restriction to small yaws is not as serious as might be expected; for during this early part of burning the velocity is sufficiently small so that the aerodynamic moment itself is rather small, and it does not matter whether or not it is computed accurately. The solutions which follow are thus valid even in the limit as the launcher length approaches zero.

The resulting linear deflection from the launcher line or Z_0 -axis is given by

$$r_w = \int_{t_p}^t v \vartheta_w dt = 2\sigma \int_{\zeta_p}^{\zeta} \zeta \vartheta_w d\zeta, \quad (16)$$

or

$$r_w = \frac{\sigma W_n}{v_\sigma} R_w(\zeta_p, \zeta). \quad (17)$$

The characteristic function R_w is given by

$$\begin{aligned} R_w(\zeta_p, \zeta) &= 2 \int_{\zeta_p}^{\zeta} \zeta \Theta_w(\zeta_p, \zeta) d\zeta \\ &= \frac{1}{\zeta_p} R_\delta(\zeta_p, \zeta) + 2(\zeta - \zeta_p), \end{aligned} \quad (18)$$

where R_δ is given explicitly by 3.35 (9).

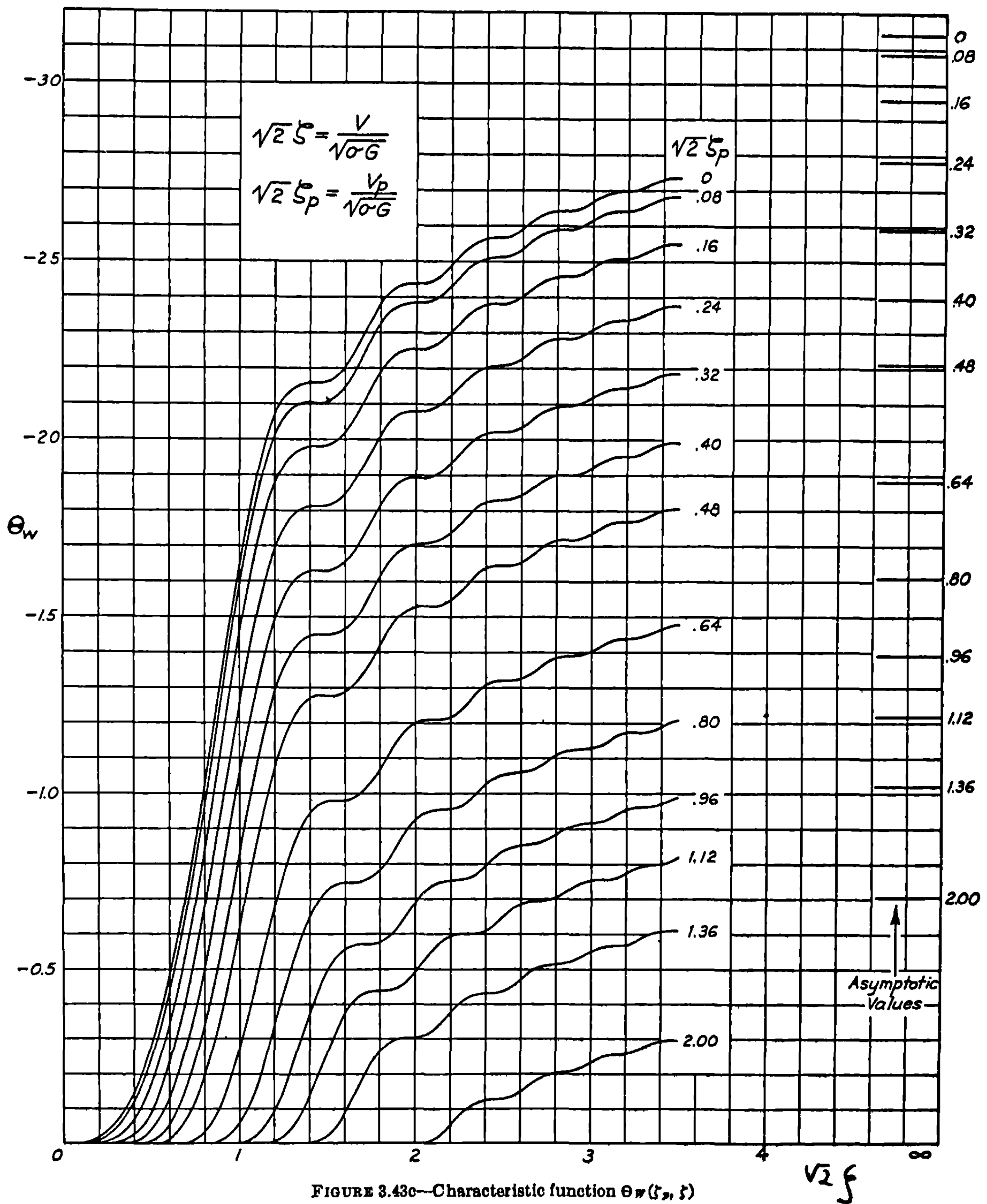
In figure 3.43c the characteristic function Θ_w is plotted as a function of $\zeta\sqrt{2}$ for a number of values of $\zeta_p\sqrt{2}$. It will be observed that the curve rises quite rapidly until the rocket has made about half a yaw oscillation, after which the function rather slowly approaches its asymptotic value. These asymptotic values to the right of the figure were attained by taking the limit of $\Theta_w(\zeta_p, \zeta)$ as $\zeta \rightarrow \infty$. The asymptotic expansion for $\Theta_w(\zeta_p, \zeta)$, namely

$$\begin{aligned} \Theta_w(\zeta_p, \zeta) &\sim \frac{1}{\zeta} + 2\pi \left\{ \left[\frac{1}{2} - C(2\zeta_p) \right] \sin 2\pi \zeta_p^2 - \left[\frac{1}{2} - S(2\zeta_p) \right] \cos 2\pi \zeta_p^2 \right\} \\ &\quad + 2\pi \sin 2\pi(\zeta^2 - \zeta_p^2) \sum_{n=0}^{\infty} \frac{(-1)^n (4n+1)!}{(2n)! 2^{6n+3} \pi^{2n+2} \zeta^{4n+3}} \\ &\quad + 2\pi \cos 2\pi(\zeta^2 - \zeta_p^2) \sum_{n=1}^{\infty} \frac{(-1)^n (4n-1)!}{(2n-1)! 2^{6n} \pi^{2n+1} \zeta^{4n+1}}, \end{aligned} \quad (19)$$

is not of much use, however, since, as can be seen from the figure, the function Θ_w cannot be approximated by its asymptotic value in the useful range of values of ζ . We note too that Θ_w is intrinsically negative, which means that the deflection ϑ_w is opposite to the direction in which the wind is blowing. This is not surprising, for during the burning period the action of the wind on the fins will tend to rotate the rocket so that it is heading into the wind, or rather into the direction of the resultant air stream. Hence the axis of thrust is deviated similarly, resulting in the deflection of the trajectory *upwind*. After burning we have the opposite effect; for the rocket will be displaced *downwind*, that is, in the direction the wind is blowing, because of the action of the downwind component of the drag.

Now (14) gives the deflection due to the component of the wind *normal* to the launcher in the plane determined by W_n and the launcher; but one is more usually interested in the effects of a cross wind or a tail wind on the deflection, and one wants the vertical and horizontal components of the deflection. If (2) is substituted in (14), one finds that

$$\vartheta_w = \vartheta_{wx} + i\vartheta_{wy} = (W_\perp + iW_\parallel \sin \theta_0) \Theta_w(\zeta_p, \zeta) / v_\sigma, \quad (20)$$

FIGURE 3.43c—Characteristic function $\Theta_W(\xi_p, \xi)$

and hence, since $\Theta_W(\xi_p, \xi)/v_\sigma$ is real, that

$$\vartheta_{WX} = \frac{W_\perp}{v_\sigma} \Theta_W(\xi_p, \xi), \quad (21)$$

and

$$\vartheta_{WY} = \frac{W_\parallel \sin \theta_0}{v_\sigma} \Theta_W(\xi_p, \xi). \quad (22)$$

To convert ϑ_{WX} into the corresponding horizontal deflection on the ground one should divide (19) by $\cos \theta_0$ as is evident from figure 3.43a.

3.44 Effect of a Uniform Wind Parallel to the Launcher Line.—We wish now to determine the effect upon the trajectory of W_z , the component of the wind parallel to the launcher, the positive direction of W_z being taken along the Z_0 -axis. It must be borne in mind that if, in the absence of this parallel wind, the rocket is undeviated from its original path as determined by the orientation of the launcher, the trajectory will remain unaltered in the presence of the parallel wind. It is only when the rocket is deviated from the launcher line due to other causes—gravity, initial yaw, wind normal to the launcher, etc.—that the wind parallel to the launcher will alter this deviation. Hence the effects that are considered below are essentially corrections to deflections due to causes other than W_z .

For the purpose at hand we consider the motion in a coordinate system $O_a X_a Y_a Z_a$ at rest with respect to the air; i. e., one moving along the Z_0 - (or Z_a -) axis with the velocity W_z , the new axes remaining parallel to the fixed axes and coinciding with them at the start of burning, $t=0$. The situation is as in the previous section, except that now the transverse velocity appears the same to the two observers. Hence $V_n=v_n$; while the Z -components of the two velocities differ, so that

$$V_z = v_z - W_z, \quad (1)$$

where, as before, V refers to velocities with respect to the air, and v refers to velocities with respect to the launcher. Thus the angles as measured by the two observers are connected by the relations

$$\varphi_a = \varphi, \quad (2)$$

$$\dot{\varphi}_a = \dot{\varphi}, \quad (3)$$

$$\vartheta_a \doteq \frac{V_n}{V_z} = \frac{v_n}{v_z} \left(1 - \frac{W_z}{v_z}\right)^{-1} \doteq \vartheta \left(1 + \frac{W_z}{v}\right), \quad (4)$$

and

$$\delta_a = \varphi_a - \vartheta_a = \delta - \frac{W_z}{v} \vartheta = \delta \left(1 + \frac{W_z}{v}\right) - \frac{W_z}{v} \varphi. \quad (5)$$

If each observer defines ζ in the usual manner as the velocity of the rocket (relative to him) divided by the parameter v_σ , then

$$\zeta_a = \frac{V}{v_\sigma} \doteq \frac{v - W_z}{v_\sigma} = \zeta - \frac{W_z}{v_\sigma} \quad (6)$$

gives the connections between the values of ζ used by the two observers. For the observer moving with the air, the problem is identical with those already solved in 3.34–3.43, and hence the solutions previously found give the solution for this observer provided we use the initial conditions and values of ζ for the air system as computed from (2)–(6). The deflection relative to the stationary observer can be computed from (4).

As an example let us compute the deflection at the end of burning due to an initial orientation φ_p when the rocket is launched in the presence of a tail wind $W_{||}$. The effect of the component $W_{||} \sin \theta_0$ normal to the launcher can be computed by the method of the previous section. Here we shall be concerned only with the effect of the component, $W_z = W_{||} \cos \theta_0$, parallel to the launcher line. In the absence of any wind, we have from 3.34 (24), (25) and (26)

$$\delta_\varphi(\zeta_p, \zeta) = 0, \quad \varphi_\varphi(\zeta_p, \zeta) = \varphi_p, \quad \vartheta_\varphi(\zeta_p, \zeta) = \varphi_p. \quad (7)$$

In the presence of W_z , the observer moving with the air will find [see (5), (2), and (3) above] the initial conditions to be

$$\delta_{ap} = -\frac{W_z}{v_p} \varphi_p, \quad (8)$$

$$\varphi_{ap} = \varphi_p, \quad (9)$$

and

$$\dot{\varphi}_{ap} = 0. \quad (10)$$

Hence, while in the ground coordinate system the rocket has only an initial orientation φ_p with $\delta_p = \dot{\varphi}_p = 0$, in the air coordinate system the rocket has not only an initial orientation φ_{ap} but an initial yaw δ_{ap} as well. As a result, the deflection in the latter system is

$$\begin{aligned} \vartheta_{a\varphi} &= \varphi_{ap} + \delta_{ap} \Theta_\delta(\zeta_{ap}, \zeta_{ab}) \\ &= \varphi_p \left[1 - \frac{W_z}{v_p} \Theta_\delta\left(\zeta_p - \frac{W_z}{v_\sigma}, \zeta_b - \frac{W_z}{v_\sigma}\right) \right]. \end{aligned} \quad (11)$$

And by (4) we have for the deflection in the ground coordinate system

$$\begin{aligned} \vartheta_\varphi &\doteq \left(1 - \frac{W_z}{v_b}\right) \vartheta_{a\varphi} \\ &= \left(1 - \frac{W_z}{v_b}\right) \varphi_p \left[1 - \frac{W_z}{v_p} \Theta_\delta\left(\zeta_p - \frac{W_z}{v_\sigma}, \zeta_b - \frac{W_z}{v_\sigma}\right) \right]. \end{aligned} \quad (12)$$

The above happens to be the only case in which one perturbing factor gives rise to two in the air coordinate system, and for that reason was chosen as the example. In similar manner it can be shown that the following are the approximate expressions for deflections in the presence of a tail wind:

$$\vartheta_\delta \doteq \left(1 - \frac{W_z}{v_b}\right) \left(1 + \frac{W_z}{v_p}\right) \delta_p \Theta_\delta\left(\zeta_p - \frac{W_z}{v_\sigma}, \zeta_b - \frac{W_z}{v_\sigma}\right), \quad (13)$$

$$\vartheta_\varphi \doteq \left(1 - \frac{W_z}{v_b}\right) \varphi_p \left[1 - \frac{W_z}{v_p} \Theta_\delta\left(\zeta_p - \frac{W_z}{v_\sigma}, \zeta_b - \frac{W_z}{v_\sigma}\right) \right], \quad (14)$$

$$\vartheta_q \doteq \left(1 - \frac{W_z}{v_b}\right) q_p t_\delta \Theta_q\left(\zeta_p - \frac{W_z}{v_\sigma}, \zeta_b - \frac{W_z}{v_\sigma}\right), \quad (15)$$

$$\vartheta_g \doteq \left(1 - \frac{W_z}{v_b}\right) \frac{ig \cos \theta_0}{G} \Theta_g\left(\zeta_g - \frac{W_z}{v_\sigma}, \zeta_b - \frac{W_z}{v_\sigma}\right), \quad (16)$$

$$\vartheta_R \doteq \left(1 - \frac{W_z}{v_b}\right) \frac{2\sigma}{K^2} R_M \Theta_R\left(\zeta_p - \frac{W_z}{v_\sigma}, \zeta_b - \frac{W_z}{v_\sigma}\right), \quad (17)$$

$$\vartheta_w \doteq \left(1 - \frac{W_z}{v_b}\right) \frac{W_n}{v_\sigma} \Theta_w\left(\zeta_p - \frac{W_z}{v_\sigma}, \zeta_b - \frac{W_z}{v_\sigma}\right). \quad (18)$$

Throughout the above expressions the values of ζ_p and ζ_b are those used in the absence of wind. It is usually satisfactory to neglect W_z/v_σ compared to ζ_b , but it may not be possible to neglect it compared to ζ_p . It must be remembered in using the approximate formulae that terms of

the order of $(W_z/v_b)^2$ and $(W_z/v_p)^2$ have been neglected compared to unity. In any case the effects of W_z are quite small and can usually be neglected.

3.5 Effect of the Damping Terms

In reducing the equations of motion to integrable form in 3.33, it was found convenient to neglect the so-called damping terms, that is the terms containing C_i , the cross-force coefficient; C_a , the aerodynamic damping coefficient; and K_{JD} , the jet damping coefficient. This was justified on the grounds that during the early part of burning, when the major features of the motion are determined, the terms containing C_i and K_{JD} were quite small compared to the aerodynamic restoring moment, and the cross force was negligible compared to the component of the jet force normal to the trajectory. It remains for us now to verify this by evaluating the effects of the damping terms on the motion of the rocket.

It is clear that if, in the absence of the damping terms, the rocket is undeviated from its original path as determined by the orientation of the launcher, the trajectory will remain unaltered when the damping terms are present. It is only when the rocket is deviated from the launcher line by disturbing factors, such as gravity, initial yaw, mallaunching, malalignment, or wind, that the damping terms will alter this deviation. Hence the yaws and deflections that are considered herein are essentially those due to causes other than the damping terms.

The complete equations of motion in terms of the dimensionless parameter ζ are, from 3.33 (8)–(10)

$$\varphi'' + \frac{C_a \rho A l^2 \sigma \zeta + t_\sigma K_{JD}}{m K^2} \varphi' + 16 \pi^2 \zeta^2 \delta = -\frac{2 \sigma R_M}{K^2} + 16 \pi^2 \zeta^2 \delta_0, \quad (1)$$

$$\zeta \vartheta' - \delta - \frac{C_i \rho A \sigma}{m} \zeta^2 \delta = \frac{g \cos \theta_0}{G} + \beta_M, \quad (2)$$

and

$$\varphi - \vartheta - \delta = 0. \quad (3)$$

In 3.3 and 3.4 these equations have been solved under the condition that $C_a = C_i = K_{JD} = 0$. We shall now attempt to determine the effects of the damping terms by considering them as perturbations to the main effects. The zero'th-order solutions already determined for $C_a = C_i = K_{JD} = 0$ will therefore be designated by the superscript zero; e. g., ϑ^0 is the unperturbed deflection resulting from gravity. Since the damping terms are small, we may expect that the perturbed values of δ , φ , ϑ will differ but little from the corresponding unperturbed quantities δ^0 , φ^0 , ϑ^0 ; and if we write

$$\delta = \delta^0 + \delta^I, \quad (4)$$

$$\varphi = \varphi^0 + \varphi^I, \quad (5)$$

and

$$\vartheta = \vartheta^0 + \vartheta^I, \quad (6)$$

we may expect δ^I , φ^I , and ϑ^I to be small. (Were it not that the symbol Δ is already used for characteristic functions, one would write $\Delta\delta$ rather than δ^I for the change in δ due to the damping coefficients.)

Substituting (4)–(6) into (1)–(3), and making use of the fact that δ^0 , φ^0 and ϑ^0 satisfy the equations

$$\varphi^{0''} + 16\pi^2 \zeta^2 \delta^0 = -(2\sigma/K^2)R_M + 16\pi^2 \zeta^2 \delta^0, \quad (7)$$

$$\zeta \vartheta^{0'} - \delta^0 = (g/G) \cos \theta_0 + \beta_M, \quad (8)$$

and

$$\varphi^0 - \vartheta^0 - \delta^0 = 0, \quad (9)$$

we have

$$\varphi^{I''} + 16\pi^2 \zeta^2 \delta^I = -\frac{C_a \rho A l^2 \sigma}{m K^2} \zeta \varphi^{0'} - \frac{K_{JD} t_\sigma}{m K^2} \varphi^{0'}, \quad (10)$$

$$\zeta \vartheta^{I'} - \delta^I = (C_i \rho A \sigma / m) \zeta^2 \delta^0, \quad (11)$$

and

$$\varphi^I - \vartheta^I - \delta^I = 0, \quad (12)$$

where the higher order terms that contain $C_a \varphi^{I'}$, $K_{JD} \varphi^{I'}$, or $C_i \delta^I$ have been neglected.

If the known functions $\delta^0(\zeta)$ and $\varphi^{0'}(\zeta)$ for the yaw and orientation due to any particular cause, for example, those due to initial yaw, are substituted into (10), (11), and (12), these equations can be solved for δ^I , φ^I , and ϑ^I , giving the desired first-order corrections. Now since (10)–(12) are similar in form to 3.37 (1)–(3), one can employ the Green's function method of that section to determine δ^I , φ^I , and ϑ^I , the Green's functions being the same as in 3.37. It is evident from (10)–(12) that the effects of the terms in C_a , K_{JD} , and C_i combine linearly and hence that the effect of each coefficient can be considered separately.

Because of the complicated nature of the integrands, it will generally not be possible to perform the indicated integrations. In some cases suitable simplifying assumptions might lead to an approximate general solution. However, when one is interested in determining the effect of one of the damping terms for some particular value of ζ the simplest procedure is to carry out the integration by numerical methods. Since no great accuracy is usually required, this can be done in a few minutes time with the aid of the Green's functions tabulated in appendix C.

3.51 Effect of the Cross Force.—It will suffice, as examples, to determine the effect of the cross force on the deflections resulting from initial yaw and mallaunching. If one is interested in the effect of the cross force on the deflection due to any other cause, the procedure is analogous to the one we now employ.

We consider first the effect of the cross force on the deflection due to initial yaw. Comparison of 3.37 (2) with 3.5 (11) shows that in this case

$$\begin{aligned} h_\delta(\zeta) &= \frac{C_i \rho A \sigma}{m} \zeta^2 \delta_\delta^0 \\ &= \frac{C_i \rho A \sigma}{m} \zeta^2 \delta_p \Delta_\delta^0(\zeta_p, \zeta), \end{aligned} \quad (1)$$

where $\Delta_\delta^0(\zeta_p, \zeta)$ is given explicitly by 3.34 (18) where the superscript was not needed. Hence, by 3.37 (10)

$$\begin{aligned} \vartheta_\delta^I(\zeta_p, \zeta) &= - \int_{\zeta_p}^{\zeta} \frac{h_\delta(u)}{u} \Theta_\delta^0(u, \zeta) du \\ &= - \frac{C_i \rho A \sigma \delta_p}{m} \int_{\zeta_p}^{\zeta} u \Delta_\delta^0(\zeta_p, u) \Theta_\delta^0(u, \zeta) du, \end{aligned} \quad (2)$$

where $\Theta_s^0(u, \zeta)$ is given explicitly by 3.34 (20). By analogy with the previously defined characteristics functions, we write

$$\vartheta_s^I(\zeta_p, \zeta) = -\frac{C_{1\rho} A \sigma \delta_p}{m} \Theta_s^I(\zeta_p, \zeta), \quad (3)$$

where

$$\Theta_s^I(\zeta_p, \zeta) = \int_{\zeta_p}^{\zeta} u \Delta_s^0(\zeta_p, u) \Theta_s^0(u, \zeta) du. \quad (4)$$

As mentioned before, this integral is best carried out by numerical methods. For our "typical" rocket with $V_b = 1,000$ ft./sec., $G = 1,000$ ft./sec.², $\sigma = 250$ feet and $p = 5$ feet, we find $\Theta_s^I = -.0068$. Under the same conditions, from figure 3.35a, $\Theta_s^0 = -0.410$. Also, from 3.32 (11), $C_{1\rho} A / 2m \approx 10^{-3}$ feet⁻¹. Hence, by 3.5 (6) the ratio of the first order correction to the unperturbed deflection is

$$\frac{\vartheta_s^I}{\vartheta_s^0} = -\frac{C_{1\rho} A \sigma}{m} \frac{\Theta_s^I}{\Theta_s^0} = -8.3 \times 10^{-3}; \quad (5)$$

which shows that the effect of the cross force on the deflection due to initial yaw is less than 1 percent.

It will be of interest to see what the cross force does in the case of mallaunching. Comparison of 3.37 (2) with 3.5 (11) shows that in this case

$$\begin{aligned} h_q(\zeta) &= \frac{C_{1\rho} A \sigma}{m} \zeta^2 \delta_q^0 \\ &= \frac{C_{1\rho} A \sigma}{m} \zeta^2 q_p t_\sigma \Delta_q^0(\zeta_p, \zeta), \end{aligned} \quad (6)$$

where Δ_q^0 is given explicitly by 3.34 (21). Hence by 3.37 (10)

$$\begin{aligned} \vartheta_q^I(\zeta_p, \zeta) &= -\int_{\zeta_p}^{\zeta} \frac{h_q(u)}{u} \Theta_s^0(u, \zeta) du \\ &= -\frac{C_{1\rho} A \sigma q_p t_\sigma}{m} \int_{\zeta_p}^{\zeta} u \Delta_q^0(\zeta_p, u) \Theta_s^0(u, \zeta) du, \end{aligned} \quad (7)$$

where Θ_s^0 is given explicitly by 3.34 (20). We now write

$$\vartheta_q^I(\zeta_p, \zeta) = -\frac{C_{1\rho} A \sigma q_p t_\sigma}{m} \Theta_q^I(\zeta_p, \zeta), \quad (8)$$

where

$$\Theta_q^I(\zeta_p, \zeta) = \int_{\zeta_p}^{\zeta} u \Delta_q^0(\zeta_p, u) \Theta_s^0(u, \zeta) du. \quad (9)$$

For a rocket having the same characteristics as stated above, we find $\Theta_q^I = -0.0105$; while, from figure 3.36a $\Theta_q^0 = 0.135$. Hence, the ratio of the first order correction to the unperturbed deflection in this case is

$$\frac{\vartheta_q^I}{\vartheta_q^0} = -\frac{C_{1\rho} A \sigma}{m} \frac{\Theta_q^I}{\Theta_q^0} = 0.038. \quad (10)$$

Although somewhat greater than in the case of initial yaw the error resulting from neglecting the cross force in computing the deflection due to mallaunching is still only 4 percent.

The errors in other cases are similarly small.

3.52 Effect of the Aerodynamic Damping Moment.—Since one would normally expect the effect of the aerodynamic damping moment to be greatest in the case of mallaunching, we shall consider only that case. The determination of the effect of the aerodynamic damping on the deflection due to any other cause is analogous.

Comparison of 3.37 (1) with 3.5 (10) shows that in this case

$$\begin{aligned} f_a(\zeta) &= -\frac{C_a \rho A l^2 \sigma}{m K^2} \zeta \varphi_a^{0'} \\ &= -\frac{C_a \rho A l^2 \sigma}{m K^2} \zeta q_p t_\sigma \Phi_a^{0'}(\zeta_p, \zeta), \end{aligned} \quad (1)$$

where, from 3.34 (22),

$$\Phi_a^{0'}(\zeta_p, \zeta) = \cos 2\pi(\zeta^2 - \zeta_p^2). \quad (2)$$

Hence, by 3.37 (7),

$$\begin{aligned} \vartheta_a^I(\zeta_p, \zeta) &= \int_{\zeta_p}^{\zeta} f_a(u) \Theta_a^0(u, \zeta) du \\ &= -\frac{C_a \rho A l^2 \sigma q_p t_\sigma}{m K^2} \int_{\zeta_p}^{\zeta} u \cos 2\pi(u^2 - \zeta_p^2) \Theta_a^0(u, \zeta) du, \end{aligned} \quad (3)$$

where Θ_a^0 is given explicitly by 3.34 (23). We now write

$$\vartheta_a^I(\zeta_p, \zeta) = -\frac{C_a \rho A l^2 \sigma q_p t_\sigma}{m K^2} \Theta_a^I(\zeta_p, \zeta), \quad (4)$$

where

$$\Theta_a^I(\zeta_p, \zeta) = \int_{\zeta_p}^{\zeta} u \cos 2\pi(u^2 - \zeta_p^2) \Theta_a^0(u, \zeta) du. \quad (5)$$

Carrying out the above integration by numerical methods for the case of our “typical” rocket whose characteristics are given in 3.51, we find $\Theta_a^I = 0.0034$. Under the same conditions, from figure 3.36, $\Theta_a^0 = 0.135$. Also from 3.32 (11), $C_a \rho A l^2 / 2m K^2 \approx 3 \times 10^{-3}$ feet⁻¹. Hence, by 3.5 (6) the ratio of the first order correction to the unperturbed deflection is

$$\frac{\vartheta_a^I}{\vartheta_a^0} = -\frac{C_a \rho A l^2 \sigma}{m K^2} \frac{\Theta_a^I}{\Theta_a^0} = -3.8 \times 10^{-2}. \quad (6)$$

We see then that the introduction of the aerodynamic damping moment introduces a very small correction to the deflection in its absence.

3.53 Effect of Jet Damping.—As with the aerodynamic damping we shall consider the effect of the jet damping on the deflection due to mallaunching only. In this case, comparison of 3.37 (1) with 3.5 (10) shows that

$$\begin{aligned} f_a(\zeta) &= -\frac{K_{JD} t_\sigma}{m K^2} \varphi_a^{0'} \\ &= -\frac{K_{JD} t_\sigma^2 q_p}{m K^2} \cos 2\pi(\zeta^2 - \zeta_p^2), \end{aligned} \quad (1)$$

where $\varphi_a^{0'}$ was taken from 3.52 (2). By 3.37 (7), the deflection is given by

$$\vartheta_a^I(\zeta_p, \zeta) = \int_{\zeta_p}^{\zeta} f_a(u) \Theta_a^0(u, \zeta) du$$

$$= -\frac{K_{JD}t_g^2 q_p}{mK^2} \Theta_q^I(\zeta_p, \zeta), \quad (2)$$

where in this case the characteristic function Θ_q^I is given by

$$\Theta_q^I(\zeta_p, \zeta) = \int_{\zeta_p}^{\zeta} \cos 2\pi(u^2 - \zeta_p^2) \Theta_q^0(u, \zeta) du. \quad (3)$$

By numerical integration of (3) we find, for the conditions of our "typical" rocket, $\Theta_q^I = 0.0018$; while $\Theta_q^0 = 0.135$. Also, from 2.26 (17), $K_{JD}/mK^2 \approx 0.4/t_b$. Hence, the ratio of the first order correction to the unperturbed deflection is

$$\frac{\vartheta_q^I}{\vartheta_q^0} = -\frac{K_{JD}t_g}{mK^2} \frac{\Theta_q^I}{\Theta_q^0} = -3.8 \times 10^{-3}. \quad (4)$$

3.6 Effects of Slow Spin

We have seen that the principal source of dispersion in well-made fin-stabilized rockets is the gas malalignment, which, in practice, produces a dispersion of about 20 mils in ground firing. One of the simplest ways to reduce the effect of the gas malalignment is to rotate the rocket about its longitudinal axis so that the malalignment tends to yaw the rocket first in one direction and then in the other, thus leaving only a small average effect. Through the use of inclined jets (see ch. 7) the rocket can be given a spin (i. e., angular velocity about the longitudinal axis) proportional to its velocity so that it rotates very rapidly at the end of burning. When this is done it is not necessary to have fins on the rocket, because, as discussed in later chapters, the gyroscopic effects of the spin will suffice for stabilization. Such rockets, called spin-stabilized rockets, not only are more accurate than nonrotating rockets but also are more convenient to store, handle, and fire than rockets having bulky and somewhat fragile fins. Both nonrotating fin-stabilized rockets and spin-stabilized rockets have been used extensively and each has its own field of special usefulness. If a case should arise in which it seems desirable to extend the field of usefulness of a particular fin-stabilized rocket by reducing its dispersion by a factor of two or three, it should be possible to do so by using some device that gives the rocket an angular velocity about its longitudinal axis. Such a spin in a fin-stabilized rocket will be referred to as *slow spin* in order to distinguish it from the more rapid spin that is characteristic of spin-stabilized rockets.

A rough estimate of the effectiveness of the slow spin in decreasing the dispersion may be obtained in the following manner. It can be shown by the methods developed in 9.25 that the effects of malalignment tend to cancel out after the first quarter of a revolution. In 3.12 it was shown that during the early part of burning the deflection of the trajectory due to a constant malalignment is proportional to the distance traveled. Hence the dispersion due to malalignment in a rocket having slow spin should be roughly proportional to the distance traveled during the first quarter of a revolution. Now the slow spin could be produced by a rifled launcher, by inclined jets, by inclined fins, or by a combination of these devices. Evidently inclined fins will be relatively ineffective in rotating the rocket during the critical period just after launching, since then the aerodynamic forces are small. It is not so clear that inclined jets are impractical, but any complications, such as excessive drift or instability, that arise because of the spin will be much worse in this case than in the case where the same average spin during the first quarter revolution is produced by a rifled launcher. Furthermore little appears to be gained by a combination of a rifled launcher and inclined jets since then one

will have most of the disadvantages of each and no more spin during the first quarter revolution than could be obtained from either alone. We shall consider in the present section only the case in which the spin is imparted by a rifled launcher or other device that acts only during launching and thus leaves the rocket with a constant angular velocity after launching. The other case, in which the spin is accelerated, can be treated by the methods of 9.25 if desired, or a rough estimate of the dispersion to be expected can be obtained by comparison with the constant spin case.

It will be shown that such a constant slow spin reduces the dispersion due to linear thrust malalignment appreciably, the ratio of the dispersions with and without spin being roughly $1/(2n_\sigma)$ where n_σ is the number of revolutions made by the rocket while it traverses the initial distance σ . Thus it should be possible to reduce the dispersion due to malalignment to the point where it is no longer the dominant source of dispersion. It must be emphasized that this is a theoretical result, experimental confirmation being necessary before one can be sure that there are no unsuspected effects that introduce appreciable dispersion. For example, one would have to be sure that the fins do not produce a large Magnus moment (see 8.24) when the rocket has slow spin. If there are no such effects, then the principal remaining sources of dispersion should be wind effects and mallaunching produced by the mechanism that provides the slow spin and by the dynamic unbalance (see 9.7).

We shall assume that the spin is slow enough so that gyroscopic effects are negligible, allowing us to use the equations of motion as previously derived. The methods developed in chapters 9 and 10 show that this assumption is justified provided n_σ is small compared to the ratio of the moment of inertia about a transverse axis through the center of mass to the moment of inertia about the longitudinal axis. In 3.24 the equations for the components of the motion of the rocket in the vertical and lateral planes through the launcher were written separately. It was shown there, also, that the complete three-dimensional motion can be represented by writing 3.24 (8)–(10) in complex form. If we substitute into these equations the expression $V=Gt$ given by 3.31 (8), we get

$$\ddot{\varphi} + \frac{C_q \rho A l^2 G t + 2K_{JD}}{2mK^2} \dot{\varphi} + \frac{C_m \rho A l G^2 t^2}{2mK^2} \delta = -\frac{GR_M}{K^2} + \frac{C_m \rho A l G^2 t^2}{2mK^2} \delta_0, \quad (1)$$

$$t\dot{\vartheta} - \delta - \frac{C_l \rho A G t^2}{2m} \delta = i(g/G) \cos \theta_0 + \beta_M, \quad (2)$$

and

$$\varphi - \delta - \vartheta = 0, \quad (3)$$

in which G_J has been replaced by G [see remarks following 3.33 (3)]. Since we omit all gyroscopic effects, these equations are still valid, if it is understood that the malalignment vectors R_M , β_M and δ_0 are no longer fixed relative to the coordinate axes. That is, if s be the angular rate of spin about the longitudinal axis in radians per second, we have

$$R_M = R_M e^{ist}, \quad (4)$$

or

$$R_{MX} = R_M \cos st, \quad (5)$$

and

$$R_{MY} = R_M \sin st, \quad (6)$$

with similar expressions for β_M and δ_0 .

Since the homogeneous terms, as well as the term in gravity, are unaffected by the rotation, it follows that the deflections resulting from initial yaw, initial orientation, initial transverse angular velocity and gravity are *unaltered* by the spin. Of the remaining terms, the deflections resulting from the angular thrust malalignment β_M and the aerodynamic fin malalignment δ_0 are too small to be concerned with at present. The significant term is that in the linear thrust malalignment R_M , and we shall devote our principal attention to its effects. The same type of analysis may be employed to determine the effects of slow spin on the deflections resulting from β_M and δ_0 .

3.61 The Vacuum Case.—It will be useful to consider first the effect of spin in the ideal vacuum case; that is, in the absence of aerodynamic forces. Setting the aerodynamic coefficients as well as the jet damping coefficient equal to zero and neglecting the terms in g and β_M , we have in lieu of 3.6 (1)–(3),

$$\ddot{\varphi} = -\frac{G}{K^2} R_M, \quad (1)$$

$$t\dot{\vartheta} - \delta = 0, \quad (2)$$

and

$$\varphi - \delta - \vartheta = 0. \quad (3)$$

The boundary conditions on this set of equations are that at $t=t_p$, the instant of launching,

$$\varphi_p = \delta_p = \vartheta_p = 0. \quad (4)$$

Substituting

$$R_M = R_M e^{ist} \quad (5)$$

in (1), and integrating twice, we get

$$\varphi = \frac{GR_M}{s^2 K^2} [\exp(ist) - \exp(ist_p) - is(t-t_p) \exp(ist_p)]. \quad (6)$$

Eliminating δ from (2) and (3), we have

$$t\dot{\vartheta} + \vartheta = \varphi, \quad (7)$$

where φ is given by (6).

Now (7) is a linear differential equation of the first order which can be solved by elementary methods. The solution is

$$\vartheta = \frac{iGR_M \exp(ist_p)}{ts^3 K^2} \{1 - \exp[is(t-t_p)] + is(t-t_p) - (s^2/2)(t-t_p)^2\}; \quad (8)$$

and hence the absolute value of the deflection is

$$\vartheta = \frac{GR_M}{ts^3 K^2} [2 - 2 \cos s(t-t_p) - 2s(t-t_p) \sin s(t-t_p) + s^2(t-t_p)^2 \cos s(t-t_p) + (s^4/4)(t-t_p)^4]^{\frac{1}{2}}. \quad (9)$$

Letting n be the number of turns which the rocket has made when it has gone a distance d ,

and n_p the number of turns made on the launcher, we have the relations

$$n = \frac{st}{2\pi} = \frac{s}{\pi} \left(\frac{d}{2G} \right)^{\frac{1}{2}}, \quad (10)$$

$$n_p = \frac{st_p}{2\pi} = \frac{s}{\pi} \left(\frac{p}{2G} \right)^{\frac{1}{2}}. \quad (11)$$

And placing the subscript s on ϑ to indicate the deflection when spin is present, we have

$$\begin{aligned} \vartheta_s = \frac{GR_M t^2}{8\pi^3 K^2 n^3} [2 - 2 \cos 2\pi(n - n_p) - 4\pi(n - n_p) \sin 2\pi(n - n_p) \\ + 4\pi^2(n - n_p)^2 \cos 2\pi(n - n_p) + 4\pi^4(n - n_p)^4]^{\frac{1}{2}}. \end{aligned} \quad (12)$$

Now, from 3.12, the deflection in vacuum in the absence of spin is

$$\vartheta = \frac{GR_M}{6K^2} \left(1 - \frac{t_p}{t} \right)^3 t^2; \quad (13)$$

hence the ratio of deflection with and without spin under the same conditions is

$$\begin{aligned} \frac{\vartheta_s}{\vartheta} = \frac{3}{4\pi^3(n - n_p)^3} [2 - 2 \cos 2\pi(n - n_p) - 4\pi(n - n_p) \sin 2\pi(n - n_p) \\ + 4\pi^2(n - n_p)^2 \cos 2\pi(n - n_p) + 4\pi^4(n - n_p)^4]^{\frac{1}{2}}. \end{aligned} \quad (14)$$

Since ϑ_s/ϑ is a function of $(n - n_p)$ alone, the relative dispersion is a function merely of the number of turns made during burning off the launcher. A good approximation to (14), accurate to about 2 percent for $0.75 \leq (n - n_p) \leq 1.5$ and to within a small fraction of 1 percent for $(n - n_p) \geq 2.0$, is given by

$$\frac{\vartheta_s}{\vartheta} = \frac{0.48}{(n - n_p)}; \quad (15)$$

or, for the spin s in *revolutions per second*,

$$\frac{\vartheta_s}{\vartheta} = \frac{0.48}{(t - t_p)} \frac{1}{s}. \quad (16)$$

We have tacitly assumed that the spin was imparted at ignition so that it would be constant throughout the entire burning period. The question now arises as to what the correct interpretations of n and n_p are when the spin is *not* constant, while the rocket is on the launcher, as would happen, say, in a rifled launcher. In such a case, n and n_p are still defined as in (10) and (11); namely,

$$n = \frac{st}{2\pi}, \quad n_p = \frac{st_p}{2\pi},$$

where s is the spin *after* launching. Physically, then, $(n - n_p)$ is the actual number of turns made during burning off the launcher; while n and n_p separately are the number of turns that would have been made during the times t and t_p , respectively, if the spin had been constant throughout burning. Since the method of imparting spin on the launcher is immaterial, it is of course necessary that the solution depend only on $(n - n_p)$.

In connection with the above equations it must be borne in mind that ϑ_s/ϑ is the ratio of the dispersion due to malalignment with spin to the dispersion of the unrotated rocket, both launched under otherwise identical conditions. Thus, for any rocket which makes at least one complete turn during burning after it has left the launcher the dispersion varies approximately inversely with the spin velocity. As an example, for our "typical" rocket with $V_b=1,000$ ft./sec. $G=1,000$ ft./sec.², and $p=5$ feet (therefore $t_b=1.0$ sec., $t_p=0.1$ sec.) the dependence of dispersion on spin is given in the following tabulation:

Spin frequency (rev./sec.)	n	n_p	$(n-n_p)$	ϑ_s/ϑ [Eq. (14)]	ϑ_s/ϑ [Eq. (15)]
0	0	0	0	1.00	-----
1	1	0.1	0.9	.548	0.533
2	2	.2	1.8	.264	.267
5	5	.5	4.5	.106	.107
10	10	1.0	9.0	.053	.053
20	20	2.0	18.0	.027	.027

The dependence of dispersion on launcher length can be seen from figure 3.61 where ϑ_s/ϑ is

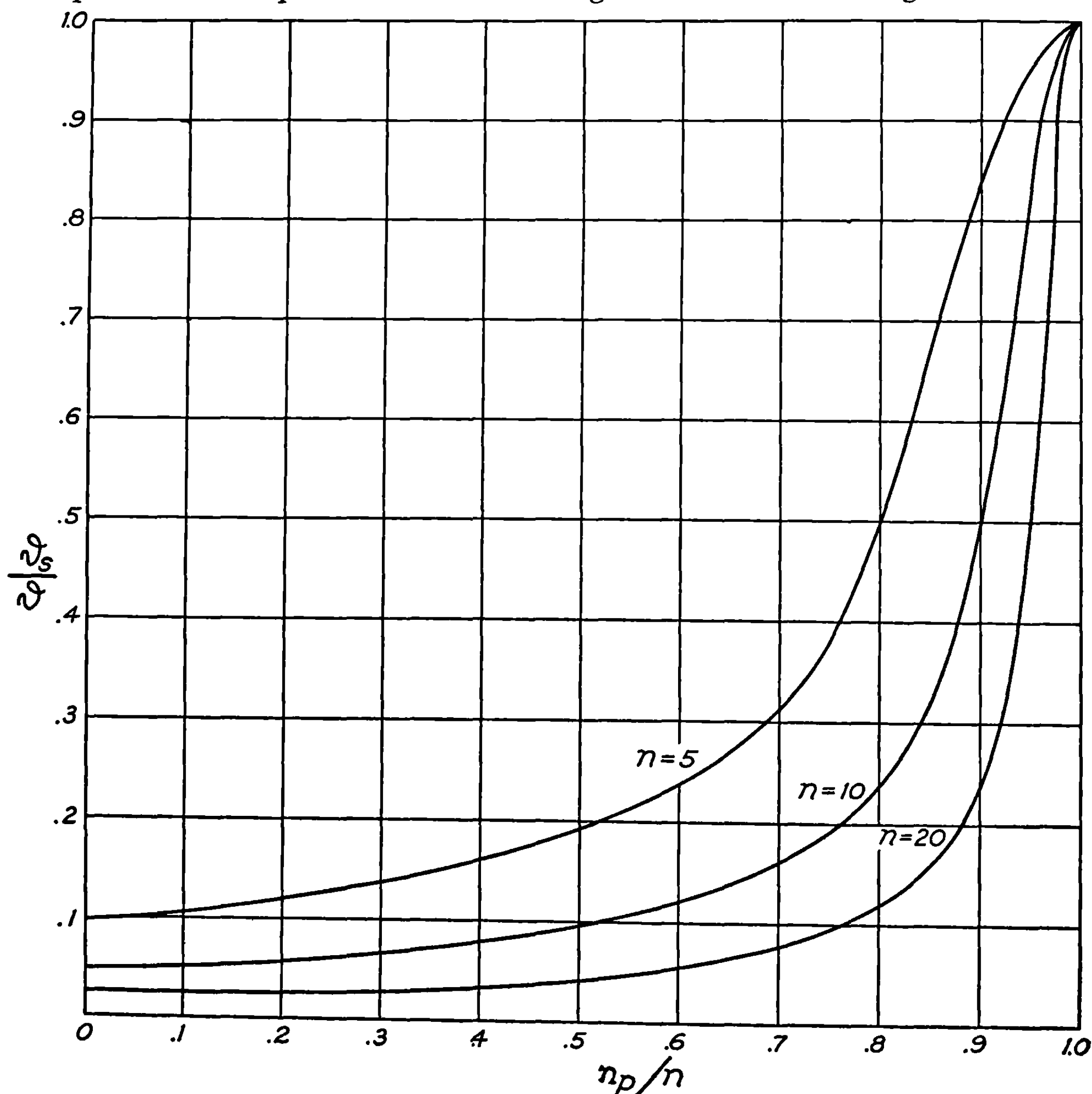


FIGURE 3.61.—Ratio of deflection with spin to deflection of unrotated rocket (vacuum case).

plotted as a function of n_p/n for a number of values of n . It follows from the figure that the relative gain in accuracy is greater the shorter the launcher; for very long launchers [$n_p/n = (p/d)^{1/2} \geq 1/2$] the relative gain in accuracy is negligible except for high rates of spin. This is in agreement with the previous conclusion that for constant spin velocity, the ratio ϑ_s/ϑ depends merely on the number of turns made during burning off the launcher.

3.62 The Aerodynamic Case.—In dealing with problems involving aerodynamic forces it is convenient to replace the moment coefficient by its value in terms of σ ; namely, from 3.32 (15)

$$\frac{C_m \rho A l}{2} = \frac{4 \pi^2 m K^2}{\sigma^2}, \quad (1)$$

and to write the equations of motion in terms of the dimensionless parameter

$$\zeta = \left(\frac{G}{2\sigma} \right)^{1/2} t = \frac{t}{t_\sigma} = \frac{V}{v_\sigma} = \left(\frac{d}{\sigma} \right)^{1/2}. \quad (2)$$

Furthermore, according to the arguments following 3.33 (10), we can neglect the terms containing C_a , K_{JD} and C_i during burning. Hence 3.6 (1)–(3) become

$$\varphi'' + 16 \pi^2 \zeta^2 \delta = -\frac{2\sigma}{K^2} R_M + 16 \pi^2 \zeta^2 \delta_0, \quad (3)$$

$$\zeta \vartheta' - \delta = i(g/G) \cos \theta_0 + \beta_M, \quad (4)$$

$$\varphi - \delta - \vartheta = 0. \quad (5)$$

We are interested here only in the effect of the spin on the deflection due to the linear thrust malalignment; and since the above set of equations is mathematically identical with 3.33 (14)–(16) we can determine this deflection by constructing the proper Green's function according to the method of 3.37. Now the complex malalignment is given by

$$R_M = R_M e^{i s t} = R_M e^{i 2 \pi n_\sigma \zeta}, \quad (6)$$

where n , the number of turns made in the time t , is given by

$$n = \frac{s t}{2 \pi} = \frac{s t_\sigma}{2 \pi} \zeta = n_\sigma \zeta, \quad (7)$$

and

$$n_\sigma = \frac{s t_\sigma}{2 \pi}. \quad (8)$$

It may be of interest to note that if s is produced by a rifled launcher in which the rocket travels ν_L feet per revolution at launching, then $s = 2 \pi V_P / \nu_L$ and

$$n_\sigma = \frac{V_P t_\sigma}{\nu_L} = \left(\frac{2 \sigma}{\nu_L} \right) \left(\frac{V_P}{v_\sigma} \right) = \left(\frac{2 \sigma}{\nu_L} \right) \zeta_p,$$

where V_P is the velocity at launching.

The effect of the linear thrust malalignment R_M is given by the characteristic functions identified by the subscript R and defined in 3.33 (23). Comparison of (3) above with 3.37 (1)

shows that in this case

$$f(\zeta) = -\frac{2\sigma}{K^2} R_M e^{i2\pi n_\sigma \zeta}.$$

Hence if we use 3.37 (5), (6) and (7) together with 3.33 (23) we find that the yaw, orientation angle, and deflection of the tangent to the trajectory are

$$\delta_{sR} = -\frac{2\sigma}{K^2} R_M \Delta_{sR}(\zeta_p, \zeta), \quad (9)$$

$$\varphi_{sR} = -\frac{2\sigma}{K^2} R_M \Phi_{sR}(\zeta_p, \zeta), \quad (10)$$

and

$$\vartheta_{sR} = -\frac{2\sigma}{K^2} R_M \Theta_{sR}(\zeta_p, \zeta). \quad (11)$$

The new characteristic functions defined above are given by

$$\Delta_{sR}(\zeta_p, \zeta) = \int_{\zeta_p}^{\zeta} e^{i2\pi n_\sigma u} \Delta_q(u, \zeta) du, \quad (12)$$

$$\Phi_{sR}(\zeta_p, \zeta) = \int_{\zeta_p}^{\zeta} e^{i2\pi n_\sigma u} \Phi_q(u, \zeta) du, \quad (13)$$

and

$$\Theta_{sR}(\zeta_p, \zeta) = \int_{\zeta_p}^{\zeta} e^{i2\pi n_\sigma u} \Theta_q(u, \zeta) du, \quad (14)$$

where Δ_q , Φ_q and Θ_q are given explicitly by 3.34 (21), (22), and (23). In the above expressions the subscript s is used to distinguish the functions in the case of spin.

Substituting from 3.34 (21) into (12) above, we have

$$\Delta_{sR}(\zeta_p, \zeta) = \frac{1}{4\pi\zeta} \int_{\zeta_p}^{\zeta} e^{i2\pi n_\sigma u} \sin 2\pi(\zeta^2 - u^2) du. \quad (15)$$

To integrate, we write the trigonometric term in the exponential form

$$\sin 2\pi(\zeta^2 - u^2) = \frac{1}{2i} [e^{i2\pi(\zeta^2 - u^2)} - e^{-i2\pi(\zeta^2 - u^2)}] \quad (16)$$

and substitute in (15). Thus

$$\Delta_{sR}(\zeta_p, \zeta) = \frac{-i}{8\pi\zeta} \left[e^{i2\pi\zeta^2} \int_{\zeta_p}^{\zeta} e^{i2\pi n_\sigma u} e^{-i2\pi u^2} du - e^{-i2\pi\zeta^2} \int_{\zeta_p}^{\zeta} e^{i2\pi n_\sigma u} e^{i2\pi u^2} du \right]. \quad (17)$$

Now

$$\begin{aligned} \int_{\zeta_p}^{\zeta} e^{i2\pi n_\sigma u} e^{-i2\pi u^2} du &= e^{i\pi n_\sigma^2/2} \int_{\zeta_p}^{\zeta} e^{-i2\pi(u - n_\sigma/2)^2} du \\ &= e^{i\pi n_\sigma^2/2} \int_{(\zeta_p - n_\sigma/2)}^{(\zeta - n_\sigma/2)} e^{-i2\pi v^2} dv \\ &= \frac{1}{2} e^{i\pi n_\sigma^2/2} [E^*(2\zeta - n_\sigma) - E^*(2\zeta_p - n_\sigma)]; \end{aligned} \quad (18)$$

while

$$\begin{aligned}
 \int_{\zeta_p}^{\zeta} e^{i2\pi n_\sigma u} e^{i2\pi u^2} du &= e^{-i\pi n_\sigma^2/2} \int_{\zeta_p}^{\zeta} e^{i2\pi(u+n_\sigma/2)^2} du \\
 &= e^{-i\pi n_\sigma^2/2} \int_{(\zeta_p+n_\sigma/2)}^{(\zeta+n_\sigma/2)} e^{i2\pi v^2} dy \\
 &= \frac{1}{2} e^{-i\pi n_\sigma^2/2} [E(2\zeta+n_\sigma) - E(2\zeta_p+n_\sigma)];
 \end{aligned} \tag{19}$$

where E and E^* are the complex and complex conjugate Fresnel integrals, defined by

$$E(x) = C(x) + iS(x) = \int_0^x e^{i\pi v^2/2} dy, \tag{20}$$

$$E^*(x) = C(x) - iS(x) = \int_0^x e^{-i\pi v^2/2} dy. \tag{21}$$

Hence, (17) becomes

$$\begin{aligned}
 \Delta_{sR}(\zeta_p, \zeta) &= \frac{i}{16\pi\zeta} \left\{ e^{-i2\pi(\zeta^2+n_\sigma^2/4)} [E(2\zeta+n_\sigma) - E(2\zeta_p+n_\sigma)] \right. \\
 &\quad \left. - e^{i2\pi(\zeta^2+n_\sigma^2/4)} [E^*(2\zeta-n_\sigma) - E^*(2\zeta_p-n_\sigma)] \right\}.
 \end{aligned} \tag{22}$$

The solution for $\Theta_{sR}(\zeta_p, \zeta)$ is not so easily found; and, in fact, one is compelled to employ numerical methods. One procedure is to determine Θ_{sR} by numerical integration of (14) above, using the values of $\Theta_q(u, \zeta)$ given in table 2C, appendix C. However, an alternate procedure is to make use of the existing relations between ϑ and δ in the differential equations. Since in (3)–(5) above we can set all the inhomogeneous terms but \mathbf{R}_M equal to zero, we have, from (4),

$$\vartheta' = \frac{1}{\zeta} \delta. \tag{23}$$

Hence,

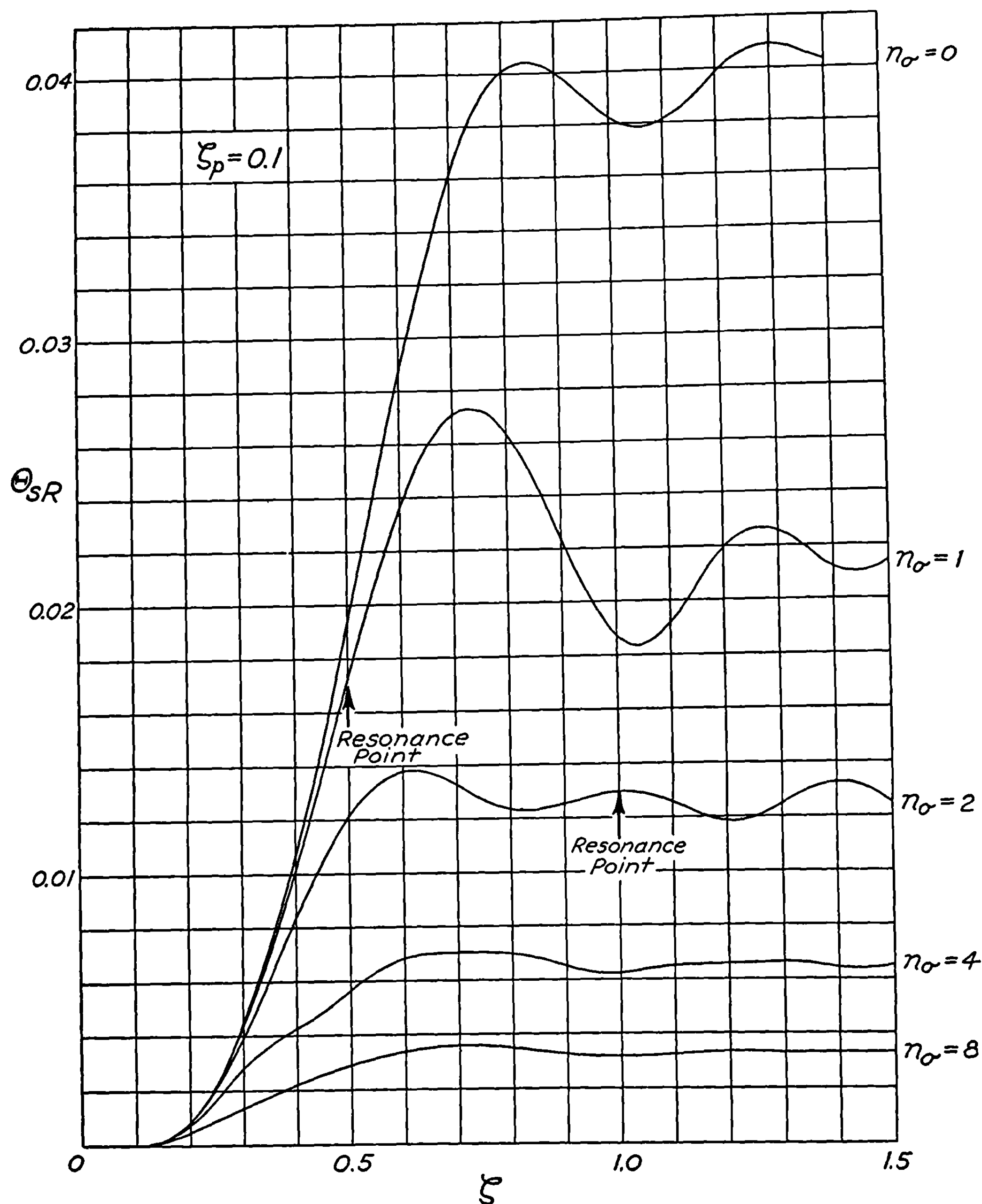
$$\vartheta_{sR} = \int_{\zeta_p}^{\zeta} \frac{1}{\zeta} \delta_{sR}(\zeta_p, \zeta) d\zeta; \tag{24}$$

and comparison with (9) and (11) shows that the characteristic function Θ_{sR} is given by

$$\Theta_{sR}(\zeta_p, \zeta) = \int_{\zeta_p}^{\zeta} \frac{1}{\zeta} \Delta_{sR}(\zeta_p, \zeta) d\zeta. \tag{25}$$

For $s=n=n_\sigma=0$, it can easily be shown that the equations reduce to those for the nonrotating rocket, and that the characteristic functions Δ_{sR} , ϕ_{sR} , and Θ_{sR} become the *real* quantities Δ_R , Φ_R , and Θ_R as given in 3.39.

Since our main interest is in the resultant dispersion and not in the components of the deflection, it is Θ_{sR} , the absolute value of Θ_{sR} , that we want for comparison with the nonrotating case. In order to see graphically how the deflection varies during burning we have plotted in figure 3.62a Θ_{sR} as a function of ζ for a series of values of the dimensionless spin parameter $n_\sigma = st_\sigma/2\pi$. The value of ζ_p is constant and equal to 0.1 for this set of curves. The curves are to be compared with the one for zero spin, that is $n_\sigma=0$. The procedure used to obtain these curves was to calculate the real and imaginary parts of Δ_{sR} by means of (22), and then to perform the integration indicated in (25) by Simpson's rule or other numerical methods. The absolute value Θ_{sR} is then the square root of the sum of the squares of the real and imaginary

FIGURE 3.62a.—Characteristic function Θ_{SR} .

parts of Θ_{SR} . It will be observed that, as with no spin (see figure 3.39), the function rises rapidly to a maximum within roughly half a yaw oscillation, and thereafter oscillates with small amplitude about a value close to its asymptotic value. The effect of spin in reducing the dispersion is quite pronounced, a spin velocity corresponding to one rotation in the distance σ ($n_\sigma=1$) reducing the dispersion for $\zeta \geq 1$ to about half of its value in the absence of spin. This is shown more effectively in figure 3.62b where the ratios $\vartheta_{SR}/\vartheta_R = \Theta_{SR}/\Theta_R$ are plotted as a function of ζ , for $\zeta_p=0.1$. As an example, for a rocket with $V_b=1,000$ ft./sec., $G=1,000$ ft./sec.², $\sigma=250$ feet and $p=2.5$ feet ($V_p=71$ ft./sec., and $\zeta_p=0.1$) the dependence of dispersion on spin is

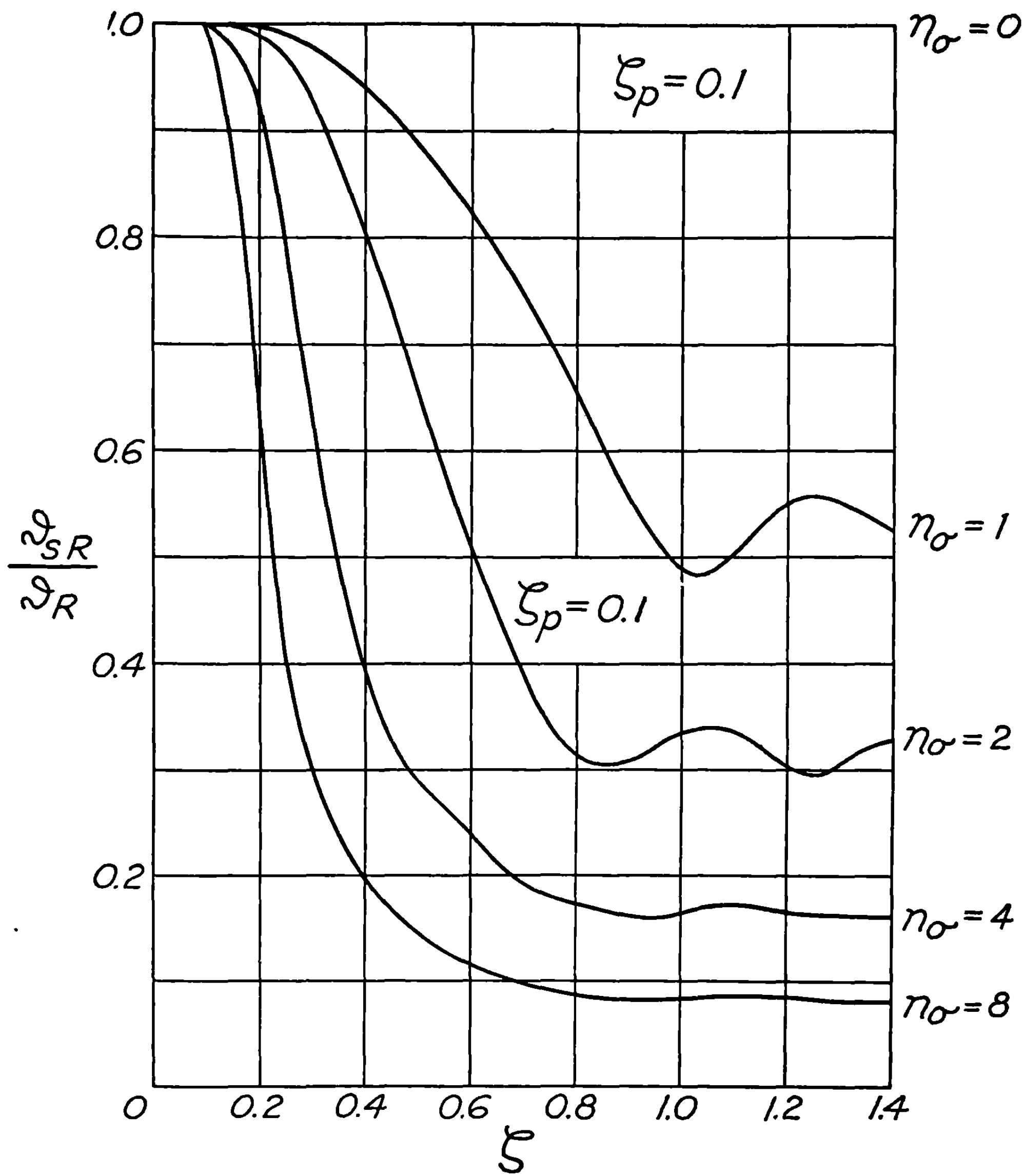


FIGURE 3.62b.—Relative decrease in dispersion due to slow spin.

given in the following tabulation which also lists the values of ν_L , the pitch of the rifling required to produce the spin.

Spin frequency (rev./sec.)	n	n_σ	ν_L	$\vartheta_{SR}/\vartheta_R$
0	0	0	∞	1. 000
1	1	0. 71	71	. 620
2	2	1. 41	35	. 432
5	5	3. 54	14	. 185
10	10	7. 07	7	. 089

It should also be noted that the relative decrease in dispersion is greater for the long-burning rockets than for the short-burning rockets, although for burning distances greater than σ (i. e., $\zeta > 1$) there is very little further improvement in accuracy. Examination of figure 3.62a

shows that in ground firing by the use of a moderate amount of spin with a long-burning rocket one can get the same low dispersion due to malalignment as with a very short-burning rocket without spin and thus have the other advantages of a long-burning rocket. For example, if $n_\sigma=4$, the dispersion for any d_b is less than that if $n_\sigma=0$ but $d_b \geq \sigma/8$.

An interesting situation occurs when the frequency of yaw oscillation V/σ , which increases linearly with time or velocity during burning, becomes equal to the spin frequency $s/2\pi$. This condition of *resonance* is reached when

$$\frac{V_{\text{res}}}{\sigma} = \frac{s}{2\pi}, \quad (26)$$

or, by (2) and (8), when

$$\zeta_{\text{res}} = \frac{n_\sigma}{2}. \quad (27)$$

Although the amplitude of oscillation of the function Θ_{sR} increases somewhat as the resonance point is reached and passed, the effect of the resonance on Θ_{sR} and hence on the dispersion is quite inappreciable, except for the very slow spin corresponding to $n_\sigma=1$. The reason is that practically all of the deflection occurs during the first half yaw oscillation, generally before the resonance point is reached, as can be seen from figure 3.62a. This is not true in the case of very slow spins, for then resonance can occur very early during burning. This is shown in the curve for $n_\sigma=1$ in figure 3.62a where the large variations in Θ_{sR} near $\zeta=0.5$ are due to the resonance.

Contrary to the effect on Θ_{sR} , the effect of the resonance on the yaw proper is quite pronounced. The characteristic function Δ_R , as well as the real and imaginary parts of Δ_{sR} for $n_\sigma=2$, are plotted in figure 3.62c, all the curves corresponding to $\zeta_p=0.1$. The increase in the

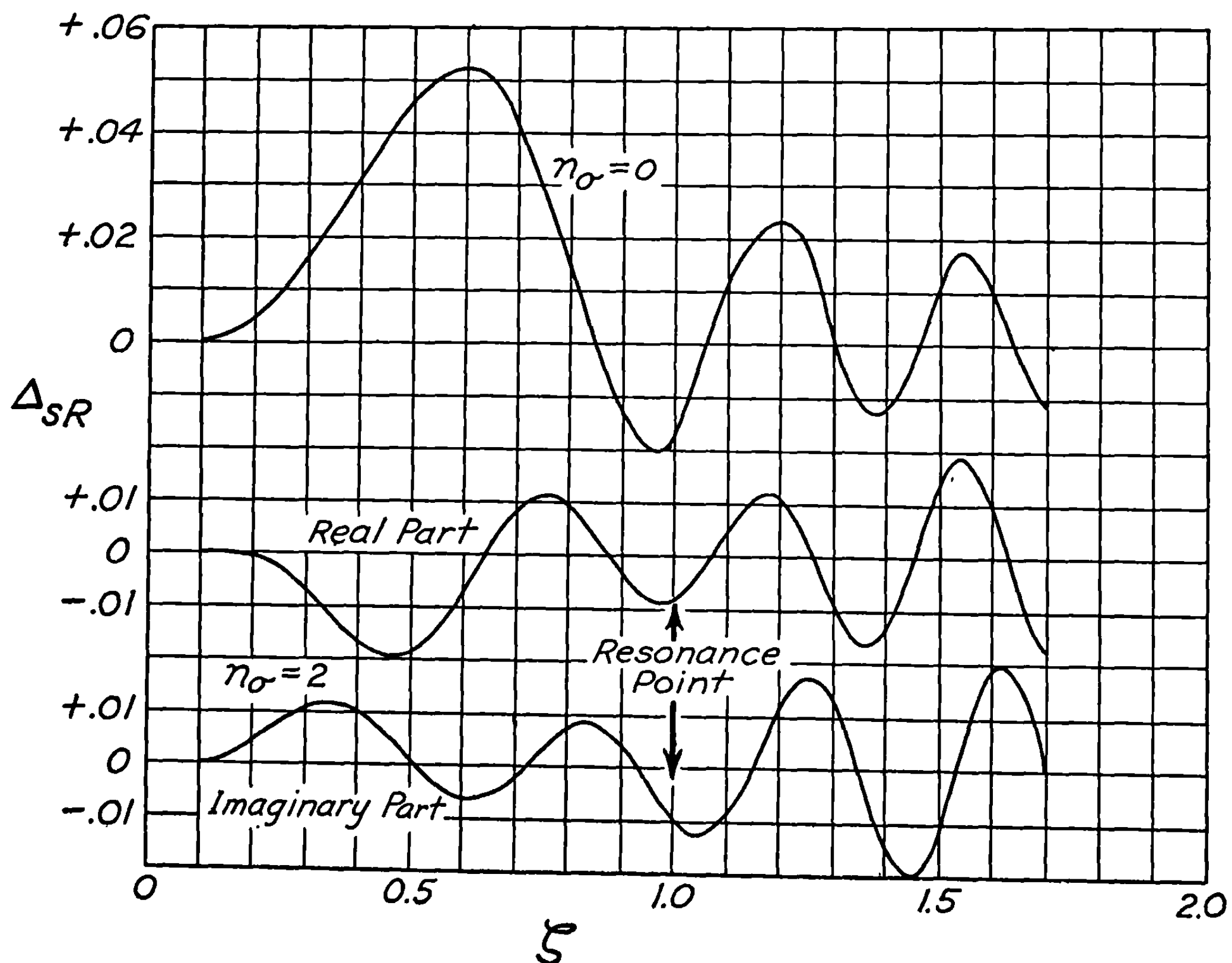


FIGURE 3.62c.—Effect of resonance on yaw.

amplitude of the yaw following the resonance point in the case of spin is in marked contrast to the normal decrease.

The question now arises as to when the resonance effects might be important. This will depend primarily on whether the frequencies of yaw oscillation and spin remain nearly equal for a number of oscillations. Hence it will not depend much on the spin, which is constant in this discussion, but on the rate of increase of the yaw oscillation frequency. If the rate of increase is slow, so that the two oscillations remain nearly in phase for a considerable time, one would expect the resonance effects to be large. On the other hand, if the rate of increase is rapid so that the two oscillations are nearly in phase for only a short time, then one would expect the resonance effects to be small. Since the rate of increase with time of the frequency of yaw oscillation is G/σ , it follows that the resonance effects are greatest for large values of σ and for small accelerations. Since $G = V_b/t_b = V_b^2/2d$, the resonance effects should also be greatest for long-burning rockets.

In any case, as pointed out earlier, the main effects of resonance will occur only when the resonance condition is reached before the rocket has built up its main deflection ($d < \sigma/2$). One danger may be noted; if the spin is slow and builds up slowly, a condition which can occur with twisted fins, the spin may resonate with the yaw oscillation along the whole trajectory and result in a much larger deflection than with no spin.

CHAPTER 4

THE LAUNCHING PROCESS

4.0 Introduction

Before firing, a rocket is supported on some device, crude or elaborate as the case may be, by which it is aimed and from which it can be fired. This device may be a trough, a tube, or a set of rails on which the rocket or projecting lugs slide. Such devices are called launchers; while the term "launching" is used for the entire motion while the rocket is in contact with the launcher or, in phrases such as at "launching," for the instant at which such contact ends. It is the purpose of the present chapter to treat the motion on the launcher, primarily in order to obtain from the position, orientation, and linear and angular velocities at launching the initial conditions for the motion described in chapter 3. That motion, it will be recalled, commenced at this instant.

The simplest assumption is that, due to the constraints imposed by the launcher, the rocket moves in a straight line without rotation about a transverse axis. Thus its position at launching is known, its orientation is that of the launcher, its linear velocity is in the same direction, and its angular velocity is zero. Actually this is not the case, since the launcher usually allows the nose of the rocket to start falling before the tail is released, and since the launcher may move or the rocket may not fit the launcher perfectly. As far as the effect on the subsequent trajectory goes, the most important deviation from the ideal state is usually the mallaunching; i. e., the transverse angular velocity. In most rockets there is a systematic mallaunching, called tip-off, due to the fact that the nose is released before the tail. Its effect is to deflect the trajectory downward and, in the case of spinners, to the left. These effects should be included in the trajectory calculations and in range tables, although it must be realized that they are functions not only of the rocket and the temperature, but also of the launcher type. In the construction of range tables the mallaunching should be determined empirically, usually by treating it as a parameter whose value is chosen so as to give the best possible correlation between trajectory calculations and the actual range firings on which the tables are based. Among the reasons that the average mallaunching thus determined by the experiment seldom agrees with the value calculated theoretically are the following: looseness of fit of the rocket in the launcher, resulting in a skittering motion in which the tail is not supported as long as would otherwise be expected; flexibility of the launcher which results in systematic launcher motion due to the weight of the rocket and the action of the jet blast on the launcher; an incorrect allowance for the deviation of the jet thrust during launching from the average value during burning; the presence of some unrecognized effect that is, at least partially, allowed for by the empirically determined mallaunching parameter. However, although the experimentally determined mallaunching is more suitable for range table calculations than the theoretical value, it is necessary to have expressions for the theoretical value as a guide in understanding the phenomena and for use when experimental data are not available or where a small amount of data must be extrapolated over a wide range.

The calculations given in this chapter are applicable both to fin- and spin-stabilized rockets. That the spin is irrelevant in the equations of motion follows from the fact that most spin-stabilized rockets make less than one revolution during the period when only the rear of the rocket is constrained. It will be shown in chapters 9 and 10 that the gyroscopic effects asso-

ciated with spin do not show up until after two or three revolutions and hence need not be considered in the motion on the launcher.

This statement must be qualified in the following cases where the spin affects the constraints or the applied forces. If a spin stabilized rocket is fired from a closely fitting tube it may roll around inside the tube and experience large centrifugal forces and peculiar kinematic constraints not contemplated in this chapter. Thus the spin can produce large amounts of mallaunching even though it does not directly enter the equations of motion. This effect does not seem to be important if the tube contains interior rails and will not be considered further since it did not seem to occur in the launchers developed at CIT. If the bourrelets, the two rings at which a spin stabilized rocket touches the launcher, are not circular or are not centered on the axis of dynamic symmetry, one gets a source of mallaunching that will be discussed in chapter 9, since the treatment is too complicated for the present chapter. Another instance in which the theory given here did not apply was the early forward firing of spinning rockets from airplanes. The experimental evidence showed clearly that the rockets received a large mallaunching, of the order of a radian per second, the nose moving horizontally away from the fuselage. No explanation of this was found and at the time there seemed to be no reasonably expected forces that could account for it. It appears that the most profitable point of view in all such cases is to assume that the equations given below hold, but to look for additional forces or constraints.

A corresponding situation can, of course, occur for fin-stabilized rockets. For instance, rockets fired forward from airplanes equipped with certain "zero length" launchers in which the rockets were, essentially, supported by two hooks that cleared the launcher as soon as the rocket moved forward an inch showed a mallaunching in which the nose lifted, although no mallaunching was to be expected since both supports were released simultaneously. This was found to be due to the forces involved in shearing the wire which held the rocket on the launcher.

There are two types of rocket support that must be considered in a treatment of launching. The first is the usual type in which during the interval in which the rocket is supported at but one point, this point is fixed on the rocket and slides along the launcher. This point of support may be a tail ring as on the barrage rocket, a lug as on the aircraft rockets, or a bourrelet as on the spinners. The second type is that in which the rocket is perfectly cylindrical over its rear portion so that the point of contact with the launcher is at the end of the launcher; thus it slides along the rocket and is fixed on the launcher. Since the first type is the more common and is easier to treat, we shall devote our main attention to it. The behavior of the second type is qualitatively the same, but the mallaunching is usually only about one half as great.

The angular deflections involved in tip-off are of the order of 10^{-3} radians; i. e., a mil, and during the early parts of the launching they are much smaller. Hence even though the round may be constrained by rails above as well as below, there is apt to be enough clearance to allow tip-off to occur unimpeded by the apparent additional constraint.

4.1 Rounds Constrained at a Point that Slides Along the Launcher

The most common rocket and launcher arrangement is one in which during the first phase of the launching the rocket is supported at two points and slides forward with only one degree of freedom. The distance traveled and the velocity as functions of time depend on the jet thrust only; and when they have been found, the motion during this period is completely determined from the shape and motion of the launcher. This phase ends when the front support point passes the end of the launcher (or bounces up off it). It is unnecessary to treat the motion during this phase because it is so simple; we regard the conditions at its end as given initial conditions for the calculation of the motion during the second phase of the

launching. During this phase the rocket is supported at one point that is fixed on the rocket and slides along the launcher. The rocket has two degrees of freedom, one of rotation about this sliding point and one corresponding to the translation of the point. We shall treat below the motion during this phase, omitting from consideration factors that merely complicate the equations without producing significant effects. This second phase ends when the rear support point passes the end of the launcher. The conditions at this instant are the initial conditions for the motion described in chapter 3.

4.11 Equations of Motion.—The situation during the second phase of launching is as shown in Fig. 4.11. The origin of the coordinate system $O_0Y_0Z_0$ is at the position occupied by the center of mass at the instant the front support point passes the end of the launcher. Z_0 is the distance traveled by the center of mass parallel to the launcher (more precisely, parallel to the axis of the rocket at this instant), Y_0 is the distance traveled downward at right angles to the launcher, and φ is the angle through which the rocket has rotated. The forces to be considered are the jet force, mG_0 , which is assumed to act along the axis of the rocket, the force of gravity, mg , and the force of reaction, F_R , which is assumed to act normal to the launcher. We can also, if we wish, assume that a torque, M , acts about a horizontal axis. We neglect friction since it either produces a small torque or, if some kind of jamming occurs, is unpredictable. Aerodynamic forces and moments are neglected since the distance traveled with respect to the air during launching is usually very small compared to the yaw oscillation distance and since the rear contact point is usually so located that the aerodynamic forces and torque will have little effect on the motion. The angle made by the launcher with the horizontal is denoted by θ_0 .

If φ is assumed to be small so that all terms containing it can be linearized, we find that the equations of motion are

$$\ddot{Z}_0 = G_0 - g \sin \theta_0 = G, \quad (1)$$

$$\ddot{Y}_0 = G_0 \varphi + g \cos \theta_0 - (F_R/m), \quad (2)$$

and

$$K^2 \ddot{\varphi} = (F_R/m) l_R + (M/m), \quad (3)$$

where m is the mass, mK^2 is moment of inertia about a transverse axis through the center of mass, and l_R is the distance from the center of mass to the rear contact point. To allow for the fact that the launcher can move and need not be straight, let Y_R be the Y coordinate of

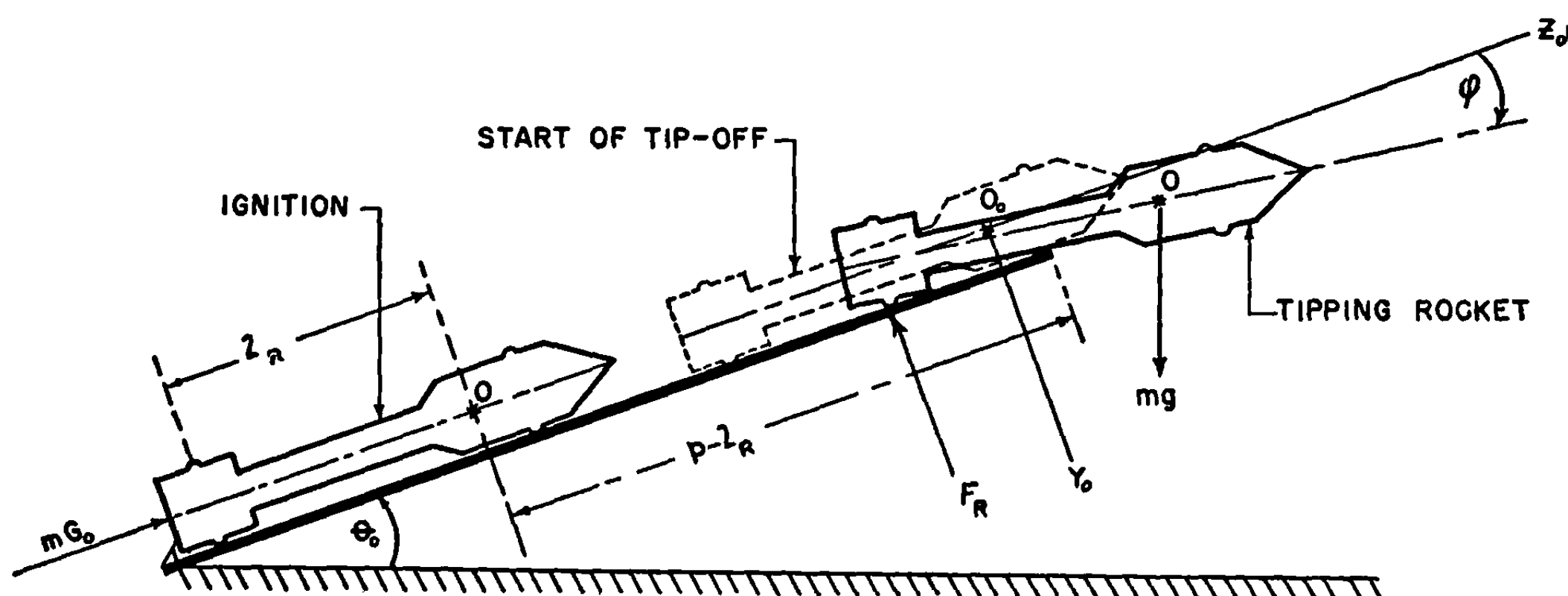


FIGURE 4.11.—A rocket of the first type in three positions during launching.

the point on the axis of the rocket opposite the rear contact point; in other words, the Y coordinate of the rear contact point is Y_R plus the radius of the rocket. Then to the approximation considered the equation of constraint is

$$Y_0 = Y_R + l_R \varphi. \quad (4)$$

We see that (1) is independent of the remaining equations and hence the translatory motion parallel to the launcher is irrelevant to our problem except in so far as it determines the times t_1 and t_p , when the front and rear contact points pass the end of the launcher. If we eliminate Y_0 and F_R between (2), (3), and (4), we get

$$(l_R^2 + K^2) \ddot{\varphi} = G_0 l_R \varphi + g l_R \cos \theta_0 + (M/m) - \ddot{Y}_R l_R, \quad (5)$$

which contains only the one unknown, φ , and is easily integrated. It may be interpreted as the equation of motion of the rocket when pivoted at the rear contact point, about which its moment of inertia is $m(l_R^2 + K^2)$, and acted upon by suitable torques. We shall see in the next section that if G is constant and the launcher length is greater than twice the distance between the support points, then no significant change is made in the tip-off if the first term on the right-hand side of (5) is dropped. It is easy to show that this applies in general and hence we see that as far as the lateral and rotational motions are concerned, the jet forces and the translational motion along the trajectory can be disregarded except for determining times. Thus in this approximation the lateral and rotational motions during tip-off are the same as the motions that occur if the rocket is supported at the front and rear contact points by sawhorses that are kicked out from under at t_1 and t_p , respectively.

The initial conditions in the simplest case are that at $t=t_1$, $\varphi=\dot{\varphi}=0$. In the more complicated case in which the launcher is moving and is not straight, we can locate the coordinate system $O_0 Y_0 Z_0$ so that at $t=t_1$, $\varphi=Y_0=Y_R=0$. If now the motion and shape of the launcher are specified, one can determine \dot{Y}_{F1} and \dot{Y}_{R1} , the lateral velocities of the front and rear contact points, respectively, in this coordinate system. We then have as the remaining initial condition $\dot{\varphi}=(\dot{Y}_{R1}-\dot{Y}_{F1})/l_B$, where l_B is the distance between the supporting points.

The results desired from the solution of the equations of motion are the values at $t=t_p$ of $q_p=\dot{\varphi}_p$, the mallaunching, φ_p , the initial cross-pointing, and δ_p , the initial yaw. The first two of these are given immediately by the solution of (5) but the last must be computed from the equation

$$\delta = \varphi - \vartheta = \varphi - (\dot{Y}_0/v) = \varphi - (l_R \dot{\varphi}/v) - (\dot{Y}_R/v), \quad (6)$$

where $v=\dot{Z}_0$ is the velocity along the trajectory computed from (1).

4.12 Tip-off.—The most important solution of the equations given in the previous section is for the ordinary gravity tip-off, the solution obtained for straight, stationary launchers, so that $Y_R=0$, and for $M=0$. It is readily seen to be

$$\varphi = \frac{g \cos \theta_0}{G_0} [\cosh \Omega(t-t_1) - 1], \quad (1)$$

$$q = \dot{\varphi} = \frac{g \cos \theta_0}{G_0} \Omega \sinh \Omega(t-t_1), \quad (2)$$

$$\delta = \frac{g \cos \theta_0}{G_0} \left[\cosh \Omega(t-t_1) - 1 - \frac{l_R}{v} \Omega \sinh \Omega(t-t_1) \right], \quad (3)$$

where

$$\Omega^2 = Gl_R / (l_R^2 + K^2), \quad (4)$$

and we have used the initial conditions $\varphi = \dot{\varphi} = 0$ at $t = t_1$. It may be worth remarking that Ω is $(G/g)^{1/2}$ times the angular frequency of the pendulum that results when the rocket is hung from a point on its axis opposite the rear contact point.

If one wishes to determine the effect of a constant torque, M , one need only replace $g \cos \theta_0$ by $M/l_R m$ in the above equations.

In the derivation of (1)–(4) it is assumed that G_0 is constant during the interval from t_1 to t_p . Since the interval is short, it is usually possible to select an average value such that this is a good approximation. If the jet thrust is constant from ignition onward, these results can be put in a very convenient form if one makes the approximation of replacing G_0 by $G = G_0 - g \sin \theta_0$ in 4.11 (2) and (5) and in (1)–(4) above. For then $\frac{1}{2} G t_p^2 = p$, the launcher length, and $\frac{1}{2} G t_1^2 = p - l_R$, the distance traveled before tip-off begins. Thus the square root of

$$\Omega^2 (t_p - t_1)^2 = \frac{2l_R p}{l_R^2 + K^2} \left[1 - \left(1 - \frac{l_B}{p} \right)^{1/2} \right]^2 \quad (5)$$

provides an easy way of determining the argument of the hyperbolic functions. If $p \geq 2l_B$, this is small enough so that the hyperbolic functions can be expanded, and we can write

$$\varphi_p \doteq \frac{p l_R g \cos \theta_0}{(l_R^2 + K^2) G} \left[1 - \left(1 - \frac{l_B}{p} \right)^{1/2} \right]^2, \quad (6)$$

$$q_p = \dot{\varphi}_p \doteq \frac{(2Gp)^{1/2} l_R g \cos \theta_0}{(l_R^2 + K^2) G} \left[1 - \left(1 - \frac{l_B}{p} \right)^{1/2} \right], \quad (7)$$

$$\delta_p = \varphi_p - l_R q_p / (2Gp)^{1/2} \quad (8)$$

These are the same as the results obtained if one omits the first term on the right in 4.11 (2) and (5). Thus we see that except for very short launchers the lateral force due to the jet is not important during launching.

Even if the jet force is not constant from ignition to the beginning of tip-off, one can use these expressions provided an effective value of p is used such that $(2Gp)^{1/2}$ is the true velocity at the end of tip-off and G is the average acceleration during tip-off.

4.13 Effects of Launcher Motion.—To simplify the treatment, we can set $M = 0$ and drop the terms in G_0 and g from 4.11 (2) and hence (5). If one has to deal with very short launchers where this is a poor approximation, solutions of the general character of those in the preceding section can be used as Green's functions to solve the exact equation. However, our problem is merely to solve

$$(l_R^2 + K^2) \ddot{\varphi} = -l_R \ddot{Y}_R \quad (1)$$

subject to the initial conditions that at $t = t_1$, $\varphi = 0$, $\dot{\varphi} = (\dot{Y}_{R1} - \dot{Y}_{F1})/l_B$, where Y_R and Y_F are regarded as known functions of t which are zero at $t = t_1$.

By integration, the solution can be found in terms of: \dot{Y}_{R1} , the lateral velocity of the rear contact point of the rocket at t_1 as precisely defined in 4.11; \dot{Y}_{F1} , the lateral velocity of the tip of the launcher and of the front contact point at t_1 ; \dot{Y}_{Rp} , the lateral velocity of the tip of the launcher and of the rear contact point at t_p ; Y_{Rp} , the lateral displacement of the tip

of the launcher during the interval from t_1 to t_p ; and $t_p - t_1$. The result for the mallaunching, which is the term having the greatest influence on the motion during burning, is

$$q_p = \dot{\varphi}_p = -\frac{l_R}{l_R^2 + K^2} \dot{Y}_{Rp} + \left(\frac{l_R}{l_R^2 + K^2} + \frac{1}{l_B} \right) \dot{Y}_{R1} - \frac{1}{l_B} \dot{Y}_{F1}. \quad (2)$$

It will be noted that if all the lateral velocities are the same, corresponding to uniform translation, there is no mallaunching. But in most other cases small velocities, those of the order of 0.1 ft./sec, produce significant mallaunching.

The less important initial conditions are found by further integration to be

$$\varphi_p = -\frac{l_R}{l_R^2 + K^2} Y_{Rp} + (t_p - t_1) \left[\dot{Y}_{R1} \left(\frac{l_R}{l_R^2 + K^2} + \frac{1}{l_B} \right) - \frac{1}{l_B} \dot{Y}_{F1} \right], \quad (3)$$

and

$$\delta_p = \varphi_p - (l_R q_p / v_p) - (\dot{Y}_{Rp} / v_p). \quad (4)$$

The expressions in this section apply to lateral motion as well as motion in the vertical plane. They also give the effect of crooked launchers since from the inclination of the launcher at the front and rear contact points to the rocket axis when the latter is in the standard position used to define the $O_0 Y_0 Z_0$ coordinate system, it is easy to compute the various Y 's by using the known velocities. If this is done, very small bumps or deviations from straightness will appear to give quite large mallaunchings. However, it must be remembered that the tendency of the rocket to skip from high point to high point along the launcher reduces the effect of small bumps and the elasticity of the launcher may either reduce or magnify these effects, depending on the relative phase of the oscillations at the two contact points. It is clear that these phenomena will usually produce dispersion and that they may produce systematic effects that should be allowed for in range tables. These systematic effects will usually have to be determined empirically.

The most obvious source of launcher motion is motion of the vehicle upon which the launcher is mounted. Also since no launcher is completely rigid, there are always vibrations present due to the forces exerted by the rocket on the launcher because of its weight and due to the blast forces produced when the jet strikes the launcher. An analysis of these effects is out of place here but studies with accurate spin stabilized rockets show that there are significant systematic differences in going from one launcher to another that most probably are due to the phenomena treated in this section. If one wishes to study rockets rather than launchers, the launchers should be very stiff, including, in the case of spin stabilized rockets, considerable torsional stiffness.

It is of interest to solve 4.11 (3) and (5) for F_R , the force of constraint applied at the rear support point. The result is

$$F_R = \frac{K^2}{K^2 + l_R^2} (m g \cos \theta_0 + m G_0 \omega - m Y_R) - \frac{M l_R}{K^2 + l_R^2}. \quad (5)$$

It will be seen from this that since $\dot{l}_R^2 \approx 3K^2$ in most cases, the force of constraint is only about one quarter of the weight or of the mass times the acceleration of the rear contact point.

4.2 Rounds Constrained at a Point that is Fixed on the Launcher

Occasionally one uses rockets that are cylindrical over most of their length and that do

not have projections that fix their points of contact with the launcher. After the center of mass of such a rocket passes the end of the launcher, the nose drops and we have tip-off, but the point of contact is at the tip of the launcher. This point of contact slides along the rocket from a point opposite its center of mass to a point at the rear as the rocket moves forward. The resulting equations of motion are considerably more difficult than those treated in the previous section; and, because of their lesser practical importance, we shall treat them less completely.

The same coordinate system used in figure 4.11 can be used here except that since tip-off begins when the center of mass of the rocket is opposite the tip of the launcher, O_0 is located at this point. Equations 4.11 (1)–(4) can be used as the basic equations of motion and constraint if l_R is replaced by Z_0 , the distance from the center of mass to the point of contact with the launcher. If next one eliminates Y_0 and F_R as before, one gets a more complicated equation in place of 4.11. (5) since $\dot{Z}_0 \neq 0$. Simplifying by the aid of 4.11 (1) and setting $Y_R = M = 0$, one gets

$$(Z_0^2 + K^2)\ddot{\phi} + 2Z_0\dot{Z}_0\dot{\phi} = gZ_0 \cos \theta_0 + gZ_0\phi \sin \theta_0. \quad (1)$$

Since the second term on the right is small compared to the first, it will be dropped. This corresponds to neglecting the difference between G and G_0 in the first term on the right-hand side of 4.11 (5).

In order to proceed without resorting to numerical integration, it is necessary that the jet thrust be constant during tip-off. If this is the case, we can now integrate (1) after dropping the last term. Using $\phi = \dot{\phi} = 0$ at $t = t_1$ (when $Z_0 = 0$) as initial conditions, we find the mallaunching due to tip-off to be

$$q = \phi = \frac{4g \cos \theta_0 (p - l_R)^{3/2}}{3(2G)^{1/2}(K^2 + Z_0^2)} \left[1 - \frac{1}{2} \left(2 - \frac{Z_0}{p - l_R} \right) \left(1 + \frac{Z_0}{p - l_R} \right)^{1/2} \right]. \quad (2)$$

Here $p - l_R$ is the distance the rocket slides before tip-off begins if the acceleration is G throughout this time; otherwise $(p - l_R)$ should be replaced by $V_1^2/2G$, where V_1 is the velocity at the time that the center of mass reaches the tip of the launcher. This formula can be integrated analytically to give ϕ , and from the result δ can be found; but in practice it is easier to proceed by numerical integration. The results are presented in figure 4.2a, b, and c.

If the ratio of the length of the rocket to the length of the launcher is great enough, the rocket will get so much mallaunching that it will rise off the launcher before the rocket has slid the distance l_R . Launching should be regarded as ending at this instant. The curves in figure 4.2 terminate at the point where this occurs. It will be obvious that unless l_R/K is much greater than in normal rockets, this phenomenon need not be considered for the launcher lengths shown in the figures. It could be prevented by the application of a constraint from above but such a constraint would probably require a complete change in the entire treatment.

The figures are not adapted to the treatment of very short launchers since then V_1 is small. The general behavior under such circumstances is given by the simple formulas for the limiting case in which the center of mass is placed at the tip of the launcher at ignition; i. e., $V_1 = 0$, $p - l_R = 0$. These formulas are easily found to be

$$\phi = q = \frac{1}{3} (2/G_0)^{1/2} g \cos \theta_0 [Z_0^{3/2}/(Z_0^2 + K^2)], \quad (3)$$

$$\varphi = (g \cos \theta_0 / 6 G_0) \ln[(Z_0^2 + K^2)/K^2], \quad (4)$$

$$\delta = (g \cos \theta_0 / 3G_0) [Z_0^2 / (Z_0^2 + K^2)]. \quad (5)$$

The point at which the rocket rises off the launcher in this case is $Z_0 = 3^{1/2}K$; this could easily be less than l_R for normal rockets.

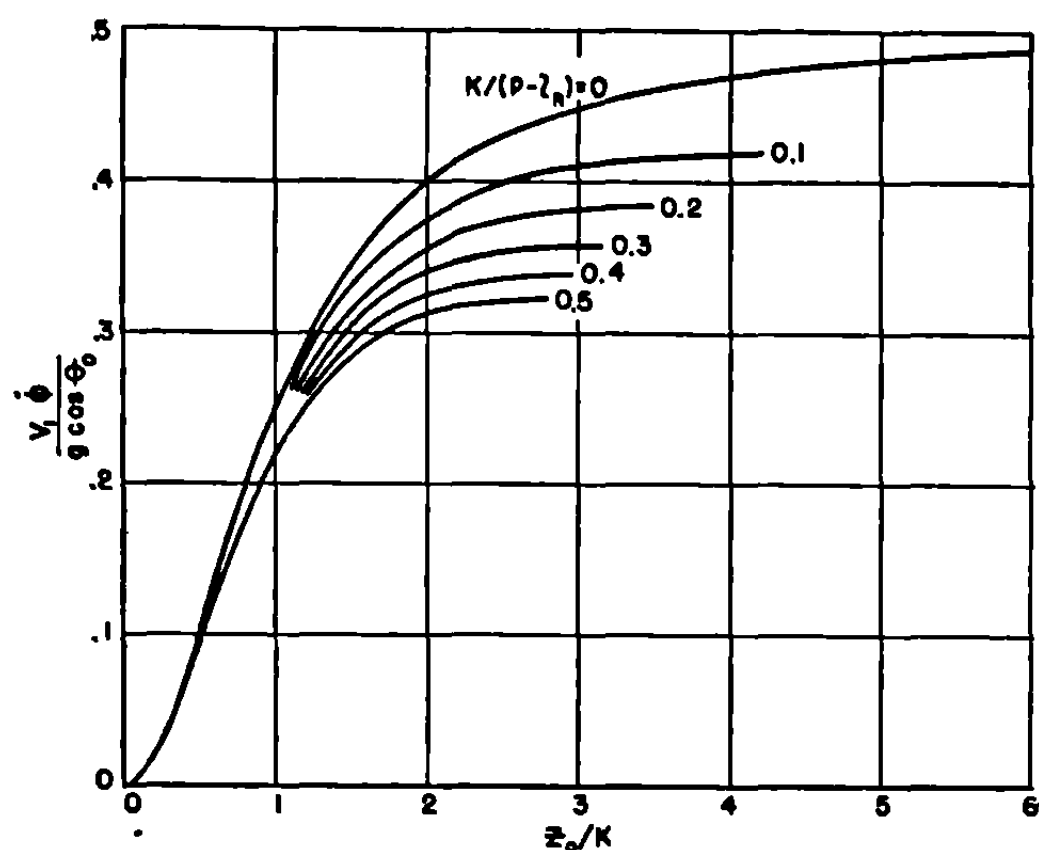


FIGURE 4.2a.—Angular velocity during tip-off when this contact point is at the tip of the launcher.

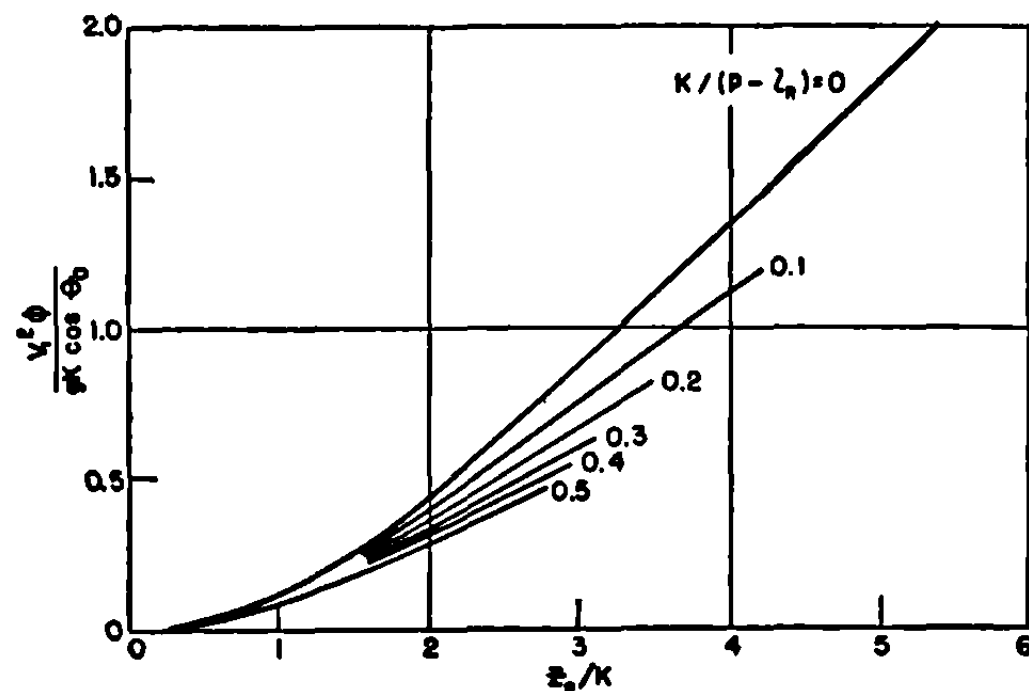


FIGURE 4.2b.—Cross-pointing during tip-off when the contact point is at the tip of the launcher.

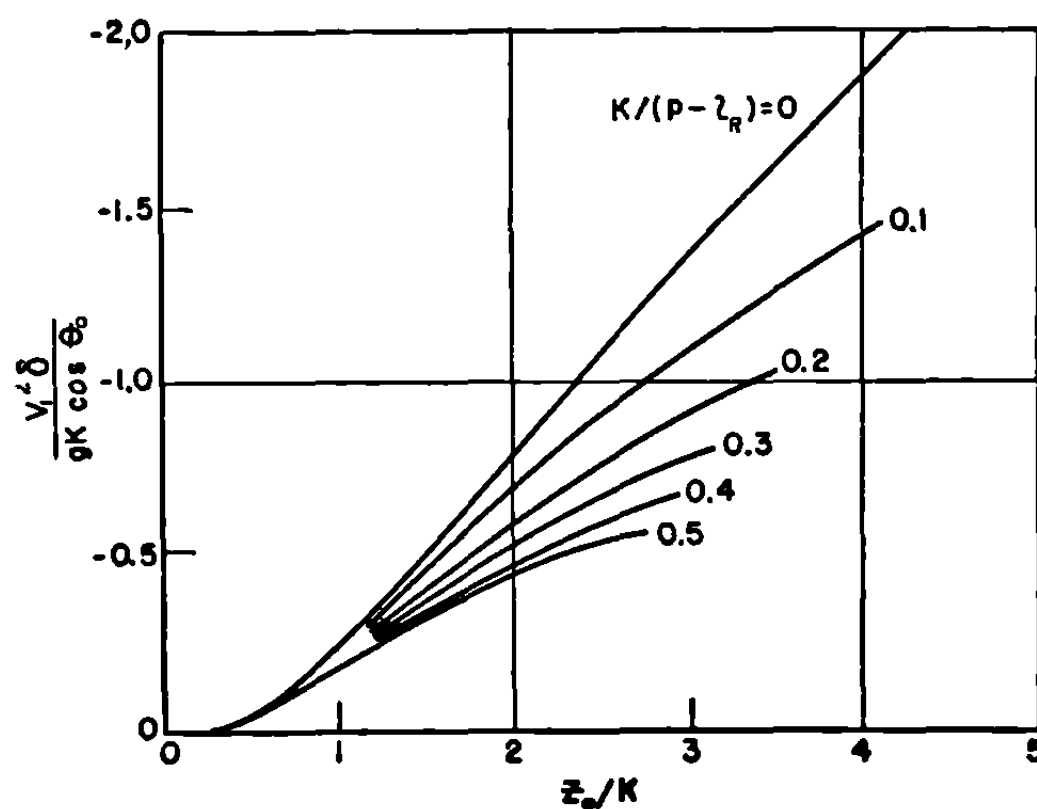


FIGURE 4.2c.—Yaw during tip-off when the contact point is at the tip of the launcher.

CHAPTER 5

THE MOTION AFTER BURNING

5.0 Introduction

In the previous chapters much attention has been devoted to the short section of the trajectory over which the rocket forces act and we have learned how to calculate the position and velocity of the rocket at the end of burning. We must now consider the much longer part where no jet forces act and the rocket moves like a shell. One might expect that this part of the motion could be treated as was the motion during burning (ch. 3) by merely setting the jet thrust equal to zero and thus greatly simplifying the equations. This would indeed be the case if one worked with the exact equations in both cases, but they are much too complicated for this to be a practical program. Instead, during burning the aerodynamic drag and gravity were regarded as small compared to the jet forces and were given relatively little weight in the approximations. After the end of burning they become the dominant forces which, since they act for a long time, must be given the major weight in the approximations appropriate to this regime. The aerodynamic lift and righting moment can be disregarded, even in computing wind effects, since it is satisfactory to assume that the moment keeps the average yaw zero. The much more complicated case in which one wishes to take account of the orientation and of the effects of forces normal to the trajectory is significant only for spin-stabilized projectiles and is treated in chapter 10. Even for such projectiles, the basic trajectory calculations neglect these effects.

Thus our problem now is to determine the motion of a projectile acted upon by gravity and a drag that depends on its velocity and the air density but not on its orientation. This is just the classical problem in ballistics and it would be possible to conclude this chapter at this point with the remark that having found the conditions at the end of burning by the methods of chapter 3, one uses the well-known methods of classical ballistics to obtain the remainder of the trajectory. However, classical ballistics is very extensive and it seems worthwhile to add a few guide posts to help the reader find his way to those parts of the subject that seem to us to be particularly useful in rocketry. It may well be, of course, that for some problems there are still more useful methods that we have overlooked.

The history of ballistics is divided into two parts by World War I. Before this period the main effort was to develop first a universal ballistics formula and, when this failed, a universal ballistics table. These efforts were reasonably successful as long as initial velocities were low, shells were short and fairly blunt, and the accuracy required was not too great. With the introduction of a variety of long slender shells fired at high velocities from accurate guns it was found necessary to base the range tables much more on numerical integrations appropriate to the particular case. Thus recent calculations are usually carried only over the range of immediate interest and have little general application. Fortunately for the ballistcian, rockets are still relatively inaccurate, low velocity, high drag projectiles, and the older methods are quite satisfactory in many cases. The rocket ballistcian can still work with universal formulas and tables which are to be looked for not in recent developments but in those of the nineteenth century. He should remember, however, that there is no point in trying to carry these methods to the extremes that were attempted by the older ballisticians and that the simple methods should not be used when so many corrections are needed that

they are no longer simple. If rockets ever have dispersions as low, and velocities as high as shells now have, it will be necessary to make much more precise measurements of the forces acting on rockets and to carry out accurate numerical integrations for the trajectories of individual rockets in order to provide satisfactory ballistic calculations.

5.1 The Equivalent Shell

The most common situation in ballistics is that in which the firing point and the impact point are at the same elevation and it is for this situation that the most extensive tables are to be found. But in the firing of rockets our basic need for these tables is as a means of computing the trajectory from the point at the end of burning to the impact point, which is lower since it is on the same level as the launcher. One procedure would be to calculate the conditions at the end of burning by the methods considered earlier, or to measure them photographically. Then the methods considered below could be used to calculate the velocity, direction of motion, time of flight, and range at the point where the elevation is the same as it is at the end of burning. A relatively simple approximate calculation would then complete the determination of the short section of trajectory between this point and the point of impact. A second, and in practice much more convenient, procedure is to determine the initial conditions for what is called the equivalent shell trajectory. This is the trajectory, shown in figure 5.11, that would be traversed by a shell fired at the level at which the rocket is fired with such initial conditions that the shell will reach the point at which the burning of the rocket ends with the same velocity and direction of motion as the rocket. The shell is assumed to have the same mass and drag as the rocket so that the remainder of the two trajectories are identical. Essentially, the process is to calculate from the state of the rocket at the end of burning the initial conditions that a shell must have in order to have the same trajectory as the rocket has after burning is over. The impact conditions are then calculated from the range tables or formulas for the shell. It is relatively easy to calculate the initial conditions of the equivalent shell, the so called "equivalent initial conditions," since only a short segment of its trajectory is involved and one can use any approximation whose errors are small compared to those involved in the determination of the trajectory of the rocket during burning. We shall see that the equivalent shell will have to be fired with a smaller quadrant angle of departure, at a later time, and, usually, from slightly farther forward than is the rocket. The initial velocity of the shell will be greater than the burnt velocity of the rocket but smaller than the corrected initial velocity, the velocity that would be imparted by the jet if there were no gravity and aerodynamic forces.

This equivalent shell procedure is most useful in the case of rockets fired at quadrant elevations above 15° at targets that are at about the same level as the launcher and provided suitable ballistics tables or formulas are available. The procedure is not useful when firing at very low quadrant elevations or when firing high velocity rockets for which the curvature of the trajectory between the end of burning and the target is small. In such cases there is a simple alternative procedure. One assumes the launcher to be horizontal and computes the conditions at the end of burning. Using these as initial conditions, one then computes a section of the subsequent trajectory by a simple modification of the Didion-Bernoulli method (5.22) or by the Siacci method (5.24). The results are put in the form of a single table showing drop below the launcher line as a function of distance along this line. This table gives a satisfactory approximation for any reasonable inclination of the launcher and launcher line provided the total curvature is less than about 30° .

5.11 The Equivalent Initial Conditions.—Let us now list a series of expressions for the equivalent initial conditions that will be satisfactory in most cases. They are calculated on rather simple assumptions; if expressions based on other assumptions seem desirable, the mode of procedure should be obvious. We assume that the motion takes place in a vertical plane through the launcher and that at the end of the burning time, t_b , the velocity of the rocket is v_b , its direction of motion makes the angle ϑ_b with the launcher, whose quadrant elevation is θ_0 , and that the distances along and normal to the launcher line are X_{0b} and Y_{0b} , respectively; (fig. 5.11). θ_0 is positive in the upward direction but ϑ and Y_0 are positive downward. By proper choice of c , the deceleration coefficient, we can assume that mcv^2 is a sufficiently accurate expression for the aerodynamic drag of both the rocket and the equivalent shell during the short period of interest.

The equations of the motion of the equivalent shell are taken to be

$$\ddot{X}_0 = -g \sin \theta_0 - cX_0^2; \quad \ddot{Y}_0 = g \cos \theta_0 - cX_0\dot{Y}_0.$$

These are integrated by successive approximations, the constants of integration being evaluated so that the motion of the shell is the same as that of the rocket at $t=t_b$, the end of burning. In this way we get the following expressions for the equivalent initial conditions, which we identify by the subscript e .

$$v_e = v_b + (g \sin \theta_0 + cv_b^2) \frac{X_{0b}}{v_b} + \left[(g \sin \theta_0 + cv_b^2) \left(-\frac{gX_{0b}^2}{2v_b^3} \csc \theta_0 + \frac{cX_{0b}^2}{2v_b} - \frac{Y_{0b}}{v_b} \cot \theta_0 + \frac{\vartheta_b X_{0b}}{v_b} \cot \theta_0 \right) \right] + \dots \quad (1)$$

$$\theta_e = \theta_0 - \vartheta_b + \frac{gX_{0b}}{v_b^2} \cos \theta_0 + \left[-\frac{g^2 X_{0b}^2}{v_b^4} (\cot \theta_0 + 2 \sin \theta_0 \cos \theta_0) - \frac{gcX_{0b}^2}{v_b^2} \cos \theta_0 - \frac{gY_{0b}}{v_b^2} \cos^2 \theta_0 \csc \theta_0 + \frac{\vartheta_b gX_{0b}}{v_b^2} \csc \theta_0 \right] + \dots, \quad (2)$$

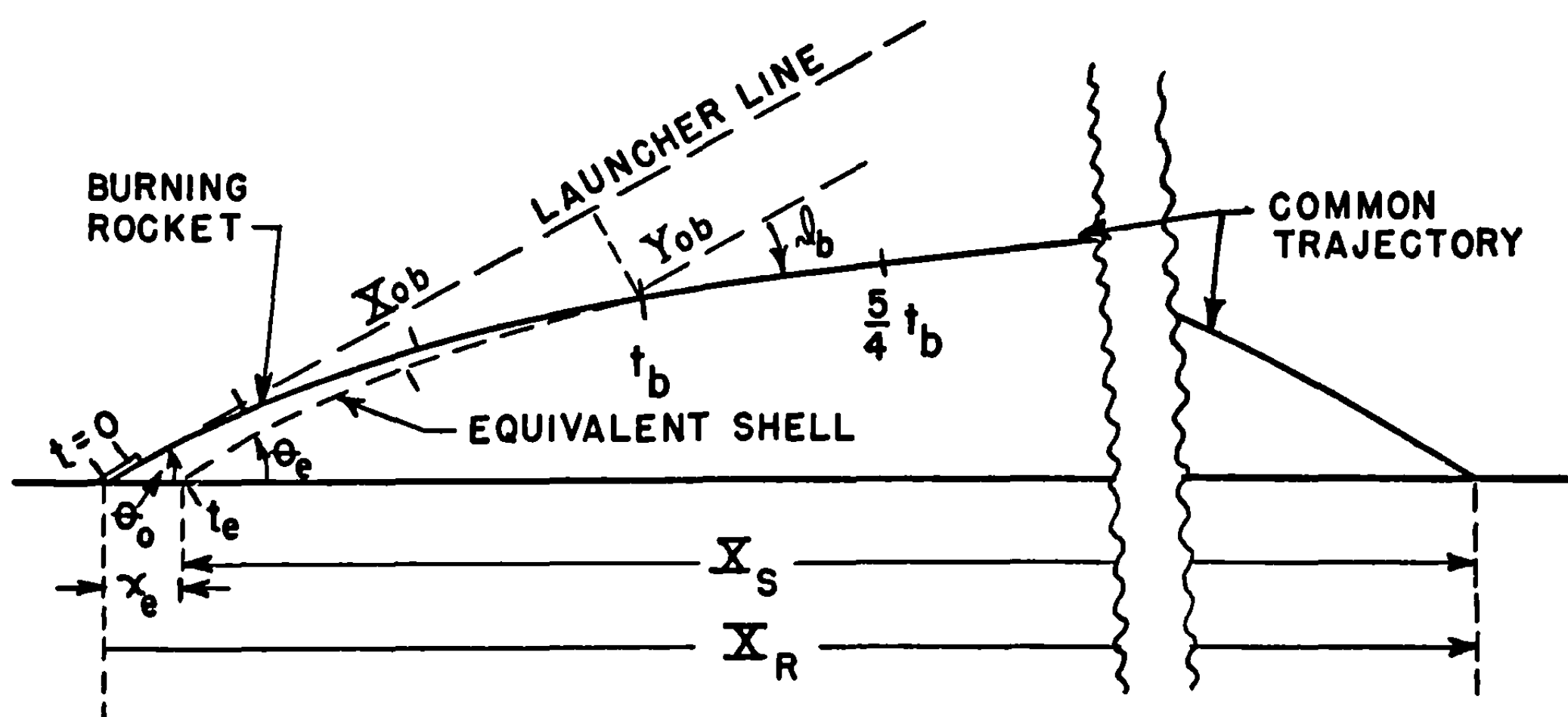


FIGURE 5.11.—Schematic comparison of the rocket trajectory during burning and the equivalent shell trajectory. Equal time intervals, of length $t_b/4$, are marked on the trajectories.

and

$$t_s = t_b - \frac{X_{0b}}{v_b} + \left[\frac{g X_{0b}^2}{2 v_b^3} \csc \theta_0 + \frac{Y_{0b}}{v_b} \cot \theta_0 + \frac{c X_{0b}^2}{2 v_b} - \frac{\vartheta_b X_{0b}}{v_b} \cot \theta_0 \right] + \dots \quad (3)$$

The distance in front of the launcher at which one must locate the equivalent gun is

$$x_s = 0 + \left[Y_{0b} \csc \theta_0 - \vartheta_b X_{0b} \csc \theta_0 + \frac{g X_{0b}^2}{2 v_b^2} \cot \theta_0 \right] + \dots \quad (4)$$

The lengthy square bracket in each of these expressions contains the terms of second order. Usually it is not necessary to evaluate these terms which are included only to enable one to estimate the accuracy of the approximation made if one stops with the lower order terms.

These expressions for the equivalent initial conditions can be simplified if it is assumed that the jet thrust is constant. We shall assume that the jet thrust is large compared to gravity and the drag. We wish also to eliminate v_b from the result since it depends on θ_0 because of the gravity. Instead we adopt v_0 , the corrected initial velocity as the appropriate measure of the velocity imparted by the jet forces considered in 2.22 because it is defined as the burnt velocity of rocket in the absence of gravity and drag. If it is known, we can compute v_b from the approximate expression

$$v_b = v_0 - (g \sin \theta_0 + \frac{1}{3} c v_0^2) t_b \quad (5)$$

This is easily derived since $-g \sin \theta_0$ is the component of the acceleration along the trajectory due to gravity and the acceleration due to drag is $-c v^2 = -c v_0^2 (t/t_b)^2$. We can also express X_{0b} in terms of v_0 and t_b by means of the approximate relation $X_{0b} = \frac{1}{2} v_0 t_b$. Thus (1) to (4) become, to terms of the first order

$$v_s \doteq v_0 - \frac{1}{2} \left(g \sin \theta_0 - \frac{1}{3} c v_0^2 \right) t_b, \quad (6)$$

$$\theta_s \doteq \theta_0 - \vartheta_b + \frac{1}{2} (g t_b / v_b) \cos \theta_0. \quad (7)$$

$$t_s \doteq \frac{1}{2} t_b, \quad (8)$$

and

$$x_s \doteq 0. \quad (9)$$

Let us now summarize the way in which these formulas are used. To calculate the range, X_R , and the time of flight, T_R , of a rocket, one computes the range, X_S , and time of flight, T_S , of the equivalent shell which is fired with quadrant elevation θ_s and velocity v_s . One then has

$$X_R = X_S + x_s, \quad (10)$$

and

$$T_R = T_S + t_s. \quad (11)$$

5.2 Ballistics of Shells

It is the purpose of this section to treat a few of the simpler methods and in the case of more complicated methods to provide some explanatory material and references that should

be consulted for more complete treatments. The methods considered are those that seem useful in rocketry.

The problem treated is the motion of a point mass acted upon by a constant gravitational force and an aerodynamic drag that is tangent to the trajectory and is a known function of velocity and perhaps the air density, which is a known function of position. An extensive survey of the various methods of attacking this problem is given by Cranz,¹ and a more modern treatment by Herrmann.²

In general, no method gives a completely accurate solution of the differential equations; the only methods whose errors can always be pushed below any preassigned limit are those based on a detailed numerical integration of the trajectories. However, there are many cases where suitable approximate formulas are sufficiently accurate and much more convenient.

5.21 The Vacuum Approximation.—Rocket motors or boosters are occasionally used to throw quite heavy objects over short distances with low initial velocities. In this case the simple vacuum approximation in which the trajectory is a parabola is useful. The formulas are well known and easily derived but it may be convenient to consult Cranz³ for a conveniently arranged and reasonably complete collection. Even in cases where aerodynamic forces are moderately important, the vacuum trajectory may be useful in obtaining rough approximations or treating small segments of the trajectory.

5.22 The Didion-Bernoulli Method.—If the quadrant angle of departure is less than about 20° and the drag is proportional to the square of the velocity, the Didion-Bernoulli method⁴ is very convenient. If only low accuracy is required, as is sometimes the case in rocketry, the quadrant elevation can be as much as 45°. By means of simple modifications it can also be applied with good accuracy to segments of steep trajectories provided the total deflection of the segment considered is less than about 30°. The requirement that the drag be proportional to the square of the velocity restricts one to rockets whose burnt velocity is less than about 800 ft./sec., although, again, if great accuracy is not needed and the range is short enough so that the change in velocity is small, the method can be used provided the final velocity is well over that of sound.

In the Didion-Bernoulli method one throws the equations of motion into a form in which θ , the inclination of the trajectory, and v , the velocity, play prominent roles. One then replaces $\sec \theta$ by a , a suitably chosen constant, in enough places to reduce the equations to an exactly integrable form. The quantities involved are: those mentioned in 5.11; X , the range or distance from firing point to an impact point at the same level; T , the time of flight; v_s , the velocity at the summit or highest point of the trajectory; ω , the striking angle or angle with the horizontal made by the trajectory at impact; v_ω , the velocity at impact; a , a constant that is approximately unity and whose evaluation will be considered below; and Z , a parameter defined by

$$Z = 2caX. \quad (1)$$

The results are given in terms of the functions $B(Z)$, $\Theta(Z)$, $J(Z)$, and $F(Z)$ by the following formulas which also contain the definitions of these functions:

$$v_s^2 \sin 2\theta_0 / gX = B(Z) \equiv 2(e^Z - Z - 1)/Z^2, \quad (2)$$

$$2ca v_s^2 \sin 2\theta_0 / g = Z B(Z), \quad (3)$$

¹ O. Cranz, "Lehrbuch der Ballistik" Vol. 1, Springer, 1925 (Edwards Bros., 1943).

² E. E. Herrmann, "Exterior Ballistics, 1935," U. S. Naval Institute, Annapolis, Md.

³ Cranz, loc. cit., p. 33.

⁴ Cranz, loc. cit., pp. 147-170.

$$gT^2/2X \tan \theta_e = \Theta(Z) \equiv 2(e^{1/2 Z} - 1)/(e^Z - Z - 1) \\ \equiv J \left(\frac{1}{2} Z \right)^2 / B(Z), \quad (4)$$

$$(v_e \cos \theta_e / v_s)^2 = J(Z) \equiv (e^Z - 1)/Z, \quad (5)$$

$$v_e^2 \cos^2 \theta_e (\tan \theta_e + \tan \omega) / gX = J(Z), \quad (6)$$

$$v_e \cos \theta_e / v_\omega \cos \omega = V(Z) \equiv e^{1/2 Z}, \quad (7)$$

$$2v_e \sin \theta_e / gT = F(Z) \equiv (e^Z - Z - 1)/Z(e^{1/2 Z} - 1) \\ \equiv B(Z) / J \left(\frac{1}{2} Z \right), \quad (8)$$

and

$$Tv_e \cos \theta_e / X = J \left(\frac{1}{2} Z \right). \quad (9)$$

The explicit expressions for the functions $B(Z)$ are given although usually one obtains their values either from figure 5.22 or, if more accuracy is needed, from suitable tables.⁶ Figure 5.22 gives the values of B , F , J , V , and ZB as functions of Θ , whose scale is along the bottom of the graph, and of Z , whose scale is along the top. By comparing the top and bottom scales one can get the relationship between Θ and Z .

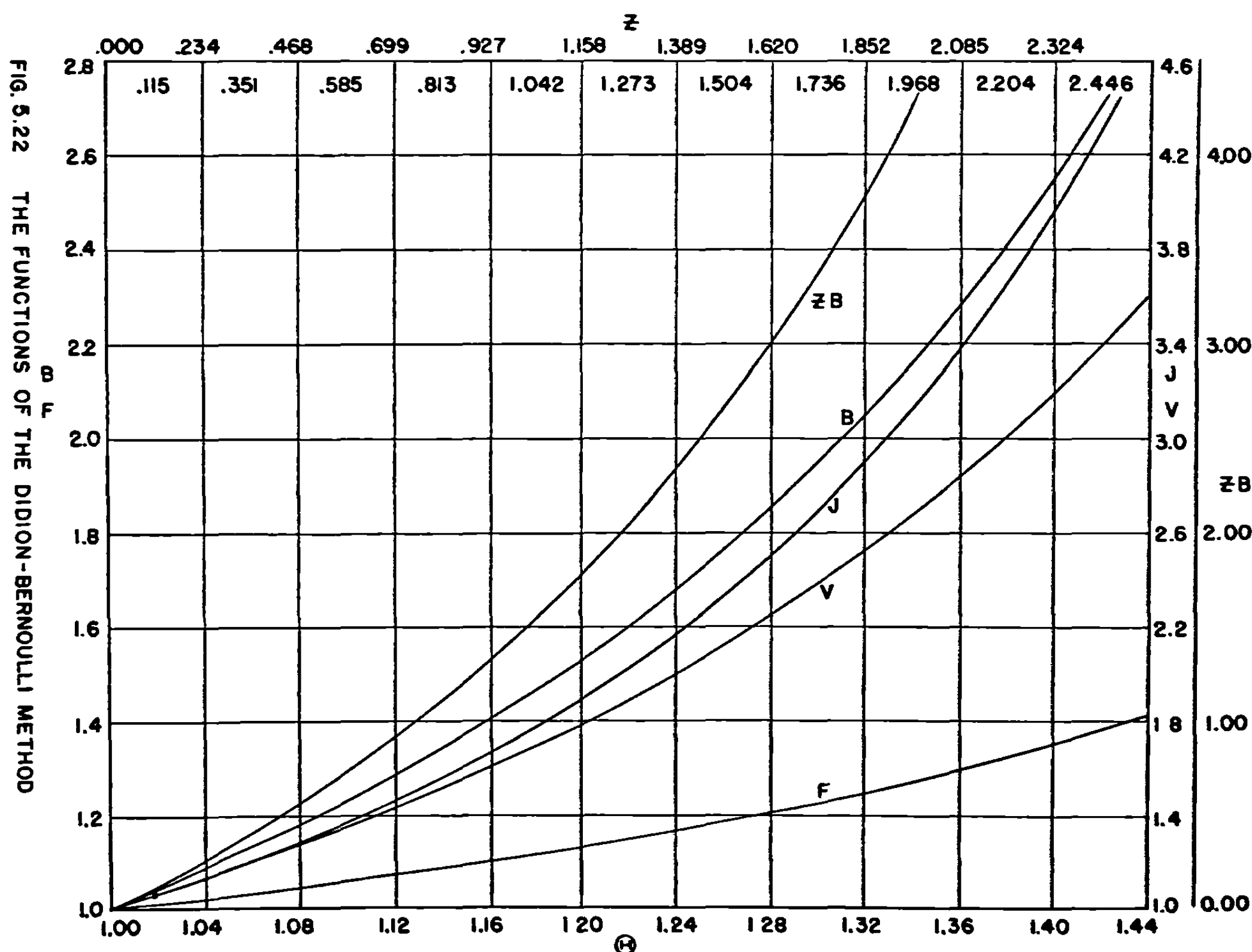


FIGURE 5.22.—The functions of the Didion-Bernoulli method

⁶ Cranz, loc. cit., table 5, pp. 569-571. Table 9, p. 607 of this reference is also convenient for this purpose if one replaces $1000 \pi(2R)^{1/2}/1,306 P$ by $0.9271 \times 10^4 c$.

Before proceeding farther it is necessary to have some means of determining α which is to be regarded as the suitably weighted average of $\sec \theta$ over the trajectory. Ideally the weighting is to be done in such a way that the above formulas give correct results in spite of their approximate derivation. It is, of course, impossible to juggle α so that more than one result is precisely correct. Hence a compromise value must be used. Various authors use various procedures at this point. In practice, it seems best merely to use the results given in Table 5.22, which is based on a table of Cranz ⁶ and to realize that if α differs markedly from unity or if it differs markedly from one method of its computation to another, then the results will not be particularly accurate in any case.

TABLE 5.22

Values of α for Different Values of θ_0 and X , the Range

θ_0 (deg.)	Range (feet)			
	0	2,000	4,000	6,000
2	1.00	1.00	----	----
4	1.00	1.00	1.00	----
6	1.00	1.00	1.00	----
8	1.01	1.01	1.00	1.00
10	1.01	1.01	1.01	1.01
12	1.01	1.01	1.01	1.01
14	1.01	1.01	1.01	1.01
16	1.02	1.02	1.02	1.02
18	1.02	1.02	1.02	1.02
20	1.03	1.03	1.03	1.03
22	1.03	1.03	1.03	1.03
24	1.04	1.04	1.04	1.04
26	1.05	1.05	1.05	1.05
28	1.06	1.05	1.05	1.05
30	1.06	1.06	1.06	1.06
32	1.08	1.08	1.07	1.07
34	1.09	1.09	1.09	1.09
36	1.10	1.10	1.10	1.10
38	1.12	1.11	1.11	1.11
40	1.13	1.13	1.13	1.13
42	1.15	1.15	1.15	1.15
44	1.17	1.17	1.16	1.16
45	1.18	1.18	1.18	1.18

In most cases the order in which the above formulas are to be used is obvious. If, for example, we are given v_0 , X , and θ_0 , we can use (2) to determine $B(Z)$. Figure 5.22 then gives us the corresponding values of Θ , Z , J , V , and F . We take α from the table and use (1), (4) or (8), (5), (6), and (7) to calculate c , T , v_s , ω , and v_ω , respectively. In some cases we must use successive approximations. For example, if we are given c , θ_0 , and v_0 , we first guess a value for α . From (3) we then compute $ZB(Z)$ so that the figure gives us Z . We next use (1) to calculate X , and table 5.22 to check our value of α . If it is necessary to correct it, we must repeat our sequence of calculations until a consistent value is found. The remaining properties of the trajectory can then be computed as in the previous example.

For small values of Z , series solutions are convenient. They are obtained by using (2)–(9) and expanding the functions on the right-hand side in power series in Z . In a similar way the additional equations given by Cranz ⁷ can be expressed in a form that is very convenient provided $Z \ll 1$.

⁶ Cranz, loc. cit., table 11, p. 674.

⁷ Cranz, loc. cit., p. 164, but note that he uses different symbols for the quantities appearing on the left-hand sides of (2)–(9).

Under the circumstances considered in this section one can often make use of what is known as the principal of the rigidity of the trajectory to tell what happens when the quadrant angle of departure is changed somewhat. The principal states that to the first approximation the trajectory behaves as though it were rigid and rigidly attached to the launcher. This principal is particularly useful in allowing for the effect of moderate changes in the elevation of the point of impact. Of course it cannot be used at large quadrant angles of departure. This is obvious if one considers firing at 45° where changing the quadrant angles does not affect the range but does change the shape of the trajectory. Even in this case the principle can be applied to the initial part of the trajectory, particularly if one uses skew coordinates as in 6.42.

5.23 The Otto-Lardillon Method.—This method is superior to the Didion-Bernoulli method in that it gives exact solutions of the equations of motion, the only approximation involved being the assumption that the drag is proportional to the square of the velocity. The procedure is to determine trajectories accurately by numerical integration and to take advantage of the fact if the drag is proportional to the square of the velocity, then it is easy to show that all trajectories having the same θ_e and the same value of one of the quantities $2cX$, cv_e^2/g , $v_e^2/2gX$, ω , v_ω/v_e , $T\sqrt{g/X}$, and y_s/X must have the same value of all the remaining ones, where the notation is as in the previous section. Thus Cranz⁸ gives tables for values of θ_e ranging from 5° to 75° in multiples of 5° that make it possible to determine very easily any of the quantities listed if enough of them are known to determine the trajectory. The method is equally accurate for all quadrant elevations and thus is perhaps the ideal method for the solution of that very common problem of rocket ballistics, the determination of the range of a rocket fired at a high quadrant elevation, usually 45° , and with a burnt velocity of 800 ft./sec.

The disadvantages of the method are that it applies only when the square law of drag can be used and that the results are given in tabular form, the tables being constructed by numerical integration. The available tables seem to have been constructed before the advent of modern methods of numerical integration and modern mechanical computing machines. Hence the entries are so widely spaced that interpolation by second differences is often needed and the tables do not seem to be as accurate as one might wish. In particular, the values given for T and y_s in the tables mentioned above seem to be inaccurate. With modern techniques it should be possible to construct very convenient tables having any desired accuracy.

Since the results are given by tables rather than formulas, they will be more useful than the Didion-Bernoulli results when one is interested in those quantities that are tabulated. Since the Didion-Bernoulli results are given by formula, they are more flexible and can be used to provide more detailed, although usually less accurate, information about the trajectory.

The Otto-Lardillon tables can of course be reduced to graphical form and if plotted on 11 by 17 inch graph paper are sufficiently accurate for many problems. This has proved to be a very convenient form in rocketry. There are also many other tables besides those mentioned above.¹⁰

Occasionally, derivatives of the range with respect to various quantities are needed in estimating corrections. These can be obtained in the usual manner from the Otto-Lardillon tables; or, if only rough values are needed, one may use the formula

$$\ln \frac{X}{X_s} \sim -(cv_e^2/g) \sin \theta_e \cos^3 \theta_e, \quad (1)$$

⁸ Cranz, loc. cit., pp. 577-582.

¹⁰ See Cranz, loc. cit., p. 550, for an extensive series of references. See Applied Mathematics Panel Report No. 77.1, November 1943, prepared for the Bureau of Ordnance, Navy Department. These tables, while not as conveniently arranged for purposes of rocket ballistics as those in Cranz, give to many significant figures complete information on the descending branch of the trajectory.

where X_v is the vacuum range,

$$X_v = g^{-1} v_e^2 \sin 2\theta_e.$$

This is an empirical formula that gives a rough fit to the Otto-Lardillon tables up to about $\theta_e = 60^\circ$ provided $\ln(X/X_v) > -2/3$. This formula is probably too inaccurate for use in calculating range directly but it may be more useful in calculating derivatives, since then we can put it in a form in which the unspecified constant of proportionality has been eliminated, thus, in effect, giving it the value most nearly appropriate to the particular trajectory considered. We now obtain in this way expressions needed later:

$$\frac{\partial X}{\partial v_e} \approx \frac{2X}{v_e} \left(1 + \ln \frac{X}{X_v} \right), \quad (2)$$

and

$$\frac{\partial X}{\partial \theta_e} \approx \frac{X}{\sin \theta_e \cos \theta_e} \left[2 \cos^2 \theta_e - 1 + \frac{1}{2} (3 \cos^2 \theta_e - 1) \ln \frac{X}{X_v} \right]. \quad (3)$$

5.24 The Siacci Method.—The methods given above are adequate for most problems in which the burnt velocity of the rocket is less than about 800 ft./sec. so that the quadratic resistance law can be used. At higher velocities it is necessary to use a procedure in which allowance can be made for the particular resistance law of the projectile under consideration. If the quadrant angle of departure is less than 15° or 20° , or if only a segment of the trajectory that turns through less than about 30° is of interest, as in forward firing from airplanes, then it is possible to use a modification of the Didion-Bernoulli method. If the resistance is assumed to vary as the n th power of the velocity, the results can be put in analytic form;¹¹ however, such a resistance law can be used but rarely. If the resistance law is given essentially as a table of the drag as a function of velocity as in the case of the Siacci law or the equivalent Gâvre law discussed in 2.441, then the method makes use of tabulated functions obtained by numerical quadrature from the drag function. There are a number of minor modifications of the procedure that can be followed. The foremost developer of the method was Siacci; convenient tables and an explanation of the latest form of his methods are given by Cranz¹² as the method of Siacci III. A modification that was popular in this country is that of Ingalls.¹³ Similar tables have also been prepared at Aberdeen for several other resistance laws. Unless one knows with fair accuracy how the resistance of the particular rocket considered varies with velocity, it is pointless to be too particular in choosing which set of tables to use. It seems sufficient to make a choice of that one of the three laws, the square law, the Gâvre (or Siacci) law, and the G_0 (or J_0) law, for which tables have been prepared at Aberdeen, that best fits what is known of the resistance of the rocket in question. Usually the ballistic coefficient will be chosen to fit range firings and hence one can expect reasonable accuracy if the trajectory is not too curved.

These modifications of the basic Didion-Bernoulli method eliminate its assumption that the drag is proportional to the square of the velocity but do approximate by treating $\sec \theta$ as a constant in some places in the equation of motion. Thus they can not be used for trajectories over which the variation in θ is too great. If one demands the accuracy of which the best guns are capable, this limits the quadrant elevation to about 5° , but with the accuracy needed for rocketry, the wider limits given earlier can be used.

¹¹ Cranz, loc. cit., p. 162.

¹² Cranz, loc. cit., p. 175 and pp. 644-673.

¹³ See Herrmann "Exterior Ballistics, 1926" and "Exterior Ballistics, 1930," Annapolis, Md.

5.25 Other Methods.—In all the methods considered up to this point it has been possible to arrange things so that a single formula or entry in a table provided information about a whole family of trajectories. Moreover the tables were obtained either by evaluating analytically expressed functions or by numerical quadratures. If, however, one considers the trajectories of projectiles fired at high quadrant elevations and at velocities greater than 800 ft./sec., the situation becomes much worse. Not only does one have minor complications such as the change of air density, and hence drag, with elevation along the trajectory and the somewhat more serious complication that the drag is given by a table; one also finds that it is necessary to solve the differential equations of motion numerically and to express the results in tables in which each entry refers only to a single point on a single trajectory. Thus it requires an exceedingly large table to cover a reasonably extensive set of trajectories. It is necessary to space the entries so widely that one must usually interpolate by second differences in each of the several independent variables, and hence such tables are somewhat troublesome to use.

The advantage of such a table is that it promises completely accurate results regardless of the quadrant elevation or velocity. In practice, of course, it can not do this because it must be based on some particular drag law, and the rocket in which one is interested always follows some other (undetermined) law. Also the tables neglect all the aerodynamic forces except the drag. The only tables available are based on the Gâvre resistance law and do not extend over the entire range of ballistic coefficients needed in rocketry. In spite of all these inconveniences and limitations, the tables can be very useful on occasion. The most extensive set of such tables seems to be that prepared at Aberdeen Proving Ground.¹⁴ Other tables of lesser scope are given by Herrmann¹⁵ and by the French A. L. V. F. Tables.¹⁶

If only a few trajectories are required, it is not difficult nor particularly time consuming to obtain them by a numerical integration done on an ordinary calculating machine. Those familiar with the numerical integration of differential equations will not need advice on how to proceed and will be expected to have their own favorite methods. Readers who are unfamiliar with the procedures will probably find the Milne method¹⁷ convenient, easy to learn, and accurate. If one wants a completely different point of view and a summary of a variety of other methods that are thought by some to be more efficient than the Milne method, one can consult Jeffries and Jeffries.¹⁸

To calculate by numerical integration a great many trajectories, as for range tables, when existing tables are not felt to be accurate enough, is a major project that should not be undertaken without a careful study to determine the most efficient procedure and the facilities and time required. Of course the best procedure is to use an automatic high-speed electrical or mechanical computer if it is available.

The reader may wonder why the best procedure is not just to let the rocket do the computing. One has only to fire it and observe where it lands. But because of the dispersion it is necessary to fire many rockets in order to determine the best mean trajectory. If photographic techniques that enable one to make accurate measurements of position, velocity, and direction of motion at the end of burning are used, one can correct for the dispersion since most of it occurs during burning. If no calculations are made, it is necessary to fire a pro-

¹⁴ Ordnance Department, U. S. Army, "Exterior Ballistic Tables Based on Numerical Integration," Vol. I, "Summital Arguments," 1924, enables one to determine the complete trajectory in terms of conditions at the summit. Vol. II, "Summital Values," 1931, gives the conditions at the summit in terms of the initial conditions. Vol. III, "Terminal Values," 1944, gives the conditions at impact in terms of the initial conditions.

¹⁵ E. E. Herrmann, "Range and Ballistic Tables, 1935," pp. 89-124, U. S. Naval Institute, Annapolis, Md.

¹⁶ Commission Artillerie Lourde sur Voie Ferrée "Tables de Balistique Extérieure," French Ministère de l'Armement, September 15, 1918. These tables were translated in 1919 by the Ordnance Department, U. S. Army. More complete tables were published by the French in 1921, but these have not been translated.

¹⁷ W. E. Milne, "Numerical Calculus," pp. 131-144, Princeton University Press, 1949.

¹⁸ H. Jeffries and B. S. Jeffries, "Methods of Mathematical Physics," Cambridge, 1946.

hibitively large number of rockets to cover the required ranges of quadrant angles of departure, temperatures, and perhaps elevations of the impact point. The usual procedure is to fire groups of rockets at a few quadrant angles and temperatures in order to obtain the basic information on the properties of the rocket. Ballistic tables and formulas are then used essentially as interpolation formulas to obtain a great many more trajectories. In this way, while it is desirable that the ballistic tables be reasonably appropriate for the projectile considered, it is not essential that they fit precisely since one can afford small errors in interpolation. A further description of this process will be found in any account of the construction of range tables.

5.3 Differential Corrections

The calculations of the preceding sections have been made with the tacit assumption that we were dealing with an ideal projectile under ideal conditions. Actually the projectile is deflected by various perturbing forces, due to its imperfections, the effects of its spin, the wind, and variations in normal air density. Further, if the trajectory tables are desired for a slightly different projectile, corrections must be applied. It is possible to make such corrections, if they are small, without an elaborate computation. The results are valid as long as the trajectory is not distorted so much that the forces are significantly different. Thus, for example, if the wind changes the time of flight so much that it acts on the projectile for much longer than the usual time of flight, then the wind deflection may be much greater than that predicted.

5.31 Green's Functions.—We are interested in the solution for the trajectory in a case which differs only slightly from a previously solved case. The particular problem may differ in initial conditions or may have additional aerodynamic forces, but their effects must be small if the approximate treatment is to hold. The differential equations of motion are

$$\dot{v} = -g \sin \theta - cf(v), \quad (1)$$

$$v\dot{\theta} = -g \cos \theta + \eta, \quad (2)$$

$$v\dot{\varphi} = \xi \sec \theta, \quad (3)$$

$$\dot{x} = v \cos \theta \cos \varphi, \quad (4)$$

$$\dot{y} = v \sin \theta, \quad (5)$$

and

$$\dot{z} = \cos \theta \sin \varphi, \quad (6)$$

where x , y , z are the coordinates of the rocket in a system in which x is along the range line, y is vertically up, and z is horizontal to the right, v is the velocity, θ is the inclination of the trajectory, φ is defined by (6) and is the azimuth of the tangent to the trajectory, assumed small, and ξ and η are components (horizontally to the right and upward normal to the trajectory, respectively) of the aerodynamic acceleration normal to the trajectory. We suppose $f(v)$ to be a specified function that gives the variation of drag with velocity. We use a subscript zero to denote the solution of these equations with

$$\xi = \eta = 0, \quad c = c_i = \text{constant}, \quad (7)$$

and with the initial conditions

$$x = y = z = \varphi = 0, \quad v = v_i, \quad \theta = \theta_i. \quad (8)$$

We suppose this solution to be known and available for use in calculating the corrections.

We now wish a solution of these equations with the initial conditions

$$x = y = z = \varphi = 0, \quad v = v_i + v_i', \quad \theta = \theta_i + \theta_i', \quad (9)$$

where

$$v_i' \ll v_i, \quad \theta_i' \ll \theta_i \quad (10)$$

and where the accelerations ξ and η are finite but

$$\xi \ll g, \quad \eta \ll g, \quad (11)$$

and the deceleration coefficient has the form

$$c = c_i + c', \quad c' \ll c_i. \quad (12)$$

We may write the solutions in the form

$$\begin{aligned} v &= v_0 + v', \\ \theta &= \theta_0 + \theta', \\ \varphi &= \varphi', \\ x &= x_0 + x', \\ y &= y_0 + y', \\ z &= z_0 + z', \end{aligned} \quad (13)$$

where the primed quantities are considered small. To the first order we may write

$$\begin{aligned} f(v) &= f(v_0) + v' \frac{df(v_0)}{dv_0}, \\ \cos \theta &= \cos \theta_0 - \theta' \sin \theta_0, \\ \sin \theta &= \sin \theta_0 + \theta' \cos \theta_0. \end{aligned} \quad (14)$$

Inserting (13) in (1) to (6), using (14) and retaining only first order terms, we obtain the two sets of linear equations

$$\left. \begin{aligned} \dot{v}' + g \cos \theta_0 \theta' + c \frac{df(v_0)}{dv_0} v' &= -c' f(v_0), \\ \dot{\theta}' - \frac{g \cos \theta_0}{v_0^2} v' - \frac{g \sin \theta_0 \theta'}{v_0} &= \frac{\eta}{v_0}, \\ \dot{x}' - v' \cos \theta_0 + v_0 \sin \theta_0 \theta' &= 0, \\ \dot{y}' - v' \sin \theta_0 - v_0 \cos \theta_0 \theta' &= 0, \end{aligned} \right\} \quad (15)$$

and

$$\left. \begin{aligned} v_0 \dot{\varphi}' &= \xi \sec \theta_0, \\ \dot{z}' - v_0 \cos \theta_0 \varphi' &= 0, \end{aligned} \right\} \quad (16)$$

and the initial conditions

$$x' = y' = z' = \varphi' = 0, \quad v' = v_i', \quad \theta' = \theta_i'. \quad (17)$$

The equations have been grouped to show that they are independent. The solution of (16) which satisfies (17) is

$$\begin{aligned} \varphi &= \int_0^t [\xi(t) \sec \theta_0(t) / v_0(t)] dt, \\ z &= \int_0^t v_0(t) \varphi(t) \cos \theta_0(t) dt. \end{aligned} \quad (18)$$

The value of ξ does not affect any of the other solutions and φ and z are unaffected by them.

We may solve equations (15) by the Green's function methods employed in 3.37 if we define the sets of Green's functions $V_v(t_0, t)$, $\Theta_v(t_0, t)$, $X_v(t_0, t)$, $Y_v(t_0, t)$, and $V_\theta(t_0, t)$, $\Theta_\theta(t_0, t)$, $X_\theta(t_0, t)$, $Y_\theta(t_0, t)$ to be the sets which satisfy the homogeneous part of (15) with the initial conditions

$$V_v(t_0, t_0) = 1, \quad \Theta_v(t_0, t_0) = X_v(t_0, t_0) = Y_v(t_0, t_0) = 0 \quad (19)$$

and

$$\Theta_\theta(t_0, t_0) = 1, \quad V_\theta(t_0, t_0) = X_\theta(t_0, t_0) = Y_\theta(t_0, t_0) = 0, \quad (20)$$

respectively. This is the definition of these functions; a much better practical method for evaluating them is explained in the next section. We then have the solutions

$$v' = v_i' V_v(0, t) + \theta_i' V_\theta(0, t) - \int_0^t c'(\tau) f[v_0(\tau)] V_v(\tau, t) d\tau + \int_0^t \frac{\eta(\tau)}{v_0(\tau)} V_\theta(\tau, t) d\tau, \quad (21)$$

$$\theta' = v_i' \Theta_v(0, t) + \theta_i' \Theta_\theta(0, t) - \int_0^t c'(\tau) f[v_0(\tau)] \Theta_v(\tau, t) d\tau + \int_0^t \frac{\eta(\tau)}{v_0(\tau)} \Theta_\theta(\tau, t) d\tau, \quad (22)$$

$$x' = v_i' X_v(0, t) + \theta_i' X_\theta(0, t) - \int_0^t c'(\tau) f[v_0(\tau)] X_v(\tau, t) d\tau + \int_0^t \frac{\eta(\tau)}{v_0(\tau)} X_\theta(\tau, t) d\tau, \quad (23)$$

and

$$y' = v_i' Y_v(0, t) + \theta_i' Y_\theta(0, t) - \int_0^t c'(\tau) f[v_0(\tau)] Y_v(\tau, t) d\tau + \int_0^t \frac{\eta(\tau)}{v_0(\tau)} Y_\theta(\tau, t) d\tau. \quad (24)$$

In practice this form is not always useful if one wishes to make a single correction of one trajectory because the Green's functions cannot be obtained in closed form; hence it is necessary to fall back on direct numerical integration of the equations defining them and then to evaluate the above integrals numerically. Actually it may be less work to obtain the solution of the varied equations than to obtain the Green's function as a first step. If, however, a large number of corrections must be made, the Green's function approach is valuable since the Green's functions need be obtained only once. This is particularly true when the effects of wind or other fluctuating forces are to be determined. Also it is not necessary to calculate the corrections with as much accuracy as would have to be used in calculating the varied trajectory. This consideration is particularly important when the standard trajectory is based in part on experimental data and is not purely a computed trajectory. Fortunately there is a simple way to evaluate the Green's functions numerically, as shown in the next section, that gives

them all as functions of τ by one numerical integration for each t at which the effects are desired. If computations at a large number of times are required, as in fitting a measured trajectory, direct integration of the differential equations of motion is probably simpler than the Green's function approach.

If we are interested in the change in velocity at impact or in change in angle of fall we may use (21) and (22), but if we are interested in the change in impact point or in the change in the time of flight we must combine (23) and (24). We find, to the first order, that the change in range is

$$\Delta X = x'(T) - y'(T) \cot \theta_0(T), \quad (25)$$

where T is the uncorrected time of flight. The change in time of flight is

$$\Delta T = \frac{y'(T)}{v_0(T) \sin \theta_0(T)}. \quad (26)$$

The change in angle of impact is

$$\Delta \omega = \theta'(T) - \Delta T \frac{g \cos \theta_0(T)}{V_0^2} \quad (27)$$

5.32 Connection Between the Green's Functions and the Adjoint Equations.—Suppose that one wishes to determine the change in range due to a change in c . Inspection of 5.31 (23), (24), and (25), shows that one must have values of $X_e(\tau, T)$ and $Y_e(\tau, T)$ as functions of the single final time, T , and a series of values of the initial time, τ , so that one can evaluate by Simpson's rule the integrals with respect to τ from 0 to T . Now the Green's functions are defined by the statement that they satisfy 5.31 (15) subject to the initial conditions 5.31 (19). Thus it would appear that their calculation would require an extensive series of numerical integrations, each starting from a different initial condition and proceeding through a range of useless intermediate values to the required final value. Each complete integration would give but one value of the desired function. Obviously, the process would be enormously shortened if we could start at $t=T$ and solve numerically a set of differential equations such that each intermediate step in the process would give a useful value of the Green's function and that only a single numerical integration would be needed to get all the values of the Green's function for the selected T . In other words, one would like to use τ rather than T , the first of the two arguments of $X_e(\tau, T)$ rather than the second, as the running variable in the numerical integration. This can be done by considering what is called the set of equations adjoint to the given set.

We shall now explain this procedure in the general case rather than the particular one considered in 5.31. Any set of linear equations can be reduced to a set of N first order equations by the introduction of additional variables; usually these are just the derivatives of the dependent variables. This step is not necessary in 5.31. In all except singular cases, the resulting linear equations can be solved for the first derivatives and put in the form

$$\frac{dy_i}{dt} = \sum_{k=1}^N a_{ik}(t) y_k(t) + b_i(t), \quad i=1, \dots, N, \quad (1)$$

where the N dependent variables are now denoted by y_i , $i=1, \dots, N$, and a_{ik} and b_i are specified functions of the time only. To solve (1) we must first obtain N independent solutions of the homogeneous equations obtained by setting all $b_i=0$. Let us designate by $y_i^{(n)}(\tau, t)$ the solution that satisfies the initial conditions

$$y_i^{(n)}(\tau, \tau) = \delta_i^n, \quad (2)$$

where δ_i^n is, as usual, equal to unity if $i=n$ and is zero otherwise. Each function has two arguments, the primary argument, t , which is the independent variable in (1) and the subsidiary argument, τ , which is the value of t at the time (2) is imposed. The upper index, n , tells which one of the various sets of solutions is being considered; the lower index, i , tells which variable is being considered. By letting n run from 1 to N we get the required N independent sets of solutions. The general solution of (1) is obtained by adding a general linear combination of these $y_i^{(n)}(\tau, t)$ to a particular solution of the nonhomogeneous form of (1). We saw in 3.37 that the particular solution, $y_{iP}(t)$, that satisfied the initial conditions ²⁰

$$y_{iP}(0) = 0, \quad i = 1, \dots, N, \quad (3)$$

was

$$y_{iP}(t) = \sum_{n=1}^N \int_0^t b_n(\tau) y_i^{(n)}(\tau, t) d\tau, \quad i = 1, \dots, N. \quad (4)$$

If complete generality were desired the 0 on the left in (3) and the lower limits of (4) and (9) could be replaced by t_0 .

It now remains to obtain the $y_i^{(n)}(\tau, t)$ as functions of τ for the time $t=T$ of particular interest. If analytical solutions of (1) with $b_i=0$ are obtainable, no more need be said. Often, however, these solutions must be obtained by a series of numerical integrations. As we stated above, this process was simplified if the adjoint equations were used. These equations are defined to be

$$\frac{du_i(\tau)}{d\tau} = - \sum_{k=1}^N a_{ki}(\tau) u_k(\tau), \quad i = 1, \dots, N. \quad (5)$$

Here τ is the independent variable, $u_i(\tau)$ is the set of dependent variables, and the coefficients on the right-hand side are obtained by transposing the matrix of the coefficients in (1). Let us designate by $u_i^{(n)}(t, \tau)$ the solution that satisfies the initial conditions

$$u_i^{(n)}(t, t) = \delta_i^n, \quad (6)$$

where here τ is primary argument of $u_i^{(n)}(t, \tau)$ and t is the subsidiary argument that gives the value of τ when (6) is imposed. We note that $u_i^{(n)}(t, \tau)$ is obtainable as a function of τ by a single numerical integration over τ . Hence we have the desired simplification as a consequence of the theorem that

$$y_i^{(s)}(\tau, t) = u_j^{(s)}(t, \tau). \quad (7)$$

To prove this theorem we replace the independent variable in (1) by τ . It is then easy to see from (5) and (1) that

$$\begin{aligned} \frac{d}{d\tau} \sum_{j=1}^N [u_j^{(s)}(t, \tau) y_{jP}(\tau)] &= - \sum_{j,k=1}^N a_{kj}(\tau) u_k^{(s)}(t, \tau) y_{jP}(\tau) \\ &\quad + \sum_{j,k=1}^N u_j^{(s)}(t, \tau) a_{jk}(\tau) y_{kP}(\tau) + \sum_{j=1}^N u_j^{(s)}(t, \tau) b_j(\tau). \end{aligned} \quad (8)$$

²⁰ The derivation in 3.37 was carried out for a special case and with different notation, but it is clear that the proof applies to the general case.

The two double sums cancel out. Hence integrating from $\tau=0$ to $\tau=t$ and simplifying the left-hand side by (6) and (3) we get

$$\sum_{j=1}^N \left[u_j^{(s)}(t, \tau) y_{jP}(\tau) \right]_0^t = y_{jP}(t) = \sum_{j=1}^N \int_0^t b_j(\tau) u_j^{(s)}(t, \tau) d\tau. \quad (9)$$

If this is compared with (4) it is seen that (7) follows from the fact that these equations must hold for any b_i .

If the particular solution for which $y_j=c_j$ at $t=0$ is required, it is

$$y_i(t) = \sum_{j=1}^N c_j u_j^{(i)}(t, 0) + \sum_{j=1}^N \int_0^t b_j(\tau) u_j^{(i)}(t, \tau) d\tau. \quad (10)$$

The subject of differential corrections is treated by Bliss²¹ from the point of view of functions of lines, and the use of the adjoint equation is illustrated by the calculation of the effect of wind on the trajectory. It is instructive to compare these different approaches to the subject, both of which lead to the same result.

In chapter 10 we shall be interested in the change in range due to the aerodynamic force, η . Hence as an example we now work out the appropriate formulas in detail. To put 5.31 (15) in the form of (1), take $v'=y_1$, $\theta'=y_2$, $x'=y_3$, $y'=y_4$. The corresponding adjoint equations are

$$\begin{aligned} \frac{du_1}{d\tau} &= c \frac{df(v_0)}{dv_0} u_1 - \frac{g \cos \theta_0}{v_0^2} u_2 - \cos \theta_0 u_3 - \sin \theta_0 u_4, \\ \frac{du_2}{d\tau} &= g \cos \theta_0 u_1 - \frac{g \sin \theta_0}{v_0} u_2 + v_0 \sin \theta_0 u_3 - v_0 \cos \theta_0 u_4, \\ \frac{du_3}{d\tau} &= 0, \end{aligned}$$

and

$$\frac{du_4}{d\tau} = 0. \quad (11)$$

Here v_0 , θ_0 , and $f(v_0)$ are regarded as known functions of τ . Since we are treating only the effect of η , the only nonzero b_i is $b_2 = \eta/v_0$. From 5.31 (25) we see that we want $y_{3P}(T)$ and $y_{4P}(T)$. From (4) and (7) we now see that we need only $y_3^{(2)} = u_2^{(3)}$ and $y_4^{(2)} = u_2^{(4)}$. The initial conditions that define $u_j^{(3)}(T, \tau)$ are that at $\tau = T$,

$$u_1^{(3)}(T, T) = u_2^{(3)}(T, T) = u_4^{(3)}(T, T) = 0, \quad u_3^{(3)}(T, T) = 1. \quad (12)$$

Hence, by (11), $u_3^{(3)}(T, \tau) = 1$, $u_3^{(4)}(T, \tau) = 0$. The initial conditions that define $u_j^{(4)}$ are,

$$u_1^{(4)}(T, T) = u_2^{(4)}(T, T) = u_3^{(4)}(T, T) = 0, \quad u_4^{(4)}(T, T) = 1. \quad (13)$$

Hence, by (11), $u_4^{(3)}(T, \tau) = 0$, $u_4^{(4)}(T, \tau) = 1$.

Consideration of 5.31 (25) shows us that it is desirable to define the new functions

$$U_j(T, \tau) = u_j^{(3)}(T, \tau) - u_j^{(4)} \cot \theta_0(T), \quad j=1, 2 \quad (14)$$

where the case $j=2$ is the useful one. If we now evaluate $dU_j/d\tau$ with the aid of (14) and (11) we find that

²¹ G. A. Bliss, "Mathematics for Exterior Ballistics," pp. 63-97, Wiley & Sons, 1944.

$$\begin{aligned}\frac{dU_1}{d\tau} &= c \frac{df(v_0)}{dv_0} U_1 - \frac{g \cos \theta_0}{v_0^2} U_2 + \frac{\sin [\theta_0(\tau) - \theta_0(T)]}{\sin \theta_0(T)}, \\ \frac{dU_2}{d\tau} &= g \cos \theta_0 U_1 - \frac{g \sin \theta_0}{v_0} U_2 + v_0 \frac{\cos [\theta_0(\tau) - \theta_0(T)]}{\sin \theta_0(T)}.\end{aligned}\quad (15)$$

From (12) and (13) we see that the initial conditions are

$$U_1(T, T) = U_2(T, T) = 0. \quad (16)$$

With $U_2(T, \tau)$ defined in this way, the change in range due to the aerodynamic force, η is

$$\Delta X = \int_0^T \frac{\eta(\tau) U_2(T, \tau) d\tau}{v_0(\tau)}. \quad (17)$$

It is possible to eliminate U_1 from (15) and define U_2 by a single second degree equation, but this equation is neither easier to handle analytically nor simpler to integrate numerically.

5.33 Some Approximate Differential Corrections.—If one has approximate formulas, such as those given by the Didion-Bernoulli method, for the range or other quantities of interest, it is easy to obtain by differentiation the various differential corrections. For example, if the quadrant angle of departure and burnt velocity are low enough so that 5.22 (2) holds, then we have

$$\frac{\partial X}{\partial v_e} = \frac{ZB(Z)}{c \alpha v_e} \left/ \frac{d}{dZ} [ZB(Z)] \right., \quad (1)$$

and

$$\frac{\partial X}{\partial \theta_e} = \frac{ZB(Z)}{c \alpha} \left/ \frac{d}{dZ} [ZB(Z)] \right., \quad (2)$$

where $ZB(Z)$ and its derivative can be estimated from figure 5.22. For quadrant elevations where the Otto-Lardillon method must be used, 5.23 (2) and (3) provide corresponding expressions that can also be used at low quadrant elevations in place of (1) and (2) if desired.

The approximate expression 5.23 (1) may also be used to estimate the effects of change in velocity, drag, or mass. The effect of a change in the equivalent initial velocity, v_e , is seen from 5.23 (2) to be

$$\frac{\Delta X}{X} \approx \frac{\Delta v_e}{v_e} \left(2 + 2 \ln \frac{X}{X_v} \right). \quad (3)$$

The effect of a change in the deceleration coefficient is obtained by differentiating 5.23 (1) and is

$$\frac{\Delta X}{X} \approx \frac{\Delta c}{c} \ln \frac{X}{X_v}. \quad (4)$$

The effect of a change in mass may be obtained from these last two expressions. Since

$$\frac{\Delta v_e}{v_e} = -\frac{\Delta m}{m} \text{ and } \frac{\Delta c}{c} = -\frac{\Delta m}{m}, \quad (5)$$

we have

$$\frac{\Delta X}{X} = -\frac{\Delta m}{m} \left(2 + 3 \ln \frac{X}{X_v} \right). \quad (6)$$

Of these formulas, (6) is the most accurate for large drag, as shown by comparison with

other range tables. None of these expressions should be used when $\ln(X/X_0) < -2/3$, since then 5.23 (1) is no longer even a passable approximation. In fact, for $\ln(X/X_0) < -1$, equation (3) becomes ridiculous. However, though all formulas based on 5.23 (1) must be used with discretion, they are useful for short range rockets where it is difficult to obtain direct experimental values for the various effects.

5.4 The Effect of Wind

In the last section wind was mentioned as one of the perturbing influences which can be handled by the method of differential corrections. This is done by Bliss ²² so that we shall not repeat it here, but instead shall give an approximate treatment which is suitable in many circumstances. The advantage of this procedure is that very convenient formulas, which do not involve much computation, may be obtained for the wind effect in the case in which the wind is nearly independent of altitude.

After a small initial transient the motion of the projectile relative to the moving air is the same as it is relative to still air because both stabilizing mechanisms, fins and gyroscopic effects, orient the projectile relative to the direction of motion through the air. Then the effect of wind is caused, not by cross force, but by the downwind component of the drag, since, relative to the ground, the drag now has a component normal to the range line.²³ We shall calculate the effect of wind by transforming to coordinate axes moving with the air.

5.41 Derivation of Formulas.—Let us first consider the cross-wind deflection. During the flight of the shell, the coordinate system fixed in the air moves the distance $w_{\perp} T_e$, where w_{\perp} is the cross-wind velocity and T_e is the time of flight of the equivalent shell. With respect to the moving system, the initial direction of motion of the shell is at an angle $w_{\perp}/v_e \cos \theta_e$ up-wind, and hence the shell lands a distance $w_{\perp} X/v_e \cos \theta_e$ up-wind. Combining these we have the net cross-wind deflection

$$\Delta z = w_{\perp} \left(T_e - \frac{X}{v_e} \cos \theta_e \right), \quad (1)$$

and the deflection in radians is

$$\Delta \varphi = w_{\perp} \left(\frac{T_e}{X} - \frac{1}{v_e} \cos \theta_e \right), \quad (2)$$

where X is the range, v_e the velocity, and θ_e the quadrant elevation of the equivalent shell.

To obtain the effect of range wind we also use a coordinate system moving with the air. Again, the displacement of the coordinate system at impact is $w_{\parallel} T_e$, where w_{\parallel} is the range wind velocity. In the moving system, the shell has the approximate quadrant elevation $(\theta_e + w_{\parallel} \sin \theta_e / v_e)$ and velocity $V_e = (v_e - w_{\parallel} \cos \theta_e)$ with respect to the air. Hence the change in range is given by

$$\Delta X = w_{\parallel} \left(T_e + \frac{\sin \theta_e}{v_e} \frac{\partial X}{\partial \theta_e} - \cos \theta_e \frac{\partial X}{\partial v_e} \right). \quad (3)$$

Both (2) and (3) are nearly exact for small wind velocities but (3) is hard to evaluate experimentally because the derivative in the last term is not easily measurable. It is possible to obtain a good approximation to (3) by means of the Otto-Lardillon theory when the trajectory does not differ extensively from the vacuum trajectory and along which the drag varies as the square of the velocity. Using the expressions for the derivatives 5.23 (2) and (3), we have

$$\Delta X \approx w_{\parallel} \left[T_e - \left(\frac{X}{v_e \cos \theta_e} \right) \left(1 + \frac{1 + \cos \theta_e}{2} \ln \frac{X}{X_0} \right) \right]. \quad (4)$$

²² Ibid.

²³ E. E. Herrmann, "Exterior Ballistics, 1935," p. 139, Annapolis, Md.

This equation is approximately valid only for the case $\ln X/X_0 > -2/3$ because the approximation 5.23 (1) is only good to this point. In the cases of supersonic velocities and of large drag it is necessary to evaluate the derivatives in (3) by some other method. If they are evaluated by numerical integration of the equations (15), it is not much more work to obtain the Green's function and to treat the deflection rigorously. The derivatives may be evaluated in many cases by using the tables of the trajectories based on the Gavre law which are published by Aberdeen Proving Ground.

CHAPTER 6

THE BALLISTICS OF ROCKETS FIRED FORWARD FROM AIRCRAFT

6.0 Introduction

Up to this point we have been concerned solely with the ballistics of rockets launched from stationary emplacements on the ground. The ballistics of rockets launched from vehicles moving up to about 50 or perhaps 100 ft./sec. can be handled by the methods introduced in the treatment of wind effects. However, such methods are not satisfactory at the higher velocities involved in firing from aircraft. In practice, it is necessary to fire a fin-stabilized projectile *forward* from a rapidly moving vehicle; that is, the angle between the launcher axis and the direction of motion of the launcher must be small, in order that the yaw at launching be small. If this condition is violated, the deflection of the trajectory and the dispersion will tend to be large; while if the initial yaw is small the behavior of the rocket tends to be satisfactory and to be calculable theoretically by the methods of the previous chapters, which are valid only for small yaw ($\delta \ll 1$). It will be the aim of the present chapter to extend the previously given theory to allow for the initial conditions appropriate to this mode of launching and also to investigate any new problems that arise thereby.

Although we shall consider only the problem of firing from aircraft, the results will include a number of more special cases. By setting the dive angle equal to zero, one gets the trajectory for forward firing from a moving launcher on the ground, in a more convenient form than from the methods used in treating wind effects. Furthermore, if the dive angle is set equal to the negative of the quadrant elevation of the launcher and the aircraft speed is set equal to zero, the equations and solutions reduce to those for ground firing given in chapters 3 and 5.

There are several outstanding differences between forward firing from aircraft and ground firing. The high velocity with respect to the air at launching in the former case means that the aerodynamic restoring moment is large even at small yaw and hence the dispersion introduced by thrust malalignment is much smaller in forward firing than in ground firing. Since the velocity of the airplane is added to that of the rocket, the final velocity of a forward-fired rocket is considerably greater than that of the same rocket fired on the ground. Trajectory calculations are usually simpler in the case of forward firing because the portion of the trajectory considered is less curved. This results from the higher velocity just mentioned and also from the fact that in forward firing one does not try to attain the maximum possible range by firing up at 45° and thus getting a highly curved path with large changes in velocity.

A complete understanding of the behavior of rockets fired from airplanes requires an understanding of the motion of the airplane and the flow of air around it. We shall barely touch this part of the problem, taking only the simplest case in which the airplane dives in a straight line with constant velocity and no side slipping. If these conditions are not met, the rocket in turning to head into the onrushing airstream will be deflected by unpredictable amounts and inaccurate fire will result, unless the maneuvers being executed are well standardized.

6.1 Trajectory During Burning

The trajectory problem in forward firing is much the same as that in ground firing, with only minor differences arising from the fact that the initial velocity at time $t=0$ is no longer

zero but is equal to the speed of the aircraft. The force system acting on the rocket is of course the same as that in ground firing, except that in aircraft firing the aerodynamic forces are important even at the start of burning. In view of these similarities, we shall borrow as freely as possible from the material of chapter 3 without repeating the arguments therein. In all cases adequate references to the original text will be given. Our study of the trajectory will be limited to the motion in the vertical plane, since we are interested mainly in the over-all trajectory drop due to gravity and initial launching conditions. The effects of the various malalignments will be shown to be small in the case of forward firing; and in any event they can be superimposed on the normal gravity drop.

6.11 Connection Between Forward Firing and Ground Firing—Equations of Motion.—

It will be convenient for this purpose to refer the motion to a coordinate system at rest with respect to the air, with the origin at the center of mass of the rocket at the instant of ignition. In the absence of wind this coordinate system is also at rest with respect to the ground; but in the presence of a uniform wind (the possibility of a nonuniform wind is ruled out in this discussion) the entire frame of reference and the trajectory will be moving with the wind relative to the ground. The direction of motion of the aircraft—the so-called *flight line*—will be taken as the x -axis; while the y -axis is taken as perpendicular to the x -axis and pointing downward. (See fig. 6.11.) The aircraft is assumed to be in a straight-line glide of angle α down from the horizontal and to be traveling with the constant speed V_A between the time of ignition and the launching of the rocket, during which time the launcher axis is at some angle λ with the flight line.

This system of coordinates is essentially the same as that employed in the description of the motion in ground firing (3.21) with the exception that the x -axis replaces the Z_0 -axis, y is written in lieu of Y_0 , and α is the negative of the quadrant elevation θ_0 . The angles δ , φ , and ϑ representing the yaw, orientation, and tangent angle to the trajectory are measured in the same manner as previously; that is, from the x -axis. (In ground firing, from the Z_0 or Z -axis.) Hence the equations of motion in the present case are identical with 3.24 (1), (8)–(10) for the

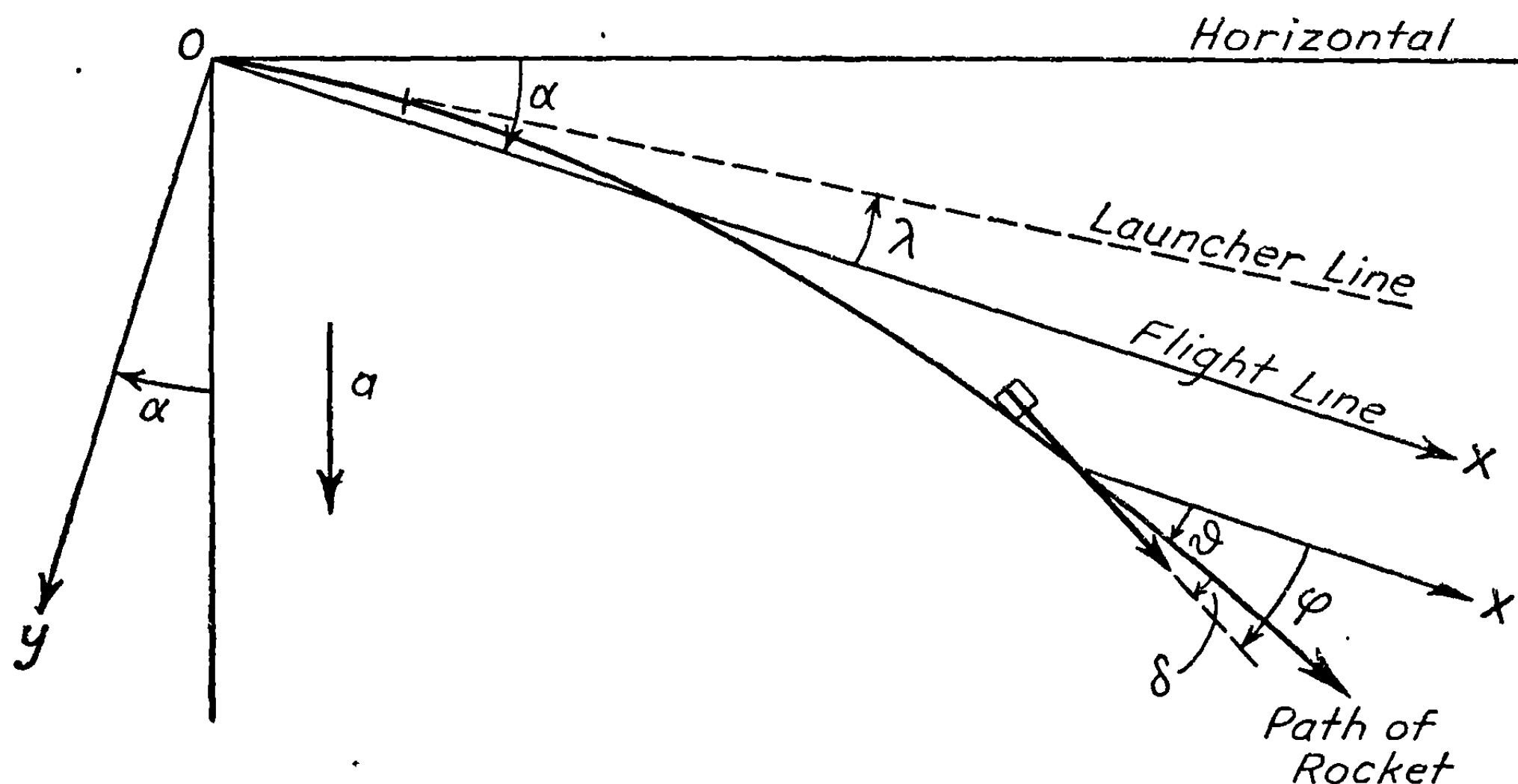


FIGURE 6.11.—Coordinate system in forward firing from aircraft.

motion in the vertical plane; namely,

$$m\dot{V} = m\ddot{x} = mG_J + mg \sin \alpha - \frac{1}{2} C_D \rho A V^2, \quad (1)$$

$$\ddot{\phi} + \frac{(C_{\phi} \rho A l^2 V + 2K_{JD})}{2mK^2} \dot{\phi} + \frac{C_m \rho A l V^2}{2mK^2} \delta = -\frac{G_J R_M}{K^2} + \frac{C_m \rho A l V^2}{2mK^2} \delta_0, \quad (2)$$

$$V\dot{\vartheta} - G_J \delta - \frac{C_l \rho A V^2}{2m} \delta = G_J \beta_M + g \cos \alpha, \quad (3)$$

and

$$\varphi - \delta - \vartheta = 0. \quad (4)$$

The boundary conditions on (1) are that at the instant of ignition, namely $t=0$, the position and velocity are given by

$$x(0) = 0,$$

$$V(0) = \dot{x}(0) = V_A. \quad (5)$$

To specify completely the boundary conditions on (2), (3), and (4) it is sufficient to give the values of δ , ϕ , and $\dot{\phi}$ at the instant $t=t_p$ at which the final constraint of the launcher is removed. These are

$$\delta(t_p) = \delta_p,$$

$$\phi(t_p) = \phi_p,$$

and

$$\dot{\phi}(t_p) = \dot{\phi}_p = q_p. \quad (6)$$

6.12 Effect of Air Drag on Velocity and Acceleration.—Because of the higher velocity of the rocket in forward firing, we must investigate carefully the effect of the air drag on the velocity and acceleration during burning. Since in any case it will be necessary to assume a constant *effective* acceleration in order to solve the equations in 6.11 in terms of a simple parameter such as ζ , we should allow for the over-all effects of the drag in as simple a manner as possible. Writing the drag coefficient, C_D , in terms of the deceleration coefficient, c ; namely,

$$\frac{1}{2} C_D \rho A = mc, \quad (1)$$

we have, in lieu of 6.11 (1),

$$\frac{dV}{dt} = G_J + g \sin \alpha - cV^2. \quad (2)$$

Since G_J , the effective jet acceleration of the rocket, is known or can be determined by the methods of 2.22, and since the deceleration coefficient is a known empirical function of V , the velocity at the end of burning can best be determined by numerical integration of (2). It is sufficiently accurate to replace V by $V_A + G_J t$ on the right side and to evaluate the integral by the trapezoidal rule, dividing the burning period into five or six intervals.

The determination of the *effective* acceleration to be used during the burning period is less straightforward. Since the rocket takes up practically all of its deflection by the time it has completed a single yaw oscillation, we shall assume that the *effective* acceleration is the average acceleration during the first yaw oscillation. If we let V_1 be the velocity of the rocket

6.1 TRAJECTORY DURING BURNING

after it has traversed the distance σ with respect to the air (including distance traveled on the launcher), and t_1 the time since the start of burning at which this velocity is reached, then on the assumption of constant acceleration we have ¹

$$V_1^2 = (V_A + Gt_1)^2 \quad (3)$$

$$\begin{aligned} &= V_A^2 + 2G(V_A t_1 + \frac{1}{2} Gt_1^2), \\ &= V_A^2 + 2G\sigma = V_A^2 + v_\sigma^2. \end{aligned} \quad (4)$$

The average acceleration over this period is then

$$G = G_J + g \sin \alpha - (cV^2)_{av}. \quad (5)$$

Since, for the type of rockets and aircraft in use at present, V_1 will be less than the velocity of sound, the value of c to be used in (5) is the roughly constant deceleration coefficient for velocities below that of sound. In that case

$$(cV^2)_{av}. = \frac{c}{t_1} \int_0^{t_1} V^2 dt, \quad (6)$$

$$= \frac{c}{t_1} \int_0^{t_1} (V_A^2 + G^2 t^2) dt, \quad (7)$$

$$= c \left(V_A^2 + V_A Gt_1 + \frac{1}{3} G^2 t_1^2 \right). \quad (8)$$

Substituting for t_1 from (3), we get

$$(cV^2)_{av}. = \frac{c}{3} (V_1^2 + V_1 V_A + V_A^2). \quad (9)$$

Hence, using (4) we find that

$$(cV^2)_{av}. = \frac{1}{3} c V_A^2 \left[2 + \frac{v_\sigma^2}{V_A^2} + \left(1 + \frac{v_\sigma^2}{V_A^2} \right)^{\frac{1}{2}} \right] \quad (10)$$

is the desired correction to the acceleration in vacuum in order to allow for the effect of the drag.

For a typical rocket, which may be supposed to have $G_J = 1,000$ ft./sec.², $\sigma = 250$ feet, and $c = 3 \times 10^{-5}$ feet⁻¹ launched from an aircraft traveling at 500 ft./sec., we have from (10)

$$\begin{aligned} (cV^2)_{av}. &= \frac{1}{3} \times 3 \times 10^{-5} \times 25 \times 10^{-4} (2 + 2 + 3^{\frac{1}{2}}) \\ &= 14 \text{ ft./sec.}^2 \approx 1.9c V_A^2. \end{aligned}$$

The relative correction to the acceleration is $(cV^2)_{av.}/G$ or only 1.4 percent. Of course for larger values of c and for greater airplane speeds this figure will be considerably greater.

6.13 Solution for the Deflection of the Tangent to the Trajectory.—As in 3.32, we express the aerodynamic restoring moment in terms of σ , the yaw oscillation distance,² by the relation 3.32 (15),

¹ Note that V represents velocities relative to the air, and v represents velocities relative to the moving airplane (launcher). In ground firing in the absence of wind, $V = v$.

² The value of σ to be used is, as before, that corresponding to velocities less than the velocity of sound.

$$\frac{C_m \rho A l}{2mK^2} = \frac{4\pi^2}{\sigma^2}; \quad (1)$$

and we write the equations of motion in terms of the dimensionless velocity parameter

$$\zeta = \frac{V}{v_\sigma}, \quad (2)$$

where, as before,³

$$v_\sigma = (2G\sigma)^{\frac{1}{2}}. \quad (3)$$

Following the argument of 3.33, we neglect the terms containing C_q , K_{JD} and C_i and let the ratio $G_J/G=1$. Thus 6.11 (2), (3) and (4) become

$$\varphi'' + 16\pi^2 \zeta^2 \delta = -(2\sigma/K^2)R_M + 16\pi^2 \zeta^2 \delta_0, \quad (4)$$

$$\zeta \vartheta' - \delta = (g/G) \cos \alpha + \beta_M, \quad (5)$$

$$\varphi - \vartheta - \delta = 0. \quad (6)$$

The initial conditions subject to which (4) — (6) are to be solved are that at the instant $t=t_p$ or

$$\zeta = \zeta_p = \frac{V_p}{v_\sigma} = \frac{V_A + v_p}{v_\sigma} = \frac{V_A + Gt_p}{v_\sigma},$$

at which the final constraint of the launcher is removed,

$$\delta(\zeta_p) = \delta_p,$$

$$\varphi(\zeta_p) = \varphi_p,$$

$$\varphi'(\zeta_p) = \varphi_p' = t_\sigma q_p.$$

Now the above equations and boundary conditions are identical with 3.33 (14) to (18); hence their solutions in terms of ζ_p and ζ are the same as those derived in chapter 3. At the moment we are not interested in the effects of the various malalignments but rather in the over-all predictable trajectory; the contributions of the terms in R_M , β_M , and δ_0 to the dispersion will be considered in 6.7. As a result, the solution for ϑ contains only the contributions due

³ In ground firing (3.33), ζ has the same form as above except that then $V=Gt=(2Gd)^{1/2}$; whereas in forward firing $V=V_A+Gt=V_A+v$. Hence in ground firing the parameter is also expressible as $\zeta=t/t_\sigma=(d/\sigma)^{1/2}$, where $t_\sigma=(2\sigma/G)^{1/2}$. In any case the expression for ζ valid for both ground firing and forward firing is given by (2) above, where v_σ is the velocity of the rocket relative to the launcher after it has traversed the initial distance σ relative to the launcher.

In terms of the equivalent time,

$$\tau = t + \frac{V_A}{G},$$

that it would have taken the rocket to acquire the same speed in ground firing as it has in forward firing, the equations for V and ζ become

$$V = V_A + Gt = G\tau,$$

$$\zeta = \frac{V}{(2G\sigma)^{\frac{1}{2}}} = \left(\frac{G}{2\sigma}\right)^{\frac{1}{2}} \left(t + \frac{V_A}{G}\right) = \frac{\tau}{t_\sigma},$$

For $V_A=0$ we have $\tau=t$ and the equations reduce simply to those for ground firing.

to gravity, g ; initial orientation, ϕ_P ; initial yaw, δ_P ; and initial angular velocity, q_P . That is,

$$\vartheta = \vartheta_g + \vartheta_\phi + \vartheta_\delta + \vartheta_q, \quad (7)$$

or

$$\vartheta = \frac{g \cos \alpha}{G} \Theta_g(\zeta_P, \zeta) + \phi_P + \delta_P \Theta_\delta(\zeta_P, \zeta) + q_P t_\sigma \Theta_q(\zeta_P, \zeta), \quad (8)$$

where the characteristic functions Θ_g , Θ_δ and Θ_q are given 3.38 (11), 3.34 (20) and 3.34 (23), respectively. Similarly, the linear deflection of the rocket from the flight line is given by ⁴

$$y = y_g + y_\phi + y_\delta + y_q, \quad (9)$$

or

$$y = \frac{\sigma g \cos \alpha}{G} R_g(\zeta_P, \zeta) + \sigma \phi_P (\zeta^2 - \zeta_P^2) + \sigma \delta_P R_\delta(\zeta_P, \zeta) + \sigma q_P t_\sigma R_q(\zeta_P, \zeta), \quad (10)$$

where R_g , R_δ , and R_q are given by 3.38 (22), 3.35 (9), and 3.36 (6), respectively.

6.14 The Gravity Term and Effective Launching Line.—The contribution to the deflection of the tangent to the trajectory due to the action of gravity alone ⁵ is, from 6.13 (8)

$$\vartheta_g = \frac{g \cos \alpha}{G} \Theta_g(\zeta_P, \zeta), \quad (1)$$

while the linear gravity drop of the rocket from the flight line is, from 6.13 (10),

$$y_g = \frac{\sigma g \cos \alpha}{G} R_g(\zeta_P, \zeta). \quad (2)$$

Since these terms are independent of the mode of launching—that is, of initial orientation, yaw, or angular velocity—but depend rather only on the properties of the rocket and the launching speed, it is convenient to describe another path in addition to those shown in figure 6.11. This, the *effective launching path* (ELP), is so defined that the tangent angle and linear deflection of the rocket from the ELP at any instant during burning are merely the gravity terms ϑ_g and y_g above. (See fig. 6.14.) That is, we might say that the total deflection ϑ of the trajectory from the flight line is made up of two parts: the gravity term, ϑ_g ; and the term,

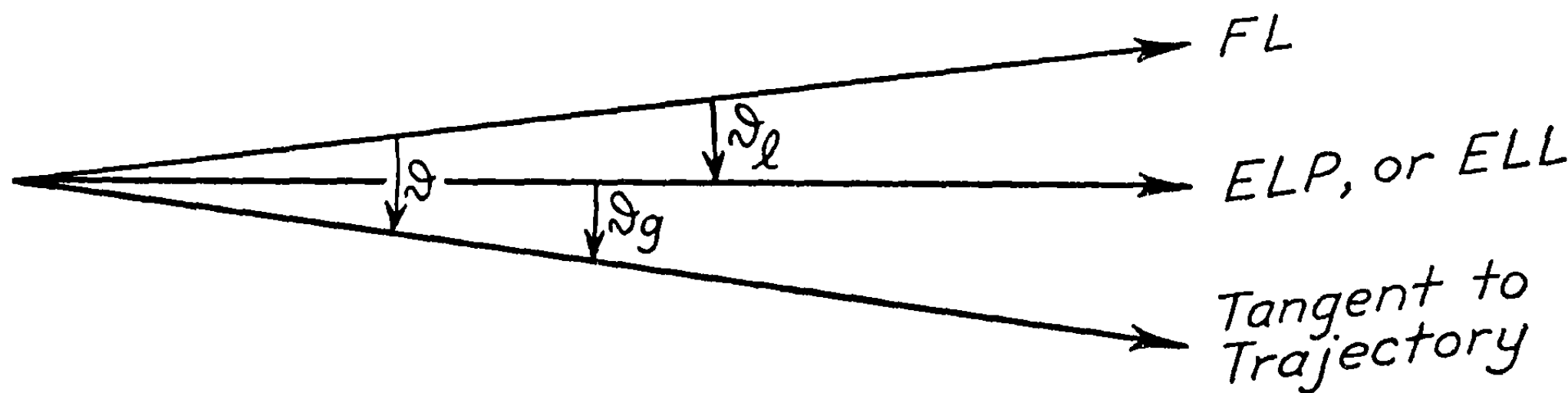


FIGURE 6.14.—Effective launching path (ELP).

⁴ The r of ch. 3 is replaced here by y .

⁵ In a strict sense the other terms in 6.13 (8) are also dependent somewhat on g , since ζ involves the term $G = G_J + g \sin \alpha + cV^2$. However, since $g \ll G_J$, the influence of gravity on ζ and the terms containing ζ is of minor importance.

$$\vartheta_1 \equiv \vartheta - \vartheta_g = \vartheta_\phi + \vartheta_\delta + \vartheta_a, \quad (3)$$

arising from the initial launching conditions ϕ_p , δ_p , and g_p . This term ϑ_1 is of course the deflection of the tangent to the trajectory in the absence of gravity.

Since one is usually interested in conditions at the end of burning, the *effective launching line* (ELL) may be defined as the direction in which the rocket would be traveling at the *end of burning*, if gravity did not act. This is the same as the direction of the effective launching path at the end of burning. The ELP and ELL are often used interchangeably. This is of no consequence as long as one knows whether the reference is to conditions during, or at the end of, burning. The reasons for the introduction of the effective launching line will become clear in subsequent sections.

For the purpose of calculating trajectories one may use either the formulas 3.38 (11) and (22) for Θ_g and R_g , the curves in figure 3.38a and b, or the tables in the appendix. In any event it must be remembered that the dimensionless parameter ζ contains the airspeed V_A implicitly.

6.15 The Launching Factor.—In the expression for the deflection of the tangent to the trajectory; namely,

$$\vartheta = \vartheta_g + \vartheta_\phi + \vartheta_\delta + \vartheta_a, \quad (1)$$

the sum

$$\vartheta_\phi + \vartheta_\delta = \varphi_p + \delta_p \Theta_\delta(\zeta_p, \zeta) \quad (2)$$

represents the deviation of the trajectory in the absence of gravity and mallaunching. In the case under consideration, where both φ_p and δ_p result from the fact that the launcher is not parallel to the flight line rather than from vibrations or other causes that would leave them independent, the angles are connected by the relations (see fig. 6.15)

$$\delta_p = \varphi_p - \vartheta_p = \varphi_p - \frac{\dot{y}_p}{\dot{x}_p} = \varphi_p - \frac{v_p \varphi_p}{V_A v_p} = \frac{\varphi_p}{1 + (v_p/V_A)}, \quad (3)$$

where $v_p = Gt_p = (2Gp)^{1/2}$ is the velocity of the rocket *relative to the launcher* at the instant of launching.

It is convenient then to introduce the quantity f such that

$$\vartheta_\phi + \vartheta_\delta = \varphi_p + \delta_p \Theta_\delta(\zeta_p, \zeta) = (1-f)\varphi_p, \quad (4)$$

where $f\varphi_p$ represents the amount by which the trajectory is turned from the launcher line into the direction of the flight line due to initial yaw. Schematically this is shown in figure 6.15, in which the f -line⁶ represents the direction of the effective launching line (see 6.14) in

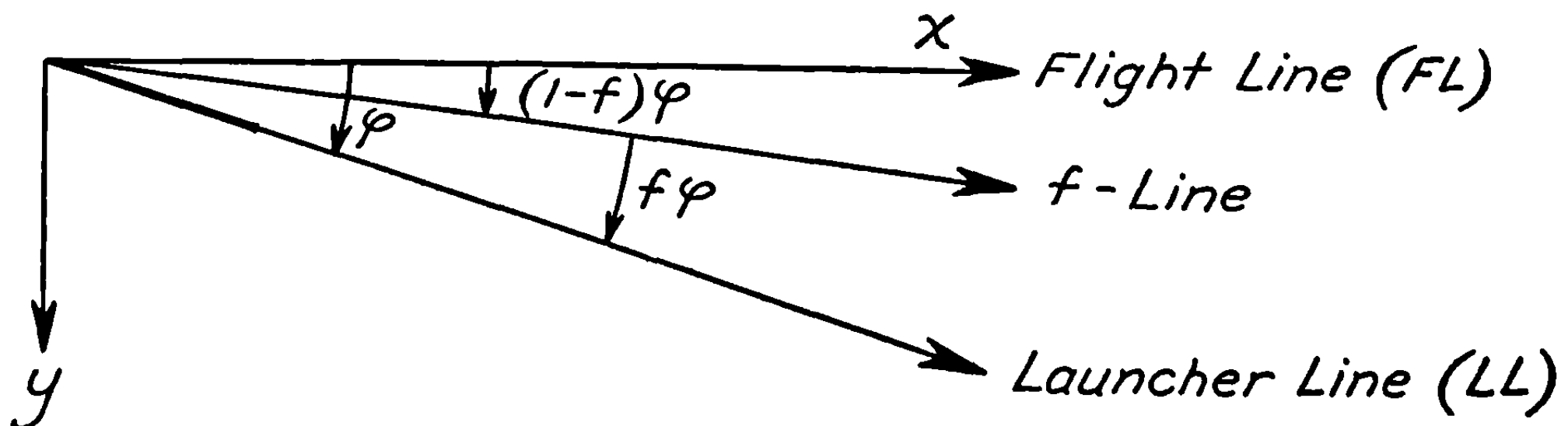


FIGURE 6.15.—Relation of the f -line to the flight line (FL) and launcher line (LL).

⁶ To simplify the drawing, the launcher line and f -line are drawn through the same origin, since the small displacements due to curved trajectories are always negligible in practice.

the absence of mallaunching. From (3) and (4), we find that

$$f = -\frac{\Theta_s(\zeta_p, \zeta)}{1 + (v_p/V_A)}. \quad (5)$$

Since Θ_s is intrinsically negative, see figure 3.34, the launching factor f is a positive quantity. Moreover, because of the relatively large values of ζ_p and ζ in forward firing, and because very short launchers are generally used on aircraft, f in most cases is very close to unity.

6.16 The Angular Velocity Factor.—We can now easily tie in the f -line with the effective launching line (ELL). Since the ELL is merely the direction of the tangent to the trajectory in the absence of gravity, we have

$$\begin{aligned} \vartheta_t &= \vartheta_p + \vartheta_s + \vartheta_a \\ &= (1-f) \varphi_p + q_p t_\sigma \nu, \end{aligned} \quad (1)$$

where ν has been written in place of the characteristic function $\Theta_a(\zeta_p, \zeta)$. In forward firing, the quantity ν is generally referred to as the *angular velocity factor*, since the dimensionless angular velocity, $q_p t_\sigma$ multiplied by ν represents the contribution to the trajectory deflection resulting from initial angular velocity. The relationships among the various angles and directions are shown schematically in figure 6.16.

6.17 Summary.—In terms of the functions defined above, the deflection of the trajectory from the flight line during burning may be written as

$$\vartheta = \vartheta_g + \vartheta_p + \vartheta_s + \vartheta_a. \quad (1)$$

In the case of firing from a launcher which can introduce an angular velocity without altering the initial orientation, this reduces to

$$\vartheta = \frac{g \cos \alpha}{G} \Theta_s + (1-f) \varphi_p + q_p t_\sigma \nu. \quad (2)$$

It should be observed that the only term in the above expressions which is significantly affected by changes in dive angle is ϑ_g , the deflection of the trajectory from the effective

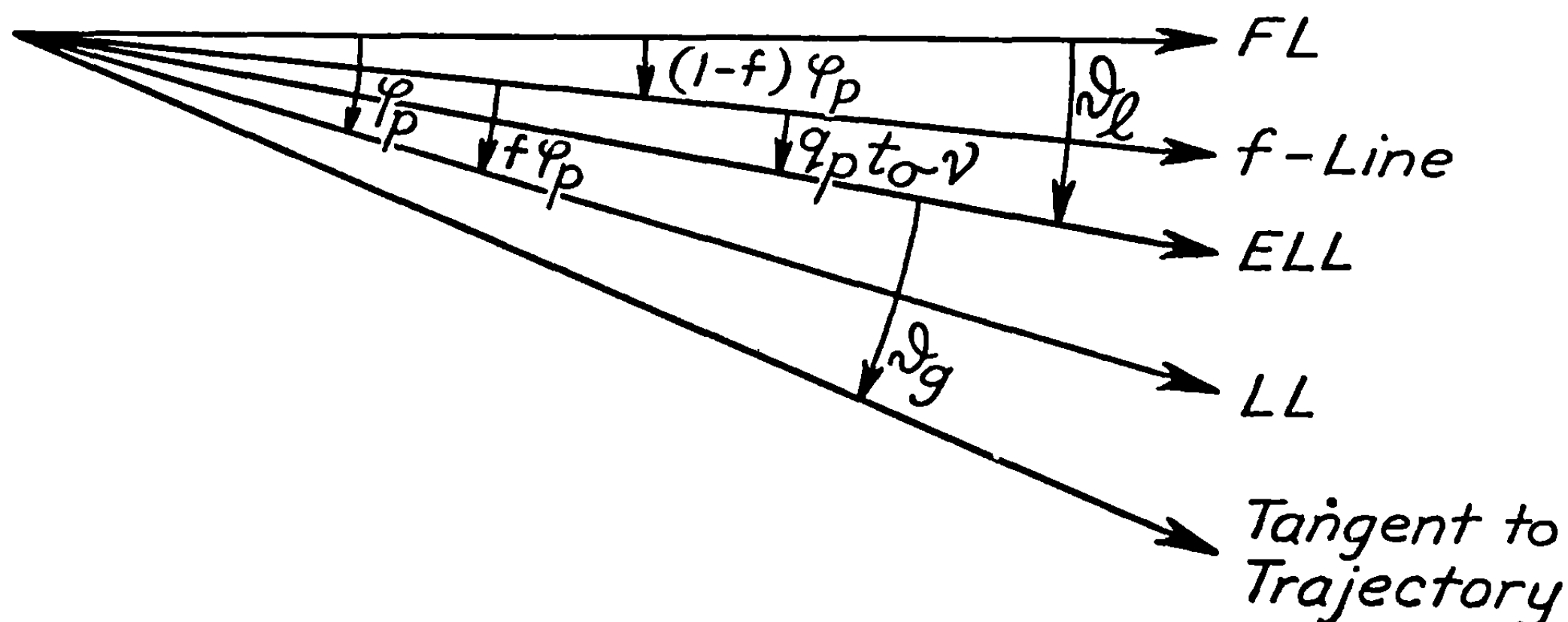


FIGURE 6.16.—Various reference lines.

launching line. This quantity is, moreover, very nearly proportional to the cosine of the dive angle; while the f and ν factors are, for all practical purposes, independent of the dive angle.

Sighting and trajectory tables for rockets fired from aircraft are often developed on the assumption that $q_p=0$, in which case the term involving q_p in the above formula is superfluous. It should be included only when a source of systematic mallaunching is present. If the rocket slides only an inch or so before lugs clear the launcher, there is ordinarily no significant mallaunching except that occasionally it appears to be introduced by shear-wires. If rail launchers are used, tip-off will ordinarily produce a systematic mallaunching of the order of 250 mils/sec. as discussed in chapter 4.

6.2 Approximate Trajectory During Burning—Equations and Solutions for $\sigma=0$

In many cases of forward firing one can get a very good approximation to the actual trajectory during burning by the simple device of assuming $\sigma=0$. This is equivalent to the assumption that the stabilizing action of the fins is great enough (infinite restoring moment) to keep the axis of the rocket always parallel to its direction of motion relative to the air; that is, the rocket axis is always tangent to the trajectory. Hence, the yaw, δ , is always zero, and $\varphi=\vartheta$.

The appropriate equations for this case are 6.11 (1) and (3) (with $\beta_M=0$); namely,

$$\ddot{x}=G_J+g \sin \alpha-\frac{C_D \rho A V^2}{2m} \equiv G, \quad (1)$$

and

$$V \dot{\vartheta}=g \cos \alpha, \quad (2)$$

where, as before, G is assumed constant. In terms of the equivalent time ⁷

$$\tau=t+\frac{V_A}{G},$$

we have from (1) and (2)

$$\dot{x}=V=V_A+Gt=C\tau, \quad (3)$$

$$\frac{d\vartheta}{d\tau}=\frac{g \cos \alpha}{G} \cdot \frac{1}{\tau}. \quad (4)$$

Hence the deflection from the flight line is

$$\vartheta_0=\vartheta_p+\frac{g \cos \alpha}{G} \ln \frac{\tau}{\tau_p}, \quad (5)$$

where ϑ_p is the deflection at the instant of launching $\tau=\tau_p$, and the subscript zero on ϑ indicates that it holds only for $\sigma=0$. It should be noted that ϑ_p is not the same as the angle φ_p which the launcher makes with the flight line; rather it is the angle between the flight line and the direction of motion of the rocket at launching. That is

$$\vartheta_p \doteq \frac{v_p \sin \varphi_p}{V_A+v_p \cos \varphi_p} \doteq \frac{v_p \varphi_p}{V_A+v_p}. \quad (6)$$

Evidently

$$\dot{y}=V \sin \vartheta \doteq G \tau \vartheta. \quad (7)$$

⁷ Same as footnote 3.

Thus, integrating (7) with the aid of (5), we have for the linear drop normal to the flight line

$$y_0 = \frac{1}{2} g \tau^2 \cos \alpha \ln \frac{\tau}{\tau_p} + \left(\frac{G \vartheta_p}{2} - \frac{g \cos \alpha}{4} \right) (\tau^2 - \tau_p^2). \quad (8)$$

As with the case for $\sigma \neq 0$, it is convenient to define an effective launching line such that the deflection from the ELL is merely the *gravity* term in (5). Hence,

$$\vartheta_{0g} = \frac{g \cos \alpha}{G} \ln \frac{\tau}{\tau_p} = \frac{g \cos \alpha}{G} \ln \frac{V_A + v}{V_A + v_p} = \frac{g \cos \alpha}{G} \ln \frac{V}{V_p}; \quad (9)$$

and, similarly,

$$y_{0g} = \frac{1}{2} g \tau^2 \cos \alpha \left[\ln \frac{\tau}{\tau_p} - \frac{1}{2} \left(1 - \frac{\tau_p^2}{\tau^2} \right) \right]. \quad (10)$$

The launching factor for $\sigma = 0$ is defined in (11) in the same way as that for $\sigma \neq 0$ in 6.15. That is

$$\vartheta_0 = \vartheta_{0g} + \vartheta_p = \vartheta_{0g} + (1 - f_0) \varphi_p. \quad (11)$$

Therefore, in view of (6),

$$f_0 = \frac{V_A}{V_A + v_p}. \quad (12)$$

Since, from 6.15 (5),

$$f = \frac{V_A}{V_A + v_p} \Theta_\delta(\zeta_p, \zeta),$$

we see that the characteristic function Θ_δ plotted in figure 3.35 a and b is also the ratio $-f/f_0$.

In spite of the limitations imposed by the assumption that $\sigma = 0$, the above expressions are of extreme practical importance. First, in a majority of cases of forward firing the values derived through the use of (9) and (10) differ from those derived through the use of the more accurate expressions that hold for $\sigma \neq 0$ by not more than 1 or 2 mils. Where errors of this order are tolerable, the $\sigma = 0$ approximation thus affords a rapid and simple means for calculating trajectories. An example of the relative values of ϑ_{0g} and y_{0g} as compared with ϑ_g and y_g is shown in figure 6.2a for the 3.5 AR. In this case the difference between ϑ_{0g} and ϑ_g at the end of burning is only 1 mil, for $\alpha = 0^\circ$ and $V_A = 350$ ft./sec. At the higher air speeds and steeper dive angles the difference would be considerably less.

In addition, the $\sigma = 0$ approximation offers a simple analytical expression which can be used, where the expressions for $\sigma \neq 0$ cannot, for rapidly estimating relative effects of the various parameters on rocket trajectories. (See 6.45.)

An estimate of the errors to be expected through the use of the $\sigma = 0$ approximation can be obtained from figure 6.2b, where the quantity $(G/g \cos \alpha) (\vartheta_{0g} - \vartheta_g)$ is plotted as a function of $\sqrt{2} \zeta$ and $\sqrt{2} \zeta_p$. Since $\sqrt{2} \zeta_p \geq 0.80$ in most cases of forward firing, it is apparent from the figure that the approximation for $\sigma = 0$ will generally give values of the gravity deflection to a fairly high order of accuracy. In such cases, for $G \geq 25 g$, $(\vartheta_{0g} - \vartheta_g) \leq 1.3$ mils.

6.3 Trajectory After Burning

In the previous sections we find all of the equations necessary for determining the conditions of flight of the rocket at the end of burning, namely values of V_b , x_b , y_b , and ϑ_b . The calculation of the remainder of the trajectory involves nothing particularly characteristic of rockets alone, and the usual methods of exterior ballistics are applicable. The proper method

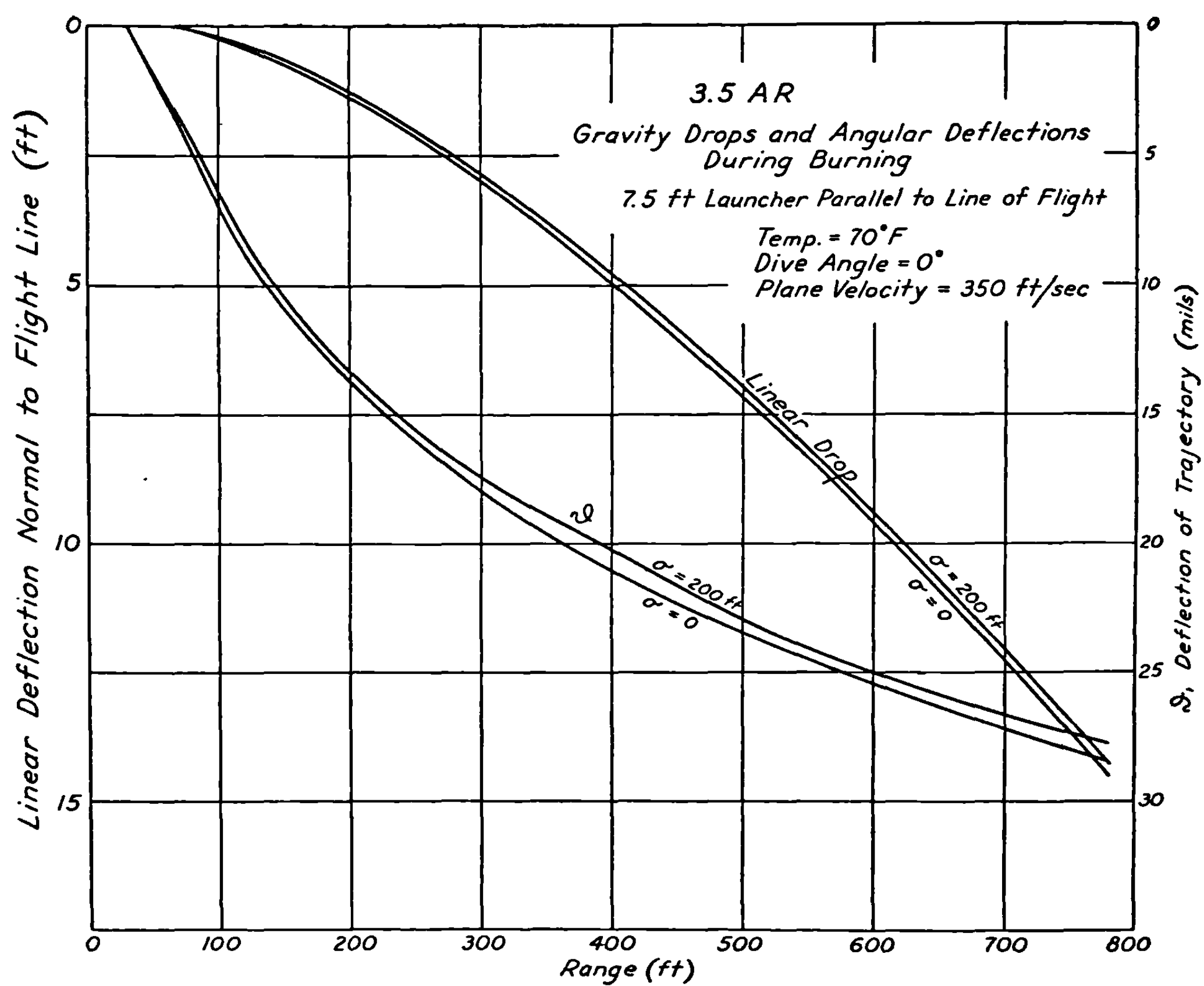


FIGURE 6.2a.—Variation of gravity drop and angular deflection with range during burning.

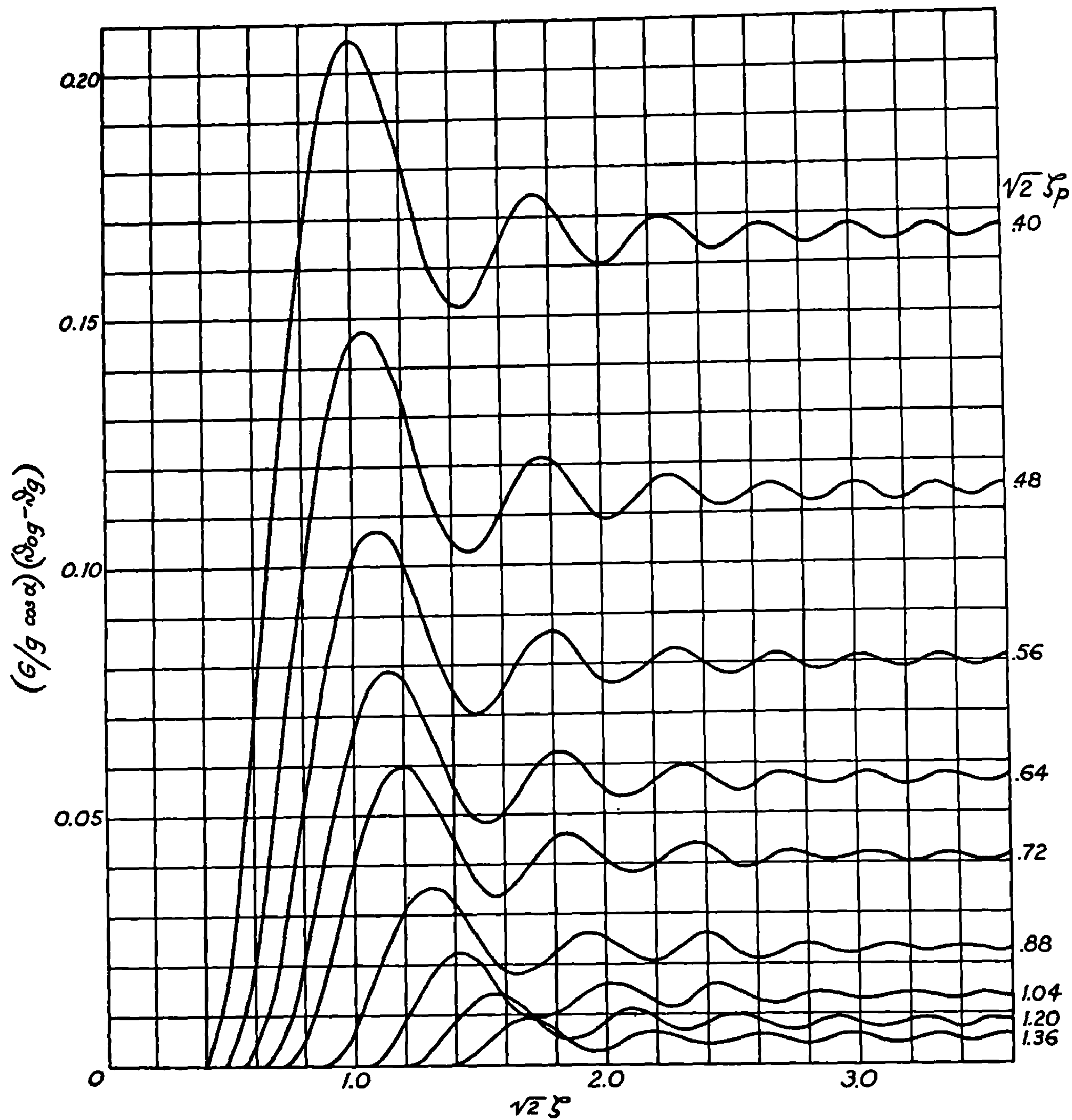


FIGURE 6.2b.—Error due to the assumption that $\sigma=0$.

to use will depend upon the particular form of the drag function of the rocket and the desired accuracy. One that proves to be very useful in many cases of forward firing is that based upon the Didion-Bernoulli treatment, described in 5.22, and the assumption that a short enough segment of the trajectory is involved so that the inclination at the end of the segment is not more than 10° greater than at the beginning.

Let S and R be the skew coordinates in a system in which the origin is at the *end* of burning, S being the distance along the tangent to the trajectory at the origin and R the vertical distance below the S -axis. Hence (see fig. 6.3) the R -axis makes the angle $\left(\frac{\pi}{2} - \alpha - \vartheta_b\right)$ with the S -axis. We then have, using the terminology of 5.22,

$$R = \frac{gS^2}{2V_b^2} B(Z), \quad (1)$$

$$V = V_b V_D^{-1}(Z), \quad (2)$$

and

$$t = t_b + \frac{S}{V_b} D(Z). \quad (3)$$

When a quadratic resistance law can be used, that is, when the velocity stays in the

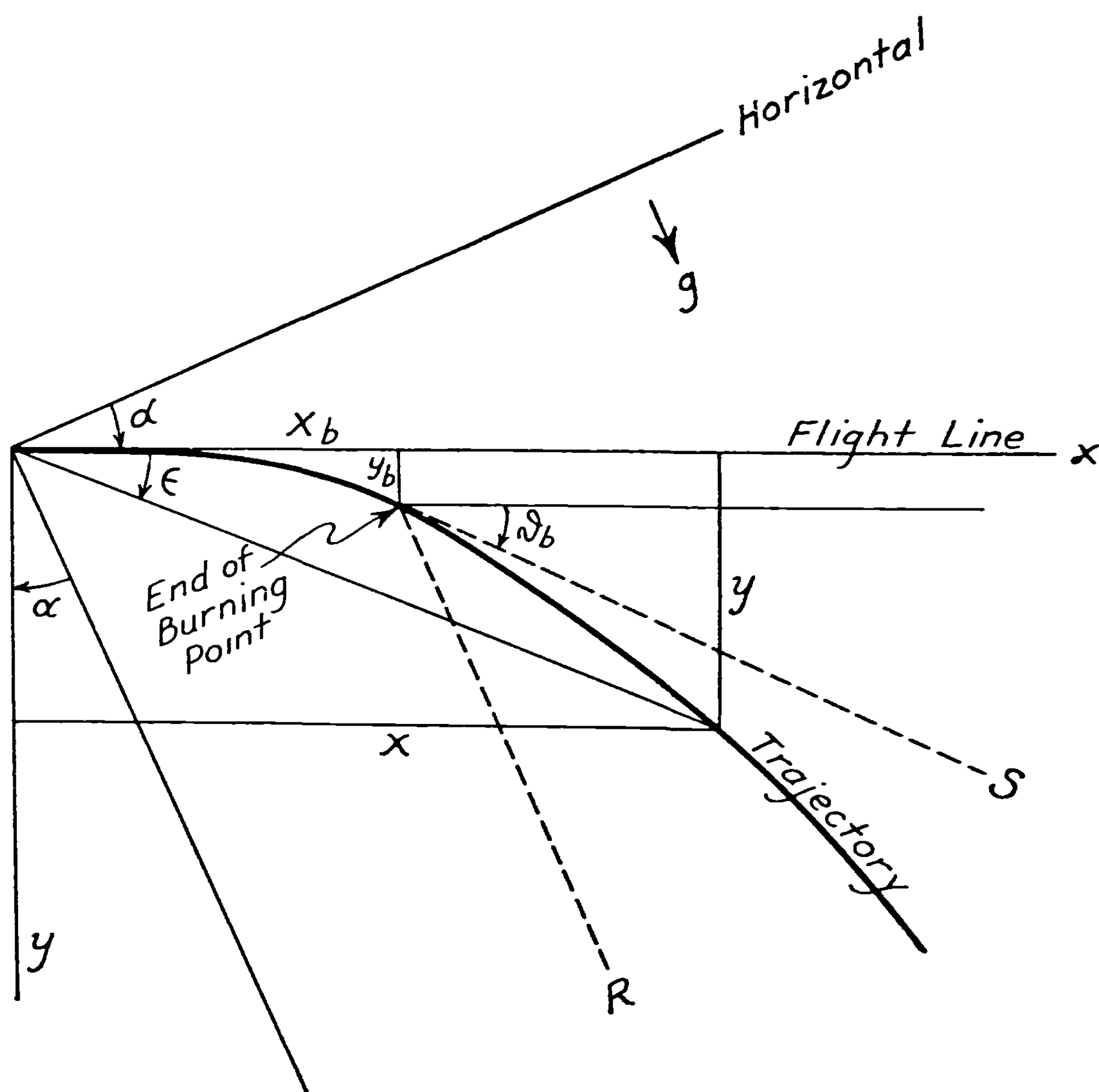


FIGURE 6.3.—Complete coordinate system in forward firing.

range of 1,250 to 1,700 ft./sec. or is less than 800 ft./sec., Z and the functions of Z are given by

$$Z = 2cS, \quad (4)$$

$$B(Z) = 2Z^{-2}(e^Z - Z - 1), \quad (5)$$

$$V_D^{-1}(Z) = e^{-Z/2}, \quad (6)$$

and

$$D(Z) = 2Z^{-1}(e^{Z/2} - 1) = J(Z/2). \quad (7)$$

These functions are tabulated in Cranz.⁸ When a quadratic resistance law cannot be used, other procedures are available, the most generally useful being mentioned in 5.24.

It remains to express the points in the x - y system originally introduced in terms of the coordinates S and R used above by means of the following equations (see fig. 6.3):
distance x along flight line

$$x = x_b + S \cos \vartheta_b + R \sin \alpha; \quad (8)$$

linear drop y normal to flight line

$$y = y_b + S \sin \vartheta_b + R \cos \alpha; \quad (9)$$

angular drop ϵ from the flight line

$$\epsilon = \tan^{-1} \frac{y}{x} \doteq \frac{y}{x}. \quad (10)$$

As we shall see when considering the sighting problem in 6.5 it is the angular drop ϵ as a function of range which is of direct importance in computing the sight setting. For that reason most of our attention in the following sections will be devoted to a consideration of the effect on ϵ of various changes in the conditions of launching.

6.4 Summary and Simplifying Procedures for Trajectory Calculations

The trajectory up to the end of burning may be calculated by the methods given in 6.11–6.17. The remainder of the trajectory can then be calculated by the methods of 6.3. The final result is the value of ϵ as given by 6.3 (10). In calculating this quantity it is generally sufficient to determine only that contribution to the trajectory resulting from gravity—that is, the drop from the effective launching line—the drop from any other reference line being determined by the method given below. For that reason we shall henceforth reserve the symbol ϵ for the angular drop of the rocket from the ELL; that is, ϵ is the angular drop due to gravity alone.

6.41 Transformation of Trajectory from Effective Launching Line to an Arbitrary Reference Line.—When only one trajectory is to be calculated, it is simple enough to compute the conditions at the end of burning by means of the equations in 6.11–6.17 and the remainder of the trajectory by the methods of 6.3. On the other hand, when trajectories have to be computed for various dive angles, temperatures, and initial launching conditions, the labor involved compels consideration of simplifying procedures. In this connection we note that the trajectory drop from the ELL for any combination of aircraft speed, dive angle and launcher length depends upon the characteristics of the rocket alone at the given temperature and is independent of the initial yaw or angular velocity.

⁸ C. Cranz, "Lehrbuch der Ballistik," vol. 1, pp. 569–571, Springer, 1925 (Edwards Bros., 1943).

It would be convenient to compute the complete trajectory from the ELL and then transform in some simple manner to any other reference line. In some of the previous figures, the flight line, launcher line, effective launching line, and tangent to the trajectory at the end of burning were drawn through the same origin. This was done merely to simplify the drawing; and as long as one considered only the direction of the tangent it was of no consequence (fig. 6.41a). However, one would like to draw the same type of figure with the actual path of the rocket instead of the tangent (fig. 6.41b). Whereas the former figure offers a means of transforming the direction of the tangent from one reference line to another, the latter offers a simple means of transforming the trajectory itself. The error involved in figure 6.41b arises from the fact that the ELL is displaced linearly from its proper position and drawn through

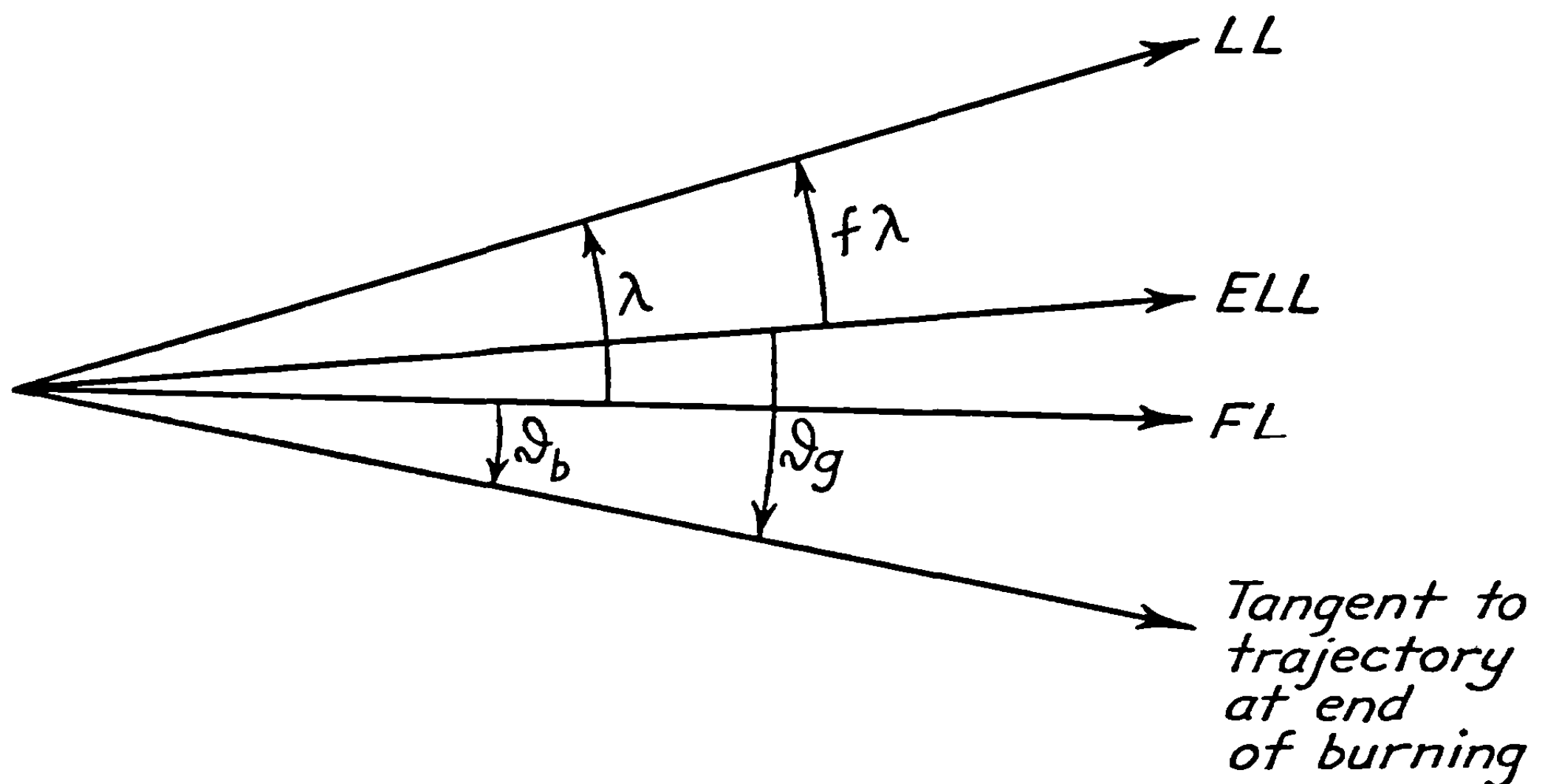


FIGURE 6.41a.—*Tangent to trajectory in relation to flight line (FL), launcher line (LL), and effective launching line (ELL).*

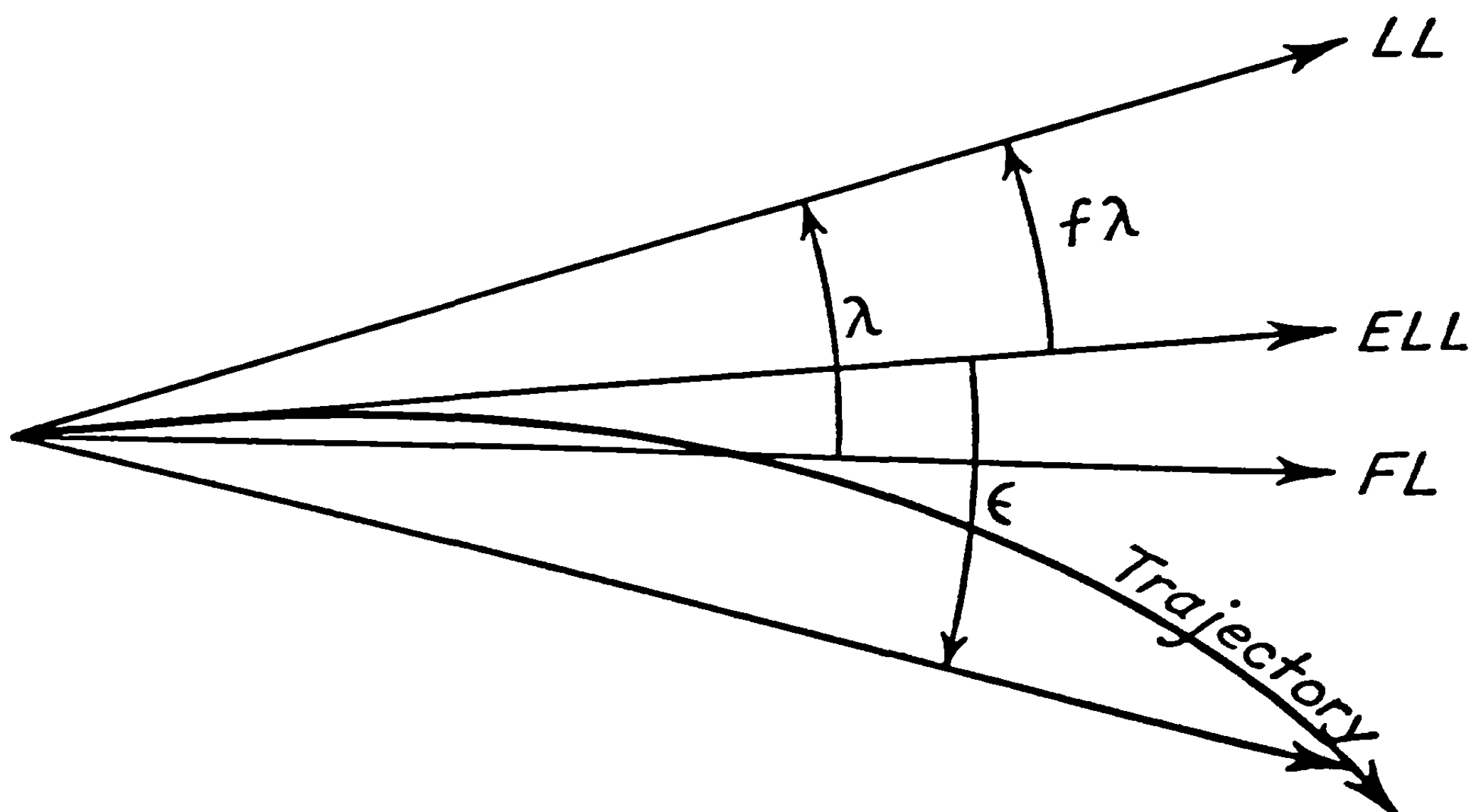


FIGURE 6.41b.—*Rocket trajectory in relation to flight line (FL), launcher line (LL), and effective launching line (ELL).*

the origin. The result is a small displacement of the entire trajectory. However, for small angles and for ranges which are large compared to the burning distance figure 6.41b is an adequate representation.

6.42 Transformation of Trajectory Drop for Various Dive Angles.—The calculation of trajectories for various angles of dive, other conditions remaining the same, may be greatly simplified by the following considerations. Let x_0 , y_0 , and $\epsilon_0 \doteq y_0/x_0$ be the range, linear drop, and angular drop, respectively, from the effective launching line for the airplane in level flight (dive angle $\alpha=0$). Then the point represented by these coordinates transforms approximately to the point x_α , y_α , and ϵ_α when the airplane is in a dive of angle α , where (see fig. 6.42)

$$x_\alpha = x_0 + y_0 \sin \alpha = x_0 (1 + \epsilon_0 \sin \alpha), \quad (1)$$

$$y_\alpha = y_0 \cos \alpha. \quad (2)$$

and

$$\begin{aligned} \epsilon_\alpha &= \tan^{-1} \frac{y_\alpha}{x_\alpha} \doteq \frac{y_\alpha}{x_\alpha} \doteq \frac{y_0}{x_0} \cos \alpha (1 - \epsilon_0 \sin \alpha), \\ &= \epsilon_0 \cos \alpha (1 - \epsilon_0 \sin \alpha). \end{aligned} \quad (3)$$

Thus, using elements x_0 , y_0 , and ϵ_0 computed for the level flight condition, one can easily arrive at approximate values for the trajectory for any dive angle by means of the above equations.

6.43 Empirical Analytic Expressions for Gravity Drop and Angle of Fall.—The trajectory beyond burning is, for short segments, very nearly parabolic; and so the angular drop, ϵ , at any distance x can be represented by an empirical equation of the form

$$\epsilon = a + bx, \quad (1)$$

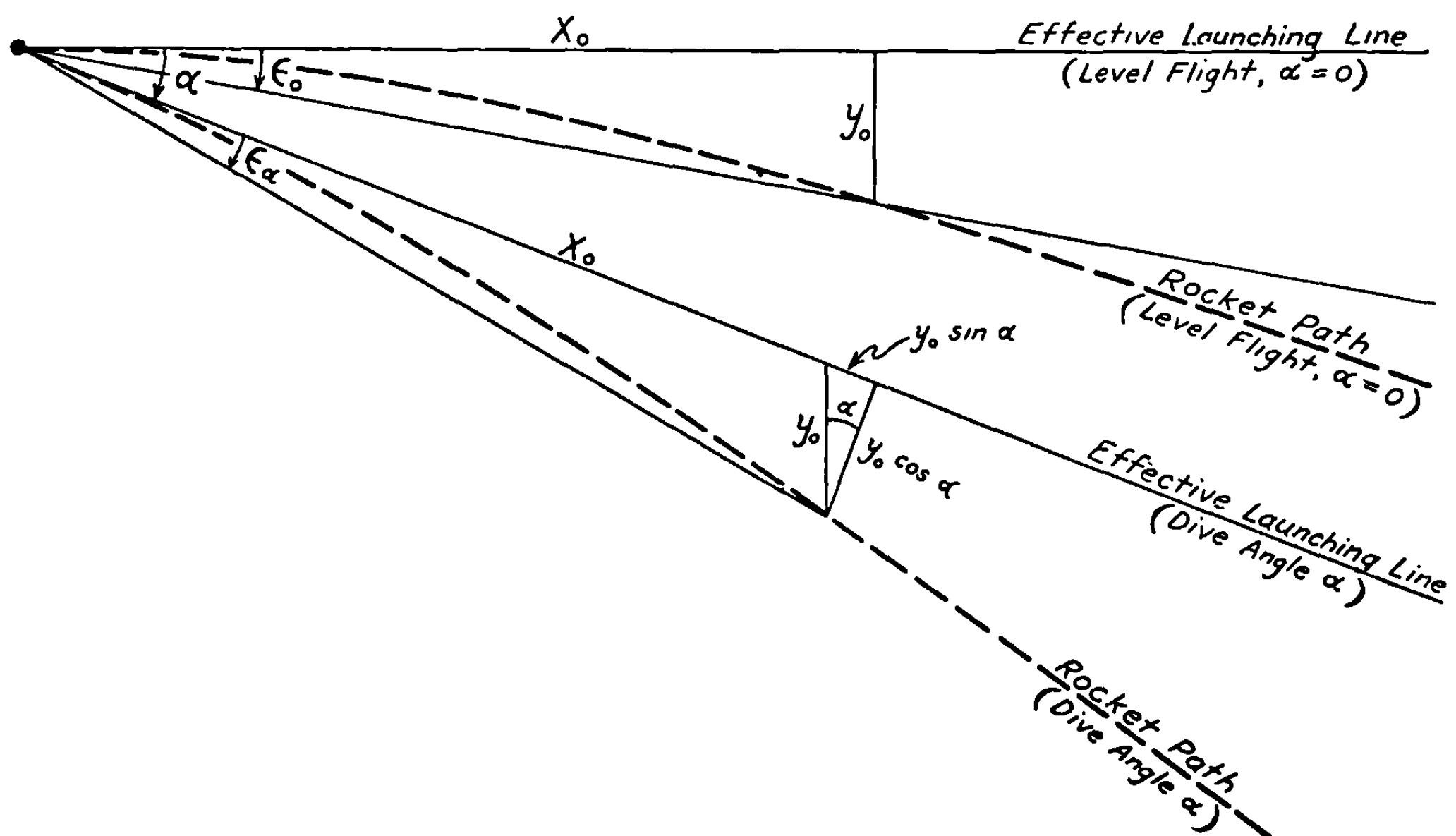


FIGURE 6.42.—Variation of ϵ with dive angle.

where the constants a and b are selected to give, over the region chosen, the best fit to the drop computed as derived above. The above equation will generally agree with the trajectory to within a mil up to a 2,000-yard range and provides a convenient analytical expression from which various properties of the trajectory can be derived. It is also useful in the design of computing sights. A quadratic expression

$$\epsilon = a_1 + b_1 x + c_1 x^2, \quad (2)$$

may be used when one is interested in including a longer portion of the trajectory.

In terms of the above coefficients the trajectory angle, or angle of fall, measured from the effective launching line at any range x is (since $y \doteq x\epsilon$) given by (linear expression)

$$\vartheta_f = \frac{dy}{dx} = \epsilon + x \frac{d\epsilon}{dx} = a + 2bx, \quad (3)$$

(quadratic expression)

$$\vartheta_f = \frac{dy}{dx} = \epsilon + x \frac{d\epsilon}{dx} = a_1 + 2b_1 x + 3c_1 x^2. \quad (4)$$

6.44 Effect of Small Changes in Burning Time and Velocity on Trajectory Drops.—It has been found that rockets loaded with propellants from different powder samples may exhibit considerable variations in their burning times and velocities. The following approximate formulas are derived for the purpose of making it possible to calculate the change in trajectory drop when the burning time and velocity of the rocket differ by small amounts from those for which the trajectory tables have been computed.

The approximation involves the consideration of variations from the vacuum trajectory after burning, and from the trajectory for $\sigma=0$ during burning. With the origin fixed with respect to the air at the position of the rocket at the instant of ignition, the slant range and linear drop from the effective launching line, as shown in figure 6.44, are given by

$$x = x_b + (v_b + V_A)t \cos \vartheta_b + \frac{1}{2}gt^2 \sin \alpha \doteq x_b + (v_b + V_A)t, \quad (1)$$

and

$$y = y_b + (v_b + V_A)t \sin \vartheta_b + \frac{1}{2}gt^2 \cos \alpha$$

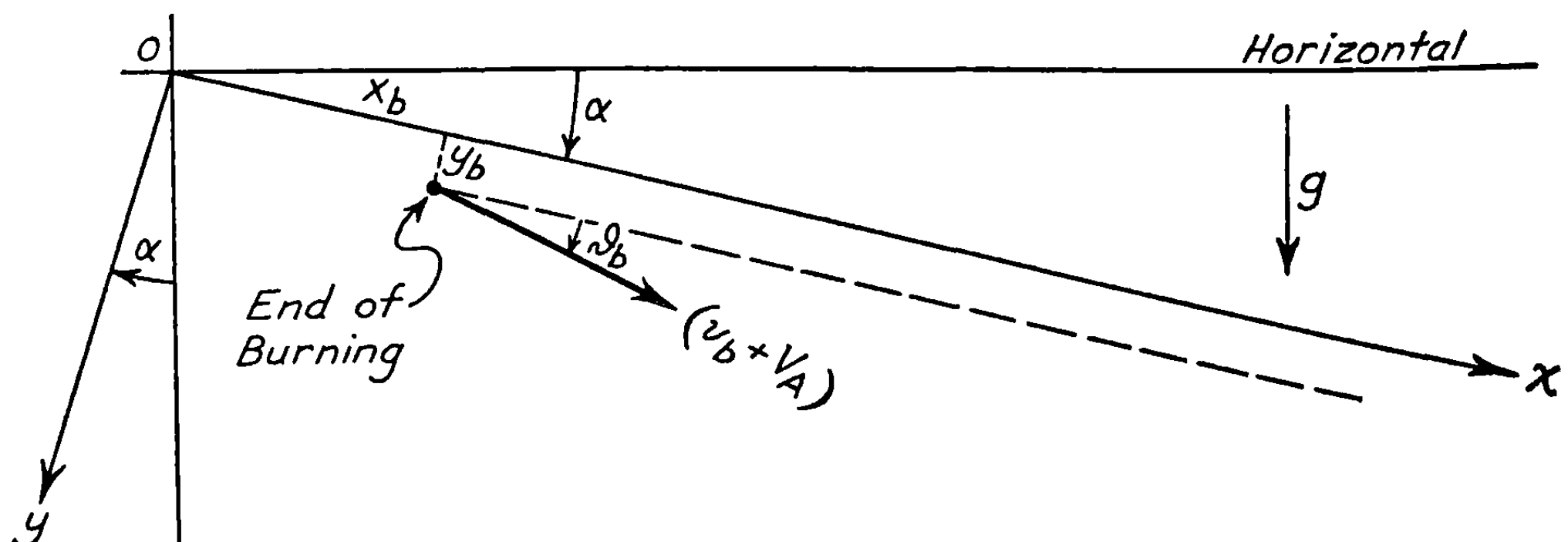


FIGURE 6.44.—Velocity and direction of motion at end of burning.

$$\doteq y_b + (v_b + V_A) t \vartheta_b + \frac{1}{2} g t^2 \cos \alpha, \quad (2)$$

where t is now the time from the end of burning.

Thus the angular drop is given by

$$\epsilon \doteq \frac{y}{x} = \frac{y_b}{x} + \left(1 - \frac{x_b}{x}\right) \vartheta_b + \left(1 - \frac{x_b}{x}\right)^2 \frac{g x \cos \alpha}{2(v_b + V_A)^2}. \quad (3)$$

Now, for $\sigma=0$ and $p=0$, we have from 6.2 (9) and (10)

$$\vartheta_b = \frac{g t_b \cos \alpha}{v_b} \ln \left(1 + \frac{v_b}{V_A}\right), \quad (4)$$

$$y_b = \frac{g t_b^2}{2} \left(1 + \frac{V_A}{v_b}\right)^2 \cos \alpha \left[\ln \left(1 + \frac{v_b}{V_A}\right) - \frac{1}{2} + \frac{1}{2(1 + v_b/V_A)^2} \right]; \quad (5)$$

while

$$x_b = \left(V_A + \frac{v_b}{2}\right) t_b + \frac{g t_b^2}{2} \sin \alpha \doteq \left(V_A + \frac{v_b}{2}\right) t_b. \quad (6)$$

For small variations in v_b , t_b , and V_A , we have from (3), (4), (5), and (6)

$$\Delta \epsilon = M \frac{\Delta v_b}{v_b} + N \frac{\Delta t_b}{t_b} + P \frac{\Delta V_A}{V_A}, \quad (7)$$

where

$$M = v_b \frac{\partial \epsilon}{\partial v_b}, N = t_b \frac{\partial \epsilon}{\partial t_b}, \text{ and } P = V_A \frac{\partial \epsilon}{\partial V_A};$$

or,

$$M = \left(1 + \frac{v_b t_b}{2x}\right) \frac{g x_b \cos \alpha}{(v_b + V_A)^2} - \frac{2 V_A}{(v_b + V_A)} \frac{y_b}{x} - \left(1 - \frac{V_A t_b}{x}\right) \vartheta_b - \left(1 - \frac{x_b}{x}\right)^2 \frac{g x v_b \cos \alpha}{(v_b + V_A)^3}, \quad (8)$$

$$N = \frac{2 y_b}{x} + \left(1 - \frac{2 x_b}{x}\right) \vartheta_b - \left(1 - \frac{x_b}{x}\right) \frac{g x_b \cos \alpha}{(v_b + V_A)^2}, \quad (9)$$

and

$$P = \frac{2 V_A}{(v_b + V_A)} \frac{y_b}{x} - \frac{V_A t_b}{x} \vartheta_b - \left[1 + \left(1 - \frac{x_b}{x}\right) \frac{V_A}{(v_b + V_A)}\right] \frac{g t_b \cos \alpha}{v_b + V_A} - \left(1 - \frac{x_b}{x}\right)^2 \frac{g x V_A \cos \alpha}{(v_b + V_A)^3}. \quad (10)$$

Since x_b is practically independent of the dive angle, while ϑ_b and y_b vary as the cosine of the dive angle, it follows that M , N , and P , and consequently $\Delta \epsilon$, will vary as $\cos \alpha$. Therefore, in computing $\Delta \epsilon$ for various dive angles it is simplest to compute the coefficients M , N , and P for level flight ($\alpha=0^\circ$) and then correct by means of the relation

$$\Delta \epsilon = \Delta \epsilon_{\alpha=0} \cos \alpha. \quad (11)$$

Example: Let us calculate the coefficients M , N , and P , for the 5.0 HVAR at a motor temperature of 70°F. , fired at 2,000-yard range from an aircraft traveling at 500 ft./sec. in a 20° dive. Under these conditions we have

$$V_A = 500 \text{ ft./sec.}, x = 2,000 \text{ yards} = 6,000 \text{ feet},$$

$$v_b = 1,320 \text{ ft./sec.},$$

$$t_f = 0.88 \text{ sec.}, \quad g = 32.2 \text{ ft./sec.}^2;$$

and for level flight, we can readily calculate that

$$\begin{aligned} x_b &= 1,025 \text{ feet}, & \vartheta_b &= 26.7 \text{ mils} \\ y_b &= 19 \text{ feet}, & &= 0.0267 \text{ rad.} \end{aligned}$$

Substituting into (8), (9), and (10), for $\alpha = 0^\circ$ we get

$$\begin{aligned} M &= -0.0444 \text{ rad} = -44.4 \text{ mils}, \\ N &= 0.0157 \text{ rad} = 15.7 \text{ mils}, \\ P &= -0.0303 \text{ rad} = -30.3 \text{ mils}. \end{aligned}$$

In the 20° dive then

$$\begin{aligned} M_{20} &= -44.4 \cos 20^\circ = -41.6 \text{ mils}, \\ N_{20} &= 15.7 \cos 20^\circ = 14.7 \text{ mils}, \\ P_{20} &= -30.3 \cos 20^\circ = -28.4 \text{ mils}. \end{aligned}$$

Therefore, the desired variation in mils is given by

$$\Delta\epsilon = -41.6 \frac{\Delta v_b}{v_b} + 14.7 \frac{\Delta t_b}{t_b} - 28.4 \frac{\Delta V_A}{V_A}.$$

6.45 Differential Corrections to Trajectory Drops for Aircraft Rockets Fired at Targets Above Sea Level.—As the altitude above sea level increases, the density of the air and hence the drag on a projectile will decrease. It is desired to investigate the effect of this change in air density on the trajectory of a rocket and to determine the necessary correction to the trajectory drop in going from sea level to targets at high altitude.

Trajectory tables presumably are computed for true air speeds of the aircraft for targets at sea level. It is assumed that in firing at targets above sea level the true aircraft speed, rocket motor temperature, dive angle, and range are known. The only corrections that need then be applied to the values of ϵ in the published tables are those for the two effects of the reduced air density, ρ : (a) The yaw oscillation distance σ will be greater at the higher altitude, for σ is inversely proportional to $\rho^{\frac{1}{2}}$; and (b) the deceleration coefficient will be less at the higher altitude, for c is directly proportional to ρ . The effect of the increased σ on ϵ , f , and ν is difficult to estimate except by computing new values corresponding to the increased σ . These changes, however, are generally small enough to be negligible. The important effect is the increase in velocity of the rocket because of the decreased drag. Since the average velocity of the rocket at the higher altitude will be greater, it will take less time and hence drop less in reaching a given range. An estimate of this effect on the angular drop, ϵ , can be obtained by neglecting the small changes in the conditions at the end of burning introduced by the difference in deceleration coefficient and by assuming that the rocket is launched as a shell with its full burnt velocity. In that case, from the equations in 6.3 we have (in the usual notation)

$$y = \left(\frac{g x^2 \cos \alpha}{2 V_b^2} \right) B(Z), \tag{1}$$

where

$$Z = 2cx,$$

c = deceleration coefficient of rocket at sea level,

and

$$B(Z) = 2Z^{-2}(e^s - Z - 1).$$

From (1)

$$\begin{aligned} \frac{\Delta y}{y} &= \frac{B'(Z)}{B(Z)} \Delta Z \\ &= \left(1 - \frac{2}{Z} + \frac{2}{ZB(Z)}\right) 2x\Delta c. \end{aligned} \quad (2)$$

Substituting for Z and $B(Z)$ in (2), and making use of the relations

$$\frac{\Delta y}{y} = \frac{\Delta \epsilon}{\epsilon},$$

and

$$\frac{\Delta c}{c} = \frac{\Delta \rho}{\rho},$$

where ρ is the air density at *sea level*, we have finally

$$\Delta \epsilon = \left[\frac{gx \cos \alpha}{V_b^2} - 2\epsilon(1 - cx) \right] \frac{\Delta \rho}{\rho}. \quad (3)$$

Unfortunately, (3) is not in a form suitable for computing purposes, since it involves the difference of two terms of a higher order than $\Delta \epsilon$. If ϵ is not actually y/x , where y is given by (1), a large error in (3) will result because of a small inaccuracy in (1). Rather than take the ϵ part of (3) from published tables and the remainder from (1), it is better to use (1) exclusively until all terms are of the same order. Making use of (1), we can put (3) in the form

$$\Delta \epsilon = 2 [cx - 1 + B^{-1}(Z)] \frac{\Delta \rho}{\rho}, \quad (4)$$

which, for $Z^2 \ll 1$, or $(cx)^2 \ll 1$, becomes

$$\Delta \epsilon = \frac{2}{3} \epsilon cx \left(1 + c \frac{x}{3}\right) \frac{\Delta \rho}{\rho}. \quad (5)$$

It is easy to use (4), especially if figure 5.22 or a table of values of $B(Z)$, such as that in Cranz, is available. Except at long ranges, however, $(cx)^2$ will generally be much less than unity, and in that case (5) is even simpler to apply.

6.5 The Sighting Problem

The foregoing material of this chapter deals with the calculation of trajectories without regard to the particular type of airplane from which the rocket may be launched. Our object now is to show how the theoretical trajectories may be used for the purpose of calculating sighting tables for correct firing from any given aircraft. For simplicity we shall assume that the airplane is in a straight-line dive at constant air speed.⁹

6.51 Speed-Attitude Relations.—It is clear from 6.13 that in order to determine the position of the effective launching line it is necessary to know the angle λ between the launcher line and the flight line; that is, the angle of attack of the launcher line. Since the launcher is set with respect to the boresight datum line (BSDL) or some other fixed line in the airplane,

⁹ Actually, however, the aircraft will generally have a forward acceleration; and, if the sight is held on the target during the dive, the plane will travel along some "curve of approach." In any refined treatment such effects must be taken into account.

it is necessary to know the attitude of the aircraft in any particular attack. Such information is generally supplied by the manufacturer in the form of graphs or tables, or in the form of constants for an analytic expression of the type

$$\eta = C \frac{L}{V_{Ai}^2} - K = C \frac{W \cos \alpha}{V_{Ai}^2} - K, \quad (1)$$

where η = angle of attack of BSDL (see fig. 6.52).¹⁰

L = lift of the wings ($L = W \cos \alpha$ in a straight-line dive),
 W = gross weight of the airplane,
 α = dive angle,
 V_{Ai} = indicated air speed of the aircraft,

and C and K are constants of the airplane.

If the airplane is not moving in a straight line the first form of (1) must be used since L may differ greatly from $W \cos \alpha$. It is the effect of this on η that is the most important source of error if rockets are fired from a maneuvering airplane.

Up to the above point no distinction has been made between the true air speed, V_A , of the aircraft relative to the air and the indicated air speed, V_{Ai} , as given by the airplane's air-speed indicator. Now air-speed indicators are merely calibrated Pitot tubes which give an index of the dynamic pressure $P = \rho V_A^2 / 2$; and for standard sea-level density, ρ_0 , the instrument is calibrated to read velocity directly instead of pressure. Since the air density ρ decreases with altitude the dynamic pressure, and thus the indicated air speed for any given true air speed, will decrease with altitude. The ratio between the two air speeds is given by

$$\frac{1}{2} \rho V_A^2 = \frac{1}{2} \rho_0 V_{Ai}^2,$$

or

$$\frac{V_{Ai}}{V_A} = \left(\frac{\rho}{\rho_0} \right)^{\frac{1}{2}}. \quad (2)$$

In the treatment of flight characteristics of an airplane flying in a straight line at constant speed, ρ and V_A always enter in the combination ρV_A^2 . By the use of (2) this can be replaced by $\rho_0 V_{Ai}^2$, a much more convenient expression since it involves ρ_0 , which is constant, and V_{Ai} , which is measured directly by means of the plane's air-speed indicator. This convenient transformation is not possible when the airplane is accelerating or when the motion of rockets is being considered, since then the quantities ρ , V_A , and V enter the fundamental equations in a variety of combinations. One can always eliminate either ρ or V_A by means of (2), introducing ρ_0 and V_{Ai} , but it is not possible to eliminate both ρ and V_A simultaneously. In such cases it is usually less confusing not to introduce V_{Ai} at all, except in (1), but rather to use the appropriate value of ρ to compute V_A from the known value of V_{Ai} . In computing rocket trajectories according to 6.1 this value of V_A plus the appropriate values of σ and c for the actual value of ρ are to be used.

6.52 Sight-Setting Equation.—Wing Launchers.—Consider first the case in which the rocket is ignited while it is on a fixed, rigid launcher attached to the aircraft, usually under the wing. In figure 6.52 are shown schematically the rocket trajectory and the various relationships among the launcher line, f -line, effective launching line, boresight datum line, and flight line. The sight line through the target at some arbitrary range from the airplane is

¹⁰ A positive (+) value for η indicates BSDL up from the flight line.

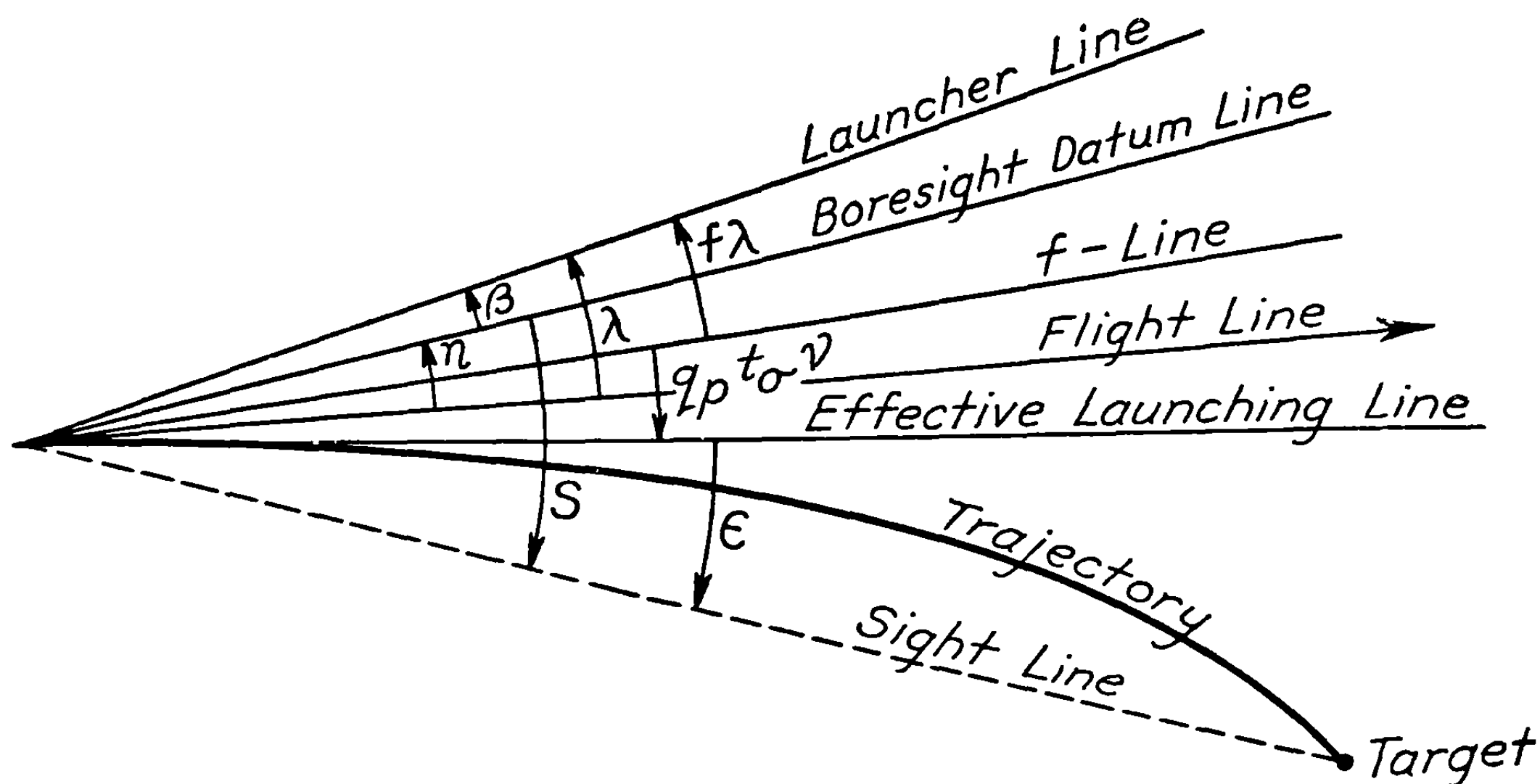


FIGURE 6.52.—Rocket trajectory and sight line in relation to various reference lines.

also indicated, with the trajectory passing through this point. The quantity β in the figure is the angle at which the launcher is set above the boresight datum line.

The sight angle, S , is the necessary depression of the line of sight from the boresight datum line in order that the trajectory cross the line of sight at the target. It is easily seen from the above figure that

$$\begin{aligned}
 S &= \epsilon + q_p t_o \nu + f \lambda - \beta \\
 &= \epsilon + q_p t_o \nu + f(\beta + \eta) - \beta \\
 &= \epsilon + q_p t_o \nu + f \eta - (1 - f) \beta.
 \end{aligned} \tag{1}$$

Actually the line of sight cannot be the one so designated in figure 6.52 for the sight is located in the cockpit of the airplane; while the launchers are set under the wings. If the distance normal to the flight line of the sight above the rocket when it is on the launcher is h , the parallax correction to (1) is h/R , where R is the range. Hence the corrected expression for S is

$$S = \epsilon + q_p t_o \nu + f \eta - (1 - f) \beta + \frac{h}{R}, \tag{2}$$

which is the fundamental equation for the sight setting. It is to be noted that the quantities ϵ , t_o , ν , and f depend only upon the rocket and the initial velocity; while the quantities q_p , η , β , and h depend upon the particular airplane used and the orientation of the launcher.

6.53 Sight-Setting Equation—Lanyard Launching.—In the launching of large rockets from aircraft there is always the danger of structural damage resulting from the rearward blast from the motor. One method of eliminating this hazard is to drop the rocket freely from under the wing or fuselage of the aircraft, and then to ignite it by means of a lanyard attached to the motor. (During the period of free fall the approximate equations of motion are (see fig. 6.53a):¹¹

¹¹ The assumptions regarding aerodynamic forces, small angles, etc., as well as the notation, are the same as in 6.1.

$$t_p = (2l)^{\frac{1}{2}}(g \cos \alpha + g_1)^{-\frac{1}{2}} + \Delta t. \quad (10)$$

At ignition, which corresponds to the time of launching in the theory of 6.1, we have

$$\delta_p = -\lambda \cos \frac{2\pi V_A}{\sigma} t_p - \frac{g \sigma \cos \alpha}{2\pi V_A^2} \sin \frac{2\pi V_A}{\sigma} t_p, \quad (11)$$

$$\varphi_p = -\lambda \cos \frac{2\pi V_A}{\sigma} t_p - \frac{g \sigma \cos \alpha}{2\pi V_A^2} \sin \frac{2\pi V_A}{\sigma} t_p + \frac{g \cos \alpha}{V_A} t_p, \quad (12)$$

and

$$q_p = \dot{\varphi}_p = \frac{2\pi V_A}{\sigma} \lambda \sin \frac{2\pi V_A}{\sigma} t_p + \frac{g \cos \alpha}{V_A} \left(1 - \cos \frac{2\pi V_A}{\sigma} t_p\right). \quad (13)$$

In the above equation, σ is the actual yaw oscillation distance of the rocket, and V_A is the true air speed of the aircraft. Since both σ and the indicated air speed, V_{Ai} , vary inversely as the square root of the air density we have

$$\frac{\sigma}{\sigma_0} = \left(\frac{\rho_0}{\rho}\right)^{\frac{1}{2}} = \frac{V_{Ai}}{V_A},$$

where σ_0 is the value of σ at standard air density ρ_0 . Hence, if we wish to use the standard value σ_0 in the above equations, we simply replace the quantity σ/V_A everywhere by σ_0/V_{Ai} .

Now, from 6.13 (7) and (8), the total deflection of the trajectory from the flight line at the end of burning is

$$\vartheta = \vartheta_g + \vartheta_\varphi + \vartheta_\delta + \vartheta_q = \frac{g \cos \alpha}{G} \Theta_g + \varphi_p + \delta_p \Theta_\delta + q_p t_p \Theta_q, \quad (14)$$

where φ_p , δ_p , and q_p are given by (11)–(13) above. In terms of the f and ν factors, (14) becomes (note that $v_p = 0$ in the present case)

$$\vartheta = \vartheta_g + \varphi_p - \delta_p f + q_p t_p \nu. \quad (15)$$

Hence the angle between the effective launching line and the flight line is given by

$$\Delta = \varphi_p - \delta_p f + q_p t_p \nu. \quad (16)$$

We desire now to determine the correct sight setting corresponding to *release at R_1* (contact range)¹³ and *ignition at R_2* (ignition range). From figure 6.53b we have

$$S_1 = \eta + \frac{R_2}{R_1} (\Delta + \epsilon_2) = (\eta + \Delta + \epsilon_2) - \frac{(R_1 - R_2)}{R_1} (\Delta + \epsilon_2), \quad (17)$$

where ϵ_2 is the gravity drop from the effective launching line corresponding to the range R_2 .

Allowing for the linear displacement, h , normal to the flight line of the rocket at ignition from the position of the sight at contact (parallax correction), we have, finally,

$$S_1 = \frac{R_2}{R_1} (\epsilon_2 + \varphi_p - \delta_p f + q_p t_p \nu) + \eta + \frac{h}{R_1}. \quad (18)$$

There are a number of peculiar effects observed in connection with the motion during

¹³ By contact range is meant the range at the instant the firing key is depressed to start the drop; by ignition range is meant the range at the instant the propellant is ignited.

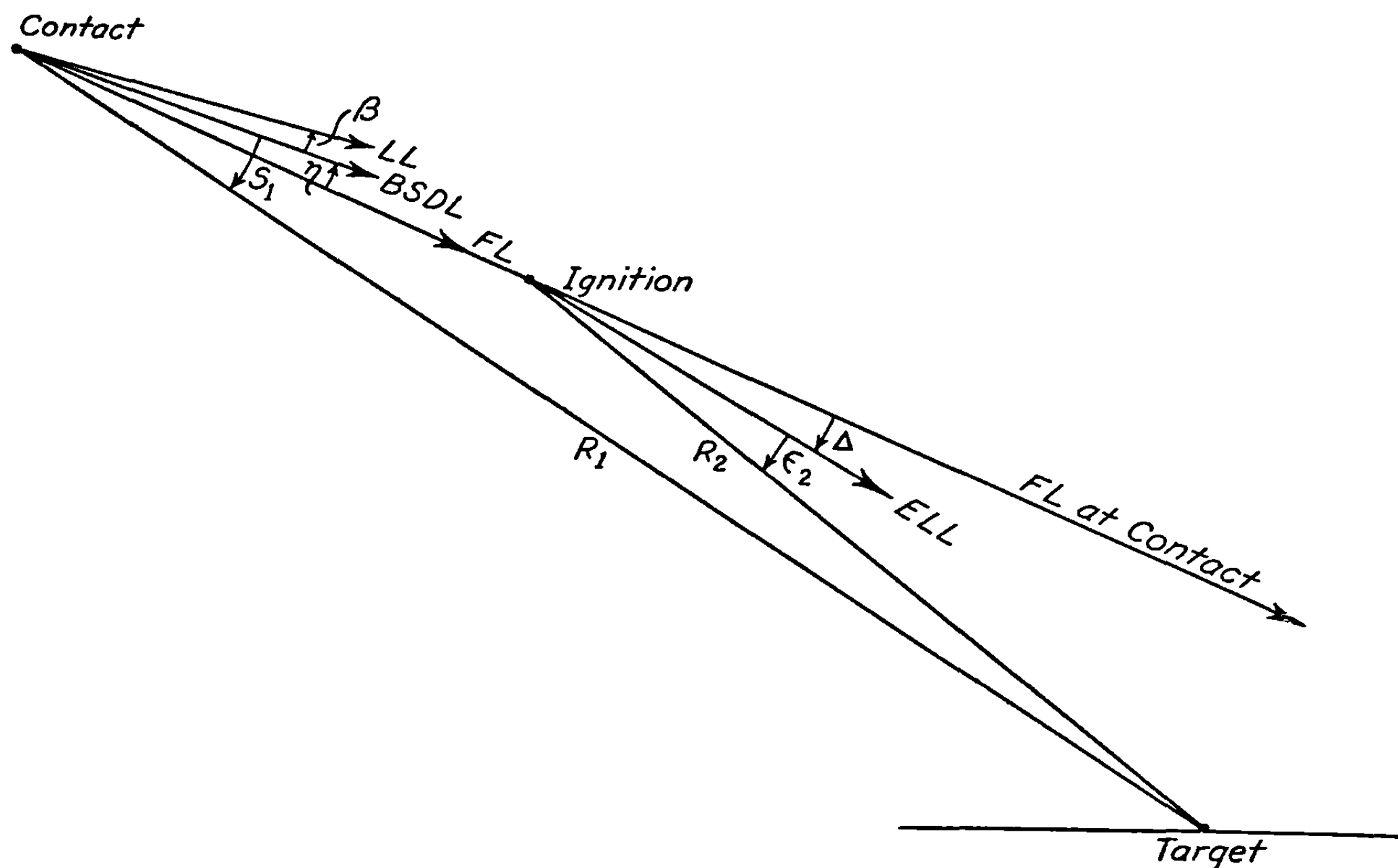


FIGURE 6.53b.—Various ranges and reference lines used in lanyard launching

“free” fall in drop launching, but as yet little is known as to their true nature. It might be that the flight path of the airplane is anomalous, or there might be unexpected aerodynamic forces on the rocket, since the flow pattern near the airplane is certainly more complicated than that assumed above. Hence it is best to use empirical methods, determining experimentally as many as possible of φ_p , δ_p , q_p .

6.54 Effective Angle of Attack of Aircraft for Rocket Firing.—The angle of attack is probably the most uncertain quantity in ordinary forward-firing problems. The following paragraphs indicate in merely the barest outline the difficulties encountered and the method of determining the *effective* angle of attack.

As defined in 6.51, the angle of attack of the boresight datum line is the angle which the BSDL makes with the line of flight of the aircraft. In other words, it is the angle between the BSDL and the direction of the *undisturbed air flow* at a great distance from the airplane. The direction of air flow adjacent to the aircraft bears very little relation to the flight line, for the effects of the propeller, fuselage and, most of all, the wings will result in a flow which is uniform neither in magnitude nor direction.

In the calculation of trajectories and sight settings, however, the assumption was made of a uniform air stream. To circumvent this difficulty the concept of *effective angle of attack* for rocket firing has been adopted, the effective angle of attack being the value of η which makes 6.52 (2) agree with experiment. That is

$$\eta = \frac{1}{f} \left[S - \epsilon - q_p t_o \nu + (1 - f) \beta - \frac{h}{R} \right],$$

where the sight setting S has been determined by experiment. Two values of η , determined for different conditions, will suffice to determine the constants C and K in 6.51 (1). In practice, however, many test firings are conducted, C and K being determined from the results

of all by statistical methods. These values of C and K are then used to determine the angle of attack and hence the sight setting for all other conditions. In this connection, it should be mentioned that the observed value of the coefficient C generally agrees fairly well with the manufacturer's value, but that this is not true for the constant K .

This method of determining the effective angle of attack will lead to reasonably accurate sighting tables even though some relevant factor may be omitted. For example, it is usually assumed that there is no systematic mallaunching, but with some launchers this is not the case. With rail launchers there will be tip-off, and other launchers at times introduce surprisingly large and consistent mallaunching velocities. These then account for part of the difference between the true and the effective angles of attack. Nevertheless, the computed sight settings will be reasonably satisfactory as long as the firing conditions do not differ too much from those at which the effective angle of attack is determined experimentally.

6.6 A Theory for the Difference Between the True Angle of Attack and the Effective Angle of Attack

The true angle of attack of a launcher on an airplane has been defined as the angle between the launcher axis and the direction of motion of the airplane with respect to the undisturbed air at infinity. The effective angle of attack is the angle of attack computed from the direction of motion of the rocket at the end of burning and the assumption that the air everywhere has the same velocity as the air at infinity. It is measured in practice by using observed impact points as a basis for the computation of angles of attack. (See 6.54.) Since the assumption of a uniform air flow is obviously incorrect, the true angle of attack and the effective angle of attack are not equal.

The purpose of the present discussion is to obtain an expression for the difference between the true and the effective angles of attack in the general case in which the direction of the air flow in the neighborhood of the wing is arbitrarily specified. The magnitude of the difference is worked out in a particular case which shows that the effect is significant under ordinary circumstances. Since an expression of the form

$$\eta = \frac{CW \cos \alpha}{V_A^2} - K \quad (1)$$

(see 6.51) should hold for the true angle of attack, and since from the aerodynamic theory of the airplane it should be possible to obtain the flow pattern as a function of the air speed and the true angle of attack, it should be possible by the use of the theory given below to deduce the variation of the effective angle of attack with airplane speed, dive angle, and airplane weight. Thus the validity of using (1) as an expression for the effective angle of attack could be investigated.

In computing the difference between the true and effective angles of attack we can neglect gravity and initial angular velocity since these would only introduce the same additional curvature into each trajectory. If in any particular circumstance we compute that with the actual velocity distribution around the airplane the direction of motion (the f -line) makes the angle ϑ_b with the launcher at the end of burning, then the effective angle of attack is ϑ_b/f , where f is the launching factor for those conditions. If we choose to make these calculations for a case in which the launcher is parallel to the direction of motion with respect to the air at infinity, the true angle of attack will be zero, and hence ϑ_b/f will be the difference between the true and effective angles of attack. For any particular rocket this difference depends

only on the flow pattern around the airplane, the air speed of the airplane, the type of rocket, and the propellant temperature. It does not depend on the orientation of the launcher, the presence or absence of gravity, malalignment, initial angular velocity, or the dive angle. Hence these latter quantities are to be given any values that are convenient for simplifying the calculation of the difference between the true and effective angles of attack.

Let us consider a coordinate system in which the axes are fixed with respect to the air at infinity, the x -axis being the direction of flight of the airplane and the y -axis being perpendicular to it and pointing downward. The origin is taken at the center of mass of the rocket at the instant of ignition, V is the velocity of the rocket in this system, and V_A the velocity of the airplane. When we need to refer quantities to a coordinate system at rest with respect to the airplane, we shall use the corresponding lower case symbols. We shall let d be the distance forward as measured by an observer in the airplane. In the neighborhood of the airplane the velocity of the air in the fundamental coordinate system is not zero but is $V_\perp(d)$ in the direction parallel to the y -axis. We shall refer to this as the cross velocity of the air at the point. It is convenient to let

$$\eta_F(d) = \frac{V_\perp(d)}{V_A}, \quad (2)$$

since η_F is the angle between the direction of the air flow at infinity and the direction of the air flow a distance d ahead of the airplane as seen by an observer in the airplane. The fact that $\eta_F(\infty) = 0$ corresponds to the fact that the true angle of attack of the x -axis, which we use as our datum line, is zero. $\eta_{F0} \equiv \eta_F(0)$ gives the direction of flow at the launcher, and $V_{\perp 0} \equiv V_\perp(0) = V_A \eta_{F0}$ gives the cross velocity at the launcher. The angles φ , ϑ , and $\delta = \varphi - \vartheta$ are, as shown in figure 6.11, the orientation of the rocket, the direction of motion with respect to an observer in the xy -coordinate system, and the yaw in this system, respectively. The yaw as seen by an observer who is at rest with respect to the air at the point occupied by the rocket is

$$\begin{aligned} \delta_a &= \delta + \frac{V_\perp}{V} = \delta + \eta_F \frac{V_A}{V} \\ &= \delta + \eta_F \frac{V_A}{v_\sigma \zeta}. \end{aligned} \quad (3)$$

Hence the equations of motion in the absence of gravity and malalignments are [cf. 6.13 (4), (5), and (6), as well as 6.11 (2), (3), and (4)]:

$$\varphi'' + 16\pi^2 \zeta^2 \delta_a = 0, \quad (4)$$

$$\zeta \vartheta' - \delta = 0, \quad (5)$$

and

$$\varphi - \vartheta - \delta = 0. \quad (6)$$

If we substitute from (3) for δ_a and write $V_A/v_\sigma = \zeta_p$, since for post launchers $V_A = V_p$, (4) becomes

$$\varphi'' + 16\pi^2 \zeta^2 \delta = -16\pi^2 \zeta_p \zeta \eta_F(\zeta). \quad (7)$$

In (7) η_F can be regarded as a function of ζ rather than of d on the basis of the change of variables

$$\zeta = \frac{V}{v_\sigma} = \frac{v}{v_\sigma} + \frac{V_A}{v_\sigma} = \left(\frac{d}{\sigma}\right)^{\frac{1}{2}} + \left(\frac{d_A}{\sigma}\right)^{\frac{1}{2}}, \quad (8)$$

and

$$d_A = \sigma V_A^2 / v_\sigma^2 = V_A^2 / 2G. \quad (9)$$

The solution of (5), (6), and (7), which are of the form considered in 3.37, can be carried out by the Green's function method for arbitrary $\eta_F(\zeta)$; and the solution can be written in the form

$$\vartheta_b = -16\pi^2 \eta_{F0} \zeta_p \int_{\zeta_p}^{\zeta_b} \left(\frac{\eta_F(u)}{\eta_{F0}} \right) [u \Theta_q(u, \zeta_b)] du, \quad (10)$$

where ζ_b is the value of ζ at the end of burning, and Θ_q is the characteristic function for mal-launching as given by 3.34 (23).

The integral in (10) is readily evaluated by means of Simpson's rule with the aid of the table of Θ_q given in the appendix. Useful information, however, is readily obtained from a graph such as that in figure 6.6a, which contains curves of $16\pi^2 u \Theta_q(u, \zeta_b)$ plotted as a function of u for several values of ζ_b corresponding to various possible burning distances of the rocket under consideration. For long-burning rockets we can take $\zeta_b = \infty$, which leads to

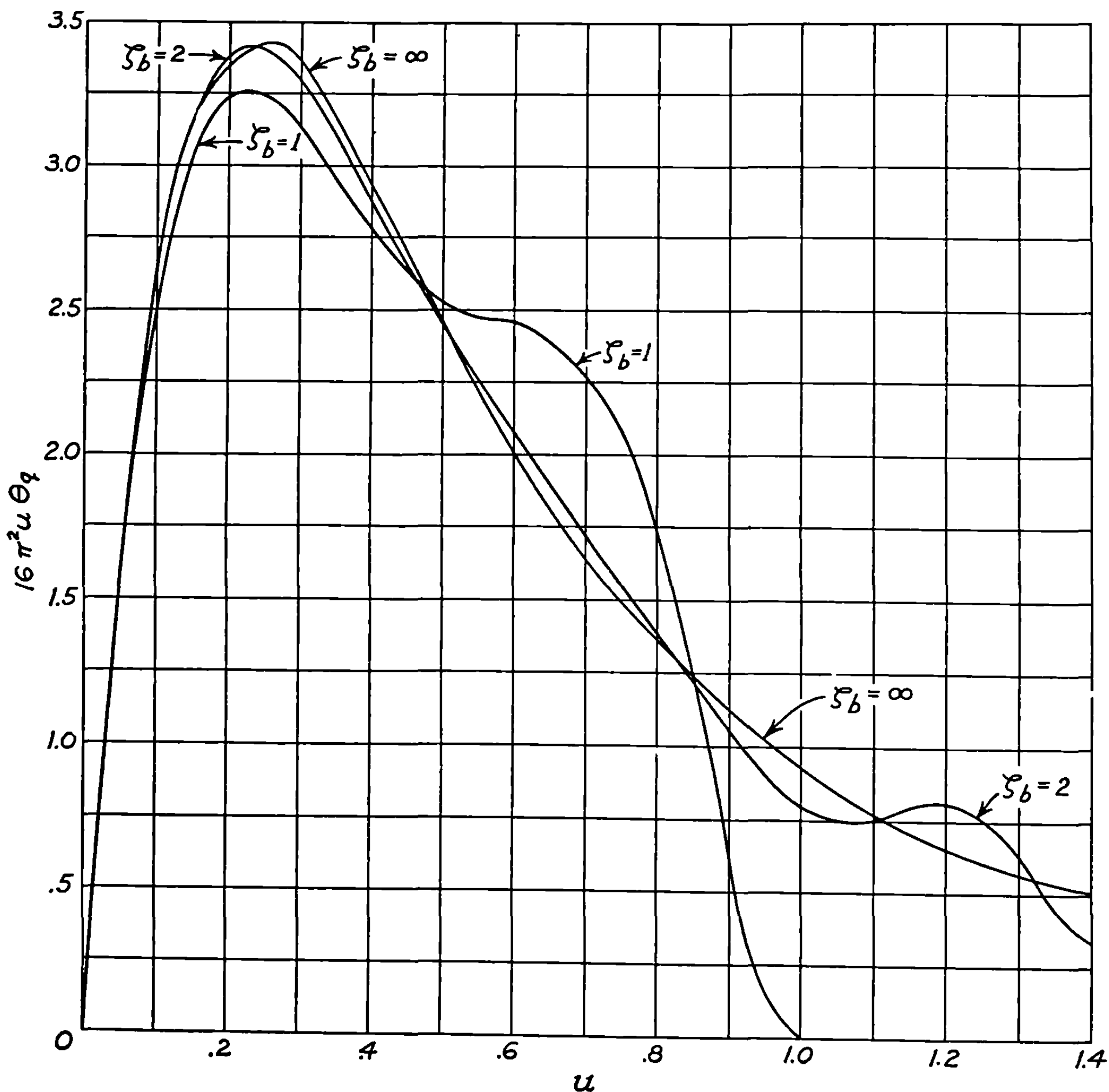


FIGURE 6.6a.—Green's function, $16\pi^2 u \Theta_q(u, \zeta_b)$, for various burning distances.

$$u\theta_q(u, \infty) = \frac{1}{2}u \left\{ \cos 2\pi u^2 \left[\frac{1}{2} - C(2u) \right] + \sin 2\pi u^2 \left[\frac{1}{2} - S(2u) \right] \right\}. \quad (11)$$

To show how figure 6.6a is used in a particular case, let us consider the example shown in figure 6.6b. If we are interested in the 5.0 HVAR at 70° F. with $V_A = 400$ ft./sec., then $\zeta_b = 1.75$ and we use the curve for $\zeta_b = 2$. Also, we add a scale giving the correspondence between d and u for $d_a = 51$ feet and $\sigma = 320$ feet. Note that $d = 0$ on this scale corresponds to $u = \zeta_p$ for a zero-length launcher. By using this scale, $\eta_F(d)/\eta_{F0}$ can be plotted for any desired variation of η_F with d . The particular form shown is assumed for illustrative purposes only; it is not the result of a study of the direction of air flow around a wing, and is probably a very poor approximation to reality. The product of the two curves may then be integrated with respect to u from $u = \zeta_p$ to $u = \zeta_b$. This result, multiplied by ζ_p , is denoted by I . Then $\vartheta_b = -\eta_{F0}I$ is the direction of motion at the end of burning, and $\eta_{F0}I/f$ is the difference between

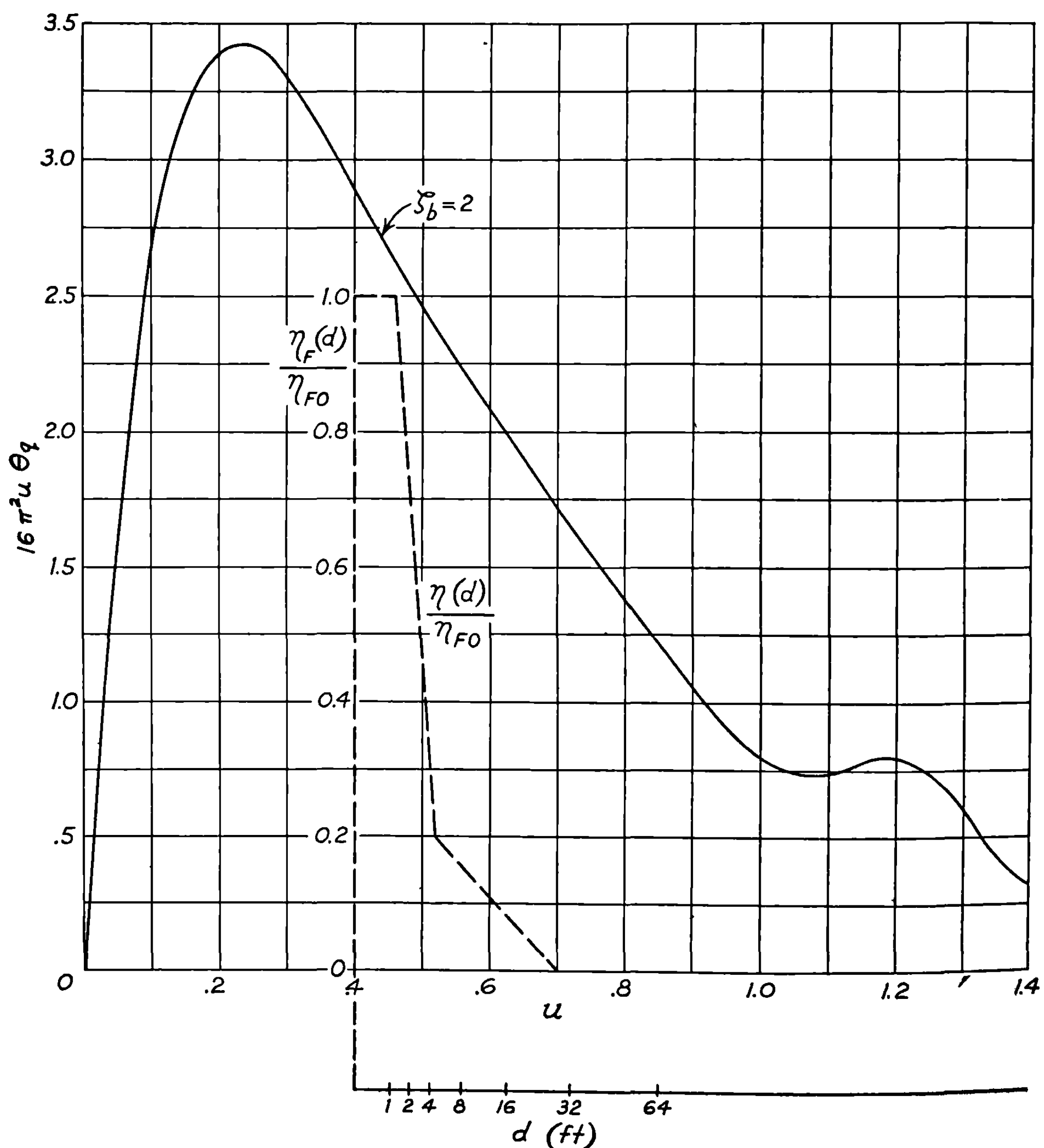


FIGURE 6.6b.—Sample calculation using Green's function.

the true and the effective angles of attack. It may be of interest to note that if $\eta_F(d)/\eta_{F0}=1$, then $I=f$. This result follows since the given condition is equivalent to the statement that the launcher is set at an angle η_{F0} to a uniform air stream.

It is possible to get considerable qualitative information from a consideration of figure 6.6b without actually carrying out an integration. For example, it is relatively easy to estimate the effect of a change in the function assumed for $\eta_F(d)$.

As an example of the quantitative information that is given by numerical integration, we can carry it out by the trapezoidal formula, using intervals of length $\Delta u=0.06$, and get

$$I=(0.4) (0.06) \left[\frac{1}{2} (2.87) (1.00) + (2.62) (1.00) + (2.37) (0.20) \right. \\ \left. + (2.15) (0.13) + (.194) (0.06) + \frac{1}{2} (1.71) (0.00) \right] = 0.118. \quad (12)$$

Since $f=0.82$ for the 5.0 HVAR at 70° F. when $V_A=400$ ft./sec., the difference between the true and the effective angles of attack for the distribution of cross velocities shown in figure 6.6b is $0.14 \eta_{F0}$. If, as an estimate, η_{F0} is of the order of 40 mils when $V_A=400$ ft./sec., the difference is 6 mils. The difference will be much larger at lower speeds.

One complication that should not be overlooked when such a calculation is carried out with values of $\eta_F(d)$ determined from aerodynamic theory is that the length of a rocket is of the same order as the chord of the airplane wing; hence, the value of $\eta_F(d)$ that is to be used may not be the direction of air flow at the point d . It would probably be better to take it as the equilibrium position of a rocket whose center of mass is at d .

6.7 Sources of Error and Dispersion

The factors which determine the pattern of striking points in rocket fire from aircraft are mentioned below. It is proposed to point out some of the more important sources of error and dispersion, without going into the details of estimating them, except in the case of the rocket malalignments. All systematic effects due to gravity will be neglected, since the small deflections arising from the various causes herein discussed are to be superposed on the normal gravity drops.

6.71 Effect of Linear Thrust Malalignment.—In 6.13 it was pointed out that the equations of motion of the rocket in terms of the dimensionless parameter

$$\zeta = \frac{V}{v_\sigma} = \frac{V_A + Gt}{(2G\sigma)^{\frac{1}{2}}} \quad (1)$$

were the same in forward firing as in ground firing. Hence the solution for the deflection of the tangent resulting from the linear thrust malalignment is, from 3.39 (11),

$$\vartheta_R = -\frac{2\sigma R_M}{K^2} \Theta_R(\zeta_p, \zeta), \quad (2)$$

where the characteristic function Θ_R is given explicitly by 3.39 (8). A set of curves showing the variation of Θ_R with ζ for various values of ζ_p will be found in figure 3.39.

In order to see more clearly the effect of the airplane speed on the dispersion, we have plotted in figure 6.71 the quantity

$$-\frac{K^2 \vartheta_R}{12\sigma R_M} = \frac{1}{6} \Theta_R$$

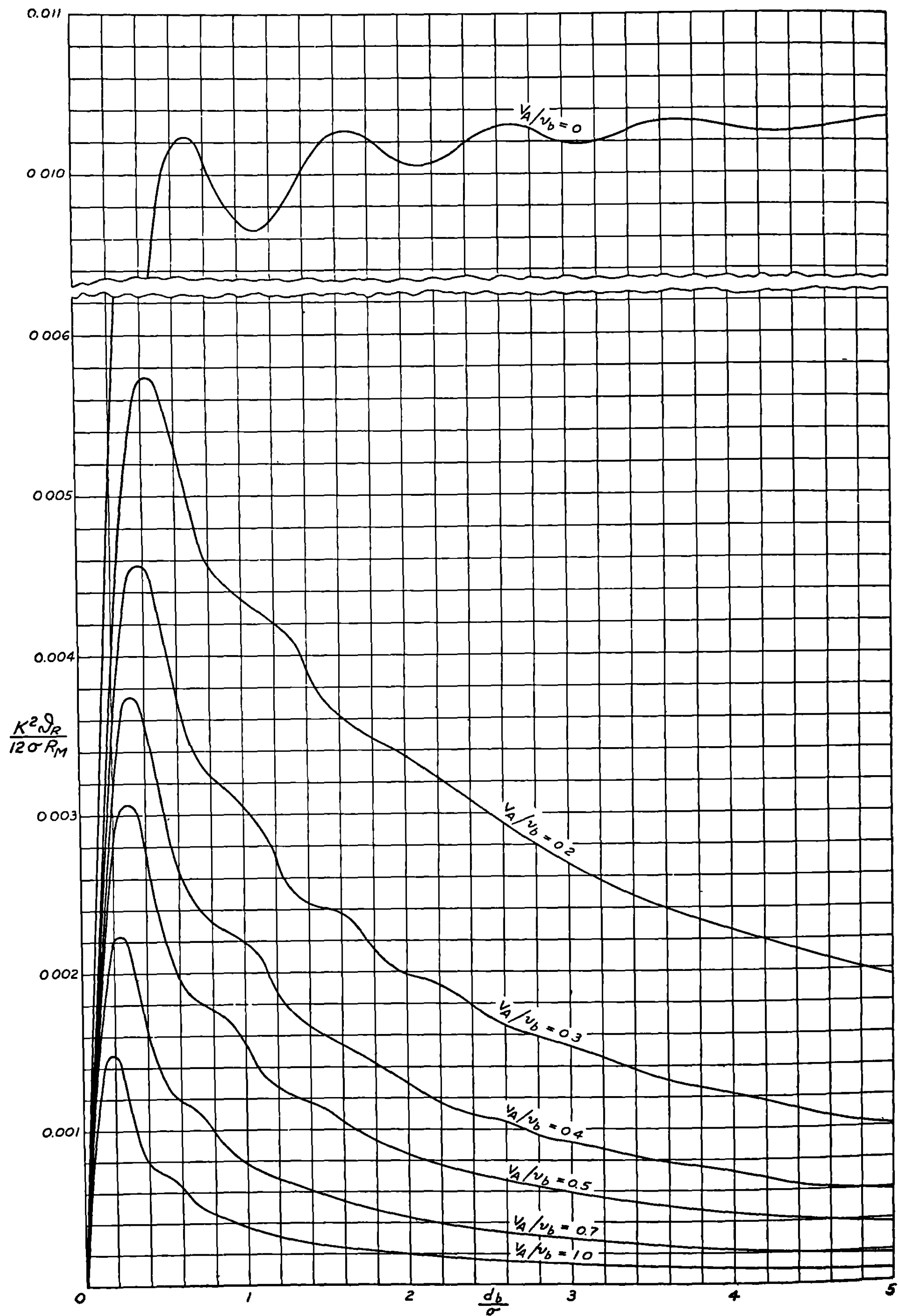


FIGURE 6.71.—Dispersion due to linear malalignment, for firing from zero-length launchers.

as a function of d_b/σ for various values of the ratio V_A/v_b , where $d_b = \frac{1}{2}Gt_b^2$ and v_b are the burning distance and the burnt velocity, respectively, relative to the moving launcher. All the curves are plotted for a zero-length launcher, $p=0$, which is the most common condition for aircraft firing. The curve for $V_A/v_b=0$ corresponds to the case of ground firing. It is observed that for a given value of V_A/v_b (excepting $V_A/v_b=0$) the deflection increases rapidly with burning distance, reaching a maximum at a value of d_b/σ between 0.2 and 0.5, depending upon the other constants chosen; it then decreases for larger values of d_b/σ , approaching zero as $d_b/\sigma \rightarrow \infty$. The dispersion can be kept below the maximum either by reducing the burning distance to an extremely small value or else by going to large values of d_b . Since the first alternative is difficult to achieve in practice, the choice of large values of the burning time (and therefore large burning distance) becomes the simplest feasible method for decreasing the dispersion due to linear malalignment of rockets fired forward from aircraft.

6.711 *Approximate formulas for long-burning rockets.*—For the present discussion it will be convenient to use distance, time, and velocity as parameters, rather than velocity and acceleration, as was done heretofore. When the acceleration is not constant throughout we use the *effective* burning time, which depends mainly upon the initial acceleration, as defined in 2.22. For forward firing considerations we define the following primed quantities:

$$\begin{aligned}
 v_b' &= v_b + V_A = V_b && \text{=total velocity of the rocket relative to the air, or relative to} \\
 &&& \text{ground in the absence of wind.} \\
 t_b' &= \frac{v_b + V_A}{v_b} t_b = \frac{V_b}{G} && \text{=time that would be necessary for the rocket to attain the velocity} \\
 &&& \text{\(V_A + v_b\) in ground firing with the acceleration } G = v_b/t_b. \\
 p' &= \frac{(v_p + V_A)^2}{2G} = \frac{V_p^2}{2G} \\
 &= \frac{[(2Gp)^{\frac{1}{2}} + V_A]^2}{2G} \\
 &= \left[p^{\frac{1}{2}} + \frac{V_A}{v_b} \left(\frac{v_b t_b}{2} \right)^{\frac{1}{2}} \right]^2 && \text{=launcher length that would be necessary to give the rocket the} \\
 &&& \text{same launching speed on the ground as it has in air firing, the} \\
 &&& \text{acceleration } G \text{ being the same in both cases.}
 \end{aligned}$$

These quantities are introduced because we can then replace the problem of firing from an airplane by the equivalent problem of firing a rocket having velocity v_b' and burning time t_b' from a stationary launcher of length p' .

Examination of figure 3.39 reveals that for long-burning rockets which obey the conditions that p' be less than half the burning distance ($p' < v_b' t_b' / 4$, or $V_p^2 < V_b^2 / 2$) and that the burning distance be greater than the yaw oscillation distance [$v_b' t_b' / 2 > \sigma$, or $V_b > (2G\sigma)^{\frac{1}{2}}$] a good approximation to the deflection produced by the linear malalignment of the jet is given by the first term of the asymptotic expression 3.39 (12); namely,

$$\frac{K^2 \vartheta_R}{\sigma R_M} = -\frac{1}{4} \left(\left\{ \frac{1}{2} - S[(4p'/\sigma)^{\frac{1}{2}}] \right\}^2 + \left\{ \frac{1}{2} - C[(4p'/\sigma)^{\frac{1}{2}}] \right\}^2 \right). \quad (1)$$

A plot of $K^2 \vartheta_R / 12 \sigma R_M$ as a function of p'/σ is shown in figure 6.711 (middle line).

6.712 *Low airplane speeds.*—For $p'/\sigma \leq 0.25$ a good approximation to 6.711 (1) is given by (cf. fig. 6.711)

$$\frac{K^2}{\sigma} \frac{\vartheta_R}{R_M} = \frac{1}{8} \exp \left[-4 \left(\frac{p'}{\sigma} \right)^{\frac{1}{2}} \right] = \frac{1}{8} \exp \left[-4 \left(\frac{p}{\sigma} \right)^{\frac{1}{2}} \right] \exp \left[-4 \frac{V_A}{v_b} \left(\frac{d_b}{\sigma} \right)^{\frac{1}{2}} \right]. \quad (1)$$

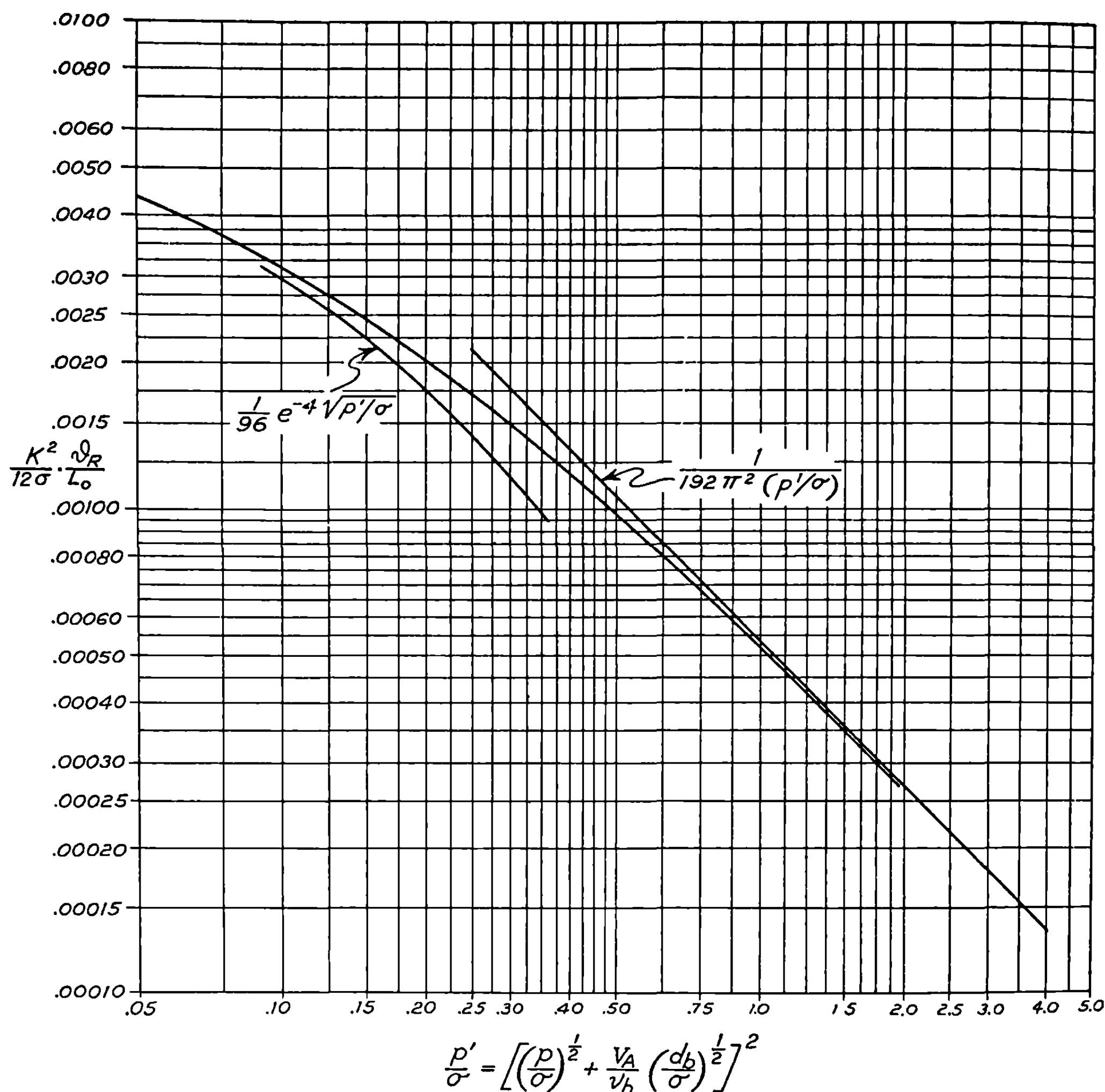


FIGURE 6.711.—Dispersion of long-burning rockets. Middle curve is exact for very long-burning rockets; side curves illustrate approximate formulae.

In the case of ground firing (again only for long-burning rockets, for which $2d_b/\sigma \geq 1$), $V_A=0$ and (1) reduces to

$$\text{Ground firing, } \frac{K^2 \vartheta_R}{\sigma R_M} = \frac{1}{8} \exp \left[-4 \left(\frac{p}{\sigma} \right)^{\frac{1}{2}} \right]. \quad (2)$$

The above inequality, $p'/\sigma \leq 0.25$, will be satisfied in the case of most of the aircraft rockets listed in Table 2.11 only for relatively low airplane speeds; namely, $V_A \leq 250$ ft./sec. In that case, (1) and (2) indicate that the *relative effect of launcher length upon the dispersion*, $\exp [-4(p/\sigma)^{\frac{1}{2}}]$, is *roughly the same both for airplane and ground firing*. Equation (1) indicates also that the relative decrease in dispersion resulting from forward firing at low airplane speeds is given by

$$\frac{\text{air dispersion}}{\text{ground dispersion}} = \exp \left[-4 \frac{V_A}{v_b} \left(\frac{d_b}{\sigma} \right)^{\frac{1}{2}} \right], \quad (3)$$

a factor which *decreases* both with increased airplane speed and with increasing burning distance or burning time.

6.713 *High airplane speeds.*—For $p'/\sigma \geq 0.35$ a good approximation to 6.711(1) is given by (see figure 6.711)

$$\frac{K^2 \vartheta_R}{\sigma R_M} = \frac{1}{16\pi^2 (p'/\sigma)} = \frac{1}{16\pi^2 \left[\left(\frac{p}{\sigma} \right)^{\frac{1}{2}} + \frac{V_A}{v_b} \left(\frac{d_b}{\sigma} \right)^{\frac{1}{2}} \right]^2} \quad (1)$$

The above inequality, $p'/\sigma \geq 0.35$, will be satisfied in the case of most of the aircraft rockets whose properties are listed in Table 2.11 only at airplane speeds above approximately 450 ft./sec. For ground firing 6.712 (2) is still applicable. Therefore, the relative decrease in angular dispersion resulting from forward firing at high airplane speeds is given by

$$\frac{\text{air dispersion}}{\text{ground dispersion}} = \frac{\exp [4(p/\sigma)^{\frac{1}{2}}]}{2\pi^2 \left[\left(\frac{p}{\sigma} \right)^{\frac{1}{2}} + \frac{V_A}{v_b} \left(\frac{d_b}{\sigma} \right)^{\frac{1}{2}} \right]^2} \quad (2)$$

a factor which decreases both with increased airplane speed and with increasing burning distance or burning time.

It should be emphasized [see 6.712 (1) and 6.713 (1)] that increasing the launcher length is less effective in reducing dispersion at high airplane speeds than it is at low, which is one reason why a post launcher; i. e., $p=0$, is satisfactory for high-velocity aircraft. It also should be borne in mind that, whereas in ground firing with long-burning rockets the dispersion is practically independent of temperature or burning time [see 6.712 (2)] *in forward firing the dispersion may depend greatly upon the temperature of the rocket motor.* This is true because the burning time and burning distance, which vary with temperature, enter into the deflections as given by the above equations. The lower the temperature (greater burning distance) the less the dispersion; while the higher the temperature (shorter burning distance) the greater the dispersion. This will not be true if the burning distance becomes so short as to violate the conditions under which 6.711 (1) is valid.

6.72 Effect of Angular Thrust Malalignment.—As with the linear malalignment, the deflection resulting from the angular thrust malalignment β_M has the same form in forward firing as in ground firing; namely,

$$\vartheta_\beta = \beta_M \Theta_\beta(\zeta_p, \zeta), \quad (1)$$

where

$$\zeta = \frac{V}{v_\sigma} = \frac{V_A + Gt}{(2G\sigma)^{\frac{1}{2}}}, \quad (2)$$

and the characteristic function Θ_β is identical with the gravity function Θ_g and therefore defined by 3.38 (11). Curves showing the variation of Θ_g with ζ for constant values of ζ_p will be found in figure 3.38a.

In order to see more clearly the effect of airplane speed on the resulting dispersion, we have plotted in figure 6.72 the quantity $\vartheta_\beta/\beta_M = \Theta_\beta$ as a function of d_b/σ for various values of the ratio V_A/v_b , where $d_b = \frac{1}{2}Gt_b^2$ and v_b are the burning distance and burnt velocity, respectively, relative to the moving launcher. All the curves are plotted for a zero-length launcher, $p=0$. The curve for $V_A/v_b=0$ corresponds, of course, to the case of ground firing. Whereas in ground firing the deflection increases without limit as $d_b/\sigma \rightarrow \infty$, it will be observed that for $V_A/v_b > 0$ the deflection approaches a finite value as $d_b/\sigma \rightarrow \infty$. Furthermore, the greater the value of V_A/v_b , the sooner does the rocket take up the major portion of its final deflection.

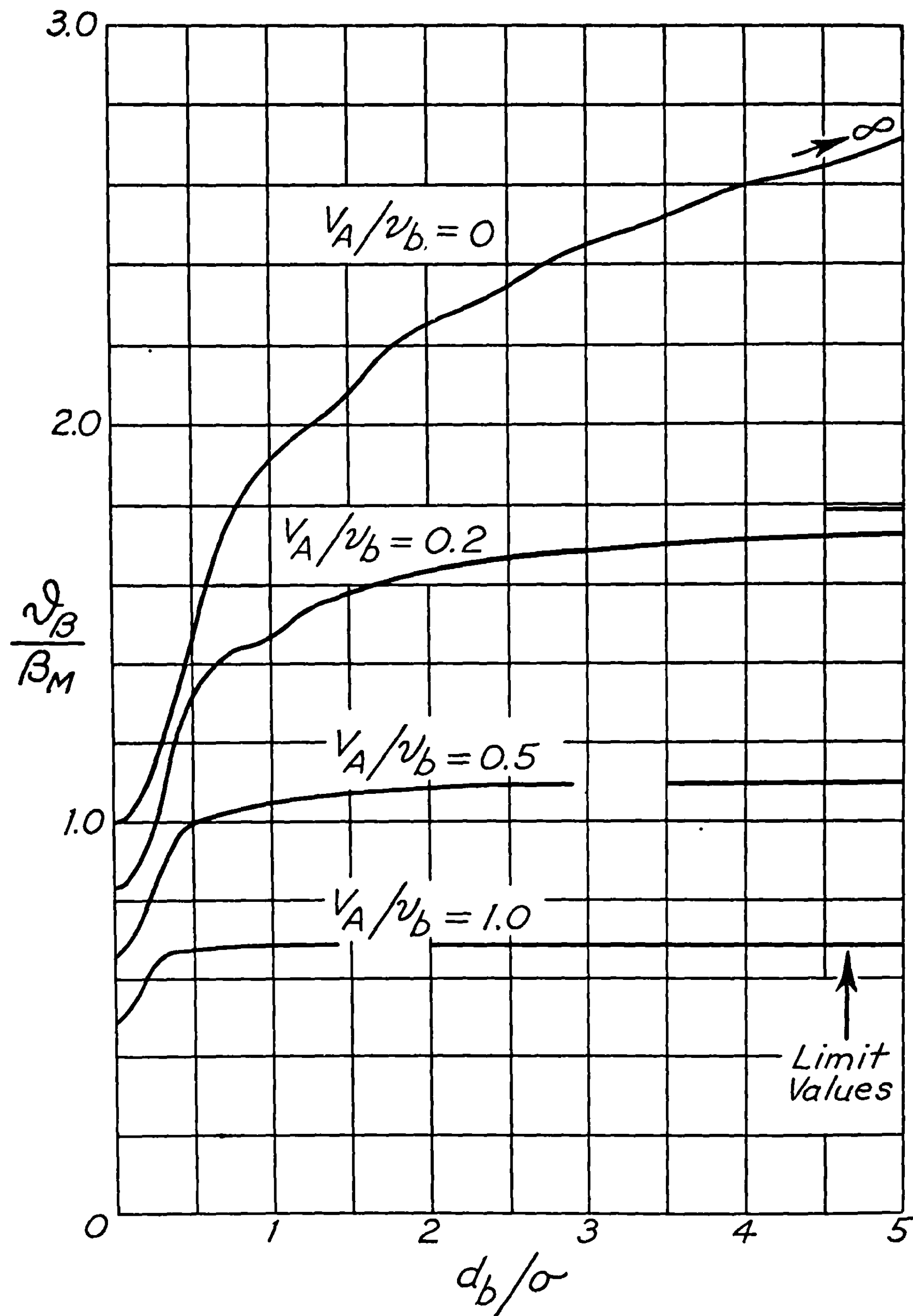


FIGURE 6.72.—Dispersion due to angular thrust malalignment for firing from zero-length launchers.

In terms of d_b and v_b ,

$$\zeta_p = \left(\frac{d_b}{\sigma}\right)^{\frac{1}{2}} \left(\frac{V_A + v_p}{v_b}\right), \quad (3)$$

and

$$\zeta_b = \left(\frac{d_b}{\sigma}\right)^{\frac{1}{2}} \left(1 + \frac{V_A}{v_b}\right). \quad (4)$$

6.7 SOURCES OF ERROR AND DISPERSION

Hence, as $d_b/\sigma \rightarrow \infty$ we note that both ζ_p and ζ_b likewise approach infinity. Therefore, from the asymptotic expansion 3.38 (18) for $\Theta_\beta = \Theta_g$, we have in the limit as $d_b/\sigma \rightarrow \infty$,

$$\frac{\vartheta_\beta}{\beta_M} = \ln \frac{\zeta_b}{\zeta_p} = \ln \frac{V_A + v_b}{V_A + v_p}. \quad (5)$$

The limit values plotted in Fig. 6.72 for $p=0$ are thus given by

$$\frac{\vartheta_\beta}{\beta_M} = \ln \left(1 + \frac{v_b}{V_A} \right). \quad (6)$$

It is interesting to note that (6) is also the value given by the $\sigma=0$ approximation [see 6.2 (9), remembering that $\vartheta_\beta/\beta_M = \vartheta_g/(g \cos \alpha/G)$]. Hence the value which ϑ_β approaches as the burning distance increases is the same as that given by the $\sigma=0$ approximation.

6.73 Effect of Fin Malalignment.—The deflection resulting from fin malalignment is, as in ground firing,

$$\vartheta_F = \delta_0 \Theta_F(\zeta_p, \zeta), \quad (1)$$

where ζ is given by 6.72 (2) and the characteristic function Θ_F is given by 3.42 (9). Curves showing the variation of Θ_F with ζ for constant values of ζ_p will be found in figure 3.42.

In order to see more clearly the effect of airplane speed on the resulting dispersion we have plotted in figure 6.73 the quantity $\vartheta_F/\delta_0 = \Theta_F$ as a function of d_b/σ for various values of the ratio V_A/v_b , and for zero launcher length. It will be noted that whereas in ground firing ($V_A/v_b=0$) the deflection increases without limit as $d_b/\sigma \rightarrow \infty$, the deflections in forward firing ($V_A/v_b > 0$) approach a finite limiting value. Furthermore, the greater the ratio V_A/v_b , the sooner does the rocket suffer the major portion of its final deflection. Following the argument of 6.72, we find that in the limit as $d_b/\sigma \rightarrow \infty$

$$\frac{\vartheta_F}{\delta_0} = \ln \frac{\zeta_b}{\zeta_p} = \ln \frac{V_A + v_b}{V_A + v_p}; \quad (2)$$

so that the limit values plotted in figure 6.72 for $p=0$ are given by

$$\frac{\vartheta_F}{\delta_0} = \ln \left(1 + \frac{v_b}{V_A} \right). \quad (3)$$

This, it will be noted, is the same as the limit value in the case of gravity and angular malalignment. The reason for this is that

$$\Theta_F = \Theta_g - \Theta_\delta - 1, \quad (4)$$

and $\Theta_\delta \rightarrow -1$ as $d_b/\sigma \rightarrow \infty$.

6.74 Other Effects.—In addition to the factors mentioned above there are a number of other causes of error and dispersion which are essentially peculiar to the problem of firing from aircraft. These arise from uncertainties in aircraft speed, propellant temperature, dive angle, range, aircraft weight, attitude of launchers, aiming errors, etc. In addition there will be deviations arising when rockets are launched while the airplane is pulling out of a dive or nosing over into one, or while the airplane is skidding or side-slipping, or when the curve of approach of the aircraft is not a straight line. These effects will not be discussed here; but it should always be remembered that good control over these factors is usually the dominant consideration in attaining accuracy when firing from aircraft. This control is to be sought both in the design of the sight and the firing system and in the training of the pilots.

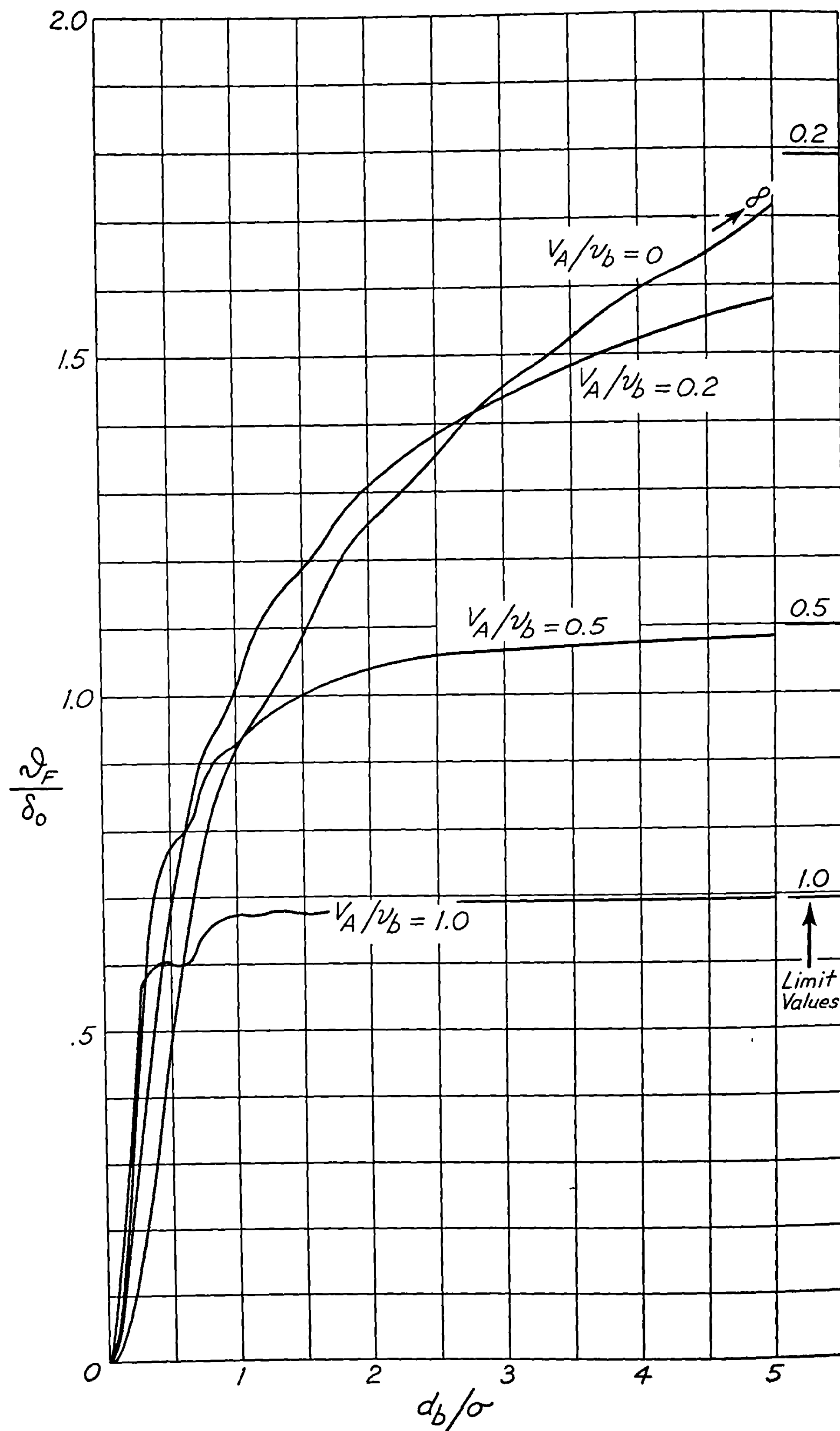


FIGURE 6.73.—Dispersion due to fin malalignment for firing from zero-length launchers.

II.

SPIN-STABILIZED ROCKETS

CHAPTER 7

INTRODUCTION TO SPIN-STABILIZED ROCKETS

7.1 Purpose

In the first three chapters it was shown that the principal source of dispersion in most well-made fin-stabilized rockets when ground-fired is the gas malalignment, which produces a dispersion of the order of 20 mils. If the rocket is rotated about its longitudinal axis so that the malalignment torque acts first in one direction and then in the other, the dispersion due to malalignment can be made negligible and the total dispersion reduced to 5 mils or less. In addition, if the rate of rotation, or spin as it is usually called, is high enough, no fins are needed, the rocket being stable against the overturning aerodynamic moment similarly to a shell fired from a rifled gun. The elimination of the bulky and somewhat fragile fins makes a rocket easier to store, handle, and fire.

Because of the low launching speed of a rocket and the desire to use light launchers that cannot withstand large forces, sufficient spin for stability cannot be imparted by a rifled launcher. Such a launcher will produce enough spin to reduce the dispersion, but fins are needed for stability. This case was treated in 3.6. A rocket can be stabilized by spin if the jets are arranged in one or more circles and each jet inclined at an angle of 10° to 20° with the longitudinal axis of the rocket. In this way the spin is roughly proportional to the linear velocity of the rocket and the distance traveled per revolution is essentially constant throughout burning. The other assumptions of the only case worked out in detail are those listed in 1.1; in particular we assume that the acceleration during burning is roughly constant and is large compared to the acceleration of gravity and the aerodynamic forces. The theory has been compared with experiment and found to be quite satisfactory for rockets having diameters of the order of 3 to 5 inches, lengths from 5 to 7 times their diameter, velocities up to 1,500 ft./sec., and a distance traveled per revolution of the order of 5 feet.

7.2 General Characteristics

Before taking up in the next three chapters the detailed treatment of the behavior of spin-stabilized rockets, let us consider a brief, nonmathematical description of some of their most important characteristics. After the end of burning, the behavior is similar to that of ordinary shells; but because the rockets have a lower density and a greater ratio of length to diameter than shells, all effects of aerodynamic forces are accentuated. During burning the orientation of the rocket depends on the conditions as it left the launcher and on the aerodynamic forces, but the behavior is profoundly modified by gyroscopic effects resulting from rotation. As in the case of fin-stabilized rockets, changes in orientation during burning lead to deflection of the trajectory since the strong jet force acts in the direction in which the rocket points.

Just as in the case of a shell, a spinning rocket tends, as it follows a long trajectory with considerable curvature, to keep its axis at all times nearly parallel to the trajectory but with a small average yaw to the right for the usual right-hand spins. The higher the rate of spin, the more aerodynamic force is required to produce the precession that tips the nose down, and the greater is the yaw. Thus after burning, rockets ordinarily drift to the right and the more rapid the spin, the greater the drift. This right yaw is greatest at the summit of the trajectory

where, because of the low velocity, the aerodynamic forces are smallest and the rate of turning of the trajectory is the greatest. If the initial quadrant elevation is high enough, this yaw at the summit may become so large that the gyroscopic stability breaks down because of the effect of the nonlinear Magnus moment. (See 10.23 and 10.26.) Thus, both to simplify fire control by reducing the drift and to allow use at the maximum possible quadrant elevation, it appears desirable that rockets fired at high quadrant elevations should be designed to have the lowest spin consistent with initial stability and satisfactory performance during launching and burning. On the other hand, if the trajectory is relatively straight, then very high spin is desirable since in this case the nose of the rocket will remain high as the trajectory drops and there will not usually be time enough for the nose to move far to the right. Thus there will be vertical drift, which can be allowed for in the range tables, but there will not be much lateral drift.

Next we may consider the phenomena of importance during burning. At present, our main interest is in factors that produce dispersion and in factors that deflect the trajectory, since then one must either contend with a complicated fire-control problem or must accept a large effective inaccuracy. Our conclusion will be that, in general, conditions during burning are more favorable with high spin.

The dispersion of spin-stabilized rockets seems to be due to a variety of factors; if any one becomes unduly large it may dominate the situation and produce a large dispersion, but if any one is eliminated, the numerous remaining effects still produce about the usual dispersion. Among the more important factors are static and dynamic unbalance due to mechanical imperfections in the rounds. If the highest accuracy is desired, the rounds should be individually balanced after manufacture. Care should also be taken that the bourrelets are not out of round. Launcher motion and rolling or bouncing of the round in the launcher are probably significant, as are nonuniformities in the rate of burning of the propellant.

If a reasonably accurate prediction of the direction of motion of a spin-stabilized rocket at the end of burning is required, one must allow at least for the temperature of the propellant, the tip-off, the wind, the length and type of launcher, and the ordinary gravity drop. However, the more rapid the spin, the less each correction will be and the simpler it will be to prepare and use range tables that take account of all these factors.

By tip-off is meant the transverse angular velocity given to a round as it leaves the launcher. In general the nose drops while the rear is supported, although the universal springiness of all launchers may give the rear end an additional transverse impulse. Because of the spin, assumed to be to the right as usual, an initial downward motion of the nose is followed by a circling to the left and then up. Due to the angular acceleration, the nose does not move in a circle but spirals toward a point below and to the left of its initial orientation. Then because the jet thrust deflects the rocket in the way it is pointing, the trajectory is deflected to the left by amounts which are typically from 15 to 30 mils and down by from 10 to 20 mils for rockets whose spin is such that their stability factor is near 2. This motion is of course complicated by the gravitational turning of the trajectory which, by itself, would produce an upward yaw. The aerodynamic overturning moment then tends to push the nose up, but the resulting gyroscopic precession moves it also to the right and then down. Thus the jet thrust drives the trajectory to the right by perhaps 5 to 30 mils and changes somewhat the gravity drop, which may range from 20 to 80 mils with temperature and rocket type. It is found that ranges and deflection vary with the type of launcher and even from one to another supposedly identical service launcher. This variation is caused by launcher motion and could be treated like tip-off, except that it is impossible to predict. It is possible to allow for some of it by means of empirical corrections, but part of the variation leads to increased dispersion.

The effects of wind during burning are quite large and annoyingly complicated. A cross-wind from left to right pushes the nose downwind; the resulting gyroscopic phenomena then make the nose drop and finally spiral off downward to the left. The jet force drives the trajectory in a similar way but with a considerable lag. Thus, depending on the rocket and the temperature, a cross wind of 1 ft./sec. from the left may deflect the trajectory to the right by as much as $\frac{1}{4}$ mil or the left by as much as 1 mil and may deflect it down by from 1 to 3 mils. Since the effect is linear in simple cases, reversing the wind reverses the deflection, and the deflection is proportional to the wind speed. The effects of range wind are usually somewhat smaller, although not negligible, and are complicated by nonlinear terms. All these numerical values apply to rockets whose stability factor (see ch. 8) is about 2. If the spin, and hence the stability factor, is considerably increased, aerodynamic torques do not change the orientation as rapidly and all deflections from the simple vacuum gravity drop become much smaller.

Thus we conclude that while it is possible to build compromise spin-stabilized rockets that are fairly satisfactory both for low-angle high-accuracy fire and for high-angle fire, it will usually be desirable to have two series. The high-spin series will have minimum wind, launcher motion, and temperature corrections and maximum accuracy for low-angle fire. The limit to the spin is set by the requirements that the rocket motor must not burst from centrifugal force plus gas pressure and that the grain must not break up. However such rockets will be unstable when fired at high quadrant elevations and will have large drifts at moderate elevations. The low-spin series will be more inaccurate at low quadrant elevation but better at high.

CHAPTER 8

DESCRIPTION OF A SPIN-STABILIZED ROCKET AND ITS FORCE SYSTEM

8.0 Introduction

It is now necessary to extend the description of chapter 2 to cover the additional parameters and forces present in the case of spin-stabilized projectiles but absent or unimportant in the cases previously considered. Since the motions to be considered and the forces that produce them are considerably more complicated than in the case of fin-stabilized rockets, new notations that are more systematic and complete will be introduced. We shall also make use of the opportunity to give a more systematic and complete treatment of aerodynamic forces.

8.1 Description of a Spin-Stabilized Rocket

In this section we give a table and figures which show the important characteristics of a number of rockets and which contain data that will permit one to obtain illustrative numerical results from the formulas to be developed. Only the average values of the most important quantities are given; additional information can be found in various catalogues and manuals.

Almost all of the quantities listed in Table 8.1 are defined as in 2.11. In addition to the quantities defined there we include k , the radius of gyration about a longitudinal axis at the end of burning, and

$$\gamma = K^2/k^2, \quad (1)$$

the ratio of the moment of inertia about a transverse axis through the center of mass to that

TABLE 8.1
CHARACTERISTICS OF SPIN-STABILIZED ROCKETS¹

Rocket	D (ft.)	l (ft.)	l_J (ft.)	K (ft.)	k (ft.)	γ	l_{gJ} (ft.)	l_g (ft.)	m (lb.)	μ_b (lb.)	m_t (lb.)
3.5/4 GPSR.....	0.292	2.03	1.12	0.556	0.112	24.8	0.63	0.83	21.5	2.5	24.0
5/1 HCSR.....	.416	2.68	1.26	.667	.162	17.0	.45	.42	49.7	3.1	53.1
5/2 HCSR.....	.416	2.68	1.28	.694	.165	17.7	.51	.52	46.7	3.9	50.9
5/5 HCSR.....	.416	2.68	1.30	.745	.165	20.4	.76	.80	44.1	5.6	50.0
5/5 SmSR.....	.416	2.74	1.26	.743	.166	21.6	.76	.80	40.0	5.6	45.9
5/9 CnSR.....	.416	2.41	1.41	.768	.163	22.1	1.12	1.35	41.2	10.0	51.6
5/10 GPSR.....	.416	2.64	1.38	.770	.161	22.8	1.12	1.35	39.4	10.0	49.8
5/14 GASR.....	.416	2.08	1.11	.592	.158	14.0	.68	.84	35.0	7.9	43.2

Rocket	v_b (ft./sec.)	s_b (rad./sec.)	t_b (sec.)	G (ft./sec. ²)	V_g (ft./sec.)	ν (ft.)	λ (ft.)	t_λ (sec.)	v_λ (ft./sec.)	S
3.5/4 GPSR.....	740	1,150	0.56	1,320	6,900	4.0	100	0.388	514	3.4
5/1 HCSR.....	400	400	.79	500	6,710	6.3	107	.651	328	2.0
5/2 HCSR.....	520	520	.86	610	6,680	6.4	113	.610	371	1.85
5/5 HCSR.....	790	820	.85	930	6,700	6.1	124	.517	480	2.45
5/5 SmSR.....	870	920	.85	1,020	6,700	6.0	128	.502	511	1.85
5/9 CnSR.....	1,480	1,490	.94	1,580	6,910	6.2	138	.419	660	2.2
5/10 GPSR.....	1,540	1,600	.94	1,640	6,910	6.1	133	.410	673	2.5
5/14 GASR.....	1,330	2,030	.75	1,770	6,620	4.1	57	.254	449	6.1

¹ Average values given. Additional data can be found in OSRD Report No. 2544, "Ballistic Data: Fin-Stabilized and Spin-Stabilized Rockets," CIT, 1946.

Meaning of symbols: D =diameter; l =length; l_J =distance of center of mass from rear (burnt); K =radius of gyration about a transverse axis through the center of mass (burnt); k =radius of gyration about a longitudinal axis (burnt); γ =ratio of transverse to longitudinal moments of inertia (burnt); l_{gJ} =distance of the center of mass of the grain from the rear; l_g =length of the grain; m =mass of projectile; μ_b =mass of propellant; m_t =mass of round; v_b =burnt velocity, 70° F.; s_b =burnt spin, 70° F.; t_b =effective burning time, 70° F.; G =effective acceleration, 70° F.; V_g =gas velocity, 70° F.; ν =distance per turn, 70° F.; λ =distance per nutation, 70° F.; t_λ =characteristic time 70° F.; v_λ =characteristic velocity, 70° F.; S =stability factor, 70° F.

about the longitudinal axis. These quantities determine the gyroscopic properties of the projectile. The spin, s , is defined to be the angular velocity about the longitudinal axis, and the value tabulated is that at the end of burning in the absence of aerodynamic deceleration. Related quantities are

$$\nu = 2\pi v/s, \quad (2)$$

the distance traveled per revolution, and

$$\lambda = \gamma \nu, \quad (3)$$

which will be shown to be the distance traveled per nutation in vacuum. It is usually proper

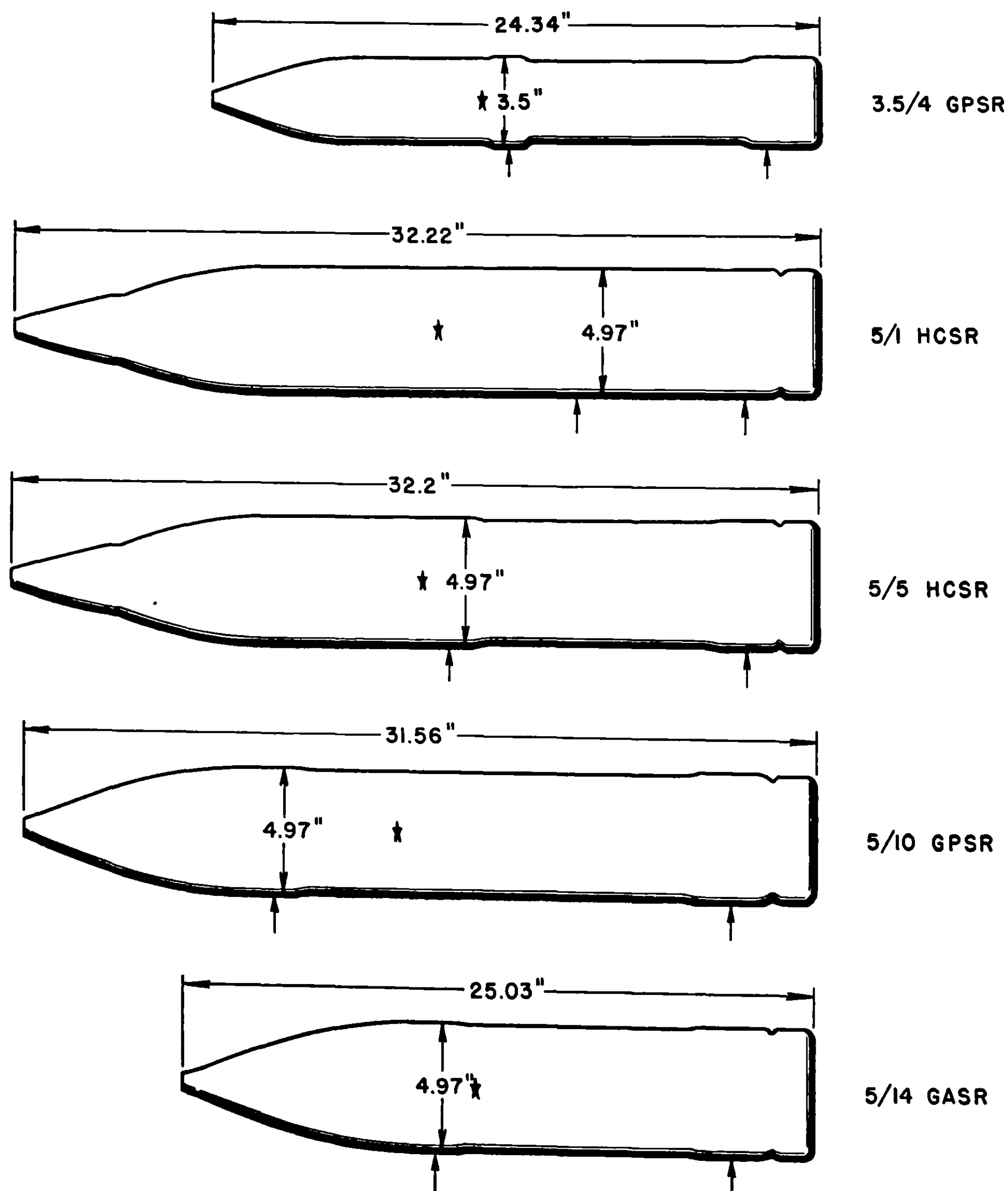


FIGURE 8.1.—Outline of typical spin-stabilized rockets.

to assume that ν is constant throughout burning; thus one usually specifies $v(t)$ and ν rather than $v(t)$ and $s(t)$.

In the case of the fin-stabilized rockets, σ was important both because it gave a convenient specification of the aerodynamic righting moment and because it measured the period of the rocket's oscillation about its mean orientation. In the case of spin-stabilized rockets the most rapid oscillations are due to the nutation rather than to aerodynamic effects and hence λ replaces σ as the characteristic distance. The same λ is used as the characteristic distance in air although the nutations are then somewhat longer; there λ characterizes the gyroscopic properties of the projectile. The characteristic velocity and time become

$$V_\lambda = (2G\lambda)^{\frac{1}{2}}, \quad (4)$$

and

$$t_\lambda = (2\lambda/G)^{\frac{1}{2}}, \quad (5)$$

respectively. The aerodynamic overturning moment, which we shall designate as $f\nu^2\delta$ is most conveniently specified in terms of the stability factor,

$$S = \frac{mK^2s^2}{4\gamma^2(f\nu^2\delta/\delta)}, \quad (6)$$

where m is the mass and δ is the yaw.

8.2 Definitions of the Aerodynamic Forces

The aerodynamic forces of greatest importance in the ballistics of spin-stabilized rockets are the drag and the overturning moment. The drag affects the velocity and hence the range, while the magnitude of the overturning moment governs most of the interactions of the rocket with the air, including its stability, the deflection during burning produced by interaction with the air, the deflection produced by cross-wind during burning, and the drift after burning. The cross-wind or lift force is important because of its effect on drift, where it is as important as the overturning moment, and because it damps the precessions, thus tending to stabilize the motion. The Magnus moment—the moment due to the type of forces that make a spinning ball curve—must be included in cases where the exponential damping or building up of the nutations and precessions are considered. The damping moment that opposes rotation about a transverse axis is also a factor in damping the nutations. The other forces and moments defined below are of relatively minor importance; the principal reason for their inclusion is to present a logically complete system.

First we shall define precisely the various forces and moments, introducing for this purpose a system of vectors describing the direction of motion, the orientation, the yaw, and the angular velocity about a transverse axis. We include a table of comparative notations that should facilitate cross-references to other treatments and that should serve as a guide to our terminology for anyone who is familiar with one of the other systems. Then in 8.3 we shall deduce a number of important relations from symmetry considerations and from the invariance of the aerodynamic force system with respect to a shift of the center of mass of the projectile. This discussion suggests an extension of the treatment of aerodynamic forces of fin-stabilized projectile beyond that given in chapter 2.

In addition to the aerodynamic forces, gravitational forces and jet forces must be considered. The gravitational force is merely the mass times the acceleration of gravity, and, since its direction is defined relative to the ground and not relative to the air or rocket, it will not be introduced quantitatively until chapter 9 when coordinate systems fixed relative to

the ground are introduced. The orientation of the jet forces is defined relative to the rocket; hence they are discussed in 8.5 where the results of 2.2 are extended to cover spinning rockets.

8.21 Introduction of Vector Notation for Yaw, Cross-Spin, and Moment About a Transverse Axis.—In order to define the forces and moments in vector form it is necessary to introduce vectors that completely describe the motion. The direction of motion is specified by a unit vector e_T drawn from the center of mass in the direction in which the rocket is moving. Since we are interested in aerodynamic forces only, all velocities that we consider will be with respect to the air. The orientation of the rocket is specified by a unit vector e_A along its axis; and the yaw, δ , is the angle between e_T and e_A . The most convenient way to represent the yaw by means of a vector is to draw a unit sphere around O , the center of gravity of the projectile, as in figures 3.21(a-d), 9.11(a), and 8.21. The unit vectors e_T and e_A terminate at the points T and A at which the tangent to the trajectory and the axis of the projectile, respectively, intersect the unit sphere. We represent the yaw by a vector δ , of length δ , tangent to the unit sphere at A and lying along the great circle away from T . We also need the vector δ_T , of length δ , which is tangent to the unit sphere at T and lies along the great circle to A . Thus

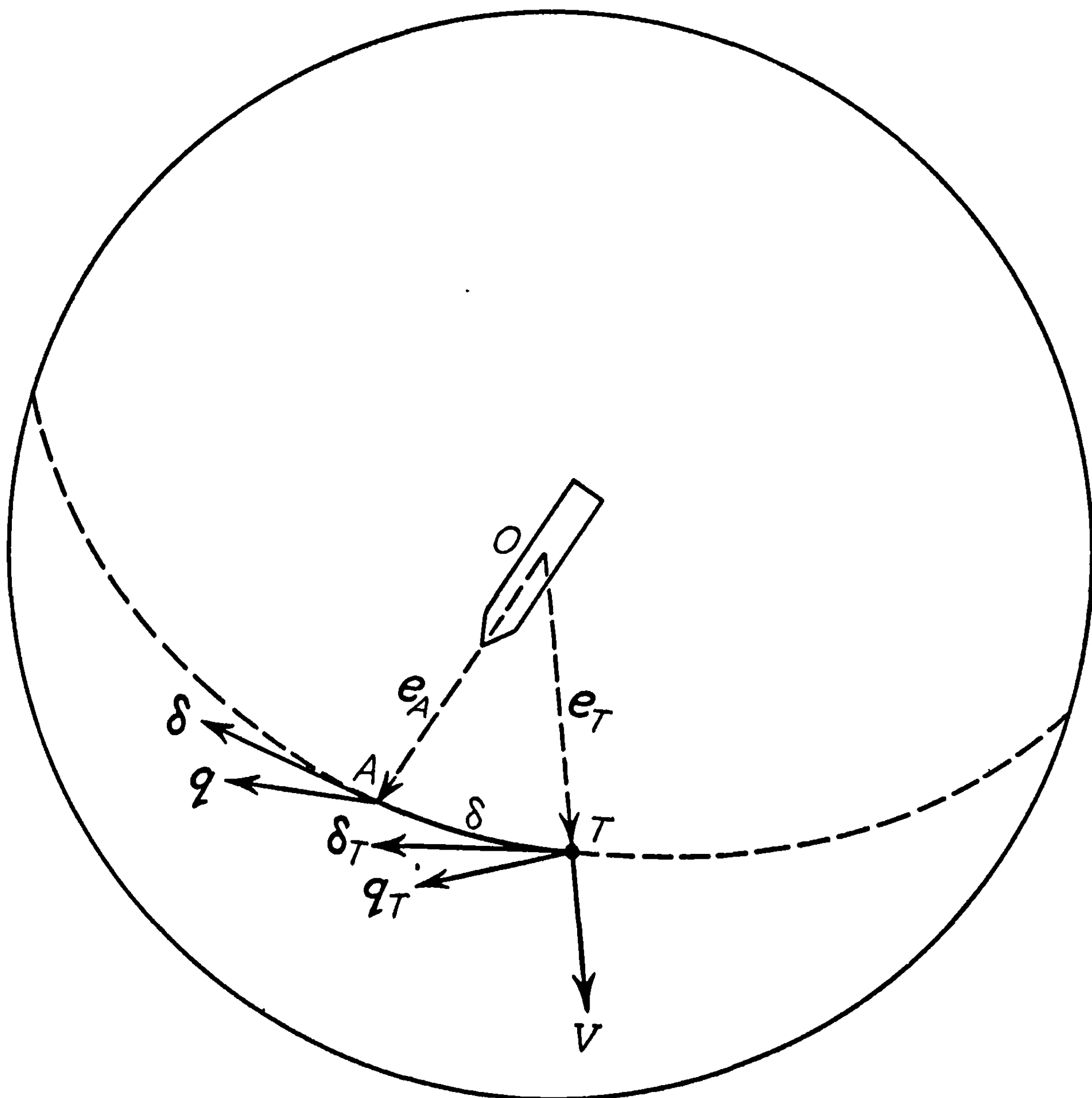


FIGURE 8.21.—Yaw and cross-spin.

both vectors δ and δ_T are of a length equal to the distance along the great circle from T to A and both lie in the same plane although they have slightly different directions.

To describe the rotation of the rocket about a transverse axis, a motion which we may call cross-spin or transverse angular velocity, we need only specify the motion of the point A . This we do by means of the vector q which is tangent to the sphere in the direction of motion of A and has a magnitude equal to the velocity of A (and to the component normal to OA of the total angular velocity). This vector is very convenient in specifying the directions of the forces and moments that depend on the cross-spin. In addition to the vector q , which is tangent to the unit sphere at A , we need the vector q_T which is tangent to the unit sphere at T , has the same length as q , and makes the same angle with δ_T that q makes with δ .

The aerodynamic forces are applied in the form of infinitesimal forces distributed continuously over the surface of the projectile. The motion depends only on the vector sum of the infinitesimal forces and on their moment about the center of mass. It is usually most convenient in dealing with the motion to resolve the total force into components along and normal to the trajectory. When studying the relations between the various forces and moments, it is often more convenient, however, to resolve the total force into components along and normal to the axis of the projectile. Most of the time we shall use the resolution along the normal to the trajectory, and so our basic notation will be devised for this time. Occasionally we shall find it necessary to introduce a subsidiary notation in order to treat the other resolution.

The resultant moment about the center of mass is always resolved into components along and normal to the axis of the projectile and these two components are treated separately instead of as a single vector. In describing the transverse component of any particular torque, it is more convenient to bypass the usual vector notation and to represent the moment by means of the force, f , that would produce this moment about the center of mass if f were applied at the point A tangent to the unit sphere. This method of treatment is reasonable from the physical point of view since it is quite natural to think, for example, of air piling up on one side of a yawed projectile and producing a torque by means of a force in the same direction as f , the only difference between the actual force and f being the point of application. In order that f produce a torque only and not contribute to the total force, we can suppose that the force $-f$ is applied at the center of mass. In using this representation of the moment we shall generally omit any reference to the force at the origin and shall treat the motion of A in a manner similar to the motion of a mass point. It should be noted that the force f and the velocity q are related in the same way as are the transverse moment and the transverse angular velocity.

It is unfortunate that the matter of terminology causes some trouble. The component of the angular velocity along the axis of the rocket is called the spin; and we shall call q the cross-spin and say that it represents the transverse angular velocity. Since we do not use the usual angular velocity vector ω , we shall sometimes call q the transverse angular velocity, or even the angular velocity, in cases where no confusion can arise and where conciseness seems preferable to precision. In a similar manner, we shall call f the moment or transverse moment, even though it would be more precise to say that it represents the moment.

8.22 Definition of the Force and Moment Due to Yaw.—Consider a projectile whose cross-spin, q , is zero but which is yawed as indicated in figure 8.22. Whatever the aerodynamic force may be, it can be expressed in terms of the three mutually perpendicular components F_{v^2} , $F_{v^2\delta}$, and $F_{v^2\delta\delta}$; where F_{v^2} is the component parallel to the direction of motion, $F_{v^2\delta}$ is the component in the plane of the yaw and normal to the direction of motion, and $F_{v^2\delta\delta}$ is the component normal to the plane of the yaw. F_{v^2} is called the drag, $F_{v^2\delta}$ the lift, and $F_{v^2\delta\delta}$ the Magnus force. It is desirable to express these forces in terms of dimensionless coefficients

that are as nearly as possible independent of the yaw, δ , of the velocity, V , of the density of the air, ρ , of the cross-sectional area of the projectile, A , and the length, l . Empirical knowledge, dimensional analysis, and the symmetry considerations treated in 8.3 combine to indicate that the proper procedure is to express the forces in the following forms:

$$F_{V^2} = -\frac{1}{2} \Gamma_{V^2} \rho A V^2 e_T = -m K_{V^2} V^2 e_T, \quad (1)$$

$$F_{V^2\delta} = \frac{1}{2} \Gamma_{V^2\delta} \rho A V^2 \delta_T = m K_{V^2\delta} V^2 \delta_T, \quad (2)$$

and

$$F_{V\delta} = -\frac{1}{2} \Gamma_{V\delta} \rho A l V s e_T \times \delta_T = -m K_{V\delta} l V s e_T \times \delta_T. \quad (3)$$

The first form in each equation, in which the dimensionless coefficient that depends on the shape of the particular projectile under consideration is designated by a Γ with appropriate subscripts, is the form usual in aerodynamic theory. The second form, in which the coefficient has the dimensions $(\text{length})^{-1}$, is convenient for use with the equations of motion where it is not desirable to carry the factor ρA and where it is desirable to introduce the factor m , the mass of the projectile. Since K_{V^2} is merely c , the deceleration coefficient, we shall frequently write c in place of K_{V^2} .

It will be noted that the forces and coefficients are identified by subscripts that indicate the major part of the variation of the force with velocity, spin, and yaw. This makes it rather easy to identify any particular force or coefficient without the need of remembering a set of arbitrary symbols.

Whatever the moment of the aerodynamic forces about the center of mass, it can be resolved into a component parallel to the axis of the rocket and a component normal to this axis. This latter component can be represented by a force f applied at A as discussed in 8.21, and f can be resolved into components lying in and normal to the plane of the yaw. Thus the aerodynamic moment is specified by M_{Vs} , which is the component of the moment parallel to the axis; by $f_{V^2\delta}$, which is the component of f in the plane of the yaw; and by $f_{Vs\delta}$, which is the component of f normal to the plane of the yaw. M_{Vs} is called the spin deceleration moment, $f_{V^2\delta}$ represents the overturning moment, and $f_{Vs\delta}$ the Magnus moment. These moments can

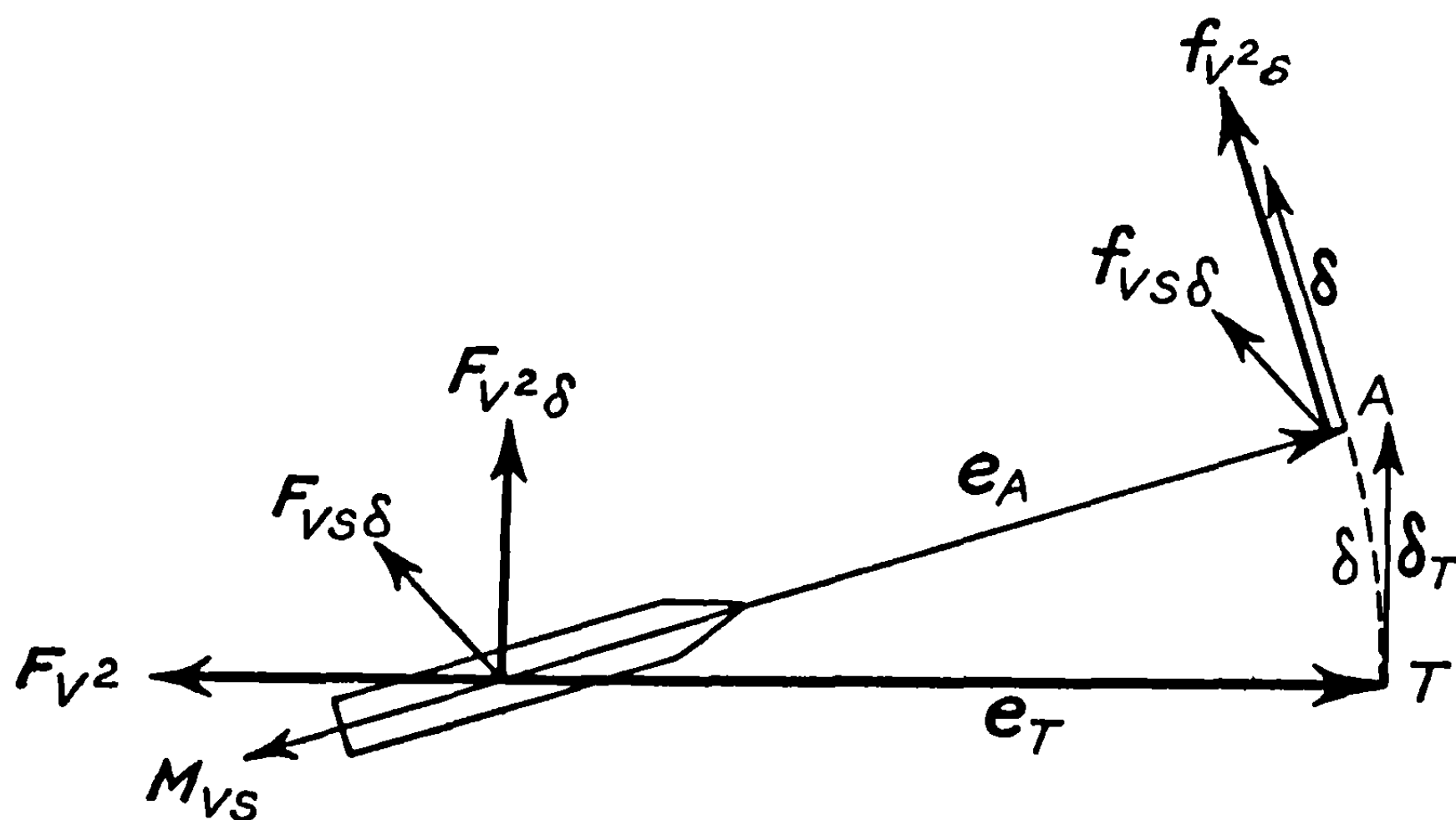


FIGURE 8.22.—Aerodynamic forces and moments due to yaw, (F_{Vs} and f_{Vs} are directed into the paper.)

be expressed in terms of dimensionless coefficients and in forms convenient for use in the equations of motion in the following manner:

$$M_{V_s} = -\frac{1}{2} \gamma_{V_s \rho} A l^2 V s e_A = -m k^2 k_{V_s} l V s e_A, \quad (4)$$

$$f_{V^2 \delta} = \frac{1}{2} \gamma_{V^2 \delta \rho} A l V^2 \delta = m K^2 k_{V^2 \delta} V^2 \delta, \quad (5)$$

and

$$f_{V s \delta} = -\frac{1}{2} \gamma_{V s \delta \rho} A l^2 V s e_A \times \delta = -m K^2 k_{V s \delta} l V s e_A \times \delta. \quad (6)$$

Here mK^2 and mk^2 are the moments of inertia about the transverse and longitudinal axes, respectively. The signs have been chosen so that the coefficients will be positive when the center of pressure in each case is ahead of the center of mass.

It is, of course, too much to expect that the various Γ 's and γ 's should be independent of everything except the shape of the projectile. At subsonic velocities, the coefficients should be nearly independent of V ; but, as discussed in 2.4, over more extended ranges they would be expected to be functions of Mach number, Reynolds number, and perhaps sR/a , where R is the radius of the projectile and a is the velocity of sound. They are also functions of the yaw, the forms given above applying for very small yaws only. We shall regard the coefficients as being functions of V and δ only, since their variation with other parameters is small. The only coefficients whose variation with yaw will be considered in detail are $\gamma_{V^2 \delta}$ and $\gamma_{V s \delta}$ which can be written as

$$\gamma_{V^2 \delta} = \gamma_{V^2 \delta, 0} + \gamma_{V^2 \delta, 1} \delta + \gamma_{V^2 \delta, 2} \delta^2 + \dots, \quad (7)$$

and

$$\gamma_{V s \delta} = \gamma_{V s \delta, 0} + \gamma_{V s \delta, 1} \delta + \gamma_{V s \delta, 2} \delta^2 + \dots \quad (8)$$

where the coefficients in the expansion are chosen in order to give a satisfactory fit over the range of interest. Under some circumstances it will be convenient to assume from symmetry that the coefficients of odd powers of δ are zero; this does not affect the possibility of approximating as closely as is desired to an arbitrary function since δ is everywhere positive. The coefficients in (7) and (8) are functions of velocity but we need not exhibit this explicitly. The other coefficients could be expanded in like manner but, since their influence on the motion is small, we shall treat them as constants. Although more convenient equations of motion are obtained if one uses the coefficients $K_{V s \delta}$, $k_{V s \delta}$, etc., rather than the coefficients $\Gamma_{V s \delta}$, $\gamma_{V s \delta}$, etc., the former are less satisfactory in a discussion of aerodynamic forces since $K_{V s \delta}$, $k_{V s \delta}$, etc., depend on the density of the air and the mass and radii of gyration of the rocket in addition to the shape, position of the center of mass, and the minor factors discussed above on which $\Gamma_{V s \delta}$, $\gamma_{V s \delta}$, etc. depend.

In the equations describing the motion, the overturning moment generally appears in conjunction with other parameters in a dimensionless parameter known as the stability factor. The stability factor, S , is defined by

$$S = \frac{mK^2}{4\gamma^2} \frac{s^2 \delta}{f_{V^2 \delta}} = \frac{mK^2}{2\rho A l \gamma_{V^2 \delta}} \left(\frac{s}{\gamma V} \right)^2 = \frac{\pi^2}{\lambda^2 k_{V^2 \delta}}. \quad (9)$$

The significance of the stability factor will best be seen from the results of chapters 9 and 10, where it will be shown that the motion is unstable unless $S > 1$ and that $4S$ is the ratio of the

gyroscopic torque to the aerodynamic overturning moment when the cross-spin is $q = s\delta/\gamma$ as it is in the circumstances discussed in 9.14 (9). In order to obtain usable equations of motion during burning, it is necessary to treat S as a constant. This is a good approximation at subsonic velocities, except when firing into a wind or forward from an airplane, since usually s is nearly proportional to V . When the velocity becomes supersonic toward the end of burning, the overturning moment increases more rapidly than the square of the velocity, and hence the stability factor decreases. However, the assumption that S has, throughout burning, the constant value appropriate at low velocities gives a good approximation for all phenomena whose character is determined during the early stages of burning.

8.23 Definition of the Forces and Moments Due to Cross-Spin.—Suppose that in addition to the yaw considered in the previous section, the projectile is rotating about a transverse axis, the direction and speed of motion being given by the vector \mathbf{q} or \mathbf{q}_T . In cases of practical interest it is reasonable to assume that $\mathbf{q}(=\mathbf{q}_T)$ is small enough so that the drag and the spin decelerating moment are independent of \mathbf{q} or \mathbf{q}_T ; in other words, we neglect¹ their variation with q since it is very much smaller than the variation with δ . The presence of the cross-spin will, however, significantly modify the force acting normal to the trajectory and the torque about an axis normal to the projectile. The additional force due to the cross-spin is found by subtracting from the total force normal to the trajectory the force normal to the trajectory when $q_T=0$. It is most convenient to resolve this added force into a component \mathbf{F}_{Vq} that is parallel (but in the opposite direction) to \mathbf{q}_T and a component \mathbf{F}_{sq} normal to \mathbf{q}_T . \mathbf{F}_{Vq} is called the lift due to cross-spin, and \mathbf{F}_{sq} the Magnus force due to cross-spin. Likewise the additional moment due to cross-spin is represented by a vector normal to the axis of the rocket, this vector being resolved into a component \mathbf{f}_{Vq} that is parallel to \mathbf{q} and a component \mathbf{f}_{sq} that is perpendicular to \mathbf{q} . \mathbf{f}_{Vq} is called the damping moment, and \mathbf{f}_{sq} is called the Magnus moment due to cross-spin. The complete transverse force and torque systems are represented in figures 8.23a and b; figure a showing the forces projected on the plane perpendicular to the trajectory at T , and figure b representing the moments by means of \mathbf{f} vectors in the plane perpendicular to the projectile axis at A . As long as the yaw is small, δ_T is nearly parallel to δ and \mathbf{q}_T to \mathbf{q} .

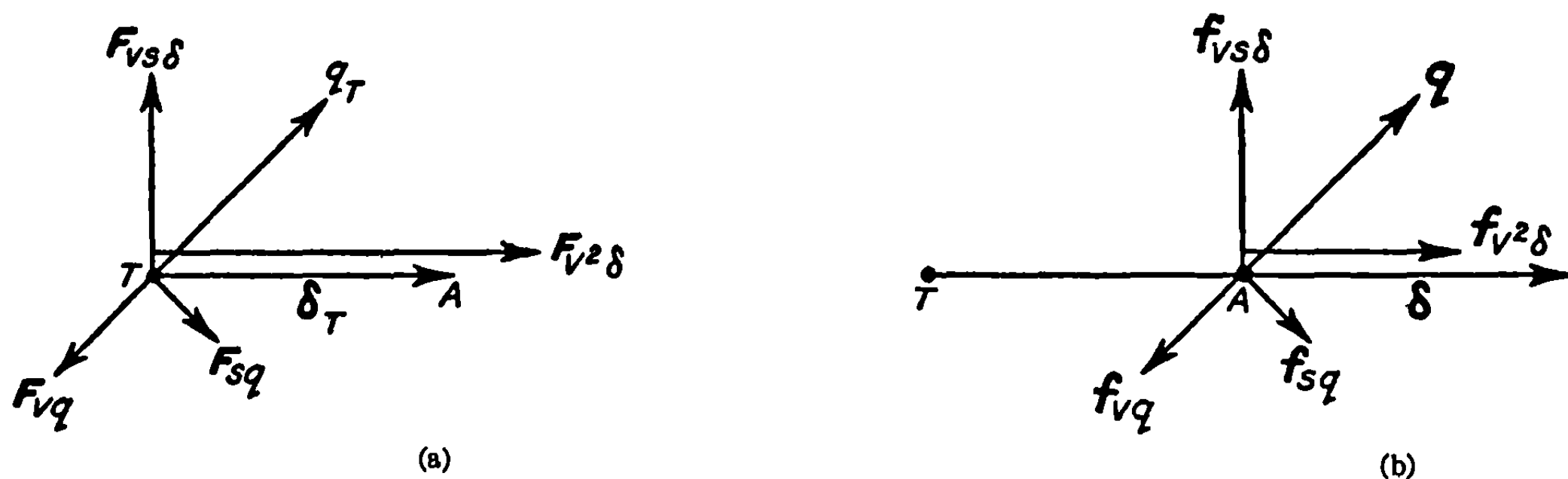


FIGURE 8.23.—Aerodynamic forces and moments as seen looking forward along the trajectory.

¹ To be strictly consistent, we should expand the aerodynamic force in a power series in q in which case the first term of the series would be the forces discussed in the previous section; the next term in the series, the linear term, would provide the forces discussed here; and the higher powers would be neglected. If this were done we would find among the terms proportional to q , contributions to the drag and the spin decelerating moment proportional to $q\delta$ and $q \times \delta$, and we would have to introduce additional forces and moments due to cross-spin. However, these terms are certainly very small and of no importance in their effects on the motion, so we shall omit further mention of them except for an occasional footnote pointing out an equation that would contain an additional very small term if one used a completely consistent system of forces. The authors, whose notations are referred to in table 8.25, do not have such a term since they expand their aerodynamic forces in a series in the two variables δ and q and disregard all quadratic and cross product terms. We prefer not to do this since we wish to retain the quadratic terms in δ in the overturning moment and the Magnus moment.

By means of the following sets of equations, these additional forces and moments can be expressed in terms of dimensionless parameters that depend principally on the shape of the projectile. The equation on the right in each case is the form that is convenient when writing the equations of motion; here the coefficient has the dimensions of $(\text{length})^{-1}$ in the case of the forces and $(\text{length})^{-2}$ in the case of the torques.

$$F_{vq} = -\frac{1}{2} \Gamma_{vq} \rho A l V q_T = -m K_{vq} l V q_T, \quad (1)$$

$$F_{sq} = \frac{1}{2} \Gamma_{sq} \rho A l^2 s e_T \times q_T = m K_{sq} l^2 s e_T \times q_T, \quad (2)$$

$$f_{vq} = -\frac{1}{2} \gamma_{vq} \rho A l^2 V q = -m K^2 k_{vq} l V q, \quad (3)$$

$$f_{sq} = \frac{1}{2} \gamma_{sq} \rho A l^3 s e_A \times q = m K^2 k_{sq} l^2 s e_A \times q. \quad (4)$$

The remarks that were applied to the coefficients that were introduced in Section 8.22 also apply to the coefficients introduced here. In addition, the new coefficients will depend to some extent on δ and on the relative orientations of δ and q . For example, one would not expect f_{vq} to have exactly the same magnitude when q is parallel to δ as it would have when q and δ are perpendicular. However, we shall neglect such effects as long as δ is sufficiently small. If desired, our expressions for the forces in terms of coefficients that are independent of δ and q can be regarded as the initial terms in an expansion in powers of δ and q .

8.24 Summary of Numerical Data.—When considering the behavior of any particular projectile it is desirable to have available some estimate of the magnitude of the aerodynamic coefficients. Since the shapes of spin-stabilized rockets resemble those of shells, there is a considerable body of useful data available. The drag coefficient or deceleration coefficient is readily obtained, as discussed in 2.44. The theoretical calculation of the drag coefficient should be relatively more accurate in the case of spin-stabilized rockets than in the case of the fin-stabilized rockets since fewer corrections for the departure from conventional shell shapes are necessary in the former case. For experimental measurements, however, the opposite is true because of the drift of the spin-stabilized rockets. Since the trajectory does not lie in a vertical plane through the position at the end of burning and the impact point, it requires difficult photographic techniques to measure accurately the velocity of a spin-stabilized rocket. Thus the determination of drag by measuring the rate of change of velocity is more difficult with spin-stabilized than with fin-stabilized rockets. This is demonstrated by the fact that with the 3.5/4 GPSR, the value of c determined from the initial conditions and the range differs so greatly from the value determined from the initial conditions and the time of flight that one is forced to conclude that when this rocket is fired at 45° quadrant elevation the vertical drift increases the range by some hundreds of yards. It appears, therefore, that the most reliable determinations of the drag of spin-stabilized rockets have been those based on theoretical calculations and those based on wind or water tunnel measurements. If an estimate of orders of magnitude only is required, the value $\Gamma_{v^2} = \frac{1}{2}$ should suffice.

Since the lateral area of a spin-stabilized rocket usually is less than the lateral area of a fin-stabilized rocket and more than the lateral area of a shell having the same cross-sectional area, the value of the cross-force coefficient for spin-stabilized rockets should be intermediate between the values for fin-stabilized rockets and those for shells. For small yaws and subsonic

velocities, a value of 3 is typical of the values for $\Gamma_{v\delta}$ given by wind and water tunnel experiments. Most experimental values of $\Gamma_{v\delta}$ are based on measurements made in a wind or water tunnel, although it is possible to deduce $\Gamma_{v\delta}$ from measurements of the stability factors of two rounds having the same external shape but different centers of mass plus the use of 8.3 (equations for the effect of shift of c. g.).

The theory of irrotational flow in hydrodynamics indicates that the Magnus force on long cylinders whose axis is perpendicular to the direction of air flow is given by

$$F_{v\delta} = 2\pi c_s \rho A l V s, \quad (1)$$

where c_s is a slippage factor that allows for the incomplete adhesion of the air to the cylinder. Experiment verifies this and yields values that are usually slightly less than $\frac{1}{2}$ for c_s . It is generally considered plausible to assume that the Magnus force is proportional to the sine of the angle between the axis of the cylinder and the direction of air flow. Thus, comparing (1) and 8.22 (3), one would expect, allowing for the taper at the nose, that $\Gamma_{v\delta}$ would be somewhat less than unity. The most promising way of determining $\Gamma_{v\delta}$ experimentally seems to be through determinations of $\gamma_{v\delta}$ from the damping of the nutations for two positions of the center of mass. All that can be said of the meager and inaccurate data obtained in this way is that so far there is no experimental evidence against the conclusion that $\Gamma_{v\delta}$ is somewhat less than unity.

Since the forces F_{vq} and F_{sq} do not influence the motion appreciably, it is difficult to obtain values of the corresponding coefficients from observation of the motion. Actually this is very satisfactory since it means that it is unnecessary to determine the value of the coefficients; they can be assumed to be zero for most purposes. The considerations to be developed in 8.3 indicate that if an estimate of orders of magnitude is required, we might assume that $\Gamma_{vq} \approx 0.3$ and $\Gamma_{sq} \approx 0.1$.

The overturning moment can be determined either by measuring the stability factor, by wind or water tunnel measurements, or from estimates based on known overturning moments of similarly shaped projectiles. The overturning moment coefficient can be computed from the stability factor by means of 8.1 (6), and the stability factor can be determined easily by means of yaw camera² records or spark range photography. Wind and water tunnel measurements give $\gamma_{v\delta}$ as a function of δ , but the water tunnel data is necessarily restricted to velocities well below that of sound, and the wind tunnel data is almost always restricted to this range. Estimates based on comparison with other projectiles are relatively inaccurate unless the only difference between the projectiles is a change in the center of mass in which case the effect on the coefficient can be calculated. Data on typical rockets show that the stability factor of spin-stabilized rockets tends to lie in the neighborhood of 2, except that rockets having high spin will have a larger S . The order of magnitude of the overturning moment coefficient at subsonic velocities can be taken to be $\frac{1}{2}$. The overturning moment at supersonic velocities can be determined from measurements of the stability factor, which is one of the easiest parameters to determine, as described in chapter 10.

In chapter 10 it will be shown that measurement of the damping rate of the nutations, say by means of the yaw camera, gives the value of

$$\gamma_{v\delta} + \frac{\gamma_{vq}}{\gamma}, \quad (2)$$

² The yaw camera technique is described in 10.3. See also L. A. Biberman, "Instrumentation for Exterior Ballistic Research in Rocketry," *Instruments*, 23, 184 (1950).

TABLE 8.25
COMPARISON OF NOTATIONS
FORCES RESOLVED ALONG THE TRAJECTORY

Notation	Fowler, Gallop, Lock, and Richmond*	Kent and McShane†**	Nielsen and Synge‡	Kelley and McShane§**	Chs. 1-6	Chs. 7-10
Drag	$R = \rho v^2 r^2 / 2$	$D = K_D \rho d^2 v^2$			$D = \frac{1}{2} C_D \rho A V^2$ $= m c V^2$	$F_{v2} = -\frac{1}{2} \Gamma_{v2} \rho A V^2 e_T$ $= -m K_{v2} V^2 e_T$
Lift, cross-wind force.....	$L = \rho v^2 r^2 \sin \delta / L$	$L = K_L \rho d^2 v^2 \sin \delta$			$L = \frac{1}{2} C_L \rho A V^2$ $= \frac{1}{2} C_L \rho A V^2 \delta$	$F_{v2} = \frac{1}{2} \Gamma_{v2} \rho A V^2 \delta_T$ $= m K_{v2} V^2 \delta_T$
Magnus force	$K = \rho v N r^2 \sin \delta / K$	$K_K \rho d^2 v N \sin \delta$				$F_{v2} = -\frac{1}{2} \Gamma_{v2} \rho A l V^2 e_T \times \delta_T$ $= -m K_{v2} l V^2 e_T \times \delta_T$
Lift due to cross-spin.....						$F_{v2} = -\frac{1}{2} \Gamma_{v2} \rho A l V q$ $= -m K_{v2} l V q_T$
Magnus force due to cross-spin.....						$F_{v2} = \frac{1}{2} \Gamma_{v2} \rho A l^2 e_T \times q_T$ $= m K_{v2} l^2 e_T \times q_T$
MOMENTS RESOLVED ALONG THE PROJECTILE						
Spin deceleration moment.....	$I = \rho v N r^4 / I$	$K_A \rho d^4 N v$	$G_2 = -\rho d^4 \omega_1 \omega_2$	$-\rho d^4 \omega_1 K_A$ $= -m d \omega_1 J_A$		$M_{v2} = -\frac{1}{2} \gamma_{v2} \rho A l^2 V e_A$ $= -m k^2 k_{v2} l V e_A$
Restoring (righting) or overturning moment; cross torque due to cross velocity.	$M = \rho v^2 r^2 \sin \delta / M$ $f_M > 0$ if $\gamma_{v2} > 0$	$M = \mu \sin \delta$ $= K_M \rho d^2 v^2 \sin \delta$ $K_M > 0$ if $\gamma_{v2} > 0$	$i P_1' \xi = -i \rho d^3 \omega f_1' \xi$ $f_1' > 0$ if $\gamma_{v2} > 0$	$-i \rho d^3 \omega K_M \xi$ $= -i m \omega J_M \xi$ $K_M > 0$ if $\gamma_{v2} > 0$	$M = \frac{1}{2} C_M \rho A l V^2$ $= \frac{1}{2} C_M \rho A l V^2 \delta$ $C_M < 0$ if $\gamma_{v2} > 0$	$f_{v2} = \frac{1}{2} \gamma_{v2} \rho A l V^2 \delta$ $= m K^2 k_{v2} V^2 \delta$
Magnus moment; Magnus torque due to cross velocity.	$J = \rho v N r^4 \sin \delta / J$	$K_J \rho d^4 v N \sin \delta$	$P_1' \xi = -\rho d^4 \omega_1 f_1' \xi$	$-\rho d^4 \omega_1 K_J \xi$ $= -m d \omega_1 J_T \xi$		$f_{v2} = -\frac{1}{2} \gamma_{v2} \rho A l^2 V e_A \times \delta$ $= -m K^2 k_{v2} l^2 V e_A \times \delta$

Damping moment; yawing moment due to yawing; cross torque due to cross-spin.	$H = \rho v w r^4 f_{11}$	$K_H \rho d^4 v \omega$	$Q_1' \eta = -\rho a^4 w g_1' \eta$	$-\rho d^2 u K_{H\eta}$ $= -m d u J_{H\eta}$	$M_c = \frac{1}{2} C_{\rho} A D V q$	$f_{Vc} = -\frac{1}{2} \gamma_V \rho A D V q_T$ $= -m K^2 k_{Vc} l V q_T$
Magnus moment due to cross-spin; Magnus torque due to cross-spin.			$i Q_2' \eta = -\rho a^4 \omega g_2' \eta$	$i \rho d^2 \omega_1 K_{X\tau\eta}$ $= i m d^2 \omega_1 J_{X\tau\eta}$		$f_{sc} = \frac{1}{2} \gamma_s \rho A D s e_T \times q_T$ $= m K^2 k_{sc} p s e_T \times q_T$
FORCES RESOLVED ALONG THE PROJECTILE						
Axial drag; axial force			$F_3 = -\rho a^2 w^2 f_3$	$-\rho d^2 u^2 K_{DA}$ $= -m J_{DA} u^2 / d$		$F_{V3}^* = -\frac{1}{2} \Gamma^* \gamma_{30} \rho A V s e_A$
Cross force; cross force due to cross velocity; normal force.			$P_1 \xi = -\rho a^2 w f_1 \xi$	$-\rho d^2 u K_{N\xi}$ $= -m J_{N\xi} u / d$		$F_{V3}^* = \frac{1}{2} \Gamma^* \gamma_{30} \rho A V s e_A$
Magnus force, Magnus cross force due to cross velocity.		$K_K \rho d^3 r N \sin \delta$	$i P_2 \xi = i \rho a^3 \omega f_2$	$+i \rho d^2 \omega_1 K_{P\xi}$ $= +i m \omega_1 J_{P\xi}$		$F_{V3}^* = -\frac{1}{2} \Gamma^* \gamma_{30} \rho A l V s e_A \times q_A$
Cross force due to cross-spin; pitching force.		$K_{Sp} d^3 v \omega$	$i Q_2 \eta = i \rho a^3 w g_2 \eta$	$i \rho d^2 \omega_1 K_{S\eta}$ $= i m u J_{S\eta}$		$F_{Vc}^* = -\frac{1}{2} \Gamma^* \gamma_{c0} \rho A l V q_A$
Magnus force due to cross-spin			$Q_{1\eta} = \rho a^4 \omega g_{1\eta}$	$\rho d^2 \omega_1 K_{X\tau\eta}$ $= m d \omega_1 J_{X\tau\eta}$		$F_{sc}^* = \frac{1}{2} \Gamma^* \gamma_{c0} \rho A l s e_A \times q_A$
OTHER NOTATIONS						
Velocity spin	$\frac{v}{N}$	$\frac{v}{N}$	w ω_3	u ω_1	$\frac{V}{s}$	$\frac{V}{s}$
Radius of projectile	r	d	a	d	$(A/\pi)^{1/2}$	$(A/\pi)^{1/2}$
Diameter of projectile						
Moment of inertia about longitudinal axis.	A	A	C	A	$m k^2$	$m k^2$
Moment of inertia about transverse axis.	B	B	A	B	$m K^2$	$m K^2$
Yaw	δ		ξ/w	ξ/u	δ	δ
Cross-spin	w	ω	η	η	q	q

*R. H. Fowler, E. G. Gallop, C. N. H. Lock, and H. W. Richmond, Roy. Soc., Trans., 221, pp. 295-387. 1921.

†R. H. Kent and E. J. McShane, Aberdeen Ballistic Laboratory Report No. 459.

‡K. L. Nielsen and J. L. Synge, "On the Motion of a Spinning Shell," *Q. App. Math.*, 3, 201 (1946).

§J. L. Kelley and E. J. McShane, Aberdeen Ballistic Laboratory Report No. 446.

**The notation used in E. J. McShane and J. L. Kelley, Aberdeen Ballistic Laboratory Memorandum Report No. 173 is a combination of the notations used by Kent and McShane† and that used by Kelley and McShane§.

which is a combination of the Magnus moment coefficient, the damping coefficient, and γ , the ratio of the moment of inertia about a transverse axis to that about the longitudinal axis. It appears probable that in the usual case the second term in (2) is enough smaller than the first that such measurements can be regarded as a rough determination of $\gamma_{v,\delta}$, the Magnus moment coefficient. In the case of the 3.5/4 GPSR, this method indicates that $\gamma_{v,\delta} \approx 0.03 - 0.001\delta^2$ out to $\delta = 6^\circ$. The rapid variation of Magnus moment coefficient with yaw indicates that the center of pressure moves backwards toward the geometrical center as soon as the yaw becomes appreciable.

The order of magnitude of the damping moment can be estimated from the expression $\gamma_{v,q} = \frac{1}{4}\Gamma_{v^2}$ obtained from 2.48 (4) for fin-stabilized rockets. It seems likely that in the case of spin-stabilized rockets the forces will not be concentrated at the ends of the round as assumed in 2.48 and that consequently the factor by which Γ_{v^2} should be multiplied would be smaller than $\frac{1}{4}$. If the centers of pressure of front and rear halves are assumed to lie at the midpoints of the halves, then the factor $\frac{1}{4}$ should be replaced by $\frac{1}{16}$. Hence a rough estimate of the value of $\gamma_{v,q}$ gives 0.4 to within a factor of 2 or 3. More accurate values could be obtained by wind tunnel measurements as described in 2.48 or by sufficiently complete and precise yaw camera measurements as described in 10.33.

Since the Magnus moment due to cross-spin has very little influence on the motion, it is both difficult and unnecessary to obtain a very good estimate of its value. Arguments of the general nature of those given in 2.48 would indicate that $\gamma_{s,q}$ was of the order of $\Gamma_{v,\delta}$ divided by a factor that should be somewhere in the range from 3 to 16 and hence could be estimated to be 0.1. Sufficiently complete yaw camera studies should throw some light on its value.

8.25 Comparison of Notations.—In order to facilitate comparisons, the notations used by a number of authors are collected in table 8.25. Since quantities in the same row are equal in magnitude, it is easy to determine the relationships among the various coefficients. For example, for the drag we have

$$\Gamma_{v^2} = C_D = mK_{v^2} \left/ \frac{1}{2} \rho A \right. = mc \left/ \frac{1}{2} \rho A \right. = 8K_D/\pi = 2f_R/\pi. \quad (1)$$

One point that should be noted carefully is that in some cases the aerodynamic forces are resolved perpendicular and parallel to the direction of motion, as in the discussion above, and in some cases they are resolved perpendicular and parallel to the axis of the rocket, as in 8.3. The former resolution is the more convenient when the principal concern is the motion of the rocket, the latter when the principal concern is the interrelations among the various aerodynamic forces and moments or the effect of a shift of the center of mass.

In some cases the directions of the forces and moments are indicated by the use of complex numbers similarly to the procedure in chapter 9. However, some care must be exercised; as in chapter 9 multiplication by i corresponds to a clockwise rotation while most authors make it correspond to a counterclockwise rotation. All authors use the same conventions for the positive directions of the forces and moments except in the case of righting moments. Thus all coefficients in any row have the same sign for any particular projectile except in the case of the righting moment, and here the signs of the coefficients are explicitly indicated.

8.3 The Detailed Analysis of the Aerodynamic Forces

We are interested in studying in some detail the forces and moments acting on a projectile with axial symmetry which were defined in the preceding sections. These forces depend on the properties of the air, on the shape and orientation of the projectile, its velocity, its angular

velocity and, to an extent that is negligible in practice, upon the derivatives of the velocities. The aerodynamic forces cannot be computed exactly from the basic equations of aerodynamics because that would involve an explicit computation of the air flow pattern around the projectile. However a large amount of information about these forces can be obtained by symmetry considerations and by approximate treatment.

While we shall not put any restriction upon the magnitude of the yaw, we shall pay special attention to the form of the forces when the yaw is small. In order to limit the problem, we assume that terms proportional to the square of the angular velocity or to the linear and angular accelerations are negligible. The ultimate justification for the neglect of these terms must come from experiment, although fairly general dimensional arguments show that the acceleration terms are small if the fractional change in velocity (or yaw, or angular velocity, etc.) is small in the time required for the projectile to travel its own length. In addition to these dynamic forces there is the buoyant effect of the air which is small and which could be taken into account, if desired, by changing the value of the acceleration of gravity in the formulas.

8.31 General Considerations.—We wish to obtain as much information about the aerodynamic forces as possible from such general principles as symmetry and the effect of changing the center of mass, since an exact calculation of the forces is impossible and any relations between the various forces will reduce appreciably the labor of experimental determinations. In particular, a means of computing the change in the aerodynamic forces when the center of mass is shifted is of direct practical use.

The air is homogeneous and isotropic and the projectile has an axis of symmetry, so that there is a plane of symmetry containing the two defined directions—the direction of motion and the direction of the projectile axis. To illustrate this point let us consider a projectile spinning about its axis of symmetry and yawed with respect to the direction of motion. If now the system, including the air, is reflected in the symmetry plane, the spin is reversed and the sign of the component of force (the Magnus force) perpendicular to the plane is changed, while the component of the aerodynamic force in the plane is unaltered. But the resulting motion is still a solution of the equations of motion of the air, because of the symmetry, so that we obtain the information that the Magnus force must be an odd function of spin, while the drag and lift are even functions of spin. We may also reflect the system in a plane perpendicular to the symmetry plane and passing through the direction of motion. Then the spin and yaw are reversed, as is the lift force. Hence both the lift and the Magnus force are odd functions of yaw, while the drag is an even function of yaw.

In the treatment, below, of the relation between the aerodynamic forces and the aerodynamic moments it is convenient to resolve the forces along the projectile axis; but in the equations of motion we wish to resolve them along the direction of motion. Hence we must define a new set of forces which are components of the total aerodynamic force resolved along the projectile axis. Because we shall not use these in later chapters, we use a temporary asterisk notation to distinguish these forces. It turns out, experimentally, that the aerodynamic coefficients are more nearly independent of yaw when the forces are resolved along the projectile axis, but they vary significantly in both cases.

To facilitate the study of these two sets of forces we introduce two suitably oriented coordinate systems which, because of the symmetry, are simply related. We use an $OXYZ$ -coordinate system with origin at the center of gravity of the projectile, with the OZ -axis along the direction of motion, and with the XZ -plane containing the axis of the projectile. We use an $Oxyz$ -system with the same origin, the Oz -axis along the axis of the projectile, the Ox -axis in the XZ plane, and with the Oy -axis coinciding with the OY -axis. We denote the angle

from the OZ -axis to the Oz -axis, measured positive toward the OX -axis, by δ . This convention, in which δ may be negative, differs from the usual convention of regarding δ as always positive. We use the unit vectors i, j, k in the $Oxyz$ -system, and I, J, K in the $OXYZ$ -system. When considering any particular force we may use x, y, z as subscripts to denote components resolved along the $Oxyz$ -axes and X, Y, Z to denote them resolved along the $OXYZ$ -axes. If it is an aerodynamic force, the system of subscripts defined in the preceding sections may also be used for components resolved along the axes of the $OXYZ$ -system; while if these subscripts are combined with an asterisk, the corresponding resolution along the axes of the $Oxyz$ -system is to be understood. Since the only difference between the two coordinate systems is a rotation through the angle δ about the Oy -axis, we have, as may be seen easily from figure 8.31a, the following relations between the components of any force, F .

$$\left. \begin{aligned} F_X &= F_x \cos \delta + F_z \sin \delta, \\ F_Y &= F_y, \\ F_Z &= -F_x \sin \delta + F_z \cos \delta, \end{aligned} \right\} \quad (1)$$

and

$$\left. \begin{aligned} F_x &= F_X \cos \delta - F_Z \sin \delta, \\ F_y &= F_Y, \\ F_z &= F_X \sin \delta + F_Z \cos \delta. \end{aligned} \right\} \quad (2)$$

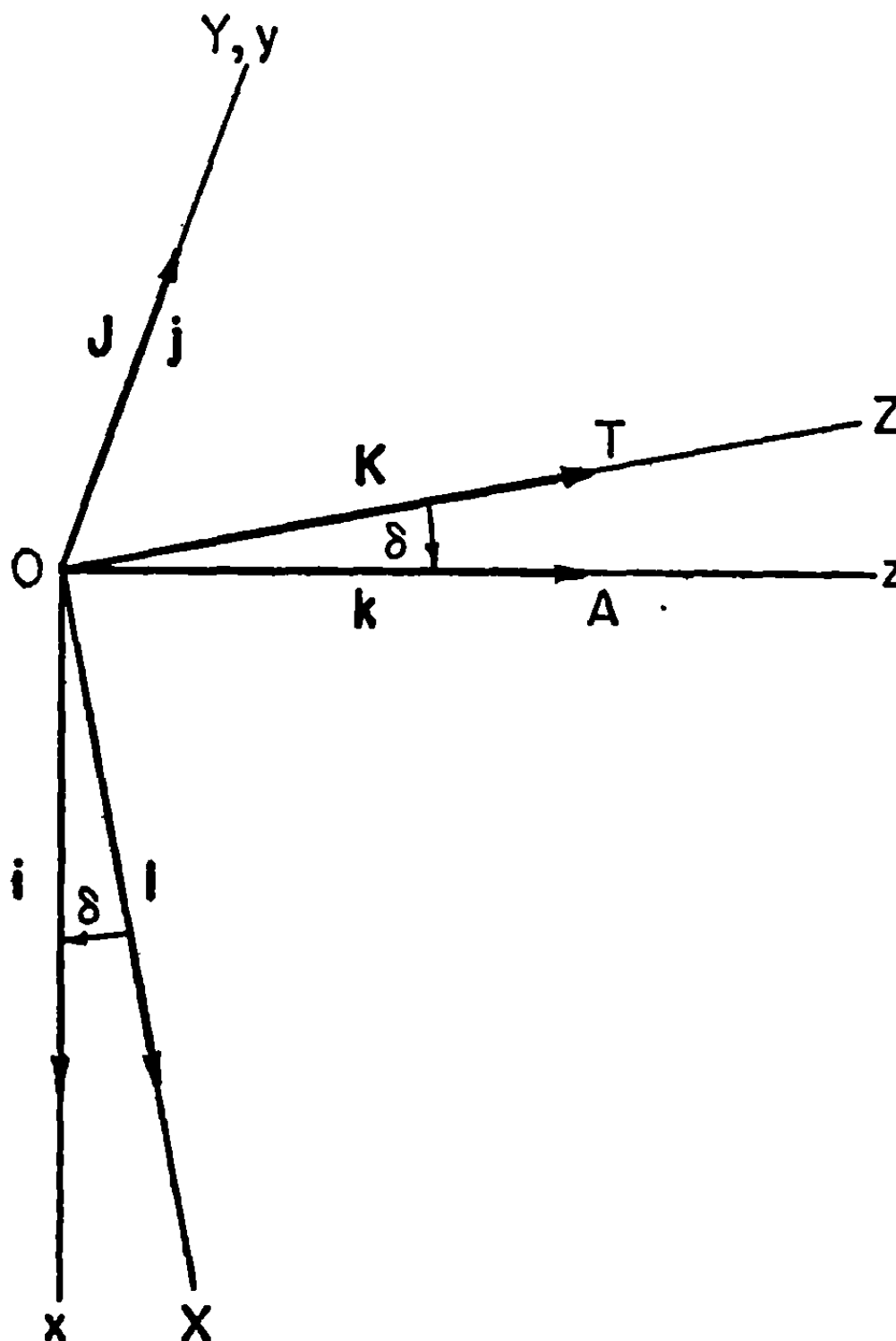


FIGURE 8.31a.—The coordinate system used in discussing the aerodynamic forces.

The moments are always resolved along the axis of the projectile so that no transformation relations are needed for them.

When the rocket has no cross-spin, the components of the total force are:

$$\left. \begin{aligned} F_x &= F_{v^2\delta} = \frac{1}{2}\Gamma_{v^2\delta}\rho AV^2\delta, \\ F_y &= -F_{vs\delta} = -\frac{1}{2}\Gamma_{vs\delta}\rho AlVs\delta, \\ F_z &= -F_{v^2} = -\frac{1}{2}\Gamma_{v^2}\rho AV^2, \end{aligned} \right\} \quad (3)$$

and

$$\left. \begin{aligned} F_x &= F^*_{v^2\delta} = \frac{1}{2}\Gamma^*_{v^2\delta}\rho AV^2\delta, \\ F_y &= -F^*_{vs\delta} = -\frac{1}{2}\Gamma^*_{vs\delta}\rho AlVs\delta, \\ F_z &= -F^*_{v^2} = -\frac{1}{2}\Gamma^*_{v^2}\rho AV^2. \end{aligned} \right\} \quad (4)$$

Substituting these in (1) and (2), we obtain the relations

$$\left. \begin{aligned} \Gamma_{v^2\delta} &= \Gamma^*_{v^2\delta} \cos \delta - \Gamma^*_{v^2} \frac{\sin \delta}{\delta} \doteq \Gamma^*_{v^2\delta} - \Gamma_{v^2}, \\ \Gamma_{v^2} &= \Gamma^*_{v^2\delta} \delta \sin \delta + \Gamma^*_{v^2} \cos \delta \doteq \Gamma^*_{v^2}, \\ \Gamma_{vs\delta} &= \Gamma^*_{vs\delta}, \end{aligned} \right\} \quad (5)$$

and the converse relations

$$\left. \begin{aligned} \Gamma^*_{v^2\delta} &= \Gamma_{v^2\delta} \cos \delta + \Gamma_{v^2} \frac{\sin \delta}{\delta} \doteq \Gamma_{v^2\delta} + \Gamma_{v^2}, \\ \Gamma^*_{v^2} &= -\Gamma_{v^2\delta} \delta \sin \delta + \Gamma_{v^2} \cos \delta \doteq \Gamma_{v^2}, \\ \Gamma^*_{vs\delta} &= \Gamma_{vs\delta}. \end{aligned} \right\} \quad (6)$$

The coefficients of the forces which depend on the cross-spin may be assumed the same in both systems, although a more accurate treatment is given in 8.34 (7) and 8.35 (3).

Let us now consider the effect of shifting the center of mass of the projectile. From these considerations we can obtain useful equations relating the aerodynamic coefficients in one projectile with those in another having a similar external shape.³ These relations may be used to estimate the magnitude of some of the forces and moments. Another important result obtainable from these considerations is a proof of the consistency and completeness⁴ of our system of forces.

The procedure we adopt is to consider a projectile with a displaced center of gravity but moving so that the motions of the external shape, and hence the air, are the same. Then the

³ Some of these relations are given by Fowler, Gallup, Lock, and Richmond, Royal Society, Trans., 221, pp. 295-387, (1921)

⁴ This seems to have been first recognized explicitly by K. L. Nielsen and J. L. Synge in their paper "On the Motion of a Spinning Shell," Q. App. Math; 3, pp. 201-226, (1946).

total aerodynamic force acting on the projectile remains the same, and the moment changes only because it is resolved about a new origin. If the center of gravity is moved forward a distance h to O' , as shown in figure 8.31b, we have the following relations among the total force and moment components:

$$F'_x = F_x, F'_y = F_y, F'_z = F_z, \quad (7)$$

and

$$f'_x = f_x - hF_x, f'_y = f_y - hF_y, M'_z = M_z. \quad (8)$$

The primes denote quantities referred to the new origin, and we use the equivalent forces defined in 8.21, to represent the transverse moments.

Unlike the $O'z'$ -axis, which is parallel to the Oz -axis, the $O'Z'$ -axis is not parallel to the OZ -axis because the velocity of O' through the air is not the same as that of O . Since the angular velocities of all points of a rigid body are the same, we have the relations

$$s' = s, q'_x = q_x, q'_y = q_y, \quad (9)$$

where q is used to represent the cross-spin as in 8.21. The velocity of O' through the air is given by adding the velocity due to the cross-spin to the velocity of O . Thus

$$V'_x = V_x + hq_x = -V \sin \delta + hq_x, \quad (10)$$

and

$$V'_y = hq_y, V'_z = V_z = V \cos \delta.$$

We may obtain V from

$$V' = \{V'^2_x + V'^2_y + V'^2_z\}^{\frac{1}{2}} = V - hq_x \sin \delta, \quad (11)$$

and δ' from

$$\delta' = \tan^{-1} \left[\frac{(V'^2_x + V'^2_y)^{\frac{1}{2}}}{V'_z} \right]$$

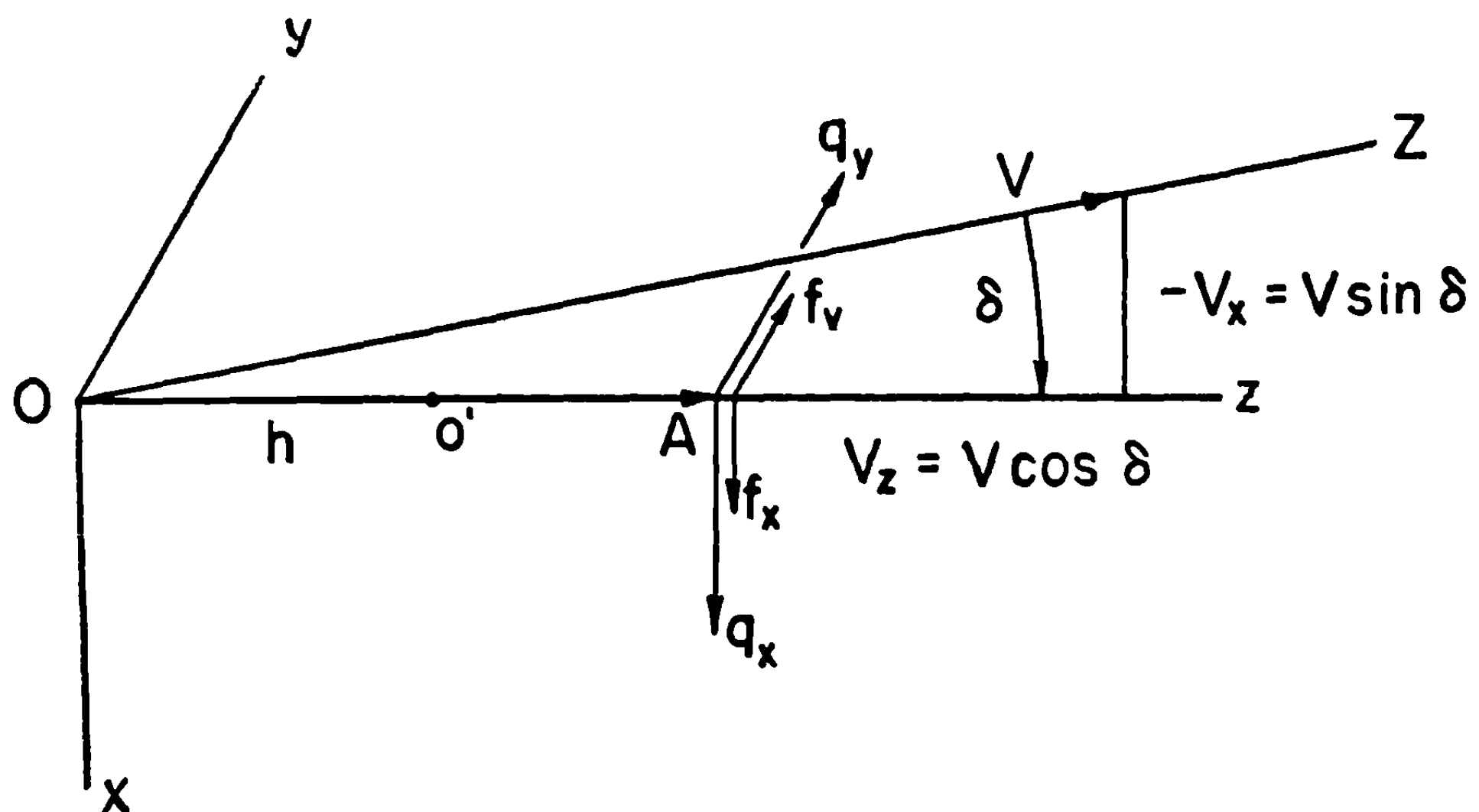


FIGURE 8.31b.—Shift of center of mass.

$$\begin{aligned}
& \doteq \tan^{-1} \left[\tan \delta - \frac{h q_x}{V \cos \delta} \right] \\
& \doteq \delta - \frac{h q_x}{V \cos \delta} \frac{d(\tan^{-1} x)}{dx} \bigg|_{x=\tan \delta} \\
& = \delta - \frac{h q_x \cos \delta}{V}.
\end{aligned} \tag{12}$$

Now we defined the xz -plane as the plane of yaw; but according to (10), O' has a velocity, and hence the projectile has a component of yaw, perpendicular to this plane. Hence we must rotate the $O'x'y'z'$ -system through an angle

$$\tan^{-1} \frac{V'_y}{V'_x} \doteq \frac{-h q_y}{V \sin \delta} \tag{13}$$

from $O'x'$ toward $O'y'$ to align the system properly. The $O'X'Y'Z'$ -system must be rotated through the component of this angle along $O'Z'$, or through the angle

$$\cos \delta \tan^{-1} \frac{V'_y}{V'_x} \doteq -\frac{h q_y}{V} \cot \delta. \tag{14}$$

The transformations (11)–(14) mix components proportional to q of the lift, drag, etc., with the forces dependent upon g and hence lead to the series of relations mentioned above.

8.32 Lift, Drag, and Overturning Moment.—Chapter 2 gives an extensive discussion of the forces acting on a projectile without spin, to which little can be added here. The treatment presented there gives some experimental values of these forces for projectiles both with and without fins, and gives a theoretical breakdown of the drag into nose drag, skin drag, and tail drag. There is, however, an interesting phenomenological argument, giving the form of the drag, which has not been presented. The argument is that the drag is equal to the forward momentum which the air acquires per unit time and hence is equal to the product of the mass of the wake generated per second (proportional to ρAV) and the velocity (proportional to V) which it acquires. Thus we have the drag

$$D = F_v = -\frac{1}{2} \rho A V^2 \Gamma_v, \tag{1}$$

where the coefficient Γ_v takes care of the proportionality factors in the above argument. Actually Γ_v is a function of the yaw and the various dimensionless parameters associated with the motion, in particular the Reynolds number and the Mach number, as described in 2.44. It is an even function of spin, as shown in 8.31, but the variation is small at small yaws. Table 8.32 gives the values of the drag as a function of yaw on a 4-in. rocket model mounted on supports and rotated at 1,210 revolutions per minute in a wind tunnel in which the air speed is 100 ft./sec. Corresponding variations are found in the lift and the overturning moment. Hence we may conclude that the effect of spin on these aerodynamic coefficients is unimportant in exterior ballistics because the yaw is generally less than 10° . We may expect, further, that its effect on the other coefficients is as small; and, because they are less important in determining the motion, we may be fairly certain that all the coefficients may be considered independent of spin.

TABLE 8.32
THE EFFECT OF SPIN AND YAW ON DRAG

Yaw	Drag	Drag
	$s=0$ $V=100$ ft./sec.	$s=1,210$ r. p. m. $V=100$ ft./sec.
	<i>Lb.</i>	<i>Lb.</i>
0°.....	0.306	0.306
5°.....	.380	.377
10°.....	.479	.484
15°.....	.595	.625
20°.....	.708	.818

The transformation from the starred to the unstarred forces has been given in 8.31 (3)-(4) and need not be repeated here. The effect of shifting the center of gravity is simple, since $q=0$, and we have

$$\begin{aligned}\Gamma'^*_{V^2\delta} &= \Gamma^*_{V^2\delta}, \quad \Gamma'^*_{V^2} = \Gamma^*_{V^2}, \\ \gamma'_{V^2\delta} &= \gamma_{V^2\delta} - \frac{h}{l} \Gamma^*_{V^2\delta} \\ &= \gamma_{V^2\delta} - \frac{h}{l} \left(\Gamma_{V^2\delta} \cos \delta + \Gamma_{V^2} \frac{\sin \delta}{\delta} \right).\end{aligned}\quad (2)$$

8.33 Magnus Force and Moment, Spin Deceleration.—When the spin of the projectile is not zero it is possible to have an aerodynamic force which is perpendicular to the XZ -plane; and, as shown in 8.31, symmetry requires that the force be an odd function of the spin and of the yaw. Experimentally a force roughly proportional to $\omega \times V$ is observed when the projectile is spinning. It is known as the Magnus force and is written in the form

$$F_{V\delta\delta} = F^*_{V\delta\delta} = -\frac{1}{2} \Gamma_{V\delta\delta} \rho A l V \delta j. \quad (1)$$

In addition to the force there is a moment when the center of pressure is not at the center of gravity. This Magnus moment may be represented by

$$f_{V\delta\delta} = -\frac{1}{2} \gamma_{V\delta\delta} \rho A l^2 V \delta j. \quad (2)$$

It is defined so that $\gamma_{V\delta\delta}$ is positive if the point of application of $F_{V\delta\delta}$ (i. e., the point at which $F_{V\delta\delta}$ would have to be applied in order to produce the same moment as does $f_{V\delta\delta}$) is ahead of the center of gravity.

The Magnus force is caused by the circulation of the air around the projectile due to the spin. The circulation is specified by the integral of the velocity around the projectile and may be written as

$$\text{Circulation} = 2\pi R V_c, \quad (3)$$

where R is the radius of the projectile and V_c is the circulation velocity. Actually V_c is not constant along the projectile because of the inertia of the air, and the circulation builds up as

the air flows back along the projectile at a rate depending on the viscosity of the air, the roughness of the projectile, etc.

In the usual treatment of the Magnus force the flow is assumed to be laminar, and the force is computed from the pressure difference on the two sides of the projectile. The pressure difference is due to the Bernoulli effect so that the pressure difference is proportional to the difference of the squares of the velocities on the two sides of the projectile. Hence we have:

$$F \sim (V \sin \delta + V_c)^2 - (V \sin \delta - V_c)^2 = 4 V V_c \sin \delta. \quad (4)$$

The analysis is given by Joos;⁵ and the force is

$$F_{V,\delta} = 2\pi\rho R l V_c V \sin \delta. \quad (5)$$

If the air next to the rocket adhered tightly we would have $V_c = sR$; but actually there is considerable slip and we have approximately

$$V_c \approx \frac{1}{4} sR. \quad (6)$$

Combining (1), (5), and (6) we might expect

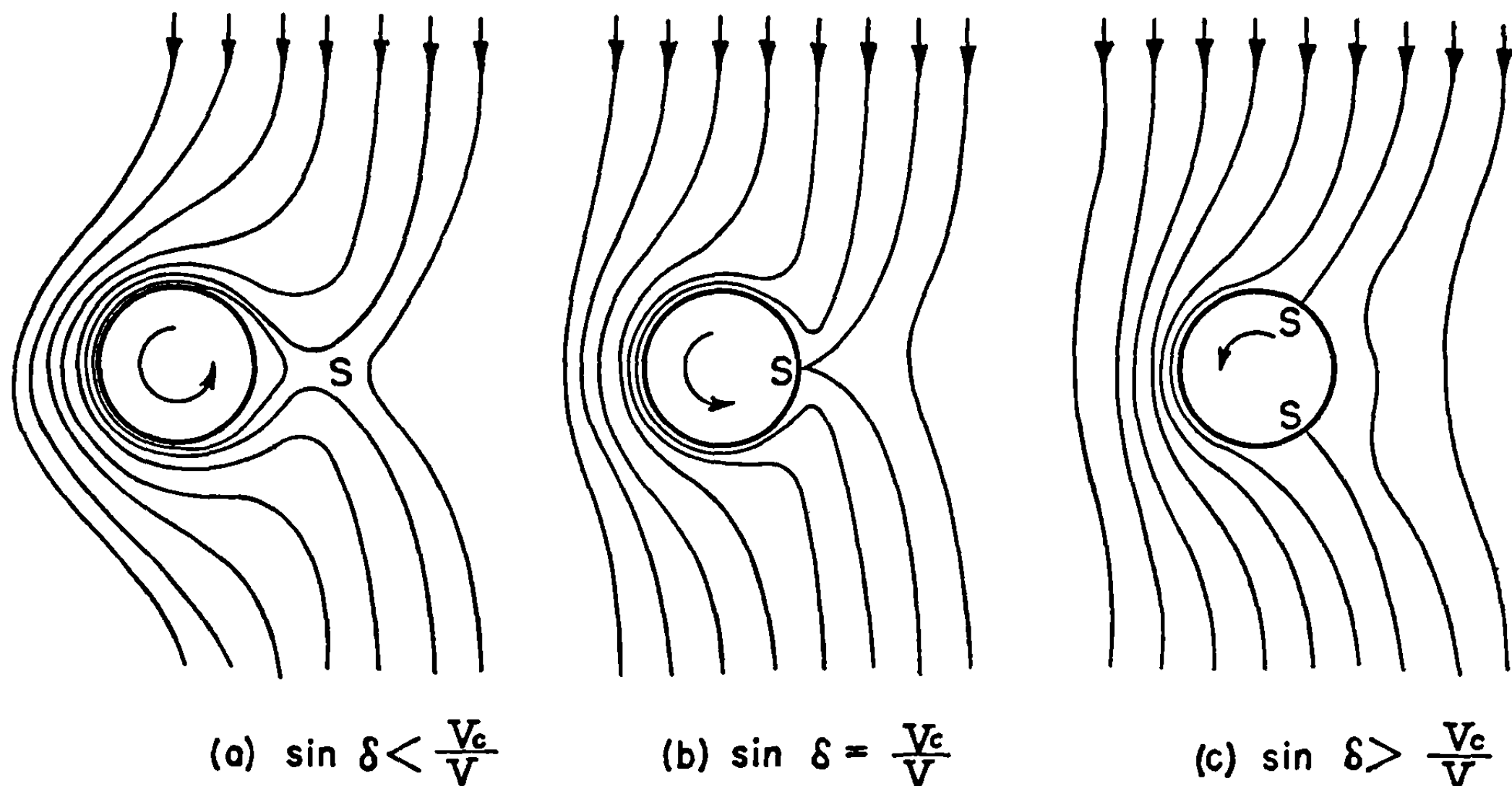
$$\Gamma_{V,\delta} \approx 1; \quad (6)$$

and this is roughly what is observed, so that we may assume that this is the actual mechanism of the Magnus force. There are several other contributions to the Magnus force by divers mechanisms but these are mostly in the $+\mathbf{j}$ rather than the $-\mathbf{j}$ direction and are very small. One flaw with this mechanism is that it would suggest that the center of pressure should be behind the center of figure since the circulation should build up as one goes along the rocket and be greater at the rear than at the nose. Actually, for subsonic velocities, the center of pressure of the Magnus force is well ahead of the center of figure at small yaw. It may be that the lesser effect of circulation at the rear is connected with the greater thickness of the turbulent boundary layer there.

It may be noted that a change in the type of air flow around the projectile takes place when $V_c = V \sin \delta$ as is shown in figure 8.33. It is apparent that for small yaw the air close to the projectile circulates in a closed path, that there is only one point where the velocity is zero, and that this point is not on the projectile boundary. The limiting case for $V_c = V \sin \delta$ has no closed paths and one point of zero velocity on the boundary. The yaw at which this transition takes place varies slightly along the projectile because the circulation is larger toward the tail; but the air flow does change character near a definite value of δ .

If the flow were purely laminar the Magnus force would be independent of the type of flow, but with turbulence this may not be true. In the first place the type of flow may change the rate of buildup of circulation and it may also modify the Bernoulli effect. These changes would not be expected to alter the Magnus force much, but the modification of the pressure distribution probably changes the center of pressure, and hence the Magnus moment, significantly. This conjecture is supported by a certain amount of experimental evidence, since the critical yaw is about 5° and this is the yaw at which the center of pressure of the Magnus force moves back. Another description of this change of character of the flow pattern is that the vorticity

⁵ Georg Joos. "Theoretical Physics" p. 196, Stechart and Co., New York, 1943.

FIGURE 8.33.—Circulation about a spinning rocket, and the stagnation points, S .

slides back along the projectile at small yaw, but slips off the lee side of the projectile at yaws larger than the critical yaw defined above.

The circulation set up by the spin of the projectile will exert a torque upon the projectile tending to slow the spin. The spin deceleration moment is written in the form

$$M_{vs} = -\frac{1}{2} \gamma_{vs} \rho A l^2 V s k. \quad (8)$$

The torque is an odd function of the spin since the projectile is assumed axially symmetric. Nielsen and Synge have pointed out that, in addition to dimensional considerations, this form for M_{vs} would be expected because the projectile leaves behind a rotating wake in which the angular velocity is proportional to the spin of the rocket, or better, to the circulation. The mass of gas to which angular velocity is imparted each second is proportional to the velocity of the projectile; and hence the torque, which is proportional to the angular momentum created per second, is proportional to the product of velocity and spin. A more quantitative computation, however, is not justified. Logically it would appear better to replace Al^2 by $A^{3/2}l$ in (8) since, if there is any simple dependence on length and diameter, the moment should be proportional to l rather than to l^2 . However, this would complicate things rather than simplify them.

When the projectile is rotating, the relative velocity of the skin and the air is not along the axis of the projectile and there is a component of the skin drag in a direction opposing the rotation. A quantitative calculation of the moment on this basis gives a deceleration in reasonable agreement with that observed. It is somewhat smaller than the experimental value, however, indicating that there may be other sources of spin deceleration.

As shown by 8.31 (5) the Magnus force coefficient is the same when the forces are resolved along the direction of motion as when resolved along the axis of the projectile. When the center of mass is shifted, the Magnus force coefficient is unaltered but the moment coefficient is changed. From 8.31 (7)–(8) we see that

$$\Gamma'_{vs\delta} = \Gamma^{*'}_{vs\delta} = \Gamma^*_{vs\delta} = \Gamma_{vs\delta}, \quad (9)$$

and

$$\gamma'_{v,\delta} = \gamma_{v,\delta} - \frac{h}{l} \Gamma^*_{v,\delta} = \gamma_{v,\delta} - \frac{h}{l} \Gamma_{v,\delta},$$

since q is zero.

8.34 The Damping Moment.—We now wish to study the additional forces and moments which are present when the projectile has cross-spin. We shall consider only those terms which are proportional to q and shall assume that the spin is zero in this section. The force due to cross-spin is very small; but the moment, the usual damping moment, is of importance. When the yaw is not zero the damping moment due to q_x , which is the component of q in the plane of the yaw, is in general not equal to that due to q_v ; but in practice the difference is not important since the yaw is usually small and they are equal at zero yaw.

Let us consider the effect of q_v first. In this case it is possible to have a force not in the plane of the yaw. If we reflect the motion in the plane of the yaw, q_v and the component normal to the plane of the yaw of the resulting force are reversed, but any component in the plane of the yaw is unaltered. Hence we conclude that the force linearly proportional to q_v is perpendicular to the plane of yaw. If the motion is reflected in the yz -plane, the yaw is changed, but q_v and the force are unaltered and we may say that the force is an even function of δ . We write the force in the form

$$F^*_{vqv} = -\frac{1}{2} \rho A l V q_v \Gamma^*_{vqv} j, \quad (1)$$

and represent the associated moment, which has the same symmetry, by

$$f_{vqv} = -\frac{1}{2} \rho A l^2 V q_v \gamma_{vqv} j. \quad (2)$$

There is one other torque proportional to q_v . This is a torque proportional to $q_v \delta$ and is not only very small but averages out in the course of the motion; hence we neglect it.⁶

When only q_x is not zero, the force must be in the plane of yaw, by symmetry, and the moment must be perpendicular to the plane of yaw. If we reflect the motion in the yz -plane, the yaw and q_x are changed in sign and the x -component of the force is reversed. Hence we conclude that the x -component is an odd function of q_x and an even function of δ , while the z -component is an even function of q_x or a function of $q_x \delta$. We write the x -component of the force in the form

$$F^*_{vqx} = -\frac{1}{2} \rho A l V q_x \Gamma^*_{vqx} i, \quad (3)$$

and represent the moment by

$$f_{vqx} = -\frac{1}{2} \rho A l^2 V q_x \gamma_{vqx} i, \quad (4)$$

and neglect the axial component of the force.⁷

When the forces are resolved along the direction of motion, the component of force along the projectile axis is mixed with that along the x -axis, so that it is not possible to write the

⁶ When the center of gravity is shifted, this torque is related to a component of the overturning moment due to the rotation of the coordinate system through the angle given by 8.31 (13).

⁷ When the center of gravity is shifted, this force is related to the change in drag due to the change in velocity and yaw given by 8.31 (11)–(12).

transformation equations explicitly without introducing notation for the axial component of force. However, using (1) and (3), the corresponding unstarred equations, and 8.31 (1)–(2), we may write the equations

$$\begin{aligned}\Gamma_{vqv} &= \Gamma^*_{vqv}, \\ \Gamma_{vqx} &= \Gamma^*_{vqx} \cos \delta + \delta \sin \delta \text{ (axial coefficient*)},\end{aligned}\tag{5}$$

and their converses

$$\begin{aligned}\Gamma^*_{vqv} &= \Gamma_{vqv}, \\ \Gamma^*_{vqx} &= \Gamma_{vqx} \cos \delta - \delta \sin \delta \text{ (axial coefficient)}.\end{aligned}\tag{6}$$

Now, since we do not even know the sign of the axial component because it depends on the position of the center of gravity, and since we are interested primarily in small yaw where we can use one coefficient Γ^*_{vq} instead of two, we write

$$\Gamma^*_{vqx} = \Gamma_{vqx} = \Gamma^*_{vqv} = \Gamma_{vqv} = \Gamma^*_{vq} = \Gamma_{vq}.\tag{7}$$

The error resulting from this approximation is negligible since, as we shall see, the effects of the force itself are not observable. Likewise we equate the two moment coefficients at small yaw, setting

$$\gamma_{vqx} = \gamma_{vqv} = \gamma_{vq}.\tag{8}$$

Physically the torque may be pictured as the result of a cross force acting on the ends of the projectile due to the additional velocity caused by q . Following this line of reasoning, as in 2.48, we find that the cross-force, which is in different directions on the two ends, nearly cancels to give a very small force, but that the resulting moments add. This concept is too crude to allow a quantitative calculation of the damping moment, but is useful in obtaining a mental picture of the motion.

A more accurate method of computing the damping moment is to treat the projectile itself as curved very slightly but having no angular velocity. The justification for this procedure comes from a consideration of the air flow. As the air passes along the projectile, the angle between the direction of the air flow and the axis changes slightly as the projectile rotates and to the air the projectile "looks" curved. Wind tunnel measurements have been made on such curved models but the size of the curvature needed to give measurable results is so large that the air flow is modified seriously at any yaw where the air flow changes rapidly with yaw. A calculation with such a model is exact, but difficult. Fortunately, sufficient information about the damping moment may be obtained by considering a displacement of the center of mass.

Let us first consider the change in Γ^*_{vqv} when the center of gravity is shifted. According to 8.32 (2), $\Gamma^*_{v2\delta}$ is unaltered by the shift, and according to 8.31 (11) and (12) the yaw and velocity are unaltered when $q_x = 0$, so that the magnitude of the cross-wind force $F^*_{v2\delta}$ is independent of the center of gravity position. However, according to 8.31 (13) the plane of the yaw, and hence the plane of $F^*_{v2\delta}$, is rotated through an angle $(-hq_y/V \sin \delta)$. Now by 8.31 (7) the total force is constant, so that the increment of F^*_{vqv} must just equal the difference of $F^*_{v2\delta}$ in its original and final orientations; i. e.,

$$F^{*'}_{vqv} - F^*_{vqv} = -[F^{*'}_{v2\delta} - F^*_{v2\delta}]$$

$$\begin{aligned}
&= -\frac{1}{2} \rho A V^2 \delta \Gamma^*_{v^2\delta} (\mathbf{i}' - \mathbf{i}) \\
&\doteq \frac{1}{2} \rho A V^2 \delta \Gamma^*_{v^2\delta} \left(\mathbf{j}' \frac{h q_y}{V \sin \delta} \right),
\end{aligned} \tag{9}$$

to the first order in q_y . On the left of (9) we may neglect the difference between \mathbf{j} and \mathbf{j}' to the accuracy with which we are concerned; and, using (7), we have

$$\Gamma^{*'}_{v_{ay}} = \Gamma^*_{v_{ay}} - \frac{\delta}{\sin \delta} \frac{h}{l} \Gamma^*_{v^2\delta}. \tag{10}$$

This expression shows that $\Gamma^*_{v_{ay}}$ may reverse as the center of gravity is moved forward, although the actual point at which this occurs can not be obtained from these arguments. However, we might estimate that this point is probably of the order of one-tenth the length of the rocket from the normal center of gravity positions; i. e.,

$$\Gamma^*_{v_{ay}} \approx \pm \Gamma^*_{v^2\delta} / 10.$$

In the case of $F^*_{v_{qx}}$ the forces are all coplanar but the yaw and velocity are different according to 8.31 (11)–(13). Using a Taylor's expansion, we have

$$F^{*'}_{v^2\delta} = F^*_{v^2\delta} - h q_x \sin \delta \frac{\partial F^*_{v^2\delta}}{\partial V} - \frac{h q_x \cos \delta}{V} \frac{\partial F^*_{v^2\delta}}{\partial \delta}, \tag{11}$$

to the first order, and hence

$$\begin{aligned}
F^{*'}_{v_{qx}} - F^*_{v_{qx}} &= -[F^{*'}_{v^2\delta} - F^*_{v^2\delta}] \\
&= \frac{1}{2} \rho A h q_x \left\{ \sin \delta \frac{\partial}{\partial V} (\Gamma_{v^2\delta} V^2 \delta) + \frac{\cos \delta}{V} \frac{\partial}{\partial \delta} (\Gamma^*_{v^2\delta} V^2 \delta) \right\} \mathbf{i} \\
&= \frac{1}{2} \rho A h V q_x \left\{ \delta \sin \delta \left[2\Gamma^*_{v^2\delta} + V \frac{\partial \Gamma^*_{v^2\delta}}{\partial V} \right] + \cos \delta \left[\Gamma^*_{v^2\delta} + \delta \frac{\partial \Gamma^*_{v^2\delta}}{\partial \delta} \right] \right\} \mathbf{i}.
\end{aligned} \tag{12}$$

Thus, using (3),

$$\Gamma^{*'}_{v_{qx}} = \Gamma^*_{v_{qx}} - \frac{h}{l} \left\{ (\cos \delta + 2\delta \sin \delta) \Gamma^*_{v^2\delta} + \delta \cos \delta \frac{\partial \Gamma^*_{v^2\delta}}{\partial \delta} + \delta \sin \delta V \frac{\partial \Gamma^*_{v^2\delta}}{\partial V} \right\}. \tag{13}$$

For small angles (10) and (13) are equivalent; thus, using (7), we have

$$\Gamma^{*'}_{v_q} = \Gamma'_{v_q} = \Gamma^*_{v_q} - \frac{h}{l} \Gamma^*_{v^2\delta}. \tag{14}$$

Since the yaw and velocity are altered when $q_x \neq 0$, there is a change in the drag, which may be computed as in (11); and thence there must be a longitudinal force, proportional to q_x , which can balance this change. This is the force mentioned above (3).

In the case of the moments due to cross-spin the shift of the center of gravity contributes two different terms. The first is the moment due to F_{v_q} at the distance h , and the second is the change in the overturning moment due to 8.31 (11)–(13). Let us first consider $f_{v_{ay}}$; then the increment due to $F^*_{v_{ay}}$ is

$$-h F^*_{v_{ay}} \doteq \frac{1}{2} \rho A l h V q_y \Gamma^*_{v_{ay}} \mathbf{j}' \tag{15}$$

to the first order, since we may neglect the difference between \mathbf{j} and \mathbf{j}' . According to 8.32 (2) the magnitude of $\mathbf{f}'_{v^2\delta}$ is equal to that of $(\mathbf{f}_{v^2\delta} - h\mathbf{F}^*_{v^2\delta})$, but the directions are now different by 8.32 (13). Hence when the various forces and moments are substituted in 8.31 (8), and the terms independent of qy are subtracted off, there is an increment to \mathbf{f}_{vqv} ; namely,

$$\mathbf{f}'_{v^2\delta} - \mathbf{f}_{v^2\delta} + h\mathbf{F}^*_{v^2\delta} = \frac{1}{2} \rho Al V^2 \delta \gamma'_{v^2\delta} (\mathbf{i}' - \mathbf{i}) \doteq \frac{1}{2} \rho Al V^2 \delta \gamma'_{v^2\delta} \frac{h q_v}{V \sin \delta} \mathbf{j}'. \quad (16)$$

Combining (15) and (16), and using (2), we have

$$\gamma'_{vqv} = \gamma_{vqv} - \frac{h}{l} \left(\Gamma^*_{vqv} + \frac{\delta}{\sin \delta} \gamma'_{v^2\delta} \right) = \gamma_{vqv} - \frac{h}{l} \left(\Gamma^*_{vqv} + \frac{\delta}{\sin \delta} \gamma_{v^2\delta} \right) + \frac{h^2}{l^2} \frac{\delta}{\sin \delta} \Gamma^*_{v^2\delta}. \quad (17)$$

In the case of \mathbf{f}_{vqx} the contribution due to \mathbf{F}_{vqx} is

$$-h\mathbf{F}^*_{vqx} = \frac{1}{2} \rho Al V q_x \Gamma^*_{vqx} \mathbf{i}', \quad (18)$$

since \mathbf{i} and \mathbf{i}' are the same when $q_v = 0$. The increment is $\mathbf{f}'_{v^2\delta}$ due to the change in yaw and velocity, 8.31 (11)–(12), is

$$\begin{aligned} \mathbf{f}'_{v^2\delta} - \mathbf{f}_{v^2\delta} + h\mathbf{F}^*_{v^2\delta} &\doteq -h q_x \sin \delta \frac{\partial \mathbf{f}'_{v^2\delta}}{\partial V} - \frac{h q_x \cos \delta}{V} \frac{\partial \mathbf{f}'_{v^2\delta}}{\partial \delta} \\ &= -\frac{1}{2} \rho Al h q_x \left\{ \sin \delta \frac{\partial}{\partial V} (V^2 \delta \gamma'_{v^2\delta}) + \frac{\cos \delta}{V} \frac{\partial}{\partial \delta} (V^2 \delta \gamma_{v^2\delta}) \right\} \mathbf{i}'. \end{aligned} \quad (19)$$

Combining (18) and (19) we have

$$\begin{aligned} \gamma'_{vqx} &= \gamma_{vqx} - \frac{h}{l} \left[\Gamma^*_{vqx} + (\cos \delta + 2\delta \sin \delta) \gamma_{v^2\delta} + \delta \cos \delta \frac{\partial \gamma_{v^2\delta}}{\partial \delta} + \delta \sin \delta V \frac{\partial \gamma_{v^2\delta}}{\partial V} \right] \\ &\quad + \frac{h^2}{l^2} \left[(\cos \delta + 2\delta \sin \delta) \Gamma^*_{v^2\delta} + \delta \cos \delta \frac{\partial \Gamma^*_{v^2\delta}}{\partial \delta} + \delta \sin \delta V \frac{\partial \Gamma^*_{v^2\delta}}{\partial V} \right]. \end{aligned} \quad (20)$$

For small yaw, (17) and (20) reduce to the same form, which we may write, using (8),

$$\gamma'_{vq} = \gamma_{vq} - \frac{h}{l} (\Gamma^*_{vq} + \gamma_{v^2\delta}) + \frac{h^2}{l^2} \Gamma^*_{v^2\delta}. \quad (21)$$

Differentiating (21) we see that the damping moment has a minimum at

$$h = \frac{l}{2\Gamma^*_{v^2\delta}} (\Gamma^*_{vq} + \gamma_{v^2\delta}), \quad (22)$$

for small yaw. This point will vary with yaw (and with direction of \mathbf{q}) but will remain near the point at which the overturning moment is zero. Mathematically there is no reason why this minimum should not correspond to negative damping, but physically we may say that it is positive for normal shapes. Choosing the origin at the minimum point, we have

$$\gamma'_{vq} = \gamma_{vq} + \frac{h^2}{l^2} \Gamma^*_{v^2\delta}. \quad (23)$$

Physically we may expect that the two terms are of comparable magnitude when $h \approx l/3$. That is, we may expect that the limits

$$\frac{1}{20} \Gamma^* v^2 \delta < \gamma v \delta < \frac{1}{4} \Gamma^* v^2 \delta, \quad (24)$$

are reasonable. The result is the same as that obtained in 8.24, but neither treatment is very accurate.

8.35 Magnus Moment Due to Cross-Spin.—When a spinning projectile has a cross-spin it has an additional force and a corresponding moment which are proportional to the spin times the cross-spin. When the projectile has cross-spin the two ends may be treated separately, in the first approximation as is done in 8.34 and 2.48; and hence there is a Magnus force acting on each end of the projectile. These forces give rise to a force and a moment which, for small yaw, we write in the form,

$$F^*_{sq} = \frac{1}{2} \rho A l^2 s q \Gamma^*_{sq}, \quad (1)$$

and

$$f_{sq} = \frac{1}{2} \rho A l^3 s q \gamma_{sq}, \quad (2)$$

with

$$\Gamma^*_{sq} = \Gamma_{sq}. \quad (3)$$

An analysis along the lines of the symmetry considerations carried out in the preceding sections could be made here with similar results; i. e., the force and moment depend on the direction of q and there are axial torques and forces. However, even (1) and (2) are very small and are usually neglected, so that we shall not carry out the analysis. The results of shifting the center of gravity are also similar to those in 8.34, and we find

$$\Gamma^{*'}_{sq} = \Gamma^*_{sq} - \frac{h}{l} \Gamma^*_{v\delta}, \quad (4)$$

and

$$\gamma'_{sq} = \gamma_{sq} - \frac{h}{l} [\Gamma^*_{sq} + \gamma_{v\delta}] + \frac{h^2}{l^2} \Gamma^*_{v\delta}, \quad (5)$$

for small yaw.

8.4 Aerodynamic Forces on a Projectile With Fins

As an extension of the above analysis of the aerodynamic force system acting on a symmetrical projectile, it is interesting to consider the force system on a projectile with fins. This discussion is given here rather than in chapter 3 because it follows the line of argument of 8.3 and because the effects are so small that they need not be considered in the treatment of fin-stabilized rockets given in chapters 3 and 5. No particular accuracy is claimed since what is essentially a dimensional argument is used to estimate the relative magnitudes of the various forces and moments. In determining the aerodynamic forces and moments acting on a projectile with fins we make use of the symmetry properties of the projectile and of the required invariance with respect to shift of center of gravity.

8.41 Lift, Drag, and Side Force.—We use the same coordinate system as in 8.3, but now we must add an angle to specify the rotation of the projectile about its axis. We denote the angle between a particular fin and the xz -plane by the symbol ψ . The analysis could be carried

through for any number of fins but we shall treat only the case of four fins to avoid complications. It is then necessary that the lift and drag be periodic functions of ψ with period $\pi/2$. Hence if we expand the force components in Fourier series in ψ , only terms of the form $\cos 4n\psi$ and $\sin 4n\psi$ will be present. Furthermore, by symmetry, the lift and drag are even functions of ψ , so that only the cosine terms remain. We may write the cross force and axial drag in the form

$$F^*_{v^2\delta} = \frac{1}{2} \Gamma^*_{v^2\delta} \rho A V^2 \delta i, \quad (1)$$

and

$$F^*_{v^2} = -\frac{1}{2} \Gamma^*_{v^2} \rho A V^2 k, \quad (2)$$

with

$$\Gamma^*_{v^2\delta} = \Gamma^*_{v^2\delta,0} + \Gamma^*_{v^2\delta,1} \cos 4\psi + \Gamma^*_{v^2\delta,2} \cos 8\psi + \dots, \quad (3)$$

and

$$\Gamma^*_{v^2} = \Gamma^*_{v^2,0} + \Gamma^*_{v^2,1} \cos 4\psi + \Gamma^*_{v^2,2} \cos 8\psi + \dots, \quad (4)$$

where the $\Gamma^*_{v^2,n}$ and $\Gamma^*_{v^2\delta,n}$ are slowly varying functions of velocity and yaw.

We have, as in 8.31 (5),

$$\Gamma_{v^2,n} = \Gamma^*_{v^2,n} \cos \delta + \Gamma^*_{v^2\delta,n} \sin \delta, \quad (5)$$

and

$$\Gamma_{v^2\delta,n} = \Gamma^*_{v^2\delta,n} \cos \delta - \Gamma^*_{v^2,n} \frac{\sin \delta}{\delta}. \quad (6)$$

In addition to these forces there may be a side force similar in direction to the Magnus force but resulting from the inclination of the fins rather than from axial spin; this force must be an odd function of ψ . We denote it by F^*_v , and write it

$$F^*_v = \frac{1}{2} \Gamma^*_v \rho A V^2 \delta j, \quad (7)$$

where

$$\Gamma^*_v = \Gamma^*_{v,1} \sin 4\psi + \Gamma^*_{v,2} \sin 8\psi + \dots \quad (8)$$

There is no apparent connection between the side-force and the cross-force, but in the absence of experimental data it is plausible to assume that $\Gamma_{v,n}$ will be of the same order of magnitude as $n\Gamma_{v^2\delta,n}$ both in velocity dependence and variations with yaw.⁹

Experimentally, the second term in the cross force is perhaps 10 percent of the first term; and the higher terms are negligibly small. Hence these variations with the orientation angle ψ may be neglected in computations, since the cross force enters only indirectly in the motion (3.22). The variation of drag with ψ is considerably smaller and is also negligible in practice.

8.42 Overturning Moment and Axial Torque.—Just as in the case of the cross force, we may write the overturning moment as a Fourier series in ψ . The moment takes the form

$$f_{v^2\delta} = \frac{1}{2} \gamma_{v^2\delta} \rho A l V^2 \delta i; \quad (1)$$

⁹ This specific relation between the cross-force and side-force coefficients may be obtained from the assumption that the forces are derivable from a generalized potential energy function. Then these forces are the two components of a gradient and are related as above. While there is no physical reason to suppose that such a potential actually exists, because energy is available from the motion through the air, the magnitude of the coefficients obtained by this estimate is the best that can be made without further detailed analysis of a particular structure. Thus the magnitudes of the coefficients estimated here and in 8.42 are little more than a guess.

where $\gamma_{V^2\delta}$, which is given by

$$\gamma_{V^2\delta} = \gamma_{V^2\delta,0} + \gamma_{V^2\delta,1} \cos 4\psi + \gamma_{V^2\delta,2} \cos 8\psi + \dots, \quad (2)$$

is negative in stable fin-stabilized projectiles. Now in addition to the overturning moment there may be torques about the longitudinal axis which must be odd functions of ψ and a torque similar to the Magnus torque called the side torque. Furthermore, changing the sign of δ shows that the axial torque, M_z , must be an even function of δ and the side torque f_y , an odd function of δ . We may write these torques in the form

$$M_z = \frac{1}{2} \gamma_z \rho A l V^2 \delta^2 k, \quad (3)$$

and

$$f_y = \frac{1}{2} \gamma_y \rho A l V^2 \delta j \quad (4)$$

with

$$\gamma_z = \gamma_{z,1} \sin 4\psi + \gamma_{z,2} \sin 8\psi + \dots, \quad (5)$$

and

$$\gamma_y = \gamma_{y,1} \sin 4\psi + \gamma_{y,2} \sin 8\psi + \dots \quad (6)$$

We may expect $\gamma_{z,n}$ to be given roughly by the expression (see footnote 9)

$$\gamma_{z,n} \approx 2n \gamma_{V^2\delta,n}. \quad (7)$$

Since M_z is proportional to δ^2 at small yaw, the axial torque may be neglected for sufficiently small yaw. Actually the moment is not always sufficiently small to neglect, but its effects are minor, as will be shown in 8.43. Similarly, we may expect that

$$\gamma_{y,n} \approx -2n \gamma_{V^2\delta,n}. \quad (8)$$

Both f_y and M_z tend to rotate the projectile into a position of minimum restoring moment.

By a combination of the methods of this section and those of 8.24 it is possible to obtain some information about the damping moment in the case of a projectile with fins; but since the moment is small its variation with ψ is of such little interest that it does not justify the lengthy analysis needed to obtain it. This is especially true since the component of damping moment opposing the motion is nearly constant, and the components perpendicular to the motion have no direct effect on the motion.

8.43 Effect of Unsymmetrical Forces and Moments on the Motion.—In treating the effect of the unsymmetrical forces and moments it is necessary to take account only of the moments, because the forces, by 3.22, have only an indirect effect on the motion and any variation in them would have negligible effects. It is desirable, of course, to use appropriate average values of the coefficients. Similar remarks apply to the damping moment, so that its variation is also unimportant. However, the variation of the overturning moment with orientation is not negligible and the side and axial torques contribute effects of the same magnitude as do the forces and the damping moment. Now a normal fin-stabilized rocket projectile has a transverse moment of inertia about forty times as large as its axial moment. For this reason the axial torque affects the motion appreciably even though it is small. Comparing the angular acceleration due to the axial torque to that due to the overturning moment, we have approximately

$$\frac{\frac{1}{2}\gamma_{z,1}\rho A l V^2 \delta^2}{I_z} \bigg/ \frac{\frac{1}{2}\gamma_{v^2\delta,0}\rho A l V^2 \delta}{I_x} = \frac{\gamma_{z,1}\delta}{\gamma_{v^2\delta,0}} \frac{I_x}{I_z}. \quad (1)$$

Now from 8.42 (7)

$$\gamma_{z,1} \approx 2\gamma_{v^2\delta,1} \quad (2)$$

so that the ratio (1) becomes

$$2\delta \frac{\gamma_{v^2\delta,1}}{\gamma_{v^2\delta,0}} \frac{I_x}{I_z}. \quad (3)$$

Now if we assume that the yaw is 10° , and that the overturning moment varies as much as 10 percent, then (3) has a numerical value of 1.4. This shows that the angular acceleration is sufficient to rotate the projectile about its longitudinal axis to the orientation in which the overturning moment is a minimum.

The effect of the side torque is smaller but it has the same tendency; so that, if the yaw oscillations are large, it is appropriate to take the minimum overturning moment coefficient ($\gamma_{v^2\delta,0} - \gamma_{v^2\delta,1}$) in computing σ ; but for small yaw oscillations the average moment coefficient ($\gamma_{v^2\delta,0}$) should be used. The size of the yaw for which the analysis of chapter 3 is valid may be reduced slightly by the variation of σ , but since σ does not enter into the theory critically, this limitation is not serious.

The effects of a variation of σ on the trajectory are not large but there is another effect which may be quite important. If the projectile is making elliptical or circular yaw oscillations, the axial torque will cause the projectile to rotate, and this may reduce the drift due to fin malalignment to a negligible source of dispersion. There do not seem to be any other effects of consequence caused by the unsymmetrical torques so that the analyses in chapters 3 and 5 are not altered appreciably.

8.5 The Jet Forces

The treatment in chapter 2 of the jet forces of fin-stabilized rockets covers all of the factors of interest in the case of spin-stabilized rockets except the production of the spin and the slight decrease in thrust resulting from some of the gas momentum imparting spin rather than thrust. If, in chapter 2, the gas velocity relative to the nozzle is replaced by the component of gas velocity along the longitudinal axis of the rocket, the entire discussion, including that of effective accelerations, burning times, and launcher lengths, that of malalignment, and that of the jet damping torque about a transverse axis, will apply to spin-stabilized rockets. Hence we need consider here only the calculation of the spin when the direction of the longitudinal axis remains constant.

8.51 The Thrust and the Malalignment.—The burning of the propellant produces forces that are distributed over the nozzles and the entire interior of the motor. However, we are concerned only with the resultant force and torque and with the principal components into which they are resolved. Using the notation and figures of 2.24, we see that the total jet force on the rocket is the sum of the components $mG_J e_A$ directed along the rocket axis and $mG_J \beta_M$ directed along the vector β_M , called the angular malalignment, which is normal to the axis of the rocket and is fixed in the rocket, rotating with it. The jet force should be resolved into components along and normal to the trajectory. If we neglect infinitesimals of order δ^2 compared to unity, these components of $mG_J e_A$ are $mG_J e_T$ and $mG_J \delta_T$, respectively. Now β_M is not quite perpendicular to the direction of motion and hence it is not strictly accurate to regard $mG_J \beta_M$ as normal to the trajectory. However, the error introduced by this assumption is negligible compared to the uncertainty in the value of β_M or compared to the fluctuations in the value

of β_M during burning. Hence we have for the component of the jet forces along the trajectory

$$F_{J\parallel} = mG_J e_T, \quad (1)$$

and for the component normal to the trajectory ¹⁰

$$F_{J\perp} = mG_J \delta_T + mG_J \beta_M. \quad (2)$$

The moment produced by the jet can be reduced to the sum of a component directed along the axis and a component normal to the axis. All that we need know about the component, M_{Jz} that is directed along the axis is the angular acceleration, α , produced by it. This is usually determined empirically, although the theoretical treatment to be given in 8.52 may be used. As in 3.23 (4) and (6), the component normal to the axis is resolved into two parts and represented by the vector

$$f_J = f_R + f_{JD} = -mG_J \mathbf{R}_M - K_{JD} \mathbf{q}. \quad (3)$$

Here f_R represents the moment due to thrust malalignment; and \mathbf{R}_M , called the linear thrust malalignment, is a vector that rotates with the rocket. The jet damping moment is represented by f_{JD} ; the jet damping moment coefficient, K_{JD} , is discussed in 2.26 (15).

8.52 An Elementary Theory for the Spin Produced by Inclined Jets.—Let us first consider a simple approximate method that will suffice for most problems connected with the spin produced by inclined jets in rockets whose propellant weighs less than 20 percent of the total weight. Assume that there are N nozzles, all identical, arranged with their centers equally spaced about a circle of radius R_J , called the nozzle circle. In the usual spin-stabilized rocket the axis of each nozzle is perpendicular to the radial line connecting the center of the nozzle and the center of the nozzle circle and makes the angle η with a line parallel to the rocket axis. This angle, shown in figure 8.52, is usually called the nozzle cant angle. On the basis of these assumptions there will be no malalignment. As discussed following 2.21 (9), the thrust of each jet may be written as

$$\frac{1}{N} V_g \frac{d\mu}{dt}, \quad (1)$$

where V_g is the gas velocity and $d\mu/dt$ is the rate at which burnt gas is ejected. This thrust can be resolved into the component

$$\frac{1}{N} V_g \frac{d\mu}{dt} \cos \eta$$

parallel to the axis of the rocket, and the component

$$\frac{1}{N} V_g \frac{d\mu}{dt} \sin \eta$$

normal to the radial line from the center of the nozzle circle to the center of the nozzle. Hence the resultant of the thrusts produced by the N jets is the thrust

$$V_g \frac{d\mu}{dt} \cos \eta \quad (2)$$

¹⁰ If desired, a vector β_{MT} can be derived from β_M by the same process that \mathbf{q}_T is derived from \mathbf{q} in 8.21. Then (1) and (2), with β_M replaced by β_{MT} , are obtained by neglecting $\delta\beta_M$ compared to unity.

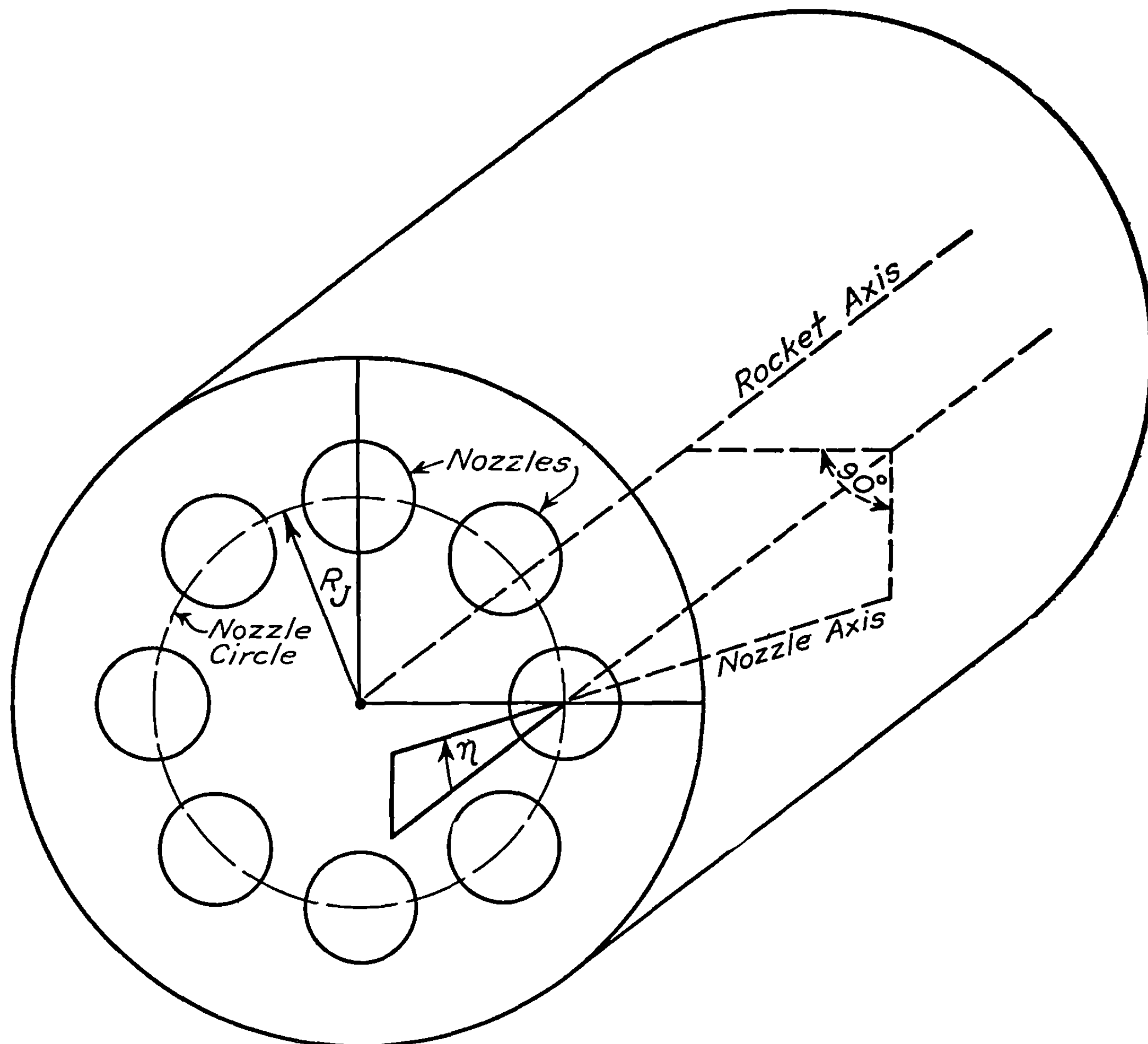


FIGURE 8.52.—Nozzle circle and the cant angle of the jet.

along the axis of the rocket, plus the torque

$$V_s \frac{d\mu}{dt} R_J \sin \eta \quad (3)$$

about this axis.

If the thrust given by (2) acts on the average mass $m_b + \frac{1}{2}\mu_b$, (where m_b is the mass of the solid parts remaining at the end of burning and μ_b is the total mass of gas ejected) for the time,

$$t_b = \mu_b \left/ \frac{d\mu}{dt} \right., \quad (4)$$

required to burn the propellant, it will impart a velocity at the end of burning given by

$$v_b = \frac{V_s \mu_b \cos \eta}{m_b + \frac{1}{2} \mu_b}. \quad (5)$$

Note that this is merely 2.21 (8) with the addition of the factor $\cos \eta$. If we let k be the radius of gyration about the longitudinal axis of the metal parts remaining after burning and κ_0 be that of the grain at the start of burning, the moment of inertia of the metal parts will be $m_b k^2$, that of the grain at the start of burning will be $\mu_b \kappa_0^2$; and we might assume that the average

moment of inertia of the rocket during burning is $m_b k^2 + \frac{1}{2} \mu_b \kappa_0^2$. If the torque given by (3) acts on a body having this moment of inertia for the time t_b , the spin at the end of burning will be

$$s_b \doteq \frac{V_g \mu_b R_J \sin \eta}{m_b k^2 + \frac{1}{2} \mu_b \kappa_0^2}. \quad (6)$$

The distance, ν_b , traveled by the rocket per revolution at the end of burning is therefore

$$\nu_b = \frac{2\pi v_b}{s_b} \doteq 2\pi \cot \eta \frac{m_b k^2 + \frac{1}{2} \mu_b \kappa_0^2}{R_J \left(m_b + \frac{1}{2} \mu_b \right)}. \quad (7)$$

When the difference between $\mu_b \kappa_0^2$ and $\mu_b k^2$ is negligible compared to $m_b k^2$, we have the simple form

$$\nu_b \doteq \frac{2\pi k^2}{R_J} \cot \eta. \quad (8)$$

This expression is also valid, to the same degree of approximation, for the distance, ν , traveled per revolution during burning, since in the above derivation it was assumed that both the linear and angular accelerations are proportional to $d\mu/dt$.

It is easy to see that (8) must break down in the case of rockets having high burnt velocities and a grain that does not rotate with the rocket. For in such cases the rocket will eventually get to spinning so fast that the gas will be able to flow backward along the motor and out the jets in a straight line, the rotation carrying the jets sideways so fast that the inclination is counteracted. In such circumstances the gas can exert no torque on the rocket. Hence v will increase while s remains constant, and therefore ν will increase during burning. In the next section a more careful analysis of such phenomena will be carried out on the basis of the principle of conservation of angular momentum. The main practical application of this more complete analysis is the determination of the factor by which ν increases during burning. This enables one to compute its value at the end of burning from measurements made near the launcher.

One point must not be overlooked if the nozzles are short. They may not be completely effective in making the gas flow along the nozzle axis, and instead the gas may tend to continue flowing parallel to the axis of the rocket. This difficulty can be met by using for the cant angle η an effective value which may be regarded as representing the amount that the inclined nozzle deflects its jet and which is to be determined so as to give agreement between the theoretical and experimental values of ν .

In the above treatment it was assumed that all nozzles had the same size, the same value of R_J , and the same cant angle. Cases not covered are those in which two or more circles of jets are used on large rockets, those in which there is a central, noninclined jet that is opened at high temperatures in order to keep the pressure in the motor from rising excessively, and those in which one set of jets is used to spin the rocket and another to drive it forward. All these cases can be covered by assuming that the nozzles are arranged in concentric circles of radii R_J' , R_J'' , R_J''' , etc. Let N' , N'' , N''' , etc. be the number of nozzles in the respective circles; η' , η'' , η''' , etc. be the corresponding nozzle cant angles; and F' , F'' , F''' be the thrusts produced by the individual jets of each circle. In case one nozzle is on the axis of the rocket, $R_J' = 0$, $N' = 1$, and $\eta' = 0$. The total thrust is

$$F_J = N'F' \cos \eta' + N''F'' \cos \eta'' + \dots, \quad (9)$$

and the total torque is

$$L_J = N'F'R_J' \sin \eta' + N''F''R_J'' \sin \eta'' + \dots, \quad (10)$$

Replacing (2) and (3) by (9) and (10), respectively, we find that (8) becomes

$$\nu = \nu_0 = 2\pi k^2 \frac{N'F' \cos \eta' + N''F'' \cos \eta'' + \dots}{N'F'R_J' \sin \eta' + N''F''R_J'' \sin \eta'' + \dots}. \quad (11)$$

Not only do these formulas enable one to estimate the value of ν to be expected for an untested rocket, but they also indicate how the nozzle should be arranged on a spin-stabilized rocket to get the maximum velocity. It is true that the decrease in velocity due to the inclination of jets is not large; but it is still desirable to minimize the effect. For example, if the inclination of each jet is 16° , the burnt velocity will be 3.9 percent less than if the jets were not inclined, and the range will be approximately 8 percent less. If the inclination of the jets is 12° , the burnt velocity will be reduced only 2.2 percent and the range only about $4\frac{1}{2}$ percent. Since in order to get satisfactory performance it is necessary to maintain a specified value of ν , it is evident that any decrease in η must be accompanied by other changes that maintain the spin and hence L_J . Evidently it is desirable to make the radius of each nozzle circle as large as possible and, if there is more than one such circle, to have as much of the thrust as possible in the largest circle, since this produces large torques with small values of η . After the best values of R , N , and F have been chosen for each circle of jets, there remains the problem of choosing the best value of η . If one wishes to maximize F_J while holding ν constant, one finds that it is necessary to have

$$\frac{\tan \eta'}{R'} = \frac{\tan \eta''}{R''} = \frac{\tan \eta'''}{R'''} = \dots = C, \quad (12)$$

where C is a constant of proportionality to be chosen so as to give the desired value of ν . If all η 's are small, so that $\cos \eta \doteq 1$ and $\sin \eta \doteq \tan \eta$, it follows from (11) that

$$C = \left(\frac{2\pi k^2}{\nu} \right) \frac{N'F' + N''F'' + \dots}{N'F'R_J'^2 + N''F''R_J''^2 + \dots}. \quad (13)$$

Minor departures from (12) do not lead to appreciable inefficiencies, but major departures may be serious. For example, since $\cos 16^\circ = 0.96$, a rocket that is both propelled and spun by a single circle of nozzles of cant angle 16° and nozzle circle radius R_J , will have a burnt velocity that is 96 percent of the velocity it would have if it were not spun and all the thrust devoted to propulsion. If this same rocket were propelled by a set of noninclined jets and were spun by a number of small jets set in a circle of radius $2R_J$ and arranged so that they tended only to spin the rocket and not to propel it forward, it would be necessary to use 13 percent of the total thrust in these latter jets in order to get the required value for ν . Hence the burnt velocity would be 87 percent of the velocity if the rocket were not spun or 91 percent of the velocity of the rocket whose nozzles were inclined at 16° .

8.53 A More Accurate Theory Based on Conservation of Angular Momentum.—In order to obtain a more accurate theory than the foregoing for the spin produced by inclined jets, it is necessary to base the treatment on the principle of the conservation of angular momentum

8.5 THE JET FORCES

and to use the assumptions of 2.21. We shall consider only the case in which there is a single circle of identical nozzles since the extension to more general cases is relatively easy.

Let us assume that the velocity with which the gas leaves a particular nozzle is V_g relative to the nozzle. Since the rocket is moving forward with linear velocity v and is spinning with angular velocity s about its longitudinal axis, the nozzle is moving forward with linear velocity v and is moving sideways with linear velocity sR_J . Hence, relative to the inertial system in which the rocket was at rest before firing, the velocity of the material in the jet is $v - V_g \cos \eta$ in the direction in which the rocket is going and $sR_J - V_g \sin \eta$ in a direction at right angles to this. Hence if in the time dt the mass of gas $d\mu$ is ejected, it will have a linear momentum along the axis of the rocket equal to $d\mu(v - V_g \cos \eta)$ and an angular momentum about this axis equal to $d\mu R_J(sR_J - V_g \sin \eta)$. This is true whether all this gas is ejected through one jet or through several. It should be noted that careful analysis might show that R_J refers to slightly different quantities in different parts of this paragraph since different points on the axis of a nozzle are at different distances from the axis of the rocket because of the nozzle cant. We shall assume however that it is sufficiently accurate throughout to use the radius of the nozzle circle.

If we made use of the theorem of the conservation of linear momentum, we would repeat the treatment of 2.21, except that V_g would be replaced by $V_g \cos \eta$ throughout. Hence we would get for the velocity at any time during burning

$$v = V_g \cos \eta \ln \frac{m_t}{m_t - \mu} = V_g \cos \eta \ln \frac{m_t}{m}; \quad (1)$$

and for the velocity at the end of burning

$$v_b = V_g \cos \eta \ln \frac{m_t}{m_b}, \quad (2)$$

where m_t is the total mass of the rocket and propellant at the start of burning, m is the total mass remaining at any time, μ is the mass of gas ejected up to any time, and m_b is the mass of the projectile after burning. Evidently μ_b is the initial mass of propellant and $\mu_b - \mu$ is the mass of unburnt propellant.

As before, let k be the radius of gyration about a longitudinal axis of the projectile after burning, so that $m_b k^2$ is the corresponding moment of inertia. We shall let κ be the radius of gyration of the propellant; hence $(\mu_b - \mu)\kappa^2$ is its moment of inertia about a longitudinal axis. This varies during burning both because μ varies and because κ may vary. Hence the total angular momentum of the rocket at any time during burning is $m_b k^2 s + (\mu_b - \mu)\kappa^2 s$, provided we assume that the propellant rotates with the same angular velocity as does the rest of the rocket. The increase in the angular momentum in the interval dt during which the mass of gas $d\mu$ is ejected is

$$m_b k^2 ds + (\mu_b - \mu)\kappa^2 ds - \kappa^2 s d\mu + 2(\mu_b - \mu)\kappa s \kappa' d\mu, \quad (3)$$

where $\kappa' = d\kappa/d\mu$. The change in the angular momentum of the gas inside the motor can be neglected since its mass is small compared to the mass of the rocket and since its flow pattern does not change appreciably during the interval dt . Since the angular momentum of the rocket plus that of the ejected gas is constant, we have

$$m_b k^2 ds + (\mu_b - \mu)\kappa^2 ds - \kappa^2 s d\mu + 2(\mu_b - \mu)\kappa \kappa' s d\mu + R_J(sR_J - V_g \sin \eta)d\mu = 0.$$

This reduces to the linear differential equation

$$\frac{ds}{d\mu} - \frac{\kappa^2 - (\mu_b - \mu)2\kappa\kappa' - R_J^2}{M_b k^2 + (\mu_b - \mu)\kappa^2} s = \frac{R_J V_g \sin \eta}{m_b k^2 + (\mu_b - \mu)\kappa^2}, \quad (4)$$

which can be solved as soon as the dependence of κ on μ is known.

We shall consider the solution of (4) in three special cases.

Case I. The grain does not rotate. The above equations are valid here, except that the terms containing $(\mu_b - \mu)\kappa^2$ are omitted throughout, since the propellant contributes nothing to the angular momentum of the system. This is equivalent to setting $\kappa=0$ throughout the above derivation of (4). The solution, readily obtained by separation of variables, is given by

$$s = \frac{V_g \sin \eta}{R_J} \left[1 - \exp\left(-\frac{\mu R_J^2}{m_b k^2}\right) \right]. \quad (5)$$

The initial condition used for this solution, as for those to follow, is that $s=0$ when $\mu=0$.

Case II.—The grain rotates with the rocket and has a constant radius of gyration $\kappa=\kappa_0$, so that $\kappa'=0$. This is an appropriate approximation in the case of cylindrical grains that burn on both the outer and inner surfaces, although strictly speaking κ decreases slightly during the burning. The solution in this case is given by

$$s = \frac{V_g R_J \sin \eta}{R_J^2 - \kappa_0^2} \left[1 - \left(1 - \frac{\mu \kappa_0^2}{m_b k^2 + \mu_b \kappa_0^2} \right)^{\frac{R_J^2 - \kappa_0^2}{\kappa_0^2}} \right], \text{ if } R_J \neq \kappa_0; \quad (6)$$

or

$$s = -\frac{V_g \sin \eta}{\kappa_0} \ln \left(1 - \frac{\mu \kappa_0^2}{m_b k^2 + \mu_b \kappa_0^2} \right), \text{ if } R_J = \kappa_0. \quad (7)$$

Case III.—Here we assume that the square of the radius of gyration of the grain is proportional to its mass so that

$$\kappa^2 = \kappa_0^2 \frac{\mu_b - \mu}{\mu_b}, \quad 2\kappa\kappa' = -\frac{\kappa_0^2}{\mu_b}. \quad (8)$$

This corresponds to the case of a solid cylinder burning on its outer surface only and should be a useful approximation for cruciform grains. The solution in closed form for this case is too complicated to be of any practical use, hence recourse is had to a power series in the moments of inertia. We find that

$$s = \frac{V_g \mu R_J \sin \eta}{m_b k^2} \left[1 - \frac{R_J^2 \mu}{k^2 m_b} - \frac{\kappa_0^2 (\mu_b - \mu)^2}{k^2 m_b \mu_b} + \frac{1}{6} \left(\frac{J_J^2 \mu}{k^2 m_b} \right)^2 \right. \\ \left. + \frac{R_J^2 \kappa_0^2 \mu (12\mu_b^2 - 20\mu_b \mu + 9\mu^2)}{12k^4 m_b^2 \mu_b} + \frac{\kappa_0^4 (\mu_b - \mu)^4}{k^4 m_b^2 \mu_b^2} + \dots \right]. \quad (9)$$

It should be noted that nowhere in the derivation of (4) is anything assumed as to the rate of burning; hence the results hold for all types of burning. The value of s_b , the spin at the end of burning, is readily obtained by setting $\mu=\mu_b$.

Although these expressions appear to have a wide diversity of form, they all lead to essentially the same expression for s_b for all usual rockets. This is shown in figure 8.53, which shows the distance traveled per turn as a function of the mass of propellant burned for two types of

rockets. By plotting $\nu/R_J \cot \eta$ against μ/μ_b a form is obtained that is independent of the values of R_J , η , V_g , and depends only on the ratios μ_b/m_b , κ_0^2/k^2 , and R_J^2/k^2 . The values of these ratios for the example in which $\mu_b/m_b=1/10$ were chosen so that the results would be applicable to an early model of the 3.5/4 GPSR, while the values in the example for which $\mu_b/m_b=1/3$ were chosen to correspond to data pertaining to a 15-cm German rocket. The value of ν was obtained from (1) and that of s from (5), (6), and (9). In addition the results obtained from the approximation of 8.52 (8) are shown. It is evident that there is an appreciable change in the value of ν between the beginning and end of burning and that whether or not the grain rotates with the round is important at the beginning of burning but not at the end. An estimate of the friction between the grain and its support indicates that the grain should rotate with the rocket.

Investigation of the solutions obtained shows that they have a number of interesting and

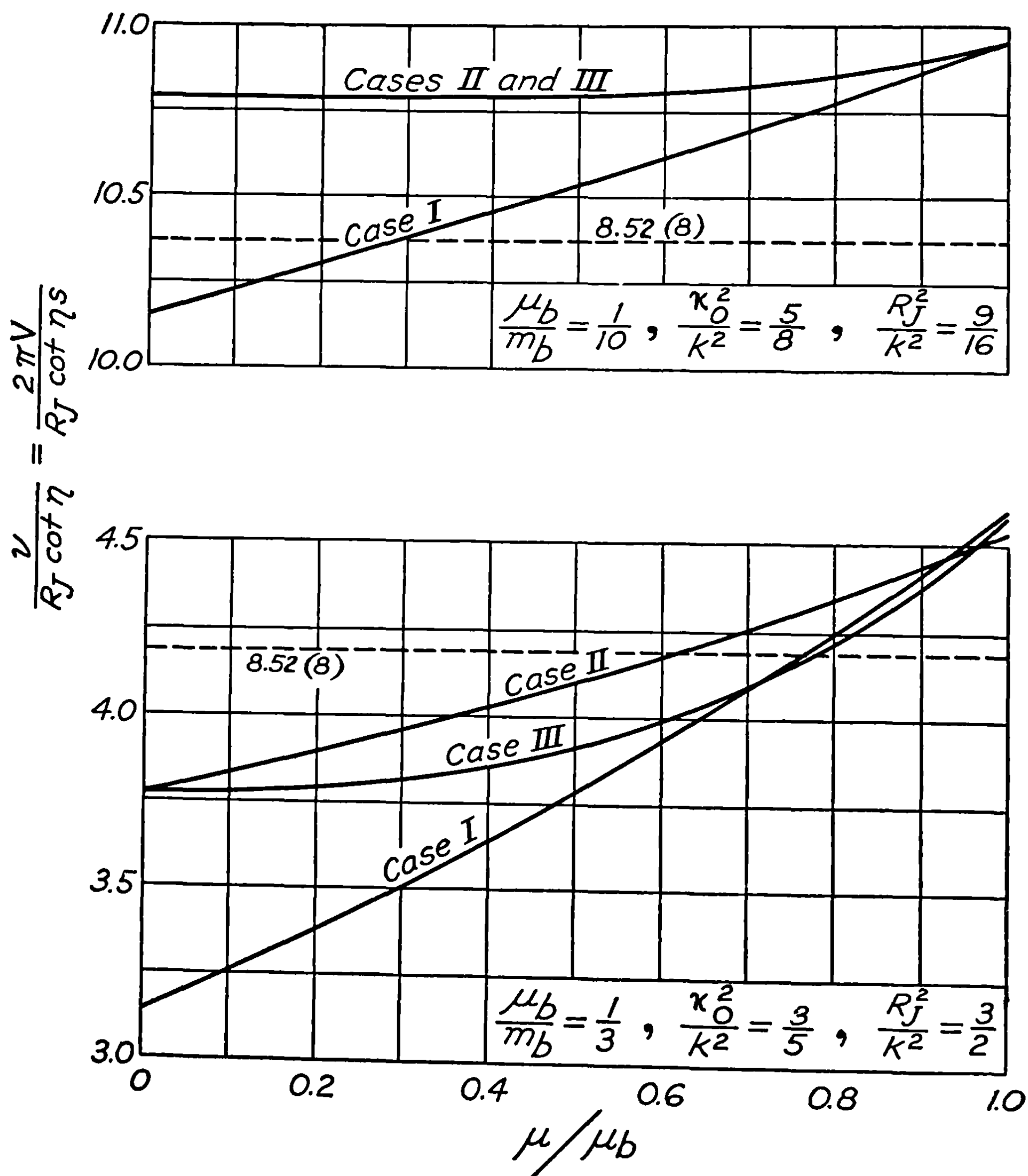


FIGURE 8.53.—Variation during burning of the distance traveled per turn, as computed from various theoretical formulas.

sometimes paradoxical properties. The approximate formula 8.52 (8) will give a value of ν at the end of burning that is too high or too low depending on whether k is greater than or less than R_J . At the start of burning the angular acceleration is obtained by dividing the torque produced by the jets, as calculated from the elementary expression 8.52 (3), by the moment of inertia of all rotating parts. If the grain rotates, the moment of inertia is greater than if it does not; hence the initial angular acceleration is greater in case I than in cases II and III. But by the end of burning the angular velocity is greatest in case II, and least in case I, with case III lying about midway between. The explanation of this paradox is easily obtained if one considers the angular momentum of the rocket and the equal and opposite angular momentum of the ejected gas. The angular velocity of the rocket during the early stages of burning is, as would be expected, smaller when the propellant must be rotated. Hence the angular velocity and angular momentum of the ejected gas in the opposite direction is larger. But at the end of burning the total angular momentum of the system is zero. Consequently the angular momentum of the rocket at the end of burning, and the equal angular momentum of the gases in the opposite direction, will be greater when the propellant rotates with the rocket.

There is another point of view that leads to the same qualitative conclusion. During the initial phase of the burning, the gas flows from the front end of the motor tube and is deflected as it passes through the nozzles, thus giving a sideways thrust to the rocket and producing spin. If, later, the gases and propellant were to have no rotation, it would be possible for the rocket to spin at such a rate that the rotation would carry the nozzles sideways fast enough to allow the burnt gases to flow straight back out of the nozzles, in a direction exactly opposite to the direction of flight of the rocket. Hence the gas would give no side thrust to the nozzle and the spin will not increase. If the propellant rotates with the motor, the gas in the motor must rotate too. Consequently the gas will be deflected as it comes out of the nozzles and will therefore produce further angular acceleration.

It is of some interest to consider the behavior of the rocket when very large propellant masses are used. Any desired linear velocity can be obtained, in theory, by making μ_b/m_b large enough. At the start of burning, large amounts of linear momentum are stored in the unburnt propellant, and much of this momentum is transferred to the rocket during the last stages of burning. The spin, on the other hand, may behave differently. Equation (5) shows that in case I the spin can never exceed $(V_g/R_J) \sin \eta$, this value being approached asymptotically if $\mu_b R_J^2 \gg m_b k^2$. This behavior is easily understood since if the grain does not rotate, no angular momentum can be stored in it to be transferred subsequently to the metal parts. This limit would be of importance only in the case of rockets for which $\mu_b R_J^2 \geq m_b k^2$. Thus its effect can be controlled both by the value of μ_b/m_b and that of R_J^2/k^2 . In the usual rocket, one never comes close to the limiting spin.

It follows from (4) that the spin stops increasing; i. e., $ds/d\mu=0$, when s equals

$$s_E = \frac{V_g \sin \eta}{R_J} \frac{R_J^2}{R_J^2 - \kappa^2 + (\mu_b - \mu) 2 \kappa \kappa'} \quad (10)$$

which we call the equilibrium spin. Hence in case II where $\kappa'=0$, s could increase indefinitely if $\kappa > R_J$; while if $\kappa < R_J$ the behavior would be similar to case I except that the limiting spin is larger. When $\kappa > R_J$ the propellant as it burns and passes out the jets draws nearer to the axis of the rocket and hence, since it conserves its angular momentum, tends to spin even faster than the rocket. Thus it can always impart torque as it passes out the nozzles. On the other hand, if $\kappa < R_J$ the gas must move outward between burning and entrance into the nozzles. Thus it enters the nozzles while spinning more slowly than the rest of the rocket

and may not be able to produce any angular acceleration. The analysis in case III is similar but more complicated because of the variation in κ which leads to a decrease in s_E during burning. At the end of burning s_E has the same value as in case I. It would even be possible for s to increase throughout most of the burning period, reaching a maximum when the decrease in s_E made it equal to s ; subsequently s would decrease but would remain slightly larger than s_E as computed from (10).

In any practical calculation of v , s , and ν on the basis of a theory of the type discussed above and in 2.2, one should not lose sight of the following complications. If one is not firing horizontally, gravity may affect v appreciably, and the aerodynamic resistance may affect both v and s in the case of high-velocity rockets. It is possible, however, to apply corrections for these effects. Quantities that are less easy to evaluate are the effective values of R_J , η , and V_g . It should be satisfactory to assume that the center of action of each nozzle is at the center of its throat and hence to fix R_J . Since the observed ν at the end of burning in the 3.5/4 GPSR agrees satisfactorily with the value computed from (2), and from (6) or (9), it seems clear that both η and V_g have about the significance ascribed above. But it has sometimes been suggested that it is not completely satisfactory to assume that the ejected gas stops interacting with the nozzle at the instant it acquires the velocity V_g and that all the jet forces should be computed on this basis. If the nozzles are underexpanded, a pressure higher than normal may be induced over the entire base of the rocket and this pressure might tend to propel the rocket without tending to spin it. This is supported by the observation that ν depends on the motor temperature of the rocket, varying in the case of one 5-in. rocket from 5.8 to 6.2 feet as T goes from 0° to 100° F. This is to be expected since the underexpansion, and hence the base pressure, are greater at high temperatures. This situation could probably be treated by using empirical values of V_g , taking different values for calculating v and s . The empirical values could be chosen to fit either the observed initial values or the observed values at the end of burning, and the theoretical expressions given above could then be used to calculate v and s throughout the burning period.

CHAPTER 9

THE MOTION DURING BURNING AND DURING LAUNCHING

9.0 Introduction

In considering the motion of spin-stabilized rockets during burning, the gyroscopic effects must be taken into account. The first section of this chapter is devoted to the introduction of coordinate systems suitable for the description of the complete motion and to the reduction of the equations of motion of a rigid body to a form adapted to computation. The techniques used for handling the angular motion of a symmetrical rigid body should be useful in most problems involving such bodies; for example, the same equations are used in chapter 10 in describing the motion of shells and rockets after burnout.

The remainder of the chapter gives the solutions of the equations of motion in enough cases so that by superposition one can find the most general motion during burning of a ground-fired, spin-stabilized rocket of the types described in 8.1. The theory has been confirmed in numerous special cases by experimental measurements. It was used in the reduction of a great deal of experimental data for the construction of range tables and gave a complete explanation of the observations. Since the theory is a logically consistent whole, confirmation of part of it tends also to support the rest. Of course, what is confirmed is not the basic laws, but, instead the assumptions concerning the properties of the rockets. If in the future rockets having more propellant and higher burnt velocities are considered, it may no longer be possible to neglect such things as the variation in the moments of inertia during burning and in this case a more elaborate theory will be required. The main residual difficulties with the theory as applied to current rockets are in connection with firing from airplanes where the mathematical difficulties in solving the equations of motion are most formidable and where the physical difficulties in a determination of the significant aerodynamic forces are as bad. There are also some mathematical difficulties in the detailed study of ground-fired spinners due to the nonlinearity of some of the forces and moments.

9.1 Derivation and Reduction of the Equations of Motion of a Symmetrical Rotating Projectile

The projectiles that we shall now consider rotate rapidly about a longitudinal axis of symmetry. When describing the motion of the projectile, we are interested principally in the direction of motion of the center of mass and in the orientation of the axis of symmetry; usually we do not care to specify the amount of rotation about this axis, although we must, of course, know the rate of rotation. The motion of the axis of symmetry is complicated by gyroscopic effects due to the spin, and an exact solution of a problem as simple as that of a top rotating under the influence of no forces except gravity is not at all convenient for computation because of the elliptic functions involved. Since we are interested in solving much more complicated problems in which the projectile is acted on by a variety of forces and moments, in particular an axial moment that accelerates the spin, it is obvious that progress can be made only by introducing judicious approximations. It will be found that very satisfactory approximate solutions are possible in the cases—those of practical importance—in which the motion of the axis of symmetry is small.

We shall first give a simple derivation of the approximate equations of motion, treating them and the properties of their solutions in some detail. This procedure introduces in a relatively simple background the important physical concepts, the coordinate systems, the differ-

ential equations of motion, and the basic methods of solving them used in most of the important phases of our study. Then, starting with 9.16, we shall introduce a more rigorous derivation of the differential equations, introducing no more approximations than seem necessary and analyzing the errors introduced by each approximation. The approximations in both treatments are based on the assumption that the various angles involved are small; and in the limit in which the angles approach zero, the simple treatment approaches the more rigorous treatment.

It would be possible, and might appear more logical, to start with exact equations of motion and to use them as long as possible in order to show clearly which results can be derived exactly and hence hold generally. One could then introduce the necessary approximations singly, estimating the effect of each as he went along. After the lengthy exact discussion, one would obtain the approximate equations of motion given toward the end of 9.11 by neglecting a number of small terms; finally he would consider the solution of the approximate equations and the estimation of the errors involved.¹ However, this method of procedure would bury most of the important concepts in a maze of less important mathematical detail.

9.11 Approximate Equations of Motion.—We describe the motion of the projectile with the aid of a right-handed Cartesian coordinate system $OX_1Y_1Z_1$ whose origin moves with the center of mass of the rocket but whose axes always remain parallel to their original directions. Thus we have a nonrotating coordinate system with an accelerated origin. As shown in figure 9.11a the OX_1 -axis is horizontal. It is taken perpendicular to the trajectory at some convenient point, usually on the launcher, and its positive direction is to the right. The positive direction of the OZ_1 -axis is down range; this axis can be either horizontal, as in 9.11a, or parallel to the launcher, whichever is more convenient. The positive direction of the OY_1 -axis is downward; it is vertical only if OZ_1 is horizontal.

We specify the direction of the axis of the projectile by means of the angle φ_x between the axis and the OY_1Z_1 -plane and the angle φ_y between the axis and the OX_1Z_1 -plane.² A

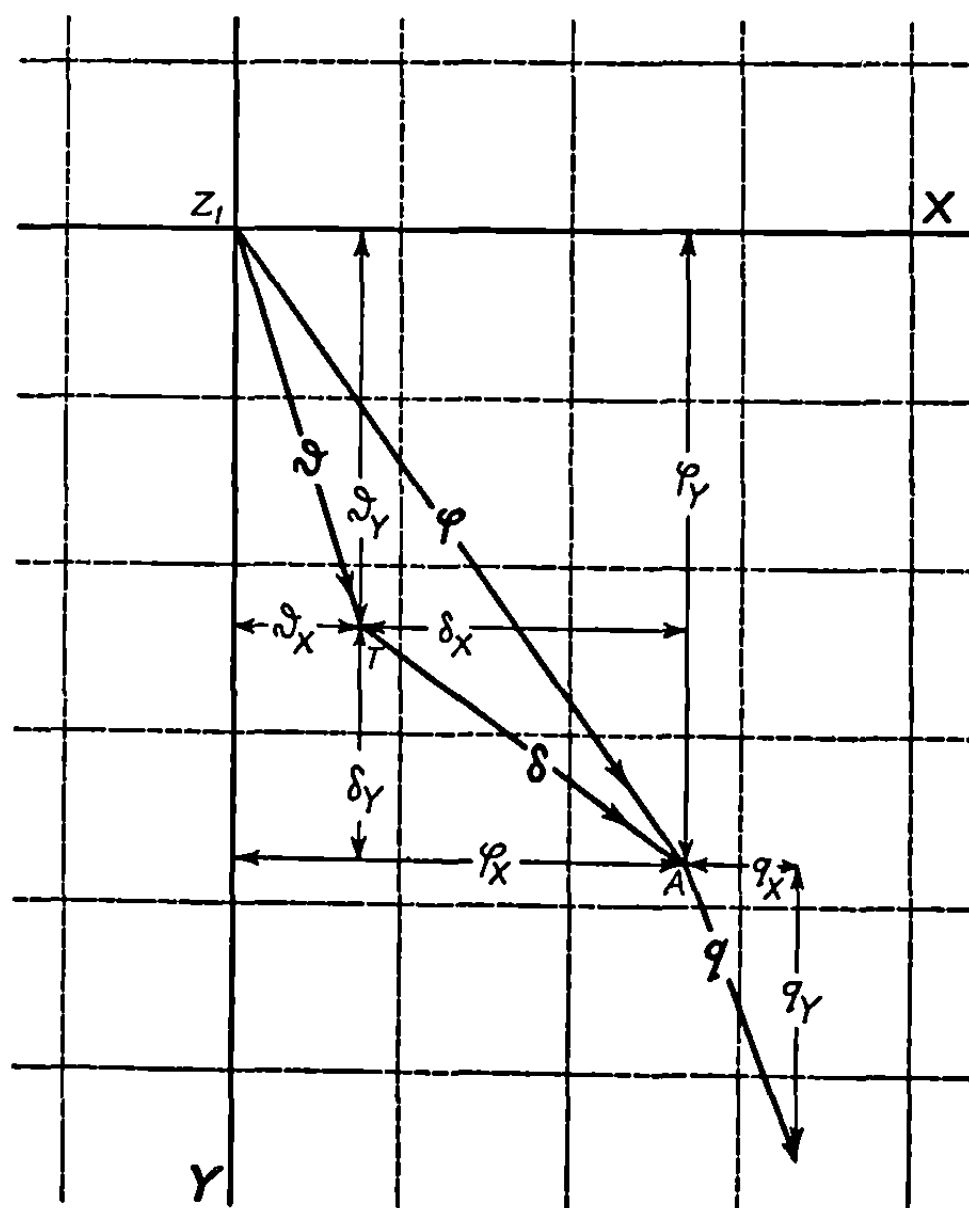
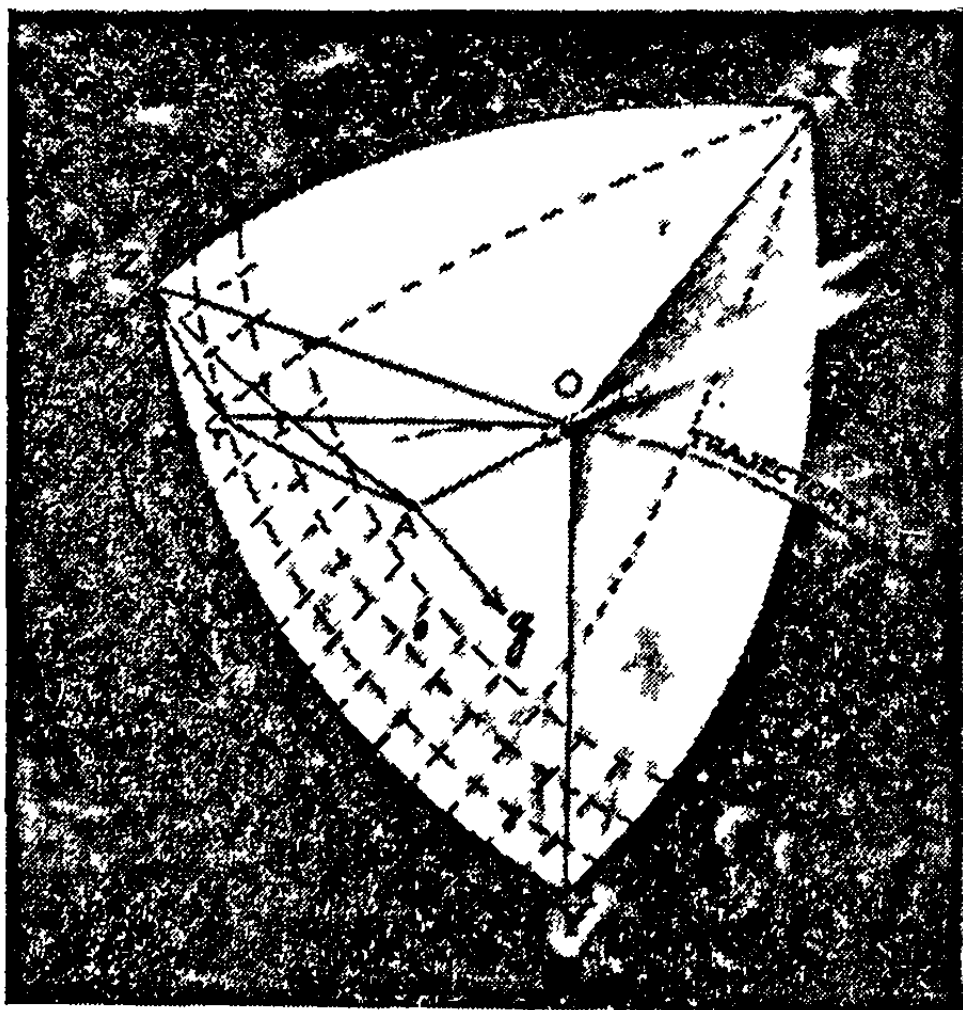


FIGURE 9.11.—The coordinate system used in the description of the motion. a. b.

¹ If this procedure is to be followed, the sections should be read in the following order: 9.14, 9.15, 9.16, 9.17, 9.18, 9.11, 9.12, 9.13, 9.19.

² Strictly, φ_y is defined as in 9.16 to be the angle between the plane in which φ_x is measured and the OX_1Z_1 -plane. When φ_x is small the two definitions are nearly equivalent and the approximate definition is the more convenient. Similar remarks hold for δ_y .

very useful way of visualizing the meaning of the coordinates φ_x and φ_r is the following. Consider the sphere shown in 9.11a having unit radius and center at O , the center of mass of the projectile. The axis of the projectile pierces the sphere at the point A . One can then regard φ_x and φ_r as the coordinates of A in an approximately Cartesian coordinate system whose origin is on the Z_1 -axis, whose X -axis starts parallel to OX_1 and whose Y -axis is wrapped around the sphere in the OY_1Z_1 -plane. A small section of this coordinate system is shown in figure 9.11b. It is then natural to introduce the single complex number φ , defined to be

$$\varphi = \varphi_x + i\varphi_r, \quad (1)$$

to specify the orientation of the axis of the projectile and to locate the point A on the sphere. Thus (1) defines the complex number associated with the point A in an Argand diagram wrapped around the sphere, and (1) can be regarded as the complex representation of the two-dimensional vector locating the point A . The absolute value or modulus of φ is denoted by

$$\varphi = (\varphi_x^2 + \varphi_r^2)^{\frac{1}{2}}, \quad (2)$$

and is, approximately, the angle between OZ_1 and the projectile axis. It should be noted that the argument of φ ; i. e. $\tan^{-1}(\varphi_r/\varphi_x)$, is measured in a clockwise, rather than a counterclockwise, direction as seen when looking in the direction in which the projectile is moving. This is necessary because of the relative orientation of the OX_1 and OY_1 axis in our right-handed coordinate system; it is convenient since the rotation, the nutation, and the precession of the projectile are all clockwise as seen from the rear. The velocity with which the point A moves on the surface of the unit sphere may be denoted by the complex number q where

$$q = q_x + iq_r = \dot{\varphi}_x + i\dot{\varphi}_r = \dot{\varphi}, \quad (3)$$

the dot denoting differentiation with respect to time.

Corresponding coordinates are used to specify the direction of rocket motion. This direction is that of the tangent to the trajectory at O . Let ϑ_x be the angle between the tangent and the OY_1Z_1 -plane and ϑ_r be the angle between the tangent (footnote 2) and the OX_1Z_1 -plane. Then ϑ_x and ϑ_r can be regarded as being the coordinates of the point T at which the tangent to the trajectory pierces the unit sphere. The direction of motion can be specified by the single complex number ϑ defined to be

$$\vartheta = \vartheta_x + i\vartheta_r \quad (4)$$

The complex number ϑ can then be regarded as the complex representation of the two-dimensional vector locating T .

The yaw of the rocket is completely specified both as to magnitude and orientation by means of the complex number

$$\delta = \varphi - \vartheta, \quad (5)$$

which can be regarded as representing the two-dimensional vector from T to A . The magnitude of the yaw is denoted by

$$\delta = (\delta_x^2 + \delta_r^2)^{\frac{1}{2}} = [(\varphi_x - \vartheta_x)^2 + (\varphi_r - \vartheta_r)^2]^{\frac{1}{2}} \quad (6)$$

in agreement with the current usage both of the symbol δ for the angle of yaw and of the symbol

δ for the absolute value of δ . The quantity designated as ϕ by Hayes³ and called angle of orientation is, in our notation, the argument of δ plus $(\pi/2)$. It must be recognized that the statements in this paragraph involve certain approximations which are considered in 9.18. As long as $\delta \ll 1$, the errors due to these approximations are negligible.

The total force acting on the rocket is the sum of the aerodynamic forces, the force of gravity, and the jet forces. The total force can be resolved into the three components F_z , F_x , and F_y , where $F_z = F_{\parallel}$ is the component parallel to the direction of motion, F_x is the component in a horizontal direction perpendicular to the direction of motion, and F_y is the component in the direction perpendicular to both F_x and F_z . The positive directions are forward, to the right, and downward, respectively. The two components normal to the direction of motion can be combined to give the complex number

$$\mathbf{F}_{\perp} = F_x + iF_y, \quad (7)$$

which can be regarded as the complex representation of a two dimensional vector.

The total torque or moment acting on the rocket is the sum of the aerodynamic torques and the jet torques. The total moment can be resolved into a component M_z along the longitudinal axis of the projectile and a component perpendicular to this axis. The component M_z changes the rate of spin of the rocket while the other component affects the orientation of the longitudinal axis. It is convenient to discuss the effect of this second component of the moment in terms of the force, \mathbf{f} , defined in 8.21, that would have to be applied perpendicular to the axis of symmetry at a point unit distance ahead of the center of mass in order to produce the moment. We may resolve \mathbf{f} into a horizontal component, f_x , and a component f_y in a direction perpendicular to both the axis of symmetry and f_x , the directions being essentially the same as those of the X and Y components of \mathbf{F}_{\perp} . The complex representation of the transverse moment is

$$\mathbf{f} = f_x + if_y. \quad (8)$$

We can now write the equations of motion of the projectile in terms of v , the velocity of the projectile; s , its spin or angular velocity in radians/sec.; m , its mass; k , its radius of gyration about the longitudinal axis; K , its radius of gyration about a transverse axis through the center of mass and γ , which equals K^2/k^2 . A dot will be used to indicate differentiation with respect to time. From Newton's second law it follows that the motion along the trajectory satisfies the equation

$$\dot{v} = F_{\parallel}/m, \quad (9)$$

and from the corresponding law for rotation about an axis it follows that the spin about the longitudinal axis satisfies the equation

$$\dot{s} = M_z/mk^2. \quad (10)$$

If Newton's second law is applied to the acceleration normal to the trajectory, one finds that the direction of motion satisfies the equation

$$v\dot{\theta} = F_{\perp}/m. \quad (11)$$

If the real and imaginary parts of this equation are considered separately, it can be regarded

³T. J. Hayes, "Elements of Ordnance," Wiley, 1938.

as derived from 3.22 (4). As will be shown in 9.16, the orientation of the longitudinal axis approximately satisfies the equation ⁴

$$\ddot{\phi} - i(s/\gamma)\dot{\phi} = f/mK^2. \quad (12)$$

The meaning of this equation can be understood from the following considerations. If the rocket were not spinning, so that $s=0$, the real part of (12) would become

$$\ddot{\phi}_x = f_x/mK^2. \quad (13)$$

This equation, as one would expect, states that the transverse angular acceleration is equal to the torque acting (f_x has the magnitude of the appropriate component of the torque) divided by the moment of inertia about a transverse axis. A similar statement holds for the imaginary part of (12). The middle term of (12) is of importance in spinning projectiles, where $s \neq 0$, since its presence is connected with the gyroscopic effects that complicate the motion. The quantity $i(s/\gamma)\dot{\phi}$ is the acceleration produced by gyroscopic effects in addition to the acceleration f/mK^2 produced by the applied torques. It is frequently convenient to think of this gyroscopic acceleration as being due to the gyroscopic torque,

$$mK^2 i(s/\gamma)\dot{\phi}, \quad (14)$$

acting normal to the direction of motion A . This is perfectly proper as long as it is remembered that (14) is not a true torque produced by the action of external bodies on the projectile. Rather it is the fictitious torque that would cause a nonspinning projectile to have the same motion that the spinning projectile has, in obedience to Newton's equations, without its application. The derivation in 9.14 of this expression for the gyroscopic acceleration can be used as the basis of an alternative derivation of (12).

Before we can consider the solutions of (9), (10), (11), and (12), expressions must be obtained for the forces and moments $F_{||}$, M_z , F_{\perp} , and f . At no time will an attempt be made to consider the complicated case in which the most general possible aerodynamic forces, jet forces, and gravitational forces act on the body. Instead, we shall consider in this and the succeeding chapter a variety of special cases in which particular forms are assumed for the various forces. There is no point in listing here all the cases that will be considered; instead, we shall limit the present discussion to a generalization of the most important case. Having

⁴ An approximate derivation of this equation can be based on the form of Euler's equation given by Leigh Page, "Introduction to Theoretical Physics," ed. 2, Van Nostrand, 1935. From equations (37-10) or (44-1) one has

$$mK^2 \dot{\omega}_x + m(k^2 - K^2)\omega_y \omega_z + mk^2 s \omega_y = M_x,$$

and

$$mK^2 \dot{\omega}_y + m(K^2 - k^2)\omega_x \omega_z - mk^2 s \omega_x = M_y,$$

where as a temporary notation, the z -axis is directed along the axis of the projectile, the x -axis is horizontal, and the y -axis is normal to the other two. The components of the angular velocity of the coordinate system are ω_x , ω_y , ω_z ; the spin of the projectile with respect to these coordinates is s ; and the components of the total moment acting on the projectile are M_x , M_y , and M_z . We can neglect the second term in each of these equations since ω_z , the z -component of the angular velocity on the coordinate system, is so much smaller than s , the spin of the projectile. If we note that

$$\dot{\phi}_x \doteq \dot{q}_x = \omega_y, \quad f_x = M_y,$$

and

$$\dot{\phi}_y \doteq \dot{q}_y = -\omega_x, \quad f_y = -M_x,$$

Euler's equations become

$$mK^2 \ddot{\phi}_x + mk^2 s \dot{\phi}_y = f_x,$$

and

$$mK^2 \ddot{\phi}_y - mk^2 s \dot{\phi}_x = f_y,$$

which correspond to the real and imaginary parts of (12).

obtained the properties of the solutions in this case, it will be easy to deduce the properties of the solution in any other case.

We assume that the linear and angular accelerations,

$$G = F_{\parallel}/m \quad (15)$$

and

$$\alpha = M_z/mk^2 \quad (16)$$

are known functions of t so that y and s can be obtained as known functions of t by integrating (9) and (10). During burning, G and α are determined principally by the jet forces, although gravity and the aerodynamic forces do influence their values to a minor extent. The only one of the transverse aerodynamic forces and moments that we include is the overturning moment $f_{v^2\delta}$, which, according to 8.22 (9), satisfies the equation

$$\frac{1}{mK^2} f_{v^2\delta} = \frac{s^2}{4\gamma^2 S} \delta, \quad (17)$$

where S is the stability factor. We assume that there is no wind so that V , the velocity with respect to the air, is equal to v , the velocity with respect to the launcher, that $f_{v^2\delta}$ is proportional to $V^2\delta$ and that during burning s is proportional to v , so that S is a constant. The linear acceleration produced by the jet forces is G_j acting along the axis of the rocket. It produces the acceleration $G_j \sin \delta$ normal to the trajectory and in the direction of the yaw. Hence when $\delta \ll 1$ and G_j is large compared to g , so that $G_j \approx G$, the contribution of the jet force to F_{\perp}/m is approximately

$$G\delta. \quad (18)$$

During burning the deflection of the trajectory is small. Hence if θ_0 is the quadrant elevation of the launcher, the contribution of gravity to F_{\perp}/m is approximately $ig \cos \theta_0$.

Hence (12), (11), and (5) become, respectively,

$$\ddot{\varphi} - i\frac{s}{\gamma} \dot{\varphi} - \frac{s^2}{4\gamma^2 S} \delta = \frac{1}{mK^2} f_I(t), \quad (19)$$

$$\dot{\vartheta} - \frac{G}{v} \delta = \frac{1}{m v} F_I(t), \quad (20)$$

and

$$\varphi - \vartheta - \delta = 0, \quad (21)$$

where $F_I(t)$ includes the gravitational force

$$img \cos \theta_0 \quad (22)$$

and any other forces, such as that due to the angular malalignment, which can be regarded as known functions of the time and which consequently are to be treated as inhomogeneous terms in the solution of the differential equations. Likewise $f_I(t)$ is the sum of all inhomogeneous terms that may come into (12) due to moments, such as that caused by the linear malalignment, which can be regarded as known functions of time.

Let us now consider the problem of developing the initial conditions subject to which these equations are to be solved. We have already assumed that the rocket starts from rest

at $t=0$. At first it slides along the launcher, both bourrelets being more or less constrained, and then there follows a period during which only the rear bourrelet is constrained. Finally, at $t=t_p$, the launching period is over and the motion becomes governed by (19), (20), and (21). We regard the values of ϕ , $\dot{\phi}=q$, and δ at this instant as being our arbitrary initial conditions. They are determined sometimes from photographic measurements and sometimes from a mathematical analysis of the motion during the launching period. When the values of these three quantities are given at this instant, (19), (20), and (21) determine the values of ϑ and of all derivatives of $\dot{\phi}$, ϑ , and δ at $t=t_p$ as well as the values of ϕ , ϑ , and δ at all later times. We might have taken ϕ and ϑ rather than ϕ and δ to define our initial conditions, but this choice would not turn out to be as convenient. We denote the values of these quantities at launching by the subscript p (chosen because the launcher was originally called a "projector") and hence write our initial conditions as being that

$$\phi = \phi_p, \delta = \delta_p, \dot{\phi} = q_p, \text{ when } t = t_p. \quad (23)$$

Occasionally it may be convenient to take t_p , the time at which the initial conditions are specified, to be sometime later than that at which all contact with the launcher is broken. In this case the functions making up the solutions have physical significance at times earlier than t_p since the solutions then give the motion that the system must have had during the time that the forces acting on it were those used in the equations of motion.

We usually find it both convenient and necessary to assume that G and α are constant throughout burning and that v and s are both zero at $t=0$, the time of ignition. Hence (9) and (10) can be integrated to give

$$v = Gt \quad (24)$$

$$d = \frac{1}{2} Gt^2 \quad (25)$$

$$s = \alpha t \quad (26)$$

and

$$\psi = \frac{1}{2} \alpha t^2 \quad (27)$$

where d is the distance traveled along the trajectory and ψ is the angle through which the rocket has rotated about its axis of symmetry since ignition. These assumptions are frequently very close to the actual situation and they give a very convenient description of it. It is necessary to make these assumptions since otherwise, except in unusual cases, the only method of procedure is the laborious one of numerical integration.

It is now possible to simplify our solutions by introducing some new parameters and making a change in the independent variable. The parameters are

$$\nu = \frac{2\pi v}{s} = \frac{2\pi G}{\alpha} = \frac{4\pi d}{\alpha t^2}, \quad (28)$$

and

$$\lambda = \gamma \nu \quad (29)$$

where ν is the distance traveled by the rocket per revolution about its longitudinal axis and λ will be found at the end of 9.14 to be the distance traveled in vacuum per nutation.⁶ For

⁶ The terms "nutation" and "precession" are used in slightly different senses by different authors. The meanings used in the present work are best described in 70.11 which the reader might well read at this time.

many rockets λ is of the order of magnitude of 100 feet. The quantities $(2\lambda/G)^{\frac{1}{2}}$ and $(2\lambda G)^{\frac{1}{2}}$ occur frequently in the solutions and will be abbreviated by the symbols

$$t_\lambda = (2\lambda/G)^{\frac{1}{2}} = (4\pi\gamma/\alpha)^{\frac{1}{2}} \quad (30)$$

and

$$v_\lambda = (2\lambda G)^{\frac{1}{2}} \quad (31)$$

since they are the time required to travel the distance λ , starting from rest, and the velocity at t_λ , respectively. The new independent variable ζ is a dimensionless parameter proportional to t and defined by the equation

$$\zeta^2 = \frac{\alpha t^2}{4\pi\gamma} = \frac{t^2}{t_\lambda^2} = \frac{d}{\lambda} = \frac{\psi}{2\pi\gamma}. \quad (32)$$

Making this change of variables and denoting differentiation with respect to ζ by a prime, we find that (19), (20), and (21) become

$$\varphi'' - 4\pi i \zeta \varphi' - \frac{4\pi^2 \zeta^2}{S} \delta = \frac{t_\lambda^2}{mK^2} f_I(\zeta) = 4\pi f_I(\zeta)/M_z, \quad (33)$$

$$\vartheta' - \frac{1}{\zeta} \delta = \frac{1}{mG\zeta} F_I(\zeta) = \zeta^{-1} F_I(\zeta)/F_{II}, \quad (34)$$

and

$$\varphi - \vartheta - \delta = 0. \quad (35)$$

We use these equations, with λ and ζ defined as above, both in air and in vacuum, but only in the latter case is λ the distance traveled per nutation.

The initial conditions must now be stated in terms of ζ , which at the instant of launching has the value

$$\zeta_p = t_p/t_\lambda = (p/\lambda)^{\frac{1}{2}} \quad (36)$$

where p is the distance traveled at $t=t_p$.

Hence (23) becomes

$$\varphi = \varphi_p, \quad \delta = \delta_p, \quad \varphi' = \varphi_p' = q_p t_\lambda, \quad \text{at } \zeta = \zeta_p. \quad (37)$$

During burning it is occasionally desirable to consider the linear or angular displacement of the rocket from the launcher line, the straight line along which a perfect rocket would travel if acted on by no forces whatever except the ideal jet forces. The coordinates of the center of mass of the rocket are X_0, Y_0, Z_0 in a right-handed Cartesian coordinate system whose origin, O_0 , remains fixed at the point occupied by the center of mass of the rocket just before ignition. The $O_0 Z_0$ axis lies along the launcher line, the $O_0 X_0$ -axis extends horizontally to the right from O_0 , and the $O_0 Y_0$ -axis lies in a vertical plane and extends downward perpendicular to $O_0 Z_0$. This is the same system that was used for fin-stabilized rockets. We describe the linear displacement of the rocket from the launcher line by the complex number

$$r = X_0 + iY_0, \quad (38)$$

and the angular displacement by

$$\epsilon = \tan^{-1} \frac{X_0}{Z_0} + i \tan^{-1} \frac{Y_0}{Z_0} \doteq \frac{r}{d}. \quad (39)$$

Once expressions for v and ϑ have been obtained, r can be found by integration since it is evident that

$$\dot{r} = v\vartheta. \quad (40)$$

This equation is a satisfactory approximation as long as $\sin \vartheta_x$ can be replaced by ϑ_x and $\cos \vartheta_x \sin \vartheta_r$ can be replaced by ϑ_r . When α and G are constant, (40) becomes

$$r' = 2\lambda\zeta\vartheta, \quad (41)$$

and the approximate form of (39) becomes

$$\epsilon = r/\lambda\zeta^2 \quad (42)$$

These equations are to be solved subject to the initial condition that $r=0$ when $\zeta=\zeta_p$.

It is occasionally convenient to define the complex number

$$u = \dot{r} = \dot{X}_0 + i\dot{Y}_0, \quad (43)$$

which can be regarded as the complex representation of the component normal to O_0Z_0 of the vector \mathbf{v} ; hence it is the cross velocity.

9.12 Properties of the Solutions.—We can now consider some properties of the solutions of the equations of motion 9.11 (33)–(35) subject to the boundary conditions 9.11 (37). The standard method for the solution of such a set of linear inhomogeneous equations is to consider first the solution of the homogeneous equations obtained by letting $f_I = F_I = 0$. Since there are three independent initial conditions, there will be three independent solutions of the homogeneous equations, any other solutions being expressible as a linear combination of the three solutions chosen as the basic ones. We shall find it convenient to choose as the first of our three basic sets of solutions the dimensionless functions $\Delta_\varphi(\zeta_p, \zeta)$, $\Phi_\varphi(\zeta_p, \zeta)$ and $\Theta_\varphi(\zeta_p, \zeta)$ defined by the fact that they satisfy the homogeneous forms of 9.11 (33)–(35) subject to the initial conditions⁶ that $\varphi=1$, $\delta=0$, and $\varphi'=0$ when $\zeta=\zeta_p$. It is useful to have a name for this set of initial conditions. We say that a rocket has initial cross pointing when it is launched in this manner and we call φ_p the initial cross-pointing. This definition may be summarized as in (1) below, and the other two basic sets of solutions are defined as in (2) and (3) by the fact that they satisfy 9.11 (33)–(35) subject to the conditions indicated. A rocket launched with the initial conditions of (2) will be said to have initial yaw, and δ_p will be called the initial yaw. A rocket launched with the initial conditions of (3) will be said to be mallaunched, and q_p will be called the mallaunching or initial cross-spin.

The characteristic functions for initial cross-pointing,

$$\left. \begin{aligned} &\Delta_\varphi(\zeta_p, \zeta), \Phi_\varphi(\zeta_p, \zeta), \Theta_\varphi(\zeta_p, \zeta), \\ &\varphi_p=1, \delta_p=\varphi'_p=f_I=F_I=0. \end{aligned} \right\} \quad (1)$$

⁶ The fact that the initial values chosen as standard involve initial cross pointing or initial yaw of one radian does not mean that the equations of motion are expected to hold for such large angles. The solutions obtained in this way will represent the true motion only when multiplied by initial yaws and orientations of reasonably small magnitude.

The characteristic functions for initial yaw,

$$\left. \begin{aligned} &\Delta_i(\zeta_p, \zeta), \Phi_i(\zeta_p, \zeta), \Theta_i(\zeta_p, \zeta), \\ &\delta_p=1, \varphi_p=\varphi'_p=f_I=F_I=0. \end{aligned} \right\} \quad (2)$$

are solutions subject to

The characteristic functions for mal launching,

$$\left. \begin{aligned} &\Delta_q(\zeta_p, \zeta), \Phi_q(\zeta_p, \zeta), \Theta_q(\zeta_p, \zeta), \\ &t_\lambda q_p=\varphi'_p=1, \delta_p=\varphi_p=f_I=F_I=0. \end{aligned} \right\} \quad (3)$$

are solutions subject to

The fact that the nine characteristic functions defined in this way depend both on ζ_p and ζ is indicated explicitly above. Frequently we shall omit writing the arguments of the functions but sometimes we shall add to the argument some parameter whose value is temporarily important in the discussion. For example, when considering how the deflection due to mal launching varies with the stability factor, S , we use the symbol $\Theta_q(S, \zeta_p, \zeta)$.

The linear combinations

$$\begin{aligned} \delta &= \delta_p \Delta_i + \phi_p \Delta_\varphi + q_p t_\lambda \Delta_q, \\ \varphi &= \delta_p \Phi_i + \varphi_p \Phi_\varphi + q_p t_\lambda \Phi_q, \\ \vartheta &= \delta_p \Theta_i + \varphi_p \Theta_\varphi + q_p t_\lambda \Theta_q, \end{aligned} \quad (4)$$

and

satisfy the homogeneous equations obtained when $f_I=F_I=0$ in 9.11 (33)–(35). This is shown by direct substitution of (4) in these equations and the use of the differential equations satisfied by the functions in (1), (2), and (3). The functions (4) also satisfy the initial conditions 9.11 (37) and hence are the general solution of the homogeneous equations.

The general solution of the inhomogeneous equations obtained when $f_I(\zeta)$ and $F_I(\zeta)$ are given functions, not both zero, is found by adding any particular solution of the inhomogeneous equations to (4). For each different set of functions f_I and F_I one gets a different set of solutions. We now introduce two more basic solutions defined by the fact that they satisfy 9.11 (33)–(35) subject to the conditions indicated below.

The functions for an arbitrary applied torque,

$$\left. \begin{aligned} &\delta_f(\zeta_p, \zeta), \varphi_f(\zeta_p, \zeta), \vartheta_f(\zeta_p, \zeta), \\ &f_I \neq 0, \delta_p=\varphi_p=\varphi'_p=F_I=0. \end{aligned} \right\} \quad (5)$$

are solutions subject to

The functions for an arbitrary applied force,

$$\left. \begin{aligned} &\delta_F(\zeta, \zeta_p), \varphi_F(\zeta_p, \zeta), \vartheta_F(\zeta_p, \zeta) \\ &F_I \neq 0, \delta_p=\varphi_p=\varphi'_p=f_I=0. \end{aligned} \right\} \quad (6)$$

are solutions subject to

In the next section we shall see that (5) and (6), the solutions of the inhomogeneous equations, can always be found by quadratures from (1), (2), and (3), the solutions of the homogeneous equation.

Now if we form the linear combinations

$$\delta = \delta_p \Delta_\delta + \varphi_p \Delta_\varphi + q_p t_\lambda \Delta_q + \delta_f + \delta_F,$$

$$\phi = \delta_p \Phi_\delta + \varphi_p \Phi_\varphi + q_p t_\lambda \Phi_q + \varphi_f + \varphi_F,$$

and

$$\vartheta = \delta_p \Theta_\delta + \varphi_p \Theta_\varphi + q_p t_\lambda \Theta_q + \vartheta_f + \vartheta_F, \quad (7)$$

direct substitution shows that the functions (7) satisfy 9.11 (33)–(35) and satisfy the initial conditions 9.11 (37). These functions are the general solution of the inhomogeneous equations.

The corresponding resolutions of the linear and angular displacements during burning are

$$r = \delta_p \lambda R_\delta + \varphi_p \lambda R_\varphi + q_p t_\lambda \lambda R_q + r_f + r_F, \quad (8)$$

and

$$\epsilon = \delta_p E_\delta + \varphi_p E_\varphi + q_p t_\lambda E_q + \epsilon_f + \epsilon_F. \quad (9)$$

Equations 9.11 (35) and (42) give connections between the characteristic functions of precisely the same forms as the connections between the complete solutions given by these equations. Thus in computing Θ_q , for example, one computes Φ_q and Δ_q and then takes the difference.

It is evident that the general solutions (7) are linear combinations of the particular solutions (1), (2), (3), (5), and (6). Thus we can develop separately the solution, Θ_q , for mal-launching only; the solution, Θ_f , for malalignment only; and those for the other ideally simple situations. Equation (7) shows that the solution of a complex problem where, say, we have both mallaunching and malalignment is obtained merely by adding together the solutions for the simple cases. It can be seen that a similar statement holds if the nonhomogeneous terms are sums of two or more terms as, for example, when F_I contains a term due to gravity and a term due to angular thrust malalignment. The solution of the complete problem is obtained by adding together the solutions obtained on the assumption that each term in F_I is present alone. We shall later consider solutions for a variety of particular nonhomogeneous terms. In each case we shall define a dimensionless characteristic function denoted by a capital letter.

The validity of this linear superposition of solutions of simple cases to give the general solution follows from the fact that the differential equations to be solved are linear, not from the particular form of 9.11 (33)–(35). Thus superposition can be used just as well with the solutions of 9.11 (19)–(21) as with (1), (2), (3), (5), and (6), which are the solutions of 9.11 (33)–(35). We have chosen to state the theorem first in the latter, less general, case since this leads to a less prolific generation of new notations. If in place of assuming that the only aerodynamic force or moment that need be considered is the overturning moment as given in 9.11 (17), we assume only that the forces and moments are linear in δ and $q = \dot{\phi}$, the coefficients of proportionality being specified functions of v and s and hence of t , then 9.11 (19)–(20) remain linear equations although additional terms in δ and $\dot{\phi}$ appear on the left in each. Since these equations are linear, the superposition principle holds in this much more general case. It breaks down, of course, when the forces or moments are not linear in δ as, for example, when the γv^2 of 8.22 is a function of δ .

It must also be remembered that the equations of motion considered throughout this section are not exact; however, as we shall see below, they are good approximations to the exact equations. Now the exact equations are not completely linear and hence the principle

of linear superposition does not hold rigorously. In order to solve the exact equations it is necessary to make enough approximations to reduce them to a linear form, in fact, to the form obtained above by our approximate derivation. An estimate of the errors introduced by this process shows that, in most of the situations of practical importance, no serious errors are introduced by using the linear superposition principle.

It was stated above that the terms f_I and F_I provide for any additional moments and forces that are given as functions of t and hence of ζ . They can also be used in obtaining a useful approximate solution in certain other cases. For example, if one wishes to consider the effect of the Magnus moment

$$f_{V\delta} = -i \frac{1}{2} \gamma_{V\delta} \rho A l^2 V \delta, \quad (10)$$

one can proceed in either of two ways. One can insert the negative of (10), multiplied by (t_λ^2/mK^2) , on the left side of 9.11 (33) in a similar position to that occupied by the term that represents the effect of the overturning moment. If one assumes that $\gamma_{V\delta}$ is independent of yaw, the equation remains linear and can be solved. The disadvantages of this process, aside from the assumption that $\gamma_{V\delta}$ is independent of δ , are that the solutions tend to be very complicated functions, that another parameter is introduced in the solution, and that no use is made of the fact that the Magnus moment is relatively small. Another method of procedure is to transfer the new term to the right side of the equation and regard it as part of f_I . Since f_I is assumed to be a function of ζ only, while the new term involves δ , which is to be solved for, this might not appear profitable. However, if we assume that the effect of the Magnus moment is relatively small, we can replace δ in this term by the function obtained from the solution when the Magnus moment is zero and thus obtain an approximation to the desired solution. If necessary the result obtained in this way for δ as a function of ζ can be substituted back for the δ in the inhomogeneous term and a second approximation obtained. It is not necessary to assume that $\gamma_{V\delta}$ is independent of δ , we assume only that it is small enough so that it does not alter the solution greatly during the time of interest. Evidently the effect of all relatively small terms can be determined in this manner as soon as we have developed a systematic method for obtaining the particular solutions of the inhomogeneous equations defined in (5) and (6).

9.13 Solution of the Inhomogeneous Equations by Means of Green's Functions.—In the previous section certain general properties of the solutions of the differential equations of motion of a spinning projectile were discussed, but nothing was said as to workable methods for actually constructing the solutions. As will be seen in later sections of this chapter, it is usually relatively easy to obtain analytic expressions for the solutions of the homogeneous equations in cases where the linear and angular accelerations are constant and where the important aerodynamic forces and moments are linear functions of δ and q . This leaves to be considered only the problem of obtaining the particular solutions of the inhomogeneous equations. These solutions could be obtained by the well-known method of the variation of parameters but we prefer to use the Green's function method developed in 3.37.

Inspection of the proof that 3.37 (5)–(10) are the solutions of the inhomogeneous equations 3.37 (1)–(3) shows that the solution of the inhomogeneous equations 9.11 (33)–(35) can be expressed in terms of the functions defined in 9.12 (2)–(6) in the form

$$\delta_f(\zeta_p, \zeta) = \int_{\zeta_p}^{\zeta} \Delta_q(u, \zeta) \frac{t_\lambda^2}{mK^2} f_I(u) du, \quad (1)$$

$$\varphi_f(\zeta_p, \zeta) = \int_{\zeta_p}^{\zeta} \Phi_q(u, \zeta) \frac{t_\lambda^2}{mK^2} f_I(u) du, \quad (2)$$

$$\vartheta_f(\zeta_p, \zeta) = \int_{\zeta_p}^{\zeta} \Theta_q(u, \zeta) \frac{t_\lambda^2}{mK^2} f_I(u) du, \quad (3)$$

$$\delta_F(\zeta_p, \zeta) = - \int_{\zeta_p}^{\zeta} \Delta_\delta(u, \zeta) \frac{F_I(u)}{mGu} du, \quad (4)$$

$$\varphi_F(\zeta_p, \zeta) = - \int_{\zeta_p}^{\zeta} \Phi_\delta(u, \zeta) \frac{F_I(u)}{mGu} du, \quad (5)$$

and

$$\vartheta_F(\zeta_p, \zeta) = - \int_{\zeta_p}^{\zeta} \Theta_\delta(u, \zeta) \frac{F_I(u)}{mGu} du. \quad (6)$$

It should be noted that in these expressions we integrate with respect to u from ζ_p , the value of ζ at launching, to the value of ζ at the instant of interest. The function that is integrated is the inhomogeneous term in the differential equation, with ζ replaced by u , multiplied by the appropriate function from 9.12 (2)–(3), with ζ_p replaced by u .

There are a number of variations in the Green's function method that are sometimes useful. Minor changes in terminology are all that is required to make the above theorems apply to 9.11 (19)–(20) rather than to 9.11 (33)–(35). If a convenient approximation for the solution is required, an expansion for the Green's function of the type found in 9.26 may yield it. An analytical evaluation of the integrals for φ is sometimes easier if one uses

$$\varphi(\zeta_p, \zeta) = \int_{\zeta_p}^{\zeta} \frac{F_I(u)}{mGu} du + \int_{\zeta_p}^{\zeta} \frac{1}{u} \frac{d[u\delta(\zeta_p, u)]}{du} du + \varphi(\zeta_p, \zeta_p), \quad (7)$$

derived as was 3.37 (11), rather than (2) and (5) above. It is frequently easier to determine ϑ from δ and φ by means of the equation

$$\vartheta = \varphi - \delta \quad (8)$$

than to solve for ϑ directly. Expressions for r_f , r_F , ϵ_f , and ϵ_F corresponding to (1)–(6) are readily obtained by analogy. In most practical cases, however, it is probably more convenient to integrate 9.11 (41) than to use the Green's function integrals.

9.14 A Rigorous Geometrical Description of the Motion; Euler's Equations.—Let us now turn our attention from the above treatment of the motion of a rocket by means of the approximate equations of motion and, instead, consider the general theorems that hold exactly for the motion of axially symmetrical rigid bodies. We shall find that this leads in a relatively simple way to some very helpful theorems and to methods of describing the motion that are both exact and very illuminating.

The motion of a rigid body having no fixed point is usually treated by considering first the motion of the center of mass and then considering the rotation of the body about the center of mass. Now the acceleration of the center of mass is equal to the vector sum of the forces acting on the rocket divided by the mass of the rocket. The nature of the resulting motion of the center of mass is relatively easily pictured, and hence we shall turn our main attention to understanding the motion due to the rotation of the body about its center of mass. Provided the torques acting on the body remain the same, the rotation is independent of the motion of the center of mass. Hence we shall discuss the rotation as it would be seen by a nonrotating observer moving with the center of mass.

The shortest method of describing the rotation of a rigid body is to specify its vector angular velocity at each instant. Thus, it will be recalled,⁷ one can say that at any particular instant the velocity of every particle is the same as though the body were rotating about a suitably chosen axis with the proper scalar angular velocity. The vector angular velocity is then a vector directed along this axis and having a magnitude that is the scalar angular velocity. In general, the angular velocity does not remain fixed in the solid body or in space. Thus it is difficult either to picture or to compute the motion even when the angular velocity is known as a function of time. There is an alternative method of describing the motion that seems more useful in case the rigid body has an axis of symmetry; it is particularly useful in the case of great interest to us in which the angular velocity remains relatively close to this axis. The alternative method specifies the motion of the axis of symmetry plus the rotation about this axis. Thus effectively it resolves the angular velocity into one component perpendicular to the axis of symmetry and one component along the axis. We find it necessary to use both methods, the first because it gives an easier derivation of the equations of motion and of expressions for such quantities as the kinetic energy; the second because it leads to a more convenient description of the motion. It will be necessary, therefore, to obtain the transformation equations between the two systems of descriptions.

We introduce the right-handed, Cartesian coordinate system Oxyz fixed in the projectile with O at the center of mass and Oz along the axis of symmetry. It must be remembered that \mathbf{e}_x , \mathbf{e}_y , and \mathbf{e}_z , which we use to denote the unit vectors in this coordinate system, rotate with the projectile and hence cannot be regarded as constants. We shall replace \mathbf{e}_z by \mathbf{e}_A when, as in chapter 8, we wish to emphasize that the vector is along the axis of the rocket and to minimize its connection with any coordinate system. Resolving the angular velocity into components along the axes of this system, we get

$$\boldsymbol{\omega} = \omega_x \mathbf{e}_x + \omega_y \mathbf{e}_y + \omega_z \mathbf{e}_z. \quad (1)$$

In the second method of description, the motion of the axis of symmetry is specified in terms of the motion of the point A , the point unit distance along the axis from the center of mass. We imagine A to be moving as shown in figure 9.14c over the surface of a nonrotating unit sphere whose center is the center of mass. The motion of A is given by \mathbf{q} , the velocity with which A moves with respect to the nonrotating sphere. The rate of rotation about the axis of symmetry is specified by means of the spin, $s = \omega_z$, the component of $\boldsymbol{\omega}$ along the axis of symmetry.

If we consider the contribution to the velocity of A due to each of the three components of $\boldsymbol{\omega}$ in turn, we see, as in figure 9.14a, that the velocity due to $\omega_z \mathbf{e}_z$ is zero, the velocity due to $\omega_y \mathbf{e}_y$ is $\omega_y \mathbf{e}_x$, and the velocity due to $\omega_x \mathbf{e}_x$ is $-\omega_x \mathbf{e}_y$. Hence

$$\mathbf{q} = q_x \mathbf{e}_x + q_y \mathbf{e}_y = \omega_y \mathbf{e}_x - \omega_x \mathbf{e}_y; \quad (2)$$

$$q_x = \omega_y, \text{ and } q_y = -\omega_x. \quad (3)$$

This result could also have been obtained directly from the theorem that \mathbf{q} , the velocity of A , is $\boldsymbol{\omega} \times \mathbf{e}_z$. Thus q , the magnitude of the velocity of A , is just the magnitude of the projection on the Oxy-plane of $\boldsymbol{\omega}$;

$$q = (\omega_x^2 + \omega_y^2)^{\frac{1}{2}}. \quad (4)$$

⁷ For a development of those general principles of dynamics that we assume, it may be convenient for the reader to have available as a reference some treatise on dynamics or theoretical physics; e. g., Leigh Page, "Introduction to Theoretical Physics," ch. I and II, Van Nostrand

The direction of the projection is perpendicular to that of \mathbf{q} . If we let \mathbf{e}_\perp be a unit vector in the direction of this projection, then we have

$$\mathbf{q}\mathbf{e}_\perp = (\omega_x\mathbf{e}_x + \omega_y\mathbf{e}_y) = \boldsymbol{\omega} - s\mathbf{e}_z, \quad (5)$$

for the component of $\boldsymbol{\omega}$ in the direction perpendicular to the axis of symmetry.

Since we have chosen to describe the motion of the axis of symmetry in terms of \mathbf{q} , which is the velocity of A , rather than in terms of $\mathbf{q}\mathbf{e}_\perp$, which is the angular velocity of the axis, we must treat \mathbf{M} , the moment acting on the body, in a similar fashion. This moment, when resolved in the $Oxyz$ system, can be written as

$$\mathbf{M} = M_x\mathbf{e}_x + M_y\mathbf{e}_y + M_z\mathbf{e}_z. \quad (6)$$

We now wish to apply to (6) an argument similar to that which led us from (1) to (2). We do this by noting that \mathbf{M} is equivalent to the sum of the moment $M_z\mathbf{e}_z$, about the OZ -axis, and the moment about the origin due to the force

$$\mathbf{f} = f_x\mathbf{e}_x + f_y\mathbf{e}_y = M_y\mathbf{e}_x - M_x\mathbf{e}_y \quad (7)$$

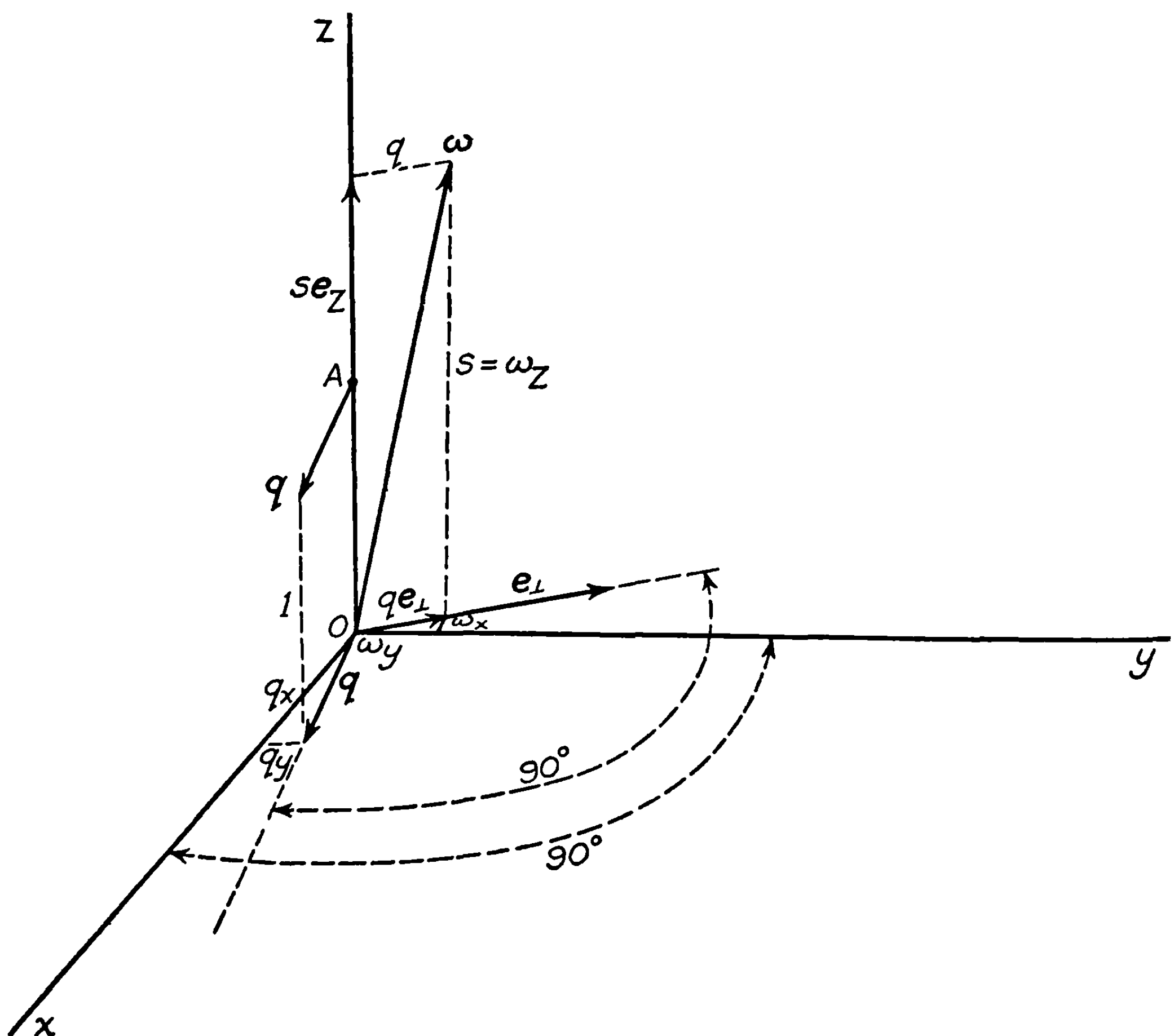


FIGURE 9.14 (a).—Velocity of A and the angular velocity.

applied at A perpendicular to the axis of symmetry. In order that the motion of the center of mass not be affected when we replace M by $M_z e_z$ and f , we must assume that a force equal in magnitude to f but oppositely directed acts at O .

Having completed our discussion of the coordinate system and the variables to be used in the description of the rotation and the applied moments, we turn our attention to the angular momentum. The angular momentum about the center of mass of a rigid axially symmetric body is

$$\begin{aligned} H &= mK^2\omega_x e_x + mK^2\omega_y e_y + mk^2\omega_z e_z \\ &= mK^2q e_\perp + mk^2s e_z, \end{aligned} \quad (8)$$

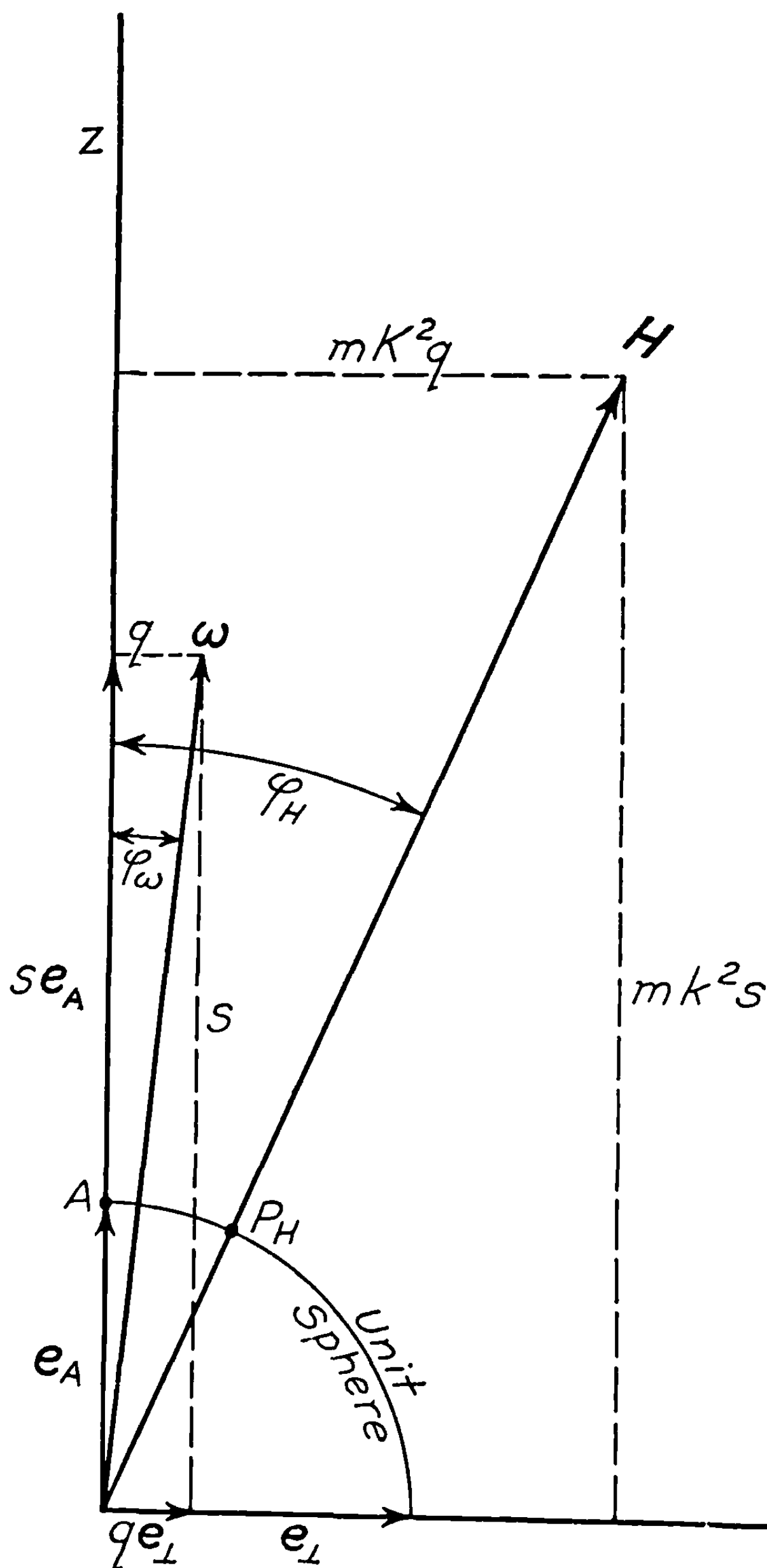


FIGURE 9.14 (b).—Connection between the Oz axis, ω , and H .

where m is the mass, K is the radius of gyration about the Ox and Oy axes, and k is the radius of gyration about the axis of symmetry. Equations (5) and (8) show that \mathbf{H} and $\boldsymbol{\omega}$ both lie in the plane containing \mathbf{e}_\perp and \mathbf{e}_z , or, as we shall now call it, \mathbf{e}_A . Hence, we can exhibit the relationships between $\boldsymbol{\omega}$, \mathbf{H} and the longitudinal axis of the rocket by means of the two-dimensional figure 9.14b, which is based on these equations. From this it can be seen that at any instant the angle, φ_H , between the longitudinal axis of the projectile and the angular momentum vector satisfies the equation

$$\tan \varphi_H = \gamma q/s = \gamma \tan \varphi_\omega, \quad (9)$$

where φ_ω is the angle between the longitudinal axis of the projectile and $\boldsymbol{\omega}$. Since $\gamma = K^2/k^2$ is ordinarily about 20 or 30, φ_ω is much less than φ_H . Since q is usually much less than s , both angles are small and we have the approximate relationship

$$\varphi_H \doteq \gamma q/s \doteq \gamma \varphi_\omega. \quad (10)$$

The basic equation of motion of a rigid body states that the rate of change of angular momentum is equal to the torque acting on the body. Applying this to (8) leads to Euler's equations of motion.

$$mK^2\dot{\omega}_x + m(k^2 - K^2)s\omega_y = M_x, \quad (11)$$

$$mK^2\dot{\omega}_y + m(K^2 - k^2)s\omega_x = M_y, \quad (12)$$

and

$$mk^2\dot{s} = M_z, \quad (13)$$

where M_x , M_y , and M_z are the components of the moment about the center of mass of the applied forces as in (6) and (7). Let us now consider the extensive information about the

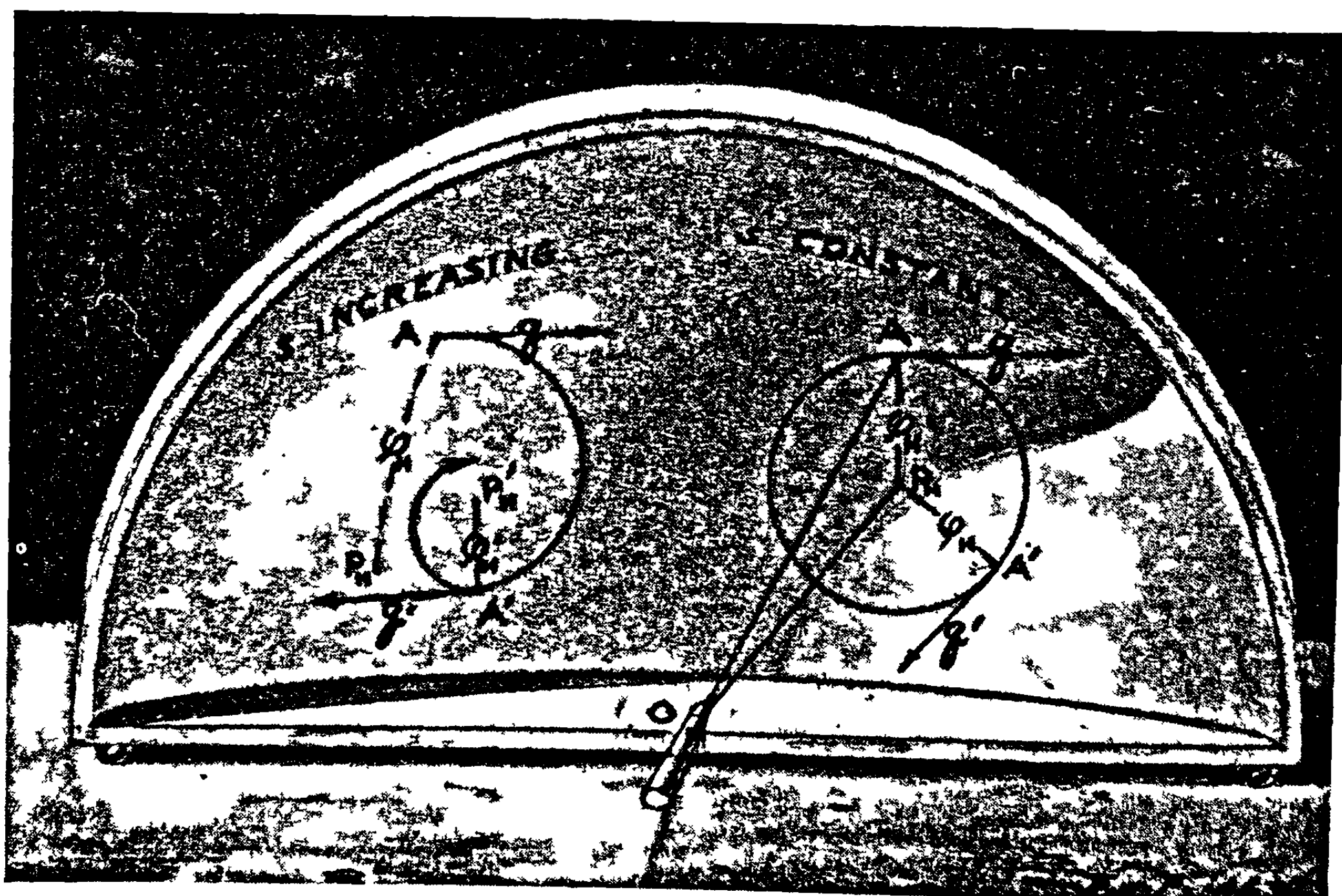


FIGURE 9.14 (c).—Motion of A on the surface of a unit sphere.

motion provided by these equations and by the equations in q and f into which we transform (11) and (12).

Since M_z is assumed to be a known function of time, we can integrate (13) directly to give the spin as a function of time. Thus

$$s = s_p + \int_{t_p}^t \frac{M_z dt}{mk^2}, \quad (14)$$

where s_p is the spin at the arbitrarily chosen initial time t_p . This shows that the spin is independent of the moments M_x and M_y . Even if, on the basis of 8.53, we regard M_z as being a function of s as well as t , (13) can be integrated to give s as a function of t .

Equations (11) and (12) can easily be combined into a single equation in $(\omega_x + i\omega_y)$ or $(q_x + iq_y)$; however, it seems preferable to use them to get the rate of change of \mathbf{q} as it appears to a nonrotating observer. It should be noted that this quantity, which we denote by $\dot{\mathbf{q}}$, must for the present be regarded as a vector and not as a complex number. For although it is entirely proper, if we wish, to regard $q_x + iq_y$ as the complex representation of the vector \mathbf{q} , $\dot{q}_x + i\dot{q}_y$ does not correspond to $\dot{\mathbf{q}}$ because of the rotation of the axes. Hence throughout the present section we do not use a complex representation of our two-dimensional vectors but continue to express them with the aid of the unit vector notation. Now

$$\dot{\mathbf{q}} = \dot{q}_x \mathbf{e}_x + \dot{q}_y \mathbf{e}_y + q_x \dot{\mathbf{e}}_x + q_y \dot{\mathbf{e}}_y = \dot{q}_x \mathbf{e}_x + \dot{q}_y \mathbf{e}_y + \boldsymbol{\omega} \times \mathbf{q}.$$

With the aid of (3), (11), (12), (7), and (5) this becomes

$$\dot{\mathbf{q}} = -q^2 \mathbf{e}_A + \frac{s}{\gamma} \mathbf{e}_A \times \mathbf{q} + \frac{\mathbf{f}}{mK^2}. \quad (15)$$

This equation states that the rate of change of \mathbf{q} , that is the acceleration of the point A , is the sum of three terms that can be regarded as independent. The first term on the right of (15) is the acceleration of A normal to the surface of the sphere and is of no further interest. The second term is just the gyroscopic acceleration discussed in the paragraph containing 9.11 (14); it should be noted that it is normal to \mathbf{q} . The third term is precisely the acceleration of A that would be produced by the applied torques if there were no spin and no gyroscopic effects. Thus we can say that the component—tangent to the surface of our unit sphere—of the acceleration of A over the surface of this sphere can be resolved into two parts. The first is the familiar acceleration \mathbf{f}/mK^2 due to the applied torques; the second is the gyroscopic acceleration $(s/\gamma)\mathbf{e}_A \times \mathbf{q}$. Since the two are independent, we can best study the nature of the motion produced by the gyroscopic acceleration in the case in which \mathbf{f} is zero.

If \mathbf{f} is zero, then (15) shows that any change in \mathbf{q} is in a direction perpendicular to \mathbf{q} so that only its direction, not its magnitude, q , changes. If in addition, $M_z = 0$ so that s is a constant, then from (9) φ_H must be constant. Also \mathbf{M} must be zero, and hence \mathbf{H} is a constant vector. This means that the motion can be pictured as the rotation of the longitudinal axis of symmetry in a cone whose half angle is φ_H about the fixed position of the angular momentum. The angular velocity, $\boldsymbol{\omega}$, moves in space on a slightly smaller cone whose half angle is $\varphi_H - \varphi_\omega \doteq (1 - \gamma^{-1})\varphi_H$. The resulting motion may be visualized by imagining that figure 9.14b is spun about \mathbf{H} with angular velocity s/γ while the rocket spins about Oz with angular velocity s with respect to a fixed reference frame and with angular velocity $s(1 - \gamma^{-1})$ with respect to figure 9.14b. An equivalent description of the motion of any axially symmetric rigid body acted on by no torques may be given in terms of the motion of the point A over that unit

sphere whose center is at O . If at some instant it is observed that the body is spinning with angular velocity s about its axis of symmetry and that the point A on this axis is moving with velocity \mathbf{q} , then throughout the subsequent motion s and q remain unaltered, while, as shown in the right half of figure 9.14c, A moves in a circle about a point P_H on the surface of the sphere. The point P_H is located as follows. Lay off a line through O making the angle $\varphi_H = \tan^{-1}(\gamma q/s)$ with the axis of the body; this line must lie in the plane perpendicular to \mathbf{q} and must be on the side of A toward which the vector $s\mathbf{e}_A \times \mathbf{q}$ points. This line, which coincides with \mathbf{H} , pierces the unit sphere at P_H . The figure shows both the initial state of the system and the state at a later time when A has moved around to A' and \mathbf{q} has become \mathbf{q}' .

If \mathbf{f} is zero but M_z is not, so that s varies, the point A does not move in a circle and \mathbf{H} remains constant neither in magnitude nor in direction. Nevertheless, according to (15), q , the speed with which A moves, remains constant and the acceleration of A depends on s but not on \dot{s} . Hence if s is known as a function of t and we are given the initial value of \mathbf{q} , we can describe the motion as follows. The body spins about OA , its axis of symmetry, with angular velocity $s(t)$. The point A moves with constant speed q in a spiral over the surface of the unit sphere as shown in the left half of figure 9.14c. The radius of curvature of the spiral varies with time, having the value required to make the acceleration of A that given by (15). Consequently the center of curvature of the spiral at each instant is P_H which is located as described above, except that now s is $s(t)$, since this gives the proper acceleration when s is constant. In this case, when A moves around to A' , P_H moves to P'_H and φ_H changes to φ'_H . P_H retains its significance as the intersection of \mathbf{H} and the sphere. When s increases monotonically, A spirals inward since φ_H decreases monotonically. This requires that P_H always move toward A ; the necessity for this follows also, as may be seen with the aid of figure 9.14b, from the fact that the rate of change of \mathbf{H} is parallel to the torque acting and in this case the torque is parallel to OA .

Let us return to the case in which M_z and \mathbf{f} are both zero so that both s and q are constants and A moves in a circle of radius $\sin \varphi_H$, where φ_H can be obtained from (9). Then in an interval of time Δt in which A moves the distance $q\Delta t$ around the circle, the direction of \mathbf{q} will change by

$$\frac{q\Delta t}{\sin \varphi_H} = \frac{s\Delta t}{\gamma \cos \varphi_H} \text{ radians,} \quad (16)$$

since \mathbf{q} is tangent to the circle and normal to its radius. But in this time the rocket rotates $s\Delta t$ radians about its axis. Hence \mathbf{q} turns $\gamma^{-1} \sec \varphi_H \doteq \gamma^{-1}$ times as fast as the rocket rotates. Since even when M_z , and hence s , are not constant, the acceleration of A and the rate of change of \mathbf{q} at any instant are determined by s and the radius of curvature of the path of A at this instant, the same conclusion holds in this more general case in which the path is a spiral. Hence, when φ_H is small, A will make one nutation, that is traverse one turn of the spiral, moving around until the tangent to the spiral becomes parallel to its original position, while the rocket spins γ times about its axis. This is a very important theorem since it is very useful in distinguishing cases in which gyroscopic effects are important from those in which they are negligible. We shall define a "nutation" in this case by saying that the rocket makes one nutation when A traverses one turn of the spiral. Ordinarily gyroscopic effects can be neglected in phenomena that take place in a small fraction of a nutation; i. e., while the projectile makes a number of revolutions that is small compared to γ . Gyroscopic effects are always important in phenomena that are spread out over a period of the order of a nutation; i. e., γ revolutions, or longer. In the usual case in which the linear velocity of a rocket is proportional to its angular velocity; λ , the distance traveled per nutation, is constant throughout burning since it is γ times ν , the distance traveled per revolution. Hence we usually say that gyroscopic effects are

unimportant while the rocket travels a distance small compared to λ but that they cannot be neglected in treating any phenomenon that is spread out over a distance as long as λ .

Having seen how we can describe and picture the motion of the body in terms of the motion of A when there is no torque \mathbf{f} acting, we can picture the motion when there is such a torque as being due to superposition of the accelerations of A . The procedure that we have followed has been completely rigorous in cases in which we have to deal with a rigid body having invariable mass and moments of inertia and having an axis of symmetry. It leads to a convenient geometrical method of describing and picturing the motion—in particular the motion due only to gyroscopic forces is described as a motion in a spiral whose radius of curvature at any instant is inversely proportional to s at that instant. It is, however, very difficult actually to carry out the integration that gives the orientation of the axis as a function of time. To get a workable expression for the orientation it is necessary to introduce the assumption that the important angles are all small and to introduce coordinate systems. Before entering upon this line of attack, we shall obtain some useful conservation theorems that hold generally, that do not involve small angle approximations.

9.15 The Energy Integrals.—It is a well-known theorem that the kinetic energy of a rigid body can be separated into two independent parts. One part, the kinetic energy of translation, is equal to $\frac{1}{2}mv^2$ where m is the mass of the body and v is the velocity of its center of mass. The other part, the kinetic energy of rotation, is just the kinetic energy that the body would have if it rotated with its center of mass held stationary. The kinetic energy of translation can be changed only by the total force applied to the body; it is not affected by moments. The kinetic energy of rotation can be changed only by moments about the center of mass; it is not affected by forces that have no moment about the center of mass.

The kinetic energy of rotation is

$$E = \frac{1}{2}mK^2\omega_x^2 + \frac{1}{2}mK^2\omega_y^2 + \frac{1}{2}mk^2\omega_z^2 = \frac{1}{2}mk^2s^2 + \frac{1}{2}mK^2q^2. \quad (1)$$

This can be separated into the spin kinetic energy,

$$E_s = \frac{1}{2}mk^2s^2, \quad (2)$$

and the nutational kinetic energy,

$$E_\perp = \frac{1}{2}mK^2q^2 = E_s \gamma^{-1} \tan^2 \varphi_H. \quad (3)$$

Although E_\perp is called “nutation kinetic energy” rather than the “kinetic energy due to transverse rotation of the longitudinal axis” it must be remembered that the more cumbersome title is the more precise. The transverse rotation is resolved into both nutations and precessions and it is really the square of a linear combination of the amplitudes of each that fixes E_\perp . The brief title is used since, unless the amplitude of the nutations is very much less than that of the precessions, the nutations contribute most of the energy.

Since we showed in 9.14 that s was affected only by M_z and not by \mathbf{f} , while q was affected only by \mathbf{f} and not by M_z , it is evident that the two components into which we have divided the kinetic energy of rotation have a considerable degree of independence. We can easily put this statement in a quantitative form that will be useful later. If we multiply 9.14 (13), the third of Euler’s differential equations of motion, by s we get

$$\frac{dE_s}{dt} = sM_z. \quad (4)$$

In similar fashion we can get from 9.14 (11) and (12), the first two of Euler's equations, and from 9.14 (3), (4), and (7)

$$\frac{dE_\perp}{dt} = f \cdot q. \quad (5)$$

9.16 Exact Definitions of the Coordinates—The Angular Motion.—We have obtained rigorous expressions for the dependence of the spin, s , on time and for the acceleration of the point A . It is relatively easy to integrate once and get the velocity of A , but it is very difficult to integrate twice and get a rigorous expression for its position. In order to go further in the study of the motion of a spinning projectile, it is desirable to make use of the simplifications that result if we use complex numbers to represent two-dimensional vectors. It is also desirable to collect together as a remainder that can usually be neglected the very small terms that normally complicate exact equations. It is necessary to introduce suitable coordinates for the description of the orientation and direction of motion of the projectile.

It may appear to be an unnecessary refinement to carry out the relatively rigorous derivations of this section, only to discard at the end enough terms to get the simple forms already considered in 9.11. Nevertheless, it is desirable to do this for several reasons. First, it enables us to give precise definitions of the various quantities to be discussed so that the exact meaning of each symbol is known even though it may be used only in approximate equations. Second, the present procedure gives a convincing derivation of some points that may appear plausible but not logically established in the previous treatment. Finally, it puts one in a position where the errors introduced by the previous approximations can be determined, if desired.

We define the orientation of the axis of symmetry and the direction of motion by reference to the right-handed Cartesian coordinate system $OX_1Y_1Z_1$ whose origin, O , moves with the center of mass of the rocket but whose axes always remain parallel to their original directions. As shown in figures 9.11a and 9.16a the OX_1 -axis is horizontal and normal to the trajectory at some convenient point, usually on the launcher. The OZ_1 -axis may be either horizontal or parallel to the axis of the launcher, and the OY_1 -axis is directed downward, being vertical when OZ_1 is horizontal.

The orientation of the axis of symmetry of the projectile is specified by the coordinates of the point A at which the axis intersects a sphere of unit radius with center at O . It is most convenient to locate A by giving its latitude φ_x and its longitude φ_y . Thus φ_x is the angle between OA and OL (OL is the projection of OA on the OY_1Z_1 -plane), φ_x being positive when A is to the right of the OY_1Z_1 -plane. The longitude of A , φ_y , is the angle from OZ_1 to OL , φ_y being positive when A is below the OX_1Z_1 -plane. An equivalent definition of these coordinates is that $\varphi_x + \frac{1}{2}\pi$ and φ_y are the coordinates of A in ordinary spherical polar coordinates, $\varphi_x + \frac{1}{2}\pi$ being the polar angle or co-latitude measured from the negative OX_1 axis and φ_y being the azimuth or longitude. It is evident from figure 9.16a that as long as φ_x is small, φ_x and φ_y are coordinates in a two-dimensional, approximately Cartesian coordinate system wrapped around the equator of a unit sphere. A little care is necessary to prevent being misled by the subscript Y , since it is only in the neighborhood of the OZ_1 -axis that a displacement in the φ_y direction is parallel to the axis OY_1 . In spite of this danger of confusion, we use this subscript since it is particularly well adapted to the complex notation that we shall soon adopt and

since we usually orient the OZ_1 -axis so that A remains near it. Since we must require that φ_x always be small, a displacement in the φ_x direction is always nearly in the OX_1 direction.

We can specify the orientation of the tangent to the trajectory at O in a similar way by giving the coordinates, ϑ_x and ϑ_y , of the point T (Fig. 9.11a) where this tangent pierces the unit sphere; and, as before, it is immaterial whether we choose to regard ϑ_x and ϑ_y as the latitude and longitude of T or whether we choose to regard $\vartheta_x + \frac{1}{2}\pi$ and ϑ_y as spherical polar coordinates.

It is convenient to define the complex numbers

$$\varphi = \varphi_x + i\varphi_y, \quad (1)$$

and

$$\vartheta = \vartheta_x + i\vartheta_y, \quad (2)$$

to specify, respectively, the orientation of the rocket and that of the tangent to the trajectory. It must be remembered that φ and ϑ are not vectors, unless all the angles involved are infinitesimals, since they do not add and subtract like vectors. For example, the yaw is not strictly $\varphi - \vartheta$ although it is a very good approximation to the yaw when both components of the yaw are under 10° . This point will be considered more carefully later.

The equations of motion involve the vectors \mathbf{q} and \mathbf{f} , where \mathbf{q} is the velocity with which A moves and \mathbf{f} is the force that would have to be applied at A in order to produce the same transverse moment or torque about the center of mass as is actually produced by the forces applied to the projectile. Both of these vectors are tangent to the surface of the sphere at A ; hence we need concern ourselves only with two components of each. The most convenient axes to introduce at A are, as indicated in figure 9.16a, the AX -axis, which is directed along the great circle of constant φ_y and the AY -axis, which is directed along the small circle of constant φ_x . We denote unit vectors in the two directions by \mathbf{e}_x and \mathbf{e}_y and write the vector \mathbf{q} in terms of its components as

$$\mathbf{q} = q_x \mathbf{e}_x + q_y \mathbf{e}_y. \quad (3)$$

Likewise,

$$\mathbf{f} = f_x \mathbf{e}_x + f_y \mathbf{e}_y. \quad (4)$$

It should be noted that AX and AY are not strictly parallel to OX_1 and OY_1 , respectively. Nevertheless, when φ is small they are nearly parallel, and our notation emphasizes this. In order to obtain an expression for the rate of change of \mathbf{q} we must determine the rate of rotation of the coordinate system based on the unit vectors \mathbf{e}_x and \mathbf{e}_y . The third unit vector in this system is \mathbf{e}_A , along the axis of symmetry. We let ω_c denote the rate of rotation of this coordinate system. If φ_y is constant, A , \mathbf{e}_x , and \mathbf{e}_A move in the stationary plane through OL and OX , hence the angular velocity of the coordinate system is $q_x \mathbf{e}_y$. If, on the other hand, φ_x is constant, A moves with velocity of q_y in a small circle of radius $\cos \varphi_x$. Hence the plane through OL and OX_1 rotates about OX_1 with angular velocity $q_y / \cos \varphi_x$, and the coordinate system rotates with just the same angular velocity. Resolving this angular velocity along OX_1 into components along \mathbf{e}_x and \mathbf{e}_A as shown in figure 9.16b and adding the angular velocity when φ_y is constant, we get

$$\omega_c = -q_y \mathbf{e}_x + q_x \mathbf{e}_y - q_y \tan \varphi_x \mathbf{e}_A. \quad (5)$$

It follows from this that

$$\begin{aligned} \dot{\mathbf{q}} &= \dot{q}_x \mathbf{e}_x + \dot{q}_y \mathbf{e}_y + q_x \dot{\mathbf{e}}_x + q_y \dot{\mathbf{e}}_y \\ &= \dot{q}_x \mathbf{e}_x + \dot{q}_y \mathbf{e}_y + \omega_c \times \mathbf{q} \\ &= \dot{q}_x \mathbf{e}_x + \dot{q}_y \mathbf{e}_y + q_y^2 \tan \varphi_x \mathbf{e}_x - q_x q_y \tan \varphi_x \mathbf{e}_y - q^2 \mathbf{e}_A. \end{aligned} \quad (6)$$

Substituting this in 9.14 (15) and taking each component separately, we get

$$\dot{q}_x + (s/\gamma)q_y + (q_y \tan \varphi_x)q_y = f_x/mK^2, \quad (7)$$

and

$$\dot{q}_y - (s/\gamma)q_x - (q_x \tan \varphi_x)q_x = f_y/mK^2. \quad (8)$$

In the future we shall find it desirable to specify the velocity of A by means of the complex number

$$q = q_x + iq_y \quad (9)$$

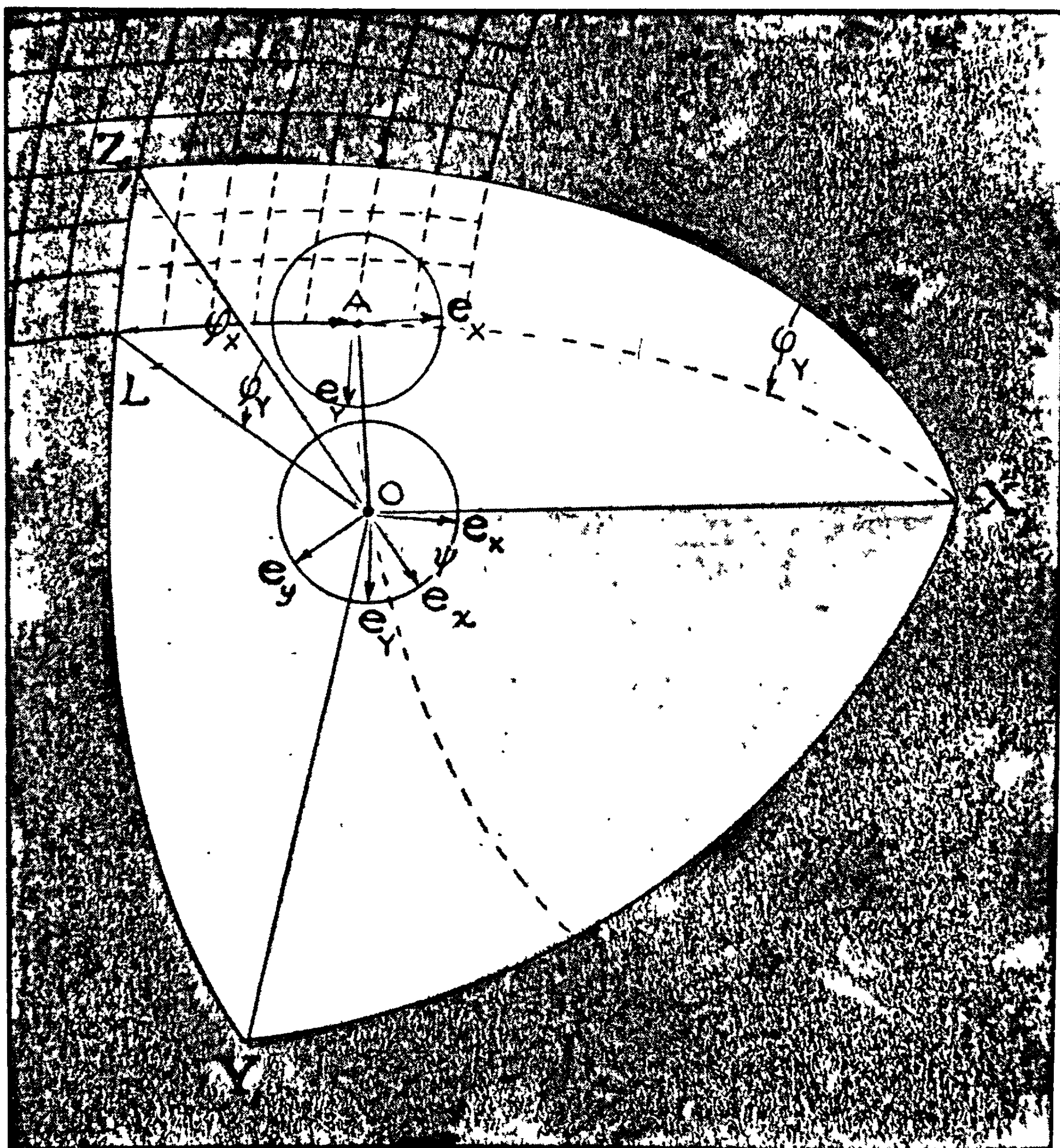


FIGURE 9.16 (a).—The coordinate system used in the description of the motion.

rather than by the vector (3). The fact that the same symbol, q , is used for both should cause no confusion. In the first place, usually it does not matter which interpretation is given to q ; either way it represents the velocity of A . In the second place, whenever it matters, one can always tell which interpretation is meant, since if unit vectors or vector products occur in an equation containing q , it should be regarded as a vector, while if $i = (-1)^{\frac{1}{2}}$ occurs, it should be regarded as a complex number. In fact, the only case in which we cannot simply state that (3) and (9) are different notations for the same thing is when derivatives of q are involved. If q is a vector, its derivative with respect to time is given by (6), while if q is a complex number.

$$\dot{q} = \dot{q}_x + i\dot{q}_y, \quad (10)$$

and there are no terms due to the rotation of the coordinate system. Since all equations containing \dot{q} will contain either i or a unit vector, one can always tell which \dot{q} is meant.

In a similar manner, the moment acting on the projectile will be described by the complex number

$$f = f_x + if_y. \quad (11)$$

Since one almost never has occasion to differentiate f , it is not as important as in the case of q to distinguish between the two notations for the moment.

It is now possible to express the equations of motion (7) and (8) in terms of the complex numbers q , f , and \dot{q} . We find that

$$\dot{q} - i \left(\frac{s}{\gamma} + q_y \tan \varphi_x \right) q = \frac{f}{mK^2}. \quad (12)$$

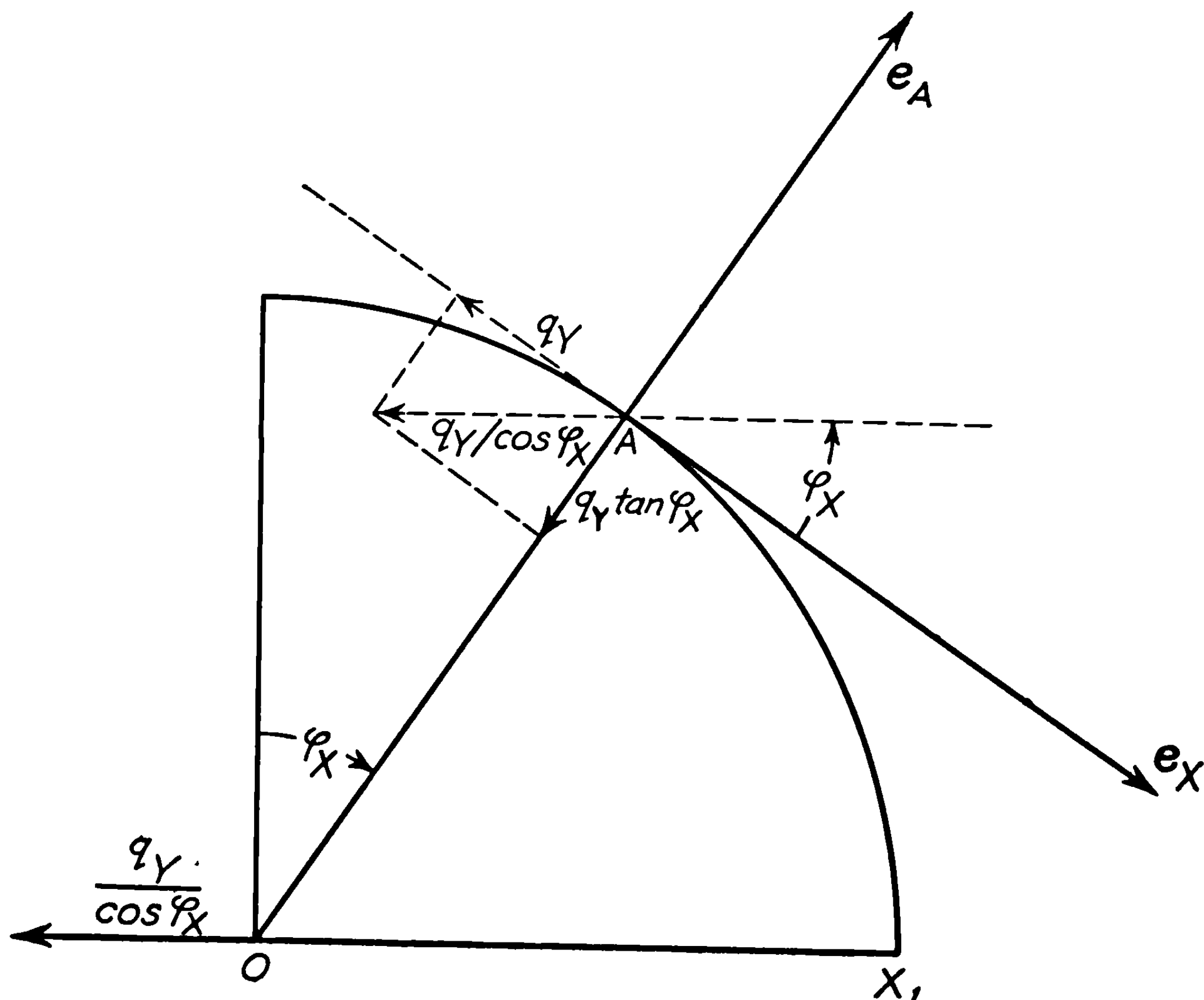


FIGURE 9.16 (b).—Components of ω , when $q_s = 0$.

The physical interpretation of this important equation was discussed in the paragraphs containing 9.11 (14) and 9.14 (15).

This equation can now be converted to an equation in φ . From figure 9.16a we see that if A is moving so that φ_x and φ_y are changing at rates $\dot{\varphi}_x$ and $\dot{\varphi}_y$, respectively, then

$$q_x = \dot{\varphi}_x, q_y = \dot{\varphi}_y \cos \varphi_x = \dot{\varphi}_y - \dot{\varphi}_y(1 - \cos \varphi_x).$$

Hence,

$$q = \dot{\varphi} - i\dot{\varphi}_y(1 - \cos \varphi_x). \quad (13)$$

There is no possible ambiguity in the meaning of $\dot{\varphi}$ since, strictly speaking φ must always be a complex number and not a vector. Substituting (13) in (12), we get

$$\ddot{\varphi} - i(s/\gamma)\dot{\varphi} = (f/mK^2) + R_1, \quad (14)$$

where we customarily neglect the higher order terms

$$R_1 = (s/\gamma)\dot{\varphi}_y(1 - \cos \varphi_x) - \dot{\varphi}_y^2 \sin \varphi_x \cos \varphi_x + 2i\dot{\varphi}_x\dot{\varphi}_y \sin \varphi_x + i\ddot{\varphi}_y(1 - \cos \varphi_x). \quad (15)$$

This completes our relatively exact discussion of φ and q , the complex numbers used to specify the position and velocity of A . In order to complete our specification of the position of the rotating projectile, we must introduce some coordinate giving the angle through which it has rotated about the axis OA . This we do by defining ψ to be the angle measured in the clockwise direction, through which the Ox and the Oy -axes, which are fixed in the projectile, have been rotated from a position in which they are parallel to the AX and AY axes, respectively. In order to show this angle in figure 9.16a we have projected the AX and the AY axes onto the parallel Oxy -plane. The coordinate ψ is rarely used except in discussions of malalignment and of dynamic unbalance.

The connection between s and $\dot{\psi}$ is easily obtained. We found in (5) above that the component along OA of the angular velocity of the AX and AY axes is $-q_y \tan \varphi_x$, and from our definition of ψ it follows that the angular velocity of the projectile with respect to the AX and AY axes is $\dot{\psi}$. But in 9.14 the component along OA of the total angular velocity of the projectile is defined to be s . Hence, using 9.14 (14),

$$s = \dot{\psi} - q_y \tan \varphi_x = \dot{\psi} - \dot{\varphi}_y \sin \varphi_x = \int (M_z/mk^2) dt, \quad (16)$$

and we see that $\dot{\psi}$ is nearly equal to s .

The coordinates φ_x , φ_y , and ψ used to specify the orientation of the projectile are closely related to the Eulerian angles frequently used for the same purpose. Although we have already obtained everything we need without making use of the fact, those familiar with the Eulerian angles may be interested in tracing the connection. The first Eulerian angle is the angle from a fixed pole, in our case the negative OX_1 -axis, to the Oz or OA -axis of the rotating coordinate system; hence it is $\varphi_x + \frac{1}{2}\pi$. The second Eulerian angle is that from a fixed line, which we will take to be the OY_1 -axis, to the line of nodes, which may be seen to be parallel to the AY -axis; hence this angle is just φ_y . The third Eulerian angle is the angle from the line of nodes to the OX -axis; hence it is $\psi - \frac{1}{2}\pi$. It is possible and somewhat more direct to express the

equations of motion in terms of the Eulerian angles and then convert to the forms given above. However, this more direct method is also somewhat more complicated than the method given above.

9.17 Motion of the Center of Mass.—In the previous section we defined the direction of motion of a projectile in terms of the coordinates ϑ_x and ϑ_y of the point T at which the tangent to the trajectory of the center of mass intersects a unit sphere with center at O ; the location of T can be specified more concisely by the single complex number $\vartheta = \vartheta_x + i\vartheta_y$. In order to get exact equations of motion analogous to the approximate equation 9.11 (9) and (11), we shall introduce unit vectors that lead to a convenient resolution of the applied forces in directions parallel to and perpendicular to the direction of motion. The unit vectors we use are e_T , e_x , and e_y , where e_T is normal to the surface of the sphere at T and is parallel to v , the velocity of the rocket, e_x is a unit vector tangent at T to the great circle on which ϑ_y is constant, and e_y is a unit vector tangent at T to the small circle on which ϑ_x is constant. Thus e_x and e_y as used here have just the same meaning as in the previous sections except that they are concerned with the point T rather than the point A . Let us now tabulate the direction cosines of e_x , e_y , and e_T with respect to OX_1 , OY_1 , OZ_1 . Each entry⁹ in table 9.17 gives the cosine of the angle between the stationary direction listed at the left of the row and the varying direction listed at the top of the column. The location considered is T ; if the corresponding results are wanted at A it is only necessary to replace e_T by e_A and ϑ by φ throughout.

TABLE 9.17
DIRECTION COSINES

	e_x	e_y	e_T
OX_1	$\cos \vartheta_x$	0.....	$\sin \vartheta_x$
OY_1	$-\sin \vartheta_x \sin \vartheta_y$	$\cos \vartheta_y$	$\cos \vartheta_x \sin \vartheta_y$
OZ_1	$-\sin \vartheta_x \cos \vartheta_y$	$-\sin \vartheta_y$	$\cos \vartheta_x \cos \vartheta_y$

To get the equations of motion of the center of mass of the rocket we start from the fact that the mass times the rate of change of velocity is equal to the total force acting on the rocket. It may be seen from figure 9.17 that the change in v over the infinitesimal interval of time dt is

$$dv = dv e_T + v d\vartheta_x e_x + v \cos \vartheta_x d\vartheta_y e_y.$$

Hence

$$m\dot{v} = m\dot{v} e_T + m v \dot{\vartheta}_x e_x + m v \cos \vartheta_x \dot{\vartheta}_y e_y \quad (1)$$

is equal to the total force, F , acting on the rocket. If we resolve this force into components F_x , F_y , and F_{\parallel} along e_x , e_y , and e_T , respectively, we get

$$F = F_x e_x + F_y e_y + F_{\parallel} e_T. \quad (2)$$

Equating corresponding components of (1) and (2) we get

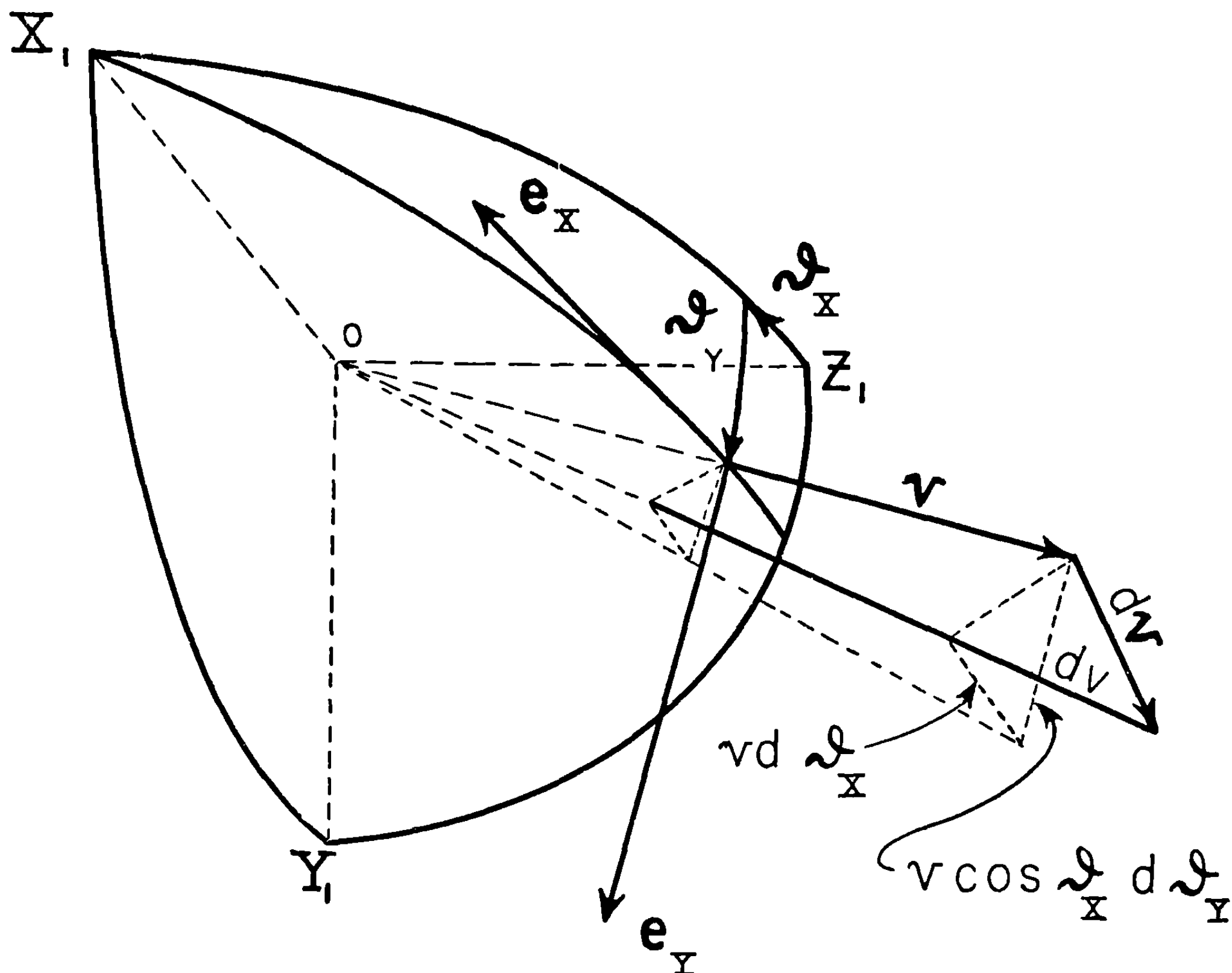
$$m v \dot{\vartheta}_x = F_x, \quad (3)$$

$$m v \dot{\vartheta}_y = F_y + m v (1 - \cos \vartheta_x) \dot{\vartheta}_x, \quad (4)$$

and

$$m \dot{v} = F_{\parallel}. \quad (5)$$

⁹ If the derivation of the entries in this table by means of Fig. 9.17 proves difficult, the reader can consult E. T. Whittaker, "Analytical Dynamics," p. 10, Dover.

FIGURE 9.17.—Proof that $dv = dv \mathbf{e}_T + v d\theta \mathbf{e}_X + v \cos \theta d\theta \mathbf{e}_Y$.

Thus far we have confined our attention to vectors; let us now use the complex notation

$$\mathbf{F}_\perp = F_X + iF_Y \quad (6)$$

for the component of \mathbf{F} normal to \mathbf{v} . We can regard the right side of (6) and $F_X \mathbf{e}_X + F_Y \mathbf{e}_Y$ as different notations for \mathbf{F}_\perp since derivatives of \mathbf{F}_\perp do not appear in our development. Combining (3) and (4) and making use of the definitions $\vartheta = \vartheta_X + i\vartheta_Y$ and (6) we get

$$v\dot{\vartheta} = (\mathbf{F}_\perp/m) + iv(1 - \cos \vartheta_X) \dot{\vartheta}_Y. \quad (7)$$

The total force, \mathbf{F} , acting on the rocket is the sum of \mathbf{F}_g , the force due to gravity; \mathbf{F}_A , the resultant of all the aerodynamic forces; and \mathbf{F}_J , the resultant of all the jet forces. Each of these three can be resolved into components, $F_{g\parallel}$, $F_{A\parallel}$, and $F_{J\parallel}$, along the trajectory and into components normal to the trajectory. In each case the two components normal to the trajectory can be combined into a single complex number by an equation analogous to (6), thus giving us

$$\mathbf{F}_\perp = \mathbf{F}_{g\perp} + \mathbf{F}_{A\perp} + \mathbf{F}_{J\perp}. \quad (8)$$

Since $\mathbf{F}_{A\perp}$ and $\mathbf{F}_{J\perp}$ depend on the yaw, we must postpone further consideration of them until the next section.

We can, however, proceed to consider the resolution of \mathbf{F}_g into $F_{g\parallel}$ and $F_{g\perp}$. In the most general case OX_1 is horizontal, while OZ_1 makes the angle θ_0 with the horizontal. \mathbf{F}_g can then

be resolved into the component $mg \cos \theta_0$ along OY_1 and the component $-mg \sin \theta_0$ along OZ_1 . By using table 9.17 we can resolve each of these into components along e_x , e_y , and e_z . Thus we get

$$\begin{aligned} F_g/m &= g \cos \theta_0 (-\sin \vartheta_x \sin \vartheta_y e_x + \cos \vartheta_y e_y + \cos \vartheta_x \sin \vartheta_y e_z) \\ &\quad - g \sin \theta_0 (-\sin \vartheta_x \cos \vartheta_y e_x - \sin \vartheta_y e_y + \cos \vartheta_x \cos \vartheta_y e_z). \end{aligned} \quad (9)$$

From this it follows that

$$F_{g\parallel}/m = -g \cos \vartheta_x \sin (\theta_0 - \vartheta_y), \quad (10)$$

$$F_{g\perp}/m = g \sin \vartheta_x \sin (\theta_0 - \vartheta_y) + ig \cos (\theta_0 - \vartheta_y). \quad (11)$$

Hence we get from (5) and (10)

$$\dot{v} = \frac{F_{J\parallel} + F_{A\parallel}}{m} - g \cos \vartheta_x \sin (\theta_0 - \vartheta_y), \quad (12)$$

and from (7) and (11)

$$v\dot{\vartheta} = \frac{F_{J\perp} + F_{A\perp}}{m} + ig \cos (\theta_0 - \vartheta_y) + R_2, \quad (13)$$

where

$$R_2 = g \sin \vartheta_x \sin (\theta_0 - \vartheta_y) + iv (1 - \cos \vartheta_x) \dot{\vartheta}_y \quad (14)$$

is always small and hence is usually neglected. The first term in R_2 is the larger and may be of importance when compared with the drift over the entire trajectory; but during burning R_2 is completely negligible. The relative sizes of the remaining terms on the right of (12) and (13) depend on the particular circumstances considered, and the smaller terms are usually either neglected or approximated by simpler expressions. For example, during burning the jet forces are generally very much larger than the gravitational force, and ϑ is generally much less than unity, so that we usually take ϑ to be zero in those terms containing g .

9.18 Complex Representation of the Forces and the Yaw.—In order to make use of the equations in complex form, we must obtain expressions for $F_{J\perp}$, $F_{A\perp}$, and f . In 8.2, vector expressions were given for these forces and moments in terms of the vectors δ and q , which are tangent to the unit sphere at A , and in terms of δ_T and q_T , which are tangent at T . Since none of these vectors has components normal to the sphere, each can be treated as a two-dimensional vector at the point of tangency and resolved into X and Y components parallel to the directions of e_x and e_y at A or at T as the case may be. Thus it is immediately possible to obtain complex representations of the form

$$\delta = \delta_x + i\delta_y, \quad (1)$$

for each of the four vectors. We also need complex representations for the cross-product of a unit vector normal to the surface of our sphere and each one of the vectors δ , δ_T , q , and q_T . The normal for δ and q is e_A while that for δ_T and q_T is e_T . It should be evident that we can set up the following correspondences between the vectors of 8.2 and complex numbers

$$e_A \times \delta \leftrightarrow i\delta, \quad (2)$$

$$e_T \times \delta_T \leftrightarrow i\delta_T, \quad (3)$$

$$\mathbf{e}_A \times \mathbf{q} \leftrightarrow i\mathbf{q}, \quad (4)$$

and

$$\mathbf{e}_T \times \mathbf{q}_T \leftrightarrow i\mathbf{q}_T. \quad (5)$$

Consequently, the expressions for the aerodynamic forces and moments given in 8.22 and 8.23 become, in complex form,

$$\mathbf{f}_A = mK^2V^2 \left\{ k_{V^2\delta} \delta - i \frac{l_s}{V} k_{Vs\delta} \delta - \frac{l}{V} k_{Vq} \mathbf{q} + i \frac{l_s^2}{V^2} k_{sq} \mathbf{q} \right\}, \quad (6)$$

and

$$\mathbf{F}_{A\perp} = mV^2 \left\{ K_{V^2\delta} \delta - i \frac{l_s}{V} K_{Vs\delta} \delta_T - \frac{l}{V} K_{Vq} \mathbf{q}_T + i \frac{l_s^2}{V^2} K_{sq} \mathbf{q}_T \right\}. \quad (7)$$

These expressions do not include the jet forces and moments. The transverse moment due to the jet may, in accordance with 8.51 (3), be represented by the vector expression

$$\mathbf{f}_J = -mG_J \mathbf{R}_M - K_{JD} \mathbf{q}. \quad (8)$$

Both \mathbf{f}_J and the second term on the right, the torque due to jet damping, are expressed in complex form merely by regarding \mathbf{f}_J and \mathbf{q} as being the complex representations of vectors. The first term, the torque due to linear malalignment, gives more trouble since the real and imaginary parts of \mathbf{f}_J are defined as components with respect to a nonrotating system while \mathbf{R}_M , the linear thrust malalignment, is a vector that rotates with the rocket. Hence it is best to resolve it into components

$$\mathbf{R}_M = R_{Mx} \mathbf{e}_x + R_{My} \mathbf{e}_y \quad (9)$$

along axes, Oxy , fixed in the rocket. We introduce

$$\mathbf{R}_M = R_{Mx} + iR_{My} \quad (10)$$

as the complex representation of the linear thrust malalignment. It must be emphasized that this complex number does not vary due to the rotation of the rocket since its real and imaginary parts are defined in terms of components with respect to axes fixed in the rocket. If we remember that the rotation of the Oxy -system beyond its position of parallelism to the OXY -system is ψ , we see that the complex number representing the torque due to the jet is

$$\mathbf{f}_J = -mG_J \mathbf{R}_M e^{i\psi} - K_{JD} \mathbf{q}. \quad (11)$$

By this we mean that the real part of (11), namely

$$-mG_J (R_{Mx} \cos \psi - R_{My} \sin \psi) - K_{JD} q_x$$

is the component of \mathbf{f}_J in the \mathbf{e}_x direction, and that the imaginary part of (11) is the component in the \mathbf{e}_y direction.

The jet force normal to the trajectory is given in vector form by 8.51 (2) as

$$\mathbf{F}_{J\perp} = mG_J \delta_T + mG_J \beta_M. \quad (12)$$

The first term on the right, the cross-force due to the fact that the rocket is not pointing along the trajectory, is readily expressed in complex form since both $\mathbf{F}_{J\perp}$ and δ_T are most natu-

rally resolved in the nonrotating system. The second term, the angular thrust malalignment, must be treated with care since the vector β_M rotates with the rocket. If, as in the case of the linear malalignment, we resolve β_M into components in the Oxy rotating system and introduce the complex number

$$\beta_M = \beta_{Mx} + i\beta_{My}, \quad (13)$$

then we can represent the transverse jet force by the complex number

$$F_{J\perp} = mG\delta_T + mG\beta_M e^{i\psi}. \quad (14)$$

Now that we have transformed these relations involving the vectors δ , δ_T , q , q_T , R_M , and β_M to relations expressed in terms of complex numbers, all that remains is to consider the connection between the complex forms of δ , δ_T , q , and q_T , and the complex numbers φ and ϑ . This can be done only in terms of complex numbers because φ and δ can not be represented by vectors. The connection between φ and q was given by 9.16 (13) and is

$$q = \dot{\varphi} + R_3 = \dot{\varphi} - i\dot{\varphi}_Y(1 - \cos \varphi_X). \quad (15)$$

The connection between φ , ϑ , and δ will be

$$\varphi - \vartheta - \delta = R_4,$$

which is just 9.11 (5) with the addition of a remainder term that is usually neglected. Let us now obtain an expression for R_4 . The quantities φ and ϑ were defined by 9.16 (1) and (2) in terms of coordinates of the points A and T . The vector δ is defined as a vector tangent to the great circle through A and T at A , its magnitude being δ , the angle between OT and OA . The complex number δ is defined in terms of the components of the vector δ along and perpendicular to the arc of the great circle through A and X_1 . Hence by applying the basic theorems of spherical trigonometry to the spherical triangle AX_1T shown in figure 9.18, we can express the complex number δ in terms of the coordinates of A and T . If we denote by Δ_T the angle between the arcs TX_1 and TA and by Δ the angle between the arcs AX_1 and TA extended, then the angles of our spherical triangle are Δ_T , $\pi - \Delta$ and $\varphi_Y - \vartheta_Y$. The sides are $\frac{1}{2}\pi - \vartheta_X$, $\frac{1}{2}\pi - \varphi_X$, and δ . Since we know $\varphi_Y - \vartheta_Y$, ϑ_X , and φ_X , we can compute the remaining unknown quantities, δ , Δ , and Δ_T . By the law of sines,

$$\sin \delta \sin \Delta = \sin (\varphi_Y - \vartheta_Y) \cos \vartheta_X, \quad (16)$$

and by the relation between two angles and three sides

$$\sin \delta \cos \Delta = \cos (\varphi_Y - \vartheta_Y) \sin \varphi_X \cos \vartheta_X - \sin \vartheta_X \cos \varphi_X. \quad (17)$$

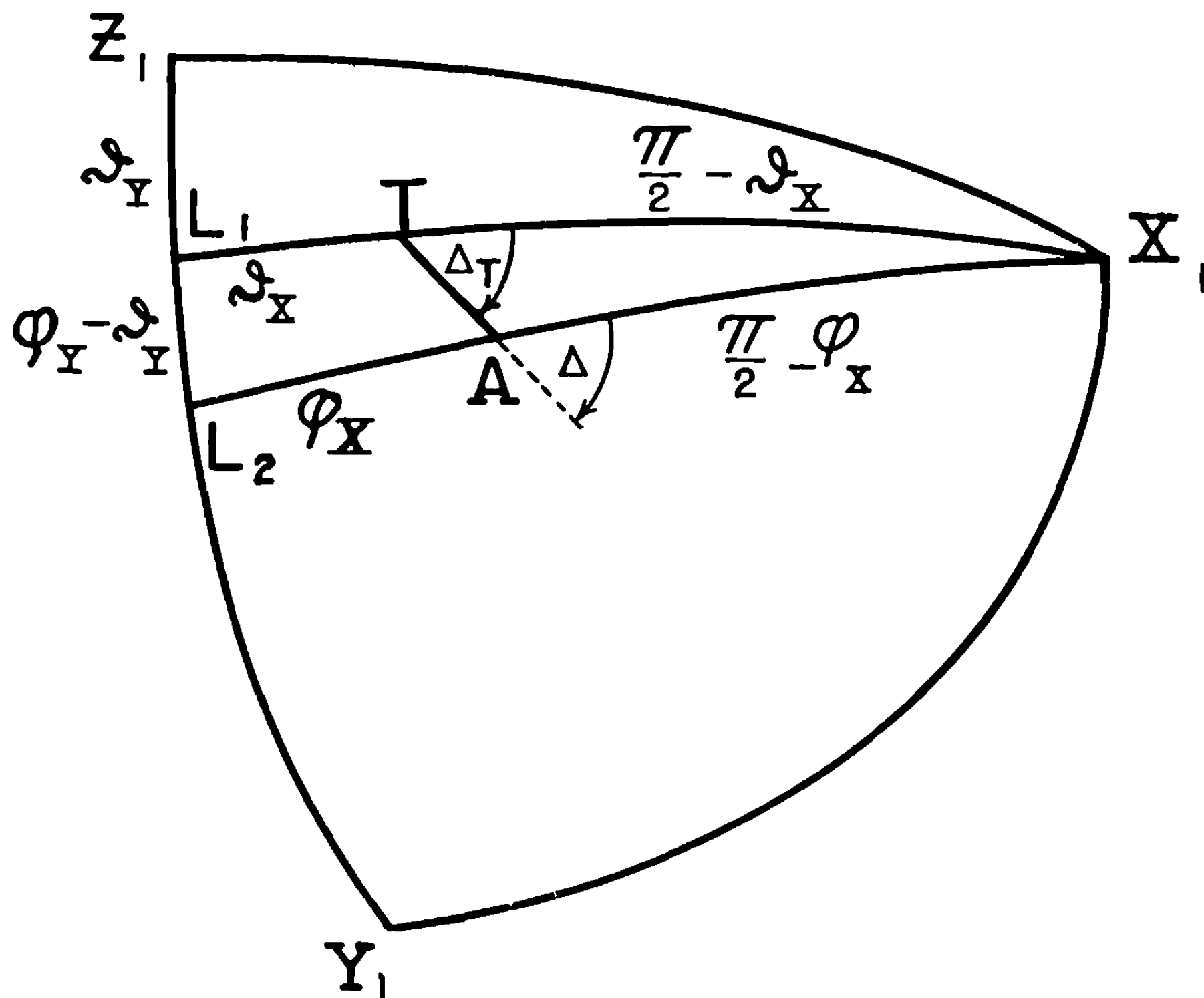
But

$$\delta_X = \delta \cos \Delta, \quad \delta_Y = \delta \sin \Delta, \quad \delta = \delta_X + i\delta_Y. \quad (18)$$

Hence

$$\begin{aligned} \varphi - \vartheta - \delta = R_4 = & \varphi_X - \sin \varphi_X \cos \vartheta_X \cos (\varphi_Y - \vartheta_Y) - \vartheta_X + \sin \vartheta_X \cos \varphi_X \\ & + i[(\varphi_Y - \vartheta_Y) - \sin (\varphi_Y - \vartheta_Y) \cos \varphi_X] - \left(1 - \frac{\sin \delta}{\delta}\right) \delta. \end{aligned} \quad (19)$$

It follows from (19) that for R_4 to be very small it is necessary that δ , φ_X , ϑ_X , and $\varphi_Y - \vartheta_Y$ be small but no restriction is put on φ_Y and ϑ_Y separately. It was to achieve this that we took the equator of our coordinate system in the OY_1Z_1 -plane.

FIGURE 9.18.—The octant X, Y, Z , as seen from the inside.

Our next problem is to inquire into the circumstances under which we can replace δ_T by δ and q_T by q in (7) and (14). The vector δ_T is defined in just the same way as was δ except that it is tangent to the great circle through A and T at T . The components along and perpendicular to the great circle through T and X_1 are the real and imaginary parts, respectively, of the complex number δ_T . Hence

$$\delta_T = \delta \cos \Delta_T + i\delta \sin \Delta_T = \delta \exp(i\Delta_T) = \delta \exp(i\Delta) \exp[i(\Delta_T - \Delta)] = \delta \exp[i(\Delta_T - \Delta)];$$

or

$$\delta_T = \delta + R_5 = \delta - \{1 - \exp[i(\Delta_T - \Delta)]\} \delta. \quad (20)$$

It is easy to obtain an estimate of $\Delta_T - \Delta$ from figure 9.18 since the sum of the angles of a spherical triangle on a unit sphere is equal to π plus the area of the triangle. Now the area of the triangle $L_1X_1L_2$ is $(\varphi_Y - \vartheta_Y)$ and the area of L_1TAL_2 is approximately

$$(\varphi_Y - \vartheta_Y) \sin \frac{1}{2} (\varphi_X + \vartheta_X),$$

provided φ_X and ϑ_X are small. This expression is exact provided $\vartheta_X = \pm \varphi_X$. Hence the area of the triangle TAX_1 is approximately

$$(\varphi_Y - \vartheta_Y) - (\varphi_Y - \vartheta_Y) \sin \frac{1}{2} (\varphi_X + \vartheta_X),$$

and the sum of its angles is

$$\Delta_T + (\pi - \Delta) + (\varphi_Y - \vartheta_Y).$$

Then, from the theorem connecting the area and the sum of the angles of a spherical triangle, we have approximately

$$\Delta_T - \Delta \doteq (\varphi_Y - \vartheta_Y) \sin \frac{1}{2} (\varphi_X + \vartheta_X). \quad (21)$$

Since \mathbf{q}_T was defined in 8.2 to be a vector tangent to the unit sphere and making the same angle with the OAT -plane as does the vector \mathbf{q} , the complex number \mathbf{q}_T is connected with \mathbf{q} by the equation

$$\mathbf{q}_T = \mathbf{q} \exp [i(\Delta_T - \Delta)] = \dot{\varphi} + \mathbf{R}_6 = \dot{\varphi} + \mathbf{R}_3 - \{1 - \exp [i(\Delta_T - \Delta)]\}(\dot{\varphi} + \mathbf{R}_3). \quad (22)$$

9.19. Exact Equations of Motion in Complex Form and the Effects of the Errors in the Approximate Equations.—Let us gather together the equations of motion derived in the last three sections. From 9.16 (14), 9.18 (11), (6), and (15) we get

$$\ddot{\varphi} - i \frac{s}{\gamma} \dot{\varphi} - \frac{s^2}{4\gamma^2 S} \delta = -\frac{GR_M}{K^2} e^{i\psi} - \frac{K_{JD}}{mK^2} \dot{\varphi} + V^2 \left\{ -i \frac{ls}{V} k_{vs\delta} \delta - \frac{l}{V} k_{vq} \dot{\varphi} + i \frac{l^2 s}{V^2} k_{sq} \dot{\varphi} \right\} + \mathbf{R}_7, \quad (1)$$

where

$$\mathbf{R}_7 = \mathbf{R}_1 + \left\{ i \frac{K_{JD}}{mK^2} + ilV k_{vq} + l^2 s k_{sq} \right\} \dot{\varphi}_Y (1 - \cos \varphi_X), \quad (2)$$

the remainder term \mathbf{R}_1 is given by 9.16 (15), and the term containing the aerodynamic overturning moment has been transferred to the left and expressed in terms of the stability factor S by means of 8.22 (9). In all applications of (1) only the terms important for the point under consideration will be retained, thus leaving a more manageable equation. From 9.17 (13), 9.18 (14), (7), (20), and (22) we get

$$v\dot{\vartheta} = ig \cos (\theta_0 - \vartheta_Y) + G\delta + G\beta_M e^{i\psi} + V^2 \left\{ K_{v^2\delta} \delta - i \frac{ls}{V} K_{vs\delta} \delta - \frac{l}{V} K_{vq} \dot{\varphi} + i \frac{l^2 s}{V^2} K_{sq} \dot{\varphi} \right\} + \mathbf{R}_8, \quad (3)$$

where the remainder term \mathbf{R}_8 is

$$\mathbf{R}_8 = \mathbf{R}_2 + \left\{ G + V^2 \left[K_{v^2\delta} - i \frac{ls}{V} K_{vs\delta} \right] \right\} \mathbf{R}_5 + V^2 \left[-\frac{l}{V} K_{vq} + i \frac{l^2 s}{V^2} \right] \mathbf{R}_6. \quad (4)$$

\mathbf{R}_2 is given by 9.17 (14), \mathbf{R}_5 by 9.18 (20), and \mathbf{R}_6 by 9.18 (22). From 9.18 (19) we have

$$\varphi - \vartheta - \delta = \mathbf{R}_4 \quad (5)$$

and the expression for the remainder term \mathbf{R}_4 .

These three equations determine the transverse motion. The motion along the trajectory and the spin about the longitudinal axis of the projectile are governed by

$$\dot{v} = -g \cos \vartheta_X \sin (\theta_0 - \vartheta_Y) + (F_{J\parallel}/m) - cV^2 \quad (6)$$

and

$$\dot{s} = (M_{J\parallel}/mk^2) - k_{vs} lVs. \quad (7)$$

The first of these equations follows directly from 9.17 (12) and 8.22 (1) while the second follows from 9.16 (16) and 8.22 (4). A final, occasionally useful, equation obtained from 9.16 (16) is

$$s = \psi - \dot{\varphi}_Y \sin \varphi_X. \quad (8)$$

The above equations are exact except possibly for the effects of changing mass, moments of inertia, and center of mass; these effects can be allowed for as discussed in 2.2. In cases in which v and s are proportional to t , the change of variables 9.11 (32) reduces (1), (3), and (5) to 9.11 (33), (34), and (35).

By neglecting the remainder terms and other small terms in these equations, systems of relatively simple equations are obtained whose solutions we shall consider at some length. It is usually easy to show that the terms that are neglected in any solution are small under the circumstances considered, but it is desirable to go further and show that there are no large cumulative effects due to the neglected terms. When considering the errors that are present in the solutions of the approximate equations of motion, it is important to note that there are two different types of error present. The first we may call the physical errors; they are due to use of approximate values of the mass, the acceleration, the stability factor, and the other physical constants that characterize a rocket. In this category we can include errors due to a variety of simplifying assumptions such as the assumption that the mass and moments of inertia are constant during burning, the assumption that the linear and angular accelerations are constant, the assumption that the aerodynamic drag, lift, and overturning moments vary as the square of the velocity, and the assumption of precise, simple initial conditions. The effects of such errors can usually be estimated satisfactorily by comparing solutions for different constant values of the mass, the acceleration, the overturning moment, etc.

The second type of error is that due to the neglect of small terms, particularly nonlinear terms such as the remainder terms, in the equations of motion and may be called a mathematical approximation.

These remainder terms may be divided into two classes of roughly equal magnitude but different time dependence. Those terms which have the same frequency as the nutations or precessions (see 10.11) give rise by resonance to cumulative effects, that is, the errors become larger as the solution is extended over longer periods of time. The other terms have roughly the same effect over part of a nutation or precession but reverse sign and cancel out by the end of a cycle so that they may be neglected over long times. Most of these latter terms arise from the distortion of the coordinate system at points not on the equator where φ_x and ϑ_x are zero. This distortion means that if, for example, the axis of the projectile describes a true circle, the representative vector should describe an oval with a ratio of the major to minor axis of $\cos \bar{\varphi}_x$, where $\bar{\varphi}_x$ is the coordinate of the center of the oval. However, if we neglect the distortion of the coordinate system in our interpretation of the results and if we neglect the parts of the remainder terms that are needed to make the equations exact in spite of the distortion, some of our errors compensate each other. By confining our attention to cases in which φ_x and ϑ_x are always small compared to unity, we can be assured that the effects of distortion are negligible. This is almost always the case in practice since, if the axis of the rocket wanders far from the vertical plane through the launcher, the motion will be characterized by large deflection and the case will be of so little practical importance that only a very approximate solution will be required.

Let us examine more closely the circumstances under which the distortion terms are negligible because the point A remains near the equator of the coordinate system. This will be the case if A moves in a spiral whose radius of curvature is small. Hence we want φ_H , as defined by 9.14 (9), to be small which requires that the transverse velocity, q , satisfy

$$\varphi_H \doteq \frac{q\gamma}{s} \ll 1. \quad (9)$$

Near the launcher, where s is small this condition may not hold, but if under such circumstances s increases rapidly enough that (9) is violated only while A moves a distance small compared to unity, A will always remain near its starting point and the effect of distortion will be small. When s is proportional to t , the time required to complete the first term of the spiral is t_λ , as defined by 9.11 (30), and the condition that must be satisfied when (9) is violated is that

$$q_p t_\lambda \ll 1 \quad (10)$$

where q_p is the angular velocity at launching. Of course we must also require that

$$\delta_p \ll 1, \text{ and } \varphi_p \ll 1 \quad (11)$$

if A is to be very near the equator of the coordinate system.

The conclusion that the fractional or percentage error vanishes when the amplitude of the motion is zero assures us that the solutions of our equations are meaningful in many cases but does not allow a determination of the error involved in any particular case. Conditions (9) and (10) apply only to errors due to the distortions of the coordinate system (and then are unnecessarily stringent), while conditions on the cumulative errors must include the time over which the solution is to hold.

In order to determine the effect of the cumulative errors, let us consider, for example, the solution of (1) in the case in which all transverse moments are zero so that the exact equation of motion is

$$\ddot{\phi} - i(s/\gamma)\dot{\phi} = R_1. \quad (12)$$

The exact solution, which is most easily obtained by the methods of 9.14, shows that the tangent to the curve traced out by the point A turns at the rate

$$\omega_N = \frac{s}{\gamma} \sec \varphi_H, \quad (13)$$

which is just the rate of nutation as defined in 10.11. On the other hand, if we neglect R_1 and solve (12) we find that the rate of nutation; i. e., the rate at which the tangent turns, is, according to our approximate solution,

$$\omega_N = s/\gamma. \quad (14)$$

To see this it is only necessary to note that $\dot{\phi}$ gives the direction of the tangent and that according to (12) the change in $\dot{\phi}$ in the time Δt is

$$\Delta \dot{\phi} = i(s/\gamma)\dot{\phi}\Delta t. \quad (15)$$

This is perpendicular to $\dot{\phi}$ so that the change in the direction of $\dot{\phi}$ is $|\Delta \dot{\phi}|/|\dot{\phi}|$ and the rate of change is s/γ . Hence the correction that must be added to the direction of the tangent as given by the approximate equation in order to get the true direction is

$$\begin{aligned} \Delta \psi_N &= \int_{t_p}^t [\omega_N (\text{exact}) - \omega_N (\text{approx.})] dt = \int_{t_p}^t \frac{s}{\gamma} [\sec \varphi_H - 1] dt \\ &= \int_{t_p}^t \left[\left(\frac{s^2}{\gamma^2} + q^2 \right)^{\frac{1}{2}} - \frac{s}{\gamma} \right] dt \doteq \int_{t_p}^t \frac{s \varphi_H^2}{2\gamma} dt. \end{aligned} \quad (16)$$

Now in the case in which the accelerations are constant so that 9.11 (26), (30), and (32) give

$$s/\gamma = 4\pi\zeta/t_\lambda; \quad t = \zeta t_\lambda, \quad (17)$$

we have

$$\begin{aligned} \Delta\psi_N &= 4\pi \int_{\zeta_p}^{\zeta} \left\{ \sqrt{\zeta^2 + \left(\frac{q_p t_\lambda}{4\pi}\right)^2} - \zeta \right\} d\zeta \\ &\doteq \frac{(q_p t_\lambda)^2}{8\pi} \ln \frac{\zeta}{\zeta_p}, \text{ when } q_p t_\lambda \ll 4\pi\zeta_p \\ &\doteq \frac{(q_p t_\lambda)^2}{8\pi} \left\{ \frac{1}{2} + \ln \frac{8\pi\zeta}{q_p t_\lambda} - \frac{8\pi\zeta_p}{q_p t_\lambda} \right\}, \text{ when } 4\pi\zeta_p \ll q_p t_\lambda \ll 2\pi\zeta. \end{aligned} \quad (18)$$

The first condition of (18) is easy to reduce to an expression for the maximum allowable value of $q_p t_\lambda$ in terms of the error $\Delta\psi_N$ which can be tolerated, but the second condition is more complicated and cannot be inverted analytically. It must be treated numerically or by successive approximations. The limits on q_p are given by

$$q_p t_\lambda < \left[\frac{8\pi\Delta\psi_N(\text{tolerated})}{\ln \zeta/\zeta_p} \right]^{\frac{1}{2}}, \text{ when } q_p t_\lambda \ll 4\pi\zeta_p$$

and

$$q_p t_\lambda < (4\pi)^{\frac{1}{2}} \{ \Delta\psi_N(\text{tolerated}) \}^{\frac{1}{2}} \left\{ \frac{1}{2} + \ln \frac{8\pi\zeta}{q_p t_\lambda} - \frac{8\pi\zeta_p}{q_p t_\lambda} \right\}^{-\frac{1}{2}}, \text{ when } 4\pi\zeta_p \ll q_p t_\lambda \ll 2\pi\zeta. \quad (19)$$

Using the values $\Delta\psi_N = \frac{\pi}{4}$, $\zeta_p = 0.2$, and $\zeta = 2$, the two conditions (19) give $q_p t_\lambda < 2$ and $q_p t_\lambda < 6$ respectively, which shows that (10) is quite stringent. The conditions (19) could also be regarded as giving the maximum allowable value of ζ in order that the cumulative error not pile up to too large a value. However, since ζ enters only in logarithmic terms the accumulation is relatively slow for all practical cases and the limit on ζ is of little importance.

After burning, the precessions must be taken into account and hence we retain the term $s^2\delta/4\gamma^2 S$ in (1). Then according to 10.11 the solution, neglecting R_1 , may be written in the form

$$\varphi = A_N \exp(i\omega_N t) + A_P \exp(i\omega_P t) \quad (20)$$

where ω_N and ω_P are constants, and $\omega_N + \omega_P = s/\gamma$. It will be shown in chapter 10 that ω_N and ω_P are the angular frequencies of the nutation and precession, respectively. If we use (20) to evaluate R_1 and obtain its effect by the Green's function technique (see 9.42 for an example of the method), we obtain

$$\Delta\psi_N = \pi N \left\{ A_N^2 + \frac{\omega_P}{8(\omega_N - \omega_P)} (10A_P^2 + 5A_N^2) \right\} \quad (21)$$

and

$$\Delta\psi_P = \pi P \left\{ \left(\frac{5}{4} A_N^2 - \frac{3}{8} A_P^2 \right) + \frac{\omega_P}{8(\omega_N - \omega_P)} (5A_P^2 + 10A_N^2) \right\} \quad (22)$$

where N is the number of nutations and P the number of precessions over which the error is computed. The fractional error in amplitude is roughly equal to the fractional error in phase and hence is quite small. When ω_P is zero, (21) reduces to the last expression in (16) as it should.

The error terms R_2 and R_4 are primarily due to the distortion of the coordinate system and hence do not give appreciable cumulative effects. These terms are of the same magnitude as R_1 , as may be seen by eliminating φ and ϑ from the left of (1), (3), and (5) (see 9.31) and thus

obtaining a single equation in δ with all the error terms combined on the right. The result of this elimination is very complicated but all the error terms are of the same magnitude when δ , φ , and ϑ are of the same order. Hence we may take (19), (21), and (22) as giving the limits of validity of the approximate equations.

9.2 The Vacuum Approximation

In order to determine the salient features in the motion of a spin-stabilized rocket during burning we first treat the case of a rocket in vacuum. A detailed treatment of the motion of a nonspinning rocket in vacuum has been given in 3.1 and the motion of a spinning rocket is in many respects the same. There are, however, several large effects caused by the spin and it is these in which we are interested. We shall start with the equations of motion derived in 9.1 and obtain the characteristic solutions immediately, since it was shown in 9.12 that the various solutions are linearly additive.

The application of the results of this section to practical cases is limited to short burning rockets and rockets with a very high stability factor. These results have been verified experimentally in cases in which they are applicable, but no general experimental check is possible, since the results give only an indication of the motion for long burning rockets. They were used in this way before the computations were carried out for the case of a finite stability factor.

The results presented in this section are obtained by a straightforward application of techniques developed in 9.1, except for the approximate treatment of malalignment. In this case use is made of physical concepts to obtain the approximations. An interesting expression for the Green's function is used in 9.26 to verify this reasoning.

9.21 Equations of Motion—The equations of motion in vacuum may be obtained from 9.11 (33)–(35) by setting the aerodynamic forces equal to zero (or $S = \infty$). These equations then become

$$\varphi'' - 4\pi i \zeta \varphi' = \frac{t_\lambda^2}{mK^2} f_I(\zeta), \quad (1)$$

$$\vartheta' - \frac{1}{\zeta} \delta = \frac{1}{mG\zeta} F_I(\zeta), \quad (2)$$

and

$$\varphi - \vartheta - \delta = 0. \quad (3)$$

We retain in the moment $f_I(\zeta)$ only the term due to linear malalignment,

$$f_I(\zeta) = -mGR_M e^{i\psi}; \quad (4)$$

and we retain in the force F_I the terms due to gravity and the angular malalignment, so that

$$F_I(\zeta) = img \cos \theta_0 + mG\beta_M e^{i\psi}. \quad (5)$$

We are to solve these equations with arbitrary initial conditions, but, by 9.12, we may single out each effect and treat it separately. We shall proceed to do this in the succeeding sections, starting with the effects of initial yaw and gravity since these solutions are the same as those given for finned rockets in 3.1.

9.22 Solutions for Initial Yaw, Initial Cross-Pointing, and Gravity.—The motion of a fin-stabilized rocket in vacuum has been considered in detail in 3.1. The spin of the rocket does not influence the motion as long as the axis of the rocket does not rotate transversely, hence, the motion with gravity and initial yaw is the same as that given in 3.1. However,

we wish to write the solution in terms of the dimensionless characteristic functions defined in 9.12 (1) and (2) rather than in terms of the time. If $f_I = F_I = 0$ and if initially $\varphi' = 0$, 9.21 (1)–(3) are immediately integrable, φ evidently being constant. If we take $\delta_p = 1$, $\varphi_p = 0$ so that we have the characteristic functions for initial yaw,

$$\Phi_\delta = 0, \Theta_\delta = -\Delta_\delta = -\frac{\zeta_p}{\zeta}, R_\delta = -2\zeta_p(\zeta - \zeta_p). \quad (1)$$

The solutions for initial cross-pointing are obtained when we take $\delta_p = 0$, $\varphi_p = 1$ and are

$$\Phi_\varphi = \Theta_\varphi = 1, \Delta_\varphi = 0, R_\varphi = (\zeta^2 - \zeta_p^2). \quad (2)$$

The solutions (1) constitute Green's functions for the applied forces and may be used to determine the effect of gravity. However, the equations are easily integrable when $F_I = imG \cos \theta_0$ and $\varphi_p = \delta_p = \varphi_p' = f_I = 0$ and the resulting gravity solution is

$$\varphi_g = \frac{g \cos \theta_0}{G} \Phi_g, \quad \vartheta_g = \frac{g \cos \theta_0}{G} \Theta_g, \quad \delta_g = \frac{g \cos \theta_0}{G} \Delta_g, \quad r_g = \frac{g \cos \theta_0}{G} \lambda R_g, \quad (3)$$

where

$$\Phi_g = 0, \Theta_g = -\Delta_g = i \left(1 - \frac{\zeta_p}{\zeta} \right), R_g = i(\zeta - \zeta_p)^2. \quad (4)$$

The presence of i in these expressions indicates that the deflection due to gravity is vertically downward. A plot of Θ_g/i may be obtained from figure 3.11 b by replacing d/p by $(\zeta/\zeta_p)^2$.

9.23 Solution for Mallaunching.—The characteristic functions for mallaunching are somewhat more complicated than those given above because of the gyroscopic effects due to the spin. The solution for φ may be obtained easily by direct integration of 9.21 (1) since it does not contain δ or ϑ . The integral of the homogeneous equation satisfying the initial conditions $\varphi_p = \delta_p = 0$, $\varphi_p' = 1$ is

$$\Phi_q = \frac{1}{2} \exp(-2\pi i \zeta_p^2) [E(2\zeta) - E(2\zeta_p)], \quad (1)$$

where $E(x)$ is the complex Fresnel integral

$$\begin{aligned} E(x) &= \int_0^x \exp\left(\frac{1}{2} i \pi y^2\right) dy \\ &= C(x) + iS(x), \end{aligned} \quad (2)$$

and $C(x)$ and $S(x)$ are the usual Fresnel integrals tabulated in appendix C.

Differentiating 9.21 (3) and eliminating ϑ' with the aid of 9.21 (2) we have

$$\delta' + \frac{\delta}{\zeta} = \frac{1}{\zeta} (\zeta \delta)' = \varphi'. \quad (3)$$

Using (3) and (1) we have

$$\begin{aligned} \Delta_q &= \frac{1}{\zeta} \int_{\zeta_p}^{\zeta} \zeta \exp\{2\pi i(\zeta^2 - \zeta_p^2)\} d\zeta, \\ &= \frac{i}{4\pi\zeta} [1 - \exp\{2\pi i(\zeta^2 - \zeta_p^2)\}], \end{aligned} \quad (4)$$

and

$$\Theta_q = \Phi_q - \Delta_q. \quad (5)$$

The solution for R_q is, by 9.11 (41),

$$\begin{aligned} R_q &= 2 \int_{\zeta_p}^{\zeta} \zeta \Theta_q d\zeta \\ &= \frac{1}{2} \left(\zeta^2 + \frac{i}{4\pi} \right) [E(2\zeta) - E(2\zeta_p)] \exp(-2\pi i \zeta_p^2) + \frac{i\zeta}{4\pi} \exp[2\pi i (\zeta^2 - \zeta_p^2)] - \frac{i(2\zeta - \zeta_p)}{4\pi}. \end{aligned} \quad (6)$$

This expression for R_q may be used to compute the displacement, but it is simpler and just as accurate to integrate $\zeta \Theta_q$ numerically. This procedure has been adopted in computing the figures described below. The functions (1), (4), (5), and (6) constitute the Green's function for an applied moment.

For most applications we desire only the value of ϑ because we are interested primarily in the direction the rocket will go at the end of burning. In some cases, however, as in dealing with yaw cards or spark photography, the values of δ and φ are desired; and for certain applications, such as firing over a mask, it is desirable to know the displacement of the rocket from the launcher line. However, publication of all four functions would require considerable space; we include large scale graphs of Θ and R only, the functions of primary interest in field work.

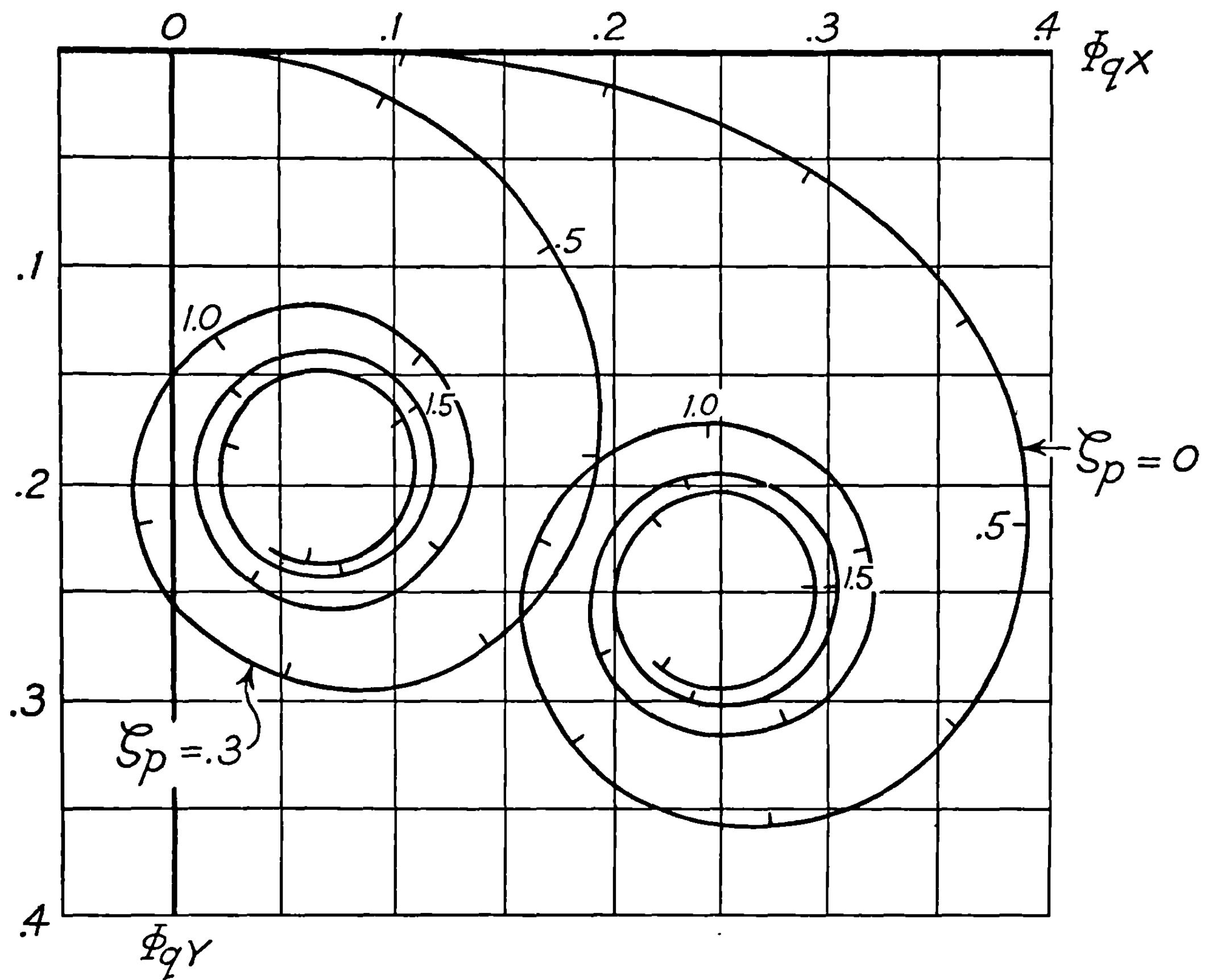
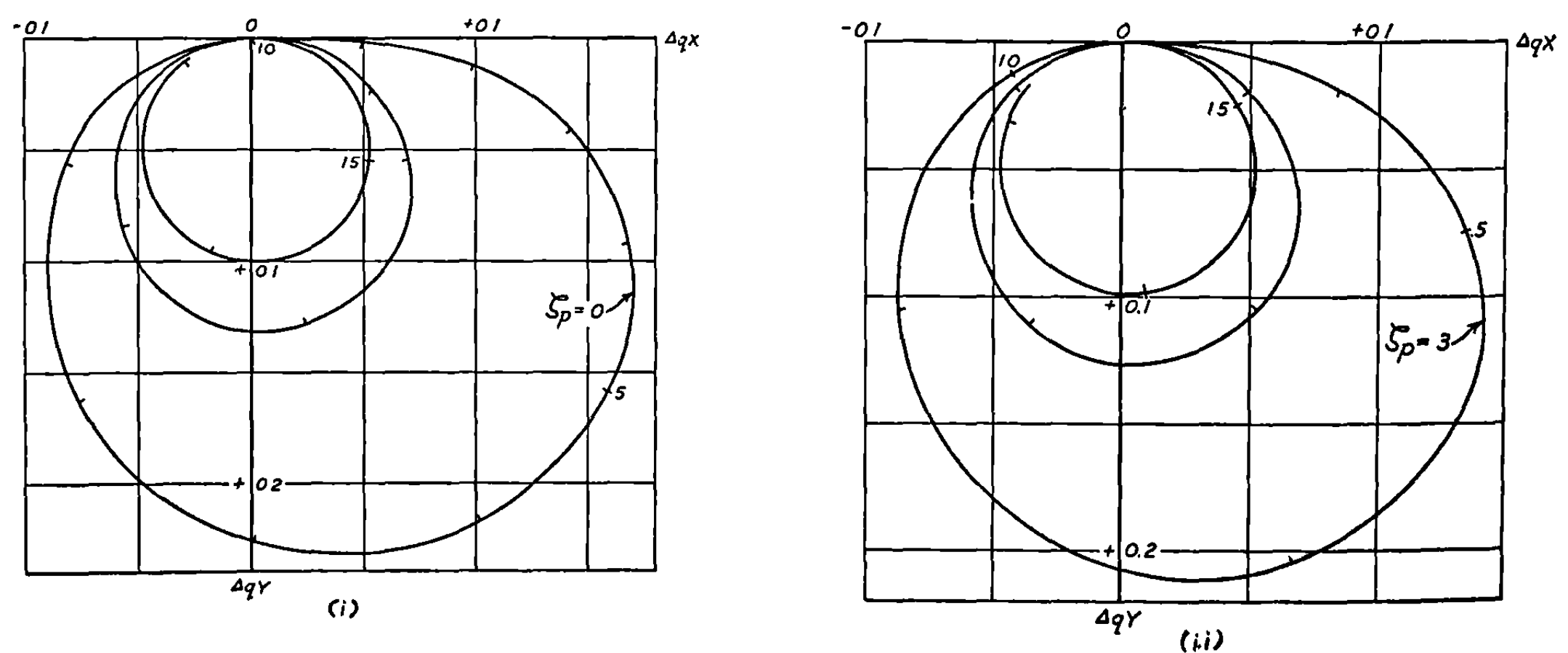
The method we employ in plotting the functions is an expression of their vector character. If one looks along the Z -axis and observes the points A and T on the unit sphere, their loci are curves on which one may mark the time. The locus of A gives a Φ curve, and the locus of T a Θ curve. We plot all the various functions in a similar manner as plane curves, with the real axis to the right and the imaginary axis down, marking the curves with the appropriate values of ζ . A plot in this form allows the motion to be visualized easily, since the figure may be rotated until the initial conditions have the correct orientation.

It may be seen from (1) that the locus of the point A is a segment of a Cornu spiral. Figure 9.23a is a plot of Φ_q for ζ_p equal to 0 and 0.3, showing the typical behavior of motion with accelerated spin. The curve for any value of ζ_p can be obtained from the curve for $\zeta_p=0$ merely by starting at the appropriate point on the latter curve. The figure shows that the motion is confined largely to the first quadrant and entirely to the first two quadrants. Furthermore, the Cornu spiral always winds around a point in the first quadrant. The character of the motion for large values of ζ is best obtained from the asymptotic expansion of (1), which may be obtained from the formulas in Appendix B. It is

$$\begin{aligned} \Phi_q &\sim \frac{1}{4} \exp(-2\pi i \zeta_p^2) \left\{ -2E(2\zeta_p) + 1 + i + \frac{\exp(2\pi i \zeta^2)}{\pi i \zeta} \left[1 + \frac{1}{4\pi i \zeta^2} + \frac{1 \cdot 3}{(4\pi i \zeta^2)^2} + \dots \right] \right\} \\ &\doteq \frac{1}{4} \exp(-2\pi i \zeta_p^2) \{ 1 + i - 2E(2\zeta_p) \} \end{aligned} \quad (7)$$

and is useful when $\zeta > 1$.

It is apparent from (4) that the imaginary part of Δ_q is always positive and that Δ_q is zero once every nutation. The rocket nutates around the angular momentum vector in a decreasing spiral, the radius of which is always just equal to the angle between the angular momentum and the trajectory. Figure 9.23b is a plot of Δ_q for ζ_p equal to 0 and 0.3, showing the general character of the motion. The yaw oscillates around the value

FIGURE 9.23 (a).—Characteristic function $\Phi_q(\xi_p, \xi)$ in vacuum.FIGURE 9.23 (b).—Characteristic function $\Delta_q(\xi_p, \xi)$ in vacuum.

$$\Delta_q \doteq \frac{i}{4\pi\zeta}, \quad (8)$$

as may be seen easily from (4), and, except for phase, is nearly independent of ζ_p for all ordinary launcher lengths.

The direction of motion, Θ_q is a composite of Δ_q and Φ_q , and hence is more complicated than either. It is a more slowly varying function since the major part of the oscillations cancel out, as may be seen from figure 9.23c in which Θ_q is plotted for ζ_p equal to 0, 0.2, and 0.3. It is apparent from the figure that Θ_q is markedly dependent upon launcher length, a result important in the determination of the optimum launcher design. The asymptotic expansion of Θ_q , as obtained from the formulas in Appendix B, is

$$\begin{aligned} \Theta_q &\sim \frac{1}{4} \exp(-2\pi i \zeta_p^2) \left\{ -2E(2\zeta_p) + 1 + i + \frac{\exp(2\pi i \zeta^2)}{\pi i \zeta} \left[\frac{1}{4\pi i \zeta^2} + \frac{1.3}{(4\pi i \zeta^2)^2} + \dots \right] \right\} - \frac{i}{4\pi\zeta} \\ &\doteq \frac{1}{4} \exp(-2\pi i \zeta_p^2) [1 + i - 2E(2\zeta_p)] - \frac{i}{4\pi\zeta}. \end{aligned} \quad (9)$$

This latter expression is very convenient for rough computations whenever ζ is greater than unity, and, since the oscillatory terms are eliminated, it is equivalent to an average over a nutation. For many purposes it is better to use this average value than the accurate value

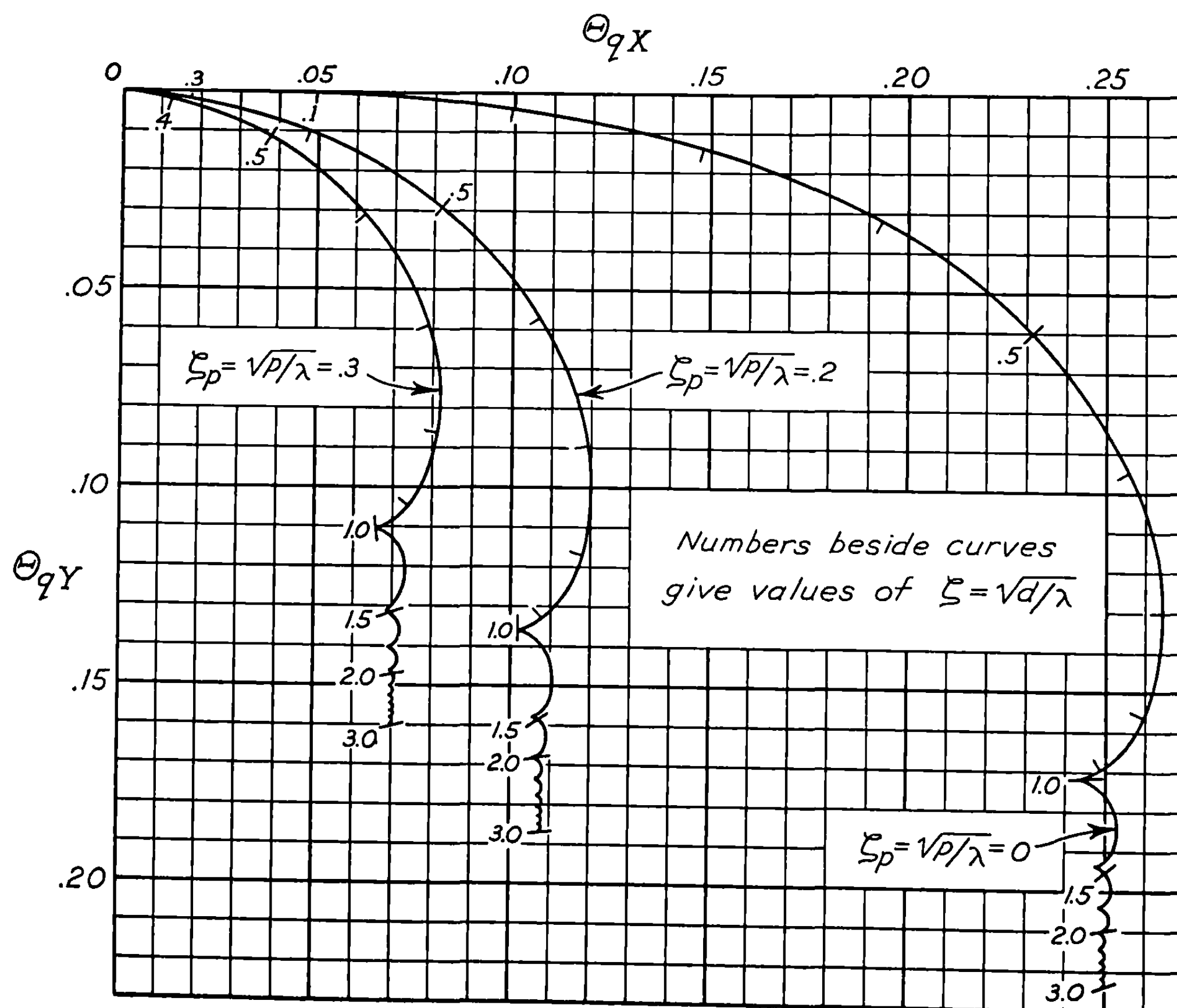


FIGURE 9.23 (c).—Characteristic function $\Theta_q(\zeta_p, \zeta)$ in vacuum.

since when ζ is large compared to unity, it is difficult to predict in any particular experimental situation just what the phase of the nutation will be at the end of burning. This is because of experimental uncertainty in the values of λ , t_b , and the effective accelerations. In such cases the average of Θ_q over a nutation may represent the average behavior to be expected while the variation during the nutation would be a source of dispersion. The dispersion due to this is very small in this case but may be larger for other functions.

If only the magnitude of Θ_q is of interest, as in the computation of dispersion from a given random malalignment, we may use the approximate expression

$$\Theta_q \approx 0.3(1 - \zeta_p)^2, \text{ for } \begin{cases} 1 < \zeta^2 < 5 \\ 0 < \zeta_p^2 < 0.1, \end{cases} \quad (10)$$

or the slightly more accurate expression

$$\Theta_q \approx 0.35 \left[\frac{1}{(1 + \zeta_p)^2} - \frac{1}{(1 + \zeta)^2} \right], \text{ for } \zeta > \zeta_p. \quad (11)$$

These two expressions have no theoretical justification but have been obtained by fitting polynomials to the computed curves.

In addition to these three curves of figure 9.23c, which may be compared directly with those that apply for a nonzero aerodynamic overturning moment (fig. 9.32 a-c), a further series of curves is shown in figures 9.23d and 9.23e. The method of plotting these curves, with magnitude in one figure and phase in another, makes it quite difficult to visualize the motion, but it is possible to get more curves on a sheet without overlapping. Ordinarily it would not be necessary to have all these curves, since the normal range of launcher lengths is not large, but they are convenient for constructing the Green's function for the numerical evaluation of small terms.

The values of R_q are given in figure 9.23f for $\zeta_p = 0, 0.2$, and 0.3 . These curves show that the linear displacement of the rocket during burning is small at first but that it increases rapidly with time after Θ_q becomes essentially constant as indicated by figure 9.23c. This behavior is characteristic of most displacements.

The function $\Theta_q(\zeta_p, \zeta)$, when regarded as a function of ζ_p , constitutes the Green's function for the solution of inhomogeneous equations, as was shown in 9.13. The analytic expression is sufficient for some applications, such as the treatment of the effect of malalignment which is given in 9.24; but it is sometimes necessary to evaluate the integral numerically. Also it is desirable to have a "feel" for the behavior of the function to be able to estimate what the effect of certain applied moments will be. Figure 9.23g is a plot of Θ_q as a function of ζ_p for $\zeta = \sqrt{2}$ and 2. In addition to representing the Green's function, these curves show very clearly the marked variation of the deflection with launcher length. It is apparent from the figure that the effect of a given applied moment is larger the nearer it is applied to the launcher.

9.24 Linear Malalignment.—It will be recalled that the linear malalignment, R_M , defined precisely in 2.24, is approximately the distance from the center of mass to the line of action of the jet thrust. In a spin-stabilized rocket the effect of malalignment is small because the rotation of the rocket tends to average out the torque. However, the effect may be important for short launchers because the spin is small as the rocket leaves such a launcher. In order to evaluate the effect of linear malalignment we must solve equations 9.21 (1)–(5) under the assumption that $F_r = 0$ and subject to the initial conditions that at $\zeta = \zeta_p$, $\varphi = \varphi' = \delta = 0$. This

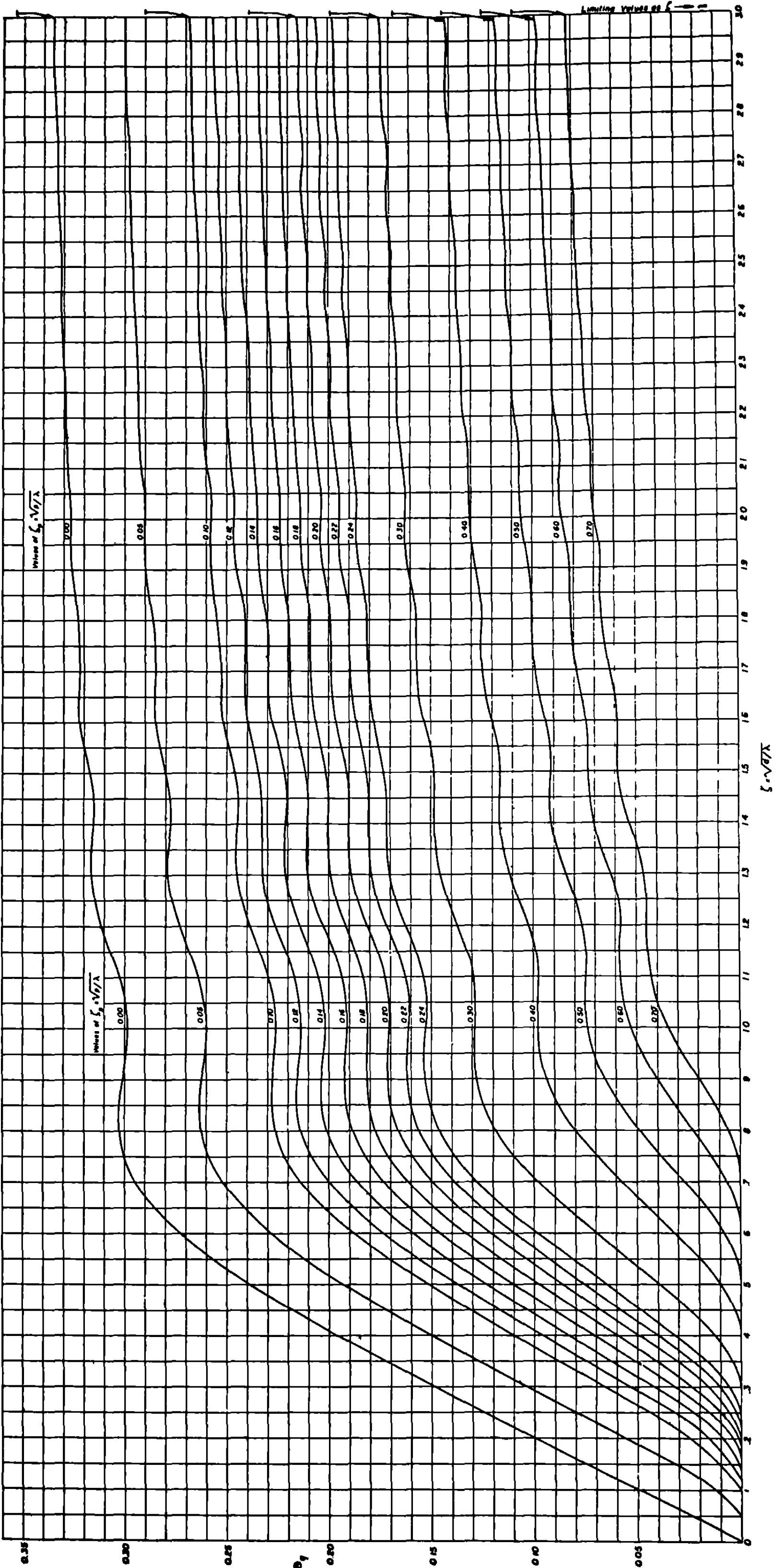


FIGURE 9.23 (d).—Absolute value, or magnitude, of $\theta_4(\xi, \eta, \lambda)$ in vacuum.

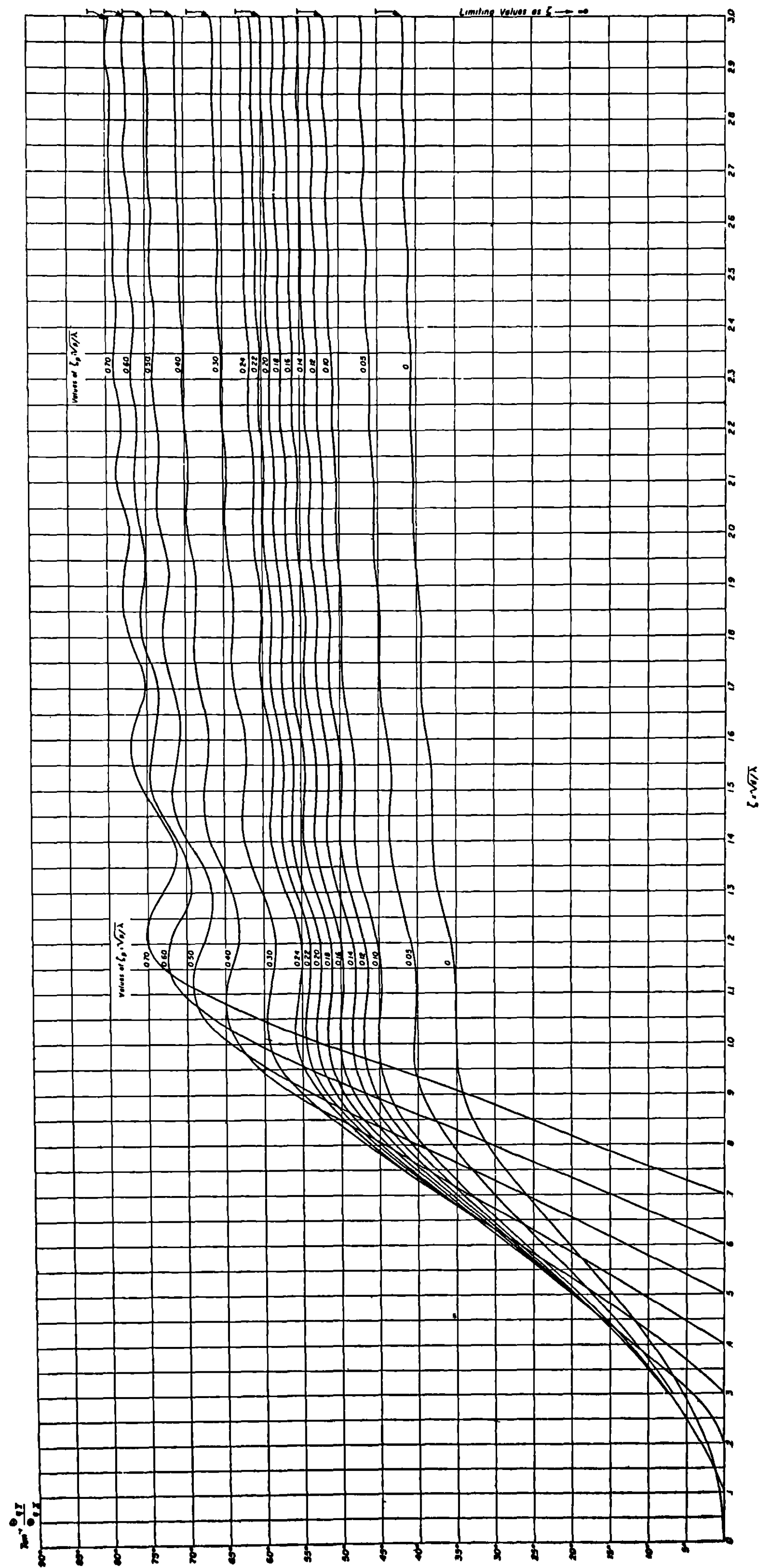


FIGURE 9.23 (e).—The phase of $\theta_q(\zeta, \zeta)$; i. e., $\tan^{-1} (\theta_q/\theta_x)$ in vacuum.

can be done by the Green's function technique, the solution being given by 9.13 (1)–(3) in terms of the functions 9.23 (1), (4), and (9), and 9.11 (32). The solution is

$$\delta_R = -\frac{t_\lambda^2 G R_M}{K^2} \int_{\xi_p}^{\xi} e^{i2\pi\gamma u^2} \Delta_q(u, \xi) du \quad (1)$$

$$\varphi_R = -\frac{t_\lambda^2 G R_M}{K^2} \int_{\xi_p}^{\xi} e^{i2\pi\gamma u^2} \Phi_q(u, \xi) du \quad (2)$$

and

$$\vartheta_R = -\frac{t_\lambda^2 G R_M}{K^2} \int_{\xi_p}^{\xi} e^{i2\pi\gamma u^2} \Theta_q(u, \xi) du = \varphi_R - \delta_R. \quad (3)$$

Let us introduce the characteristic functions for malalignment

$$\delta_R = -R_0 \Delta_R, \quad (4)$$

$$\varphi_R = -R_0 \Phi_R, \quad (5)$$

and

$$\vartheta_R = -R_0 \Theta_R, \quad (6)$$

where

$$R_0 = \frac{\nu R_M}{K^2} = \frac{t_\lambda^2 G R_M}{2\gamma K^2}. \quad (7)$$

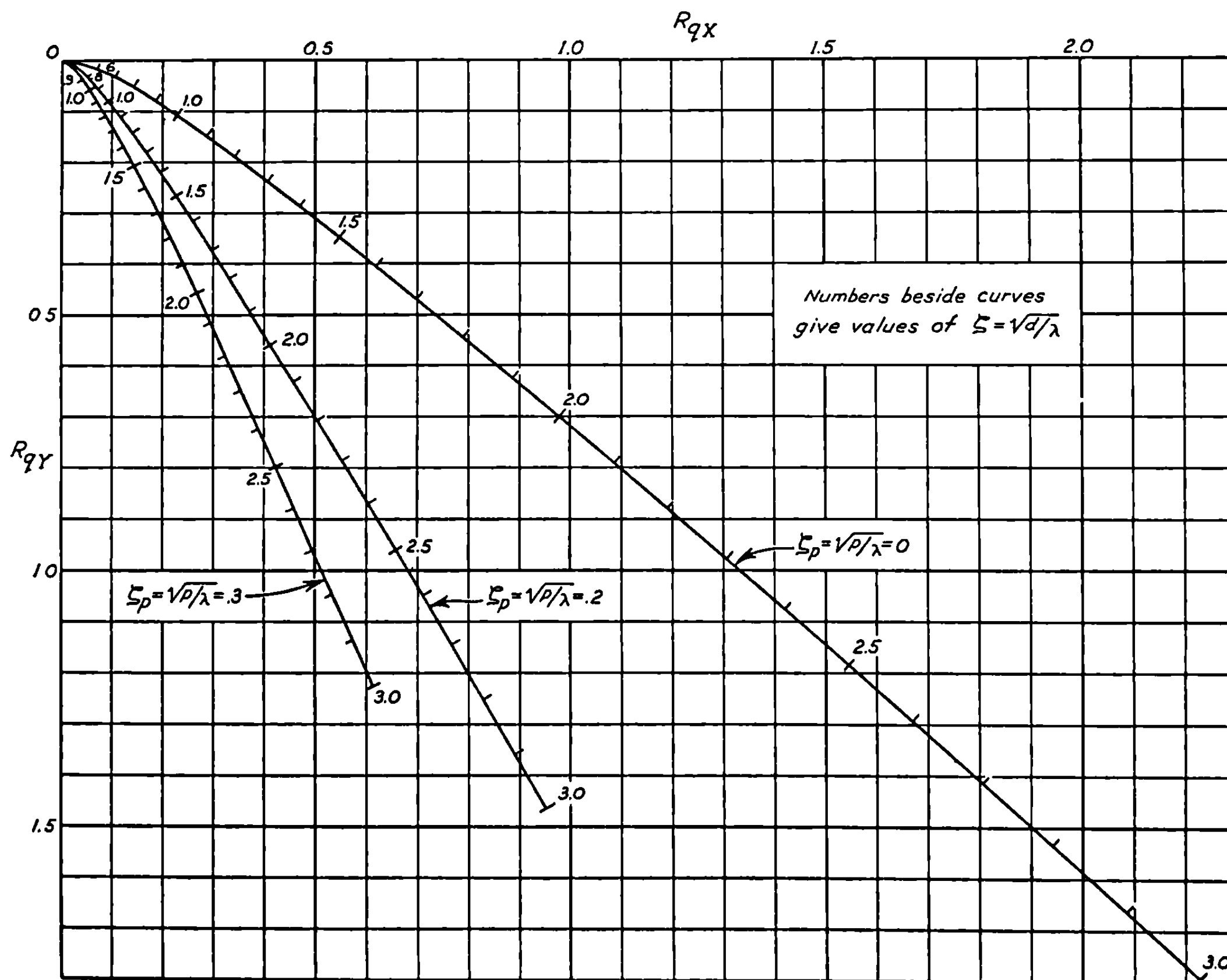


FIGURE 9.23 (f).—Characteristic function $R_q(\xi, \xi_p)$, in vacuum.

It will be noted that the characteristic functions above are not the precise analogues of the functions used with fin-stabilized rockets; there the factor γ was included with R_0 rather than with the characteristic functions. If we use the abbreviation

$$b = (\gamma - 1)^{-\frac{1}{2}}, \quad (8)$$

then

$$\begin{aligned} \Delta_R &= \frac{\gamma i}{2\pi\zeta} \int_{\zeta_p}^{\zeta} \exp(2\pi i \gamma u^2) \{1 - \exp(2\pi i \zeta^2 - 2\pi i u^2)\} du \\ &= \frac{\gamma i}{4\pi\zeta} \{ \gamma^{-\frac{1}{2}} [E(2\zeta\gamma^{\frac{1}{2}}) - E(2\zeta_p\gamma^{\frac{1}{2}})] - b e^{2\pi i \zeta^2} [E(2\zeta/b) - E(2\zeta_p/b)] \}, \end{aligned} \quad (9)$$

$$\Phi_R = \gamma \int_{\zeta_p}^{\zeta} \exp(2\pi i \gamma u^2) \exp(-2\pi i u^2) [E(2\zeta) - E(2u)] du.$$

Integration of this gives us

$$\Phi_R = \frac{b\gamma}{2} E(2\zeta) [E(2\zeta/b) - E(2\zeta_p/b)] - \gamma H(\zeta, b) + \gamma H(\zeta_p, b), \quad (10)$$

where we define

$$H(\zeta, b) = \int_0^{\zeta} \exp(2\pi i u^2/b^2) E(2u) du. \quad (11)$$

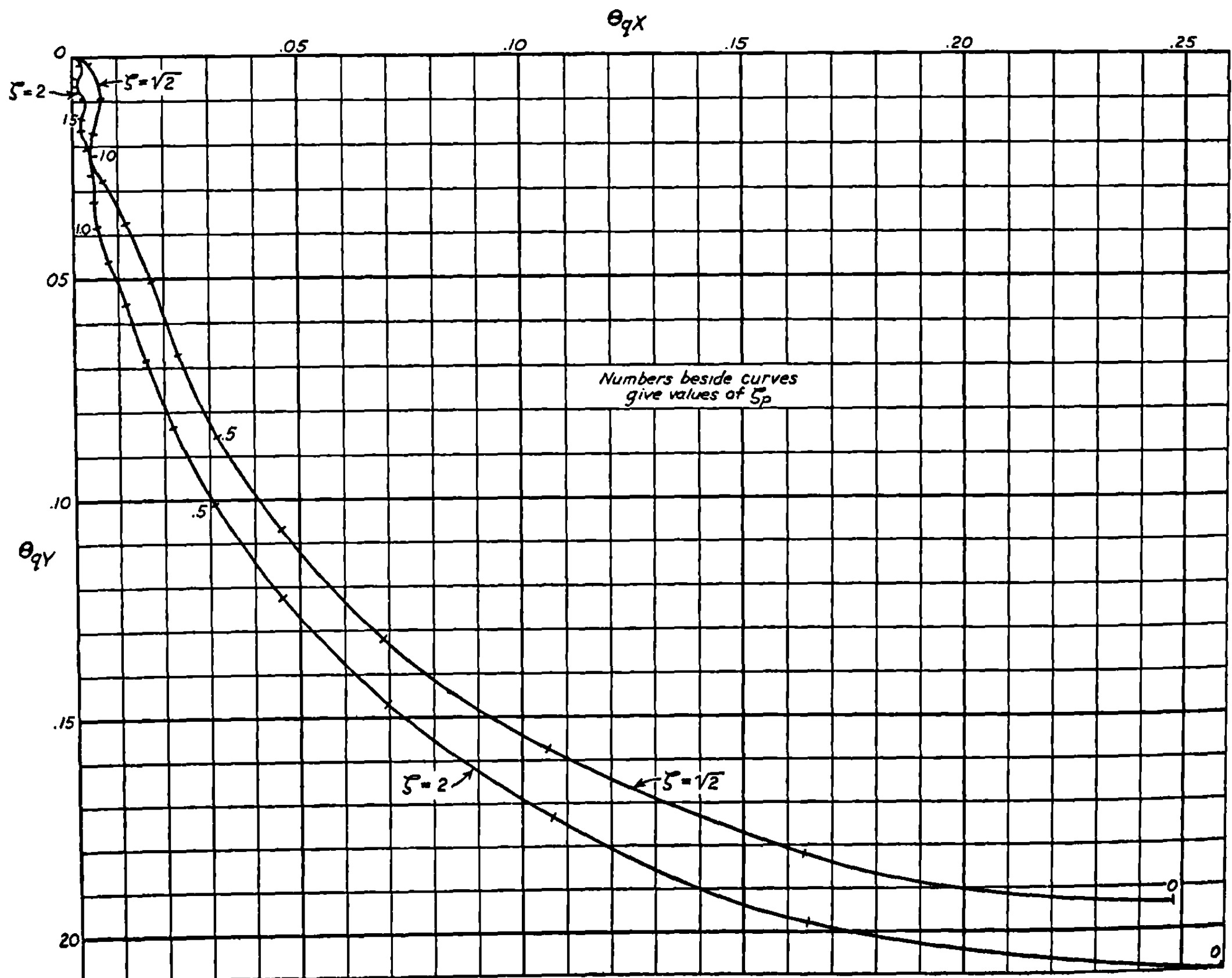


FIGURE 9.23 (g).—Green's function, $\Theta_q(\zeta_p, \zeta)$, for transverse moments in vacuum.

Finally,

$$\Theta_R = \Phi_R - \Delta_R. \quad (12)$$

The integral (11) is not expressible in terms of tabulated functions, but it is reduced to expressions suitable for calculation of numerical values in appendix B.

Because Θ_R is a function of the two parameters, γ and ζ_p , a large number of functions must be computed to cover the cases of interest. Computations of Θ_R have been made for four values of γ ; namely, 10, 15, 20, and 25, and for each of five launcher lengths, namely $\zeta_p = 0, 0.08, 0.16, 0.24$, and 0.32 . The results of these calculations are presented in figures 9.24 a-e, in each of which curves for the same ζ_p are given. These curves start out in different directions since the different rockets rotate different amounts in the launcher; but, aside from this, the curves show little variation with γ for ζ_p large. To avoid error in interpolating between these curves, it is necessary to interpolate on the amplitude and phase, rather than on the rectangular components. The curves are oriented so that they show the direction of the deflection if R_M is a negative real number; that is, if the thrust axis passes to the left of the center of mass when the rocket is placed in the firing position. The motion for any other initial orientation may be obtained by rotating the figure.

In order to show more clearly the variation of Θ_R with launcher length, values of Θ_R are plotted for $\gamma = 20$, $\zeta_p = 0, 0.08, 0.16, 0.24$, and 0.32 in figure 9.24f. It is apparent that the effect of malalignment is a rapidly decreasing function of launcher length. Here, just as in the case of mallaunching, most of the deflection occurs in the first nutation. Hence one would expect that the effect of malalignment could be reduced approximately to that of an equivalent mallaunching. It will be shown in the next section that this is a good approximation and that the equivalent mallaunching decreases with increasing launcher length.

In this treatment we neglect the relatively small effect due to the action of the malalignment during launching (see 9.75). It should also be noted that when a rocket has malalignment, it will usually have static or dynamic unbalance, and that these produce the important mallaunching treated in 9.7.

9.25 Approximate Treatment of Malalignment.—A very satisfactory treatment of malalignment can be based upon reducing its effects to those of an equivalent mallaunching. Because of the rapid rotation of the round the average of the cross torque due to the jets is small except during the first half turn of the rocket. Consequently, the malalignment is essentially equivalent to a transverse angular velocity produced in the first one or two turns. Neglecting gyroscopic terms we find that the transverse angular velocity is

$$q(\zeta) = \int_{t_p}^t \frac{f_I}{mK^2} dt = -\frac{t_\lambda G R_M}{K^2} \int_{\zeta_p}^{\zeta} e^{2\pi i \gamma \zeta^2} d\zeta \quad (1)$$

On the basis of the usual assumptions regarding the constancy of the various parameters, it is apparent that (1) is a Fresnel integral. Thus q reaches a maximum in the first turn and then decreases and oscillates about the average value

$$\begin{aligned} q_{pR} &= -(t_\lambda G R_M / K^2) \int_{\zeta_p}^{\infty} e^{2\pi i \gamma \zeta^2} d\zeta \\ &= -\frac{\gamma^{\frac{1}{2}} R_0}{t_\lambda} E_{\infty}(2\zeta_p \gamma^{\frac{1}{2}}), \end{aligned} \quad (2)$$

where

$$E_{\infty}(x) = \int_x^{\infty} e^{i\frac{\pi}{2} x^2} dx = E(\infty) - E(x). \quad (3)$$

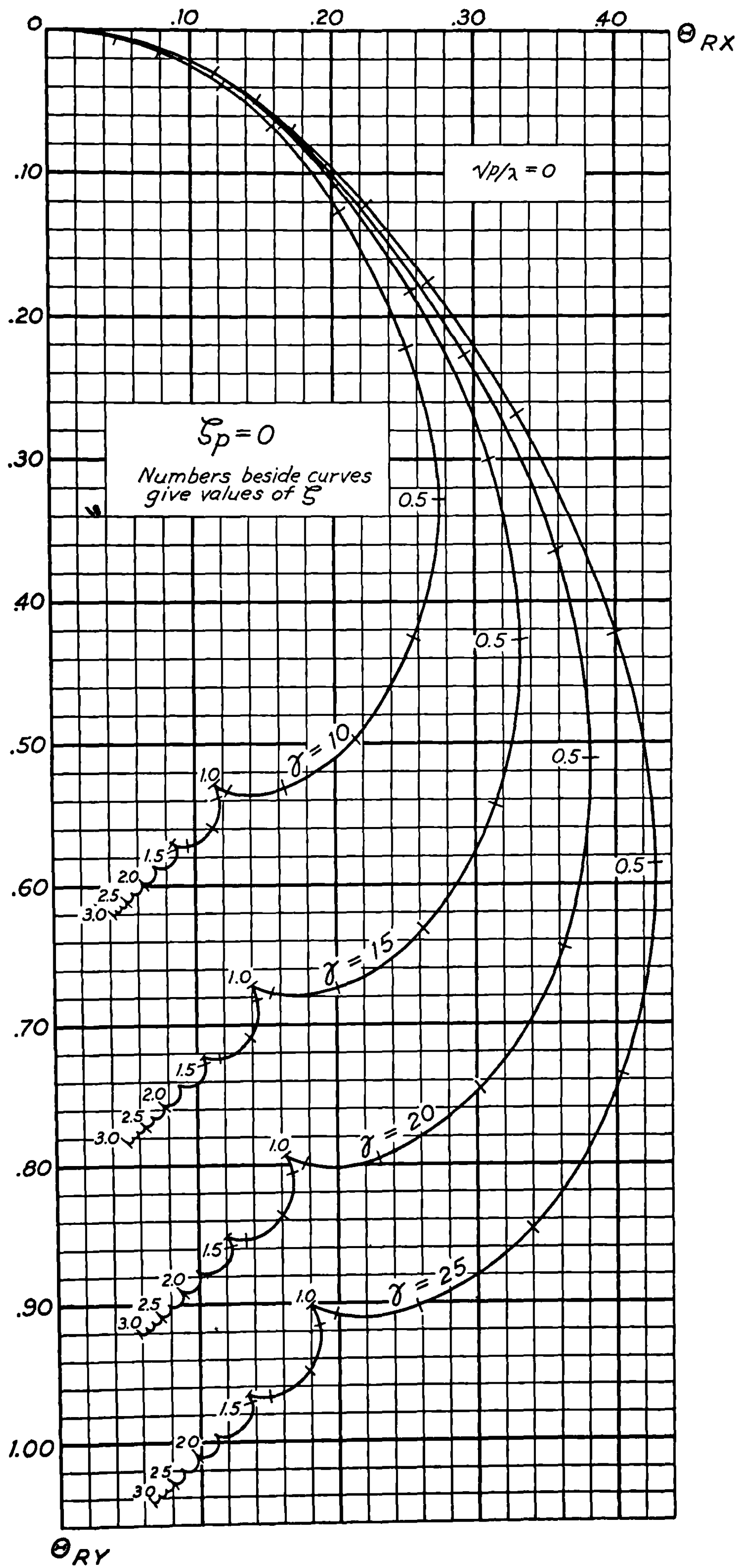


FIGURE 9.24 (a).—The characteristic function $\Theta_R(\xi_p, \xi)$, in vacuum.

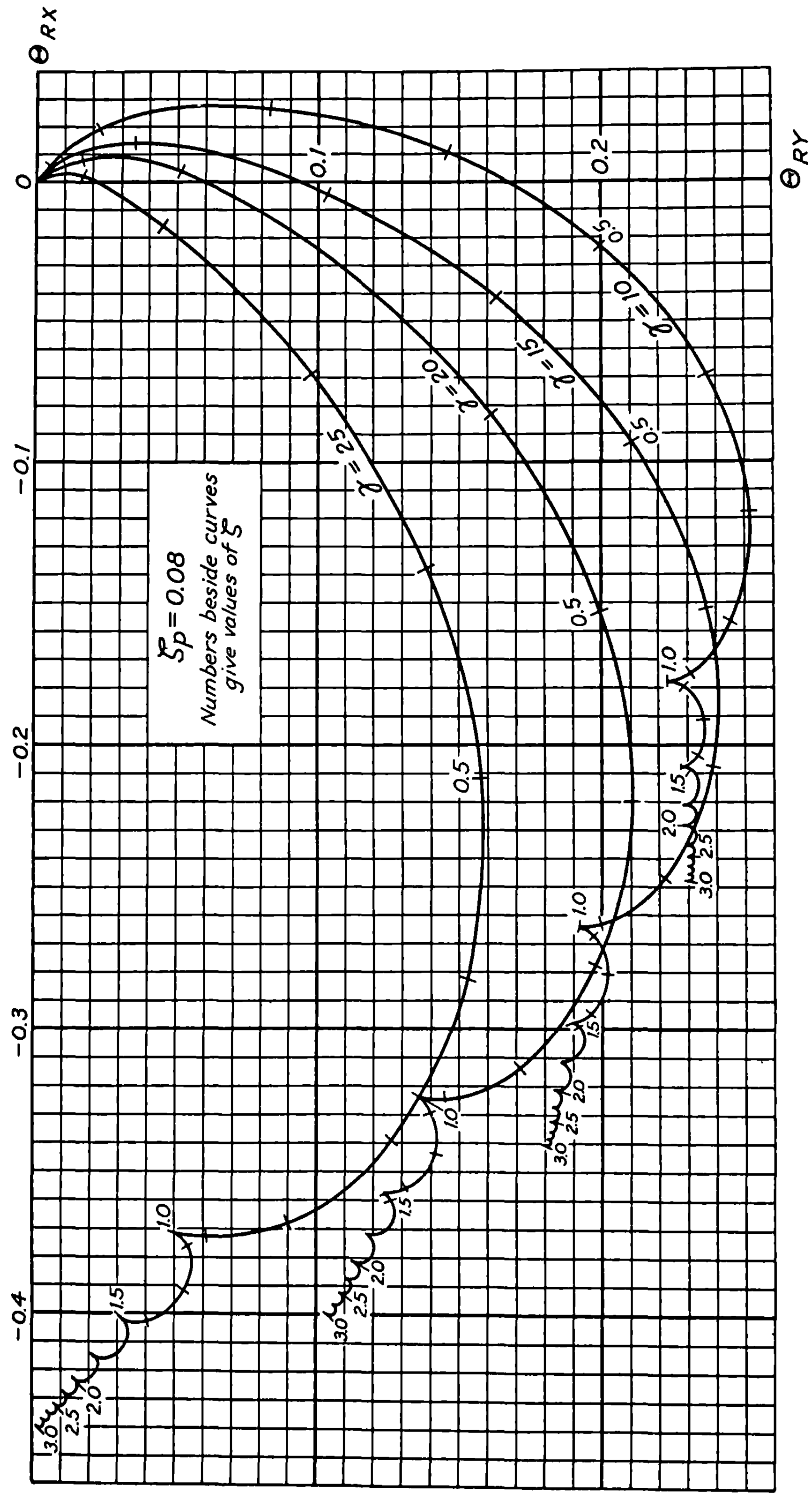


FIGURE 9.24 (b).—The characteristic function $\Theta_R(\zeta_p, \zeta)$, in vacuum.

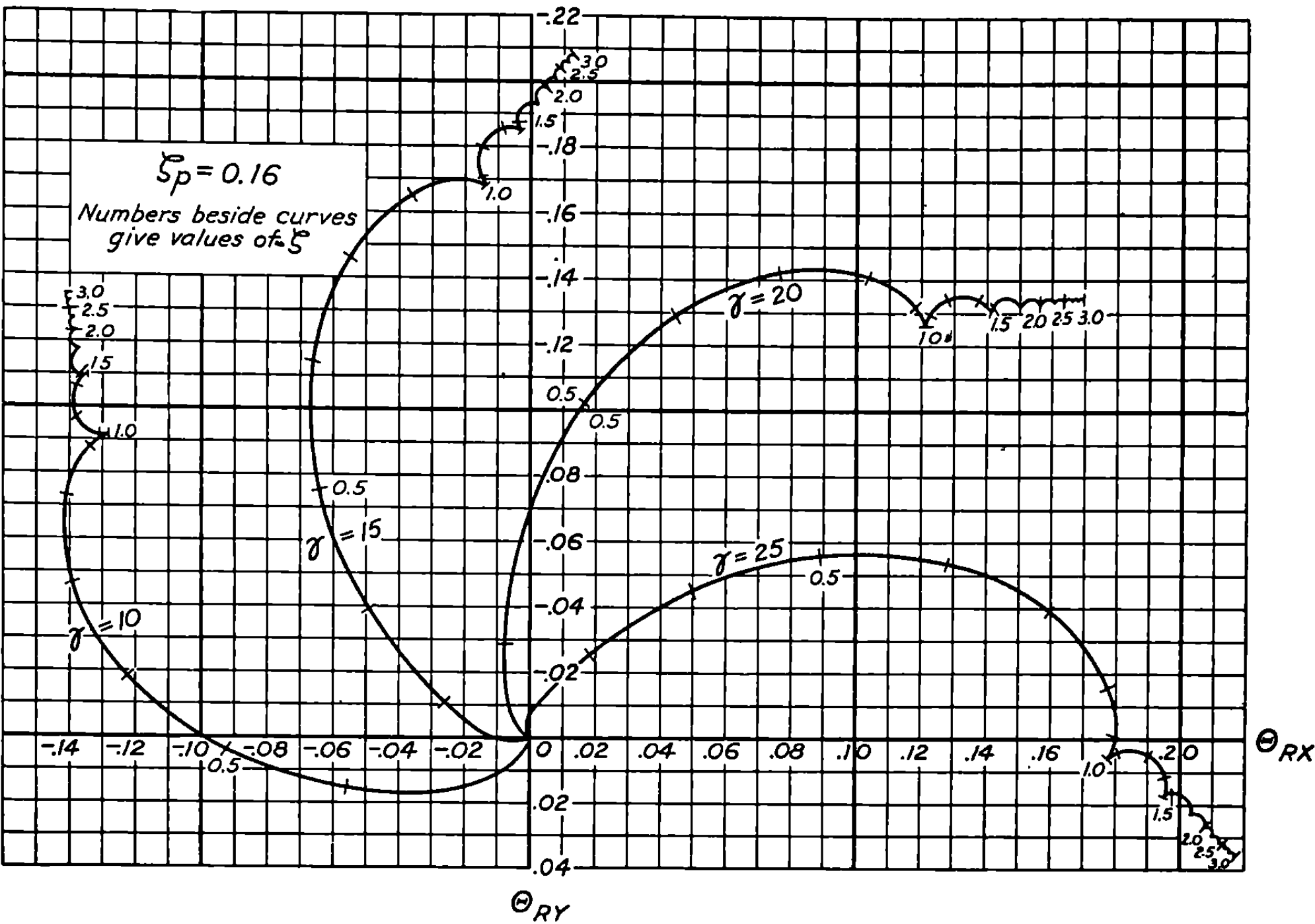


FIGURE 9.24 (c).—The characteristic function $\Theta_R(\zeta_p, \zeta)$, in vacuum.

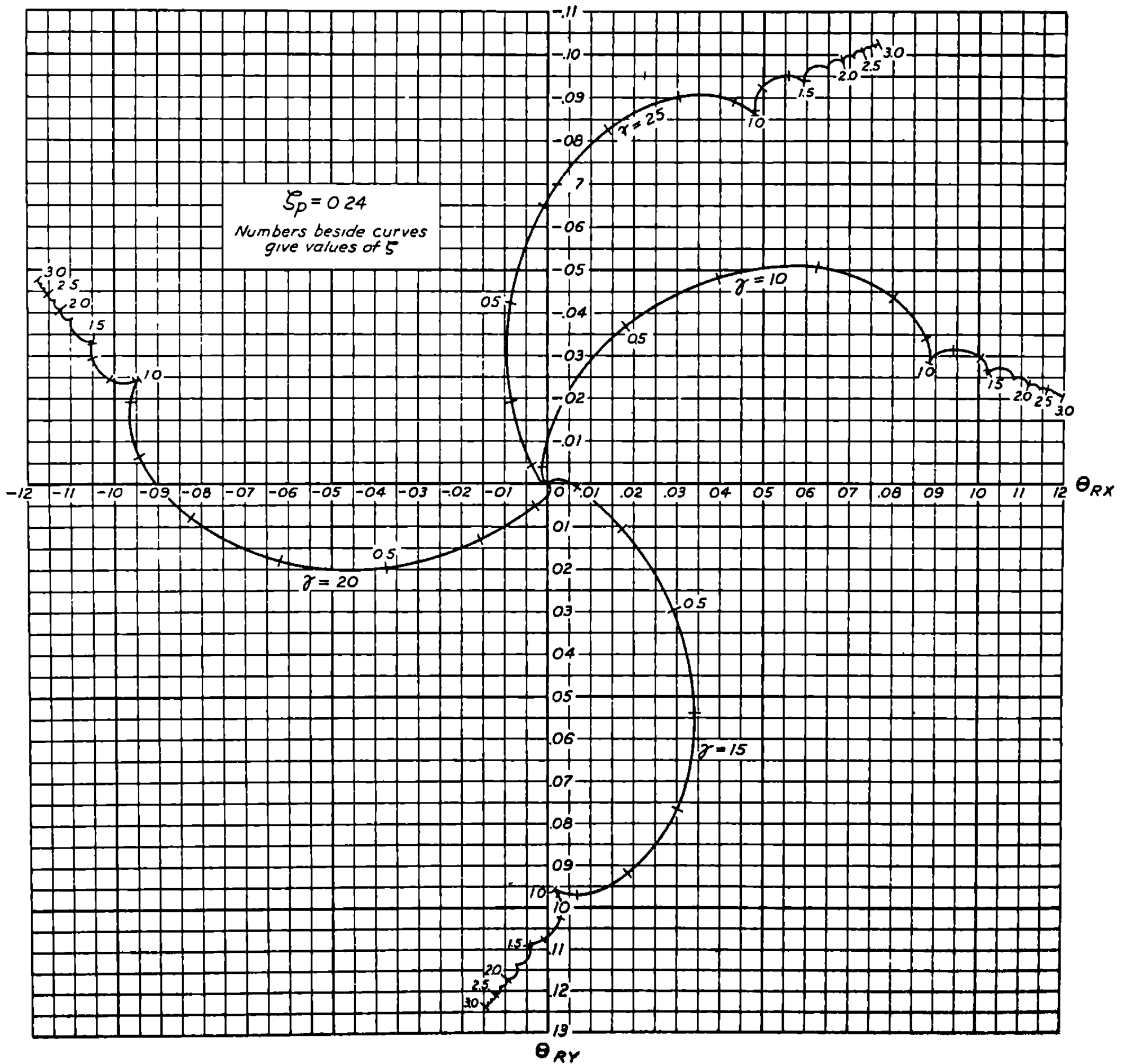


FIGURE 9.24 (d).—The characteristic function $\Theta_R(\zeta_p, \zeta)$, in vacuum.

A first approximation to the effect of the malalignment is obtained by assuming that the average transverse angular velocity as given by (2) is imparted to the round as a mallaunching and that the deflection due to this transverse velocity is given by 9.23 (11). Thus, the essential assumption is that the rocket reaches its average transverse velocity instantaneously and that its final deflection, including the gyroscopic effects, may be obtained by treating the motion as that of a projectile acted on by no transverse torques, but given an equivalent mallaunching.

A somewhat better approximation may be obtained by noticing that it is the transverse angular acceleration relative to the direction of the angular velocity that is important in determining the rate of increase in the angular velocity. The transverse angular velocity nutates at the rate given by $\exp(2\pi i \zeta^2)$ so that the exponentials in (1) and (2) should be replaced by $[\exp(2\pi i \gamma \zeta^2) \exp(2\pi i (\zeta_p^2 - \zeta^2))]$. The effect of this substitution is very small in general because γ is large ($\gamma \sim 15$ to 25), but it does change the final answer by about 5 percent. Including this effect, we have in place of (2),

$$q_{pR} = -(t_\lambda G R_M / K^2) \int_{\zeta_p}^{\infty} \exp(2\pi i \zeta^2 / b^2) \exp(2\pi i \zeta_p^2) d\zeta = -\frac{b\gamma R_0}{t_\lambda} E_\infty(2\zeta_p/b) \exp(2\pi i \zeta_p^2) \quad (4)$$

for the mallaunching equivalent to a malalignment.

To correct for the finite time required to reach this velocity we may proceed as follows. Since in the approximate treatment we give the round a "running" start, we "handicap" it by an initial orientation and yaw in the opposite direction such that, neglecting gyroscopic effects, the round would arrive at the same orientation at $t = \infty$ that it would have if we computed from (1). The initial orientation needed for this correction is easily seen to be

$$\begin{aligned} \delta_{pR} = \varphi_{pR} &= \text{Ave Lim}_{t \rightarrow \infty} \left[\int_{t_p}^t \mathbf{q} dt - \mathbf{q}_{pR}(t - t_p) \right] = \int_{\zeta_p}^{\infty} (\mathbf{q} - \mathbf{q}_p) t_\lambda d\zeta \\ &= -\frac{G t_\lambda^2 R_M}{K^2} \int_{\zeta_p}^{\infty} \int_{\infty}^{\zeta} \exp(2\pi i \gamma \zeta_1^2) d\zeta_1 d\zeta = -\frac{1}{2} R_0 F_\infty(2\zeta_p \gamma^{1/2}), \end{aligned} \quad (5)$$

where

$$F_\infty(x) = \int_x^\infty \int_\infty^y e^{i\pi u^2/2} du dy. \quad (6)$$

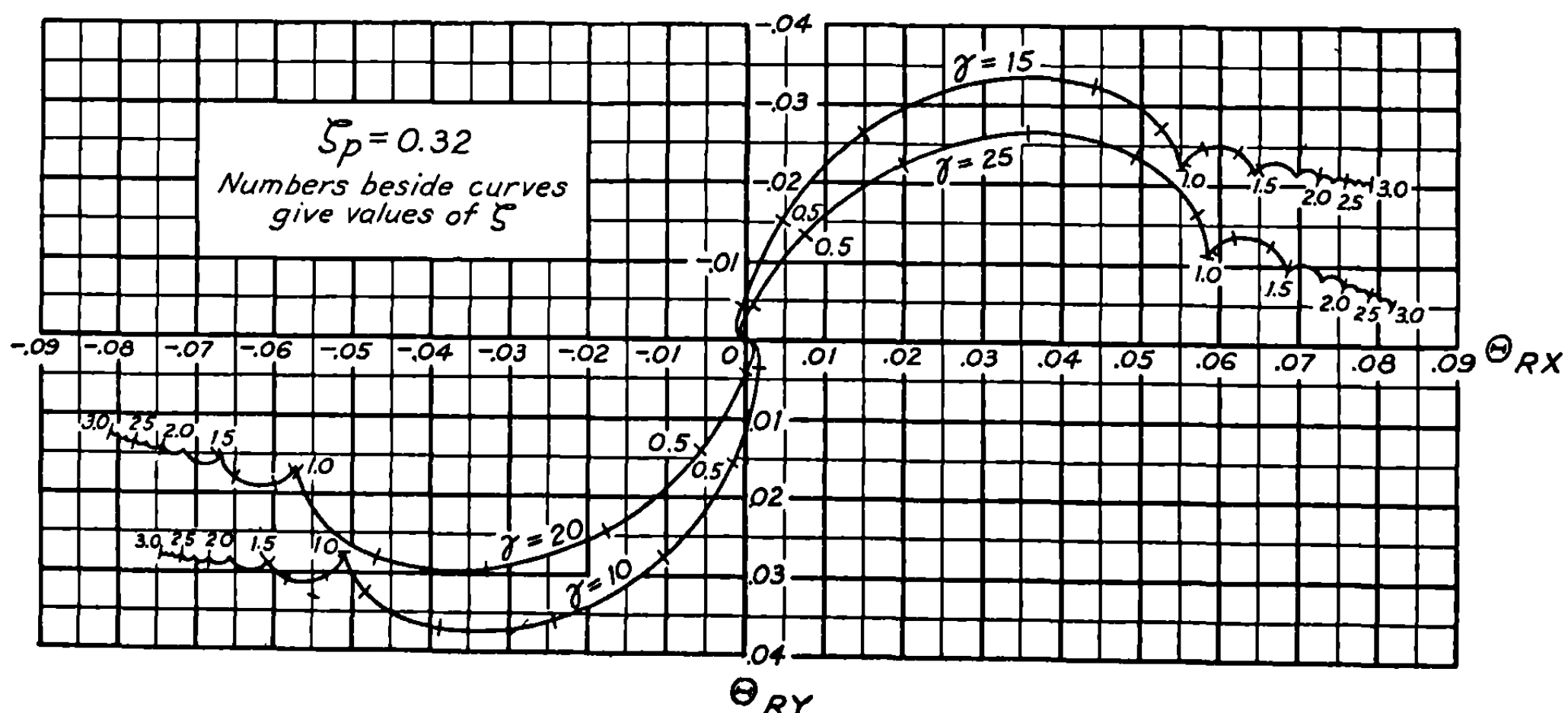
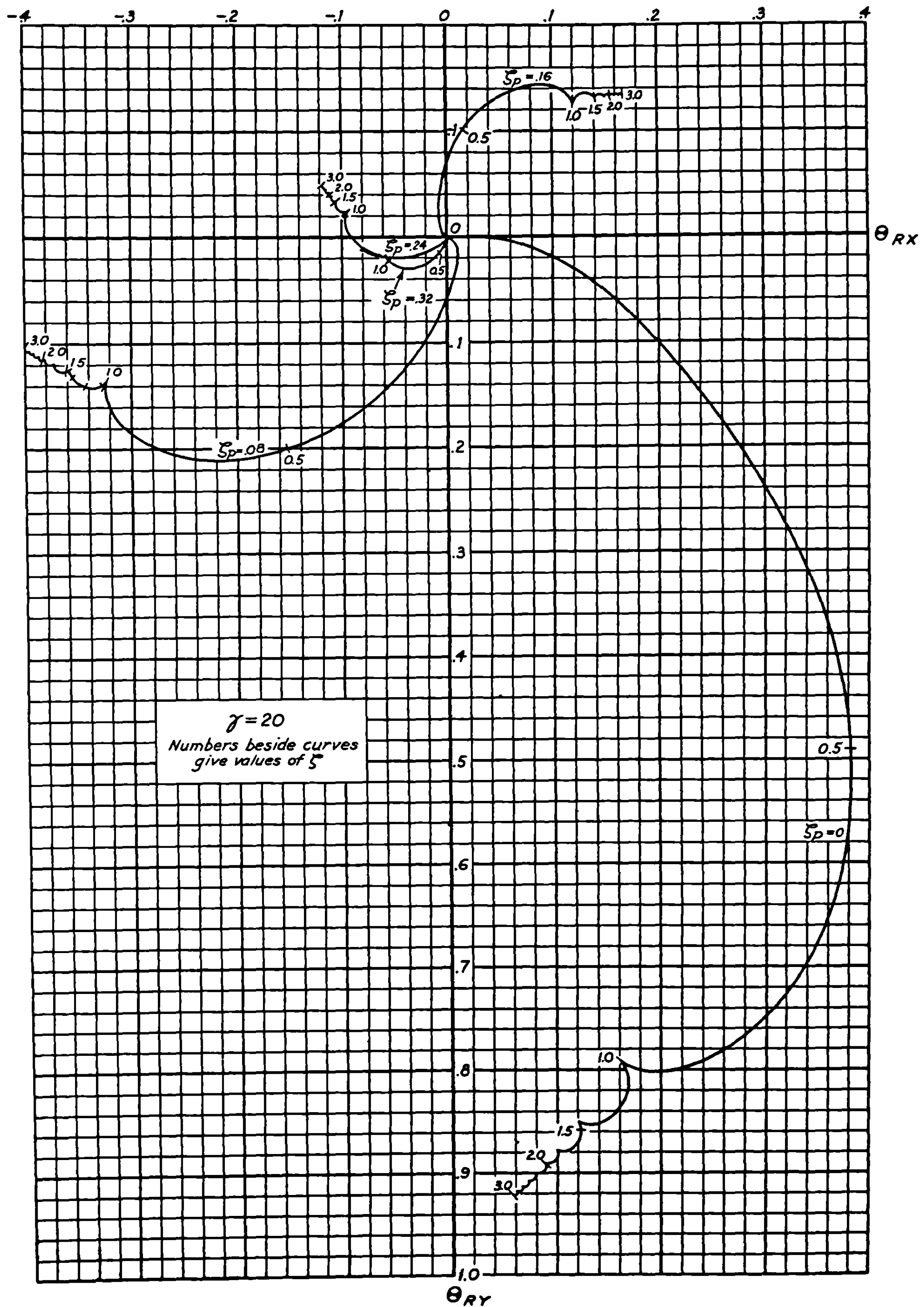


FIGURE 9.24 (e).—The characteristic function $\Theta_R(\zeta_p, \zeta)$, in vacuum.

FIGURE 9.24 (f).—Characteristic function $\Theta_R(\xi_p, \xi)$ in vacuum, for $\gamma=20$.

We started from the limit as t approached infinity because it made the integral easier to evaluate, and because it corresponds to an average over the various possible burning times. Practically, the chief contribution to the integral comes from the first few turns of the rocket and is thus independent of gyroscopic effects since they do not become important until later. The neglect of gyroscopic effects in the above integral appears justified by the fact that the major part of the effect of the malalignment occurs in the first one or two turns. A more rigorous derivation of these approximate expressions will be given in the next section by means of a Green's function technique.

The deflection due to malalignment is then given approximately by

$$\vartheta_R \doteq q_{pR} t_\lambda \Theta_q(\zeta_p, \zeta) + \varphi_{pR} + \delta_{pR} \Theta_\delta(\zeta_p, \zeta). \quad (7)$$

Using (4), (5), and 9.24 (6) we have the expression

$$\Theta_R \doteq b\gamma \exp(2\pi i \zeta_p^2) \Theta_q(\zeta_p, \zeta) E_\infty(2\zeta_p/b) + \frac{1}{2} F_\infty(2\zeta_p\gamma^{\frac{1}{2}})[1 + \Theta_\delta(\zeta_p, \zeta)]. \quad (8)$$

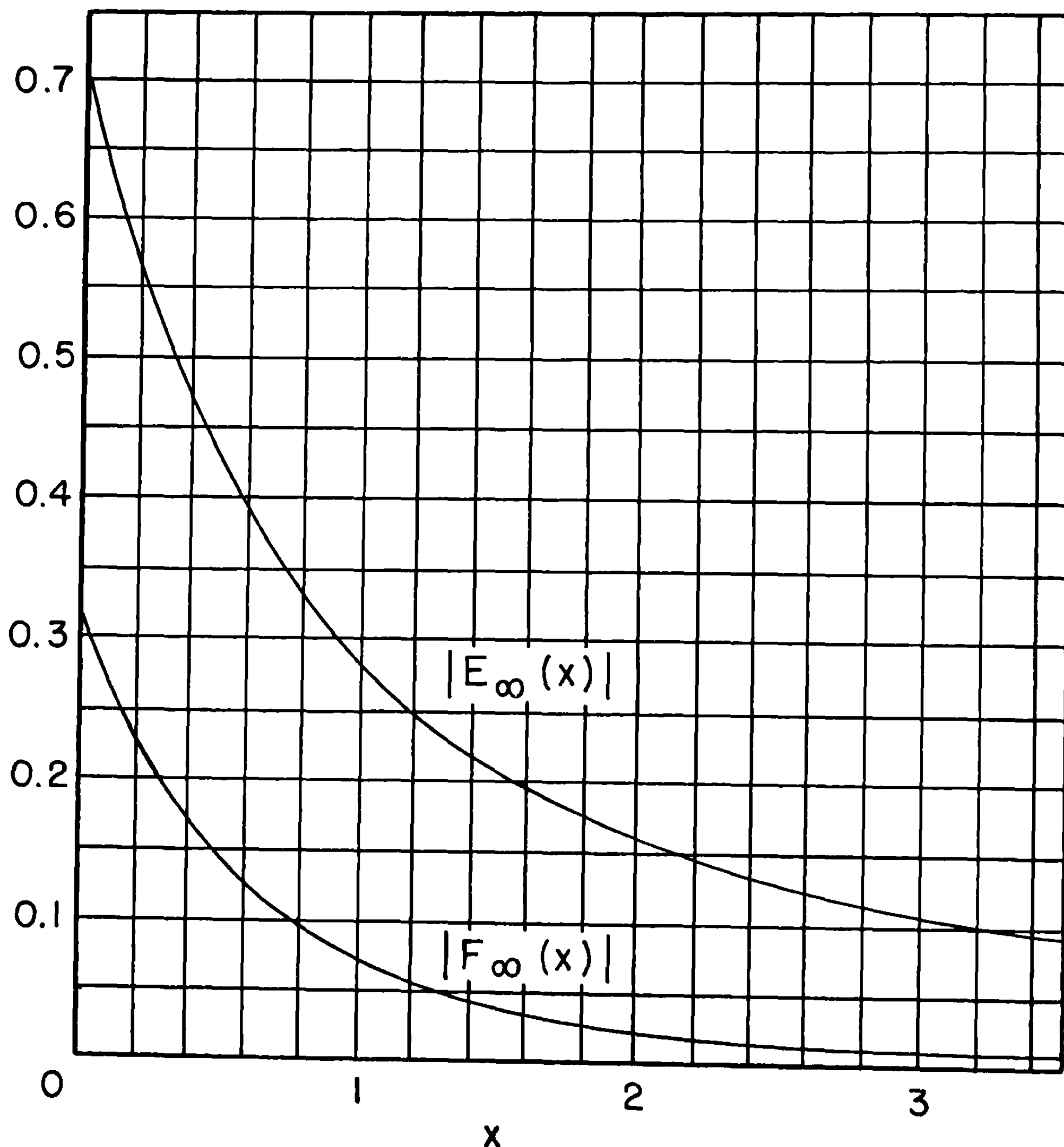


FIGURE 9.25 (a).—Absolute values of $E_\infty(x)$ and $F_\infty(x)$.

In terms of the explicit expressions for Θ_e and Θ_s this becomes

$$\Theta_R \doteq \frac{b\gamma}{2} E_\infty(2\zeta_p/b) \left\{ [E(2\zeta) - E(2\zeta_p)] + \frac{i}{2\pi\zeta} [\exp(2\pi i\zeta^2) - \exp(2\pi i\zeta_p^2)] \right\} + \frac{1}{2} \left(1 - \frac{\zeta_p}{\zeta} \right) F_\infty(2\zeta_p\gamma^{\frac{1}{2}}). \quad (9)$$

The magnitudes and phases of $E_\infty(x)$ and $F_\infty(x)$ can be conveniently represented as shown in figures 9.25a-b. The curve for $F_\infty(x)$ is obtained by reducing $F_\infty(x)$ to ordinary Fresnel integrals as given in Appendix B. The following approximate expression for the magnitude of $E_\infty(x)$ may be obtained from figure 9.25a and is convenient in conjunction with such expressions as (7) and (9).

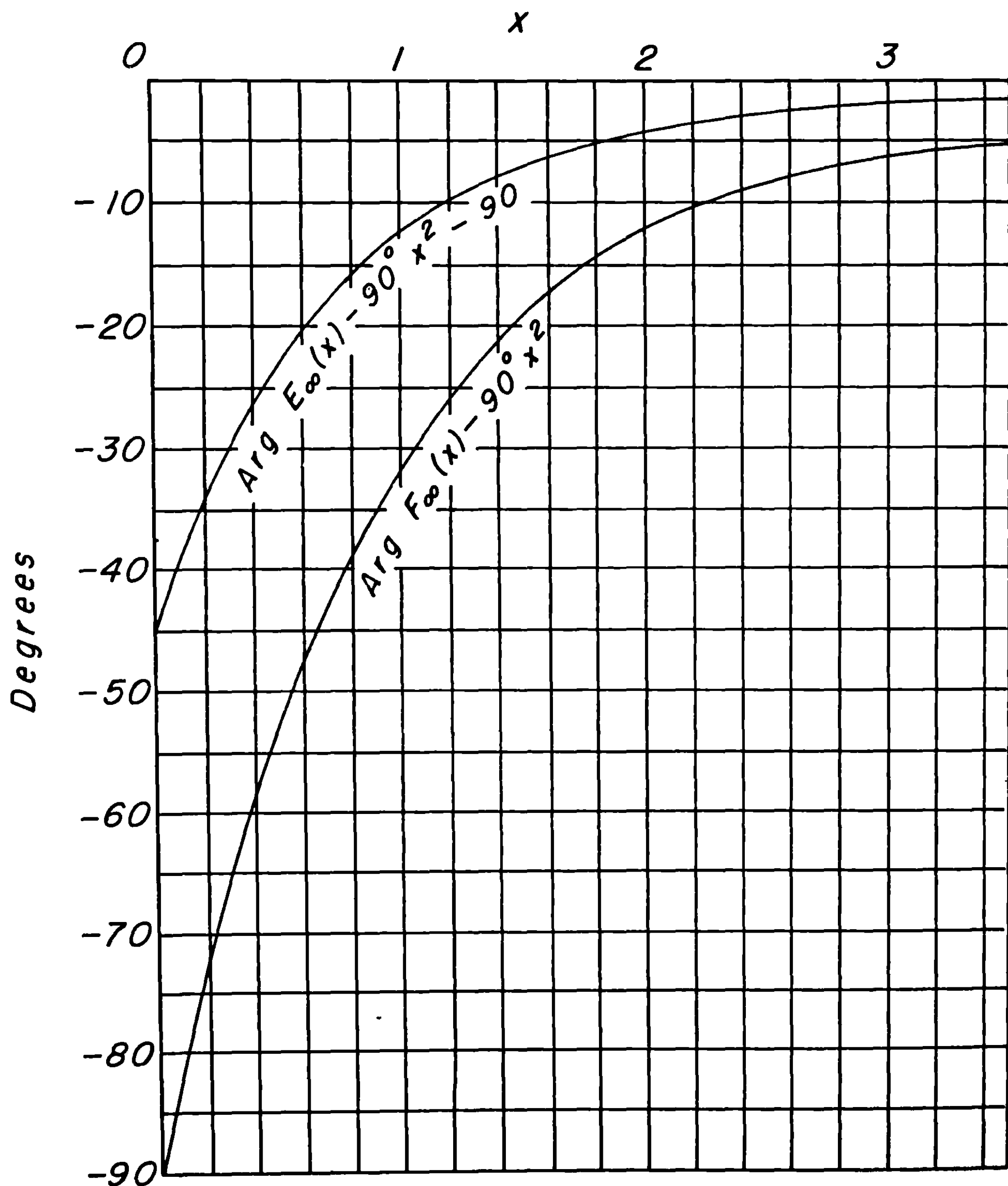


FIGURE 9.25 (b).—Arguments of $E_\infty(x)$ and $F_\infty(x)$.

9.2 THE VACUUM APPROXIMATION

$$|E_{\infty}(x)| \approx \frac{1}{\pi\sqrt{x^2+0.205}} \quad (10)$$

This expression is accurate to about one percent for all x . The asymptotic value of $|F_{\infty}(x)|$ is

$$|F_{\infty}(x)| \sim \frac{1}{\pi^2 x^2}. \quad (11)$$

The accuracy of the approximate treatment of malalignment is shown in figure 9.25c, in which the exact curve of Θ_R for $\gamma=15$ and $\zeta_p=0.24$ is compared with points computed from (9). Not only do the approximate points fall very close to the curve, they also fall at nearly the proper points along the curve and we may conclude that the approximate method is sufficiently accurate for all practical purposes.

9.26 Derivation of the Approximate Malalignment Solution from the Green's Function.—

The approximate treatment which was obtained by physical reasoning in the last section may also be obtained from Green's function in a new form on the basis of the following consideration. What is required is a transformation of 9.24 (3) from the form

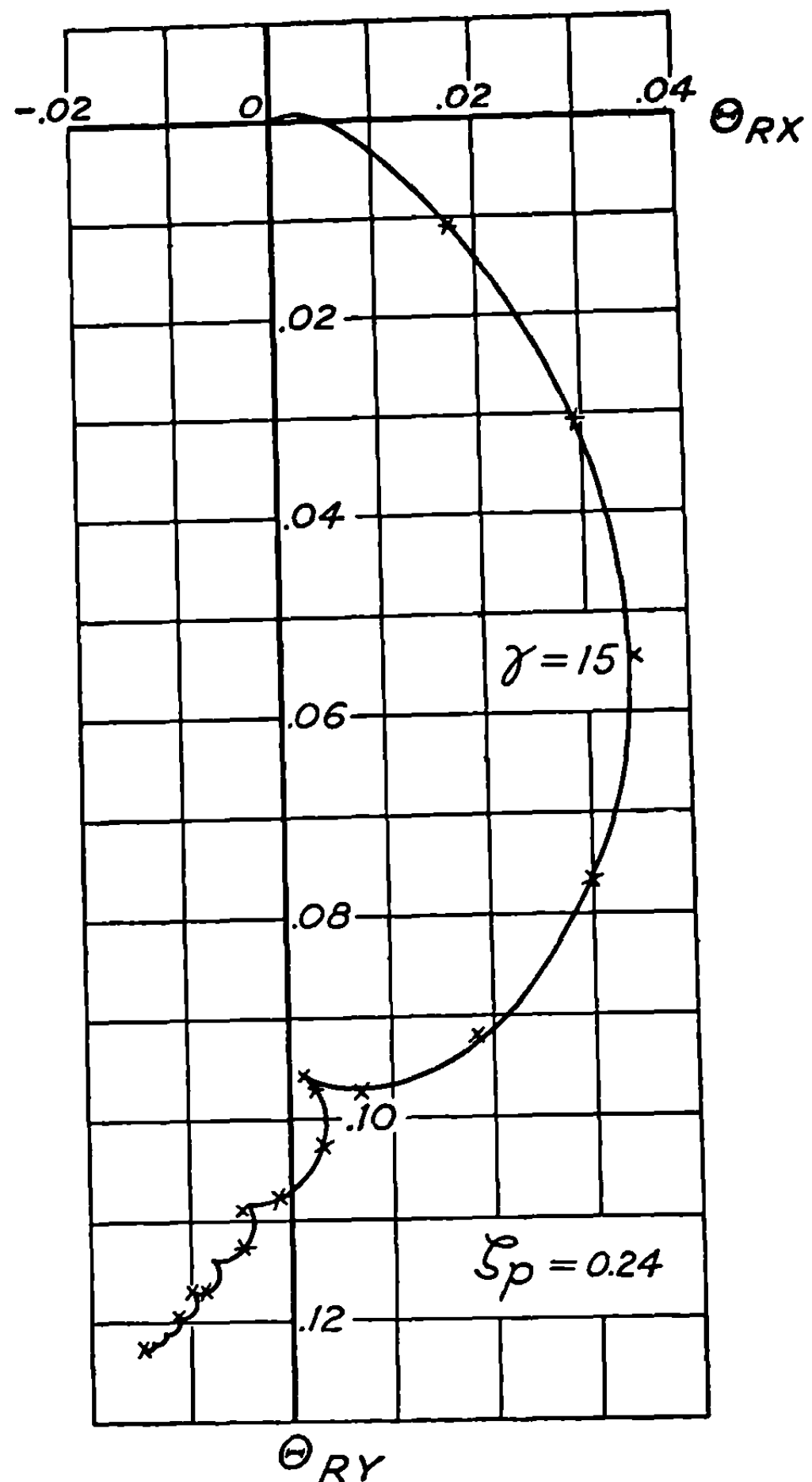


FIGURE 9.25 (c).—Comparison of the exact curve for Θ_R and points marked x , computed from the approximate equation 9.25 (9)

$$\vartheta_R(\zeta_p, \zeta) = -R_0 \Theta_R(\zeta_p, \zeta) = -2R_0 \gamma \int_{\zeta_p}^{\zeta} e^{2\pi i \gamma u^2} \Theta_q(u, \zeta) du, \quad (1)$$

to the form

$$\vartheta_R(\zeta_p, \zeta) = -R_0 [A_q(\zeta) \Theta_q(\zeta_p, \zeta) + A_\varphi(\zeta) \Theta_\varphi(\zeta_p, \zeta) + A_\delta(\zeta) \Theta_\delta(\zeta_p, \zeta)], \quad (2)$$

and a demonstration that A_q , A_φ and A_δ are nearly independent of ζ , so that they can be regarded as giving the equivalent mallaunching, equivalent cross pointing, and equivalent yaw, respectively.

If we can write

$$\Theta_q(u, \zeta) = B_q(\zeta_p, u) \Theta_q(\zeta_p, \zeta) + B_\varphi(\zeta_p, u) \Theta_\varphi(\zeta_p, \zeta) + B_\delta(\zeta_p, u) \Theta_\delta(\zeta_p, \zeta) \quad (3)$$

we will have achieved the desired transformation and will have

$$A_x(\zeta) = 2\gamma \int_{\zeta_p}^{\zeta} e^{2\pi i \gamma u^2} B_x(\zeta_p, u) du \quad (4)$$

with $x=q$, φ or δ . We now show that an equation of the form of (3) is always possible, find the expressions for the B_x 's, and show that the A_x 's are nearly independent of ζ .

If we eliminate δ and φ from the homogeneous forms of 9.21 (1)-(3) we obtain as the equation for ϑ

$$\vartheta''' + \left(\frac{3}{\zeta} - 4\pi i \zeta\right) \vartheta'' - 8\pi i \vartheta' = 0. \quad (5)$$

The general solution of this can be made up of a linear combination of any three linearly independent particular solutions. We shall take as our three basic solutions $\Theta_\varphi(\zeta_p, \zeta)$, $\Theta_\delta(\zeta_p, \zeta)$, $\Theta_q(\zeta_p, \zeta)$; their linear independence is easily demonstrated in the usual way from the nonvanishing of the Wronskian.¹¹ The validity of (3) now follows immediately since $\Theta_q(u, \zeta)$ is a solution of (5). To determine the B 's, we note that any solution of (5) may be completely characterized by giving the values of $\vartheta(\zeta)$, $\vartheta'(\zeta)$ and $\vartheta''(\zeta)$ for some specified value of ζ . Thus, although we originally characterized $\Theta_q(u, \zeta)$ by the fact that at $\zeta=u$, then $\Phi_q(u, \zeta)=0$, $\Delta_q(u, \zeta)=0$, and $d\Phi_q(u, \zeta)/d\zeta=1$, we could just as well have used 9.21 (1)-(3) and characterized $\Theta_q(u, \zeta)$ by the fact that at $\zeta=u$,

$$\Theta_q(u, \zeta) = \Phi_q(u, \zeta) - \Delta_q(u, \zeta) = 0, \quad (6)$$

$$\frac{d\Theta_q(u, \zeta)}{d\zeta} = \frac{1}{\zeta} \Delta_q(u, \zeta) = 0, \quad (7)$$

and

$$\frac{d^2\Theta_q(u, \zeta)}{d\zeta^2} = \frac{1}{\zeta} \frac{d\Phi_q(u, \zeta)}{d\zeta} - \frac{2\Delta_q(u, \zeta)}{\zeta^2} = \frac{1}{u}. \quad (8)$$

If we require that the right-hand side of (3) satisfy these three conditions, we get three equations from which the three B 's can be determined in determinantal form in a straight forward manner by differentiating (3) twice with respect to ζ and setting $\zeta=u$.

The work required for this direct procedure can be reduced if we first consider the function

$$\vartheta(\zeta_p, u; \zeta) = K(\zeta_p, u) \begin{vmatrix} \Theta_\varphi(\zeta_p, \zeta) & \Theta_\delta(\zeta_p, \zeta) & \Theta_q(\zeta_p, \zeta) \\ \Theta_\varphi(\zeta_p, u) & \Theta_\delta(\zeta_p, u) & \Theta_q(\zeta_p, u) \\ \Theta'_\varphi(\zeta_p, u) & \Theta'_\delta(\zeta_p, u) & \Theta'_q(\zeta_p, u) \end{vmatrix} \quad (9)$$

where $K(\zeta_p, u)$ is yet to be determined and the primed functions in the bottom row are the result of letting $\zeta=u$, after differentiating with respect to ζ . It will be noted that $\vartheta(\zeta_p, u; \zeta)$ is a solution of (5) since it is a linear combination of solutions, having just the form of (3). Moreover if ζ is put equal to u in either $\vartheta(\zeta_p, u; \zeta)$ or $d\vartheta(\zeta_p, u; \zeta)/d\zeta$, the result is zero, since two rows of the determinant in (9) become the same. Thus this function satisfies conditions (6) and (7). If we choose $K(\zeta_p, u)$ so that condition (8) is satisfied, (9) will give us $\Theta_q(u, \zeta)$ in just the form desired. But if we differentiate the determinant twice with respect to ζ and then replace ζ by u we have precisely the Wronskian $W(\zeta_p, u)$ of our three basic solutions, where

$$W(\zeta_p, \zeta) = \begin{vmatrix} \Theta_\varphi(\zeta_p, \zeta) & \Theta_\delta(\zeta_p, \zeta) & \Theta_q(\zeta_p, \zeta) \\ \Theta'_\varphi(\zeta_p, \zeta) & \Theta'_\delta(\zeta_p, \zeta) & \Theta'_q(\zeta_p, \zeta) \\ \Theta''_\varphi(\zeta_p, \zeta) & \Theta''_\delta(\zeta_p, \zeta) & \Theta''_q(\zeta_p, \zeta) \end{vmatrix} \quad (10)$$

Evidently then,

¹¹ See for example, E. L. Ince, "Ordinary Differential Equations," pp. 116-119, Dover, 1944.

$$K(\zeta_p, u) = \frac{1}{u W(\zeta_p, u)}. \quad (11)$$

Rather than evaluate the Wronskian by working out (10), we can make use of the theorem (footnote 11) that gives it in terms of the coefficients of (5) as

$$\begin{aligned} W(\zeta_p, \zeta) &= W(\zeta_p, \zeta_p) \exp \left\{ \int_{\zeta_p}^{\zeta} \left(-\frac{3}{\zeta} + 4\pi i \zeta \right) d\zeta \right\} \\ &= \frac{\zeta_p}{\zeta^3} \exp \left\{ 2\pi i (\zeta^2 - \zeta_p^2) \right\}. \end{aligned} \quad (12)$$

In getting this we used the value $W(\zeta_p, \zeta_p) = \zeta_p^{-2}$ obtained from (10) by evaluating the elements of the determinant with the aid of (6)–(8) and the initial conditions for the other solutions.¹² Thus we have expressed $\Theta_q(u, \zeta)$ in the form of (3) which we now write as

$$\begin{aligned} \Theta_q(u, \zeta) &= \frac{u^2}{\zeta_p} \exp [-2\pi i (u^2 - \zeta_p^2)] \left\{ \begin{vmatrix} \Theta_\varphi(\zeta_p, u) & \Theta_\delta(\zeta_p, u) \\ \Theta_\varphi'(\zeta_p, u) & \Theta_\delta'(\zeta_p, u) \end{vmatrix} \Theta_q(\zeta_p, \zeta) \right. \\ &\quad \left. + \begin{vmatrix} \Theta_\delta(\zeta_p, u) & \Theta_q(\zeta_p, u) \\ \Theta_\delta'(\zeta_p, u) & \Theta_q'(\zeta_p, u) \end{vmatrix} \Theta_\varphi(\zeta_p, \zeta) + \begin{vmatrix} \Theta_q(\zeta_p, u) & \Theta_\varphi(\zeta_p, u) \\ \Theta_q'(\zeta_p, u) & \Theta_\varphi'(\zeta_p, u) \end{vmatrix} \Theta_\delta(\zeta_p, \zeta) \right\}. \end{aligned} \quad (13)$$

If we substitute this in (1) and use 9.22 (1) and (2) we find that

$$A_q(\zeta) = 2\gamma \exp(2\pi i \zeta_p^2) \int_{\zeta_p}^{\zeta} \exp(2\pi i u^2/b^2) du = \gamma b \exp(2\pi i \zeta_p^2) [E(2\zeta/b) - E(2\zeta_p/b)], \quad (14)$$

and that $A_\varphi(\zeta)$ and $A_\delta(\zeta)$ are expressed in terms of similar integrals. Since b^{-2} is very nearly γ , $E(2\zeta/b)$ gives the coordinates of the point reached by going around a Cornu spiral approximately as many turns as the rocket has made revolutions. Hence, while $A_q(\zeta)$ will vary rapidly during the early part of burning, if one is dealing with a long-burning rocket and is interested only in the deflection at the end of burning, no appreciable error will be made if one replaces $A_q(\zeta)$ by $A_q(\infty)$. To obtain the relation between $A_q(\zeta)$ and the effective mallaunching we note that (2) would normally be written

$$\vartheta_R(\zeta_p, \zeta) = q_{pR} t_\lambda \Theta_q(\zeta_p, \zeta) + \varphi_{pR} \Theta_\varphi(\zeta_p, \zeta) + \delta_{pR}(\zeta_p, \zeta) \Theta_\delta(\zeta_p, \zeta). \quad (15)$$

Thus we may write the effective mallaunching as

$$q_{pR} = -\frac{R_0}{t_\lambda} A_q(\infty) = -\frac{R_0 b \gamma}{t_\lambda} \exp(2\pi i \zeta_p^2) [E(\infty) - E(2\zeta_p/b)], \quad (16)$$

which is just 9.25 (4). The equivalent initial yaw is

$$\begin{aligned} \delta_{pR} &= \frac{R_0 \exp(2\pi i \zeta_p^2)}{\zeta_p} \int_{\zeta_p}^{\infty} u^2 \exp(2\pi i u^2/b^2) \left\{ \frac{\exp[2\pi i (u^2 - \zeta_p^2)] - 1}{4\pi i u^2} \right\} du \\ &= \frac{R_0}{4\pi i \zeta_p} \left\{ \frac{E_\infty(2\zeta_p \gamma^{1/2})}{2\gamma^{1/2}} - \frac{b}{2} \exp(2\pi i \zeta_p^2) E_\infty(2\zeta_p/b) \right\} \end{aligned} \quad (17)$$

¹² It is not necessary that the functions used in (9) and the following equations be the characteristic functions; however they must be linearly independent or the determinant will be zero. In the general case the Wronskian, and hence the coefficient $K(\zeta_p, u)$ will be different, but the rest of the method is unaltered.

The equivalent initial cross pointing is

$$\begin{aligned}\varphi_{pR} &= \frac{R_0 \exp(2\pi i \zeta_p^2)}{\zeta_p} \int_{\zeta_p}^{\infty} u^2 \exp(2\pi i u^2/b^2) \left\{ \left(-\frac{\zeta_p}{u} \right) \frac{\exp[2\pi i(u^2 - \zeta_p^2)] - 1}{4\pi i u^2} \right. \\ &\quad \left. - \frac{\zeta_p}{u^2} \left[\frac{1}{2} \exp(-2\pi i \zeta_p^2) [E(2u) - E(2\zeta_p)] - \frac{\exp[2\pi i(u^2 - \zeta_p^2)] - 1}{4\pi i u} \right] \right\} du \\ &= \frac{1}{2} R_0 \int_{\zeta_p}^{\infty} \exp(2\pi i u^2/b^2) [E(2u) - E(2\zeta_p)] du.\end{aligned}\quad (18)$$

Neither (17) nor (18) agrees with 9.25 (5), because of the neglect of gyroscopic forces and the approximate nature of the earlier expression. The integral (18) is not expressible in terms of Fresnel integrals and although expressible in terms of $H(\zeta_p, b)$ (see Appendix B) is exceedingly complicated and hence not suited for computation. However, a numerical comparison shows that (17) and (18) are nearly equal to 9.25 (5); and, since this later expression is quite simple, we may use it for computation. Actually the contributions of (17) and (18) are only a few percent of that of (16), so that it is not necessary to evaluate them accurately, and a reasonable approximation may be obtained by neglecting them.

The technique of expanding the Green's function as in (13) can be used to derive many approximate relations; the best results are obtained when the applied force or moment is rapidly oscillating or is small except near the launcher. In such cases the integrals (16)–(18) are independent of ζ for large ζ , and the various equivalent conditions form an excellent approximation. This is shown in the case of malalignment by figure 9.25c in which the exact and approximate theories are compared.

9.27 Angular Malalignment.—The effect of angular malalignment, which is generally small compared to that of linear malalignment in spin-stabilized rockets, may be evaluated easily by means of the Green's function technique. From 9.13 (6)–(8), 9.21 (1)–(5) and 9.22 (1), we have for the deflection

$$\varphi_\beta = 0, \quad (1)$$

$$\begin{aligned}\vartheta_\beta &= -\delta_\beta = -\beta_M \int_{\zeta_p}^{\zeta} \Theta_\beta(u, \zeta) \exp(2\pi i \gamma u^2) \frac{du}{u} \\ &= \frac{\beta_M}{\zeta} \int_{\zeta_p}^{\zeta} \exp(2\pi i \gamma u^2) du \\ &= \frac{\beta_M}{2\zeta \gamma^{\frac{1}{2}}} [E(2\zeta \gamma^{\frac{1}{2}}) - E(2\zeta_p \gamma^{\frac{1}{2}})].\end{aligned}\quad (2)$$

This deflection in a typical case ($\gamma=20$, $\zeta_p=0.16$) is about one percent of the effect of linear malalignment if we make the assumption that

$$R_M \approx \frac{1}{2} \beta_M l, \quad (3)$$

which is certainly correct as to order of magnitude. The result is still small in the presence of aerodynamic forces, so that we may neglect angular malalignment completely in spin-stabilized rockets.

9.3 Motion With Finite Stability Factor and Constant Acceleration

Many of the spin-stabilized rockets used in practice have sufficiently large stability factors when ground fired that the gyroscopic forces dominate the aerodynamic forces and the general character of the motion during burning is well exemplified by the results obtained in the preceding section. The vacuum approximation is probably adequate for the treatment of such phenomena as malalignment and mallaunching where either the applied forces or the initial conditions are not known accurately in practice and where there are fluctuations from round to round. On the other hand the aerodynamic forces must be included in a treatment of wind effects, since there are no wind effects at all if there are no aerodynamic forces, and in a treatment of gravity drop expected with an ideal rocket ideally launched, since an accurate value of this gravity drop is needed for the construction of range tables and since it can be checked experimentally with considerable precision by averaging results for a series of rounds.

The dominant aerodynamic force is the overturning moment, its value being most conveniently given in terms of the stability factor. In this section we shall assume that the stability factor is constant during burning and that there are no other aerodynamic forces. This approximation gives sufficiently accurate solutions for almost all practical purposes and provides an adequate understanding of the main effects of aerodynamic forces. The more general case will be treated in later sections. Experimental tests show that the equations used in this section describe the motion during burning of ground fired spin-stabilized rockets to within the limits of experimental error, and hence that the solutions given here may be used in predicting the motion of a rocket. The most convincing specific tests were those used in checking the theoretically predicted deflections due to wind and to malalignment, the experimental results agreeing with the theory to within the experimental error. Perhaps the best check of all on the theory is the fact that it was used throughout an extensive reduction of experimental data for the construction of range tables, and no inconsistencies between theory and experiment were found.

9.31 Equations of Motion.—The equations of motion with a constant stability factor were derived in 9.11 (33)–(35) and are

$$\varphi'' - 4\pi i \zeta \varphi' - \frac{4\pi^2 \zeta^2}{S} \delta = \frac{t_\lambda^2 f_I(\zeta)}{mK^2}, \quad (1)$$

$$\vartheta' - \frac{1}{\zeta} \delta = \frac{1}{mG\zeta} F_I(\zeta), \quad (2)$$

and

$$\varphi - \vartheta - \delta = 0. \quad (3)$$

As inhomogeneous terms we shall consider only linear malalignment and gravity because the effects of angular malalignment and jet damping are so small. Hence 9.18 (11) gives us

$$f_I(\zeta) = -mGR_M e^{i\psi}, \quad (4)$$

where R_M is the linear malalignment. The component of the gravitational force normal to the trajectory is given with sufficient accuracy by

$$F_I(\zeta) = img \cos \theta_0. \quad (5)$$

First we must find the general solution of the homogeneous equations obtained when f_I and F_I are zero. This is most easily done by eliminating φ' and φ'' in (1) by means of (3) and then eliminating ϑ' and ϑ'' by means of (2), thus getting

$$\delta'' + \left(\frac{1}{\zeta} - 4\pi i \zeta \right) \delta' - \left(\frac{1}{\zeta^2} + 4\pi i + \frac{4\pi \zeta^2}{S} \right) \delta = 0. \quad (6)$$

If we write $\delta = y/\zeta$ and transform to $Z = \zeta^2$ as independent variable, (6) reduces to a linear equation with constant coefficients whose solution gives

$$\delta = C_N \zeta^{-1} \exp(2\pi i m_N \zeta^2) + C_P \zeta^{-1} \exp(2\pi i m_P \zeta^2), \quad (7)$$

where the constants m_N and m_P are

$$m_N = \frac{1}{2} \{1 + (1 - S^{-1})^{\frac{1}{2}}\}, \quad m_P = \frac{1}{2} \{1 - (1 - S^{-1})^{\frac{1}{2}}\}. \quad (8)$$

The subscripts N and P are used because the two terms correspond to the nutations and precessions discussed in 10.11.

It is desirable to express the solution as a linear combination of the characteristic functions for yaw, cross-pointing and mallaunching. Hence the constants C_N and C_P are obtained from the initial conditions which, for the various characteristic functions defined in 9.12 (1)–(3), are given by (2) and (3) to be that at $\zeta = \zeta_p$

$$\delta = 1, \delta' = -\zeta_p^{-1} \text{ for the initial yaw function } \Delta_\delta, \quad (9)$$

$$\delta = 0, \delta' = 0 \text{ for the initial cross-pointing function, } \Delta_\varphi, \quad (10)$$

and

$$\delta = 0, \delta' = 1 \text{ for the mallaunching function, } \Delta_q. \quad (11)$$

It is now easy to obtain the corresponding characteristic functions for φ and ϑ by applying 9.13 (7) to the solution for δ and by using (3) to get ϑ . A linear combination of these characteristic functions gives the general solution of the homogeneous equations and the solution of the inhomogeneous equations is obtained by the Green's function method.

The characteristic functions for R and the corresponding general solution are easily obtained by integration with the aid of 9.11 (41).

The characteristic functions obtained in this way will now be given together with a discussion of their properties and figures showing their values. They form a two parameter set, depending on both S and ζ_p , so that it is difficult to cover all cases of importance. An attempt has been made to arrange the solutions so that interpolation for cases not given is as easy as possible.

The solution (7) of the homogeneous equation for δ is the sum of two decreasing oscillations like the vacuum mallaunching solution 9.23 (4). Hence we may expect the homogeneous characteristic functions to be a sum of modified vacuum mallaunching functions, one associated with nutations and one with precessions. In this way the problem of tabulating the characteristic functions is reduced to evaluating a one-parameter set of functions. If extensive tables or sets of graphs are to be made, it will be a major economy to evaluate first the one-parameter functions $\Theta_q(\infty, \zeta_p, \zeta)$ and $\Theta_\delta^\infty(\zeta_p, \zeta)$ as defined below. The resolution of the gravity solution follows from the separation of the Green's function into nutational and precessional parts.

9.32 Solutions for Initial Cross-Pointing and for Mallaunching.—The simplest of the characteristic functions is that for initial cross-pointing, since it merely corresponds to reorientation of the launcher and is the same as in vacuum and as for nonrotating rockets. It is

$$\Delta_\varphi = 0, \Phi_\varphi = \Theta_\varphi = 1, R_\varphi = (\zeta^2 - \zeta_p^2).$$

The effect of aerodynamic forces and moments on the mallaunching solution is not large because they are proportional to the yaw and in this case the rocket starts with zero yaw and a large transverse angular velocity. The gyroscopic forces are proportional to the transverse angular velocity and are only indirectly affected by the aerodynamic forces since the latter change the transverse angular velocity appreciably only after the yaw has become large.

The solution of the equations for mallaunching is

$$\Delta_q = \frac{i}{4\pi(m_N - m_P)\zeta} \{ \exp[2\pi i m_P(\zeta^2 - \zeta_p^2)] - \exp[2\pi i m_N(\zeta^2 - \zeta_p^2)] \}, \quad (1)$$

$$\begin{aligned} \Phi_q = & \frac{m_N^{\frac{1}{2}}}{2(m_N - m_P)} \exp(-2\pi i m_N \zeta_p^2) [E(2\zeta m_N^{\frac{1}{2}}) - E(2\zeta_p m_N^{\frac{1}{2}})] \\ & - \frac{m_P^{\frac{1}{2}}}{2(m_N - m_P)} \exp(-2\pi i m_P \zeta_p^2) [E(2\zeta m_P^{\frac{1}{2}}) - E(2\zeta_p m_P^{\frac{1}{2}})], \end{aligned} \quad (2)$$

and hence

$$\Theta_q(S, \zeta_p, \zeta) = \Phi_q - \Delta_q = (m_N - m_P)^{-1} [m_N^{\frac{1}{2}} \Theta_q(\infty, \xi_p, \xi) - m_P^{\frac{1}{2}} \Theta_q(\infty, \chi_p, \chi)], \quad (3)$$

where

$$\xi = m_N^{\frac{1}{2}} \zeta, \xi_p = m_N^{\frac{1}{2}} \zeta_p, \chi = m_P^{\frac{1}{2}} \zeta, \chi_p = m_P^{\frac{1}{2}} \zeta_p. \quad (3a)$$

This solution is the sum of two vacuum case solutions as given in 9.23 and here denoted by $\Theta_q(\infty, \zeta_p, \zeta)$, but with different periods and amplitudes. Hence, it shows a somewhat more complicated behavior, although the final deflections are not much different. These functions, shown in figures 9.32a-c have been tabulated for $S=2, 4$, and 8 with $\zeta_p=0, 0.2$, and 0.3 . It is apparent by comparing these figures with 9.23c that the effect of the aerodynamic forces is small. Its main effect is to increase the angle between the plane of the mallaunching and the plane of the final deflection, although there is also a slight decrease in the magnitude of the deflection of the trajectory.

Since the deflection due to mallaunching is insensitive to aerodynamic moments, it is possible to use 9.23 (10) and (11) to approximate the magnitude of Θ_q in the present case. The asymptotic expansion of Θ_q is

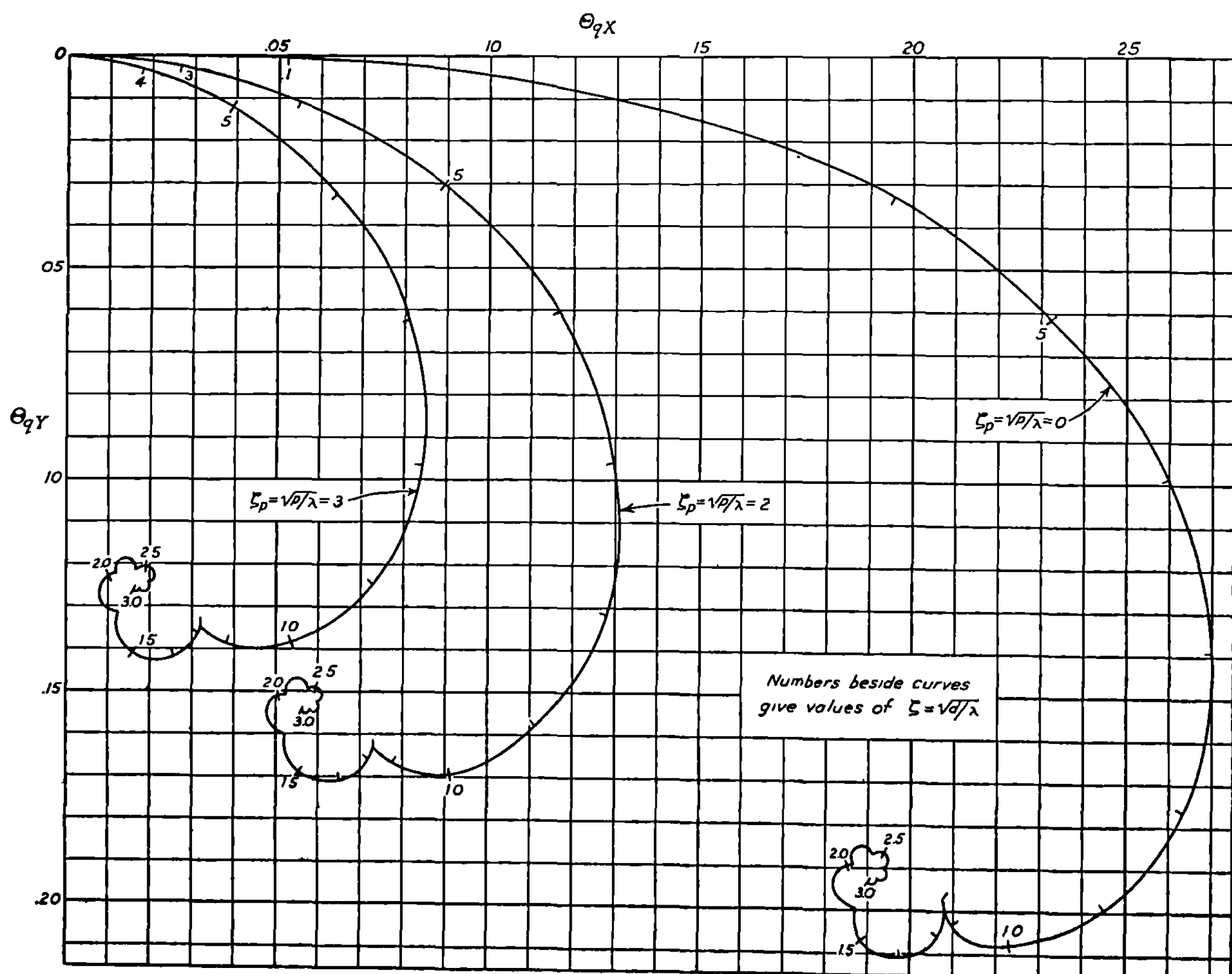


FIGURE 9.32 (a).—Characteristic function $\Theta_q(S, \zeta_p, \zeta)$ for $S=2$.

$$\begin{aligned}
\Theta_q \sim & \frac{m_N^{\frac{1}{2}}}{4(m_N - m_P)} \exp(-2\pi i m_N \zeta_p^2) [1 + i - 2E(2\zeta_p m_N^{\frac{1}{2}})] \\
& - \frac{m_P^{\frac{1}{2}}}{4(m_N - m_P)} \exp(-2\pi i m_P \zeta_p^2) [1 + i - 2E(2\zeta_p m_P^{\frac{1}{2}})] \\
& + \frac{\exp[2\pi i m_P (\zeta^2 - \zeta_p^2)]}{4\pi(m_N - m_P)\zeta} \left\{ \frac{1}{(4\pi m_P \zeta^2)} - \frac{1.3 i}{(4\pi m_P \zeta^2)^2} - \frac{1.3 \cdot 5}{(4\pi m_P \zeta^2)^3} + \dots \right\} \\
& - \frac{\exp[2\pi i m_N (\zeta^2 - \zeta_p^2)]}{4\pi(m_N - m_P)\zeta} \left\{ \frac{1}{(4\pi m_N \zeta^2)} - \frac{1.3 i}{(4\pi m_N \zeta^2)^2} - \frac{1.3 \cdot 5}{(4\pi m_N \zeta^2)^3} + \dots \right\}. \quad (4)
\end{aligned}$$

The characteristic displacement function, R_q , could be given by a complicated expression similar to 9.23 (6) which, however, is not of sufficient interest to reproduce here. Figures 9.32d-f show its value as obtained by numerical integration of the equation

$$R_q = 2 \int_{\zeta_p}^{\zeta} \zeta \Theta_q d\zeta, \quad (5)$$

for $S=2, 4$ and 8 with $\zeta_p=0, 0.2$ and 0.3 . Its behavior is very similar to that in the vacuum case and so needs no further discussion.

The mallaunching function is also the Green's function for applied torques, so that it is desirable to have plots of Θ_q with ζ_p as the independent variable. This is done in Figs. 9.32g

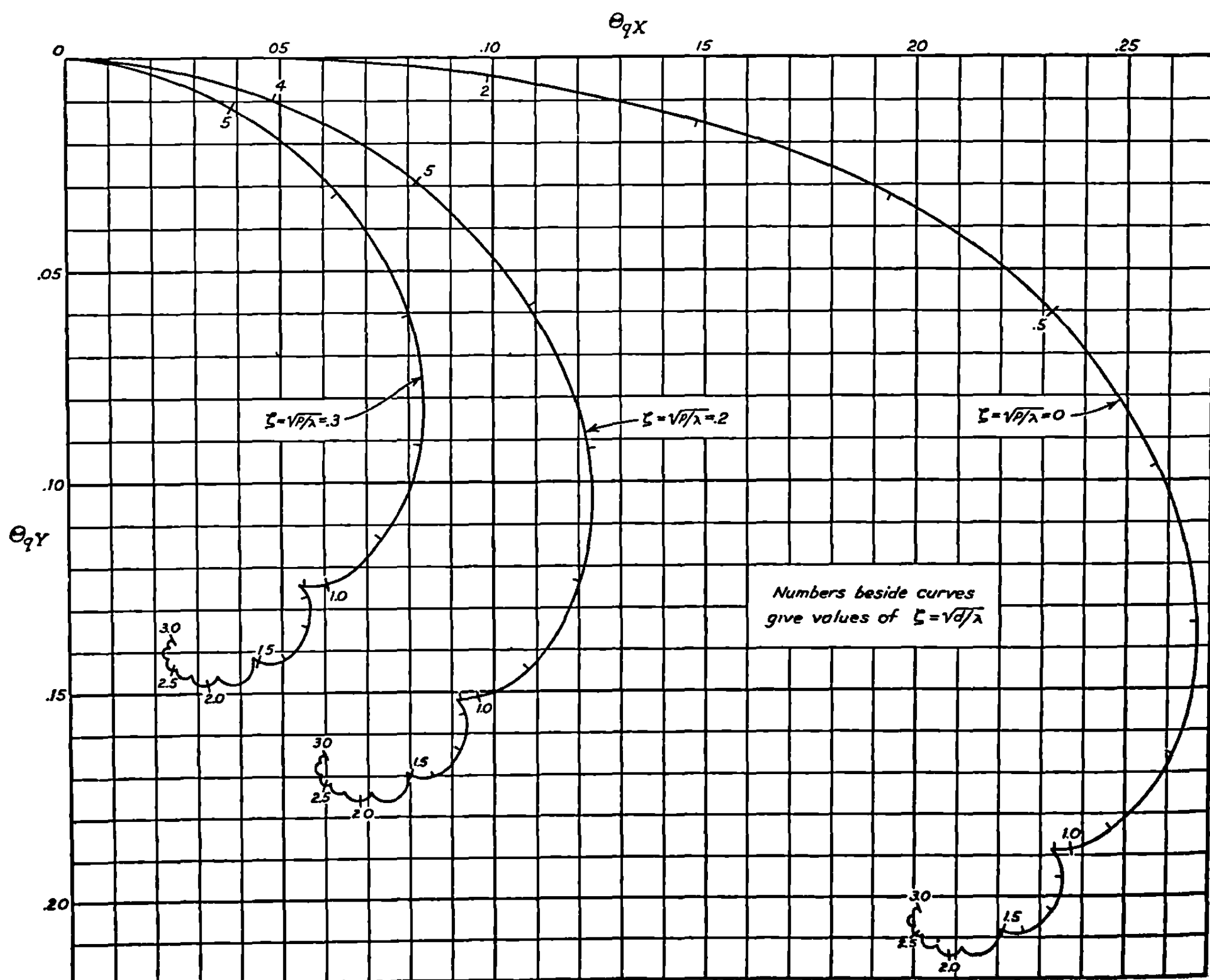


FIGURE 9.32 (b).—Characteristic function $\Theta_q(S, \zeta_p, \zeta)$ for $S=4$.

and h for $S=2$ and 4 , and $\zeta=\sqrt{2}$ and 2 , with $0 \leq \zeta_p \leq \zeta$. These functions resemble closely the curves for the vacuum case (fig. 9.23g) in that the function is large only for small ζ_p , and the magnitude is nearly the same. However the phase of Θ_e and hence the shape of the locus is somewhat different from the vacuum case.

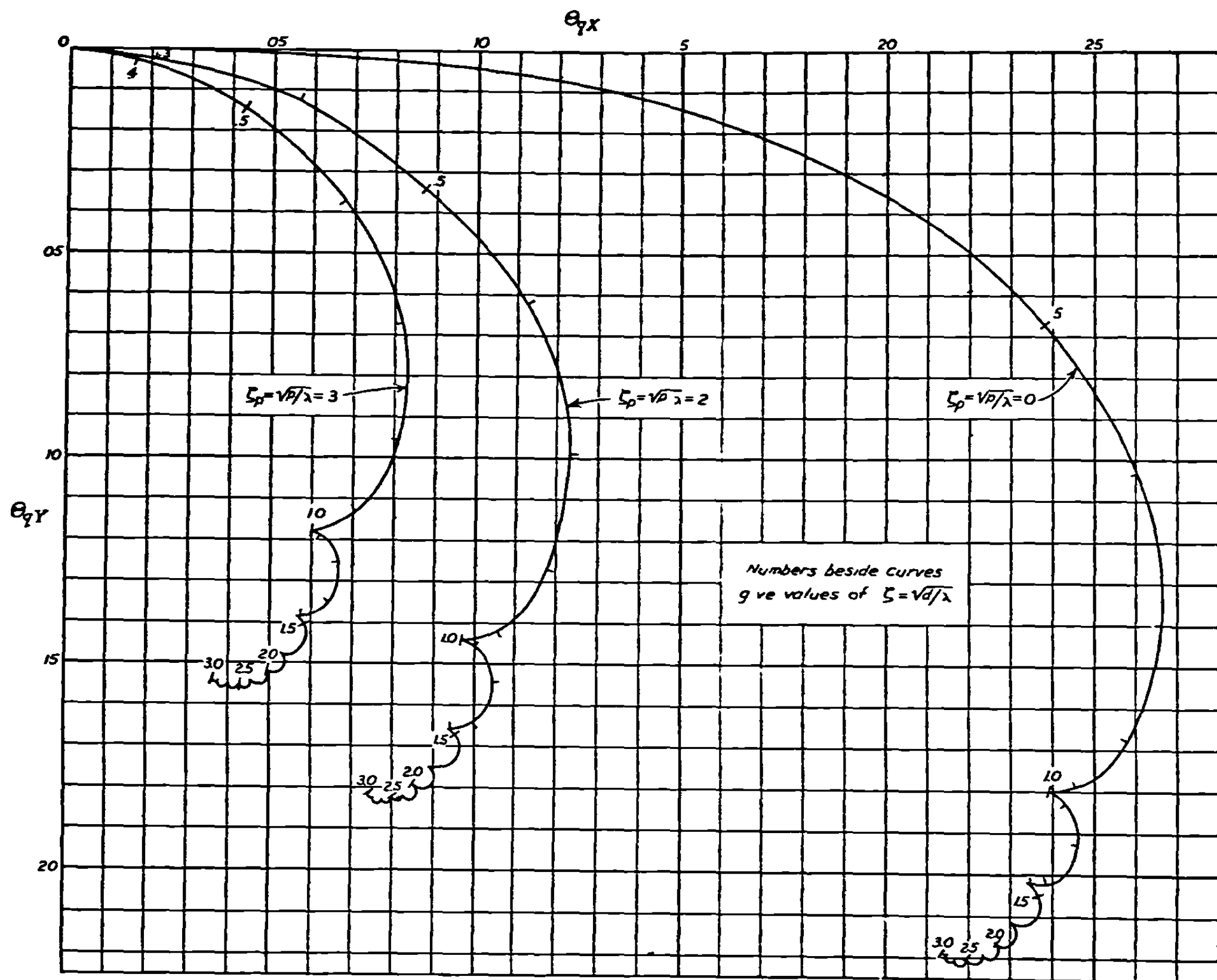
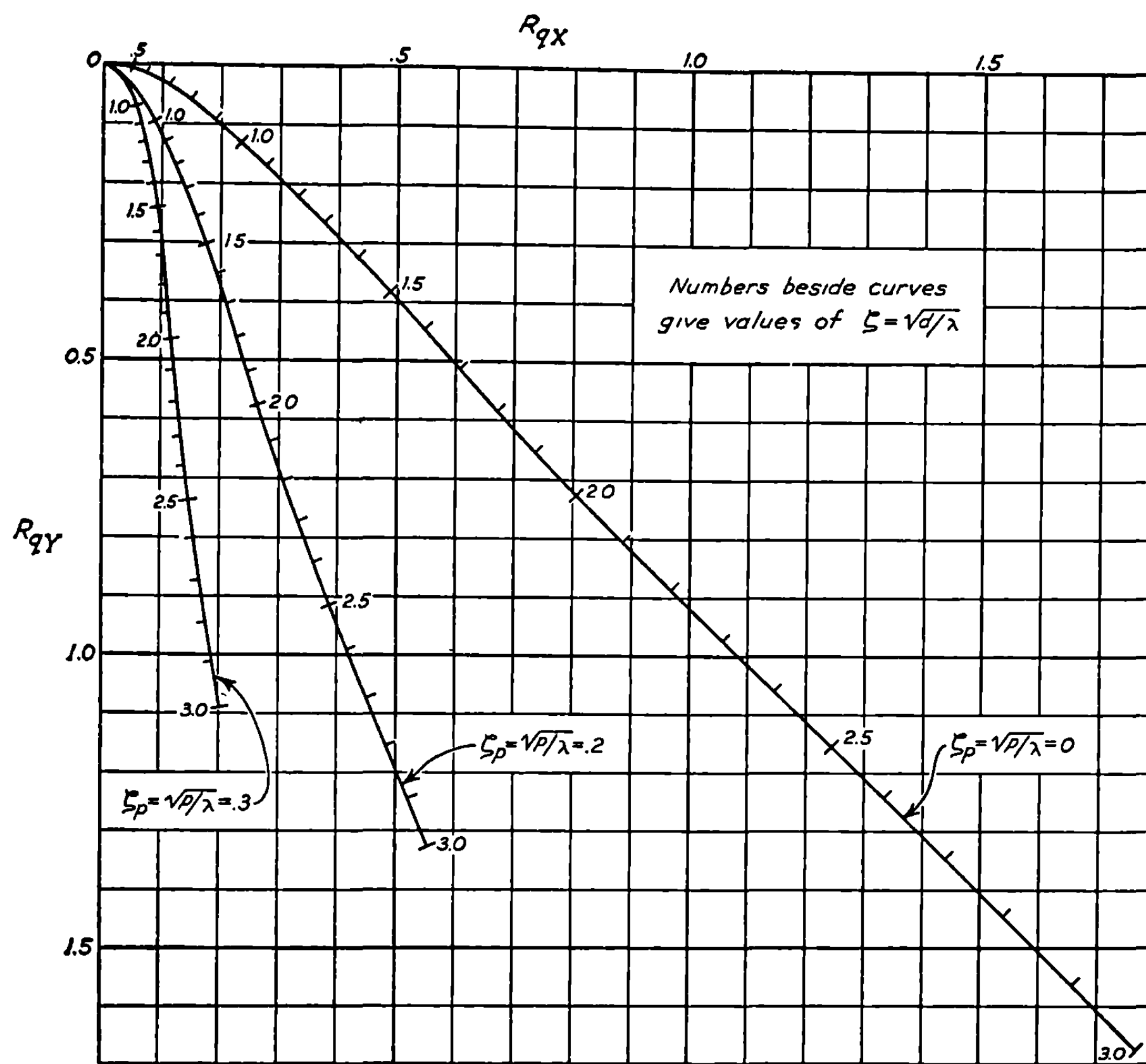
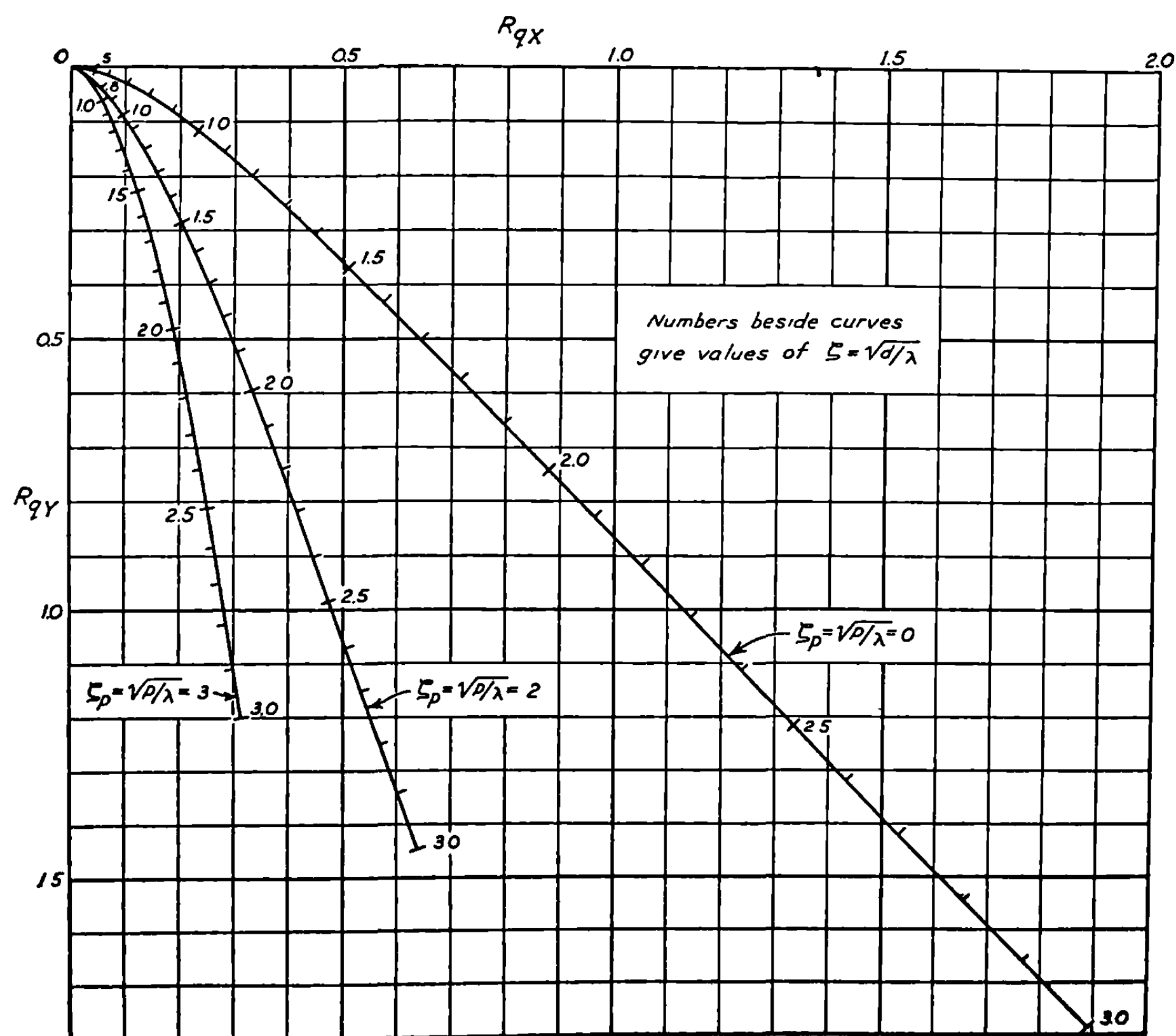


FIGURE 9.32 (c).—Characteristic function $\Theta_e(S, \zeta, \zeta_p)$ for $S=8$.

FIGURE 9.32 (d).—Characteristic function $R_q(S, \xi_p, \xi)$ for $S=2$.FIGURE 9.32 (e).—Characteristic function $R_q(S, \xi_p, \xi)$ for $S=4$.

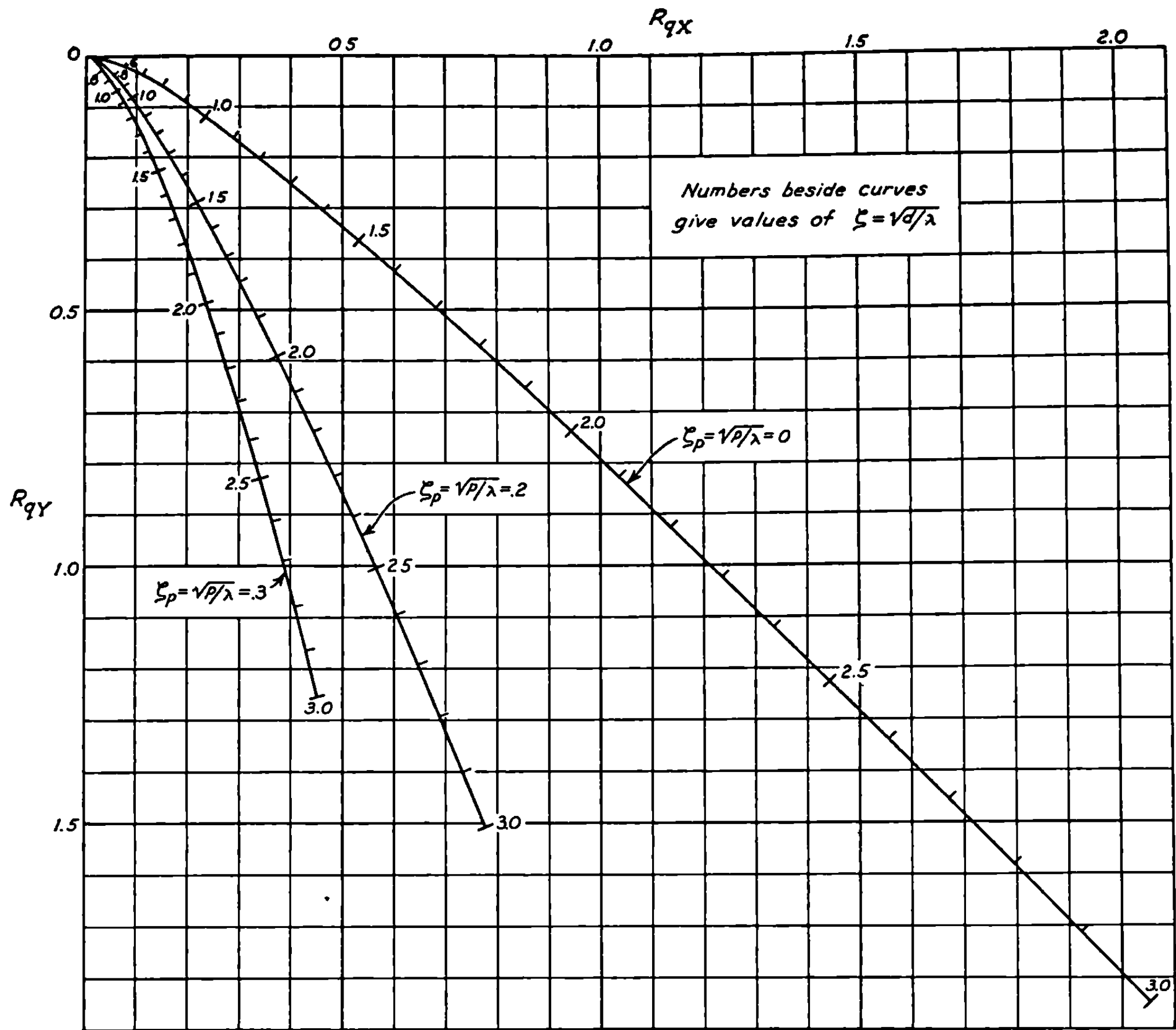
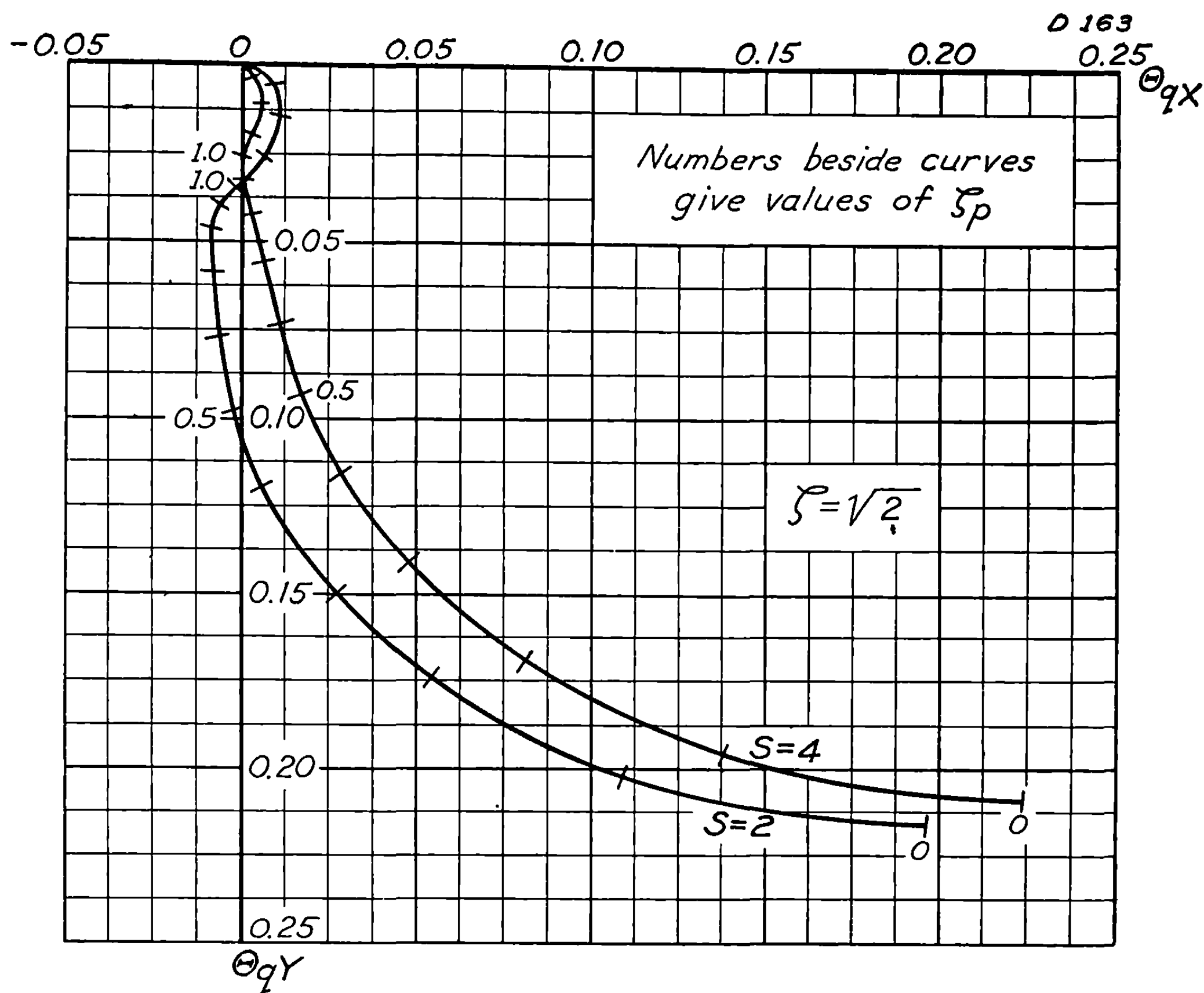
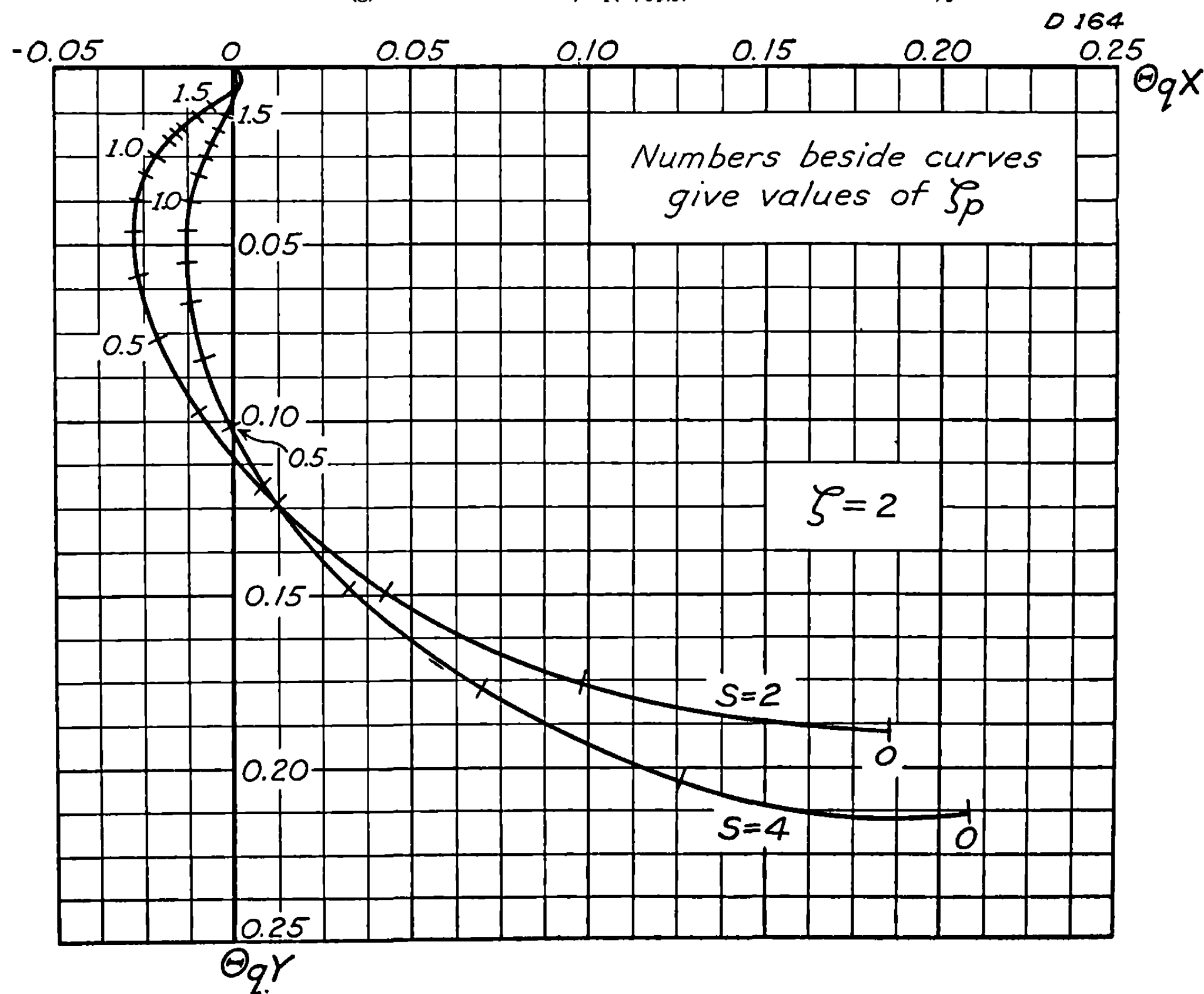


FIGURE 9.32 (f).—Characteristic function $R_q(S, \xi_p, \xi)$ for $S=8$.

FIGURE 9.32 (g).—Green's function, $\Theta_q(S, \zeta_p, \zeta)$ for transverse moments; $\zeta = 2^{1/2}$.FIGURE 9.32 (h).—Green's function, $\Theta_q(S, \zeta_p, \zeta)$ for transverse moments; $\zeta = 2$.

9.33 Solution for Initial Yaw.—The effects of initial yaw are modified from the vacuum case by the precession caused by the aerodynamic overturning moment. When we have right yaw without cross-pointing, the trajectory starts with an initial deflection to the left while the rocket points straight ahead. In vacuum the orientation would not change but the leftward deflection would decrease as the rocket picked up speed. In air the moment due to the right yaw causes the nose of the rocket to precess downward and then to the left. Thus the trajectory is deflected downward and later to the left of the vacuum trajectory. There is a small nutation superposed on the precession, but its effect on the motion is very small. The solutions for the case of initial yaw, as obtained from 9.31 (7) and (9), are

$$\Delta_\delta = \frac{m_N \zeta_p}{(m_N - m_P) \zeta} \exp [2 \pi i m_P (\zeta^2 - \zeta_p^2)] - \frac{m_P \zeta_p}{(m_N - m_P) \zeta} \exp [2 \pi i m_N (\zeta^2 - \zeta_p^2)], \quad (1)$$

$$\Phi_\delta = \frac{-i \pi \zeta_p}{2S(m_N - m_P)} \left\{ \frac{\exp(-2 \pi i m_N \zeta_p^2)}{m_N^{\frac{1}{2}}} [E(2 \zeta m_N^{\frac{1}{2}}) - E(2 \zeta_p m_N^{\frac{1}{2}})] \right. \\ \left. - \frac{\exp(-2 \pi i m_P \zeta_p^2)}{m_P^{\frac{1}{2}}} [E(2 \zeta m_P^{\frac{1}{2}}) - E(2 \zeta_p m_P^{\frac{1}{2}})] \right\}, \quad (2)$$

and hence

$$\Theta_\delta = \Phi_\delta - \Delta_\delta = -\frac{\zeta_p}{\zeta} - \frac{4 \pi i m_N^{\frac{1}{2}} m_P^{\frac{1}{2}} \zeta_p}{m_N - m_P} [m_P^{\frac{1}{2}} \Theta_q(\infty, \xi_p, \xi) - m_N^{\frac{1}{2}} \Theta_q(\infty, \chi_p, \chi)]. \quad (3)$$

A plot of Θ_δ is given in figure 9.33a, from which it may be seen that this function depends markedly on both ζ and ζ_p . Such curves are not very useful because it is difficult to interpolate accurately between the various curves. Furthermore, the solution for initial yaw is not important because the values of the yaw produced by the launching process are small. For these reasons, and because Θ_δ is easily obtained from the curves for Θ_W to be found in 9.35, no further curves of Θ_δ will be given. The function Θ_W , the deflection produced by cross-wind, is a slowly varying function of ζ and ζ_p , and is a much more important function than Θ_δ , because cross wind does produce deflections of great significance in practice. The formulas needed to obtain the characteristic functions for initial yaw from the characteristic functions for cross-wind will be derived in 9.35 but it will be useful to list the results here. They are

$$\Delta_\delta = \zeta_p (\Delta_W + \zeta^{-1}), \quad (4)$$

$$\Phi_\delta = \zeta_p \Phi_W, \quad (5)$$

$$\Theta_\delta = \zeta_p (\Theta_W - \zeta^{-1}). \quad (6)$$

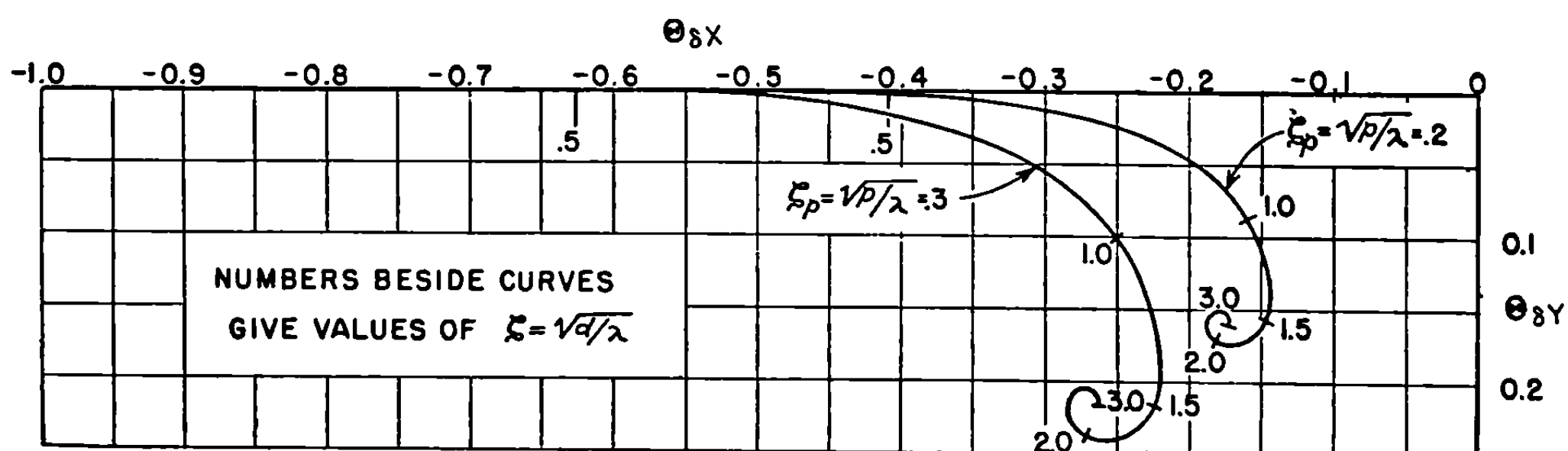


FIGURE 9.33 (a).—Characteristic function $\Theta_\delta(S, \zeta_p, \zeta)$ for $S=2$.

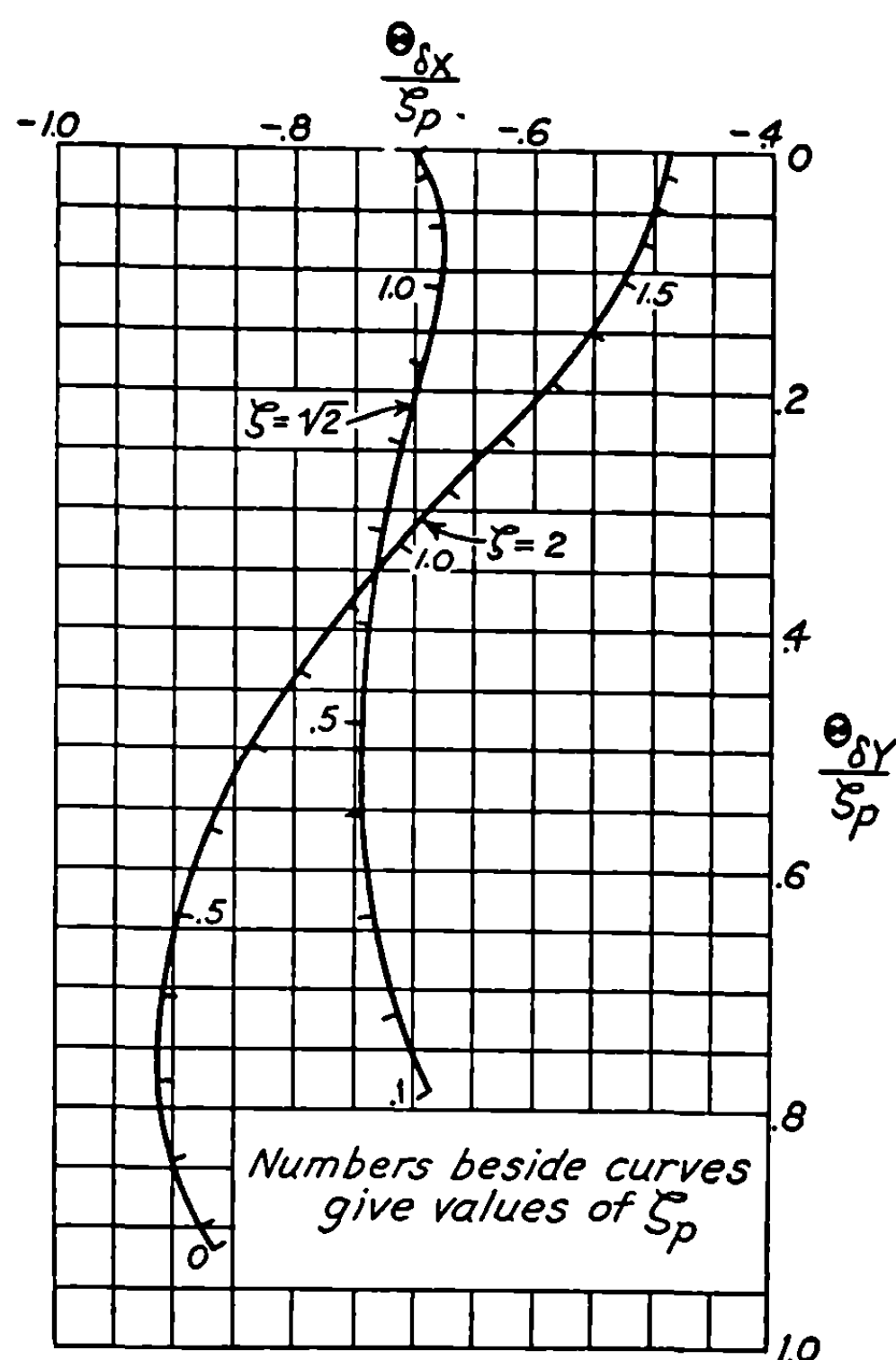


FIGURE 9.33 (b).—Green's function $\Theta_i(S, \zeta_p, \zeta)/\zeta_p$ for cross-force; $S=2$.

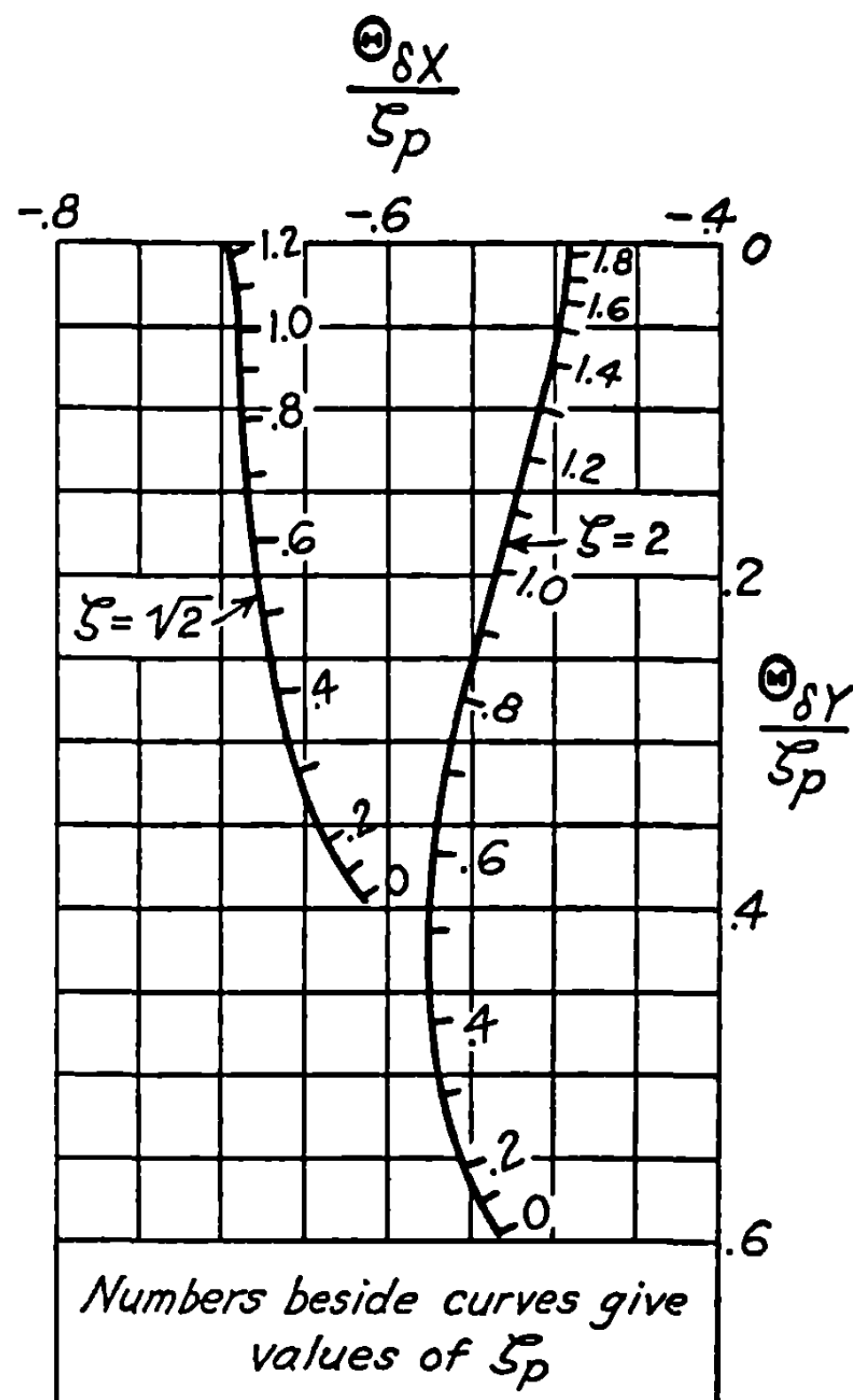


FIGURE 9.33 (c).—Green's function $\Theta_i(S, \zeta_p, \zeta)/\zeta_p$ for cross-force; $S=4$.

The solution for initial yaw is also the Green's function for applied forces. As may be seen from 9.13 (6), however, the function actually used in the integral is not Θ_i but Θ_i/ζ_p . Hence it is this latter function that is tabulated in figures 9.33b and c for $S=2$ and 4 with $\zeta=\sqrt{2}$ and 2. It may be seen from the figures that the effects of applied forces are of importance over the whole burning period, in contrast to the effects of applied moments which give significant deflections only near the launcher. The reason for this is that the inertia of the rocket stays constant while its gyroscopic stiffness; i. e., its resistance to torques, increases markedly during burning.

9.34 Solution for Gravity.—The primary effect of gravity is to deflect the trajectory downward which would leave the rocket with an up yaw if the aerodynamic forces did not then change the orientation. The first effect of the aerodynamic overturning moment is to cause the nose of the rocket to rise slightly, the nutation and precession then carrying it off to the right. The main effect after $\zeta=1$ is due to the precession produced by the overturning moment, the head precessing first to the right and then down. Hence the jet force deflects the rocket to the right of and a little below where it would go if there were no aerodynamic forces. This process is relatively slow both because precession changes the orientation slowly and because the moment that produces the precession is not applied until after gravity has deflected the trajectory. The deflection is, however, somewhat sensitive to launcher length because the rate of gravity drop depends on the launcher length.

We may obtain the solution by means of the Green's function technique. Defining the characteristic functions by the formulas

$$\delta_z = \frac{g \cos \theta_0}{G} \Delta_z, \quad \phi_z = \frac{g \cos \theta_0}{G} \Phi_z, \quad \vartheta_z = \frac{g \cos \theta_0}{G} \Theta_z, \quad r_z = \frac{g \cos \theta_0}{G} \lambda R_z \quad (1)$$

and using 9.13 (4)–(6), 9.31 (1)–(5) and 9.33 (1)–(3), we have

$$\Delta_z = -i \int_{\zeta_p}^{\zeta} \Delta_\delta(u, \zeta) \frac{du}{u} = \frac{m_P}{m_N - m_P} \Delta_z^\infty(\xi_p, \xi) - \frac{m_N}{m_N - m_P} \Delta_z^\infty(\chi_p, \chi) \quad (2)$$

where

$$\Delta_z^\infty(u_p, u) = (i/2u) \exp(2\pi i u^2) [E^*(2u) - E^*(2u_p)]. \quad (2a)$$

$$\Phi_z = -i \int_{\zeta_p}^{\zeta} \Phi_\delta(u, \zeta) \frac{du}{u} = \frac{m_P}{m_N - m_P} \Phi_z^\infty(\xi_p, \xi) - \frac{m_N}{m_N - m_P} \Phi_z^\infty(\chi_p, \chi) \quad (3)$$

where

$$\Phi_z^\infty(u_p, u) = -\pi \{ J(2u) - J(2u_p) - [E(2u) - E(2u_p)] E^*(2u_p) \} \quad (3a)$$

and

$$\Theta_z = \Phi_z - \Delta_z = (m_N - m_P)^{-1} [m_P \Theta_z^\infty(\xi_p, \xi) - m_N \Theta_z^\infty(\chi_p, \chi)]. \quad (4)$$

Here we have used the functions

$$E^*(x) = \int_0^x e^{-\pi i u^2/2} du = C(x) - iS(x), \quad (5)$$

and

$$J(x) = \int_0^x e^{\pi i u^2/2} E^*(u) du = J_R(x) + iJ_I(x), \quad (6)$$

where

$$J_R(x) = \frac{1}{2} [C^2(x) + S^2(x)] \quad (7)$$

and

$$J_I(x) = \int_0^x [C(u) \sin \pi u^2/2 - S(u) \cos \pi u^2/2] du. \quad (8)$$

Tables of these functions are given in appendix C and some of their properties are given in appendix B.

From (2) it is seen that the yaw decreases as $1/\zeta$ for large ζ and oscillates about this value in a manner similar to that for the other initial conditions. From (3) it follows that the nose of the rocket starts up slightly, then swings to the right, down, and finally spirals as the motion proceeds. This motion is shown in figure 9.34a for the case $S=2$, $\zeta_p=0$ and 0.3. It may be observed that the nutations, after the first upswing, are of only slight importance even in the orientation.

An asymptotic expansion for Θ_z can be developed by expanding (3) simultaneously in a power series in ζ_p and an asymptotic series in ζ . Unfortunately, it is of little use because it is accurate (within 10%) only after a full precession; i. e., $\zeta > 2$ for $S=2$ and $\zeta > 4$ for $S=8$. The asymptotic expansion

$$\Theta_g \sim i \ln \zeta + \pi/4 + 1.90071 i + i \frac{m_N \ln m_P - m_P \ln m_N}{2(m_N - m_P)} - (1+i) \frac{(m_N m_P)^{\frac{1}{2}}}{(m_N^{\frac{1}{2}} + m_P^{\frac{1}{2}})} \zeta_p, \zeta \gg 1, \quad (9)$$

differs considerably from the vacuum case

$$\Theta_g \sim i, \zeta \gg 1, \quad (10)$$

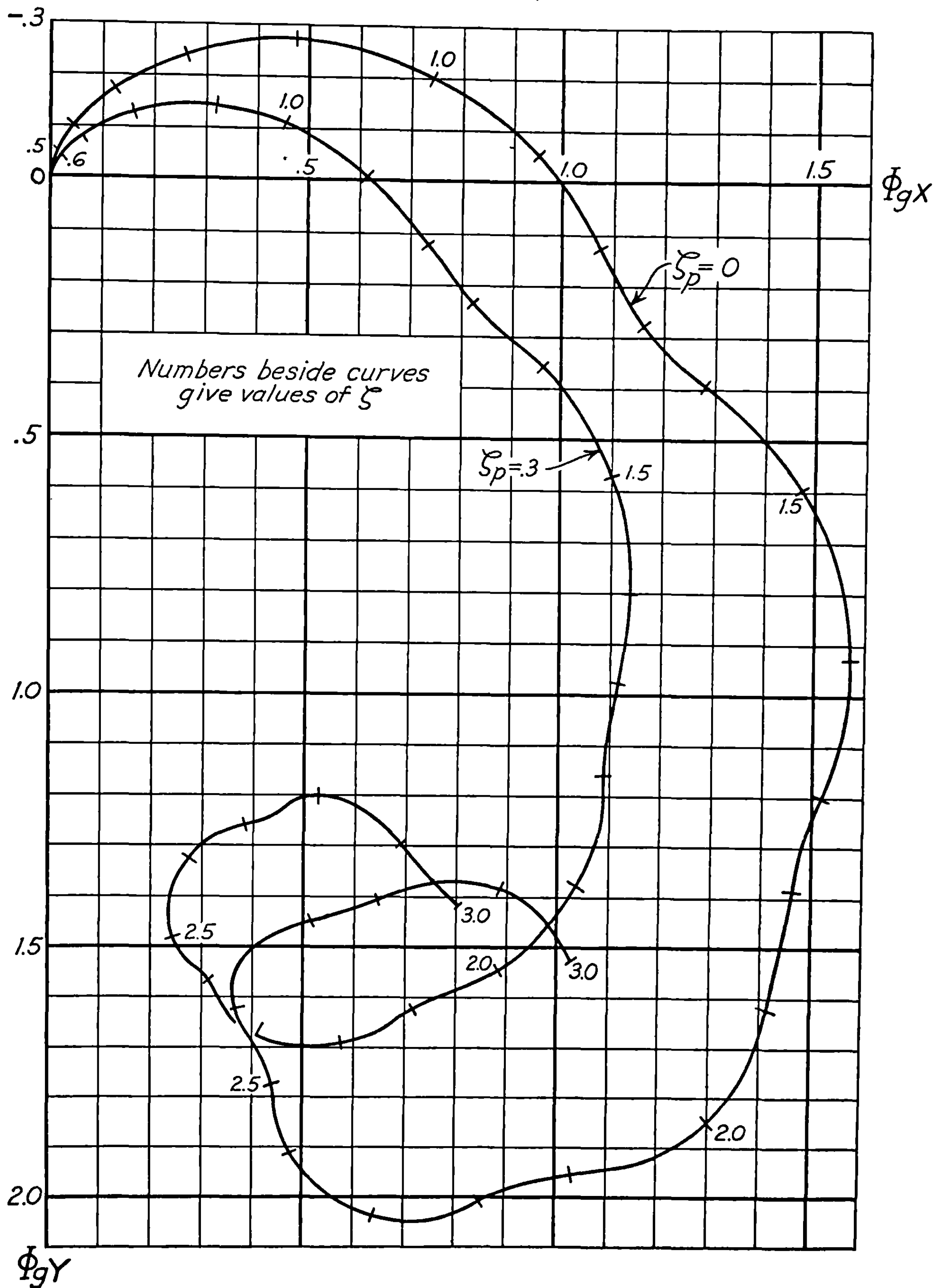
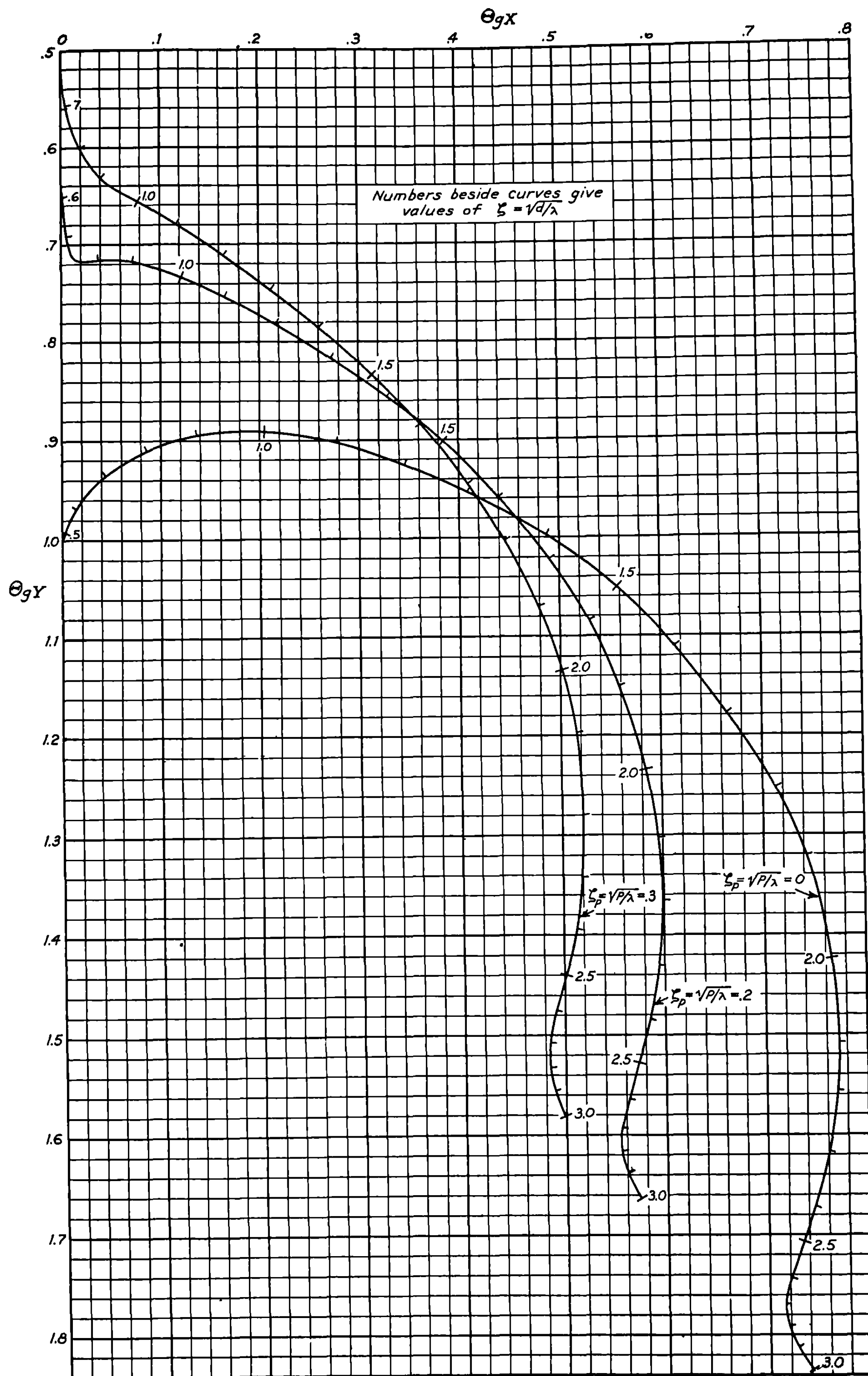


FIGURE 9.34 (a).—Characteristic function $\Phi_g(S, \zeta_p, \zeta)$ for $S=2$.

FIGURE 9.34 (b).—Characteristic function $\Theta_g(S, \xi_p, f)$ for $S=2$.

because (9) assumes that ultimately a large number of precessions will be made and no precessions occur in the vacuum case.

Exact numerical calculations are needed since (9) is not applicable to most of the cases of

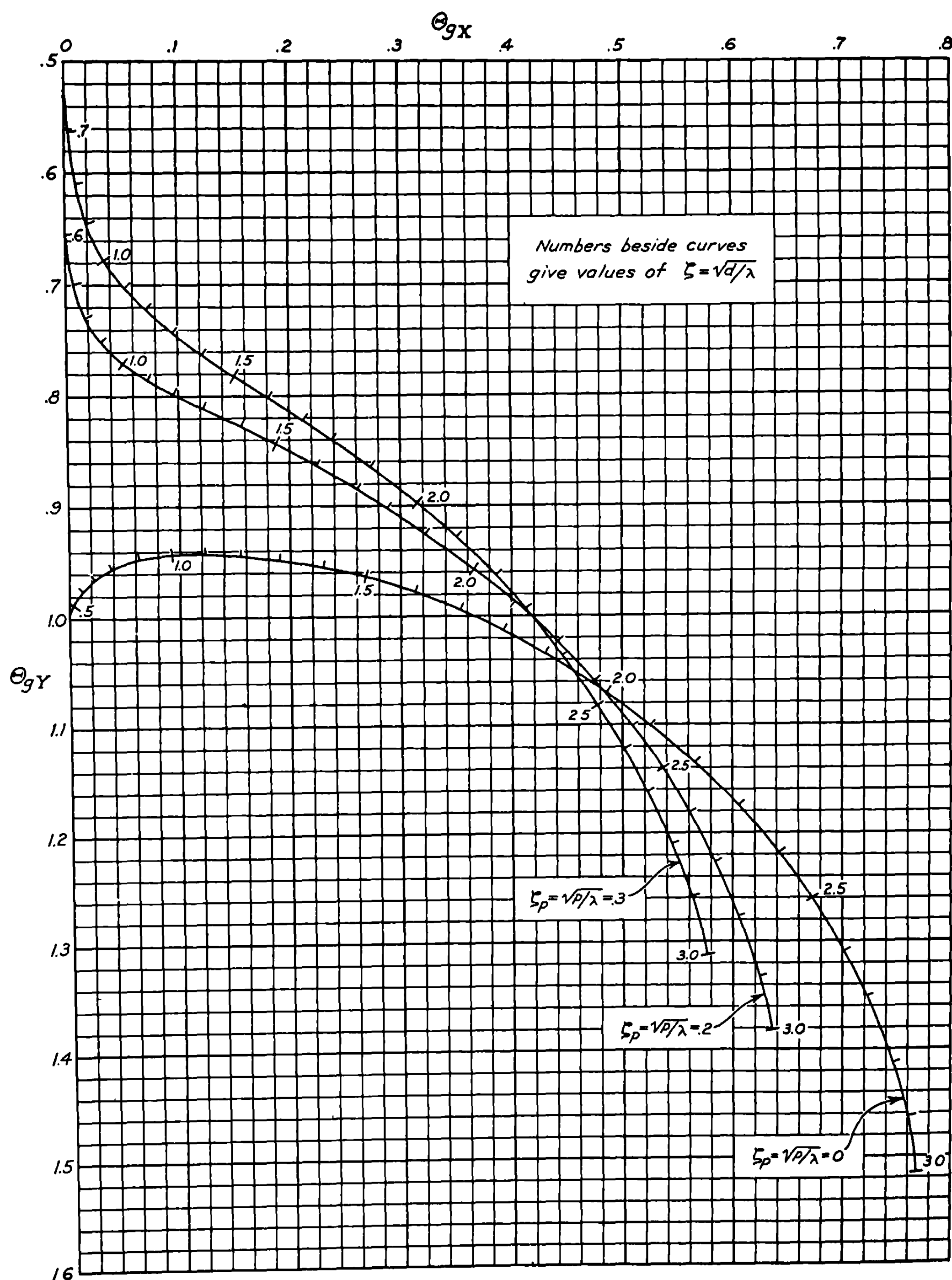


FIGURE 9.34 (c).—Characteristic function $\Theta_g(S, \zeta_p, \zeta)$ for $S=4$.

interest in practice. Plots of Θ_g for $S=2, 4$ and 8 with $\zeta_p=0, 0.2$ and 0.3 are given in figures 9.34b-d. It may be noted that these curves, while dependent upon launcher length, do not show the marked variation with launcher length shown by Θ_q . Near the launcher, where the trajectory is dropping rapidly and the aerodynamic effects are still small, the curves lie on each other along the Θ_{gY} axis, and Θ_g is difficult to determine from the graph. For this reason, this portion of the curves is not graduated. An approximate value of Θ_g in this region may be obtained from the first terms of the power series expansion, which is

$$\Theta_g \doteq i \left(1 - \frac{\zeta_p}{\zeta} \right). \quad (11)$$

Plots of R_g for $S=2, 4$, and 8 with $\zeta_p=0, 0.2$, and 0.3 are given in figures 9.34e-g. It should be noted carefully that curves are displaced horizontally, each using a different zero of R_{gX} .

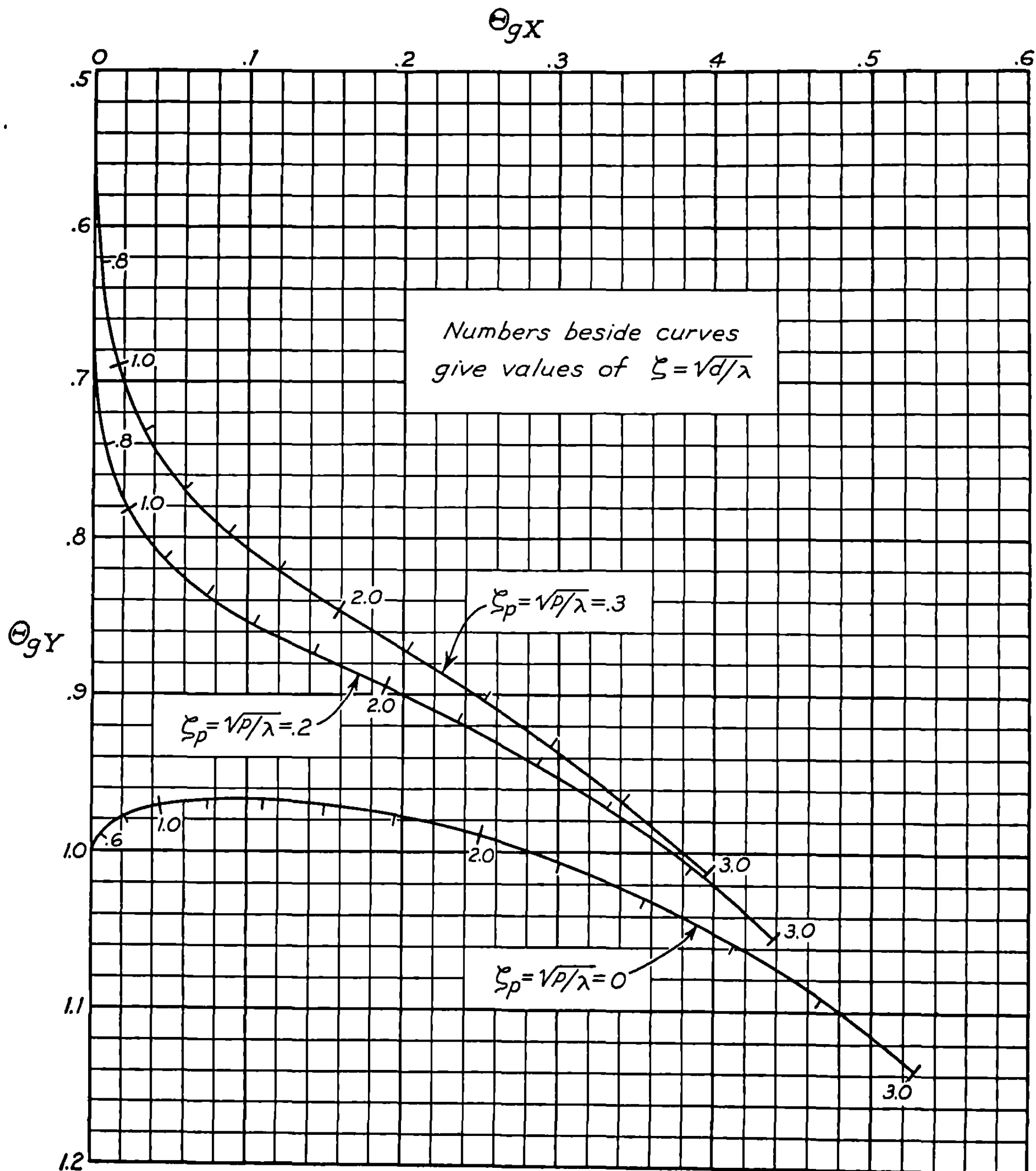
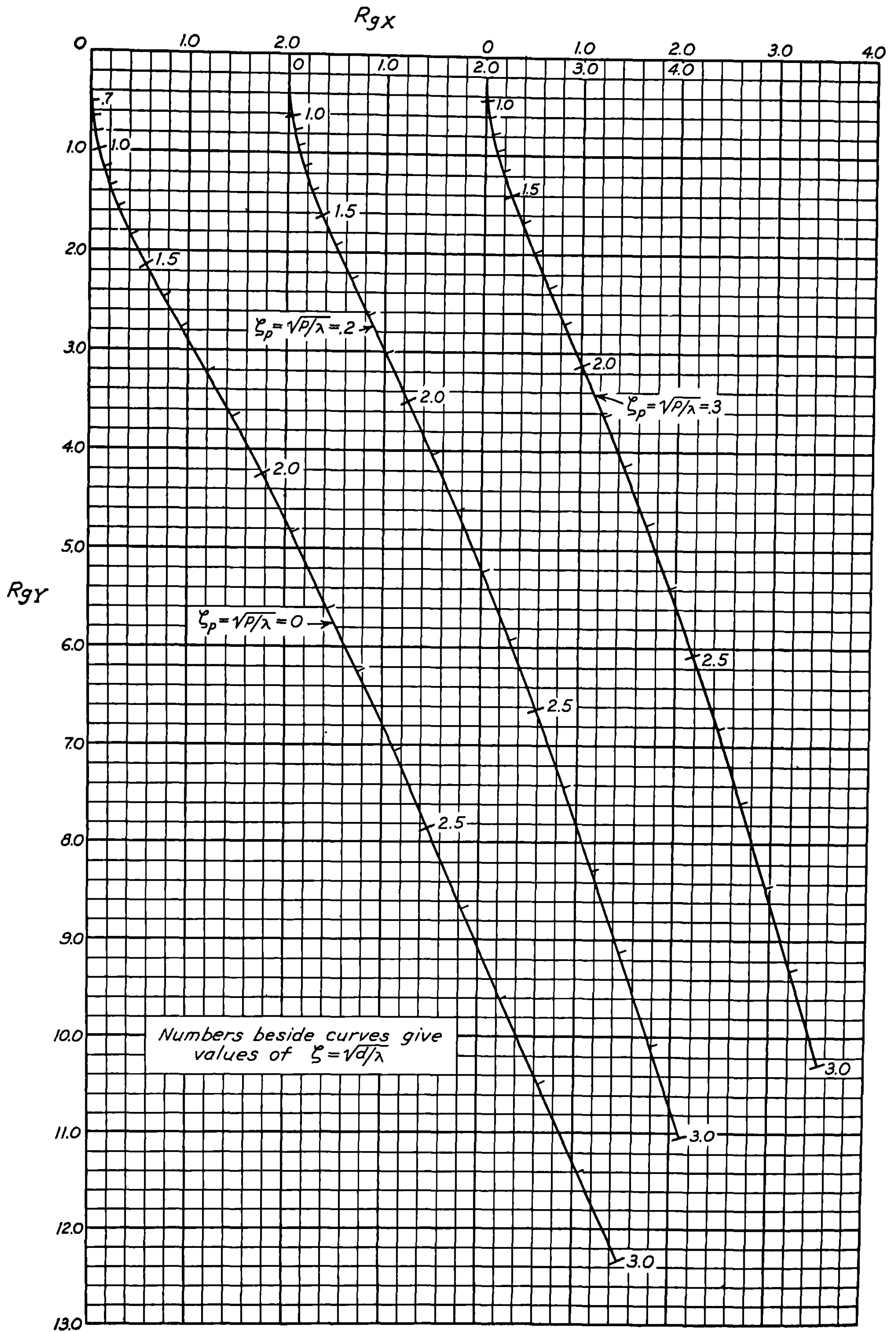


FIGURE 9.34 (d).—Characteristic function $\Theta_g(S, \zeta_p, \zeta)$ for $S=8$.

FIGURE 9.34 (e).—Characteristic function $R_g(S, \xi_p, t)$ for $S=2$.

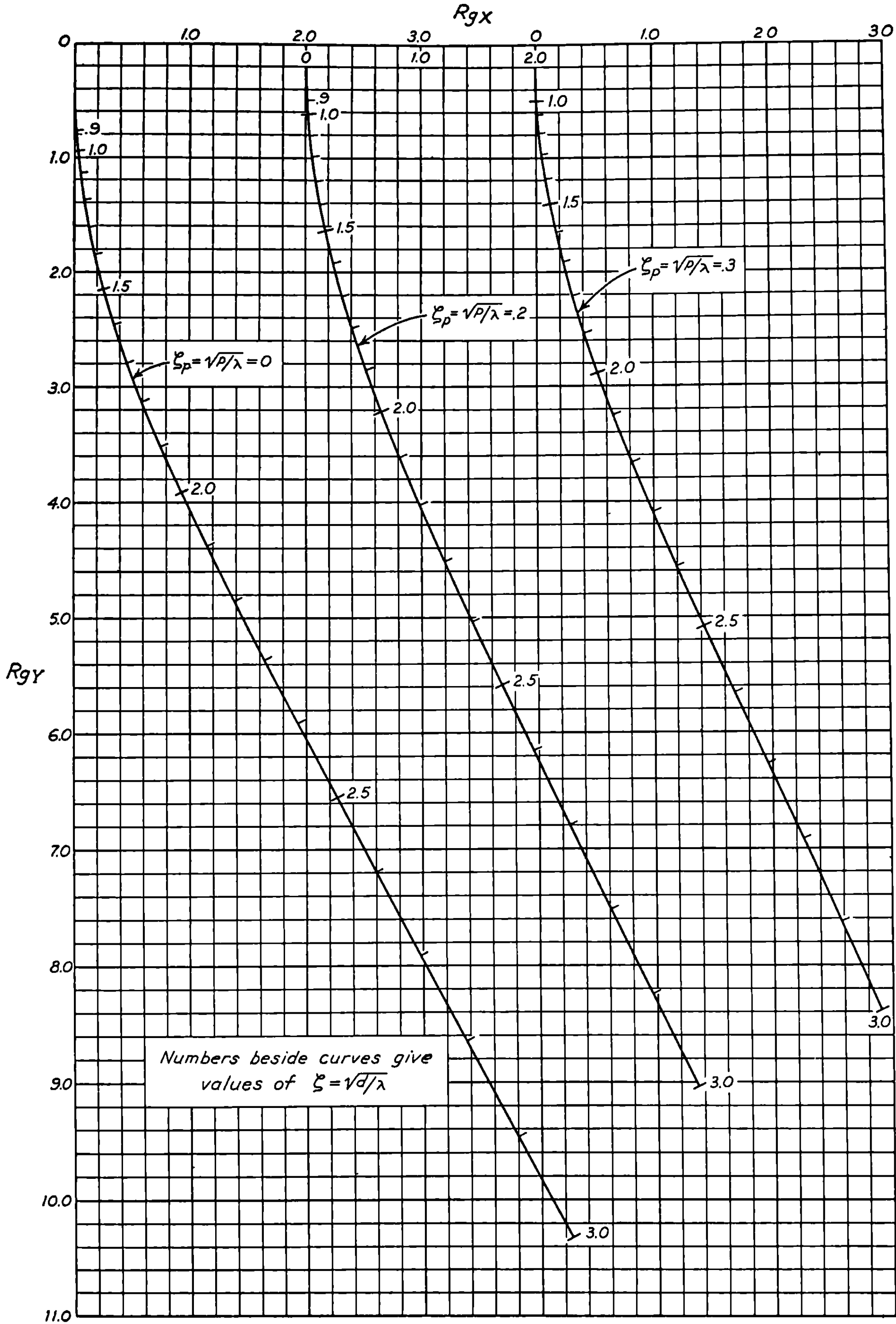


FIGURE 9.34 (f).—Characteristic function $R_g(S, \xi_p, \xi)$ for $S=4$.

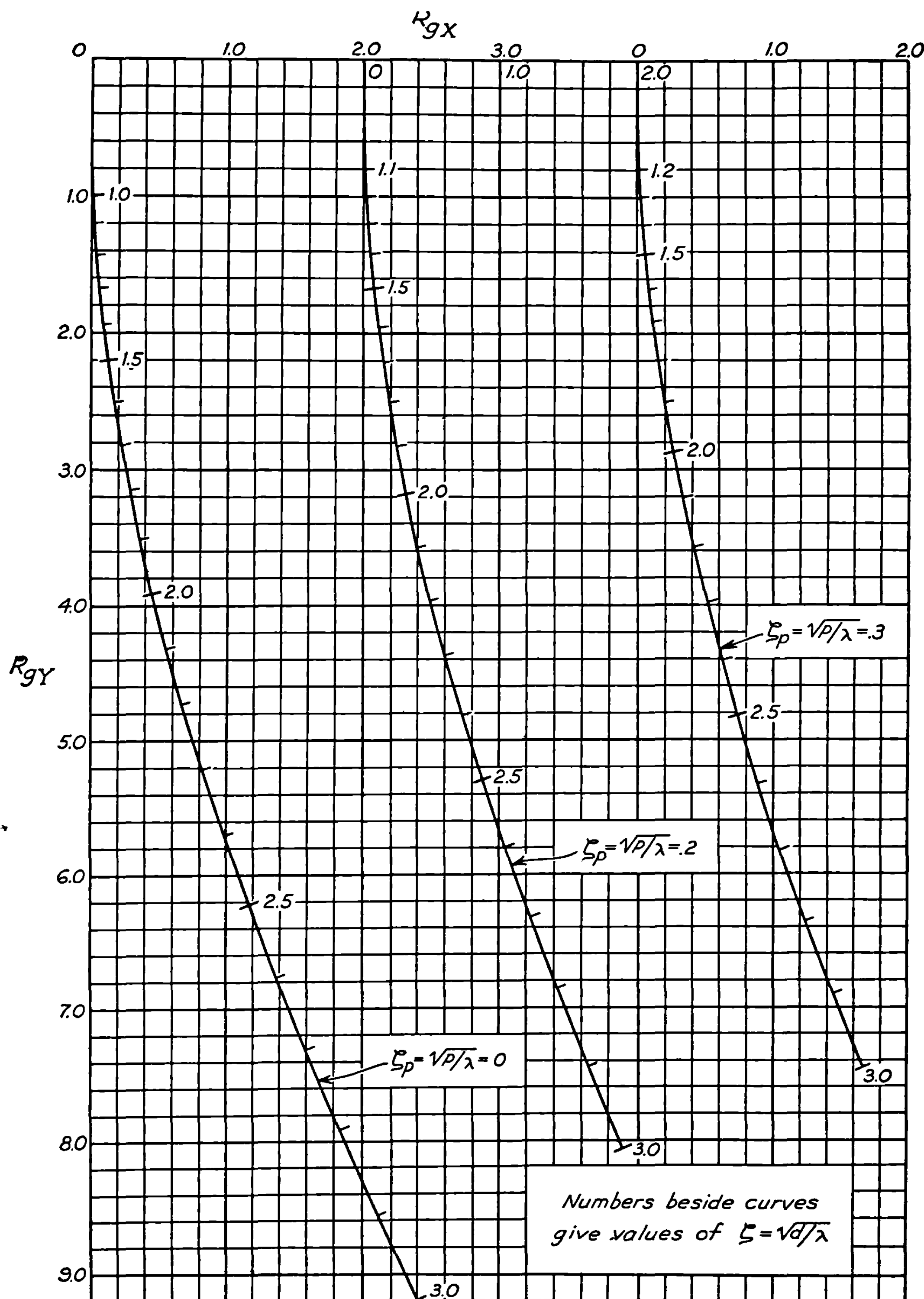


FIGURE 9.34 (g).—Characteristic function $R_g(S, \xi_p, \xi)$ for $S=8$.

9.35 Effect of a Cross Wind.—When there is a wind it is necessary to distinguish between the velocity relative to the air and the velocity relative to the ground. The former is needed to determine the aerodynamic effects and the latter is needed to determine the impact point. We use parallel coordinate systems, one fixed in the air and one fixed on the ground, and the convention that capital letters represent quantities defined relative to the air and small letters quantities defined relative to the ground. However, we use δ_a and ϑ_a for the yaw and directions of motion with respect to the air because the use of Δ and Θ would conflict with the characteristic function notation.

If the wind has a component along the trajectory, the wind deflection is a nonlinear function of the wind. This case is treated in 9.42; here we assume that the wind is purely transverse. Let

$$W = W_x + iW_y, \quad (1)$$

where W_x and W_y are the components of the wind velocity with respect to the ground along the X_0 and Y_0 axes respectively. We then have the relations, from 9.11 (43),

$$u = U + W, \quad (2)$$

and

$$v_z = V_z = \dot{\zeta} v_\lambda, \quad (3)$$

between the transverse and tangential velocity components of the rocket in the two systems. Since the effects during burning are being considered, u and U are small and we may write, from 9.11 (40),

$$\vartheta = u/\dot{\zeta} v_\lambda; \quad \vartheta_a = U/\dot{\zeta} v_\lambda \quad (4)$$

and hence

$$\vartheta_a = \vartheta - (W/\dot{\zeta} v_\lambda). \quad (5)$$

Now the orientation angle of the rocket is the same in the two systems; that is,

$$\varphi_a = \varphi, \quad (6)$$

and therefore

$$\delta_a = \delta + (W/\dot{\zeta} v_\lambda). \quad (7)$$

We are trying to find the effect of the wind on the motion of a rocket which, in the ground system, is launched with no cross-pointing, yaw, or mallaunching; i. e., $\varphi_p = \delta_p = q_p = 0$. From the point of view of the system moving with the air there is no wind and the effects are due to the fact that the rocket appears to be launched with a yaw, which is seen from (7) to be

$$\delta_{ap} = W/\dot{\zeta}_p v_\lambda. \quad (8)$$

The motion produced by initial yaw was considered in 9.33 and the appropriate solution is

$$\delta_a = (W/\dot{\zeta}_p v_\lambda) \Delta_\delta, \quad \varphi_a = (W/\dot{\zeta}_p v_\lambda) \Phi_\delta, \quad \vartheta_a = (W/\dot{\zeta}_p v_\lambda) \Theta_\delta. \quad (9)$$

From (5), (6), (7) and (9) we have

$$\delta_w = \frac{W}{v_\lambda} \left(\frac{\Delta_\delta}{\dot{\zeta}_p} - \frac{1}{\dot{\zeta}} \right), \quad \varphi_w = \frac{W}{v_\lambda} \frac{\Phi_\delta}{\dot{\zeta}_p}, \quad \vartheta_w = \frac{W}{v_\lambda} \left(\frac{\Theta_\delta}{\dot{\zeta}_p} + \frac{1}{\dot{\zeta}} \right). \quad (10)$$

where the subscript W denotes deflections, with respect to the ground system, caused by wind. We now define the characteristic functions for wind by the equations

$$\vartheta_W = \frac{W}{v_\lambda} \Theta_W, \quad \delta_W = \frac{W}{v_\lambda} \Delta_W, \quad \varphi_W = \frac{W}{v_\lambda} \Phi_W, \quad (11)$$

and therefore have from (10), (11) and 9.33 (1)–(3)

$$\Delta_W = \frac{\Delta_\delta}{\zeta_p} - \frac{1}{\zeta} = -\frac{4\pi i m_N^{\frac{1}{2}} m_P^{\frac{1}{2}}}{m_N - m_P} [m_P^{\frac{1}{2}} \Delta_q(\infty, \xi_p, \xi) - m_N^{\frac{1}{2}} \Delta_q(\infty, \chi_p, \chi)], \quad (12)$$

$$\Phi_W = \Phi_\delta / \zeta_p = -4\pi i m_N^{\frac{1}{2}} m_P^{\frac{1}{2}} (m_N - m_P)^{-1} [m_P^{\frac{1}{2}} \Phi_q(\infty, \xi_p, \xi) - m_N^{\frac{1}{2}} \Phi_q(\infty, \chi_p, \chi)], \quad (13)$$

$$\Theta_W = \Phi_W - \Delta_W = -4\pi i m_N^{\frac{1}{2}} m_P^{\frac{1}{2}} (m_N - m_P)^{-1} [m_P^{\frac{1}{2}} \Theta_q(\infty, \xi_p, \xi) - m_N^{\frac{1}{2}} \Theta_q(\infty, \chi_p, \chi)]. \quad (14)$$

These functions are slowly varying functions of ζ and ζ_p and hence quite suitable for tabulation. The character of the motion may be seen from figures 9.35a and b in which Φ_W and Δ_W are plotted for $\zeta_p = 0$ with $S = 2$ and 4. It may be seen that the nose of the rocket starts downwind to the right as the wind hits it and then precesses down and to the left. The nutation amplitude is much smaller than in the case of mallaunching, merely producing the original change in orientation and putting cusps in the curve, but is not as small as in the case of gravity.

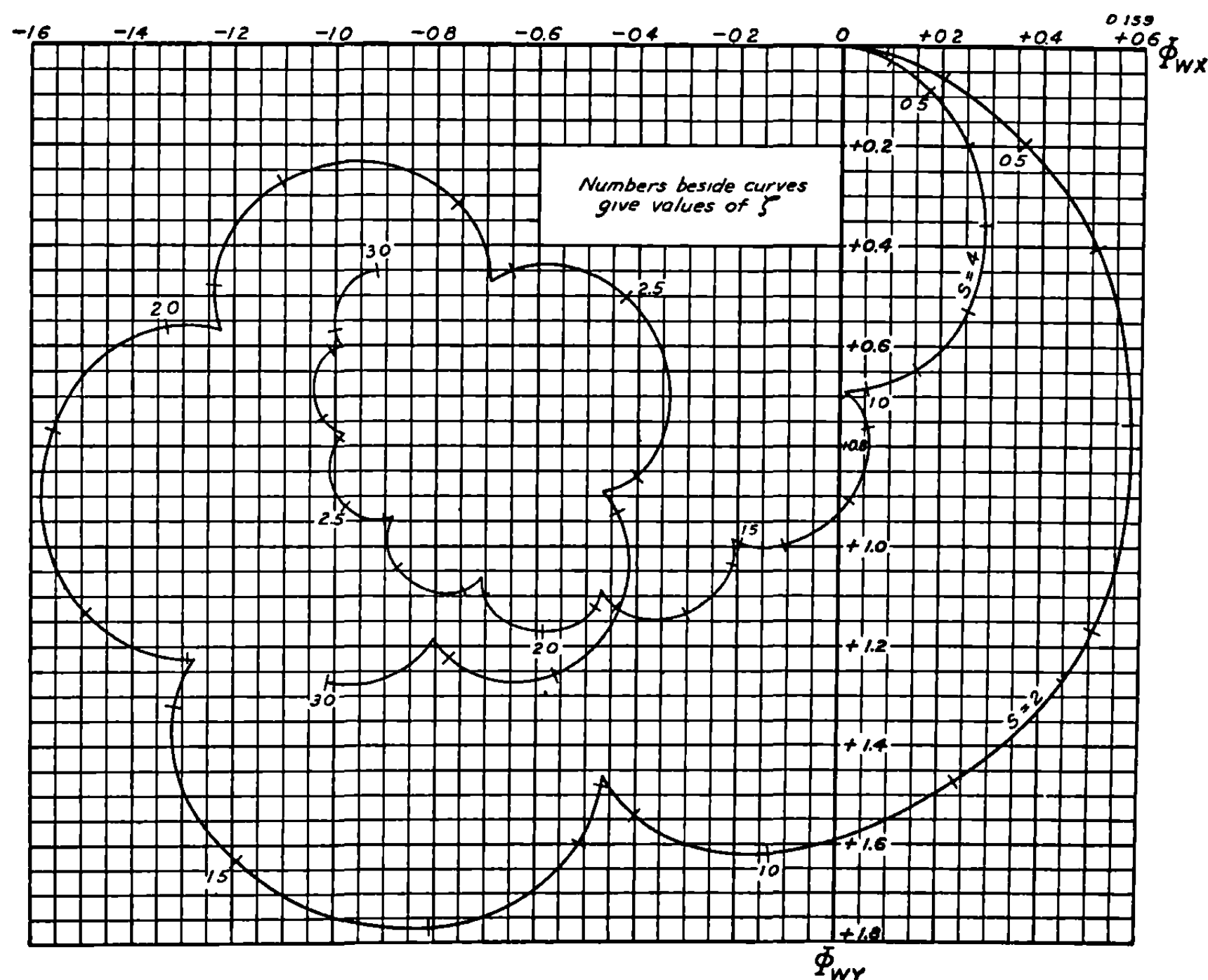


FIGURE 9.35 (a).—Characteristic function $\Phi_W(S, \zeta_p, \zeta)$ for $\zeta_p = 0$.

The function Θ_w is plotted in figures 9.35c-e for $S=2, 4$ and 8 with $\zeta_p=0$ and 0.3 . It may be noted from these figures that Θ_w varies slowly with S as well as with ζ_p and ζ . The deflection is spread out over the whole burning period rather than being nearly completed in the first nutation as in the case of mallaunching. It is for this reason that the deflection is so insensitive to launcher length. The characteristic functions R_w are plotted in figures 9.35f-h for the same cases as for Θ_w .

In order to show more clearly the variation with stability factor, plots of Θ_w for $\zeta_p=0$, with $S=2, 3$, and 4 are given in figure 9.35i and for $\zeta_p=0$ with $S=1$ in figure 9.35j. This latter motion is unstable, inasmuch as the yaw increases with time, but the Θ_w curve is convenient in showing the limiting form of the motion and in allowing more accurate interpolation in the range $1 < S < 2$.

A very convenient formula giving the variation of Θ_w with launcher length that may be used advantageously in conjunction with figure 9.35i may be obtained by expanding Θ_w in a Taylor series in ζ_p and an asymptotic series in ζ . This gives as a rough first approximation that can be used after a half precession

$$\Delta\Theta_w = \Theta_w(S, \zeta_p, \zeta) - \Theta_w(S, 0, \zeta) \doteq \frac{\zeta_p^2 \pi^2}{2S} \left\{ \frac{-1+i}{m_N^2 + m_P^2} + 2\zeta_P \right\}, \text{ for } \zeta > 1, \text{ and } \zeta_p \leq 0.3. \quad (15)$$

For ζ smaller than this, the value of $\Delta\Theta_w$ depends too strongly on ζ for use of this formula.

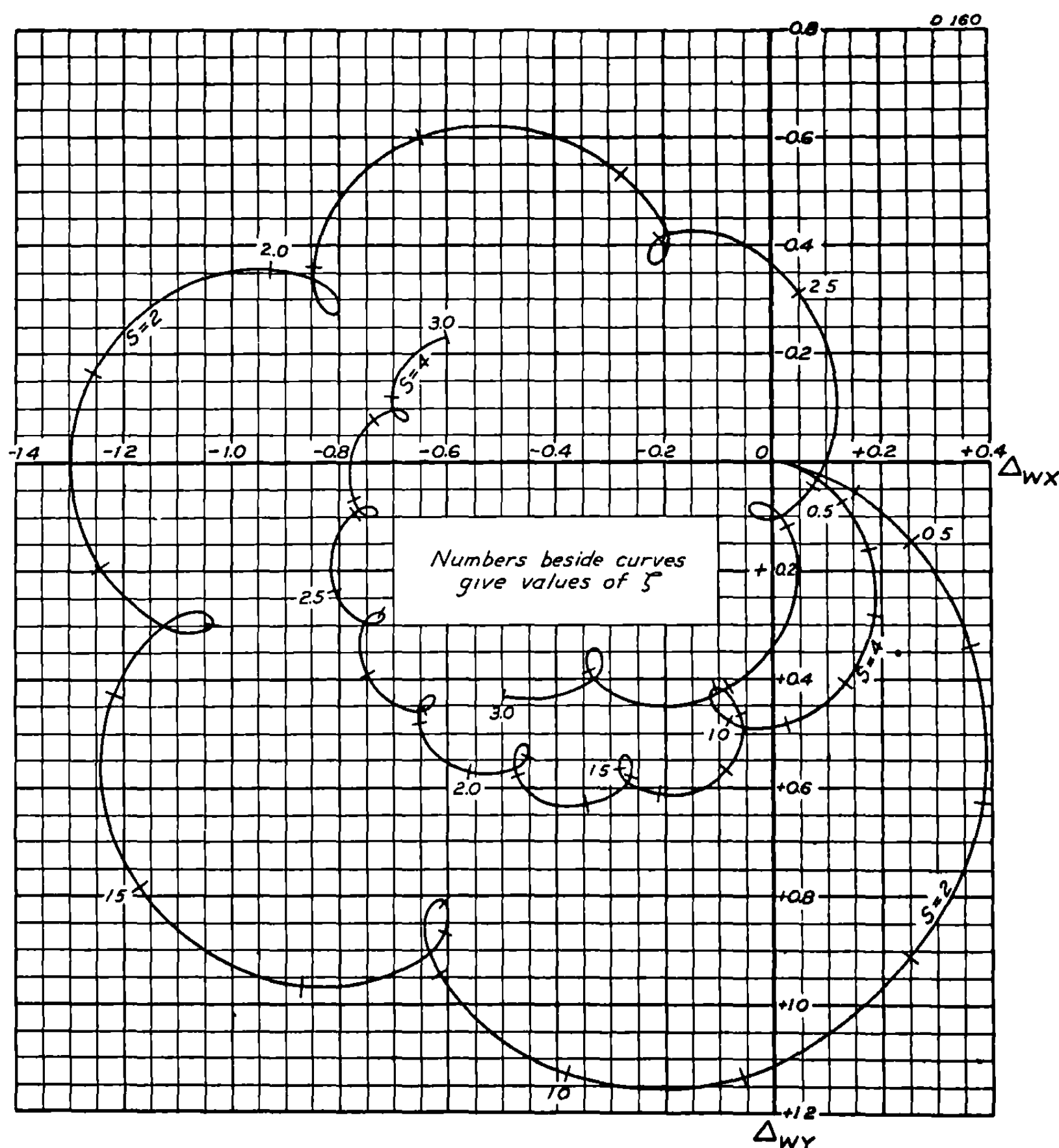


FIGURE 9.35 (b).—Characteristic function $\Delta_w(S, \zeta_p, \zeta)$ for $\zeta_p=0$.

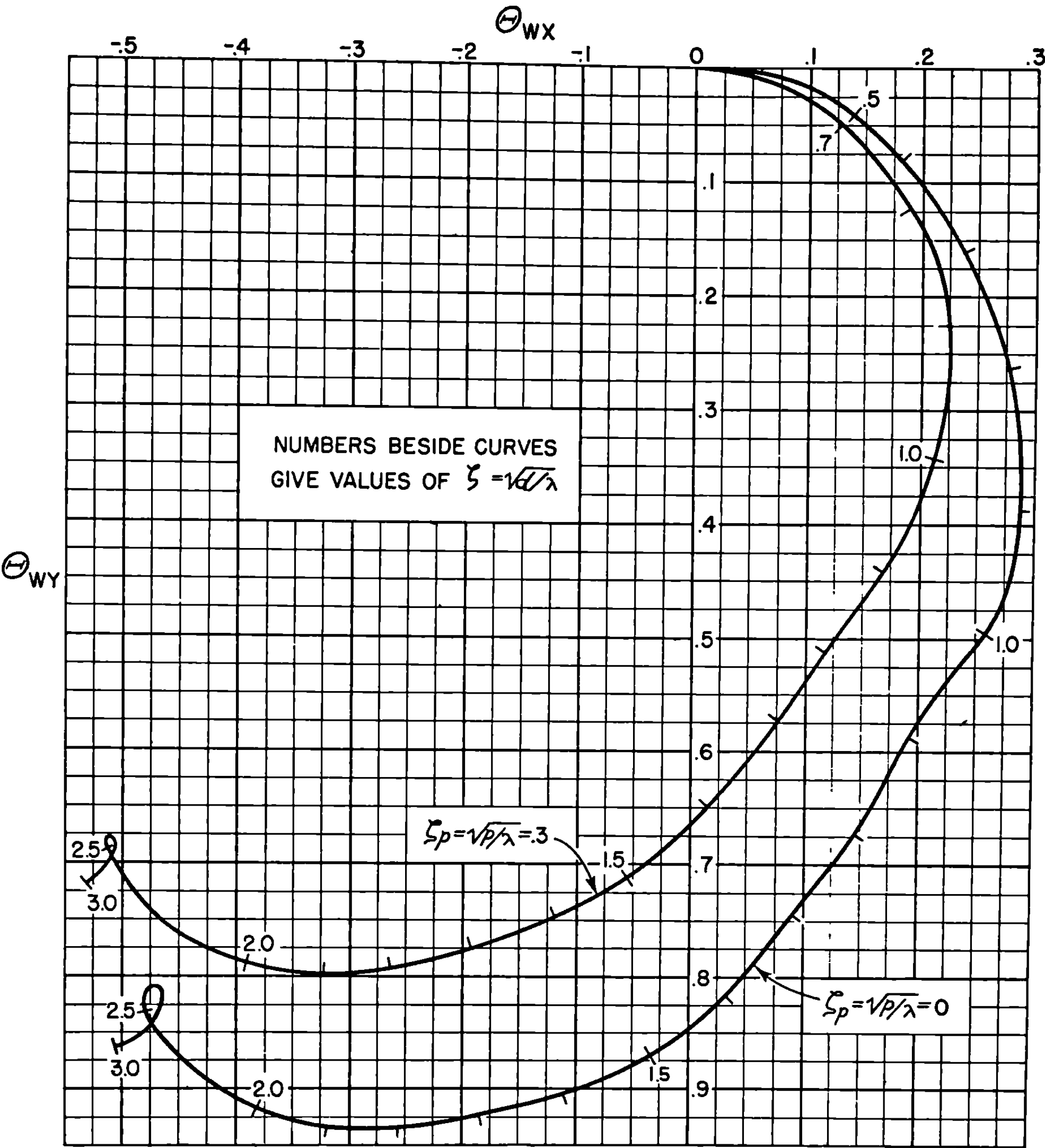


FIGURE 9.35 (c).—Characteristic function $\Theta_W(S, \zeta_p, \zeta)$ for $S=2$.

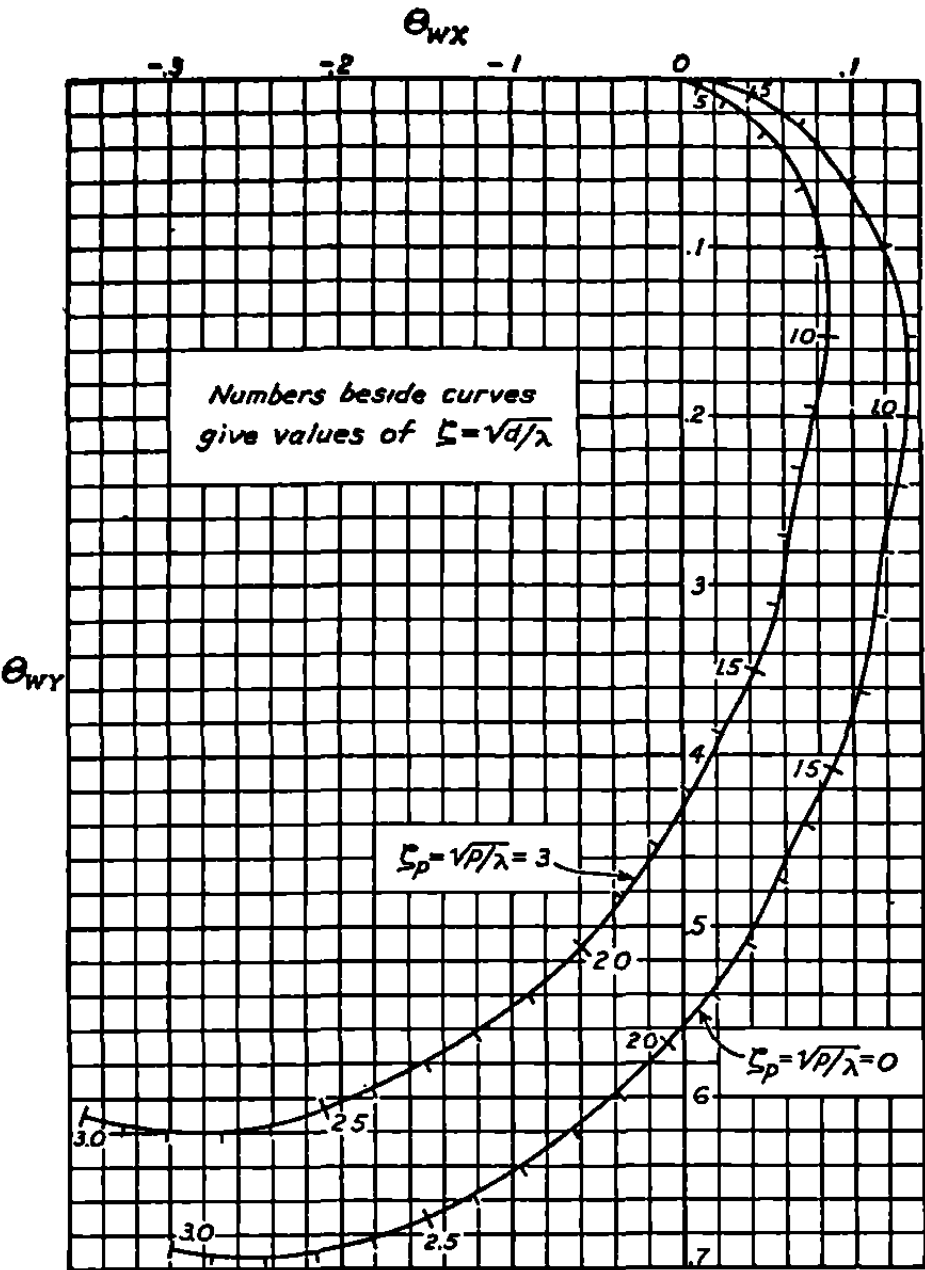


FIGURE 9.35 (d).—Characteristic function $\Theta_W(S, \zeta_p, \zeta)$ for $S=4$.

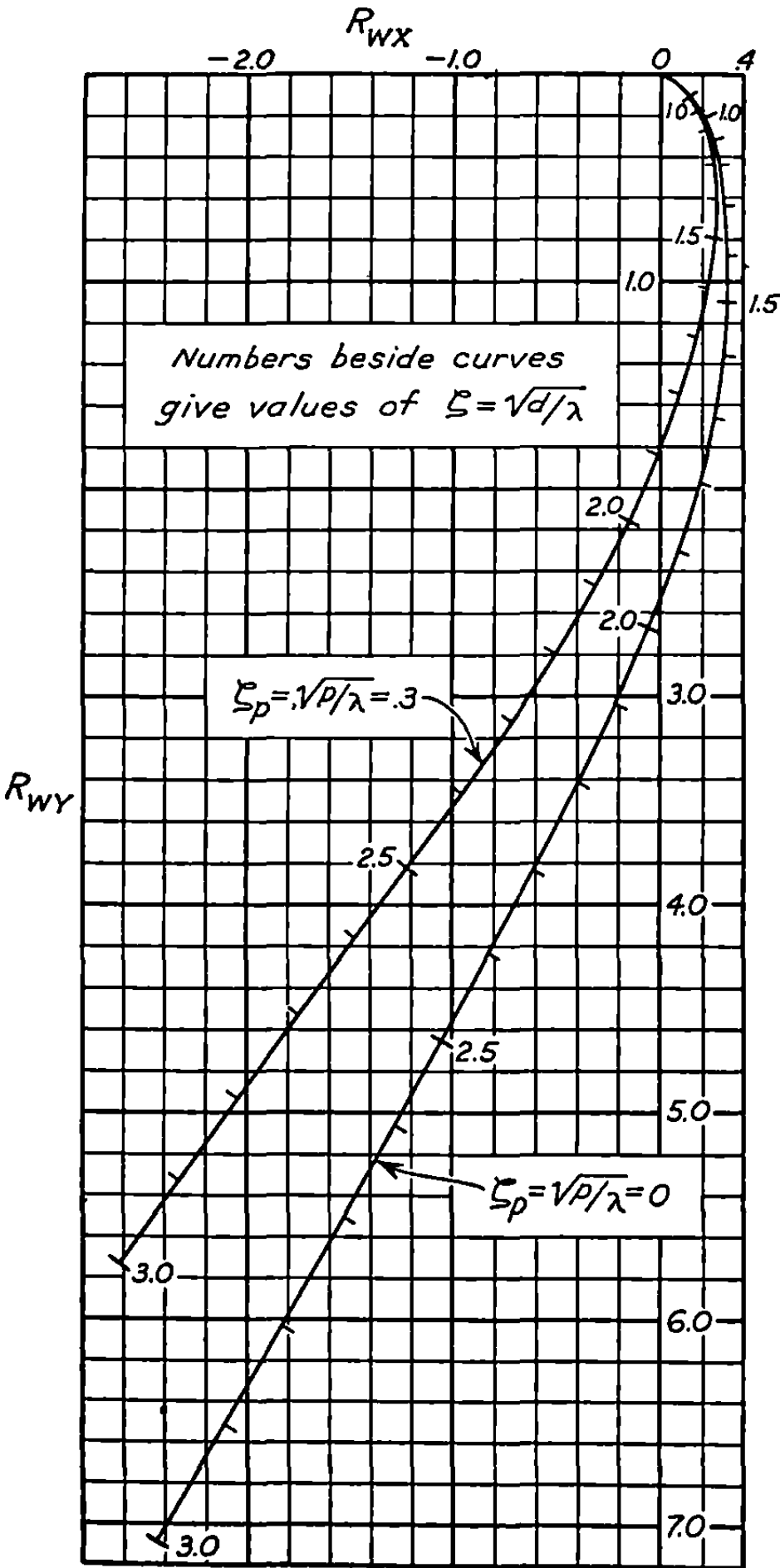


FIGURE 9.35 (f).—Characteristic function $R_W(S, \zeta_p, \zeta)$ for $S=2$.

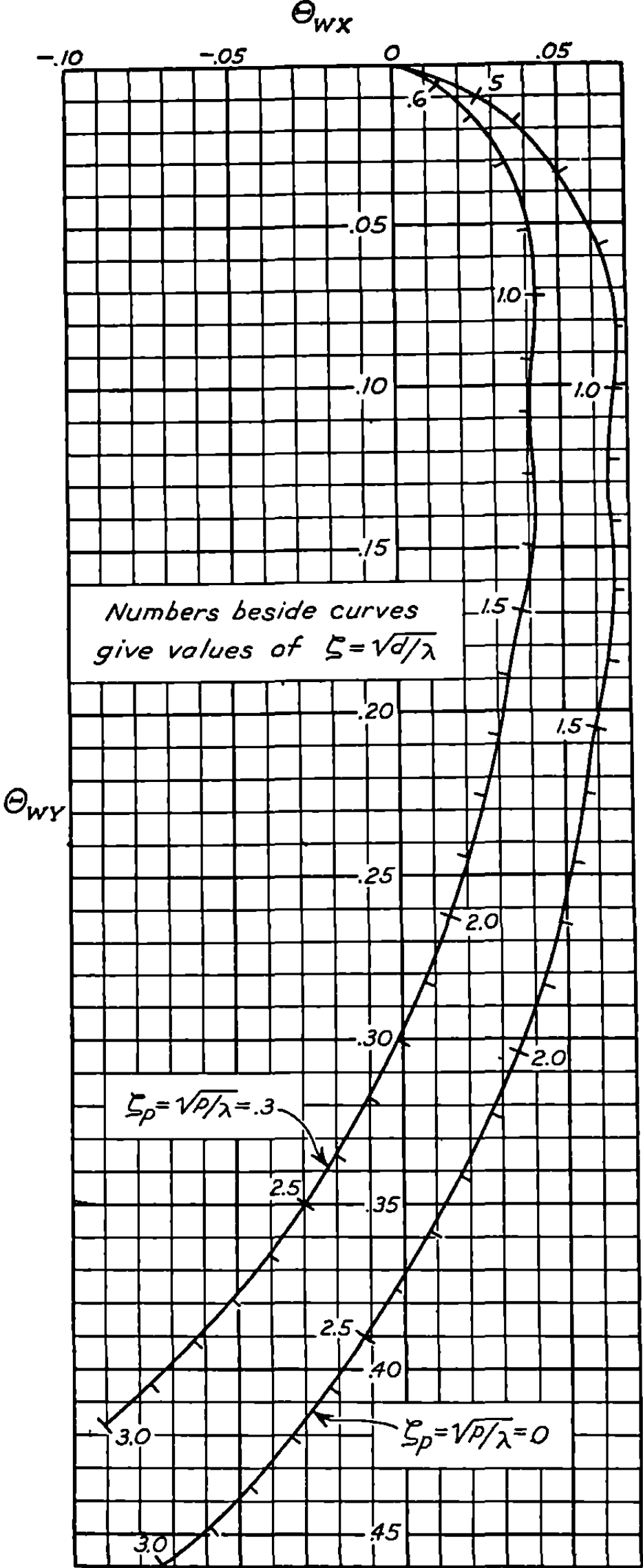


FIGURE 9.35 (e).—Characteristic function $\Theta_W(S, \zeta_p, \zeta)$ for $S=8$.

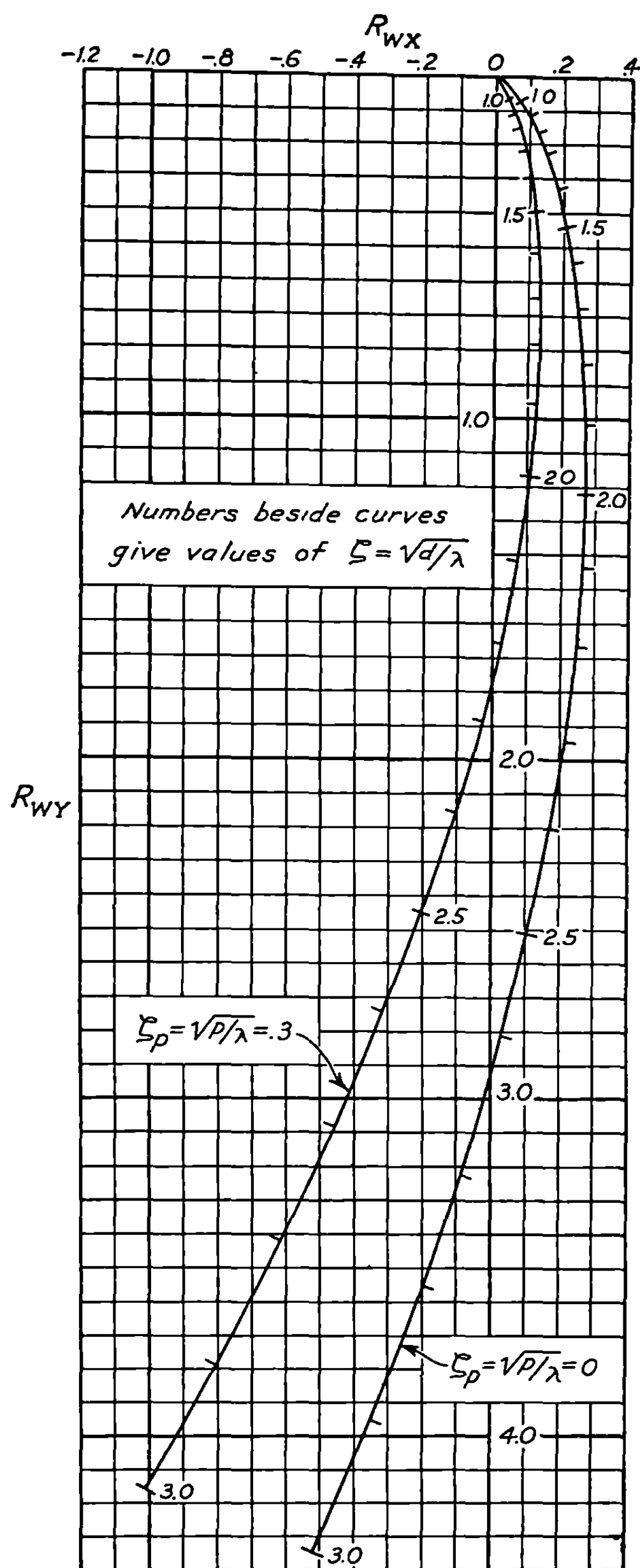
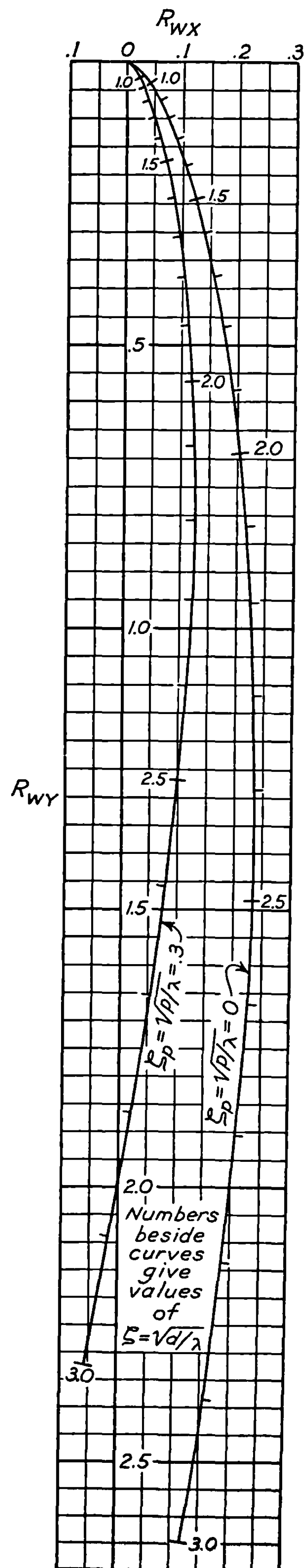


FIGURE 9.35 (g) and (h).—Characteristic function $R_W(S, \xi_p, \xi)$; $S=4$ in (g) and $S=8$ in (h).



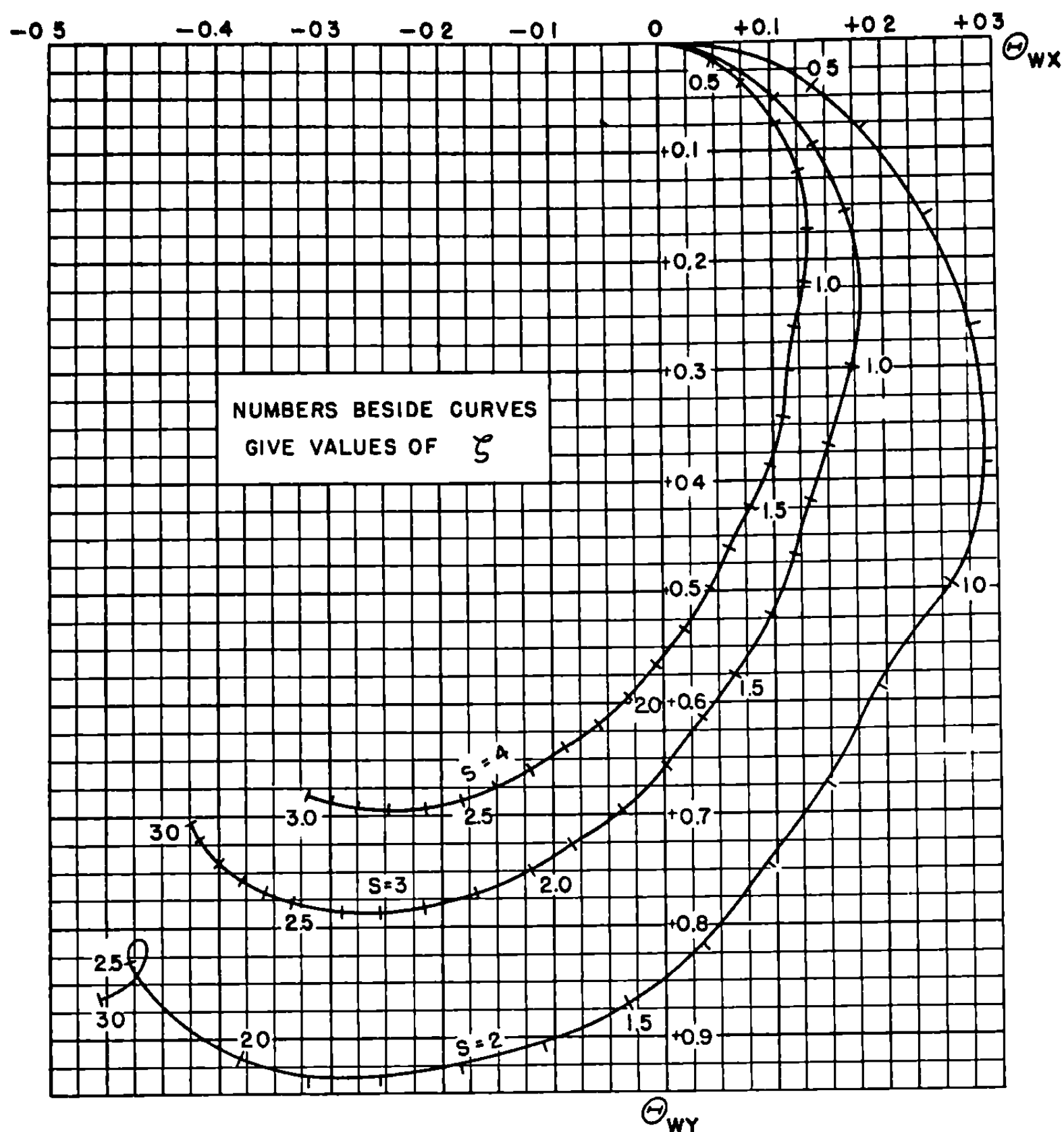


FIGURE 9.35⁵(i).—Characteristic function $\Theta_W(S, \zeta_p, \xi)$ for $\zeta_p=0$.

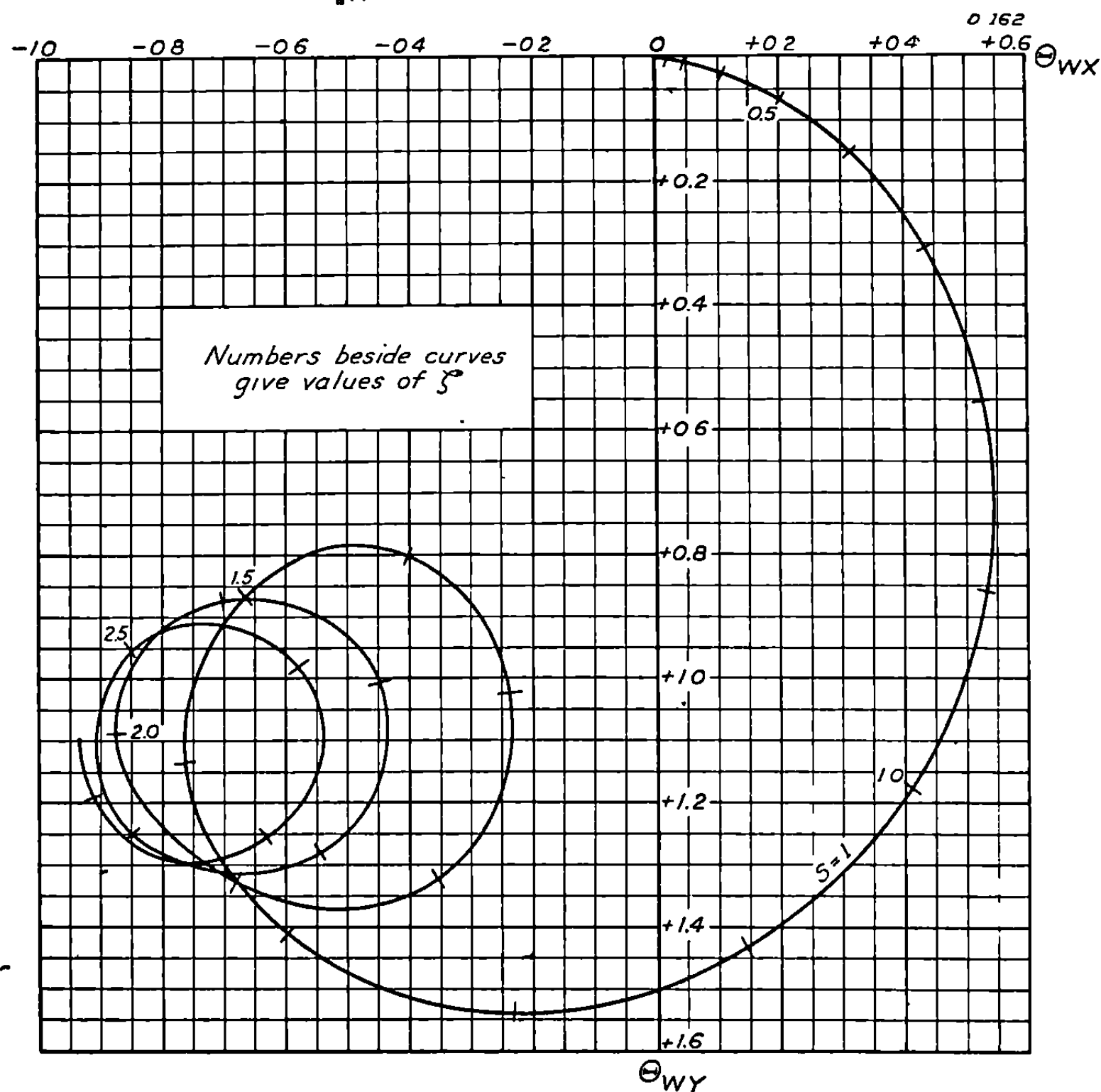


FIGURE 9.35 (j).—Characteristic function $\Theta_W(S, \zeta_p, \zeta)$ for $S=1$ and $\zeta_p=0$.

9.36 Malalignment.—The effect of malalignment was shown in 9.25 to be nearly equivalent to a mallaunching and an initial yaw. This approximation is still valid in the presence of aerodynamic forces because the equivalent mallaunching is generated in the first one or two turns and at that time the yaw is still very small. Hence the aerodynamic forces, which are proportional to the yaw, are negligible and the approximations in 9.25 may be used. The aerodynamic forces are taken into account by the use of the formulas and curves of 9.32 and 9.33, instead of those of 9.22 and 9.23, for the effects produced by the equivalent mallaunching and initial yaw.

The effect of malalignment may be taken into account rigorously by the use of the Green's function technique exactly as in the vacuum case 9.24. The expression for the deflection involves the same functions as in the vacuum case but is more complicated and contains the stability factor as an additional parameter. It may be obtained in a straightforward manner following the method of 9.24, but the expression is not reproduced here because of its length and the fact that the approximate method described above is so accurate and simple that there is no reason to use the exact formula. If the justification of the approximate method is carried out as in 9.26, an expression for the equivalent mallaunching is obtained which is more complicated than 9.25 (4) but which has nearly the same numerical value.

9.4 General Aerodynamic Effects During Burning

In the preceding two sections the general character of the motion during burning has been shown by the solutions of simplified forms of the equations of motion, unimportant forces and torques having been omitted. The introduction of the full set of aerodynamic forces leads to solvable equations, but the solution is dependent upon too many parameters to allow tabulation of the solutions. Fortunately, however, the effects of these additional forces upon the motion are small, and the general motion is represented sufficiently closely for most purposes by the curves of 9.3. In cases where the effects of the additional forces and torques are of interest, it is usually adequate to obtain approximate expressions for the modification they produce in the motion.

9.41 The Equations of Motion.—We assume here that the aerodynamic forces are linear and that the motion takes place with constant acceleration so we may obtain the equations of motion from those in 9.31 or 9.11. If we neglect malalignment, we have the following forces and moments to put into 9.11 (33) and (34).

$$f_I = -mK^2l(ik_{vs\delta}Vs\delta + k_{vq}Vq - ilk_{sq}sq), \quad (1)$$

and

$$F_I = img \cos \theta_0 + m(K_{v^2\delta}V^2\delta - ilK_{vs\delta}Vs\delta), \quad (2)$$

where we have omitted F_{vq} and F_{sq} because they are small. The resulting equations are:

$$\varphi'' - A\zeta\varphi' - B\zeta^2\delta = 0, \quad (3)$$

$$\vartheta' - (\zeta^{-1} + C\zeta)\delta = D\zeta^{-1}, \quad (4)$$

$$\varphi - \vartheta - \delta = 0, \quad (5)$$

where we have introduced as abbreviations the constants,

$$A = 4\pi i - 2l\lambda \left(k_{vq} - \frac{2\pi il}{v} k_{sq} \right),$$

$$\begin{aligned}
B &= \frac{4\pi^2}{S} (1 - i\tau), \\
C &= 2\lambda \left(K_{v^2\delta} - \frac{2\pi i l}{\nu} K_{v\delta} \right), \\
D &= \frac{ig \cos \theta_0}{G} \\
\tau &= \frac{2\pi l k_{v\delta}}{\nu k_{v^2\delta}} = \frac{f_{v\delta}}{f_{v^2}}.
\end{aligned} \tag{6}$$

The three equations of motion can be reduced to a single equation in δ by the usual procedure of eliminating φ from (3) by (5) and then eliminating ϑ' and ϑ'' by (4). This gives

$$\delta'' - (A - C - \zeta^2)\zeta \delta' - (B\zeta^2 + \zeta^{-2} + A - C + AC\zeta^{-2})\delta = D\zeta^{-2} + AD. \tag{7}$$

Treat first the homogeneous equation obtained by setting the gravity terms containing D equal to zero. If we let $\delta = y/\zeta$ and $Z = \zeta^2$, we obtain the equation

$$\frac{d^2 y}{dZ^2} - \frac{1}{2}(A - C) \frac{dy}{dZ} - \frac{1}{4}(B + 4AC)y = 0 \tag{8}$$

This is a linear equation with constant coefficients of the form

$$\frac{d^2 y}{dZ^2} - 2\pi i a \frac{dy}{dZ} + 4\pi^2 b y = 0. \tag{9}$$

It has the general solution,

$$y = C_N \exp(2\pi i m_N Z) + C_P \exp(2\pi i m_P Z), \tag{10}$$

where

$$m_N = \frac{1}{2}(a + \sqrt{a^2 - 4b}), \tag{11}$$

and

$$m_P = \frac{1}{2}(a - \sqrt{a^2 - 4b}).$$

These quantities are, in general, complex and reduce to those defined in 9.31 (8) when all the aerodynamic forces other than the overturning moment are set equal to zero. Hence the general solution of (7) is

$$\delta = C_N \zeta^{-1} \exp(2\pi i m_N \zeta^2) + C_P \zeta^{-1} \exp(2\pi i m_P \zeta^2). \tag{12}$$

By putting this in (4) and (5) it is possible to obtain the corresponding solutions for φ and ϑ . These solutions are similar to those derived in 9.3; but they are of no use for computation because the Fresnel integrals involved have complex arguments and are not tabulated.

We can see from (12) that if the imaginary parts of m_N and m_P are positive the yaw damps out exponentially, while if either imaginary part is negative the corresponding oscillation will build up exponentially. This latter behavior is not serious during burning because the short duration of the burning means that large amplitudes will not be built up. However considera-

tion of the stability conditions after burning, when stability is essential, shows that it is necessary to have the imaginary parts of both m_N and m_P positive. These criteria will be discussed more thoroughly in chapter 10 where the motion after burning is treated. The solutions for φ and ϑ have essentially the same behavior as δ so that no more need be said about them.

The solutions of (3) to (5) depend on the seven parameters ζ_p , $k_{v^2\delta}$, k_{v^2q} , k_{sq} , $K_{v^2\delta}$, and $K_{vs\delta}$. The aerodynamic coefficients enter in the complex numbers m_N and m_P and through the term involving $\left(K_{v^2\delta} - \frac{2\pi i l}{\nu} K_{vs\delta}\right)$ when φ and ϑ are determined. Hence, while (12) and the related functions are solutions of (3)–(5), they are expressed in terms of untabulated functions with an unmanageable number of parameters and therefore are of little use. We shall derive more manageable expressions in the next section.

9.42 Approximate Solutions of the Equations of Motion.—The basis of our treatment of the aerodynamic forces, other than the overturning moment, is that their effects are small and hence they may be treated as perturbations. We transfer these small terms to the right-hand side of the equation and express them as functions of ζ by using the approximate values of δ and q given in 9.3 for the case in which these small forces are zero. The resulting inhomogeneous equation is treated by means of the usual Green's function technique. If more accuracy is required, these new solutions may be used to compute the aerodynamic forces and the process repeated, but this leads to a great amount of work, and generally the first approximation is sufficient. Such a process converges if the effect of these additional terms is small, as it is in this case.

The effect of these additional terms may be looked upon as a modification of the effect of the overturning moment. It was pointed out in 9.32 that the overturning moment changed the mallaunching solution but little; hence we may expect that these additional aerodynamic forces will have little effect upon the motion of a mallaunched rocket and will not consider this case. However, in the cases of gravity and wind, the effects of the overturning moment are large, so that in these cases the additional aerodynamic terms may be expected to have an appreciable effect. We treat here the effect on the gravity solution and reserve to the next section the effect on the wind solution including the effects of the nonlinearity due to the large yaws encountered. In order to determine the modification of the gravity solution due to the additional forces, we substitute the gravity solutions 9.34 (2)–(4) in 9.41 (1)–(2) and use these forces in 9.31 (1)–(2). This gives, in terms of the abbreviations of 9.41 (6), the equations

$$\phi'' - 4\pi i \zeta \phi' - \frac{4\pi^2 \zeta^2}{S} \delta = -\frac{4\pi^2 i \Upsilon}{S} \zeta^2 \frac{g \cos \theta_0}{G} \Delta_\epsilon + (A - 4\pi i) \zeta \frac{g \cos \theta_0}{G} \Phi'_\epsilon, \quad (1)$$

$$\vartheta' - \frac{1}{\zeta} \delta = C \zeta \frac{g \cos \theta_0}{G} \Delta_\epsilon, \quad (2)$$

and

$$\varphi - \vartheta - \delta = 0, \quad (3)$$

Hence, using the Green's function technique of 9.13, we have as the increment to the characteristic function:

$$\begin{aligned} \Delta \Theta_\epsilon = & -i \Upsilon \int_{\zeta_p}^{\zeta} \frac{4\pi^2}{S} \Delta_\epsilon(S, \zeta_p, u) \Theta_\epsilon(S, u, \zeta) u^2 du + (A - 4\pi i) \int_{\zeta_p}^{\zeta} \Phi'_\epsilon(S, \zeta_p, u) \Theta_\epsilon(S, u, \zeta) u du \\ & - C \int_{\zeta_p}^{\zeta} \Delta_\epsilon(S, \zeta_p, u) \Theta_\epsilon(S, u, \zeta) u du. \end{aligned} \quad (4)$$

The values of these integrals must be obtained by numerical integration; the results are tabulated in table 9.42 for $S=2$ and certain values of ζ_p and ζ .

TABLE 9.42
INTEGRALS FROM EQUATION (4) FOR $S=2$

ζ	ζ_p	$\frac{4\pi^2}{S} \int_{\zeta_p}^{\zeta} \Delta_z(S, \zeta_p, u) \Theta_z(S, u, \zeta) u^2 du$	$\int_{\zeta_p}^{\zeta} \Phi'_z(S, \zeta_p, u) \Theta_z(S, u, \zeta) u du$	$\int_{\zeta_p}^{\zeta} \Delta_z(S, \zeta_p, u) \Theta_z(S, u, \zeta) u du$
$\sqrt{2}$	0	$0.609+0.197i$	$-0.01+0.10i$	$-0.327+0.566i$
$\sqrt{2}$	0.3	$0.356+0.094i$	$-0.003-0.06i$	$-0.219-0.342i$
2	0	$0.180+0.766i$	$-0.13+0.030i$	$-0.778+0.548i$
2	0.3	$0.123+0.559i$	$-0.088+0.029i$	$-0.635+0.463i$

Now let us obtain numerical values for the effects of these additional forces. From Chapter 8 we have

$$\tau \approx 0.2,$$

$$l\lambda k_{vq} \approx 0.001,$$

$$\lambda K_{v^2\delta} \approx 0.02.$$

For the case, $S=2$, $\zeta_p=0$, $\zeta=2$ we have as the values of the three correction terms

$$0.153-0.036i; 0.00026-0.00006i; 0.031-0.022i. \quad (6)$$

These are to be compared with $\Theta_z(2, 0, 2)=0.765+1.423i$ as obtained from figure 9.34b and $\Theta_z(\infty, 0, 2)=i$ for the case where there is no overturning moment. It is apparent that the only correction term of importance comes from the Magnus moment. Here the correction is ten percent of Θ_z and over twenty percent of the contribution of the overturning moment. The effects due to the terms containing k_{sq} and $K_{v^2\delta}$ are at least as small as the last two sets of terms in (6) and hence can be neglected.

From this result we may conclude that during burning the only aerodynamic moments that need be considered are the overturning moment and the Magnus moment and we may further conclude that a more accurate solution than that given in 9.3, one including the effects of Magnus force, is needed. Actually, the situation is not as bad in practice as appears here, because the Magnus moment is decidedly nonlinear; and if the yaw is not small, which it will not be if there is any wind blowing or any mallaunching, the nonlinearity reduces the contributions of the Magnus moment considerably. This may be the reason that good agreement has been obtained in all the experimental checks of the theory.

9.43 Effects of Wind During Burning.—In addition to the wind effect treated in 9.35 there are three other effects due to wind. These are the effects of the remaining aerodynamic moments, the effect of the nonlinearity of the overturning moment, and the effect of a tail wind in changing the air speed and hence, indirectly, the moments. The last two effects are nonlinear in the wind strength so that it is necessary to treat them together in order to obtain the total effect. A wind may be specified by giving the components W_{\parallel} , along the range line, and W_{\perp} from the left perpendicular to the range line. Using these components we have the complex vector

$$W = W_{\perp} + iW_{\parallel} \sin \theta_0, \quad (1)$$

as in 3.43 (2), and the component along the launcher

$$W_z = W_{\parallel} \cos \theta_0. \quad (2)$$

The cross-velocity relative to the air is therefore

$$U = u - W, \quad (3)$$

where u is the cross-velocity relative to the ground, and the velocity relative to the air is

$$V_z = v_z - W_z = \zeta v_{\lambda} - W_z, \quad (4)$$

where v_z is the velocity relative to the ground. Now, since

$$\vartheta_a \doteq U/V_z = (u - W)/(\zeta v_{\lambda} - W_z), \quad \vartheta \doteq u/v_z = u/\zeta v_{\lambda}, \quad (5)$$

and since

$$\varphi_a = \varphi, \quad (6)$$

it follows that

$$\begin{aligned} \delta_a &= \varphi_a - \vartheta_a \doteq \delta + (u/\zeta v_{\lambda}) - (u - W)/(\zeta v_{\lambda} - W_z) \\ &= \delta + (W/\zeta v_{\lambda}) + \dots \end{aligned} \quad (7)$$

The aerodynamic forces depend on $V_z^2 \delta_a$ and $V_z \delta_a$. If these are expressed in terms of δ , ϑ , W , and W_z by means of (4) and (7) and if no terms that are higher than the second order in these quantities are retained we get

$$V_z \delta_a \doteq \zeta v_{\lambda} \delta + W - W_z \delta - W_z \vartheta \quad (8)$$

$$V_z^2 \delta_a \doteq \zeta^2 v_{\lambda}^2 \delta + \zeta v_{\lambda} W - 2 \zeta v_{\lambda} W_z \delta - W_z W - \zeta v_{\lambda} W_z \vartheta. \quad (9)$$

The effects of the terms involving ϑ are small and they may be neglected in most cases.

Here we shall represent the nonlinearity of the overturning and Magnus moments by quadratic expressions in δ based on the first two terms of 8.22 (7) and (8). If a cubic, based on the first two terms of 10.22 (1), were used, there would be a singularity for zero length launchers. The results of 9.42 indicate that of the aerodynamic moments, the overturning and the Magnus moments are the only ones that are likely to effect the motion in a wind. Hence we omit the other aerodynamic moments and write for the angular acceleration about a transverse axis due to aerodynamic moments

$$\begin{aligned} f_A/mK^2 &= (k_{v^2\delta,0} + k_{v^2\delta,1}\delta_a) V_z^2 \delta_a - il(k_{vs\delta,0} + k_{vs\delta,1}\delta_a) V_z s \delta_a \\ &= [k_{v^2\delta,0} - (2\pi il/\nu) k_{vs\delta,0}] (\zeta^2 v_{\lambda}^2 \delta + \zeta v_{\lambda} W) \\ &\quad - W_z k_{v^2\delta,0} (2 \zeta v_{\lambda} \delta + W) - \frac{2\pi il}{\nu} W_z k_{vs\delta,0} \zeta v_{\lambda} \delta \\ &\quad + (k_{v^2\delta,1} - \frac{2\pi il}{\nu} k_{vs\delta,1}) \zeta^2 v_{\lambda}^2 \left(\delta + \frac{W}{\zeta v_{\lambda}} \right) \left| \delta + \frac{W}{\zeta v_{\lambda}} \right|. \end{aligned} \quad (10)$$

We have retained only the leading terms in each of the corrections because if higher order terms become important the whole method, which is based on small corrections, breaks down. The

form of (10) can be simplified by using $4\lambda^2 k_{v^2\delta,0} = 4\pi^2/S$ and 9.41 (6). If the resulting expression for the moment is substituted into the equations of motion and the leading term transferred to the left, we have

$$\begin{aligned} \varphi'' - 4\pi i \zeta \varphi' - \frac{4\pi^2 \zeta^2}{S} \delta = \frac{4\pi^2}{S} \left\{ \frac{W}{v_\lambda} \zeta - i\Upsilon \frac{W}{v_\lambda} \zeta - i\Upsilon \zeta^2 \delta - \frac{W_z}{v_\lambda} \left[\left(2\zeta \delta + \frac{W}{v_\lambda} \right) - i\Upsilon \zeta \delta \right] \right. \\ \left. + \left(\frac{k_{v^2\delta,1}}{k_{v^2\delta,0}} - i\Upsilon \frac{k_{v^2\delta,1}}{k_{v^2\delta,0}} \right) \left(\zeta \delta + \frac{W}{v_\lambda} \right) \left| \zeta \delta + \frac{W}{v_\lambda} \right| \right\}, \end{aligned} \quad (11)$$

$$\vartheta' - \frac{\delta}{\zeta} = 0, \quad (12)$$

$$\varphi - \delta - \vartheta = 0. \quad (13)$$

The first term on the right of (11) is the largest; and, if the others are neglected, we can obtain as a solution, the first approximation

$$\delta = (W/v_\lambda) \Delta_W,$$

$$\varphi = (W/v_\lambda) \Phi_W,$$

and

$$\vartheta = (W/v_\lambda) \Theta_W. \quad (14)$$

This is just the linearized wind solution given in 9.35 and is obtained because we have neglected all the terms but one. If this result is sought by the Green's function method, we obtain the identity

$$\Theta_W(S, \zeta_p, \zeta) \equiv (4\pi^2/S) \int_{\zeta_p}^{\zeta} u \Theta_q(S, u, \zeta) du. \quad (15)$$

Now we can put the approximate value of δ from (14) in the terms on the right of (11) since they are relatively small. Solving the resulting inhomogeneous equations by the Green's function technique gives

$$\vartheta = \frac{W}{v_\lambda} \left\{ (1 - i\Upsilon) \Theta_W(S, \zeta_p, \zeta) - i\Upsilon a_1 - \frac{W_z}{v_\lambda} (a_2 - i\Upsilon a_3) + \frac{W}{\lambda} \left(\frac{k_{v^2\delta,1}}{k_{v^2\delta,0}} - i\Upsilon \frac{k_{v^2\delta,1}}{k_{v^2\delta,0}} \right) a_4 \right\}, \quad (16)$$

where W is the magnitude of \mathbf{W} and the \mathbf{a} 's are abbreviations, defined below, for the integrals that result.

$$a_1 = (4\pi^2/S) \int_{\zeta_p}^{\zeta} u^2 \Delta_W(S, \zeta_p, u) \Theta_q(S, u, \zeta) du, \quad (17)$$

$$a_2 = (4\pi^2/S) \int_{\zeta_p}^{\zeta} [2u \Delta_W(S, \zeta_p, u) + 1] \Theta_q(S, u, \zeta) du \quad (18)$$

$$a_3 = (4\pi^2/S) \int_{\zeta_p}^{\zeta} u \Delta_W(S, \zeta_p, u) \Theta_q(S, u, \zeta) du, \quad (19)$$

and

$$a_4 = (4\pi^2/S) \int_{\zeta_p}^{\zeta} [u \Delta_W(S, \zeta_p, u) + 1] |u \Delta_W(S, \zeta_p, u) + 1| \Theta_q(S, u, \zeta) du. \quad (20)$$

Values of these integrals as obtained by numerical integration are given in table 9.43 for several cases. For purposes of comparison we also give the values of Θ_W as obtained from the

curves of 9.35. It should be noted that interpolation in table 9.43 is satisfactory for the a 's but not for Θ_w , which must be obtained from curves to give sufficient accuracy.

TABLE 9.43
COEFFICIENTS FOR NONLINEAR WIND CONVECTIONS

S	ζ	ζ_p	Θ_w	a_1	a_2	a_3	a_4
2	$\sqrt{2}$	0.0	0.025+0.825i	-0.453+0.043i	-0.37+2.39i	-0.417+0.009i	-0.040+2.552i
		.1	.020+.800i	-.453+.043i	-.69+1.94i	-.417+.009i	-.357+2.102i
		.2	.005+.735i	-.453+.043i	-.85+1.54i	-.417+.009i	-.552+1.697i
		.3	.005+.660i	-.453+.043i	-.92+1.19i	-.417+.007i	-.594+1.353i
	2	.0	-.380+.915i	-.328-.521i	-.67+1.00i	-.293-.703i	-.538+1.597i
		.1	-.390+.900i	-.328-.521i	-.96+.60i	-.293-.703i	-.834+1.203i
		.2	-.395+.850i	-.328-.522i	-1.00+.26i	-.293-.703i	-.973+.853i
		.3	-.390+.790i	-.328-.525i	-1.15-.03i	-.293-.704i	-1.016+.558i
4	$\sqrt{2}$.0	.100+.368i	-.075+.034i	.30+1.14i	.068+.021i	.370+1.143i
		.1	.090+.365i	-.075+.034i	.11+.93i	.068+.021i	.189+.935i
		.2	.075+.350i	-.075+.034i	.00+.74i	.068+.021i	.079+.749i
		.3	.055+.320i	-.075+.034i	-.06+.58i	.068+.021i	.016+.590i
	2	.0	-.010+.568i	-.178-.039i	-.11+1.19i	-.200-.070i	.043+1.276i
		.1	-.020+.560i	-.178-.039i	-.28+.97i	-.200-.070i	-.122+1.160i
		.2	-.040+.545i	-.178-.039i	-.37+.78i	-.200-.070i	-.216+.867i
		.3	-.060+.512i	-.178-.040i	-.42+.62i	-.200-.070i	-.262+.803i

From the table it is apparent that the nonlinear terms in the wind deflection; i. e., those involving a_2 , a_3 , and a_4 , are quite sensitive to the launcher length. This is in sharp contrast to the linear terms, which are only slightly affected by launcher length. The quadratic terms are also more sensitive to the stability factor than is the linear term, but this variation is masked in the table by the sensitivity to ζ . The marked variation with ζ is due to the fact, which may be seen from figure 9.35b, that the phase of the precession is critically dependent on both ζ and S .

In addition to the above effects, any wind changes somewhat the mallaunching, initial yaw, and gravity solutions, because of the change in the aerodynamic forces. A treatment similar to the above can be used for rockets fired from the ground; in 9.53 and 9.54 we treat the case of rockets fired forward from aircraft, where the effect is more important.

9.5 Aircraft Firing of Spin-Stabilized Rockets

The firing of spin-stabilized rockets from aircraft is exceedingly difficult to carry out successfully in practice and is correspondingly difficult to treat theoretically. The experimental difficulties arise mainly from the fact that, due to the airplane's velocity, aerodynamic forces are much larger than in the case of ground firing and that the difference is particularly great during the early part of burning when the spin and hence the gyroscopic stability are small. An important complicating factor may be the instability at large yaw due to a nonlinear Magnus moment. (See 10.22.) Theoretical treatment is difficult because the spin is no longer proportional to the velocity with respect to the air. As a consequence, the problem can not be reduced to the problem of a ground fired rocket by a change of origin as was possible for fin-stabilized rockets. Indeed, the solutions of the differential equations are not expressible in terms of tabulated, elementary functions or even in terms of known functions. Furthermore, the number of parameters is such that an extensive amount of computation is needed to cover the cases of interest. For these reasons it is desirable to develop approximate methods to give orders of magnitude for design purposes. It is not possible to obtain very satisfactory approximate formulas, and it appears that future work may have to be based on a program of computations using the differential analyzer or some other automatic computing machine that will give a

series of curves that can be used to explain the behavior of rockets and that are useful for the computation of sighting tables.

A consideration of the problems involved in designing spin-stabilized rockets that will have small dispersion when fired from airplanes and in developing sights for these rockets indicates that it will be very difficult to surmount the various obstacles. On the other hand, the obvious advantages that spin-stabilized rockets have over fin-stabilized rockets with their bulky and fragile fins will justify a vigorous attack on the problems.

9.51 Qualitative Discussion of Aircraft Fired Spinners.—When a spin-stabilized rocket is fired on the ground in still air, the spin and velocity remain nearly proportional and the stability factor, $S = (k^2 s / K^2 V)^2 / 4k_{V^2\delta}$, which must be greater than unity for stability, has throughout burning essentially the same value that it has at the end of burning. When the same rocket is fired forward from an airplane, its velocity through the air is increased by the airspeed of the airplane but its spin is unaffected. Hence the stability will increase during burning, starting at zero at ignition and never getting as great as for the ground fired rocket. During the stage when S is less than unity the yaw and transverse angular velocity tend to increase very rapidly and the motion is very sensitive to slight fluctuations in initial conditions. After S is greater than unity the motion is like that of a ground fired rocket in a head wind and can be treated by the methods of 9.43 provided the yaw has not become so large that the Magnus moment produces instability.

It is desirable that aircraft rockets have as much spin as possible in order to increase the stability factor. The upper limit is the spin at which the rocket bursts because of the combination of centrifugal force and motor pressure; the limitation that the spin be small enough so that the rocket is stable near the summit of a high quadrant elevation trajectory applies to some ground fired rockets but is not relevant here. Thus rockets for aircraft firing should be designed so that they can withstand as much spin as possible and should have enough cant to the jets to produce the maximum safe spin. In addition, it would be highly desirable if the rocket could be provided with an initial spin or if the spin could be increased very fast compared to the velocity increase while $S < 1$, thus shortening this undesirable stage without leading to excessive spin at the end of burning. A considerable number of such devices have been proposed but the authors know of none that does not appear to have more drawbacks than advantages. Besides having high spin, aircraft rockets should also be relatively short. This reduces the tendency to instability due to the Magnus moment at large yaw, and it increases S by increasing the value of k/K , and tending to reduce $k_{V^2\delta}$. If the rocket can be designed so that its center of mass is well forward this will reduce $k_{V^2\delta}$ and hence increase S ; but if it is too far forward it may increase the Magnus moment to the point of instability. It will be recalled that $k_{V^2\delta}$ is a function of the airspeed near and above the velocity of sound, and that it increases markedly at the velocity of sound. However, the time when a low moment is most important is when the rocket has just come off the launcher and here the airspeed will be less than the velocity of sound.

Firing sideways is more complicated but experiment has shown that it is possible and that the rocket may have a stable motion. In this case the yaw is very large initially and the rocket must have a low aerodynamic moment at large yaw and must acquire spin rapidly in order to maintain its orientation until the velocity has increased enough to reduce the yaw.

When a rocket is fired backward from an airplane it would appear to be unstable initially but as its air speed is decreasing while its spin increases it becomes stable much sooner than when fired forward. On the other hand nothing is known as to the aerodynamic moments during this state of the motion; wind and water tunnel data being useless because of the great disturbance produced in the airflow by the jet. At the instant the rocket stops moving backward the sta-

bility is infinite, S then decreasing but never getting as small as when the rocket is ground fired. It might be satisfactory to assume that the motion is nearly that given in 9.2 for the vacuum case, there being some deviations toward the motion described in 9.3 for the case where S is constant and the effect of the short unstable period being expressed in terms of a mallaunching. The same quantities that make a rocket satisfactory for firing forward should be desirable for firing backward except that perhaps the center of mass should not be located so far forward, thus decreasing the aerodynamic effects during the unstable period.

9.52 Equations of Motion.—We shall treat only the case of an overturning moment because, just as in ground firing, the other forces and moments do not usually modify the motion very much during burning. There may be instances in which the nonlinear Magnus moment contributes to the instability at large yaw but here a detailed solution is not needed since unstable cases are of no practical importance and since the nature of the instability is illustrated by the treatment of 10.22. We use small letters to denote velocities relative to the airplane and capital letters for velocities relative to the air, and denote the airplane speed by V_A . We use the subscript a on an angle to indicate that it is measured in a coordinate system that is stationary with respect to the air while angles measured in a coordinate system moving with the airplane will have no subscript. The subscript a on a characteristic function will indicate that both the function and the corresponding initial condition are measured in the air coordinate system. Thus our coordinate system is similar to that of 9.43 except that $-V_A$ replaces W_z and $W=0$; we can derive from the equations given there the equations

$$V_z = v_z + V_A, \quad (1)$$

$$\varphi = \varphi_a, \quad (2)$$

$$\vartheta \doteq \left(1 + \frac{V_A}{v_z}\right) \vartheta_a, \quad (3)$$

and

$$\delta \doteq \delta_a - (V_A/v_z) \vartheta_a. \quad (4)$$

Since we shall work exclusively in the air coordinate system, the principal use of (2)–(4) will be to translate results back to the coordinate system moving with the airplane if such a transformation is required. If this is done for the characteristic functions great care must be taken with the initial conditions and 3.44 should be consulted.

The overturning moment is given by

$$f_{V^2\delta} = mK^2 k_{V^2\delta} (v_z + V_A)^2 \delta_a, \quad (5)$$

and if we write

$$\mu = \frac{V_A}{v_\lambda}, \quad (6)$$

then we may write

$$\frac{t_\lambda^2}{mK^2} f_{V^2\delta} = \frac{4\pi^2}{S} (\zeta + \mu)^2 \delta_a, \quad (7)$$

where S is the stability factor of the rocket when ground fired. If we put (7) into the equations of motion we have

$$\varphi''_a - 4\pi i \zeta \varphi'_a - \frac{4\pi^2}{S} (\zeta + \mu)^2 \delta_a = 0, \quad (8)$$

$$\vartheta'_a - \frac{1}{(\zeta + \mu)} \delta_a = \frac{ig}{G(\zeta + \mu)}, \quad (9)$$

and

$$\varphi_a - \delta_a - \vartheta_a = 0. \quad (10)$$

Using (10) to eliminate φ_a and (9) to eliminate ϑ_a , we obtain the equation in δ_a

$$\begin{aligned} \delta''_a + [(\zeta + \mu)^{-1} - 4\pi i \zeta] \delta'_a - [(\zeta + \mu)^{-2} + 4\pi i \zeta (\zeta + \mu)^{-1} + (4\pi^2/S)(\zeta + \mu)^2] \delta_a \\ = i(g/G)[(\zeta + \mu)^{-2} + 4\pi i \zeta (\zeta + \mu)^{-1}]. \end{aligned} \quad (11)$$

If we now change variables, writing

$$\delta_a = y/(\zeta + \mu), \quad (12)$$

$$Z = (\zeta + \mu)^2, \quad (13)$$

we have

$$\frac{d^2 y}{dZ^2} - 2\pi i \left(1 - \frac{\mu}{Z^{1/2}}\right) \frac{dy}{dZ} - \frac{\pi^2}{S} y = \frac{ig}{4G} \left[\frac{1}{Z^{3/2}} + 4\pi i \frac{Z^{1/2} - \mu}{Z} \right]. \quad (14)$$

Except when we want the gravity solution, $g/G=0$, and we have an especially simple form for numerical integration. Due to the presence of the term in $Z^{-1/2}$, (14) does not lend itself to analytical investigation except in the trivial case of cross-pointing.

Next we must consider the initial conditions to be imposed on y and dy/dZ if from the general solution of (14) we are to obtain particular solutions that can be used to generate the various characteristic functions. These initial conditions on y are easily computed by means of (9), (10), (12), and (13) from the conditions on φ_a , φ'_a , and δ_a , at $\zeta = \zeta_p$ used as the basic definition. The derivation is indicated in table 9.52, which lists the results and some of the intermediate steps.

TABLE 9.52

VALUES OF THE DEPENDENT VARIABLES AT $\zeta = \zeta_p$ FOR VARIOUS CHARACTERISTIC SOLUTIONS

	δ	φ	φ'	g/G	δ'	y	y'	dy/dZ
Yaw.....	1	0	0	0	$-(\zeta + \mu)^{-1}$	$(\zeta + \mu)$	0	0
Cross pointing.....	0	1	0	0	0	0	0	0
Malfunctioning.....	0	0	1	0	1	0	$(\zeta + \mu)$	$\frac{1}{2}$
Gravity.....	0	0	0	1	$-i(\zeta + \mu)^{-1}$	0	$-i$	$-\frac{1}{2}i(\zeta + \mu)^{-1}$

9.53 Approximate Gravity Solution.—It was pointed out in 9.34 that the nutation amplitude is very small in the gravity solution because the rocket starts out with zero yaw and zero transverse angular velocity, so that no large torques act upon it. In the case of forward firing from aircraft a similar situation would be expected because the trajectory drops so slowly. Hence we should make little error by neglecting the nutations and their angular accelerations. This means that we neglect the term in φ''_a in 9.52 (8) because it is small. If this is done and the equations are then treated as in the last section, it is easy to obtain

$$y' - \frac{\pi i (\zeta + \mu)^2}{S \zeta} y = -\frac{ig}{G}. \quad (1)$$

This is a linear equation of the first order and may be integrated by quadratures. Table 9.52 shows that the characteristic function of the gravity solution is obtained by solving (1) for $g/G=1$ subject to $y=0$ at $\zeta = \zeta_p$, the condition $y' = -i$ being consistent with (1). The desired solution is

$$y = -i \exp \left[\int_{\zeta_p}^{\zeta} \frac{\pi i (\zeta + \mu)^2}{S \zeta} d\zeta \right] \int_{\zeta_p}^{\zeta} \exp \left[- \int_{\zeta_p}^{\zeta} \frac{\pi i (\zeta + \mu)^2}{S \zeta} d\zeta \right] d\zeta. \quad (2)$$

It may be remarked that (2) holds even if the overturning moment is not proportional to V^2 , in which case S is a function of ζ . Now using 9.52 (9) and (12) and the initial condition that $\delta_a = \varphi_a - \delta_a = 0$, we have the characteristic function

$$\Theta_{ga} = i \ln \frac{\mu + \zeta}{\mu + \zeta_p} - i \int_{\zeta_p}^{\zeta} \left\{ \frac{\exp \left[\int_{\zeta_p}^{\zeta} \frac{i(x + \mu)^2}{Sx} dx \right]}{(\zeta + \mu)^2} \int_{\zeta_p}^{\zeta} \exp \left[- \int_{\zeta_p}^{\zeta} \frac{\pi i(x + \mu)^2}{Sx} dx \right] d\zeta \right\} d\zeta. \quad (3)$$

This expression has been evaluated for the conditions $\zeta_p = 0.15$ and 0.25 , $\mu = 0.5$, and 1.0 , and

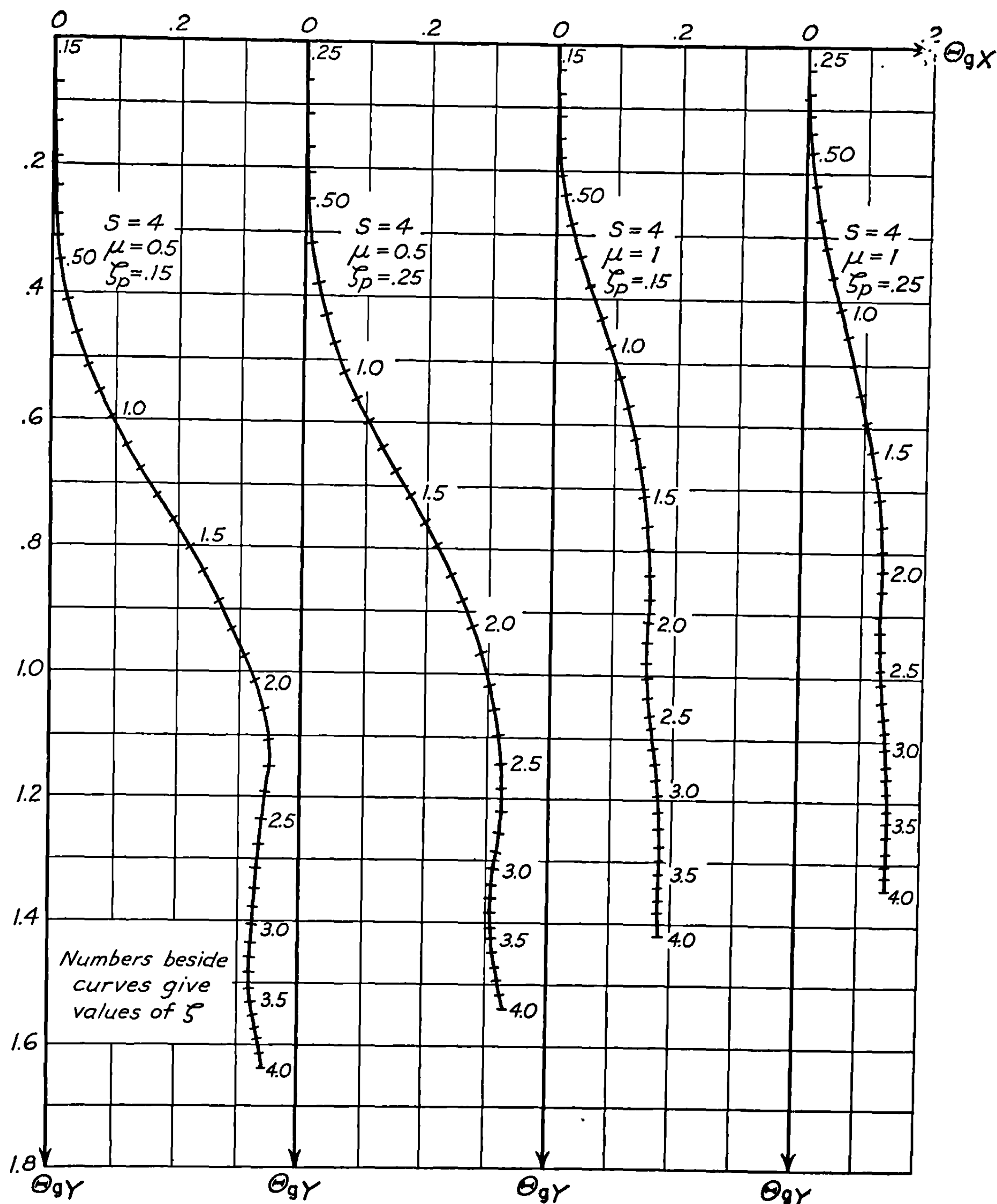


FIGURE 9.53.—Characteristic function $\Theta_g(S, \zeta_p, \zeta)$ for the deflection with respect to a coordinate system fixed in the air when firing forward from an airplane.

$S=4$; the results are shown in figure 9.53. It may be noted that the functions are very similar to those for ground fired rockets.

Unfortunately, it is not possible to use the above approximation in the case of initial yaw or mallaunching, because the nutations are not small enough; hence other techniques are needed.

9.54 Discussion of the Solutions for Initial Yaw and Mallaunching.—Since it is nearly impossible to maintain the launcher parallel to the line of flight of an airplane under all circumstances in which a spin-stabilized rocket is to be fired forward, it is essential to consider the effect of initial yaw on the trajectory. Likewise it is necessary to consider the effect of the mallaunching which will always be present due to tipoff, dynamic unbalance, and perhaps other causes. Now, when a forward fired rocket leaves the launcher, it is, in general, unstable until the spin has had time to build up sufficiently to compensate for the initial air speed. If, because it is launched with initial yaw or because mallaunching is rapidly producing yaw, the rocket has an appreciable yaw during this period, the large aerodynamic forces will produce a large transverse angular velocity and hence nutations and precessions of considerable amplitude. In some cases the Magnus moment makes the rocket unstable but even in the favorable cases where the nutations are strongly damped, the oscillations during burning are large and hence it is difficult to predict accurately the ultimate direction of motion. Furthermore, the direction of motion at the end of burning does not equal its asymptotic value because of the large amplitude of the nutations and precessions. Because of these factors there does not appear to be any simple expression which gives the behavior of the rocket.

The effective value of S is given by

$$S_{\text{eff}} = \left(\frac{\zeta}{\zeta + p} \right)^2 S. \quad (1)$$

Now

$$S_{\text{eff}} \geq 1 \text{ for } \zeta \geq \zeta_{\text{crit}} = \frac{\mu}{\sqrt{S}-1}. \quad (2)$$

This value of ζ_{crit} is a strong function of both μ and S . Until this time the rocket will gyrate wildly and the solution will be sensitive to μ , S and ζ_p . To illustrate this motion, the characteristic functions Φ_q for $\mu=1$, $S=4$ and 8 are given in figure 9.54(a). The large difference between the solution for $S=4$ ($\zeta_{\text{crit}}=1$) and that for $S=8$ ($\zeta_{\text{crit}}=.547$) is due to the long time before the missile becomes stable for $S=4$.

The solutions of the equations have been obtained by an electric analog computer and are on the average accurate to 2 or 3 percent. However, errors up to 10 percent may exist in the following solutions, especially near the end of the trajectory where the errors may accumulate. The accuracy could be improved by using a digital computer for the solution of the equations. However, there seems to be no advantage to tabulating these functions extensively for the forward fired case since the variation in aerodynamic coefficients in the vicinity of Mach 1 requires a special integration for each rocket. While the general availability of modern computing equipment eliminates the advantage of extensive figures of rocket performance, a set of figures has been prepared to demonstrate the order of magnitude of the characteristic functions.

In figures 9.54(b)–(e) the characteristic functions Θ_q have been plotted for $\mu=1$ and 2, $S=4$, 8 and 16. The larger values of stability are appropriate in the aircraft case because at higher altitudes the decrease in air density leads to a much larger effective stability factor. At 35,000 feet the air density is approximately $\frac{1}{4}$ of the sea level value and hence the stability factor is four times the corresponding sea level figure. However, the higher aircraft speeds at high altitude nullify the advantage of the increased stability. For $S=8$, $\mu=2$, $\zeta_{\text{crit}}=1.09$ which com-

pares closely with $\zeta_{\text{crit}}=1$ for $S=4$, $\mu=1$. The solutions [figures 9.54(b) and (d)] show many of the same characteristics. It is apparent that any practical rocket and launcher design must have larger ζ_p or S in order to get decent performance.

In figures 9.54(f)–(i) the characteristic functions for cross pointing are plotted. These functions differ from both the cross pointing and the initial yaw solutions defined in 9.22. Just as it was more convenient to tabulate wind functions than it was to tabulate the initial yaw functions, here it is useful to plot the function Θ_φ obtained with the initial condition

$$\begin{aligned}\Phi_\varphi &= \Delta_\varphi = 1, \\ \Phi'_\varphi &= \Theta_\varphi = 0 \quad \text{at } \zeta = \zeta_p.\end{aligned}\tag{3}$$

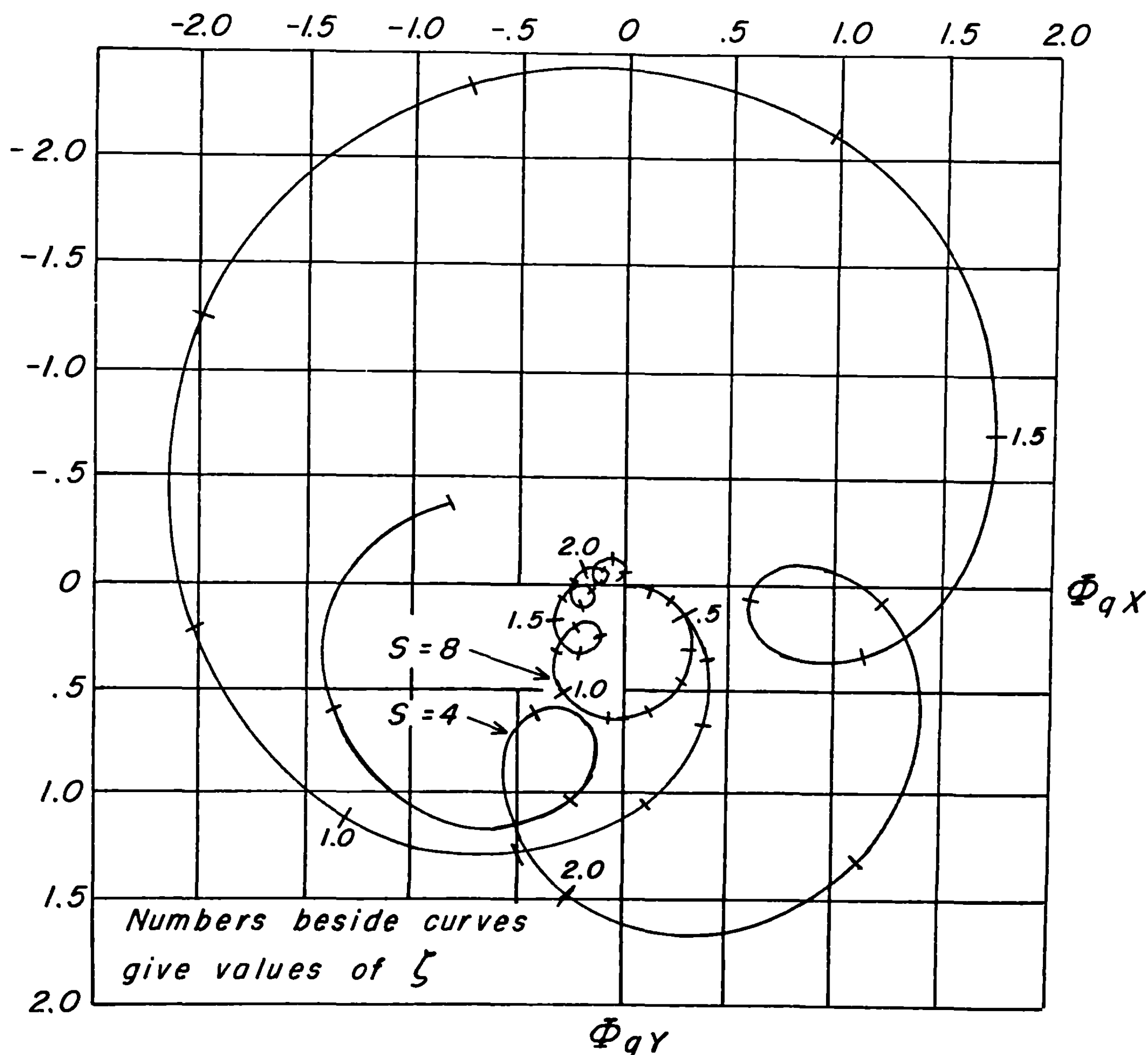
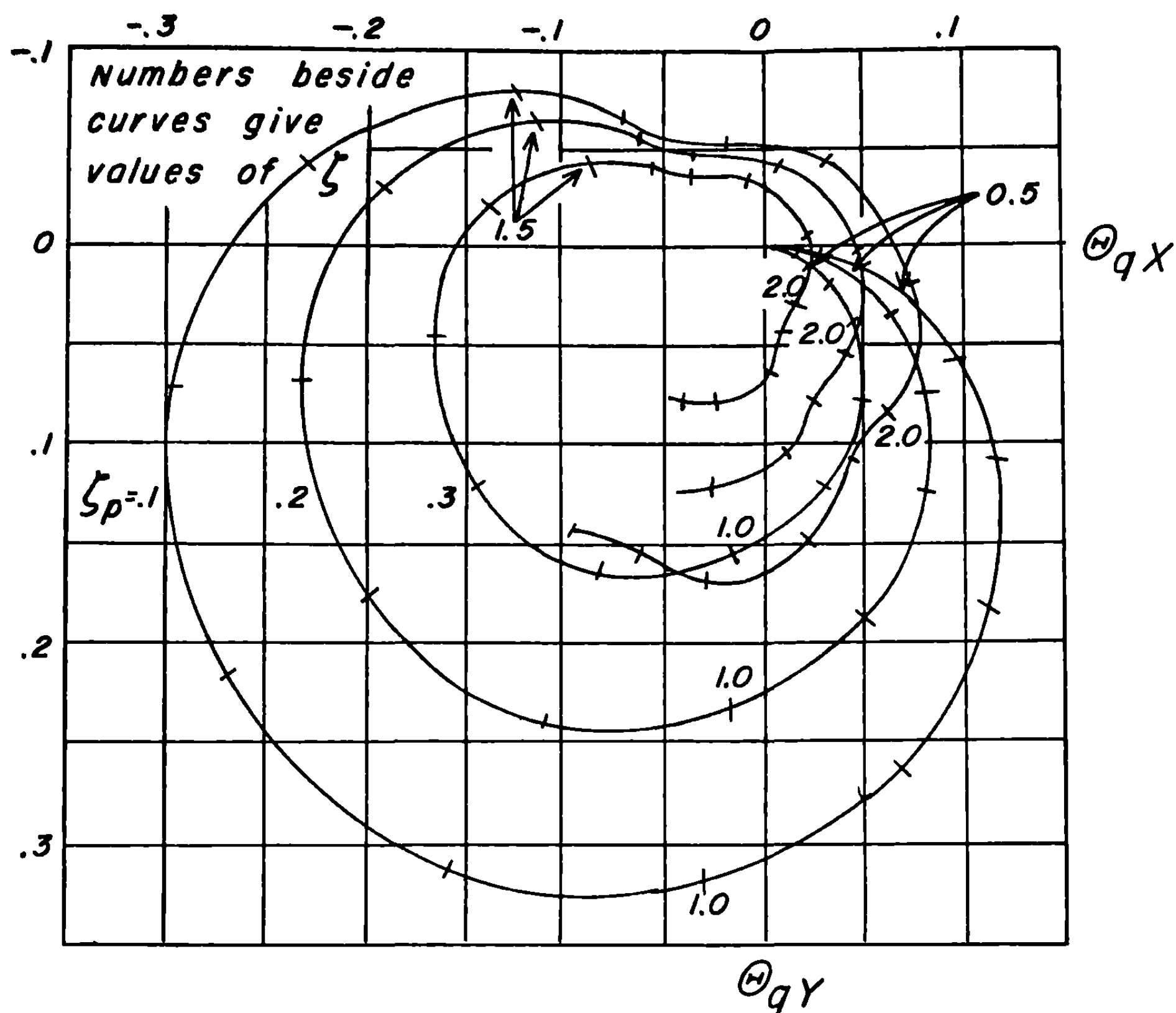
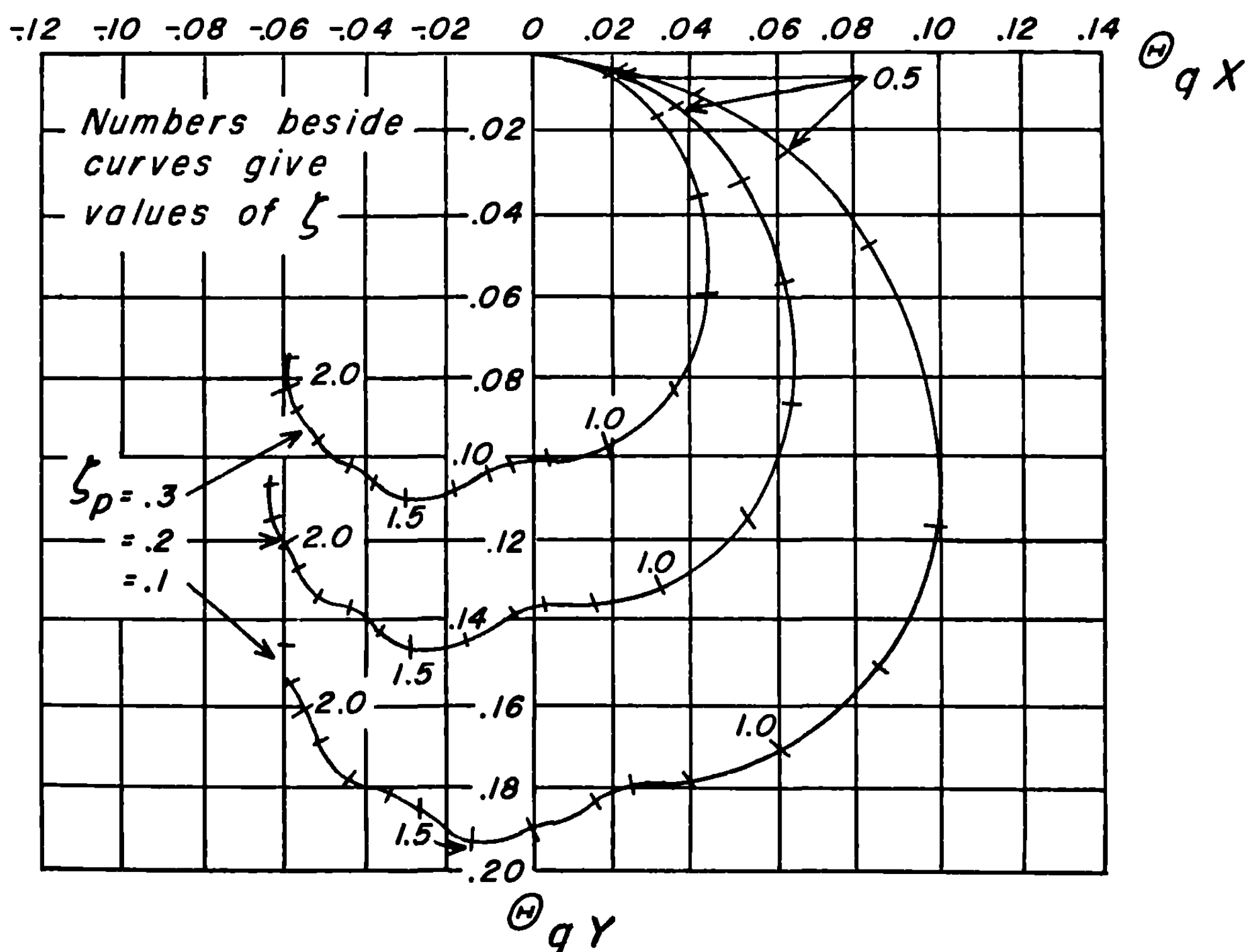
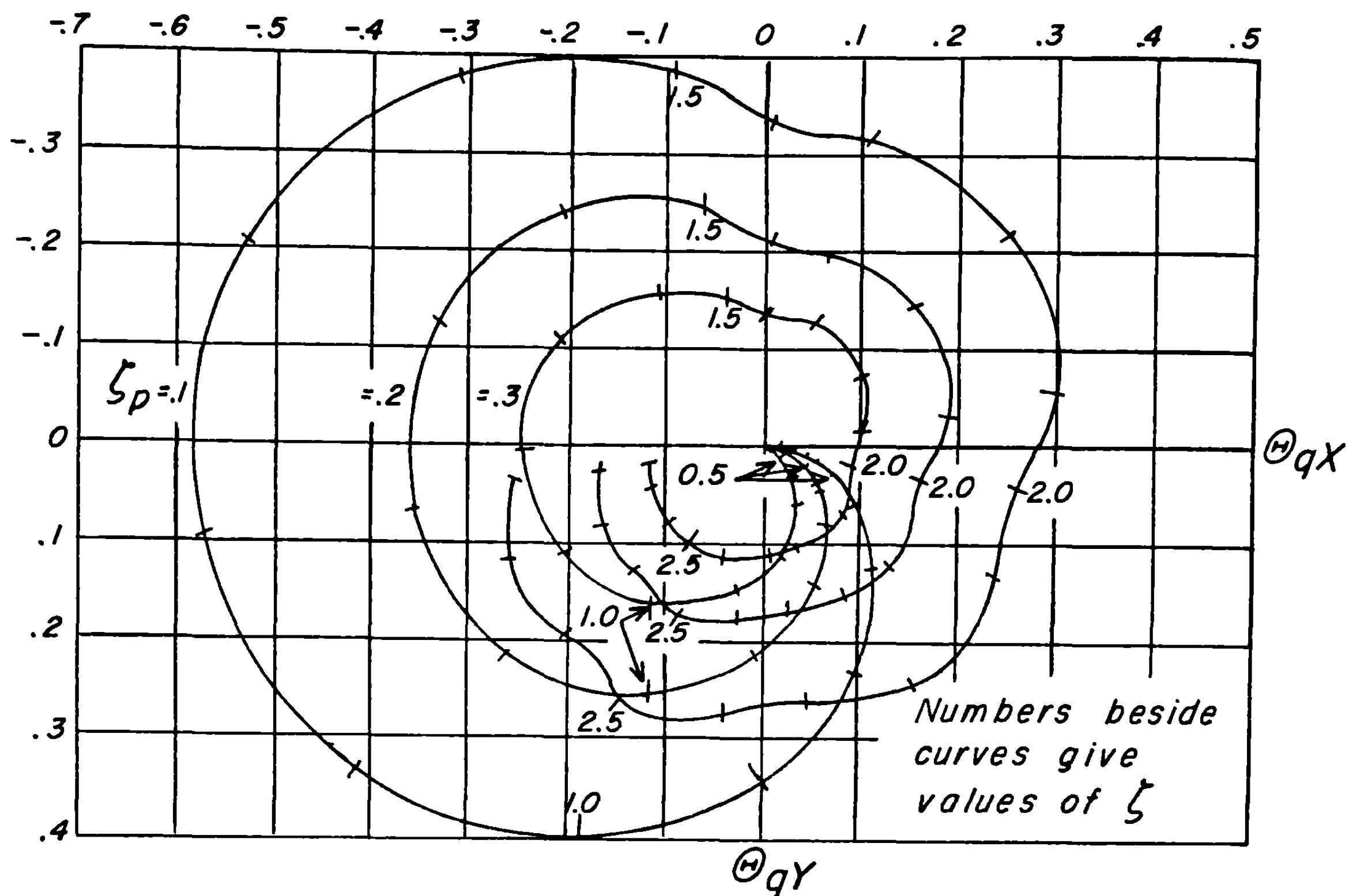
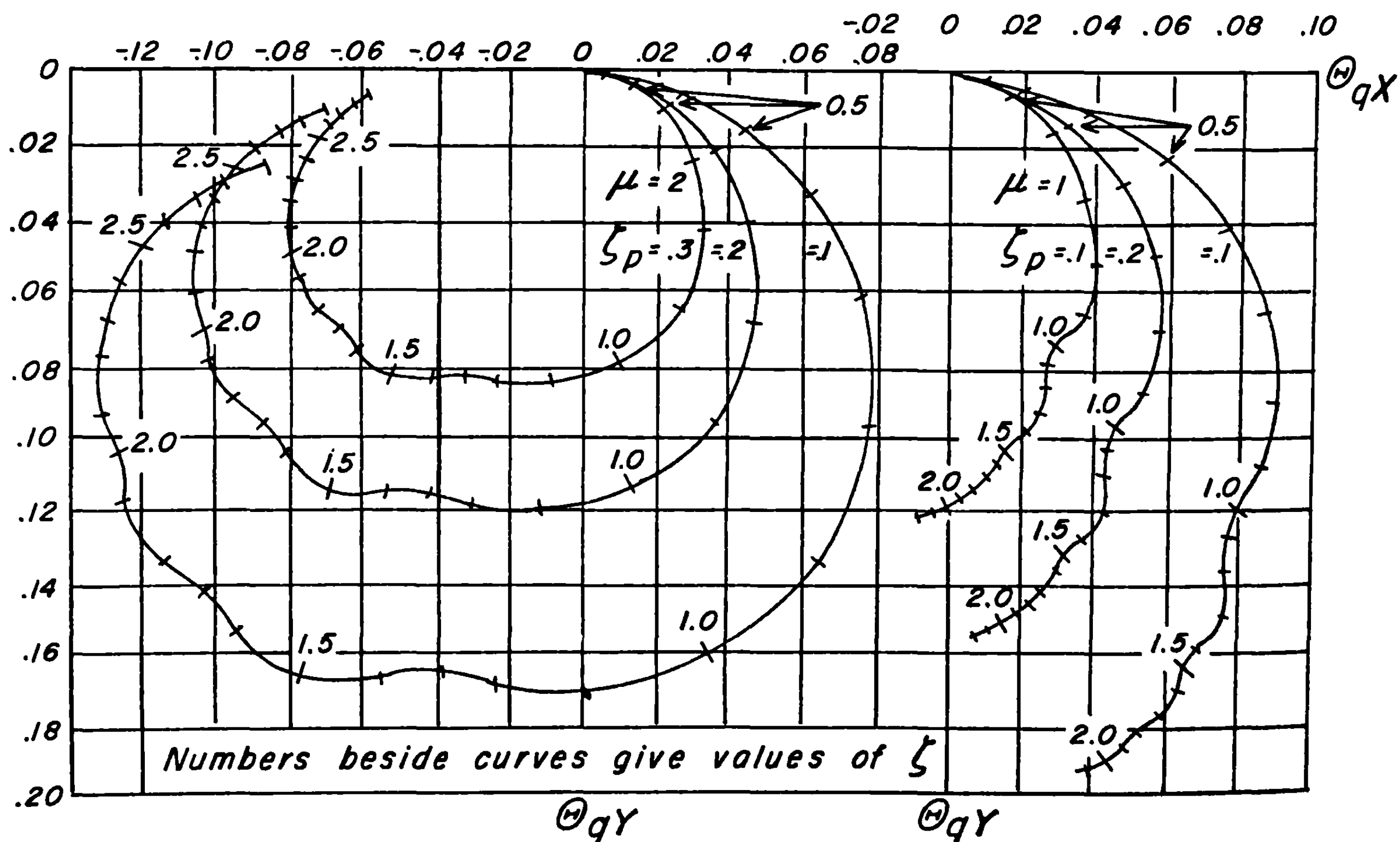


FIGURE 9.54 (a).—Characteristic functions Φ_q for aircraft firing when $\zeta_p=.2$, $\mu=1$, $S=4$ and 8.

FIGURE 9.54 (b).—Characteristic functions Θ_q for aircraft firing when $S=4$, $\mu=1$.FIGURE 9.54 (c).—Characteristic functions Θ_q for aircraft firing when $S=8$, $\mu=1$.

FIGURE 9.54 (d).—Characteristic functions Θ_q for aircraft firing when $S=8$, $\mu=2$.FIGURE 9.54 (e).—Characteristic functions Θ_q for aircraft firing when $S=16$, $\mu=1$ and 2 .

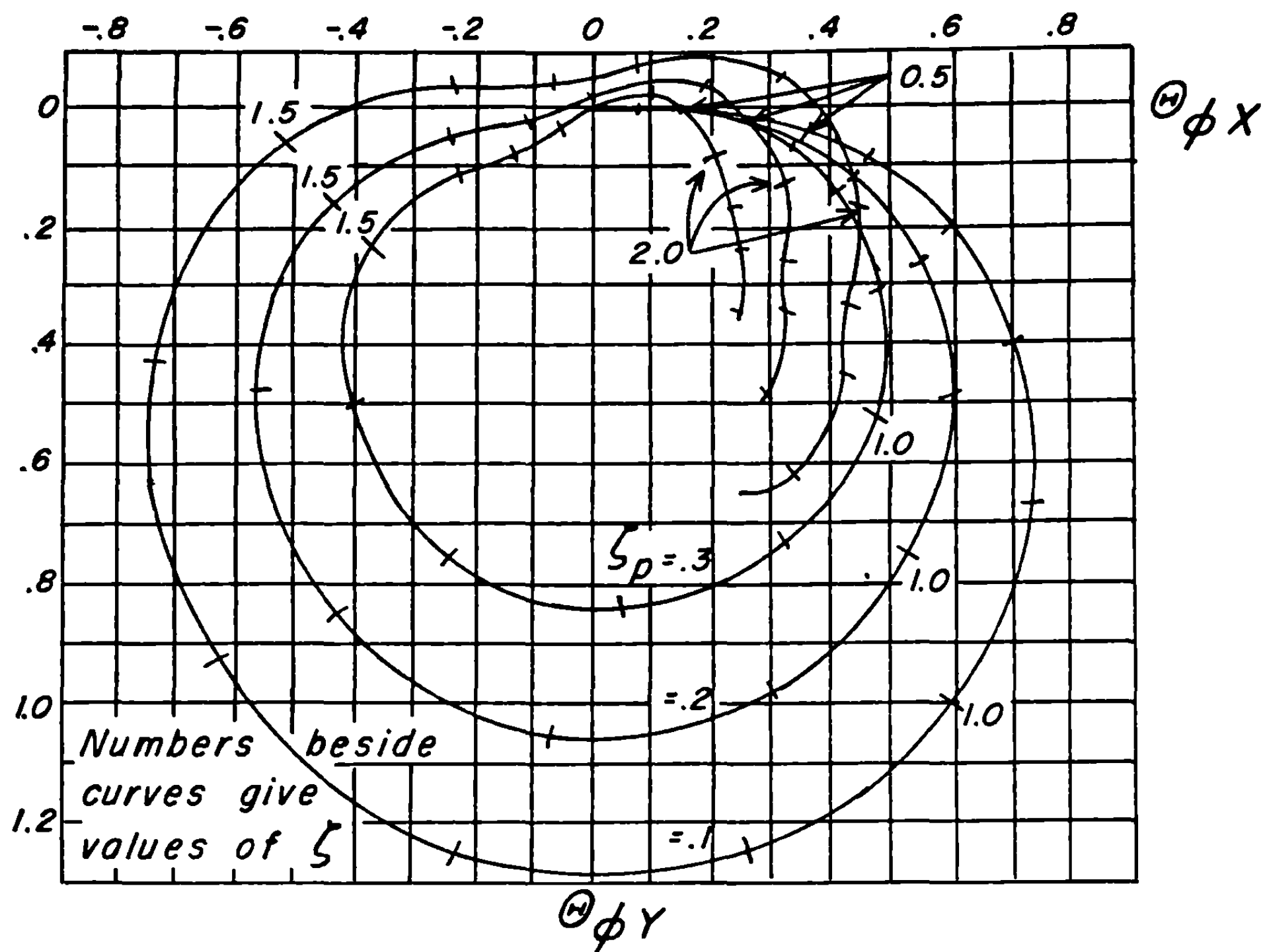


FIGURE 9.54 (f).—Characteristic functions $\Theta\phi$ for aircraft firing when $S=4$, $\mu=1$.

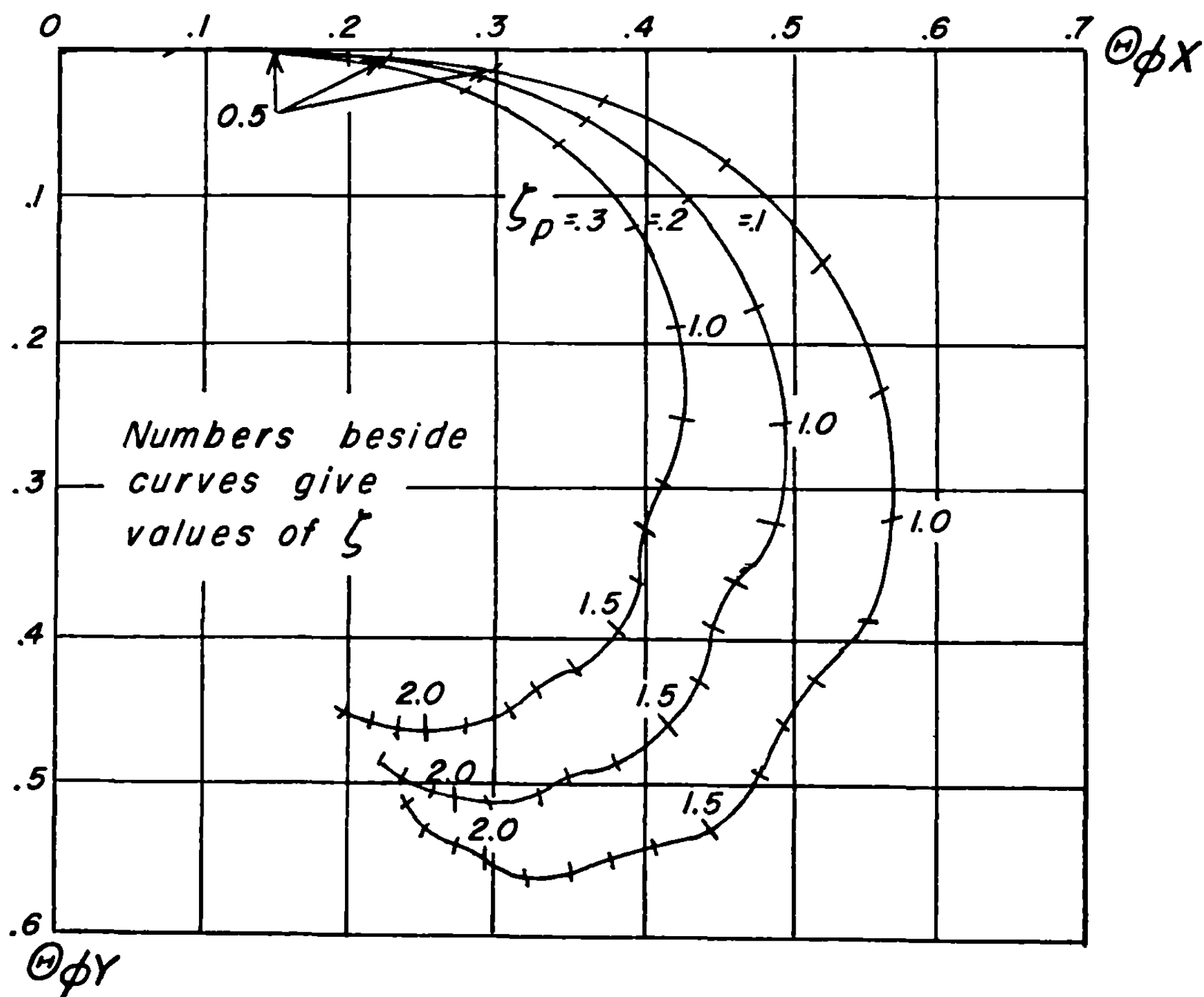
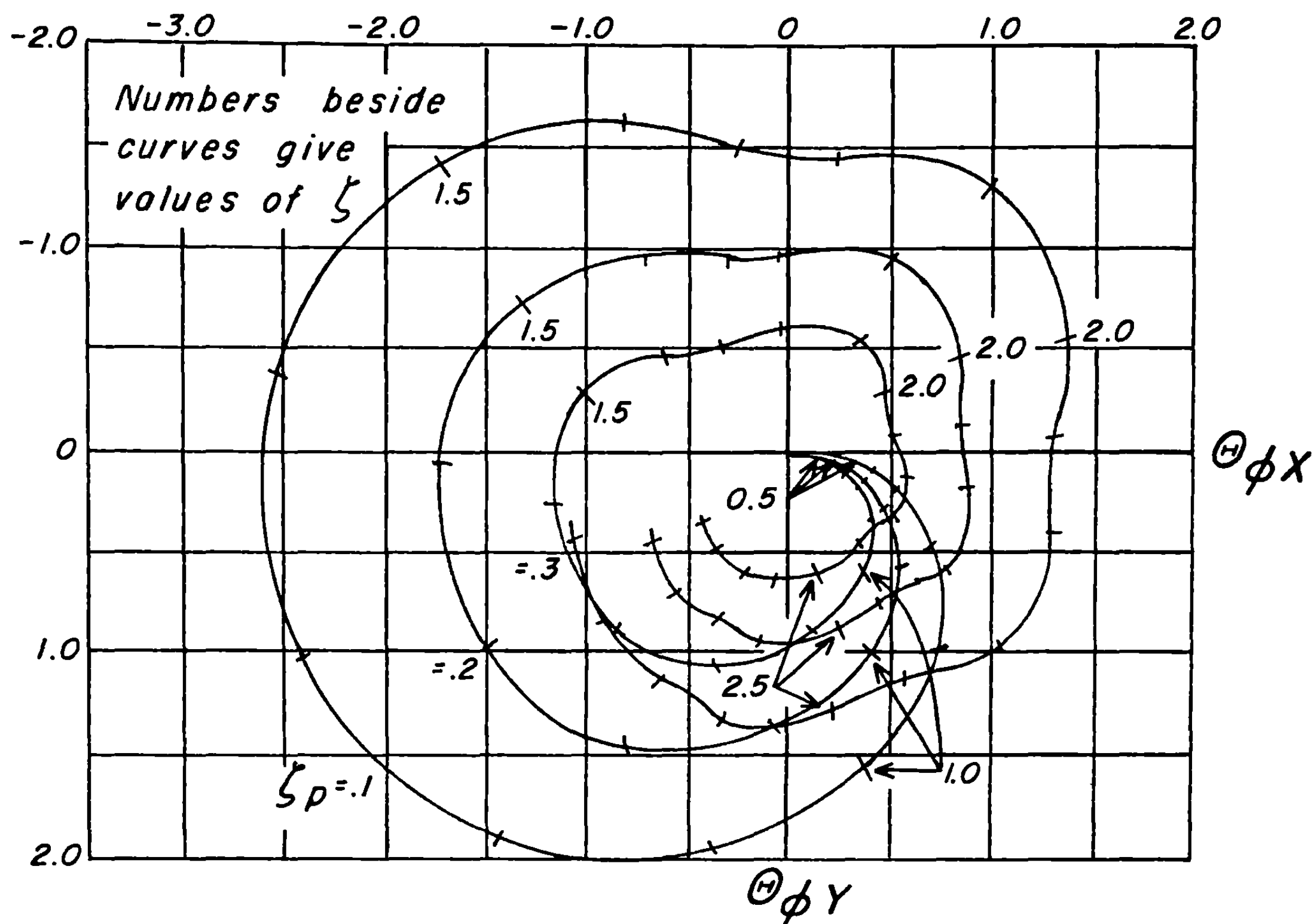
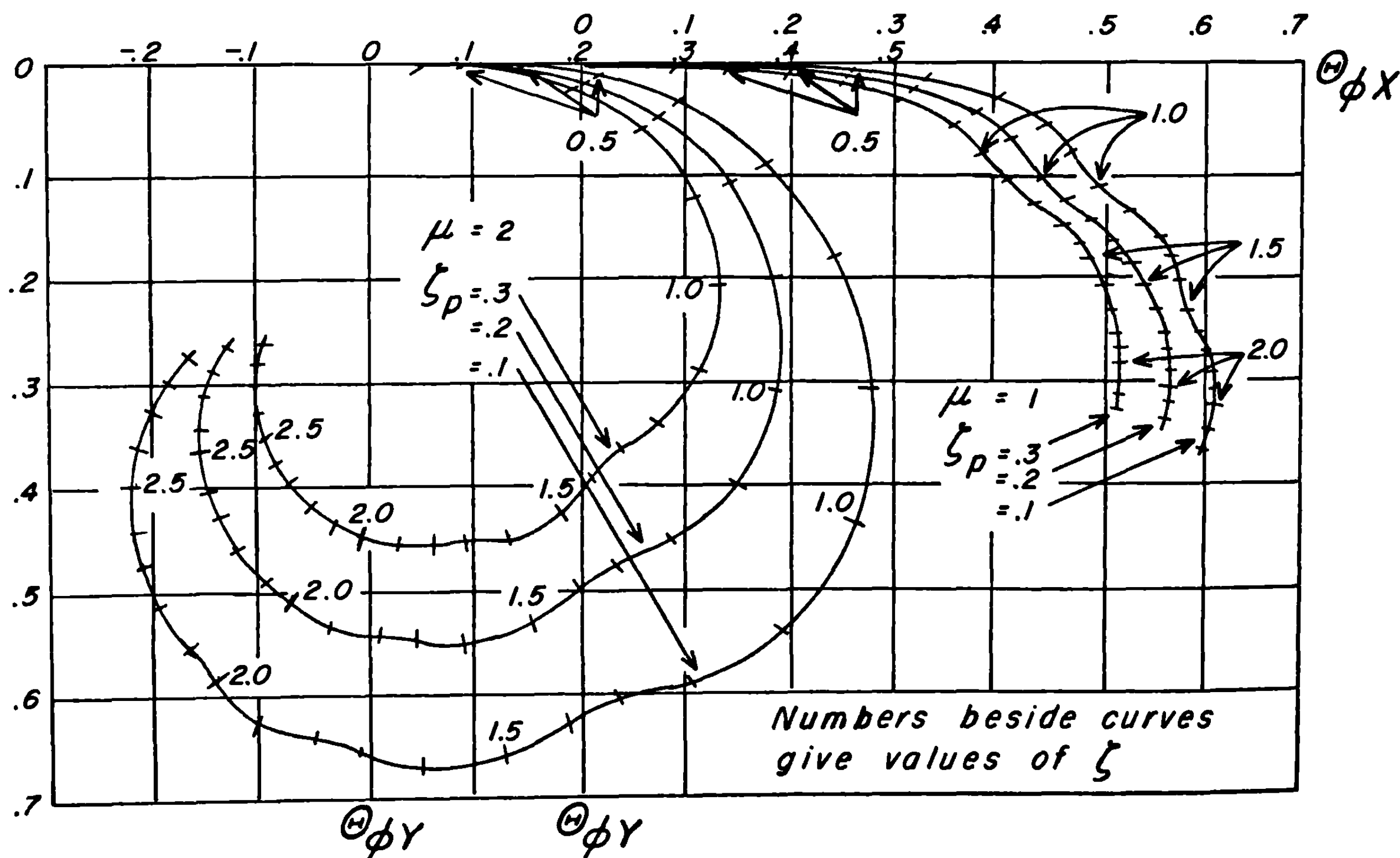


FIGURE 9.54 (g).—Characteristic functions $\Theta\phi$ for aircraft firing when $S=8$, $\mu=1$.

FIGURE 9.54 (h).—Characteristic functions $\Theta\phi$ for aircraft firing when $S=8$, $\mu=2$.FIGURE 9.54 (i).—Characteristic functions $\Theta\phi$ for aircraft firing when $S=16$, $\mu=1$ and 2 .

Note that this notation (which is used only in this section) is at variance with 9.32. If the reference axis is put along φ_p , the component of airspeed perpendicular to the reference is called a cross wind, and μ is set equal to zero, then these solutions are proportional to the wind functions defined in 9.35. The same dependence of the character of the solutions on ζ_{crit} is to be noted.

In addition to the variation of aerodynamic coefficients near Mach 1 there are three other factors which modify the solutions given above. First, all the aerodynamic forces and moments are most important; in particular, the aerodynamic lift is large. The correct equations may be obtained from 9.41(3)–(5) by replacing ζ by $(\zeta + \mu)$ where velocity factors are involved; for instance, 9.41(4) becomes

$$\vartheta - \left(\zeta^{-1} + 2\lambda K_{v^2}(\zeta + \mu) - \frac{4\pi i l \lambda}{\nu} K_{v, \delta} \zeta \right) \delta = D(\zeta + \mu)^{-1}. \quad (4)$$

The second effect is that large angles of attack are present unless the rocket is fired forward and the change of stability with angle of attack leads to very complicated behavior of the rocket. The third effect is the effect of drag and non-uniform burning. These cause similar effects (which are discussed in 9.61) tending to decrease the deflection. As a consequence of these large perturbations of the trajectory it is clear that high-speed computers should be used for any future analyses.

9.55 Sighting of Forward Fired Spinners.—The sighting problem for forward fired spinners is very much more difficult than that for fin-stabilized rockets described in chapter 6 because the rocket does not remain in a vertical plane. By the use of complex notation, the horizontal and vertical components of the deflections due to gravity and initial yaw can be expressed as a single complex number and correspondingly the horizontal and vertical components of the sight setting can be expressed as a single complex number. If this is done, the sighting equation, 6.52 (3), remains valid. It will probably be feasible to build an automatic sight, but the problem will be very difficult both because it must deal with both lateral and vertical deflections and because the effects of initial yaw will be so difficult to deal with.

In the case of fin-stabilized rockets fired forward from an airplane the rocket does not go in the direction in which the launcher is pointed but, as discussed in 6.15, goes much more nearly along the direction in which the airplane is moving. This happens because the fins turn the rocket toward the flight line. This phenomena is frequently disadvantageous because it means that the airplane must be carefully flown in a specified manner during the two seconds previous to firing in order to bring the flight line into a specified relation to the launcher line. Also it is very difficult to aim rockets at a large angle to the flight line. It appears to be one of the obvious advantages of spin-stabilized rockets that they do not turn toward the flight line. However, we feel that unless their design can be greatly improved, this apparent advantage is largely illusory. Spin-stabilized rockets turn away from the flight line and nutate in a spiral, the total deflection of the trajectory from the launcher line being at least as large as that of a fin-stabilized rocket. Thus just as much care is needed in flying the airplane, no more freedom to fire while maneuvering is obtained, and just as much dispersion is introduced by unexpected yaws. An improperly oriented launcher is not serious for fin-stabilized rockets since the deflection of the trajectory is $1-f$, i. e., about 0.1, times the deflection of the launcher. In the case of spin-stabilized rockets the deflection of the trajectory will be of the order of twice the deflection of the launcher. It is true that firing to the side will be easier with spin-stabilized rockets because such a rocket will have a much smaller aerodynamic moment at very large yaw than will a fin-stabilized rocket of the same moment of inertia about a transverse axis.

Another factor that may have to be considered in the case of spin-stabilized rockets is the mallaunching. Not only will small random mallaunchings due to imperfection in the launcher or round produce a relatively large dispersion due to the large aerodynamic forces, but any systematic mallaunching will produce relatively large deflections that must be allowed for in sighting. One source of systematic mallaunching is tipoff, the resulting mallaunching depending on dive angle and on the launching velocity which in turn depends on propellant temperature. Another source of mallaunching was evident in the early experiments with spin-stabilized rockets fired forward from airplanes, but no reason for it could be found, since there did not seem to be any torques acting during the launching period that were large enough to produce it. Nevertheless, the data indicated that mallaunching as large as one radian per second were present, the nose of the rocket moving roughly outward from the fuselage. Either such effects will have to be eliminated or their cause will have to be discovered and their dependence on air speed, dive angle, propellant temperature, and the other relevant factors will have to be determined before satisfactory sighting tables can be computed.

9.6 Miscellaneous Effects During Burning

There are several miscellaneous effects during burning which are not very important but which should be mentioned. These include the effects of regressive burning, of the variation of the overturning moment coefficient with velocity, and of a liquid pay load. We shall give here merely a qualitative discussion of the first two of these effects because they do not warrant numerical computations by the Green's function technique.

9.61 Effect of Regressive Burning.—It was pointed out in chapter 2 that the jet thrust is usually nearly constant during the first three-quarters of burning and that it drops off during the last quarter of burning. Because the effective acceleration is chosen as an average over the first three-quarters of burning, the equations of motion should be accurate over this portion of burning and the regression should modify only the motion during the last quarter. At this stage of the motion, the gyroscopic forces are large and the orientation as a function of time is only slightly modified by the change in axial jet torque. If, as a first approximation, we assume that the orientation of the axis remains in agreement with the earlier theory, then it is apparent that because the burning lasts longer, the axis will precess farther during burning, and the resultant average rocket thrust will be oriented in a somewhat different direction and hence give a different direction of motion at the end of burning. Furthermore, consideration of the δ and ϑ loci in 9.3 indicates that the effect of this increased precession is primarily to deflect the ϑ locus in the direction of increasing the curvature; that is, the point corresponding to ϑ is projected inward along the normal to the curve.

The effects of the regression are unimportant in the mallaunching solution because the amplitude of the precession is small and the motion during the last part of burning has nearly reached an asymptote, so that the resultant is the same whatever the thrust-time curve. In the case of the gravity solution, the effects are more pronounced because the rocket axis precesses to keep up with the trajectory. In addition to this forced precession there is a precession about the equilibrium yaw, and it is primarily this that is altered by the regression. This latter precession contributes only a part of the motion so that the effect of the regression is of the same character but is not as large as for the wind solution, in which the entire precession contributes to the effect of the regression. The effect expected on the wind solution is shown qualitatively in figure 9.61 in which the solid line is taken from figure 9.35(i) and dashed line represents the motion expected for $S=2$ and $\vartheta_p=0$, if the acceleration drops to one-half of its original value at $\vartheta=1.5$.

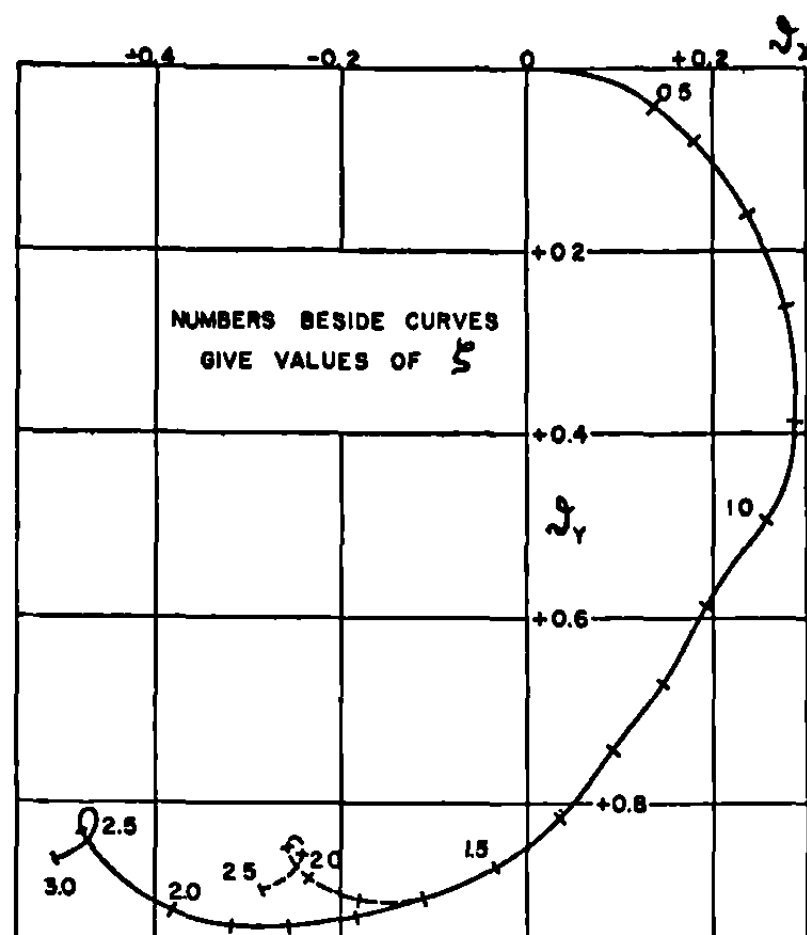


FIGURE 9.61.—Deflection produced by wind when the burning is regressive.

9.62 Effect of Varying Stability Factor.—The decrease in the stability factor near the velocity of sound causes the projectile to precess faster than usual. This increased precession rate, which will generally occur near the end of burning, changes the orientation of the rocket thrust in a manner very similar to regressive burning so that the same general statements may be made about the deflection. Here however, the equilibrium yaw is reduced so that there is a somewhat larger correction to the gravity solution. Actually the equilibrium yaw is proportional to $1/\zeta^2$ and hence even this effect is very small.

9.63 Effect of a Liquid Pay Load.—In a spin-stabilized rocket with a liquid pay load the fluid does not rotate with the rigid body at first but lags behind due to its inertia. The relaxation time is slightly longer than the burning time so that the transient effects of the fluid motion are important. The relaxation time is long compared to a nutation so that the fluid does not take part in the nutation. It does, however, take part in the precessions.

While the fluid does not rotate with the metal part during a nutation it does partake of the translational motion of the axis and hence acts like a mass point on the axis. Thus the effective transverse moment of inertia for nutations is less than that expected by I_T , the transverse moment of inertia of the fluid about its own center of gravity. Likewise the longitudinal moment of inertia is decreased by I_A , the axial moment of inertia of the fluid. Thus we can define the ratio of moments of inertia for nutations

$$\gamma_N = \frac{mK^2 - I_T}{mk^2 - I_A}, \quad (1)$$

and reserve γ for the ratio

$$\gamma = \frac{mK^2}{mk^2}. \quad (2)$$

The initial spin rate should be computed from the moment of inertia, $mk^2 - I_A$, because the fluid does not rotate appreciably, hence we have the initial feet per turn

$$\nu_{\text{initial}} \propto mk^2 - I_A, \quad (3)$$

and, hence, the initial nutation distance λ_N is

$$\lambda_N = \gamma_N \nu_{\text{initial}} \propto mK^2 - I_T. \quad (4)$$

Since $I_T \ll mK^2$ and hence $\lambda_N \doteq \lambda$, the effects of mallaunching and malalignment are the same as they would be for a solid payload because the dominant effects occur during the first nutation.

The effects of wind and gravity are important throughout burning so that the change of ν during burning cannot be neglected. The fluid partakes in the precessional motion only to a limited extent since the period is less than the buildup time of the fluid motion. However the transfer of angular momentum to the fluid from the metal parts increases the rate of precession under the influence of the aerodynamic moments and hence leads to an apparent reduction of the stability factor compared to that for a solid payload. The correction factor for the stability factor is equal to the square of the initial value of ν divided by the square of the mean value of ν during the first precession. In addition, the value of λ_N must be multiplied by the ratio $\nu_{\text{mean}}/\nu_{\text{initial}}$ because of the change in the nutation rate.

9.7 The Launching Process

All the launching effects discussed in chapter 4 are present whether or not the rocket is spinning; if there is spin the launching is complicated by a number of additional effects. These are not due to gyroscopic action since the nutation is negligible during launching but they are best regarded as kinematic effects producing mallaunching. This is obviously true of elliptical bourrelets and of the rolling around of the rocket inside of a tubular launcher. In a similar way dynamic and static unbalance produce a mallaunching that is perhaps the largest source of dispersion in spin-stabilized rockets. If rockets having very small dispersion are needed, they should be balanced on a dynamic balancing machine.

9.71 Description of Motion During Launching.—The longitudinal translation and the spin of a rocket are affected slightly by the friction on the launcher and by changes in the jet forces due to interactions with the launcher, but such effects are small and we shall neglect them completely. Thus we shall be concerned only with changes in the orientation and direction of motion of the rocket.

As shown in figure 8.1, most spin-stabilized rockets have two rings, called bourrelets, whose diameter is slightly larger than the outside diameter of the rest of the rocket. All contact between the rocket and the launcher is made at the bourrelets. For the present we shall assume that all frictional effects can be neglected and that the bourrelets are circular; hence we need consider only the motion of the centers of the bourrelets. We shall also assume that each bourrelet fits snugly in the launcher so that until it moves beyond the end of the launcher, the center of the bourrelet must coincide with the axis of the launcher.

During the first phase of launching both bourrelets are constrained so that the rocket rotates about the bourrelet axis—the line joining the bourrelet centers—and this axis coincides with the launcher axis. During the second phase of launching the rocket pivots about the center of the rear bourrelet, which slides along the launcher axis, thus giving a motion like that of a top whose point is accelerated along a fixed line. When the rear bourrelet slides clear of the launcher, launching is over and the motion at this instant provides the initial conditions for the unconstrained motion considered previously.

Consider now the description of the motion during the second phase when the rocket is pivoting about R , the center of the rear bourrelet, and R is sliding along the rocket axis. It will be convenient to denote the center of mass of the rocket by O , the vector from O to R by r_R , and the velocity of R by v_R . The mass of the rocket is m , and its angular velocity is ω . In 4.1 we showed that the rotational motion about the sliding point R can be treated in the same way as is the motion of a free body about its center of mass. The only differences in the treatment are that the tensor of inertia is referred to R rather than to O and that the torque applied

to the body is not the torque of applied forces about O but is the torque about R plus the term $m \mathbf{r}_R \times \dot{\mathbf{v}}_R$. The same conclusion will be reached if one regards the rocket as a body, say a top, pivoting about a fixed point, the acceleration $\dot{\mathbf{v}}_R$ being replaced by the equivalent gravitational field.

From the discussion of the motion of a free body in 9.14 it follows that the motion can be described in terms of a rotation about a longitudinal axis A_R plus the motion of this axis. The axis A_R is the longitudinal principal axis of the tensor of inertia with respect to the center of the rear bourrelet. In general this will coincide neither with the bourrelet axis nor with A_D , the dynamic axis; i. e., the longitudinal principal axis of the tensor of inertia with respect to O . Fortunately the gyroscopic forces, and hence the nutations, can be neglected in the treatment of the launching process because rockets usually make only a quarter, or at most a half turn during the second phase of launching while gyroscopic forces do not appreciably modify the motion until the number of turns is comparable to γ . Moreover the value of γ that applies here is $(K^2 + r_R^2)/k^2$, not the smaller K^2/k^2 , since the transverse moment of inertia is about an axis through R , not O . Thus γ is of the order of 50 and the error in the deflection due to neglect of the nutations is of the order of one percent of the deflection. Hence if the applied torques are negligible, the longitudinal axis rotates about R with constant angular velocity. If the applied torques are not negligible, we need not consider the nutations or the precessions, but we must consider that the axis is accelerated by the torque in just the same way that it would be if the rocket were not rotating.

It is now easy to describe the motion. At the instant the front bourrelet clears the launcher, the rocket is rotating about the bourrelet axis, which coincides with the launcher axis. Thus, assuming the mass distribution to be known, the motion of the axis A_R at this instant is easily found. During the second phase of the launching, the axis A_R pivots about R with its initial angular velocity if there are no applied torques or with the acceleration produced by the applied torques if they are present. Meanwhile, of course, the rocket is spinning about A_R with angular velocity $s(t)$. It is then possible to determine the orientation and motion of the dynamic axis, A_D , and the cross-velocity of the center of mass at the instant the rear bourrelet clears the launcher. A_D was the longitudinal axis used throughout our previous treatment of a free rocket; it is the axis about which an unconstrained rocket can spin smoothly without nutations. Hence the angular velocity and orientation of A_D gives the mallaunching, \mathbf{q}_p , and initial orientation, φ_p ; the cross-velocity enables one to compute the initial yaw, δ_p . The subsequent deflection of the trajectory is obtainable from 9.2, 9.3, or 9.4.

Since we have seen that gyroscopic effects are negligible, it is clear that the only effects of spin to be considered here are those that are essentially kinematic. Dynamic effects, such as those due to tipoff or launcher motion and discussed in chapter 4 for nonspinning rockets, are independent of spin provided the bourrelet axis, the dynamic axis A_D , and the axis A_R all coincide. Elliptical bourrelets and the rolling of a rocket in a loose-fitting launcher produce precisely the same effects as does the appropriate launcher motion. Static and dynamic unbalance destroy the coincidence of the three axes and the rocket spins about first one, then another as described above. To treat unbalance, therefore, we must determine the relative positions of the axes and work out the kinematics of the motion.

9.72 Theory of the Mallaunching Produced by Unbalance.—An ideal rocket is completely symmetrical dynamically about its longitudinal axis but any actual rocket will deviate from this ideal construction. These deviations produce the malalignment, which has already been considered, and the unbalance, which we must now define. A rocket is said to have static unbalance if the center of gravity does not coincide with the bourrelet axis. Static unbalance can be detected, if the bourrelets are circular, by laying a round on a plane, level surface and

seeing whether there is any tendency to roll. A rocket is said to have dynamic unbalance if A_D , the longitudinal principal axis of the tensor of inertia with respect to the center of mass, is not parallel to the bourrelet axis. Dynamic unbalance can be detected by rotating the rocket about the bourrelet axis. If the rocket exerts on the constraints a couple about a transverse axis fixed in the rocket, it is dynamically unbalanced. If the rocket exerts a force only, it is statically unbalanced. When we wish to speak of a combination of the two kinds or to speak of one without specifying which, we shall always use the term unbalance. Care must be taken to avoid confusion since sometimes the term dynamic unbalance has been used for both kinds.

Except in the present section we define the axis of the rocket to be the dynamic axis A_D since this is the only axis about which the rocket can spin smoothly without nutations in the absence of applied torques. Here it is more convenient to base our coordinate system on the bourrelet axis because initially it lies along the launcher and the initial direction of the angular velocity must coincide with it. We use a coordinate system of $O'xyz$ that is fixed in the rocket with the $O'z$ -axis along the bourrelet axis. It is convenient to choose the origin so that the center of mass is in the $O'xy$ -plane and to orient the $O'x$ -axis so that while the rocket is on the launcher but before it has begun to move the $O'x$ -axis extends horizontally to the right, coinciding with the OX -axis of figure 9.16a. We denote the coordinates of O , the center of mass, by $(x_s, y_s, 0)$, the S reminding us that our main interest in O at present is in its effect on the static unbalance. We shall usually measure the static unbalance by giving the complex number

$$R_s = x_s + iy_s. \quad (1)$$

The coordinates of the centers of the rear and front bourrelets may be denoted by $(0, 0, z_R)$ and $(0, 0, z_R + l_B)$, respectively, the bourrelet spacing being l_B . The dynamic unbalance may be specified by the angle β_{Dx} which the dynamic axis, A_D , makes with the $O'yz$ plane and the angle β_{Dy} which it makes with the $O'xz$ plane, the angles being positive when A_D is in the first octant at infinity. The specification can also be given in terms of the complex angle:

$$\beta_D = \beta_{Dx} + i\beta_{Dy}. \quad (2)$$

Expressions from which R_s and β_D can be computed in some cases are given in the next section. We assume here that they are known for the rocket under consideration either from such a computation or from experimental measurements with a dynamic balancing machine.

Next we must find the orientation with respect to the $O'xyz$ system of A_R , the longitudinal principal axis of the tensor of inertia with respect to R , the center of the rear bourrelet. The tensor of inertia with respect to principal axes through the center of mass is

$$m \begin{vmatrix} K^2 & 0 & 0 \\ 0 & K^2 & 0 \\ 0 & 0 & k^2 \end{vmatrix}, \quad (3)$$

where m is the mass of the rocket and any small difference between the moments about the two transverse axes has been neglected since it will have no effect on the motion. If we rotate the axes through the small angle $-\beta_{Dx}$ about the y -axis and through the small angle β_{Dy} about the x -axis, we obtain¹³ the tensor of inertia for a system with origin at O and axes parallel to those of the $O'xyz$ system, the result being

¹³ E. T. Whittaker, "Analytical Dynamics," ch. V. Dover, 1944. J. O. Slater and N. H. Frank, "Mechanics," p. 96, p. 272. McGraw-Hill.

$$m \begin{vmatrix} K^2 & 0 & -(K^2 - k^2)\beta_{Dx} \\ 0 & K^2 & -(K^2 - k^2)\beta_{Dy} \\ -(K^2 - k^2)\beta_{Dx} & -(K^2 - k^2)\beta_{Dy} & k^2 \end{vmatrix}. \quad (4)$$

To go from O to R we must undergo displacements $-x_s$, $-y_s$, and z_R parallel to the $O'x$, the $O'y$ and the $O'z$ axes, respectively. By the usual theorem for the translation of axes (footnote 13), the tensor of inertia for a system with origin at R and axes parallel to those of the $O'xyz$ system is found to be, neglecting terms of order x_s^2 , y_s^2 or x_sy_s ,

$$m \begin{vmatrix} (K^2 + z_R^2) & 0 & -(K^2 - k^2)\beta_{Dx} + z_R x_s \\ 0 & K^2 + z_R^2 & -(K^2 - k^2)\beta_{Dy} + z_R y_s \\ -(K^2 - k^2)\beta_{Dx} + z_R x_s & -(K^2 - k^2)\beta_{Dy} + z_R y_s & k^2 \end{vmatrix}. \quad (5)$$

The orientation of A_R with respect to $O'xyz$ is specified by the complex angle β_R in just the same way that the orientation of A_D is specified by β_D . By reversing the general procedure that carried us from (3) to (4) we can rotate axes until (5) is referred to principal axes and thereby obtain

$$\beta_R = \frac{K^2 - k^2}{K^2 - k^2 + z_R^2} \beta_D - \frac{z_R}{K^2 - k^2 + z_R^2} R_s. \quad (6)$$

We are now ready to consider the motion of the rocket during launching. We use the subscript f to denote the value of a quantity at the instant the front bourrelet leaves the launcher and, as usual, the subscript p to denote the value of a quantity when the rear bourrelet leaves. Thus we denote by ψ_f and ψ_p the angles through which the rocket has rotated about its longitudinal axis during the intervals t_f and t_p , respectively. At t_f the angular velocity lies along the $O'z$ axis and can be resolved into a spin s_f about A_R plus the motion of A_R described in the usual way by the vector \mathbf{q}_f which gives the transverse velocity of the point on A_R unit distance ahead of R . Since β_R is the angle between $O'z$ and A_R , the magnitude of this velocity is $\beta_R s_f$. The velocity is normal to the plane of β_R and hence in the $O'xyz$ system is specified by the complex number $i\beta_R s_f$. But the $O'xyz$ system rotates with the rocket and has turned through the angle ψ_f with respect to the fixed system in which we measure \mathbf{q} . Hence

$$\mathbf{q}_f = i\beta_R s_f \exp(i\psi_f). \quad (7)$$

For the present we assume that no torques, except the axial torque that produces spin, need be considered and we saw above that the nutations can always be ignored between t_f and t_p . This corresponds to neglecting k^2 compared to K^2 , which we do throughout the rest of this section. Hence at t_p the transverse motion of A_R is still given by (7) but the spin about A_R is now s_p . At this instant we wish to transfer from A_R to A_D , which will be the longitudinal axis used to describe the subsequent motion. The spin about A_D may be taken to be s_p ; the transverse motion is obtained by adding to the transverse motion of A_R the motion due to the spin of A_D about A_R with angular velocity s_p , the angle between the axes being $\beta_D - \beta_R$. By the same argument that led to (7) this last term is seen to be

$$i(\beta_D - \beta_R)s_p \exp(i\psi_p), \quad (8)$$

and hence the motion during launching is the sum of (7) and (8). If now we use (6) plus the relations for a uniformly accelerated rocket:

$$\begin{aligned}\psi_p &= 2\pi\gamma\zeta_p^2, & \psi_f &= \left(1 - \frac{l_B}{p}\right) 2\pi\gamma\zeta_p^2, \\ s_p &= \frac{4\pi\gamma\zeta_p}{t_\lambda}, & s_f &= \sqrt{1 - \frac{l_B}{p}} \frac{4\pi\gamma\zeta_p}{t_\lambda}\end{aligned}\quad (9)$$

we obtain for the mallaunching due to static and dynamic unbalance,

$$\begin{aligned}q_p &= \frac{4\pi i\gamma\zeta_p}{t_\lambda} \exp(2\pi i\gamma\zeta_p^2) \left\{ R_s \frac{z_R}{K^2 + z_R^2} \left[1 - \sqrt{1 - \frac{l_B}{p}} \exp \frac{(-2\pi i\gamma\zeta_p^2 l_B)}{p} \right] \right. \\ &\quad \left. + \beta_D \left[\frac{z_R^2}{K^2 + z_R^2} + \frac{K^2}{K^2 + z_R^2} \sqrt{1 - \frac{l_B}{p}} \exp \frac{(-2\pi i\gamma\zeta_p^2 l_B)}{p} \right] \right\}.\end{aligned}\quad (10)$$

In (10) the contributions of static and dynamic unbalance are separated and it may be seen that their resultant could be much smaller than either if the dynamic axis is skewed in the right direction. However, in such case mirroring the mass distribution in the Oxz plane (thus changing β_D to its conjugate) or spinning the rocket in the opposite direction will change the mallaunching enormously even though the mass distribution is apparently but little changed.

In addition to the mallaunching, dynamic unbalance causes an initial cross-pointing and an initial yaw, but these terms are small and may be neglected. They may be computed if desired by keeping track of the motion of the center of mass and of the orientation of A_D in the above discussion.

The static and dynamic unbalance are separated because the experimental data indicate that they are independent and because, as discussed in 9.74, it may be desirable to add a term depending on the malalignment due to the static unbalance. As an example of the type of unbalance present in rockets and its effect on the trajectory, the results of measurements of R_s and β_D for 100 3.5/4 GPSR are given in table 9.71 together with the computed values of the mallaunching and the deflection of the trajectory in vacuum.

TABLE 9.71
DYNAMIC UNBALANCE IN 3.5/4 GPSR

Average measured displacement of CG	$R_s=0.0035''$
Average measured angular displacement of dynamic axis....	$\beta_D=0.00053$ radians
Average theoretical mallaunching.....	$q_p=0.064$ radians/sec.
Average theoretical deflection due to mallaunching.....	$\vartheta_s=0.0054$ radians
Average theoretical total deflection (including effects of malalignment, crosspointing and initial yaw).....	$\vartheta_t=0.0059$ radians

Detailed study of the unbalance of these and other rounds showed that each Cartesian component of the deflection had essentially a Gaussian distribution. No correlation was found between the dynamic and static unbalance and the unbalance could not be traced to a single component of the rocket, approximately equal contributions coming from the body and from the motor.

9.73 Expressions for the Unbalance Due to the Addition of a Small Mass.—It is useful to have expressions for the values of R_s and β_D for a perfect rocket of mass m to which a small mass m_1 is added at the point (x_1, y_1, z_1) . It may be shown that with an error of order $(m_1/m)^2$,

$$R_s = m_1 \left(\frac{x_1 + iy_1}{m + m_1} \right), \quad (1)$$

and

$$\beta_D = m_1 z_1 \frac{(x_1 + iy_1)}{m(K^2 - k^2)}. \quad (2)$$

In addition there is a longitudinal shift of the center of mass but this can be neglected. If several such masses are added, the results are additive as long as the resultants are small. If a mass is removed, one has only to use a negative mass for m_1 . These formulas can also be used to tell how to add or remove mass to balance an unbalanced round.

9.74 Effect of Unbalance on Malalignment.—If a rocket is perfect except for a non-uniformly filled head or for a small mass added at a point, the same maldistribution of mass that produces unbalance will produce jet malalignment. We therefore consider now the possibility that the jet malalignment can be split into two parts, one the malalignment relative to the bourrelet axis, the other that due to unbalance. Such a resolution is always possible; it will be useful when the two are essentially independent or when one is considering the effect on the dispersion of changes in mass distribution that do not affect the relation between the jet forces and the bourrelet axis.

The two sources of malalignment are, to a considerable extent, independent in the case of rockets whose bourrelets are on the motor for the manufacture of a rocket is based on geometric not dynamic, controls. Therefore, any error in the location of nozzles, any lack of uniformity in nozzle size, any skewness of the plate containing the nozzles, and any errors in turning out the bourrelets tends to produce mechanical malalignment with respect to the bourrelet axis rather than with respect to the dynamic axis. Gas malalignment, which is due to non-uniform flow of the gas in the absence of any mechanical causes, also depends on the geometry of the rocket rather than on the location of the center of mass and hence is properly measured with respect to the bourrelet axis. Some of these factors may introduce some unbalance also but in general they will not produce much.

On the other hand anything that shifts the mass distribution without changing the relation of the nozzles to the bourrelet axis will introduce both malalignment and unbalance, the malalignment being expressible in terms of the unbalance. Important factors of this kind are lack of symmetry of the head or fuse, skewness in the junction of the head and motor, and the addition or removal of weight as in dynamic balancing. When any of these factors are to be considered their simultaneous influence on unbalance and malalignment is best accounted for by expressing their contribution to the malalignment in terms of the unbalance.

The linear and angular malalignments, R_M and β_M , were defined in 2.24 in terms of statement that the jet forces acting on the rocket are equivalent to a force mG_J acting along the dynamic axis A_D , a force $mG_J\beta_M$ acting normal to this axis at the center of mass, an axial torque

$$mk^2\alpha = \frac{2\pi mk^2 G_J}{\nu}, \quad (1)$$

and a transverse torque equal to that produced by a transverse force $-mG_J R_M$ acting on A_D unit distance ahead of the center of mass. In the treatment of malalignment given in 9.2 it was necessary to base this resolution of forces on the dynamic axis. Now, however, it is desirable to base it on the bourrelet axis and we shall say in this section that the jet forces are equivalent to a thrust mG'_J along the bourrelet axis, a force $mG'_J\beta_M$ acting normal to this axis at O' , which is the foot of the perpendicular from the center of mass to the bourrelet axis, an axial torque $mk^2\alpha' \approx 2\pi mk^2 G'_J/\nu$, and a transverse torque equal to that produced by a transverse force $-mG'_J R'_M$ acting on the bourrelet axis unit distance ahead of O' .

Next consider the relations connecting β_M and R_M with β'_M , R'_M , β_D , and R_S . The force mG'_J along the bourrelet axis can, to a good approximation, be taken to be equal to the force mG_J along A_D plus the force $-mG_J\beta_D$ normal to A_D . To get $mG_J\beta_M$, the total force normal to A_D , we must add to $-mG_J\beta_D$ the force $mG'_J\beta'_M \approx mG_J\beta'_M$ which is normal to the bourrelet axis. Hence, approximately, the angular malalignment is

$$\beta_M = \beta'_M - \beta_D. \quad (2)$$

In a similar way we get for the linear malalignment,

$$R_M = R'_M - R_S - \frac{2\pi i k^2}{\nu} \beta_D, \quad (3)$$

the last term coming from the fact that the torque along the bourrelet axis has a component normal to A_D .

The deflection of the trajectory due to angular malalignment can be neglected but the deflection due to linear malalignment should be considered by the inclusion of an effective mallaunching due to malalignment as discussed in 9.25. By 9.25 (2) the effective mallaunching is

$$q_p = -\frac{v_\lambda E_\infty (2\gamma^{\frac{1}{2}} \zeta_p)}{2\gamma^{\frac{1}{2}} K^2} \left[R'_M - R_S - \frac{2\pi i k^2}{\nu} \beta_D \right]. \quad (4)$$

When this is added to 9.72 (10) it is natural to combine the last two terms of (4) with the corresponding terms of 9.72 (10) to give the effect due to unbalance. This is not quite the total effect as the action of malalignment during launching, which will be considered next, is still to be included.

9.75 Effect of Malalignment During Launching.—In our discussion of unbalance we assumed that the transverse torque was zero whereas we should have taken it to be the torque about R due to the applied forces plus the torque $m\mathbf{r}_R \times \dot{\mathbf{v}}_R$. Of the applied forces, friction and aerodynamic forces are probably negligible during this phase of the motion. Gravitational forces need not be considered here since the tip-off produced in this way has been determined in 4.2. Hence we need consider only the jet forces and the torque $m\mathbf{r}_R \times \dot{\mathbf{v}}_R$. In an ideal rocket these torques would be zero, hence they may be thought of as being due to malalignment. It turns out that the effect of the malalignment during launching is small enough, usually of the order of 10 percent of the effect of the unbalance, so that it can usually be neglected. If the jet forces are resolved with respect to the bourrelet axis and hence described in terms of the primed symbols of the last section, then the torque about R due to jet forces is the same as that due to the application of a transverse force,

$$-mG'_J R'_M - mG_J z_R \beta'_M \approx -mG_J (R'_M + z_R \beta'_M), \quad (1)$$

to the bourrelet axis unit distance ahead of R . The first term is the torque about O' , the second is due to the application of the force $mG'_J \beta'_M$ at a point $|z_R| = -z_R$ ahead of R . In addition to this transverse torque there is the torque $2\pi m k^2 G_J / \nu$ spinning the rocket about the bourrelet axis.

The transverse torque that we require is that normal to A_R , the longitudinal principal axis of the tensor of inertia with respect to R . Hence to (1) we must add $2\pi i m G_J k^2 \beta_R / \nu$, the component normal to A_R of the torque along the bourrelet axis. In addition we must consider the torque $m\mathbf{r}_R \times \dot{\mathbf{v}}_R$, where \mathbf{r}_R is the vector from the center of mass to R and $\dot{\mathbf{v}}_R$ is the acceleration of

R along the launcher. If we let e_L be a unit vector along the launcher and if we locate A_R with respect to the launcher axis by means of the complex vector φ_R in exactly the same way that A_D is located by means of φ , then we have

$$\dot{v}_R \approx G_J e_L, \quad (2)$$

and

$$r_R \approx z_R(e_L + \varphi_R - \beta_R) - R_S. \quad (3)$$

Hence the torque $m r_R \times \dot{v}_R$ is the same as that produced by a transverse force

$$m G_J (R_S - z_R \varphi_R + z_R \beta_R) \quad (4)$$

applied unit distance ahead of R along A_R . Thus the total transverse torque to be considered is

$$m G_J \left[-z_R \varphi_R + R_S + \left(z_R + \frac{2\pi i k^2}{\nu} \right) \beta_R - R'_M - z_R \beta'_M \right]. \quad (5)$$

As long as this equation is written in terms of vectors and is derived by vector diagrams, no reference to transverse coordinate systems is needed, and no difficulty is caused by the fact that for the complex notation φ_R is resolved into components with respect to stationary axes while the remaining vectors are based on a coordinate system that rotates with the rocket. In order to express (5) in terms of complex numbers whose real and imaginary parts refer to the components of the force with respect to stationary axes, it is necessary to multiply all but the first term of (5) by

$$\exp(i\psi) = \exp(2\pi i \gamma \zeta^2). \quad (6)$$

The moment of inertia of the rocket about a transverse axis through R is $m(K^2 + z_R^2)$. Since, as was shown above, the gyroscopic forces can be neglected during launching, the equation of motion is

$$m(K^2 + z_R^2) \ddot{\varphi}_R = -m G_J z_R \varphi_R + m G_J \left[R_S + \left(z_R + \frac{2\pi i k^2}{\nu} \right) \beta_R - R'_M - z_R \beta'_M \right] e^{i\psi}. \quad (7)$$

If the independent variable is changed from t to ζ and if we let

$$a^2 = -\frac{2\lambda z_R}{K^2 + z_R^2}, \quad (8)$$

where a will ordinarily be of the order of 10, we get

$$\varphi''_R - a^2 \varphi_R = a^2 \left[\frac{R_S - R'_M}{-z_R} - \left(1 + \frac{2\pi i k^2}{\nu z_R} \right) \beta_R + \beta'_M \right] \exp(2\pi i \gamma \zeta^2) = a^2 \beta_i \exp(2\pi i \gamma \zeta^2), \quad (9)$$

where

$$\begin{aligned} \beta_i &= \frac{R_S - R'_M}{-z_R} - \left(1 - \frac{2\pi i k^2}{\nu z_R} \right) \beta_R + \beta'_M \\ &= \beta_M - \frac{R_M}{-z_R} + \left(1 - \frac{2\pi i k^2}{\nu z_R} \right) (\beta_D - \beta_R) \\ &= \frac{z_R^2}{K^2 - k^2 + z_R^2} \left(1 - \frac{2\pi i k^2}{\nu z_R} \right) \left(\beta_D - \frac{R_S}{z_R} \right) - \frac{R_M}{-z_R} + \beta_M. \end{aligned} \quad (10)$$

Equation (9) is to be solved subject to the initial conditions that at $\zeta = \zeta_f$,

$$\varphi_R = \beta_R \exp(i\psi_f), \quad \varphi'_R = i t_{\lambda} s_f \beta_R \exp(i\psi_f), \quad (11)$$

the second condition being obtained from 9.72 (7). The solution may be obtained by the Green's function method; it is easily verified that it is

$$\varphi_R = \beta_R \exp(i\psi_f) \left\{ \cosh a(\zeta - \zeta_f) + \frac{it_{\lambda} s_f}{a} - \sinh a(\zeta - \zeta_f) \right\} + a\beta_f \int_{\zeta_f}^{\zeta} \sinh a(\zeta - u) \exp(2\pi i \gamma u^2) du. \quad (12)$$

Our main interest is in q_p . If we subtract 9.72 (7) from the value of $\dot{\varphi}_R(t_p) = \varphi'_R(\zeta_p)/t_{\lambda}$ obtained by differentiating (12) and evaluating the integral approximately by substitution of a power series expansion for $\cosh a(\zeta_p - u)$, we get as the correction to 9.72 (10) due to the refinements now under consideration

$$\begin{aligned} \Delta q_p = & \frac{\beta_R}{t_{\lambda}} \exp(2\pi i \gamma \zeta_f^2) \{ a \sinh a(\zeta_p - \zeta_f) + 4\pi i \gamma \zeta_f [\cosh a(\zeta_p - \zeta_f) - 1] \} \\ & + \frac{a^2 \beta_f}{2\gamma^{\frac{1}{2}}} \left\{ [E(2\gamma^{\frac{1}{2}} \zeta_p) - E(2\gamma^{\frac{1}{2}} \zeta_f)] + \frac{i a^2}{4\pi \gamma} \left[\left(\frac{1}{2} - 2\pi i \gamma \zeta_p^2 \right) (E(2\gamma^{\frac{1}{2}} \zeta_p) - E(2\gamma^{\frac{1}{2}} \zeta_f)) \right. \right. \\ & \left. \left. + \gamma^{\frac{1}{2}} \zeta_p \exp(2\pi i \gamma \zeta_p^2) - \gamma^{\frac{1}{2}} (2\zeta_p - \zeta_f) \exp(2\pi i \gamma \zeta_f^2) \right] + \dots \right\}, \end{aligned} \quad (13)$$

where

$$\zeta_f = \sqrt{1 - \frac{l_B}{p}} \zeta_p. \quad (14)$$

This expression can be regarded as giving the contribution to the mallaunching due to the action of the malalignment over the launching period. To get the complete mallaunching due to both unbalance and malalignment, one must add together 9.72 (10), 9.74 (4) and (13). Ordinarily (13) is much smaller than the other two terms.

9.76 Variation of Dispersion With Launcher Length for Rigid Launchers.—The dispersion of spin-stabilized rockets is due largely to unbalance and to malalignment. The various other effects—dispersion in launching velocity and hence in tip-off, elliptical bourrelets, etc.—are not important in discussing the variation of the total dispersion with launcher length. We use 9.23 (10) to give the approximate deflection due to mallaunching and assume that static and dynamic unbalance and malalignment are all independent. A plot of the deflection due to a static unbalance amounting to 0.0003 foot and corresponding malalignment for the 3.5/4 GPSR is given in figure 9.76a. The deflection has a shallow minimum at $p = 1.3$ feet, but the curve is generally smooth with small variation. The effects of a dynamic unbalance of $\beta_D = 0.0005$ radians and of a malalignment of $R_M = 0.001$ foot are also shown in the figure. Combining these three deflections at random and dividing by $\sqrt{2}$ to obtain the average component in a given direction, we have the result shown in figure 9.76(b). Also given is the resultant dispersion when $R_M = 0.002$ foot. It is apparent from these curves that the dispersion is nearly independent of the launcher length when the latter is greater than 2 feet.

The optimum launcher length may be then chosen for other reasons such as portability or the fact that with a long launcher the tipoff and its variation with temperature are less, so that the sighting problem is simplified. The standard launcher length adopted for the 3.5/4

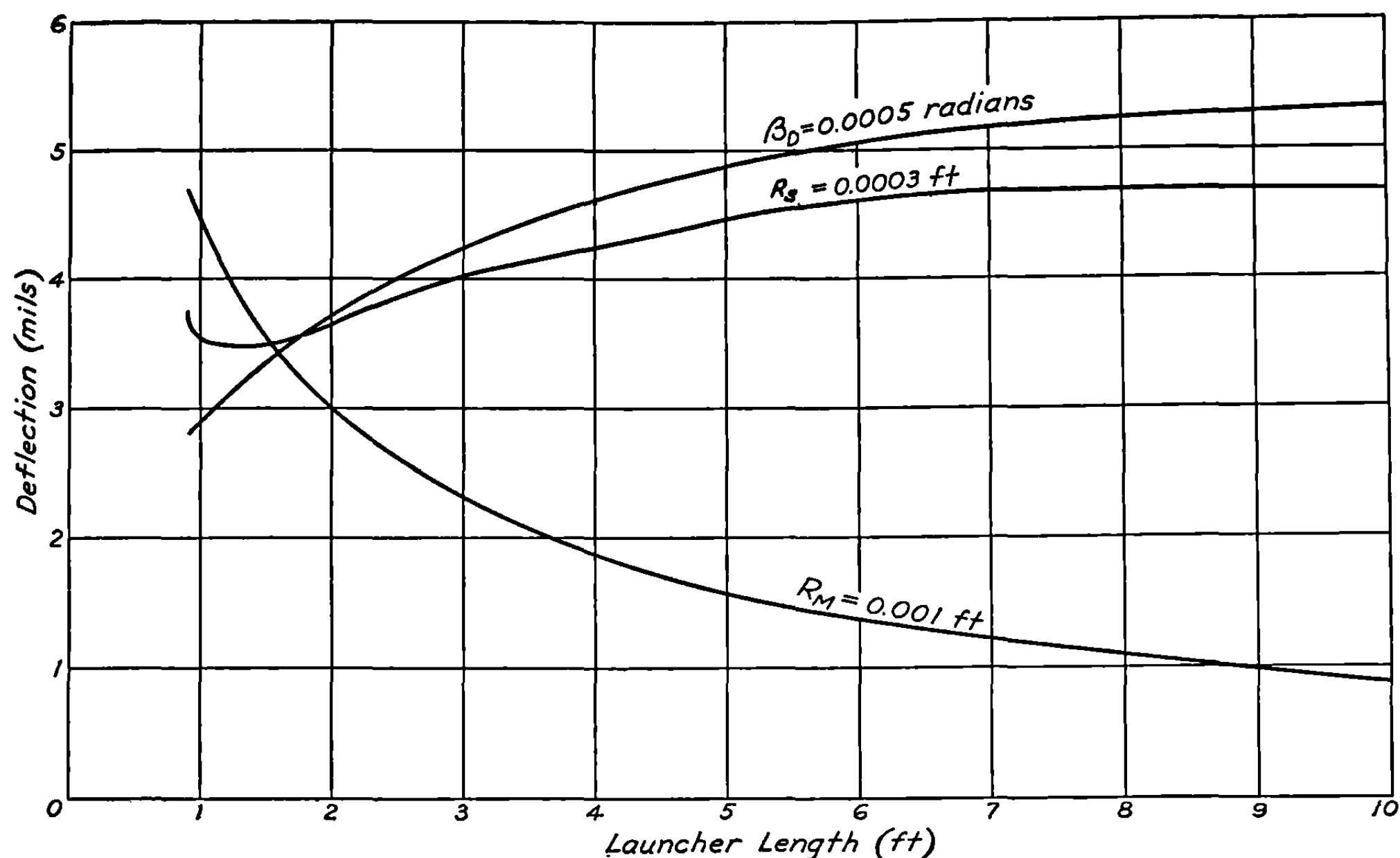


FIGURE 9.76 (a).—Effects of dynamic unbalance, of static unbalance, and of malalignment as functions of launcher length for the 3.5/4 GPSR.

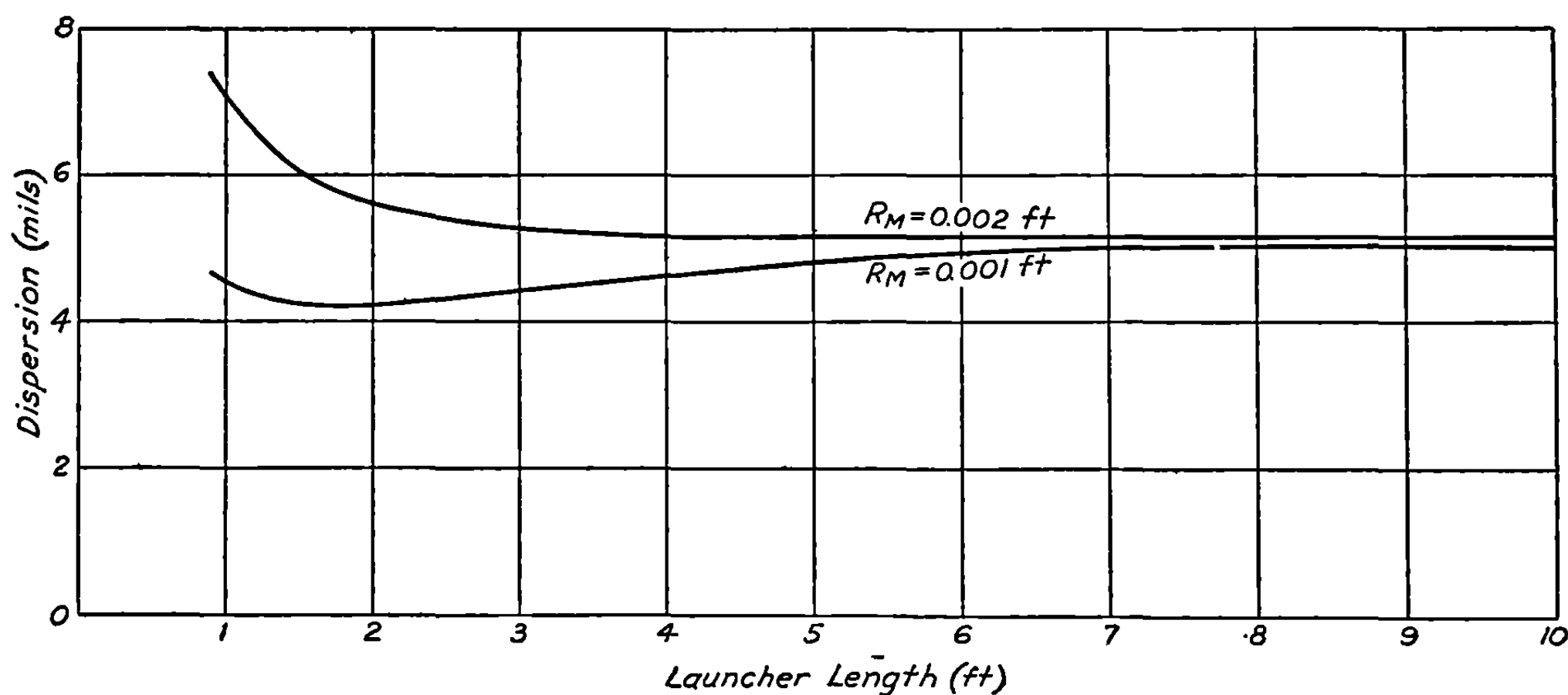


FIGURE 9.76 (b).—Combined effects of unbalance and malalignment as a function of launcher length for the 3.5/4 GPSR.

GPSR after considerable experiment was 2.8 feet, in excellent agreement with the above considerations about dispersion.

9.77 Effect of Elliptical Bourrelets.—We have thus far assumed the bourrelets to be circular and dealt with the mallaunching produced when the dynamic axis does not pass through the centers of the bourrelets. If now we assume that the bourrelets are not circular, then as they rotate against fixed rails, the centers are given transverse velocities which we shall compute below. The mallaunching that results is given by 4.13 (2) since it is just the same as though the bourrelets were circular and the motion of their centers was produced by launcher motion.

We describe a slightly non-circular bourrelet by giving the radius from the dynamic axis as a function of χ , the angle from the $O'xz$ plane of 9.72 around clockwise to r . If we expand r in a Fourier series we can write

$$r=r_0[1+\epsilon \cos 2(\chi-\chi_0)+\dots], \quad (1)$$

where $\epsilon \ll 1$ and the terms in $\sin \chi$ and $\cos \chi$ are omitted since they produce only a circular motion of the dynamic axis and hence are taken care of when we treat dynamic and static unbalance. We also neglect the higher order terms since we wish to consider only the order of magnitude of the effect and since if the short bumps that produce such terms are low enough so that the bourrelet maintains contact with the rails as the rocket rotates only negligible transverse velocities are produced. Effectively then we are supposing the bourrelet to be slightly elliptical.

Suppose the rocket to be firmly pressed by gravity or springs against two parallel rails whose separation is $2r_0 \sin \alpha$, thus defining the angle α . Let X, Y be the coordinates of the center of the rocket in a stationary system whose origin is at the center of an ideal bourrelet and whose X -axis is parallel to the plane of the rails. Then, if ψ is the angle that $O'x$ has rotated through, a somewhat lengthy geometrical calculation shows that, neglecting term of order ϵ^2 , the transverse velocity of the center of the rocket is, in complex notation,

$$\dot{q} = \dot{X} + i\dot{Y} = -2\epsilon r_0 s \left[\frac{\sin 2\alpha}{\sin \alpha} \cos 2(\psi + \chi_0) + i \frac{\cos 2\alpha}{\cos 2} \sin 2(\psi + \chi_0) \right]. \quad (2)$$

This expression can be applied to either the front or rear bourrelet if appropriate values of ϵ and χ_0 are used. Thus from 4.13 (2) an expression for the mallaunching can be developed and from this the deflection of the trajectory is obtained in the usual manner.

Production testing of one 5-inch rocket shows that ϵr_0 averages 0.002 inch for the front and rear bourrelets and that there is no correlation between the two values of χ_0 . It follows that the dispersion due to the elliptical bourrelets is 2 mils, about half of that due to unbalance. In this case, then, the presence of this much ellipticity does not greatly increase the total dispersion. Thus it appears that in rocket production it is necessary to keep in mind the possibility of dispersion due to elliptical bourrelets, but that no more than reasonable care is needed to keep it within bounds.

9.8 Inertial Forces on Spinning Rockets

In the design of rockets it is necessary to consider the forces acting on the various parts in order to be sure that the parts and joints are strong enough and that such devices as the fuzes will operate properly. In this connection gravitational and aerodynamic forces are negligible for spin-stabilized artillery rockets, except in cases where the fuzes might be operated by means of aerodynamic forces. Jet forces, including principally the effects of motor pressure, are very important but their study belongs to interior ballistics. This leaves for consideration here the inertial forces, that is, the forces required to produce the accelerations of the parts of the rocket. The largest of these is the centrifugal force, although the set-back force during burning is far from negligible. A nutational motion, such as that caused by mallaunching, produces very small inertial forces and it will be shown that such forces, as well as the much smaller forces associated with the precessional motion, may be neglected for design purposes.

9.81 Acceleration of the Parts of the Rocket.—The inertial forces on a part of a rocket are equal to its mass times its acceleration; hence we concern ourselves here with the accelerations at various points on a spinning rocket. To indicate orders of magnitude, our results will be illustrated by numerical values for a rocket similar to the 5/5 HCSR at 70° F. We shall assume that the rocket has a linear acceleration, G , of 30 g , a burnt velocity, v_b , of 800 ft./sec., that ν , the feet per turn, is 6.28, and that $\gamma=20$. We shall consider first the case of an ideal

rocket with no mallaunching; consequently it rotates about the dynamic axis. If no parts of the rocket move with respect to it, there are only three accelerations to be considered during burning. First, there is the set-back, the acceleration parallel to the axis of the rocket. This acceleration is G in general and is $30 g$ for our example. Second, at the distance R from the axis there is the acceleration $\alpha R = 2\pi G r \nu$ due to the angular acceleration, α . This acceleration is normal to the axis and to R . For our typical rocket it is $3 g$ at 0.1 feet from the axis. Third, and most important, there is the centrifugal acceleration $s^2 R$ which builds up from zero as the square of the spin, s , to $4\pi^2 v_b^2 R / \nu^2$ at the end of burning. For the typical rocket the centrifugal acceleration at the end of burning is $2000 g$ at 0.1 feet from the axis. If, as is the case with some fuzes, a part of the rocket moves with respect to the rest of the rocket, there is the Coriolis acceleration. This is equal in magnitude to $2s v_{\perp}$, where v_{\perp} is the velocity normal to the axis, and hence builds up from zero to $4\pi v_b v_{\perp} / \nu$ at the end of burning. For the typical rocket, the Coriolis acceleration at the end of burning is $50 g$ if v_{\perp} is 1 ft./sec. Hence, it may be very large if the transverse velocities are large. This force is at right angles to the relative velocity, but may hinder the motion by causing excessive friction. After the end of burning only the centrifugal acceleration and the Coriolis acceleration remain, and these have the same magnitude they had at the end of burning. There are, of course, forces due to the aerodynamic forces decelerating the velocity and spin, but these are very small.

If the rocket is imperfect there may be large forces due to centrifugal forces acting on the displaced parts. Thus if the fuze lies 0.005 feet from the dynamic axis, it is acted on by an acceleration of $100 g$. If the dynamic axis passes 0.001 feet from the center of gravity of the head there is a torque of 300 lb./ft. acting on the joint between the body and the motor.

If the rocket is mallaunched or acquires nutations in any other way, the axis of the rocket wobbles as described in 9.14. It might appear that this would impose large accelerations on the parts of the rocket but the following calculation shows that this is not so. Since the motion may be described as the motion of the axis in a cone plus a rotation about the axis, the acceleration is the vector sum of the accelerations due to the motion of the axis and the rotation. The rotation produces the large centrifugal acceleration considered above. If the mallaunching, or in general the transverse angular velocity of the axis, is q then the axis moves in a cone of half angle $\gamma q / s$ and a point on the axis at a distance l from the center of mass moves in a circle of radius $l \gamma q / s$ with velocity $q l$. Consequently the acceleration of this point, and the acceleration due to the nutation of any point in the same transverse plane, is

$$(q l)^2 \frac{s}{l \gamma q} = \frac{q l s}{\gamma} = \frac{2 \pi v q l}{\lambda}.$$

Hence if we take l to be 1 foot and give q the very large value of 1 radian per second, the acceleration at the end of burning is only $1\frac{1}{4} g$ which is trivial. It is apparent that the only accelerations that will have an appreciable effect on fuze operation or the structural safety of the rocket are centrifugal forces, set-back, and, occasionally, Coriolis forces.

CHAPTER 10

THE MOTION AFTER BURNING

10.0 Introduction

The study of the motion of a spin-stabilized rocket during burning is considerably simplified by the fact that the jet forces are dominant and the burning distance is relatively short. Thus it is possible to regard the velocity and spin as known functions of the time, disregarding in their computation the effects of aerodynamic forces and moments; and even in considering the orientation and direction of motion it is not necessary to consider in detail all of the forces and moments acting on the rocket. On the other hand, after burning nearly all of the aerodynamic forces and moments have observable consequences because they act over such a long time. Moreover, the effects of gravity and drag on the velocity and of gravity on the direction of motion produce large alterations in the trajectory that cannot be described in terms of small, linearized functions. As a result the complete analysis of the motion after burning becomes very involved. The most desirable attack, therefore, appears to be the consideration of a series of simplified examples that illustrate the general character of the motion and that exhibit the various special features in as simple a way as possible. After a feeling for the various characteristics of the motion of a spinning projectile is thus developed, a more elaborate and connected attack on the complete problem is possible.

The simplest, and most important, case is that in which all effects of yaw are neglected; this forms the basis for most trajectory calculations. Chapter 5 is devoted to this case and gives the most important features of the trajectory. There remains for the present chapter only a consideration of cases where the orientation is not parallel to the trajectory. The basic description of the motion is obtained from the case in which the velocity and spin are constant and the only aerodynamic force is a linear overturning moment. The motion is found to consist of the sum of a nutation and a precession, just as during burning. The effect of more general forces in modifying the motion is then considered. This case, using appropriate average values of the spin and velocity, is useful in practice for approximate studies of the motion for limited time intervals since the rates of variation of velocity and spin are usually small. It also provides the basis for an extensive study of stability. These theoretical results are then combined with experimental data obtained from the solar yaw camera to give values of some of the aerodynamic coefficients. All of this leads to both a qualitative and, in some respects, a quantitative understanding of the motion; but there is no close obvious connection with the trajectory calculations of chapter 5 nor with the extension of these calculations to cover the effects on the trajectory of the yaw. These effects include drift to the right (for right-handed spin) and range effects. An attack on the complete problem, including the variation of velocity over the complete trajectory, is therefore attempted. Very complicated expressions result that are difficult to put in explicit, easily interpreted forms. However, expressions for some of the effects of greatest practical importance are reduced to forms that are not too complicated for computation.

It may be wondered why such an involved subject is not dismissed with a statement of the equations of motion and the remark that they can be integrated easily if one uses a suitable high-speed computing machine. It is obvious that this is the best procedure if one wishes to determine the motion of a rocket having specified properties and specified initial conditions—provided the machine is available. But in addition to the cases where the machine is not

available, there are many situations where analytical treatments or physical arguments lead to a better understanding of the character of the behavior than would a numerical calculation.

10.1 The Motion With Linear Aerodynamic Moments and Constant Velocity and Spin

The first case to be considered is that in which the aerodynamic moments and forces are assumed to be linear functions of the yaw, that is, the moment and force coefficients are independent of yaw, and the velocity and spin are assumed to be constant. In this way the equations of motion are reduced to easily handled linear equations with constant coefficients and several small terms are eliminated. Since the aerodynamic forces and moments are approximately linear for small yaw and since the velocity and spin are slowly changing functions, the general character of the motion is given by simplified equations.

10.11 Motion With an Overturning Moment Only.—The coordinates used to describe the motion and the equations of motion can be taken from the previous chapter. It will be recalled that φ denotes the orientation of the rocket, ϑ the direction of motion, δ the yaw, s the spin, γ the ratio of the moments of inertia, m the mass, mK^2 the moment of inertia about a transverse axis, f and F_{\perp} the transverse torque and force, respectively, and S the stability factor. We suppose here that v , the velocity with respect to the ground, equals V , the velocity with respect to the air, and both V and s are constant. Hence the equations of motion are, from 9.11 (5), (11), and (12),

$$\ddot{\varphi} - \frac{is}{\gamma} \dot{\varphi} = \frac{f}{mK^2}, \quad (1)$$

$$V\dot{\vartheta} = \frac{F_{\perp}}{m}, \quad (2)$$

and

$$\varphi - \vartheta - \delta = 0. \quad (3)$$

We are considering the case in which there are no forces and the only torque is the overturning moment, $mK^2k_{v^2\delta}V^2\delta$, so that $F_{\perp}=0$ and

$$\frac{f}{mK^2} = k_{v^2\delta}V^2\delta = \frac{s^2\delta}{4\gamma^2S}. \quad (4)$$

If we orient our axes along the direction of motion, it follows from (2) and (3) that

$$\vartheta = 0, \quad \varphi = \delta. \quad (5)$$

Substitution in (1) gives

$$\ddot{\delta} - \frac{is}{\gamma} \dot{\delta} - \frac{s^2}{4\gamma^2S} \delta = 0. \quad (6)$$

This equation is linear with constant coefficients and has the solution

$$\varphi = \delta = A_N \exp(i\omega_N t) + A_P \exp(i\omega_P t), \quad (7)$$

where

$$\omega_N = \frac{m_N s}{\gamma} = \frac{s}{2\gamma} \left(1 + \sqrt{1 - \frac{1}{S}} \right) = \frac{s}{\gamma} \left(1 - \frac{1}{4S} + \dots \right)$$

and

$$\omega_P = \frac{m_P s}{\gamma} = \frac{s}{2\gamma} \left(1 - \sqrt{1 - \frac{1}{S}} \right) = \frac{s}{4\gamma S} \left(1 + \frac{1}{4S} + \dots \right). \quad (8)$$

If $A_P=0$, the point where the axis intersects the unit sphere moves in a circle of radius A_N with the constant velocity ω_N . Such a motion is called a nutation. As the stability factor approaches infinity; i. e., as the overturning moment approaches zero, the motion approaches the nutational motion in vacuum described in 9.14; while for finite S the motion is somewhat slower. If $A_N=0$, the motion is again circular but now the radius is A_P and the velocity is ω_P . Such a motion is called a precession. It is always slower than the nutation and the velocity approaches zero as S approaches infinity. As S approaches unity, ω_N and ω_P approach $s/2\gamma$ from opposite sides; but (7) does not hold for $S=1$. The general motion described by (7) is epicyclic; that is, it is the sum of the two circular motions that constitute the nutation and precession. It is most helpful to visualize the situation as a rapid motion, the nutation, in a circle about a center whose slow motion constitutes the precession. Usually the nutation has the smaller amplitude. It is important to note that a nutation period is defined by the time required to complete a full revolution in the fixed coordinate system, not by the somewhat longer time required to complete a rotation relative to the rotating radius vector $A_P \exp(i\omega_P t)$. It is useful to note that the nutation and precession may be considered to be the two normal modes of motion of the system.

It follows immediately from these definitions that the number of rotations of the rocket about its longitudinal axis per nutation is

$$R_N = \frac{s}{\omega_N} = \frac{2\gamma}{1 + \sqrt{1 - \frac{1}{S}}}, \quad (9)$$

the number of rotations per precession is

$$R_P = \frac{s}{\omega_P} = \frac{2\gamma}{1 - \sqrt{1 - \frac{1}{S}}}, \quad (10)$$

and the number of nutations per precession is

$$N_P = \frac{R_P}{R_N} = \frac{\omega_N}{\omega_P} = S \left(1 + \sqrt{1 - \frac{1}{S}} \right)^2. \quad (11)$$

These equations can be solved for γ and S very simply, giving

$$\gamma = \frac{R_P}{1 + N_P}, \quad (12)$$

and

$$S = \frac{(1 + N_P)^2}{4N_P}. \quad (13)$$

These relations allow a very simple determination of the stability factor and the ratio of the moments of inertia if measurements are made of R_P and N_P . This can be done very simply by means of the solar yaw camera, described in 10.3, which makes the presence or absence of stability obvious on inspection.

The breakdown of the motion into nutations and precessions is valid in general, but the frequencies are modified by the other aerodynamic moments, and the motion is damped so that the amplitudes of the two component motions vary. In spite of this variation, the relations (12) and (13) hold to a high degree of accuracy.

10.12 Motion With Overturning and Magnus Moments Only.—As the next most simple system, we now treat the motion in the presence of the Magnus moment, $-imK^2k_{v,s}lVs\delta$, as well as the usual overturning moment. In this case we have $F_{\perp}=0$ and

$$\frac{f}{mK^2} = k_{v^2s}V^2\delta - ik_{v,s}lVs\delta = \frac{s^2}{4\gamma^2S}(l-i\Upsilon)\delta, \quad (1)$$

where Υ is the ratio of the Magnus moment to the overturning moment. As in the previous case we have

$$\vartheta=0, \varphi=\delta; \quad (2)$$

but, now, substitution of (1) and (2) in 10.11 (1) gives

$$\ddot{\delta} - \frac{is}{\gamma}\dot{\delta} - \frac{s^2}{4\gamma^2S}(1-i\Upsilon)\delta = 0. \quad (3)$$

The solution of (3) is

$$\varphi=\delta=A_N \exp(i\omega_N t) + A_P \exp(i\omega_P t), \quad (4)$$

where now,

$$\omega_N = \frac{s}{2\gamma} \left(1 + \sqrt{1 - \frac{1-i\Upsilon}{S}} \right),$$

and

$$\omega_P = \frac{s}{2\gamma} \left(1 - \sqrt{1 - \frac{l-i\Upsilon}{S}} \right). \quad (5)$$

Just as in the previous paragraph, the motion is the sum of two normal modes, the rapid one being called the nutation and the slow one the precession (fig. 10, 12). However, since the frequencies are complex, each mode does not consist of uniform circular motion. Suppose that for one mode the frequency is $\omega = \omega_R + i\omega_I$. Then the motion in that mode is

$$\varphi=\delta=A \exp(-\omega_I t) \exp(i\omega_R t), \quad (6)$$

where A is a constant. Thus the motion in each mode follows an equi-angular spiral, the radius vector being $|A| \exp(-\omega_I t)$. If $\omega_I > 0$, the damping is positive and the motion proceeds toward the center of the spiral; if $\omega_I < 0$, the damping is negative and as one proceeds around the spiral in a clockwise direction (since $\omega_R > 0$), one gets farther from the center, corresponding to an increasing amplitude of oscillation. If $k_{v,s}$ is positive, Υ is positive, the imaginary part of ω_N is

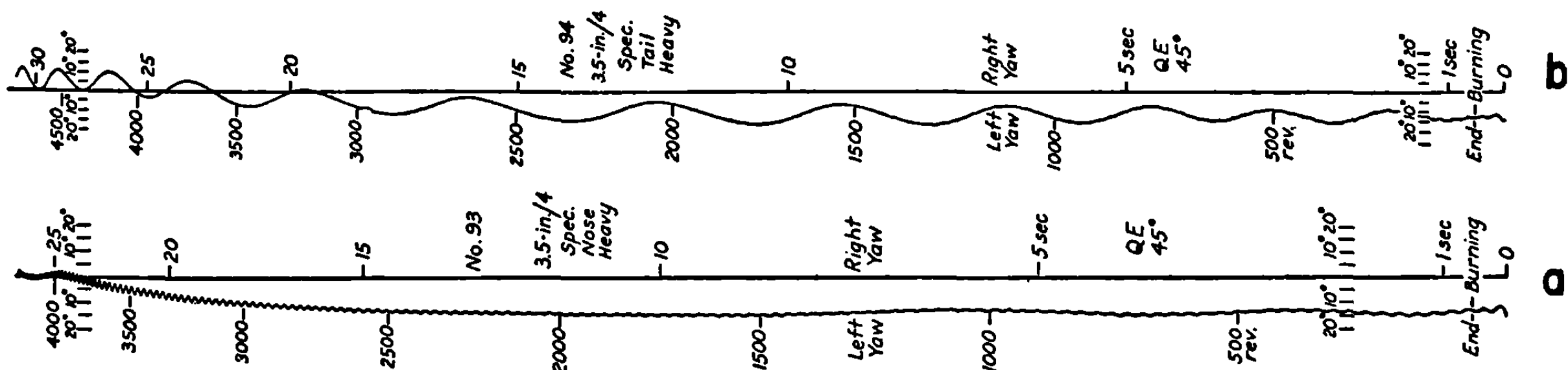


FIGURE 10.12.—Yaw camera records showing one component of the orientation for two rounds whose only essential difference is that the center of mass of round *a* is 2 inches farther forward than that of round *b*. The resulting change in the Magnus moment will account for the differences in the behavior of the nutations, which are the very short oscillations, and the precessions, which are the longer ones. The nutations are strongly damped in case *b*, but in case *a* maintain their amplitude over most of the trajectory and are negatively damped at the summit. The precessions show the reverse behavior, being rapidly damped to zero in case *a* and showing negative damping in case *b*.

therefore positive, and hence the nutation is damped as shown in figure 10.12b. Since the imaginary part of ω_P is the negative of that of ω_N , the damping of the precession will be negative. It is clear that the spiral for the precession will have a few widely spaced turns that are traversed slowly while that for the nutation will have many closely spaced turns that are traversed more rapidly, the magnitudes of the fractional changes in radius per unit time being the same. If $k_{V,s}$ is negative, the damping of the nutation is negative while that of the precession is positive as shown in figure 10.12a. This damping is the principal effect of the Magnus moment although the frequencies of the nutation and precession are also changed slightly.

Experience does not agree with this prediction that either the precession or the nutation will increase exponentially and hence that, unless the initial conditions are precisely right or the Magnus moment is zero, the projectile will always be unstable. Thus we are led to consider the effect of the remaining aerodynamic forces where we shall find that theory predicts a zone of values for the Magnus moment coefficient within which the projectile is stable for arbitrary initial conditions.

10.13 Motion With All Transverse Aerodynamic Forces and Moments.—In the presence of aerodynamic forces the motion is somewhat more complicated because the center of mass moves along a complicated helix-like path as the projectile precesses and nutates. The general behavior is the same as for the simpler cases, however, and we can treat the motion in the same way.

Suppose gravity is absent and V and s are constant so that we have the following forces and moments:

$$\frac{\mathbf{F}_\perp}{m} = (K_{V^2\delta} V^2 - i l k_{V s \delta} V s) \boldsymbol{\delta} + (-l K_{V q} V + i l^2 K_{s q} s) \boldsymbol{\varphi} = A \boldsymbol{\delta} + B \dot{\boldsymbol{\varphi}}, \quad (1)$$

$$\frac{\mathbf{f}}{m K^2} = (k_{V^2\delta} V^2 - i l k_{V s \delta} V s) \boldsymbol{\delta} + (-l k_{V q} V + i l^2 k_{s q} s) \dot{\boldsymbol{\varphi}} = C \boldsymbol{\delta} + D \dot{\boldsymbol{\varphi}}, \quad (2)$$

where we assume the aerodynamic force and moment coefficients to be independent of velocity and yaw. The equations of motion are

$$\ddot{\boldsymbol{\varphi}} - \left(\frac{i s}{\gamma} + D \right) \dot{\boldsymbol{\varphi}} - C \boldsymbol{\delta} = 0 \quad (3)$$

$$V \dot{\boldsymbol{\vartheta}} - B \dot{\boldsymbol{\varphi}} - A \boldsymbol{\delta} = 0 \quad (4)$$

$$\boldsymbol{\varphi} - \boldsymbol{\vartheta} - \boldsymbol{\delta} = 0 \quad (5)$$

where A , B , C , and D are defined by (1) and (2). Eliminating $\boldsymbol{\vartheta}$ by (5) and $\boldsymbol{\varphi}$ by (4), we get from (3)

$$\ddot{\boldsymbol{\delta}} - \left(\frac{i s}{\gamma} - \frac{A}{V} + D \right) \dot{\boldsymbol{\delta}} - \left[\frac{A}{V} \left(\frac{i s}{\gamma} + D \right) + (V - B) \frac{C}{V} \right] \boldsymbol{\delta} = 0. \quad (6)$$

This equation is of the form

$$\ddot{\boldsymbol{\delta}} - i(a + i b) \frac{s}{\gamma} \dot{\boldsymbol{\delta}} - (c + i d) \frac{s^2}{\gamma^2} \boldsymbol{\delta} = 0, \quad (7)$$

where

$$a = 1 + \gamma l K_{V s \delta} + \gamma l^2 k_{s q} \quad (8)$$

$$\begin{aligned} &\approx 1 + \gamma l K_{v\delta}, \\ b &= \frac{\gamma V}{s} (K_{v^2\delta} + l k_{vq}), \end{aligned} \quad (9)$$

$$c = +\frac{1}{4S} (1 + l K_{vq}) - \gamma^2 l^3 K_{sq} k_{v\delta} + \gamma l K_{v\delta} - \gamma^2 \frac{l V^2}{S^2} K_{v^2\delta} k_{vq} + \gamma^2 l^3 K_{v\delta} k_{sq} \quad (10)$$

$$\approx \frac{1}{4S} + \gamma l K_{v\delta},$$

and

$$\begin{aligned} d &= \frac{\gamma V}{s} \{ K_{v^2\delta} + \gamma l^2 K_{v\delta} k_{vq} + \gamma l^2 K_{v^2\delta} k_{sq} - \gamma l k_{v\delta} - \gamma l^2 K_{vq} k_{v\delta} - \gamma l^2 K_{sq} k_{v^2\delta} \} \\ &\approx -\frac{\gamma V}{s} \{ \gamma l k_{v\delta} - K_{v^2\delta} \}, \end{aligned} \quad (11)$$

are constant coefficients.

Solutions of (7) are found by substituting $\delta = A \exp(i\omega t)$ and determining ω by means of the algebraic equation

$$\omega^2 - (a + ib)(s/\gamma)\omega + (c + id)(s/\gamma)^2 = 0. \quad (12)$$

The general solution is

$$\delta = A_N \exp(i\omega_N t) + A_P \exp(i\omega_P t), \quad (13)$$

where

$$\omega_N = \frac{s}{\gamma} (m_N + i\mu_N) = \frac{s}{2\gamma} [a + ib + \sqrt{a^2 - b^2 - 4c + 2i(ab - 2d)}], \quad (14)$$

and

$$\omega_P = \frac{s}{\gamma} (m_P + i\mu_P) = \frac{s}{2\gamma} [a + ib - \sqrt{a^2 - b^2 - 4c + 2i(ab - 2d)}]. \quad (15)$$

Thus each of the normal modes consists of a motion in an equiangular spiral as described in the previous section but the relations between the two modes are somewhat more complicated. In particular, because of the presence of the term ib , it is possible for both modes to have positive or both to have negative damping. If one solves for ϑ or φ one finds that they are also given by expressions of the form of (13) with the same values of ω_N and ω_P but with different values of the constants A_N and A_P .

In order that the motion be stable, both the nutations and precessions must be positively damped; thus necessary and sufficient conditions for stability are that μ_N and μ_P be positive. It is obvious from (14) and (15) that if b is negative the motion must be unstable and that if b is zero it is unstable unless d is also zero. If both b and d are zero, then μ_N and μ_P are zero and we have oscillations of constant amplitude, a situation which could be classed as neutral equilibrium, neither stable nor unstable. Evidently, then, the necessary and sufficient conditions for stability are that b must be greater than zero and greater than the imaginary part of the square root in (14). By the use of the formula¹

$$\text{Im}(u + iv)^{\frac{1}{2}} = \left[-\frac{1}{2}u + \frac{1}{2}(u^2 + v^2)^{\frac{1}{2}} \right]^{\frac{1}{2}}, \quad (16)$$

and considerable manipulation, the latter condition can be put in the form

¹ H. B. Dwight, "Table of Integrals," Revised Ed., Eq. 58.1 to 58.3, New York: Macmillan, 1947.

$$d^2 - abd + b^2c < 0. \quad (17)$$

Let us now convert these conditions to a more usual and useful form. Consider the parabola

$$y = x^2 - abx + b^2c.$$

It is clear that y is greater than zero if x is large enough and is less than zero only if the parabola has real intersections with $y=0$ and if x lies between these intersections. Thus d must lie between these roots if (17) is to hold. Hence, necessary and sufficient conditions for stability are that all of the following hold:

$$b > 0, \quad (18)$$

$$a^2 - 4c > 0, \quad (19)$$

$$d < \frac{b}{2} [a + \sqrt{a^2 - 4c}] \doteq b m_N, \quad (20)$$

and

$$d > \frac{b}{2} [a - \sqrt{a^2 - 4c}] \doteq b m_P. \quad (21)$$

The approximate forms are derived on the assumption that b and d are relatively small compared to a . If we substitute from (8) and (10) in (19) and neglect the smaller terms we find that (19) is equivalent to

$$S > 1 + 2\gamma l K_{V\delta} - 2\gamma l^2 k_{sq} + l K_{Vq} \approx 1 + 2\gamma l K_{V\delta}. \quad (19')$$

This corresponds to the elementary condition that $S > 1$. If (19') is barely satisfied it becomes difficult to satisfy (20) and (21). If we substitute from (9) and (11) in (18) and the approximate forms of (20) and (21), we get

$$\frac{\gamma V}{s} \{ K_{V^2\delta} + k_{Vq} l \} > 0, \quad (18')$$

$$\frac{\gamma V}{s} \{ k_{V\delta} \gamma l - (1 - m_N) K_{V^2\delta} + m_N k_{Vq} l \} > 0, \quad (20')$$

and

$$\frac{\gamma V}{s} \{ -k_{V\delta} \gamma l + (1 - m_P) K_{V^2\delta} - m_P k_{Vq} l \} > 0. \quad (21')$$

If $2(ab - 2d) \ll a^2 - b^2 - 4c$ so that the first two terms of the binomial expansion can be used in (14) and (15), then the left sides of (20') and (21') become just $m_N - m_P = (a^2 - b^2 - 4c)^{\frac{1}{2}}$ times μ_N and μ_P , respectively; and in this case these conditions are equivalent to the requirement that μ_N and μ_P be positive. If further, we let $a=1$, $c=1/4S$, then m_N and m_P are given by 10.11 (8). If we set $a=1$ and $c=1/4S$ in the exact forms of (20) and (21) and expand the square root by the binomial expansion, we find that they are approximately equivalent to

$$k_{V\delta} \gamma l - \frac{K_{V^2\delta}}{4S} + \left(1 - \frac{1}{4S}\right) k_{Vq} l > 0, \quad (20'')$$

and

$$-k_{V\delta} \gamma l + \left(1 - \frac{1}{4S}\right) K_{V^2\delta} - \frac{k_{Vq} l}{4S} > 0. \quad (21'')$$

These expressions show that when all the forces and moments are considered it is possible for both the nutations and precessions to be stable in contrast to the result when only overturning and Magnus moments are considered. Condition (18) is always satisfied and (19) will always be satisfied if the projectile is spun fast enough. Condition (20'') and (21'') show that the Magnus moment and the damping moment tend to damp the nutations and undamp (i. e., give negative damping to) the precessions while the aerodynamic lift has the opposite effect. But, particularly for large S , the aerodynamic lift is much more important in affecting the precessions than the nutations while the converse is true for the damping moment. Thus there is a range of values of the Magnus moment coefficient where (20'') and (21'') are both satisfied.

The above considerations form a suitable introduction to the problem of stability and are sufficient to enable one to understand the observed motion in many cases of practical interest. However, the assumptions made are too restricted to allow any understanding of the instability that appears near the summit of trajectories having high quadrant elevation. The solar yaw camera (see 10.3) shows that the instability is due to negative damping of the nutations but (20'') gives no indication of this. Since the projectiles are stable near the beginning of the trajectory, (20'') is positive there. As the velocity decreases, $1/S$ decreases, and (20'') must continue to be satisfied at the summit. The curvature of the trajectory does not provide a direct explanation of the instability since, as will be shown in 10.14, it merely adds a slowly varying equilibrium yaw to the solutions already obtained. The correct explanation is that the Magnus moment coefficient is smaller at the summit, where the equilibrium yaw is large, than it is initially, where the yaw is small. Such nonlinear moments will be studied in 10.2.

Necessary and sufficient conditions for stability essentially equivalent to (17) have been given by, among others, Nielsen and Synge² and Kelley and McShane.³ Nielsen and Synge include (19) as an independent condition; but we have seen that this is a consequence of (17). Kelley and McShane reduce their result to a form corresponding to that obtained by adding $s/(4\gamma VS)$ times (18') to (20'') and (21''). The resulting necessary conditions for stability are obviously very convenient, but the fact that they, together with (18') and (19'), are not sufficient conditions for stability make them somewhat less satisfactory than the set (18'), (19'), (20''), and (21''). If one is concerned with the stability of a particular projectile for which the coefficients are known or assumed, perhaps the best procedure is to evaluate (footnote 1) ω_N and ω_P from (14) and (15). If the imaginary parts are positive, the projectile is stable; if one is negative but small compared to the reciprocal of the time during which stability is required, then the lack of stability is unimportant. If the application under consideration requires a definite rate of damping of nutations or precessions rather than mere stability, this too is easily investigated. On the other hand, if one is interested in the effects of the various forces and moments on the stability of projectiles in general, conditions of the form of (20'') and (21'') are the most useful.

In using observations of the motion to determine the aerodynamic coefficients, it is advantageous to measure the fractional increase per nutation in the nutation amplitude, φ_N . This is given by

$$\frac{\Delta\varphi_N \text{ (per nutation)}}{\varphi_N} = -\frac{2\pi\mu_N}{m_N}$$

² K. L. Nielsen and J. L. Synge, "On the Motion of a Spinning Shell," Quarterly of Applied Mathematics, 4: pp. 201-226, 1946.

³ J. K. Kelley and E. J. McShane, Aberdeen Proving Ground Report 446.

$$\begin{aligned}
&\approx -\frac{2\pi\gamma V}{sm_N(m_N-m_P)}\{k_{V\delta}\gamma l-(1-m_N)K_{V^2\delta}+m_N k_{Vq}l\} \\
&\approx -\frac{2\pi\gamma V}{s}\left(1+\frac{3}{4S}\right)\left\{k_{V\delta}\gamma l-\frac{K_{V^2\delta}}{4S}+\left(1-\frac{1}{4S}\right)k_{Vq}l\right\}, \quad (22)
\end{aligned}$$

where the various approximations are the same as in the derivation of (20''). Of the various quantities that determine the value of the expression in braces, this is the most convenient to determine by means of the yaw camera (see 10.3), although $s\mu_N/\gamma$ could be obtained and is the basic quantity measured by some devices. We may denote the amplitude of the precession by φ_P and find in a similar way that

$$\begin{aligned}
\frac{\Delta\varphi_P \text{ (per precession)}}{\varphi_P} &= -\frac{2\pi\mu_P}{m_P} \\
&\approx -\frac{2\pi\gamma V}{sm_P(m_N-m_P)}\{-k_{V\delta}\gamma l+(1-m_P)K_{V^2\delta}-m_P k_{Vq}l\}, \\
&\approx -\frac{2\pi\gamma V}{s}(4S+1)\left\{-k_{V\delta}\gamma l+\left(1-\frac{1}{4S}\right)K_{V^2\delta}-\frac{K_{Vq}l}{4S}\right\}. \quad (23)
\end{aligned}$$

In general, it is more convenient to compute the relative increase per nutation in the precession amplitude since V and S may vary significantly over a precession and since the length of the precession and the value of S vary so much over the trajectory that errors may arise in the interpretation of (23). The required formula is

$$\begin{aligned}
\frac{\Delta\varphi_P \text{ (per nutation)}}{\varphi_P} &= -\frac{2\pi\mu_P}{m_N} \\
&\approx -\frac{2\pi\gamma V}{sm_N(m_N-m_P)}\{k_{V\delta}\gamma l+(1-m_P)K_{V^2\delta}-m_P k_{Vq}l\} \\
&\approx -\frac{2\pi\gamma V}{s}\left(1+\frac{3}{4S}\right)\left\{k_{V\delta}\gamma l+\left(1-\frac{1}{4S}\right)K_{V^2\delta}-\frac{k_{Vq}l}{4S}\right\}. \quad (24)
\end{aligned}$$

Now let us consider the effect of the inclusion of the remaining aerodynamic forces on the expressions for γ and S given by 10.11 (12) and (13). We must now write

$$\frac{\text{Rl } \omega_N}{s} = \frac{1}{R_N}, \quad (25)$$

and

$$\frac{\text{Rl } \omega_P}{s} = \frac{1}{R_P}, \quad (26)$$

where Rl indicates the real part. Now from (14) and (15)

$$\frac{\text{Rl}(\omega_N + \omega_P)}{s} = \frac{a}{\gamma} \quad (27)$$

so that

$$\gamma = \frac{R_N R_P}{R_N + R_P} \quad a = \frac{R_P}{1 + N_P} \quad a = \frac{R_P}{1 + N_P} \{1 + \gamma l K_{V\delta} + \gamma l^2 k_{s\delta}\}, \quad (28)$$

which is just 10.11 (12) except for the factor a , which differs from unity by less than one percent;

hence it is not possible to determine $K_{vs\delta}$ from a knowledge of γ , R_P , and N_P with the present accuracy of measurement.

Using the relation (footnote 1)

$$\text{Rl}(u+iv)^{\frac{1}{2}} = \left[\frac{u}{2} + \frac{1}{2} (u^2 + v^2)^{\frac{1}{2}} \right]^{\frac{1}{2}}, \quad (29)$$

we have, by means of the following reduction and elimination of small terms,

$$\begin{aligned} (\text{Rl } \omega_N)(\text{Rl } \omega_P) &= \frac{s^2}{4\gamma^2} \{ a^2 - [\text{Rl} \sqrt{a^2 - b^2 - 4c + 2i(ab - 2d)}]^2 \} \\ &= \frac{s^2}{4\gamma^2} \left\{ 4c + b^2 - \frac{(ab - 2d)^2}{(a^2 - b^2 - 4c)} + \dots \right\} \\ &\doteq \frac{s^2 c}{\gamma^2}. \end{aligned} \quad (30)$$

From (10), (25), (26), and (30) we then get

$$S \doteq \frac{R_N R_P}{4\gamma^2} \left[1 - \left(\frac{R_N R_P}{4\gamma^2} \right) 4\gamma l K_{vs\delta} \right]^{-1}, \quad (31)$$

where the factor in square brackets is very close to unity. Using (28) we have approximately

$$S \approx \frac{(1 + N_P)^2}{4N_P} \left[1 + \left(\frac{R_N R_P}{\gamma^2} - 2 \right) \gamma l K_{vs\delta} \right], \quad (32)$$

which is 10.11 (13) with an additional correction term which generally is less than five percent of S .

So far we considered only the complex frequencies, ω , which are the same for the oscillations of δ , φ , and ϑ . Because of the yaw, the aerodynamic forces give the center of mass of the projectile a helical motion. To determine the relation between the amplitude of the associated oscillations in ϑ and that of the yaw, we put (13) in (4). We have, neglecting the terms in φ since they can be shown to have only a small effect, an expression that can be immediately integrated to give

$$\vartheta = \frac{\gamma A}{isV} \left[\frac{A_N \exp(i\omega_N t)}{m_N + i\mu_N} + \frac{A_P \exp(i\omega_P t)}{m_P + i\mu_P} \right] \quad (33)$$

The effect due to precession is generally dominant since $|m_N + i\mu_N| > |m_P + i\mu_P|$. Thus the amplitude of the oscillation in ϑ may be taken to be

$$|\vartheta| \approx \frac{\gamma |A| \delta_P}{sV |m_P + i\mu_P|} \approx \frac{4S\gamma V}{s} K_{v^2\delta} \delta_P, \quad (34)$$

where δ_P is the amplitude of the precession of the yaw and (1) and $|m_P + i\mu_P| \approx 1/4S$ have been used in the approximation. This shows that $|\vartheta|$ is of the order of $0.02 \delta_P$ for typical rockets, which shows that the motion is nearly rectilinear and that $\delta \approx \varphi$.

Because of this corkscrew motion of the center of mass there will be a deflection of the trajectory that depends on the phase of the precession at the end of burning and that is of the

order of $0.02 \delta_P$, an effect that may generally be neglected. The distance of the trajectory from the axis of the helix is of the order of one-fourth of the distance traveled per precession times $|\varphi|$ as given by (34). Hence it is about $0.02S\lambda\delta_P$, a quantity that is usually small compared to the diameter of the rocket.

10.14 Effect of Gravity.—Up to now we have considered the motion of the projectile with constant spin and velocity, except for the small deflections caused by the aerodynamic forces. Gravity has two effects, first, to change the magnitude of the velocity, and second, to curve the trajectory. The decrease in velocity means that the coefficients in the equations of motion are no longer constant, but vary slowly with time. This variation does not change the solution over a limited portion of the trajectory but will modify it over a distance in which the coefficients change by an appreciable percentage, and in this case it is necessary to use other methods to solve the equations. A complete treatment is given in 10.4.

The principal result of the curvature of the trajectory is that the rocket has a finite equilibrium yaw such that the aerodynamic moment causes the rocket axis to precess downward at the same rate that the trajectory turns. We may compute the equilibrium yaw by adding to the right-hand side of 10.13 (1) $ig \cos \theta$, the component normal to the trajectory of the acceleration of gravity. Then 10.13 (6) becomes

$$\ddot{\delta} - \left(\frac{is}{\gamma} - \frac{A}{V} + D \right) \dot{\delta} - \left[\frac{A}{V} \left(\frac{is}{\gamma} + D \right) + (V - B) \frac{C}{V} \right] \delta = -\frac{g}{V} \cos \theta \left(\frac{s}{\gamma} - iD \right). \quad (1)$$

The general solution of this equation is obtained by adding to the solution considered in the previous section the particular integral

$$\begin{aligned} \delta_e &= \frac{g \cos \theta (s - i\gamma D)}{A(is + \gamma D) + \gamma(V - B)C} \approx \frac{sg \cos \theta}{\gamma VC} \\ &= \frac{sg \cos \theta}{\gamma V(k_{V^2s} V^2 - ilk_{Vs} Vs)} = \frac{4\gamma Sg \cos \theta}{Vs(1 - iT)}, \end{aligned} \quad (2)$$

where it must be remembered that in the last form S varies with V and s along the trajectory. The general solution is interpreted as the superposition of the oscillations discussed in the previous section on the equilibrium yaw given by (2). For a projectile that spins to the right, the yaw is to the right and, assuming the Magnus moment coefficient to be positive, down. One important effect of the equilibrium yaw is to increase the total yaw and hence increase the nonlinear effects.

The most important result of this equilibrium yaw is that the aerodynamic lift and Magnus force have a resultant to the right and hence the projectile is deflected to the right of the corresponding point trajectory. There is also a vertical drift that affects the range. If δ , as given by the sum of (2) and 10.13 (13) is substituted in 10.13 (4), the solution is just that given by 10.13 (33) plus the term

$$\vartheta_e = \frac{A}{V} \delta_e t = \frac{4\gamma Sg \cos \theta (K_{V^2s} V^2 - ilK_{Vs} Vs)}{V^2 s (1 - iT)} t. \quad (3)$$

Thus the drift is always to the right for projectiles with a right-hand spin and may be up or down depending on whether the center of pressure of the Magnus force is ahead or behind that of the overturning moment.

This gives the average deflection of the trajectory over any time short enough so that V , s , and θ can be regarded as constants. The exact evaluation of the drift in trajectories

where V , s , or θ vary appreciably is very difficult, and simple, accurate formulas for it do not seem to exist. However, fairly good approximations will be obtained later.

10.2 Motion With Nonlinear Aerodynamic Moments and Constant Velocity and Spin

The assumptions that the aerodynamic coefficients are independent of yaw and that the velocity and spin are constant has lead us to relatively simple equations of motion that were solved analytically in the previous paragraphs. Experimental measurements of the overturning moment by means of wind tunnels or water tunnels show that it is not a linear function of yaw; i. e., the coefficient is not constant for yaws greater than about 10° . Records obtained with the solar yaw camera show that the Magnus moment has an even more marked nonlinearity. Since these nonlinearities occur within the range of yaw of practical interest, it is necessary to consider their effects on the motion. This will lead to results of considerable practical importance in a treatment of stability.

If the nonlinearity over the range from zero out to the yaw of interest is not great, then it can be ignored if suitable average constant values, that may depend on the average yaw, are used for the aerodynamic coefficients. In any case this gives a good deal of information about the general character of the motion but there are some features where even qualitative information cannot be obtained with taking explicit account of the nonlinearity.

When the aerodynamic moments are nonlinear, the motion is quite complicated and the equations of motion are intractable analytically. It is necessary to proceed by approximate methods developed from physical concepts. The nutations and precessions cannot be defined in terms of independent normal modes of motion. However, when the stability factor is large enough, the motion will be recognized to consist of approximately circular oscillations whose angular frequency is about s/γ superposed on a much slower motion. The slow motion is defined as the precession, the oscillations as the nutation. This resolution is particularly useful when the amplitude of the nutations is small, the case to which we will devote the most attention. In this case the nutations do not react on the precession, which may be treated as though it alone were present. This is done in 10.23 and 10.24. The nutations are treated on the assumption that the average value of the yaw is known and that all that matters are the values of the aerodynamic coefficients, and perhaps their rates of change, at this yaw, which is determined as a function of time from the precessional motion. The neglect of the change in velocity and spin is a quite satisfactory approximation in the case of the nutations since the changes are usually small even over the period of several nutations needed to treat damping. It is much less satisfactory in the case of the precessions since for steep trajectories the change in velocity from one precession to the next may have more effect on their shape than does the damping computed on the assumption that the velocity is constant.

10.21 Description of the Motion in Terms of Nutations and Precessions.—When the equations of motion are linear, the solution can be expressed in terms of independent normal modes of motion which provide the most satisfactory definitions of the terms nutation and precession. Our problem now is to generalize these definitions to cover the nonlinear case where the equations can not be solved analytically and the motion can not be resolved into normal modes since superposition does not hold vigorously. We have found that a convenient way of describing these normal modes is to say that the axis of the projectile moves around a circle of varying radius, the center of the circle also moving. The former motion is called the nutation and the latter the precession; and we say that the orientation of the rocket is given by $\varphi = \varphi_N + \varphi_P$, where φ_P locates the center of the circle and φ_N defines its radius. Any motion can be resolved into two components in this manner; indeed it can be done in infinitely many

the first term producing a modification of the circular motion produced by the gyroscopic force, f_g . We shall consider only cases in which the modification is small so that the basic circular motion is easily apparent.

The motion produced by \bar{f} is easily found by taking F_\perp to be zero and $f = \bar{f}$ to be constant in 10.11 (1)–(3). The solution is the cycloidal motion

$$\vartheta = 0, \quad \varphi = \delta = \frac{i\gamma\bar{f}}{mK^2s} t + \varphi_N \exp\left(\frac{ist}{\gamma}\right), \quad (3)$$

where φ_N is one of the constants of integration and the others, whose values do not affect the character of the motion, have been set equal to zero. This motion consists of uniform motion about a circle whose center moves with a constant velocity at right angles to the applied force. The first term of (3) gives the velocity of the center of the circle and defines the precession in this case; the second term defines the nutation. The presence of the precessional velocity, q_P , which is given by (3) as

$$q_P = \frac{i\gamma\bar{f}}{mK^2s} \quad (4)$$

is easily understandable since the effect of \bar{f} is to speed A up on the top half of the circle of figure 10.21a and to slow it down on the bottom half. In accordance with (1), the radius of curvature must be somewhat greater on the right where the speed is more than the average and \bar{f} works against f_g and somewhat less on the left where the speed is less than the average and \bar{f} adds to f_g . Hence, instead of a circle the path of A is epicycloidal as indicated in figure 10.21b.

If \bar{f} and f_t are zero and f_r is constant, then A moves in a circle but the connection between the radius and the speed is no longer given by (1), and the angular frequency of the nutations is no longer $\omega_N = s/\gamma$. If we use the relation $q = \omega_N \varphi_N$ and equate the mass times the radial acceleration of A to the radial force, we get

$$mK^2\omega_N^2\varphi_N = (mK^2s/\gamma)\omega_N\varphi_N - f_r,$$

where f_r is taken to be positive if f_r is directed outward. Solving for ω_N we get

$$\omega_N = \frac{s}{2\gamma} \left(1 + \sqrt{1 - \frac{4\bar{f}_r\gamma^2}{mK^2\varphi_N s^2}} \right), \quad (5)$$

where \bar{f}_r has been written to indicate the average over a nutation of f_r , since, if f_r is not constant, this is the relevant quantity. This result is valid even if f and f_t are not zero. It is obvious that (5) is equivalent to the value of ω_N given by 10.11 (8) since by 10.11 (4) $\bar{f}/mK^2 = s^2\delta_P/4\gamma^2S$ and $f_r/mK^2 = s^2\varphi_N/4\gamma^2S$.

Finally we must consider the effect on the motion of f_t acting alone. If we resolve the forces and accelerations tangentially we see that

$$mK^2\dot{q} = -f_t,$$

where the positive direction of f_t is taken to be the direction opposite to q . By integrating this over the period of one nutation we can get the change in q and, by (1), we find the relative

decrease in the nutation amplitude to be

$$\frac{-\Delta\varphi_N \text{ (per nutation)}}{\varphi_N} = -\frac{\gamma\Delta q \text{ (per nutation)}}{s\varphi_N} = \frac{\gamma}{s\varphi_N} \int_0^{2\pi/\omega_N} \frac{f_t}{mK^2} dt \quad (6)$$

Since $q = d\varphi_N/dt$,

$$f_t dt = -\frac{\mathbf{f}_t \cdot \mathbf{q}}{q} dt = -\frac{\gamma \mathbf{f}_t \cdot d\varphi_N}{s\varphi_N}.$$

Also, if Φ_N is the angle through which φ_N has turned as indicated in fig. 10.21a, $|d\varphi_N| = \varphi_N d\Phi_N$ and

$$f_t dt = \frac{\gamma f_t d\Phi_N}{s}.$$

Hence (6) can be put in the forms

$$\frac{-\Delta\varphi_N \text{ (per nutation)}}{\varphi_N} = \frac{\gamma^2}{s^2\varphi_N^2} \oint \frac{-\mathbf{f}_t \cdot d\varphi_N}{mK^2} = \frac{\gamma^2}{s^2\varphi_N} \int_0^{2\pi} \frac{f_t d\Phi_N}{mK^2}. \quad (7)$$

These expressions for the nutational damping are satisfactory even when $\bar{\mathbf{f}}$ and \mathbf{f}_r are not zero, in which case it is permissible to replace $-\mathbf{f}_t$ by $-\mathbf{f}$ if desired.

There is an interesting physical interpretation that can be given to the first form of (7). The numerator in the integrand is the work done by the projectile against the force \mathbf{f}_t , and hence against \mathbf{f} . As was shown in 9.15 this work is done at the expense of the "nutational" kinetic energy, which is

$$E_{\perp} = \frac{1}{2} mK^2 q^2 = \frac{1}{2} m^2 K^2 (s^2/\gamma^2) \varphi_N^2.$$

If one computes from this how much φ_N must decrease when the "nutational" kinetic energy is decreased by the computed amount, one gets (7).

Since \mathbf{f}_{vq} is always directed oppositely to \mathbf{q} so that its contribution to \mathbf{f}_t is always positive, it is easy to see from (7) that the damping moment always increases the stability of the nutations as indicated by 10.13 (20''). If the Magnus moment is a linear function of yaw and $k_{v\delta}$ is positive so that the nose of the projectile tends to rise when it is yawed to the right, it is clear that f_t is positive and the nutations are stable as indicated by 10.13 (20'') and by 10.12. This case is shown by figure 10.21a in which $\bar{\mathbf{f}}$, \mathbf{f}_r , and \mathbf{f}_t are drawn to scale for $\Upsilon = \frac{1}{2}$. (This is purely an illustrative example; in practice Υ is much smaller.) In fact, if the Magnus and overturning moments are both linear, it follows from 10.12 (1) that

$$\bar{\mathbf{f}}/mK^2 = (s^2/4\gamma^2 S)(1 - i\Upsilon) \delta_P,$$

$\mathbf{f}_t = (s^2/4\gamma^2 S)(-i\Upsilon) \varphi_N$. Hence it follows from (6) that $-\Delta\varphi_N/\varphi_N = (2\pi/\omega)(s\Upsilon/4\gamma S)$ while a series expansion of 10.12 (5) and (6) gives the same result multiplied by $(1 - S^{-1})^{-\frac{1}{2}}$. This indicates that (7) is a satisfactory approximation. It is even possible to see qualitatively why, as indicated by the presence of a term in K_v^2 in 10.13 (20''), the aerodynamic lift contributes to the instability of the nutations. The variation in lift during a nutation causes T to move in a small circle with angular velocity ω_N , the displacement of T being 90° behind A since the position of T depends on the transverse velocity. This means that in figure 10.21a T will be displaced toward P_c when A is in the lower of the indicated positions. The consequent change in δ reduces f_t , thus reducing the stability produced by the Magnus moment.

Equations (5) and (7) enable us to treat the nutations for any force system but it is desirable to generalize (3) and (4) somewhat to enable us to deal with precessions in the general case.

The precessional motion is one where $\ddot{\varphi}$ plays as minor a role as possible, and which is not influenced at all by \mathbf{f} , and \mathbf{f}_r . Hence we write the equations of motion, 10.11 (1)–(3) in the form

$$\dot{\varphi} = \frac{i\gamma\bar{\mathbf{f}}}{mK^2s} - \frac{i\gamma\ddot{\varphi}}{s}, \quad (8)$$

$$V\dot{\vartheta} = \frac{\mathbf{F}_\perp}{m}, \quad (9)$$

and

$$\varphi - \vartheta - \delta = 0, \quad (10)$$

and neglect the last term of (8). This leaves us with a set of equations whose solution contains one less arbitrary constant than before, the amplitude of the nutations being the constant that is suppressed. This solution is regarded as the first approximation to the precession. Ordinarily this is all that is required, but if not, the first approximation can be substituted in the last term of (8) and the next approximation obtained. Some appreciation for the connection between this procedure and the definitions adopted in 10.1 can be derived by considering the case treated in 10.11, where $\mathbf{f}/mK^2 = s^2\delta/4\gamma^2S$. From (8), (9), and (10), one can readily obtain the result that the precessional motion is $\varphi_P = A_P \exp(i\omega_P t)$, where in the first approximation $\omega_P = s/4\gamma S$ and in the second $\omega_P = (s/4\gamma S)(1 + \frac{1}{4}S^{-1})$. Comparison with 10.11 (8) shows that the above procedure is equivalent to expanding the solution in powers of $1/S$ and that, when only the first approximation is used, the error is likely to be of the order of this approximation divided by $4S$.

Our confidence in this procedure should be increased by the observation that it provides a relatively simple physical understanding of the various terms in 10.13 (21''). In this case the basic precessional motion of P_c is a circle and we are interested in the modifications of the circular motion. We see from figure 10.21a, which is drawn for the case in which $k_{v,s}$ is positive, that the effect of a positive Magnus moment coefficient is to rotate $\bar{\mathbf{f}}$ counterclockwise from the direction of δ_P . By (4), the direction of \mathbf{q}_P is then such that as P_c moves along it, δ_P increases and the precessions increase in amplitude. If the nutation amplitude is zero, then the damping moment, \mathbf{f}_{vq} , will contribute to \mathbf{f} a small term directed along $-\mathbf{q}_P$; and even when φ_P is not zero, the precessional motion will add such a term to $\bar{\mathbf{f}}$. The effect of this force on the precession is, by (4), to deflect \mathbf{q}_P to the right of where it would otherwise be directed, producing negative damping. The interaction of the aerodynamic lift and the precessional motion causes T to move approximately in a circle which is larger than that associated with the nutation since the force acts longer in one direction, T always staying 90° behind P_c . Thus δ_P , and hence $\bar{\mathbf{f}}$ and \mathbf{q}_P are rotated clockwise from the position they would occupy if the lift were zero, and this leads to a damping of the precession.

It is worth noting that the division of the motion into nutations and precessions was not made in terms of the angular momentum, \mathbf{H} . The division is always made by locating P_c , and the criteria that we have used are that its motion should be as smooth as possible and that $P_c A = \varphi_H$ should change as slowly as possible. Now it happens that for the usual motions of a projectile, the point, P_H , where \mathbf{H} pierces the unit sphere with center at the center of mass lies near our point P_c , the velocity of P_H is $i\gamma\mathbf{f}/mK^2s$, which has the same average value of \mathbf{q}_P , and it is easier to locate P_H unambiguously than to locate our P_c . Hence the division into nutations and precessions is sometimes made by requiring that P_c coincide with P_H . We do not do this since the motion of P_H contains oscillations of frequency ω_N and we want to include them in the nutations.

10.22 Nutations and Precessions With an Overturning Moment Only.—We consider first the important case in which there are no aerodynamic forces and the only aerodynamic moment is the overturning moment.

$$\mathbf{f}_{V^2\delta} = mK^2k_{V^2\delta}V^2\delta = mK^2V^2\delta(k_{V^2\delta,0} + k_{V^2\delta,2}\delta^2 + k_{V^2\delta,4}\delta^4 + \dots). \quad (1)$$

We neglect gravity so that we can take the equilibrium yaw to be zero; although the results can be applied in cases where it is not zero if it is sufficiently small. Then if the nutations are small, $\bar{\mathbf{f}}$ is directed along δ_P , which here equals φ_P . An obvious solution of 10.21 (8) is obtained if the precession consists of motion in a circle with constant yaw at the constant angular velocity

$$\omega_P = \frac{s}{2\gamma} \left[1 - \sqrt{1 - \frac{1}{S}} \right]. \quad (2)$$

For since the yaw is constant, $\bar{\mathbf{f}}$ is constant in magnitude, the rocket cannot tell whether the overturning moment is linear or not, and the solution for a linear overturning moment holds when S and hence ω_P are given values that depend appropriately on δ . The stability factor, S , in (2) is defined as in 8.22 (9) by

$$S = s^2/4\gamma^2V^2k_{V^2\delta}, \quad (3)$$

where $k_{V^2\delta}$ now depends on δ .

Now consider small nutations superposed on the precessions. By 10.21 (7) we can conclude that there is no change in the amplitude of the nutations if we can show that $\mathbf{f}_{V^2\delta}$ does no net work during a complete nutation. Figure 10.22a shows a typical nonlinear variation of $f_{V^2\delta}$ with δ . Figure 10.22b shows two different possible nutational motions, one with small average yaw and one with large. For convenient comparison with Figure 10.22a the center of the circle has been taken on the X -axis in each case, but this does not affect the result. It is not necessary to assume that the average yaw is to the right. The circles indicate the motion of the axis of the rocket; the straight arrows show how the forces producing the aerodynamic moment vary with the position of the axis. The magnitudes of the forces are obtained from figure 10.22a. It is evident that, because of the symmetry, the forces are essentially conservative and do no net work over a nutation. Hence, there is no change in the amplitude of the nutations.

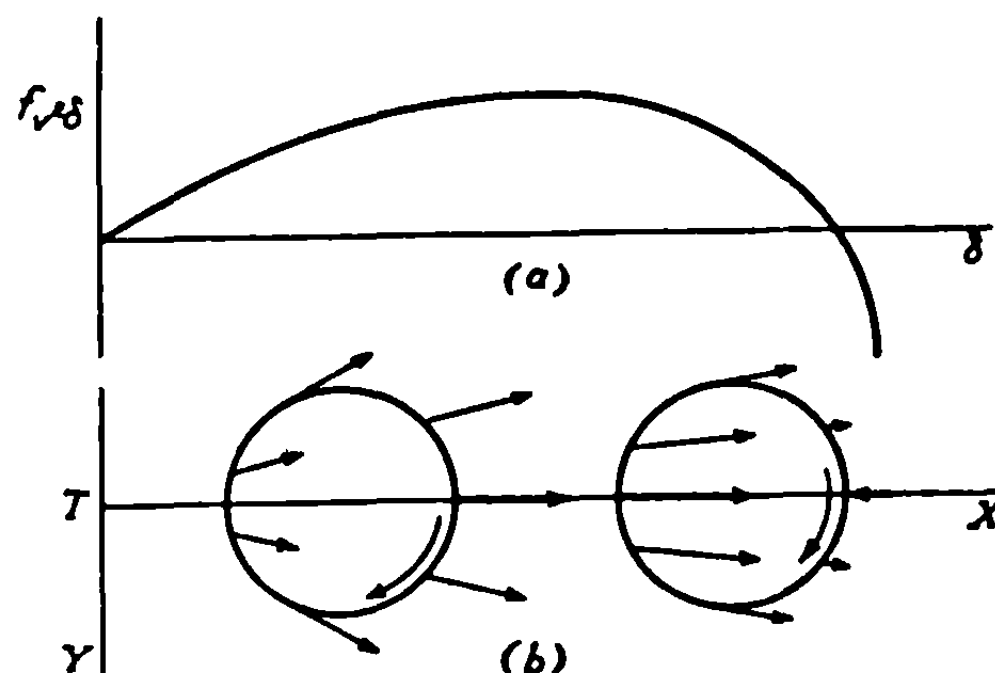


FIGURE 10.22 (a), (b).—Diagram showing that the overturning moment does no net work during a nutation.

The frequency of the nutations will be given by 10.21 (5) if we determine \bar{f}_r . Now, when φ_N is parallel to δ_P , f_r is $\varphi_N \partial f_{v^2\delta}/\partial\delta$; while when φ_N is perpendicular to δ_P , f_r is $\varphi_N f_{v^2\delta}/\delta$ since

$$f_r/\varphi_N = f/\delta.$$

Hence we can assume that

$$\begin{aligned}\bar{f}_r &= \frac{1}{2} \varphi_N \left(\frac{f_{v^2\delta}}{\delta} + \frac{\partial f_{v^2\delta}}{\partial\delta} \right) = mK^2 \varphi_N V^2 \left(k_{v^2\delta} + \frac{1}{2} \delta \frac{\partial k_{v^2\delta}}{\partial\delta} \right) \\ &= mK^2 \varphi_N V^2 (k_{v^2\delta,0} + 2k_{v^2\delta,2} \delta^2 + 3k_{v^2\delta,4} \delta^4 + \dots).\end{aligned}\quad (4)$$

If we define

$$S_N = \frac{s^2}{4\gamma^2 V^2} \left(k_{v^2\delta} + \frac{1}{2} \delta \frac{\partial k_{v^2\delta}}{\partial\delta} \right)^{-1} \quad (5)$$

as the effective stability factor for nutations, then the expression for the nutation frequency takes the form

$$\omega_N = \frac{s}{2\gamma} \left[1 + \sqrt{1 - \frac{1}{S_N}} \right]. \quad (6)$$

Under these circumstances 10.11 (12) and (13) do not hold and it is necessary to have a knowledge of γ to obtain the stability factor. We have

$$S = \frac{R_P^2}{4\gamma(R_P - \gamma)}, \quad (7)$$

$$S_N = \frac{R_N^2}{4\gamma(R_N - \gamma)}, \quad (8)$$

and

$$\frac{S}{S_N} = \frac{N_P^2(R_N - \gamma)}{(R_P - \gamma)}. \quad (9)$$

These relations may be used to determine the nonlinearity in the overturning moment, but unfortunately, not very accurately because S_N depends on the small difference between the nearly equal numbers R_N and γ .

Summing up we may say that the nutation frequency depends primarily upon the derivatives of the moments while that of the precessions depends upon the magnitude of the moments. In the rare cases in which the precession amplitude is small compared to the equilibrium yaw, its frequency also depends upon the derivatives of the moments. In the intermediate case there is no simple expression for the precessions.

10.23 Damping of the Nutations.—We now consider the nutational motion in the presence of all the aerodynamic forces and moments. We treat the case in which the nutations are small compared to the precessions and in which the remaining aerodynamic moments are small compared to the overturning moment so that we may use the motion given in 10.21 as a first approximation. Thus we can use 10.21 (7) to compute the damping of the nutations by computing the work done by the aerodynamic forces per cycle.

We shall make the computation on the assumption that $f_{v\delta}$ and $f_{s\delta}$ are linear but that $f_{v^2\delta}$ and $f_{v\delta\delta}$ are nonlinear. We saw in the previous section that $f_{v^2\delta}$ does no work and hence does not influence the damping. From figure 8.23b it may be seen that $f_{s\delta}$ is always at right

angles to the motion and hence does no work. It may also be seen that $f_{v\alpha}$ always opposes the motion and hence always damps the nutation. The effect of this term is computed below and is shown to be too small to account for the damping observed. Thus the main aerodynamic moment to be considered is the Magnus moment, which may be seen from figure 10.23a and b to do work during the cycle. Figure 10.23a shows an assumed variation of Magnus moment with yaw, and figure 10.23b shows the arrows representing the corresponding forces for two possible motions. The lengths of the arrows are obtained as a function of the yaw from figure 10.23a; their directions are at right angles to the line representing the yaw. It is evident from the left half of the figure that for small yaw the Magnus moment removes kinetic energy, and hence damps the nutation. For sufficiently large yaws, such as that shown in the right half of the figure, the Magnus moment adds kinetic energy so that the nutation is negatively damped and the motion is unstable. The arrows have the directions shown in figure 10.23b when the center of the pressure of the Magnus force is ahead of the center of mass. When the center of pressure is behind the center of mass, the arrows and the forces and moments they represent are reversed. Also the curve for $f_{vs\delta}$ lies below the horizontal axis. If $f_{vs\delta}$ is proportional to δ , it is evident that whatever the yaw, the Magnus moment will tend to damp out the nutations whenever the center of pressure of the Magnus force is ahead of the center of mass. On the other hand, whenever the center of pressure of the Magnus force is behind the center of mass, so that the curve of figure 10.23a is a straight line having a negative slope, one will tend to have negative damping. This is the well-known result obtained in 10.12 and 10.13.

The present method of analysis will show that for nonlinear variations of Magnus moment with yaw, whether one gets positive or negative damping due to the Magnus moment depends on whether $(f_{vs\delta}/\delta + \partial f_{vs\delta}/\partial \delta)$ is greater or less than zero. Figure 10.23a gives the equivalent geometrical method of locating the dividing point between stable and unstable nutational motion. That this point is not the point of maximum Magnus moment, as one would at first expect, is due to the fact that the arrows in figure 10.23b are not perpendicular to the TX -axis except where the circles cross this axis. Consequently, even if the center of the circle corresponds to the yaw at which $f_{vs\delta}$ is a maximum, and if the corresponding forces on the right and left halves of the circle are equal, the forces at the top and bottom of the circle are not perpendicular to the motion but, instead, oppose it, while the forces on the right do more work than do the equal, but differently directed forces on the left of the circle. This is true even for infinitesimally small nutations.

Let us now treat the effect of the Magnus moment quantitatively. We describe the motion of the projectile by the coordinates shown in figure 10.23c. The orientation of the

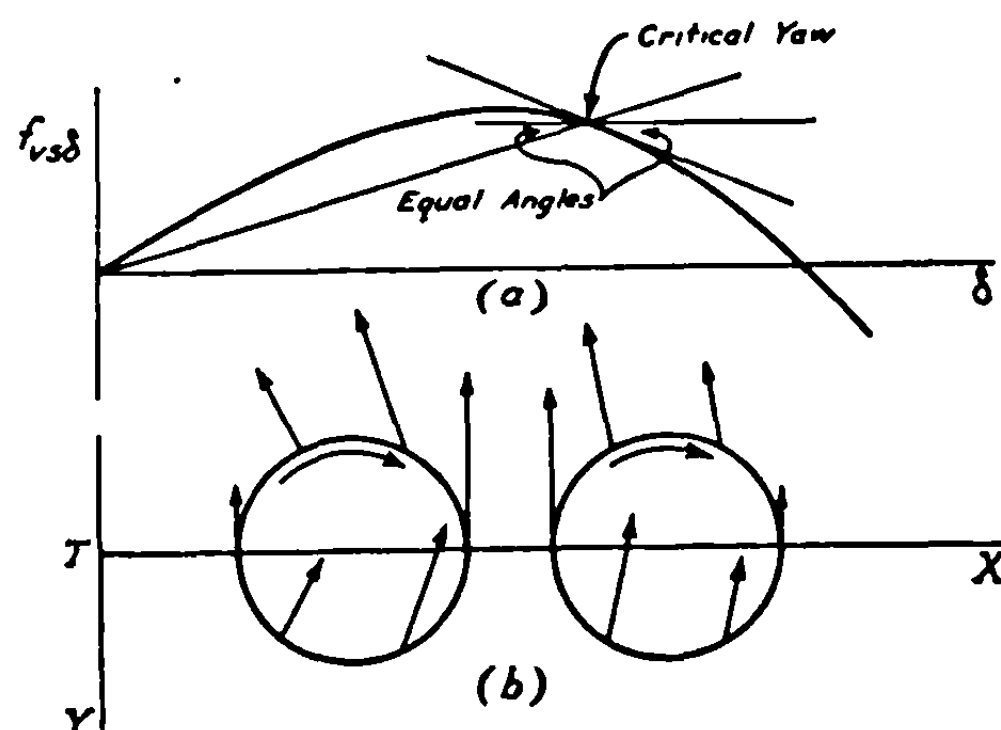


FIGURE 10.23 (a), (b).—Diagram showing that the Magnus moment may remove or add kinetic energy during a nutation.

projectile is located with respect to the tangent to the trajectory by the polar angles δ and D ; the center of the circle about which it nutates is described by the polar angles δ_P and Δ_P ; and the orientation relative to this direction by the polar angles φ_N and Φ_N . We also use the unit vectors \mathbf{i}_z , \mathbf{i}_r , and \mathbf{i}_q , which are along the Z , φ_N , and Φ_N directions, respectively. We have the relations

$$\varphi_N = \varphi_N \mathbf{i}_r, \quad (1)$$

$$\delta_P = \delta_P [\mathbf{i}_r \cos (\Phi_N - \Delta_P) - \mathbf{i}_q \sin (\Phi_N - \Delta_P)], \quad (2)$$

$$\delta = \varphi_N + \delta_P = \mathbf{i}_r [\varphi_N + \delta_P \cos (\Phi_N - \Delta_P)] - \mathbf{i}_q \delta_P \sin (\Phi_N - \Delta_P), \quad (3)$$

$$\delta^2 = \delta_P^2 + \varphi_N^2 + 2\delta_P \varphi_N \cos (\Phi_N - \Delta_P). \quad (4)$$

The Magnus moment is represented by the power series

$$\mathbf{f}_{vs\delta} = \delta \times \mathbf{i}_z m K^2 V s l \sum_n k_{vs\delta, 2n} \delta^{2n}. \quad (5)$$

The element of path length is

$$ds = \mathbf{i}_q \varphi_N d\Phi_N, \quad (6)$$

and the element of work done by the Magnus moment, which is equal to the increase in the kinetic energy, is

$$\begin{aligned} d(KE)_{vs\delta} &= \mathbf{f}_{vs\delta} \cdot d\mathbf{s} = \delta \times \mathbf{i}_z \cdot \mathbf{i}_q \varphi_N m K^2 V s l \sum_n k_{vs\delta, 2n} \delta^{2n} d\Phi_N \\ &= -\delta \cdot \mathbf{i}_r \varphi_N m K^2 V s l \sum_n k_{vs\delta, 2n} \delta^{2n} d\Phi_N \\ &= -[\delta_P \cos (\Phi_N - \Delta_P) + \varphi_N] \varphi_N m K^2 V s l \sum_n \{ k_{vs\delta, 2n} [\delta_P^2 + \varphi_N^2 + 2\delta_P \varphi_N \cos (\Phi_N - \Delta_P)]^n \} d\Phi_N, \end{aligned} \quad (7)$$

where the subscript on the energy (KE), indicates the source of the energy. The work done by the Magnus moment per nutation is

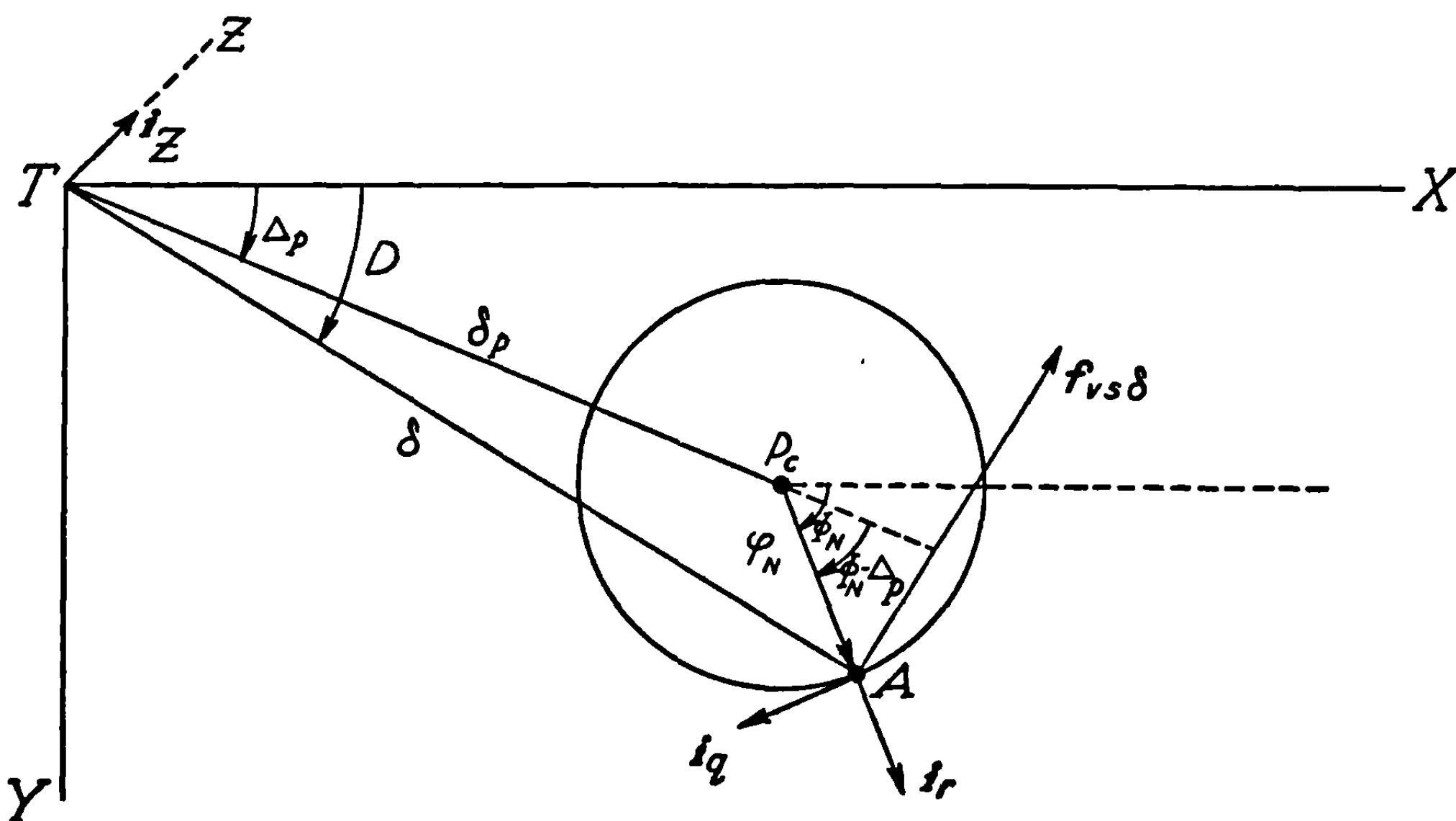


FIGURE 10.23 (c).—The coordinate system used in computing the effect of the Magnus moment.

$$\begin{aligned}\Delta(KE)_{vs\delta} &= \int_0^{2\pi} \frac{d(KE)_{vs\delta}}{d\Phi_N} d\Phi_N \\ &= -2\pi mK^2 \varphi_N^2 lVs [k_{vs\delta,0} + k_{vs\delta,2}(\varphi_N^2 + 2\delta_P^2) + \dots].\end{aligned}\quad (8)$$

For small nutations the term in φ_N^2 is negligible and it is easy to show that the condition that (8) be zero, and hence that the amplitude is constant, is as shown in figure 10.23a.

Let us now compute the work done by the damping moment. We have

$$f_{vq} = -i_q mK^2 k_{vq} lVq, \quad (9)$$

and

$$q = \frac{s}{\gamma} m_N \varphi_N, \quad (10)$$

so that, using (6),

$$d(KE)_{vq} = -\frac{mK^2 k_{vq} lVs m_N \varphi_N^2}{\gamma} d\Phi_N; \quad (11)$$

and, hence,

$$\Delta(KE)_{vq} = -\frac{2\pi mK^2 lVs m_N \varphi_N^2}{\gamma} k_{vq}. \quad (12)$$

Hence, the total change in nutational energy per nutation is

$$\Delta(KE) = -2\pi mK^2 lVs \varphi_N^2 \left[k_{vs\delta,0} + m_N \frac{k_{vq}}{\gamma} + k_{vs\delta,2}(\varphi_N^2 + 2\delta_P^2) + \dots \right]. \quad (13)$$

Now the nutational energy is

$$(KE) = \frac{1}{2} mK^2 q^2 = \frac{mK^2 m_N^2 s^2 \varphi_N^2}{2\gamma^2}. \quad (14)$$

Differentiating, we get

$$d(KE)/d\varphi_N = mK^2 m_N^2 s^2 \varphi_N / \gamma^2. \quad (15)$$

Hence,

$$\frac{\Delta\varphi_N}{\varphi_N} = \frac{1}{\varphi_N} \frac{\Delta(KE)}{d(KE)/d\varphi_N} = -\frac{2\pi\gamma V}{m_N^2 s} \left[l\gamma k_{vs\delta,0} + lm_N k_{vq} + l\gamma k_{vs\delta,2}(\varphi_N^2 + 2\delta_P^2) + \dots \right] \quad (16)$$

gives the logarithmic decrement of the nutations. It depends on the stability factor only through m_N so that it is not very sensitive to the overturning moment or to its nonlinearity. The magnitude of the damping due to the damping moment is about twenty percent of that due to the Magnus moment at small yaw. An interesting feature of the nonlinearity is that the damping rate depends not only on the average yaw but also upon the amplitude of the nutation. If $k_{vs\delta,s}$ is negative, as it usually is, the nutations will build up if they are larger than a critical amplitude but diminish if they are smaller. Thus, if they once exceed this critical amplitude, they are self-sustaining and are very hard to eliminate.

There is one additional effect on the nutations due to aerodynamic forces. What we have computed is the decrease in the nutational energy and hence the decrease in q . By (10), φ_N is proportional to q/s ; and hence, if s changes, the change in φ_N is given by

$$\frac{\Delta\varphi_N}{\varphi_N} = -\frac{\Delta s}{s}. \quad (17)$$

Now, according to 8.22 (4), we have

$$\frac{ds}{dt} = \frac{M_{v_s}}{mk^2} = -lVs k_{v_s}; \quad (18)$$

and, since the nutation period is $\frac{2\pi\gamma}{m_N s}$ we have

$$\frac{\Delta\varphi_N}{\varphi_N} = -\frac{2\pi\gamma}{m_N s} \frac{1}{s} \frac{ds}{dt} = \frac{2\pi\gamma l V}{m_N s} k_{v_s}. \quad (19)$$

Physically the effect of the spin deceleration is to cause the axis to spiral out on the Cornu spiral shown in figure 9.23a rather than in, as during burning. The damping given by (19) is very small, usually about two or three percent of the total, but it should be added to (16) to give the total damping of the nutations. A change in the velocity of the projectile has no direct effect on the amplitude of the nutations.

If the nonlinear terms in (16) are dropped and the result compared with the second form of 10.13 (22), we see that the results are the same except that $m_N(m_N - m_P)$ has become m_N^2 and that the energy method omitted the small term $K_{v^2\delta}/4S$, both small effects. The latter arises from the spiraling of the trajectory due to the lift force, an effect resulting in the motion in a small circle of the point T in figure 10.23c. If this is allowed for, one can obtain the desired term from the contribution of $f_{v^2\delta}$ to f_t in 10.21 (7); but it is easier just to accept the term from 10.13 (22). Hence, the total damping is

$$\frac{\Delta\varphi_N}{\varphi_N} = -\frac{2\pi\gamma V}{m_N^2 s} \left[l\gamma k_{v_s\delta,0} + lm_N k_{v_q} - lm_N k_{v_s} - m_P K_{v^2\delta} + l\gamma k_{v_s\delta,2}(\varphi_N^2 + 2\delta_P^2) + \dots \right]. \quad (20)$$

10.24 Precessions With a Nonlinear Overturning Moment Only.—The treatment of nutations given in the preceding section could be fairly complete because the nutations have a very simple motion. The period is only slightly affected by the aerodynamic forces and the motion of the axis is nearly circular. On the other hand, the precessional motion is determined entirely by the aerodynamic forces and gravity, and is strongly sensitive to nonlinearity in any of the moments. Also, as mentioned in 10.2, the effect of the change in velocity along the trajectory is more damaging to the accuracy of our approximations when dealing with precessions.

We can give a fairly satisfactory description of the precessions by assuming that the nutations are zero and that, at any instant, the angular momentum precesses in the direction of the applied moment. This assumption means that the kinetic energy associated with the precession is small and hence that the stability factor is high. Essentially we are expanding the motion in inverse powers of the stability factor and taking the first term, a procedure which may lead to fractional errors of order of $\frac{1}{4S}$ but which does give the general character of the motion. Neglecting the kinetic energy is equivalent to neglecting the angular accelerations and hence we may set $\ddot{\varphi} = 0$ in the equations of motion. The total moment is given in this approximation by 10.22 (1) and the total force by

$$\frac{F_{\perp}}{m} = ig \cos \theta, \quad (1)$$

so that the equations of motion are

$$-\frac{\dot{s}}{\gamma}\dot{\varphi}=k_{V^2\delta}V^2\delta=\left[k_{V^2\delta,0}+k_{V^2\delta,2}\delta^2+\dots\right]V^2\delta, \quad (2)$$

$$V\dot{\vartheta}=ig\cos\theta, \quad (3)$$

and

$$\varphi-\delta-\vartheta=0. \quad (4)$$

We shall now take $\theta=0$, although if it is desired to consider inclined trajectories it is only necessary to replace g by $g\cos\theta$ throughout. Eliminating φ by means of (4) and ϑ by means of (3) we have

$$\dot{\delta}-i\frac{\gamma V^2}{s}k_{V^2\delta}(\delta)\delta=-\frac{ig}{V}. \quad (5)$$

This is a nonlinear equation of the first order with complex coefficients, and it is not possible to obtain a solution in closed form; but there do exist certain simple particular integrals in which δ remains constant. If we let $\dot{\delta}=0$ in (5) we see that we must have

$$\delta=\delta_e \quad (6)$$

where δ_e is a real root of

$$k_{V^2\delta}(\delta)\delta=\frac{sg}{\gamma V^3}. \quad (7)$$

Now, in general, $k_{V^2\delta}(\delta)\delta$ somewhat resembles a cubic in δ as shown in figure 10.24a. The roots are located by drawing horizontal lines as shown for two possible values of $sg/\gamma V^3$. Thus for small values of $sg/\gamma V^3$ there are three roots, two positive and one negative; while for large values there is only a single negative root. It is desirable that the constants be such that one has the former case, since then the normal behavior of the projectile is to make small precessions about δ_{e1} ; that is, to have a small equilibrium yaw to the right. If, as the projectile slows down at the summit, $sg/\gamma V^3$ should become large enough that there is only the single root on the left, the projectile must start precessing about δ_{e2} ; that is, it will have precessions of large amplitude about a large equilibrium yaw to the left. As $sg/\gamma V^3$ decreases on the descending branch of the trajectory, the equilibrium yaw will usually only shift toward δ'_{e1} although rarely it may return to δ_{e1} . There are no stable precessions about the larger positive root at δ''_{e1} so that the projectile will never remain there long.

The motion may be visualized by plotting the various loci on which the projectile axis may move. Since the loci form closed curves when the only moment is the overturning moment and s and V are constant, the precessional motion progresses around and around the curve on which it is started. These loci might be constructed by a series of numerical integrations, but considerable information about them may be obtained by some simple geometrical considerations and by an investigation of the motion near each of the equilibrium yaws.

To investigate the small precessions around the equilibrium yaw we write

$$\delta=\delta_e+\xi+i\eta, \quad (8)$$

where ξ and η are small. Then since $\delta=\delta_e+\xi$ if we neglect second order terms, we find on expansion of $k_{V^2\delta}$ in a Taylor's series about δ_e that (7) and (8) enable us to reduce (5) to

$$\dot{\xi}+i\dot{\eta}-\frac{i\gamma V^2}{s}\left\{k_{V^2\delta}(\xi+i\eta)+\delta_e\frac{\partial k_{V^2\delta}}{\partial\delta}\xi\right\}=0, \quad (9)$$

if we retain only first order terms and remember that $k_{v^2\delta}$ and $\partial k_{v^2\delta}/\partial\delta$ are to be evaluated at δ_e . Equating real and imaginary parts we obtain two equations whose simultaneous solution is easily found (as may be verified by substitution) to be

$$\xi = \xi_0 \cos \omega_P (t - t_0), \quad \eta = \eta_0 \cos \omega_P (t - t_0), \quad (10)$$

with

$$\omega_P = \frac{\gamma V^2}{s} \left[k_{v^2\delta} \frac{\partial (\delta k_{v^2\delta})}{\partial \delta} \right]_{\delta_e}^{\frac{1}{2}} \doteq \frac{s}{4\gamma S_N}, \quad (11)$$

$$\eta_0 = \left[\frac{1}{k_{v^2\delta}} \frac{\partial (\delta k_{v^2\delta})}{\partial \delta} \right]_{\delta_e}^{\frac{1}{2}} \xi_0 \doteq \frac{S}{S_N} \xi_0, \quad (12)$$

where S and S_N are defined by 10.22 (3) and (5) and we consider only oscillations about stable equilibrium yaws, the ones where the square roots are real. Hence the projectile precesses in an ellipse about the equilibrium yaw with the ratio of major to minor axis independent of the amplitude. If $\ddot{\varphi}$ had not been ignored in (2) we should have found the angular velocity

$$\omega_P = \frac{s}{2\gamma} \left[1 - \left(1 - \frac{1}{S_N} \right)^{\frac{1}{2}} \right] \quad (13)$$

instead of (11), but the error is not large.

At the other equilibrium yaw where $k_{v^2\delta}$ and $\partial k_{v^2\delta}/\partial\delta$ have opposite signs, ω_P becomes imaginary. Hence the motion is unstable and no small precessions exist. In this case the solution has the form

$$\xi = \xi_1 e^{p't} + \xi_2 e^{-p't}, \quad \eta = -R\xi_1 e^{p't} + R\xi_2 e^{-p't}, \quad (14)$$

with

$$p = \frac{\gamma V^2}{s} \left[-k_{v^2\delta} \frac{\partial (\delta k_{v^2\delta})}{\partial \delta} \right]_{\delta_e}^{\frac{1}{2}}, \quad (15)$$

and

$$R = \left[-\frac{1}{k_{v^2\delta}} \frac{\partial (\delta k_{v^2\delta})}{\partial \delta} \right]_{\delta_e}^{\frac{1}{2}}. \quad (16)$$

Hence as long as ξ and η are sufficiently small, the precession is a motion along a hyperbolic path whose asymptotes have the slope $\pm R$. For large values of ξ and η , the motion is much more complicated.

Let us consider an illustrative numerical example. Suppose that

$$k_{v^2\delta} = \frac{1}{2} (3 - \delta^2), \quad sg/\gamma V^2 = \frac{1}{2}, \quad (17)$$

which corresponds to the lower line of figure 10.24a. We find from the roots of (7) that the stable equilibrium yaw to the right is at $\delta_e = 0.347$ radians and that for small oscillations about this point $\eta_0/\xi_0 = 0.99$ and $\omega_P/\omega_{P1} = 0.95$, where ω_{P1} is the precessional frequency when only the linear term is retained so that $k_{v^2\delta} = 3/2$. Thus the motion around the normal equilibrium yaw is only slightly affected by the nonlinearity even in this case where a decrease of 26 percent in the velocity would remove this equilibrium yaw, leaving only the one on the left. Returning to the roots of (7), we find that the other stable equilibrium yaw is at $\delta_e = -1.879$ radians and that $\eta_0/\xi_0 = 3.78$ and $\omega_P/\omega_{P1} = 0.67$. Here the motion is completely different from the linear case as would be expected, since then the only equilibrium yaw is at $\delta_e = +0.333$ radians. The unstable root of (7) is at $\delta_e = 1.532$ radians with $R = 2.49$ and $p/\omega_{P1} = 0.54$.

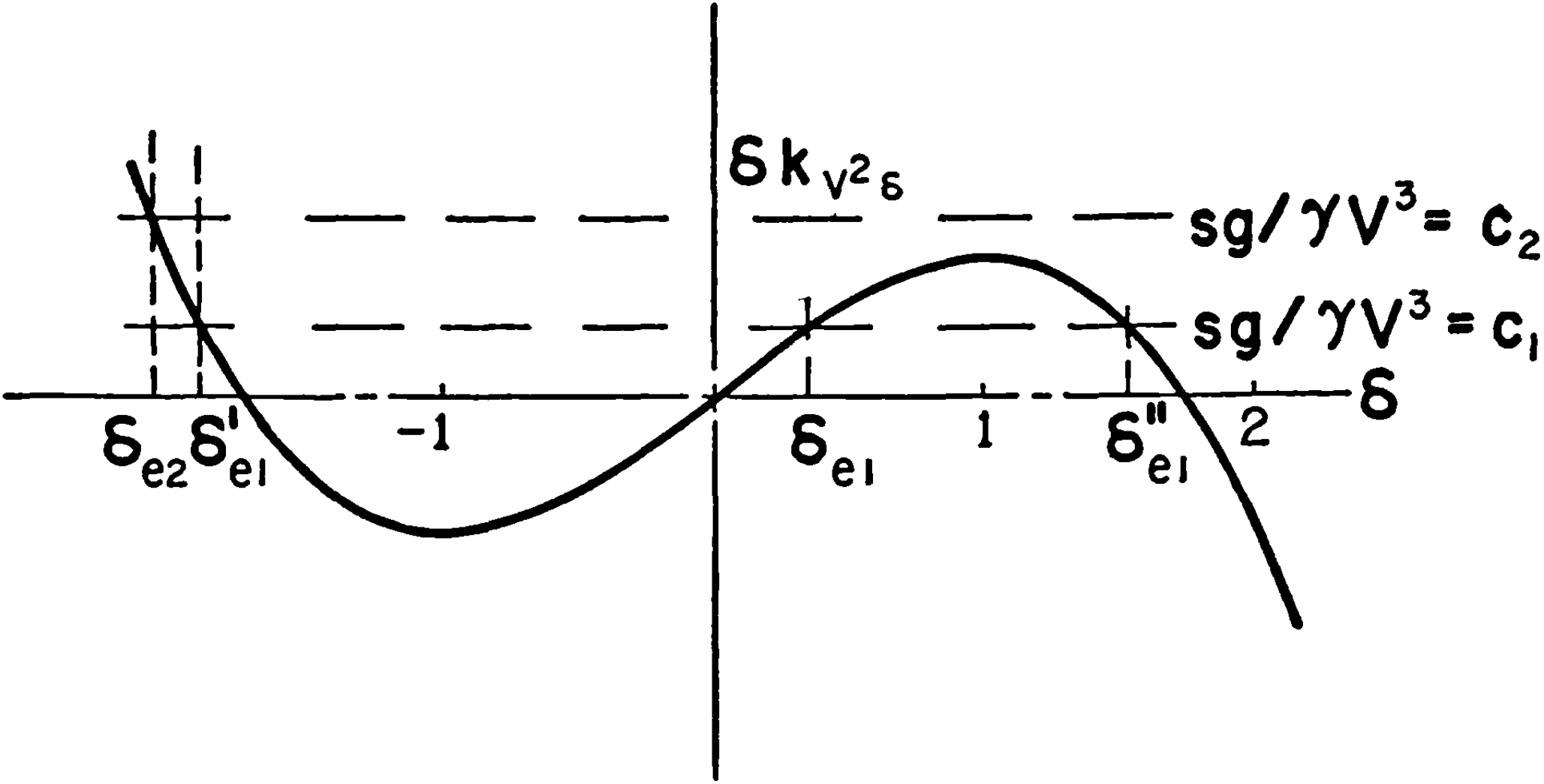


FIGURE 10.24 (a).—Determination of the equilibrium yaw.

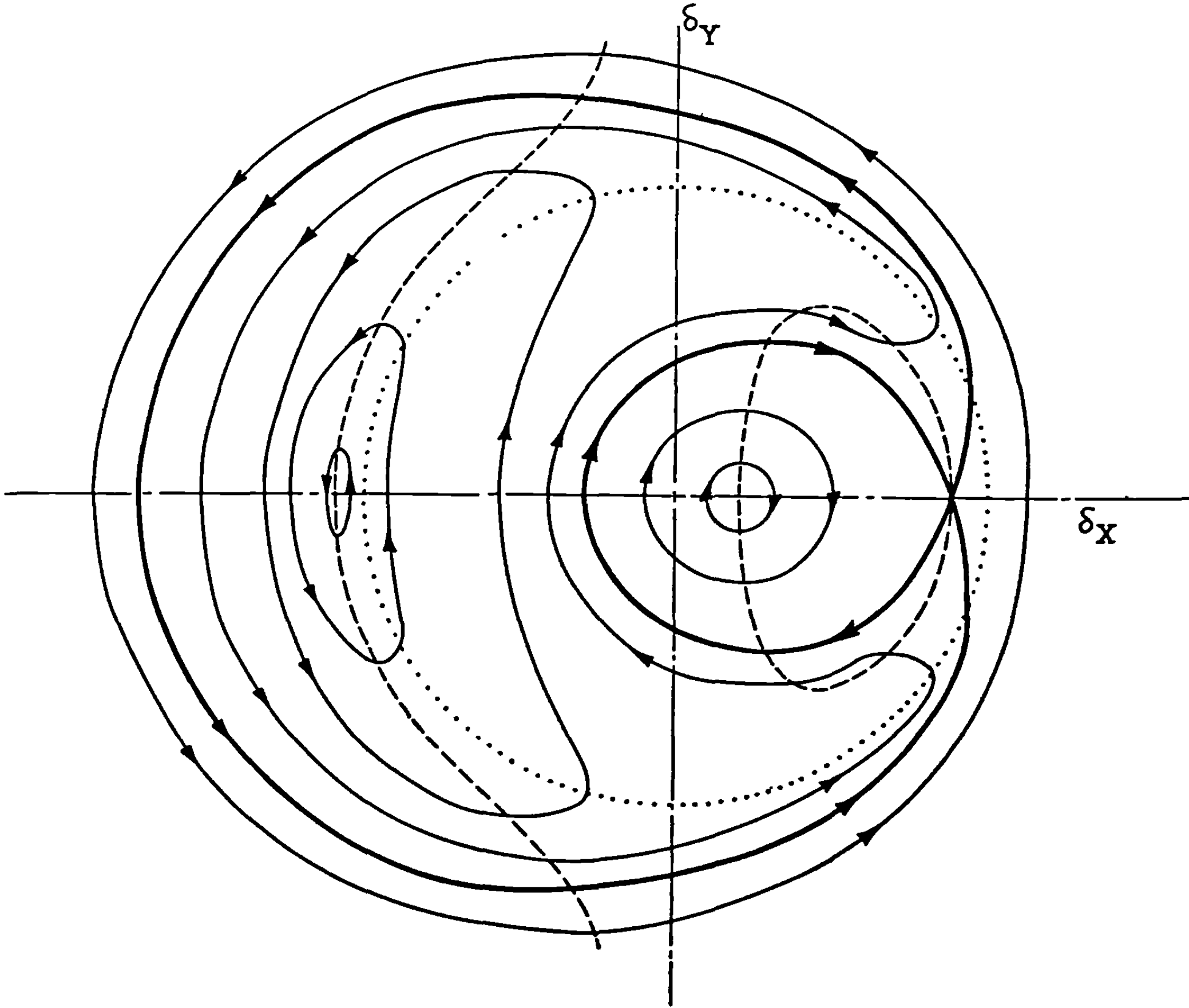


FIGURE 10.24 (b).—Precessional motion with a nonlinear overturning moment only.

The motion when the precessions are large is more complicated, but may be obtained geometrically fairly easily if too great accuracy is not required. We can learn several things about the motion which allow us to draw its loci in most circumstances. First, we know the character of the motion near the equilibrium yaws. Second, we know that it is only near the critical points (the equilibrium yaws) of the differential equation that the motion changes discontinuously. Third, we see that on the real axis, and on the circle on which $k_{v^2\delta}$ and the moment are zero, the loci have a vertical tangent because the rate of precession in the X -direction is zero. Fourth, we may obtain the locus of the horizontal tangents by putting $\dot{\delta}_v = 0$ in the imaginary part of (5), getting, with the aid of 10.22 (1),

$$\delta_x = \frac{sg}{\gamma V^3} \frac{1}{k_{v^2\delta,0} + k_{v^2\delta,2}\delta^2}. \quad (18)$$

The locus (18) is plotted dashed in figure 10.24b for the case of (17). Shown dotted is the circle $f_{v^2\delta} = 0$ where the precessions are vertical. It may be noted that the equilibrium yaws are at the juncture of the locus of horizontal tangents and the real axis where the tangents are vertical. Actually both velocity components are zero and the slopes are indeterminate at these points. From this information the general shapes of the loci are easily obtainable, and if necessary it is possible to compute the slope of the loci at several points to guide us in drawing the curves. The heavy solid lines are tangent to the asymptotes at the unstable equilibrium point and divide the remainder of the loci into three groups, two enclosing only one stable equilibrium yaw and one enclosing all three equilibrium yaws. The general character of each of these three groups of loci are shown along with the small amplitude case in the first two groups. It is apparent that even for precessions large compared to the stable right equilibrium yaw the precessions are still only slightly deformed. Experimentally only these precessions have been observed, so that in the future we shall concentrate our attention upon them, ignoring the precessions about the left equilibrium yaw. This procedure will allow us to study the effects of the other aerodynamic forces without excessive complication. The effect of the other aerodynamic forces and gravity is twofold; first they shift the positions of the equilibrium yaws slightly, and second, they generally change the closed curves into spirals which may either wind onto or unwind from the stable equilibrium yaws, although they may leave some isolated closed loci under certain circumstances. The motion about the unstable equilibrium yaw is not greatly altered although the asymptotes are reoriented.

10.25 Precessions With General Nonlinear Aerodynamic Moments.—We now wish to determine the precessions in a more general case involving other aerodynamic forces and moments. The completely general case is very complicated, and therefore we shall neglect several aerodynamic forces and make assumptions concerning the magnitude of the others. We assume that the projectile has constant velocity and spin and has linear lift and Magnus forces, a linear damping moment, but nonlinear overturning and Magnus moments. We also assume that the overturning moment is dominant and that the equilibrium yaw is to the right.

Thus we have the forces

$$\frac{1}{mK^2} \mathbf{f} = (k_{v^2\delta,0} + k_{v^2\delta,2}\delta^2) V^2 \delta - i(k_{v\delta,0} + k_{v\delta,2}\delta^2) V s l \delta - k_{vq} V l q, \quad (1)$$

and

$$\frac{1}{m} F_{\perp} = K_{v^2\delta} V^2 \delta - i K_{v\delta} V s l \delta + i g, \quad (2)$$

where again if inclined trajectories are to be considered, it is necessary to replace g by $g \cos \theta$. The remaining aerodynamic forces have negligible effects. The equations for the precessional motion are

$$\left(k_{vq}Vl - \frac{is}{\gamma}\right)\dot{\varphi} = (k_{v^2\delta,0} + k_{v^2\delta,2}\delta^2)V^2\delta - i(k_{vs\delta,0} + k_{vs\delta,2}\delta^2)Vsl\delta, \quad (3)$$

$$V\dot{\vartheta} = ig + K_{v^2\delta}V^2\delta - iK_{vs\delta}Vsl\delta, \quad (4)$$

and

$$\varphi = \vartheta + \delta. \quad (5)$$

Eliminating φ and ϑ by means of (5) and (4), we have the equation

$$\dot{\delta} + \left\{K_{v^2\delta}V - iK_{vs\delta}sl - \frac{i\gamma/s}{(1 + ik_{vq}\gamma Vl/s)} [(k_{v^2\delta,0} + k_{v^2\delta,2}\delta^2)V^2 - i(k_{vs\delta,0} + k_{vs\delta,2}\delta^2)Vsl]\right\}\delta = -\frac{ig}{V}. \quad (6)$$

The damping moment has very little effect since the term containing it is small compared to unity. We may approximate its effect by expanding the denominator and retaining only the largest term. Doing so, and regrouping the terms, we have

$$\dot{\delta} = \left\{\left[-K_{v^2\delta}V + \frac{k_{vq}}{4S}Vl + k_{vs\delta,0}\gamma Vl + k_{vs\delta,2}\gamma Vl\delta^2\right] + \frac{i\gamma}{s}\left[K_{vs\delta}\frac{s^2l}{\gamma} + k_{v^2\delta,0}V^2 + k_{v^2\delta,2}V^2\delta^2\right]\right\}\delta - \frac{ig}{V} \quad (7)$$

Just as with a nonlinear overturning moment the equation has constant particular integrals corresponding to the equilibrium yaws. Under certain circumstances only one such solution will exist but we are interested in the usual case in which there are three and in particular in the motion about the stable right equilibrium yaw. Equation (7) is of the form

$$\dot{\delta} = (A + iB)\delta - (C + iD)\delta^2\delta - iE, \quad (8)$$

where the coefficients are all positive, except A , which may have either sign but is generally positive.

The equilibrium yaw, δ_e , is found by setting $\dot{\delta} = 0$ in (8) and solving by successive approximations. We may obtain information about the small oscillations about the equilibrium yaw by writing

$$\delta = \delta_e + \xi + i\eta. \quad (9)$$

We shall neglect certain small terms containing the imaginary part of δ_e since the phase of δ_e is small, being the ratio of the Magnus moment to the overturning moment. Expanding (8) and retaining only first order terms we obtain

$$\dot{\xi} + i\dot{\eta} = [(A - C\delta_e^2) + i(B - D\delta_e^2)](\xi + i\eta) - 2(C + iD)\delta_e^2\xi. \quad (10)$$

Separating real and imaginary parts we have

$$\dot{\xi} = (A - 3C\delta_e^2)\xi - (B - D\delta_e^2)\eta, \quad (11)$$

and

$$\dot{\eta} = (B - 3D\delta_e^2)\xi + (A - C\delta_e^2)\eta. \quad (12)$$

Differentiating (11) and eliminating $\dot{\eta}$ and η by (12) and (11) respectively, we have

$$\ddot{\xi} - 2(A - 2C\delta_e^2)\dot{\xi} + [(B - D\delta_e^2)(B - 3D\delta_e^2) + (A - C\delta_e^2)(A - 3C\delta_e^2)]\xi = 0. \quad (13)$$

The solution of this equation is

$$\xi = \xi_0 e^{pt} \cos \omega t, \quad (14)$$

where

$$p = A - 2C\delta_e^2, \quad (15)$$

$$\omega = [(B - 2D\delta_e)^2 - (C^2 + D^2)\delta_e^4]^{\frac{1}{2}} \doteq B - 2D\delta_e^2 \doteq \frac{s}{4\gamma S_N}. \quad (16)$$

The solution for η may be obtained by substitution in (11). It has the same frequency and exponential factor. The condition that the precessions be stable is that

$$A - 2C\delta_e^2 < 0, \quad (17)$$

or

$$K_{V^2\delta} - \frac{k_{V\delta}l}{4S} - k_{V\delta,0}\gamma l - 2k_{V\delta,2}\delta_e^2\gamma l > 0. \quad (18)$$

This, however, is essentially condition 10.13(21'') with the addition of a term to take account of the nonlinearity of the Magnus moment. The term $-K_{V^2\delta}/4S$ is lacking from the (18) because of the neglect of $\ddot{\phi}$ in the equations of motion. Neither change in velocity or spin has any direct effect upon the amplitude of the precessions.

Comparison of (18) with 10.23(20) shows that a nonlinearity of the Magnus moment with $k_{V\delta,2} < 0$ tends to increase the damping of small precessions while it decreases that of small nutations. This result could also be obtained by retaining the term in $\ddot{\phi}$ in the equation of motion and in the expansion (10). The resulting equation would then have solutions for nutations and precessions and the damping rates would be as given above.

If (18) is not satisfied the precessions will get larger, but as they do, the effect of the nonlinearity increases and the precession stabilizes at a finite amplitude. To compute the amplitude of this limiting precession or limit cycle we must investigate possible periodic solutions of (8). We shall not attempt to obtain an exact solution because of the mathematical difficulties of treating nonlinear equations. We can, however, obtain a solution which satisfies (8) on the average. By this we mean that the difference between the true and approximate solutions vanishes when averaged over a complete precession.

When integrated over a cycle, the left-hand side of (8) vanishes for a periodic solution, and we obtain as one condition to be satisfied by our approximate solution

$$0 = (A + iB)\bar{\delta} - (C + iD)\bar{\delta}^2\delta - iE, \quad (19)$$

the bars denoting average values. We obtain another condition from the equation

$$\begin{aligned} \frac{d}{dt} \delta^2 &= \delta \frac{d\delta^*}{dt} + \delta^* \frac{d\delta}{dt} \\ &= 2A\delta^2 - 2C\delta^4 + iE(\delta - \delta^*), \end{aligned} \quad (20)$$

where the asterisk indicates complex conjugate. Integrating over a cycle we obtain

$$2A\bar{\delta}^2 - 2C\bar{\delta}^4 + iE(\bar{\delta} - \bar{\delta}^*) = 0. \quad (21)$$

It is possible to obtain additional conditions by averaging derivatives of higher powers of δ , but these are sufficient for our present purposes. Equation (21) is real and imposes one condition upon the motion, while (19) is complex and hence represents two conditions. With these three conditions we may determine three characteristics of the locus of the motion. We shall take them to be δ_0 and the two parts of δ_{e1} in

$$\delta = \delta_{e1} + \delta_0 e^{i\omega t}, \quad (22)$$

which describes a motion in a circle of radius δ_0 with center at δ_{e1} , which we may assume is near, but not coincident with, the equilibrium yaw δ_e of (9). We have the average values

$$\bar{\delta} = \delta_{e1},$$

$$\bar{\delta}^2 = \delta_{e1}^2 + \delta_0^2,$$

$$\bar{\delta}^4 = \delta_{e1}^4 + \delta_0^4 + 4\delta_{e1}^2 \delta_0^2,$$

and

$$\bar{\delta}^2 \delta = (\delta_{e1}^2 + 2\delta_0^2) \delta_{e1}. \quad (23)$$

Inserting these expressions in (19) and (21) and separating real and imaginary parts, we have

$$A\delta_{e1X} - B\delta_{e1Y} - (\delta_{e1}^2 + 2\delta_0^2)(C\delta_{e1X} - D\delta_{e1Y}) = 0, \quad (24)$$

$$A\delta_{e1Y} + B\delta_{e1X} - (\delta_{e1}^2 + 2\delta_0^2)(C\delta_{e1Y} + D\delta_{e1X}) = E, \quad (25)$$

and

$$A(\delta_{e1}^2 + \delta_0^2) - C(\delta_{e1}^4 + \delta_0^4 + 4\delta_{e1}^2 \delta_0^2) = E\delta_{e1Y}. \quad (26)$$

Multiplying (24) by δ_{e1X} and (25) by δ_{e1Y} , adding, and then subtracting from (26) we have

$$A\delta_0^2 - C(\delta_0^4 + 2\delta_{e1}^2 \delta_0^2) = 0. \quad (27)$$

Equation (27) will have a finite real root for δ_0 if (17), the condition for damped precessions, is violated. From (27) we have

$$\delta_0^2 = \frac{A - 2C\delta_{e1}^2}{C}, \quad (28)$$

so that the diameter of the locus decreases as δ_{e1} increases and becomes zero; i. e., even small precessions are damped, when $\delta_{e1}^2 = A/2C$.

We must approximate further to evaluate δ_{e1} . We assume that B , which contains the overturning moment, is large compared to the quantities

$$A, C\delta_{e1}^2, \text{ and } D\delta_{e1}^2, \quad (29)$$

and that these terms are of the same order of magnitude. Then, by (24), δ_{e1Y} is small compared to δ_{e1X} and we may write

$$\delta_{e1}^2 \doteq \delta_{e1X}^2. \quad (30)$$

Using (30) we see that (25) has three roots which give the three equilibrium yaws. These are

⁴ It would be natural to use the notation δ_F in place of δ_e except that δ_F was used in 10.23 for the quantity we now denote by δ , that is, the yaw after the nutational motion has been removed.

located close to their positions when only an aerodynamic moment is present, as given by 10.24 (7), and two of them may also vanish under certain circumstances. We are interested only in the stable right equilibrium yaw which, neglecting δ_{e1} in (25) and using (28), is approximately

$$\begin{aligned}\delta_{e1x} &\doteq \frac{EC}{BC-2AD+3CD\delta_{e1}^2} \\ &\doteq \frac{EC}{BC-2AD+\frac{3CDE^2}{B^2}}.\end{aligned}\quad (31)$$

Putting (31) in (24) we obtain

$$\delta_{e1y} \doteq \frac{EC^2}{B^2} \frac{(3CE^2-AB^2)}{\left[BC-2AD+\frac{3CDE^2}{B^2}\right]^2}.\quad (32)$$

Using (30) and (31) we have, from (28),

$$\delta_0^2 \approx \frac{A}{C} - \frac{2E^2}{B^2},\quad (33)$$

as a crude approximation. The solutions (31)–(33) may be refined somewhat if desired, but they do give the general character of the motion. A desirable improvement would be to use more parameters in the solution in conjunction with additional conditions similar to (19) and (21). Such a computation, however, becomes bogged down in the algebra and will not be carried out here. The amplitude of the equilibrium precession is sufficiently small so that its locus should be nearly circular, as indicated by figure 10.24b.

Figure 10.25a is a plot of the amplitude of the limit cycle as a function of δ_{e1} . This curve is an ellipse and shows that the limit cycle has nearly constant amplitude for small δ_{e1} and then decreases rapidly to zero as δ_{e1} approaches $\delta_{cp} = (A/2C)^{\frac{1}{2}}$, the yaw at which small pre-

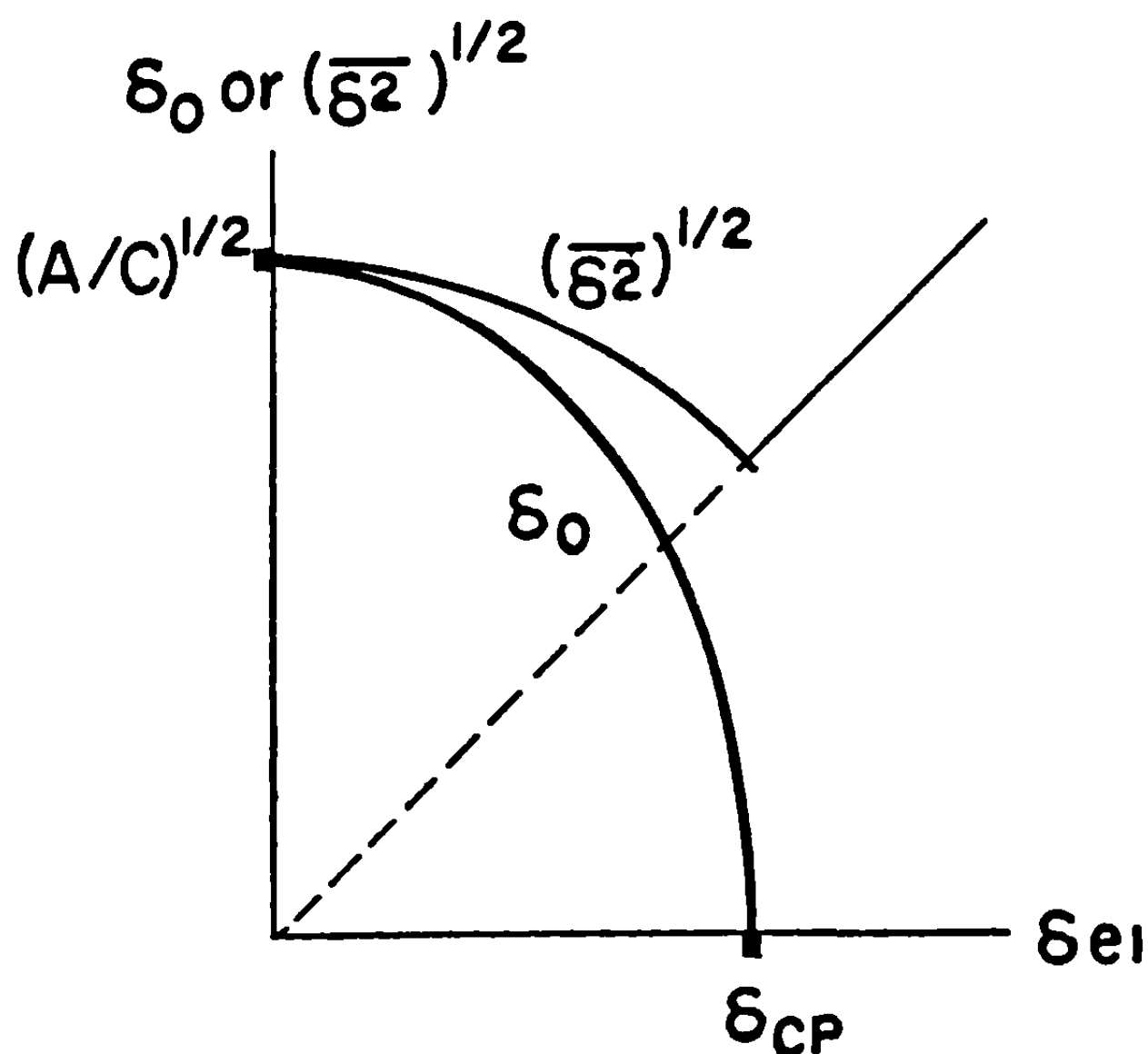


FIGURE 10.25 (a).—Dependence of δ_p and $(\overline{\delta^2})^{\frac{1}{2}}$ on δ_{e1} .

cessions are damped. In the same figure there is a plot of the root mean square yaw $(\bar{\delta}^2)^{\frac{1}{2}}$ as a function of δ_e , showing the sharp minimum at δ_{eP} .

The frequency of the limiting precession may be obtained by noting that

$$\frac{i}{4} [\delta d\delta^* - \delta^* d\delta] = \frac{1}{2} (\delta_X d\delta_Y - \delta_Y d\delta_X) \quad (34)$$

is just the area enclosed by the triangle with vertices at the origin, at δ , and at $\delta + d\delta$. Hence integrating (34) over a cycle we obtain the area of the limit cycle. Substituting (8) in (34) and integrating, we have

$$\pi \delta_0^2 = \frac{i}{4} \int_0^{2\pi/\omega} (\delta \dot{\delta}^* - \delta^* \dot{\delta}) dt = \frac{\pi}{\omega} [B \bar{\delta}^2 - D \bar{\delta}^4 - E \delta_{e1X}]. \quad (35)$$

Multiplying (24) by δ_{e1Y} and (25) by δ_{e1X} , subtracting, and using the result to eliminate the term $E \delta_{e1X}$ from (35) we obtain

$$\omega = B - D(\delta_0^2 + 2\delta_{e1}^2), \quad (36)$$

which differs only slightly from (16) when the limiting precession is small. Using (28) we have

$$\omega = B - \frac{AD}{C}, \quad (37)$$

which shows that the frequency of the limiting precession is independent of the equilibrium yaw and that, as would be expected, it depends markedly upon the nonlinearity of the aerodynamic moments. It is possible to express the results (28)–(37) in terms of the aerodynamic coefficients, but the expressions do not simplify and are too unwieldy for further manipulation.

It must be remembered that only the limiting motion has been derived and that in practice the projectile will generally start out with a small but finite precession and either die down to zero or build up to the limit cycle, but that the transient behavior will take several precessions during which changes in velocity may be important. The rate of build-up of the precessions toward the limit cycle will decrease markedly as they near the limit cycle and the frequency will decrease uniformly from that given by (16) to that given by (37). Because of the small damping and undamping rates in the vicinity of the limit cycle, the actual precession will lag behind the equilibrium value as δ_e changes and the motion will be very complicated mathematically.

An interesting result may be obtained by averaging the damping rate of the nutations as given in 10.23 (20) over a precession and using (23) and (28). Setting $\delta_P^2 = \bar{\delta}^2$, substituting for A and C , and reducing, we have approximately

$$\overline{\frac{1}{\varphi_N} \frac{d\varphi_N}{dt}} \approx -\frac{V}{m_N} \{K_{V^2\delta} + lk_{Vq} - lk_{Vs} + l\gamma k_{V\delta\delta,2} \delta_0^2\} \quad (38)$$

$$\approx -\frac{V}{m_N} \{2K_{V^2\delta} + lk_{Vq} - lk_{Vs} - l\gamma k_{V\delta\delta,0} - 2l\gamma k_{V\delta\delta,2} \delta_{e1}^2\}, \quad (39)$$

where $\bar{\delta}_N^2$ has been omitted, since, if it is not small, it affects δ_0 . Equation (38) shows that when the equilibrium yaw is such that δ_0 is small, the nutations are damped on the average around the limit cycle, provided their original amplitude is small so that $\bar{\delta}_N^2$ can be neglected. When the equilibrium yaw is small, the damping may be obtained most easily from (39). If

the fourth term in (39) is larger than the first two, as it often is, the nutations will be undamped on the average during the limit cycle. This result is due to the fact that the mean square yaw has a minimum when the limit cycle vanishes and is considerably larger at zero equilibrium yaw.

We demonstrate this behavior graphically for one possible case in figure 10.25b. At the top of the figure is a typical plot of Magnus moment showing the critical yaw, δ_c , at which the Magnus moment contributes zero damping to small nutations and precessions. Also shown are δ_{cN} and δ_{cP} , the critical yaws at which small nutations and precessions are just stable when all aerodynamic forces are included. Underneath the graph are two bars indicating the regions in which small nutations and small precessions are stable; the full bar indicating the case when only Magnus moments are considered and the extensions indicating the general case. At the bottom the root mean square yaw curve of figure 10.25a is inverted for comparison with the

δ vs δ

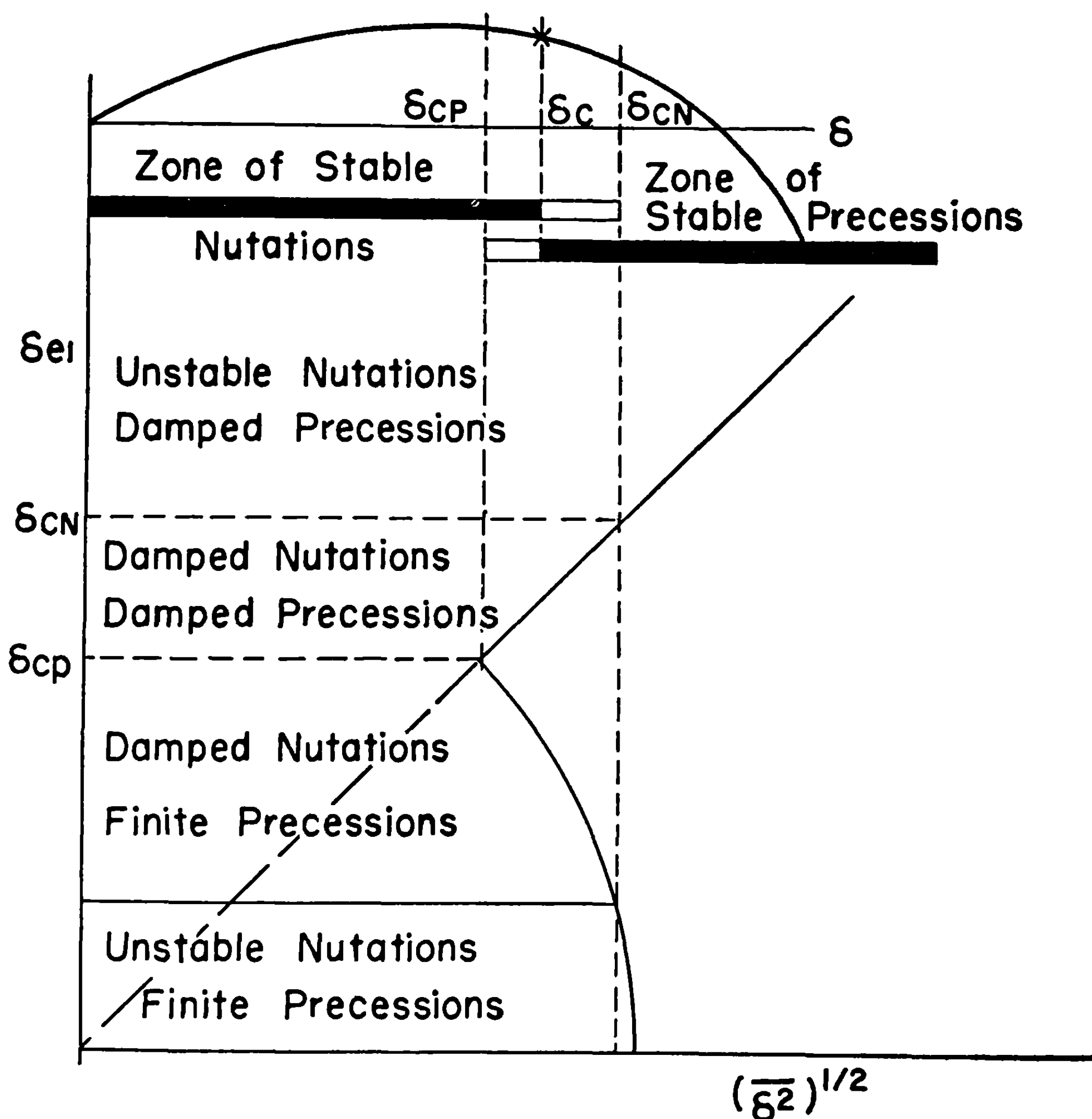


FIGURE 10.25 (b).—Zones of stable nutations and damped precessions.

critical yaws. The equilibrium yaw is plotted at the left and it may be seen that for large δ_{a1} there is a region in which precessions are damped but nutations are undamped. At somewhat smaller δ_{a1} the nutations are damped for both small precessions and for the finite limit cycle precessions. For small δ_{a1} there may be a region in which the nutations are undamped on the average around the limit cycle. This region does not exist if $\delta_{cN} > 1.41\delta_{cP}$, a condition equivalent to requiring that (39) give damping for $\delta_{a1} = 0$. At supersonic velocities the cross force and damping moment coefficients increase markedly and this condition is generally satisfied.

It must be remembered that, even though the nutations are damped on the average, they will build up during part of a precession and diminish during the remainder of the cycle but will always remain small. During the time it takes for the precession to build up to the limit cycles, the nutations will be more stable than given by (38) and (30); thus if the limit cycle is never reached, they may not become unstable before impact, even if they are unstable on the limit cycle. However, if at any time the nutation amplitude becomes too large, the term in ϕ_N^2 in 10.23 (20) shows that the nutation amplitude will then rapidly increase without limit.

10.26 Types of Instability in Spin-Stabilized Projectiles.—There are several different definitions which could be made of instability, and, although they are similar, they must be distinguished carefully in setting up criteria for the stability of the motion. In dealing with terminal ballistics and fuse design the important consideration is the yaw at impact. It is necessary for the yaw to be small for proper fuse function and to be very small if the projectile must penetrate the target. When dealing with fire control, stability means that the dispersion is low and that the range and deflection do not vary more drastically than is normal with quadrant elevation, wind, or any extraneous influence. Part of this definition is tied up with manufacturing tolerances but it also implies that small external disturbances, such as gusts of wind or minor variations in initial conditions, do not change the trajectory much, and that small manufacturing changes do not change the aerodynamic or other behavior so that the trajectory is seriously altered. One might mean by stability that the projectile always has a small yaw; in which case it satisfies the previous criteria and also has its smallest drag and longest range. We shall adopt this definition and shall also require that the yaw make no abrupt transitions such as from the right equilibrium yaw to the left equilibrium yaw, because the point at which such a transition occurs varies markedly with small changes in circumstances, thus introducing significant dispersion even though the yaws are small, since the transition changes the aerodynamic forces and the motion.

With this definition of stability we may tabulate the various types of instability and the stability criteria. There are five types of instability which we distinguish and correspondingly five criteria which must be satisfied. One of these refers to the stability factor, two to nutations, and two to precessions. The various criteria are as follows:

1. *Stability factor.*—This gives the most important stability condition, since, if it is not met, the gyroscopic forces are unable to overbalance the aerodynamic forces and the projectile turns nearly broadside very rapidly. When only overturning moments are present, the stability factor enters, as shown in 10.11 (7), in expressions of the form

$$\exp\left\{\frac{is}{2\gamma}\left[1 \pm \left(1 - \frac{1}{S}\right)^{1/2}\right]\right\}. \quad (1)$$

If S is less unity, one of the solutions builds up exponentially at a rapid rate. For example, if $S = 0.96$ the nutation amplitude is multiplied by 3.5 every nutation, so that the motion is completely unstable. Hence we must require that

$$S \equiv \frac{s^2}{4\gamma^2 V^2 k_{V^2\delta}} \geq 1. \quad (2)$$

This puts a lower limit on the spin the projectile may have and be stable. If other aerodynamic forces are present the condition becomes, from 10.13 (19')

$$S \geq 1 + 2K_{V\delta}\gamma l - 2k_{s\delta}\gamma l^2 + lK_{V\delta}, \quad (3)$$

an expression which is generally slightly greater than one. If the overturning moment is nonlinear, S_N should be substituted for S in (3).

This condition is the classical stability condition and is attributed to Sir George Greenhill. Projectiles are generally designed to have a stability factor of about two or higher so that they will still be stable when fired into a head wind and, in the case of rockets, since a large stability factor reduces the deflections during burning. Therefore one might suppose that it is always desirable to give a rocket as much spin as possible, the upper limit being set by the energy one can afford to devote to spin and by the structural strength of the round and its grain. But although these considerations are dominant for applications where the trajectories are relatively straight, it is essential to consider further stability conditions for all cases in which the trajectory turns through angles of the order of 90° .

2. *Stability of nutations.*—The next most important stability condition in practice is that the nutations should be damped. We saw in 10.23 and 10.25 that this is favored by a small average yaw and that it is undesirable for the equilibrium yaw, δ_e , to be too large. But δ_e is proportional to s/V^3 . Thus it is undesirable from this point of view for s to be too large, particularly when firing at high quadrant elevations where V is small and δ_e large at the summit.

The rate of damping of nutations is given in 10.23 (20) for the case in which the Magnus moment is nonlinear. For these large yaws the precessions are highly damped and we may assume that the average yaw is just the equilibrium yaw. The condition that small nutations always be damped is

$$k_{V\delta,0} + m_N k_{V\delta} - m_P l^{-1} K_{V^2\delta} - m_N k_{V\delta} > -k_{V\delta,2} \delta_{e1}^2, \quad (4)$$

where it should be noted that $k_{V\delta,2}$ is negative, so that (4) gives a maximum yaw for stable nutations. Now, as a crude approximation, neglecting the nonlinearity of the overturning moment, and all other moments, we have from 10.14 (2)

$$\delta_{e1} = \frac{sg \cos \theta}{V^3 k_{V^2\delta}}. \quad (5)$$

A better approximation is not necessary here because of the low accuracy of the rest of the calculation. According to 5.22 (5) the velocity at the summit is given by ⁵

$$\frac{1}{V_s^2} = \frac{J(Z)}{V_e^2 \cos^2 \theta_e}. \quad (6)$$

Using (5) and (6) in (4) we have the condition for the maximum quadrant elevation

⁵ Alternative expressions for V , both at the summit and elsewhere, are given by O. Cranz, "Lehrbuch der Ballistik" 1: pp. 120-121, eq. 12, p. 585, and p. 158, Springer, 1925 (Edwards Bros., 1943).

$$\gamma k_{v\delta,0} + m_N k_{vq} - m_P l^{-1} K_{v^2\delta} - m_N k_{vs} > - \frac{s^2 g^2 k_{v\delta,2}}{\gamma k_{v^2\delta,0}} \frac{J^3}{V_e^6 \cos^6 \theta_e} \quad (7)$$

If the projectile is fired at quadrant elevation satisfying (7), the nutations will be damped along the whole trajectory. However (7) does not give the maximum quadrant elevation such that the over-all motion is stable. Actually, at the maximum quadrant elevation, the nutations are damped originally, are undamped at the summit for a length of time such that they reach roughly their original amplitude, and then are again damped on the descending portion of the trajectory. This requirement may be stated in a form involving the integral of the damping rate over the trajectory. Using 10.23 (20) and (10) and assuming that the spin is essentially constant we obtain as a necessary condition for stability that for all t

$$\begin{aligned} \ln \frac{\varphi_N}{\varphi_{Ne}} &= \int_{t_e}^t \frac{1}{\varphi_N} \frac{d\varphi_N}{dt} dt = \int_{t_e}^t \frac{\Delta\varphi_N}{\varphi_N} \frac{\Phi_N}{2\pi} dt \\ &= - \int_{t_0}^t \frac{Vl}{m_N} \{ k_{v\delta,0} + m_N k_{vq} - m_N k_{vs} - m_P l^{-1} K_{v^2\delta} + 2\gamma k_{v\delta,2} \delta_{e1}^2 \} dt \\ &\approx \frac{l}{g} \int_{\theta_e}^{\theta} \left\{ \gamma k_{v\delta,0} + k_{vq} - k_{vs} - \frac{K_{v^2\delta}}{4Sl} + 2k_{v\delta,2} \frac{s^2 g^2 \cos^2 \theta}{\gamma V^6 k_{v^2\delta}} \right\} \frac{V^2 d\theta}{\cos \theta} \leq 0. \end{aligned} \quad (8)$$

Using suitable formulas (footnote 5), we may eliminate V in (8) and integrate over θ . This integral must be carried out numerically, and hence considerable computation is needed to determine the maximum allowed value for θ_e . In view of the uncertainty in formulating this stability criterion it does not seem desirable to carry this calculation further. It is probably sufficient to put the value of δ_{e1} , averaged over the summit of the trajectory, on the right side of (4) to estimate the maximum quadrant elevation.

If the nutations are once allowed to build up to the point where, as described below 10.23 (16), they are self-sustaining, then regardless of any subsequent decrease of δ_{e1} on the descending portion of the trajectory the nutations will continue to increase, reaching an amplitude near 90° and giving the appearance of tumbling. At such large yaws the projectile produces a characteristic roar best described as a "wow-wow", which is the descriptive name given to this type of instability. Because of its large yaw, a "wow-wow" exhibits large drag and hence a short range. It also usually has a drift to the left rather than to the right. This is the type of instability that limits the quadrant elevation at which most spin-stabilized rockets can be fired.

It is apparent from (8) that the maximum quadrant elevation is dependent upon the spin of the projectile and if a high quadrant elevation is desirable the projectile should have low spin; that is, a low stability factor. On the other hand a high stability factor is required to reduce the deflections during burning, especially the wind deflections, to a small value. Since these requirements conflict it is necessary to accept a compromise or to develop two sets of rockets, one with high spin for accurate low-angle fire, and one with low spin for long-range, high angle barrages.

There is a second, less important, condition that must be imposed under some circumstances if the nutations are to be stable. As pointed out in 10.25, if the equilibrium yaw is very small, the precessions may be unstable and may build up toward a limit cycle on which the nutations can sometimes be, on the average, undamped. The condition that they be damped is that

$$2K_{v^2\delta} + lk_{vq} - k_{v\delta,0} - lk_{vs} > 0. \quad (9)$$

This condition is not very important in most cases, however, because the nutations are damped

until the precessions build up nearly to the limit cycle. At this point the nutations are very small and build up slowly because the rate of undamping is small. Before the nutations become large the projectile will usually either have reached the target, if fired at low quadrant elevation, or reached a part of the trajectory where the equilibrium yaw is too large for the effect to occur, if fired at high quadrant elevation.

3. *Stability of precessions.*—There are two conditions the precessional motion must satisfy to be stable in the strictest sense. First, the spin must be such that the equilibrium right yaw always exists, in order to avoid transitions to the equilibrium left yaw. It is also necessary that, if small precessions are negatively damped, a limit cycle shall exist about the equilibrium right yaw. In actual rocket design this condition is not important. It cannot be written explicitly because it depends upon the velocity at the summit where the equilibrium yaw is largest. If no other condition limits the maximum quadrant elevation of stable motion, this one will, but the condition on the nutations is generally more severe.

The second condition is that the precessions be damped or that the limit be sufficiently small so that the yaw at impact will be that required. It is easy to show from 10.25 (28) that the maximum value of $\delta_{e1} + \delta_0$ is, in the notation of the last section,

$$(\delta_{e1} + \delta_0)_{\max} = \left(\frac{3A}{2C} \right)^{\frac{1}{2}}. \quad (10)$$

Hence, if the maximum permissible yaw be denoted by δ_M , we must satisfy the relation

$$3A < 2C\delta_M^2,$$

or

$$3K_{v^2\delta} - \frac{3k_{vql}}{4S} - 3k_{v\delta,0}\gamma l - 2k_{v\delta,2}\delta_M^2 > 0. \quad (11)$$

A somewhat less stringent condition is sometimes possible in the cases in which δ_{e1} is known at impact for all quadrant elevations of interest.

It has been found in dealing with rockets that neither of these conditions is particularly important because instability enters first in the nutations. However, in some projectiles these conditions may be more important and merit further study. An integration of the motion over the whole trajectory is carried out in 10.4 and it may be used for a more careful analysis of the stability conditions for precessions. Because the Magnus moment reverses at small yaw the limit cycle is small and the precessions do not get large. If the moments were linear, further study of the precessions would be necessary.

10.3 The Solar Yaw Camera

We have seen in the previous sections the way in which aerodynamic forces modify the pure nutational motion that would be observed in a vacuum. An important problem is the determination of the aerodynamic forces from the observed motion. We shall not attempt here a complete treatment of all the methods that can be used. Instead we shall briefly mention a variety of standard methods for which adequate discussions are available elsewhere and shall treat more extensively only the solar yaw camera method since it is perhaps less fully discussed elsewhere and since we have had the most experience with it, obtaining much of our aerodynamic data on spin-stabilized rockets with its aid.

10.31 Methods of Exterior Ballistics Measurements.—The early exterior ballistics measurements were concerned primarily with measuring velocity and drag. The methods

used include the ballistic pendulum, the Boulengé chronograph and later the solenoid chronograph.⁶ More recently measurements of the orientation of the projectile have been made with the object of determining all the aerodynamic forces. The first method⁷ of doing this was to fire the projectile through a series of cardboard targets and measure the shape and orientation of the holes punched by the projectile.

Most modern measurements are carried out photographically; methods of getting the drag and yaw oscillation distance have been described in 2.441 and 2.45. However, these latter methods are not precise enough to allow an accurate determination of the aerodynamic forces on spin-stabilized rockets. It is impossible to measure the position with sufficient accuracy to obtain the forces directly by differentiation and it is necessary, instead, to calculate the coefficients from the results of the preceding sections. Suitable measurements can be made with some such facility as the spark range; this consists of a group of camera stations past which the projectile is fired. At these stations the projectile is illuminated by intense sparks or other light sources of short duration and sufficient photographs showing one or perhaps both components of the orientation are taken to allow determination of the amplitude and phase of the nutations and precessions. Then using the results of consecutive stations it is possible to determine the entire motion. From the frequencies and damping rates, it is possible to determine some of the aerodynamic coefficients. The rest may be obtained from firings of geometrically similar projectiles, with displaced centers of gravity, by means of formulas from 8.3.

There are, however, several disadvantages of this method. Unless the projectiles are shot from guns or unless very long launchers are used with rocket propelled projectiles, the dispersion by the end of burning requires large lateral dimensions and reduced accuracy. Also, measurements can be made only at isolated points and only on the short horizontal portion of a trajectory. The last objection is not serious because the projectile may be fired with different velocities and spins to cover the cases of interest, but the second makes it very difficult to measure and interpret the effects of nonlinear aerodynamic moments. The solar yaw camera, which was invented by W. R. Smythe, eliminates these difficulties but, in some applications, introduces the difficulty of determining the direction of motion exactly, since the camera measures one component of the orientation. As shown schematically in figure 10.31, it consists of a pinhole camera which takes a picture of the sun once every rotation and thus records the angle between the axis of the projectile and the line to the sun over the whole trajectory. The film is driven through a gear train by the differential angular velocity between the projectile and a flywheel which is initially at rest. The device is mounted in a specially designed head which may, however, be used more than once. The versatility of the device is shown by its use for either high or low quadrant elevation shots and for firing from airplanes. It can be used to obtain values of the aerodynamic coefficients, information about the character of the motion and stability on different sections of a long trajectory, and values of the initial conditions, such as the mallaunching for rounds fired from aircraft. The photographic record consists of a straight base line and a series of dots, one for each revolution of the rocket, the distance from the base line to the dot measuring the angle between the axis and the line to the sun. The record may be analyzed in much the same way in which spark range data are treated. Examples of such records will be found below and in figure 10.12.

The velocity and spin of the projectile must be obtained separately for the interpretation of yaw camera-data. The spin may be obtained by an interesting technique using microwaves.

⁶ T. J. Hayes, "Elements of Ordnance," New York, Wiley, 1938.

⁷ Fowler, Gallop, Lock, and Richmond, Roy. Soc., Trans., 221: pp. 295-387, 1921.

If a proximity fuze with a dipole antenna is used, the signal it sends out goes through a minimum twice every revolution as the dipole axis points toward the receiver. By measuring the frequency modulating the received signal, a very easy measurement, the rate of spin can be obtained at all points of the trajectory. This method is very straightforward and allows an immediate evaluation of the spin deceleration coefficient.

The velocity may be obtained experimentally, or theoretically by the formulas of chapter 5. The methods of measuring the velocity along the trajectory include two radar and two photographic techniques. The radar measurements may be made by a radar tracker which plots the position along the trajectory so that the velocity may be determined by differentiation, or the radial component of velocity may be measured directly by a Doppler radar which measures the frequency shift due to the velocity. Neither method would give, in 1945, an accuracy sufficient to permit an evaluation of the forces acting on the projectile but the velocities were useful in conjunction with yaw camera studies.

A photographic method for the complete trajectory has been developed by W. R. Smythe. This method involves the use of a special projectile head which ejects a flash of magnesium powder at periodic intervals. At night the entire trajectory may be recorded on one photo-

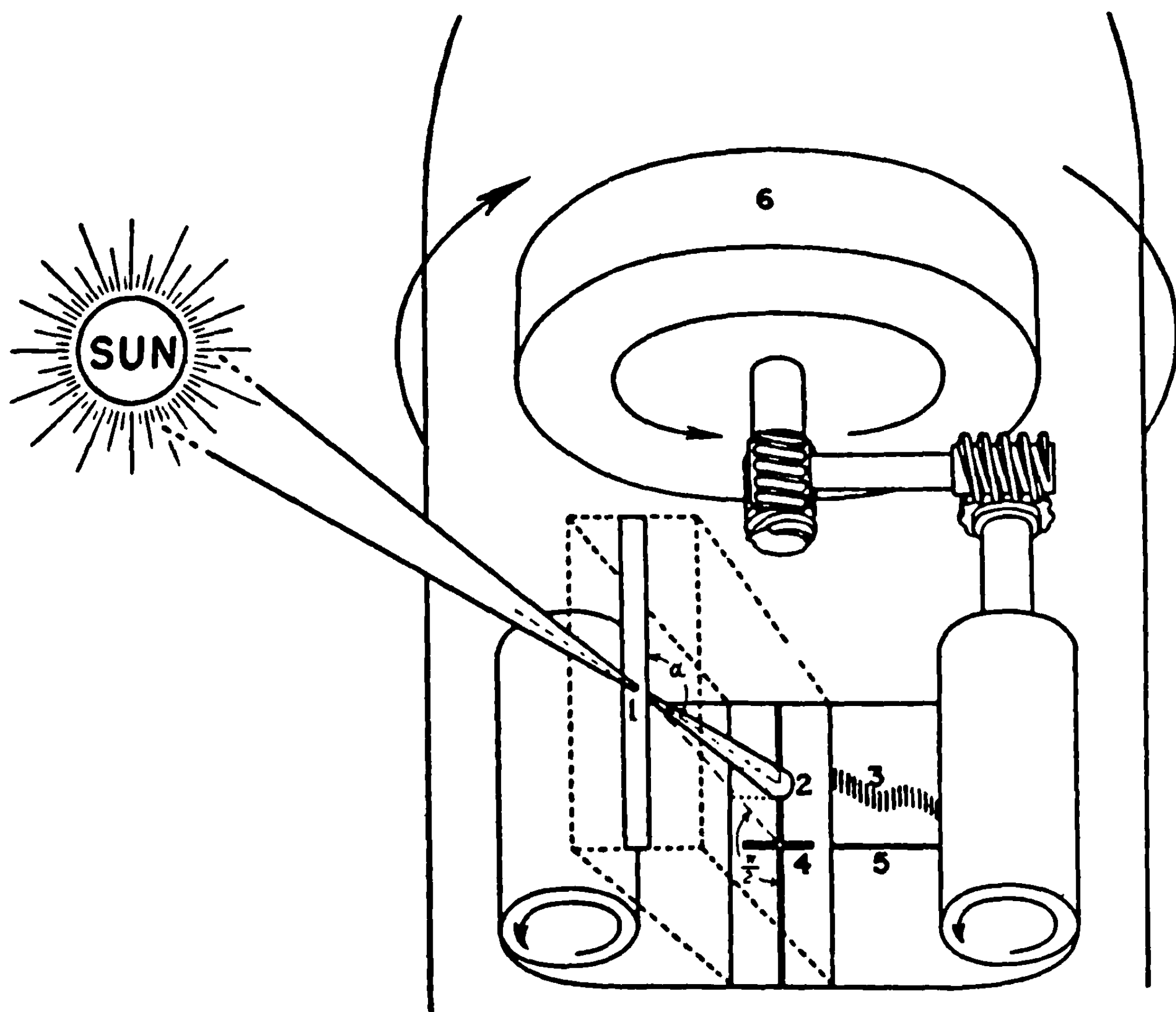


FIGURE 10.31.—Schematic diagram of the yaw camera: 1, pinhole; 2, image of solar disk; 3, successive exposures on film; 4, cross-slit; 5, exposure through cross-slit (by skylight) forming base line; 6, flywheel.

graphic plate, and, if pictures are taken from several angles and the flashes are accurately timed, excellent results can be obtained. On the first test using this technique the three position coordinates were obtained to within two or three feet over the course of a trajectory 13,000 feet long and the time was obtained to within 0.002 seconds as measured with an unstandardized clock. Considerable improvement in the measurement both of position and time seemed possible. One advantage of the night firing is that atmospheric refractive troubles are less than during the day. It occasionally happened that the magnesium charges were not completely ejected, the residue burning in the rocket and forming a streak on the film. The streak is modulated by the spin of the rocket, and allows a photographic determination of the spin rate and feet per turn at this point.

I. S. Bowen has developed a special camera for photographing the trajectory of a projectile. It makes a substantial number of accurately timed exposures on a single large plate, a slotted focal plane shutter being suitably tracked so that each exposure covers only the part of the plate in the neighborhood of the image of the projectile.

10.32 Analysis of Yaw Camera Records.—As shown schematically in figures 10.31 and 10.32, the dots which constitute a yaw camera record lie on a curve that forms the projection

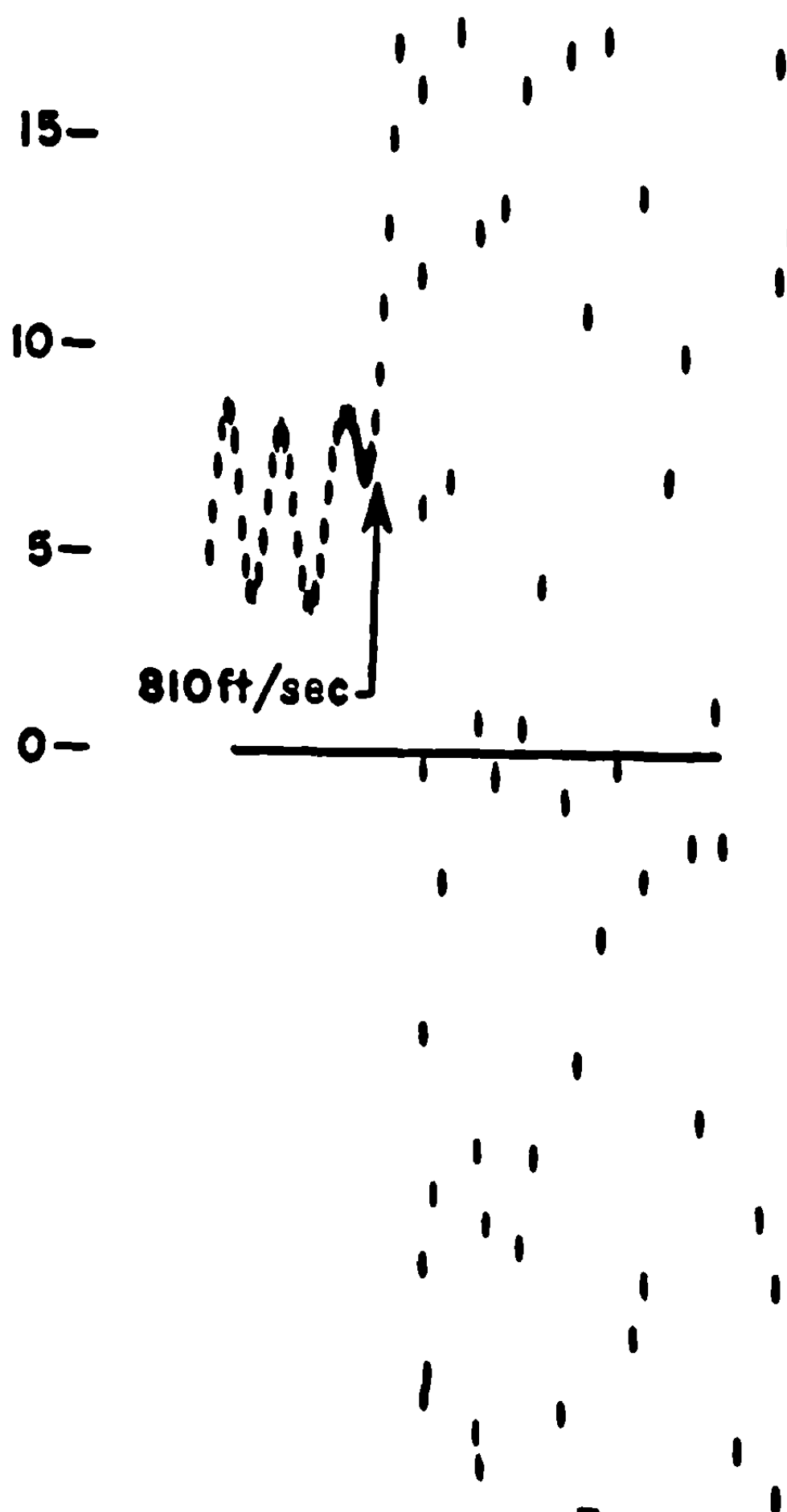


FIGURE 10.32.—Yaw camera record during acceleration of a rocket having constant spin, showing the onset of instability at a time when it was known to have a velocity of 810 ft./sec.

of an epicyclic motion on a plane. Before considering the analysis of data obtained by measurement of the film with a comparator, let us consider the information to be obtained by visual inspection of the record. A casual examination of the record shows the general character of the motion and the type and approximate time of occurrence of any instability that may be present. As a somewhat unusual example, consider figure 10.32 which shows an enlargement of the record of a test in which a rocket with noninclined nozzles was fired from a spinning launcher. Thus the spin remained constant at 62 rev./sec. while the velocity, which was measured by a camera placed at the side, increased. The record shows that the motion was stable, until the velocity reached the critical value at which the stability factor was equal to unity; then it shows that the yaw increased exponentially. One sees clearly how rapidly the yaw increases when the stability factor is less than one, as discussed in 10.26. The overturning moment may be obtained by the analysis of records such as this, but since it is difficult to identify the exact point at which the rocket becomes unstable, higher accuracy is possible by using equation (1) below.

From direct inspection of the record it is easy to obtain by counting approximate values of R_N the number of revolutions per nutation; i. e., the number of dots in one of the shorter waves, and N_P , the number of nutations per precession; i. e., the number of short waves in a long wave. From these, one obtains the stability factor and the ratio of the moments of inertia from

$$S = (1 + N_P)^2 / 4N_P, \quad (1)$$

and

$$\gamma = R_P / (1 + N_P), \quad (2)$$

results derived in 10.11 (12) and (13).

Next, consider the more extensive information that can be obtained by careful measurement of the records. The motion of the rocket, and in particular its orientation, depends on all the aerodynamic coefficients. It is theoretically possible to reverse the dependance and determine most of the coefficients from a knowledge of the orientation and direction of motion as a function of time. However the experimental error in the measurements and the fact that only a finite number of measurements are made means that for each position of the center of mass only certain combinations of the coefficients can be determined. Fortunately, these may be obtained from the yaw camera record with only a small amount of measurement and computation. If the same measurements are made on a round with the same external shape, but with a displaced center of gravity, different combinations of the coefficients are obtained and it is possible to separate the various coefficients.

In proceeding with the analysis it is necessary to start with the variation of the velocity and spin along the trajectory and with the values of the drag and spin deceleration coefficients, since these are not obtainable from the yaw camera record. For the order of accuracy required it is simplest to obtain the remaining coefficients by a successive approximations procedure, first obtaining rough values of the overturning moment, cross force, and Magnus moment coefficients, using these to calculate the smaller coefficients, and then using the latter to refine the values of the larger coefficients. We use primes to denote the coefficients obtained from rounds with the displaced centers of mass.

The first step is to obtain an approximate value for the stability factor and the ratio of moments of inertia (if not already known by direct measurement) for two rounds of the same external shape but different centers of mass.

The overturning moment coefficients γ_{v^2} and γ'_{v^2} may be obtained from 8.22 (9)

$$\gamma_{V^2\delta} = (mK^2/2\rho AlS) (s/\gamma V)^2. \quad (3)$$

From these the cross force coefficient is, according to 8.32 (2)

$$\Gamma_{V^2\delta} \doteq (l/h) (\gamma_{V^2\delta} - \gamma'_{V^2\delta}) - \Gamma_{V^2}, \quad (4)$$

where h is the displacement of the center of gravity and Γ_{V^2} is the drag coefficient. We may convert from Γ 's and γ 's to K 's and k 's if desired by table 8.25.

Now the rates of damping of the nutations and precessions can be obtained relatively easily from the yaw camera film by direct measurement of the peaks of the nutations and precessions at several points. The rate of damping is most conveniently expressed in terms of the fractional change in amplitude of the nutation per nutation and of the precession per nutation. Then we may use 10.13 (22) and (24).

$$\frac{\Delta\varphi_N}{\varphi_N} = -\frac{2\pi\gamma V}{s} \left(1 + \frac{3}{4S}\right) \left\{ \gamma l k_{V\delta\delta} + \left(1 - \frac{1}{4S}\right) l k_{Vq} - \frac{K_{V^2}}{4S} \right\}, \quad (5)$$

$$\frac{\Delta\varphi_P}{\varphi_P} = -\frac{2\pi\gamma V}{s} \left(1 + \frac{3}{4S}\right) \left\{ \left(1 - \frac{1}{4S}\right) K_{V^2\delta} - \gamma l k_{V\delta\delta} - \frac{l k_{Vq}}{4S} \right\}. \quad (6)$$

Using the value of S and $\Gamma_{V^2\delta}$ obtained above, it is easy to solve these equations simultaneously for $k_{V\delta\delta}$ and k_{Vq} . With the values of $\gamma_{V\delta\delta}$ and γ_{Vq} obtained from these for rounds with normal and with displaced centers of gravity, the corresponding force coefficients may be obtained from 8.33 (9), 8.34 (21), 8.31 (6), and 8.34 (7). The required expressions are:

$$\Gamma_{V\delta\delta} = (l/h) (\gamma_{V\delta\delta} - \gamma'_{V\delta\delta}), \quad (7)$$

$$\Gamma_{Vq} = (l/h) (\gamma_{Vq} - \gamma'_{Vq}) - \gamma_{V^2\delta} + (h/l) (\Gamma_{V^2\delta} + \Gamma_{V^2}). \quad (8)$$

From the values of the Magnus force coefficient, $\Gamma_{V\delta\delta}$, the corrected value of S may be determined by 10.13 (31) and (32) which give

$$S = \frac{1}{4} (1 + N_P)^2 N_P^{-1} [1 + (4S_{\text{approx}} - 2)\gamma l k_{V\delta\delta}]. \quad (9)$$

The values of $\gamma_{V^2\delta}$ and $\Gamma_{V^2\delta}$ are next redetermined as above. Then the more accurate value $K_{V^2\delta}$ may be inserted in (5) and (6) to give the final values of the Magnus and damping moment coefficients. Finally, with the corrected value of $\Gamma_{V\delta\delta}$, the value of the coefficient of the Magnus moment due to cross spin, γ_{sq} , could theoretically be obtained from 10.13 (28),

$$\gamma = R_P (1 + N_P)^{-1} \{1 + \gamma l K_{V\delta\delta} + \gamma l^2 k_{sq}\}, \quad (10)$$

provided γ is taken from direct measurement and not from (2). In practice (10) will usually be satisfied within the experimental error by setting k_{sq} and hence γ_{sq} equal to zero. However, in cases where this moment does not affect the motion sufficiently to enable us to determine its value, knowledge of its value is not necessary. If γ_{sq} and γ'_{sq} are obtainable from the measurements, then we may obtain Γ_{sq} from 8.35 (5),

$$\Gamma_{sq} = (l/h) (\gamma_{sq} - \gamma'_{sq}) - \gamma_{V\delta\delta} + (h/l) \Gamma_{V\delta\delta}. \quad (11)$$

If the aerodynamic forces and moments are nonlinear the analysis becomes much more difficult, but fortunately the only case of importance in practice is that in which only the Magnus

moment coefficient depends on yaw. In this case the analysis is tractable, although difficult, since it is necessary to determine the yaw at all points and to measure the damping rates at various values of the yaw. The procedure is to obtain first the stability factor and cross force coefficient in the same manner as in the linear case. Next it is necessary to determine the absolute value of the yaw. To do this we compute the equilibrium yaw from 10.14 (2), setting $\tau=0$ if no estimate of its value is available. Then the amplitude and phase of the precessions are measured and combined with the equilibrium yaw to give the total yaw (the spherical trigonometry involved is elementary but tedious). In measuring the damping it is no longer possible to measure the nutation amplitude at long intervals, because of the experimental error and the rapid change of yaw, every nutation must be measured. The amplitudes are then plotted on semilog graph paper as a function of the nutation number. The positions of the minima and maxima of the yaw are indicated on the graph because here the yaw remains nearly constant for several nutations. The slopes of the amplitude curve are then taken at each of these points where the yaw is known. Then, using 10.23 (20),

$$\Delta\varphi_N/\varphi_N = (-2\pi\gamma V/sm_N^2) \{ \gamma lk_{vs\delta,0} + m_N lk_{vq} - m_N lk_{vs} - m_P K_{V^2\delta} + \gamma lk_{vs\delta,2} \delta^2 \}, \quad (12)$$

the expression in the brace may be obtained as a function of yaw. If this is plotted against δ and a parabola is fitted to the points, the value of $k_{vs\delta,2}$ and the value of the linear part of the damping are obtained.

This linear damping corresponds to (5) and in order to determine $k_{vs\delta,0}$ and k_{vq} separately it is necessary to obtain an expression analagous to (6). We may do this if the amplitude of the precession is small or if the precessions are in the limit cycle. In the first case we have, by 10.25 (14)–(18),

$$\frac{\Delta\varphi_P(\text{per nutation})}{\varphi_P} = -\frac{2\pi\gamma V}{sm_N} \left\{ K_{V^2\delta} - \gamma lk_{vs\delta,0} - \frac{lk_{vq}}{4S} - 2\gamma lk_{vs\delta,2} \delta^2 \right\}. \quad (13)$$

It is then possible to solve (12) and (13) simultaneously for $k_{vs\delta,0}$ and k_{vq} ; after this, the procedure is the same as that following (5) and (6).

If the precession has an amplitude corresponding to the limit cycle the coefficients may be obtained from 10.25 (28),

$$-K_{V^2\delta} + (lk_{vq}/4S) + \gamma lk_{vs\delta,0} = \gamma lk_{vs\delta,2} [\delta_0^2 + 2\delta_{e1}^2] = \gamma lk_{vs\delta,2} [\delta_0^2 + (32g^2\gamma^2 S^2/V^2 s^2)]. \quad (14)$$

Here also the coefficients may be obtained by simultaneous solution of (12) and (14). If the precession amplitude does not satisfy the conditions of either (13) or (14) then the analysis is no longer feasible. Some information may be obtained by substituting the measured precession in 10.25 (7) and adjusting the coefficients to fit the data, but the accuracy is very poor.

In order to obtain the force coefficients it is necessary to fire a round with a displaced center of gravity just as in the linear case. The nonlinear term $k_{vs\delta,2}$ may be expected to be the same for both positions of the center of mass since the Magnus force is a linear function of yaw.

It should be noted that yaw camera data on a single round is adequate for most applications since the combinations of coefficients in (5) and (6), or (12) and (13) or (14) are those needed for a determination of the stability of slightly modified rockets or the motion with modified initial conditions. The reason for this simplicity is that all the large terms in (5) and (6) are multiplied by $\gamma V/s$ and the value of S enters only in small terms. Hence the effect of a change of V or s due to a change in the rocket or to a different quadrant elevation or wind may be computed very easily.

10.4 The Effect of Aerodynamic Forces on the Trajectory

The effect of the drag on the trajectory has been treated in chapter 5. We now consider the significant further modifications of the trajectory arising from the equilibrium right yaw and the remaining aerodynamic forces. The most important effect, and the one that usually receives the most attention since it is the easiest to compute and to recognize experimentally, is the drift to the right due to the cross-force. The Magnus force tends to support the rocket and thus increase the range over that computed by the methods of chapter 5. It also affects the time of flight and angle of fall, but the change in range is the most important effect and we neglect the others. Since the drag increases with yaw and the equilibrium yaw increases with the quadrant elevation, the effective drag coefficient is slightly larger than its value at zero yaw and it increases with the quadrant elevation. The chief effect of this modified drag is to decrease the terminal velocity. The tendency of the increased drag to reduce the range is overbalanced by the increase due to the Magnus force. The presence of these various factors means that the impact velocity cannot be computed with much accuracy from the initial conditions and an effective drag coefficient which is chosen to give the observed range.

In the approximate investigations below of the drift to the right and the effect of the Magnus lift, the nutations may be completely ignored because their amplitude is small and their frequency high. Likewise, the precessions may be ignored for most projectiles and the yaw taken to be the equilibrium yaw, as given by 10.14; (2). We neglect the small modifications due to the amplitude of the precessions and to the phase of the precession at the end of burning.

10.41 Approximate Treatment of Right Drift.—There is no simple method of computing the drift to the right unless the air drag is small enough so that the trajectory does not deviate greatly from the vacuum case. However, we can derive a relatively simple formula if we assume that the only aerodynamic forces that need be considered are the overturning moment and the cross-force. Then, according to 10.26 (5), the equilibrium yaw is

$$\delta_e = \frac{sg \cos \theta}{V^3 k_{v^2\delta}}. \quad (1)$$

The corresponding cross-force is

$$\begin{aligned} F_{v^2\delta} &= m K_{v^2\delta} V^2 \delta_e \\ &= \frac{m g s \cos \theta}{V} \frac{K_{v^2\delta}}{k_{v^2\delta}} = \frac{m g K^2 s \cos \theta}{l V} \frac{\Gamma_{v^2\delta}}{\gamma_{v^2\delta}} \end{aligned} \quad (2)$$

by table 8.25. The linear deflection is therefore

$$Z = \int_0^T \int_0^t \frac{g s \cos \theta}{V} \frac{K_{v^2\delta}}{k_{v^2\delta}} dt dt, \quad (3)$$

where T is the total time of flight and s , θ , and V are functions of t , the time elapsed since firing. On the above assumptions there are no aerodynamic forces in the vertical plane and hence $V\dot{\theta} = -g \cos \theta$ (cf. 5.31 (2)) is the acceleration normal to the trajectory in this plane. Thus (3) becomes

$$Z = \int_0^T \int_{\theta_0}^{\theta} s (K_{v^2\delta}/k_{v^2\delta}) (-d\theta) dt, \quad (4)$$

where so far the only assumptions are those as to the nature of the aerodynamic moments and transverse forces.

To proceed, we assume that the spin is constant, which means that (4) can be integrated to give

$$Z = s (K_{V^2\delta}/k_{V^2\delta}) \int_0^T (\theta_0 - \theta) dt. \quad (5)$$

If we assume that θ depends on t as in a vacuum trajectory, then

$$\int_0^T \theta dt = 0, \quad (6)$$

and we have

$$Z = s \theta_0 T (K_{V^2\delta}/k_{V^2\delta}) = s \theta_0 T (K^2 \Gamma_{V^2\delta}/l \gamma_{V^2\delta}). \quad (7)$$

The angular deflection is

$$\Delta_\phi = s (\theta_0 T/X) (K_{V^2\delta}/k_{V^2\delta}) = s (\theta_0 T/X) (K^2 \Gamma_{V^2\delta}/l \gamma_{V^2\delta}) \quad (8)$$

where X is the range.

This result holds only for nearly parabolic trajectories since the vertical components of all aerodynamic forces, the left-hand side of (6), and the change in spin have been neglected. It is, however, adequate for most subsonic projectiles. For other cases, a direct numerical integration of (4) is necessary.

10.42 Approximate Treatment of Lift.—The effect of the Magnus force and torque on the range can be computed by the use of 5.32 (17); i. e., by the Green's function technique. However, an explicit analytic expression for the Green's function and for the change in range can be obtained only when the unperturbed trajectory is taken to be the vacuum trajectory. In order to use 5.32 (17) we must first solve 5.32 (15) to get U_2 and then must obtain a convenient expression for η .

In the vacuum case these equations for U_2 become

$$\frac{dU_1}{d\tau} = -\frac{g \cos \theta}{V^2} U_2 + \frac{\sin (\theta - \theta_T)}{\sin \theta_T}, \quad (1)$$

and

$$\frac{dU_2}{d\tau} = g \cos \theta U_1 - \frac{g \sin \theta}{V} U_2 + \frac{V \cos (\theta - \theta_T)}{\sin \theta_T},$$

where all quantities except U_1 and U_2 refer to the vacuum trajectory and we now use θ_T for $\theta_0(T)$. We also need the relations

$$V = V_x \sec \theta,$$

and

$$\frac{d\theta}{d\tau} = -g \frac{\cos \theta}{V} = \frac{g \cos^2 \theta}{V_x}. \quad (2)$$

Changing to the new independent variable $\mu = \sin \theta$, we get for (1)

$$\begin{aligned} \frac{dU_1}{d\mu} &= \frac{U_2}{V_x} - \frac{V_x}{g \sin \theta_T} \sec^3 \theta \sin (\theta - \theta_T), \\ \frac{\cos^2 \theta}{V_x} \frac{dU_2}{d\mu} &= -U_1 + \frac{\sin \theta}{V_x} U_2 - \frac{V_x}{g \sin \theta_T} \sec^2 \theta \cos (\theta - \theta_T). \end{aligned} \quad (3)$$

Differentiating the second of these equations, and eliminating $dU_1/d\mu$ by means of the first, we obtain

$$(1-\mu^2) \frac{d^2 U_2}{d\mu^2} - 3\mu \frac{dU_2}{d\mu} = -\frac{2V_x^2}{g} \sec^4 \theta. \quad (4)$$

The initial conditions for U_2 are

$$\left. \begin{aligned} U_2 &= 0 \\ \frac{dU_2}{d\mu} &= -\frac{V_x^2}{g} \frac{\sec^4 \theta_T}{\sin \theta_T} = -\frac{V_x^2}{g\mu_T} \frac{1}{(1-\mu_T^2)^2} \end{aligned} \right\} \text{ at } \mu = \mu_T, \quad (5)$$

where $\mu_T = \sin \theta_T$.

By using the integrating factor $(1-\mu^2)^{\frac{1}{2}}$ this can be integrated to give

$$\begin{aligned} U_2(T, \mu) &= \frac{2V_x^2}{g} \left\{ \cot 2\theta_T \left[\frac{\mu_T}{(1-\mu_T^2)^{\frac{1}{2}}} - \frac{\mu}{(1-\mu^2)^{\frac{1}{2}}} \right] + \frac{1}{2(1-\mu_T^2)} - \frac{1}{2(1-\mu^2)} \right\} \\ &= \frac{2V_x^2}{g} \left\{ \cot 2\theta_T (\tan \theta_T - \tan \theta) + \frac{1}{2} (\sec^2 \theta_T - \sec^2 \theta) \right\}. \end{aligned} \quad (6)$$

While this function is correct only for a vacuum trajectory, it is only slightly in error for most subsonic trajectories.

To get η we must find the contribution to the lift due to the presence of the Magnus effects. The lift acting on the projectile is composed of two parts, that due to the Magnus force and the component of the cross force in the vertical direction due to the effect of the Magnus moment in generating a vertical component of the equilibrium yaw. If we take the only aerodynamic moments to be linear overturning and Magnus moments, then the equilibrium yaw is, by 10.14(2)

$$\delta_e = \frac{sg \cos \theta}{\gamma V^3} \left[k_{V^2\delta} - \frac{ils}{V} k_{V\delta} \right]^{-1}. \quad (7)$$

If we take only the aerodynamic forces to be linear cross and Magnus forces, then by 10.13 (1) the total force is

$$\begin{aligned} F_{\perp} &= m V^2 \left[K_{V^2\delta} - \frac{ils}{V} K_{V\delta} \right] \delta_e \\ &= \frac{m s g \cos \theta}{\gamma V} \frac{K_{V^2\delta}}{k_{V^2\delta}} \left\{ 1 - \frac{ils}{V} \left(\frac{K_{V\delta}}{K_{V^2\delta}} - \frac{k_{V\delta}}{k_{V^2\delta}} \right) \right\}, \end{aligned} \quad (8)$$

where in all cases the Magnus effects are assumed to be relatively small. To this order the drift is unaltered by the inclusion of the Magnus effects, and the lift may have either sign. Thus, the vertical aerodynamic acceleration to be substituted in 5.32 (17) is

$$\eta = \frac{ls^2 g \cos \theta}{\gamma V^2} \left(\frac{K_{V\delta}}{k_{V^2\delta}} - \frac{K_{V^2\delta} k_{V\delta}}{k_{V^2\delta}^2} \right). \quad (9)$$

The change in range is

$$\Delta X = \int_0^T \frac{U_2(T, \tau)}{V} \frac{ls^2 g \cos \theta}{\gamma V^2} \left(\frac{K_{V\delta}}{k_{V^2\delta}} - \frac{K_{V^2\delta} k_{V\delta}}{k_{V^2\delta}^2} \right) d\tau$$

$$= \int_{\mu_0}^{\mu_T} U_2(T, \mu) \frac{ls^2 \cos \theta}{\gamma V_x^2} \left(\frac{K_{V_{s\delta}}}{k_{V_{2\delta}}} - \frac{K_{V_{2\delta}} k_{V_{s\delta}}}{k_{V_{2\delta}}^2} \right) (-d\mu). \quad (10)$$

Since this is to be evaluated along the vacuum trajectory on which the spin, s , and V_x are constant, it becomes

$$\Delta X = \frac{ls^2}{\gamma V_x^2} \left(\frac{K_{V_{s\delta}}}{k_{V_{2\delta}}} - \frac{K_{V_{2\delta}} k_{V_{s\delta}}}{k_{V_{2\delta}}^2} \right) \int_{\mu_T}^{\mu_0} U_2(T, \mu) (1 - \mu^2)^{\frac{1}{2}} d\mu. \quad (11)$$

When (6) is substituted in (11), the integral can be evaluated and gives as the change in range

$$\Delta X = \frac{ls^2}{\gamma g} \left(\frac{K_{V_{s\delta}}}{k_{V_{2\delta}}} - \frac{K_{V_{2\delta}} k_{V_{s\delta}}}{k_{V_{2\delta}}^2} \right) \sin 2\theta_0. \quad (12)$$

For very low angle firing this result may be obtained in a simpler manner. In this case, the aerodynamic force due to Magnus effects is constant and vertical along the trajectory. Therefore the change in range can be computed by computing the effect of a corresponding small change in gravity. For a vacuum trajectory the range is

$$X = \frac{V_x^2}{g} \frac{\sin 2\theta_0}{\cos^2 \theta_0} \doteq \frac{2 V_0^2 \theta_0}{g}, \quad (13)$$

and the change in range satisfies

$$\frac{\Delta X}{X} = -\frac{\Delta g}{g}. \quad (14)$$

The η of (9) is just the appropriate value of $-\Delta g$ if θ_0 is set equal to zero. Hence we have

$$\Delta X \doteq \frac{2ls^2\theta_0}{\gamma g} \left(\frac{K_{V_{s\delta}}}{k_{V_{2\delta}}} - \frac{K_{V_{2\delta}} k_{V_{s\delta}}}{k_{V_{2\delta}}^2} \right). \quad (15)$$

While the latter derivation is simpler and demonstrates the physics of the situation more clearly, it is not as satisfying since its accuracy cannot be determined for high-angle fire. The derivation using the Green's function gives a result valid for all quadrant elevations as long as the drag is small. If the spin is not constant or if the effects of nonlinear terms or the other aerodynamic forces and moments are to be included, the Green's function approach is mandatory.

The nonlinear character of the Magnus moment is sufficient at large quadrant elevations to reduce the moment to zero at the equilibrium yaw. Hence the yaw will be entirely to the right and the second term in the parenthesis in (13) should be omitted. Thus the increased range due to lift at high quadrant elevation is not partially compensated by the effects of Magnus moment as it is at lower quadrant elevation and the apparent "drag" coefficient varies markedly with elevation.

1.
2.
3.

APPENDIX A

GLOSSARY OF SYMBOLS

Listed here are the important symbols used, together with the name of the quantity designated by each and the sections where it is defined. In a few cases a brief definition is also given. Symbols not listed here are either used very briefly and defined where used or, occasionally, are part of the standard body of symbols of physics. For example, xyz and XYZ are used for rectangular coordinate axes.

A dot over a symbol indicates differentiation with respect to time; a prime indicates differentiation with respect to ζ . Vector quantities, as well as complex numbers, are indicated by **bold-face** type. As abbreviations, FSR means fin-stabilized rocket while SSR means spin-stabilized rocket.

All equations are valid in any absolute system of units. Thus one can measure mass, length, time and force in pounds, feet, seconds and poundals, respectively; or in kilograms, meters, seconds, and Newtons; or in slugs, feet, seconds, and pounds, etc.

Glossary of Symbols

a , velocity of sound in air (2.41).

$a_0=1,120$ ft./sec., velocity of sound in air under standard ballistic conditions (2.41).

A , cross-sectional area of projectile (2.41).

b , as a subscript denotes value at end of burning.

$b=(\gamma-1)^{\frac{1}{2}}$, constant describing inertial characteristics of SSR (9.24).

$B(Z)$, Didion-Bernoulli function (5.22).

c , deceleration coefficient (2.41).

C , ballistic coefficient (2.441).

$C(x)$, the Fresnel integral $\int_0^x \cos(\pi u^2/2) du$ (App. B).

C_D , aerodynamic drag coefficient (2.41; 8.25).

$C_l=C_L/\delta$, aerodynamic lift (cross-force) coefficient (2.41; 3.5; 8.25).

C_L , aerodynamic lift coefficient (2.41; 8.25).

$C_m=C_M/\delta$, aerodynamic restoring moment coefficient (2.41; 8.25).

C_M , aerodynamic restoring moment coefficient (2.41; 8.25).

C_q , aerodynamic damping moment coefficient (2.41; 3.5; 8.25).

d , diameter of projectile (2.41).

d , distance traveled by rocket, usually from start of burning.

d_b , burning distance; usually effective burning distance.

$d_{b,eff}=v_b^2/2G_{eff}$, effective burning distance (2.22).

D , diameter of projectile (8.1).

D , aerodynamic drag (2.41; 8.25).

$D(Z)$, Didion-Bernoulli function (6.3).

e_A , unit vector along axis of rocket (8.21).

e_r , unit vector in direction of motion of rocket (8.21).

$E(x)=C(x)+iS(x)$, complex Fresnel integral (appendix B).

$E^*(x)$, complex conjugate of $E(x)$.

$E_{\infty}(x)=E(\infty)-E(x)$, mathematical function (appendix B).

- f , factor measuring deflection toward flight line in aircraft firing of FSR (6.15).
- \bar{f} , measure of a transverse moment or torque; the vector force which, when applied unit distance from the center of mass, would produce this moment (3.22; 8.21).
- $\bar{f} = f_x + if_y$, complex representation of the transverse moment (3.22; 8.21).
- f_J , moment due to jet forces (8.51).
- f_{JD} , moment due to jet damping (8.51).
- f_M , aerodynamic moment (3.23).
- f_q , aerodynamic damping moment (3.23).
- f_R , moment due to thrust malalignment (8.51).
- f_{sq} , Magnus moment due to cross spin (8.23; 8.25).
- $f_{v^2\delta}$, aerodynamic restoring or overturning moment (8.22; 8.25).
- f_{vq} , damping moment due to cross spin (8.23; 8.25).
- $f_{vs\delta}$, Magnus moment (8.22; 8.25).
- $F(Z)$, Didion-Bernoulli function (5.22).
- F_\perp , vector force on projectile perpendicular to direction of motion; $F_\perp = F_x + iF_y$, complex representation of the vector (3.22; 9.11).
- F_A , total aerodynamic force on rocket (2.41).
- $F_{A\perp}$, component of F_A perpendicular to direction of motion (3.23).
- F_{AZ} , component of F_A along direction of motion (3.23).
- $F_g = mg$, force due to gravity (3.23).
- F_J , thrust due to jet action (2.22).
- $F_{J\parallel}$, component of jet force parallel to the trajectory (8.51).
- $F_{J\perp}$, component of jet force normal to the trajectory (8.51).
- F_{sq} , Magnus force due to cross spin (8.23; 8.25).
- F_{v^2} , aerodynamic drag (8.22; 8.25).
- $F_{v^2\delta}$, aerodynamic lift (8.22; 8.25).
- F_{vq} , lift due to cross spin (8.23; 8.25).
- $F_{vs\delta}$, Magnus force (8.22; 8.25).
- F_Z , component of force F along the direction of motion (3.23).
- $F_\infty(x)$, mathematical function (appendix B).
- g , acceleration due to gravity.
- G , acceleration of rocket (usually effective acceleration) (3.31).
- G_{eff} , effective acceleration of rocket (2.22).
- G_J , acceleration due to jet forces alone (2.21).
- H , angular momentum of rocket about center of mass (9.14).
- $H(\zeta, b)$, mathematical function (appendix B).
- $i \equiv \sqrt{-1}$.
- i , form factor of projectile (2.441).
- \mathbf{i} , unit vector (usually along X -axis).
- $I = mK^2$, moment of inertia of rocket about transverse axis through the center of mass (2.26).
- \mathbf{j} , unit vector (usually along Y -axis).
- $\mathbf{J}(x)$, complex mathematical function (appendix B).
- $J_R(x)$, real part of $\mathbf{J}(x)$ (appendix B).
- $J_I(x)$, imaginary part of $\mathbf{J}(x)$ (appendix B).
- $J(Z)$, Didion-Bernoulli function (5.22).
- k , radius of gyration of projectile about longitudinal axis through center of mass.
- \mathbf{k} , unit vector (usually along Z -axis).

- k_{sq} , Magnus moment coefficient due to cross spin (8.23; 8.25).
 k_{v^2s} , aerodynamic overturning moment coefficient (8.22; 8.25).
 k_{vq} , aerodynamic damping moment coefficient due to cross spin (8.23; 8.25).
 k_{vs} , aerodynamic spin deceleration moment coefficient (8.22; 8.25).
 k_{vss} , Magnus moment coefficient (8.22; 8.25).
 K , radius of gyration of projectile about transverse axis through center of mass.
 K_{JD} , jet damping torque coefficient (2.26).
 K_{sq} , Magnus force coefficient due to cross spin (8.23; 8.25).
 K_{v^2} , aerodynamic drag coefficient (same as deceleration coefficient c) (8.22).
 K_{v^2s} , aerodynamic lift coefficient (8.22; 8.25).
 K_{vq} , lift coefficient due to cross spin (8.23; 8.25).
 K_{vss} , Magnus force coefficient (8.22; 8.25).
 l , over-all length of rocket (2.41).
 l_g , length of the grain (8.1).
 l_{gr} , distance from center of mass of grain to rear end of rocket (8.1).
 l_J , distance from center of mass of rocket to rear end of rocket (8.1).
 l_L , distance from center of lift to center of mass (2.41).
 $\ln = \log_e$.
 l_P , distance from center of pressure to center of mass (2.41).
 L , aerodynamic lift (2.41; 8.25).
 m , mass of rocket (usually a function of time).
 m_b , mass of rocket after burning (2.21).
 m_i , total mass of rocket before burning (2.21).
 m_N , constant related to the nutational motion (9.31).
 m_P , constant related to the precessional motion (9.31).
 M , aerodynamic restoring moment (2.41; 8.25).
 M_J , effective moment of force about center of mass produced by the jet forces (2.24).
 M_{JD} , jet damping torque (2.26).
 M_q , aerodynamic damping moment (2.41).
 M_{vs} , aerodynamic spin deceleration moment (8.22; 8.25).
 n , number of turns resulting from spin about longitudinal axis (a function of time) (3.61).
 n_σ , number of turns resulting from constant spin in traversing the characteristic distance σ (3.62).
 N , as a subscript refers to nutational motion (10.11).
 N , number of nozzles in any rocket (8.52).
 $N_P = \omega_N / \omega_P$, number of nutations per precession (10.11).
 p , as a subscript denotes value of quantity at the instant of launching; i. e., when all constraints of the launcher are removed.
 p , launcher length (usually effective launcher length) (3.1).
 p_{eff} , effective launcher length (2.23).
 P , as a subscript refers to precessional motion (10.11).
 P_0 , air pressure under standard ballistic conditions (750 mm of Hg) (2.41; 8.21).
 q , magnitude of transverse angular velocity; as a subscript it refers to mallaunching (2.41; 8.21; 9.24).
 \mathbf{q} , vector cross spin (or transverse angular velocity, $\dot{\phi}$) (2.41; 8.21).
 $q_p = \dot{\phi}_p$, mallaunching; the angular velocity of the rocket about a transverse axis at instant of launching.
 $q_p = \dot{\phi}_p$, complex mallaunching.

- \mathbf{r} , linear deflection of rocket from launcher line ($\mathbf{r} = X_0 + iY_0$) (3.35; 9.11).
 \mathbf{r}_F , linear deflection of FSR from launcher line resulting from fin malalignment δ_0 (3.42).
 \mathbf{r}_g , linear deflection of rocket from launcher line resulting from gravity (3.38; 9.22).
 \mathbf{r}_q , linear deflection of rocket from launcher line resulting from mallaunching \mathbf{q}_p (3.36).
 \mathbf{r}_R , linear deflection of rocket from launcher line resulting from linear malalignment \mathbf{R}_M (3.39).
 \mathbf{r}_W , linear deflection of rocket from launcher line resulting from crosswind \mathbf{W}_n (3.43).
 \mathbf{r}_β , linear deflection of rocket from launcher line resulting from angular malalignment β_M (3.41).
 \mathbf{r}_δ , linear deflection of rocket from launcher line resulting from initial yaw δ_p (3.35).
 R , radius of projectile (8.22).
 R , usual symbol for range.
 $R_F(\xi_p, \xi)$, characteristic function for determining \mathbf{r}_F (FSR) (3.42).
 $R_g(\xi_p, \xi)$, characteristic function for determining \mathbf{r}_g (FSR) (3.38).
 $\mathbf{R}_g(\xi_p, \xi)$, characteristic function for determining \mathbf{r}_g (SSR) (9.22).
 R_J , radius of nozzle circle (8.52).
 R_M , magnitude of linear malalignment (2.24).
 \mathbf{R}_M , linear malalignment vector, or complex linear malalignment (2.24).
 $R_N = s/\omega_N$, number of spin rotations per nutation (10.11).
 $\mathbf{R}_0 = \nu \mathbf{R}_M / K^2$, dimensionless constant proportional to \mathbf{R}_M for SSR (9.24).
 $R_P = s/\omega_P$, number of spin rotations per precession (10.11).
 $R_q(\xi_p, \xi)$, characteristic function for determining \mathbf{r}_q (FSR) (3.36).
 $\mathbf{R}_q(\xi_p, \xi)$, characteristic function for effects of mallaunching in SSR (9.32).
 $R_R(\xi_p, \xi)$, characteristic function for determining \mathbf{r}_R (FSR) (3.39).
 $R_W(\xi_p, \xi)$, characteristic function for determining \mathbf{r}_W (FSR) (3.43).
 $R_\beta(\xi_p, \xi)$, characteristic function for determining \mathbf{r}_β (FSR) (3.41).
 $R_\delta(\xi_p, \xi)$, characteristic function for determining \mathbf{r}_δ (FSR) (3.35).
 $\mathbf{R}_\varphi(\xi_p, \xi)$, characteristic function for effects of initial cross-pointing in SSR (9.32).
 s , angular velocity of spin of rocket (3.6; 8.1).
 s_b , spin at end of burning (8.1).
 S , stability factor (8.1).
 S , sighting angle in forward firing from aircraft (6.52).
 $S(x)$, the Fresnel integral $\int_0^x \sin(\pi u^2/2) du$ (appendix B).
 S_N , effective stability factor for nutations (10.22).
 t , time (usually from start of burning).
 t_b , burning time (usually effective burning time).
 $t_{b, \text{eff}}$, effective burning time (2.22).
 t_p , time at which rocket leaves launcher (3.1).
 $t_\lambda \equiv (2\lambda/G)^{1/2}$, characteristic time for SSR (8.1).
 $t_\sigma \equiv (2\sigma/G)^{1/2}$, characteristic time for FSR (2.11).
 T , effective rocket temperature (2.31).
 T_a , air temperature (2.31).
 T_e , time of flight of equivalent shell (5.11).
 T_0 , air temperature under standard ballistic conditions (59° F.).
 $\mathbf{u} = \dot{\mathbf{r}}$, the cross velocity (9.11).
 v , velocity of rocket relative to launcher; in firing from a stationary launcher in the absence of wind $v = V$ (3.33).
 v_b , velocity of rocket at end of burning (2.22).
 v_e , velocity of equivalent shell (5.11).

- v_0 , burnt velocity of rocket in absence of gravity and drag (2.22).
 v_p , velocity of rocket at instant of launching.
 $v_\lambda \equiv (2G\lambda)^{\frac{1}{2}}$, characteristic velocity for SSR (8.1).
 $v_\sigma \equiv (2G\sigma)^{\frac{1}{2}}$, characteristic velocity for FSR (2.11).
 V , velocity of rocket relative to surrounding air (2.41; 3.33).
 V_A , velocity of airplane in forward firing (6.11).
 V_{At} , indicated air speed of the aircraft (6.51).
 $V_D(Z)$, Didion-Bernoulli function (6.3).
 V_g , velocity of efflux of the jet gases (2.21).
 W , as a subscript refers to effect of wind.
 $W = W_x + iW_y$, complex wind velocity (3.43; 9.35).
 $W_{||}$, component of wind velocity parallel to range line (3.43).
 W_{\perp} , component of wind velocity perpendicular to range line (3.43).
 $W_n = W_{\perp} + iW_{||} \sin \theta_0$, component of wind velocity normal to launcher line (3.43).
 $W_z = W_{||} \cos \theta_0$, component of wind velocity parallel to the launcher line (3.44).
 y_g , linear gravity drop of rocket from flight line in forward firing from aircraft (6.14).
 Z , dimensionless parameter in Didion-Bernoulli method (5.22).
 α , dive angle of aircraft (6.11).
 α , angular acceleration of spin (9.11).
 β , angle between launcher line and aircraft boresight datum line (6.52).
 β_M , magnitude of angular malalignment (2.24).
 β_M , angular malalignment vector, or complex angular malalignment (2.24).
 $\gamma = K^2/k^2$, ratio of moments of inertia (8.1).
 γ_{sq} , Magnus moment coefficient due to cross spin (8.23).
 $\gamma_{v^2\delta}$, aerodynamic overturning moment coefficient (8.22).
 γ_{vq} , aerodynamic damping moment coefficient due to cross spin (8.23).
 γ_{vs} , aerodynamic spin deceleration moment coefficient (8.22).
 $\gamma_{vs\delta}$, Magnus moment coefficient (8.22).
 Γ_{sq} , Magnus force coefficient due to cross spin (8.23).
 Γ_{v^2} , aerodynamic drag coefficient (8.22).
 $\Gamma_{v^2\delta}$, aerodynamic lift coefficient (8.22).
 Γ_{vq} , aerodynamic lift coefficient due to cross spin (8.23).
 $\Gamma_{vs\delta}$, Magnus force coefficient (8.22).
 δ , angle of yaw (2.41).
 $\delta = \delta_x + i\delta_y$, complex designation of yaw angle (3.21).
 δ_a , yaw with respect to surrounding air (wind effects) (9.35).
 δ_0 , fin (aerodynamic) malalignment (2.47).
 δ_F , complex yaw resulting from fin malalignment (3.33).
 δ_g , complex yaw resulting from gravity (3.33).
 δ_q , complex yaw resulting from mallaunching (3.33).
 δ_R , complex yaw resulting from linear malalignment (3.33).
 δ_{sR} , complex yaw resulting from linear malalignment in case of constant slow spin of FSR (3.62).
 δ_β , complex yaw resulting from angular malalignment (3.33).
 δ_i , complex yaw resulting from initial yaw (3.33).
 δ_φ , complex yaw resulting from initial cross pointing (3.33).
 $\Delta(\zeta_p, \zeta)$, dimensionless characteristic function for determining the yaw for FSR (3.33).
 $\Delta_F(\zeta_p, \zeta)$, characteristic function for effects of fin malalignment (3.33).

- $\Delta_g(\zeta_p, \zeta)$, characteristic function for effects of gravity for FSR (3.33).
 $\Delta_q(\zeta_p, \zeta)$, characteristic function for effects of mallaunching for FSR (3.33).
 $\Delta_R(\zeta_p, \zeta)$, characteristic function for effects of linear malalignment for FSR (3.33).
 $\Delta_\beta(\zeta_p, \zeta)$, characteristic function for effects of angular malalignment for FSR (3.33).
 $\Delta_\delta(\zeta_p, \zeta)$, characteristic function for effects of initial yaw for FSR (3.33).
 $\Delta_\varphi(\zeta_p, \zeta)$, characteristic function for effects of cross pointing for FSR (3.33).
 $\Delta_q(\zeta_p, \zeta)$, characteristic function for effects of mallaunching for SSR (9.12).
 $\Delta_R(\zeta_p, \zeta)$, characteristic function for effects of linear malalignment for SSR (9.24).
 $\Delta_{sR}(\zeta_p, \zeta)$, characteristic function for effects of linear malalignment in case of constant slow spin of FSR (3.62).
 $\Delta_\delta(\zeta_p, \zeta)$, characteristic function for effects of initial yaw for SSR (9.12).
 $\Delta_\varphi(\zeta_p, \zeta)$, characteristic function for effects of initial cross pointing for SSR (9.12).
 ϵ , angular gravity drop of rocket from effective launching line in forward firing from aircraft (6.3)
 $\epsilon = r/d$, angular displacement of rocket from launcher line as seen from launcher (9.11).
 ϵ_q , angular displacement resulting from mallaunching for SSR (9.12).
 ϵ_δ , angular displacement resulting from initial yaw for SSR (9.12).
 ϵ_φ , angular displacement resulting from initial cross-pointing for SSR (9.12).
 $E(\zeta_p, \zeta)$, characteristic function for determining the angular displacement ϵ (9.12).
 $E_q(\zeta_p, \zeta)$, characteristic function for effects of mallaunching for SSR (9.12).
 $E_\delta(\zeta_p, \zeta)$, characteristic function for effects of initial yaw for SSR (9.12).
 $E_\varphi(\zeta_p, \zeta)$, characteristic function for effects of initial cross-pointing for SSR (9.12).
 ζ , dimensionless measure of time (or of velocity) used during burning. For FSR in ground firing, $\zeta = t/t_\sigma = V/v_\sigma = (d/\sigma)^{\frac{1}{2}}$ (3.33). For SSR, $\zeta = t/t_\lambda = V/v_\lambda = (d/\lambda)^{\frac{1}{2}}$ (9.11).
 ζ_p , value of ζ at launching.
 η , coefficient of viscosity of air (2.41).
 η , effective angle of attack of aircraft boresight datum line (6.51).
 η , nozzle cant angle (8.52).
 θ_e , quadrant elevation of equivalent shell (5.11).
 θ_0 , quadrant elevation of launcher (2.22).
 ϑ , angle between tangent to trajectory and the launcher line; i. e., deflection of tangent from initial direction of motion (3.21).
 $\vartheta = \vartheta_x + i\vartheta_y$, complex representation of deflection of trajectory (3.21).
 $\vartheta_{g, vac}$, deflection of trajectory due to gravity in vacuum case (3.1).
 $\vartheta_{q, vac}$, deflection of trajectory due to mallaunching in vacuum case (3.13).
 $\vartheta_{R, vac}$, deflection of trajectory due to linear malalignment in vacuum case (3.12).
 $\vartheta_{\beta, vac}$, deflection of trajectory due to angular malalignment in vacuum case (3.12).
 ϑ_a , deflection of trajectory with respect to surrounding air (wind effects) (9.35).
 ϑ_F , deflection of trajectory resulting from fin malalignment (3.33).
 ϑ_g , deflection of trajectory resulting from gravity (3.33).
 ϑ_q , deflection of trajectory resulting from mallaunching (3.33).
 ϑ_R , deflection of trajectory resulting from linear malalignment (3.33).
 ϑ_{sR} , deflection of trajectory resulting from linear malalignment in case of constant slow spin of FSR (3.62).
 ϑ_w , deflection of trajectory resulting from cross-wind (3.43).
 ϑ_β , deflection of trajectory resulting from angular malalignment (3.33).
 ϑ_δ , deflection of trajectory resulting from initial yaw (3.33).
 ϑ_φ , deflection of trajectory resulting from cross-pointing (3.33).

- $\theta(\zeta_p, \zeta)$, dimensionless characteristic function for determining the deflection of the tangent to the trajectory for FSR (3.33).
- $\theta_F(\zeta_p, \zeta)$, characteristic function for effects of fin malalignment (3.33).
- $\theta_g(\zeta_p, \zeta)$, characteristic function for effects of gravity for FSR (3.33).
- $\theta_L(\zeta_p, \zeta)$, characteristic function for effects of mallaunching for FSR (3.33).
- $\theta_R(\zeta_p, \zeta)$, characteristic function for effects of linear malalignment for FSR (3.33).
- $\theta_W(\zeta_p, \zeta)$, characteristic function for effects of wind for FSR (3.43).
- $\theta_\beta(\zeta_p, \zeta)$, characteristic function for effects of angular malalignment for FSR (3.33).
- $\theta_\delta(\zeta_p, \zeta)$, characteristic function for effects of initial yaw for FSR (3.33).
- $\theta_\varphi(\zeta_p, \zeta)$, characteristic function for effects of cross-pointing for FSR (3.33).
- $\theta_L(\zeta_p, \zeta)$, characteristic function for effects of mallaunching for SSR (9.12).
- $\theta_R(\zeta_p, \zeta)$, characteristic function for effects of linear malalignment for SSR (9.24).
- $\theta_{LR}(\zeta_p, \zeta)$, characteristic function for effects of linear malalignment in case of constant slow spin of FSR (3.62).
- $\theta_\delta(\zeta_p, \zeta)$, characteristic function for effects of initial yaw for SSR (9.12).
- $\theta_\varphi(\zeta_p, \zeta)$, characteristic function for effects of initial cross-pointing for SSR (9.12).
- $\theta(Z)$, Didion-Bernoulli function (5.22).
- κ , radius of gyration of propellant about its longitudinal axis (8.52).
- λ , angle of attack of launcher line in forward firing from aircraft (6.11).
- λ , characteristic oscillation distance for SSR. ($\lambda = \gamma\nu$, the distance traveled per nutation) (8.1).
- $\mu = V_A/v_\lambda$, dimensionless airplane velocity in aircraft firing of SSR (9.52).
- $\mu(t)$, mass of propellant ejected up to time t during burning (2.21).
- μ_b , total mass of gas ejected (initial mass of propellant) (2.21).
- ν , angular velocity factor in aircraft firing of FSR (6.16).
- $\nu = 2\pi v/s$, distance traveled per spin revolution of SSR (8.1).
- $\xi = m_N^{\frac{1}{2}}\zeta$, dimensionless variable (9.32—9.35).
- $\xi_p = m_N^{\frac{1}{2}}\zeta_p$, dimensionless variable (9.32—9.35).
- ρ , density of air (2.41).
- ρ_0 , density of air under standard ballistic conditions (0.07513 lb./ft.³).
- σ , characteristic yaw oscillation distance for FSR (3.32).
- $\tau = t + V_A/G$, "equivalent" time in aircraft firing of FSR (6.2).
- $T = f_{V\delta\delta}/f_{V^2\delta}$, ratio of Magnus to overturning moment (9.41).
- φ , orientation angle; angle through which rocket axis has rotated from its initial direction on the launcher (3.21).
- $\varphi = \varphi_X + i\varphi_Y$, complex representation of orientation angle (3.21).
- φ_p , initial cross-pointing; orientation angle at instant of launching.
- φ_H , angle between rocket axis and angular momentum vector \mathbf{H} (9.14).
- φ_ω , angle between rocket axis and angular velocity vector $\boldsymbol{\omega}$ (9.14).
- φ_a , orientation angle with respect to surrounding air (wind effects) (9.35).
- φ_F , orientation angle resulting from fin malalignment (3.33).
- φ_g , orientation angle resulting from gravity (3.33).
- φ_L , orientation angle resulting from mallaunching (3.33).
- φ_R , orientation angle resulting from linear malalignment (3.33).
- φ_{LR} , orientation angle resulting from linear malalignment in case of constant slow spin of FSR (3.62).
- φ_β , orientation angle resulting from angular malalignment (3.33).
- φ_δ , orientation angle resulting from initial yaw (3.33).
- φ_φ , orientation angle resulting from initial cross-pointing (3.33).

- $\Phi(\zeta_P, \zeta)$, dimensionless characteristic function for determining the orientation angle for FSR (3.33).
- $\Phi_F(\zeta_p, \zeta)$, characteristic function for effects of fin malalignment (3.33).
- $\Phi_g(\zeta_p, \zeta)$, characteristic function for effects of gravity for FSR (3.33).
- $\Phi_a(\zeta_p, \zeta)$, characteristic function for effects of mallaunching for FSR (3.33).
- $\Phi_R(\zeta_p, \zeta)$, characteristic function for effects of linear malalignment for FSR (3.33).
- $\Phi_\beta(\zeta_p, \zeta)$, characteristic function for effects of angular malalignment for FSR (3.33).
- $\Phi_\delta(\zeta_p, \zeta)$, characteristic function for effects of initial yaw for FSR (3.33).
- $\Phi_\varphi(\zeta_p, \zeta)$, characteristic function for effects of initial cross-pointing for FSR (3.33).
- $\Phi_a(\zeta_p, \zeta)$, characteristic function for effects of mallaunching for SSR (9.12).
- $\Phi_R(\zeta_p, \zeta)$, characteristic function for effects of linear malalignment for SSR (9.24).
- $\Phi_{sR}(\zeta_p, \zeta)$, characteristic function for effects of linear malalignment in case of constant slow spin of FSR (3.62).
- $\Phi_\delta(\zeta_p, \zeta)$, characteristic function for effects of initial yaw for SSR (9.12).
- $\Phi_\varphi(\zeta_p, \zeta)$, characteristic function for effects of initial cross-pointing for SSR (9.12).
- $\chi = m_P \zeta$, dimensionless variable (9.32—9.35).
- $\chi_p = m_P \zeta_p$, dimensionless variable (9.32—9.35).
- ψ , angle of rotation resulting from spin (9.11).
- $\omega = \dot{\varphi}$, angular velocity of rocket about a transverse axis (2.26).
- ω_N , angular frequency of nutation (9.19).
- ω_P , angular frequency of precession (9.19).

APPENDIX B

INTEGRALS, SERIES, AND ASYMPTOTIC EXPANSIONS

A complete mathematical discussion of the Fresnel integral and associated functions used in chapters 3 and 9 to describe the motion of rockets during burning would take a long chapter in its own right. Such a discussion (with, however, considerably different notation) is given by Rosser,¹ and some properties of the more simple functions may be found in more elementary treatises such as that by Jahnke and Emde.² Here our aim is to present a list of the more important properties of these functions with, at most, only an indication of the proof.

The chief mathematical functions used in the text are:

$$C(x) = \int_0^x \cos(\pi u^2/2) du = 2 \int_0^{x/2} \cos 2\pi y^2 dy, \quad (1)$$

$$S(x) = \int_0^x \sin(\pi u^2/2) du = 2 \int_0^{x/2} \sin 2\pi y^2 dy. \quad (2)$$

These functions are the well known Fresnel integrals used in the theory of diffraction of light by a plane slit and are frequently plotted as rectangular coordinates to give the Cornu Spiral.² This spiral is just the locus, in the complex plane, of the function

$$E(x) = \int_0^x \exp(i\pi u^2/2) du = C(x) + iS(x). \quad (3)$$

This function enters into the theory in the text because of the symmetry of the missiles in the x and y directions. Most of the integrals of $C(x)$ and $S(x)$ are expressible in simple terms. The most important one not so expressible is

$$\begin{aligned} J(x) &= \int_0^x \exp(i\pi u^2/2) E^*(u) du \\ &= J_R(x) + iJ_I(x), \end{aligned} \quad (4)$$

where the asterisk indicates the complex conjugate, $E^* = C - iS$. Here

$$\begin{aligned} J_I(x) &= \int_0^x [C(u) \sin \pi u^2/2 - S(u) \cos \pi u^2/2] du \\ &= C_S(x) - S_C(x), \end{aligned} \quad (5)$$

where

$$C_S(x) = \int_0^x C(u) \sin \pi u^2/2 du = \frac{1}{2} C(x)S(x) + \frac{1}{2} J_I(x), \quad (6)$$

and

¹ J. B. Rosser, "Theory and Application of $\int_0^z e^{-x^2} dx$ and $\int_0^z e^{-x^2 y^2} dy \int_0^y e^{-x^2} dx$," Brooklyn; reproduced by arrangement with Office of Technical Services, Department of Commerce, by Mapleton House, 1948.

² Eugene Jahnke and Fritz Emde, "Tables of Functions With Formulae and Curves," Dover Publications, 1943.

$$S_c(x) = \int_0^x S(u) \cos \pi u^2/2 du = \frac{1}{2} C(x)S(x) - \frac{1}{2} J_I(x), \quad (7)$$

and

$$\begin{aligned} J_R(x) &= \int_0^x [C(u) \cos \pi u^2/2 + S(u) \sin \pi u^2/2] du \\ &= \frac{1}{2} [C^2(u) + S^2(u)]. \end{aligned} \quad (8)$$

The functions C , S , and J_I are tabulated in appendix C; C_s , S_c , and J_R are then easily found. Two other related functions are

$$Si(x) = \int_0^x \sin u \, du/u, \quad (9)$$

i. e.,

$$\int_0^x \sin (\pi u^2/2) du/u = \frac{1}{2} Si(\pi x^2/2), \quad (10)$$

and

$$Ci(x) = - \int_x^\infty \cos u \, du/u, \quad (11)$$

i. e.,

$$\int_x^\infty \cos (\pi u^2/2) du/u = -\frac{1}{2} Ci(\pi x^2/2). \quad (12)$$

Some simple numerical values of these functions are

$$S(\infty) = C(\infty) = 2 J_R(\infty) = \frac{1}{2}, \quad (13)$$

and

$$Si(\infty) = \pi/2. \quad (14)$$

In the following list of integrals most of the formulas are given in complex form to simplify them and because this is the form generally required. It is an easy matter to separate the real and imaginary parts if desired. Other formulas used in the text either can be obtained by integration by parts or can be verified by differentiation.

$$\int_0^x \exp(i\pi u^2/2) u \, du = (i/\pi)[1 - \exp(i\pi x^2/2)]. \quad (15)$$

$$\int_0^x \exp(i\pi u^2/2) u^2 du = -(i x/\pi) \exp(i\pi x^2/2) + (i/\pi) E(x). \quad (16)$$

$$\int_0^x \exp(i\pi u^2/2) u^n du = -\frac{i x^{n-1}}{\pi} \exp(i\pi x^2/2) + \frac{(n-1)i}{\pi} \int_0^x \exp(i\pi u^2/2) u^{n-2} du. \quad (17)$$

$$\int_0^\infty \exp(i\pi u^2/2) du/u = -\frac{1}{2} [Ci(\pi x^2/2) + iSi(\pi x^2/2) - (i\pi/2)] \quad (18a)$$

Numerical tables of these functions are available or one can use (33), (48), and (49).

$$\int_x^\infty \exp(i\pi u^2/2) du/u^2 = \frac{1}{2} \pi(-1+i) + (1/x) \exp(i\pi x^2/2) - i\pi E(x). \quad (18b)$$

$$\int_x^\infty \exp(i\pi u^2/2) du/u^n = \frac{1}{(n-1)x^{n-1}} \exp(i\pi x^2/2) + \frac{i\pi}{n-1} \int_x^\infty \exp(i\pi u^2/2) du/u^{n-2}. \quad (19)$$

$$\int_0^x E(u) du = xE(x) + (i/\pi) [\exp(i\pi x^2/2) - 1]. \quad (20)$$

$$\int_0^x E(u) u du = (ix/2\pi) \exp(i\pi x^2/2) + \frac{1}{2} (x^2 - i/\pi) E(x). \quad (21)$$

$$\int_0^x E(u) u^n du = [x^{n+1}/(n+1)] E(x) - [1/(n+1)] \int_0^x \exp(i\pi u^2/2) u^{n+1} du. \quad (22)$$

$$\int_0^x S(u) du/u^2 = -(1/x) S(x) + \frac{1}{2} Si(\pi x^2/2). \quad (23)$$

$$\int_x^\infty C(u) du/u^2 = (1/x) C(x) - \frac{1}{2} Ci(\pi x^2/2). \quad (24)$$

Since $\exp(i\pi x^2/2)$ is an analytic function throughout the complex plane, it and its integrals may be expanded in power series convergent for all finite values of the argument. The simplest method of obtaining these series is to integrate term by term after expanding the integrands (multiplication of these series by each other is justified by their absolute convergence and the resulting series has the same property).

$$\begin{aligned} E(x) &= \int_0^x \sum_{n=0}^{\infty} \frac{1}{n!} \left(\frac{i\pi u^2}{2} \right)^n du \\ &= \sum_{n=0}^{\infty} \frac{(i\pi/2)^n x^{2n+1}}{n!(2n+1)}. \end{aligned} \quad (25)$$

$$\begin{aligned} C(x) &= \sum_{n=0}^{\infty} \frac{(-1)^n}{4n+1} \frac{(\pi/2)^{2n}}{(2n)!} x^{4n+1} \\ &= x - \frac{\pi^2}{40} x^5 + \frac{\pi^4}{3456} x^9 - \dots \end{aligned} \quad (26)$$

$$\begin{aligned} S(x) &= \sum_{n=0}^{\infty} \frac{(-1)^n}{4n+3} \frac{(\pi/2)^{2n+1}}{(2n+1)!} x^{4n+3} \\ &= \frac{\pi}{6} x^3 - \frac{\pi^3}{336} x^7 + \frac{\pi^5}{4224} x^{11} - \dots \end{aligned} \quad (27)$$

$$J(x) = \frac{1}{2} \sum_{n=0}^{\infty} \frac{(i\pi/2)^n x^{2n+2}}{n+1} \sum_{r=0}^n \frac{(-1)^r}{(2r+1)(n-r)!r!} \quad (28)$$

$$\begin{aligned} J_R(x) &= \frac{1}{2} \sum_{n=0}^{\infty} \frac{(-1)^n (\pi/2)^{2n} x^{4n+2}}{(2n+1)} \sum_{r=0}^{2n} \frac{(-1)^r}{(2r+1)(2n-r)!r!} \\ &= 0.5 x^2 - 0.1096623 x^6 + 0.0103089 x^{10} - 0.0005082 x^{14} + \dots \end{aligned} \quad (29)$$

$$\begin{aligned} J_I(x) &= \frac{1}{4} \sum_{n=0}^{\infty} \frac{(-1)^n (\pi/2)^{2n+1} x^{4n+4}}{(n+1)} \sum_{r=0}^{2n+1} \frac{(-1)^r}{r!(2n-r+1)!(2r+1)} \\ &= 0.261799 x^4 - 0.0369122 x^8 + 0.002453259 x^{12} - 0.0000931267 x^{16} + \dots \end{aligned} \quad (30)$$

$$C_s(x) = \frac{1}{4} \sum_{n=0}^{\infty} \frac{(-1)^n (\pi/2)^{2n+1} x^{4n+4}}{n+1} \sum_{r=0}^n \frac{1}{(4r+1)(2r)!(2n-2r+1)!}$$

$$= 0.392699 x^4 - 0.12919281 x^8 + 0.02361263 x^{12} - 0.002817055 x^{16} + \dots \quad (31)$$

$$S_c(x) = \frac{1}{4} \sum_{n=0}^{\infty} \frac{(-1)^n (\pi/2)^{2n+1} x^{4n+4}}{n+1} \sum_{r=0}^n \frac{1}{(4r+3)(2r+1)!(2n-2r)!}$$

$$= 0.13089969 x^4 - 0.09228058 x^8 + 0.021159365 x^{12} - 0.002723928 x^{16} + \dots \quad (32)$$

$$Si(x) = \sum \frac{(-1)^n x^{2n+1}}{(2n+1)(2n+1)!} = x - \frac{x^3}{18} + \frac{x^5}{600} - \dots \quad (33a)$$

$$Ci(x) = \ln x + \gamma + \sum_{n=1}^{\infty} \frac{(-1)^n x^{2n}}{2n(2n)!} = \ln x + 0.577215 \dots - \frac{x^2}{4} + \frac{x^4}{96} - \dots \quad (33b)$$

The asymptotic expansions of these functions can be derived most easily by repeated integration by parts. The validity of the expansion can be verified by examination of the remainder after N integrations and once verified it is permissible to multiply series and integrate term by term (differentiation is in general not permissible with asymptotic expansions). For $E(x)$ we have

$$E(x) = \int_0^{\infty} \exp(i\pi u^2/2) du - \int_x^{\infty} \exp(i\pi u^2/2) du$$

$$= \frac{1}{2}(1+i) - \left[\frac{1}{u} \frac{\exp(i\pi u^2/2)}{i\pi} \right] \Big|_x^{\infty} - \int_x^{\infty} \frac{\exp(i\pi u^2/2)}{i\pi u^2} du$$

$$= \frac{1}{2}(1+i) - \exp(i\pi x^2/2) \left\{ \frac{i}{\pi x} + \sum_{n=0}^{N-2} \frac{(-i)^n (2n+1)!}{n! 2^n \pi^{n+2} x^{2n+3}} \right\} + R_N, \quad (34)$$

where the remainder after N integrations is

$$R_N = \int_x^{\infty} \frac{1 \cdot 3 \cdot 5 \cdot 7 \dots (2N-1)}{(i\pi u^2)^N} \exp(i\pi u^2/2) du. \quad (35)$$

Now

$$|R_N| \leq \int_x^{\infty} \frac{1 \cdot 3 \cdot 5 \cdot 7 \dots (2N-1)}{x(\pi u^2)^N} du = \frac{1 \cdot 3 \cdot 5 \dots (2N-3)}{(i\pi) x^{2N-1}}, \quad (36)$$

so that for fixed N , $R_N(x) \rightarrow 0$ as required for an asymptotic series. We omit the proof that $\lim_{N \rightarrow \infty} R_N(x) \rightarrow \infty$. Thus the asymptotic expansion of $E(x)$ is

$$E(x) \sim \frac{1}{2}(1+i) - \exp(i\pi x^2/2) \left\{ \frac{i}{\pi x} + \sum_{n=0}^{\infty} \frac{(-i)^n (2n+1)!}{n! 2^n \pi^{n+2} x^{2n+3}} \right\}$$

$$= \frac{1}{2}(1+i) + \frac{\exp(i\pi x^2/2)}{i\pi x} \left\{ 1 + \frac{1}{i\pi x^2} + \frac{1 \cdot 3}{(i\pi x^2)^2} + \frac{1 \cdot 3 \cdot 5}{(i\pi x^2)^3} + \dots \right\}. \quad (37)$$

The expansions for $C(x)$ and $S(x)$ follow from this by separation of real and imaginary parts.

$$C(x) \sim \frac{1}{2} - \cos(\pi x^2/2) \left\{ \frac{0.10132118}{x^3} - \frac{0.1539897}{x^7} + \dots \right\}$$

$$+ \sin(\pi x^2/2) \left\{ \frac{0.318309886}{x} - \frac{0.09675459}{x^5} + \dots \right\}. \quad (38)$$

$$S(x) \sim \frac{1}{2} - \sin(\pi x^2/2) \left\{ \frac{0.10132118}{x^3} - \frac{0.1539897}{x^7} + \dots \right\} \\ - \cos(\pi x^2/2) \left\{ \frac{0.318309886}{x} - \frac{0.09675459}{x^5} + \dots \right\}. \quad (39)$$

The asymptotic series for $J(x)$ may be obtained from the expression

$$J(x) = \lim_{T \rightarrow \infty} \left\{ \int_0^T \exp(i\pi u^2/2) E^*(u) du - \int_x^T \exp(i\pi u^2/2) E^*(u) du \right\}, \quad (40)$$

where we substitute the asymptotic expansion for $E^*(u)$ in the second integral. Thus

$$J(x) \sim \lim_{T \rightarrow \infty} \left\{ \int_0^T \exp(i\pi u^2/2) E^*(u) du - \int_x^T \exp(i\pi u^2/2) \frac{1}{2}(1-i) du \right. \\ \left. - \int_x^T \frac{1}{-i\pi u} \left[1 + \frac{1}{(-i\pi u^2)} + \frac{1 \cdot 3}{(-i\pi u^2)^2} + \dots \right] du \right\} \\ = \text{const.} + \frac{1}{2}(1-i) \frac{\exp(i\pi x^2/2)}{i\pi x} \left\{ 1 + \frac{1}{(i\pi x^2)} + \frac{1 \cdot 3}{(i\pi x^2)^2} + \dots \right\} \\ + \frac{i}{\pi} \left[\ln x - \frac{i}{2\pi x^2} + \frac{1 \cdot 3}{4(\pi x^2)^2} + \frac{1 \cdot 3 \cdot 5 i}{6(\pi x^2)^3} - \frac{1 \cdot 3 \cdot 5 \cdot 7}{8(\pi x^2)^4} - \dots \right], \quad (41)$$

where the constant is given by

$$\text{const.} = \lim_{T \rightarrow \infty} \left\{ \int_0^T \exp(i\pi u^2/2) E^*(u) du - \frac{i}{\pi} \ln T \right\}. \quad (42)$$

The real part of the const. is $\frac{1}{4}$, since $J_R(\infty) = \frac{1}{4}$; but the imaginary part can only be evaluated by rather complicated transformations of (42). However, its numerical value could be obtained by equating the power series and asymptotic series at some intermediate value of x . As shown by Rosser, its value is

$$\text{const.} = \frac{1}{4} + (i/2\pi)(\gamma + \ln 2\pi) \\ = 0.25 + 0.384375 i, \quad (43)$$

where γ is Euler's constant. Separating real and imaginary parts we have

$$J_R(x) \sim \frac{1}{4} + \frac{1}{2\pi^2 x^2} - \frac{5}{2\pi^4 x^6} + \dots - \cos(\pi x^2/2) \left\{ \frac{1}{2\pi x} + \frac{1}{2\pi^2 x^3} - \frac{3}{2\pi^3 x^5} + \dots \right\} \\ + \sin(\pi x^2/2) \left\{ \frac{1}{2\pi x} - \frac{1}{2\pi^2 x^3} - \frac{3}{2\pi^3 x^5} + \dots \right\}; \quad (44)$$

$$J_I(x) \sim 0.384375 + \frac{1}{\pi} \ln x + \frac{3}{4\pi^3 x^4} - \dots - \cos(\pi x^2/2) \left\{ \frac{1}{2\pi x} - \frac{1}{2\pi^2 x^3} - \frac{3}{2\pi^3 x^5} + \dots \right\} \\ - \sin(\pi x^2/2) \left\{ \frac{1}{2\pi x} + \frac{1}{2\pi^2 x^3} - \frac{3}{2\pi^3 x^5} + \dots \right\}. \quad (45)$$

Additional asymptotic expansions are

$$C_s(x) \sim 0.3171875 + 0.159155 \ln x + \frac{0.0120943}{x^4} + \dots$$

$$- \sin(\pi x^2/2) \left\{ \frac{0.0506606}{x^3} - \frac{0.0769948}{x^7} + \dots \right\} - \cos(\pi x^2/2) \left\{ \frac{0.15915494}{x} - \frac{0.04837730}{x^5} + \dots \right\}$$

$$+ \cos \pi x^2 \left\{ \frac{0.016125766}{x^4} + \dots \right\} - \frac{1}{2} \sin \pi x^2 \left\{ \frac{0.0506606}{x^2} - \frac{0.0359309}{x^6} + \dots \right\}; \quad (46)$$

$$S_c(x) \sim -0.0671875 - 0.159155 \ln x - \frac{0.0120943}{x^4} + \dots$$

$$- \cos \frac{1}{2}(\pi x^2/2) \left\{ \frac{0.0506606}{x^3} - \frac{0.0769948}{x^7} + \dots \right\}$$

$$+ \sin \pi x^2/2 \left\{ \frac{0.15915494}{x} - \frac{0.04837730}{x^5} + \dots \right\}$$

$$+ \cos \pi x^2 \left\{ \frac{0.016125766}{x^4} + \dots \right\} - \left(\frac{1}{2}\right) \sin \pi x^2 \left\{ \frac{0.050660593}{x^2} - \frac{0.035930934}{x^6} + \dots \right\}; \quad (47)$$

$$Si(x) \sim \frac{\pi}{2} - \cos x \left(\frac{1}{x} - \frac{2}{x^3} + \frac{2 \cdot 3 \cdot 4}{x^5} + \dots \right) - \sin x \left(\frac{1}{x^2} - \frac{2 \cdot 3}{x^4} + \dots \right); \quad (48)$$

and

$$Ci(x) \sim \sin x \left(\frac{1}{x} - \frac{2}{x^3} + \frac{2 \cdot 3 \cdot 4}{x^5} + \dots \right) - \cos x \left(\frac{1}{x^2} - \frac{2 \cdot 3}{x^4} + \dots \right). \quad (49a)$$

$$Ci(x) + i Si(x) - (i\pi/2) \sim e^{ix} \left[\frac{1}{ix} + \frac{1}{(ix)^2} + \frac{2}{(ix)^3} + \frac{2 \cdot 3}{(ix)^4} + \dots \right]. \quad (49b)$$

In addition to the above functions, which have general applicability throughout the book, two functions were defined in 9.24 and 9.25 which are needed in the theory of malalignment. One, $F_\infty(x)$, is expressible in terms of $E(x)$;

$$F_\infty(x) = \int_x^\infty \int_\infty^y \exp(i\pi u^2/2) du dy$$

$$= \text{Ave} \lim_{T \rightarrow \infty} \int_x^T \int_T^y \exp(i\pi u^2/2) du dy$$

$$= \text{Ave} \lim_{T \rightarrow \infty} \{x[E(T) - E(x)] + (i/\pi)[\exp(i\pi T^2/2) - \exp(i\pi x^2/2)]\}$$

$$= \frac{1}{2}(1+i)x - xE(x) - (i/\pi) \exp(i\pi x^2/2). \quad (50)$$

The other function is

$$H(x, b) = \int_0^x \exp(2\pi i u^2/b^2) E(2u) du. \quad (51)$$

The special case

$$H(2x, i) = \frac{1}{2} J^*(4x), \quad (52)$$

is not computable from the formulas to be developed because the expansions fail to converge. Substituting $w = -2\pi i u^2/b^2$, expanding $E(2u)$ in a power series, and integrating to ∞ , we have

$$H(\infty, b) = \int_0^\infty e^{-w} \sum_{n=0}^\infty \frac{(-b^2 w)^n}{n! (2n+1)} \frac{i b^2}{2\pi} dw = \frac{i b^2}{2\pi} \sum_{n=0}^\infty \frac{(-1)^n b^{2n}}{2^{n+1}} = \frac{i b}{2\pi} \tan^{-1} b. \quad (53)$$

The derivation of (53) is valid for $|b| < 1$ only, but by analytic continuation it may be extended to all b such that the integral converges. The singularities at $b = \pm i$ are related to the asymptotic behavior of $J(x)$ as $x \rightarrow \infty$.

For small b and x a convenient series may be obtained by integrating (53) to a finite limit and rearranging terms. The retention of the exponential cuts down significantly the number of terms needed in the following expansion as compared to the usual type of power series.

$$H(x, b) = \frac{i b}{2\pi} \tan^{-1} b (1 - e^{2\pi i x^2/b^2}) - \frac{i b^2}{2\pi} e^{2\pi i x^2/b^2} \left\{ \left[\frac{1}{3} - \frac{b^2}{5} + \frac{b^4}{7} - \dots \right] 2\pi i x^2 \right. \\ \left. + \left[\frac{1}{5} - \frac{b^2}{7} + \frac{b^4}{9} - \dots \right] \frac{(2\pi i x^2)^2}{2!} + \left[\frac{1}{7} - \frac{b^2}{9} + \frac{b^4}{11} - \dots \right] \frac{(2\pi i x^2)^3}{3!} + \dots \right\}. \quad (54)$$

The asymptotic expansion of $H(x, b)$ may be obtained by substituting the asymptotic expansion of $E(2u)$ in (51) and integrating from x to ∞ .

$$H(x, b) \sim \frac{i b}{2\pi} \tan^{-1} b - \int_x^\infty \exp \frac{2\pi i u^2}{b^2} \left\{ \frac{1+i}{2} + \frac{\exp(2\pi i u^2)}{2\pi i u} \left[1 + \frac{1}{4\pi i u^2} + \frac{1 \cdot 3}{(4\pi i u^2)^2} + \dots \right] \right\} du \\ = \frac{i b}{2\pi} \tan^{-1} b + \frac{(1+i)}{8\pi i x} \exp \frac{2\pi i x^2}{b^2} \sum_{n=0}^\infty \frac{(2n)!}{n!} \left(\frac{b^2}{8\pi i x^2} \right)^n \\ - \frac{b^2}{8\pi^2 (1+b^2) x^2} \exp \frac{2\pi i (1+b^2) x^2}{b^2} \sum_{n=0}^\infty \left\{ n! \left(\frac{b^2}{2\pi i (1+b^2) x^2} \right)^n \sum_{t=0}^n \frac{(2t)!}{(t!)^2} \left(\frac{1+b^2}{4b^2} \right)^t \right\}. \quad (55)$$

For large values of b , $H(x, b)$ may be computed by use of the identity

$$H(x, b) = (b/2) E(2x/b) E(2x) - b^2 H(x/b, 1/b). \quad (56)$$

APPENDIX C

TABLES OF FRESNEL INTEGRALS AND CHARACTERISTIC FUNCTIONS

A satisfactory numerical evaluation of the functions used to describe the behavior of rockets usually can be made from the various graphs presented in connection with the formulas. In some cases, however, it may be desirable to use tables. Accordingly in table C1 we give the basic integrals to five decimal places and in tables C2 to C8 we give the more important characteristic functions for fin stabilized rockets arranged for use as Green's functions. Second central differences, δ^2 , are listed in table C1 in case it is desired to interpolate using second differences by means of the familiar Everett's formula; however the use of Lagrangian interpolation coefficients is probably more convenient if suitable tables and computing machines are available. The definitions of the various functions and the curves giving their values may be found from the following list:

Table	Function	Definition	Figures
C1-----	$C(x)$ -----	3.34 (14) and B (1)-----	9.23a, $\zeta_p=0$, R1.Pt.
C1-----	$S(x)$ -----	3.34 (15) and B (2)-----	9.23a, $\zeta_p=0$, Im.Pt.
C1-----	$J_I(x)$ -----	3.38 (9) and B (5)-----	
C2-----	$\Theta_q(\zeta_p, \zeta)$ -----	3.34 (23)-----	3.36.
C3-----	$\Theta_s(\zeta_p, \zeta)$ -----	3.34 (20)-----	3.35.
C4-----	$\Theta_r(\zeta_p, \zeta)$ -----	3.38 (11)-----	3.38.
C5-----	$\Theta_R(\zeta_p, \zeta)$ -----	3.39 (8)-----	3.39.
C6-----	$\Phi_q(\zeta_p, \zeta)$ -----	3.34 (22)-----	
C7-----	$\Phi_s(\zeta_p, \zeta)$ -----	3.34 (19)-----	
C8-----	$\Phi_R(\zeta_p, \zeta)$ -----	3.39 (7)-----	

Care must be exercised in using the tables and the figures since the functions there may differ in argument and in simple multiplicative factors from the functions listed above.

With the exception of the first two rows and the last column of tables C2 to C8, which were computed under our supervision, all the tables in this appendix are taken from a slightly more extensive set of tables computed by Dr. A. S. Peters of the Ballistic Research Laboratory with the help of Miss Geraldine Rice and Miss Helen Saunders. We are most grateful for permission to use these tables. We have rearranged the tables slightly and changed the arguments by a factor or two, but have not changed the tabulated entries. This is the origin of the multiplicative factors mentioned above.

These tables are arranged to give the functions of interest relatively directly. However the primary functions listed in table C1 have an oscillatory character and hence require closely spaced entries to give moderate accuracy. It is possible to define monotonic functions, for which interpolation is easy, from which these oscillatory functions can be computed by means of simple auxiliary formulas involving trigonometric functions. This procedure is most desirable if one needs more than five significant figures. An extensive table of such monotonic functions together with an extensive discussion of their mathematical properties is given by Rosser, Newton, and Gross.¹ A shorter table whose entries have fewer decimal places is given by Rankin.² By comparing definitions one can express our functions in terms of theirs and thus make use of their results.

¹ J. B. Rosser, R. B. Newton, and G. L. Gross, "Mathematical Theory of Rocket Flight," McGraw-Hill, 1947

² E. A. Rankin, "On the mathematical theory of the motion of rotated and unrotated rockets," Phil. Trans. A-241, pp. 457-585, 1948-49.

TABLE C1

TABLE OF FRESNEL INTEGRALS AND RELATED INTEGRALS

x	$C(x)$	δ^2	$S(x)$	δ^2	$J_I(x)$	δ^2	x	$C(x)$	δ^2	$S(x)$	δ^2	$J_I(x)$	δ^2
0.00	0.00000	----	0.00000	----	0.00000	----	.50	0.49234	-5	0.06473	15	0.01622	7
.01	.01000	0	.00000	----	.00000	0	.51	.50155	-6	.06863	15	.01754	8
.02	.02000	0	.00000	1	.00000	0	.52	.51070	-8	.07268	14	.01894	8
.03	.03000	0	.00001	1	.00000	0	.53	.51977	-6	.07687	16	.02042	9
.04	.04000	0	.00003	1	.00000	0	.54	.52878	-8	.08122	15	.02199	9
.05	.05000	0	.00006	2	.00000	1	.55	.53771	-8	.08572	15	.02365	8
.06	.06000	0	.00011	2	.00001	-1	.56	.54656	-8	.09037	16	.02539	10
.07	.07000	0	.00018	2	.00001	0	.57	.55533	-9	.09518	15	.02723	9
.08	.08000	0	.00027	2	.00001	1	.58	.56401	-9	.10014	16	.02916	10
.09	.09000	0	.00038	3	.00002	0	.59	.57260	-9	.10526	16	.03119	9
.10	.10000	0	.00052	4	.00003	0	.60	.58110	-11	.11054	16	.03331	12
.11	.11000	-1	.00070	3	.00004	0	.61	.58949	-11	.11598	16	.03555	10
.12	.11999	1	.00091	3	.00005	1	.62	.59777	-10	.12158	15	.03789	11
.13	.12999	0	.00115	5	.00007	1	.63	.60595	-12	.12733	17	.04034	11
.14	.13999	-1	.00144	4	.00010	0	.64	.61401	-12	.13325	16	.04290	11
.15	.14998	0	.00177	4	.00013	1	.65	.62195	-13	.13933	16	.04557	12
.16	.15997	0	.00214	6	.00017	1	.66	.62976	-13	.14557	16	.04836	13
.17	.16996	0	.00257	5	.00022	0	.67	.63744	-13	.15197	17	.05128	11
.18	.17995	0	.00305	6	.00027	2	.68	.64499	-15	.15854	15	.05431	13
.19	.18994	-1	.00359	6	.00034	1	.69	.65239	-14	.16526	16	.05747	14
.20	.19992	0	.00419	6	.00042	1	.70	.65965	-15	.17214	16	.06077	12
.21	.20990	-1	.00485	6	.00051	1	.71	.66676	-17	.17918	15	.06419	13
.22	.21987	0	.00557	8	.00061	2	.72	.67370	-16	.18637	16	.06774	13
.23	.22984	-1	.00637	6	.00073	2	.73	.68048	-17	.19372	15	.07142	15
.24	.23980	0	.00723	8	.00087	1	.74	.68709	-17	.20122	16	.07525	14
.25	.24976	-1	.00817	8	.00102	2	.75	.69353	-19	.20888	14	.07922	14
.26	.25971	-1	.00919	9	.00119	3	.76	.69978	-19	.21668	15	.08333	13
.27	.26965	-1	.01030	7	.00139	2	.77	.70584	-19	.22463	15	.08757	16
.28	.27958	-2	.01148	9	.00161	2	.78	.71171	-20	.23273	14	.09197	15
.29	.28949	0	.01275	10	.00185	3	.79	.71738	-21	.24097	13	.09652	14
.30	.29940	-2	.01412	8	.00212	2	.80	.72284	-21	.24934	14	.10121	14
.31	.30929	-1	.01557	10	.00241	4	.81	.72809	-21	.25785	13	.10604	18
.32	.31917	-1	.01712	11	.00274	3	.82	.73313	-23	.26649	13	.11105	13
.33	.32904	-3	.01878	9	.00310	3	.83	.73794	-23	.27526	12	.11619	16
.34	.33888	-1	.02053	9	.00349	4	.84	.74252	-24	.28415	12	.12149	16
.35	.34871	-3	.02239	11	.00392	4	.85	.74686	-24	.29316	11	.12695	15
.36	.35851	-2	.02436	10	.00439	3	.86	.75096	-25	.30228	11	.13256	15
.37	.36829	-2	.02643	12	.00489	5	.87	.75481	-25	.31151	10	.13832	16
.38	.37805	-3	.02862	12	.00544	5	.88	.75841	-26	.32084	9	.14424	16
.39	.38778	-3	.03093	12	.00604	4	.89	.76175	-27	.33026	10	.15032	15
.40	.39748	-3	.03336	12	.00668	5	.90	.76482	-26	.33978	8	.15655	17
.41	.40715	-3	.03591	12	.00737	6	.91	.76763	-28	.34938	7	.16295	14
.42	.41679	-4	.03858	13	.00812	4	.92	.77016	-28	.35905	7	.16949	15
.43	.42639	-4	.04138	13	.00891	6	.93	.77241	-29	.36879	7	.17618	16
.44	.43595	-4	.04431	15	.00976	7	.94	.77437	-29	.37860	5	.18303	16
.45	.44547	-5	.04737	13	.01068	5	.95	.77604	-29	.38846	4	.19004	14
.46	.45494	-4	.05056	15	.01165	7	.96	.77742	-30	.39836	4	.19719	14
.47	.46437	-5	.05390	13	.01269	6	.97	.77850	-31	.40830	3	.20448	16
.48	.47375	-5	.05737	14	.01379	8	.98	.77927	-30	.41827	2	.21193	13
.49	.48308	-7	.06098	14	.01497	7	.99	.77974	-31	.42826	1	.21951	16
.50	.49234	-5	.06473	15	.01622	7	1.00	.77990	-32	.43826	0	.22725	13

TABLE C1—Continued

x	$C(x)$	δ^2	$S(x)$	δ^2	$J_1(x)$	δ^2	x	$C(x)$	δ^2	$S(x)$	δ^2	$J_1(x)$	δ^2
1.00	.77990	-32	.43826	0	.22725	13	1.50	.44526	19	.69750	-43	.64343	-32
1.01	.77974	-32	.44826	-1	.23512	13	1.51	.43612	19	.69346	-43	.64801	-33
1.02	.77926	-31	.45825	-3	.24312	13	1.52	.42717	23	.68899	-43	.65226	-33
1.03	.77847	-33	.46821	-2	.25125	13	1.53	.41845	25	.68409	-40	.65618	-35
1.04	.77735	-32	.47815	-4	.25951	12	1.54	.40998	26	.67879	-41	.65975	-34
1.05	.77591	-33	.48805	-6	.26789	12	1.55	.40177	29	.67308	-40	.66298	-34
1.06	.77414	-32	.49789	-6	.27639	11	1.56	.39385	31	.66697	-37	.66587	-37
1.07	.77205	-33	.50767	-8	.28500	11	1.57	.38624	33	.66049	-37	.66839	-36
1.08	.76963	-33	.51737	-9	.29372	11	1.58	.37896	35	.65364	-36	.67055	-36
1.09	.76688	-32	.52698	-9	.30255	8	1.59	.37203	36	.64643	-33	.67235	-36
1.10	.76381	-33	.53650	-12	.31146	10	1.60	.36546	39	.63889	-32	.67379	-37
1.11	.76041	-33	.54590	-12	.32047	9	1.61	.35928	41	.63103	-31	.67486	-36
1.12	.75668	-33	.55518	-14	.32957	5	1.62	.35351	42	.62286	-28	.67557	-36
1.13	.75262	-31	.56432	-15	.33872	9	1.63	.34816	44	.61441	-26	.67592	-36
1.14	.74825	-32	.57331	-16	.34796	6	1.64	.34325	46	.60570	-24	.67591	-36
1.15	.74356	-32	.58214	-17	.35726	5	1.65	.33880	46	.59675	-22	.67554	-36
1.16	.73855	-31	.59080	-20	.36661	5	1.66	.33481	49	.58758	-19	.67481	-35
1.17	.73323	-31	.59926	-19	.37601	4	1.67	.33131	50	.57822	-18	.67373	-35
1.18	.72760	-30	.60753	-22	.38545	1	1.68	.32831	50	.56868	-14	.67230	-32
1.19	.72167	-30	.61558	-23	.39490	4	1.69	.32581	52	.55900	-12	.67055	-33
1.20	.71544	-29	.62340	-24	.40439	0	1.70	.32383	52	.54920	-9	.66847	-33
1.21	.70892	-28	.63098	-25	.41388	0	1.71	.32237	54	.53931	-7	.66606	-30
1.22	.70212	-28	.63831	-26	.42337	-2	1.72	.32145	54	.52935	-3	.66335	-30
1.23	.69504	-27	.64538	-29	.43284	-1	1.73	.32107	54	.51936	-1	.66034	-28
1.24	.68769	-25	.65216	-28	.44230	-4	1.74	.32123	55	.50936	2	.65705	-27
1.25	.68009	-25	.65866	-31	.45172	-3	1.75	.32194	54	.49938	6	.65349	-26
1.26	.67224	-24	.66485	-32	.46111	-6	1.76	.32319	55	.48946	9	.64967	-24
1.27	.66415	-23	.67072	-32	.47044	-7	1.77	.32499	54	.47963	11	.64561	-23
1.28	.65583	-22	.67627	-34	.47970	-7	1.78	.32733	54	.46991	15	.64132	-20
1.29	.64729	-20	.68148	-36	.48889	-8	1.79	.33021	54	.46034	17	.63683	-18
1.30	.63855	-19	.68633	-35	.49800	-11	1.80	.33363	53	.45094	21	.63216	-17
1.31	.62962	-18	.69083	-37	.50700	-11	1.81	.33758	51	.44175	24	.62732	-15
1.32	.62051	-16	.69496	-39	.51589	-13	1.82	.34204	50	.43280	27	.62233	-13
1.33	.61124	-15	.69870	-39	.52465	-12	1.83	.34700	49	.42412	30	.61721	-10
1.34	.60182	-13	.70205	-39	.53329	-16	1.84	.35245	48	.41574	33	.61199	-8
1.35	.59227	-12	.70501	-41	.54177	-15	1.85	.35838	45	.40769	36	.60669	-6
1.36	.58260	-10	.70756	-42	.55010	-18	1.86	.36476	45	.40000	38	.60133	-3
1.37	.57283	-8	.70969	-42	.55825	-18	1.87	.37159	41	.39269	41	.59594	-2
1.38	.56298	-7	.71140	-43	.56622	-19	1.88	.37883	39	.38579	45	.59053	+2
1.39	.55306	-4	.71268	-44	.57400	-21	1.89	.38646	38	.37934	46	.58514	+4
1.40	.54310	-3	.71352	-43	.58157	-22	1.90	.39447	34	.37335	48	.57979	7
1.41	.53311	-1	.71393	-44	.58892	-23	1.91	.40282	31	.36784	52	.57451	8
1.42	.52311	1	.71390	-45	.59604	-24	1.92	.41148	29	.36285	53	.56931	12
1.43	.51312	3	.71342	-45	.60292	-25	1.93	.42043	25	.35839	55	.56423	14
1.44	.50316	6	.71249	-45	.60955	-26	1.94	.42963	23	.35448	57	.55929	16
1.45	.49326	7	.71111	-45	.61592	-29	1.95	.43906	18	.35114	58	.55451	20
1.46	.48343	9	.70928	-45	.62200	-28	1.96	.44867	15	.34838	60	.54993	21
1.47	.47369	12	.70700	-44	.62780	-28	1.97	.45843	12	.34622	61	.54556	24
1.48	.46407	14	.70428	-45	.63332	-31	1.98	.46831	7	.34467	61	.54143	26
1.49	.45459	15	.70111	-44	.63853	-31	1.99	.47826	4	.34373	63	.53756	28
1.50	.44526	19	.69750	-43	.64343	-32	2.00	.48825	1	.34342	62	.53397	3

TABLE C1—Continued

x	$C(x)$	δ^2	$S(x)$	δ^2	$J_I(x)$	δ^2	x	$C(x)$	δ^2	$S(x)$	δ^2	$J_I(x)$	δ^2
2.00	.48825	-1	.34342	251	.53397	124	3.00	.60572	-375	.49631	0	.67966	186
2.02	.50820	-32	.34468	251	.52775	139	3.02	.60384	-372	.51619	-71	.69265	149
2.04	.52783	-65	.34845	248	.52292	152	3.04	.59824	-354	.53536	-141	.70713	105
2.06	.54681	-96	.35470	240	.51961	165	3.06	.58910	-322	.55312	-208	.72266	56
2.08	.56483	-128	.36335	227	.51795	176	3.08	.57674	-278	.56880	-267	.73875	+4
2.10	.58157	-159	.37427	211	.51805	182	3.10	.56160	-224	.58181	-317	.75488	-48
2.12	.59672	-186	.38730	190	.51997	185	3.12	.54422	-158	.59165	-358	.77053	-101
2.14	.61001	-213	.40223	164	.52374	186	3.14	.52526	-86	.59791	-384	.78517	-150
2.16	.62117	-234	.41880	137	.52937	182	3.16	.50544	-9	.60033	-395	.79831	-196
2.18	.62999	-252	.43674	103	.53682	174	3.18	.48553	70	.59880	-392	.80949	-232
2.20	.63629	-269	.45571	68	.54601	170	3.20	.46632	148	.59335	-373	.81835	-260
2.22	.63990	-276	.47536	31	.55690	149	3.22	.44859	220	.58417	-337	.82461	-281
2.24	.64075	-281	.49532	-7	.56928	134	3.24	.43306	287	.57162	-289	.82806	-288
2.26	.63879	-279	.51521	-48	.58300	114	3.26	.42040	340	.55618	-225	.82863	-284
2.28	.63404	-273	.53462	-88	.59786	89	3.28	.41114	381	.53849	-151	.82636	-268
2.30	.62656	-258	.55315	-127	.61361	64	3.30	.40569	408	.51929	-71	.82141	-240
2.32	.61650	-241	.57041	-164	.63000	36	3.32	.40432	415	.49938	13	.81406	-202
2.34	.60403	-215	.58603	-200	.64675	+6	3.34	.40710	405	.47960	102	.80469	-153
2.36	.58941	-185	.59965	-231	.66356	-25	3.36	.41393	379	.46084	186	.79379	-98
2.38	.57294	-151	.61096	-258	.68012	-58	3.38	.42455	332	.44394	261	.78191	-36
2.40	.55496	-110	.61969	-280	.69610	-85	3.40	.43849	271	.42965	328	.76967	+27
2.42	.53588	-68	.62562	-295	.71123	-117	3.42	.45514	197	.41864	381	.75770	91
2.44	.51612	-22	.62860	-306	.72519	-143	3.44	.47376	111	.41144	415	.74664	152
2.46	.49614	25	.62852	-308	.73772	-168	3.46	.49319	19	.40839	433	.73710	205
2.48	.47641	73	.62536	-302	.74857	-190	3.48	.51341	-76	.40967	430	.72961	252
2.50	.45741	120	.61918	-289	.75752	-208	3.50	.53257	-167	.41525	404	.72464	285
2.52	.43961	166	.61011	-270	.76439	-218	3.52	.55006	-254	.42487	360	.72252	305
2.54	.42347	207	.59834	-241	.76908	-226	3.54	.56501	-328	.43809	297	.72345	312
2.56	.40940	245	.58416	-208	.77151	-228	3.56	.57668	-388	.45428	219	.72750	303
2.58	.39778	278	.56790	-165	.77166	-224	3.58	.58447	-430	.47266	127	.73458	277
2.60	.38894	303	.54999	-120	.76957	-215	3.60	.58796	-450	.49231	28	.74443	238
2.62	.38313	321	.53088	-70	.76533	-196	3.62	.58695	-448	.51224	-74	.75666	185
2.64	.38053	330	.51107	-16	.75913	-174	3.64	.58148	-422	.53143	-174	.77074	123
2.66	.38123	332	.49110	40	.75119	-148	3.66	.57179	-372	.54888	-267	.78605	+52
2.68	.38525	322	.47153	96	.74177	-116	3.68	.55838	-302	.56366	-346	.80188	-24
2.70	.39249	304	.45292	148	.73119	-79	3.70	.54195	-217	.57498	-409	.81747	-96
2.72	.40277	277	.43579	200	.71982	-39	3.72	.52335	-117	.58221	-451	.83210	-167
2.74	.41582	239	.42066	246	.70806	+1	3.74	.50358	-9	.58493	-468	.84506	-232
2.76	.43126	195	.40799	285	.69631	+42	3.76	.48372	101	.58297	-459	.85570	-280
2.78	.44865	145	.39817	317	.68498	86	3.78	.46487	207	.57642	-425	.86354	-318
2.80	.46749	87	.39152	341	.67451	125	3.80	.44809	304	.56562	-366	.86820	-335
2.82	.48720	26	.38828	352	.66529	162	3.82	.43435	382	.55116	-286	.86951	-336
2.84	.50717	-36	.38856	354	.65769	193	3.84	.42443	443	.53384	-186	.86746	-315
2.86	.52678	-101	.39238	345	.65202	221	3.86	.41894	477	.51466	-76	.86226	-275
2.88	.54538	-160	.39965	322	.64856	240	3.88	.41822	483	.49472	42	.85431	-223
2.90	.56238	-219	.41014	291	.64750	253	3.90	.42233	461	.47520	158	.84413	-153
2.92	.57719	-269	.42354	247	.64897	257	3.92	.43105	412	.45726	267	.83242	-72
2.94	.58931	-312	.43941	196	.65301	252	3.94	.44389	335	.44199	361	.81999	+11
2.96	.59831	-346	.45724	136	.65957	240	3.96	.46008	237	.43033	434	.80767	98
2.98	.60385	-367	.47643	69	.66853	217	3.98	.47864	123	.42301	482	.79633	180
3.00	.60572	-375	.49631	0	.67966	186	4.00	.49843	0	.42051	500	.78679	248

TABLE C1—Continued

x	$C(x)$	δ^2	$S(x)$	δ^2	$J_I(x)$	δ^2
4.00	.49843	0	.42051	500	.78679	248
4.02	.51822	-126	.42301	488	.77973	306
4.04	.53675	-244	.43039	441	.77573	342
4.06	.55284	-349	.44218	367	.77515	357
4.08	.56544	-434	.45764	270	.77814	351
4.10	.57370	-490	.47580	150	.78464	319
4.12	.57706	-514	.49546	20	.79433	268
4.14	.57528	-505	.51532	-112	.80670	195
4.16	.56845	-461	.53406	-240	.82102	109
4.18	.55701	-385	.55040	-354	.83643	+16
4.20	.54172	-281	.56320	-443	.85200	-82
4.22	.52362	-156	.57157	-503	.86675	-175
4.24	.50396	-18	.57491	-529	.87975	-256
4.26	.48412	122	.57296	-519	.89019	-321
4.28	.46550	256	.56582	-468	.89742	-363
4.30	.44944	374	.55400	-386	.90102	-381
4.32	.43712	466	.53832	-273	.90081	-370
4.34	.42946	524	.51991	-138	.89690	-330
4.36	.42704	545	.50012	8	.88969	-271
4.38	.43007	523	.48041	157	.87977	-184
4.40	.43833	464	.46227	294	.86801	-84
4.42	.45123	368	.44707	412	.85541	+21
4.44	.46781	240	.43599	500	.84302	129
4.46	.48679	95	.42991	548	.83192	226
4.48	.50672	-62	.42931	556	.82308	308
4.50	.52603	-216	.43427	519	.81732	366
4.52	.54318	-352	.44442	440	.81522	398
4.54	.55681	-465	.45897	325	.81710	393
4.56	.56579	-540	.47677	181	.82291	358
4.58	.56937	-571	.49638	20	.83230	297
4.60	.56724	-556	.51619	-142	.84466	207
4.62	.55955	-494	.53458	-297	.85909	+97
4.64	.54692	-390	.55000	-428	.87449	-21
4.66	.53039	-250	.56114	-525	.88968	-136
4.68	.51136	-90	.56703	-577	.90351	-245
4.70	.49143	83	.56715	-580	.91489	-332
4.72	.47233	249	.56147	-534	.92295	-392
4.74	.45572	397	.55045	-439	.92709	-418
4.76	.44308	510	.53504	-303	.92705	-407
4.78	.43554	579	.51660	-141	.92294	-362
4.80	.43379	598	.49575	38	.91521	-280
4.82	.43802	561	.47728	215	.90468	-173
4.84	.44786	474	.45996	374	.89242	-51
4.86	.46244	341	.44638	500	.87965	+80
4.88	.48043	174	.43780	584	.86768	203
4.90	.50016	-9	.43506	611	.85774	310
4.92	.51980	-196	.43843	581	.85090	388
4.94	.53748	-366	.44761	497	.84794	430
4.96	.55150	-500	.46176	361	.84928	432
4.98	.56052	-590	.47952	191	.85494	390
5.00	.56364	-624	.49919	0	.86450	310

x	$C(x)$	δ^2	$S(x)$	δ^2	$J_I(x)$	δ^2
5.00	.56364	-624	.49919	0	.86450	310
5.02	.56052	-595	.51886	-193	.87716	201
5.04	.55145	-507	.53660	-371	.89183	+67
5.06	.53731	-368	.55063	-513	.90717	-71
5.08	.51949	-189	.55953	-604	.92180	-211
5.10	.49978	11	.56239	-635	.93432	-321
5.12	.48018	210	.55890	-602	.94363	-407
5.14	.46268	392	.54939	-506	.94887	-451
5.16	.44910	536	.53482	-356	.94960	-446
5.18	.44088	622	.51669	-168	.94587	-395
5.20	.43888	647	.49688	40	.93819	-304
5.22	.44335	602	.47747	248	.92747	-176
5.24	.45384	490	.46054	430	.91499	-32
5.26	.46923	326	.44791	568	.90219	+120
5.28	.48788	126	.44096	645	.89059	+261
5.30	.50779	-94	.44046	654	.88160	+371
5.32	.52676	-303	.44650	589	.87632	+447
5.34	.54270	-482	.45843	458	.87551	+469
5.36	.55382	-607	.47494	274	.87939	+442
5.38	.55887	-668	.49419	59	.88769	+361
5.40	.55724	-651	.51403	-167	.89960	+242
5.42	.54910	-560	.53220	-377	.91393	+92
5.44	.53536	-403	.54660	-544	.92918	-71
5.46	.51759	-198	.55556	-649	.94372	-228
5.48	.49784	33	.55803	-681	.95598	-356
5.50	.47842	262	.55369	-633	.96468	-448
5.52	.46162	462	.54302	-507	.96890	-486
5.54	.44944	611	.52728	-321	.96826	-465
5.56	.44337	685	.50833	-94	.96297	-389
5.58	.44415	678	.48844	194	.95379	-267
5.60	.45171	588	.47004	372	.94194	-107
5.62	.46515	425	.45536	556	.92902	+65
5.64	.48284	205	.44624	671	.91675	+231
5.66	.50258	-38	.44383	702	.90679	371
5.68	.52194	-284	.44844	647	.90054	465
5.70	.53846	-493	.45952	510	.89894	501
5.72	.55005	-643	.47570	303	.90235	472
5.74	.55521	-711	.49491	59	.91048	386
5.76	.55326	-688	.51471	-98	.92247	244
5.78	.54443	-576	.53253	-430	.93690	+72
5.80	.52984	-386	.54605	-608	.95205	-111
5.82	.51139	-144	.55349	-710	.96609	-283
5.84	.49150	121	.55383	-715	.97730	-419
5.86	.47282	369	.54702	-627	.98432	-498
5.88	.45783	575	.53394	-453	.98636	-514
5.90	.44859	700	.51633	-215	.98326	-458
5.92	.44635	733	.49657	54	.97558	-341
5.94	.45144	666	.47735	318	.96449	-174
5.96	.46319	506	.46131	541	.95166	+18
5.98	.48000	272	.45068	691	.93901	+209
6.00	.49953	----	.44696	----	.92845	----

TABLE C2—Continued

$2\theta_e(\zeta_p, \zeta) 10^3$

ζ_p	ζ																	
	1.75	1.80	1.85	1.90	1.95	2.00	2.10	2.20	2.30	2.40	2.50	2.60	2.70	2.80	2.90	3.00	3.50	∞
0.00	498	500	502	502	500	498	501	499	500	500	500	500	500	500	500	500	500	500
.05	406	408	410	409	407	406	409	407	408	408	408	408	408	408	408	408	408	408
.10	328	330	332	332	330	329	332	330	331	331	331	331	331	330	331	330	331	331
.15	265	266	269	269	267	266	268	267	267	267	267	267	267	267	267	267	267	267
.20	213	215	217	217	215	214	216	215	215	216	215	216	215	215	216	215	215	215
.25	171	173	175	175	174	172	174	173	173	174	173	174	174	174	174	173	174	174
.30	138	139	141	142	141	139	141	140	140	141	140	141	140	140	140	140	140	140
.35	111	112	114	115	114	112	114	114	113	114	113	114	113	114	114	113	113	114
.40	90	90	92	94	93	91	92	93	91	93	92	93	92	92	92	92	92	92
.45	74	73	75	77	77	75	75	76	74	76	74	76	75	76	75	75	75	75
.50	61	60	61	63	63	62	61	63	61	63	61	62	61	62	61	62	61	62
.55	51	49	49	51	53	52	50	52	50	52	50	52	50	51	51	51	51	51
.60	43	41	40	42	44	43	41	43	41	43	42	43	42	43	42	43	42	42
.65	37	35	33	34	36	37	34	36	35	36	35	36	35	36	35	36	35	35
.70	32	30	28	28	30	31	28	30	29	30	30	30	29	30	29	30	30	30
.75	27	26	24	23	25	26	24	25	25	25	25	25	25	25	25	25	25	25
.80	23	23	21	19	20	22	21	21	22	21	22	21	22	21	21	22	21	21
.85	19	20	19	17	17	18	19	17	19	17	19	17	19	18	18	18	18	18
.90	15	18	17	15	14	15	17	14	17	15	16	15	16	15	16	15	16	15
.95	12	14	16	14	12	12	15	12	14	13	14	13	14	13	14	13	14	14
1.00	10	11	13	13	11	10	13	11	12	12	12	12	12	11	12	11	12	12
1.05	8	9	11	12	11	9	11	10	10	11	10	11	10	10	10	10	10	10
1.10	8	7	8	10	10	9	9	10	8	10	8	10	8	9	9	9	9	9
1.15	8	6	6	8	10	9	7	7	7	9	7	9	7	9	8	8	8	8
1.20	9	7	5	6	8	9	6	8	6	7	7	7	7	8	7	7	7	7
1.25	9	7	5	4	6	8	6	6	6	6	7	6	6	6	6	7	6	6
1.30	7	8	6	4	4	6	6	5	6	5	6	5	6	5	6	6	6	6
1.35	5	7	7	5	3	4	6	4	6	4	6	4	6	4	5	5	5	5
1.40	3	5	6	6	4	3	6	4	5	4	5	4	5	4	4	4	4	4
1.45	2	3	5	6	5	3	4	4	4	5	4	4	4	4	4	4	4	4
1.50	3	2	3	5	5	4	3	5	3	5	3	4	3	4	3	4	3	4
1.55	5	2	1	3	5	5	2	4	3	4	3	4	3	4	3	4	3	3
1.60	5	4	2	1	3	4	2	3	3	3	3	3	3	3	3	3	3	3
1.65	4	5	4	1	1	3	3	2	4	2	4	2	3	2	3	3	3	3
1.70	1	4	5	3	1	1	4	1	3	2	3	2	3	2	3	2	2	2
1.75	----	1	4	4	3	1	3	2	2	3	2	3	2	2	3	2	2	2
1.80	----	----	1	3	4	2	1	3	1	3	1	3	2	3	2	2	2	2
1.85	----	----	----	1	3	3	1	3	1	2	2	2	2	2	1	2	2	2
1.90	----	----	----	----	1	3	1	2	2	1	2	1	2	2	2	2	2	2
1.95	----	----	----	----	----	1	3	1	3	1	2	1	2	1	2	2	2	2
2.00	----	----	----	----	----	----	3	1	2	2	2	2	2	1	2	1	2	2
2.05	----	----	----	----	----	----	1	2	1	2	1	2	1	2	1	1	1	1
2.10	----	----	----	----	----	----	----	2	1	2	1	2	1	2	1	2	1	1
2.15	----	----	----	----	----	----	----	1	2	1	2	1	2	1	1	2	1	1
2.20	----	----	----	----	----	----	----	----	2	0	2	1	2	1	2	1	1	1
2.25	----	----	----	----	----	----	----	----	1	1	1	1	1	1	1	1	1	1
2.30	----	----	----	----	----	----	----	----	----	2	0	2	0	2	1	1	1	1
2.35	----	----	----	----	----	----	----	----	----	1	1	1	1	1	1	1	1	1
2.40	----	----	----	----	----	----	----	----	----	2	0	2	0	1	1	1	1	1
2.45	----	----	----	----	----	----	----	----	----	1	1	1	1	1	1	0	1	1
2.50	----	----	----	----	----	----	----	----	----	----	2	0	0	1	1	1	1	1

TABLE C3—Continued

$-\Theta_s(\zeta_v, \zeta) 10^3$

ζ_v	ζ																	
	1.75	1.80	1.85	1.90	1.95	2.00	2.10	2.20	2.30	2.40	2.50	2.60	2.70	2.80	2.90	3.00	3.50	∞
0.00	0	0	0	0	0	0	0	0	0	0	0	0	0	0	0	0	0	0
.05	155	154	155	156	155	155	155	155	155	155	155	155	155	155	155	155	155	155
.10	299	298	298	300	300	299	299	300	298	300	299	300	299	299	299	299	299	299
.15	426	425	426	428	428	427	426	428	426	428	426	427	426	427	426	427	426	427
.20	536	533	534	537	538	537	535	537	535	537	535	537	535	537	535	536	536	536
.25	627	624	625	628	630	628	625	629	625	628	626	628	626	628	626	627	627	627
.30	703	699	698	702	705	703	699	704	700	703	701	703	701	703	701	702	701	702
.35	764	759	758	762	765	765	759	765	760	764	761	763	761	763	761	763	762	762
.40	814	808	805	809	814	814	807	813	809	812	809	811	809	812	809	811	810	811
.45	854	848	843	846	851	853	845	851	847	850	848	849	848	850	847	850	849	849
.50	886	880	874	875	881	884	876	881	879	879	879	879	879	880	878	881	879	879
.55	911	907	899	897	903	908	901	904	904	902	904	903	904	904	902	905	904	903
.60	931	928	920	915	920	927	921	922	924	920	924	921	923	922	922	924	923	922
.65	944	946	938	931	932	940	938	935	941	934	940	935	939	936	938	938	938	937
.70	953	959	953	944	942	949	952	945	954	945	953	946	952	947	950	949	950	949
.75	958	967	966	957	951	955	964	953	963	955	962	955	962	956	961	958	960	958
.80	960	972	976	968	959	960	973	961	970	963	969	964	969	963	969	964	967	966
.85	961	972	982	979	968	964	979	968	974	971	973	971	973	970	975	970	972	972
.90	964	971	984	987	978	969	981	976	976	979	975	979	976	976	979	974	976	977
.95	970	969	981	991	987	976	981	984	976	985	977	984	978	982	981	979	979	981
1.00	979	970	977	991	994	984	979	990	977	990	979	988	980	987	982	984	982	984
1.05	991	976	974	986	997	993	978	994	980	991	982	990	983	990	983	988	985	986
1.10	1002	987	975	980	994	999	980	994	985	990	987	990	986	991	985	992	988	988
1.15	1007	999	983	977	988	1000	986	991	992	987	993	988	991	991	988	993	991	991
1.20	1003	1007	994	980	981	995	994	986	998	985	997	987	996	989	992	993	994	992
1.25	991	1007	1006	989	980	987	1002	984	1001	986	999	988	998	988	996	991	995	993
1.30	979	998	1010	1002	985	982	1005	986	998	991	996	991	997	990	998	990	995	993
1.35	975	984	1004	1010	997	983	1000	994	992	998	991	997	993	994	997	991	994	994
1.40	984	976	990	1008	1008	993	991	1003	987	1003	988	1001	990	999	994	994	993	996
1.45	1003	982	979	996	1010	1005	984	1007	987	1003	990	1001	991	1001	991	998	994	997
1.50	1017	999	981	982	1001	1011	986	1002	994	997	997	997	995	999	992	1001	996	997
1.55	1015	1015	996	980	986	1005	997	992	1004	990	1003	991	1001	995	997	999	999	996
1.60	996	1016	1012	993	980	991	1009	985	1007	989	1005	990	1004	992	1001	995	1000	997
1.65	976	998	1017	1011	990	981	1010	990	1002	996	999	996	1000	994	1002	993	998	996
1.70	977	978	1001	1017	1008	988	999	1002	991	1005	991	1004	994	1000	998	995	995	998
1.75	----	978	980	1003	1017	1006	985	1011	987	1007	990	1005	991	1004	993	1000	995	1000
1.80	----	----	978	982	1004	1016	985	1006	995	999	998	999	996	1002	993	1004	998	999
1.85	----	----	----	979	984	1006	1001	991	1008	989	1007	991	1004	995	999	1001	1001	998
1.90	----	----	----	----	980	986	1014	985	1010	990	1006	992	1005	992	1004	995	1001	999
1.95	----	----	----	----	----	981	1009	996	997	1002	995	1001	998	997	1003	993	998	998
2.00	----	----	----	----	----	----	989	1012	986	1010	989	1008	991	1005	995	999	995	1000
2.05	----	----	----	----	----	----	982	1010	992	1003	996	1002	995	1004	993	1005	998	1000
2.10	----	----	----	----	----	----	----	992	1009	989	1008	991	1005	996	999	1002	1002	1000
2.15	----	----	----	----	----	----	----	984	1011	990	1007	992	1007	992	1006	995	1002	1000
2.20	----	----	----	----	----	----	----	----	994	1006	993	1004	996	999	1002	994	997	1000
2.25	----	----	----	----	----	----	----	985	1011	989	1009	990	1007	993	1002	995	1001	1001
2.30	----	----	----	----	----	----	----	----	996	1003	997	1000	1002	994	1006	1000	1000	1000
2.35	----	----	----	----	----	----	----	----	986	1011	989	1009	992	1005	998	1004	1004	1000
2.40	----	----	----	----	----	----	----	----	----	998	1000	1001	995	1006	992	999	1000	1000
2.45	----	----	----	----	----	----	----	----	----	987	1011	990	1007	995	1000	995	1001	1001
2.50	----	----	----	----	----	----	----	----	----	----	1000	997	1004	993	1007	1000	1000	1001

TABLE C4

$$\Theta_{\pm}(\zeta_p, \zeta) 10^3$$

ζ_p	ζ														
	0.25	0.30	0.35	0.40	0.45	0.50	0.55	0.60	0.65	0.70	0.75	0.80	0.85	0.90	0.95
0.00	1010	1021	1039	1065	1102	1152	1215	1291	1377	1472	1568	1664	1749	1821	1878
.05	826	846	883	920	964	1015	1076	1149	1231	1320	1412	1504	1588	1660	1719
.10	602	673	729	779	828	882	942	1011	1088	1172	1260	1347	1430	1502	1563
.15	400	502	578	641	697	754	814	879	952	1031	1114	1198	1279	1351	1413
.20	200	334	431	507	572	632	692	756	825	899	977	1057	1136	1208	1271
.25	----	167	286	378	452	517	579	641	706	776	850	926	1002	1073	1138
.30	----	----	143	251	336	408	472	534	597	663	732	804	877	948	1012
.35	----	----	----	125	223	303	372	435	496	559	624	692	762	830	895
.40	----	----	----	----	111	201	275	341	403	463	525	589	655	722	786
.45	----	----	----	----	----	100	182	253	316	375	434	495	558	621	684
.50	----	----	----	----	----	----	91	167	234	294	352	409	468	529	590
.55	----	----	----	----	----	----	----	83	154	217	275	331	387	444	502
.60	----	----	----	----	----	----	----	----	77	143	203	258	312	366	422
.65	----	----	----	----	----	----	----	----	----	71	134	190	243	296	348
.70	----	----	----	----	----	----	----	----	----	----	67	126	179	230	281
.75	----	----	----	----	----	----	----	----	----	----	----	63	118	169	218
.80	----	----	----	----	----	----	----	----	----	----	----	----	59	112	161
.85	----	----	----	----	----	----	----	----	----	----	----	----	----	56	106
.90	----	----	----	----	----	----	----	----	----	----	----	----	----	----	53

ζ_p	ζ														
	1.00	1.05	1.10	1.15	1.20	1.25	1.30	1.35	1.40	1.45	1.50	1.55	1.60	1.65	1.70
0.00	1922	1956	1988	2024	2067	2116	2166	2210	2246	2274	2301	2331	2367	2404	2437
.05	1765	1801	1834	1870	1912	1960	2008	2053	2090	2119	2146	2176	2211	2247	2280
.10	1611	1650	1684	1720	1761	1806	1854	1899	1936	1967	1994	2024	2058	2094	2127
.15	1464	1505	1541	1576	1616	1660	1707	1751	1789	1821	1849	1879	1912	1947	1980
.20	1324	1368	1405	1441	1479	1520	1567	1611	1651	1683	1713	1741	1773	1808	1841
.25	1193	1238	1277	1314	1351	1392	1436	1480	1520	1554	1584	1612	1644	1678	1711
.30	1069	1117	1158	1195	1232	1271	1314	1357	1398	1433	1463	1492	1523	1556	1589
.35	953	1004	1046	1084	1121	1159	1201	1243	1284	1320	1351	1380	1410	1442	1476
.40	845	897	942	981	1018	1056	1095	1137	1177	1214	1247	1276	1306	1337	1370
.45	743	797	844	885	923	959	998	1038	1078	1116	1150	1180	1209	1239	1271
.50	649	703	752	795	834	870	907	946	986	1024	1059	1090	1119	1148	1179
.55	560	615	666	711	750	787	823	861	899	938	973	1005	1035	1064	1094
.60	478	533	584	631	672	710	745	781	819	857	893	926	956	985	1014
.65	402	455	507	555	598	637	673	708	744	781	818	852	882	911	940
.70	332	383	434	483	528	568	604	639	674	710	747	781	813	842	870
.75	267	316	366	414	460	502	540	575	609	644	680	715	747	777	805
.80	208	255	302	350	396	439	479	514	548	582	617	652	685	715	744
.85	163	198	244	290	335	379	420	457	491	524	558	592	625	657	686
.90	101	146	189	233	278	321	363	401	437	470	502	535	569	601	631
.95	50	96	139	181	224	267	308	348	384	418	450	482	515	547	578
1.00	----	48	92	133	174	215	256	296	334	369	401	432	464	496	527
1.05	----	----	45	88	128	167	207	246	285	321	354	385	416	447	478
1.10	----	----	----	44	84	123	161	199	238	274	308	340	371	401	432
1.15	----	----	----	----	42	81	118	155	192	229	264	297	328	357	387
1.20	----	----	----	----	----	39	78	114	150	186	221	255	286	316	345
1.25	----	----	----	----	----	----	38	75	110	145	180	214	246	276	305
1.30	----	----	----	----	----	----	----	37	72	106	140	174	207	238	267
1.35	----	----	----	----	----	----	----	----	36	70	102	135	168	200	230
1.40	----	----	----	----	----	----	----	----	----	35	67	99	131	163	194
1.45	----	----	----	----	----	----	----	----	----	----	33	65	96	127	158
1.50	----	----	----	----	----	----	----	----	----	----	----	32	63	93	123
1.55	----	----	----	----	----	----	----	----	----	----	----	----	31	61	91
1.60	----	----	----	----	----	----	----	----	----	----	----	----	----	30	89
1.65	----	----	----	----	----	----	----	----	----	----	----	----	----	----	29

TABLE C4—Continued

$\Theta_s(\zeta_v, \zeta) 10^3$

ζ_v	ζ																	
	1.75	1.80	1.85	1.90	1.95	2.00	2.10	2.20	2.30	2.40	2.50	2.60	2.70	2.80	2.90	3.00	3.50	4.00
0.00	2463	2486	2512	2542	2572	2596	2640	2692	2732	2778	2816	2858	2893	2932	2964	3000	3153	3287
.05	2307	2330	2356	2385	2415	2440	2484	2535	2576	2621	2660	2701	2737	2775	2808	2844	2997	---
.10	2154	2178	2203	2232	2262	2288	2331	2382	2423	2468	2507	2548	2584	2622	2656	2691	2844	2979
.15	2008	2033	2058	2086	2115	2141	2186	2236	2278	2322	2362	2402	2439	2476	2510	2545	2699	2833
.20	1870	1895	1920	1948	1977	2003	2048	2097	2140	2184	2224	2264	2301	2338	2372	2407	2560	2694
.25	1741	1766	1791	1818	1846	1873	1918	1967	2011	2054	2094	2134	2171	2208	2242	2277	2431	2565
.30	1619	1645	1670	1697	1725	1752	1798	1846	1890	1932	1973	2012	2050	2087	2121	2156	2310	2444
.35	1506	1533	1558	1584	1611	1639	1685	1732	1777	1819	1861	1899	1937	1974	2008	2043	2197	2331
.40	1401	1428	1453	1479	1506	1533	1580	1627	1672	1714	1756	1794	1833	1868	1904	1938	2092	2226
.45	1302	1331	1356	1381	1408	1435	1483	1529	1575	1616	1658	1696	1735	1771	1806	1840	1994	2128
.50	1211	1240	1266	1291	1316	1343	1392	1438	1484	1525	1567	1605	1644	1679	1715	1749	1903	2037
.55	1125	1155	1181	1206	1231	1258	1308	1353	1399	1440	1482	1520	1559	1594	1630	1664	1818	1952
.60	1045	1075	1102	1127	1152	1178	1229	1273	1319	1360	1402	1441	1479	1515	1551	1584	1739	1872
.65	970	1000	1028	1053	1078	1103	1154	1199	1245	1286	1328	1366	1405	1440	1476	1510	1664	1798
.70	899	929	958	984	1009	1033	1084	1129	1174	1217	1258	1297	1335	1371	1406	1440	1594	1728
.75	833	863	891	918	943	968	1018	1061	1108	1151	1192	1231	1269	1305	1340	1374	1528	1662
.80	772	800	829	856	882	906	955	1002	1046	1089	1129	1169	1206	1243	1278	1312	1466	1600
.85	713	741	769	797	823	848	896	944	987	1031	1070	1111	1148	1184	1219	1253	1407	1541
.90	658	686	713	741	768	792	840	888	931	975	1015	1055	1092	1129	1163	1198	1352	1485
.95	606	633	660	688	714	740	787	835	878	922	962	1002	1039	1076	1110	1145	1299	1432
1.00	556	583	610	637	664	689	737	784	828	871	912	951	989	1025	1060	1094	1248	1382
1.05	508	536	562	588	615	641	689	736	781	823	864	903	941	977	1012	1046	1200	1334
1.10	462	490	517	543	569	595	644	690	735	777	818	857	895	931	966	1000	1155	1288
1.15	417	446	473	499	525	550	600	646	691	733	774	813	851	887	923	956	1111	1244
1.20	374	403	431	458	483	508	558	603	649	691	732	771	809	845	880	914	1068	1202
1.25	334	362	391	417	443	467	517	563	608	651	691	731	768	805	840	873	1028	1161
1.30	295	323	351	378	404	429	478	525	569	612	652	692	729	766	801	835	989	1122
1.35	258	285	313	340	367	392	440	487	531	574	614	654	692	728	763	797	951	1085
1.40	222	250	277	304	330	356	404	451	495	538	579	618	655	692	727	761	915	1049
1.45	188	216	242	268	295	321	369	416	460	503	544	583	621	657	692	726	880	1014
1.50	153	182	209	235	261	287	336	382	427	469	510	549	587	623	658	692	847	980
1.55	120	149	177	203	228	254	303	349	394	436	477	516	554	590	626	659	814	947
1.60	83	117	145	172	197	222	271	318	362	405	445	485	523	559	594	628	782	916
1.65	58	86	114	141	167	192	240	287	331	374	415	454	492	528	563	597	751	885
1.70	29	56	83	110	137	162	210	258	301	344	385	424	462	499	533	568	722	855
1.75	----	28	55	81	108	133	182	228	273	315	356	395	433	470	505	539	693	826
1.80	----	----	27	53	79	105	154	200	245	287	328	367	405	441	477	510	665	798
1.85	----	----	----	26	52	77	127	173	217	260	301	340	378	414	449	483	637	771
1.90	----	----	----	----	26	51	100	146	191	233	274	313	351	387	423	456	611	744
1.95	----	----	----	----	----	25	73	121	164	208	248	288	325	362	396	430	585	718
2.00	----	----	----	----	----	----	48	95	139	182	223	262	300	336	371	405	559	693
2.05	----	----	----	----	----	----	24	70	115	157	198	237	275	311	347	381	535	668
2.10	----	----	----	----	----	----	----	46	91	133	174	213	251	287	323	356	511	644
2.15	----	----	----	----	----	----	----	23	67	110	150	190	227	264	299	333	487	621
2.20	----	----	----	----	----	----	----	----	44	87	127	167	204	241	276	310	464	598
2.25	----	----	----	----	----	----	----	21	64	105	144	182	219	254	288	322	475	609
2.30	----	----	----	----	----	----	----	----	42	83	122	160	196	232	266	300	453	587
2.35	----	----	----	----	----	----	----	----	21	62	101	139	175	210	244	278	431	565
2.40	----	----	----	----	----	----	----	----	----	40	80	117	154	189	223	257	411	545
2.45	----	----	----	----	----	----	----	----	----	20	59	97	133	168	202	236	389	523
2.50	----	----	----	----	----	----	----	----	----	----	39	77	113	148	182	216	369	503

TABLE C5

$$4\pi\theta_R(\zeta_p, \zeta) 10^3$$

ξ_p	ξ														
	0.25	0.30	0.35	0.40	0.45	0.50	0.55	0.60	0.65	0.70	0.75	0.80	0.85	0.90	0.95
0.00	130	186	251	323	399	478	554	624	708	730	760	772	770	758	744
.05	66	108	159	216	280	348	415	479	559	579	609	624	626	616	605
.10	28	55	92	136	188	244	303	360	412	454	485	503	507	502	491
.15	8	23	47	79	119	165	214	264	311	352	383	403	411	409	400
.20	1	7	20	41	69	105	145	188	230	269	300	321	332	333	327
.25	-----	1	6	17	36	62	93	128	165	200	231	253	267	271	268
.30	-----	-----	1	5	15	32	55	83	114	145	174	197	213	220	220
.35	-----	-----	-----	1	5	14	29	49	74	101	127	151	168	178	180
.40	-----	-----	-----	-----	1	4	12	26	44	66	90	112	130	142	148
.45	-----	-----	-----	-----	-----	1	4	11	24	40	60	80	98	111	120
.50	-----	-----	-----	-----	-----	-----	0	3	10	21	36	54	72	85	95
.55	-----	-----	-----	-----	-----	-----	-----	0	3	9	20	33	48	62	74
.60	-----	-----	-----	-----	-----	-----	-----	-----	0	3	9	18	30	43	55
.65	-----	-----	-----	-----	-----	-----	-----	-----	-----	0	3	8	17	27	39
.70	-----	-----	-----	-----	-----	-----	-----	-----	-----	-----	0	2	7	15	25
.75	-----	-----	-----	-----	-----	-----	-----	-----	-----	-----	-----	0	2	7	14
.80	-----	-----	-----	-----	-----	-----	-----	-----	-----	-----	-----	-----	0	2	7
.85	-----	-----	-----	-----	-----	-----	-----	-----	-----	-----	-----	-----	-----	0	2
.90	-----	-----	-----	-----	-----	-----	-----	-----	-----	-----	-----	-----	-----	-----	0

ξ_p	ξ														
	1.00	1.05	1.10	1.15	1.20	1.25	1.30	1.35	1.40	1.45	1.50	1.55	1.60	1.65	1.70
0.00	731	727	734	747	762	772	774	768	761	758	761	769	776	776	771
.05	592	589	593	605	617	629	632	626	620	624	619	626	634	634	630
.10	481	476	478	488	500	510	514	512	506	502	504	510	516	518	515
.15	391	385	386	394	405	415	420	419	414	410	411	416	422	424	422
.20	319	313	312	318	328	337	343	343	339	335	335	340	345	348	347
.25	261	255	253	257	265	275	281	282	280	276	275	278	283	287	286
.30	215	210	207	209	215	224	230	233	231	228	227	229	233	237	237
.35	178	173	170	170	175	182	189	193	192	190	188	189	193	197	198
.40	147	144	140	139	142	148	155	160	161	159	156	157	160	164	166
.45	122	120	117	115	116	121	127	132	135	133	131	131	133	137	139
.50	100	101	98	96	95	99	104	110	133	113	111	110	111	114	117
.55	81	84	83	80	79	81	85	90	94	96	94	93	93	96	99
.60	64	69	70	68	67	67	70	74	79	81	81	79	79	81	84
.65	49	56	58	58	57	56	57	61	65	69	69	68	67	68	71
.70	35	43	48	49	49	47	47	50	54	58	59	59	58	58	60
.75	23	31	38	41	42	41	40	41	44	48	51	51	50	50	51
.80	13	21	28	33	35	35	34	34	36	39	43	44	44	43	43
.85	6	12	19	25	29	30	30	29	30	32	35	38	39	38	38
.90	2	6	11	17	22	25	26	25	25	26	29	32	33	33	33
.95	0	2	5	10	16	20	22	22	22	22	23	26	28	29	29
1.00	-----	0	2	5	10	14	18	19	19	19	19	21	24	25	26
1.05	-----	-----	0	2	5	9	13	16	17	16	16	17	19	22	23
1.10	-----	-----	-----	0	2	4	8	12	14	15	14	14	16	18	20
1.15	-----	-----	-----	-----	0	2	4	8	11	12	13	12	13	14	16
1.20	-----	-----	-----	-----	-----	0	1	4	7	10	11	11	11	12	13
1.25	-----	-----	-----	-----	-----	-----	0	1	4	7	9	10	10	10	10
1.30	-----	-----	-----	-----	-----	-----	-----	0	1	3	6	8	9	9	9
1.35	-----	-----	-----	-----	-----	-----	-----	-----	0	1	3	6	7	8	8
1.40	-----	-----	-----	-----	-----	-----	-----	-----	-----	0	1	3	5	7	7
1.45	-----	-----	-----	-----	-----	-----	-----	-----	-----	-----	0	1	3	5	6
1.50	-----	-----	-----	-----	-----	-----	-----	-----	-----	-----	-----	0	1	3	4
1.55	-----	-----	-----	-----	-----	-----	-----	-----	-----	-----	-----	-----	0	1	3
1.60	-----	-----	-----	-----	-----	-----	-----	-----	-----	-----	-----	-----	-----	0	1
1.65	-----	-----	-----	-----	-----	-----	-----	-----	-----	-----	-----	-----	-----	-----	0

TABLE C5—Continued

$4\pi\Theta_R(\zeta_p,\zeta)10^3$

ζ_p	ζ																	
	1.75	1.80	1.85	1.90	1.95	2.00	2.10	2.20	2.30	2.40	2.50	2.60	2.70	2.80	2.90	3.00	3.50	∞
0.00	768	769	775	778	777	773	777	778	777	780	778	781	779	780	781	780	782	783
.05	626	627	633	635	636	632	635	637	636	638	636	638	637	638	638	638	640	640
.10	511	512	516	520	519	516	518	520	519	522	520	523	521	523	523	523	524	528
.15	419	418	422	426	426	423	425	427	425	429	426	429	428	430	429	429	430	434
.20	344	343	346	350	350	348	349	352	350	353	351	354	352	354	354	354	355	358
.25	284	282	285	288	289	288	288	291	289	292	290	293	291	293	293	293	294	298
.30	235	234	235	239	240	239	238	242	240	243	241	244	242	244	243	244	245	249
.35	196	195	195	198	200	200	198	202	200	203	202	204	203	204	204	205	205	209
.40	165	163	163	165	168	168	166	170	168	171	170	171	171	172	171	173	173	177
.45	139	137	137	139	141	142	140	143	142	144	144	145	145	146	145	146	147	150
.50	118	117	116	117	119	120	119	122	121	122	123	123	123	124	124	125	126	129
.55	100	100	99	99	101	103	102	104	104	104	105	105	106	107	106	107	108	111
.60	86	86	84	84	86	88	87	89	90	90	91	91	92	92	92	93	94	97
.65	73	74	73	72	73	75	76	76	78	77	79	78	80	79	80	80	82	85
.70	62	64	63	63	63	65	66	66	68	67	69	68	69	69	70	70	71	74
.75	53	55	55	55	54	56	58	57	59	59	60	60	61	61	61	61	63	66
.80	45	47	48	48	47	48	51	50	52	51	53	53	54	53	54	54	56	59
.85	38	40	42	42	42	42	44	44	45	45	46	47	47	47	48	48	49	53
.90	33	34	36	37	37	37	39	39	40	40	41	41	42	42	43	43	44	47
.95	29	29	31	33	33	32	34	35	35	36	36	37	37	38	38	38	39	43
1.00	25	25	27	28	29	29	29	31	31	32	32	33	33	34	34	34	35	39
1.05	23	22	23	24	26	26	26	28	27	29	29	30	30	30	30	31	32	35
1.10	20	20	20	21	22	23	23	24	25	25	26	26	27	27	27	28	29	32
1.15	18	18	18	18	19	20	20	21	22	23	23	24	24	25	25	25	26	30
1.20	15	16	16	16	16	18	18	19	20	20	21	21	22	22	23	23	24	27
1.25	12	14	14	14	14	15	17	16	18	18	19	19	20	20	21	21	22	25
1.30	10	11	12	13	12	13	15	15	16	16	17	17	18	18	19	19	20	23
1.35	8	9	10	11	11	11	13	13	14	15	15	16	16	17	17	17	18	22
1.40	7	7	8	10	10	10	11	12	12	13	13	14	14	15	15	16	17	20
1.45	6	6	7	8	9	9	9	11	11	12	12	13	13	14	14	14	16	19
1.50	5	5	5	6	7	8	8	10	10	11	11	12	12	13	13	13	14	18
1.55	4	5	5	5	6	7	7	8	9	9	10	10	11	11	12	12	13	16
1.60	2	4	4	4	4	5	7	7	8	8	9	9	10	10	11	11	12	15
1.65	1	2	3	4	4	4	6	6	7	8	8	9	9	9	10	10	11	14
1.70	0	1	2	3	4	4	5	6	6	7	7	8	8	9	9	9	10	14
1.75	----	0	1	2	3	3	4	5	5	6	6	7	7	8	8	9	10	13
1.80	----	----	0	1	2	3	3	4	5	5	6	6	7	7	7	8	9	12
1.85	----	----	----	0	1	2	3	3	4	4	5	6	6	6	7	7	8	12
1.90	----	----	----	----	0	1	2	2	4	4	5	5	6	6	6	7	8	11
1.95	----	----	----	----	----	0	2	2	3	4	4	5	5	5	6	6	7	10
2.00	----	----	----	----	----	----	1	2	2	3	3	4	4	5	5	6	7	10
2.05	----	----	----	----	----	----	0	1	2	3	3	4	4	4	5	5	6	9
2.10	----	----	----	----	----	----	----	1	2	2	3	3	4	4	4	5	6	9
2.15	----	----	----	----	----	----	----	0	1	2	2	3	3	3	4	4	5	9
2.20	----	----	----	----	----	----	----	----	1	1	2	2	3	3	4	4	5	8
2.25	----	----	----	----	----	----	----	0	1	1	2	2	3	3	3	3	5	8
2.30	----	----	----	----	----	----	----	----	1	1	2	2	2	2	3	3	4	8
2.35	----	----	----	----	----	----	----	----	0	1	1	1	2	2	3	3	4	8
2.40	----	----	----	----	----	----	----	----	----	1	1	1	1	2	2	2	4	7
2.45	----	----	----	----	----	----	----	----	----	0	1	1	1	2	2	2	3	7
2.50	----	----	----	----	----	----	----	----	----	----	0	0	1	1	2	2	3	6

TABLE C6

$$4\zeta_p \Phi_a(\zeta_p, \zeta) 10^3$$

ζ_p	ζ														
	0.25	0.30	0.35	0.40	0.45	0.50	0.55	0.60	0.65	0.70	0.75	0.80	0.85	0.90	0.95
0.00	0	0	0	0	0	0	0	0	0	0	0	0	0	0	0
.05	39	48	56	63	67	69	67	62	55	46	36	28	32	24	30
.10	59	77	94	107	117	121	119	111	96	77	58	41	32	32	43
.15	59	88	114	136	152	161	160	149	129	102	72	46	30	29	43
.20	40	79	115	148	173	188	192	182	158	124	85	48	23	17	33
.25		50	98	142	178	204	216	210	186	148	99	51	15	1	14
.30			60	116	167	206	230	233	214	175	110	61	11	-16	-10
.35				69	135	190	230	248	240	205	148	79	15	-28	-35
.40					79	152	212	249	259	236	184	110	32	-31	-57
.45						89	169	231	265	263	223	152	63	-18	-69
.50							98	185	248	275	259	201	111	13	-65
.55								108	201	263	281	248	170	64	-38
.60									117	215	275	282	231	133	14
.65										126	279	285	278	207	90
.70											135	242	292	270	178
.75												144	253	296	256
.80													153	264	298
.85														162	274
.90															170

ζ_p	ζ														
	1.00	1.05	1.10	1.15	1.20	1.25	1.30	1.35	1.40	1.45	1.50	1.55	1.60	1.65	1.70
0.00	0	0	0	0	0	0	0	0	0	0	0	0	0	0	0
.05	39	49	54	54	46	37	30	30	37	47	51	47	38	31	34
.10	62	81	93	92	79	59	45	44	58	77	87	79	61	48	53
.15	70	99	119	120	102	73	49	46	66	95	111	102	74	53	59
.20	66	105	135	140	119	81	48	40	63	101	127	118	82	52	55
.25	51	100	141	155	135	90	45	28	51	98	135	131	89	47	45
.30	28	85	139	165	150	101	44	15	33	87	136	142	97	43	30
.35	-3	59	126	169	165	116	48	2	10	67	131	150	108	41	14
.40	-37	24	102	164	178	136	60	-4	-13	40	117	155	122	46	0
.45	-70	-19	66	147	185	159	81	-1	-34	7	93	154	139	59	-9
.50	-95	-64	17	115	181	181	112	15	-47	-28	58	144	155	81	-9
.55	-103	-104	-39	66	161	195	148	45	-45	-60	15	119	165	110	5
.60	-85	-128	-95	3	119	193	182	89	-25	-80	-34	79	163	141	33
.65	-36	-124	-138	-67	56	167	204	141	17	-80	-78	25	141	166	74
.70	44	-84	-153	-131	-25	111	201	188	77	-54	-107	-37	97	175	121
.75	144	-3	-126	-168	-107	28	163	214	145	3	-107	-95	31	157	163
.80	239	106	-50	-161	-170	-69	86	202	201	81	-69	-130	-47	106	183
.85	297	218	65	-95	-186	-156	-20	141	222	163	6	-124	-116	26	167
.90	282	293	193	23	-136	-200	-129	36	188	220	104	-68	-150	-67	105
.95	178	290	286	164	-20	-171	-202	-90	94	221	194	32	-129	-142	7
1.00		187	296	277	133	-62	-199	-192	-42	148	235	147	-44	-165	-100
1.05			195	301	265	100	-102	-218	-170	13	194	228	83	-112	-170
1.10				202	305	250	66	-139	-229	-138	70	228	200	9	-164
1.15					210	308	234	30	-173	-230	-96	125	245	154	-65
1.20						217	309	215	-6	-202	-222	-48	175	244	92
1.25							224	309	195	-42	-225	-205	4	215	225
1.30								231	308	172	-78	-242	-179	58	243
1.35									238	306	148	-112	-253	-145	111
1.40										244	302	123	-144	-257	-105
1.45											251	297	96	-173	-253
1.50												257	291	69	-200
1.55													262	284	41
1.60														268	276
1.65															273

TABLE C6—Continued

$4\zeta_v\Phi_q(\zeta_v,\zeta) 10^3$

ζ	ζ																	
	1.75	1.80	1.85	1.90	1.95	2.00	2.10	2.20	2.30	2.40	2.50	2.60	2.70	2.80	2.90	3.00	3.50	∞
0.00	0	0	0	0	0	0	0	0	0	0	0	0	0	0	0	0	0	0
.05	44	50	45	36	33	40	45	34	48	34	47	35	46	36	44	41	45	41
.10	72	84	75	57	50	65	75	53	80	53	79	54	78	56	73	65	75	66
.15	86	106	98	67	56	76	95	60	101	60	99	62	98	65	91	78	94	80
.20	90	119	110	73	54	78	109	58	114	60	111	62	110	64	102	81	104	86
.25	86	126	121	75	46	71	118	51	121	56	116	58	116	59	109	76	108	87
.30	73	126	129	79	37	58	126	41	123	50	116	52	118	50	114	67	107	84
.35	55	120	137	85	28	40	131	30	121	45	111	47	115	41	117	53	102	79
.40	30	106	142	96	24	19	134	22	114	43	101	45	108	33	118	38	93	74
.45	3	84	143	110	26	-1	133	19	99	47	84	49	95	29	115	22	80	68
.50	-23	54	137	127	37	-18	125	24	78	58	61	59	76	32	108	9	61	62
.55	-44	17	119	143	58	-26	107	39	49	76	32	75	50	42	93	1	40	56
.60	-53	-24	88	151	87	-22	77	63	14	98	1	95	20	60	70	2	16	51
.65	-43	-60	43	145	120	-1	36	94	-22	120	-28	114	-11	83	40	14	-7	46
.70	-12	-82	-11	120	148	37	-11	124	-51	134	-48	127	-37	106	4	37	-22	41
.75	41	-80	-64	72	159	85	-57	145	-65	131	-50	124	-50	122	-30	69	-25	38
.80	105	-46	-101	6	144	134	-86	143	-55	106	-30	100	-42	120	-53	100	-12	34
.85	163	18	-107	-64	95	164	-87	112	-16	56	14	54	-9	95	-55	120	13	31
.90	192	99	-70	-116	18	160	-50	50	46	-10	72	-7	43	46	-29	117	59	28
.95	169	171	9	-127	-68	110	21	-29	112	-74	125	-66	99	-17	22	83	97	26
1.00	89	199	107	-80	-132	20	107	-100	158	-109	151	-99	138	-73	83	23	114	24
1.05	-31	160	187	17	-140	-81	171	-130	155	-94	127	-85	135	-97	130	-46	98	22
1.10	-143	52	203	131	-76	-150	177	-94	91	-23	53	-20	81	-70	134	-93	44	20
1.15	-190	-87	131	206	46	-144	107	3	-16	79	-48	74	-11	5	83	-91	-28	18
1.20	-131	-186	-10	191	168	-50	-20	121	-119	162	-126	151	-98	98	-9	-29	-85	17
1.25	22	-180	-153	73	219	95	-141	194	-155	172	-131	160	-130	156	-97	67	-89	16
1.30	188	-51	-207	-94	149	208	-178	165	-89	86	-44	81	-74	133	-125	143	-28	15
1.35	258	137	-118	-207	-19	204	-90	32	54	-57	91	-51	48	29	-63	142	68	14
1.40	160	257	74	-174	-181	64	82	-128	184	-165	186	-151	158	-97	61	48	136	13
1.45	-60	202	240	6	-211	-130	219	-197	196	-147	158	-135	169	-152	161	-82	117	12
1.50	-243	-12	236	208	-63	-227	201	-102	60	1	9	2	53	-79	149	-148	10	11
1.55	-223	-226	38	259	163	-127	17	100	-131	172	-152	160	-110	79	17	-83	-105	11
1.60	13	-243	-203	87	270	108	-189	238	-209	211	-179	195	-177	189	-133	74	-125	10
1.65	266	-16	-258	-175	134	268	-220	167	-82	57	-24	54	-69	134	-157	182	-16	9
1.70	278	256	-44	-270	-141	177	-19	-71	150	-158	177	-145	128	-53	-13	122	128	8
1.75	-----	282	244	-72	-276	-103	288	-242	247	-210	213	-194	212	-188	166	-64	155	8
1.80	-----	-----	287	232	-99	-278	244	-142	81	-19	19	-17	71	-111	180	-183	17	8
1.85	-----	-----	-----	291	218	-125	-20	144	-184	218	-202	202	-156	113	-10	-83	-142	7
1.90	-----	-----	-----	-----	294	204	-268	279	-229	209	-177	193	-195	221	-192	137	-125	7
1.95	-----	-----	-----	-----	-----	298	-174	68	32	-65	90	-59	27	56	-126	202	65	7
2.00	-----	-----	-----	-----	-----	-----	173	-240	275	-259	261	-238	235	-187	126	4	188	6
2.05	-----	-----	-----	-----	-----	-----	304	-216	151	-87	80	-80	130	-170	222	-202	60	6
2.10	-----	-----	-----	-----	-----	-----	-----	139	-196	233	-222	215	-166	110	4	-112	-156	6
2.15	-----	-----	-----	-----	-----	-----	-----	309	-251	220	-189	204	-213	244	-224	166	-134	6
2.20	-----	-----	-----	-----	-----	-----	-----	-----	104	-139	158	-127	88	3	-96	201	114	5
2.25	-----	-----	-----	-----	-----	-----	-----	-----	312	-276	268	-254	267	-247	208	-88	194	5
2.30	-----	-----	-----	-----	-----	-----	-----	-----	-----	66	-72	61	2	-73	176	-231	-49	5
2.35	-----	-----	-----	-----	-----	-----	-----	-----	-----	315	-291	291	-271	249	-165	42	-207	5
2.40	-----	-----	-----	-----	-----	-----	-----	-----	-----	-----	27	1	-46	133	-207	253	20	5
2.45	-----	-----	-----	-----	-----	-----	-----	-----	-----	-----	316	-295	286	-235	154	-2	227	4
2.50	-----	-----	-----	-----	-----	-----	-----	-----	-----	-----	-----	-12	74	-146	234	-261	3	4

TABLE C7—Continued

$$-\left(\frac{1}{2\pi\zeta_p}\right)\Phi_3(\zeta_p, \zeta) 10^3$$

ζ_p	ζ																	
	1.75	1.80	1.85	1.90	1.95	2.00	2.10	2.20	2.30	2.40	2.50	2.60	2.70	2.80	2.90	3.00	3.50	∞
0.00	415	492	575	566	475	421	563	462	516	497	499	497	514	470	546	447	500	500
.05	408	484	568	560	468	414	556	456	508	490	491	491	506	464	539	440	492	493
.10	389	463	548	545	456	397	536	442	488	477	471	477	486	449	520	423	473	476
.15	364	433	521	525	439	374	509	424	459	459	443	458	459	430	494	400	446	453
.20	336	397	489	503	422	350	477	405	425	440	410	439	426	409	464	375	415	427
.25	308	358	452	480	406	326	442	388	388	422	374	420	390	390	430	350	382	399
.30	283	319	413	456	393	306	403	373	350	405	338	402	353	373	395	328	348	372
.35	263	280	371	430	383	291	363	362	311	390	302	387	317	359	359	309	315	347
.40	250	244	327	401	375	281	321	354	274	377	268	372	282	347	322	294	284	323
.45	244	214	282	369	367	278	279	348	241	363	239	358	250	338	285	285	257	300
.50	247	192	238	332	358	281	238	342	213	346	216	341	223	328	250	280	234	280
.55	258	181	197	289	343	289	201	332	193	325	201	320	203	317	218	279	218	261
.60	274	182	165	243	320	297	172	316	183	298	196	294	192	301	192	279	210	245
.65	289	195	144	196	288	300	154	292	184	263	200	261	190	279	175	277	208	229
.70	298	218	138	154	245	295	150	257	195	223	213	223	198	249	168	269	213	216
.75	294	244	150	123	197	276	161	215	214	181	229	183	212	213	172	252	221	203
.80	271	265	177	110	148	242	184	169	234	143	242	147	227	174	186	226	227	192
.85	229	270	210	120	110	194	212	128	245	117	245	122	236	140	203	191	227	182
.90	172	252	239	149	91	142	235	102	241	110	232	115	231	117	217	153	215	173
.95	114	209	250	188	99	98	240	98	216	124	200	127	209	112	219	121	190	164
1.00	72	149	232	222	132	77	220	119	173	153	156	153	171	127	203	104	156	157
1.05	62	91	184	233	176	87	175	156	122	187	111	184	126	155	168	107	122	149
1.10	90	56	121	210	212	125	118	193	82	206	81	201	91	182	126	130	99	143
1.15	145	61	66	155	218	173	72	209	70	198	80	193	79	194	90	161	96	137
1.20	198	106	46	90	183	206	57	189	92	159	109	157	97	177	78	181	155	132
1.25	217	167	73	46	120	199	84	138	137	104	152	106	135	136	95	175	144	126
1.30	183	206	133	49	59	149	137	78	178	61	181	66	170	88	132	141	164	122
1.35	109	193	188	100	37	81	183	45	185	56	174	61	175	61	164	94	158	117
1.40	39	128	196	164	70	36	185	61	146	94	128	95	141	72	165	62	124	113
1.45	22	50	144	193	136	47	135	116	82	146	70	144	86	114	128	67	82	109
1.50	73	18	64	158	183	107	64	167	38	172	42	167	48	154	76	106	60	106
1.55	153	58	17	79	167	168	27	169	50	143	66	140	58	155	48	146	76	102
1.60	190	139	45	19	94	173	56	112	109	78	123	80	107	109	67	148	116	99
1.65	143	184	125	34	24	108	126	42	160	32	159	37	150	54	118	105	141	96
1.70	49	144	178	111	25	31	169	25	149	49	133	52	141	40	148	52	122	93
1.75	----	50	144	171	98	18	133	80	80	113	66	111	82	82	122	42	73	91
1.80	----	----	51	144	164	85	51	147	22	154	25	149	32	135	61	85	43	88
1.85	----	----	----	52	144	157	11	148	40	120	57	117	47	135	31	133	65	86
1.90	----	----	----	----	53	144	62	73	114	44	125	47	109	76	67	124	113	84
1.95	----	----	----	----	----	54	141	11	150	18	141	23	140	26	125	64	124	82
2.00	----	----	----	----	----	----	143	42	96	76	79	76	94	50	126	26	79	80
2.05	----	----	----	----	----	----	56	125	18	140	16	135	27	115	63	62	34	78
2.10	----	----	----	----	----	----	----	141	26	114	42	111	33	127	21	121	52	76
2.15	----	----	----	----	----	----	----	58	109	30	119	34	104	62	62	112	106	74
2.20	----	----	----	----	----	----	----	----	138	15	126	19	128	15	122	43	111	72
2.25	----	----	----	----	----	----	----	----	60	93	46	91	62	61	102	22	53	71
2.30	----	----	----	----	----	----	----	----	----	134	8	129	10	123	29	83	25	69
2.35	----	----	----	----	----	----	----	----	----	62	77	62	62	91	26	120	74	68
2.40	----	----	----	----	----	----	----	----	----	130	5	124	16	99	62	112	66	66
2.45	----	----	----	----	----	----	----	----	----	63	63	78	36	111	12	64	65	65
2.50	----	----	----	----	----	----	----	----	----	----	125	6	112	34	64	18	64	64

TABLE C8—Continued

$$8\Phi_R(\zeta_p, \zeta)10^3$$

ζ_p	ζ																	
	1.75	1.80	1.85	1.90	1.95	2.00	2.10	2.20	2.30	2.40	2.50	2.60	2.70	2.80	2.90	3.00	3.50	∞
0.00	456	588	624	521	404	425	611	406	588	435	567	440	575	425	579	449	547	500
.05	359	480	526	440	330	335	512	328	485	358	464	361	473	344	482	359	448	410
.10	280	388	443	377	271	262	429	267	397	297	377	300	388	280	402	286	365	336
.15	215	312	373	326	228	205	360	220	324	251	305	253	316	231	336	227	296	276
.20	164	247	314	286	196	160	302	186	262	216	245	217	257	194	280	181	239	228
.25	124	192	263	253	173	127	251	161	209	190	194	190	206	166	233	146	192	190
.30	95	146	217	225	158	103	206	144	165	171	151	169	163	146	192	120	153	158
.35	75	108	176	200	148	88	167	133	127	156	116	154	127	132	157	101	120	133
.40	64	77	139	176	141	80	131	126	95	145	88	142	97	122	125	89	94	113
.45	60	55	105	151	136	77	100	122	70	134	66	131	73	115	98	82	74	96
.50	62	40	75	126	129	80	72	117	51	123	50	120	55	109	74	79	59	82
.55	68	33	51	101	120	84	50	111	39	110	41	107	43	102	55	78	49	71
.60	77	33	32	75	108	88	34	103	33	95	38	92	37	93	40	78	44	62
.65	85	40	22	51	91	90	25	90	34	78	41	76	36	82	32	77	43	54
.70	89	51	19	31	71	88	23	74	40	59	46	58	40	68	28	73	46	47
.75	87	62	24	17	50	80	27	55	48	40	53	40	46	52	30	66	49	42
.80	78	71	35	12	30	65	37	36	56	25	59	26	52	36	36	55	52	37
.85	62	73	48	16	15	47	48	21	60	15	60	16	56	23	42	41	52	34
.90	41	66	59	26	8	28	56	11	59	12	55	13	54	14	48	28	47	30
.95	21	52	62	40	11	13	58	10	50	17	44	17	46	13	48	16	39	27
1.00	7	32	57	51	22	6	51	17	36	26	30	26	34	17	43	11	28	25
1.05	4	14	42	54	36	9	37	28	20	37	16	35	20	26	32	12	17	22
1.10	12	4	23	48	46	20	20	39	8	43	7	41	10	34	19	19	10	21
1.15	28	5	8	32	48	34	7	44	5	40	7	38	6	37	9	27	9	19
1.20	42	17	2	14	38	43	3	38	11	30	15	29	11	33	6	33	14	17
1.25	47	33	9	3	22	41	10	25	23	16	26	15	21	22	11	31	22	16
1.30	39	43	24	4	7	29	24	10	33	5	33	5	30	10	20	23	27	15
1.35	21	40	37	16	1	12	34	2	35	4	31	4	31	4	28	11	26	14
1.40	5	25	39	31	9	2	35	6	25	12	21	12	23	6	28	4	18	13
1.45	1	7	28	37	24	4	24	18	11	24	8	23	11	16	20	5	8	12
1.50	12	0	10	30	34	17	9	29	2	30	2	28	3	24	8	14	4	11
1.55	29	9	0	13	31	30	1	29	4	24	7	22	5	25	2	22	7	10
1.60	36	25	6	1	16	31	7	18	16	10	18	10	15	15	6	23	15	10
1.65	27	34	22	4	2	18	20	4	26	1	25	2	23	5	16	14	20	9
1.70	9	26	32	19	2	4	28	1	24	5	20	5	21	2	22	4	16	9
1.75	-----	9	26	30	16	1	22	11	11	16	8	15	10	10	17	2	7	8
1.80	-----	-----	9	25	28	13	7	23	1	24	1	22	1	19	6	10	2	8
1.85	-----	-----	-----	9	24	26	0	23	4	18	6	17	4	19	1	18	6	7
1.90	-----	-----	-----	-----	9	24	9	11	17	5	18	5	15	9	7	17	14	7
1.95	-----	-----	-----	-----	-----	9	22	0	23	1	21	1	20	1	17	7	16	7
2.00	-----	-----	-----	-----	-----	-----	22	5	14	10	10	9	12	5	17	1	8	6
2.05	-----	-----	-----	-----	-----	-----	9	19	2	20	1	19	2	15	7	6	1	6
2.10	-----	-----	-----	-----	-----	-----	-----	21	3	16	5	15	3	17	0	15	4	6
2.15	-----	-----	-----	-----	-----	-----	-----	9	15	4	16	3	13	7	7	14	12	6
2.20	-----	-----	-----	-----	-----	-----	-----	-----	20	1	17	1	17	0	15	4	13	5
2.25	-----	-----	-----	-----	-----	-----	-----	-----	8	12	6	12	7	7	13	1	5	5
2.30	-----	-----	-----	-----	-----	-----	-----	-----	-----	18	0	17	0	15	2	9	1	5
2.35	-----	-----	-----	-----	-----	-----	-----	-----	-----	8	10	8	7	11	2	15	7	5
2.40	-----	-----	-----	-----	-----	-----	-----	-----	-----	-----	17	0	16	1	12	7	12	4
2.45	-----	-----	-----	-----	-----	-----	-----	-----	-----	-----	8	8	9	4	13	0	6	4
2.50	-----	-----	-----	-----	-----	-----	-----	-----	-----	-----	-----	16	0	13	3	7	0	4

INDEX

- Aberdeen, 5.24, 5.25, 5.41,
- Acceleration, effect of air drag on, 6.12.
- Adjoint equations, 5.32.
- Aerodynamic acceleration, 10.42.
- Aerodynamic case, 3.62.
- Aerodynamic damping moment, 3.23, 3.52.
- Aerodynamic drag, 2.11, 5.0.
- Aerodynamic effect during burning, 9.4.
- Aerodynamic forces, 2.4, 3.23, 3.32:
 - determination of precessional motion by, 10.24.
 - effect on initial yaw, 9.33.
 - effect on mallaunching, 9.32.
 - fin-stabilized rockets, 8.4.
 - linear, 9.41.
 - spin-stabilized rocket, 8.2, 8.3.
- Aerodynamic malalignment, 2.47, 3.42.
- Aerodynamic moment, 3.12, 3.32, 10.25.
- Aerodynamic restoring moment, 2.11, 3.5, 3.22, 3.33.
- Aerodynamic theory, 6.6.
- After-burning, 2.443.
- Air coordinate system, 9.52.
- Aircraft rockets, desirable characteristics, 9.51.
- Air density, 2.42.
- Airplane speeds:
 - high, 6.713.
 - low, 6.712.
- Air-speed indicators, 6.51.
- Angle of attack, 6.51, 6.54, 6.6.
- Angle of fall, 6.43.
- Angular acceleration, 2.26, 3.22, 9.25, 9.43.
- Angular deflection, 10.41.
- Angular drop, 6.4.
- Angular malalignment, 2.24, 3.12, 3.23, 3.25, 3.33, 9.27.
- Angular momentum, 8.53.
- Angular motion, 9.16.
- Angular thrust malalignment, 3.41, 6.72.
- Angular velocity, 6.16, 6.17, 9.25, 10.24.
- Applied torque, 3.22.
- Approximate equations of motion for rotating projectile, 9.11.
- Approximate formulas, 3.393.
- Arrangement, rocket and launcher, 4.1, 4.2.
- Asymptotic expansion, 9.32, 9.34, appendix B.
- At launching, 4.0.
- Ballistics:
 - classical problem in, 5.0.
 - coefficient, 2.441.
 - common problem, 5.23.
 - history of, 5.0.
 - of aircraft rockets, 6.0.
 - of shells, 5.2.
- Ballistics—Continued
 - measurements, 10.31.
 - pendulum, 10.31.
 - tables, 5.0, 5.1.
- Boosters, use of, 5.21.
- Bonlengé chronograph, 10.31.
- Boundary conditions, 3.11, 3.12, 6.11.
- Bourrelets, 4.0, 9.77.
- Bowen, I. S., 10.31.
- Burning:
 - effects during, 9.6.
 - regressive, 9.6.
 - time, 6.713.
- Burning distance, 3.1, 3.12, 3.31, 6.71, 6.713.
- Burnt velocity, 3.12, 6.71.
- Cauchy's method, 3.37.
- Center of lift, 2.412.
- Characteristic:
 - functions, 3.25, 3.33.
 - time, 3.33.
 - velocity, 3.33.
- Commission de Gâvre, 2.441.
- Computing sights, 6.43.
- Constant torque, 4.12.
- Contact range, 6.53.
- Coordinate forces, 3.21.
- Coordinate systems, 3.21.
- Coriolis acceleration, 9.81.
- Cornu spiral, 9.26, 10.23, appendix B.
- Critical yaw, 10.25.
- Cross-force, 2.41, 3.32, 3.51, 10.32, 10.4, 10.41.
- Cross pointing, 9.12, 9.52:
 - characteristic functions, 3.25, 3.33, 3.34, 9.31.
 - equivalent, 9.26.
 - initial, 3.13, 4.11.
 - solutions for, 9.32.
- Cross spin, 8.21, 8.23.
- Cross velocity, 6.63:
 - at launcher, 6.6.
 - initial, 3.13.
- Cross wind, 9.33:
 - effect of, 9.35.
 - force, 3.43.
- Curve of approach, 6.5.
- Damping, 3.33, 3.5, 10.12, 10.13, 10.2, 10.21, 10.23.
- Damping moment, 2.48, 8.34, 10.25.
- Deceleration coefficient, 2.11, 2.41, 3.31, 6.45.
- Deflection:
 - due to angular malalignment, 3.12.
 - due to gravity, 3.11.
 - due to linear malalignment, 3.12, 3.6, 3.62.
 - due to malalignment, 9.25.

Deflection—Continued

- due to mallaunching, 3.13, 3.52, 3.53.
- due to tail wind, 3.44.
- magnitude of, 3.21.
- Deflection of tangent, 3.42, 6.71:
 - due to gravity, 3.38.
 - due to linear malalignment, 3.39.
- Deflection of trajectory from flight line, 6.53.
- Didion-Bernoulli method, 5.1, 5.22, 5.23, 5.33, 6.3.
- Differential corrections, 5.3, 5.33, 6.45.
- Diffraction of light, appendix B.
- Dimensionless velocity parameter, 6.13.
- Direction, integrable equations for, 3.33.
- Dispersion, 10.31:
 - causes of, 6.74.
 - due to gas malalignment, 3.6.
 - due to rocket motor temperature, 6.713.
 - effect of launcher length on, 6.712, 9.76.
 - relative decrease in, 6.713.
 - sources of, 6.7.
- Distance functions, 3.31.
- Dive angles, trajectory drop for, 6.42.
- Doppler radar, 10.31.
- Down-wind, 3.43.
- Drag, 2.44, 2.442, 3.31, 5.11, 5.33, 8.32, 10.4.
- Drift, 10.4.
- Dynamical equations, 3.22.
- Effect of changes of mass, 2.43.
- Effect of changes of position of center of mass, 2.43.
- Effective acceleration, 2.22, 6.12.
- Effective burning distances, 2.22.
- Effective burning time, 2.22, 6.711.
- Effective launching line, 6.14, 6.15, 6.16, 6.17, 6.2, 6.41, 6.51.
- Effective launching path, 6.14.
- Effective rocket temperature, 2.3.
- Element, 10.23.
- Energy integrals, 9.15.
- Equations of constraint, 4.11.
- Equations of motion, 3.12, 3.13, 3.21, 3.32, 4.0, 4.11, 4.2, 6.1, 6.6, 9.31, 9.41, 9.52, 10.13, 10.21.:
 - approximate solution, 9.42.
 - during burning, 3.11, 3.2.
 - in two dimensions, 3.24.
 - of equivalent shell, 5.11.
 - rotating projectile, 9.1.
- Equations of rotation, 3.12.
- Equilibrium yaw, 10.14, 10.22, 10.23, 10.24, 10.25, 10.32, 10.42.
- Equivalent initial conditions, 5.1, 5.11.
- Equivalent shell, 5.1.
- Equivalent time, 6.13.
- Error, 6.7, 6.74.
- Euler's constant, appendix B.
- Euler's equations, 9.14.

- Fin malalignment, 2.47, 3.23, 3.25, 3.33, 3.42, 6.73.
- Fin size, effect of, 3.391.
- Fin-stabilized rockets:
 - with slow spin, 3.6.
 - advantages and disadvantages of, 9.55.
- Firing:
 - in absence of wind, 3.2.
 - in presence of wind, 3.43.
- Flight line, 6.11, 6.14, 6.15, 6.16, 6.2, 6.3.
- Force of constraint, 4.2.
- Formulas, derivation of, 5.41.
- Forward firing, 6.711:
 - connection with ground firing, 6.11.
 - uncertain quantity in, 6.54.
- Freedom:
 - one degree of, 4.1.
 - two degrees of, 4.1.
- Free fall, 6.53.
- Fresnel integral, appendix B.
- Fresnel and Related integrals, table C1.
- G₀ law, 5.24.
- Gas malalignment, 2.2, 2.24, 3.394, 3.6.
- Gâvre law, 5.24, 5.25, 5.41.
- General solution, reduction of, 3.25.
- Geometrical malalignment, 3.394.
- Gravity, 9.52:
 - as dominant force, 5.0.
 - characteristic functions of, 3.25, 3.33.
 - deflection, 6.2.
 - determination of precessional motion by, 10.24.
 - drop, 6.43, 6.53, 6.7.
 - effect of, 3.1, 3.12, 3.23, 3.38, 10.14.
 - for equivalent shell, 5.11.
 - motion due to, 3.38.
 - notation, 3.1.
 - solution for, 9.34, 9.53.
 - term, 6.14, 6.2.
- Greenhill, Sir George, 10.26.
- Green's functions, 3.5, 3.37, 3.41, 3.62, 4.13, 5.31, 6.6, 9.13, 9.25, 9.26, 9.31, 9.34, 9.36, 9.42, 9.43, 9.54, 10.42.
- Ground firing, 6.11, 6.712.
- Head wind, 9.43, 9.54.
- Homogeneous equations, 3.25, 3.34, 9.31.
- Horizontal tangents, locus of, 12.24.
- Ignition range, 6.53.
- Inclined jets, 8.52.
- Inertial forces on spinning rockets, 9.8.
- Inhomogeneous equations and terms, 3.25, 3.37, 9.31.
- Initial cross-spin, 9.12.
- Initial velocity, 5.1, 5.33, 6.1.
- Initial yaw, 3.33, 3.34, 3.35, 9.12.

- Jet acceleration, 3.31.
- Jet damping:
 - effect of, 3.53.
 - torque, 2.26.
 - torque coefficient, 2.26.
- Jet force, 3.23, 4.12, 8.5, 9.34.
- Jet thrust, 4.2, 5.11.
- J_0 law, 5.24.

- Lanyard launching, 6.53.
- Lateral displacement, 3.35, 4.13,
- Lateral motion, 3.33, 3.35, 3.36.
- Lateral velocity, 4.11, 4.13.
- Launcher length, 3.12, 3.39, 6.711, 6.712, 6.713.
- Launchers, 4.0:
 - crooked, 4.13.

 - zero-length, 3.12, 3.14, 4.0, 6.17, 6.71, 6.72.
- Launching, 4.0, 4.2.
 - factor, 6.15.
 - line, 6.14.
 - motion, 4.13.
 - process, 9.7, 9.71.
- Lift, 2.46, 8.32, 10.42.
- Limiting motion, 10.25.
- Linear damping, 10.32.
- Linear deflection, 3.36, 10.41.
- Linear malalignment, 2.24, 3.23, 9.27.
 - effect of, 3.12, 3.39.
 - characteristic functions, 3.25, 3.33.
- Linear thrust, 2.25.
- Linear thrust malalignment, 3.6, 6.71.
- Liquid payload, 9.6.

- Long-burning rockets, 3.62, 6.711.

- Magnus force, 8.33, 10.25, 10.4, 10.42.
- Magnus moments, 3.6, 8.2, 8.33, 9.42, 9.51, 10.12, 10.13, 10.14, 10.2, 10.21, 10.23, 10.32.
- Malalignment, 6.7:
 - approximate treatment of, 9.25.
 - approximate solution of, 9.26.
 - effect of, 9.36.
 - effect of during launching, 9.75.
 - effect of unbalance on, 9.74.
- Mallaunching, 4.0, 4.11, 4.13, 6.17, 6.54, 6.6, 9.55:
 - characteristic functions 3.25, 3.33, 3.34, 9.31.
 - effective, 9.26.
 - effect of, 3.12.
 - effect on initial angular velocity, 3.36.
 - equivalent, 9.25, 9.26.
 - solutions for, 9.32, 9.54.
 - produced by unbalance, 9.72.
- Mass, 3.12, 3.22.
- Mechanical malalignment, 2.25.
- Milne method, 5.25.
- Moments of inertia, 3.12, 3.22, 3.6, 10.11, 10.32.
- Moments, 3.25.
- Motion:
 - after burning, 5.0, 10.0.
 - during burning, 3.0.
 - in a single plane, 3.12.
 - in terms of nutations and precessions, 10.21.
 - in two planes, 3.12, 3.21.
 - with constant acceleration, 9.3.
 - with finite stability, 9.3.
 - with linear aerodynamic moments, 10.1.
 - with nonlinear aerodynamic moments, 10.2.
 - with overturning moment, 10.11.
 - with overturning and magnus moments, 10.12.
 - with transverse aerodynamic forces and moments, 10.13.
- Moving vehicles, rockets launched from, 6.0.

- Near contact points, 4.12.
- Neutral equilibrium, 10.13.
- Newton's law, 3.22.
- Nutation, 9.14, 9.31, 10.0, 10.11, 10.12, 10.2, 10.21:
 - amplitude, 10.13.
 - damped, 10.13, 10.23.
 - frequency, 10.22.
 - per precession, 10.11.
 - stable, 10.13, 10.26.
 - with overturning moment, 10.22.
- Nutational kinetic energy, 9.15.

- Orientation, 3.42:
 - due to gravity, 3.38.
 - due to linear malalignment, 3.39.
 - initial, 9.25.
 - integrable equations for, 3.33.
- Orientation angle, 3.12, 3.21.
- Oscillation constant amplitude, 10.13.
- Otto-Lardillon method, 5.23.
- Overturning moment, 8.32, 9.42, 9.52, 9.53, 9.6, 10.11, 10.12, 10.2, 10.21, 10.22, 10.24, 10.32, 10.41:
 - effect of, 9.34.
 - linear, 10.25.

- Payload, 9.63,
- Pitot tubes, 6.51.
- Post launcher, 6.713.
- Precession, 9.31, 10.0, 10.11, 10.12, 10.13, 10.2, 10.21, 10.22:
 - damped, 10.13.
 - stable, 10.13.
 - with general nonlinear aerodynamic moments, 10.25.
 - with nonlinear overturning moment, 10.24.
 - with overturning moment, 10.22.
- Proximity fuze, 10.31.

- Quadratic resistance law, 6.3.

- Radar tracker, 10.31.
- Radius of gyration, 3.12.
- Rapid-spin rockets, 3.6.
- Reaction time, 2.22.
- Resistance law, table 2.441.
- Resonance, 3.62.
- Restoring moment, 2.45, 3.32.
- Rigorous geometrical description of motion, 9.14.
- Rocket motors, use of, 5.21.
- Rotations:
 - per nutation, 10.11.
 - per precession, 10.11.
- Siacci, 2.441.
- Siacci method, 5.1, 5.24.
- Sight angle, 6.52.
- Sighting problem, 6.5.
- Sight setting, 6.3, 6.54.
- Sight-setting equations, 6.52, 6.53.
- Simpson's rule, 6.6.
- Slow spin:
 - effect of, 3.6.
 - danger in, 3.62.
- Smythe, W. R., 10.31.
- Solar yaw camera, 10.0, 10.11, 10.13, 10.2, 10.3.
- Solenoid chronograph, 10.31.
- Solution of inhomogeneous equations by Green's functions, 9.13.
- Spark range, 10.31.
- Speed-attitude relations, 6.51.
- Spin:
 - effect of, 3.62.
 - in vacuum case, 3.61.
- Spin deceleration, 8.33.
- Spinners:
 - aircraft fired, 9.51.
 - sighting of, 9.55.
- Spin-stabilized rocket:
 - advantages and disadvantages of, 9.55
 - aircraft firing of, 9.5.
 - description of, 8.1.
 - instability in, 10.26.
 - motion during burning, 9.0, 10.0.
 - motion during launching, 9.0.
- Square law, 5.24.
- Stability, 10.13:
 - after burning, 9.41.
 - definition of, 10.26.
 - of nutations, 10.25.
- Stability factor, 8.22, 9.51, 9.54, 9.62, 10.11, 10.22, 10.24, 10.26, 10.32.
- Striking points, pattern of, 6.7.
- Table of notations, 8.25.
- Tangent deflection to trajectory, 6.13.
- Tangential acceleration, 3.22, 3.3.
- Taylor's series, 9.35, 10.24.
- Theory, limitations of, 3.394.
- Thrust malalignment, 6.0.
- Time to attain total velocity, 6.711.
- Tip-off, 4.0, 4.12, 6.17, 9.54, 9.55.
- Torque:
 - effect of 3.12, 10.42.
 - jet damping, 3.23.
 - ratio of, 3.33.
- Trajectory:
 - after burning, 6.3.
 - approximate, during burning, 6.2.
 - calculations for any aircraft, 6.5.
 - change in velocity along, 10.24.
 - deflection of tangent to, 3.12, 3.35, 6.13.
 - during burning, 3.0, 6.1, 6.17.
 - effect of aerodynamic forces on, 10.4.
 - of equivalent shell, 5.1.
 - of forward-fired rockets, 6.0, 6.1.
 - of rocket, 5.1.
 - rigidity of, 5.22.
 - subsonic, 10.42.
 - vacuum, 10.42.
- Trajectory calculation procedures, 6.4.
- Trajectory drops:
 - effect of small changes in burning time on, 6.44.
 - effect of small changes in velocity on, 6.44.
 - for various dive angles, 6.42.
- Transverse angular velocity, 3.37, 8.21.
- Trapezoidal formula, 6.6.
- True air speed, 6.53.
- Unbalance:
 - dynamic, 9.54, 9.72.
 - effect of additional small mass on, 9.73.
 - effect on malalignment, 9.74.
 - static, 9.72.
- Uniform wind, 6.11:
 - effect of, 3.43.
 - normal to launcher, 3.43.
 - parallel to launcher, 3.44.
- Unsymmetrical forces, 8.43.
- Unsymmetrical moments, 8.43.
- Upwind, 3.43.

Vacuum approximation, 3.1, 5.21, 9.2, 9.3.

Vacuum case, effect of spin in, 3.61.

Velocity:

effect of air drag on, 6.12.

functions of, 3.31.

total, 6.711.

Vertical motion, 3.36.

Wind:

effect during burning, 9.43.

effect of, 5.4.

Wing launchers, 6.52.

"Wow-wow" projectiles, 10.26.

Wronskian, 9.26.

Yaw, 3.42, 9.52.

angle of, 3.21.

camera records, 10.32.

characteristic functions, 3.25, 9.31.

due to gravity, 3.38.

due to linear malalignment, 3.39.

equivalent, 9.26.

initial, 4.11, 6.0.

in resonance, 3.62.

integrable equations for, 3.33.

oscillation, 6.45.

oscillation after burning, 3.34.

oscillation distance, 3.32, 6.53.

oscillation during burning, 3.34.

solution for, 9.33, 9.54.

Zero length launchers, 9.43.

